0099871

[0093583]

U.S. DEPARTMENT OF ENERGY

Prepared for the U.S. Department of Energy
under Contract DE-AC05-76RL01830

RPP-RPT-49990, Rev. 0
PNNL-20739

Single-Shell Tank Integrity Project Analysis of Record

Hanford Type III Single-Shell Tank Thermal and Operating Loads and Seismic Analysis

Report to Washington River Protection Solutions

MW Rinker
SK Bapanapalli
JE Deibler
CE Guzman-Leong
FG Abatt
BM Larsen
LJ Julyk
KI Johnson
NK Karri
SP Pilli
SE Sanborn
JA Dewberry
KL Stoops

RECEIVED
OCT 27 2011
EDMC

September 2011

Pacific Northwest
NATIONAL LABORATORY

Proudly Operated by **Battelle** *Since 1965*

Single-Shell Tank Integrity Project Analysis of Record Hanford Type III Single-Shell Tank Thermal and Operating Loads and Seismic Analysis

Author Name: R.S. Rast
Washington River Protection Solutions

Richland, WA 99352
U.S. Department of Energy Contract DE-AC27-08RV14800

EDT/~~ECN~~: 824659 UC:
Cost Center: Charge Code:
B&R Code: Total Pages: 561

Key Words: Single Shell Tank, SST, 758000 gallon, structural, analysis of record, dome, concrete, rebar, thermal, operating, seismic, soil structure interaction, finite element analysis, ANSYS

Abstract: This report documents the structural analysis of record of Hanford 758000 gallon (Type III) Single-Shell Tanks. The analysis concludes that for the imposed loading, the reinforced concrete tank structure meets the requirements of the American Concrete Institute (ACI) 349 code and thereby the International Building Codes (IBC). Analyses include the effects and combinations of seismic, dead, live, soil, thermal, hydrostatic, concentrated loads. The analysis also addresses the effects of concrete pits and associated penetrations. Limit load and buckling analyses are also performed to provide insight as to the response of the tank structure to increased concentrated and distributed loads applied at the ground surface. The analysis of record has been peer reviewed by recognized industry experts.

TRADEMARK DISCLAIMER. Reference herein to any specific commercial product, process, or service by trade name, trademark, manufacturer, or otherwise, does not necessarily constitute or imply its endorsement, recommendation, or favoring by the United States Government or any agency thereof or its contractors or subcontractors.

OCT 05 2011
DATE:
STA: 15
HANFORD RELEASE
ID: 65

Nancy A Fouad 10/5/2011
Release Approval Date

Release Stamp

Approved For Public Release

DISCLAIMER

This report was prepared as an account of work sponsored by an agency of the United States Government. Neither the United States Government nor any agency thereof, nor Battelle Memorial Institute, nor any of their employees, makes **any warranty, express or implied, or assumes any legal liability or responsibility for the accuracy, completeness, or usefulness of any information, apparatus, product, or process disclosed, or represents that its use would not infringe privately owned rights**. Reference herein to any specific commercial product, process, or service by trade name, trademark, manufacturer, or otherwise does not necessarily constitute or imply its endorsement, recommendation, or favoring by the United States Government or any agency thereof, or Battelle Memorial Institute. The views and opinions of authors expressed herein do not necessarily state or reflect those of the United States Government or any agency thereof.

PACIFIC NORTHWEST NATIONAL LABORATORY
operated by
BATTELLE
for the
UNITED STATES DEPARTMENT OF ENERGY
under Contract DE-AC05-76RL01830

This document was printed on recycled paper.
(9/2003)

RPP-RPT-49990, Rev. 0
PNNL-20739

Single-Shell Tank Integrity Project Analysis of Record

Hanford Type III Single-Shell Tank Thermal and Operating Loads and Seismic Analysis

Report to Washington River Protection Solutions

MW Rinker
SK Bapanapalli
JE Deibler
CE Guzman-Leong
FG Abatt1[1]
BM Larsen[1]
LJ Julyk[1]
KI Johnson
NK Karri
SP Pilli
SE Sanborn
JA Dewberry[1]
KL Stoops[1]

September 2011

Prepared for
the U.S. Department of Energy
under Contract DE-AC05-76RL01830

Pacific Northwest National Laboratory
Richland, Washington 99352

[1] M&D Professional Services, Inc., Richland, Washington

This page intentionally left blank.

Summary

This report, prepared by Pacific Northwest National Laboratory and M&D Professional Services, Inc. for Washington River Protection Solutions, documents the Type III (758-kgal storage capacity) single-shell tank (SST) detailed modeling results for the thermal and operating loads analysis (TOLA) and seismic analyses under the Single-Shell Tank Analysis of Record (SST AOR) Project.

The SST AOR project supports the U.S. Department of Energy's (DOE's) Office of River Protection (ORP) mission for obtaining a better understanding of the structural integrity of Hanford SSTs. Phase I of the SST AOR Project included the Evaluation Criteria report, Johnson et al. (2010), to guide the AOR of the Hanford SSTs, and the Preliminary Modeling Plan for Thermal and Operating Loads, found in Rinker et al. (2010), to determine the number of analyses required for adequate bounding of each of the SST types. Phase II of the SST AOR performs detailed modeling of thermal, operating, and seismic loads for each of the Hanford SST types. This Type III SST report is one of the Phase II deliverables for the SST AOR Project.

The analyses documented in this report used modern finite element (FE) modeling techniques with ANSYS®,[1] version 12.0 for the axisymmetric static thermal and operating loads analysis (TOLA) model. The 90° TOLA appurtenance model and both dynamic seismic analyses (baseline and appurtenance models) used ANSYS®, version 13.0. The versions 12.0 and 13.0 of ANSYS® software were fully verified and validated per the project quality assurance requirements on each of the computers used in the structural analyses. The TOLA static model includes the Type III geometry and the steel reinforcement detailed in the tank drawings. The static analysis evaluated the effects of waste level, waste temperature, and soil overburden loads. The effects of time (creep) and temperature on material properties, concrete cracking, and soil properties were also considered. A separate TOLA model evaluated the effects of tank appurtenances such as pump pits and/or sluice pits. A tank limit analysis was also conducted with the TOLA static model. The dynamic seismic model evaluated a range of soil properties, and evaluated tanks with and without waste during a seismic event. A separate seismic model evaluated the effects of tank appurtenances such as pump pits and/or sluice pits. Tank buckling was also evaluated using theoretical buckling solutions with appropriate knockdown factors for geometric imperfections, creep, cracking of reinforced concrete, and inelastic concrete deformation.

The SSTs are evaluated as Performance Category 2 (PC-2) structures, and DOE-STD-1020-2002, Section 2 (DOE 2002), requires that the ground motions for PC-2 shall be developed following the 2000 International Building Code (IBC 2000) requirements. The Tank Operations Contractor standard (TFC-ENG-STD-06) recognizes the State of Washington Administrative Code (WAC) 51-50-003, which currently adopts the 2009 edition of the International Building Code. The SST ground motions are developed as 2/3 of the Hanford Site-Specific Maximum Considered Earthquake (MCE) ground motions. The MCE ground motions are defined as the ground motions with a mean annual frequency of exceedance of 4×10^{-4} (2% probability of exceedance in 50 years). In this analysis, the site-specific design response spectra (DRS) for the SST facilities site uses the Rohay and Reidel (2005) Hanford Waste Treatment Plant (WTP) design spectra as a reasonable assessment of the current state of knowledge of the hazard levels at the 200 East and 200 West areas. The 2005 spectra are conservative relative to data documented in Geomatrix (2007), but this choice was made to protect against the chance that Hanford seismic hazard levels will be increased in the near future.

[1] ANSYS® is a registered trademark of ANSYS, Inc., Canonsburg, Pennsylvania.

While the IBC does not explicitly address underground tanks, provisions are made within the code to satisfy its requirements by demonstrating compliance with the requirements of the American Concrete Institute (ACI) code for concrete structures. Chapter 19 of the IBC states that structural concrete shall be designed in accordance with the requirements of ACI 318. The commentary on ACI 349 describes the additional conservatisms for nuclear structures that exceed those in ACI 318. Therefore, the Evaluation Criteria report (Johnson et al. 2010) specified that the American Concrete Institute code for nuclear safety-related structures (ACI 349-06) be used to evaluate the SST reinforced concrete structures. ACI 349-06 defines specific combinations of static, thermal, and seismic loads that must be checked. For the static plus seismic load combination, the concrete forces and moments from the dynamic seismic analyses were added to the static TOLA results as prescribed in ACI 349. The SST Type III results reported in this report demonstrate that the steel reinforced concrete SSTs meet the requirements of ACI 349-06 and by inference the IBC (2009).

The structural evaluations completed with the TOLA and seismic tank models do not reveal any deficiencies with the structural integrity of the Type III SSTs. In addition, rebar yielding was not observed in any of the analysis runs performed. The analyses evaluate 59 years of use, which extends to the oldest tanks in service. The temperature loads imposed on the TOLA model are taken from the S-104 thermal history, which is significantly more severe than any of the other Type III tank thermal histories. Bounding material properties were also selected to analyze the most limiting combinations.

The Type III tank model was subjected to a 200 kip concentrated load on the soil surface, a 40 lb/ft^2 surface load, a typical waste load, and a 59-year thermal history that peaked at 300°F. Eleven feet of soil at 125 lb/ft3 was modeled over the tank dome to bound the maximum 10.38 ft soil depth measured over the TX-108, Type III tank (Rifaey 2002). The ACI 349-06 code evaluations show that tank demands are lower than the capacities for all locations in the dome, upper haunch, and wall. The best estimate condition of the Type III tanks with 11 feet of soil overburden and best estimate material properties is that the non-seismic ACI 349-06 load demands are at most 34%, 73%, and 53% of the meridional, hoop, and shear capacities, respectively, at any section in the dome, upper haunch, and wall. One case under TOLA analysis and several analysis cases when TOLA and seismic demands are combined, show demands higher than capacities at a few locations in the bottom slab, indicating that cracking of the slab likely occurred due to radial thermal expansion followed by contraction. However, the slab is supported on soil, and the cracking and displacements are displacement controlled. Cracks in the slab do not affect the structural stability of the tank dome, walls, and footing. Additional finite element analyses were performed with the slab separated from the tank footing to further evaluate the effect of possible cracking and shear offset of the concrete there. The studies presented in Appendix E of this report demonstrate that even in the event of local slab shear cracking, the slab-to-footing offset deformation is predicted to be less than 0.06 inch. For reference, this is less than one-sixth of the original nominal liner thickness of 0.375 inch. The bottom and knuckle of the tank are also covered with a tar-based mastic material that would cushion the transition. Therefore, it is likely that the liner would bridge the small displacement offset without being damaged. Disconnecting the slab and footing at this location would not reduce the tank's structural stability. The soil overburden is the largest load on the tank and the largest contributor to the static tank demands. Waste and soil surface loads produced only secondary effects. Thermal loads were significant in the slab and lower wall where the temperatures were highest (about 300°F). Including the load-relieving effects of concrete creep reduces the demands by 5–16%. The material combination of upper bound concrete modulus and lower bound soil modulus increased the concrete section demands.

The seismic model input (horizontal and vertical) motions were defined as acceleration time histories. These motions were carefully analyzed to ensure that they resulted in surface-level and tank foundation-level responses that met or exceeded appropriate spectral matching criteria. The resulting input motions were generally conservatively biased. The maximum tank section forces and moments over the time history were extracted from the seismic model and combined with the non-seismic forces and moments to evaluate the ACI seismic load combination. Again, the seismic ACI evaluation results indicate that tank demands are lower than the ACI 349-06 capacities for all locations in the dome, upper haunch, and wall. For the best estimate material property runs, either with or without waste, the seismic ACI load combination resulted in demands that were at most 28%, 73%, and 46% of the meridional, hoop, and shear capacities, respectively, in the dome, upper haunch, and wall.

To assess the impact of tank appurtenances (pits), appurtenance models were also evaluated according to the ACI code. As with the tank model without the appurtenances, the ACI evaluation results indicated the tank demands were lower than the capacities in the dome, haunch, and wall. The results from the appurtenance model when compared with the results from models without appurtenances under ACI load combinations indicated that there is an increase in demands in the sections closer to the pits. However, the increases in demands are restricted to local regions and diminish when sections farther away from the pits are considered. The results at sections farther away from the pits and at all other locations are close to the baseline TOLA model without pits. It should be noted that the appurtenance configuration modeled is a conservative combination of the heaviest pits on the Type III tanks along with 11 ft of soil overburden. This actual configuration does not exist on any of the Type III tanks. The Type III-specific appurtenance modeling results show that it is not necessary to conduct a full series of analyses over the entire range of material property combinations. For the Type III SSTs, the baseline material properties were adequate to evaluate the effects of the appurtenances.

Additional Type III SST analysis of record evaluations included tank limit load and buckling analyses. The limit loads were evaluated for both uniform and concentrated loads over the tank dome. The uniform load was applied over the entire soil surface, while the concentrated load was applied over a 20-ft-diameter area at the center of the tank. The limit loads were estimated by increasing the load until the tank model offered little or no resistance to additional load. The buckling analysis evaluated three tank conditions for the Type III SSTs: 1) the baseline tank analysis – the maximum Type III thermal history with a bounding soil overburden depth of 11 ft; 2) maximum thermal history with the actual overburden; and 3) actual thermal history for the tank with maximum overburden. The tank limit load and buckling analyses both demonstrated adequate margins with demands lower than capacities. The results of the tank limit load analyses confirm the adequacy of the current dome load limits.

Additional analyses, documented as appendices to this report, were conducted to address the external reviewer comments and recommendations while performing the Type-II AOR. The appendices address the use of 11-ft soil overburden, the pits configuration used in the analysis based on Type III tank features, the extent of backfill in the seismic model, improvements in modeling soil above the tanks (using soil rings), the waste height sensitivity (empty vs. full tank scenarios), slab detachment scenarios, buckling analyses in Mathcad™, and the details of the ACI evaluations. In addition, load contribution plots showing the effects of individual load components, alternate load factor studies, and force and moment plots for Run #6 with nominal strength concrete, are included in these appendices to gain a more complete understanding of the Type III SSTs and to ensure that the models present an accurate representation of tank structural integrity.

This page intentionally left blank.

Acknowledgments

Project Management would like to thank the static and seismic modeling teams for their tenacity in the completion of task deliverables. In addition, appreciation is extended to the following individuals for their dedicated administrative, contracts, scheduling and budget support, and technical editing and formatting support, respectively: Theresa Vancorbach, Lori Bisping, Kelle Airhart, Dave Payson, Megan Peters, Meghan Chalk, and Kay Hass.

This page intentionally left blank.

Acronyms

ACI	American Concrete Institute
AOR	analysis of record
APDL	ANSYS® parametric design language
ASA	Accelerated Safety Analysis
ASCE	American Society of Civil Engineers
ASME	American Society of Mechanical Engineers
ASTM	American Society for Testing and Materials
AWS	American Welding Society
BBI	Best-Basis Inventory
BES	best estimate soil
CTL	Construction Technology Laboratory
DBE	design-basis (event/earthquake)
D/C	demand/capacity ratio
DF	damping factor
DOE	U.S. Department of Energy
DOE-RL	U.S. Department of Energy's Richland Operations Office
DRS	design response spectra
DST	double-shell tank
DW	dead weight
EDP	Extended Drucker-Prager
EED	Energy and Environment Directorate
EPA	U.S. Environmental Protection Agency
FCC	fully cracked concrete
FE	finite element
FIRS	foundation input response spectra
HEW	Hanford Engineering Works
HW	Hanford Works
HWS	Hanford Works Specification
IBC	International Building Code
IDMS	Integrated Data Management System
kip	thousand pounds
LBS	lower bound soil
MP	material properties
NER	no external rebar
NRA	not readily available
ORP	DOE Office of River Protection

PNNL	Pacific Northwest National Laboratory
PQAP	Project Quality Assurance Plan
QA	Quality Assurance
QAPD	Quality Assurance Program Description
R&D	research and development
SACS	Surveillance Analysis Computer System
SSI	soil-structure interaction
SST	single-shell tank
TOLA	Thermal and Operating Loads Analysis
TWINS	Tank Waste Information Network System
UBS	upper bound soil
WRPS	Washington River Protection Solutions

Contents

Summary iii
Acknowledgments vii
Acronyms ix
1.0 Introduction and Objective 1.1
1.1 Quality Assurance 1.1
2.0 Scope 2.1
2.1 TOLA and Seismic Results Roadmap 2.1
3.0 Type III SST Background 3.1
3.1 Design 3.1
4.0 Guidance 4.1
4.1 Acceptance Criteria 4.1
4.1.1 Material Properties 4.1
4.1.2 Loads 4.2
4.1.3 Static Load Combinations 4.3
4.2 Post Design Evaluation Input 4.6
5.0 Static Thermal and Operating Loads Analysis 5.1
5.1 Introduction 5.1
5.2 Geometry 5.1
5.3 ANSYS® Model Construction 5.1
5.4 Real Constants 5.6
5.5 Loads and Boundary Conditions 5.9
5.6 The TOLA Run Matrix 5.10
5.7 Temperature Profile and the Thermal Model 5.11
6.0 Seismic Analysis 6.1
6.1 Seismic Model Overview 6.1
6.2 Model Geometry 6.4
6.2.1 Model Development 6.4
6.2.2 Soil and Concrete Properties 6.4
6.2.3 Model Organization 6.4
6.2.4 Input and Output Files 6.4
6.2.5 Organization and Identification System 6.6
6.2.6 Tank Concrete 6.8
6.2.7 Contact Interfaces 6.12
6.2.8 Surface Loads 6.21
6.2.9 Boundary Conditions 6.21
6.2.10 Model Excitation 6.23

6.2.11 Seismic Input 6.23
6.2.12 Post-Processing 6.24
6.2.13 Concrete Tank Elements 6.24
6.2.14 Contact Elements 6.27
6.2.15 Enveloping Process 6.28
6.3 Material Properties 6.29
6.3.1 Tank Concrete Properties 6.29
6.3.2 Waste 6.37
6.3.3 Soil Model 6.38
6.3.4 Soil Properties 6.39
6.3.5 Excavated Backfill Soil 6.44
6.3.6 Native Soil 6.47
6.4 Run Descriptions 6.49
6.4.1 Seismic Run Matrix 6.49
6.4.2 Results Extraction 6.49
7.0 Soil Column Properties, Base Motion Inputs, and Spectral Matching 7.1
7.1 Introduction 7.1
7.2 SHAKE Soil Column Descriptions 7.1
7.3 Characterization of the SHAKE Soil Columns 7.6
7.3.1 Amplification Factors for Three Soil Profiles – Horizontal Motion 7.6
7.3.2 Amplification Factors for Three Soil Profiles – Vertical Motion 7.8
7.4 Development of Time Histories at the Base of the SSI Profiles to be Used as Input to ANSYS® SSI Models 7.10
7.5 Generation of Target Spectra Using SHAKE 7.11
7.6 Description of the ANSYS® Soil Column Models 7.14
7.6.1 Element Geometry and Layer Thickness 7.15
7.6.2 Boundary Conditions 7.20
7.6.3 Seismic Loading 7.21
7.6.4 ANSYS® Soil Column Material Properties 7.21
7.7 Calibration of ANSYS® Damping Parameters 7.25
7.8 Characterization of the ANSYS® Soil Columns Dynamic Response 7.29
7.9 Spectral Matching Methodology and Acceptance Criteria 7.34
7.9.1 Spectral Matching for the Simplified Soil Column 7.35
7.9.2 Spectral Matching for the Full ANSYS® SSI Model 7.42
7.10 Backfill Properties 7.74
7.11 Harmonic Analysis for the Full SSI Model with BE Soil Profile 7.79
7.11.1 Conclusions Regarding Spectral Matching for the BE Soil Profile 7.84
7.12 Harmonic Analysis for the Full SSI Model with LB Soil Profile 7.86
7.12.1 Conclusions Regarding Spectral Matching for the LB Soil Profile 7.91

7.13 Harmonic Analysis for the Full SSI Model with UB Soil Profile 7.93
7.13.1 Conclusions Regarding Spectral Matching for the UB Soil Profile 7.97
8.0 Static Modeling Results 8.1
8.1 Introduction 8.1
8.2 ACI Evaluations – Structural Concrete 8.1
8.3 Run 1, Baseline Case with Best Estimate Material Properties 8.11
8.4 Run 2, Nominal Soil Modulus, Nominal Concrete Modulus, Near Zero Concrete Tensile Strength, and No Creep 8.15
8.5 Run 3, Nominal Soil Modulus, High Concrete Modulus, Near Zero Concrete Tensile Strength, and No Creep 8.20
8.6 Run 4, Low Soil Modulus, High Concrete Modulus, Near Zero Concrete Tensile Strength, and No Creep 8.23
8.7 Run 5, Low Soil Modulus, Nominal Concrete Modulus, Near Zero Concrete Tensile Strength, and No Creep 8.26
8.8 Run 6, Nominal Soil Modulus, Nominal Concrete Modulus, Nominal Concrete Tensile Strength with Creep 8.28
8.9 Run 7, Low Soil Modulus, Nominal Concrete Modulus, Near Zero Concrete Tensile Strength with Creep 8.28
8.10 Run 8, High Soil Modulus, Nominal Concrete Modulus, Near Zero Concrete Tensile Strength with Creep 8.31
8.11 TOLA Run Matrix Conclusions 8.33
8.12 Shear Friction at Construction Joints 8.37
9.0 Seismic Results 9.1
9.1 Concrete Tank 9.1
9.1.1 Summary of Seismic Demands 9.16
9.2 Soil Contact Results 9.17
9.2.1 Summary of Contact Results 9.22
9.3 TOLA and Seismic Combination Procedure 9.23
9.4 ACI Load Combination 4 Results 9.25
9.5 LC4 Combined Results Summary 9.35
10.0 Tank Appurtenances 10.1
10.1 Type III SST TOLA Appurtenance Models 10.3
10.2 Type III SST Seismic Modeling with Appurtenances 10.9
10.2.1 Type III SST Pit Appurtenances Model Development 10.9
10.2.2 Pit Appurtenances Model Soil and Concrete Properties 10.9
10.2.3 Type III SST Pit Appurtenances Model Description 10.10
10.2.4 Type III SST Seismic Pit Appurtenances Model Run Matrix 10.15
10.2.5 Pit Appurtenances Type III SST Seismic Results 10.16
10.3 Appurtenance Demand to Capacity Ratios 10.26
10.4 Summary of the Type III Appurtenance Model Evaluations 10.32

11.0 Tank Limit Analysis 11.1
12.0 Concrete Shell Buckling Analysis 12.1
12.1 Unfactored Theoretical Buckling Loads 12.2
12.1.1 Dome Buckling 12.2
12.1.2 Cylindrical Wall Buckling 12.5
12.2 Buckling Load-Reduction Factors 12.6
12.3 Buckling Load-Interaction and Safety Factors 12.10
12.4 Results of the Type III Tank Buckling Evaluation 12.11
12.5 Summary of the Type III Tank Buckling Evaluation 12.16
13.0 Conclusions 13.1
14.0 References 14.1
Appendix A – SST AOR Guidance, March 28, 2011 ..... A.1
Appendix B – Appurtenance Review B.1
Appendix C – Backfill Soil Evaluation C.1
Appendix D – Waste Height Sensitivity Analysis D.1
Appendix E – Slab Removal Study E.1
Appendix F – Run 1, Baseline Case with Best EstimateMaterial Properties: Load Contributions F.1
Appendix G – Alternate Load Factor Study G.1
Appendix H – Run 6, Forces and Moments H.1
Appendix I – Buckling Calculation in MathCADTM I.1
Appendix J – Details of ACI-349 Demand/Capacity Calculations J.1
Appendix K – Seismic Soil Overburden Modeling Technique K.1
Appendix L – External Reviewer Comments L.1

Figures

Figure 3.1. Typical 758,000-Gallon Single-Shell Waste Tank and Riser Configuration for Type III Tanks 241BY, 241S, 241TX, and 241TY (not to scale) 3.2
Figure 3.2. Type III SST, BY Tank Farm Cascade Series Configuration, Hanford Drawing H-2-1308 ..... 3.3
Figure 4.1. Typical Layout of a Single-Shell Tank (not to scale) 4.4
Figure 4.2. Flow Plan for SST AOR Analyses 4.5
Figure 5.1. Slice Model Showing Type III SST and Surrounding Soil 5.3
Figure 5.2. Finite Element Mesh of Tank and Soil 5.4
Figure 5.3. Close-up Showing Mesh of Haunch with Reinforced Concrete Elements 5.4
Figure 5.4. Close-up Showing Mesh of Footing with Reinforced Concrete Elements 5.5
Figure 5.5. The Peak Temperature History Profile and Waste Height Profile Used for Detailed Analysis of the Type III Tanks 5.9
Figure 5.6. Temperature History Data for Tanks S-101 and S-104 for the Period 1953-1960 Obtained from Mercier et al. (1981) 5.12
Figure 5.7. The 2-D Thermal Model Showing the Element in the Tank Structure and the Element in the Waste Surface 5.13
Figure 5.8. Temperature Distribution in Concrete Tank at the End Time Step 2 (peak temperature of 300°F) 5.15
Figure 6.1. Element Plot of Complete Best Estimate Soil Full Tank Seismic Model 6.2
Figure 6.2. Element Plot Detail of Best Estimate Soil Baseline Seismic Model Showing Tank, Waste, and Backfill 6.3
Figure 6.3. Element Plot Detail of Best Estimate Soil Baseline Seismic Model Showing Tank, Waste, and Overburden Soil 6.3
Figure 6.4. Seismic Model Concrete Tank Profile Showing Shell Element Thickness 6.8
Figure 6.5. Seismic Model Concrete Tank Angled View Showing Shell Element Thickness 6.9
Figure 6.6. Seismic Model Concrete Tank Angled View Showing Elements at ACI Sections 6.9
Figure 6.7. Seismic Model Concrete Tank Profile Showing Material Properties and ACI Section Locations 6.10
Figure 6.8. Seismic Model Concrete Tank Angled View Showing Shell Element Orientation 6.11
Figure 6.9. Shell Element Orientation Detail 6.11
Figure 6.10. Seismic Model Concrete Tank Material Property Assignment 6.12
Figure 6.11. Seismic Model Interface Elements Real Property Assignment – Soil-to-Concrete Tank 6.13
Figure 6.12. Seismic Model Soil/Concrete Contact Element Normal Pressure for At-Rest Calibration – Gravity Only 6.14
Figure 6.13. Seismic Model Interface Elements Real Property Assignment – Waste-to-Concrete Tank 6.15
Figure 6.14. Seismic Model Interface Elements Real Property Assignment – Near Soil to Far Soil 6.17
Figure 6.15. Seismic Model Excavated Backfill Soil –Soil Slip Planes 6.18

Figure 6.16. Gravity Only Contact Pressure Plot 6.19
Figure 6.17. Seismic Model Maximum Soil Height above the Dome 6.20
Figure 6.18. Seismic Model Mass Elements – Soil Surface 6.21
Figure 6.19. Seismic Model Boundary Conditions – Symmetry Plane and Soil Base 6.22
Figure 6.20. Seismic Model Boundary Conditions – Slaved Boundary Conditions 6.22
Figure 6.21. Seismic Model Boundary Condition – Concrete Tank 6.23
Figure 6.22. SHELL 181 Element Force and Moment Vector Orientations 6.25
Figure 6.23. Seismic Model Concrete Tank Elements at ACI Sections 6.27
Figure 6.24. Typical Multilayer Reinforced Concrete Section (left) and Schematic Net Tension Section Transformed Steel Areas (right) 6.31
Figure 6.25. Concrete Tank Alpha and Beta Damping Ratios 6.34
Figure 6.26. Seismic Model Detail – Element Plot of Waste 6.38
Figure 6.27. Seismic Model BES – Excavated Backfill Soil Detail 6.45
Figure 6.28. Seismic Model LBS Excavated Backfill Soil Material Property Assignment 6.45
Figure 6.29. Seismic Model BES Excavated Backfill Soil Material Property Assignment 6.46
Figure 6.30. Seismic Model UBS Excavated Backfill Soil Material Property Assignment 6.46
Figure 6.31. Seismic Model LBS Far-Field Soil Layering and Material Property Assignment 6.47
Figure 6.32. Seismic Model BES Far-Field Soil Layering and Material Property Assignment 6.48
Figure 6.33. Seismic Model UBS Far-Field Soil Layering and Material Property Assignment 6.48
Figure 7.1. SHAKE91 Best Estimate Amplification Factors from Horizontal Input Motion at Soil Column Base 7.6
Figure 7.2. SHAKE91 Lower Bound Amplification Factors from Horizontal Input Motion at Soil Column Base 7.7
Figure 7.3. SHAKE91 Upper Bound Soil Amplification Factors from Horizontal Input Motion at Soil Column Base 7.7
Figure 7.4. SHAKE91 Best Estimate Amplification Factors from Vertical Input Motion at Soil Column Base 7.8
Figure 7.5. SHAKE91 Lower Bound Soil Amplification Factors from Vertical Input Motion at Soil Column Base 7.9
Figure 7.6. SHAKE91 Upper Bound Amplification Factors from Vertical Input Motion at Soil Column Base 7.9
Figure 7.7. Best Estimate Horizontal Target Spectra 7.11
Figure 7.8. Best Estimate Vertical Target Spectra 7.12
Figure 7.9. Lower Bound Horizontal Target Spectra 7.12
Figure 7.10. Lower Bound Vertical Target Spectra 7.13
Figure 7.11. Upper Bound Horizontal Target Spectra 7.13
Figure 7.12. Upper Bound Vertical Target Spectra 7.14
Figure 7.13. Elevation View of Typical ANSYS® Soil Column Model 7.15
Figure 7.14. Top View of ANSYS® Soil Column Model 7.20
Figure 7.15. Mass Proportional Damping vs. Frequency for Alpha=1.0 ..... 7.27

Figure 7.16. Stiffness Proportional Damping vs. Frequency 7.27
Figure 7.17. Composite Rayleigh Damping for Lower Bound Soil 7.28
Figure 7.18. Composite Rayleigh Damping for Best Estimate Soil 7.28
Figure 7.19. Composite Rayleigh Damping for Upper Bound Soil 7.29
Figure 7.20. SHAKE91 vs. ANSYS® Free Field Horizontal Amplification Factors for Best Estimate 7.30
Figure 7.21. SHAKE91 vs. ANSYS® Free Field Horizontal Amplification Factors for Lower Bound 7.31
Figure 7.22. SHAKE91 vs. ANSYS® Free Field Horizontal Amplification Factors for Upper Bound 7.31
Figure 7.23. SHAKE91 vs. ANSYS® Free Field Vertical Amplification Factors for Best Estimate 7.32
Figure 7.24. SHAKE91 vs. ANSYS® Free Field Vertical Amplification Factors for Lower Bound 7.33
Figure 7.25. SHAKE91 vs. ANSYS® Free Field Vertical Amplification Factors for Upper Bound 7.33
Figure 7.26. Best Estimate Surface and Tank Foundation Spectra from Horizontal Time History Comparison between ANSYS® and Target Spectra 7.36
Figure 7.27. Lower Bound Surface and Tank Foundation Spectra from Horizontal Time History Comparison Between ANSYS® and Target Spectra 7.37
Figure 7.28. Upper Bound Surface and Tank Foundation Spectra from Horizontal Time History Comparison Between ANSYS® and Target Spectra 7.38
Figure 7.29. Best Estimate Surface and Tank Foundation Spectra from Vertical Time History Comparison Between ANSYS® and Target Spectra 7.39
Figure 7.30. Lower Bound Surface and Tank Foundation Spectra from Vertical Time History Comparison Between ANSYS® and Target Spectra 7.40
Figure 7.31. Upper Bound Surface and Tank Foundation Spectra from Vertical Time History Comparison Between ANSYS® and Target Spectra 7.41
Figure 7.32. Comparison of Best Estimate Horizontal Surface Spectra with 5% Spectral Damping from the ANSYS® SSI Model with an Empty Tank 7.42
Figure 7.33. Comparison of Best Estimate Horizontal Tank Foundation Spectra with 5% Spectral Damping from the ANSYS® SSI Model with an Empty Tank 7.43
Figure 7.34. Comparison of Upper Bound Horizontal Surface Spectra with 5% Spectral Damping from the ANSYS® SSI Model with an Empty Tank 7.44
Figure 7.35. Comparison of Upper Bound Horizontal Tank Foundation Spectra with 5% Spectral Damping from the ANSYS® SSI Model with an Empty Tank 7.45
Figure 7.36. Comparison of Lower Bound Horizontal Surface Spectra with 5% Spectral Damping from the ANSYS® SSI Model with an Empty Tank 7.45
Figure 7.37. Comparison of Lower Bound Horizontal Tank Foundation Spectra with 5% Spectral Damping from the ANSYS® SSI Model with an Empty Tank 7.46
Figure 7.38. Surface Spectra Curves for Horizontal Time Histories 7.47
Figure 7.39. Surface Spectra Ratio Curves and Maximum Envelope Curve for Horizontal Time Histories 7.47
Figure 7.40. Comparison of Best Estimate Horizontal Surface Spectra with 5% Spectral Damping from the ANSYS® SSI Model with High Shear Stiffness Tank Waste 7.48

Figure 7.41. Comparison of Best Estimate Horizontal Tank Foundation Spectra with 5% Spectral Damping from the ANSYS® SSI Model with High Shear Stiffness Tank Waste 7.49
Figure 7.42. Comparison of Upper Bound Horizontal Surface Spectra with 5% Spectral Damping from the ANSYS® SSI Model with High Shear Stiffness Tank Waste 7.50
Figure 7.43. Comparison of Upper Bound Horizontal Tank Foundation Spectra with 5% Spectral Damping from the ANSYS® SSI Model with High Shear Stiffness Tank Waste 7.50
Figure 7.44. Comparison of Lower Bound Horizontal Surface Spectra with 5% Spectral Damping from the ANSYS® SSI Model with High Shear Stiffness Tank Waste 7.51
Figure 7.45. Comparison of Lower Bound Horizontal Tank Foundation Spectra with 5% Spectral Damping from the ANSYS® SSI Model with High Shear Stiffness Tank Waste 7.51
Figure 7.46. Surface Spectra Curves for Horizontal Time Histories for SSI Full Model with High Shear Stiffness Tank Waste 7.53
Figure 7.47. Surface Spectra Ratio Curves and Maximum Envelope Curve for Horizontal Time Histories for SSI Full Model with High Shear Stiffness Tank Waste 7.53
Figure 7.48. Comparison of Best Estimate Horizontal Surface Spectra with 5% Spectral Damping from the ANSYS® SSI Model with Low Shear Stiffness Tank Waste 7.54
Figure 7.49. Comparison of Best Estimate Horizontal Tank Foundation Spectra with 5% Spectral Damping from the ANSYS® SSI Model with Low Shear Stiffness Tank Waste 7.55
Figure 7.50. Comparison of Upper Bound Horizontal Surface Spectra with 5% Spectral Damping from the ANSYS® SSI Model with Low Shear Stiffness Tank Waste 7.55
Figure 7.51. Comparison of Upper Bound Horizontal Tank Foundation Spectra with 5% Spectral Damping from the ANSYS® SSI Model with Low Shear Stiffness Tank Waste 7.56
Figure 7.52. Comparison of Lower Bound Horizontal Surface Spectra with 5% Spectral Damping from the ANSYS® SSI Model with Low Shear Stiffness Tank Waste 7.57
Figure 7.53. Comparison of Lower Bound Horizontal Tank Foundation Spectra with 5% Spectral Damping from the ANSYS® SSI Model with Low Shear Stiffness Tank Waste 7.57
Figure 7.54. Surface Spectra Curves for Horizontal Time Histories for SSI Full Model with Low Shear Stiffness Tank Waste 7.58
Figure 7.55. Surface Spectra Ratio Curves and Maximum Envelope Curve for Horizontal Time Histories for SSI Full Model with Low Shear Stiffness Tank Waste 7.59
Figure 7.56. Comparison of Best Estimate Vertical Surface Spectra with 5% Spectral Damping from the ANSYS® SSI Model with Empty Tank 7.60
Figure 7.57. Comparison of Best Estimate Vertical Tank Foundation Spectra with 5% Spectral Damping from the ANSYS® SSI Model with Empty Tank 7.60
Figure 7.58. Comparison of Upper Bound Vertical Surface Spectra with 5% Spectral Damping from the ANSYS® SSI Model with Empty Tank 7.61
Figure 7.59. Comparison of Upper Bound Vertical Tank Foundation Spectra with 5% Spectral Damping from the ANSYS® SSI Model with Empty Tank 7.61
Figure 7.60. Comparison of Lower Bound Vertical Surface Spectra with 5% Spectral Damping from the ANSYS® SSI Model with Empty Tank 7.62
Figure 7.61. Comparison of Lower Bound Vertical Tank Foundation Spectra with 5% Spectral Damping from the ANSYS® SSI Model with Empty Tank 7.63
Figure 7.62. Surface Spectra Envelop Curves for Vertical Time Histories with Empty Tank 7.63

Figure 7.63. Surface Spectra Ratio Curves and Maximum Envelope Curve for Vertical Time Histories for SSI Full Model with Empty Tank 7.64
Figure 7.64. Comparison of Best Estimate Vertical Surface Spectra with 5% Spectral Damping from the ANSYS® SSI Model with High Shear Stiffness Tank Waste 7.65
Figure 7.65. Comparison of Best Estimate Vertical Tank Foundation Spectra with 5% Spectral Damping from the ANSYS® SSI Model with High Shear Stiffness Tank Waste 7.65
Figure 7.66. Comparison of Upper Bound Vertical Surface Spectra with 5% Spectral Damping from the ANSYS® SSI Model with High Shear Stiffness Tank Waste 7.66
Figure 7.67. Comparison of Upper Bound Vertical Tank Foundation Spectra with 5% Spectral Damping from the ANSYS® SSI Model with High Shear Stiffness Tank Waste 7.66
Figure 7.68. Comparison of Lower Bound Vertical Surface Spectra with 5% Spectral Damping from the ANSYS® SSI Model with High Shear Stiffness Tank Waste 7.67
Figure 7.69. Comparison of Lower Bound Vertical Tank Foundation Spectra with 5% Spectral Damping from the ANSYS® SSI Model with High Shear Stiffness Tank Waste 7.68
Figure 7.70. Surface Spectra Curves for Vertical Time Histories with High Shear Stiffness Tank Waste 7.68
Figure 7.71. Surface Spectra ANSYS® to SHAKE Ratio Curves and Maximum Envelope Curve for Vertical Time Histories of the SSI Full Model with High Shear Stiffness Tank Waste 7.69
Figure 7.72. Comparison of Best Estimate Vertical Surface Spectra with 5% Spectral Damping from the ANSYS® SSI Model with Low Shear Stiffness Tank Waste 7.70
Figure 7.73. Comparison of Best Estimate Vertical Tank Foundation Spectra with 5% Spectral Damping from the ANSYS® SSI Model with Low Shear Stiffness Tank Waste 7.70
Figure 7.74. Comparison of Upper Bound Vertical Surface Spectra with 5% Spectral Damping from the ANSYS® SSI Model with Low Shear Stiffness Tank Waste 7.71
Figure 7.75. Comparison of Upper Bound Vertical Tank Foundation Spectra with 5% Spectral Damping from the ANSYS® SSI Model with Low Shear Stiffness Tank Waste 7.71
Figure 7.76. Comparison of Lower Bound Vertical Surface Spectra with 5% Spectral Damping from the ANSYS® SSI Model with Low Shear Stiffness Tank Waste 7.72
Figure 7.77. Comparison of Lower Bound Vertical Tank Foundation Spectra with 5% Spectral Damping from the ANSYS® SSI Model with Low Shear Stiffness Tank Waste 7.73
Figure 7.78. Surface Spectra Envelop Curves for Vertical Time Histories with Low Shear Stiffness Tank Waste 7.73
Figure 7.79. Surface Spectra ANSYS® to SHAKE Ratio Curves and Maximum Envelope Curve for Vertical Time Histories of the SSI Full Model with Low Shear Stiffness Tank Waste 7.74
Figure 7.80. Best Estimate Soil Profile Comparison: Far Field to Backfill Shear Velocities 7.75
Figure 7.81. Lower Bound Soil Profile Comparison: Far Field to Backfill Shear Wave Velocity 7.76
Figure 7.82. Upper Bound Soil Profile Comparison: Far Field to Backfill Shear Wave Velocity 7.78
Figure 7.83. SST Type III Tank Model with Tank Features Shown 7.80
Figure 7.84. Horizontal Amplification Factors at the Far Field Boundary at the Tank Foundation, Haunch, Dome Apex, and Surface Elevations 7.81
Figure 7.85. Horizontal Amplification Factors of the Dome Apex and Haunch Normalized to the Tank Foundation 7.82

Figure 7.86. Vertical Amplification Factors at the Far Field Boundary for the Elevation of the Tank Foundation, Haunch, Dome Apex, and Surface 7.83

Figure 7.87. Vertical Amplification Factors of the Dome Apex, and Haunch Normalized to the Tank Foundation Amplitude 7.84

Figure 7.88. Horizontal spectra for SSI Model with Best Estimte Soil Profile Shown as a Percentage Above Target Spectra Along with the Natural Frequencies of the Soil Column and the Fundamental Natural Frequency of the Dome 7.85

Figure 7.89. Vertical Spectra for SSI Model with Best Estimate Soil Profile Shown as a Percentage Above Target Spectra Along with the Fundamental Natual Frequencies of the Soil Column and Dome 7.86

Figure 7.90. Horizontal Amplification Factors at the Far Field Boundary at the Tank Foundation, Haunch, Dome Apex, and Surface Elevations 7.88

Figure 7.91. Horizontal Amplification Factors of the Dome Apex and Haunch Normalized to the Tank Foundation 7.89

Figure 7.92. Vertical Amplification Factors at the Far Field Boundary for the Elevation of the Tank Foundation, Haunch, Dome Apex, and Surface 7.90

Figure 7.93. Vertical Amplification Factors of the Dome Apex, and Haunch Normalized to the Tank Foundation Amplitude 7.91

Figure 7.94. Horizontal spectra for SSI Model with Best Estimte Soil Profile Shown as a Percentage Above Target Spectra Along with the Natural Frequencies of the Soil Column and the Fundamental Natural Frequency of the Dome. 7.92

Figure 7.95. Vertical Spectra for SSI Model with Best Estimate Soil Profile Shown as a Percentage Above Target Spectra Along with the Fundamental Natual Frequencies of the Soil Column and Dome 7.93

Figure 7.96. Horizontal Amplification Factors at the Far Field Boundary at the Tank Foundation, Haunch, Dome Apex, and Surface Elevations 7.94

Figure 7.97. Horizontal Amplification Factors of the Dome Apex and Haunch Normalized to the Tank Foundation 7.95

Figure 7.98. Vertical Amplification Factors at the Far Field Boundary for the Elevation of the Tank Foundation, Haunch, Dome Apex, and Surface 7.96

Figure 7.99. Vertical Amplification Factors of the Dome Apex, and Haunch Normalized to the Tank Foundation Amplitude 7.97

Figure 7.100. Horizontal Spectra for SSI Models with Upper Bound Soil Profile Shown as Percentage Above the Target Spectra Along with the Natural Frequencies of the Soil Column and the Fundamental Natural Freuquency of the Dome. 7.98

Figure 7.101. Vertical Spectra for SSI Model with Upper Bound Soil Profile Shown as Percentage Above Target Spectra Along with the Fundamental Natural Frequency of the Soil Column and Dome 7.99

Figure 8.1. Reinforced Concrete Sections 8.3

Figure 8.2. ACI Demand/Capacity Ratio Definition 8.7

Figure 8.3. ACI – Force-Moment Diagram for Section 13. The results are for Run1 with best estimate material properties at the maximum tank temperature (Loadstep 6) and ACI load factors equal to 1.0 ..... 8.7

Figure 8.4. ACI – Force-Moment Diagram for Section 14. The results are for Run1 with best estimate material properties at the maximum tank temperature (Loadstep 6) and ACI load factors equal to 1.0. 8.8
Figure 8.5. ACI – Force-Moment Diagram for Section 15. The results are for Run1 with best estimate material properties at the maximum tank temperature (Loadstep 6) and ACI load factors equal to 1.0. 8.8
Figure 8.6. ACI – Force-Moment Diagram for Section 16. The results are for Run1 with best estimate material properties at the maximum tank temperature (Loadstep 6) and ACI load factors equal to 1.0. 8.9
Figure 8.7. ACI – Force-Moment Diagram for Section 30. The results are for Run1 with best estimate material properties at the maximum tank temperature (Loadstep 6) and ACI load factors equal to 1.0. 8.9
Figure 8.8. ACI – Force-Moment Diagram for Section 31. The results are for Run1 with best estimate material properties at the maximum tank temperature (Loadstep 6) and ACI load factors equal to 1.0. 8.10
Figure 8.9. ACI – Force-Moment Diagram for Section 32. The results are for Run1 with best estimate material properties at the maximum tank temperature (Loadstep 6) and ACI load factors equal to 1.0. 8.10
Figure 8.10. Run 1, ACI D/C Ratios at Peak Temperature. ACI load factors are equal to 1.0. 8.12
Figure 8.11. Run 1, ACI D/C Ratios for LC1 8.13
Figure 8.12. Run 1, ACI D/C Ratios for LC4 (TOLA results only – no seismic) 8.13
Figure 8.13. Run 1, ACI D/C Ratios for LC9 8.14
Figure 8.14. Run 2, ACI D/C Ratios at Peak Temperature. ACI load factors are equal to 1.0. 8.15
Figure 8.15. Run 2, ACI D/C Ratios for LC1 8.16
Figure 8.16. Run 2, ACI D/C Ratios for LC4 (TOLA results only – no seismic) 8.16
Figure 8.17. Run 2, ACI D/C Ratios for LC9 8.17
Figure 8.18. Run 2, Concrete Stress (Sy in psi) in the Haunch and Wall 8.18
Figure 8.19. Run 2, Meridional Rebar Stress (psi) in Haunch, Wall and Knuckle Region 8.19
Figure 8.20. Run 2, Hoop Rebar Stress (psi) in Haunch, Wall and Knuckle Region 8.20
Figure 8.21. Run 3, ACI D/C Ratios at Peak Temperature. ACI load factors are equal to 1.0. 8.21
Figure 8.22. Run 3, ACI D/C Ratios for LC1 8.22
Figure 8.23. Run 3, ACI D/C Ratios for LC4 (TOLA results only – no seismic) 8.22
Figure 8.24. Run 3, ACI D/C Ratios for LC9 8.23
Figure 8.25. Run 4, ACI D/C Ratios at Peak Temperature. ACI load factors are equal to 1.0. 8.24
Figure 8.26. Run 4, ACI D/C Ratios for LC1 8.24
Figure 8.27. Run 4, ACI D/C Ratios for LC4 (TOLA results only – no seismic) 8.25
Figure 8.28. Run 4, ACI D/C Ratios for LC9 8.25
Figure 8.29. Run 5, ACI D/C Ratios at Peak Temperature. ACI load factors are equal to 1.0. 8.26
Figure 8.30. Run 5, ACI D/C Ratios for LC1 8.27
Figure 8.31. Run 5, ACI D/C Ratios for LC4 (TOLA results only – no seismic) 8.27
Figure 8.32. Run 5, ACI D/C Ratios for LC9 8.28
Figure 8.33. Run 7, ACI D/C Ratios at Peak Temperature. ACI load factors are equal to 1.0. 8.29

Figure 8.34. Run 7, ACI D/C Ratios for LC1 ..... 8.29
Figure 8.35. Run 7, ACI D/C Ratios for LC4 (TOLA results only – no seismic) 8.30
Figure 8.36. Run 7, ACI D/C Ratios for LC9 ..... 8.30
Figure 8.37. Run 8, ACI D/C Ratios at Peak Temperature. ACI load factors are equal to 1.0 ..... 8.31
Figure 8.38. Run 8, ACI D/C Ratios for LC1 ..... 8.32
Figure 8.39. Run 8, ACI D/C Ratios for LC4 (TOLA results only – no seismic) 8.32
Figure 8.40. Run 8, ACI D/C Ratios for LC9 ..... 8.33
Figure 8.41. Construction Joints in Type III Tanks (Drawing H-2-2244, Rev. 2) Highlighted on the Type III ACI Sections 8.37
Figure 9.1. Best Estimate Soil (BES): Concrete Tank Meridional Force – Seismic Only 9.2
Figure 9.2. Best Estimate Soil (BES): Concrete Tank Hoop Force – Seismic Only 9.2
Figure 9.3. Best Estimate Soil (BES): Concrete Tank Meridional Moment – Seismic Only 9.3
Figure 9.4. Best Estimate Soil (BES): Concrete Tank Hoop Moment – Seismic Only 9.3
Figure 9.5. Best Estimate Soil (BES): Concrete Tank Through-Wall Shear Force – Seismic Only 9.4
Figure 9.6. Best Estimate Soil (BES): Concrete Tank In-Plane Shear Force – Seismic Only 9.4
Figure 9.7. Lower Bound Soil (LBS): Concrete Tank Meridional Force – Seismic Only 9.5
Figure 9.8. Lower Bound Soil (LBS): Concrete Tank Hoop Force – Seismic Only 9.5
Figure 9.9. Lower Bound Soil (LBS): Concrete Tank Meridional Moment – Seismic Only 9.6
Figure 9.10. Lower Bound Soil (LBS): Concrete Tank Hoop Moment – Seismic Only 9.6
Figure 9.11. Lower Bound Soil (LBS): Concrete Tank Through-Wall Shear Force – Seismic Only 9.7
Figure 9.12. Lower Bound Soil (LBS): Concrete Tank In-Plane Shear Force – Seismic Only 9.7
Figure 9.13. Upper Bound Soil (UBS): Concrete Tank Meridional Force – Seismic Only 9.8
Figure 9.14. Upper Bound Soil (UBS): Concrete Tank Hoop Force – Seismic Only 9.8
Figure 9.15. Upper Bound Soil (UBS): Concrete Tank Meridional Moment – Seismic Only 9.9
Figure 9.16. Upper Bound Soil (UBS): Concrete Tank Hoop Moment – Seismic Only 9.9
Figure 9.17. Upper Bound Soil (UBS): Concrete Tank Through-Wall Shear Force – Seismic Only 9.10
Figure 9.18. Upper Bound Soil (UBS): Concrete Tank In-Plane Shear Force – Seismic Only 9.10
Figure 9.19. Seismic Results: Concrete Tank Meridional Force – Seismic Only 9.11
Figure 9.20. Seismic Results: Concrete Tank Hoop Force – Seismic Only 9.12
Figure 9.21. Seismic Results: Concrete Tank Meridional Moment – Seismic Only 9.13
Figure 9.22. Seismic Results: Concrete Tank Hoop Moment – Seismic Only 9.14
Figure 9.23. Seismic Results: Concrete Tank Through-Wall Shear Force – Seismic Only 9.15
Figure 9.24. Seismic Results: Concrete Tank In-Plane Shear Force – Seismic Only 9.16
Figure 9.25. Soil/Concrete Contact Element Normal Pressure – Gravity Only 9.18
Figure 9.26. Soil/Concrete Contact Element Bounding Normal Pressure – Seismic Only 9.19
Figure 9.27. Soil/Concrete Contact Element Meridional Shear – Seismic Only 9.20
Figure 9.28. Soil/Concrete Contact Element Hoop Shear – Seismic Only 9.21

Figure 9.29. Soil/Concrete Contact Element Lateral Displacement (Sliding) – Seismic Only 9.22
Figure 9.30. Example P-M Diagram with Four Possible Seismic Combinations 9.24
Figure 9.31. LC4 Combined Run 1 ACI D/C Ratios 9.26
Figure 9.32. Section 33 Hoop Capacity and LC4 Combined Run 1 Demands 9.27
Figure 9.33. LC4 Combined Run 2 ACI D/C Ratios 9.28
Figure 9.34. LC4 Combined Run 3 ACI D/C Ratios 9.28
Figure 9.35. LC4 Combined Run 4 ACI D/C Ratios 9.29
Figure 9.36. LC4 Combined Run 5 ACI D/C Ratios 9.30
Figure 9.37. LC4 Combined Run 6 ACI D/C Ratios 9.30
Figure 9.38. LC4 Combined Run 7 ACI D/C Ratios 9.31
Figure 9.39. LC4 Combined Run 8 ACI D/C Ratios 9.32
Figure 9.40. LC4 Combined Run 9 ACI D/C Ratios 9.32
Figure 9.41. In-Plane Shear D/C Ratios for all Nine Seismic Runs 9.33
Figure 10.1. Centerline Cut View of TY-101/102 Appurtenance Configuration. Units in feet 10.2
Figure 10.2. Plan View of Appurtenance Configuration used in Appurtenance Models. Units in feet. 10.2
Figure 10.3. Centerline Cut View of Appurtenance Configuration used in Appurtenance Models. Units in feet 10.3
Figure 10.4. Plan View of TOLA Appurtenance Configuration. Hatched area is modeled with symmetric boundary conditions. 10.4
Figure 10.5. TOLA Appurtenance Model with Mesh. Coloring is by material properties after thermal degradation of the concrete has occurred. 10.5
Figure 10.6. Appurtenance Model Thermal History Compared to Axisymmetric Thermal History 10.6
Figure 10.7. Appurtenance Loading History Flow Plan 10.6
Figure 10.8. Temperature Profile at Peak Temperature in Appurtenance Model 10.7
Figure 10.9. Temperature Profile at 80°F in Appurtenance Model 10.8
Figure 10.10. Type III SST Seismic Model Plan View with Pit Appurtenances (net weights indicated) 10.11
Figure 10.11. Type III SST Seismic Model Section View with Pit Appurtenances 10.11
Figure 10.12. Type III SST Seismic Pit Appurtenances Model Configuration 1 ..... 10.12
Figure 10.13. Type III SST Seismic Pit Appurtenances Model Configuration 2 ..... 10.12
Figure 10.14. Type III SST Seismic Pit Appurtenances ANSYS® Model Configuration 1 ..... 10.13
Figure 10.15. Type III SST Seismic Pit Appurtenances ANSYS® Model Configuration 2 ..... 10.13
Figure 10.16. Type III SST ANSYS® Seismic Pit Appurtenances Model Elemental Plot 10.14
Figure 10.17. Type III SST ANSYS® Seismic Pit Appurtenances Model Contact Surfaces 10.15
Figure 10.18. Type III SST ANSYS® Seismic Pit Appurtenances Model ACI Locations 10.16
Figure 10.19. Concrete Tank Maximum Meridional Force: Type III SST (BES, Empty) Pit Appurtenances Model Configuration 1 (Seismic Only) 10.17
Figure 10.20. Concrete Tank Maximum Hoop Force: Type III SST (BES, Empty) Pit Appurtenances Model Configuration 1 (Seismic Only) 10.18

Figure 10.21. Concrete Tank Maximum Meridional Moment: Type III SST (BES, Empty) Pit Appurtenances Model Configuration 1 (Seismic Only) 10.18
Figure 10.22. Concrete Tank Maximum Hoop Moment: Type III SST (BES, Empty) Pit Appurtenances Model Configuration 1 (Seismic Only) 10.19
Figure 10.23. Concrete Tank Maximum Through-Wall Shear Force: Type III SST (BES, Empty) Pit Appurtenances Model Configuration 1 (Seismic Only) 10.19
Figure 10.24. Concrete Tank Maximum In-Plane Shear Force: Type III SST (BES, Empty) Pit Appurtenances Model Configuration 1 (Seismic Only) 10.20
Figure 10.25. Concrete Tank Maximum Meridional Force: Type III SST (BES, Empty) Pit Appurtenances Model Configuration 2 (Seismic Only) 10.20
Figure 10.26. Concrete Tank Maximum Hoop Force: Type III SST (BES, Empty) Pit Appurtenances Model Configuration 2 (Seismic Only) 10.21
Figure 10.27. Concrete Tank Maximum Meridional Moment: Type III SST (BES, Empty) Pit Appurtenances Model Configuration 2 (Seismic Only) 10.21
Figure 10.28. Concrete Tank Maximum Hoop Moment: Type III SST (BES, Empty) Pit Appurtenances Model Configuration 2 (Seismic Only) 10.22
Figure 10.29. Concrete Tank Maximum Through-Wall Shear Force: Type III SST (BES, Empty) Pit Appurtenances Model Configuration 2 (Seismic Only) 10.22
Figure 10.30. Concrete Tank Maximum In-Plane Shear Force: Type III SST (BES, Empty) Pit Appurtenances Model Configuration 2 (Seismic Only) 10.23
Figure 10.31. Concrete Tank Maximum Meridional Force – Type III SST (BES, Empty) Comparison with and without Pit Appurtenances (Seismic Only) 10.23
Figure 10.32. Concrete Tank Maximum Hoop Force – Type III SST (BES, Empty) Comparison with and without Pit Appurtenances (Seismic Only) 10.24
Figure 10.33. Concrete Tank Maximum Meridional Moment – Type III SST (BES, Empty) Comparison with and without Pit Appurtenances (Seismic Only) 10.24
Figure 10.34. Concrete Tank Maximum Hoop Moment – Type III SST (BES, Empty) Comparison with and without Pit Appurtenances (Seismic Only) 10.25
Figure 10.35. Concrete Tank Maximum Through-Wall Shear – Type III SST (BES, Empty) Comparison with and without Pit Appurtenances (Seismic Only) 10.25
Figure 10.36. Concrete Tank Maximum In-Plane Shear – Type III SST (BES, Empty) Comparison with and without Pit Appurtenances (Seismic Only) 10.26
Figure 10.37. Peak Temperature D/C Ratios for Through Wall Shear (top), Meridional (middle), and Hoop (bottom) 10.27
Figure 10.38. ACI LC1 D/C Ratios for through Wall Shear (top), Meridional (middle), and Hoop (bottom) 10.28
Figure 10.39. ACI LC9 D/C Ratios for Through Wall Shear (top), Meridional (middle), and Hoop (bottom) 10.29
Figure 10.40. ACI LC4 D/C Ratios for Through Wall Shear (top), Meridional (middle), and Hoop (bottom) 10.31
Figure 10.41. ACI LC4 D/C Ratios for In-Plane Shear 10.32
Figure 11.1. Equivalent Local Surface Load Calculation 11.2
Figure 11.2. Equivalent Uniform Surface Load Calculation 11.3

Figure 11.3. Equivalent Local Load 11.3
Figure 11.4. Load-Displacement Response of Nominal Concrete under Local Load 11.4
Figure 11.5. Load-Displacement Response of Lower Bound Concrete under Uniform Surface Load 11.5
Figure 11.6. Local Load Tank Deformation (Scale Factor = 40) 11.5
Figure 11.7. Uniform Surface Load Tank Deformation (Scale Factor = 40) 11.6
Figure 11.8. Load-Displacement Response of Nominal Concrete under Uniform Surface Load 11.7
Figure 11.9. Load-Displacement Response of Lower Bound Concrete under Local Load 11.7
Figure 11.10. Load-Displacement Response of Nominal Concrete under 6.85 ft of Soil with Uniform Load 11.8
Figure 11.11. Load-Displacement Response of Nominal Concrete under 6.85 ft of Soil with Local Load 11.8
Figure 11.12. Load-Displacement Response of Lower Bound Concrete under 6.85 ft of Soil with Uniform Load 11.9
Figure 11.13. Load-Displacement Response of Lower Bound Concrete under 6.85 ft of Soil with Local Load 11.9
Figure 12.1. Theoretical Buckling Loads for Clamped Spherical Cap Under Concentrated Load (Figure 10-34 of Baker et al. 1972) 12.3
Figure 12.2. Buckling and Post-Buckling Behavior of a Spherical Cap Under Distributed Load (Fitch and Budiansky 1970) 12.5
Figure 12.3. Values of ψ for Effect of Concrete Cracking and Amounts and Type of Reinforcement (Figure 4 of Scordelis 1981) 12.8
Figure 12.4. Effect of Geometric Imperfections on Buckling Load (Figure 3 of Scordelis 1981) 12.8
Figure 12.5. Reduction Factor α_3 for Concrete Cracking and Amounts and Type of Reinforcement (Figure 5 of Scordelis 1981) 12.9

Tables

Table 3.1. Type III SST Geometry 3.4
Table 3.2. Type III SST Waterproofing Description 3.5
Table 3.3. Type III SST Waste Design Parameters 3.6
Table 3.4. Type III SST Design Equipment Loads 3.7
Table 3.5. Type III SST Soil Density 3.7
Table 3.6. Type III SST Soil Bearing 3.7
Table 3.7. Type III SST Soil Cover 3.7
Table 3.8. Type III SST Backfill Description 3.8
Table 4.1. TOLA Run Matrix (Material Combination Strategy) used in the Type II SST AOR 4.2
Table 4.2. SST Analysis Load Conditions 4.3
Table 4.3. Load Combinations 4.4
Table 4.4. TOLA Load Step Numbers for Reference 4.5
Table 5.1. Source Drawings for Type III ANSYS® Model Construction 5.2
Table 5.2. Dome Concrete Rebar Volume Ratios 5.7
Table 5.3. Haunch Concrete Rebar Volume Ratios 5.7
Table 5.4. Wall Concrete Rebar Volume Ratios 5.8
Table 5.5. Foundation Concrete Rebar Volume Ratios 5.8
Table 5.6. TOLA Run Matrix (Material Combination Strategy) for Type III SST AOR 5.11
Table 5.7. Temperature History and Waste Height Data Used in the Type III Tank AOR 5.14
Table 6.1. ANSYS® Model Input File Description (pre-processing phase) 6.5
Table 6.2. ANSYS® Model Input File Description (solution phase) 6.6
Table 6.3. ANSYS® Model Input File Description (post-processing phase) 6.6
Table 6.4. ANSYS® Model Output File Description 6.7
Table 6.5. List of Model Components 6.7
Table 6.6. Summary of Soil-to-Concrete Tank Friction Properties 6.13
Table 6.7. Summary of Soil-to-Soil Friction Properties 6.16
Table 6.8. Selected SHELL181 Output Quantities and Sequence Numbers 6.24
Table 6.9. Tank Concrete ACI Section Data Output (Sample Excerpt) 6.26
Table 6.10. Selected CONTA173 Output Quantities 6.27
Table 6.11. Fully Cracked Orthotropic Concrete Properties 6.35
Table 6.12. Seismic Model Waste Properties 6.37
Table 6.13. Lower Bound Excavated Backfill Soil Properties 6.39
Table 6.14. Strain Compatible Lower Bound Native Soil Properties 6.40
Table 6.15. Best Estimate Excavated Backfill Soil Properties 6.41
Table 6.16. Strain Compatible Best Estimate Native Soil Properties 6.42
Table 6.17. Upper Bound Excavated Backfill Soil Properties 6.43

Table 6.18. Strain Compatible Upper Bound Native Soil Properties 6.44
Table 6.19. Seismic Model Run Matrix 6.49
Table 7.1. SSI Profile Geometry 7.2
Table 7.2. The LB SSI Profile 7.2
Table 7.3. The BE SSI Profile 7.4
Table 7.4. The UB SSI Profile 7.5
Table 7.5. Maximum Allowable Element Sizes for Best Estimate Soil 7.16
Table 7.6. Maximum Allowable Element Sizes for Lower Bound Soil 7.17
Table 7.7. Maximum Allowable Element Sizes for Upper Bound Soil 7.19
Table 7.8. Strain Compatible Best Estimate Soil Properties 7.22
Table 7.9. Strain Compatible Upper Bound Soil Properties 7.23
Table 7.10. Strain Compatible Lower Bound Soil Properties 7.24
Table 7.11. Soil Column Modal Frequencies for Horizontal Excitation 7.32
Table 7.12. Soil Column Modal Frequencies for Vertical Displacement 7.34
Table 7.13. Best Estimate Backfill Properties 7.75
Table 7.14. Lower Bound Backfill Properties 7.77
Table 7.15. Upper Bound Back Fill Properties 7.78
Table 8.1. Computed Shear, Meridional, and Circumferential (hoop) Forces and Moments at Critical Sections Under Peak Temperatures for Run 1 ..... 8.4
Table 8.2. Section Properties in Meridional Direction 8.5
Table 8.3. Section Properties in Circumferential Direction 8.6
Table 8.4. Meridional ACI Demand/Capacity Ratio Range 8.34
Table 8.5. Hoop/Circumferential ACI Demand/Capacity Ratio Range 8.35
Table 8.6. Shear ACI Demand/Capacity Ratio Range 8.36
Table 8.7. Section 18 Shear Friction D/C Ratios 8.39
Table 8.8. Section 22 Shear Friction D/C Ratios 8.40
Table 8.9. Section 26 Shear Friction D/C Ratios 8.41
Table 8.10. Section 30 Shear Friction D/C Ratios 8.42
Table 9.1. Combined Seismic and TOLA Runs 9.23
Table 9.2. LC4 Combined TOLA and Seismic ACI Demand/Capacity Ratio Range 9.25
Table 9.3. LC4 Combined Shear Friction D/C Calculations for Section 18 ..... 9.33
Table 9.4. LC4 Combined Shear Friction D/C Calculations for Section 22 ..... 9.34
Table 9.5. LC4 Combined Shear Friction D/C Calculations for Section 26 ..... 9.34
Table 9.6. LC4 Combined Shear Friction D/C Calculations for Section 30 ..... 9.34
Table 9.7. LC4 Combined Shear Friction D/C Calculations for Reduction in Steel at Section 30 ..... 9.35
Table 10.1. Type III SST Pit Appurtenances Maximum Net Weights 10.9
Table 10.2. Type III SST Pit Appurtenances Model Weights 10.10
Table 10.3. Type III SST Pit Appurtenances Dome Load 10.10
Table 10.4. Type III SST Seismic Pit Appurtenance Model Loading Conditions 10.10

Table 10.5. Summary of Type III SST Seismic Pit Appurtenances Model Interface Friction Properties 10.15
Table 10.6. Type III SST Seismic Pit Appurtenances Model Run Matrix 10.16
Table 10.7. Shear Friction D/C Ratios for LC4 Appurtenance Model 10.32
Table 11.1. Summary of Limit Load Analysis 11.4
Table 12.1. Tank Dimensions for the Buckling Analysis 12.12
Table 12.2. Summary Results of the Dome Buckling Analysis 12.13
Table 12.3. Summary Results of the Wall Buckling Analysis 12.15

1.0 Introduction and Objective

The U.S. Department of Energy (DOE) Office of River Protection (ORP) has determined the need to better understand the structural integrity of the single-shell tanks (SSTs) on the Hanford Site in Washington State. To address this need, Pacific Northwest National Laboratory (PNNL) has performed an SST Analysis of Record (AOR) for Washington River Protection Solutions (WRPS). Completion of this work supports the Hanford Federal Facility Agreement and Consent Order (HFFACO) and the Tri-Party Agreement Milestone, M-45-10-01.

The primary objective of the SST AOR Project is to perform a comprehensive structural AOR for the SSTs in order to understand the existing SST structural integrity as a result of past usage and natural hazard phenomena. Seismic analysis is included to assess the structural integrity of the tanks in the event that a design basis earthquake occurs in the future. PNNL has performed the static analysis of the thermal and operating loads while M&D Professional Services, Inc. (M&D) was subcontracted to perform the seismic analysis of the SSTs.

The first phase of the SST AOR Project, preliminary analysis documentation, conducted an extensive review of SST reports, specifications, drawings, and supporting documents, followed by finite element model development, exploratory calculations, and benchmarking resulting in recommendations for subsequent phases. Phase II of the SST AOR project is to perform detailed analyses of the thermal and operating loads and the seismic loads for each of the four tank types. The analyses described in this report document the structural integrity assessment for the Type III (758-kgal storage capacity) SSTs.

This report summarizes the AOR detailed modeling results for Type III SSTs. Hanford Type III SSTs are located at the BY, S, TX, and TY Tank Farms. Acceptance criteria and recommendations given in Johnson et al. (2010) guided the modeling effort. The AOR evaluates the structural consequences of both the static and seismic loads.

1.1 Quality Assurance

The PNNL Quality Assurance (QA) Program is based on the requirements of 10 CFR 830, "Energy/Nuclear Safety Management," Subpart A—"Quality Assurance Requirements" (i.e., the Quality Rule) and the U.S. Department of Energy (DOE) Order 414.1C, "Quality Assurance." Compliance with these documents requires the development of a Quality Assurance Program consistent with a national or international consensus standard. (In addition, DOE Order 414.1C requires that software activities be performed consistent with ASME NQA-1-2000, Subpart 2.7, or an equivalent national or international consensus standard). PNNL has developed its Quality Assurance Program, in a graded approach, using ASME NQA-1-2000, Part IV, Subpart 4.2, "Guidance on Graded Application of Quality Assurance (QA) for Nuclear-Related Research and Development" for both research and development activities and management systems. A QA Program Description (QAPD) describes PNNL's Quality Assurance Program.

Consistent with the structure of ASME NQA-1, other parts of this standard (i.e., NQA-1) are applied, where appropriate, to nuclear and radiological work. For example, by applying the following consensus standards, as appropriate:

ASME NQA-1: "Quality Assurance Requirements for Nuclear Facility Applications, Part 1, Requirements for Quality Assurance Programs for Nuclear Facilities"

ASME NQA-1, Part II, Subpart 2.7: "Quality Assurance Requirements for Computer Software for Nuclear Facility Applications."

The implementing procedures and processes, described in the DOE-approved PNNL QAPD, are made available in a web-based system for the delivery of PNNL requirements and laboratory-level workflow and procedures.

Because the efforts of the SST AOR Project are beyond those defined as research and development (R&D), such as Subpart 4.2 of NQA-1, a Quality Assurance Program to Parts I and II of NQA-1 (using a graded approach) is necessary and is required per the project Statement of Work. PNNL-NQA-EQAM-1, Energy and Environment Directorate (EED) Quality Assurance Plan, provides that NQA-1 Quality Assurance Program (plan). PNNL-NQA-EQAM-1 provides the general, or high-level, overview of the implementation of NQA-1-2008. PNNL-NQA-EQAM-1 is supported by administrative procedures (APs) which provide the more specific requirements for implementation of NQA-1 requirements. The Project Quality Assurance Plan (PQAP), Single-Shell Tank Integrity Project Analysis of Record Project (57926-QAP, Revision 1), is subordinate to PNNL-NQA-EQAM-1 and uses the processes and procedures of PNNL-NQA-EQAM-1 to provide the applicable quality assurance requirements for the specific work activities for the Project (based on client requirements and PNNL requirements) and is compliant with the QAPD.

The requirements contained in the PQAP will satisfy the requirements of DOE Order 414.1C and 10 CFR 830 (when applicable).

2.0 Scope

The objective of the Single-Shell Tank Analysis of Record (SST AOR) Project is to perform a comprehensive structural analysis of record for each of the four tank types of the Hanford single-shell tanks (SSTs). This report provides the detailed finite element (FE) modeling results for the Type III SSTs. The Type III SST structural integrity was evaluated by performing thermal and operating loads analysis, as well as seismic analysis. These analyses include loading conditions described in the Evaluation Criteria report (Johnson et al. 2010). Loading conditions considered in the Type III detailed FE models included: waste thermal loads and hydrostatic pressure, soil overburden, soil surface uniform and concentrated loads, and seismic loads; temperature effects on material properties; creep; concrete cracking; tank appurtenances; and tank limit loads. Additional closed form calculations were performed for the buckling analysis. Two types of models were used, one addressed the static thermal and operating loads analysis (TOLA), and the second addressed seismic loads. The TOLA and seismic models were analyzed independently, and then selected TOLA and seismic results were combined to obtain demand-to-capacity ratios in accordance with the American Concrete Institute code, ACI 349-06 (ACI 2007). The resulting demands on the FE models of the Type III tanks were compared to the capacities at various locations on the tank profile to evaluated the structural integrity of Type III SSTs.

Similar to the Type II structural and seismic analyses reported in Rinker et al. (2011a), the current analysis for the Type III tanks does not consider tank-to-tank interaction, because the previous Brookhaven study (BNL, 1995) concluded that the interaction of tanks separated by one-half the tank radius or more did not cause any significant increase in stress levels. However, tank-to-tank interaction will be evaluated in the detailed analyses for the Type IV tanks because some of the Type IV tanks are spaced closer than one half the radius. Depending on the tank-to-tank interaction results for the Type IV tanks, tank-to-tank interaction effects for the Type II and III tanks may be considered at a later date as appropriate.

2.1 TOLA and Seismic Results Roadmap

Two structural models (TOLA and seismic) were used to evaluate the structural integrity of Type III SSTs. Given the number of TOLA and seismic analyses conducted on the Type III FE models, this chapter describes the sequence in which the analyses and their results are presented in this report.

Independent run matrices were established for the TOLA and seismic models to evaluate results' sensitivities to material property variations and loading scenarios. TOLA and seismic results were then combined for selected best estimate and bounding combinations.

The analytical portion of the report begins with background information on the Type III SSTs in Chapter 3. This chapter summarizes the design information including tank dimensions, dates of construction and specifications, and design parameters.

Chapter 4 lists the applicable codes and standards, acceptance criteria, and loads described in the Evaluation Criteria report, which apply to both the TOLA and seismic modeling efforts. The TOLA material property run matrix (Table 4.1) used in the Type II AOR (Rinker et al. 2010) is presented for reference as the starting point for the TOLA Type III SST run matrix. The material property run matrix evaluates the sensitivity of the analysis results to the expected variations in soil, concrete, and waste

properties, and their combinations. The TOLA Type III SST run matrix is presented in Table 5.6, while the Seismic Run Matrix is presented in Table 9.1. The combined TOLA + Seismic runs are listed in Table 9.2. Chapter 4 also presents the ACI 349-06 load combinations and load factors that are applicable to the SST TOLA and seismic analyses.

Chapter 5 describes the TOLA model, including the geometry, boundary conditions, material properties, and the applied loads. Material property combinations are summarized in the TOLA run matrix (Table 5.6). Figure 5.5 shows the temperature and waste-level histories that were applied in the TOLA analyses.

Chapter 6 describes the seismic model, including the geometry, loads, boundary conditions, and material properties. The section stiffness properties of the seismic model include the effects of concrete cracking and thermally degraded elastic modulus. Section 6.3 describes the analytical methods used to calculate the finite element stiffness properties. Waste properties are summarized in Table 6.12. Background information on waste properties is included in Appendix N of Rinker et al. (2011a). The soil properties used in the seismic modeling are discussed in Section 6.3.4. The far-field soil properties are provided by AMEC Geomatrix and documented in the *Development of Inputs for SSI Analyses of SSTs*, AMEC Geomatrix report in Appendix R of Rinker et al. (2011a). The backfill soil properties are provided in Appendix O of Rinker et al. (2011a). The seismic run matrix is given in Table 6.19.

Chapter 7 provides the details of the three soil columns used for the seismic analysis, and their associated properties defined in the AMEC Geomatrix report referenced in the paragraph above. Chapter 7 also summarizes the spectral matching calculations that were performed to confirm that input motions to the seismic model produced the appropriate free-field responses in the seismic model.

Chapter 8 lists the TOLA model results independent of the seismic modeling results for the TOLA matrix runs. The ACI 349-06 meridional, hoop, and through-wall shear demand to capacity (D/C) ratios are reported for each of the TOLA runs (refer to Sections 8.3 through 8.6). Tables 8.4 through 8.6 summarize the D/C ratios at several load steps for the dome, haunch, wall, and slab sections of the tank. Since the slab section was the only location where tank demands exceeded the ACI 349-06 capacities, the slab element removal side studies were performed and documented in Appendix E; similar slab removal analyses were performed in Sections 8.4.1 and 8.6.1 of Rinker et al. (2011a). The slab was detached from the footing to further evaluate possible cracking and shear offset displacement of the concrete there. The analysis (in Appendix E) showed that disconnecting the slab and footing would not alter the tank's structural stability. The displacement offset is also small compared to the liner thickness and therefore it is likely that the liner would bridge the discontinuity without being damaged. Section 8.12 summarizes the shear friction D/C ratios for the construction joints in the Type III SSTs.

Chapter 9 summarizes the seismic modeling results. Section 9.1 presents the seismic demands for each of the nine runs in Table 6.19. These results are independent of the TOLA results. Section 9.4 summarizes the combined TOLA + Seismic results. Table 9.2 lists the combined demand-to-capacity ratios for the selected cases in Table 9.1. Tables 9.3 through 9.7 give the TOLA + Seismic combined shear friction D/C ratios for the Type III SST construction joints.

Chapter 10 evaluates the effect of appurtenances (e.g., pits, risers, piping, pads) on the tank structural integrity. Tank appurtenances have not been examined in the past other than in the SST AOR Type II report (Rinker et al, 2011a). Two independent models (TOLA and seismic) were used to evaluate the

bounding Type III SST appurtenances. Both the TOLA and seismic models were constructed to represent the same appurtenance configuration: one central pump pit and two offset sluice pits. A thorough review of Type III SST appurtenances is summarized in Appendix B. Sections 10.1 discusses the TOLA appurtenance model. Section 10.2 discusses seismic model and results. Section 10.3 discusses the D/C ratios for the peak temperatures and all applicable ACI load combinations. The Type III SST appurtenance study is summarized in Section 10.4.

Chapter 11 summarizes the tank limit load analysis performed for Type III SSTs. The limit loads were evaluated for both uniform and concentrated loads over the tank dome. The uniform load was applied over the entire soil surface, while the concentrated load was applied over a 20-ft-diameter area at the center of the tank. The limit loads were estimated by increasing the load until the tank model offered little or no resistance to additional load. The limit load results are summarized in Table 11.1.

Chapter 12 presents the buckling analyses performed for the Type III SSTs. Three tank conditions were evaluated for the Type III SSTs: 1) the baseline tank analysis – the maximum Type III thermal history with the bounding soil overburden depth of 11 ft; 2) the maximum thermal history with the actual overburden; and 3) the actual thermal history for the tank with the maximum overburden. Results for the three loading conditions are discussed in Section 12.4. The buckling calculations performed in Mathcad™ are found in Appendix I.

Chapter 13 gives the overall conclusions of the tank modeling results.

The references cited in the report are listed in Chapter 14.

Appendices A through K provide supplemental information on the Type III SST thermal, operating, and seismic analyses described in this report. Appendix L includes the external reviewer comments on this report.

This page intentionally left blank.

3.0 Type III SST Background

In response to Hanford's plutonium production, a total of 149 underground tanks were constructed between 1943 and 1964 to contain the nuclear waste in twelve separate tank farms in the 200 East and West areas of the Hanford Site. Forty-eight of these underground tanks, each with a 758,000-gallon capacity and 75-foot internal diameter, were built among four tank farms (BY, S, TX, and TY) between 1947 and 1952 and are designated as the Type III single-shell tanks (SSTs). These SSTs were first used in the TX Tank Farm in 1949 (Boomer 2009). By 1980, however, discharge operations to the SSTs ended pursuant with the congressional mandate. Interim stabilization was completed by 2004 when target supernate and interstitial liquid were removed from all SSTs (Berman 2009). Subsequent sections in this chapter summarize the Type III SST design information.

3.1 Design

The Type III SSTs are 758,000-gallon reinforced concrete tanks with a 75-foot internal diameter. The Type III tanks include the BY, S, TX, and TY tank farms. Each of the Type III tank farms was built from a different set of construction drawings (Hanford Engineering Works [HEW] drawings). Each SST is an underground, reinforced concrete structure with a carbon steel liner along the base and cylindrical walls. The Type III tanks have an internal height of approximately 37 feet from the floor to the dome center, while the steel liners have a height of approximately 24 feet. Additional tank geometry details are provided in greater detail in Han (1998).

Protection for the tanks' steel liners and concrete structures included asphaltic waterproofing and paint on their surfaces. Figure 3.1 illustrates the basic tank design features. Appendix B provides tank-to-tank piping and appurtenance information. The Type III tanks have dish-shaped bottoms and are arranged in several layouts including: 4 rows of 3 tanks in the BY and S, 3 rows of 4 and 2 rows of 3 tanks in the TX, and 2 rows of 3 tank in the TY tank farms. Furthermore, the tanks in each row have overflow piping connecting them in a cascade series where the first tank overflows to the next tank (Hanford Engineering Works [HEW] drawings). Figure 3.2 illustrates one of the cascade series arrangements (BY Tank Farm) of the Type III SSTs.

Table 3.1 summarizes the geometrical characteristics for the Type III SSTs, while Table 3.2 describes the asphaltic waterproofing for the tanks. However, waterproofing layers, and the steel liners, were not included in the structural models as discussed in Section 4.2 of Rinker et al. (2010). Waste loading characteristics were obtained from the construction specifications and technical drawings and are presented in Table 3.3. Current tank contents are not presented in this report, but tank-specific data and current status are provided in the Best-Basis Inventory (BBI) within the Tank Waste Information Network System (TWINS). The BBI is the official database for tank waste inventory estimates at the DOE Hanford Site.

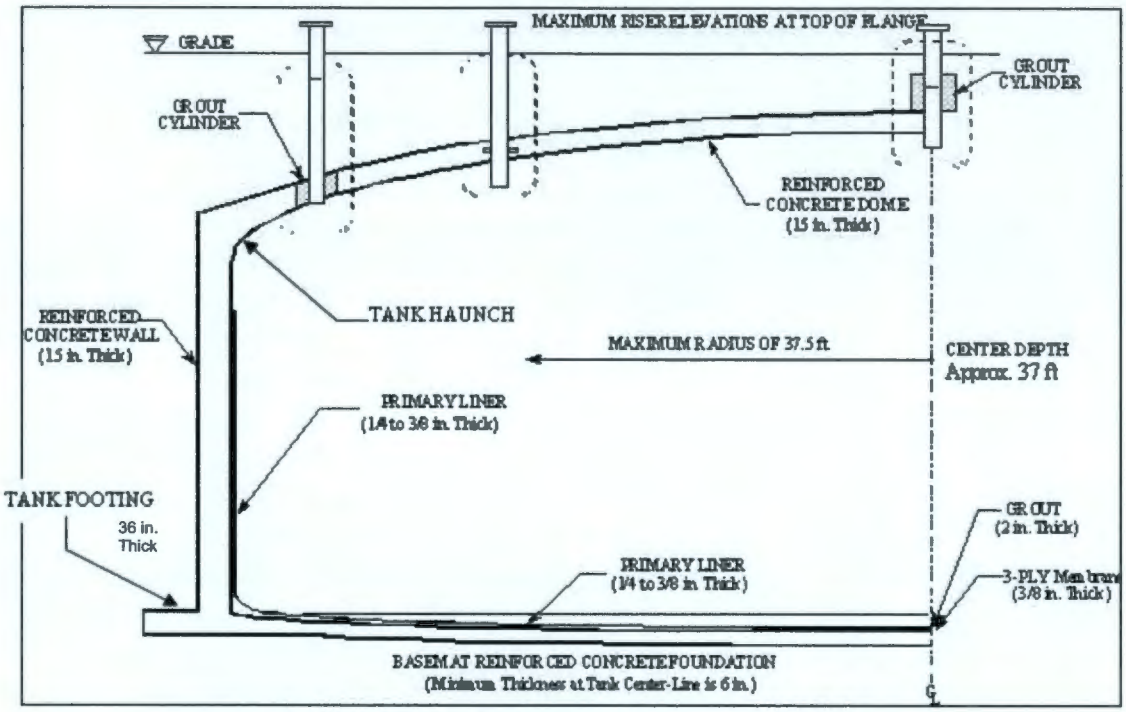

Figure 3.1. Typical 758,000-Gallon Single-Shell Waste Tank and Riser Configuration for Type III Tanks 241BY, 241S, 241TX, and 241TY (not to scale)

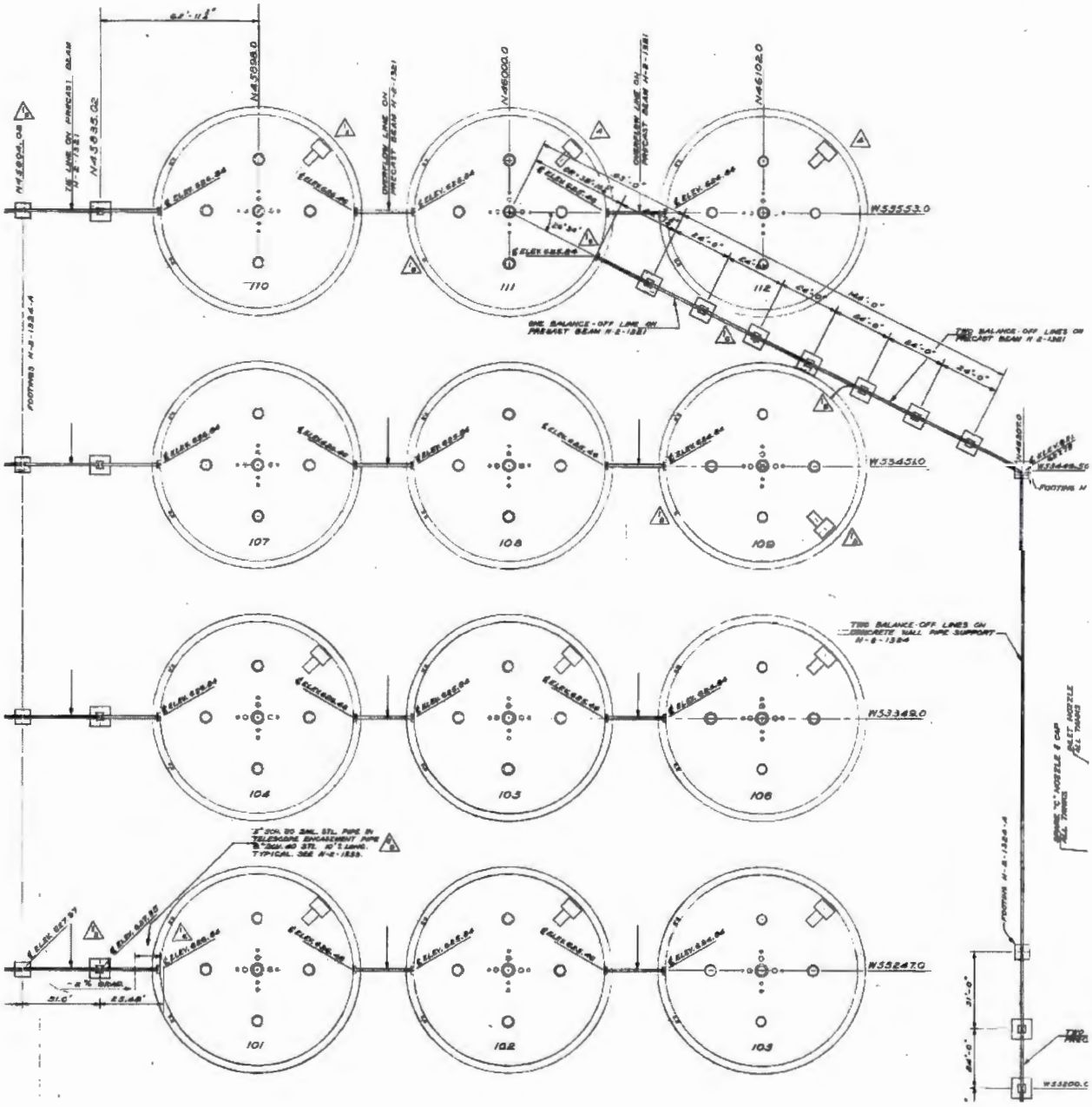

Figure 3.2. Type III SST, BY Tank Farm Cascade Series Configuration, Hanford Drawing H-2-1308

Table 3.1. Type III SST Geometry

Tank Farm	Footing Thickness (in.)	Concrete Foundation Centerline Thickness (in.)	Reinforced Concrete Wall Thickness (in.)	Reinforced Concrete Dome Thickness (in.)	Steel Liner Height (in.)	Reference (Drawings)	Steel Liner Centerline Thickness (in.)
BY, S, TX, and TY	36	6[a]	~15	15	~287 to ~288	BY: H-2-1312[b], S: H-2-1783[b], TX: H-2-808[b], and TY: H-2-2244[b] **For steel liner thickness**: BY: H-2-1313[b], S: H-2-1784[b], TX: H-2-809, TY: H-2-2245[b]	0.375

(a) Dished bottom.
(b) Checked for as-built.

Table 3.2. Type III SST Waterproofing Description

Tank Farm	Steel Liner Foundation	Steel Liner Walls	Concrete Exterior	Reference
BY	3 ply asphaltic membrane waterproofing 3/8" thick, 2" grout reinforced with wire mesh 2" openings (only reinforce near knuckle, ends at 29' from center of tank)	3 ply asphaltic membrane waterproofing covered with asphalt, 3/8" to ½" thick, and 5/8" thick gunite reinforced with 2" opening wire mesh	3/4" gunite reinforced with wire mesh 2" openings over 3/8" thick 3 ply asphaltic membrane waterproofing, covers top of dome and ~6' down side wall	Drawing H-2-1312[a]
S	3 ply asphaltic membrane waterproofing 3/8" thick, 2" grout reinforced with 2"x2" -14ga. Galv. Welded fabric (only reinforce near knuckle, ends at 32' 1" from center of tank)	3 ply asphaltic membrane waterproofing covered with asphalt, 3/8" to ½" thick, and 5/8" thick gunite reinforced with 2"x2" 14ga. Galv. Welded fabric	3/4" gunite reinforced with 2"x2" -14 Ga. Galv. Welded fabric over 3/8" 3 ply asphaltic membrane waterproofing, covers top of dome and 1' below side wall-haunch transition except at nozzles	H-2-1783[a]
TX	3 ply 3/8" thick asphaltic membrane, 2" thick grout reinforced with 2" opening wire mesh	3 ply asphaltic membrane waterproofing covered with asphalt, 3/8" to ½" thick, and 5/8" thick gunite reinforced with 2" opening wire mesh	3/8" thick 3 ply asphaltic membrane waterproofing covered with 3/4" thick gunite reinforced with 2" opening wire mesh, covers top of dome and ~6' down side wall	Drawing H-2-808[a]
TY	3 ply 3/8" thick asphaltic membrane, 2" thick grout reinforced with 2"x2" 14 ga. Galv. Welded fabric (only reinforce near knuckle, ends at 32'1" from center of tank), 55# roll roofing over grout pad to top of footings	3 ply asphaltic membrane waterproofing 3/8" to 1/2" thick, 5/8" thick gunite reinforced with 2"x2" 14 ga. Galv welded fabric	3 ply 3/8" thick asphaltic membrane waterproofing, covered with 3/4" gunite reinforced with 2"x2" 14ga. Galv. Welded fabric, covers top of dome and 1' below side wall-haunch transition except at nozzles	H-2-2244[a]

(a) Checked for as-built.

Table 3.3. Type III SST Waste Design Parameters

Tank Farm	Max Specific Gravity	Reference	Height (in.)	Reference	Storage Pressure (psi)	Reference	Max Liquid Design Temperature (°F)	Reference	pH	Reference
BY, S, TX, and TY	1.5	Stivers 1955 and Rifaey 2002	282	Smith 1955	Atmospheric	Stivers 1957 and/or Harvey 1970	220	Stivers 1957 and Harvey 1970	8 to 10	Stivers 1957 and Harvey 1970

The loads defined in the Evaluation Criteria report (Johnson et al. 2010) were used for the analysis detailed in this document (see Table 4.2). Johnson et al. (2010) requires that a concentrated surface load be used but does not designate a value other than to mention the "encroachment of heavy crawler cranes near the tank dome." Table 3.4 summarizes the limited information on Type III tank loads that was found during the review of historical documents. Rifaey (2002) reiterates the 2 × 35,000 lb. concentrated load found in Stivers (1955). The Analysis of Record Summary for Single-Shell Tanks (Mackey and Julyk 2004b) makes mention of a 110 ton crane for the double-shell tanks (DSTs). The 200 kip concentrated load design limit appears in Ramble (1983). Subsequent analysis (Mackey 2004b) has shown this limit to be conservative when considered with soil depth and density. Additional background is discussed in Appendix A.

Table 3.4. Type III SST Design Equipment Loads

Tank Farm	Equipment Loading	Reference
BY, S, TX, and TY	2×35,000-lb tractors, 1'-3" concrete slab at 150 psf	Stivers 1955

Refer to Table 3.5 for soil density values, to Table 3.6 for design soil-bearing values, to Table 3.7 for soil cover, and to Table 3.8 for backfill. A more recent effort in Mackey and Julyk (2004a) provides soil cover results on a detailed soil survey from field walk-downs and revises soil height data above the DSTs and the SSTs at the Hanford Site. However, the soil cover and soil density values listed in Section 4.2, Post Design Evaluation Input, will be used in the Type III detailed analyses.

Table 3.5. Type III SST Soil Density

Tank Farm	Soil Density Specification (lb_f/ft^3)	Reference
BY, S, TX, and TY	110	Harvey 1970 and Mercier 1981

Table 3.6. Type III SST Soil Bearing

Tank Farm	Soil-Bearing Value (lb_f/ft^2)	Reference
BY, S, TX, and TY	6000	Harvey 1970 and Mercier 1981

Table 3.7. Type III SST Soil Cover

Tank Farm	Soil Cover Depth from Top of Dome Apex to Finished Backfill Grade (in.)	Reference
BY	96	Drawing H-2-1312[a] and GE 1953a
S	~74.6	Drawing H-2-1783[a]
TX	96	Drawing H-2-808[a] and GE 1953b
TY	~74.6	Drawing H-2-2244[a]

(a) Checked for as-built.

Table 3.8. Type III SST Backfill Description

Tank Farm	Backfill Description	Reference
BY	Backfill will be placed in layers 6" to 24" deep.	Rutherford 1948
S	The top layer of backfill coarse gravel 4" deep. Backfill placed in layers no deeper than 24".	Rutherford 1949
TX	Backfill will be done in 6" to 24" layers uniformly around and over structure so that all weight and pressures are equally distributed.	Overbeck 1946
TY	Bank-rum sand is placed at least 1' below foundation grade and ~2' above and shaped to cradle the catch tanks. Top layer of backfill coarse gravel 4" deep. Backfill placed in layers no deeper than 24".	Rutherford 1951

4.0 Guidance

This chapter summarizes the guidance documents and design input used in the detailed finite element (FE) models of the Type III single-shell tanks (SSTs).

4.1 Acceptance Criteria

The Evaluation Criteria report by Johnson et al. (2010) provides the acceptance criteria, codes and standards, and the recommended analysis methods for application in the SST structural integrity evaluations. Subsequent sections of this chapter describe the material properties, loads, and load combinations considered in the Type III tank analyses in this report.

4.1.1 Material Properties

Material property data for concrete, soil, and reinforcing steel are provided in the Evaluation Criteria report (Johnson et al. 2010). Best estimate, lower bound, and upper bound concrete strength and elastic modulus are provided as a function of temperature. Elastic modulus versus temperature is provided for the reinforcing steel. Best estimate, lower bound, and upper bound values are provided for the static stiffness properties of Hanford soils. The nominal concrete density of 145 lbf/ft^3 used in the analysis is representative of unreinforced Hanford concrete. The added weight of the rebar was accounted for by the ANSYS software in the reinforcement layers. However, the steel volume is a small fraction of the total tank section volume so this has a very small effect on the overall density of the reinforced concrete.

A material property sensitivity matrix was presented in the Preliminary Analysis report (Rinker et al. 2010) for the thermal and operating loads analysis of the SSTs. The matrix covered the uncertainty in concrete strength and modulus and the soil modulus. In Rinker et al. (2010), sensitivity studies were conducted on the material property variables to develop the recommended TOLA run matrix for the detailed analyses. This material property sensitivity run matrix was updated in the Type II report (Rinker et al. 2011a) based on the literature review and reviewer recommendations on the use of concrete tensile strength in finite element models. Table 4.1 shows the TOLA run matrix used in the Type II SST AOR. Table 4.1 was updated for the SST Type III analysis to include additional runs for compatibility with the seismic runs. The final Type III TOLA run matrix is presented in Section 5.6.

Table 4.1. TOLA Run Matrix (Material Combination Strategy) used in the Type II SST AOR

Case/ Run	Soil Modulus	Concrete Modulus	Concrete Tensile Strength	Concrete Creep		Notes
1	N	N	Near Zero (10 psi)	Yes		Best Estimate Properties
2	N	N	Near Zero (10 psi)	No	"Worst-Case Combinations" using available material property bounds	
3	N	H	Near Zero (10 psi)	No		Depending on depth, low soil modulus is lower by 20% to 50% when compared to best estimate values.
4	L	H	Near Zero (10 psi)	No		Depending on temperature, high concrete modulus is higher by 15% to 30% when compared to best estimate values.
5	L	N	Near Zero (10 psi)	No		
6	N	N	N	Yes		
7	N	N	N	No		

H = High.
L = Low.
N = Nominal/Mean (Best Estimate).

4.1.2 Loads

The design and operating loads for the SSTs are established by their construction specifications, safety analysis reports, or other basis documents for the tank farm of interest (Johnson et al. 2010). The loads for evaluation at each of the SST farms were summarized in several reports, including Chapter 2 of Johnson et al. (2010) and Appendix A of Rifaey (2002). The SST design loadings include those associated with normal operation, abnormal conditions, and extreme conditions. Table 4.2 lists the loading conditions used in this analysis. The 1.7 value of specific gravity chosen for the static TOLA analysis represents a conservative average waste density for the Type III tanks. Note that it is slightly lower than the revised operating limit on specific gravity of 1.8 given in Rifaey (2002) for the Type III tanks (BY, S, TX, and TY). However, the sensitivity analysis in Appendix D shows that the waste is not a significant contributor to the static load demands on the tank. Therefore, specific gravities of 1.7 and 1.8 will give nearly the same results.

Table 4.2. SST Analysis Load Conditions

Design Load	Value	Notes
Design Life	25 to 35 years	A 59-year (1953–2012) design life is used
Soil Cover	11 ft @ 125 lb/ft^3	Relative to dome apex
Hydrostatic	variable height @ SpG = 1.7	Specific gravity (SpG) = 1.7
Live Load	40 lb/ft^2	Uniform surface load
	200,000 lb	Concentrated over 10 ft radius
Thermal	300°F	Maximum temperature of waste (tank center bottom)
Seismic	--	See Section 6.3

4.1.3 Static Load Combinations

The classification of loading conditions and events is key to determining the appropriate load factors and combinations to analyze in the tank structural integrity evaluations. Section 9.2 of the American Concrete Institute (ACI) 349-06 (ACI 2007) code specifies the factored load combinations that must be used in evaluating the required design strength. The Evaluation Criteria report provides a complete list of load combinations followed by a short list of load combinations applicable to the SSTs. In summary, the applicable load combinations from the Evaluation Criteria report are:

Load Combination 1 (LC1). $$U = 1.4D + 1.4F + 1.7L + 1.7H \quad (4.1a)$$

Load Combination 4 (LC4). $$U = D + F + L + H + T_o + E_{ss} \quad (4.1b)$$

Load Combination 9 (LC9). $$U = 1.05D + 1.05F + 1.3L + 1.3H + 1.05T_o \quad (4.1c)$$

where
- D = Dead loads including tank self weight, piping and equipment dead loads. (Where the structural effects of differential settlement, creep, or shrinkage may be significant, they shall be included with the dead load D.)
- L = Live loads, including impact effects of moving loads
- F = Lateral and vertical pressure of liquids
- H = Loads due to weight and pressure of soil, water in soil, or other materials, or related internal moments and forces
- T_o = Internal moments and forces caused by temperature distribution within the concrete during normal operation and shutdown
- E_{ss} = Safe Shutdown Earthquake (SSE) effects = Design-Basis Event/Earthquake (DBE) effects

Although the Evaluation Criteria report provides a list of load combinations applicable to the SSTs, the sub-classification of the soil over and around the tanks into dead or live loads is somewhat open to interpretation. The previous analysis of the C-106 tank provides a detailed discussion of the classification of soil and other loads (Bander et al. 1994). That analysis, along with the guidance from the tank operating contractor (WRPS), was considered when defining the dead and live loads. Table 4.3 lists the loading conditions and the corresponding load factors used in the Type III SST analysis of record. Figure 4.1 shows a typical layout of an SST along with the soil boundaries used in the load and load factor definitions applicable to the ACI 349-06 evaluation of TOLA loads only.

Table 4.3. Load Combinations

Loading Type	Load	Nominal Value (LC4)	Load Factor (LC1)	Load Factor (LC9)	Alternative Load Factors
Structure	Body Load (D)	1 g	1.4	1.05	1.4
Structure	Soil Cover (D) (depth at apex of dome)	11 ft	N/A (density is factored)	N/A (density is factored)	N/A (density is factored)
Structure	Soil Density – backfill overburden (D)	125 lb_f/ft^3	1.4	1.05	1.4
	Soil Density – backfill side soil (H)	125 lb_f/ft^3	1.7	1.3	0.9
	Soil Density – undisturbed	110 lb_f/ft^3	N/A	N/A	N/A
Normal Op	Uniform Surface Load (L)	40 lb_f/ft^2	1.7	1.3	1.7
Extended Op	Concentrated Load at dome center (L)	200 kip	1.7	1.3	1.7
Normal Op	Waste Specific Gravity (F)	1.7	1.4	1.05	1.4
Normal Op	Waste Level	120 in	N/A (density is factored)	N/A (density is factored)	N/A (density is factored)
Normal Op	Thermal cycle as shown in Figure 5.5	Peak of 300°F (tank center bottom)	N/A	1.05	N/A
Seismic	Horizontal	See Section 6.2	N/A	N/A	N/A
	Vertical		N/A	N/A	N/A

N/A = Not applicable.

In addition to the load combinations shown in Equations 4.1a-c, Section 9.2.3 of ACI 349-06 (ACI 2007) states that "*If any load reduces the effects of other loads, the load factors for that load shall be reduced to 0.9 if it is always present or occurs simultaneously with other loads. Otherwise the load factors for that load shall be taken as zero in the additional load case.*" An alternative load factor run was performed using run #1 to understand the effect of the reduced load factors. The results are provided in Appendix G.

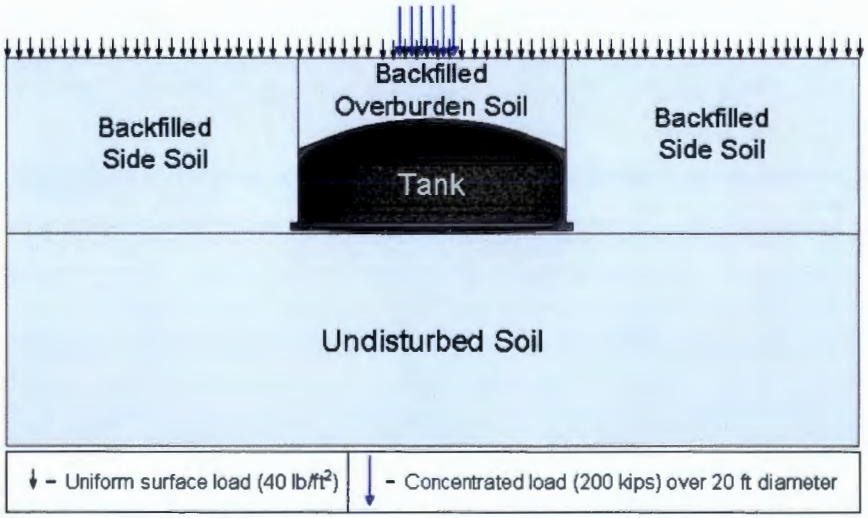

Figure 4.1. Typical Layout of a Single-Shell Tank (not to scale)

Figure 4.2 shows the flow chart used to model the 59 years of thermal loads and creep with appropriate intervals for the ACI structural evaluation. Mechanical loads (gravity, waste load, and concentrated load) were applied in load steps 1 through 3. Thermal and waste-level histories were applied in load steps 4 through 16, with load step 16 corresponding to a maximum waste temperature of 110°F. Details of the waste temperature and level are provided in Section 5.6. The analyses were then carried in two separate steps for respective ACI evaluations. In one step, the entire model was cooled down to 50°F after which the ACI load combination 1 load factors were applied for tank evaluation. In the other step, the waste was cooled to 80°F during which the ACI load combination 4 was evaluated followed by the evaluation of ACI load combination 9. Table 4.4 shows the load step numbers and the corresponding thermal and waste-level history; Figure 5.5 illustrates the temperature and waste height profiles used for the detailed analysis of the Type III tanks.

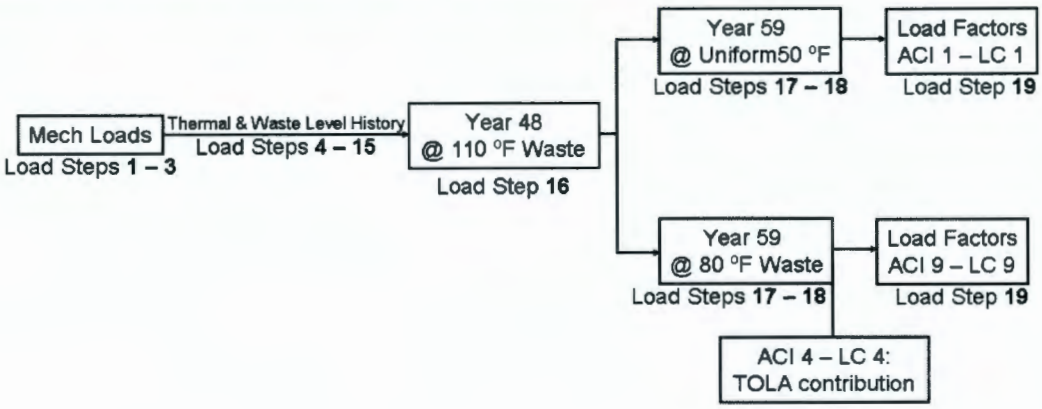

Figure 4.2. Flow Plan for SST AOR Analyses

Table 4.4. TOLA Load Step Numbers for Reference

Load Step No.	Time		Max Temp (tank center bottom) (°F)	Waste Height (inches)	Notes	
	Days	Years				
1	1	0.003	53	0	Gravity	Mech Loads
2	2	0.005	53	275	Waste Load	
3	3	0.008	53	275	Conc. and Live Loads	
4	154	0.42	300	275	-	Thermal & Waste Level History Loads
5	398	1.09	300	275	Material Property Change	
6	399	1.09	300	275	-	
7	1479	4.05	260	275	-	
8	2388	6.54	200	275	-	
9	3168	8.68	200	275	-	
10	3290	9.01	200	300	-	
11	4020	11.01	200	300	-	
12	5024	13.76	138	300	-	
13	5481	15.02	110	300	-	
14	6608	18.10	110	120	-	
15	7703	21.10	110	120	-	
16	17535	48.04	110	120		

Table 4.4. (contd)

Load Step No.	Time		Max Temp (tank center bottom) (°F)		Waste Height (inches)	Notes	
	Days	Years					
17	20091	55.04	53 (LC1)	80 (LC9)	120	Back to Initial Temperature/Current Temperature	-
18	21552	59.05	53 (LC1)	80 (LC9)	120	Steady State at 50°F/80°F	-
19	21553	59.05	53 (LC1-LF)	80 (LC9-LF)	120	Load Factors	ACI Load Factors

LC = Load Combination.
LF = Load Factors.

4.2 Post Design Evaluation Input

Per the WRPS email on 3/28/2011, 16:00 - Appendix A, an 11-ft soil overburden will be used in the detailed SST Type III modeling. In addition to the soil overburden - as previously prescribed in the SST Type II detailed analyses, a 125-lb_f/ft^3 soil density, as identified in Johnson et al. (2010), and a 200-kip live load applied over a 10-ft radius area, as recommended in Rinker et al. (2010), are to be used for each of the tank type SST AOR detailed analyses.[3] The 11-ft soil overburden bounds the maximum soil overburden reported in Mackey (2004a) for the Type III SSTs (10.38 ft for tank TX-108). The prescribed soil density is an upper bound estimate recommended by Johnson et al. (2010). The concentrated load at the dome center over a 10-ft radius is specified as an operating limit in Mackey (2004a).

[3] Current Allowable Concentrated Dome Loads are given in Mackey 2004b, and Mackey and Julyk, 2004b. These are based on analytical results from Julyk and Mackey 2003 (which references Julyk 2003 and Ramble 1983) and data from Mackey and Julyk 2004a and Mackey and Julyk 2004c.

5.0 Static Thermal and Operating Loads Analysis

5.1 Introduction

This chapter describes the ANSYS® finite element (FE) model developed for the Type III SST Thermal and Operating Loads Analysis (TOLA). The geometry details of the Type III tanks were taken from the pertinent construction drawings database collected during Phase I of the Single-Shell Tank Analysis of Record (SST AOR) Project. The following sections describe the steps involved in developing the model, the element types used, and the boundary conditions applied for the structural and thermal analyses models.

5.2 Geometry

The Type III tanks are 758,000-gallon, underground, reinforced-concrete tanks with a 75-foot internal diameter located in the TX, BY, S and TY tank farms. The tanks in the TX farm were constructed in 1947 through 1948 followed by the BY tank farm (1948 through 1949), the S tank farm (1949 through 1951), and the TY tank farm (1951 through 1952). Although the TX, BY, S and TY tank farms were constructed from different specifications, they are geometrically identical and have the same material properties with minor differences in reinforcing steel arrangements. The Type III tanks have base slabs of 6-inch-thick reinforced concrete at the centerline of the tanks. The top surface of the base slab has an inverted dome shape with a radius of 569.82 feet while the bottom surface is flat. The dished top surface and horizontal bottom surface result in a 18-inch-thick slab at a radius of 33feet, 8⅞ inches. The tanks cylindrical side walls have an inside radius of 37 feet, 7¼ inches with a thickness of 15 inches. The circular footing under the wall is 3 feet thick and extends 3 feet radially beyond the outer face of the cylindrical wall. The outer radius of the footing is about 41 feet, 10¼ inches. Similar to other SSTs, the steel liner in the Type III tanks is not attached to the cylindrical wall and does not contribute significantly to the structural integrity of the reinforced concrete tank shell. The purpose of the liner is only to serve as a leak barrier and hence it is not included in the structural analysis.

5.3 ANSYS® Model Construction

The Type III tank finite element model closely resembles the Type II AOR model except for minor changes in the tank geometry. ANSYS® Version 12.0 was used in all the TOLA analyses of the Type III SSTs, except for the TOLA appurtenance analysis. The TOLA appurtenance modeling used ANSYS® Version 13.0. The FE model was developed using ANSYS® parametric design language (APDL) macros and input files. The geometric details of the Type III tanks were taken from the construction drawings listed in Table 5.1. The Type III FE model is a 3-D slice model. While building the 3-D model, the 2-D geometry was initially created to represent the cross-section, and it was swept (rotated) about the central axis through two degrees to get the 3-D slice model. The rotation angle was chosen to obtain elements of good aspect ratios in the FE model. The Type III tanks were modeled with a soil overburden of 11 ft, bounding the maximum value reported for the Type III tanks. Similar to the Type II AOR model, the sub-grade undisturbed soil depth was specified at 168 ft below the foundation and the radial extent of the soil (lateral soil dimension) was modeled to a radial distance of 240 ft. The compacted backfill excavation slope boundary that distinguishes backfill soil from undisturbed soil was not modeled in the TOLA analysis and instead the backfill soil was modeled throughout the radial extent of the soil. The Type III model includes seven layers of backfill soil above the tank foundation level. The undisturbed

soil underneath the tanks was modeled with eight stratigraphic soil layers to a depth of 168-feet. The material properties for the concrete and soil are summarized in the SST Evaluation Criteria report (Johnson et al. 2010).

Table 5.1. Source Drawings for Type III ANSYS® Model Construction

Tank Farm	Composite Tank Details	Wall and Floor Reinforcement	Dome Reinforcement
TX	H-2-808, Rev 7	H-2-812, Rev 3	H-2-813, Rev 2
BY	H-2-1312, Rev 2	H-2-1314, Rev 2	H-2-1315, Rev 2
S	H-2-1783, Rev 3	H-2-1785, Rev 1	H-2-1786, Rev 1
TY	H-2-2244, Rev 2	H-2-2246, Rev 2	H-2-2247, Rev 2

The ANSYS® SOLID65 (3-D Reinforced Concrete Solid) elements were used to represent concrete regions with and without reinforcement bars (rebars). SOLID65 elements have the ability to simulate concrete cracking in tension, crushing in compression and creep. The reinforced concrete is divided into regions that have different steel reinforcement ratios, where it is assumed that each reinforcing layer is one inch thick (approximately the thickness of the crossed meridional and hoop rebar layers). The reinforcement model in the SOLID65 elements is a smeared model and requires specifying the amount of steel in each element as a volume fraction of the total element volume. The volume fractions of steel and concrete near the inner and the outer faces of the tank cross-section were calculated at various locations around the tank cross-section and assigned to the elements in the 1-inch-thick reinforced layers. The reinforcement properties are input as real constants which include the material number, the volume ratio, and the orientation angles. In these regions the element coordinate system is defined such that the element x-axis is parallel to the direction of a vector connecting the centroids of the current and adjacent elements and the y-axis is defined normal to this vector. These local coordinate systems are defined on the plane passing through the z-centroids (the plane passing through half the angle of the 2-degree slice) of the elements. The z-axis (for hoop reinforcement) for these elements is automatically defined normal to the x-y plane. The soil surrounding the tank is modeled with SOLID185 elements, with the Extended Drucker-Prager material model. The nonlinear contacts at the concrete and the soil interface use TARGE170 and CONTA173 elements. Figure 5.1 through Figure 5.4 show various details of the FE model of Type III tanks.

Since the rebar was not explicitly modeled, it is not required to prescribe the exact location of each rebar. While calculating the volume fraction of steel for real constants, careful consideration was given to match the total amount of steel in the meridional and the hoop directions. The locations of the 1-inch-thick reinforcement layers were also accurately defined in the cross-section thickness to accurately model the bending resistance of the reinforcing bars. The locations of the assigned hoop steel region in the haunch region are more approximate; however, the fraction of reinforcement steel prescribed in this region (Figure 5.3) matches the steel volume in this region. This ensures minimal error in the global structural response of the haunch region.

The ANSYS® concrete model has no provision for simulating the post-cracking tension stiffening behavior of reinforced concrete. The reinforced concrete elements instantly lose their total stiffness upon cracking resulting in numerical instability leading to solution convergence difficulties. In order to overcome the convergence issues, the unreinforced concrete elements were also given negligible but non-zero reinforcement by assigning a reinforcement volume fraction of 0.01% of the element volume. The use of this augmented stiffness greatly enhanced the numerical stability of the model and it was demonstrated to have no significant impact on the resulting force, moment, stress, or strain calculations.

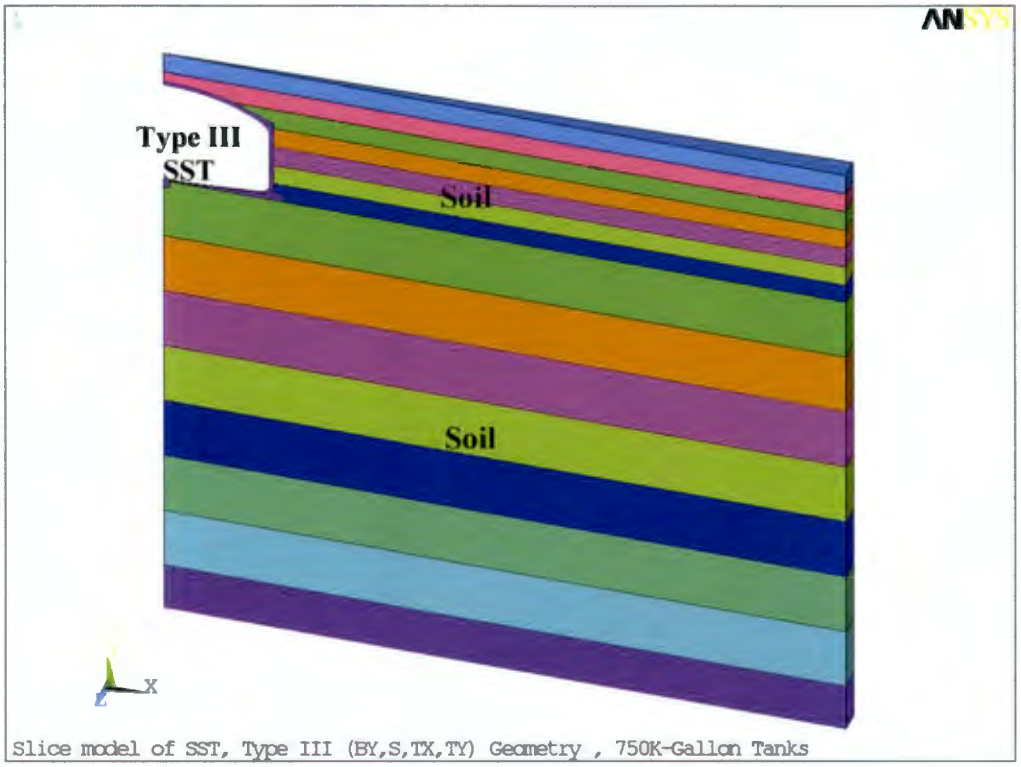

Figure 5.1. Slice Model Showing Type III SST and Surrounding Soil

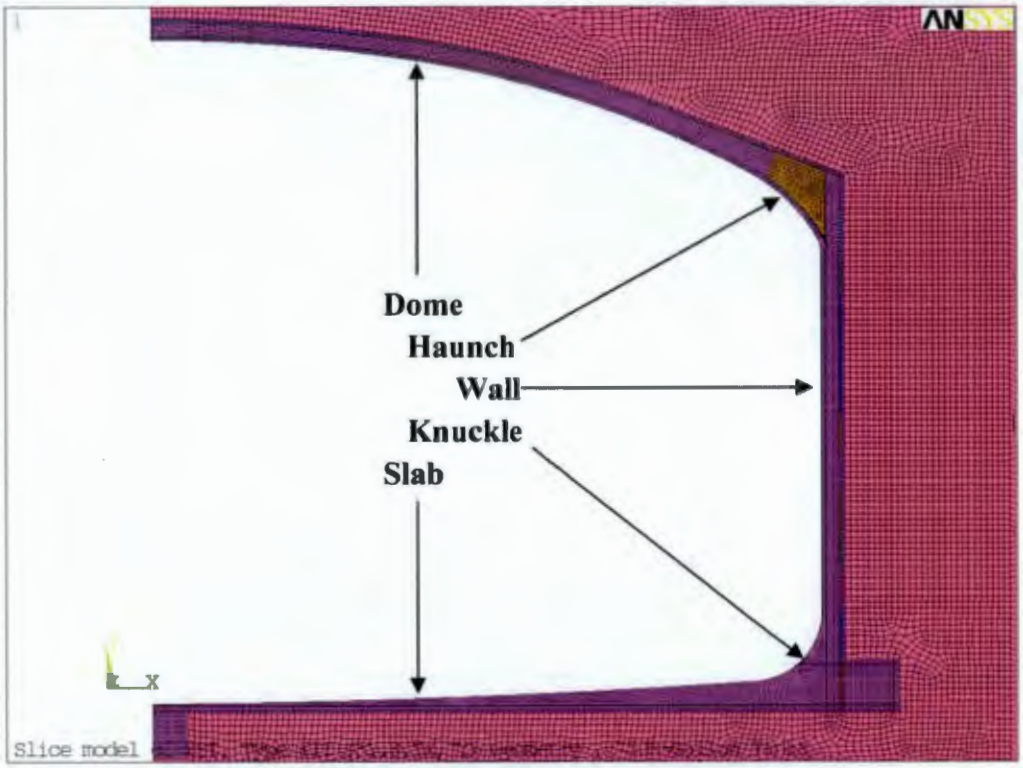

Figure 5.2. Finite Element Mesh of Tank and Soil

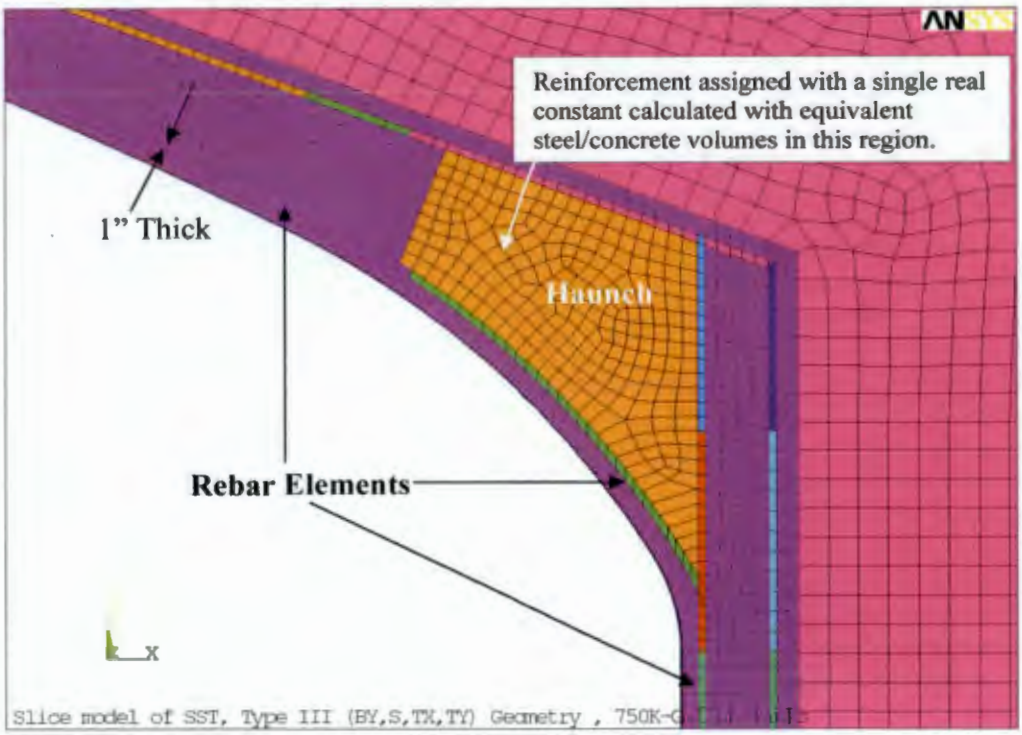

Figure 5.3. Close-up Showing Mesh of Haunch with Reinforced Concrete Elements

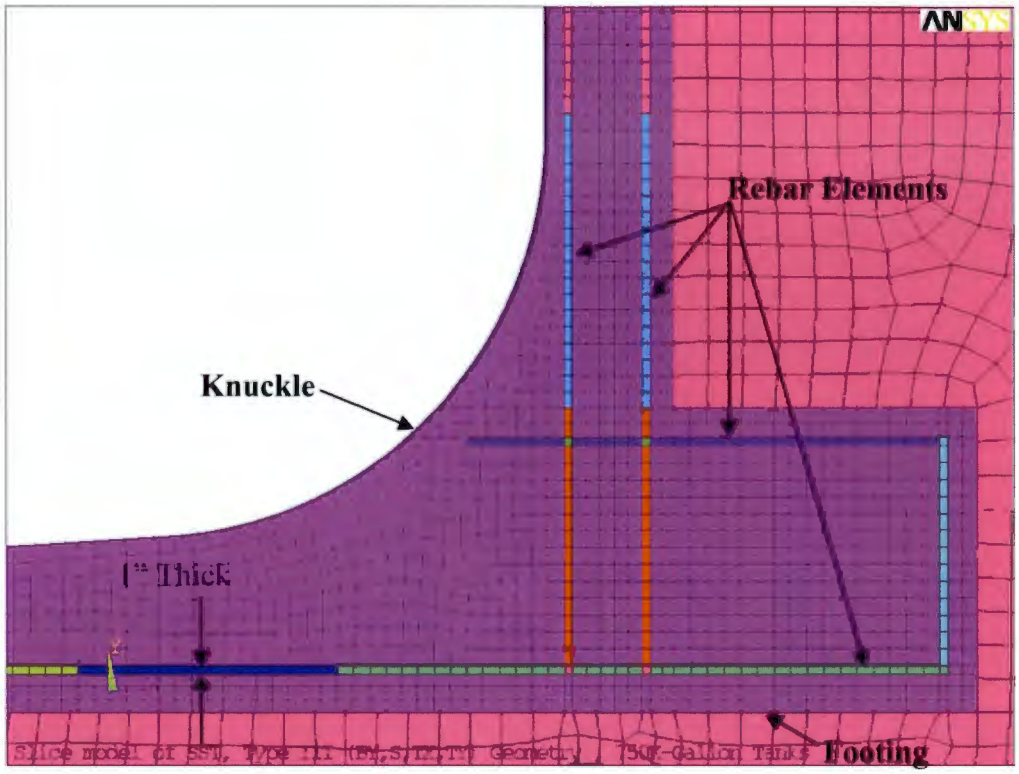

Figure 5.4. Close-up Showing Mesh of Footing with Reinforced Concrete Elements

The ANSYS® concrete material model that allows for cracking and crushing, as well as variable shear transfer for open/closed cracks, is used for the SOLID65 elements. In addition, a custom creep model for concrete as described in Section A.2.4 of the Evaluation Criteria report is also input to account for thermally induced creep throughout the tank thermal history.

The soil elements use the Extended Drucker-Prager (EDP) constitutive model, which has an internal friction angle, cohesion, and dilatancy angle as material properties. A small positive value of cohesion is used to represent the Hanford cohesionless soils, and the dilatancy angle is assumed to be equal to the friction angle. The ANSYS® EDP material model also requires specification of yield surface and flow potentials. A linear yield function and linear flow potential function are prescribed for the soil EDP material behavior in these analyses models.

The soil-structure interaction (SSI) between the tank and surrounding soil is modeled using surface-to-surface contact elements with sliding friction coefficient values prescribed in Section A.5.6 of the Evaluation Criteria report (Johnson et al. 2010).

5.4 Real Constants

ANSYS® uses real constants to define element properties for certain element types (e.g., thickness for shell elements, friction for contacts, steel-to-concrete volume fractions for reinforced concrete elements). The concrete reinforcing steel is modeled by using rebar capabilities of the ANSYS® SOLID65 element. Elements of 1-inch thickness were defined in the appropriate location in the dome, haunch, wall, knuckle, and foundation slab to model the steel reinforcement at those locations. There are three possible rebar directions in ANSYS® for rebar elements, and each of these directions include the following real constants:

- The rebar material ID
- Steel volume ratio
- Two angles used to orient the rebar directions relative to the element coordinate system.

Table 5.2 through Table 5.5 show the calculated steel volume ratios of the concrete rebar elements. Initially these real constants are defined in the model input file and are then assigned to the reinforcement elements by location. The following nomenclature is applicable to Tables 5.2 through 5.5:

Elevation: The height of any section from the tank's origin that is at the top of slab along the tank's axis in the model.

Radius: The radial distance of any section where the rebar volume fraction is calculated

Spacing: The distance between the reinforcement bars along hoop or meridional direction

Volume Ratio: The ratio of the steel volume to the total volume (concrete + steel) at any section when the rebar steel is assumed to be distributed in a 1" thick element as shown in Figures 5.3 or 5.4. In the tables, the Top/Bottom refers to top or bottom layup of reinforcements in the dome and similarly Inner/Outer refers to inner or outer layup of reinforcement in the wall or floor.

Real Constant: The real constant number assigned to a section in the ANSYS® model that contains details of volume fractions of steel in the meridional and hoop directions.

Table 5.2. Dome Concrete Rebar Volume Ratios

Description:	**Dome**								
Elevation[a] (in.)	Radius (in.)	Size	Meridional Spacing[b] (in.)	# Bars[b]	Volume Ratio (Top=Bot)	Size[c]	Hoop Spacing (in.)	Volume Ratio (Top=Bot)	Real Constant
NA	0–90	6	12	NA	0.0368	6	12	0.0368	55
	90–150	6	NA	57	0.0334	6	12	0.0368	54
	150–270	6	NA	114	0.0382	6	12	0.0368	53
	270–364	6	NA	228	0.0506	6	12	0.0368	52
	364–404	6	NA	228	0.0418	1"□	9	0.1111	51/151
	404–415	6	NA	556[d]	0.0783	1"□	8.06	0.1240	50
	415-454(t)	6	6	228[d]	0.0738	1¼"□	7.12	0.2193	49
	415-454(b)	6	12	556[d]	0.0369	1¼"□	8	0.1953	149

(a) Considering bottom of the slab at centerline is origin.
(b) The drawings used to obtain this information specify rebar by spacing or number of (#) bars or both; therefore, where a measurement for meridional spacing along with information for # bars is given, both are recorded; otherwise, neither is recorded.
(c) Square symbols imply square bars were used as noted in the as-built drawings.
(d) Only 228 bars were considered in FE model to account for ACI splicing length requirements.
NA = Not applicable.

Table 5.3. Haunch Concrete Rebar Volume Ratios

Description:	**Haunch**								
Elevation[a] (in.)	Radius (in.)	Size	Meridional Spacing[b] (in.)	# Bars[b]	Volume Ratio (Inner=Outer)	Size[c]	Hoop # Bars	Volume Ratio (Inner=Outer)	Real Constant
337–360	NA	6	6	556[d]	0.0736	1¼"□	5	0.3125	46
337–365	NA	5	24	NA	0[e]	1¼"□	5	0.3125	48
NA	427–440[f]	5	6[f]	114	0[f]	1¼"□	21[f]	0.0355	150

(a) Considering bottom of the slab at centerline is origin.
(b) The drawings used to obtain this information specify rebar by spacing or number of (#) bars or both; therefore, where a measurement for meridional spacing along with information for # bars is given, both are recorded; otherwise, neither is recorded.
(c) Square symbols imply square bars were used as noted in the as-built drawings.
(d) Only 556 bars (6C1 and 6C2) were considered in FE model to a distance accounting for ACI splicing length requirements.
(e) The meridional bars (vertical bars #504-9) are not included in this region to account for development length requirements.
(f) Real constant assigned as a single value (bulk) in this region for composite section of the haunch. Meridional bars are not included in this region (considering development lengths) and hoop bars considered are 1¼"□ bars those not included (twenty one 1¼"□ bars) in the volume fraction calculations of outer and inner haunch regions (real constants 45 through 48)
NA = Not applicable.

Table 5.4. Wall Concrete Rebar Volume Ratios

Description:	**Wall**								
Elevation[a] (in.)	Radius[b] (in.)	Size	Meridional Spacing[c] (in.)	# Bars[b]	Vol. Ratio (In=Out)	Size[e]	Hoop Spacing (in.)	Volume Ratio (Inner=Outer)	Real Constant
4.25–36	453/463	6	12	240	0.0368	NA	NA	0.0000	36
36–72	453/463	6	12	240	0.0368	8	6	0.1309	37
72–100	453/463	6	12	240	0.0368	8	7	0.1122	38
100–126	453/463	6	12	240	0.0368	7	6	0.1002	39
126–151	453/463	6	12	240	0.0368	7	7	0.0859	40
151–176	453/463	6	12	240	0.0368	7	8	0.0752	41
176–204	453/463	6	12	240	0.0368	7	9	0.0668	42
204–282	453/463	6	12	240	0.0368	7	10	0.0601	43
282–308	453/463	6	12	240	0.0368	7	5.5	0.1093	44
308–337(out)	453/463	6	12	556	0.0368	1¼"□	5	0.3125	45
308–337(in)	453/463	6	24	NA	0.0000[d]	1¼"□	5	0.3125	47

(a) Considering bottom of the slab at centerline is origin.
(b) The radial distance to inner and outer rebar in the wall.
(c) The drawings used to obtain this information specify rebar by spacing or # bars or both; therefore, where a measurement for meridional spacing along with information for # bars is given, both are recorded; otherwise, neither is recorded.
(d) The meridional bars (vertical bars #504-9) are not included in this region to account for development length requirements.
(e) Square symbols imply square bars were used as noted in the as-built drawings.
NA = Not applicable.

Table 5.5. Foundation Concrete Rebar Volume Ratios

Description:	**Slab**								
Elevation[a] (in.)	Radius (in.)	Size	Meridional Spacing[b] (in.)	# Bars[b]	Volume Ratio	Size[c]	Hoop Spacing (in.)	Volume Ratio	Real Constant
NA	0–396	4	12	NA	0.0164	4	12	0.0164	31
NA	396–430	4	12	NA	0.0164	4	12	0.0164	32
Description:	**Footing**								
Elevation (in.)	Radius (in.)	Size	Meridional Spacing (in.)	# Bars	Volume Ratio	Size	Hoop Spacing (in.)	Volume Ratio	Real Constant
Footing-top	444–498	4	24	120	0.0082	1"□	8.75	0.1143	35
Footing-side	498	6	8	360	0.0552	NA	NA	NA	34
Footing-bot	430–501	6	8	360	0.0552	1"□	8.75	0.1143	33

(a) Considering bottom of the slab at centerline is origin.
(b) The drawings used to obtain this information specify rebar by spacing or # bars or both; therefore, where a measurement for meridional spacing along with information for # bars is given, both are recorded; otherwise, neither is recorded.
(c) Square symbols imply square bars were used as noted in the as-built drawings.
(d) There is an overlap of 1'8" between bars from slab and 6A1 bars from footing.
NA = Not applicable.

5.5 Loads and Boundary Conditions

The Type III TOLA models consider the following mechanical live and dead loads.

- Soil load (soil overburden of 11 ft at 125 lb/ft^3) and self-weight of the tank applied by gravity.
- Historical hydrostatic loads due to waste (variable height at Specific Gravity of 1.7) applied as pressure loads on the inner surface of the tank
- 40 lb/ft^2 uniform surface live load to account for snow and ash fall applied as pressure on the top surface of the soil
- 200,000-lb concentrated live load distributed over a 20-ft-diameter circular area concentric with the tank applied as a pressure load at the top surface of the soil.

The mechanical loads were applied to the model in three load steps; the first load step applies the gravity load (self weight and soil overburden), the second load step applies the initial hydrostatic waste load, and the third load step applies the additional surface live loads. The transient thermal loads along with variable hydrostatic waste loads were applied to the model in several load steps beginning from load step four. The historical thermal and waste load profiles are shown in Figure 5.5, and these loads are solved in steps 4 through 16 in the analysis.

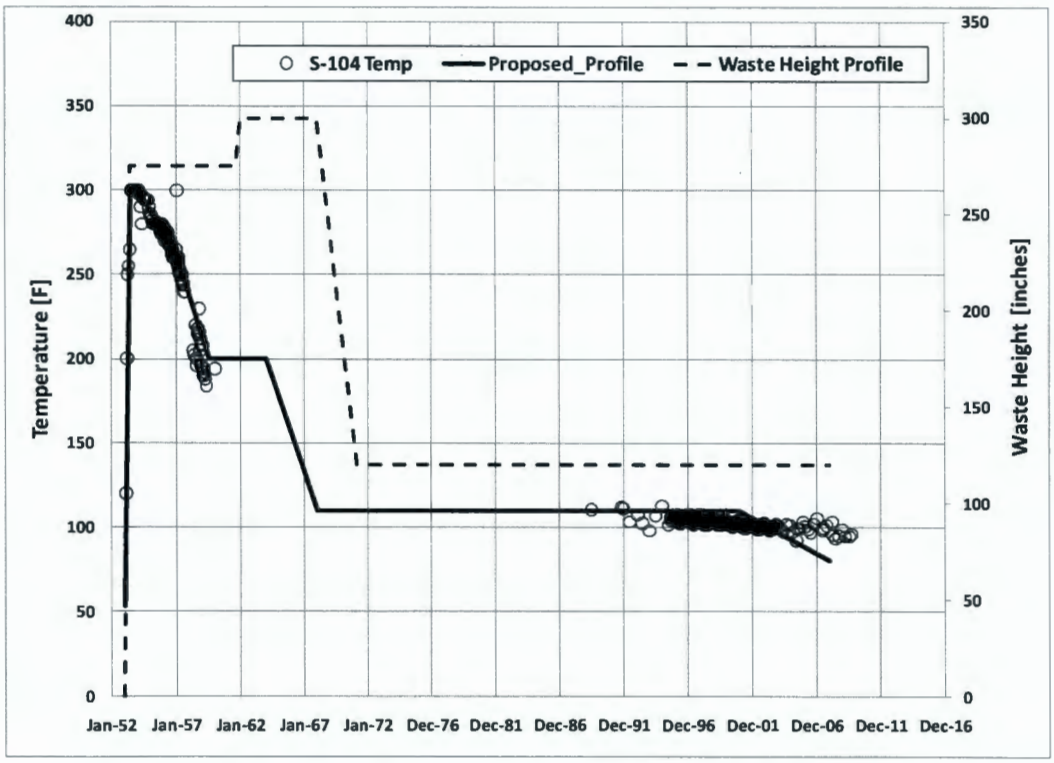

Figure 5.5. The Peak Temperature History Profile and Waste Height Profile Used for Detailed Analysis of the Type III Tanks

In the FE model, the base of the soil column is constrained in the vertical direction. Similarly, the soil column is confined radially at the outer (240 ft.) radial surface. The front and back faces of the 2 degree slice are given symmetric boundary conditions (constrained circumferentially). These boundary conditions are applicable to structural models with mechanical as well as thermal loads.

The thermal loads on the tank (temperature profiles) at any point of time during the tank's operating history are dependent on the waste temperature and level in the tank. These thermal loads were determined from a 2-D axisymmetric, transient thermal model that was developed to bound the operational histories of the Type III tanks. Section 5.7 describes in detail the transient thermal analysis model.

The temperature distributions in the tank and the soil were output as *.temp data files containing the temperature histories of all the nodes at specific times of interest. These thermal distributions were obtained from a 2-D thermal model and imposed on the 3-D structural model to account for the historical thermal loads on the tanks.

The model considers the thermal degradation of concrete properties during the tank's service history. The property degradation is incorporated in the model by locking in the degraded material properties when the tank sections reach the peak temperatures in time. This prevents the degradation from reversing as the tank cools.

5.6 The TOLA Run Matrix

The TOLA run matrix for the Type III SST AOR was developed based on the results of the Type II AOR (Rinker et al. 2011a). The following text describes the progression of analyses that were run for the Type II analysis and the resulting makeup of the Type III run matrix. The initial Type II run matrix (Table 4.1 in this report) included five runs with different combinations of soil modulus, concrete modulus/strength and creep. A sixth run with nominal soil modulus, nominal concrete modulus/strength and creep was also performed for the SST Type II AOR and the results were presented in Appendix F of the Type II report. Appendix H in this report includes the forces and moments of Run 6 for the Type III analysis. An additional run using upper bound soil modulus was also performed to combine with the LC4 seismic demands in the SST Type-II detailed analysis. The Type III run matrix also includes the UBS run as Run 8 in Table 5.6. Run 5 with creep was also added to the Type III TOLA run matrix (Run 7 in Table 5.6) to be consistent with the seismic demands for the same material property combination.

Table 5.6. TOLA Run Matrix (Material Combination Strategy) for Type III SST AOR

Case/ Run	Soil Modulus	Concrete Modulus	Concrete Tensile Strength	Concrete Creep		Notes
1	N	N	Near Zero (10 psi)	Yes		Best Estimate Properties
2	N	N	Near Zero (10 psi)	No	"Worst-Case Combinations" Runs 2 – 8, use available material property bounds	Depending on depth, low soil modulus is lower by 20% to 50% when compared to best estimate values.
3	N	H	Near Zero (10 psi)	No		
4	L	H	Near Zero (10 psi)	No		
5	L	N	Near Zero (10 psi)	No		
6	N	N	N	Yes		Depending on temperature, high concrete modulus is higher by 15% to 30% when compared to best estimate values.
7	L	N	Near Zero (10 psi)	Yes		
8	H	N	Near Zero (10 psi)	Yes		

H = High.
L = Low.
N = Nominal/Mean (Best Estimate).

5.7 Temperature Profile and the Thermal Model

Type III single-shell tanks have a capacity to hold 758,000 gallons of waste and belong to the Tank Farms BY, S, TX, and TY. Limited temperature history data is available for Type III tanks. The Rifaey et al. (2002) report presents the historic peak temperature data for all Type III tanks. However, literature review points to the fact that historic peak temperature values for some of the tanks may not have been obtained from direct temperature readings data. For example, most of the tanks from Tank Farm BY and TX were assigned a historic peak temperature value of 240°F based on the design specification in McKnight (1970) that specifies that the inter-tank piping should be designed for waste at 240°F. In some cases where the historic peak temperatures were in the range of 300°F, temperature history records are available to corroborate the peak temperature values. Tanks S-101 and S-104 attained peak temperatures of 300°F in the early years of their operation (1953) and evidence of this is documented in the letter by E. R. Irish (1953). Rifaey et al. (2002) presents the peak temperature values for tanks BY-101, BY-102, and BY-112 as 322°F. However, the 322°F value could not be verified from the references provided in the Rifaey et al. (2002) report and also could not be corroborated from any other available sources. Therefore, the peak temperature value of 322°F was not considered for the Type III detailed analysis. Based on the available data on S tanks and interactions with WRPS staff, it was decided that temperature histories of tanks S-101 and S-104 should be used as the worst case scenarios for the Type III detailed analysis.

Additional data were available for the temperature histories of the tanks in Tank Farm S and could be extracted from Mercier et al. (1981). Tanks S-101 and S-104 clearly appear to be the bounding cases with peak temperatures of 300°F. Figure 5.6 shows the recorded temperature history values for these two tanks from 1953 to 1960. All other S-farm tanks had peak temperatures values lower than 300°F. Clearly, Tank S-104 experienced higher temperatures for a longer period of time and, therefore, its temperature history was selected for the detailed analysis. Figure 5.5 shows the assumed temperature and waste height history profiles of Tank S-104 that were used for the thermal and structural analysis. The

temperature history data starting from 1989 was obtained from the TWINS database. Peak temperature values were gradually decreased from 105°F to 80°F in order to analyze the tanks with a current peak temperature value of 80°F. Based on discussions with WRPS, the temperature at the knuckle region was assumed to be 85% of the peak temperature value. The temperature at the waste surface was assumed to be 225°F for periods when the peak temperature was above 260°F and 75% of the peak temperature value when the peak temperature was below 260°F. Data for generation of the waste height profile were obtained from Ewer et al. (1997).

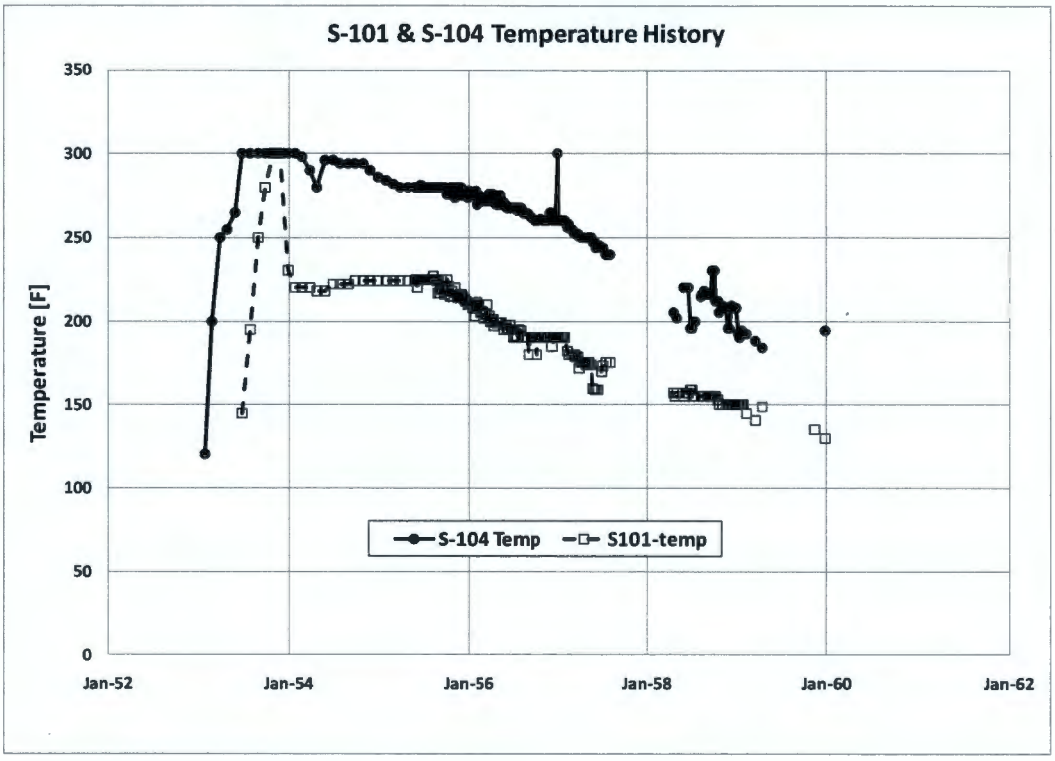

Figure 5.6. Temperature History Data for Tanks S-101 and S-104 for the Period 1953-1960 Obtained from Mercier et al. (1981)

Thermal analysis was carried out using a 2-D axisymmetric model, which is a subset of the two-degree slice model. It was generated by suppressing the two-degree rotation in the slice model. Elements were changed from structural to thermal elements. The soil extent in the model was the same as that in the two-degree slice model. One addition to the 2-D thermal model was the waste surface as shown in Figure 5.7. This waste surface was added to simulate radiation and convection heat transfer from the waste surface to the tank dome and walls. The waste surface in the model is not physically linked to the rest of the tank elements. Therefore, there is no conduction between the waste surface elements and the tank elements. Radiation surfaces have been identified in Figure 5.7 with the aid of red and blue arrows. ANSYS® calculates the radiation view factors for all element surfaces based on the axisymmetric model.

Loads on the thermal model were specified in the form of temperatures on the inner surface of the tank. Waste temperatures were imposed in the model by assigning the waste temperature values to the nodes on the inner surface of the tank that are located at or below the waste height. Waste temperature was assumed to vary linearly from the tank bottom temperature to the knuckle region (Figure 5.7). The radial coordinate (x-coordinate) of the nodes was used to specify the linearly varying temperature from

the tank bottom to the knuckle region. Similarly, the temperature was assumed to vary linearly from the knuckle to the liquid surface temperature. In this case, the vertical coordinate (y-coordinate) of the nodes was used to specify the linearly varying temperature from the knuckle region to the waste surface. Temperature variations imposed on the inner surface of the tank slab and tank wall are schematically illustrated with black arrows in Figure 5.7. The temperature specifications (thermal load) on the tank inner surface and the liquid surface were imposed in the form of ramped boundary conditions. That is, the imposed temperature within a step is varied (increased or decreased) linearly with time over the time period of the step.

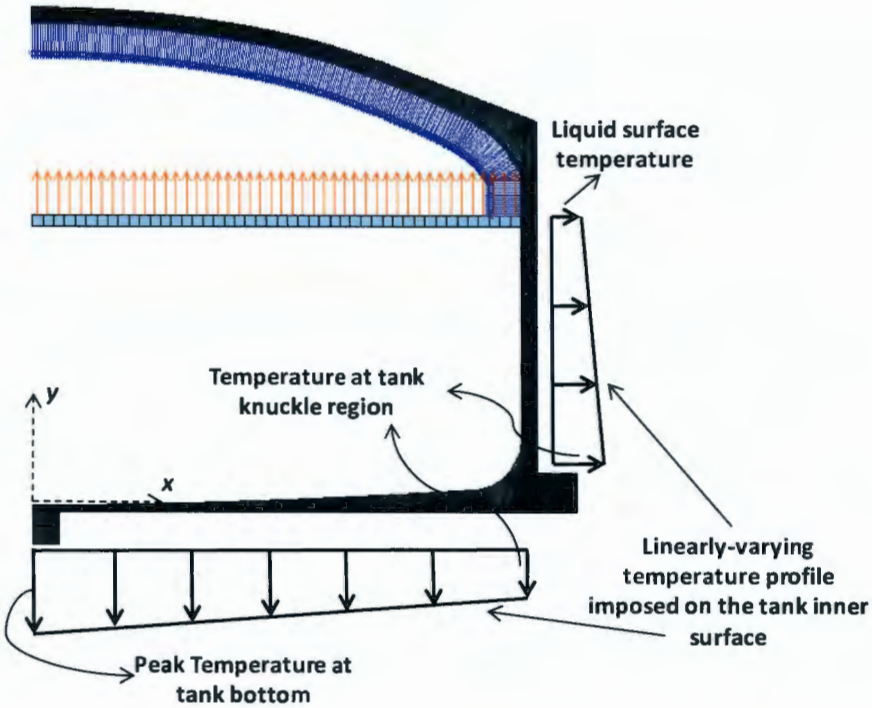

Figure 5.7. The 2-D Thermal Model Showing the Element in the Tank Structure and the Element in the Waste Surface

Boundary conditions were imposed on the top and the bottom surfaces of the soil in the model. The bottom surface was assigned an isothermal boundary condition with a temperature value of 55°F and the top surface was assigned an isothermal boundary condition with a temperature value of 53°F. There was no specified boundary condition on the right end of soil in the model. ANSYS® assumes an adiabatic boundary condition (default) on this surface.

Table 5.7 shows the data in Figure 5.5 in a tabulated form. The waste height profile shows 3 different waste heights throughout the history of tank S-104. In order to account for the variation in waste height, the thermal analysis was split into 3 different sub-analyses (Column 2 of Table 5.7). Geometrically, the only difference between each sub-analysis model is the position of the waste surface. At the end of each sub-analysis, the temperature values of all the nodes in the model were stored in an array, which was then used in the next sub-analysis to specify the initial temperature of each node. Each sub-analysis had two or more intermediate time steps corresponding to different temperature points.

Nodal temperatures obtained from the thermal analysis were imposed as body forces on the nodes of the two-degree slice model in the thermal stress analysis. The nodal temperatures at the end of each time step were written to text files, which were read into the structural analysis to define the temperature dependent material properties and calculate the thermal stresses.

Figure 5.8 shows the temperature distribution in the tank at the peak temperature value of 300°F.

Table 5.7. Temperature History and Waste Height Data Used in the Type III Tank AOR

Time Step Number	Sub-Analysis Number	Date	Waste Height (in.)	Center Bottom Temperature(°F)	Knuckle Temperature (°F)	Liquid Surface Temperature (°F)
--	0[a]	1/1/1953	0	53	53	53
1	1	6/1/1953	275	300	255	225
2	1	2/1/1954	275	300	255	225
3	1	1/16/1957	275	260	221	225
4	1	7/14/1959	275	200	170	150
5	1	9/1/1961	275	200	170	150
6	2	1/1/1962	300	200	170	150
7	2	1/1/1964	300	200	170	150
8	2	10/1/1966	300	138	117	104
9	2	1/1/1968	300	110	94	83
10	3	2/1/1971	120	110	94	83
11	3	1/1/2001	120	110	94	88
12	3	1/1/2008	120	80	68	64

(a) Initial temperature of all nodes in the model was assumed to be 53°F.

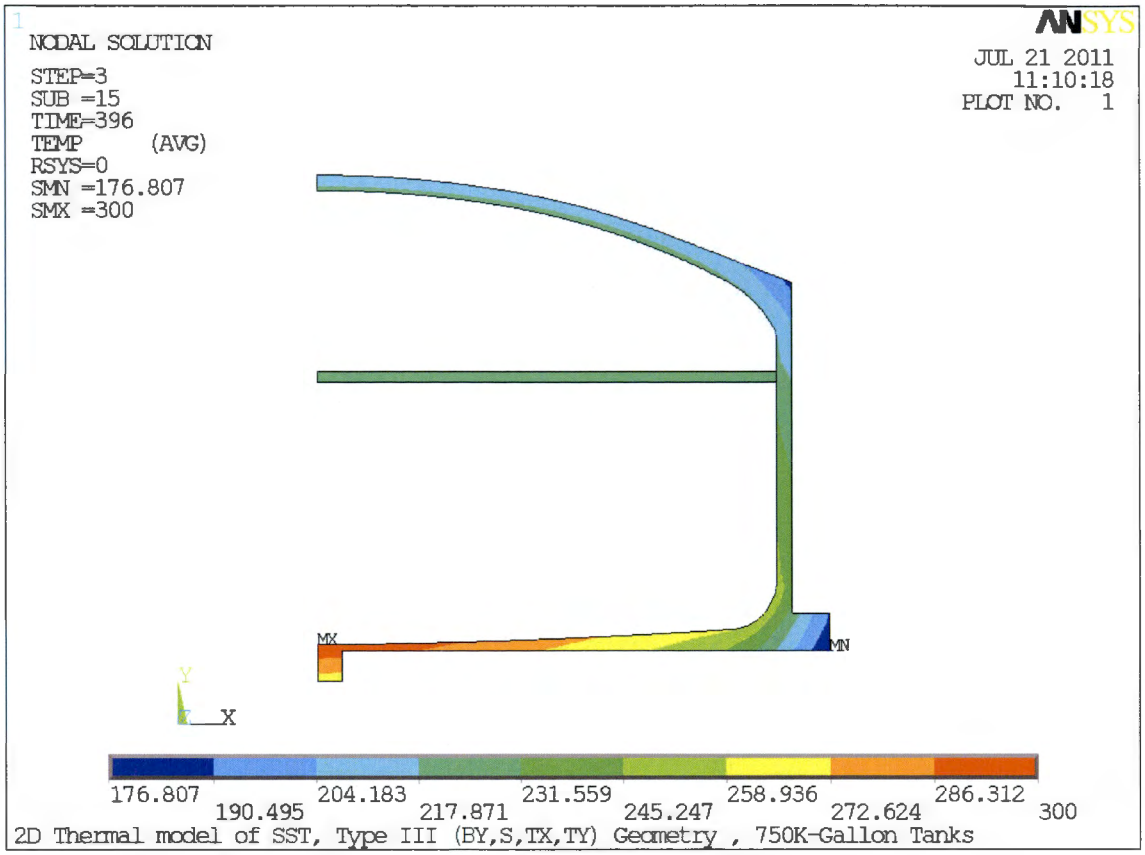

Figure 5.8. Temperature Distribution in Concrete Tank at the End Time Step 2 (peak temperature of 300°F)

This page intentionally left blank.

6.0 Seismic Analysis

M&D Professional Services, Inc. (M&D) was subcontracted by PNNL to perform the seismic analysis of the Type III single-shell tanks (SSTs) for the Analysis of Record (AOR), which supports completion of the Hanford Federal Facility Agreement and Consent Order (HFFACO) and the Tri-Party Agreement Milestone, M-45-10-01. This chapter provides the results of that seismic analysis.

The SSTs are evaluated as Performance Category 2 (PC-2) structures and DOE-STD-1020-2002, Section 2 (DOE 2002), requires that the ground motions for PC-2 shall be developed following the 2003 International Building Code (IBC 2003). The SST ground motions are developed as 2/3 of Hanford Site-Specific Maximum Considered Earthquake (MCE) ground motions. The MCE ground motions are defined as the ground motions with a mean annual frequency of exceedance of 4×10^{-4} (2% probability of exceedance in 50 years). In this analysis, the site-specific design response spectra (DRS) for the SST facilities site uses the Rohay and Reidel (2005) Hanford Waste Treatment Plant (WTP) design spectra as a reasonable assessment of the current state of knowledge of the hazard levels at the 200 East and 200 West Areas. The 2005 spectra are conservative relative to data documented in Geomatrix (2007), but this choice was made to protect against the chance that Hanford seismic hazard levels will be increased in the near future.

The seismic analysis documented here assesses the impacts of potentially non-conservative assumptions used in previous analysis. These assumptions included addressing: updating site-specific seismic hazard, variation of backfill properties, the effects of material degradation, additional thermal profiles applied to the full structure including the soil-structure response with footings, the non-rigid (low frequency) response of the tank dome, the asymmetric seismic-induced soil loading, the asymmetric seismic-induced waste loading and current methodology for defining seismic loads for both the tank foundation and surface of soil, and incorporating "at-rest" soil pressure loading on the exterior wall of the tank surface.

The seismic analysis considers interaction of the tank with the surrounding soil, and the effects of the tank waste. The SST and the surrounding soil are modeled as a system of finite elements. The depth and width of the soil incorporated into the analysis model are sufficient to obtain appropriately accurate analytical results. The analyses required to support the work statement differ from previous analyses of the SSTs in that soil-structure interaction model includes nonlinear contact surfaces between the tank and the supporting soil. The contained waste was modeled explicitly in order to capture the interaction behavior between the concrete tank and contained waste.

6.1 Seismic Model Overview

A model of a Hanford Type III SST was created and analyzed using version 13.0 of the general-purpose finite element program ANSYS®. The seismic model for the AOR of Type III tanks was developed from the drawings for tanks BY, S, TX, and TY (drawings H-2-1783, H-2-2225) and it is typical of the Type III tanks.

The seismic ANSYS® Type III SST geometry is modeled as a centerline shell model – also known as a mid-thickness shell model in the literature. The Type III SST shell model includes stiffness properties calculated assuming Fully Cracked Concrete (FCC) properties as described in Section 6.3. FCC properties were created at element shell locations of the ANSYS® seismic model.

A half-symmetry (180°) model of the SST, including the concrete tank and surrounding soil, was developed to evaluate the soil-structure interaction seismic loading on the Type III SST. Details for each part of the model are discussed in the following sections. The complete model, including the SST and surrounding soil, is shown in Figure 6.1.

The global origin is above the center of the tank at grade elevation. The x-axis is radial and the positive z-axis points upward. The y-axis completes the right-hand triad, and in a cylindrical coordinate system defines the rotational angle. The model is located between 0° and 180° angles. Where shown, tank geometry is presented in a likewise oriented coordinate system with an origin at the tank footing elevation. The tank and excavated soil meshes are based on 9-degree slices over the half model, for a total of twenty slices. The native soil is modeled in 9-degree slices, for a total of twenty slices. Plots of the model are shown in Figure 6.2 and Figure 6.3 with selective transparency to enhance visibility of hidden features. The unit system used in the model is kip, foot, second.

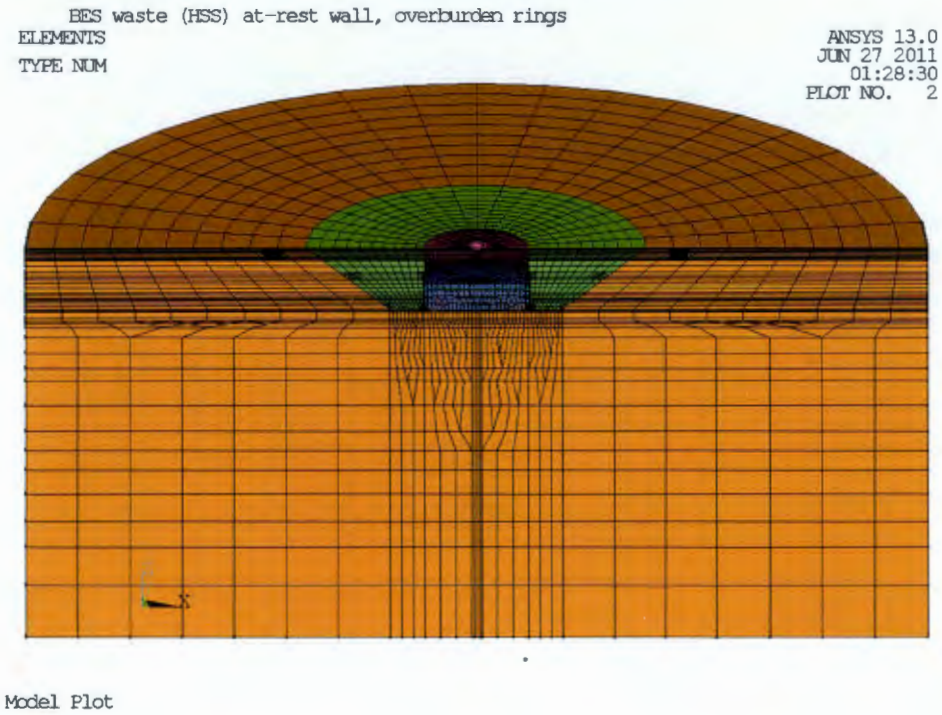

Figure 6.1. Element Plot of Complete Best Estimate Soil Full Tank Seismic Model

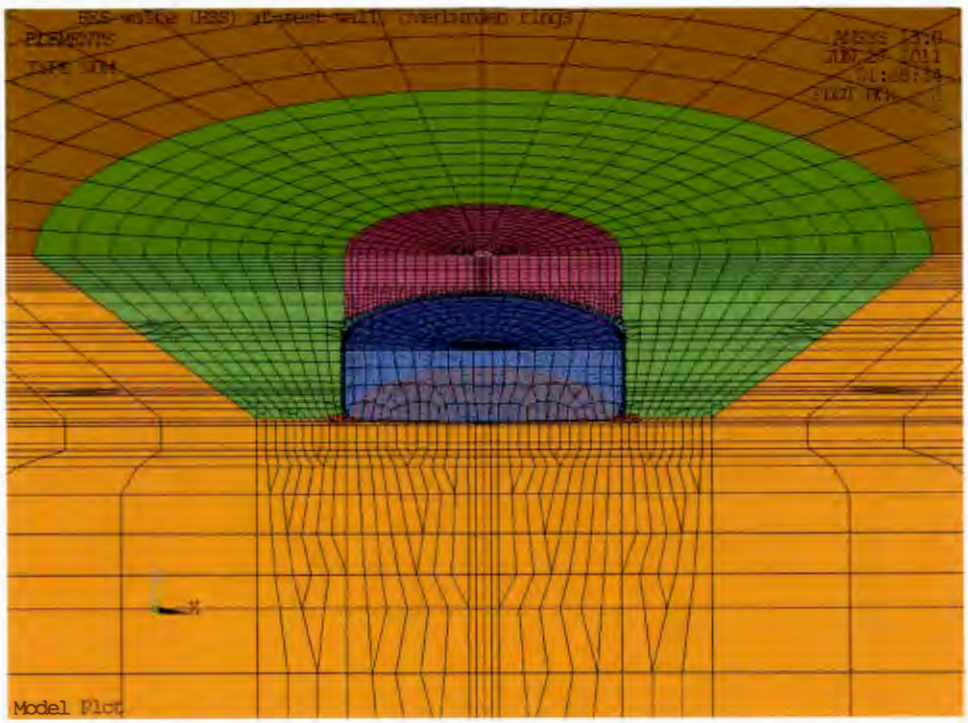

Figure 6.2. Element Plot Detail of Best Estimate Soil Baseline Seismic Model Showing Tank, Waste, and Backfill

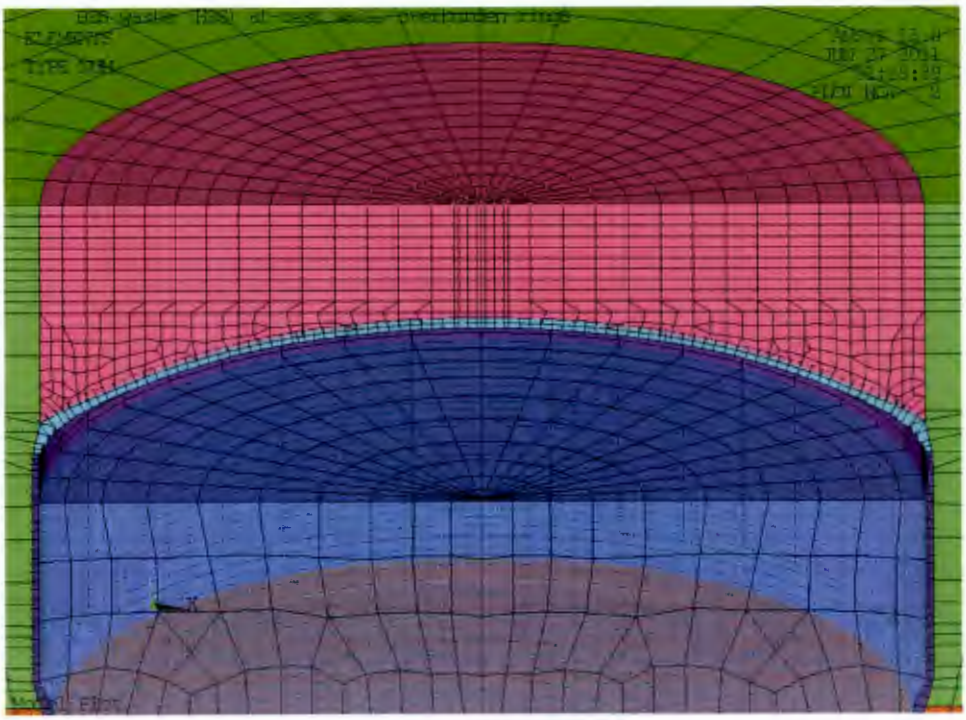

Figure 6.3. Element Plot Detail of Best Estimate Soil Baseline Seismic Model Showing Tank, Waste, and Overburden Soil

6.2 Model Geometry

6.2.1 Model Development

Since there are many similarities between the double-shell and single-shell tanks, many of the methodologies of the previous DST analysis (Rinker et al. 2008) and SST Type II (Rinker et al. 2011a) are incorporated in this SST analysis. Thus, it is not necessary to repeat all of the studies performed previously. A detailed description of the model is provided in this section. Where other studies have been performed supporting the development of this model, these will be referenced as appropriate.

6.2.2 Soil and Concrete Properties

Three combinations of soil and concrete properties have been considered in this analysis. These combinations are:

- Lower Bound Soil (LBS), Fully Cracked Concrete (FCC) properties
- Best Estimate Soil (BES), FCC properties (baseline model)
- Upper Bound Soil (UBS), FCC properties

The three variations in soil properties address the uncertainty as required by ASCE (2000). The fully cracked concrete case is consistent with the no-tension hypothesis described in Section 5.6 of Rinker et al. (2011a).

Since the seismic model used linear concrete properties, the effects of concrete cracking were implemented by integrating fully cracked orthotropic properties discussed in Sections 6.3.1.2 and 6.3.1.3.

Each configuration is run as a full nonlinear (interface elements are the only nonlinear elements in seismic model) seismic time history including gravity, and separately as a gravity-only analysis. The difference between the two cases represents the seismic-only effects.

6.2.3 Model Organization

The model has been divided into distinct components, each with its own input file. Each component may be modified and meshed independently to facilitate development of alternate configurations. The model is progressively defined as each input file is executed. Each input file integrates into the model by reading the model data from preceding input files. The model configuration may be changed by removing or renaming the input file for changes in individual features. A number of global reference points are also created before geometry generation to define critical locations and locate the local coordinate systems used in the component input files.

6.2.4 Input and Output Files

The files used, along with a short description of each file, are provided in Table 6.1 through Table 6.4. The model description addresses the model parts in the order that they are executed – tank components first, then the surrounding soil, followed by solution and post-processing phases.

Table 6.1. ANSYS® Model Input File Description (pre-processing phase)

File Name	Use	Description
Assembly.inp	All	Calls each input for development of model.
Plotmacrolib.inp	All	Contains macros for plotting model. Macros are called for easy manipulation of display.
TKCD.inp	Geometry	Creates tank concrete dome geometry. Concrete geometry set to match PNNL ACI section cut locations. Not connected to other tank items (within this input file).
TKCW.inp	Geometry	Creates tank concrete sidewall geometry. Concrete geometry set to match PNNL ACI section cut locations. Not connected to other tank items (within this input file).
TKCF.inp	Geometry	Creates tank concrete floor geometry. Concrete geometry set to match PNNL ACI section cut locations. Not connected to other tank items (within this input file).
WAST.inp	Geometry (optional)	Creates model of waste. Uses Solid45 elements with low shear modulus. Matches tank geometry.
SOIL_properties.inp	Properties	Defines specific soil material properties and layering. Excavated region and native soil have different material properties. Properties vary by layer.
SOFO.inp	Geometry	Creates soil fill overburden for excavated region above tank. Matches tank dome geometry. Reads soil properties and layers from the SOIL properties input file.
B.SOFOIII.inp	Geometry	Creates appurtenances pits and soil fill overburden for excavated region above tank. Creates contact surfaces for appurtenances pits and soil fill overburden. Reads soil properties and layers from the SOIL properties input file.
SOFA.inp	Geometry	Creates soil fill for excavated region around tank. Matches tank sidewall, dome, and soil overburden geometry. Reads soil properties and layers from the SOIL properties input file.
SOUD.inp	Geometry	Creates far-field/undisturbed (native) soil. Matches tank floor, soil fill around geometry. Reads soil properties and layers from the SOIL properties input file.
Surface_load.inp	Geometry	Creates surface loads, including concentrated surface load masses.
prepost.inp	All	Prepares model data for post-processing – set up data arrays, select elements at ACI sections.
Connect.inp	Geometry	Creates contact interfaces between model components: • Tank and waste • Tank dome and soil fill overburden/soil fill around tank • Tank sidewall and soil fill around tank • Tank floor and undisturbed soil • Soil fill overburden and soil fill around tank • Soil fill and undisturbed soil portions of the model
BC.inp	Geometry	Creates boundary conditions: • Symmetry plane • Slaved (coupled) boundary conditions around exterior of model to control shear behavior • Spar elements at edge of soil model when couples and boundary conditions cannot both be applied to the same node • Places large mass at bottom of model for excitation force
modify.inp	All	Modifies as-generated model. Applies orthotropic tank concrete properties.
Plots.inp	All	Generates model plots.

Table 6.2. ANSYS® Model Input File Description (solution phase)

File Name	Use	Description
Solution.inp	Gravity	Executes solution static, pseudostatic phase of model.
Solution_TH.inp	Seismic	Executes solution time history phase of model.
th-10ms-h.inp	Seismic	Time History acceleration input (horizontal) – tabular data.
th-10ms-v.inp	Seismic	Time History acceleration input (vertical) – tabular data.

Table 6.3. ANSYS® Model Input File Description (post-processing phase)

File Name	Use	Description
post1.inp	Static	Post processes model static POST1 results. Creates tabular and graphical summaries of results.
postproc.inp	Transient	Post processes model transient (pseudo-static/time history) POST26 results for tank concrete elements. Creates tabular and graphical summaries of results.
post-cont.inp	Transient	Post processes model transient (pseudo-static/time history) results for contact elements. Creates tabular and graphical summaries of results.
subtract_gravity.inp	Seismic	Read in gravity-only results from previous output, subtract gravity from seismic+gravity. Creates tabular and graphical summaries of tank concrete seismic-only results.
subtract_cont.inp	Seismic	Read in gravity-only results from previous output, subtract gravity from seismic+gravity. Creates tabular and graphical summaries of contact seismic-only results.
spectra.inp	Seismic	Determines response spectra results. Creates tabular and graphical summaries of response spectra results.
spectra_target.inp	Seismic	Contains SHAKE target response spectra (horizontal and vertical) for comparison to SSI model results – tabular data.
SC-SPTR-H.txt	Seismic	Contains soil column target response spectra (horizontal) for comparison to SSI model results – tabular data.
SC-SPTR-V.txt	Seismic	Contains soil column target response spectra (vertical) for comparison to SSI model results – tabular data.

6.2.5 Organization and Identification System

Where possible, items are organized in a hierarchical manner. Each model component is assigned a tag and a number to easily distinguish its attributes (coordinate systems, element MAT/REAL/TYPE/ SECT properties, etc.) from other components (Table 6.5). The tag enables both alphabetic and numeric hierarchical organization. The tag is used in labeling and identifying model components and variables, beginning with the component, then with subcomponent(s), and ending with a letter designating the modeling item (i.e., area, element, etc.). The tag itself is assigned a numeric value so that it can also be used as a variable within numerically organized aspects of the model.

Table 6.4. ANSYS® Model Output File Description

File Name	Use	Description
QAoutput.out	General	Run information for QA control and run identification.
Model_GEO_data.OUT	All	Summary of model geometry data: Tank Concrete Dome Penetration geometry data (as applicable) Tank Concrete Dome geometry and ACI section data Tank Concrete Sidewall geometry and ACI section data Tank Concrete Floor geometry and ACI section data Soil Fill Overburden geometry data Soil Fill Around geometry data Soil Undisturbed geometry data Tank Concrete ACI section data details
Model_MAT_data.OUT	All	Summary of model material property data.
TKC_ACI_angles.OUT	All	List of ESOL minimum/maximum results for Tank Concrete elements.
TKC_ACI_SUM#.OUT	All	Summary of results for Tank Concrete elements. Used in both gravity and seismic runs, where # is the load step number.
TKC_ACI_MIN#.OUT	All	List of minimum results for Tank Concrete elements. Used in both gravity and seismic runs, where # is the load step number.
TKC_ACI_MAX#.OUT	All	List of maximum results for Tank Concrete elements. Used in both gravity and seismic runs, where # is the load step number.
TKC_ACI_seismic_only _SUM.OUT	Seismic	Summary of seismic-only results for Tank Concrete elements.
SPTR-accel.out	Seismic	List of acceleration and response spectra results at far field soil
SPTR-disp.out	Seismic	List of displacement and response spectra results at far field soil

Table 6.5. List of Model Components

Component	Tag	Number
Tank Concrete Dome	TKCD	100
Tank Concrete Sidewall	TKCW	200
Tank Concrete Floor	TKCF	300
Tank Waste	WAST	400
Soil Fill Overburden (above tank)	SOFO	500
Soil Fill Around (remaining fill)	SOFA	600
Soil Undisturbed	SOUD	700
Contacts	CONT	800
Target surfaces	TARG	900

Elements constituting a given component have attributes beginning with the component number. Contact interface pair real numbers are organized using a hierarchical method as well. For example, element type 815 is a contact (8xx) interface element between the tank concrete dome (1xx) and the soil backfill overburden (5xx). In a few cases, the numbering scheme must be modified, such as when multiple items are used, but would be assigned the same number according to the organization system.

6.2.6 Tank Concrete

The tank concrete is divided into the floor, sidewall, and dome using input files TKCF.inp, TKCW.inp, and TKCD.inp. The input files contain geometry coordinates and locations of ACI sections. Orthotropic material properties and associated thicknesses are found in input file modify.inp. Because the tank concrete subcomponents are integral, they are merged together using the input file connect.inp.

The Type III SST profile and centerline of the tank initially was created using a 2-D CAD model. The centerline locations from the CAD geometry for the profile were used in the creation of the centerline shell seismic ANSYS® model, shown in Figure 6.7. In all parts, the basic geometry is created first, and then cut to create locations for which concrete forces and moments are extracted and combined with TOLA results to perform an ACI evaluation. These locations are referred to as ACI sections. Element type SHELL181 (4-node finite strain shell) was chosen to model the tank concrete vault. Detailed output quantities are described in Section 6.2.13. Because the model uses shell elements, the geometry is based on the centerline of the actual geometry. The geometry is therefore approximate when the section is irregular (e.g., upper haunch, lower knuckle) or has misalignments (e.g., outer footing vs. floor). Figure 6.4, Figure 6.5, and Figure 6.6 show the concrete tank shell model with shell thicknesses displayed.

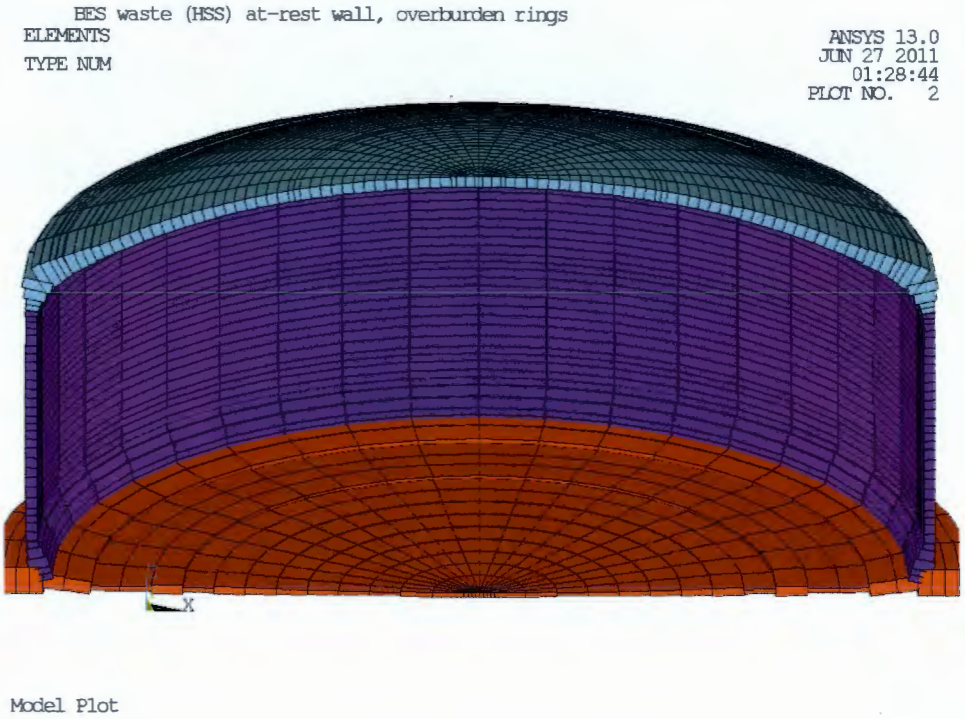

Figure 6.4. Seismic Model Concrete Tank Profile Showing Shell Element Thickness

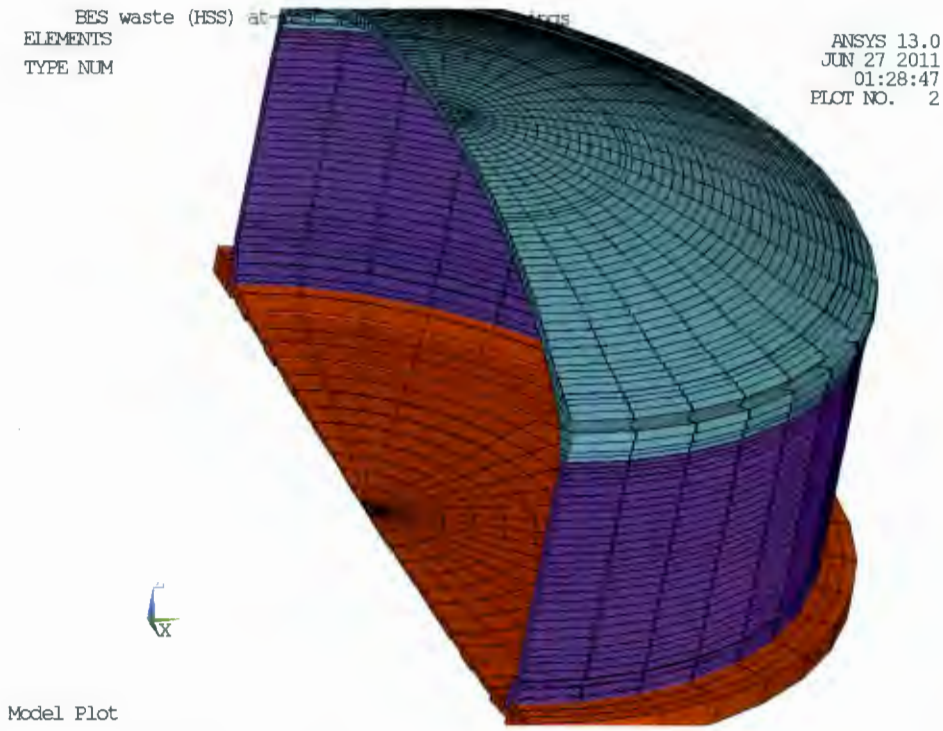

Figure 6.5. Seismic Model Concrete Tank Angled View Showing Shell Element Thickness

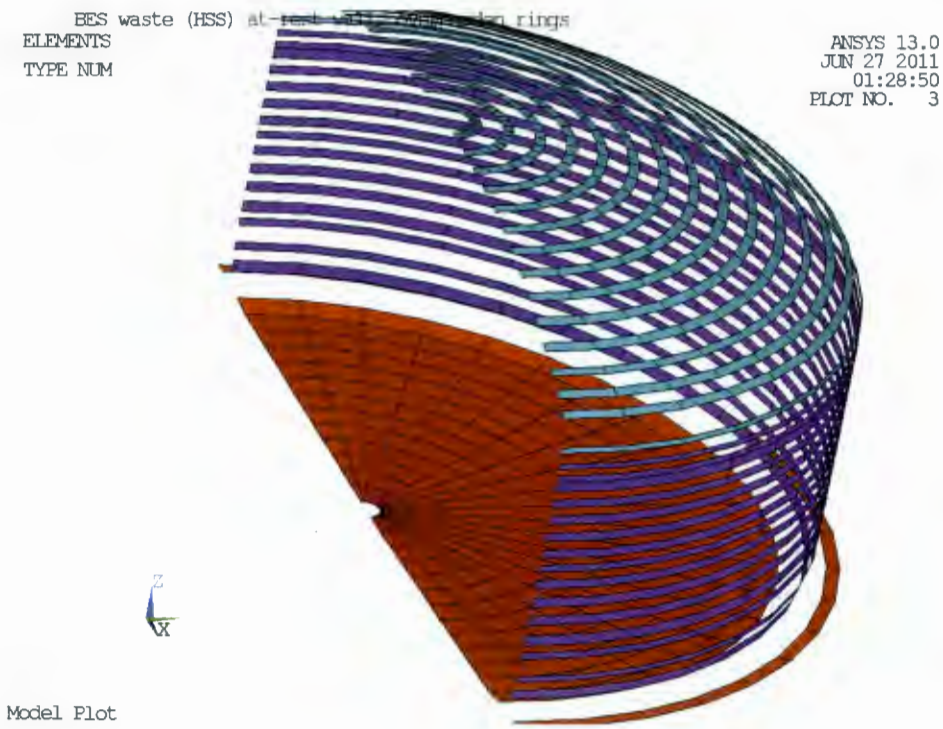

Figure 6.6. Seismic Model Concrete Tank Angled View Showing Elements at ACI Sections

Due to the differences between static (TOLA) and time history (seismic) modeling and post-processing methods, some ACI sections are at slightly different locations in the TOLA and seismic models because the TOLA model uses results extracted at nodes, and the baseline seismic model uses results from element centroids. This difference is due to the fact that the TOLA model used solid elements to represent the tank and the seismic model uses shell elements. To match the seismic ACI section locations as closely as practical with the TOLA model ACI section locations, the baseline seismic model uses a mesh that is offset to align the baseline seismic model element centroids with TOLA node locations. A graphical display of the ACI section locations and material numbers is shown in Figure 6.7.

TOLA ACI Section No.	Seismic Model Element Location
1	101
2	104
3	107
4	110
5	113
6	117
7	120
8	123
9	126
10	129
11	132
12	135
13	138
14	141
15	145
16	201
17	203
18	204
19	206
20	208
21	210
22	212
23	214
24	216
25	218
26	220
27	222
28	224
29	227
30	229
31	301
32	305
33	306
34	307
35	308
36	309
37	310
38	311
39	312
40	313
41	314
42	315
43	316
44	317

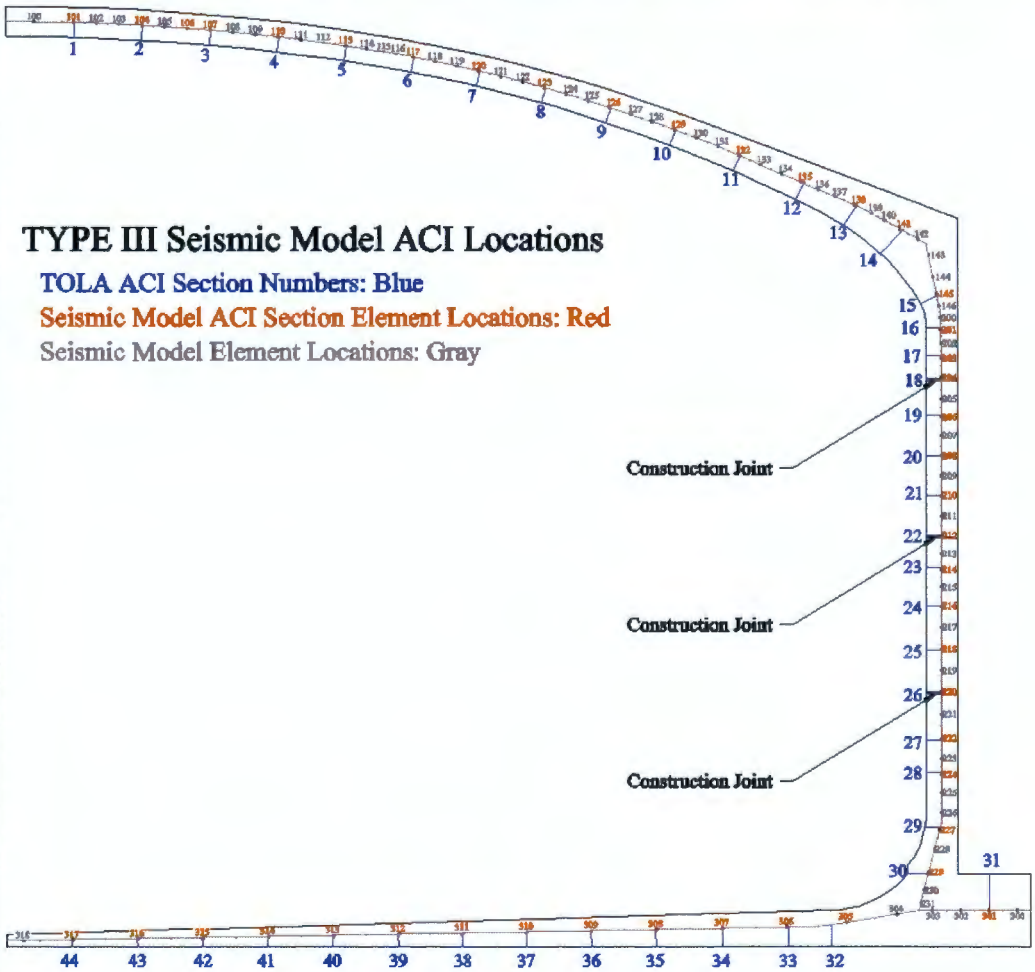

Figure 6.7. Seismic Model Concrete Tank Profile Showing Material Properties and ACI Section Locations

The tank shell elements are oriented such that the positive element x-axis is aligned in the meridional direction, initially pointing away from the dome apex. The element y-axis is aligned in the hoop direction. This orientation allows for extraction of meridional and hoop results and application of orthotropic material properties. The meridional and hoop axes are indicated in Figure 6.8 as black and yellow triad lines, respectively. Each ring of elements has unique properties defined in order to maximize accuracy and ensure smooth transitions. Shell element orientation is shown in Figure 6.9 and concrete tank material properties are shown in Figure 6.10.

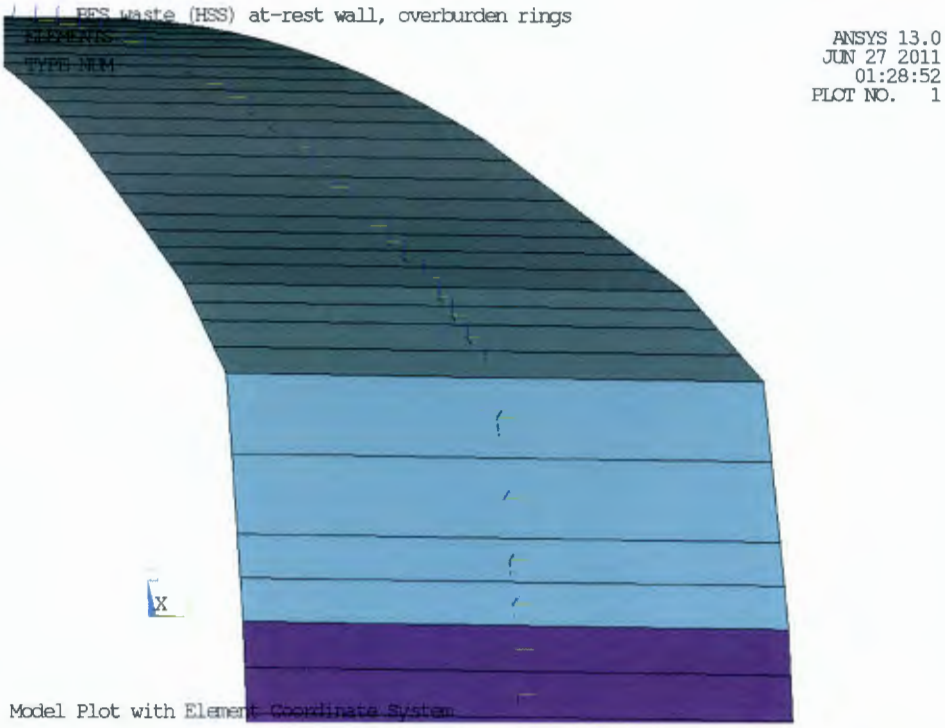

Figure 6.8. Seismic Model Concrete Tank Angled View Showing Shell Element Orientation

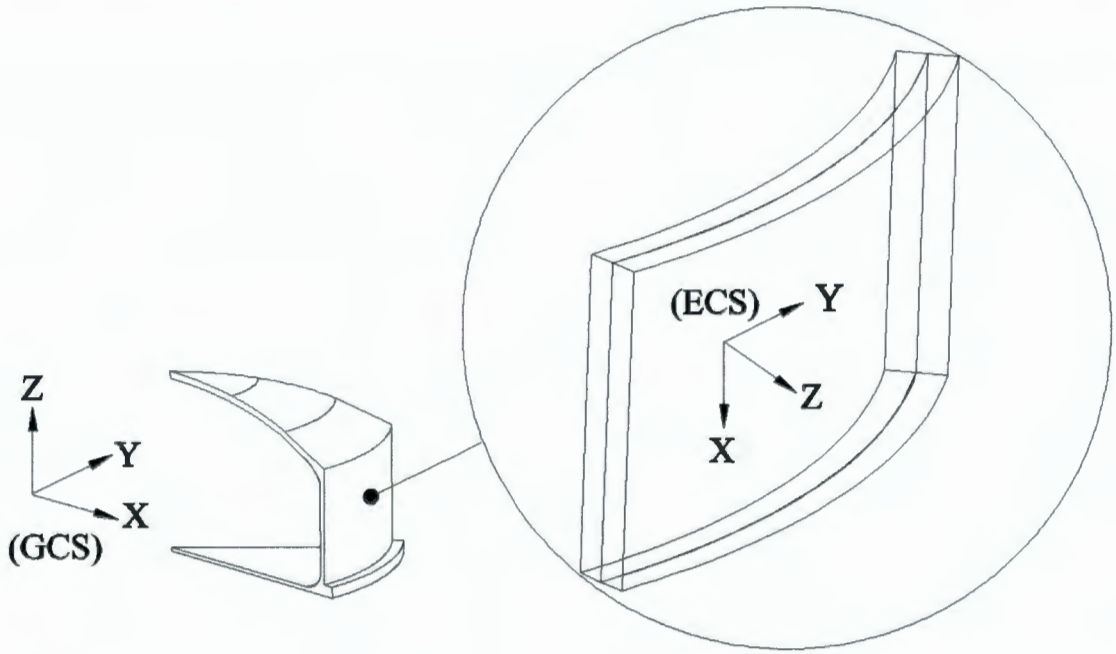

(GCS) = Global Coordinate System
(ECS) = Elemental Coordinate System

Figure 6.9. Shell Element Orientation Detail

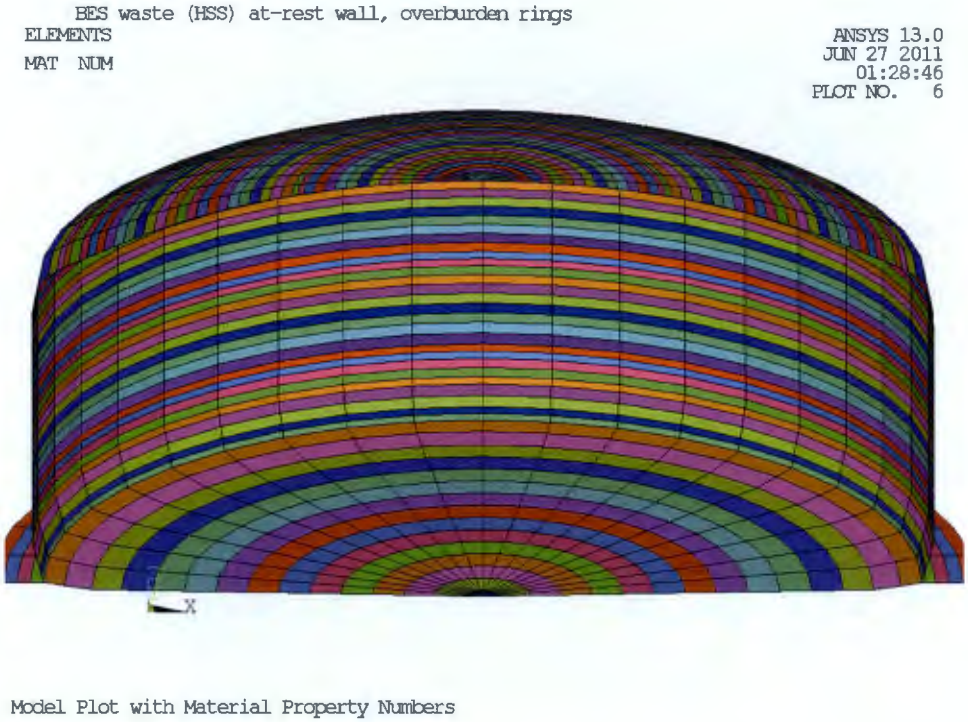

Figure 6.10. Seismic Model Concrete Tank Material Property Assignment

6.2.7 Contact Interfaces

The use of contact interface surfaces allows independent components to have dissimilar meshes, as well as controlling model behavior across designated boundaries such as near and far-field soil. Interface elements are overlaid (ESURF) on the underlying components to create contact/target surface pairs. Interfaces use element types TARGE170 and CONTA173. The interfaces are applied after the model geometry is created, using the input file connect.inp. The following interfaces are supported by the model:

1. Concrete tank to excavated soil over and around the tank
2. Concrete tank to native soil below the tank
3. Excavated backfill soil to native soil
4. Between subcomponents of the excavated backfill soil

The behavior of the interfaces between the concrete tank and the soil has a direct effect on the loads in the concrete tank. The interface between the soil subcomponents is included to enable dissimilar meshing and improve the geostatic behavior. Additional details on these interfaces are found in the following sections.

6.2.7.1 Soil/Concrete Tank Interface

A combination of TARGE170 and CONTA173 elements is used to model the interface between the soil and the concrete tank. The presence of this interface surface is important to establish a proper initial

geostatic stress state (see Section 6.2.7.2) and also to allow for the possibility of sliding or separation between the concrete vault and the surrounding soil. The surfaces are allowed to slide and separate (standard contact). The soil is the contact surface and the concrete tank is the target surface. The soil/concrete tank interface elements are shown in Figure 6.11.

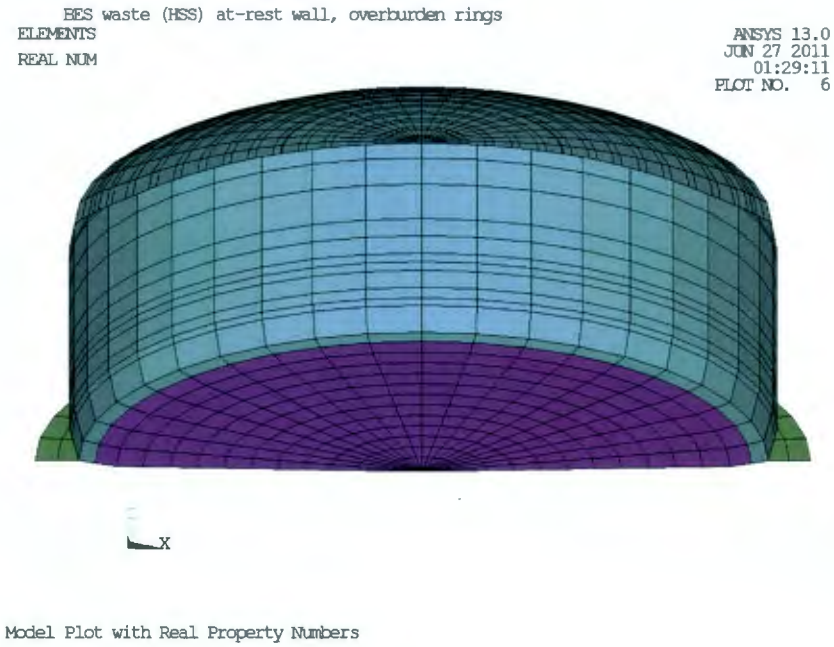

Figure 6.11. Seismic Model Interface Elements Real Property Assignment – Soil-to-Concrete Tank

The friction coefficients used in the seismic model during the application of dead weight are artificially low in order to prevent the development of unrealistically high compressive loads in the sidewall from artificially induced drag down loads due to high friction loads between the concrete and in-place modeled soil. During construction the backfill soil was placed in 6- to 24-inch compacted layers, thus high concrete-to-soil friction induced drag down loads would not have developed. Hence, the friction coefficients between the concrete and soil were reduced to minimize the development of high drag down loads in the initial geostatic analysis of the full in-place modeled backfill soil as gravity is turned on.

The dome and wall friction coefficients used during both phases of the seismic analysis are summarized in Table 6.6. Per the reviewers comment, studies were performed that showed little sensitivity in the solution to friction values as discussed in Rinker et al. (2011a). Therefore, these friction values are consistent with the TOLA friction values as discussed in Section 5.3.

Table 6.6. Summary of Soil-to-Concrete Tank Friction Properties

	Initial Gravity Step	Seismic Time History
Dome down to top of sidewall	0.3	0.3
Sidewall	0.05	0.5
Footing top surface	0.6	0.6
Basemat	0.6	0.6

6.2.7.2 At-Rest Soil Pressure at Tank Wall

Initially, the sidewall pressure of the seismic SST model did not follow the linear trend of the at-rest pressure estimate of 0.5ρgh during gravity loading. To achieve the correct at-rest pressure on the side wall of the seismic SST model during gravity loading, the contact interference between the soil and the side wall of the tank was adjusted by defining a small initial contact adjustment using real constants for CONTA173 elements. This initial contact adjustment allows the gravity-only contact pressure to be approximately the theoretical at-rest pressure of 0.5ρgh for the side wall of the tank. As shown in Figure 6.12, the theoretical sidewall pressure 0.5ρgh is shown in red. The adjusted at-rest sidewall pressure for the seismic model configurations is shown along with the at-rest wall pressure during gravity loading.

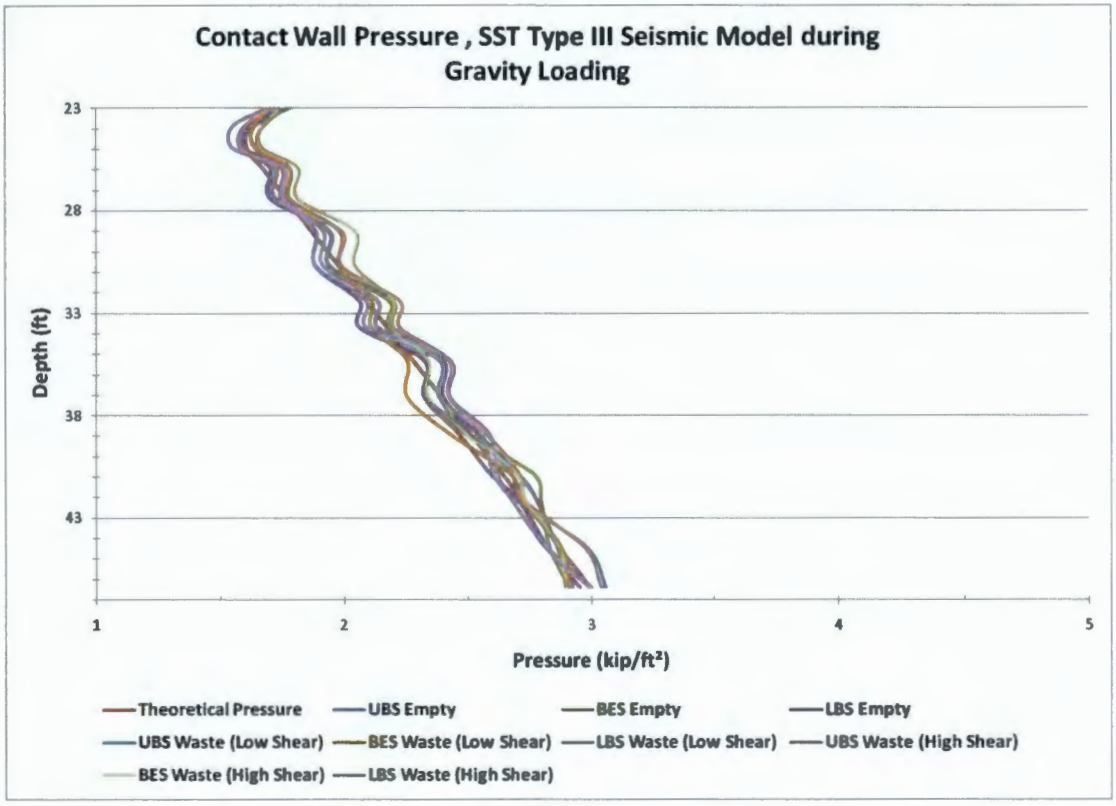

Figure 6.12. Seismic Model Soil/Concrete Contact Element Normal Pressure for At-Rest Calibration – Gravity Only

6.2.7.3 Waste/Concrete Tank Interface

A combination of TARGE170 and CONTA173 elements is used to model the interface between the waste and the concrete tank. The presence of this interface is important to establish a realistic relationship between the relatively low-stiffness waste and the concrete tank. The relatively flexible behavior of the waste is best modeled by allowing the waste to move independently of the tank. A frictionless contact surface was used at this interface in order to simulate a yield mechanism for the waste. The surfaces are allowed to slide but not separate. Separation is not permitted due to contact instabilities encountered during solution of preliminary Type III runs. The contact stiffness of the Low Shear Stiffness (LSS)

waste was increased to match the High Shear Stiffness (HSS) waste to improve solution stability. The adjustment does not alter the global load transfer to the wall for either case. The waste is the contact surface and the concrete tank is the target surface. The waste/concrete tank interface elements are shown in Figure 6.13.

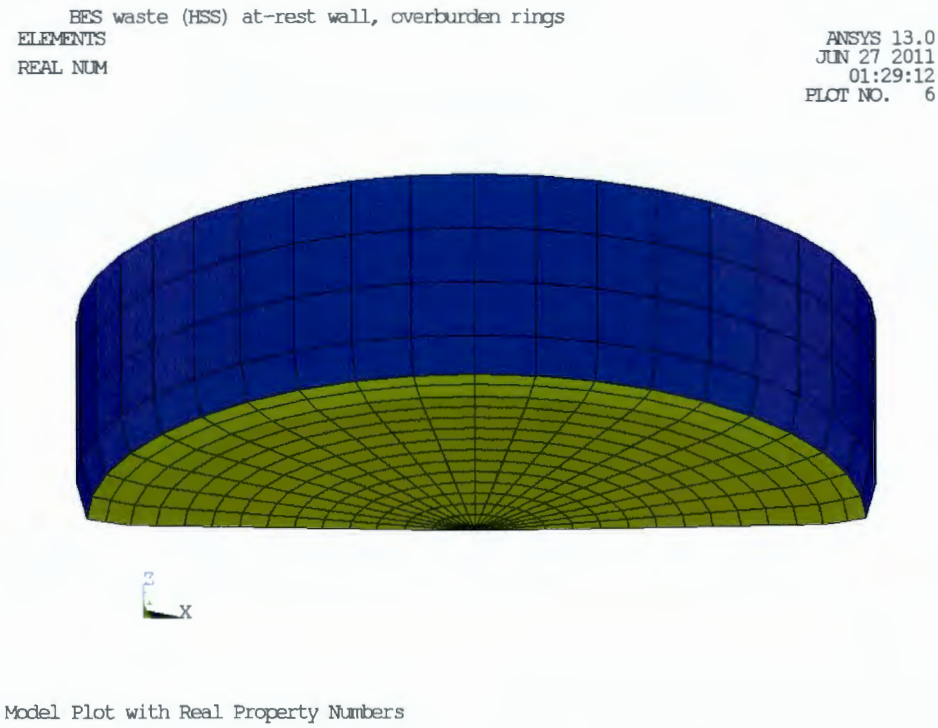

Figure 6.13. Seismic Model Interface Elements Real Property Assignment – Waste-to-Concrete Tank

6.2.7.4 Soil-to-Soil Interfaces

A combination of TARGE170 and CONTA173 elements is used to model the interface between the native and excavated backfill soils. The excavated soil is the contact surface and the native soil is the target surface. Initial geometrical penetration or gap and offset are both excluded. The contact behavior is specified as "no separation," since separation of the native soil from the backfill is nonphysical. This allows for the potential of sliding between the surfaces, but the surfaces remain in contact.

This surface is included to improve the initial conditions for the transient analysis by allowing an initial displacement between the native and excavated soil. This is necessary due to the modeling approach, where the backfill is already present at the initial application of gravity. Thus, the native soil is not able to develop its own pre-existing initial condition before the addition of the backfill. The interface surface provides a slip plane that permits the backfill to "settle" independently, more like the actual construction sequence. This prevents artificial stresses at the soil interface, since no initial stress existed after backfill.

An initial coefficient of friction of 0.3 (slope lateral boundary) and 0.6 (bottom) (see Figure 6.14) is used for the gravity (static) analysis. The coefficient of friction on both the slope lateral boundary and the bottom is changed to 0.7 for the transient analysis (Table 6.7; Figure 6.14). The methodology and friction coefficients were found to be effective in studies performed for the DST analysis (Rinker et al. 2008).

Vertical slip planes are inserted into the soil overburden (soil above the dome within the radius of the wall) to prevent or minimize soil arching. More detailed discussionof soil arching is found in the next section and in Appenidx L. The locations of the contact surfaces are consistently placed halfway between the ACI sections to ensure uniform loading. Separation of the surfaces is not allowed, to improve solution stability. The stiffness of the slip plane contacts was adjusted to give similar contact stiffness across all three soil configurations. Appendix K discusses the vertical slip planes for the soil overburden modeling technique in further detail. To establish the initial conditions, a low coefficient of friction of 0.05 is used, which lets the soil settle consistently with the dome deformation. A coefficient of friction of 0.2 is used during the seismic analysis. A sensitivity study in Appendix K compares a Type III, SST, Best-Estimate Soil (BES), empty tank with a 0.2 and 0.5 coefficients of friction. The higher friction causes resistance to upward movement in the soil rings, which increases the demand in portions of the dome during a seismic time history. A higher coefficient of friction between the soil rings leads to unrealistic soil arching which is not expected for the ground shaking during the seismic event. For this reason, the friction coefficient of 0.2 was selected to provide a more realistic dynamic response of the soil overburden during the seismic analysis.

Table 6.7. Summary of Soil-to-Soil Friction Properties

	Initial Gravity Step	Seismic Time History
Excavated soil overburden slip planes	0.05	0.2
Excavated soil to native soil	0.3 (slope lateral boundary), 0.7 (bottom)	0.7 (all)

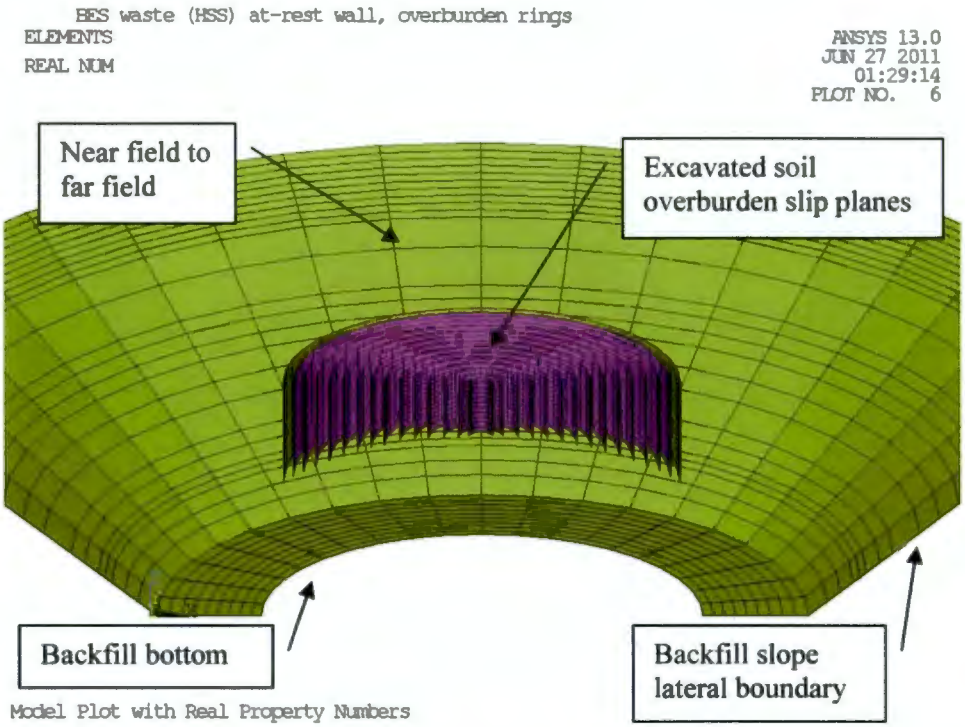

Figure 6.14. Seismic Model Interface Elements Real Property Assignment – Near Soil to Far Soil

6.2.7.5 Soil Arching

When linear elastic material properties are used to model soils, there is potential for developing artificial tensile zones. When the tensile zone is part of a beam type behavior forming a self-supporting condition, the soil is said to be arching. When this occurs there is a potential for soil loads to be transferred away from the tank dome into the surrounding soil. While localized tensile zones (i.e., not forming a continuous arch) will have only a limited impact on the results, excessive arching behavior will result in underestimating the vertical loads on the concrete dome and tank sidewalls. Discussion of soil arching is also found in Rinker et al. 2008.

Arching will not occur where a yield method (e.g., Drucker-Prager as in the TOLA model) or other displacement mechanism is provided. In the seismic model, vertical contact surfaces are inserted into the overburden to create annular rings of soil that are free to displace vertically consistently with the tank dome, but, allows the load to be transferred laterally during horizontal motion. This effectively creates a nonlinear yield mechanism that acts in the vertical direction only and allows for horizontal load transfer from one ring to the other ring. A low coefficient of friction is used, thereby ensuring that the majority of the soil load is carried by the tank dome. Studies performed during preliminary modeling determined that higher coefficients of friction caused the soil to be too stiff, thus a low coefficient of friction was found to be most effective.

Table 6.7 shows the friction coefficient for the soil overburden slip planes in the initital gravity step (static) to be 0.05 as compared to the value of 0.2 for the seismic transient.

Figure 6.15 shows rings in soil overburden with slip planes. The plot is of displacement contours under gravity loading, which shows the increasing vertical displacement of the soil rings from the tank wall radius toward the tank dome apex. The stepwise displacement contour of each adjacent ring confirms the ability of each soil rings to displace according to the dome deformation and confirms the overburden load is transferred correctly to the tank dome.

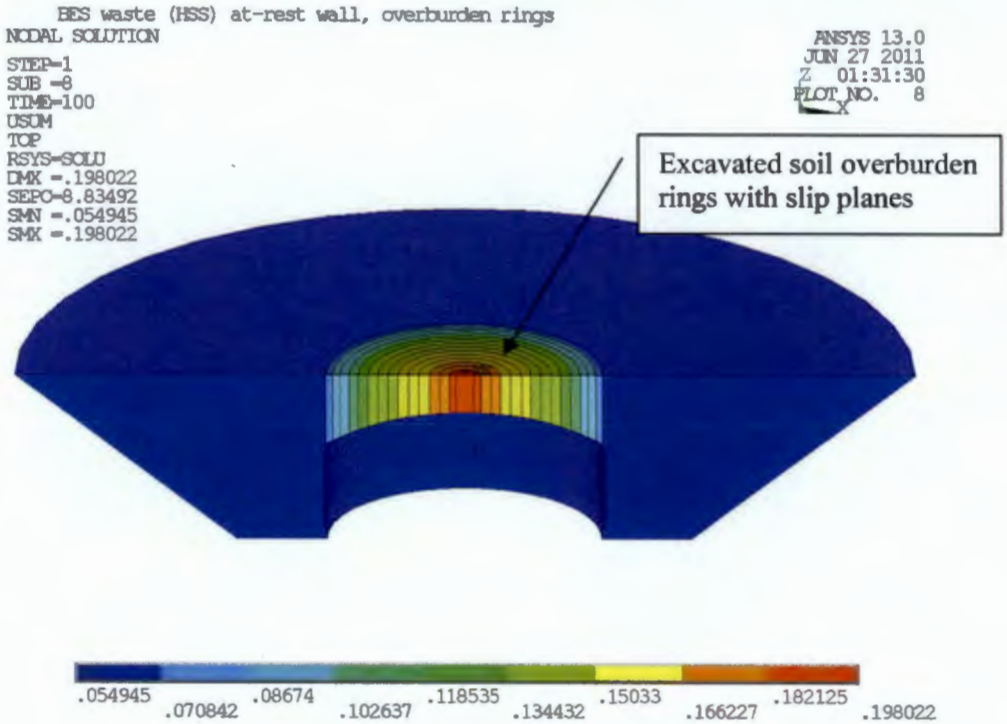

Figure 6.15. Seismic Model Excavated Backfill Soil –Soil Slip Planes

The dead weight contact pressure in Figure 6.16 demonstrates the effectiveness of the overburden soil slip rings technique by showing contact pressure in the dome close to theoretical pressure (note: the concentrated surface load is not included). The increase in contact pressure toward the haunch is additional load from soil immediately outside the tank wall radius. This is due to the tank wall being vertically stiffer than the soil adjacent to the tank. There is also a small effect from unadjusted at-rest pressure in the dome, according to the horizontal vector component of the dome. The soil overburden contact slip plane method for reducing soil arching is therefore demonstrated to be effective.

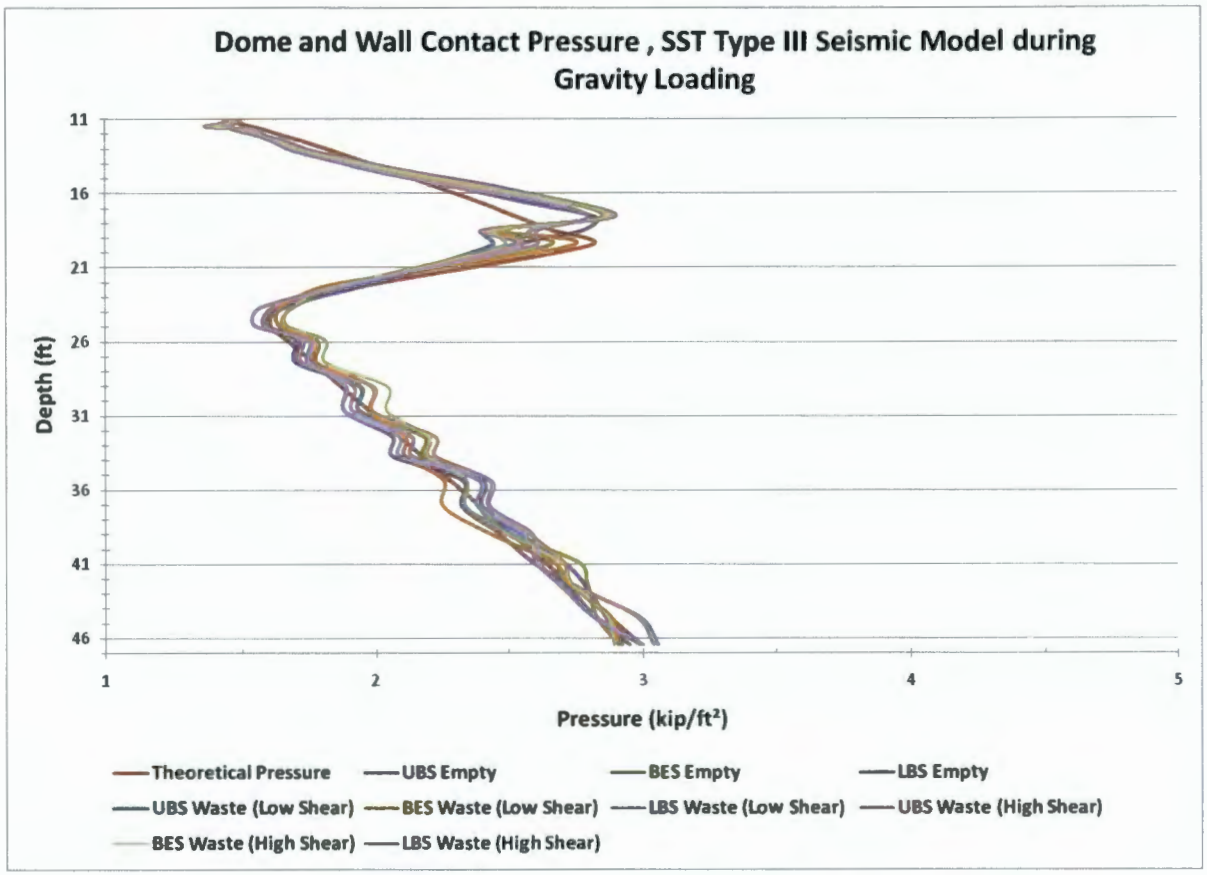

Figure 6.16. Gravity Only Contact Pressure Plot

6.2.7.6 Soil to Dome Contact Stiffness

The overburden soil rings above the dome have larger sized elements than the elements in the concrete dome. This meshing difference results in localized uneven contact pressure, which is nonphysical. This is easily resolved by softening the contact stiffness to smooth out the loading. However, care must be taken to ensure that the contact is not too soft, creating a nonphysical situation where the soil mode becomes decoupled from the dome mode. This is especially important at the dome, which is the only part of the tank capable of having a modal response independent of the soil column response. Thus, the contact stiffness for the dome to the soil overburden was verified to ensure that the contact stiffness was rigid (33 Hz or greater). Figure 6.16 shows the depth of the soil to the dome apex to be 11-feet. The maximum soil depth of the haunchis 20.2 ft and was rounded to a conservative value of 21 ft for this calculation.

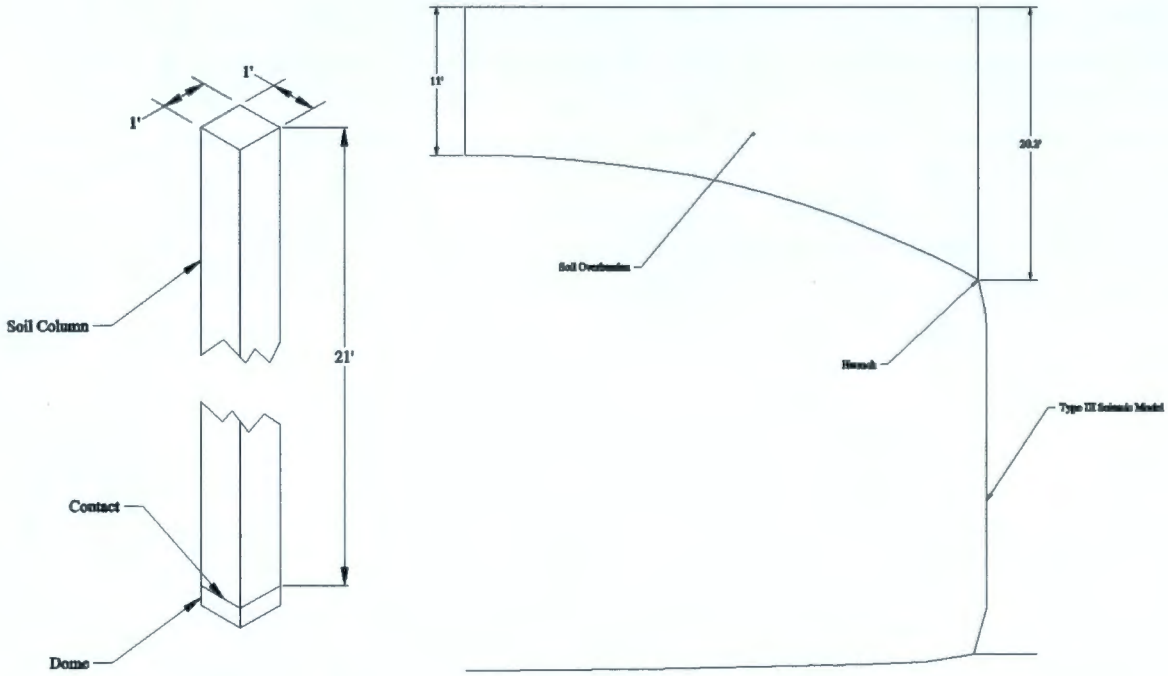

Figure 6.17. Seismic Model Maximum Soil Height above the Dome

The following calculation determines the minimum contact stiffness between the soil overburden and the dome:

$$f = \frac{\sqrt{\frac{k}{m}}}{2\pi} \quad \text{Frequency} \tag{6.1}$$

$$f = 33Hz \quad \text{Target Frequency} \tag{6.2}$$

$$\rho = 129\frac{lbm}{ft^3} \quad \text{Soil Density of Backfill (see Section 7.10)} \tag{6.3}$$

$$m_{haunch} = 21 \cdot ft \cdot (1ft)^2 \cdot \rho = 2709lb \quad \text{Mass above the Haunch} \tag{6.4}$$

$$k = [f \cdot (2\pi)]^2 \cdot m_{haunch} = 3620\frac{kip}{ft} \quad \text{Minimum Contact Stiffness} \tag{6.5}$$

Thus, the contact stiffness between the soil overburden and the dome must be 3620 kip/ft or greater to create a rigid contact.

6.2.8 Surface Loads

Three-dimensional point mass MASS21 elements with three translational and three rotational degrees-of-freedom were added to the soil surface on a 10-foot-radius circle over the center of the dome to create a concentrated load over the tank dome. The mass provides an equivalent weight of 200,000 lbf, which is the nominal allowable concentrated load for a 100-series SST with the maximum allowable soil overburden. Because the gravity results are subtracted from the gravity plus seismic results to produce seismic-only results, the seismic-only results only retain the inertial effect of the concentrated load. The dead weight contribution is added back in when the seismic-only results are combined with the TOLA results. The surface load is developed using the input file SOUD.inp. Mass elements are on top of the soil elements as shown in Figure 6.18.

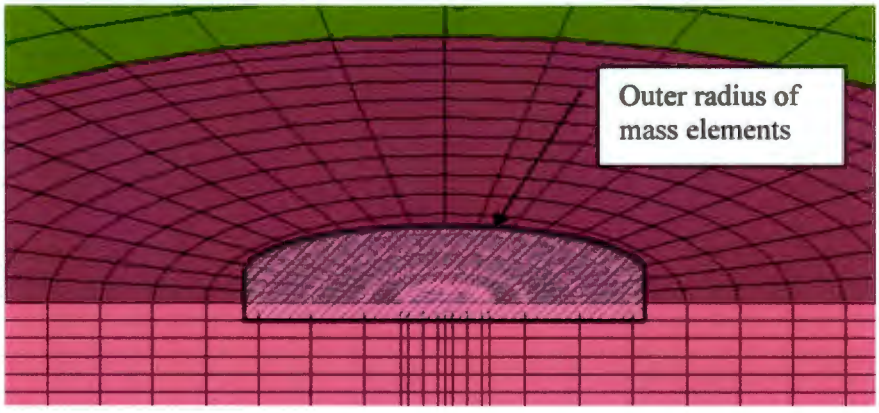

Figure 6.18. Seismic Model Mass Elements – Soil Surface

6.2.9 Boundary Conditions

Boundary conditions and supporting elements are developed in input file BC.inp.

6.2.9.1 Soil Boundary Conditions

All nodes at the base of the model are coupled together to create a rigid region (see Figure 6.19). The soil elements support three translational degrees of freedom, thus the symmetry plane for the soil has all nodes fixed for translation across the symmetry plane.

All nodes on the outside edge (radius = 320 ft) have been "slaved" to a single node at each layer. Couples are used in each of the three translations to force the soil to behave essentially as a shear beam. This approach is used to create the appropriate conditions for vertical and horizontal waves to pass through the model (see Figure 6.20). The effectiveness of this approach is documented in Rinker et al. (2006).

LINK8 elements with a high stiffness are used to connect the native soil slaved nodes on each layer to the symmetry plane. These are required because the slaved node of a couple cannot also support an applied boundary condition. Therefore, to maintain the desired soil behavior, the link elements effectively complete the coupling of the outside soil node at each layer.

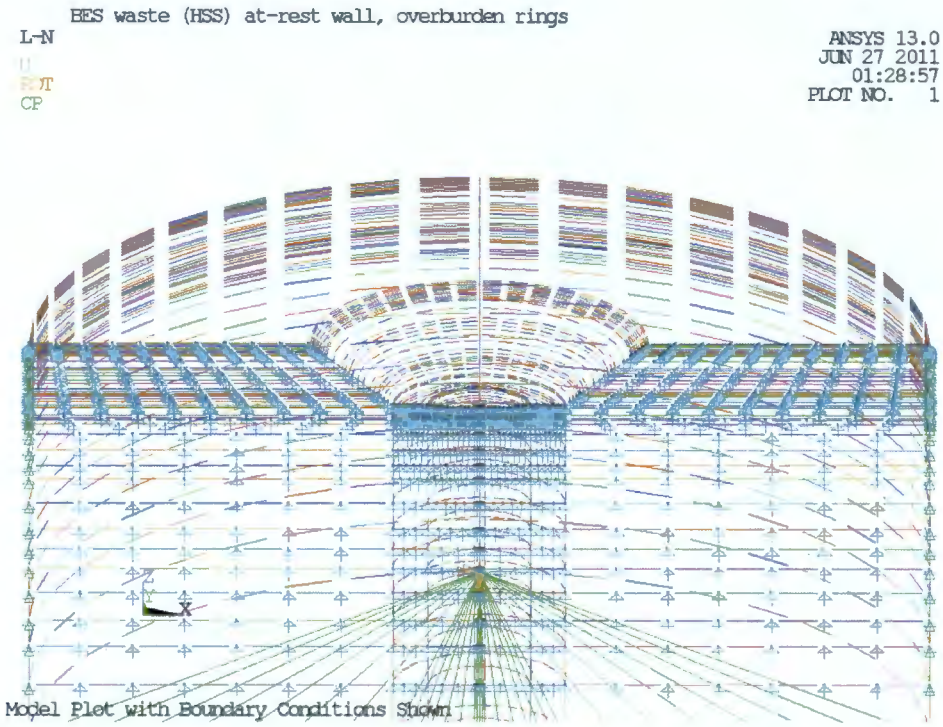

Figure 6.19. Seismic Model Boundary Conditions – Symmetry Plane and Soil Base

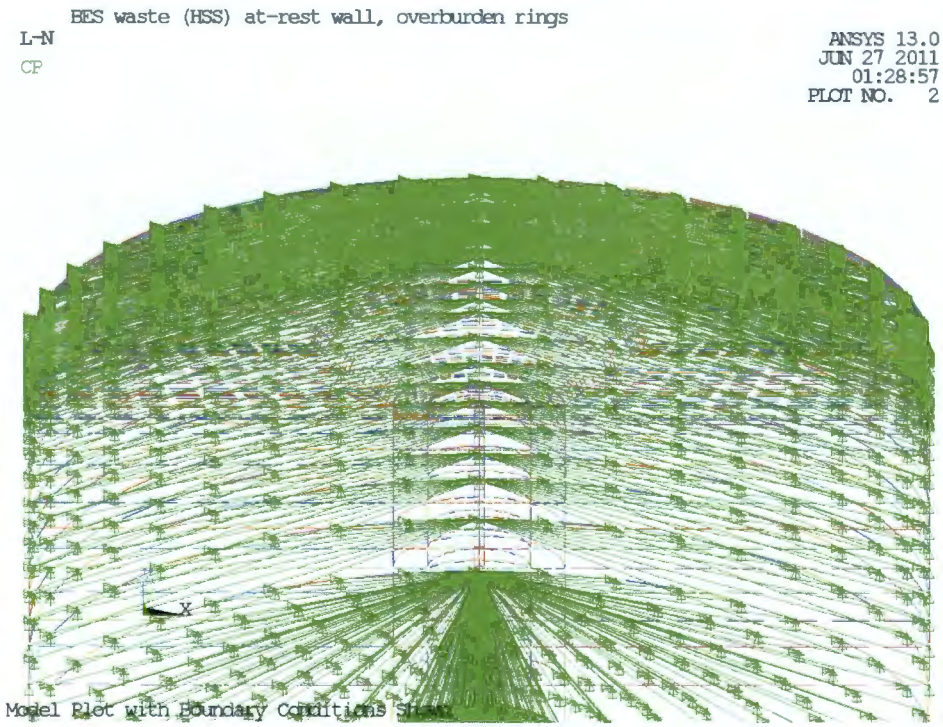

Figure 6.20. Seismic Model Boundary Conditions – Slaved Boundary Conditions

6.2.9.2 Tank Boundary Conditions

The tank model shell elements support six degrees of freedom; thus, all nodes on the symmetry plane are fixed from translation normal to the symmetry plane and for rotations about the two axes in the symmetry plane (see Figure 6.21).

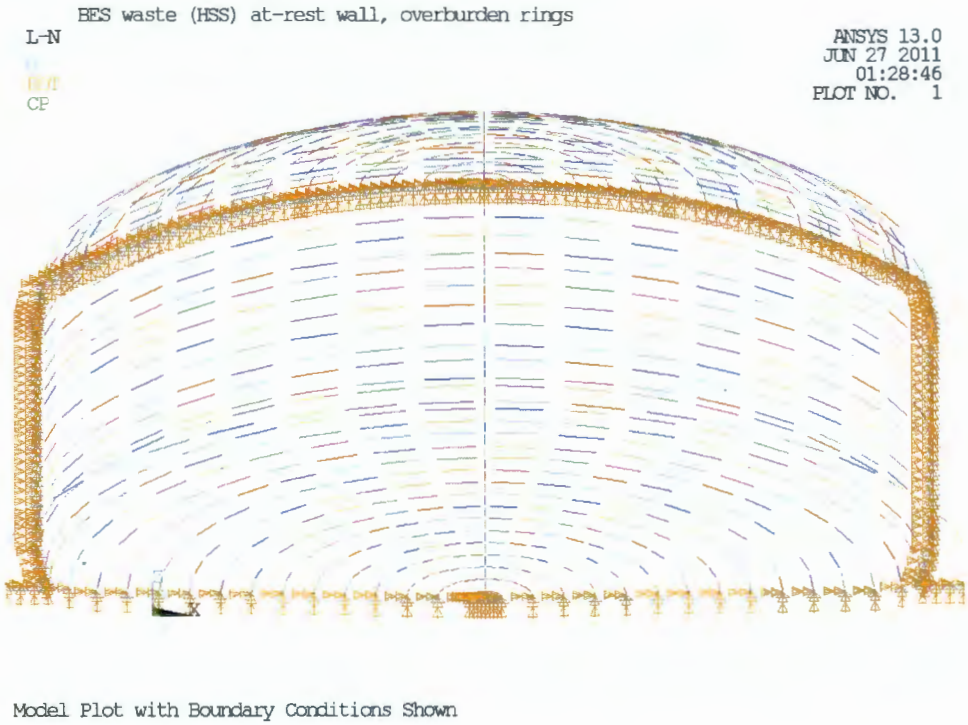

Figure 6.21. Seismic Model Boundary Condition – Concrete Tank

6.2.10 Model Excitation

A very large mass element is located at the base of the model and a seismic excitation is applied at that node as a force time history. The force is the product of the point mass and the acceleration for that time step of the seismic acceleration time history. The point mass used is greater than 100 times the mass of the full model to simulate seismic ground motion.

6.2.11 Seismic Input

Two input motions (horizontal and vertical) have been defined as acceleration time histories consisting of 4,096 time steps. However, only 2,048 time steps were used for the analysis since the time increment of the seismic input is 0.01 seconds based on a 20.48 second event. Discussion of spectra comparisons is provided in Chapter 8.

6.2.12 Post-Processing

The methods for post-processing described below are typical for all of the studies and seismic runs used with the seismic model. Information about the run configuration (see Section 6.4.1) is recorded in the output files to aid identification and checking.

6.2.13 Concrete Tank Elements

Concrete tank forces and moments at each of the ACI sections are extracted from the model in 9-degree slices. The ACI section sequence starts near the center of the dome and moves radially along the dome, down the sidewall, then across the footing from the outside to the center of the tank lower slab. The results presented for the concrete forces and moments are enveloped minima/maxima around the circumference of the tank.

The SHELL181 element used for the concrete tank supports the following output used in this analysis (Table 6.8):

Table 6.8. Selected SHELL181 Output Quantities and Sequence Numbers

Output Quantity Name	Item	Sequence Numbers	Description
N11	SMISC	1	Meridional force (per unit length)
N22	SMISC	2	Hoop force (per unit length)
N12	SMISC	3	In-plane shear force (per unit length)
M11	SMISC	4	Meridional moments (per unit length)
M22	SMISC	5	Hoop moments (per unit length)
M12	SMISC	6	Twisting moment – not used
Q13	SMISC	7	Transverse (through-wall) shear force (per unit length)
Q23	SMISC	8	Transverse (through-wall) shear force (per unit length)

Figure 6.22 shows the SHELL181 element force and moment vector and element coordinate system (ECS) relative to the tank model coordinate system. Results for through-wall shear forces are the envelope of SMISC7 and SMISC8. Results are not presented for SMISC6, the element in-plane twisting moment, as this is not used in the ACI evaluation.

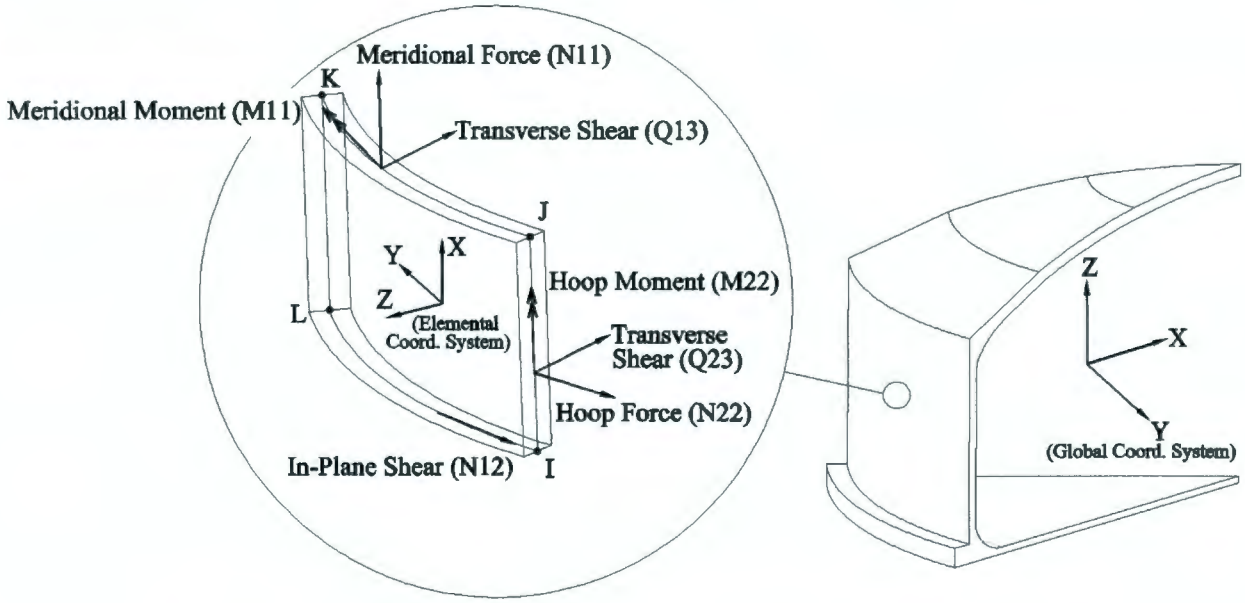

Figure 6.22. SHELL 181 Element Force and Moment Vector Orientations

The elements for post-processing are determined by selecting the elements whose centroids most closely match the locations defined as ACI sections. A sample excerpt of the element selection is shown as Table 6.9 for the first angle slice. The first four columns (ACI#, LocX/Y/Z) describe the ACI sections by sequence number and location. The next four columns (Elem/X/Y/Z) identify the element at that location, and the location of the element centroid. All locations are in a cylindrical coordinate system with its origin at the elevation of the sidewall bottom. The element path (PathE) is the cumulative sum of each successive element centroid spacing. The vector components of the slope (SlopeX, SlopeZ) of the element are reported for checking purposes.

Table 6.9. Tank Concrete ACI Section Data Output (Sample Excerpt)

Tank Concrete elements angle 1 (0°) ACI section data

ACI#	LocX	LocY	LocZ	Elem	ElemX	ElemY	ElemZ	PathE	SlopeX	SlopeZ
1	2.79	4.41	36.84	493	2.76	4.50	36.82	33.1	1.000	0.024
2	5.58	4.41	36.73	463	5.54	4.50	36.70	66.5	0.999	0.053
3	8.38	4.41	36.54	433	8.32	4.50	36.50	100.0	0.997	0.082
4	11.16	4.41	36.27	403	11.10	4.50	36.22	133.5	0.994	0.111
5	13.93	4.41	35.92	373	13.84	4.50	35.86	166.7	0.990	0.140
6	16.70	4.41	35.48	333	16.62	4.50	35.39	200.4	0.984	0.180
7	19.44	4.41	34.92	303	19.35	4.50	34.81	233.9	0.975	0.221
8	22.16	4.41	34.24	273	22.05	4.50	34.11	267.4	0.965	0.262
9	24.85	4.41	33.45	243	24.73	4.50	33.30	301.0	0.953	0.303
10	27.49	4.41	32.55	213	27.37	4.50	32.38	334.6	0.939	0.343
11	30.10	4.41	31.51	183	29.95	4.50	31.32	368.0	0.916	0.402
12	32.67	4.41	30.38	153	32.43	4.50	30.22	400.6	0.916	0.402
13	34.77	4.41	29.46	123	34.60	4.50	29.27	429.0	0.916	0.402
14	36.65	4.41	28.49	93	36.41	4.50	28.28	453.8	0.866	0.500
15	38.48	4.41	25.84	53	37.92	4.50	25.59	490.8	0.196	0.981
16	38.21	4.41	24.34	1263	38.08	4.50	24.10	508.7	0.034	0.999
17	38.23	4.41	23.10	1243	38.11	4.50	22.93	522.9	0.000	1.000
18	38.23	4.41	22.13	1233	38.11	4.50	22.13	532.5	0.000	1.000
19	38.23	4.41	20.63	1213	38.11	4.50	20.51	551.8	0.000	1.000
20	38.23	4.41	18.95	1193	38.11	4.50	18.88	571.4	0.000	1.000
21	38.23	4.41	17.30	1173	38.11	4.50	17.22	591.4	0.000	1.000
22	38.23	4.41	15.63	1153	38.11	4.50	15.56	611.3	0.000	1.000
23	38.23	4.41	14.32	1133	38.11	4.50	14.16	628.1	0.000	1.000
24	38.23	4.41	12.71	1113	38.11	4.50	12.62	646.5	0.000	1.000
25	38.23	4.41	10.88	1093	38.11	4.50	10.85	667.8	0.000	1.000
26	38.23	4.41	9.13	1073	38.11	4.50	9.08	689.1	0.000	1.000
27	38.23	4.41	7.13	1053	38.11	4.50	7.14	712.3	0.000	1.000
28	38.23	4.41	5.80	1033	38.11	4.50	5.64	730.3	0.000	1.000
29	38.07	4.41	3.50	1003	38.03	4.50	3.32	758.2	0.253	0.967
30	37.57	4.41	1.60	983	37.58	4.50	1.58	779.7	0.253	0.967
31	40.34	4.41	0.00	1644	40.01	4.50	0.00	814.6	0.000	0.000
32	33.69	4.41	-0.67	1693	34.24	4.50	-0.49	884.1	0.000	0.000
33	32.00	4.41	-0.71	1703	31.85	4.50	-0.69	912.9	0.000	0.000
34	29.33	4.41	-0.76	1713	29.27	4.50	-0.74	943.9	0.000	0.000
35	26.67	4.41	-0.81	1723	26.61	4.50	-0.79	975.8	0.000	0.000
36	24.00	4.41	-0.86	1733	23.95	4.50	-0.83	1007.7	0.000	0.000
37	21.33	4.41	-0.91	1743	21.29	4.50	-0.88	1039.6	0.000	0.000
38	18.67	4.41	-0.96	1753	18.64	4.50	-0.93	1071.5	0.000	0.000
39	16.00	4.41	-1.01	1763	15.98	4.50	-0.98	1103.4	0.000	0.000
40	13.33	4.41	-1.05	1773	13.32	4.50	-1.03	1135.3	0.000	0.000
41	10.67	4.41	-1.10	1783	10.66	4.50	-1.08	1167.2	0.000	0.000
42	8.00	4.41	-1.15	1793	8.00	4.50	-1.13	1199.1	0.000	0.000
43	5.33	4.41	-1.20	1803	5.34	4.50	-1.18	1231.0	0.000	0.000
44	2.67	4.41	-1.25	1813	2.69	4.50	-1.23	1263.0	0.000	0.000

Concrete tank forces and moments at each of the ACI sections are extracted from the model in 9-degree slices. The ACI section sequence starts near the center of the dome and moves radially along the dome, down the sidewall, then across the footing from the outside to the center of the tank lower slab. The results presented for the concrete forces and moments are enveloped minima/maxima around the circumference of the tank (Figure 6.23).

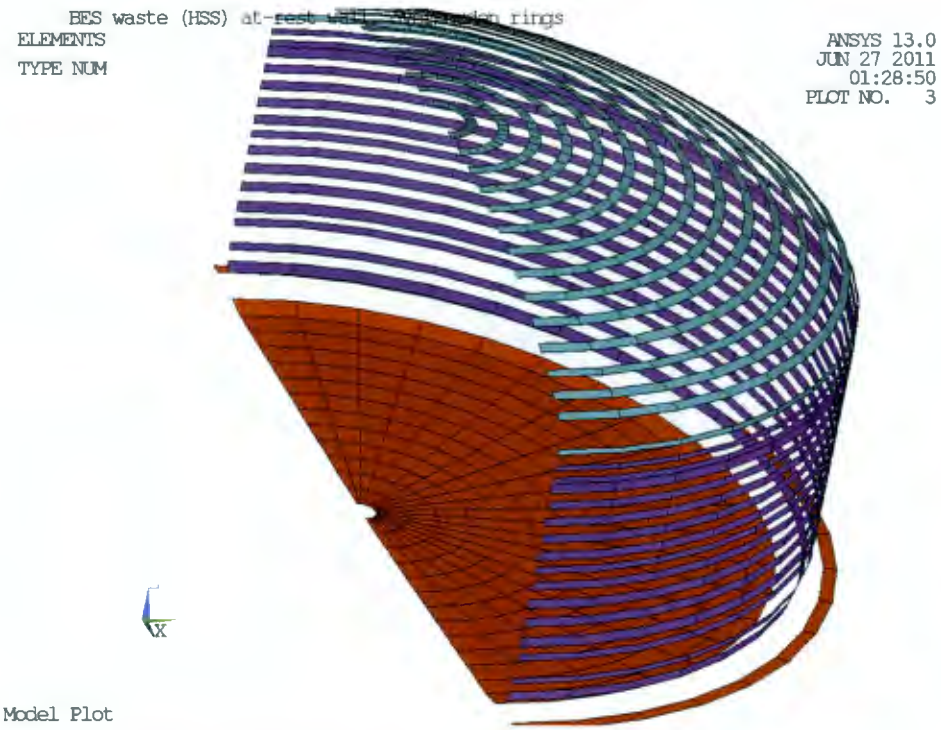

Figure 6.23. Seismic Model Concrete Tank Elements at ACI Sections

6.2.14 Contact Elements

Soil contact data are extracted from the contact elements overlying the tank ACI sections. The location (i.e., mesh) of the soil contact elements is not as strictly controlled as the tank ACI section locations, but is of sufficient detail and proximity to show meaningful trends along the tank profile.

The CONTA173 element used for the contact surfaces supports the following output used in this analysis (Table 6.10):

Table 6.10. Selected CONTA173 Output Quantities

Output Quantity Name	Description
CONT:PRES	Normal contact pressure
CONT-GAP	Contact Gap Distance
CONT-STAT	Contact Status (Open, Closed, Sliding)

Just as with the tank elements, ANSYS® determines the contact elements for post-processing by selecting the elements whose centroids most closely match the locations defined as ACI sections.

6.2.15 Enveloping Process

The transient analysis consists of an initial gravity step plus 2,048 transient time steps. To condense the amount of data that is generated by the time history analysis, the following enveloping process is used:

1. At every element at all ACI section locations, the maximum and minimum results are extracted over the entire time history. Built-in ANSYS® functions are used to determine the maximum and minimum results.
2. From these extreme results, the bounding result from each min/max result pair is determined and the result with the greatest magnitude is identified and the sign is retained.
3. The results at each ACI section are summarized by determining the bounding results at any angle around the tank. The result with the greatest magnitude is identified and the sign is retained.

These steps are performed within ANSYS® post-processing using array parameter operations. The results of each step are output in tabular text format. See Section 6.2.4 for a list of output files generated during post-processing. Because of the enveloping process used, the maximum values shown on results plots may occur at different times and different locations.

For subtraction of gravity from the seismic plus gravity results, the minima and maxima results are each subtracted separately to maintain accuracy. The subtracted results are then summarized according to the same process described above. As a result of taking the bound of subtracting the minima and maxima separately, the bounding seismic results may not match the difference in the bounding values of the gravity and seismic plus gravity steps. Thus, caution must be used when comparing only the bounded results. This step is also performed within ANSYS® post-processing after the seismic run. The gravity results are read in via the minima/maxima results text output previously generated. The seismic-only results are reported as absolute values only.

6.2.15.1 Post-Processing Example

Since the post-processing is a complex process, a simplified example is demonstrated below.

1. The following minima and maxima results at each angle within an ACI section are extracted by ANSYS® from the results time history. These hypothetical results are chosen to demonstrate different mathematical combinations that may be encountered. The bounding min/max values are determined for each angle.

Gravity-only results

	Min	Max	Bound
Angle 1	-10	10	10
Angle 2	-10	-9	-10
Angle 3	-10	-9	-10

Gravity + seismic results

	Min	Max	Bound
Angle 1	10	10	10
Angle 2	-100	-99	-100
Angle 3	-99	100	100

2. The bounding values at each angle are reduced to a single bounding value for the entire ACI section. These are the bounding values reported for the respective cases.

	Gravity-only results
	Bound
Any angle	10

	Gravity + seismic results
	Bound
Any angle	100

3. Subtract minimum and maximum gravity-only results from the gravity plus seismic results and repeat previous enveloping steps on the subtracted values.

	Seismic-only results		
	Min	Max	Bound
Angle 1	20	0	20
Angle 2	-90	-90	-90
Angle 3	-89	-81	-89

4. Final seismic-only bounding value at an ACI section:

	Seismic-only results
	Bound
Any angle	90

Observations:

- The bounding seismic value at angle 1 (20) does not match the difference in the bounding values of the gravity and seismic plus gravity steps (10-10=0). Thus, the subtracted bounding values should not be directly compared to the separate bounding values.
- The values at angles 2 and 3 represent a situation where the seismic activity causes the structure to oscillate at nearly equal values of alternating sign. However, since the enveloping process captures only the bounding values, it would appear that the structure experiences load reversals from one location to the next. This is obviously nonphysical, so this phenomenon should be kept in mind when bounding results show sign reversals between values of similar magnitude. The results are not as discontinuous as they would appear.

6.3 Material Properties

6.3.1 Tank Concrete Properties

The shell element properties for the seismic model are determined for the predicted present-day condition of the concrete as determined by load step 27 (80°F) of TOLA Run 1 (see Sections 4.1.1 and 4.1.3). The concrete in TOLA Run 1 has a nominal modulus and near zero tensile strength. After being subjected to the thermal cycle the concrete is cracked in all tank sections in both the hoop and meridional directions. The shell element properties (Young's modulus, thickness, and density) for the seismic model are determined following the procedure presented in the C-106 seismic analysis (Day et al. 1994, Appendix U). This procedure matches shell axial and bending stiffnesses to the stiffnesses of the cracked

or uncracked reinforced concrete sections. In addition to adjusting the properties for cracking, the procedure also accounts for the degradation of the concrete due to the thermal cycle and the current temperature of the steel.

The C-106 seismic analysis (Day et al. 1994, Appendix U) assumes a linear strain profile through the section. The actual area of steel is converted to the transformed area of steel using the ratio of the thermal history dependent steel and concrete moduli, $n = E_{st}/E_{conc}$. If there is a bending moment, concrete on the tension side of the section does not carry any load. The neutral axis of the section is calculated as the location where the strain is zero. The effective moment of inertia is also calculated. From this, the axial and bending stiffness of the section are matched to the axial and bending stiffness of the shell. Matching the axial and bending behaviors determines one unique shell value of Young's modulus and one unique shell thickness. The density of the shell is then adjusted based on this thickness so that the overall weight of the section remains the same.

Within the SST AOR, the procedure described in the C-106 seismic analysis is followed with two alterations: 1) sections that are in net axial tension are assigned axial and bending behavior consistent with the reinforcement properties only; and 2) rather than use isotropic shell properties, orthotropic shell properties are used to accurately model the different behavior due to differing reinforcement and net tension in the meridional and hoop directions.

6.3.1.1 Net Tension Sections

At the end of the thermal cycle, most sections are in net compression in the meridional direction. Those that are in net tension, a few sections near the center of the slab, have insignificant net tension values of less than 1 kip/ft net tension. However, in the hoop direction many sections in the outer dome, haunch, wall, and slab are in significant net tension. Because concrete can carry no tensile load, the behavior of the shells in these net tension sections should depend on the reinforcing steel alone. In addition, if a section is in net tension or compression at the end of the thermal cycle, then it remains in net tension or compression respectively throughout the earthquake. The shell elements used in the seismic model are linear and do not have the ability to switch behaviors based on the net axial load direction. Also, the bending in the net tension section is small enough that no concrete is in compression.

The axial stiffness of the section can be calculated by transforming the steel areas. Transformed steel areas for a typical reinforced concrete section are shown in Figure 6.24. Unlike the transforming of a compressive section, the ratio $n = E_{st}/E_{conc}$ is not used for the transformed areas. Axial stiffness for the section is simply the sum of these steel areas times the temperature-dependent modulus of steel. Following C-106 seismic analysis (Day et al. 1994, Appendix U), the axial stiffness of the section must be equal to the axial stiffness of the shell:

$$(EA)_{shl} = E_{shl} t_{shl} = E_{st} \sum_i A_{st}^i \tag{6.6}$$

where the summation is done from i = 1,2, …, number of steel layers.

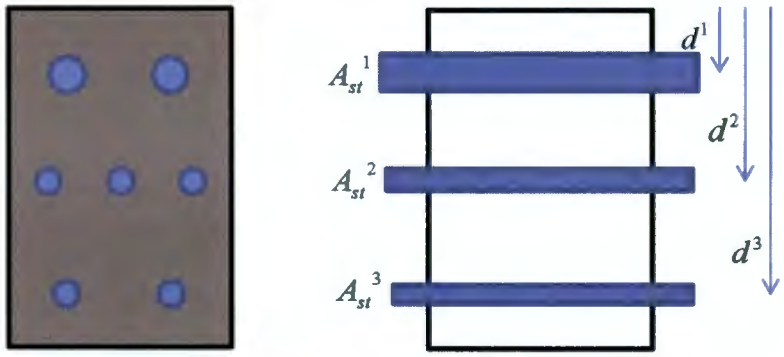

Figure 6.24. Typical Multilayer Reinforced Concrete Section (left) and Schematic Net Tension Section Transformed Steel Areas (right)

The bending stiffness of the section can be calculated by first getting the effective moment of inertia of the section.

$$I_{eff} = \sum_i A_{st}^i (d^i - X_{na})^2 \tag{6.7}$$

where d^i is the depth of the reinforcement layer as defined in Figure 6.21 and the neutral axis location is:

$$X_{na} = \sum_i A_{st}^i d^i / \sum_i A_{st}^i \tag{6.8}$$

The bending stiffness of the section is then calculated as:

$$(12EI)_{shl} = E_{shl} t_{shl}^3 = 12 E_{st} I_{eff} \tag{6.9}$$

Again the bending stiffness of the section is set equal to the bending stiffness of the shell.

Using Equations (6.6) and (6.9), the effective value of Young's modulus for the shell element can be solved as:

$$E_{shl} = \sqrt{(EA)_{shl}{}^3 / (12EI)_{shl}} \tag{6.10}$$

Then the effective thickness and effective density of the concrete is solved in succession by:

$$t_{shl} = (EA)_{shl} / E_{shl} \tag{6.11}$$

$$\gamma_{shl} = (t / t_{shl}) \gamma_{conc} \tag{6.12}$$

For net tension sections in the slab, there is only one layer of rebar in both the hoop and meridional directions (section 28 only has two layers of rebar in the meridional direction). Any net tension sections with only one layer of rebar will have a zero bending stiffness. For these slab sections in net tension, the hoop thickness t_{shl}^{hoop} is assumed to be the thickness of the slab, 6 inches. E_{shl}^{hoop} is then calculated from Equation (6.6) rather than Equation (6.10). The bending stiffness behavior is then not accurate but the difference in bending stiffness is acceptable as the hoop moments in the slab are generally small.

6.3.1.2 Orthotropic Shells

Orthotropic shell properties are necessary to allow different behavior in the meridional and hoop direction. This accounts for the significant differences in meridional and hoop reinforcement in the haunch as well as different behaviors for net compression and tension sections. Orthotropic shell properties allow unique assignment of effective Young's modulus in the meridional and hoop directions. Unfortunately only one value of thickness and one value of density is allowed per shell element. The thickness corresponding to one direction will be chosen. Then, the effective Young's modulus in the other direction can be adjusted to match either the correct axial stiffness or the correct bending stiffness. Because the hoop moments are generally small compared to the other forces and moments, the hoop bending stiffness accuracy was given second priority in order to accurately represent the meridional axial and bending behavior and hoop axial behavior.

The correct effective Young's modulus and effective thickness in the meridional direction are used. The new effective Young's modulus in the hoop direction, which accurately captures the hoop axial behavior, is then the old effective Young's modulus factored by the thickness ratio of the hoop thickness to the meridional thickness:

$$E_{shl}^{hoop_new} = E_{shl}^{hoop}(t_{shl}^{hoop}/t_{shl}^{merid}) \tag{6.13}$$

This means that the bending stiffness in the hoop direction that uses the meridional thickness t_{shl}^{merid} and the new hoop stiffness $E_{shl}^{hoop_new}$ is too stiff by a factor of $(t_{shl}^{hoop}/t_{shl}^{merid})^2$ compared to what it should be. This factor is in the range of 0.69 to 2.93 for the sections of the dome, haunch, and wall. It is important to note however, that the use of orthotropic properties that can accurately model the axial tension in the hoop direction is a significant improvement over simply using isotropic properties even with this inexact hoop bending stiffness. If isotropic shells are used (by assigning meridional properties in all directions) the hoop axial stiffness would be off by a factor ranging from 0.36 to 5.76 for sections of the dome, haunch, and wall instead of matching exactly as in the orthotropic case. In addition, the use of isotropic shells would still leave the hoop bending stiffness off by a factor ranging from 0.34 to 2.60 for sections of the dome, haunch, and wall.

In addition, orthotropic properties require the assignment of: E_z, the through thickness effective Young's modulus; υ_{mh}, υ_{hm}, υ_{mz}, υ_{zm}, υ_{hz}, and υ_{zh}, the six Poisson's ratios; and G_{mh}, G_{hz}, and G_{zm}, the three shear moduli. E_z is simply assigned as the degraded concrete modulus.

Due to symmetry, the six Poisson's ratios are not independent. One Poisson's ratio is related to another through their moduli:

$$\upsilon_{ij}/E_i = \upsilon_{ji}/E_j; \text{ where i or j = m, h, or z} \tag{6.14}$$

The recommended Hanford concrete Poisson's ratio values (Johnson et al. 2010) are assigned to υ_{mh}, υ_{zm}, and υ_{zh}, and the corresponding υ_{hm}, υ_{mz}, and υ_{hz} values are computed using Equation (6.14). This order of Poisson's ratio dependence was chosen because of the differences in the meridional, hoop, or through-wall moduli. If this process is reversed, some sections would have physically unreasonable values for the ratios.

Finally, the three shear moduli are three additional independent material properties. The only restriction on the shear moduli is that they must be greater than zero. For isotropic materials, the shear modulus is related to Young's moduli and poisson's ratio by:

$$G = E/(2(1+\upsilon)) \tag{6.15}$$

Because of this, no guidance exists in the Structural Evaluation Criteria (Johnson et al. 2010) as to what the orthotropic shear moduli should be. Chen and Saleeb (1994) detail an approximation for the in-plane shear moduli of an orthotropic material for plane stress under monotonic loading. This approximation is generalized for the three dimensional case here as:

$$G_{ij} = \frac{E_i E_j}{E_i + E_j + 2\sqrt{\upsilon_{ij}\upsilon_{ji}E_i E_j}}; \text{ where i or j = m, h, or z} \tag{6.16}$$

In the case where the concrete is isotropic, then Equation (6.16) reduces to the isotropic formula of Equation (6.15).

6.3.1.3 Seismic Modeling Orthotropic Concrete Properties

Orthotropic concrete properties discussed above were used in seismic modeling. Since there is no significant post-construction seismic event experienced by the SSTs, the earthquake is assumed to occur at present day or in the future. The tank concrete properties for the seismic analysis include the effects of thermal and operating loads. Thus, the thermal degraded cracked section concrete properties as determined in the TOLA model analysis are used in the seismic analysis. In addition, concrete damping properties are applied for the dynamic seismic analysis.

ANSYS® uses Rayleigh damping in which the critical damping is given by

$$\varsigma = \alpha/2\omega + \beta\omega/2 \tag{6.17}$$

where ς is the % critical damping = 7% for concrete (ASCE 4-98) and $\omega = 2\pi f$, where f is the frequency. That is, critical damping (ς) is a function of alpha (α) and beta (β) damping. Alpha damping and beta damping are used to define Rayleigh damping constants α and β. Alpha damping is based on mass, while beta damping is based on stiffness. Alpha damping is a global option for the model, and has already been set by the soil column damping requirements. Beta damping is applied at the material property level.

The concrete tank is in contact with the soil at all points and as such closely follows the displacement of the soil. The only independent modes experienced by the tank will be a diaphragm action in the dome. Thus, the beta damping value is calibrated to produce 7% critical damping when combined with the existing alpha damping.

The alpha, beta, and critical damping ratios are shown in Figure 6.25. As shown graphically in the figure, the critical damping ratio (Z) is 0.07 (7%) where it intersects with the tank dome primary response mode.

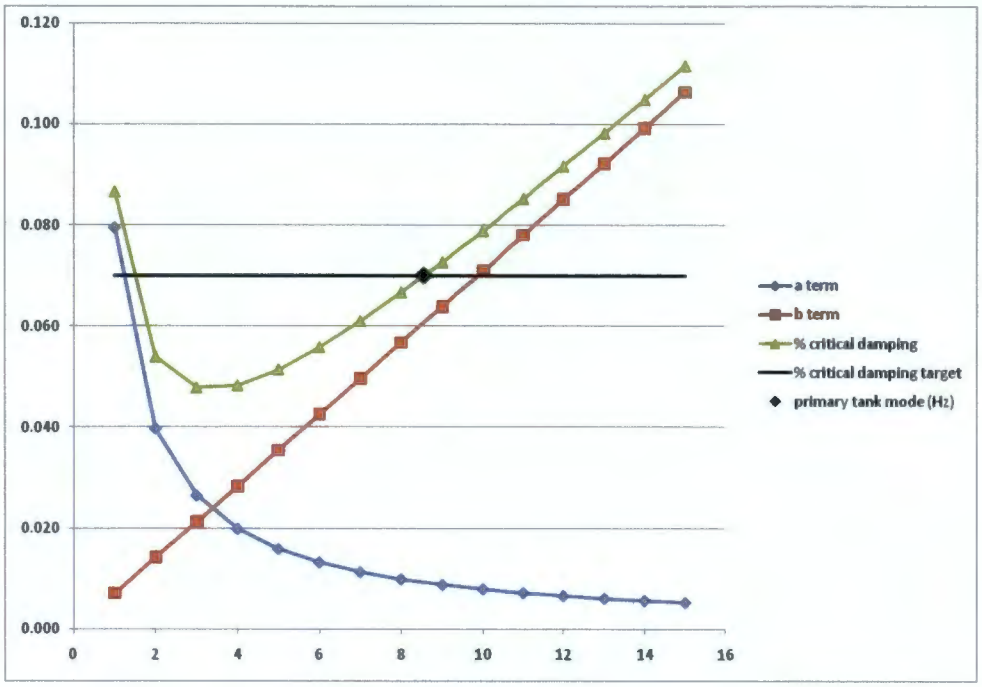

Frequency (Hz)

Figure 6.25. Concrete Tank Alpha and Beta Damping Ratios

The fundamental natural frequencies of the dome in response to vertical harmonic motion are 8.8 Hz from the best estimate soil, 6.7 Hz from the lower bound soil, and 10.2 Hz from the upper bound soil. The beta damping for the entire concrete tank is based on the average of the theese fundamental natural frequencies of the dome to be 8.6 Hz. Section 7.11 shows the details fo the vertical harmonic analysis and results. During final checking, the beta damping value for concrete was zero instead of the intended value, which adds more conservatism to the final results.

Orthotropic properties are applied in the modify.inp input file. The thickness is based on the properties in the meridional direction, and the Young's modulus in the hoop direction is adjusted to match the thickness. Table 6.11 provides orthotropic concrete section properties assuming all sections are cracked. Refer to Figure 6.7 for locations of the material numbers and ACI sections. The nomimal concrete density is 145 lb/ft^3. The concrete densities shown in the following table are adjusted values.

Table 6.11. Fully Cracked Orthotropic Concrete Properties

Concrete Material Number	Eshl Merid (EX) (psi)	Shell Thickness t-shl (in.)	Shell Density, Rho-shl (lb/in^3)	Eshl Hoop (EY) (using merid. thickness) (psi)	Ez (psi)	ν_{mh} (PRXY)	ν_{mz} (PRXZ)	ν_{hz} (PRYZ)	G_{mh} (GXY) estimate (psi)	G_{hz} (GYZ) estimate (psi)	G_{zm} (GXZ) estimate (psi)
100	8.81E+05	11.57	0.1088	8.81E+05	3.51E+06	0.15	0.04	0.04	3.83E+05	6.65E+05	6.65E+05
101	8.81E+05	11.57	0.1088	8.81E+05	3.51E+06	0.15	0.04	0.04	3.83E+05	6.65E+05	6.65E+05
102	8.81E+05	11.57	0.1088	8.81E+05	3.51E+06	0.15	0.04	0.04	3.83E+05	6.65E+05	6.65E+05
103	8.81E+05	11.57	0.1088	8.81E+05	3.51E+06	0.15	0.04	0.04	3.83E+05	6.65E+05	6.65E+05
104	8.81E+05	11.57	0.1088	8.81E+05	3.51E+06	0.15	0.04	0.04	3.83E+05	6.65E+05	6.65E+05
105	8.81E+05	11.57	0.1088	8.81E+05	3.51E+06	0.15	0.04	0.04	3.83E+05	6.65E+05	6.65E+05
106	8.81E+05	11.57	0.1088	8.81E+05	3.51E+06	0.15	0.04	0.04	3.83E+05	6.65E+05	6.65E+05
107	9.06E+05	12.46	0.1010	8.32E+05	3.51E+06	0.15	0.04	0.04	3.79E+05	6.36E+05	6.79E+05
108	8.75E+05	12.28	0.1025	8.44E+05	3.51E+06	0.15	0.04	0.04	3.74E+05	6.43E+05	6.61E+05
109	8.45E+05	12.10	0.1041	8.57E+05	3.51E+06	0.15	0.04	0.04	3.70E+05	6.50E+05	6.44E+05
110	8.17E+05	11.92	0.1057	8.70E+05	3.51E+06	0.15	0.03	0.04	3.65E+05	6.58E+05	6.27E+05
111	7.96E+05	11.77	0.1070	8.81E+05	3.51E+06	0.15	0.03	0.04	3.61E+05	6.64E+05	6.15E+05
112	9.98E+05	12.94	0.0973	8.01E+05	3.51E+06	0.15	0.04	0.03	3.92E+05	6.18E+05	7.29E+05
113	9.71E+05	12.81	0.0983	8.09E+05	3.51E+06	0.15	0.04	0.03	3.88E+05	6.23E+05	7.14E+05
114	9.50E+05	12.72	0.0991	8.15E+05	3.51E+06	0.15	0.04	0.03	3.85E+05	6.26E+05	7.03E+05
115	9.35E+05	12.64	0.0998	8.20E+05	3.51E+06	0.15	0.04	0.04	3.83E+05	6.29E+05	6.94E+05
116	9.23E+05	12.58	0.1003	8.24E+05	3.51E+06	0.15	0.04	0.04	3.81E+05	6.32E+05	6.88E+05
117	9.06E+05	12.50	0.1010	8.30E+05	3.51E+06	0.15	0.04	0.04	3.79E+05	6.35E+05	6.78E+05
118	8.88E+05	12.44	0.1018	8.35E+05	3.51E+06	0.15	0.04	0.04	3.76E+05	6.38E+05	6.68E+05
119	8.70E+05	12.39	0.1026	8.40E+05	3.51E+06	0.15	0.04	0.04	3.72E+05	6.41E+05	6.58E+05
120	8.52E+05	12.33	0.1034	8.45E+05	3.51E+06	0.15	0.04	0.04	3.69E+05	6.44E+05	6.48E+05
121	8.36E+05	12.32	0.1041	8.48E+05	3.51E+06	0.15	0.04	0.04	3.66E+05	6.46E+05	6.38E+05
122	8.20E+05	12.31	0.1049	8.52E+05	3.51E+06	0.15	0.04	0.04	3.62E+05	6.47E+05	6.29E+05
123	8.05E+05	12.30	0.1056	8.55E+05	3.51E+06	0.15	0.03	0.04	3.59E+05	6.49E+05	6.20E+05
124	1.02E+06	13.72	0.0956	7.70E+05	3.51E+06	0.15	0.04	0.03	3.89E+05	5.99E+05	7.40E+05
125	9.99E+05	13.77	0.0961	7.70E+05	3.51E+06	0.15	0.04	0.03	3.85E+05	5.99E+05	7.30E+05
126	9.79E+05	13.83	0.0966	7.70E+05	3.51E+06	0.15	0.04	0.03	3.81E+05	5.99E+05	7.19E+05
127	9.60E+05	13.92	0.0971	7.69E+05	3.51E+06	0.15	0.04	0.03	3.77E+05	5.99E+05	7.08E+05
128	9.42E+05	14.02	0.0975	7.68E+05	3.51E+06	0.15	0.04	0.03	3.73E+05	5.98E+05	6.98E+05
129	9.23E+05	14.12	0.0980	7.67E+05	3.51E+06	0.15	0.04	0.03	3.69E+05	5.97E+05	6.88E+05
130	9.03E+05	14.31	0.0985	7.63E+05	3.51E+06	0.15	0.04	0.03	3.64E+05	5.95E+05	6.77E+05
131	8.84E+05	14.51	0.0989	7.59E+05	3.51E+06	0.15	0.04	0.03	3.59E+05	5.93E+05	6.66E+05
132	8.65E+05	14.71	0.0994	8.47E+05	3.51E+06	0.15	0.04	0.04	3.73E+05	6.45E+05	6.55E+05
133	8.19E+05	14.05	0.1090	4.63E+05	3.51E+06	0.15	0.03	0.02	2.67E+05	3.95E+05	6.29E+05
134	7.91E+05	14.68	0.1090	4.43E+05	3.51E+06	0.15	0.03	0.02	2.56E+05	3.81E+05	6.12E+05
135	7.68E+05	15.24	0.1091	4.27E+05	3.51E+06	0.15	0.03	0.02	2.48E+05	3.69E+05	5.98E+05
136	9.00E+05	18.47	0.0957	3.73E+05	3.56E+06	0.15	0.04	0.02	2.42E+05	3.28E+05	6.77E+05
137	8.68E+05	19.58	0.0957	3.51E+05	3.56E+06	0.15	0.04	0.01	2.30E+05	3.11E+05	6.59E+05
138	8.36E+05	20.78	0.0958	4.52E+05	3.56E+06	0.15	0.04	0.02	2.65E+05	3.88E+05	6.40E+05
139	7.85E+05	23.42	0.0959	1.42E+06	3.56E+06	0.15	0.03	0.06	4.24E+05	9.36E+05	6.10E+05
140	7.48E+05	25.67	0.0963	1.41E+06	3.56E+06	0.15	0.03	0.06	4.09E+05	9.30E+05	5.88E+05
141	7.12E+05	28.29	0.0971	1.40E+06	3.56E+06	0.15	0.03	0.06	3.93E+05	9.25E+05	5.65E+05
142	6.82E+05	31.09	0.0978	1.39E+06	3.56E+06	0.15	0.03	0.06	3.81E+05	9.22E+05	5.46E+05
143	6.90E+05	30.20	0.0970	1.41E+06	3.56E+06	0.15	0.03	0.06	3.86E+05	9.30E+05	5.51E+05
144	7.86E+05	22.32	0.0959	1.47E+06	3.56E+06	0.15	0.03	0.06	4.28E+05	9.55E+05	6.10E+05
145	7.37E+05	15.60	0.1095	1.75E+06	3.56E+06	0.15	0.03	0.07	4.28E+05	1.07E+06	5.81E+05
146	7.74E+05	14.17	0.1101	2.16E+06	3.56E+06	0.15	0.03	0.09	4.67E+05	1.21E+06	6.03E+05
200	8.25E+05	12.66	0.1114	1.38E+06	3.56E+06	0.15	0.03	0.06	4.35E+05	9.18E+05	6.34E+05
201	8.85E+05	11.12	0.1132	5.79E+05	3.56E+06	0.15	0.04	0.02	3.13E+05	4.78E+05	6.69E+05
202	8.85E+05	11.12	0.1132	5.79E+05	3.56E+06	0.15	0.04	0.02	3.13E+05	4.78E+05	6.69E+05
203	8.85E+05	11.12	0.1132	5.79E+05	3.56E+06	0.15	0.04	0.02	3.13E+05	4.78E+05	6.69E+05
204	8.78E+05	11.14	0.1129	5.78E+05	3.51E+06	0.15	0.04	0.02	3.11E+05	4.76E+05	6.62E+05

Table 6.11. (contd)

Concrete Material Number	Eshl Merid (EX) (psi)	Shell Thickness t-shl (in.)	Shell Density, Rho-shl (lb/in^3)	Eshl Hoop (EY) (using merid. thickness) (psi)	Ez (psi)	ν_{mh} (PRXY)	ν_{mz} (PRXZ)	ν_{hz} (PRYZ)	G_{mh} (GXY) estimate (psi)	G_{hz} (GYZ) estimate (psi)	G_{zm} (GXZ) estimate (psi)
205	8.81E+05	12.02	0.1047	2.95E+05	3.51E+06	0.15	0.04	0.01	2.05E+05	2.66E+05	6.64E+05
206	8.74E+05	12.05	0.1045	1.08E+06	3.47E+06	0.15	0.04	0.05	4.14E+05	7.68E+05	6.58E+05
207	8.74E+05	12.05	0.1045	1.08E+06	3.47E+06	0.15	0.04	0.05	4.14E+05	7.68E+05	6.58E+05
208	8.74E+05	12.05	0.1045	1.08E+06	3.47E+06	0.15	0.04	0.05	4.14E+05	7.68E+05	6.58E+05
209	8.67E+05	12.07	0.1043	1.07E+06	3.42E+06	0.15	0.04	0.05	4.11E+05	7.61E+05	6.52E+05
210	8.67E+05	12.07	0.1043	1.07E+06	3.42E+06	0.15	0.04	0.05	4.11E+05	7.61E+05	6.52E+05
211	8.67E+05	12.07	0.1043	1.07E+06	3.42E+06	0.15	0.04	0.05	4.11E+05	7.61E+05	6.52E+05
212	8.60E+05	12.09	0.1041	1.06E+06	3.38E+06	0.15	0.04	0.05	4.08E+05	7.54E+05	6.46E+05
213	8.60E+05	12.09	0.1041	1.12E+06	3.38E+06	0.15	0.04	0.05	4.16E+05	7.85E+05	6.46E+05
214	8.60E+05	12.09	0.1041	1.12E+06	3.38E+06	0.15	0.04	0.05	4.16E+05	7.85E+05	6.46E+05
215	8.60E+05	12.09	0.1041	1.12E+06	3.38E+06	0.15	0.04	0.05	4.16E+05	7.85E+05	6.46E+05
216	8.53E+05	12.12	0.1039	1.19E+06	3.34E+06	0.15	0.04	0.05	4.23E+05	8.13E+05	6.40E+05
217	8.53E+05	12.12	0.1039	1.22E+06	3.34E+06	0.15	0.04	0.05	4.26E+05	8.25E+05	6.40E+05
218	8.53E+05	12.12	0.1039	1.31E+06	3.34E+06	0.15	0.04	0.06	4.37E+05	8.67E+05	6.40E+05
219	8.53E+05	12.12	0.1039	1.31E+06	3.34E+06	0.15	0.04	0.06	4.37E+05	8.67E+05	6.40E+05
220	8.53E+05	12.12	0.1039	1.31E+06	3.34E+06	0.15	0.04	0.06	4.37E+05	8.67E+05	6.40E+05
221	8.53E+05	12.12	0.1039	1.43E+06	3.34E+06	0.15	0.04	0.06	4.49E+05	9.17E+05	6.40E+05
222	8.47E+05	12.14	0.1037	1.41E+06	3.30E+06	0.15	0.04	0.06	4.46E+05	9.08E+05	6.35E+05
223	8.47E+05	12.14	0.1037	1.51E+06	3.30E+06	0.15	0.04	0.07	4.55E+05	9.48E+05	6.35E+05
224	8.47E+05	12.14	0.1037	1.51E+06	3.30E+06	0.15	0.04	0.07	4.55E+05	9.48E+05	6.35E+05
225	8.32E+05	11.53	0.1114	1.61E+06	3.30E+06	0.15	0.04	0.07	4.58E+05	9.84E+05	6.27E+05
226	8.40E+05	11.73	0.1120	6.57E+05	3.26E+06	0.15	0.04	0.03	3.26E+05	5.21E+05	6.29E+05
227	8.34E+05	11.97	0.1118	6.44E+05	3.22E+06	0.15	0.04	0.03	3.22E+05	5.11E+05	6.24E+05
228	7.84E+05	16.40	0.1093	4.70E+05	3.22E+06	0.15	0.04	0.02	2.64E+05	3.95E+05	5.95E+05
229	7.10E+05	22.02	0.1062	3.50E+05	3.22E+06	0.15	0.03	0.02	2.13E+05	3.07E+05	5.52E+05
230	7.10E+05	22.02	0.1062	3.50E+05	3.22E+06	0.15	0.03	0.02	2.13E+05	3.07E+05	5.52E+05
231	7.10E+05	22.02	0.1062	3.50E+05	3.22E+06	0.15	0.03	0.02	2.13E+05	3.07E+05	5.52E+05
300	6.24E+05	28.61	0.1056	2.34E+05	3.65E+06	0.15	0.03	0.01	1.57E+05	2.16E+05	5.11E+05
301	6.24E+05	28.61	0.1056	2.34E+05	3.65E+06	0.15	0.03	0.01	1.57E+05	2.16E+05	5.11E+05
302	6.07E+05	28.83	0.1048	2.32E+05	3.51E+06	0.15	0.03	0.01	1.55E+05	2.14E+05	4.96E+05
303	5.92E+05	29.04	0.1040	2.30E+05	3.38E+06	0.15	0.03	0.01	1.53E+05	2.12E+05	4.82E+05
304	4.63E+05	15.30	0.1263	3.15E+04	3.22E+06	0.15	0.02	0.00	2.89E+04	3.11E+04	3.90E+05
305	4.82E+05	13.78	0.1264	3.50E+04	3.22E+06	0.15	0.02	0.00	3.19E+04	3.45E+04	4.03E+05
306	7.24E+05	4.83	0.3371	1.29E+06	3.18E+06	0.15	0.03	0.06	3.89E+05	8.43E+05	5.59E+05
307	7.18E+05	4.84	0.3028	1.19E+06	3.14E+06	0.15	0.03	0.06	3.77E+05	7.96E+05	5.54E+05
308	5.31E+05	10.24	0.1284	4.70E+04	3.14E+06	0.15	0.03	0.00	4.22E+04	4.61E+04	4.36E+05
309	7.13E+05	4.85	0.2427	9.94E+04	3.10E+06	0.15	0.03	0.00	8.41E+04	9.54E+04	5.49E+05
310	5.86E+05	7.85	0.1340	6.14E+04	3.10E+06	0.15	0.03	0.00	5.40E+04	5.99E+04	4.70E+05
311	6.17E+05	6.76	0.1388	7.12E+04	3.07E+06	0.15	0.03	0.00	6.19E+04	6.91E+04	4.89E+05
312	6.54E+05	5.76	0.1457	8.37E+04	3.03E+06	0.15	0.03	0.00	7.17E+04	8.08E+04	5.11E+05
313	7.04E+05	4.83	0.1557	9.98E+04	3.03E+06	0.15	0.03	0.00	8.43E+04	9.57E+04	5.41E+05
314	7.58E+05	4.00	0.1692	1.20E+05	3.00E+06	0.15	0.04	0.01	9.98E+04	1.14E+05	5.70E+05
315	8.22E+05	3.27	0.1878	1.47E+05	2.96E+06	0.15	0.04	0.01	1.19E+05	1.38E+05	6.04E+05
316	6.91E+05	4.88	0.1156	9.87E+04	2.96E+06	0.15	0.04	0.00	8.32E+04	9.46E+04	5.30E+05
317	6.86E+05	4.89	0.1079	3.77E+05	2.93E+06	0.15	0.04	0.02	2.20E+05	3.23E+05	5.26E+05
318	6.86E+05	4.89	0.1041	3.46E+05	2.93E+06	0.15	0.04	0.02	2.09E+05	3.00E+05	5.26E+05

6.3.2 Waste

All analyses that include waste are run with a waste height of 20.3 ft, which represents the maximum depth of waste in any Type III SST (tank TX-113) per App. H of Weber (2009). Waste shear modulus data, with relevance to Hanford waste, are summarized in Appendix N of Rinker et al. (2011a). The consideration of both an empty and a "full" tank is considered bounding. The waste is modeled using SOLID45 solid elements. The material properties are as follows in Table 6.12:

Specific gravity of 1.94[4]

Poisson's ratio of 0.49, which is consistent with undrained saturated clays/silts/sediments

No additional damping beyond the global mass-proportional damping is applied to the waste. Figure 6.26 shows the waste elements.

Waste with Low Shear Stiffness (LSS):

G_{low}=50,000 Pa=1.04 kip/ft^2 (soft waste)
E_{low}1.49 × 10^5 Pa=3.1 kip/ft^2

Waste with High Shear Stiffness (HSS):

G_{high}=7,000 kPa=146 kip/ft^2 (stiff waste)
E_{high}=20.9 × 10^6 Pa=436 kip/ft^2

Table 6.12. Seismic Model Waste Properties

Waste	Specific Gravity[1]	Poisson's Ratio	G	E
Low Shear Stiffness (LSS)	1.94	0.49	1.04 kip/ft^2	3.1 kip/ft^2
High Shear Stiffness (HSS)	1.94	0.49	146 kip/ft^2	436 kip/ft^2

Note:
1. Mean plus standard deviation of non-convective waste density for bounding Type III tank BY-105 per Appendix H of Weber (2009).

[4] Mean plus standard deviation of non-convective waste density for bounding Type III tank BY-105 per Appendix H of Weber (2009).

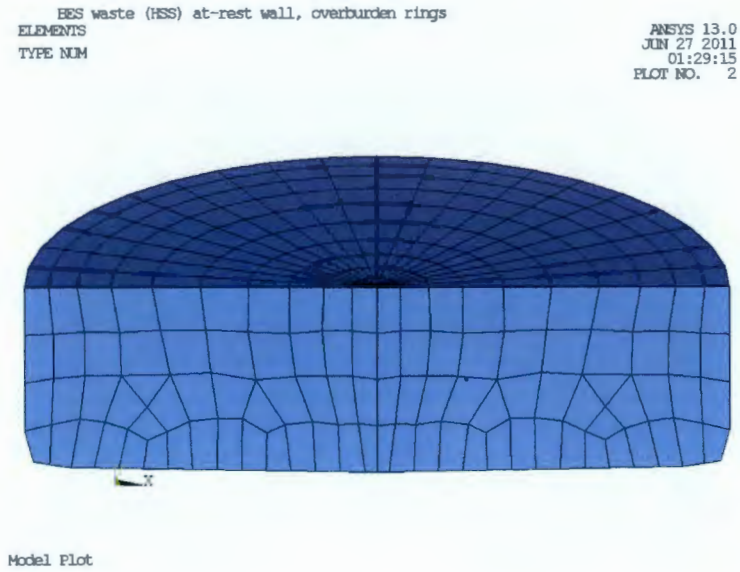

Figure 6.26. Seismic Model Detail – Element Plot of Waste

6.3.3 Soil Model

The soil surrounding the tank is modeled in two groups, the excavated backfill soil and the far-field soil. The backfill soil fills the near volume surrounding the concrete tank and is bounded by the slope matching the soil removed during construction. The far-field soil comprises all other soil out to a radius of 320 ft. Both regions are modeled using SOLID45 elements, which is an eight-node element with three translational degrees-of-freedom at each node.

Three sets of soil properties are considered:

- Lower Bound Soil (LBS)
- Best Estimate Soil (BES)
- Upper Bound Soil (UBS)

The properties for the two soil subcomponents are used consistently, so that the BES native soil is used with the BES backfill, etc.

Each set of soil properties has different layering, maximum depth, and material properties. To simplify model configuration control, the specific properties and layering are maintained in an input file (SOIL_properties.inp) separate from the remainder of the soil modeling inputs. Thus, the file containing parameters that differ between the soil property sets can be modified independently of other input files. In all configurations, the soil mesh is designed to transition to a coarser mesh away from regions of interest, in order to minimize the amount of elements. The excavated backfill soil uses the same layering as the native soil, except near the dome apex where layers are combined to prevent poor element aspect ratios at the tangent of the dome curve and the horizontal layer division. Appendix C includes a comparison of tank demands from the Type III seismic baseline model to the tank demands of the Type III seismic extended backfill model.

6.3.4 Soil Properties

Far-field soil properties are provided by AMEC Geomatrix and documented in the *Development of Inputs for SSI Analyses of SSTs*, Rev. 0 in Appendix R of Rinker et al. (2011a). The dynamic materials model uses the linear elastic relationship and the shear and compression wave velocities as constants for each soil layer. Backfill soil properties are provided in Appendices O and P in Rinker et al. (2011a). The soil properties used in the models are summarized in the following tables:

- Table 6.13. Lower Bound Excavated Backfill Soil Properties
- Table 6.14. Strain Compatible Lower Bound Native Soil Properties
- Table 6.15. Best Estimate Excavated Backfill Soil Properties
- Table 6.16. Strain Compatible Best Estimate Native Soil Properties
- Table 6.17. Upper Bound Excavated Backfill Soil Properties
- Table 6.18. Strain Compatible Upper Bound Native Soil Properties

Table 6.13. Lower Bound Excavated Backfill Soil Properties

Elevation (ft)	Damping (in Decimal)	Unit Weight (kip/ft^3)	Strain-Compatible Vs (ft/sec)	Poisson's Ratio	Shear Modulus (kip/ft^2)	Modulus of Elasticity (kip/ft^2)	Material Property No.
-1	0.01540	0.129	560	0.28	1256	3216	501, 601
-2	0.02120	0.129	575	0.28	1325	3391	502, 602
-3	0.02830	0.129	590	0.28	1395	3570	503, 603
-4	0.03720	0.129	605	0.28	1466	3754	504, 604
-5	0.04340	0.129	620	0.28	1540	3942	505, 605
-6	0.04290	0.129	635	0.28	1615	4135	506, 606
-7	0.04300	0.129	650	0.28	1693	4333	507, 607
-8	0.04740	0.129	665	0.28	1772	4535	508, 608
-9	0.05090	0.129	680	0.28	1852	4742	509, 609
-10	0.04210	0.129	695	0.28	1935	4954	510, 610
-14	0.04350	0.1227	755	0.28	2172	5561	511, 611
-19	0.04620	0.1122	830	0.28	2400	6145	512, 612
-21	0.04960	0.108	860	0.28	2481	6350	613
-23	0.04990	0.108	880	0.28	2597	6649	614
-25	0.05520	0.108	900	0.28	2717	6955	615
-28	0.05600	0.108	930	0.28	2901	7426	616
-31	0.05710	0.108	960	0.28	3091	7913	617
-35	0.05360	0.108	1000	0.28	3354	8586	618
-37	0.06110	0.108	1020	0.28	3490	8933	619
-39	0.06140	0.108	1040	0.28	3628	9287	620
-40	0.05580	0.108	1050	0.28	3698	9466	621
-41	0.05580	0.108	1060	0.28	3769	9648	622
-42	0.05080	0.108	1070	0.28	3840	9830	623
-43	0.05080	0.108	1080	0.28	3912	10015	624
-45	0.05080	0.108	1100	0.28	4058	10389	625
-48	0.05180	0.108	1130	0.28	4283	10964	626

Table 6.14. Strain Compatible Lower Bound Native Soil Properties

Elevation (ft)	Damping (in Decimal)	Unit Weight (kip/ft^3)	Strain-Compatible Vs (ft/sec)	Vp (ft/sec)	Poisson's Ratio	Shear Modulus (kip/ft^2)	Modulus of Elasticity (kip/ft^2)	Material Property No.
-1	0.01540	0.106	438	1047.6	0.39	632	1761	700
-2	0.02120	0.106	438	1047.6	0.39	632	1761	701
-3	0.02830	0.106	438	1047.6	0.39	632	1761	702
-4	0.03720	0.106	438	1047.6	0.39	632	1761	703
-5	0.04340	0.106	438	1047.6	0.39	632	1761	704
-6	0.04290	0.106	540	1047.6	0.32	960	2532	705
-7	0.04300	0.106	540	1047.6	0.32	960	2532	706
-8	0.04740	0.106	540	1047.6	0.32	960	2532	707
-9	0.05090	0.106	540	1047.6	0.32	960	2532	708
-10	0.04210	0.106	680	1099.0	0.19	1522	3622	709
-14	0.04350	0.106	680	1099.2	0.19	1522	3623	710
-19	0.04620	0.106	787	2027.4	0.41	2039	5755	711
-21	0.04960	0.106	815	2027.4	0.40	2187	6138	712
-23	0.04990	0.106	860	2027.4	0.39	2435	6770	713
-25	0.05520	0.106	860	2027.4	0.39	2435	6770	714
-28	0.05600	0.106	860	2027.4	0.39	2435	6770	715
-31	0.05710	0.106	900	2313.1	0.41	2666	7524	716
-35	0.05360	0.106	970	2313.1	0.39	3097	8631	717
-37	0.06110	0.106	970	2313.1	0.39	3097	8631	718
-39	0.06140	0.106	970	2313.1	0.39	3097	8631	719
-40	0.05580	0.106	1047	2313.1	0.37	3609	9896	720
-41	0.05580	0.106	1047	2313.1	0.37	3609	9896	721
-42	0.05080	0.106	1089	2313.1	0.36	3904	10600	722
-43	0.05080	0.106	1089	2313.1	0.36	3904	10600	723
-45	0.05080	0.106	1089	2313.1	0.36	3904	10600	724
-48	0.05180	0.106	1089	2313.1	0.36	3904	10600	725
-49	0.05170	0.106	1089	2313.1	0.36	3904	10600	726
-50	0.05170	0.106	1089	2313.1	0.36	3904	10600	727
-54	0.04990	0.106	1089	2313.1	0.36	3904	10600	728
-55	0.05210	0.106	1190	2313.1	0.32	4662	12307	729
-57	0.05210	0.106	1190	2313.1	0.32	4662	12307	730
-59	0.05210	0.106	1190	2313.1	0.32	4662	12307	731
-63	0.05250	0.106	1210	2313.1	0.31	4820	12643	732
-71	0.05650	0.106	1210	2313.1	0.31	4820	12643	733
-82	0.05580	0.106	1210	2313.1	0.31	4820	12643	734
-94	0.06140	0.106	1210	2313.1	0.31	4820	12643	735
-120	0.06430	0.106	1210	2313.1	0.31	4820	12643	736
-160	0.06490	0.106	1210	2313.1	0.31	4820	12643	737
-205	0.08060	0.106	1149	2313.1	0.34	4346	11614	738
-215	0.08060	0.127	1210	2313.1	0.31	5775	15148	739
-225	0.07500	0.127	1210	2313.1	0.31	5775	15148	740
-235	0.07500	0.127	1210	2313.1	0.31	5775	15148	741
-285	0.08320	0.127	1210	2313.1	0.31	5775	15148	742
-295	0.06580	0.135	1560	3470.1	0.37	10203	28025	743
-315	0.06570	0.135	1560	3470.1	0.37	10203	28025	744
-335	0.07030	0.135	1560	3470.1	0.37	10203	28025	745
-355	0.08130	0.135	1400	3470.1	0.40	8217	23055	746
-380	0.05510	0.135	1580	3470.1	0.37	10466	28662	747
-405	0.05880	0.135	1580	3470.1	0.37	10466	28662	748

Table 6.15. Best Estimate Excavated Backfill Soil Properties

Elevation (ft)	Damping (in Decimal)	Unit Weight (kip/ft^3)	Strain-Compatible Vs (ft/sec)	Poisson's Ratio	Shear Modulus (kip/ft^2)	Modulus of Elasticity (kip/ft^2)	Material Property No.
-1	0.01143	0.129	750	0.28	2253	5769	501, 601
-2	0.01525	0.129	770	0.28	2375	6081	502, 602
-3	0.01960	0.129	790	0.28	2500	6401	503, 603
-4	0.02230	0.129	810	0.28	2628	6729	504, 604
-5	0.02435	0.129	830	0.28	2760	7065	505, 605
-6	0.02973	0.129	850	0.28	2894	7410	506, 606
-7	0.02848	0.129	870	0.28	3032	7763	507, 607
-8	0.03235	0.129	890	0.28	3173	8124	508, 608
-9	0.03073	0.129	910	0.28	3318	8493	509, 609
-10	0.02903	0.129	930	0.28	3465	8870	510, 610
-14	0.035750	0.1227	1010	0.28	3887	9951	511, 611
-19	0.035950	0.1122	1110	0.28	4293	10991	512, 612
-21	0.036980	0.108	1150	0.28	4436	11355	613
-23	0.037950	0.108	1177	0.28	4644	11888	614
-25	0.037800	0.108	1203	0.28	4857	12433	615
-28	0.040450	0.108	1243	0.28	5185	13273	616
-31	0.040680	0.108	1283	0.28	5524	14141	617
-35	0.034850	0.108	1337	0.28	5993	15341	618
-37	0.034850	0.108	1363	0.28	6234	15959	619
-39	0.035150	0.108	1390	0.28	6480	16590	620
-40	0.035150	0.108	1403	0.28	6605	16909	621
-41	0.035480	0.108	1417	0.28	6731	17232	622
-43	0.035150	0.108	1443	0.28	6987	17887	623
-45	0.035150	0.108	1470	0.28	7248	18554	624
-48	0.035480	0.108	1510	0.28	7648	19578	625

Table 6.16. Strain Compatible Best Estimate Native Soil Properties

Elevation (ft)	Damping (in Decimal)	Unit Weight (kip/ft^3)	Strain-Compatible Vs (ft/sec)	Vp (ft/sec)	Poisson's Ratio	Shear Modulus (kip/ft^2)	Modulus of Elasticity (kip/ft^2)	Material Property No.
-1	0.011430	0.106	710	1283.3	0.28	1659	4246	700
-2	0.015250	0.106	710	1283.3	0.28	1659	4246	701
-3	0.019600	0.106	710	1283.3	0.28	1659	4246	702
-4	0.022300	0.106	720	1283.3	0.27	1707	4336	703
-5	0.024350	0.106	720	1283.3	0.27	1707	4336	704
-6	0.029730	0.106	720	1283.3	0.27	1707	4336	705
-7	0.028480	0.106	775	1283.3	0.21	1977	4797	706
-8	0.032350	0.106	775	1283.3	0.21	1977	4797	707
-9	0.030730	0.106	775	1283.3	0.21	1977	4797	708
-10	0.029030	0.106	987	1595.0	0.19	3207	7631	709
-14	0.030100	0.106	987	1595.0	0.19	3207	7631	710
-19	0.031750	0.106	1086	1755.0	0.19	3882	9238	711
-21	0.034500	0.106	1158	2483.3	0.36	4414	12016	712
-23	0.035750	0.106	1158	2483.3	0.36	4414	12016	713
-25	0.035950	0.106	1158	2483.3	0.36	4414	12016	714
-28	0.036980	0.106	1158	2483.3	0.36	4414	12016	715
-31	0.037950	0.106	1280	2833.3	0.37	5393	14797	716
-35	0.037800	0.106	1280	2833.3	0.37	5393	14797	717
-37	0.040450	0.106	1280	2833.3	0.37	5393	14797	718
-39	0.040680	0.106	1280	2833.3	0.37	5393	14797	719
-40	0.034850	0.106	1344	2833.3	0.35	5946	16112	720
-41	0.034850	0.106	1344	2833.3	0.35	5946	16112	721
-43	0.035150	0.106	1383	2833.3	0.34	6296	16920	722
-45	0.035150	0.106	1383	2833.3	0.34	6296	16920	723
-48	0.035480	0.106	1416	2833.3	0.33	6600	17604	724
-49	0.033130	0.106	1526	2833.3	0.30	7666	19865	725
-50	0.033130	0.106	1526	2833.3	0.30	7666	19865	726
-55	0.034100	0.106	1526	2833.3	0.30	7666	19865	727
-57	0.034450	0.106	1526	2833.3	0.30	7666	19865	728
-59	0.034450	0.106	1526	2833.3	0.30	7666	19865	729
-62	0.035900	0.106	1526	2833.3	0.30	7666	19865	730
-70	0.037880	0.106	1526	2833.3	0.30	7666	19865	731
-82	0.040400	0.106	1526	2833.3	0.30	7666	19865	732
-94	0.041930	0.106	1526	2833.3	0.30	7666	19865	733
-104	0.032480	0.106	1780	2877.0	0.19	10430	24822	734
-123	0.034250	0.106	1780	4816.7	0.42	10430	29641	735
-143	0.028330	0.106	2424	4816.7	0.33	19343	51468	736
-158	0.018450	0.135	2638	4816.7	0.29	29176	75027	737
-173	0.019100	0.135	2638	4935.2	0.30	29176	75858	738
-192	0.020000	0.135	2638	4935.2	0.30	29176	75858	739
-213	0.020700	0.135	2638	4935.2	0.30	29176	75858	740
-233	0.008130	0.156	3350	6267.3	0.30	54370	141362	741
-263	0.008150	0.156	3350	6267.3	0.30	54370	141362	742
-303	0.008450	0.156	3350	6267.3	0.30	54370	141362	743

Table 6.17. Upper Bound Excavated Backfill Soil Properties

Elevation (ft)	Damping (in Decimal)	Unit Weight (kip/ft^3)	Strain-Compatible Vs (ft/sec)	Poisson's Ratio	Shear Modulus (kip/ft^2)	Modulus of Elasticity (kip/ft^2)	Material Property No.
-1	0.008700	0.129	960	0.28	3692	9451	501, 601
-2	0.010200	0.129	988	0.28	3910	10011	502, 602
-3	0.012200	0.129	1016	0.28	4135	10586	503, 603
-4	0.015200	0.129	1044	0.28	4366	11178	504, 604
-5	0.016400	0.129	1072	0.28	4603	11785	505, 605
-6	0.017700	0.129	1100	0.28	4847	12409	506, 606
-7	0.018300	0.129	1128	0.28	5097	13049	507, 607
-8	0.016300	0.129	1156	0.28	5353	13705	508, 608
-9	0.017700	0.129	1184	0.28	5616	14377	509, 609
-10	0.016400	0.129	1212	0.28	5884	15065	510, 610
-14	0.019500	0.1227	1324	0.28	6679	17100	511, 611
-19	0.019500	0.1122	1464	0.28	7468	19118	512, 612
-21	0.020400	0.108	1520	0.28	7749	19837	613
-23	0.022700	0.108	1558	0.28	8141	20842	614
-25	0.021000	0.108	1596	0.28	8543	21871	615
-28	0.022900	0.108	1653	0.28	9164	23461	616
-31	0.020400	0.108	1710	0.28	9807	25107	617
-35	0.021700	0.108	1786	0.28	10698	27388	618
-37	0.024400	0.108	1824	0.28	11158	28566	619
-39	0.026400	0.108	1862	0.28	11628	29769	620
-40	0.021200	0.108	1881	0.28	11867	30379	621
-41	0.021200	0.108	1900	0.28	12108	30997	622
-43	0.019800	0.108	1938	0.28	12597	32249	623
-45	0.019800	0.108	1976	0.28	13096	33526	624
-48	0.021900	0.108	2033	0.28	13863	35488	625

Table 6.18. Strain Compatible Upper Bound Native Soil Properties

Elevation (ft)	Damping (in Decimal)	Unit Weight (kip/ft^3)	Strain-Compatible Vs (ft/sec)	Vp (ft/sec)	Poisson's Ratio	Shear Modulus (kip/ft^2)	Modulus of Elasticity (kip/ft^2)	Material Property No.
-1	0.008700	0.106	1089	1760.3	0.19	3904	9291	700
-2	0.010200	0.106	1089	1760.3	0.19	3904	9291	701
-3	0.012200	0.106	1089	1760.3	0.19	3904	9291	702
-4	0.015200	0.106	1089	1760.3	0.19	3904	9291	703
-5	0.016400	0.106	1089	1760.3	0.19	3904	9291	704
-6	0.017700	0.106	1089	1760.3	0.19	3904	9291	705
-7	0.018300	0.106	1089	1760.3	0.19	3904	9291	706
-8	0.016300	0.106	1280	2069.1	0.19	5393	12837	707
-9	0.017700	0.106	1280	2069.1	0.19	5393	12837	708
-10	0.016400	0.106	1280	2069.1	0.19	5393	12837	709
-14	0.019500	0.106	1379	2229.0	0.19	6260	14898	710
-19	0.020900	0.106	1423	3041.0	0.36	6666	18129	711
-21	0.020400	0.106	1423	3041.0	0.36	6666	18129	712
-23	0.022700	0.106	1520	3041.0	0.33	7606	20284	713
-25	0.021000	0.106	1520	3041.0	0.33	7606	20284	714
-28	0.022900	0.106	1630	3041.0	0.30	8746	22713	715
-31	0.020400	0.106	1732	3041.0	0.26	9875	24884	716
-35	0.021700	0.106	1732	3469.7	0.33	9875	26348	717
-37	0.024400	0.106	1732	3469.7	0.33	9875	26348	718
-39	0.026400	0.106	1732	3469.7	0.33	9875	26348	719
-40	0.021200	0.106	1732	3469.7	0.33	9875	26348	720
-41	0.021200	0.106	1732	3469.7	0.33	9875	26348	721
-43	0.019800	0.106	1732	3469.7	0.33	9875	26348	722
-45	0.019800	0.106	1732	3469.7	0.33	9875	26348	723
-48	0.021900	0.106	1950	3469.7	0.27	12518	31774	724
-49	0.022300	0.106	1950	3469.7	0.27	12518	31774	725
-50	0.022300	0.106	1950	3469.7	0.27	12518	31774	726
-55	0.020400	0.106	1950	3469.7	0.27	12518	31774	727
-57	0.021100	0.106	1950	3469.7	0.27	12518	31774	728
-59	0.021100	0.106	1950	3469.7	0.27	12518	31774	729
-62	0.023800	0.106	1950	3469.7	0.27	12518	31774	730
-70	0.023800	0.106	1950	3469.7	0.27	12518	31774	731
-82	0.025400	0.106	1950	3469.7	0.27	12518	31774	732
-94	0.027400	0.106	1950	3469.7	0.27	12518	31774	733
-99	0.015900	0.135	2351	5899.6	0.41	23173	65144	734
-104	0.015900	0.135	2351	5899.6	0.41	23173	65144	735
-113	0.016900	0.135	2351	5899.6	0.41	23173	65144	736
-123	0.016900	0.135	2351	5899.6	0.41	23173	65144	737

6.3.5 Excavated Backfill Soil

The excavated backfill soil is subdivided into two subgroups – one for soil above the tank (overburden) and one for soil around the tank. The backfill soil portion of the soil is developed using the input files SOFO.inp and SOFA.inp. The input files contain geometry coordinates and uniform generic layering and material properties. Specific soil layering and material properties are found in input file SOIL_properties.inp. Figure 6.27 shows the excavated region of the backfill soil in the seismic model. Figures 6.28 through 6.30 show the excavated backfill soil material property assignments for the seismic model LBS, BES, and UBS, respectively.

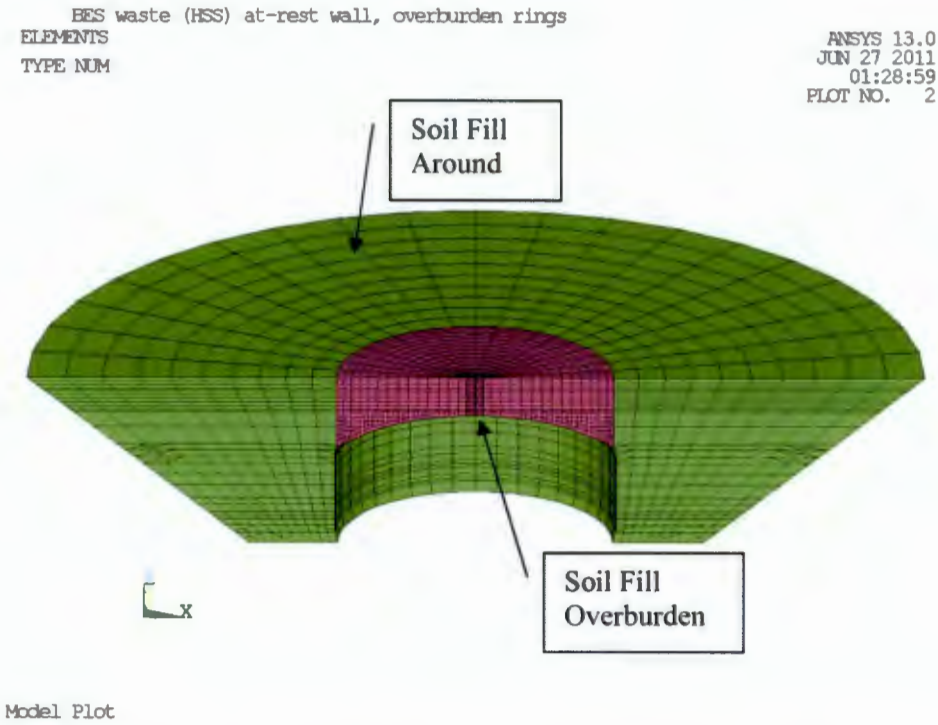

Figure 6.27. Seismic Model BES – Excavated Backfill Soil Detail

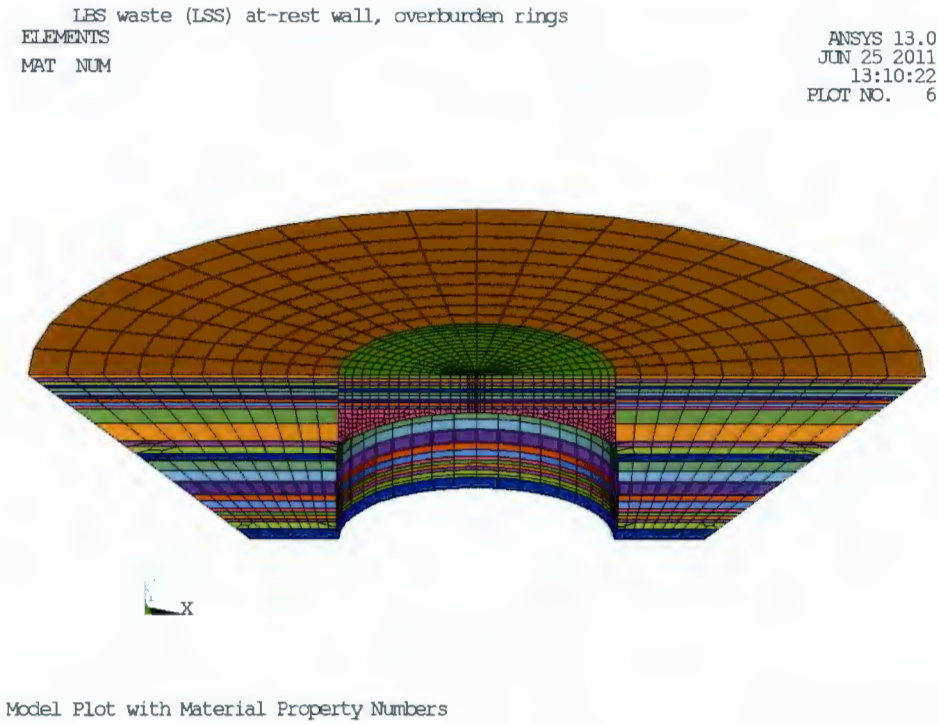

Figure 6.28. Seismic Model LBS Excavated Backfill Soil Material Property Assignment

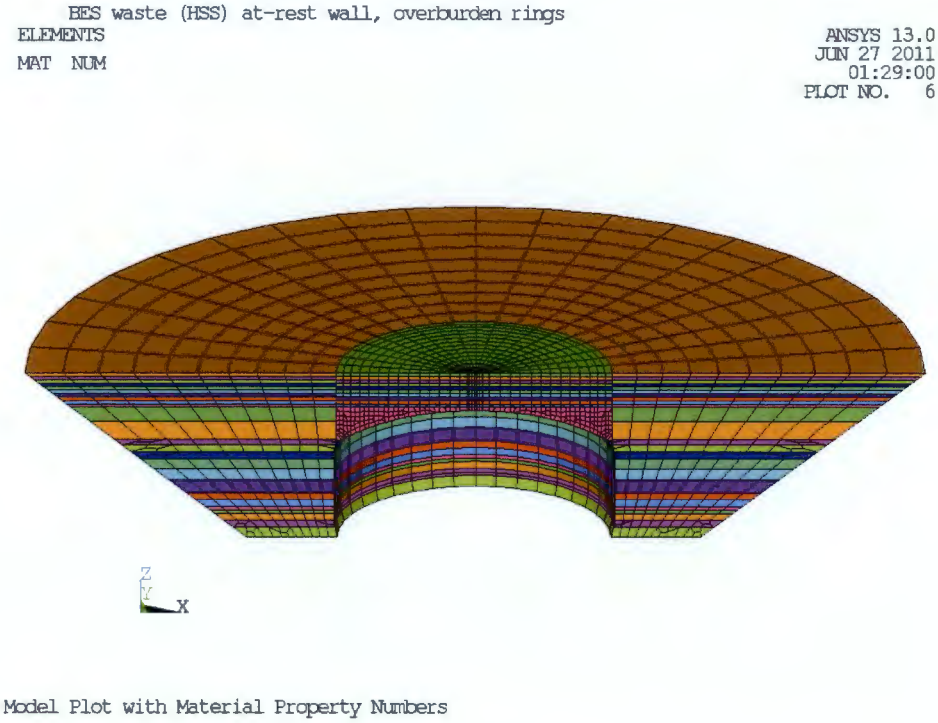

Figure 6.29. Seismic Model BES Excavated Backfill Soil Material Property Assignment

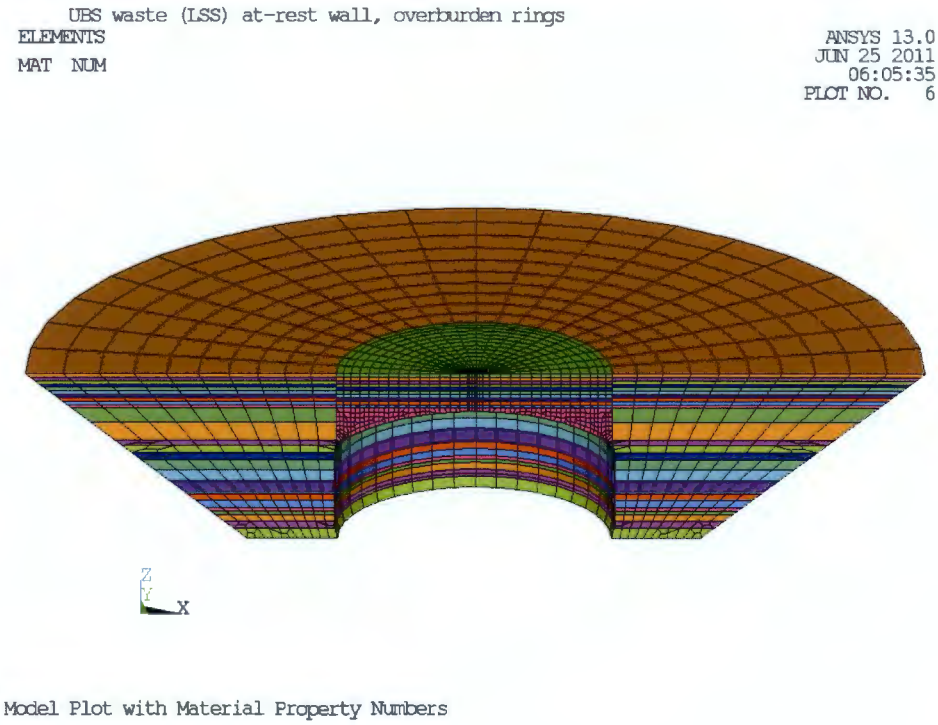

Figure 6.30. Seismic Model UBS Excavated Backfill Soil Material Property Assignment

6.3.6 Native Soil

The native ("undisturbed") soil region of the model is developed using input file SOUD.inp. The input file contains geometry coordinates and uniform generic layering and material properties. Specific soil layering and material properties are found in input file SOIL_properties.inp. SOLID45 elements are used and the material properties are discussed above. Figure 6.31 through Figure 6.33 show the soil layering in the native soil portion of the model.

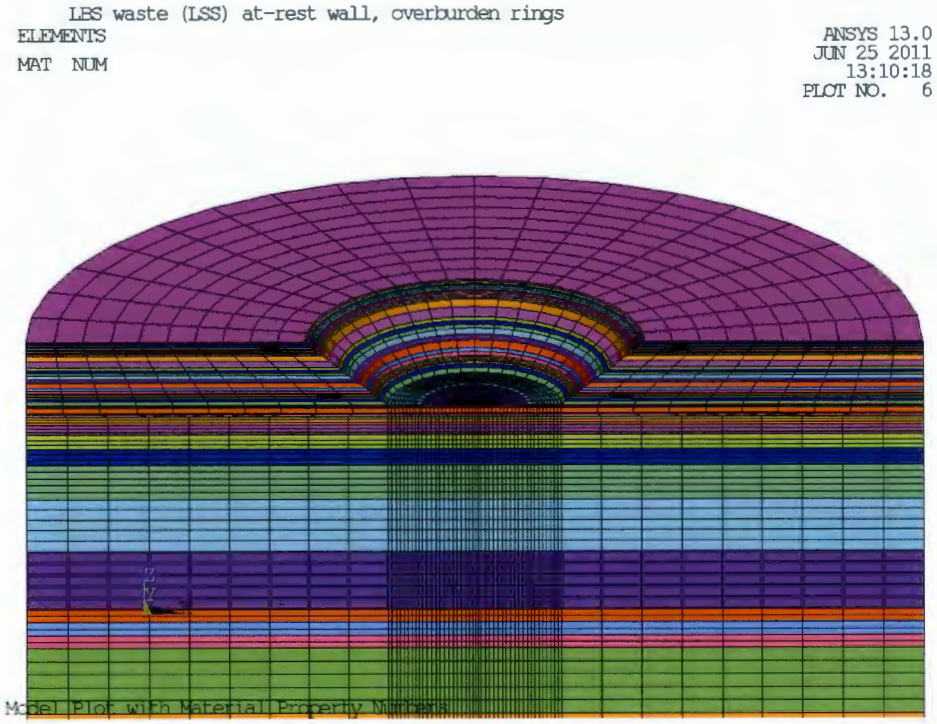

Figure 6.31. Seismic Model LBS Far-Field Soil Layering and Material Property Assignment

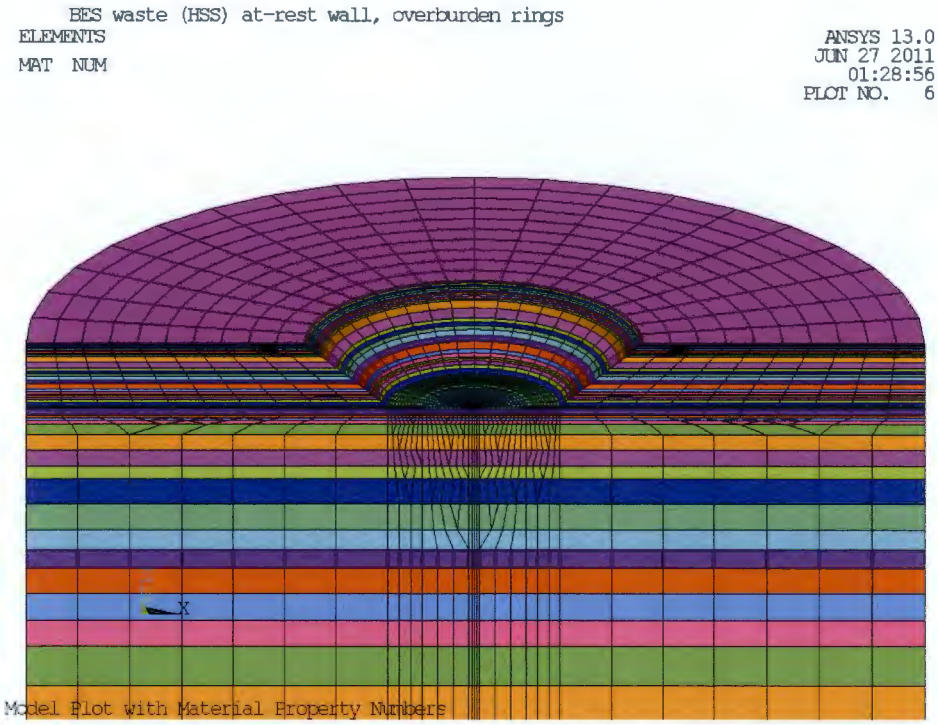

Figure 6.32. Seismic Model BES Far-Field Soil Layering and Material Property Assignment

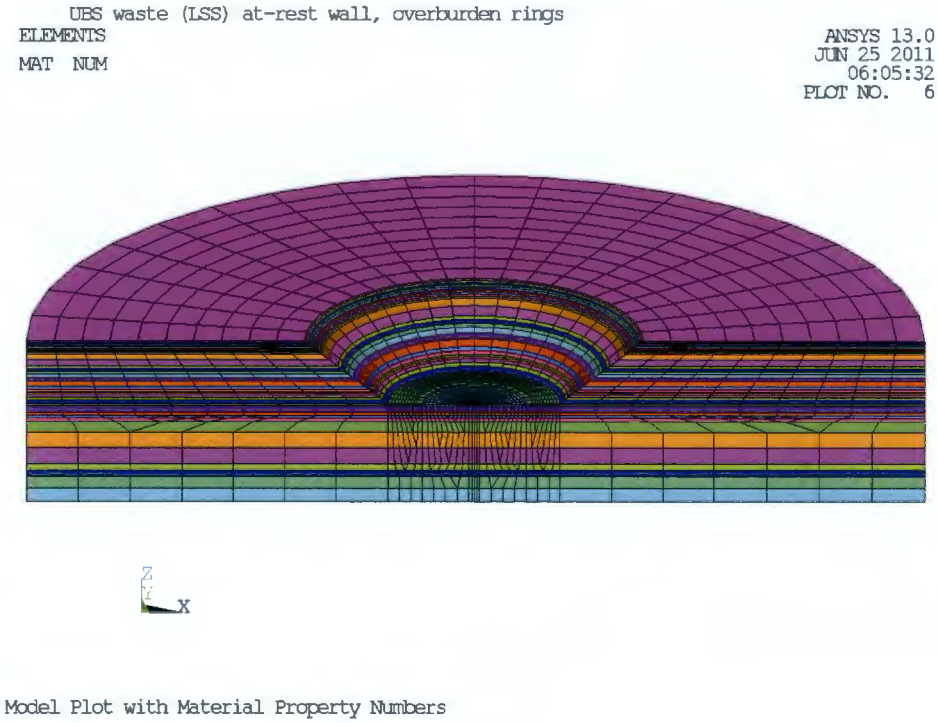

Figure 6.33. Seismic Model UBS Far-Field Soil Layering and Material Property Assignment

6.4 Run Descriptions

6.4.1 Seismic Run Matrix

The combinations used for the seismic matrix runs are listed in Table 6.19. A full tank is defined as a waste height of 20.3 ft, which represents the current maximum depth of waste in any Type III SST, per Appendix H of Weber (2009). See Section 6.3.2 for definition of low modulus (soft) and high modulus (stiff) waste properties. All seismic runs used thermal degraded, orthotropic, fully cracked concrete (FCC) properties as determined in TOLA analysis. Results for the seismic matrix runs are presented in Chapter 9.

Table 6.19. Seismic Model Run Matrix

Run	Soil	Backfill	Time History	Tank Concrete	Waste	At-rest
1	BES	BE	BES H + V	FCC	Empty	Wall
2	BES	BE	BES H + V	FCC	Full soft (LSS)	Wall
3	BES	BE	BES H + V	FCC	Full stiff (HSS)	Wall
4	LBS	LB	LBS H + V	FCC	Empty	Wall
5	LBS	LB	LBS H + V	FCC	Full soft (LSS)	Wall
6	LBS	LB	LBS H + V	FCC	Full stiff (HSS)	Wall
7	UBS	UB	UBS H + V	FCC	Empty	Wall
8	UBS	UB	UBS H + V	FCC	Full soft (LSS)	Wall
9	UBS	UB	UBS H + V	FCC	Full stiff (HSS)	Wall

FCC = Fully Cracked concrete.
LSS = Low Shear Strength for waste properties.
HSS = High Shear Strength for waste properties.

6.4.2 Results Extraction

The following data are recorded for the gravity and transient analyses.

- Nodes — Displacements at all locations
- Reactions — None applicable
- Concrete Tank — Element results
- Soil Contacts — Element results
- Waste Contacts — None
- Excavated Backfill Soil — None
- Excavated Backfill Soil Contacts — None
- Native Soil — None
- Waste — None

The following results have been extracted from the analyses.

• Nodes	Displacements and accelerations
• Reactions	None
• Concrete Tank Elements	Element Forces and Moments
• Soil Contact Elements	Pressures, gaps, status
• Waste Contact Elements	None
• Excavated Backfill Soil Elements	None
• Excavated Backfill Soil Contact Elements	None
• Native Soil Elements	None
• Waste Elements	None

For each of the results listed above, all time history results have been extracted into text files. Minima and maxima data were also obtained for all the above-listed results. In general, only the resulting minima and maxima data are used in this report. Results are obtained throughout the model and then summarized around the circumference for presentation. A detailed description of the post-processing methods is found in Section 6.2.12.

7.0 Soil Column Properties, Base Motion Inputs, and Spectral Matching

7.1 Introduction

The previous chapter described the ANSYS® SSI model in detail, but it did not describe the details of the soil columns used for the analysis, the input motions used for the analysis, or the spectral matching performed to confirm that the input motions to the model produced the appropriate free-field responses in the model. The purpose of this chapter is to summarize the SSI profile properties that were developed in the AMEC Geomatrix report in Appendix R of Rinker et al. (2011a), describe the process for developing the input motions to the ANSYS® SSI model, characterize the dynamic SHAKE and ANSYS® soil columns, characterize the dynamic response of the soil in the full ANSYS® SSI model, and perform spectral matching to ensure that the ANSYS® SSI model reproduces an appropriate free-field response.

Three soil columns and their associated properties were defined in the subject AMEC Geomatrix report. The three columns are necessary to address the uncertainty of the soil properties in the SSI analysis. The three soil columns are referred to as the lower bound (LB), best estimate (BE), and upper bound (UB) columns. Each column had a different depth and different dynamic properties. As stated in the subject AMEC Geomatrix report, normally the range in SSI properties is intended to cover the uncertainty in properties at a single site. In this case, that range of properties has been extended to cover the uncertainty in properties and column depths over a broader geographical area represented by the SST sites.

7.2 SHAKE Soil Column Descriptions

A single set of LB, BE, and UB SSI profiles is specified for analysis of the Hanford SST sites. The LB profile is taken to be the 200 East LB profile because it has lower shear wave velocities and greater depth to a major velocity contrast. The BE profile is chosen to be the 200 West BE profile because it produces higher relative displacements than the 200 East BE profile, representing the larger relative displacements computed for the 200 West LB profile. The UB profile is chosen to be the 200 West UB profile because it clearly represents the stiffest and shallowest soil profile among the SST sites. The SSI profile geometry for each of the soil types is shown in Table 7.1.

Tables 7.2 through 7.4 list the final set of LB, BE, and UB SSI profiles used in the SHAKE evaluations. Included in these tables are values of compression wave (V_P) and Poisson's ratio. The Vp values are calculated based on results presented in Rohay and Brouns (2007, Table 4.1) with imposition of a minimum Poisson's ratio of 0.19 based on minimum value reported in Shannon and Wilson (2000). Figures 4.9a and 4.9b in the subject AMEC Geomatrix report show the three shear wave velocity profiles.

The base of the SSI profiles is placed in accordance with ASCE (2000) such that the shear wave velocity at the base is greater than or equal to 3,500 ft/s, or else the base is at least three times the maximum foundation dimension below the foundation (approximately 285 ft). The depth of the LB SSI profile was set at 405 ft, with a corresponding shear wave velocity of over 4,000 ft/s, which meets both of the criteria above. The depth of the BE profile was set at 303 ft, with a corresponding shear wave velocity of 3,350 ft/s, which meets the second criterion above. The depth of the UB profile was set at

123 ft with a corresponding shear wave velocity of 4,552 ft/s, which meets the first criterion above. In the cases of the LB and UB profiles, the base of the SSI profile corresponds with the first large velocity contrast encountered (e.g., basalt).

Table 7.1. SSI Profile Geometry

Soil Type	Extending Depth	Number of Layers
Best estimate	303 ft	44
Upper bound	123 ft	38
Lower bound	405 ft	49

Table 7.2. The LB SSI Profile

Lower Bound (LB)						
Layer Number	Thickness (ft)	Damping (in decimal)	Unit Weight (kip/ft^3)	Strain-Compatible Vs (ft/sec)	Vp (ft/sec)	Poisson's Ratio
1	1	0.0154	0.106	438	1048	0.394
2	1	0.0212	0.106	438	1048	0.394
3	1	0.0283	0.106	438	1048	0.394
4	1	0.0372	0.106	438	1048	0.394
5	1	0.0434	0.106	438	1048	0.394
6	1	0.0429	0.106	540	1048	0.319
7	1	0.0430	0.106	540	1048	0.319
8	1	0.0474	0.106	540	1048	0.319
9	1	0.0509	0.106	540	1048	0.319
10	1	0.0421	0.106	680	1099	0.190
11	4	0.0435	0.106	680	1099	0.190
12	5	0.0462	0.106	787	2027	0.411
13	2	0.0496	0.106	815	2027	0.404
14	2	0.0499	0.106	860	2027	0.390
15	2	0.0552	0.106	860	2027	0.390
16	3	0.0560	0.106	860	2027	0.390
17	3	0.0571	0.106	900	2313	0.411
18	4	0.0536	0.106	970	2313	0.393
19	2	0.0611	0.106	970	2313	0.393
20	2	0.0614	0.106	970	2313	0.393
21	1	0.0558	0.106	1047	2313	0.371
22	1	0.0558	0.106	1047	2313	0.371
23	1	0.0508	0.106	1089	2313	0.358
24	3	0.0508	0.106	1089	2313	0.358
25	3	0.0518	0.106	1089	2313	0.358
26	2	0.0517	0.106	1089	2313	0.358

Table 7.2. (contd)

Lower Bound (LB)						
Layer Number	Thickness (ft)	Damping (in decimal)	Unit Weight (kip/ft^3)	Strain-Compatible Vs (ft/sec)	Vp (ft/sec)	Poisson's Ratio
27	4	0.0499	0.106	1089	2313	0.358
28	1	0.0521	0.106	1190	2313	0.320
29	4	0.0521	0.106	1190	2313	0.320
30	4	0.0525	0.106	1210	2313	0.312
31	8	0.0565	0.106	1210	2313	0.312
32	11	0.0558	0.106	1210	2313	0.312
33	12	0.0614	0.106	1210	2313	0.312
34	26	0.0643	0.106	1210	2313	0.312
35	40	0.0649	0.106	1210	2313	0.312
36	45	0.0806	0.106	1149	2313	0.336
37	10	0.0806	0.127	1210	2313	0.312
38	10	0.0750	0.127	1210	2313	0.312
39	10	0.0750	0.127	1210	2313	0.312
40	10	0.0832	0.127	1210	2313	0.312
41	10	0.0832	0.127	1210	2313	0.312
42	10	0.0832	0.127	1210	2313	0.312
43	20	0.0832	0.127	1210	2313	0.312
44	10	0.0658	0.135	1560	3470	0.373
45	20	0.0657	0.135	1560	3470	0.373
46	20	0.0703	0.135	1560	3470	0.373
47	20	0.0813	0.135	1400	3470	0.403
48	25	0.0551	0.135	1580	3470	0.369
49	25	0.0588	0.135	1580	3470	0.369
50		0.0397	0.175	4006	6939	0.250

Table 7.3. The BE SSI Profile

Best Estimate (BE)						
Layer Number	Thickness (ft)	Damping (in decimal)	Unit Weight (kip/ft^3)	Strain-Compatible Vs (ft/sec)	Vp (ft/sec)	Poisson's Ratio
1	1	0.0114	0.106	710	1283	0.279
2	1	0.0153	0.106	710	1283	0.279
3	1	0.0196	0.106	710	1283	0.279
4	1	0.0223	0.106	720	1283	0.270
5	1	0.0244	0.106	720	1283	0.270
6	1	0.0297	0.106	720	1283	0.270
7	1	0.0285	0.106	775	1283	0.213
8	1	0.0324	0.106	775	1283	0.213
9	1	0.0307	0.106	775	1283	0.213
10	1	0.0290	0.106	987	1595	0.190
11	4	0.0301	0.106	987	1595	0.190
12	5	0.0318	0.106	1086	1755	0.190
13	2	0.0345	0.106	1158	2483	0.361
14	2	0.0358	0.106	1158	2483	0.361
15	2	0.0360	0.106	1158	2483	0.361
16	3	0.0370	0.106	1158	2483	0.361
17	3	0.0380	0.106	1280	2833	0.372
18	4	0.0378	0.106	1280	2833	0.372
19	2	0.0405	0.106	1280	2833	0.372
20	2	0.0407	0.106	1280	2833	0.372
21	1	0.0349	0.106	1344	2833	0.355
22	1	0.0349	0.106	1344	2833	0.355
23	4	0.0352	0.106	1383	2833	0.344
24	3	0.0355	0.106	1416	2833	0.334
25	2	0.0331	0.106	1526	2833	0.296
26	5	0.0341	0.106	1526	2833	0.296
27	4	0.0345	0.106	1526	2833	0.296
28	3	0.0359	0.106	1526	2833	0.296
29	8	0.0379	0.106	1526	2833	0.296
30	12	0.0404	0.106	1526	2833	0.296
31	12	0.0419	0.106	1526	2833	0.296
32	10	0.0325	0.106	1780	2877	0.190
33	19	0.0343	0.106	1780	4817	0.421
34	20	0.0283	0.106	2424	4817	0.330
35	15	0.0185	0.135	2638	4817	0.286
36	15	0.0191	0.135	2638	4935	0.300
37	19	0.0200	0.135	2638	4935	0.300
38	21	0.0207	0.135	2638	4935	0.300
39	20	0.0081	0.156	3350	6267	0.300
40	30	0.0082	0.156	3350	6267	0.300
41	40	0.0085	0.156	3350	6267	0.300
42		0.0088	0.156	3350	6267	0.300

Table 7.4. The UB SSI Profile

Upper Bound (UB)						
Layer Number	Thickness (ft)	Damping (in decimal)	Unit Weight (kip/ft^3)	Strain-Compatible Vs (ft/sec)	Vp (ft/sec)	Poisson's Ratio
1	1	0.0087	0.106	1089	1760	0.190
2	1	0.0102	0.106	1089	1760	0.190
3	1	0.0122	0.106	1089	1760	0.190
4	1	0.0152	0.106	1089	1760	0.190
5	1	0.0164	0.106	1089	1760	0.190
6	1	0.0177	0.106	1089	1760	0.190
7	1	0.0183	0.106	1089	1760	0.190
8	1	0.0163	0.106	1280	2069	0.190
9	1	0.0177	0.106	1280	2069	0.190
10	1	0.0164	0.106	1280	2069	0.190
11	4	0.0195	0.106	1379	2229	0.190
12	5	0.0209	0.106	1423	3041	0.360
13	2	0.0204	0.106	1423	3041	0.360
14	2	0.0227	0.106	1520	3041	0.333
15	2	0.0210	0.106	1520	3041	0.333
16	3	0.0229	0.106	1630	3041	0.298
17	3	0.0204	0.106	1732	3041	0.260
18	4	0.0217	0.106	1732	3470	0.334
19	2	0.0244	0.106	1732	3470	0.334
20	2	0.0264	0.106	1732	3470	0.334
21	1	0.0212	0.106	1732	3470	0.334
22	1	0.0212	0.106	1732	3470	0.334
23	4	0.0198	0.106	1732	3470	0.334
24	3	0.0219	0.106	1950	3470	0.269
25	2	0.0223	0.106	1950	3470	0.269
26	5	0.0204	0.106	1950	3470	0.269
27	4	0.0211	0.106	1950	3470	0.269
28	3	0.0238	0.106	1950	3470	0.269
29	8	0.0238	0.106	1950	3470	0.269
30	12	0.0254	0.106	1950	3470	0.269
31	12	0.0274	0.106	1950	3470	0.269
32	5	0.0159	0.135	2351	5900	0.406
33	5	0.0159	0.135	2351	5900	0.406
34	9	0.0169	0.135	2351	5900	0.406
35	10	0.0169	0.135	2351	5900	0.406
36		0.0053	0.156	4552	8516	0.300

7.3 Characterization of the SHAKE Soil Columns

7.3.1 Amplification Factors for Three Soil Profiles – Horizontal Motion

SHAKE91 (Idriss and Sun 1992) inputs for the three soil profiles include the soil properties and the final horizontal time histories to compute the amplification of ground motion through the soil column. The amplitude curves show the natural frequencies of the soil column. The following figures show the amplification factors at the surface and the three tank foundation levels, which are -41ft (E1), -49 ft (E2) and -57 ft (E3). The full soil column depths for BE, UB, and LB full are -303 ft, -123 ft, and -405 ft.

Figure 7.1 shows the amplification factors for the full BE soil column computed with SHAKE91. The natural frequencies of the full soil column are seen at the amplitude peaks. Figure 7.2 shows the amplification factors for the full LB soil column computed from SHAKE. Figure 7.3 shows the amplification factors computed by SHAKE91 for the full UB soil column.

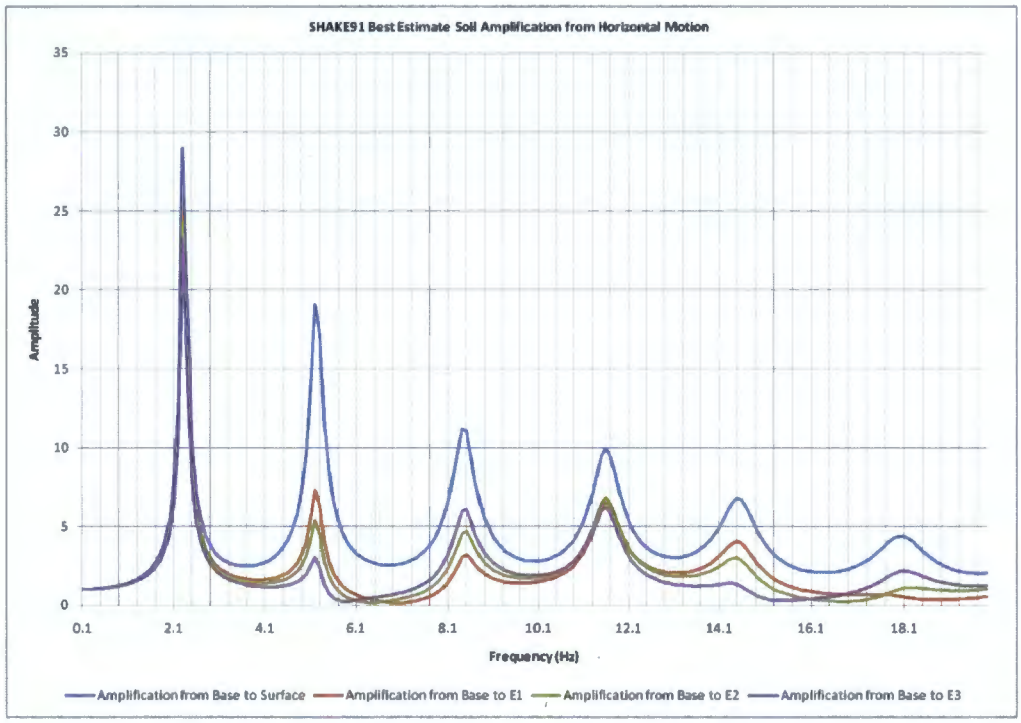

Figure 7.1. SHAKE91 Best Estimate Amplification Factors from Horizontal Input Motion at Soil Column Base

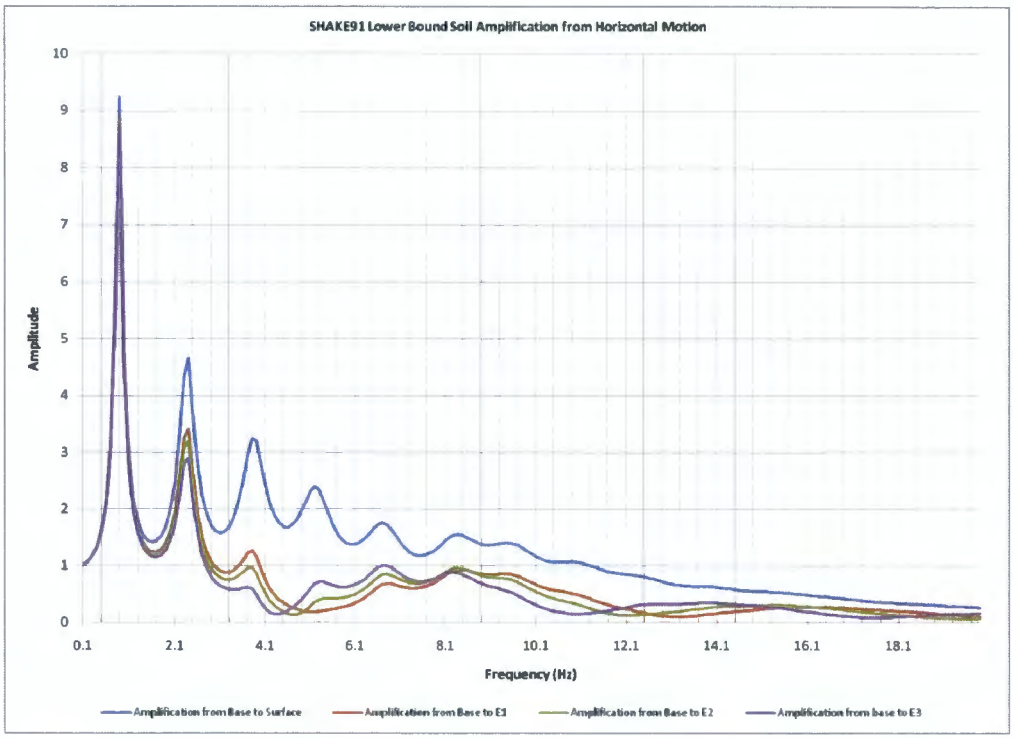

Figure 7.2. SHAKE91 Lower Bound Amplification Factors from Horizontal Input Motion at Soil Column Base

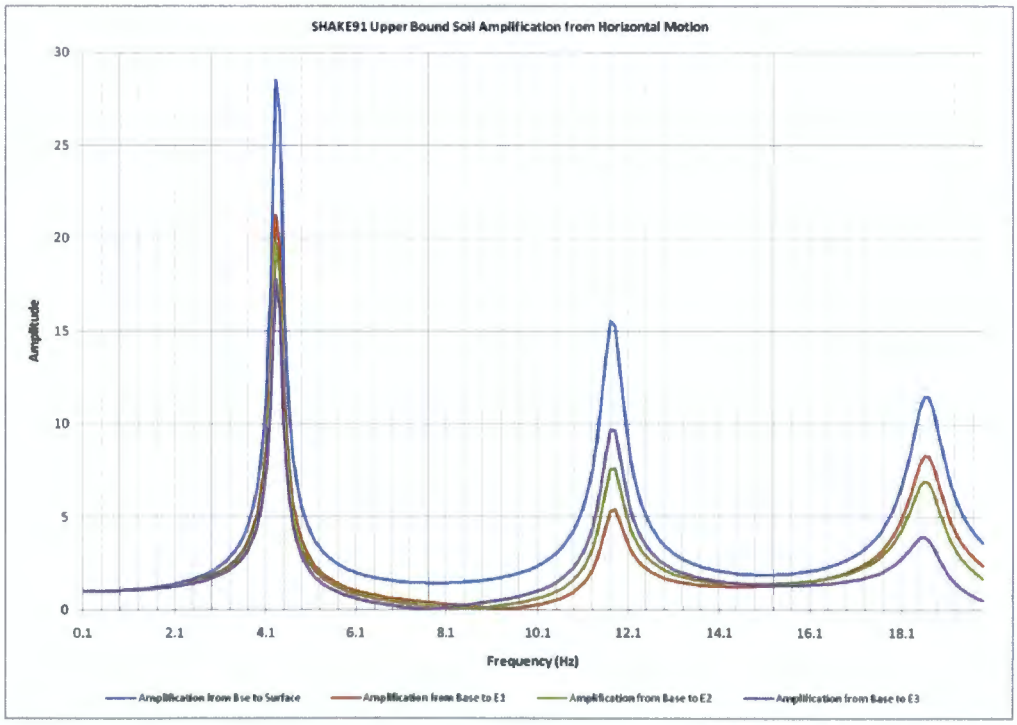

Figure 7.3. SHAKE91 Upper Bound Soil Amplification Factors from Horizontal Input Motion at Soil Column Base

7.3.2 Amplification Factors for Three Soil Profiles – Vertical Motion

The subsurface horizontal time histories cannot be directly used to represent vertical seismic because the vertical control motion is different than the horizontal control motion.

The SHAKE inputs for vertical spectra use the same soil layering, soil density and soil damping as the SHAKE inputs for horizontal spectra. The soil layer velocities are different, namely, compression velocities (Vp) values are used instead of the Vs values. The Vp values for the three soil profiles are shown in Section 7.6.4, Table 7.8, Table 7.9, and Table 7.10.

Figure 7.4 shows the amplification factors for the full BE soil column computed from the final vertical time history. The fundamental frequencies of the full soil column are seen at the amplitude peaks. Figure 7.5 shows the amplification factors for the full LB soil column computed from the final vertical time histories. Figure 7.6 shows the amplification factors computed by SHAKE91 for the full UB soil column.

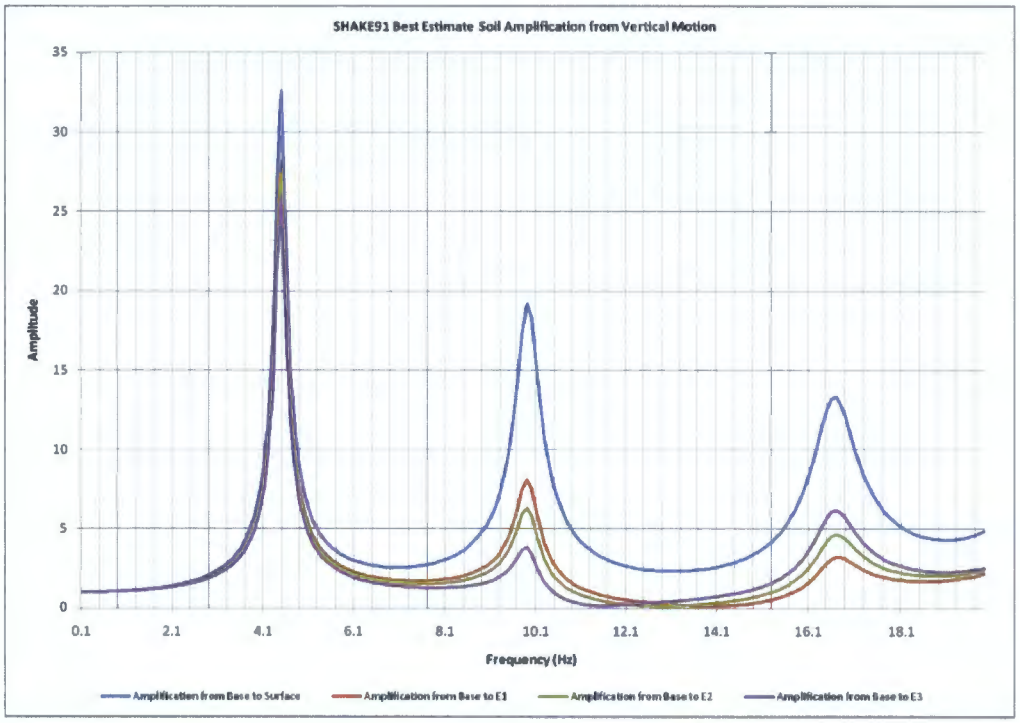

Figure 7.4. SHAKE91 Best Estimate Amplification Factors from Vertical Input Motion at Soil Column Base

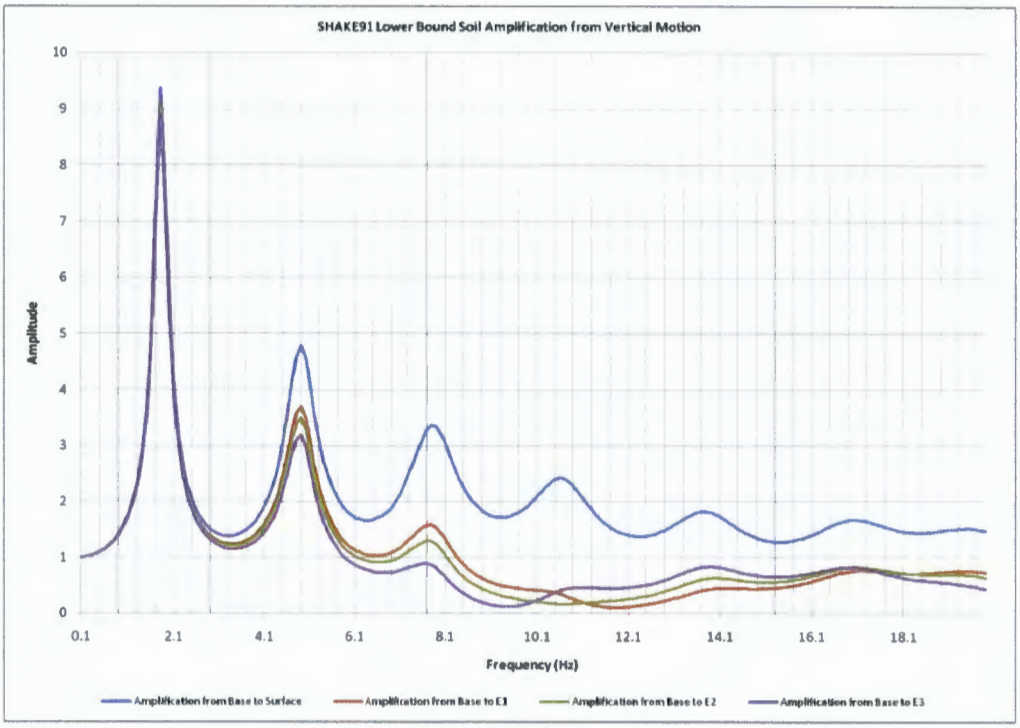

Figure 7.5. SHAKE91 Lower Bound Soil Amplification Factors from Vertical Input Motion at Soil Column Base

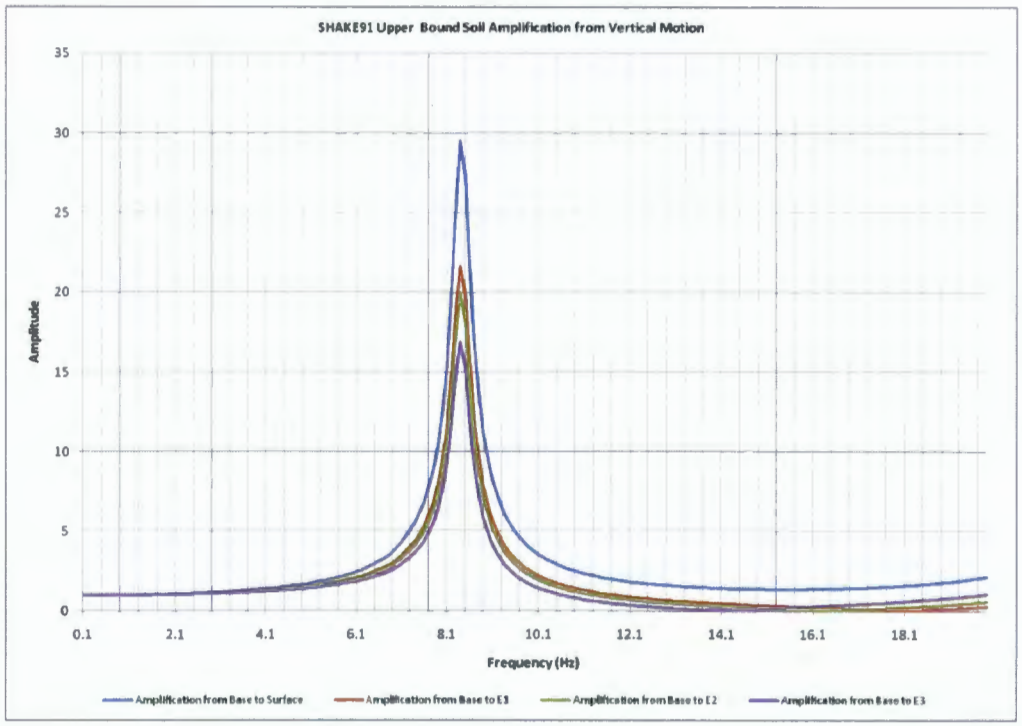

Figure 7.6. SHAKE91 Upper Bound Amplification Factors from Vertical Input Motion at Soil Column Base

7.4 Development of Time Histories at the Base of the SSI Profiles to be Used as Input to ANSYS® SSI Models

The ANSYS® SSI models require that acceleration time histories be provided as input at the base of the SSI profiles. The time histories were developed in a consistent manner following the guidance presented in Section 3.2.3 of NEI (2009). A more complete description of this process appears in the AMEC Geomatrix report in Appendix R of Rinker et al. (2011a). The first step is to develop soil column outcrop response (SCOR)-based foundation input response spectra (FIRS) corresponding to the foundation depths of the various SST types. Acceleration time histories are then spectrally matched these FIRS. The spectrally matched acceleration time histories are then input into the SSI profiles to compute in-column motions at the three foundation depths and at the base of the SSI profiles using SHAKE. The above steps are performed by AMEC Geomatrix and documented in the AMEC Geomatrix report.

The resulting base motions are then used to compute foundation level and surface motions in the ANSYS® SSI models. The computed foundation level and surface motions are compared to the foundation level and surface-level targets to ensure that the SSI model is producing adequate levels of ground shaking. Because pseudo-outcrop motions are not available from ANSYS®, the foundation-level target is the in-column motion from SHAKE that is consistent with the time history that is spectrally matched to the FIRS at the corresponding elevation.

More explicitly, the procedure for developing the time histories to be used as input to the SSI models consists of the following steps:

1. Specification of design surface spectra.
2. Specification of dynamic properties of the three soil profiles. These are defined in terms of the LB, BE, and UB SSI profiles.

Development of input time histories for the ANSYS® SSI models.

3a. From the site response analyses conducted to develop the soil properties, obtain pseudo-outcrop motions at the SST foundation levels.

3b. Construct FIRS at the tank foundation levels using the results of Step 3a.

3c. Create time histories that are spectrally matched to FIRS at the tank foundation levels.

3d. Deconvolve the foundation-level inputs from Step 3c to the base of the SSI profiles using SHAKE, and then extract as in-column motions at the base.

3e. Apply the in-column motions from Step 3d as input to the ANSYS® SSI full models.

3f. Verify that these foundation-level spectra and surface spectra from the ANSYS® models meet appropriate matching criteria.

3g. Adjust the time histories as necessary to meet the matching criteria. The outcome of this step is a specific set of input time histories to be used for a specific SSI profile, that is one set for the LB profile, one set for the BE profile, and one set for the UB profile.

Steps 1, 2, 3a through 3d are documented in the subject AMEC Geomatrix report. Step 3e is performed as part of this evaluation, and steps 3f and 3g are performed jointly by AMEC Geomatrix and M&D and are documented here and in the subject AMEC Geomatrix report.

7.5 Generation of Target Spectra Using SHAKE

Target spectra are produced in SHAKE and are the benchmark for determining if the free-field response in the ANSYS® model is correct. The surface target spectrum for the ANSYS® SSI model is simply the PC-2 surface spectrum documented in the AMEC Geomatrix report in Appendix R of Rinker et al. (2011a). This spectrum is referred to as the surface design response spectra (DRS) and is equal to two-thirds of the site-specific maximum considered earthquake (MCE). The surface spectrum is the same for the LB, BE, and UB profiles.

The initial foundation-level target spectra are probabilistically developed foundation input response spectra (FIRS) for each of the three soil columns. A bounding FIRS is defined for each soil column that is the upper bound of the E1, E2, and E3 level FIRS. As mentioned above, pseudo-outcrop motions are not available from ANSYS®, so the actual foundation-level targets used for spectral matching between ANSYS® and SHAKE are the in-column spectra from SHAKE that are consistent with the time history that is spectrally matched to the FIRS at the corresponding elevation.

Figure 7.7 through Figure 7.12 show the Target Spectra for all three soil profiles as a result of the horizontal and vertical input base motion.

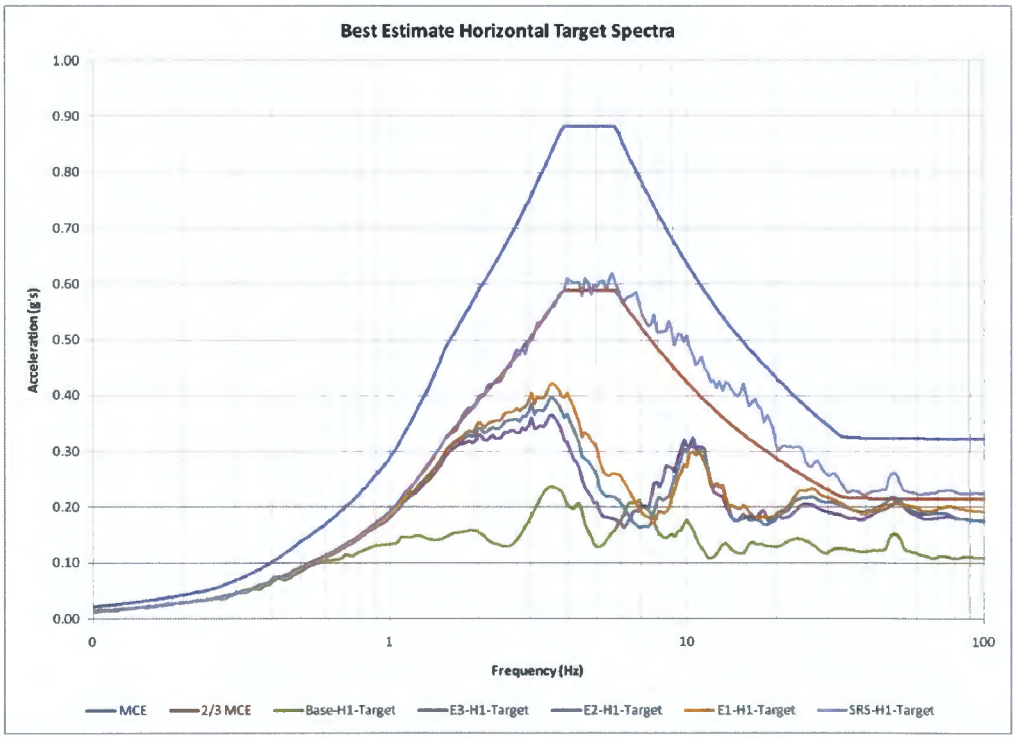

Figure 7.7. Best Estimate Horizontal Target Spectra

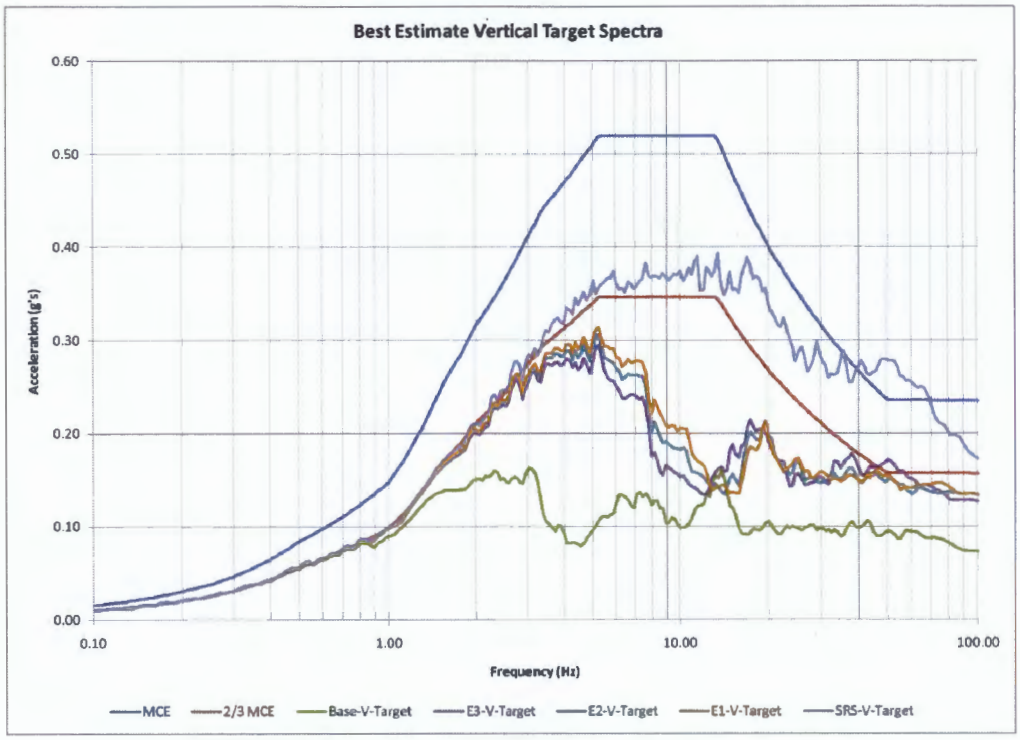

Figure 7.8. Best Estimate Vertical Target Spectra

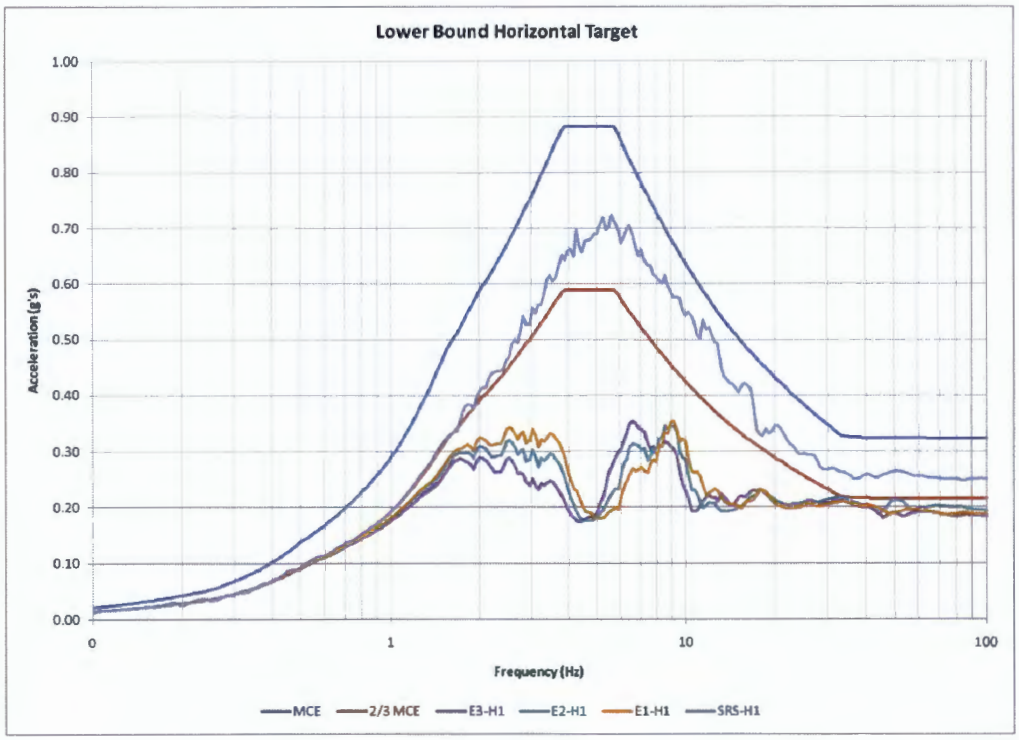

Figure 7.9. Lower Bound Horizontal Target Spectra

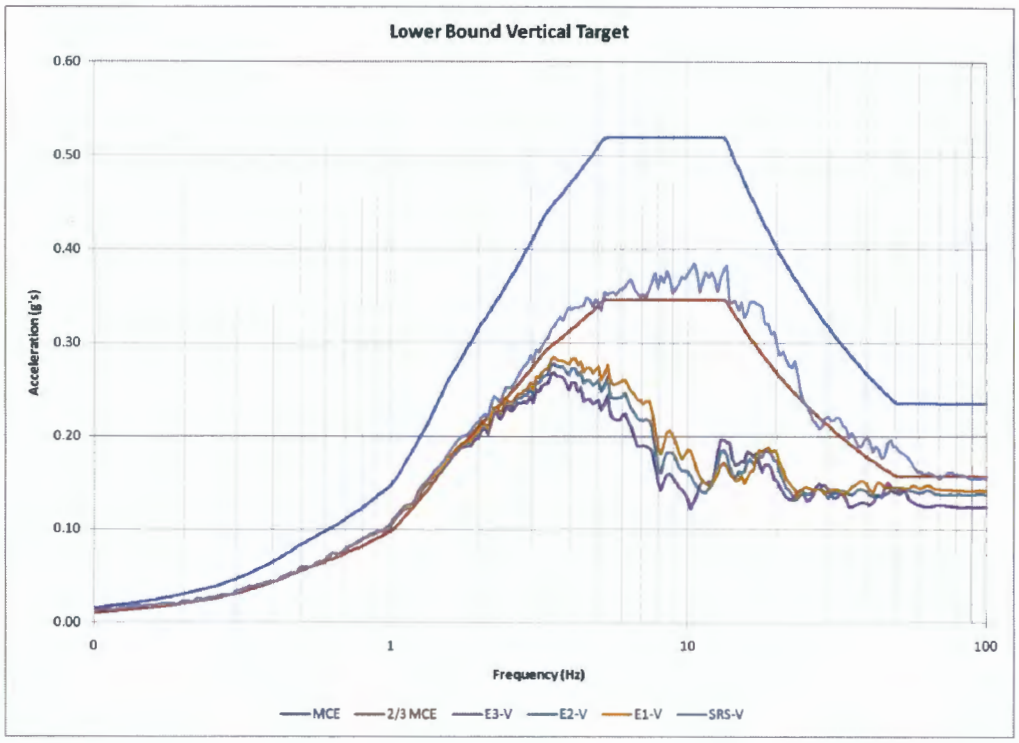

Figure 7.10. Lower Bound Vertical Target Spectra

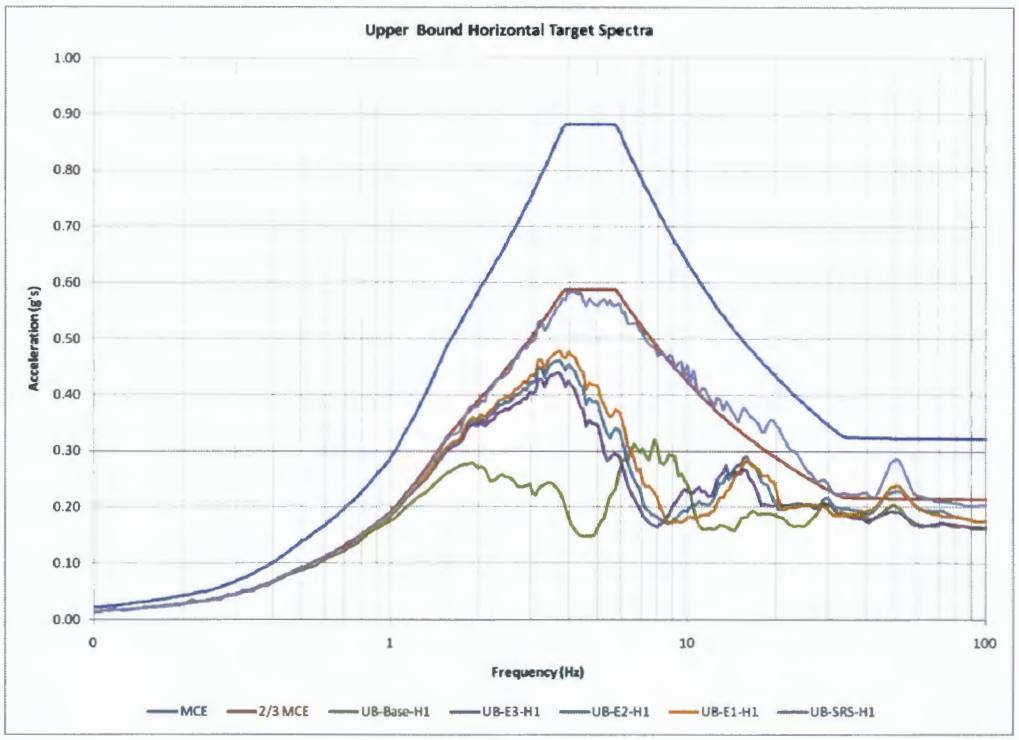

Figure 7.11. Upper Bound Horizontal Target Spectra

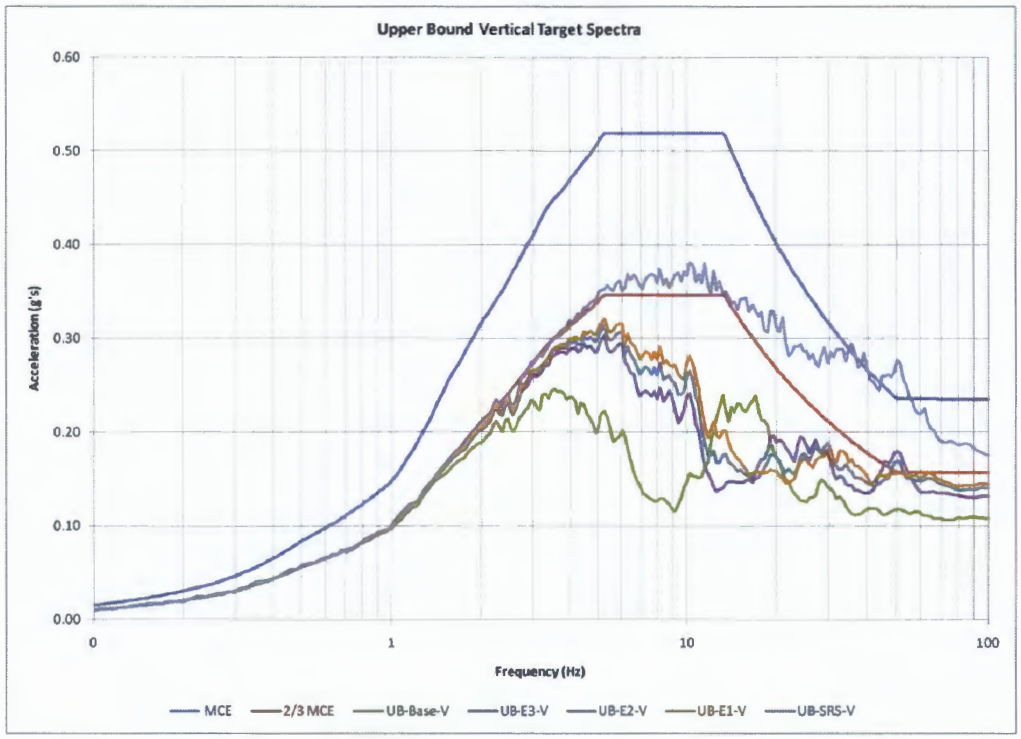

Figure 7.12. Upper Bound Vertical Target Spectra

7.6 Description of the ANSYS® Soil Column Models

As stated in the introduction to this chapter, it is necessary to perform spectral matching between the ANSYS® SSI models and the SHAKE models to determine if the free-field response is adequately reproduced in the ANSYS® models. As an intermediate step, simplified soil column models are generated in ANSYS®, the appropriate dynamic properties are assigned, the Rayleigh damping parameters are established, and spectral matching is checked. This step serves the purpose of establishing damping parameters and spectral matching in simpler models than the full ANSYS® SSI models. This saves time while demonstrating that ANSYS® can adequately reproduce the target free-field response. The final spectral matching with the full SSI model is then performed as a confirmatory step.

The ANSYS® column was 40 ft wide by 10 ft wide and had the depth of the individual soil profile being considered (LB, BE, or UB). The individual soil column depths are listed in Section 7.3.1. The soil models have four elements across the width and one element through the depth. The ANSYS® soil column model uses SOLID45 elements for the soil and incorporates strain compatible elastic properties for the soil. The ANSYS® soil column model is shown in Figure 7.13.

Solid elements were used to model the soil layers, where each layer is assigned unique soil properties including the elastic modulus, the density, Poisson's ratio and soil layer damping known as beta damping. The elastic modulus for each layer is calculated from the strain compatible shear modulus using the relationship shown in Section 7.6.4. The shear wave speeds, densities, and Poisson's ratios are given from the SHAKE models described in Section 7.2. The elastic (extensional) modulus (E) is determined from the elastic relations shown below.

Shear Modulus: $$G = \rho \cdot V_s^2 \quad (7.1)$$

Modulus of Elasticity: $$E = 2G(1+\upsilon) \quad (7.2)$$

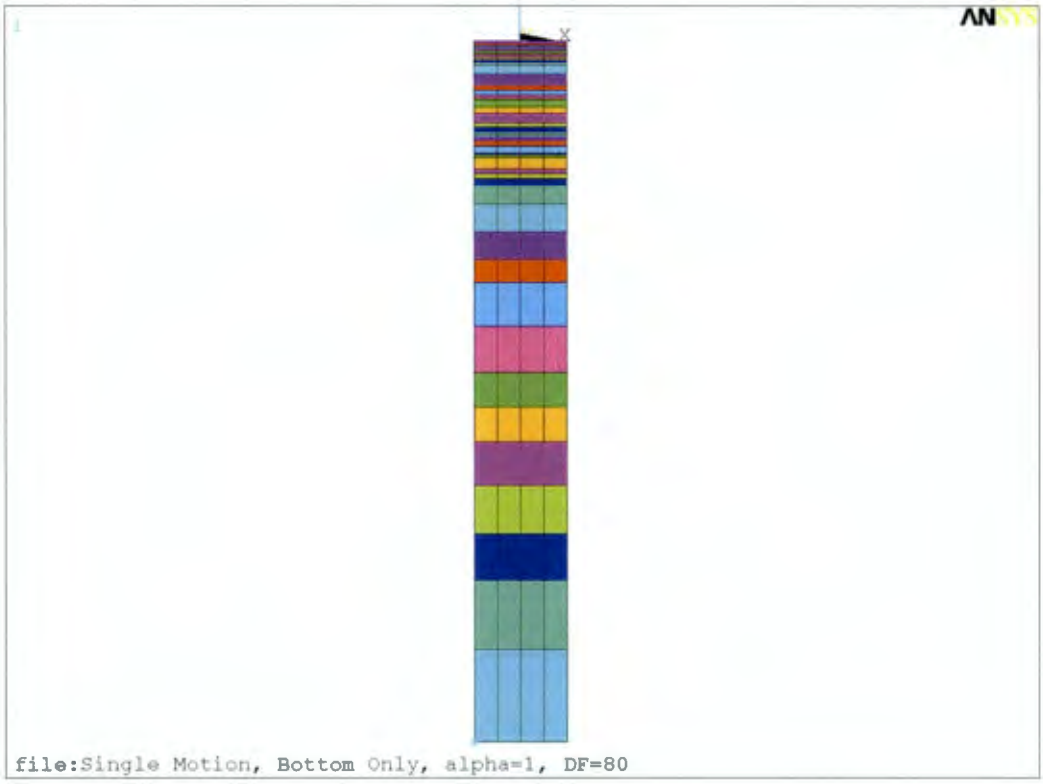

Figure 7.13. Elevation View of Typical ANSYS® Soil Column Model

7.6.1 Element Geometry and Layer Thickness

For a finite element model to effectively represent seismic wave propagation, the resolution of the mesh must be sufficient to transmit the highest frequency of interest. Table 7.5 shows the element thicknesses for the best estimate soil profile. In addition to the element thicknesses used in the model, the table displays the maximum element thicknesses consistent with having five, eight, or ten elements per wavelength based on a cutoff frequency of 25 Hz.

The SSI profile layering was documented in the AMEC Geomatrix report in Appendix R of Rinker et al. (2011a). However, in the ANSYS® model, some layers were subdivided in order to be consistent with the above considerations maximum passing frequencies and in a few cases layers were merged for convenience. A sensitivity analysis was performed for the BE soil column because Layers 32–44 have thicknesses that exceed the 1/5th wavelength guideline. The results showed slightly higher accelerations at peak acceleration points and slightly lower accelerations than the lowest acceleration points. It was concluded that mesh refinements did not improve spectral matching between the SHAKE and the ANSYS® soil column model. Therefore, no further mesh adjustments were implemented.

Table 7.5. Maximum Allowable Element Sizes for Best Estimate Soil

Layer Number	Vs (ft/sec)	Vp (ft/sec)	Cutoff Frequency (Hz)	Cut-off Wave Length (ft)	Maximum Allowable Element Thickness (ft)			Actual Element Thickness (ft)
					1/5th Wave Length	1/8th Wave Length	1/10th Wave Length	
1	710	1283	25	28	6	4	3	1.0
2	710	1283	25	28	6	4	3	1.0
3	710	1283	25	28	6	4	3	1.0
4	720	1283	25	29	6	4	3	1.0
5	720	1283	25	29	6	4	3	1.0
6	720	1283	25	29	6	4	3	1.0
7	775	1283	25	31	6	4	3	1.0
8	775	1283	25	31	6	4	3	1.0
9	775	1283	25	31	6	4	3	1.0
10	987	1595	25	39	8	5	4	1.0
11	987	1595	25	39	8	5	4	4.0
12	1086	1755	25	43	9	5	4	5.0
13	1158	2483	25	46	9	6	5	2.0
14	1158	2483	25	46	9	6	5	2.0
15	1158	2483	25	46	9	6	5	2.0
16	1158	2483	25	46	9	6	5	3.0
17	1280	2833	25	51	10	6	5	3.0
18	1280	2833	25	51	10	6	5	4.0
19	1280	2833	25	51	10	6	5	2.0
20	1280	2833	25	51	10	6	5	2.0
21	1344	2833	25	54	11	7	5	1.0
22	1344	2833	25	54	11	7	5	1.0
23	1383	2833	25	55	11	7	6	2.0
24	1383	2833	25	55	11	7	6	2.0
25	1416	2833.	25	57	11	7	6	3.0
26	1526	2833	25	61	12	8	6	1.0
27	1526	2833	25	61	12	8	6	1.0
28	1526	2833	25	61	12	8	6	5.0
29	1526	2833	25	61	12	8	6	2.0
30	1526	2833	25	61	12	8	6	2.0
31	1526	2833	25	61	12	8	6	3.0
32	1526	2833	25	61	12	8	6	8.0
33	1526	2833	25	61	12	8	6	12.0
34	1526	2833	25	61	12	8	6	12.0
35	1780	2877	25	71	14	9	7	10.0
36	1780	4816	25	71	14	9	7	19.0
37	2424	4816	25	97	19	12	10	20.0
38	2638	4816	25	106	21	13	11	15.0
39	2638	4935	25	106	21	13	11	15.0
40	2638	4935	25	106	21	13	11	19.0
41	2638	4935	25	106	21	13	11	21.0
42	3350	6267	25	134	27	17	13	20.0
43	3350	6267	25	134	27	17	13	30.0
44	3350	6267	25	134	27	17	13	40.0
Mode Value					12	8	6	--

The relationship between element size and cutoff frequencies for LB and UB soil profiles are shown in Table 7.6 and Table 7.7, respectively.

The LB soil column spectra at the surface and tank foundation did not consistently match with the target spectra despite adjustments with damping parameters and time histories. Several layer thicknesses exceeded 10 feet, the maximum element thickness consistent with the 1/5th wavelength guideline. Layers 35–49 have soil layers that are greater than 10 feet thick and these layers are subdivided so that there are ten elements for wavelength at the 25 Hz cutoff frequency. In addition, Layers 33–34 that are adjacent to Layer 35 were also subdivided. Table 7.6 and Table 7.7 show the actual layer thickness and the subdivided layer thickness in the last two columns.

Table 7.6. Maximum Allowable Element Sizes for Lower Bound Soil

Layer Number	Vs (ft/sec)	Vp (ft/sec)	Cutoff Frequency	Cutoff Wave Length	Maximum Allowable Element Thickness (ft)			Actual Element Thicknes s (ft)	Mesh Refinements Thickness (ft)
					1/5th Wave Length	1/8th Wave Length	1/10th Wave Length		
1	438	1047	25	18	4	2	2	1	1.0
2	438	1047	25	18	4	2	2	1	1.0
3	438	1047	25	18	4	2	2	1	1.0
4	438	1047	25	18	4	2	2	1	1.0
5	438	1047	25	18	4	2	2	1	1.0
6	540	1047	25	22	4	3	2	1	1.0
7	540	1047	25	22	4	3	2	1	1.0
8	540	1047	25	22	4	3	2	1	1.0
9	540	1047	25	22	4	3	2	1	1.0
10	680	1099	25	27	5	3	3	1	1.0
11	680	1099	25	27	5	3	3	4	4.0
12	787	2027	25	31	6	4	3	5	5.0
13	815	2027	25	33	7	4	3	2	2.0
14	860	2027	25	34	7	4	3	2	2.0
15	860	2027	25	34	7	4	3	2	2.0
16	860	2027	25	34	7	4	3	3	3.0
17	900	2313	25	36	7	5	4	3	3.0
18	970	2313	25	39	8	5	4	4	4.0
19	970	2313	25	39	8	5	4	2	2.0
20	970	2313	25	39	8	5	4	2	2.0
21	1047	2313	25	42	8	5	4	1	1.0
22	1047	2313	25	42	8	5	4	1	1.0
23	1089	2313	25	44	9	5	4	1	1.0
24	1089	2313	25	44	9	5	4	1	1.0
25	1089	2313	25	44	9	5	4	2	2.0
26	1089	2313	25	44	9	5	4	3	3.0
27	1089	2313	25	44	9	5	4	1	1.0
28	1089	2313	25	44	9	5	4	1	1.0
29	1089	2313	25	44	9	5	4	4	4.0
30	1190	2313	25	48	10	6	5	1	1.0

Table 7.6. (contd)

Layer Number	Vs (ft/sec)	Vp (ft/sec)	Cutoff Frequency	Cutoff Wave Length	Maximum Allowable Element Thickness (ft)			Actual Element Thickness (ft)	Mesh Refinements Thickness (ft)
					1/5th Wave Length	1/8th Wave Length	1/10th Wave Length		
31	1190	2313	25	48	10	6	5	2	2.0
32	1190	2313	25	48	10	6	5	2	2.0
33	1210	2313	25	48	10	6	5	4	2 elements 2.0-ft
34	1210	2313	25	48	10	6	5	8	3 elements 2.67-ft
35	1210	2313.	25	48	10	6	5	11	3 elements 3.67-ft
36	1210	2313	25	48	10	6	5	12	3 elements 4.0-ft
37	1210	2313	25	48	10	6	5	26	5 elements 5.20-ft
38	1210	2313	25	48	10	6	5	40	5 elements 8.0-ft
39	1149	2313	25	46	9	6	5	45	5 elements 9.0-ft
40	1210	2313	25	48	10	6	5	10	2 elements 5.0-ft
41	1210	2313	25	48	10	6	5	10	2 elements 5.0 ft
42	1210	2313	25.	48	10	6	5	10	2 elements 5.0 ft
43	1210	2313	25	48	10	6	5	50	5 elements 10.0-ft
44	1560	3470	25	62	12	8	6	10	2 elements 5.0-ft
45	1560	3470	25	62	12	8	6	20	3 elements 6.67-ft
46	1560	3470	25	62	12	8	6	20	3 elements 6.67-ft
47	1400	3470	25	56	11	7	6	20	3 elements 6.67-ft
48	1580	3470	25	63	13	8	6	25	4 elements 6.25-ft
49	1580	3470	25	63	13	8	6	25	4 elements 6.25-ft
Mode Value					10	6	5	--	--

Table 7.7. Maximum Allowable Element Sizes for Upper Bound Soil

Layer Number	Vs (ft/sec)	Vp (ft/sec)	Cutoff Frequency	Cut off Wave Length	Maximum Allowable Element Thickness (ft)			Actual Element Thickness (ft)
					1/5th Wave Length	1/8th Wave Length	1/10th Wave Length	
1	1089	1760	25	44	9	5	4	1.0
2	1089	1760	25	44	9	5	4	1.0
3	1089	1760	25	44	9	5	4	1.0
4	1089	1760	25	44	9	5	4	1.0
5	1089	1760	25	44	9	5	4	1.0
6	1089	1760	25	44	9	5	4	1.0
7	1089	1760	25	44	9	5	4	1.0
8	1280	2069	25	51	10	6	5	1.0
9	1280	2069	25	51	10	6	5	1.0
10	1280	2069	25	51	10	6	5	1.0
11	1379	2229	25	55	11	7	6	4.0
12	1423	3041	25	57	11	7	6	5.0
13	1423	3041	25	57	11	7	6	2.0
14	1520	3041	25	61	12	8	6	2.0
15	1520	3041	25	61	12	8	6	2.0
16	1630	3041	25	65	13	8	7	3.0
17	1732	3041	25	69	14	9	7	3.0
18	1732	3469	25	69	14	9	7	4.0
19	1732	3469	25	69	14	9	7	2.0
20	1732	3469	25	69	14	9	7	2.0
21	1732	3469	25	69	14	9	7	1.0
22	1732	3469	25	69	14	9	7	1.0
23	1732	3469	25	69	14	9	7	2.0
24	1732	3469	25	69	14	9	7	2.0
25	1950	3469	25	78	16	10	8	3.0
26	1950	3469	25	78	16	10	8	1.0
27	1950	3469	25	78	16	10	8	1.0
28	1950	3469	25	78	16	10	8	5.0
29	1950	3469	25	78	16	10	8	2.0
30	1950	3469	25	78	16	10	8	2.0
31	1950	3469	25	78	16	10	8	3.0
32	1950	3469	25	78	16	10	8	8.0
33	1950	3469	25	78	16	10	8	12.0
34	1950	3469	25	78	16	10	8	12.0
35	2351	5899	25	94	19	12	9	5.0
36	2351	5899	25	94	19	12	9	5.0
37	2351	5899	25	94	19	12	9	9.0
38	2351	5899	25	94	19	12	9	10.0
Mode Value					16	10	8	--

7.6.2 Boundary Conditions

Rinker et al. (2008) demonstrated that the best results were achieved when so-called "slaved" boundary conditions were applied. Accordingly, slaved boundary conditions are applied to the lateral boundaries of the ANSYS® SSI full model and the ANSYS® soil column models. At each elevation, the nodes on the exterior lateral faces (faces with ±x-direction normal) were coupled such that the horizontal (±x-direction) and vertical (±z-direction) displacements were the same at a given elevation. These boundary conditions support the horizontal shear and vertical compression modes associated with vertically propagating shear and compression waves, but do not allow displacements that are not consistent with the soil behavior.

All nodes in the soil column models were constrained against out-of-plane (y-direction) motion. In the case of horizontal seismic input (±x-direction), the bottom of the models was fixed vertically. In the case of vertical seismic input (±z-direction), the base of the models was fixed in both horizontal directions, but was free vertically.

Consistent with the Abatt and Rinker (2008), the boundary constraints of the soil column meet the ASCE-4 guidance on boundary conditions (Section C3.3.3.3): "*When vertically propagating waves are used, horizontal roller boundaries are used for shear waves, and vertical roller boundaries are specified for compression waves.*"

The nodes at each soil layer are coupled instead of fixing vertical displacements to allow for vertically propagating compressions waves. The coupling includes horizontal displacements allows for shear wave displacements. Therefore, coupling the exterior model nodes results in the same condition as given in ASCE-4, but allows both vertical and horizontal excitation of the model simultaneously. The boundary conditions of the ANSYS® soil column model are shown in Figure 7.14.

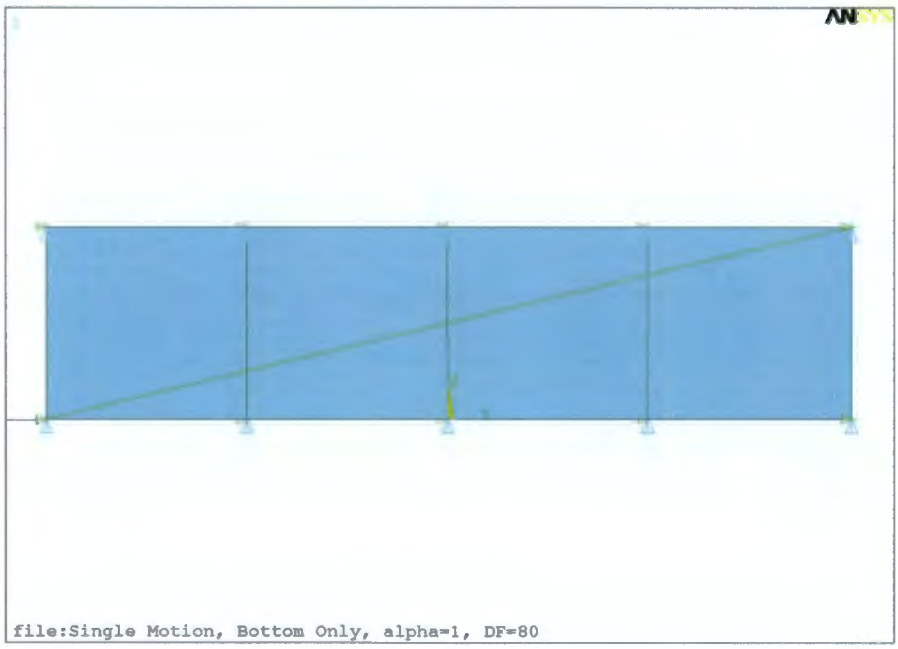

Figure 7.14. Top View of ANSYS® Soil Column Model

7.6.3 Seismic Loading

The base excitation for the soil models was determined from the output acceleration time history from the SHAKE model at various elevations corresponding to the base of the soil column models for each soil type.

Acceleration time history input is applied to the ANSYS® model as a force time history at a large mass at the base of the model. The base mass was simulated with a MASS21 element having a mass approximately 1,000 times greater than the total soil mass, thus simulating seismic ground motion. The nodes at the bottom of the ANSYS® model were coupled together to form a rigid region effectively providing a single point force time history input to the soil column.

7.6.4 ANSYS® Soil Column Material Properties

The soil properties used in the ANSYS® models are linear elastic, isotropic properties. These properties are developed based on the linear elastic relationships and the strain-compatible V_s and V_p wave velocities. The strain-compatible dynamic soil properties used in the ANSYS® models are summarized in Table 7.8, Table 7.9, and Table 7.10.

Table 7.8. Strain Compatible Best Estimate Soil Properties

Elevation (ft)	Damping (in decimal)	Unit Weight (kip/ft^3)	Vs (ft/sec)	Vp (ft/sec)	Poisson's Ratio	Shear Modulus (kip/ft^2)	Modulus of Elasticity (kip/ft^2)
-1	0.011430	0.106	710	1283	0.279	1659	4246
-2	0.015250	0.106	710	1283	0.279	1659	4246
-3	0.019600	0.106	710	1283	0.279	1659	4246
-4	0.022300	0.106	720	1283	0.270	1707	4336
-5	0.024350	0.106	720	1283	0.270	1707	4336
-6	0.029730	0.106	720	1283	0.270	1707	4336
-7	0.028480	0.106	775	1283	0.213	1977	4797
-8	0.032350	0.106	775	1283	0.213	1977	4797
-9	0.030730	0.106	775	1283	0.213	1977	4797
-10	0.029030	0.106	987	1595	0.190	3207	7631
-14	0.030100	0.106	987	1595	0.190	3207	7631
-19	0.031750	0.106	1086	1755	0.190	3882	9238
-21	0.034500	0.106	1158	2483	0.361	4414	12016
-23	0.035750	0.106	1158	2483	0.361	4414	12016
-25	0.035950	0.106	1158	2483	0.361	4414	12016
-28	0.036980	0.106	1158	2483	0.361	4414	12016
-31	0.037950	0.106	1280	2833	0.372	5393	14797
-35	0.037800	0.106	1280	2833	0.372	5393	14797
-37	0.040450	0.106	1280	2833	0.372	5393	14797
-39	0.040680	0.106	1280	2833	0.372	5393	14797
-40	0.034850	0.106	1344	2833	0.355	5946	16112
-41	0.034850	0.106	1344	2833	0.355	5946	16112
-43	0.035150	0.106	1383	2833	0.344	6296	16920
-45	0.035150	0.106	1383	2833	0.344	6296	16920
-48	0.035480	0.106	1416	2833	0.334	6600	17604
-49	0.033130	0.106	1526	2833	0.296	7666	19865
-50	0.033130	0.106	1526	2833	0.296	7666	19865
-55	0.034100	0.106	1526	2833	0.296	7666	19865
-57	0.034450	0.106	1526	2833	0.296	7666	19865
-59	0.034450	0.106	1526	2833	0.296	7666	19865
-62	0.035900	0.106	1526	2833	0.296	7666	19865
-70	0.037880	0.106	1526	2833	0.296	7666	19865
-82	0.040400	0.106	1526	2833	0.296	7666	19865
-94	0.041930	0.106	1526	2833	0.296	7666	19865
-104	0.032480	0.106	1780	2877	0.190	10430	24822
-123	0.034250	0.106	1780	4817	0.421	10430	29641
-143	0.028330	0.106	2424	4817	0.330	19343	51468
-158	0.018450	0.135	2638	4817	0.286	29176	75027
-173	0.019100	0.135	2638	4935	0.300	29176	75858
-192	0.020000	0.135	2638	4935	0.300	29176	75858
-213	0.020700	0.135	2638	4935	0.300	29176	75858
-233	0.008130	0.156	3350	6267	0.300	54370	141362
-263	0.008150	0.156	3350	6267	0.300	54370	141362
-303	0.008450	0.156	3350	6267	0.300	54370	141362

Table 7.9. Strain Compatible Upper Bound Soil Properties

Elevation	Damping (in decimal)	Unit Weight (kip/ft^3)	Vs (ft/sec)	Vp (ft/sec)	Poisson's Ratio	Shear Modulus (kip/ft^2)	Modulus of Elasticity (kip/ft^2)
-1	0.008700	0.106	1089	1760	0.190	3904	9291
-2	0.010200	0.106	1089	1760	0.190	3904	9291
-3	0.012200	0.106	1089	1760	0.190	3904	9291
-4	0.015200	0.106	1089	1760	0.190	3904	9291
-5	0.016400	0.106	1089	1760	0.190	3904	9291
-6	0.017700	0.106	1089	1760	0.190	3904	9291
-7	0.018300	0.106	1089	1760	0.190	3904	9291
-8	0.016300	0.106	1280	2069	0.190	5393	12837
-9	0.017700	0.106	1280	2069	0.190	5393	12837
-10	0.016400	0.106	1280	2069	0.190	5393	12837
-14	0.019500	0.106	1379	2229	0.190	6260	14898
-19	0.020900	0.106	1423	3041	0.360	6666	18129
-21	0.020400	0.106	1423	3041	0.360	6666	18129
-23	0.022700	0.106	1520	3041	0.333	7606	20284
-25	0.021000	0.106	1520	3041	0.333	7606	20284
-28	0.022900	0.106	1630	3041	0.298	8746	22713
-31	0.020400	0.106	1732	3041	0.260	9875	24884
-35	0.021700	0.106	1732	3470	0.334	9875	26348
-37	0.024400	0.106	1732	3470	0.334	9875	26348
-39	0.026400	0.106	1732	3470	0.334	9875	26348
-40	0.021200	0.106	1732	3470	0.334	9875	26348
-41	0.021200	0.106	1732	3470	0.334	9875	26348
-43	0.019800	0.106	1732	3470	0.334	9875	26348
-45	0.019800	0.106	1732	3470	0.334	9875	26348
-48	0.021900	0.106	1950	3470	0.269	12518	31774
-49	0.022300	0.106	1950	3470	0.269	12518	31774
-50	0.022300	0.106	1950	3470	0.269	12518	31774
-55	0.020400	0.106	1950	3470	0.269	12518	31774
-57	0.021100	0.106	1950	3470	0.269	12518	31774
-59	0.021100	0.106	1950	3470	0.269	12518	31774
-62	0.023800	0.106	1950	3470	0.269	12518	31774
-70	0.023800	0.106	1950	3470	0.269	12518	31774
-82	0.025400	0.106	1950	3470	0.269	12518	31774
-94	0.027400	0.106	1950	3470	0.269	12518	31774
-99	0.015900	0.135	2351	5900	0.406	23173	65144
-104	0.015900	0.135	2351	5900	0.406	23173	65144
-113	0.016900	0.135	2351	5900	0.406	23173	65144
-123	0.016900	0.135	2351	5900	0.406	23173	65144

Table 7.10. Strain Compatible Lower Bound Soil Properties

Elevation	Damping (in decimal)	Unit Weight (kip/ft^3)	Compatible Vs (ft/sec)	Vp (ft/sec)	Poisson's Ratio	Shear Modulus (kip/ft^2)	Modulus of Elasticity (kip/ft^2)
-1	0.01540	0.106	438	1048	0.394	632	1761
-2	0.02120	0.106	438	1048	0.394	632	1761
-3	0.02830	0.106	438	1048	0.394	632	1761
-4	0.03720	0.106	438	1048	0.394	632	1761
-5	0.04340	0.106	438	1048	0.394	632	1761
-6	0.04290	0.106	540	1048	0.319	960	2532
-7	0.04300	0.106	540	1048	0.319	960	2532
-8	0.04740	0.106	540	1048	0.319	960	2532
-9	0.05090	0.106	540	1048	0.319	960	2532
-10	0.04210	0.106	680	1099	0.190	1522	3622
-14	0.04350	0.106	680	1099	0.190	1522	3623
-19	0.04620	0.106	787	2027	0.411	2039	5755
-21	0.04960	0.106	815	2027	0.404	2187	6138
-23	0.04990	0.106	860	2027	0.390	2435	6770
-25	0.05520	0.106	860	2027	0.390	2435	6770
-28	0.05600	0.106	860	2027	0.390	2435	6770
-31	0.05710	0.106	900	2313	0.411	2666	7524
-35	0.05360	0.106	970	2313	0.393	3097	8631
-37	0.06110	0.106	970	2313	0.393	3097	8631
-39	0.06140	0.106	970	2313	0.393	3097	8631
-40	0.05580	0.106	1047	2313	0.371	3609	9896
-41	0.05580	0.106	1047	2313	0.371	3609	9896
-42	0.05080	0.106	1089	2313	0.358	3904	10600
-43	0.05080	0.106	1089	2313	0.358	3904	10600
-45	0.05080	0.106	1089	2313	0.358	3904	10600
-48	0.05180	0.106	1089	2313	0.358	3904	10600
-49	0.05170	0.106	1089	2313	0.358	3904	10600
-50	0.05170	0.106	1089	2313	0.358	3904	10600
-54	0.04990	0.106	1089	2313	0.358	3904	10600
-55	0.05210	0.106	1190	2313	0.320	4662	12307
-57	0.05210	0.106	1190	2313	0.320	4662	12307
-59	0.05210	0.106	1190	2313	0.320	4662	12307
-63	0.05250	0.106	1210	2313	0.312	4820	12643
-71	0.05650	0.106	1210	2313	0.312	4820	12643
-82	0.05580	0.106	1210	2313	0.312	4820	12643
-94	0.06140	0.106	1210	2313	0.312	4820	12643
-120	0.06430	0.106	1210	2313	0.312	4820	12643
-160	0.06490	0.106	1210	2313	0.312	4820	12643
-205	0.08060	0.106	1149	2313	0.336	4346	11614
-215	0.08060	0.127	1210	2313	0.312	5775	15148
-225	0.07500	0.127	1210	2313	0.312	5775	15148
-235	0.07500	0.127	1210	2313	0.312	5775	15148
-285	0.08320	0.127	1210	2313	0.312	5775	15148
-295	0.06580	0.135	1560	3470	0.373	10203	28025
-315	0.06570	0.135	1560	3470	0.373	10203	28025
-335	0.07030	0.135	1560	3470	0.373	10203	28025
-355	0.08130	0.135	1400	3470	0.403	8217	23055
-380	0.05510	0.135	1580	3470	0.369	10466	28662
-405	0.05880	0.135	1580	3470	0.369	10466	28662

7.7 Calibration of ANSYS® Damping Parameters

The full time-integration algorithm for structural analysis in ANSYS®, utilizes Rayleigh damping formulation consisting of mass and stiffness proportional damping parameters α and β, respectively. In the ANSY®S soil column model, each soil layer was assigned a unique stiffness proportional (beta) damping value. Mass proportional (alpha) damping was also employed in the ANSYS® model, although the alpha damping parameter is limited to a global application in the model rather than on an element-by-element basis.

In this evaluation, the effects of changing both the alpha and beta terms were evaluated with respect to the ability to match the soil column behavior from SHAKE to ANSYS® computed spectra. A wide range of both alpha and beta terms were initially tested; however, only the final values are presented here.

Values for mass proportional (alpha) damping ranged from 0.3 to 2.0. After testing, an alpha value of 1.0 resulted in the best match for all three soil columns.

In contrast to mass proportional damping, which is applied globally to the model, stiffness proportional (beta) damping can be applied to specific materials, and therefore can be defined in an almost unlimited number of combinations. For simplicity, beta damping was varied uniformly across the model by using a single scaling factor on the damping values taken from SHAKE. Specifically, damping values output by SHAKE were assigned to each material layer in ANSYS® and then divided by the scaling factor (DF) to define the beta damping for each layer.

For example, if the damping for the soil layer was 2.0% of critical damping, the material damping property applied in ANSYS® would be (0.02)/DF. Studies were run varying the DF value from 25 to 100. A DF value of 80 resulted in the best match for the best estimate and upper bound soil columns. A DF value of 40 is the best match for the lower bound soil column.

Varying alpha has a significant effect on lower frequencies, but does not significantly affect the composite damping over the full range of frequencies of interest (0–20 Hz). Varying the DF factor (and therefore beta) affects primarily the composite damping at higher frequencies. To evaluate the performance of the ANSYS® soil column model, response spectra were extracted at the soil surface and at theses tank foundation levels (-43-ft, -49-ft, and -57-ft).

Damping parameters alpha and DF were selected by matching response spectra between ANSYS® and SHAKE without explicitly considering a target frequency or target composite damping. However, it is informative to relate the selected parameters to the critical damping level as a function of frequency. The relationship between the mass proportional damping parameter alpha, the critical damping level, and frequency is straightforward since a single value of alpha is applied globally.

$$\xi_a = \frac{\alpha}{4\pi f} = \frac{1.0}{4\pi f} \tag{7.3}$$

The relationship between stiffness proportional damping and frequency is slightly more complicated because the stiffness proportional damping parameter DF depends on the frequency-independent damping from the SHAKE analysis. The stiffness proportional damping in ANSYS® was entered layer-by-layer by dividing the frequency independent critical damping ratio reported from SHAKE by the parameter DF. This results in layer-by-layer frequency dependent stiffness proportional damping in ANSYS®.

$$\xi_{\beta i} = \xi_{\beta i}(\xi_{SHAKEi}, f) \tag{7.4}$$

For a given frequency independent critical damping ratio from SHAKE, the stiffness dependent critical damping ratio can be calculated as a function of frequency through the following equations:

$$\beta_i = \frac{\xi_{SHAKEi}}{DF} \tag{7.5}$$

and

$$\xi_{\beta i} = \pi \beta_i f = \pi \left(\frac{\xi_{SHAKEi}}{DF} \right) f \tag{7.6}$$

where DF equals 80 for the best estimate and upper bound soil columns and DF equals 40 for the lower bound soil column.

Figure 7.15 shows the percent critical damping as a function of frequency ranging from 0.1–20 Hz using an alpha value of 1.0. The mass proportional damping curve shown in Figure 7.15 is applicable to all soil profiles because the value of alpha does not change for any of the soil profiles. Figure 7.16 shows the stiffness proportional damping as a function of frequency for typical SHAKE damping values.

Figure 7.17 shows the composite Rayleigh damping for the LB soil profile. The fundamental frequency of the LBS column is shown as 0.9 Hz and the frequency of the fifth mode is 13.6 Hz. This frequency range establishes an important frequency range for quantifying the composite damping for the soil. Similarly, Figure 7.18 shows the composite Rayleigh damping for the BE soil profile. The fundamental frequency of the BE column is shown as 2.3 Hz and the frequency of the fifth mode is 14.4 Hz. Figure 7.19 shows the composite damping for the UB soil profile. In this case the fundamental mode is at 4.3 Hz and the third mode is at 18.7 Hz.

The important point in Figure 7.17, Figure 7.18, and Figure 7.19 is that in each case, the composite damping in the frequency range of interest is between the minimum and maximum damping specified in SHAKE. That is, the values of alpha and beta resulting from optimizing the spectral matching process correspond to physically realistic values for the critical damping in each of the soil columns in physically meaningful frequency ranges.

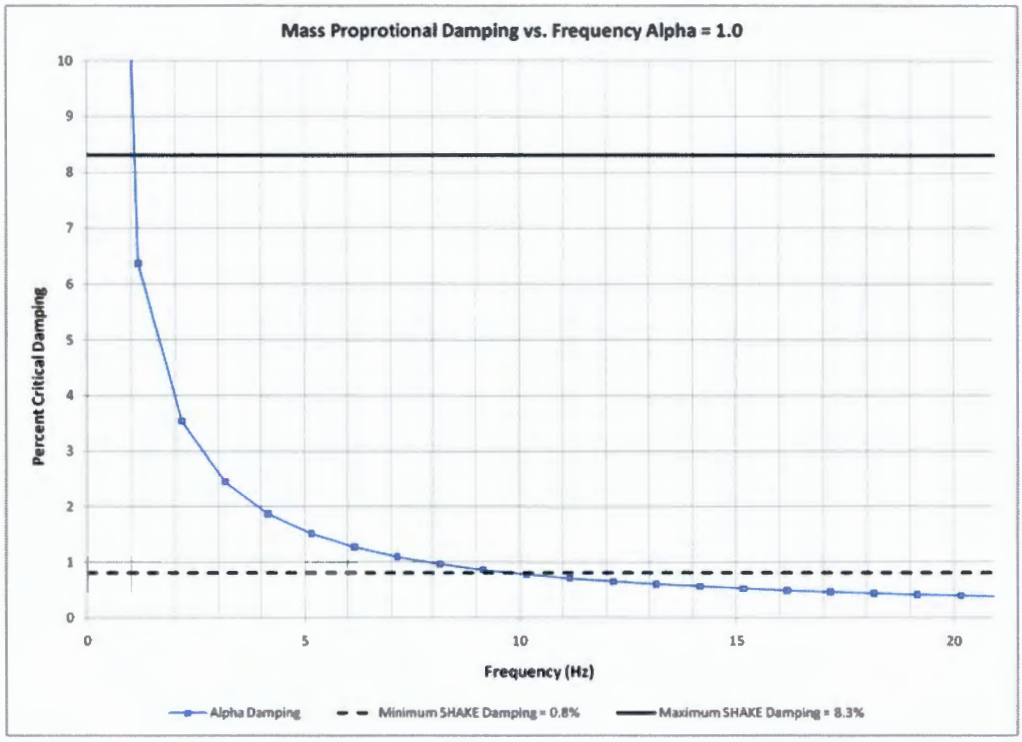

Figure 7.15. Mass Proportional Damping vs. Frequency for Alpha=1.0

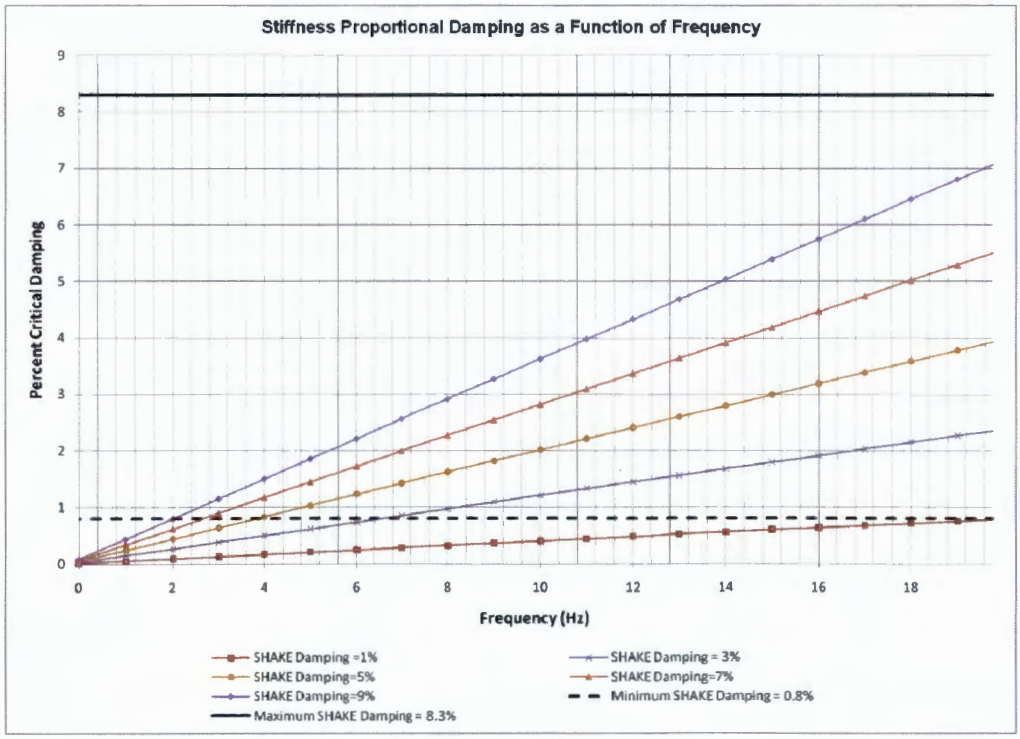

Figure 7.16. Stiffness Proportional Damping vs. Frequency

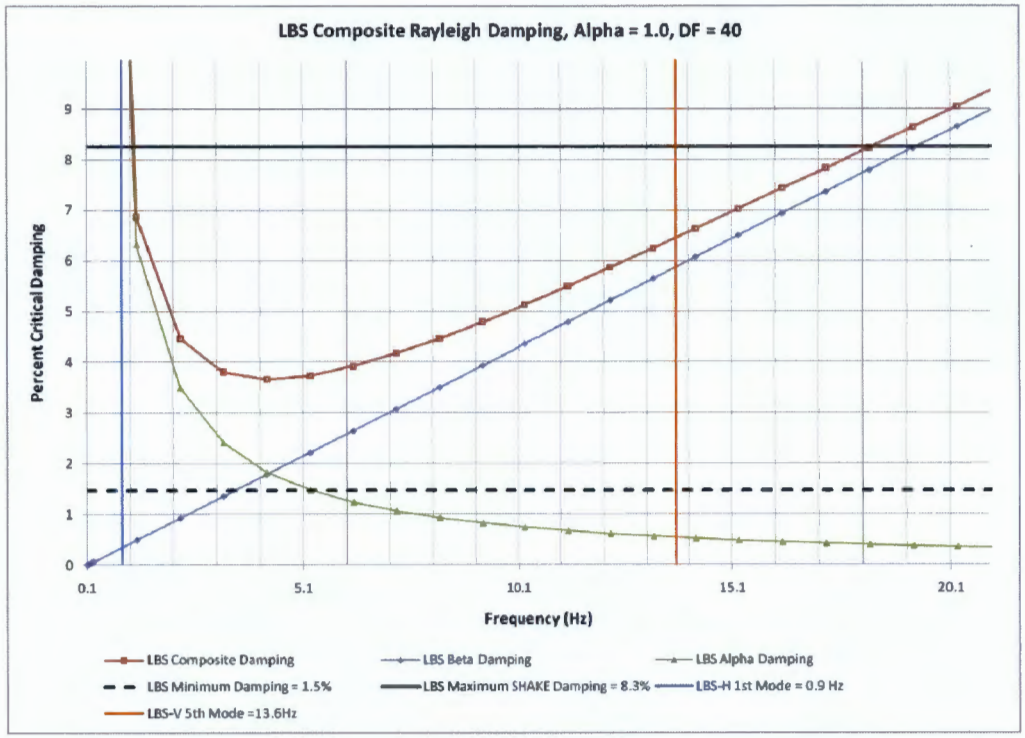

Figure 7.17. Composite Rayleigh Damping for Lower Bound Soil

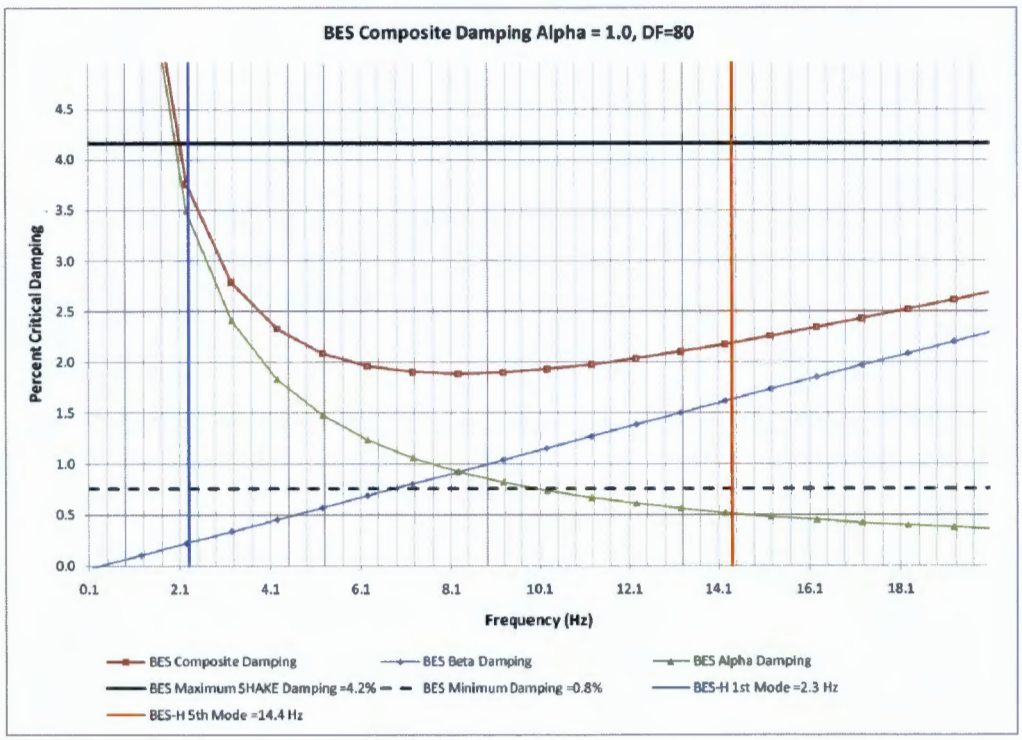

Figure 7.18. Composite Rayleigh Damping for Best Estimate Soil

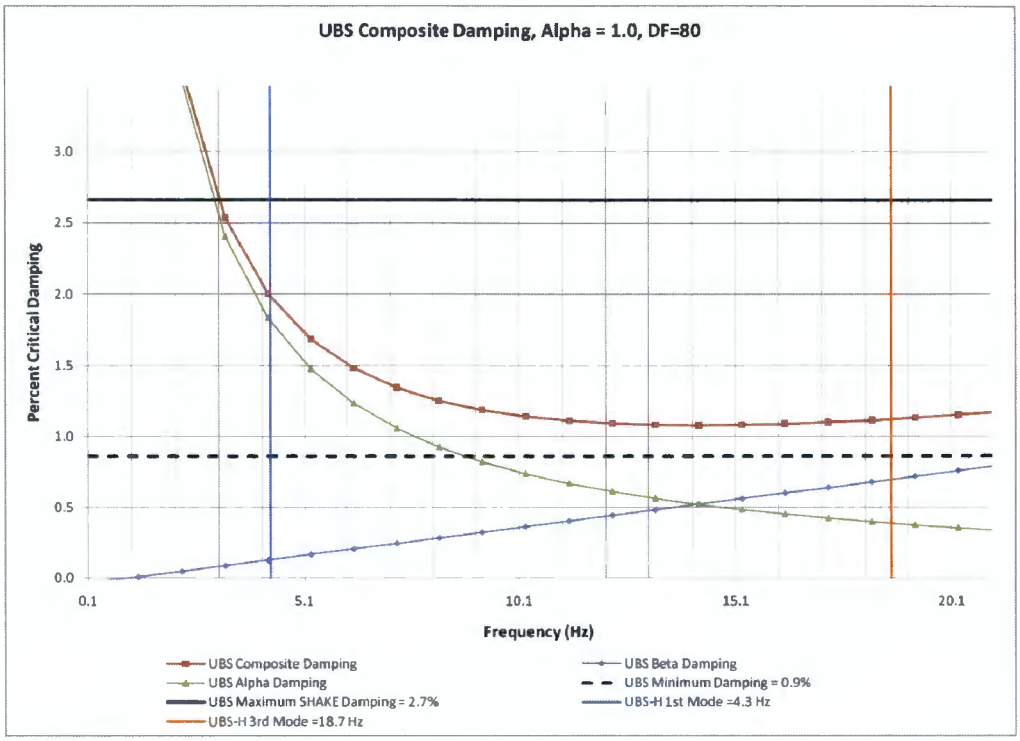

Figure 7.19. Composite Rayleigh Damping for Upper Bound Soil

7.8 Characterization of the ANSYS® Soil Columns Dynamic Response

Using the three soil profiles, a harmonic analysis of the each soil types is performed in ANSYS® to benchmark the soil column, provide insight for the alpha/beta optimization used in the time domain evaluations, ensure that the boundary conditions are appropriate, and that the isotropic material properties used in ANSYS® are correct.

The amplification factors shows the amplification of the base motion to the surface or the tank foundations (-43 ft, -49 ft, and -57 ft). The full soil column depths are best estimate full column soil depth is 303 ft, the upper bound soil column depth is 123 ft and the lower bound soil column depth is 405 ft. Full soil column amplification factors from ANSYS® and SHAKE91 are compared to show reasonable matches at each elevation.

The SHAKE91 models include layer-by-layer damping. The ANSYS® harmonic analysis omits the individual material layer damping and incorporates a constant damping ratio applied globally. The upper bound amplitude spectra agree will between SHAKE91 and ANSYS® when a constant damping ratio of 2.3% of critical is specified in the ANSYS® harmonic analysis. Similarly, good matches between SHAKE91 and ANSYS® amplitude spectra result for the BE and LB columns when the damping ratio in ANSYS® is set to 3.5% and 5.5% of critical, respectively.

Figure 7.20 shows the SHAKE91 and ANSYS® amplification factors for the BE soil column. The peak amplifications occur at the BE soil column natural frequencies of 2.3 Hz, 5.2 Hz, 8.5 Hz, and 11.6 Hz, respectively, and the SHAKE91 and ANSYS® results are in good agreement.

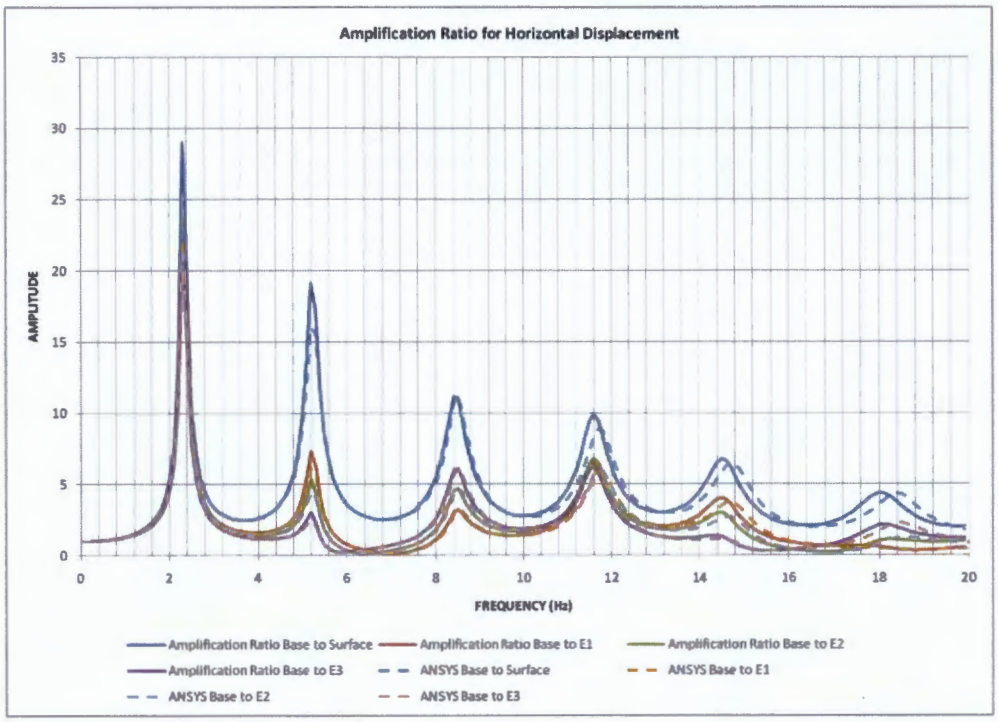

Figure 7.20. SHAKE91 vs. ANSYS® Free Field Horizontal Amplification Factors for Best Estimate

Figure 7.21 and Figure 7.22 show similar results for the LB and UB soil columns. The ANSYS® and SHAKE91 natural frequencies for horizontal excitation of the BE, LB, and UB soil columns are summarized in Table 7.11.

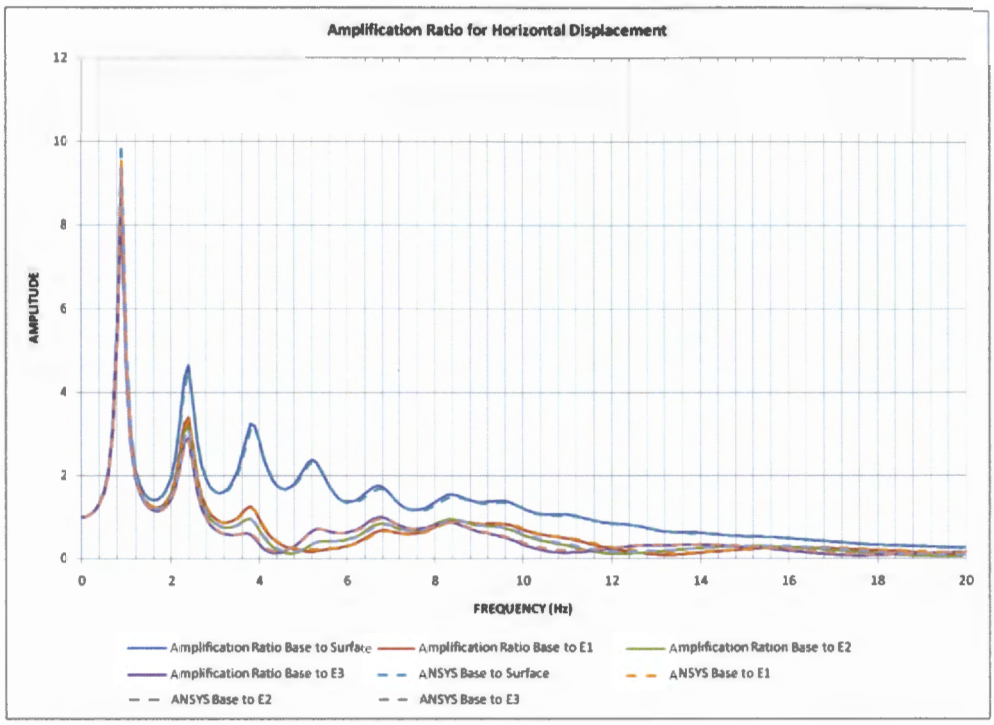

Figure 7.21. SHAKE91 vs. ANSYS® Free Field Horizontal Amplification Factors for Lower Bound

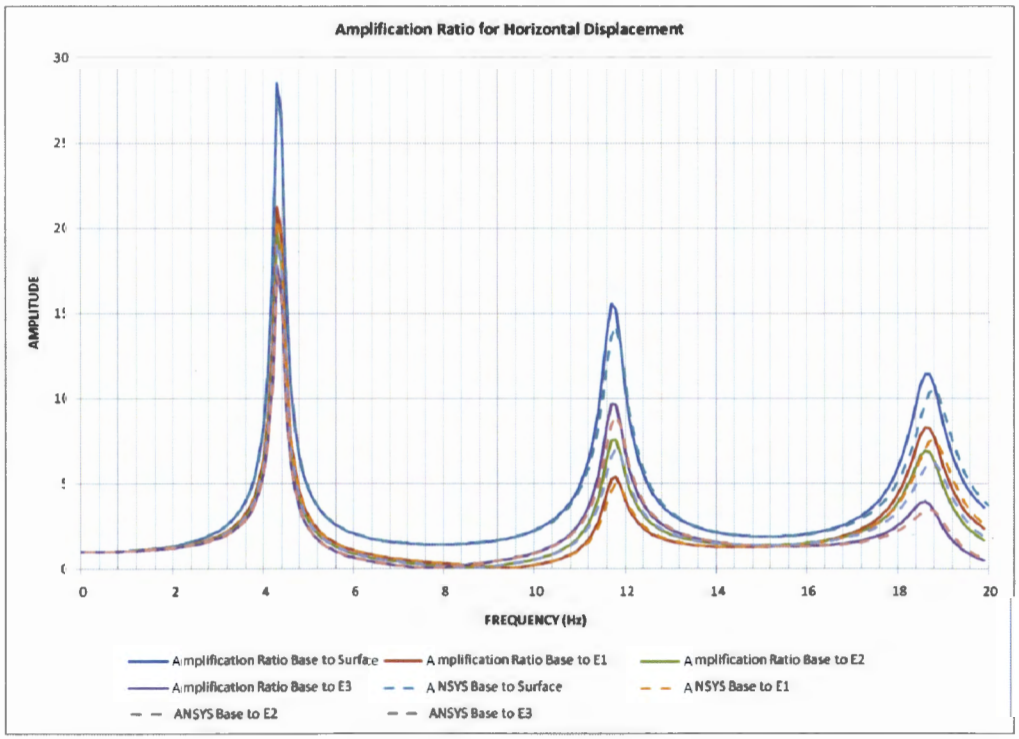

Figure 7.22. SHAKE91 vs. ANSYS® Free Field Horizontal Amplification Factors for Upper Bound

Table 7.11. Soil Column Modal Frequencies for Horizontal Excitation

Frequency (Hz)	Best Estimate		Lower Bound		Upper Bound	
	Horizontal		Horizontal		Horizontal	
	SHAKE91	ANSYS®	SHAKE91	ANSYS®	SHAKE91	ANSYS®
1	2.3	2.3	0.9	0.9	4.3	4.3
2	5.2	5.2	2.4	2.4	11.7	11.8
3	8.5	8.5	3.8	3.9	18.7	18.8
4	11.6	11.7	5.2	5.2	--	--
5	14.5	14.7	6.7	6.7	--	--

7.8.1.1 Soil Column Harmonic Analysis – Vertical Excitation

Ultimately, the seismic excitations are applied to ANSYS® models as force time histories based on acceleration time histories determined via SHAKE. Although the horizontal and vertical input motions are different, the soil column properties remain the same for the two directions.

Amplification factors for vertical displacement comparing SHAKE91 and ANSYS® with the best estimate soil properties is shown in Figure 7.23. Similarly, Figure 7.24 and Figure 7.25 show the vertical displacement amplification spectra for the LB and UB columns. Table 7.12 summarizes the natural frequencies of the three soil columns for vertical excitation.

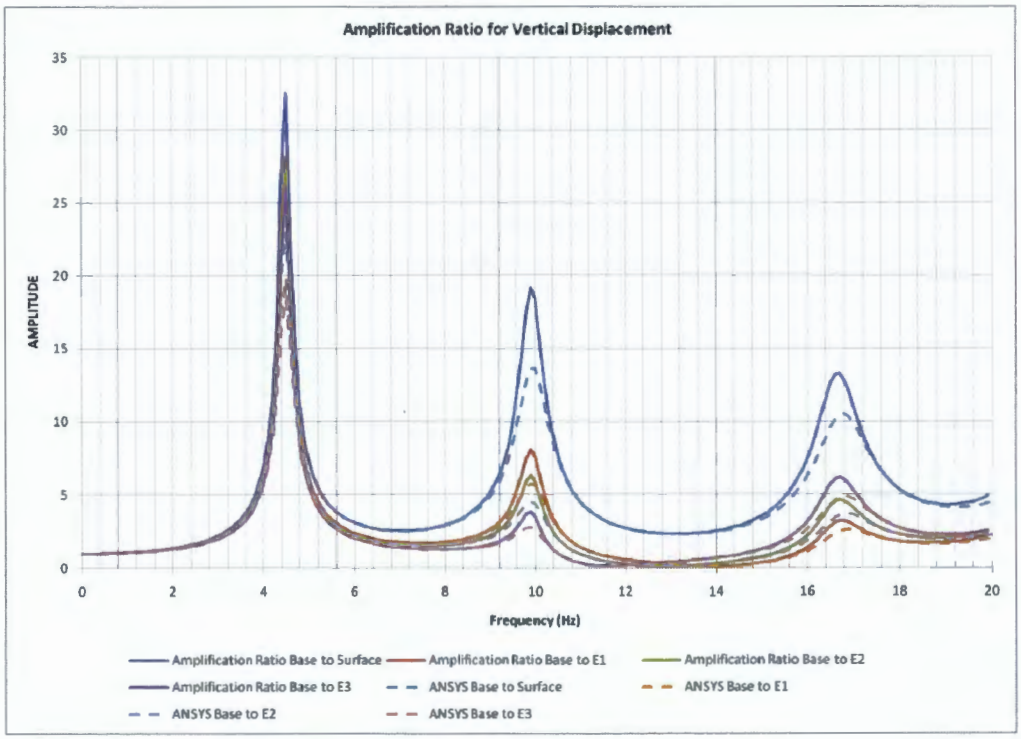

Figure 7.23. SHAKE91 vs. ANSYS® Free Field Vertical Amplification Factors for Best Estimate

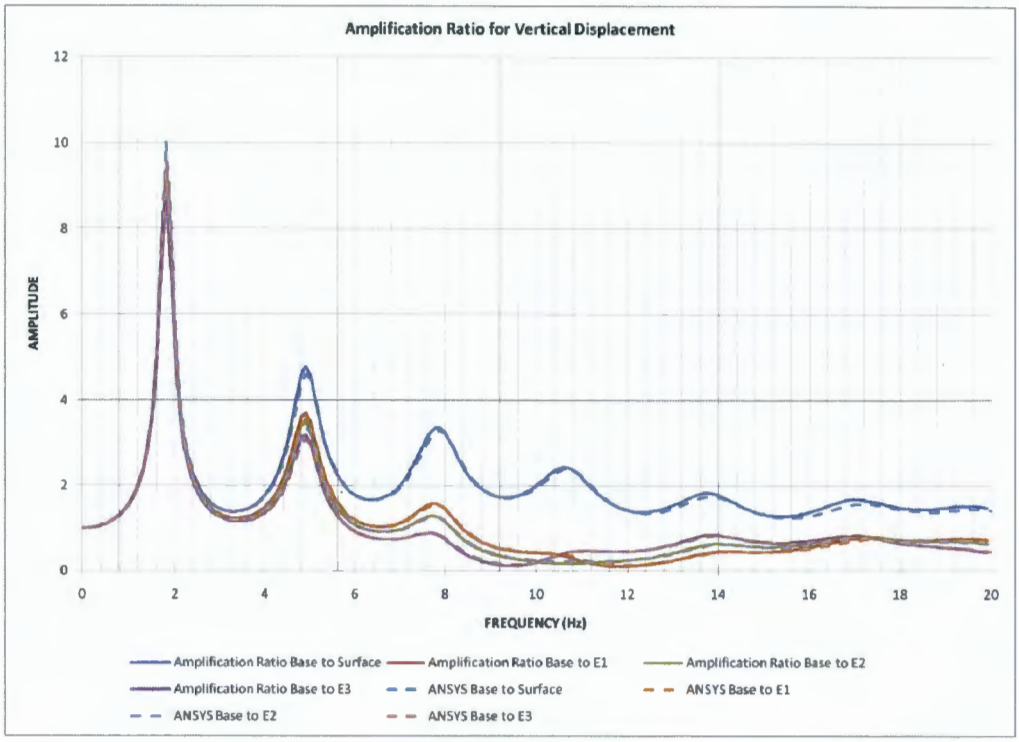

Figure 7.24. SHAKE91 vs. ANSYS® Free Field Vertical Amplification Factors for Lower Bound

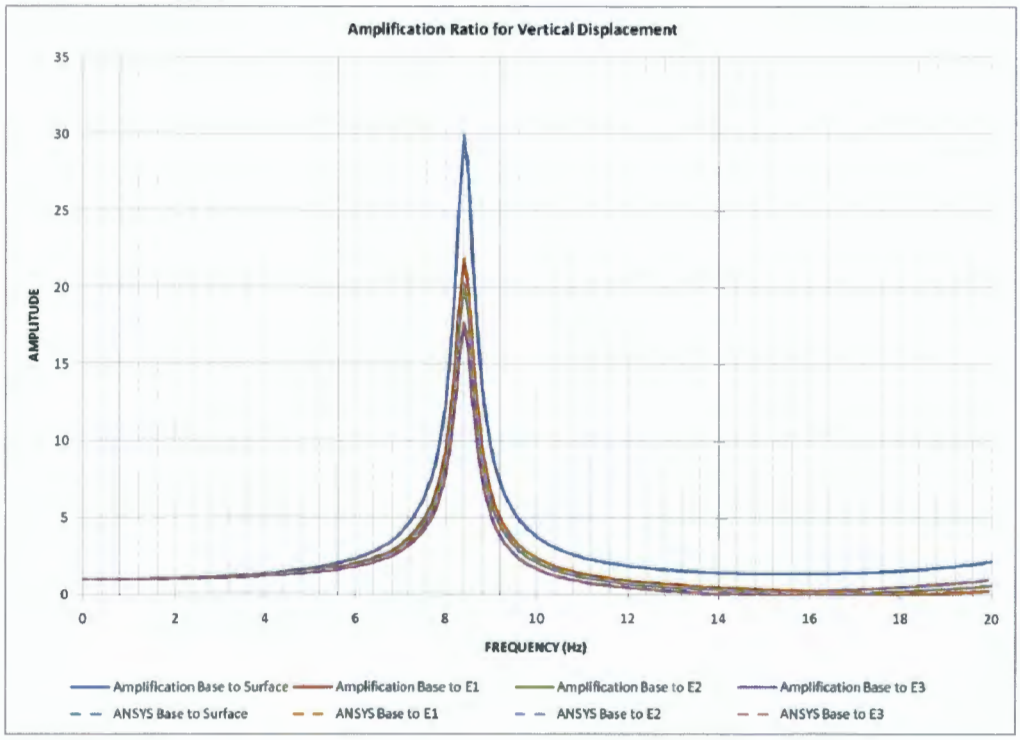

Figure 7.25. SHAKE91 vs. ANSYS® Free Field Vertical Amplification Factors for Upper Bound

Table 7.12. Soil Column Modal Frequencies for Vertical Displacement

Frequency (Hz)	Best Estimate Vertical		Lower Bound Vertical		Upper Bound Vertical	
	SHAKE91	ANSYS®	SHAKE91	ANSYS®	SHAKE91	ANSYS®
1	4.5	4.5	1.8	1.8	8.4	8.4
2	9.9	9.9	4.9	4.9	--	--
3	16.7	16.8	7.8	7.9	--	--
4	--	--	10.6	10.7	--	--
5	--	--	13.8	13.8	--	--

7.9 Spectral Matching Methodology and Acceptance Criteria

As described in the AMEC Geomatrix report in Appendix R of Rinker et al. (2011a), smooth target spectra have been developed at the surface and at the tank foundation levels using SHAKE. The surface target spectrum is the DRS (2/3 of the site-specific MCE) and the foundation-level target spectra are the three FIRS described previously in this section, there is one FIRS for each SSI profile and for each foundation level. Because the SSI evaluation is performed using ANSYS®, it must be verified that the spectral matching is preserved at the foundation level and at the surface in the ANSYS® SSI model when the base time histories are input to the SSI models. As stated in Section 7.4, the foundation-level targets for ANSYS® are the in-column spectra that are compatible with the time histories that are spectrally matched to the FIRS. Although the only one bounding FIRS is used for each soil column, when the spectrally matched motion is deconvolved to the base in SHAKE and convolved back up in ANSYS®, the process results in nine in-column targets to be considered in ANSYS®. That is, one target for each foundation elevation for each SSI profile.

The time histories spectrally matched to the target response spectra shown in the subject Geomatrix report were input as pseudo-outcrop motion into SHAKE91 and the in-column motions at the three foundation elevations E1, E2, and E3 as well as the in-column motion at the base of the SSI profiles were obtained. The motions at the base of the SSI profiles were then baseline corrected and applied as input to the ANSYS® SSI models.

The acceptance criteria for spectral matching were that the in-column spectra at each foundation level for each of the three soil columns should individually match the target (in-column) spectra from SHAKE according to the criteria below from McGuire et al. (2001) for a mean-based fit.

- Comparison between the time history response spectrum and the target response spectrum is made for 300 frequencies spaced uniformly in log frequency, 100 frequencies per log decade.
- The 5% damped response spectrum of the acceleration time history shall not fall more than 10% below the target response spectrum at any one frequency.
- The spectral ordinates for no more than 9 adjacent frequencies shall lie below the target spectrum.

At the surface, the same criteria were applied to the upper bound envelope of the three surface spectra corresponding to the three SSI profiles. Any deficiencies in the ANSYS® motions were noted. If significant valleys were present in the ANSYS® spectra over narrow frequency ranges, they were minimized as described below. If only a minor broad-banded adjustment was required, the time history could simply be scaled uniformly. Although some modifications to the time histories at the base of the SSI profiles were made to minimize significant narrow-banded valleys, no corrections were made to reduce peaks in the ANSYS® spectra.

To minimize significant valleys in the ANSYS® spectra relative to the target spectra, the base time history was modified by adjusting the appropriate FIRS target spectrum smoothly upward in the frequency range where the ANSYS® motions were deficient, and a new spectrally matched time history was obtained. This modified time history was then input into SHAKE91 and deconvolved to obtain a new base input motion for ANSYS®. The process was repeated until the response spectra for the ANSYS® in-column motions at the three foundation levels and at the surface adequately matched the response spectra for the SHAKE91 in-column motions obtained using the initial spectrally matched time history. This process was repeated separately for the LB, BE, and UB runs. It is important to understand that the adjustment to the target FIRS was done only within SHAKE simply for generating a modified time history. The target FIRS used for spectral matching in ANSYS® remained unaltered. This iterative process was followed for both the horizontal and vertical input motions.

7.9.1 Spectral Matching for the Simplified Soil Column

The spectral matching results for the simplified soil column introduced in Section 7.6 are presented below for the three soil columns and two directions of motion. From this point forward, the rest of the chapter focuses on spectral matching at the Type III tank foundation level (E2), which is at -49 ft. Figure 7.26, Figure 7.27, and Figure 7.28 show the spectral matching results for the ANSYS® soil column in the horizontal direction. In each figure, the upper panel shows the spectral match at the surface, and the lower panel shows the spectral match at the Type III tank foundation elevation (E2). The upper panel depicts the smooth surface spectrum (2/3 of the horizontal MCE), the SHAKE surface response spectrum from the particular soil profile (e.g., Target), and the ANSYS® surface response spectrum for the particular soil profile (e.g., ANSYS® Surface). The corresponding spectral accelerations are read off the left-hand scale.

Also shown in each of the plots is the percentage ratio between the SHAKE surface response spectrum and the ANSYS® surface response spectrum. In these plots the ratio was based on the SHAKE surface response spectrum from the specific soil profile as the "target" spectrum. However, the ultimate acceptance criterion is based on the smooth surface spectrum as the surface target. The percentage ratio in the two curves is read off of the right-hand scale. The two heavy horizontal black lines are also read off of the right-hand scale and indicate the 90% and 100% ratios that are helpful in visualizing the acceptance criteria. Similar plots for the vertical direction are shown in Figure 7.29, Figure 7.30, and Figure 7.31. The plots indicate that for the simplified soil columns, the ANSYS® responses exceed the target responses at both the tank foundation level and the surface.

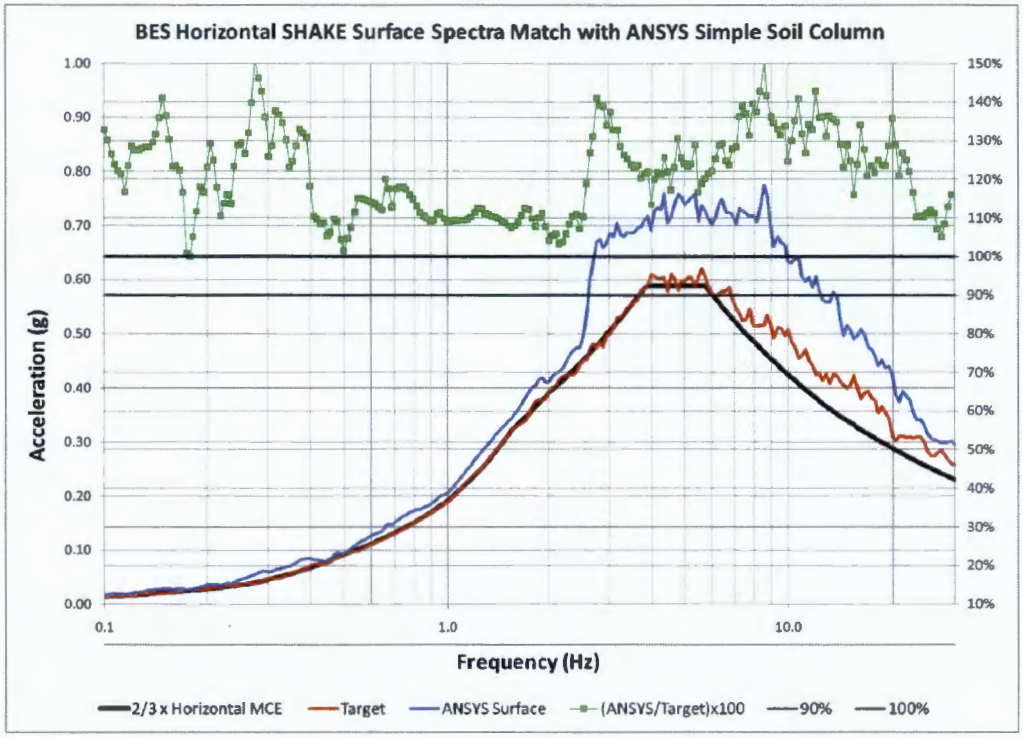

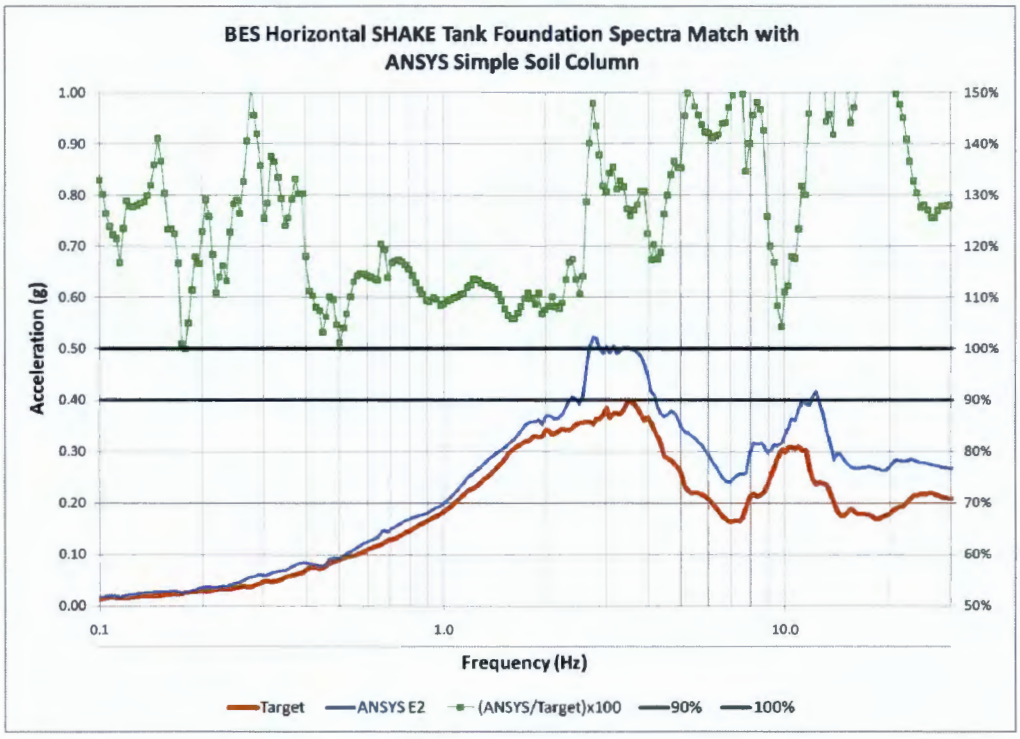

Figure 7.26. Best Estimate Surface and Tank Foundation Spectra from Horizontal Time History Comparison between ANSYS® and Target Spectra

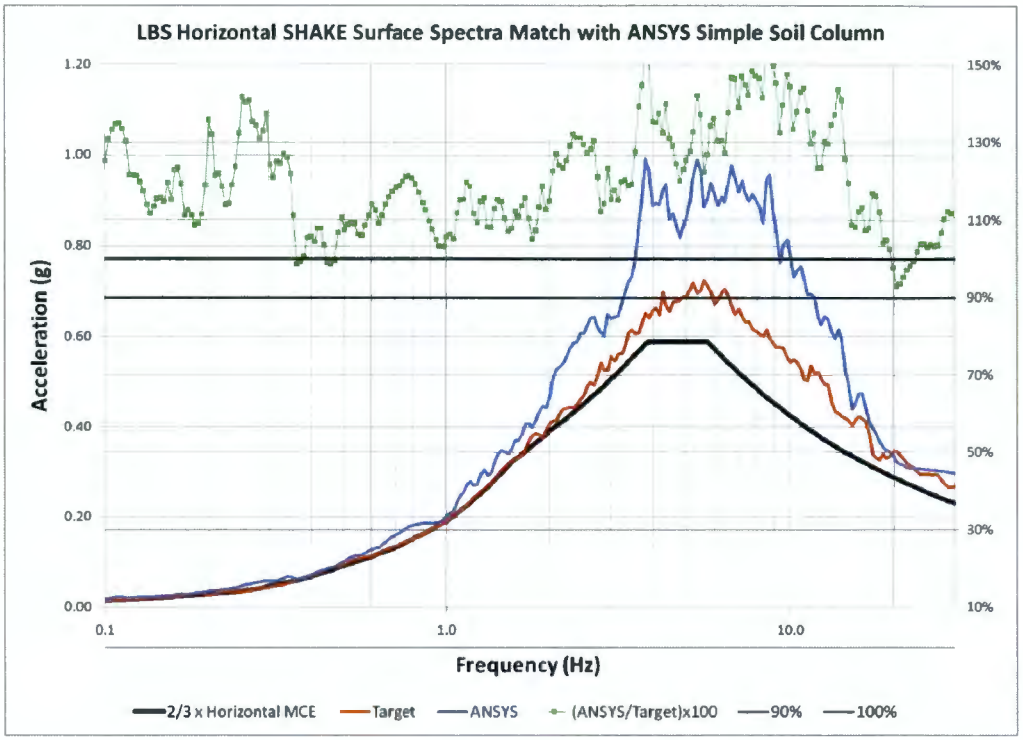

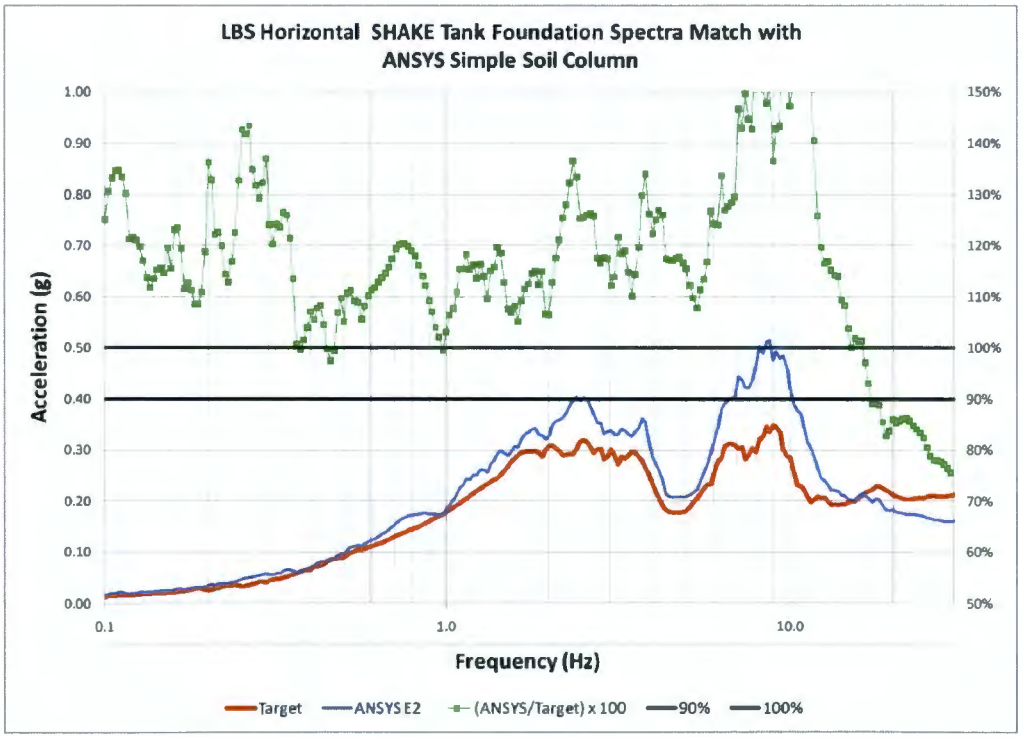

Figure 7.27. Lower Bound Surface and Tank Foundation Spectra from Horizontal Time History Comparison Between ANSYS® and Target Spectra

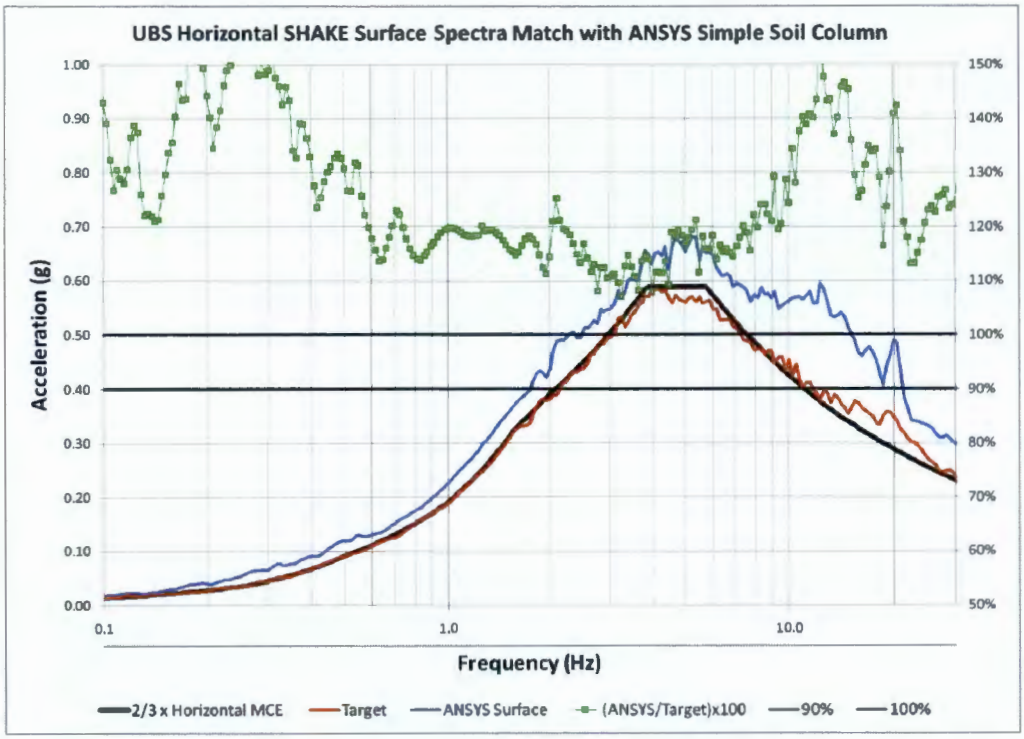

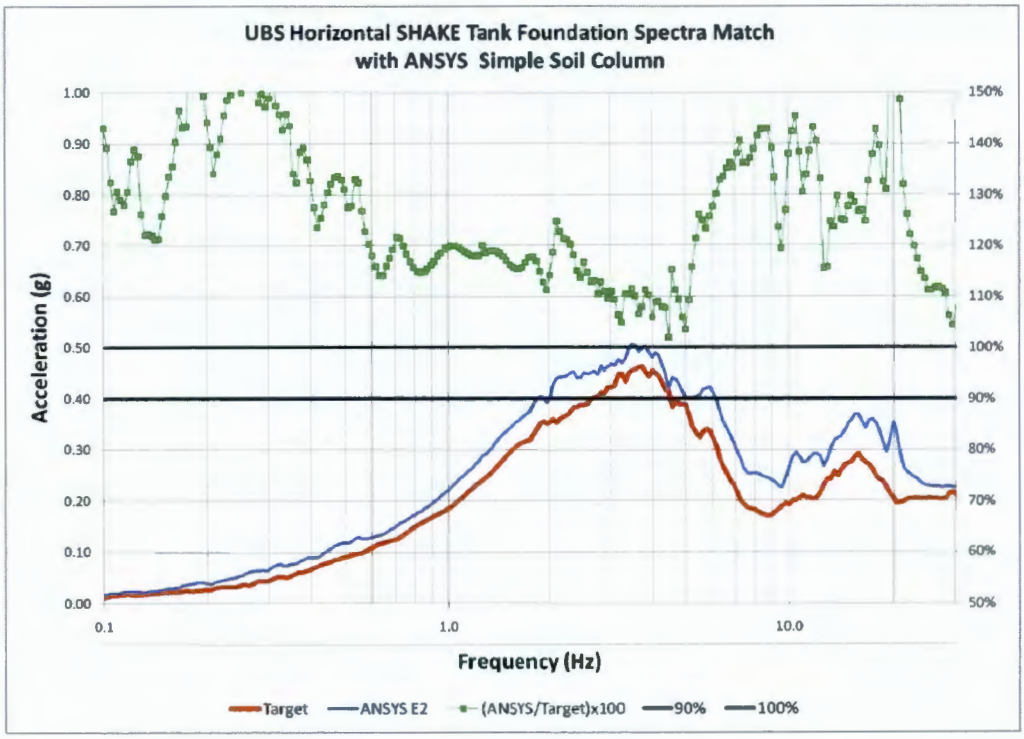

Figure 7.28. Upper Bound Surface and Tank Foundation Spectra from Horizontal Time History Comparison Between ANSYS® and Target Spectra

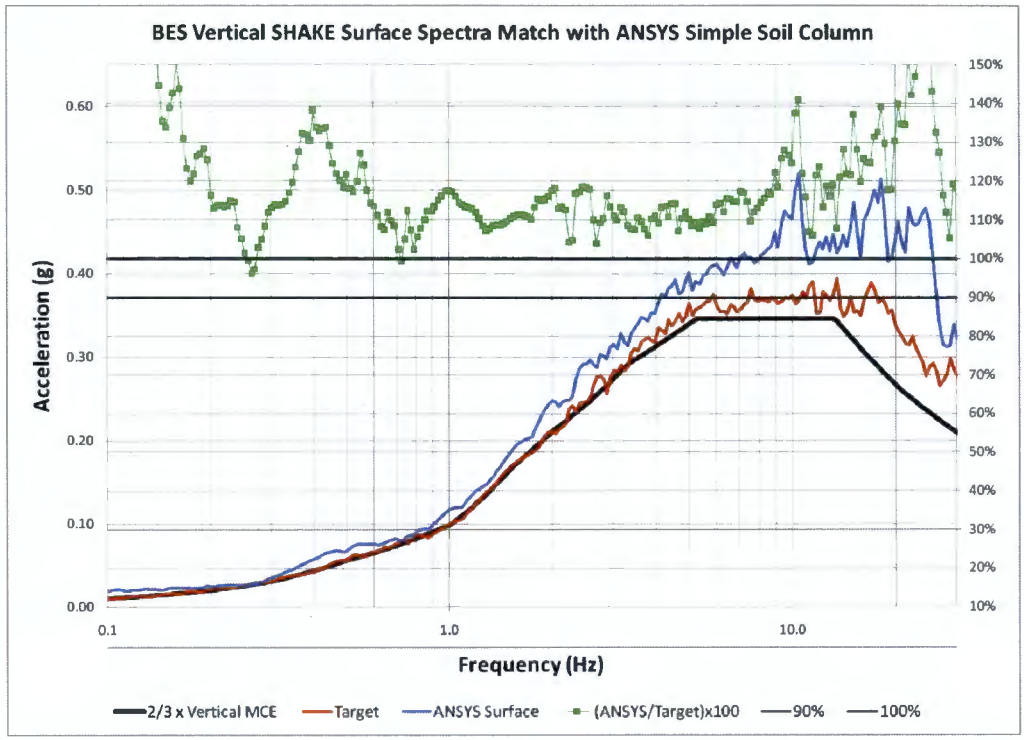

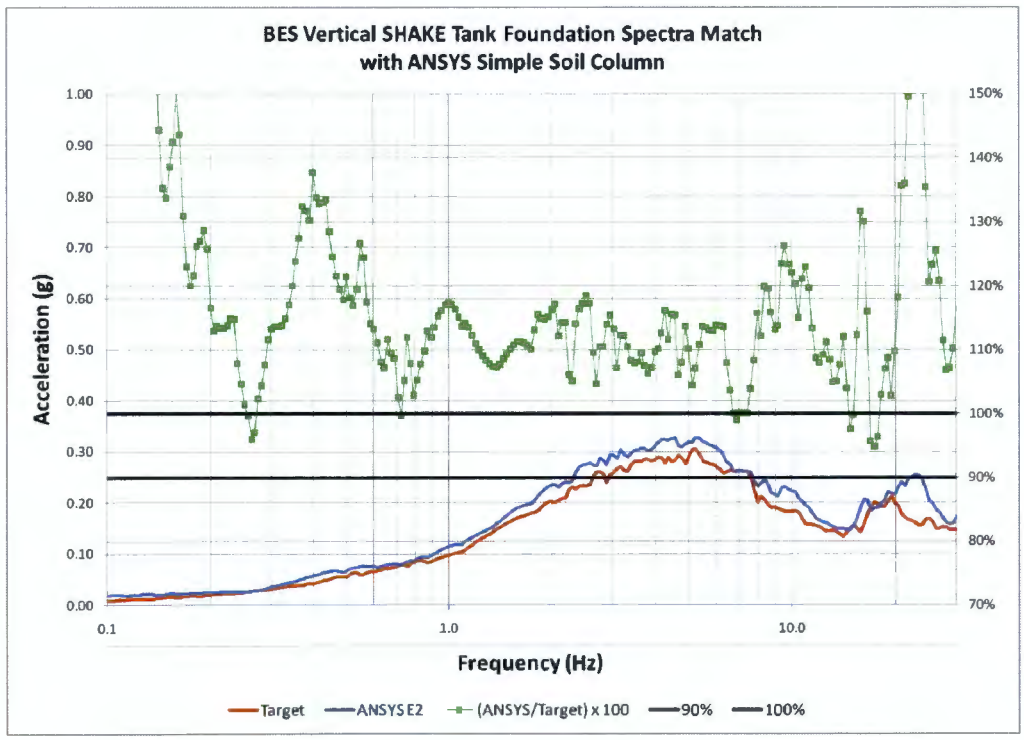

Figure 7.29. Best Estimate Surface and Tank Foundation Spectra from Vertical Time History Comparison Between ANSYS® and Target Spectra

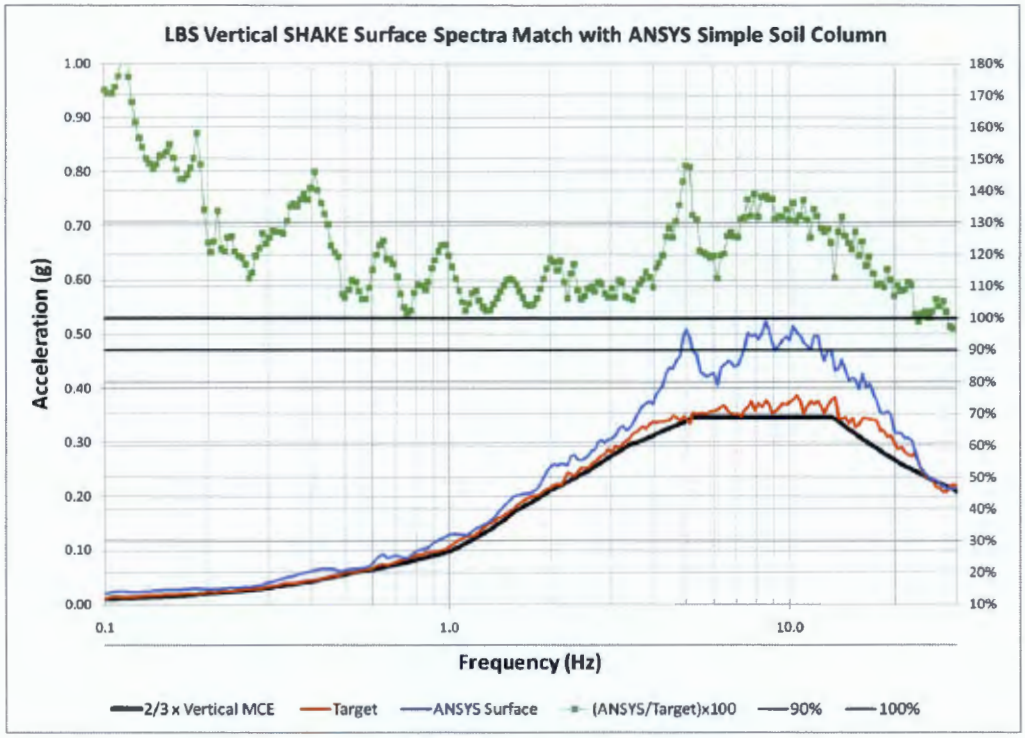

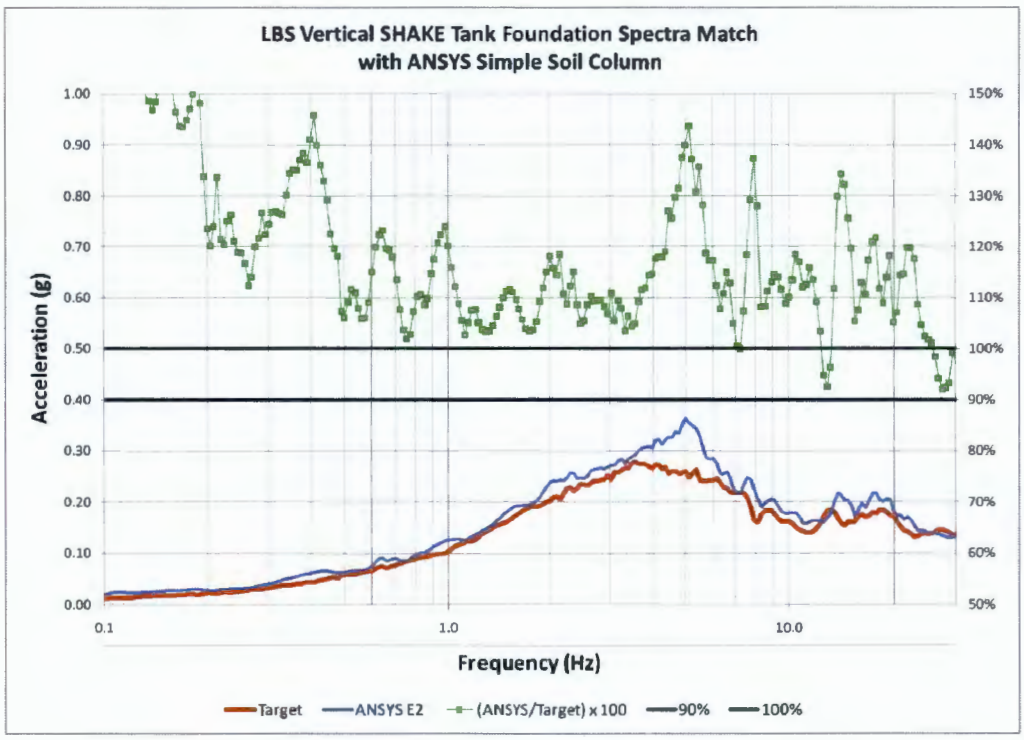

Figure 7.30. Lower Bound Surface and Tank Foundation Spectra from Vertical Time History Comparison Between ANSYS® and Target Spectra

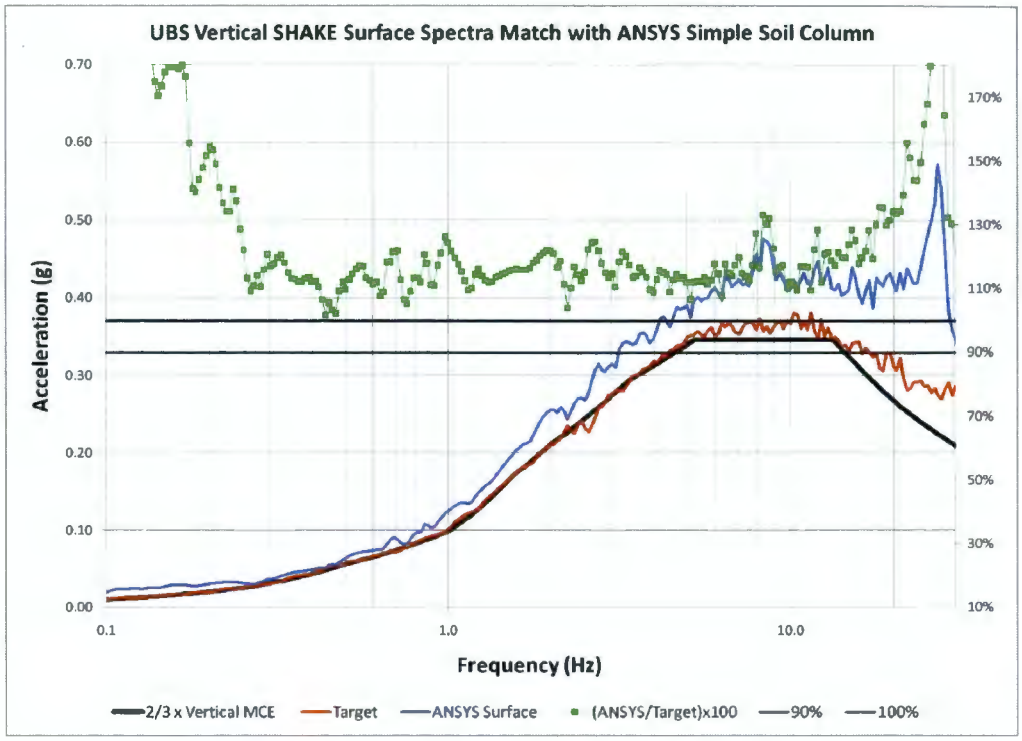

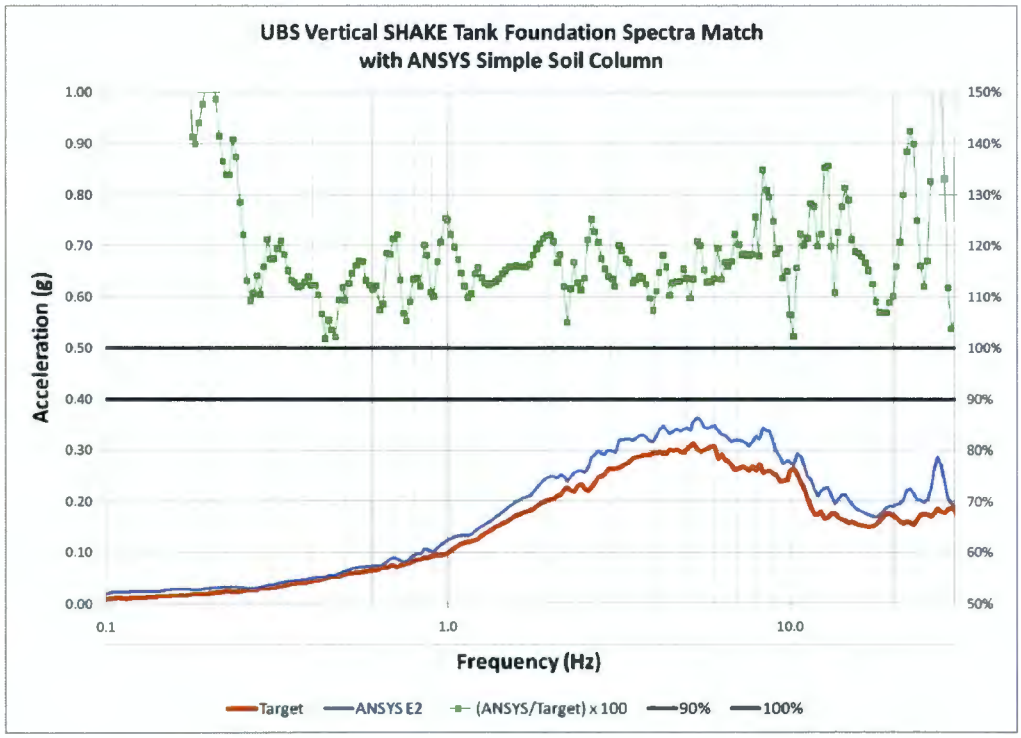

Figure 7.31. Upper Bound Surface and Tank Foundation Spectra from Vertical Time History Comparison Between ANSYS® and Target Spectra

7.9.2 Spectral Matching for the Full ANSYS® SSI Model

7.9.2.1 Empty Tank Spectral Results for SSI Full Model with Horizontal Time Histories

The ultimate test of the input motions is the response of the full ANSYS® SSI models to those motions. To check this response and compare the spectra to the targets, the ANSYS® SSI models were used to compute motions at the lateral boundary of the models (intended to simulate the free-field motion) at the surface and at the Type III tank foundation elevation (E2), which is at elevation -49 ft. The surface spectra and (in-column) foundation spectra were extracted from ANSYS® and compared to the DRS and in-column targets developed in SHAKE.

The spectral matching results for the full ANSYS® SSI model are presented below for the three soil columns and two directions of motion for the empty tank case. Figure 7.32 and Figure 7.33 show the spectral matching results for the BE column at the surface and at the tank foundation elevation, respectively. At the surface, the plot shows the smooth surface spectrum (2/3 of the horizontal MCE), the SHAKE surface spectrum (the legend shows this as 'Target'), and the ANSYS® surface spectrum (ANSYS® Surface). The plot also shows the ratio of the ANSYS® spectrum to the target as a percentage. As was the case for the simplified soil columns, the surface target is defined as the deterministic SHAKE surface spectrum. The foundation-level plot shows the in-column SHAKE target spectrum (Target), the ANSYS® SSI model spectrum (ANSYS® E2), and the ratio of the two curves.

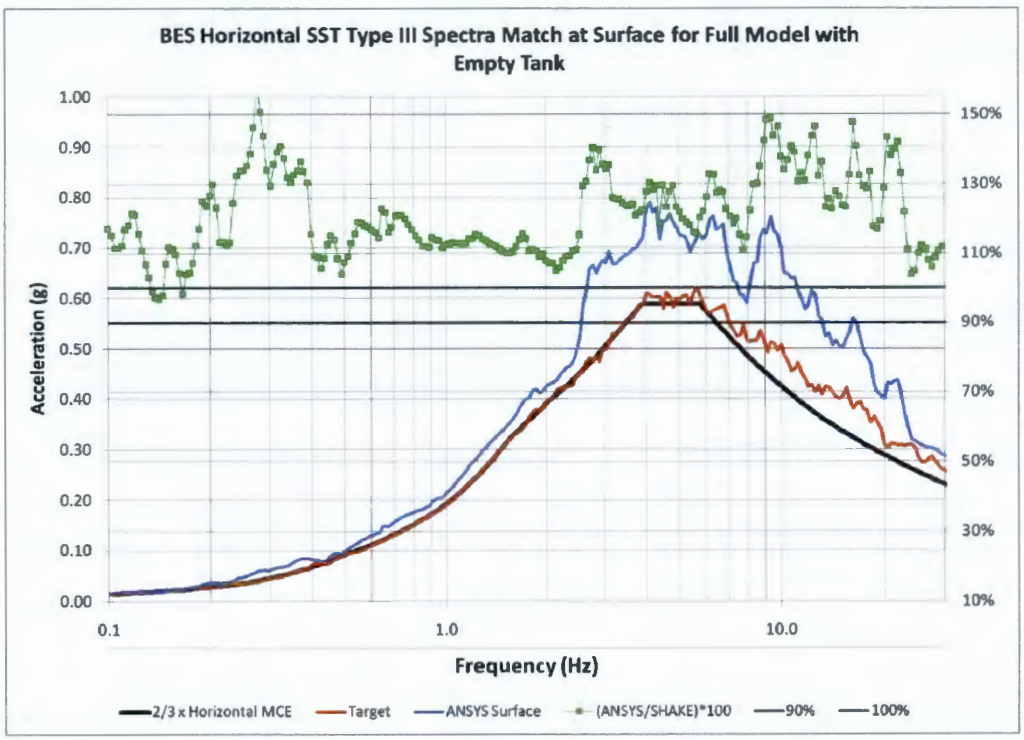

Figure 7.32. Comparison of Best Estimate Horizontal Surface Spectra with 5% Spectral Damping from the ANSYS® SSI Model with an Empty Tank

Figure 7.32 shows the surface spectrum from the ANSYS® SSI model and the SHAKE surface spectrum from the BE soil profile along with the smooth target spectrum. The ratio of the ANSYS® to SHAKE spectra is greater than 1.0 from 0.17 to 30 Hz.

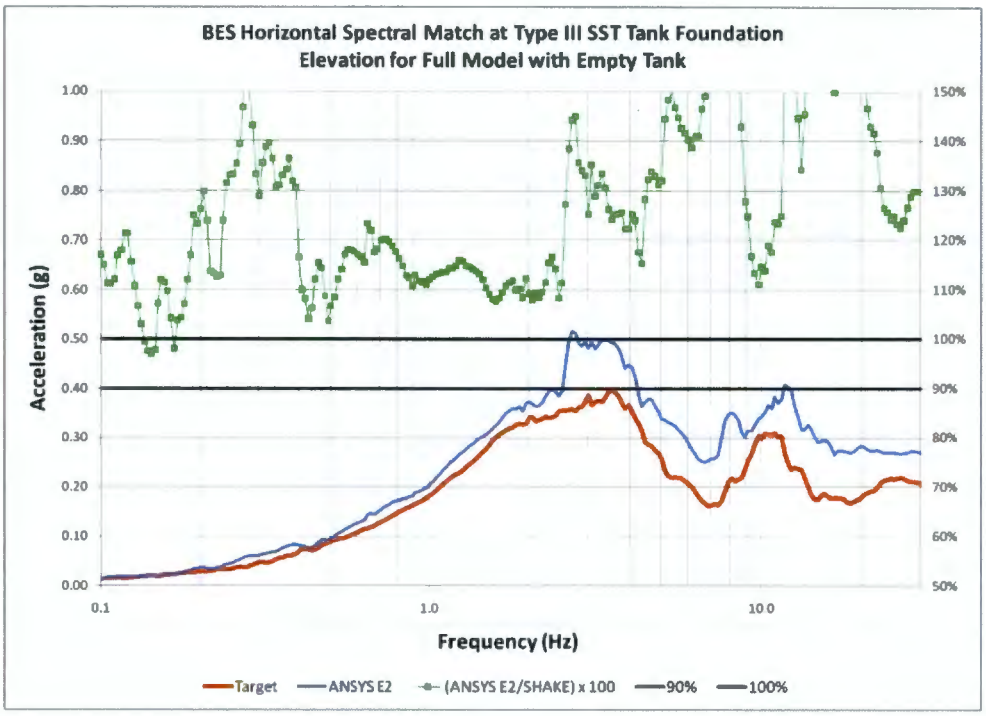

Figure 7.33. Comparison of Best Estimate Horizontal Tank Foundation Spectra with 5% Spectral Damping from the ANSYS® SSI Model with an Empty Tank

Figure 7.33 shows the foundation-level response spectra for the BE soil profile. The plot indicates that the spectrum for the ANSYS® SSI model exceeds the target in-column spectrum between 0.17 and 30 Hz. That is, the BE foundation spectrum meets the acceptance criteria described in Section 7.9.

Figure 7.34 shows the ANSYS® surface and the SHAKE surface spectrum for UB soil profile. Also shown is the smooth surface spectrum. The ratio of the ANSYS® to SHAKE surface spectra is greater than 1.0 except in a narrow band from approximately 4.37 to 4.65 Hz. However, in that frequency range, only two points fall below the ratio of 1.0 and everywhere the ratio of the two curves is always greater than 0.9, so the acceptance criteria is met.

Figure 7.35 shows the foundation-level response spectra for the UB soil profile. The ratio of the two curves is greater than 1.0 except in a narrow frequency band from approximately 4.37 to 5.0 Hz. In that frequency range, only 7 points fall below the ratio of 1.0, but a single point falls below 0.9 at 4.46 Hz. This single point does not meet the spectral acceptance criteria. As mentioned previously, scaling the time histories by a factor is proposed when the spectral acceptance criteria is not met. However, the tank demands and demand-to-capacity (D/C) ratios are further analyzed for acceptable tank performance. The D/C ratios plots for UB empty tank case, which are shown in the next section, have sufficient and wide margins. So by inspection of the D/C ratio, scaling the time histories for a single point would not change the results. Therefore, it is justified to accept the single point not meeting the spectral matching criteria because the tank performance is acceptable.

Figure 7.36 shows the ANSYS® surface spectrum along with the SHAKE surface spectrum and the smooth target surface spectrum for the LB soil profile. The ratio of ANSYS® and SHAKE spectra is greater than 1.0 between 0.15 and 25.13 Hz and is greater than 0.9 between 0.1 and 30.0 Hz.

Figure 7.37 shows the ANSYS® foundation spectrum and the LB soil profile target spectrum. The ratio of the two curves is greater than or equal to 1.0 between 0.15 and 16.2 Hz, after which two points fall below 1.0 followed by a single point below 0.9. The ratio of the two curves falls below 0.9 at 17.79 Hz.

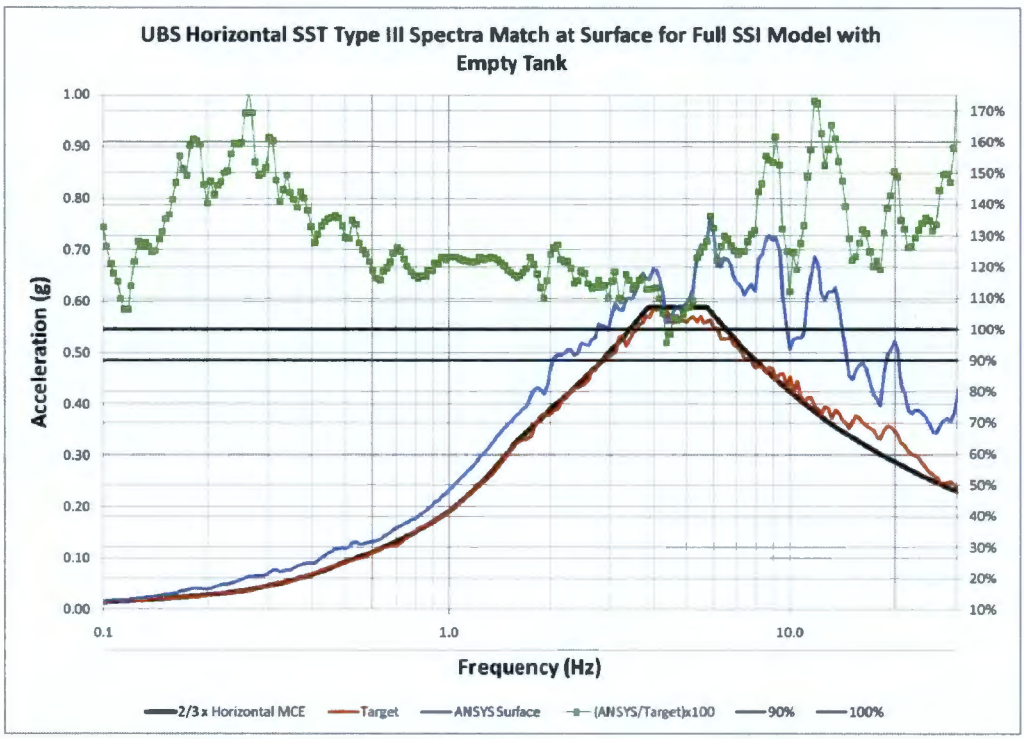

Figure 7.34. Comparison of Upper Bound Horizontal Surface Spectra with 5% Spectral Damping from the ANSYS® SSI Model with an Empty Tank

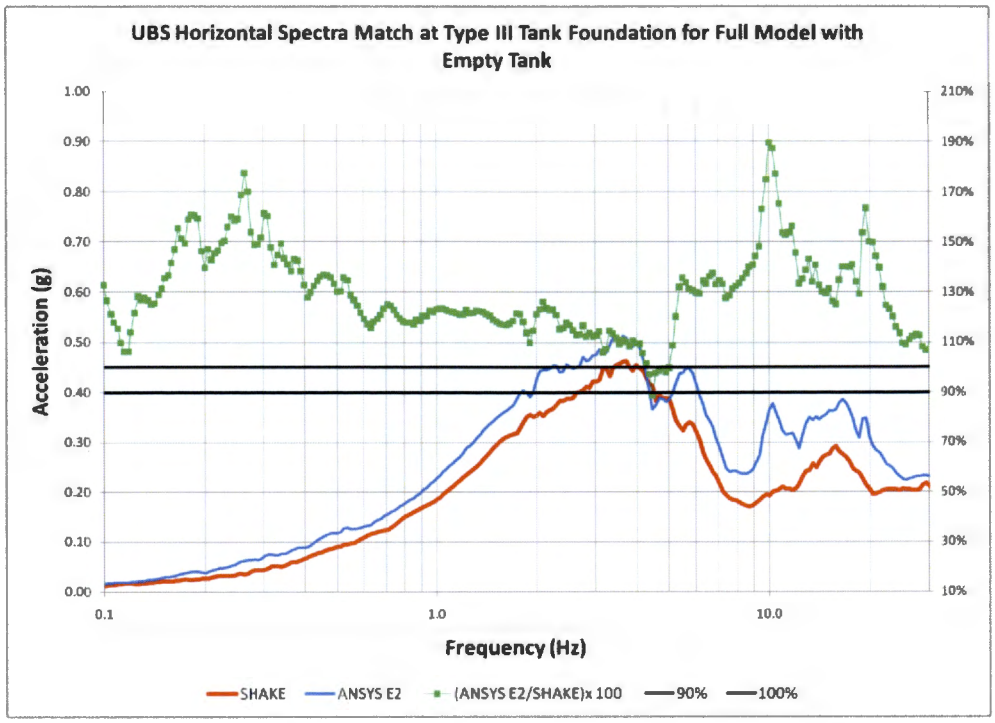

Figure 7.35. Comparison of Upper Bound Horizontal Tank Foundation Spectra with 5% Spectral Damping from the ANSYS® SSI Model with an Empty Tank

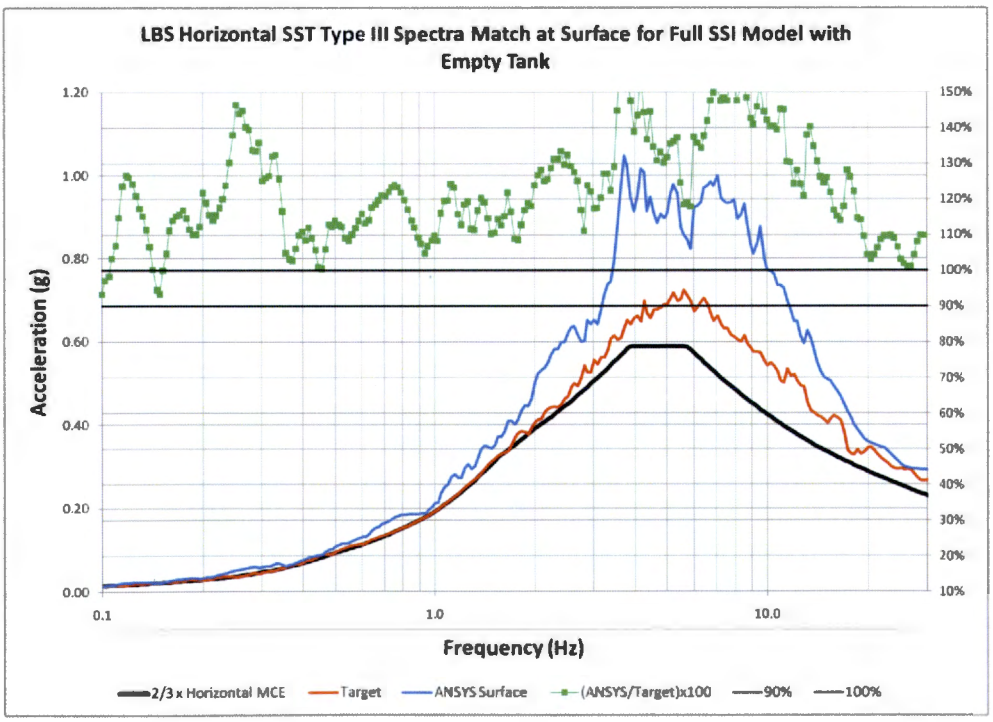

Figure 7.36. Comparison of Lower Bound Horizontal Surface Spectra with 5% Spectral Damping from the ANSYS® SSI Model with an Empty Tank

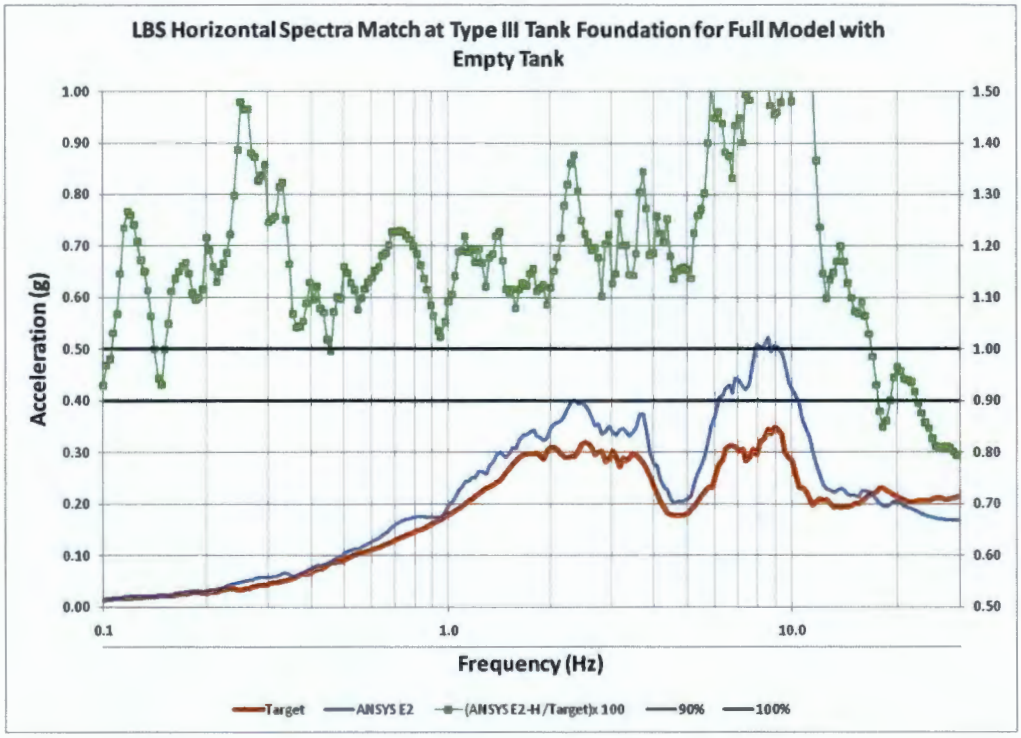

Figure 7.37. Comparison of Lower Bound Horizontal Tank Foundation Spectra with 5% Spectral Damping from the ANSYS® SSI Model with an Empty Tank

Figure 7.38 shows the three soil profile surface spectra plotted against the smooth target spectrum. Figure 7.39 shows the surface spectral ratio curves for each soil profile and the maximum surface envelope (heavy black curve). It is clear that the upper bound envelope of ANSYS® SSI model surface spectra ratio exceeds 1.0 and 0.9 of the target spectrum for all of the frequencies shown.

The conclusion from this section is that adequate spectral matching has been achieved between the ANSYS® SSI model and the target spectra generated by SHAKE in the frequency range of 0.1 to 30.0 Hz. Adequate spectral matching between the ANSYS® SSI model and target spectra for the LB soil profile has a slightly smaller frequency range of 0.1 to 17.79 Hz. The limiting run is the UB soil profile, where at the tank foundation; the spectra response at 4.46 Hz has a single point that is 0.89 of target. If this case were excluded, there are adequate spectra matching between 0.1 and 17.79 Hz. In general, there is a very conservative bias in the input time histories.

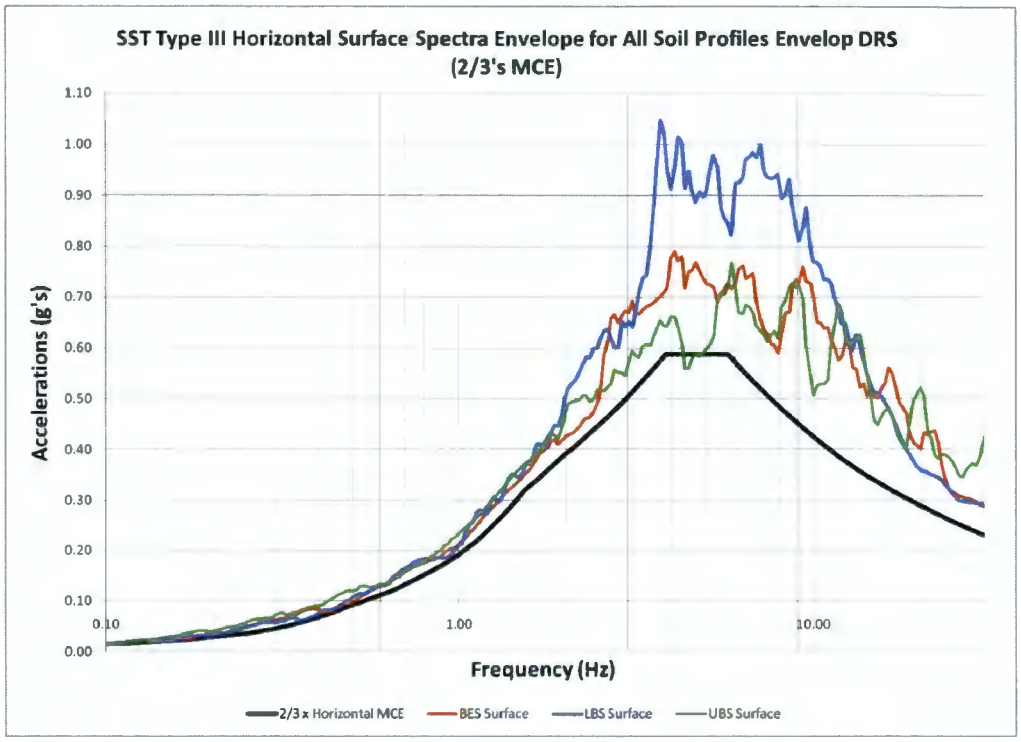

Figure 7.38. Surface Spectra Curves for Horizontal Time Histories

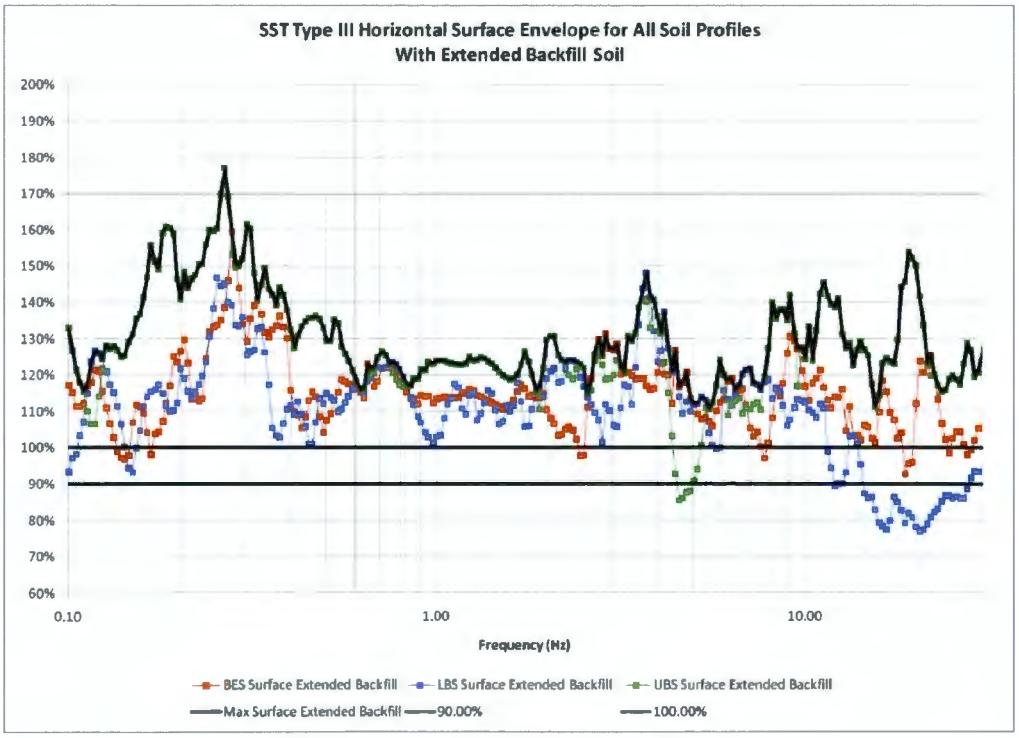

Figure 7.39. Surface Spectra Ratio Curves and Maximum Envelope Curve for Horizontal Time Histories

7.9.2.2 Spectral Results for SSI Full Model with High Shear Stiffness Tank Waste with Horizontal Time Histories

This section shows the spectral matching results for the full ANSYS® SSI model from the three soil columns for tank waste characterized with high shear stiffness properties. Figure 7.40 and Figure 7.41 show the spectral matching results for the BE column at the surface and at the tank foundation elevation, respectively. The nomenclature presented in the previous section applies to the following figures.

Figure 7.40 shows the surface spectrum from the ANSYS® SSI model and the SHAKE surface spectrum from the BE soil profile along with the smooth target spectrum. The ratio of the ANSYS® to SHAKE spectra is greater than 1.0 from 0.1 to 30 Hz with a few points that fall below 1.0, but none that fall below 0.9 of target.

Figure 7.41 shows the foundation-level response spectra for the BE soil. The plot indicates that the spectrum for the ANSYS® SSI model exceeds the target in-column spectrum between 0.1 and 30 Hz with a few points that fall below 1.0, but no points fall below 0.9. That is, the BE foundation spectrum meets the acceptance criteria described in Section 7.9 between 0.1 Hz and 30 Hz.

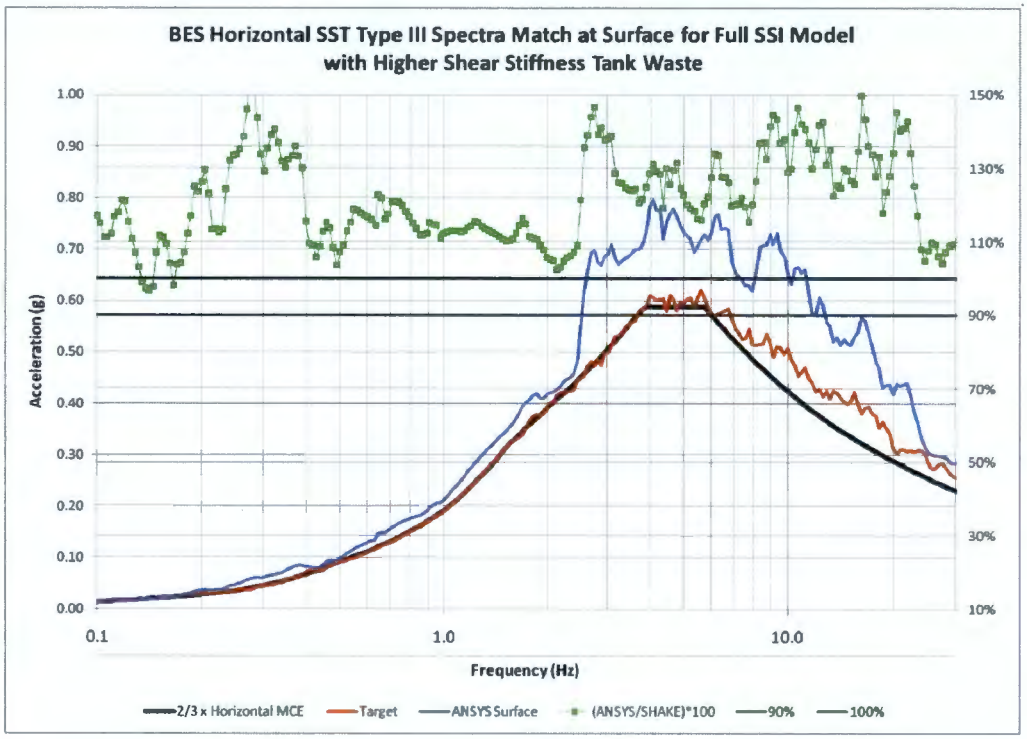

Figure 7.40. Comparison of Best Estimate Horizontal Surface Spectra with 5% Spectral Damping from the ANSYS® SSI Model with High Shear Stiffness Tank Waste

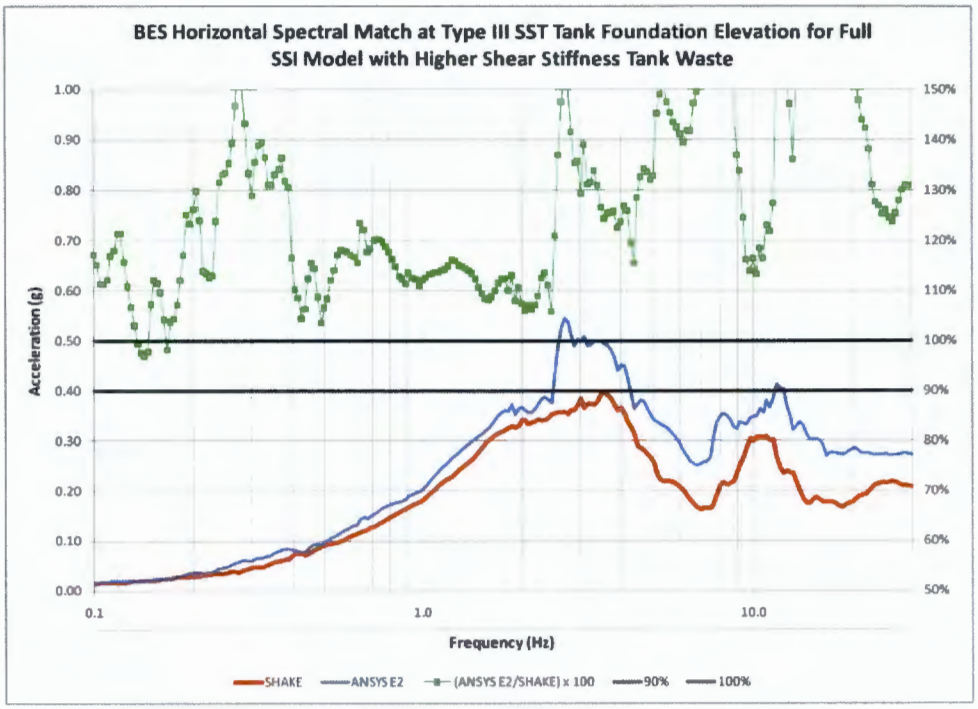

Figure 7.41. Comparison of Best Estimate Horizontal Tank Foundation Spectra with 5% Spectral Damping from the ANSYS® SSI Model with High Shear Stiffness Tank Waste

Figure 7.42 shows the ANSYS® surface and the SHAKE surface spectrum for UB soil. Also shown is the smooth surface spectrum. The ratio of the ANSYS® to SHAKE surface spectra is greater than 1.0 from approximately 0.1 to 30.0 Hz with a few points falling below 1.0, but always greater than 0.9. The ratio of the two curves meets the acceptance criteria described in Section 7.9 in the range of approximately 0.1 to 30.0 Hz.

Figure 7.43 shows the foundation-level response spectra for the UB soil. The ratio of the two curves is greater than 1.0 except in a narrow band from approximately 4.36 to 5.0 Hz. In this frequency range, 7 adjacent points fall below the ratio of 1.0, and a single point falls below 0.9 at 4.46 Hz. This single point does not meet the spectral acceptance criteria. As discussed previously, the time histories could be scaled by a factor to increase the spectrum so that the 0.9 spectral criterion can be met. However, the tank demands and demand-to-capacity (D/C) ratios show acceptable tank performance and have sufficient and wide margins. By inspection of the D/C ratio, scaling the time histories for a single point would not change the results. Therefore, scaling the time histories is not considered justifiable for a single point because the tank performance is acceptable.

Figure 7.44 shows the ANSYS® surface spectrum and the LB soil SHAKE surface spectrum and the smooth target surface spectrum. The ratio of ANSYS® and SHAKE spectra is greater than 1.0 between 0.15 and 30 Hz and is greater than 0.9 between 0.1 and 30 Hz.

Figure 7.45 shows the ANSYS® foundation spectrum and the LB soil profile target spectrum. The ratio of the two curves falls below 1.0 at several intervals between 0.1 to 16.2 Hz with two points that fall below 1.0 followed by a single point that is less than 0.9 at 17.79 Hz. The ratio of the two curves does meet the acceptance criteria between 0.1 and 17.79 Hz.

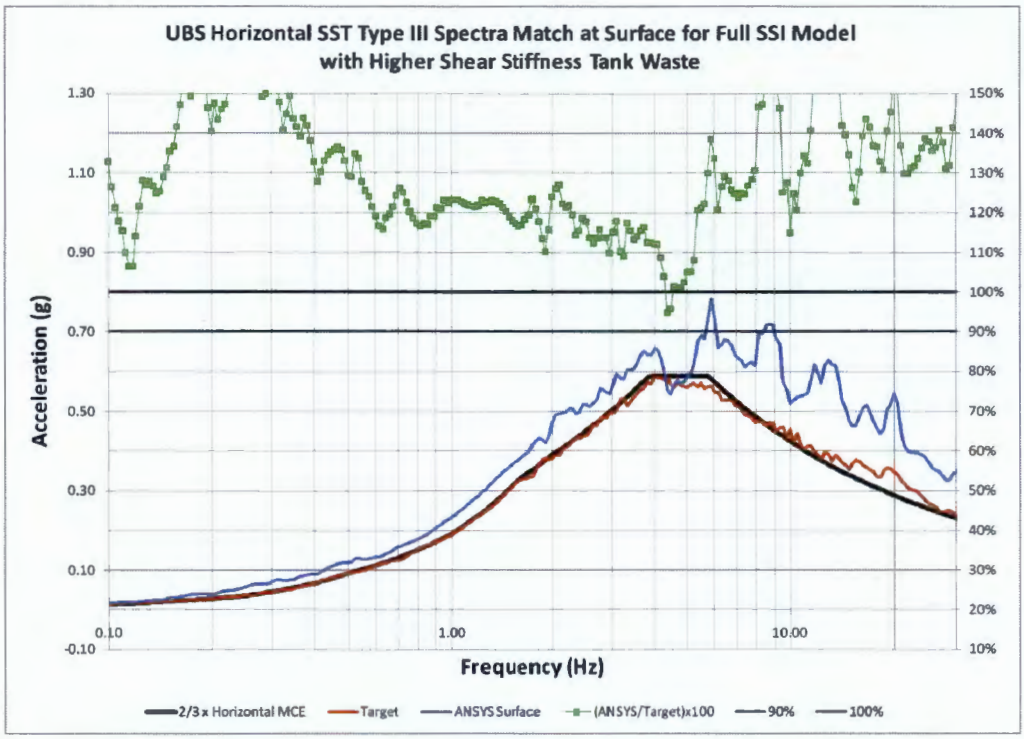

Figure 7.42. Comparison of Upper Bound Horizontal Surface Spectra with 5% Spectral Damping from the ANSYS® SSI Model with High Shear Stiffness Tank Waste

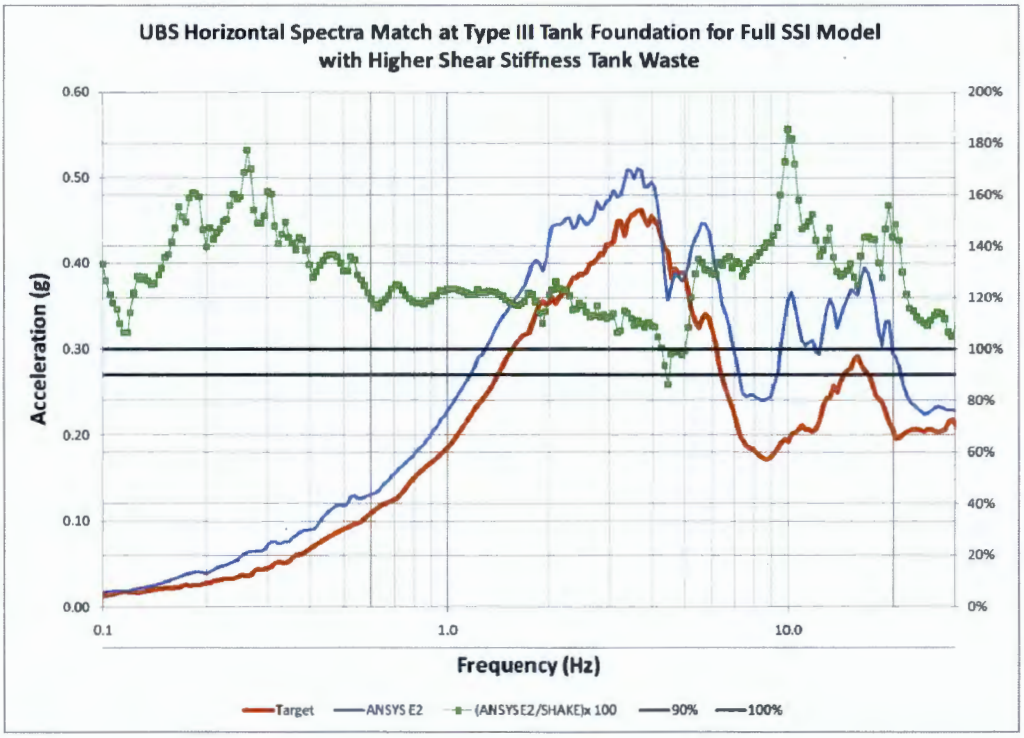

Figure 7.43. Comparison of Upper Bound Horizontal Tank Foundation Spectra with 5% Spectral Damping from the ANSYS® SSI Model with High Shear Stiffness Tank Waste

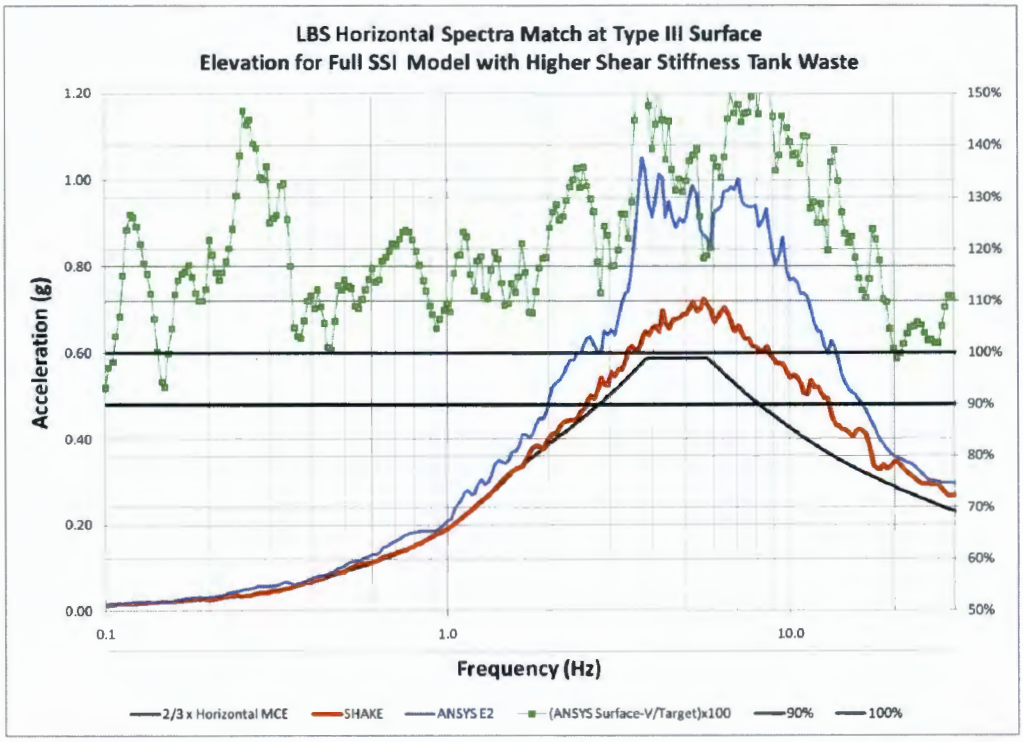

Figure 7.44. Comparison of Lower Bound Horizontal Surface Spectra with 5% Spectral Damping from the ANSYS® SSI Model with High Shear Stiffness Tank Waste

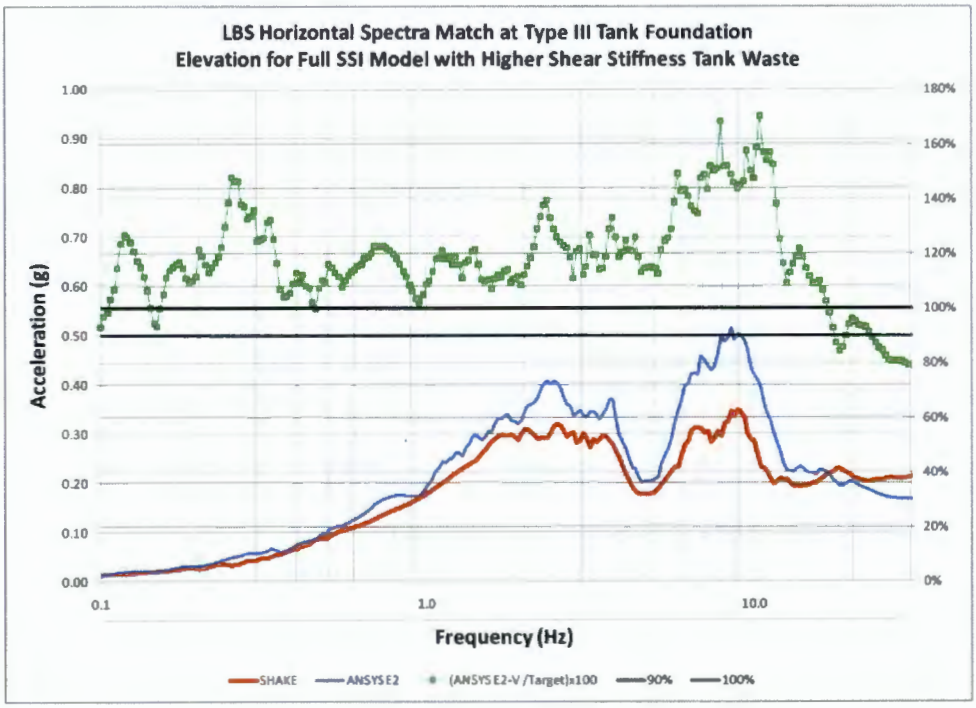

Figure 7.45. Comparison of Lower Bound Horizontal Tank Foundation Spectra with 5% Spectral Damping from the ANSYS® SSI Model with High Shear Stiffness Tank Waste

Figure 7.46 shows the three soil profile surface spectra plotted against the smooth target spectrum. Figure 7.47 shows the surface spectral ratio curves for each soil profile and the maximum surface envelope (heavy black curve). It is clear that the upper bound envelope of ANSYS® SSI model surface spectra ratio exceeds the 1.0 and 0.9 of the target for nearly all of the frequencies shown.

The conclusion from this section is that adequate spectral matching has been achieved between the ANSYS® SSI model and the target spectra generated by SHAKE in the frequency range of 0.1 to 17.79 Hz. The UB and LB soil profiles are the limiting the cases. For the LB soil profile, acceptable spectra results are shown from 0.1 to 17.79 Hz. The UB soil profile has acceptable results are from 0.1 to 30.0 Hz, except a single point falls below 0.9 of target at frequency 4.46 Hz. Excluding the single point with the UB soil profiles, the spectral matching is adequate from 0.1 to 17.79 Hz. In general, there is a very conservative bias in the input time histories.

Because the UB soil profile showed a single point below 0.9 of the target, a sensitivity study was performed to investigate whether the model boundary is far enough away from the tank and the results are discussed in this section. The study is to extend the model boundary from 320-ft radius to 400-ft and 600-ft radius and evaluate the spectral response of the UB soil profile at the model boundary. The tank foundation spectral ratio curves of ANSYS® to the target for both the 400-ft and 600-ft case meet the spectral acceptance criteria. More specifically, the ordinate at 4.46 Hz of the spectral ratio curve of ANSYS® to the target is above 0.9 and there less than 3 ordinates below 1.0 in the frequency band of 4.36 to 5.0 Hz for both cases. However, there was no change to tank demands. Scaling the time histories by a factor is an option for the baseline model radius, but the conclusions for the tank demands and D/C ratios would not change. Therefore, even though there is a single point below 0.9 of the target, the spectral matching is considered acceptable because the tank demands and D/C ratios will have sufficiently wide margins and the conclusions would not change.

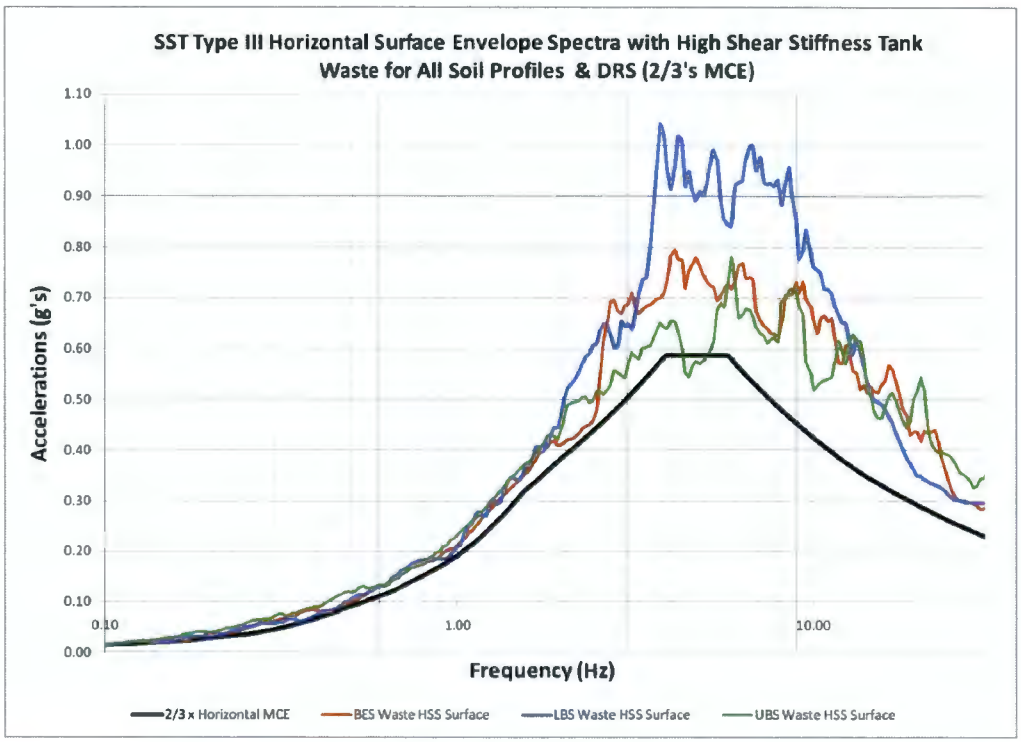

Figure 7.46. Surface Spectra Curves for Horizontal Time Histories for SSI Full Model with High Shear Stiffness Tank Waste

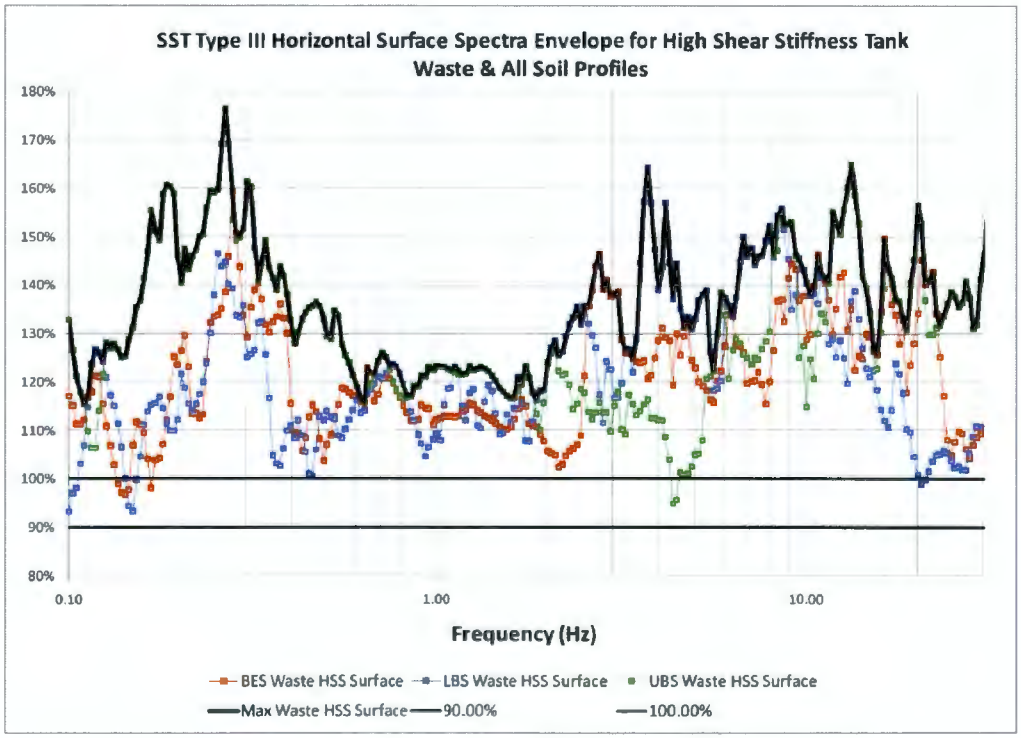

Figure 7.47. Surface Spectra Ratio Curves and Maximum Envelope Curve for Horizontal Time Histories for SSI Full Model with High Shear Stiffness Tank Waste

7.9.2.3 Spectral Results for SSI Full Model with Low Shear Stiffness Tank Waste with Horizontal Time Histories

This section presents the spectral matching results for the full ANSYS® SSI model from the three soil columns and two directions of motion. The full SSI model includes the tank waste that is characterized with low shear stiffness properties.

Figure 7.48 shows the surface spectrum from the ANSYS® SSI model and the SHAKE surface spectrum from the BE soil profile along with the smooth target spectrum. The ratio of the ANSYS® to SHAKE spectra is greater than 1.0 from 0.1 to 30 Hz.

Figure 7.49 shows the foundation-level response spectra for the BE soil. The plot indicates that the spectrum for the ANSYS® SSI model exceeds the target in-column spectrum between 0.1 and 30 Hz. That is, the BE foundation spectrum meets the acceptance criteria described in Section 7.9.

Figure 7.50 shows the ANSYS® surface and the SHAKE surface spectrum for UB soil. Also shown is the smooth surface spectrum. The ratio of the ANSYS® to SHAKE surface spectra is greater than 1.0 from 0.1 to 30.0 Hz with a few points that fall below the ratio of 1.0, but the ratio are greater than 0.9 of the target. The ratio of the two curves meets the acceptance criteria described in Section 7.9 in the range of approximately 0.1 to 30.0 Hz.

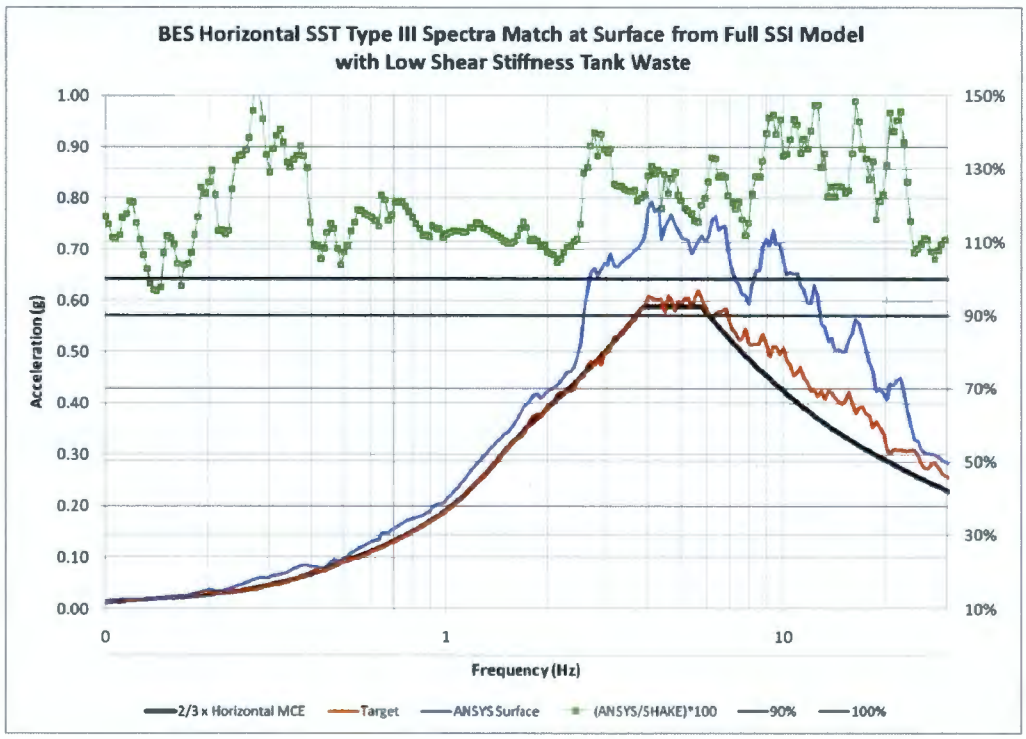

Figure 7.48. Comparison of Best Estimate Horizontal Surface Spectra with 5% Spectral Damping from the ANSYS® SSI Model with Low Shear Stiffness Tank Waste

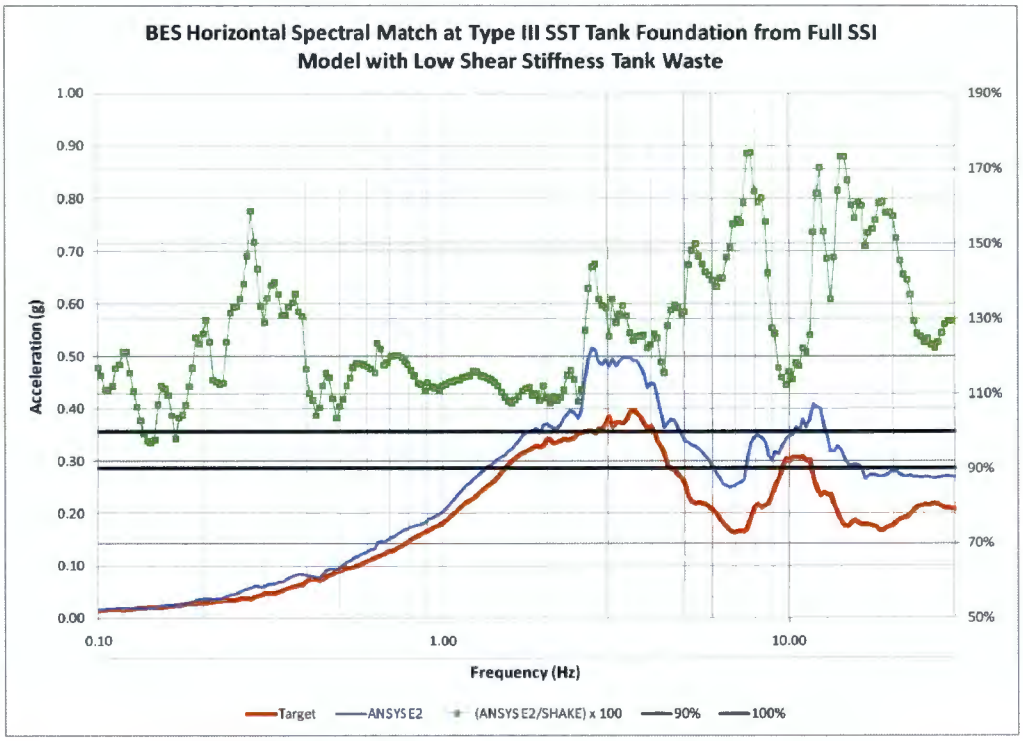

Figure 7.49. Comparison of Best Estimate Horizontal Tank Foundation Spectra with 5% Spectral Damping from the ANSYS® SSI Model with Low Shear Stiffness Tank Waste

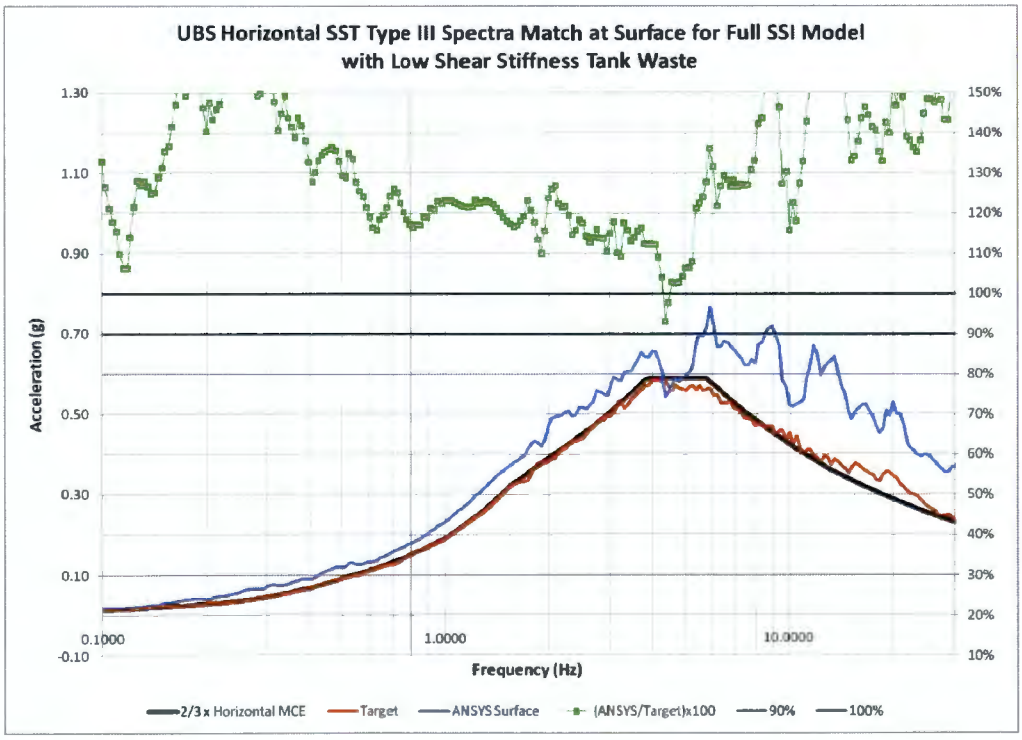

Figure 7.50. Comparison of Upper Bound Horizontal Surface Spectra with 5% Spectral Damping from the ANSYS® SSI Model with Low Shear Stiffness Tank Waste

Figure 7.51 shows the foundation-level response spectra for the UB soil. The ratio of the two curves is greater than 1.0 from approximately 0.1 to 30.0 Hz with several points that fall below 1.0 of the target. In that frequency range between 4.36 to 5.0 Hz, there are 7 adjacent points fall below the ratio of 1.0, and a single point falls below 0.9 at 4.46 Hz. This single point does not meet the spectral acceptance criteria. However, the tank demands and D/C ratios for this case are acceptable with wide margin. Even though the single point does not meet the spectral acceptance criteria, scaling the time histories would not change the conclusions. Therefore, the spectrum for this case is acceptable because the tank performance is acceptable.

Figure 7.52 shows the ANSYS® surface spectrum and the LB soil SHAKE surface spectrum and the smooth target surface spectrum. The ratio of ANSYS® and SHAKE spectra is greater than 1.0 between 0.15 and 30.0 Hz with one interval where a two points fall below 1.0. Between 0.1 and 30 Hz, none of the points fall below 0.9.

Figure 7.53 shows the ANSYS® foundation spectrum and the LB soil profile target spectrum. The ratio of the two curves has is greater than 1.0 between 0.107 Hz and 16.2 Hz with a few points that fall below 1.0. At 17.79 Hz, the ratio of the two curves falls below 0.9. The ratio of the two curves meets the acceptance criteria described in Section 7.9 between for 0.1 to 17.79 Hz.

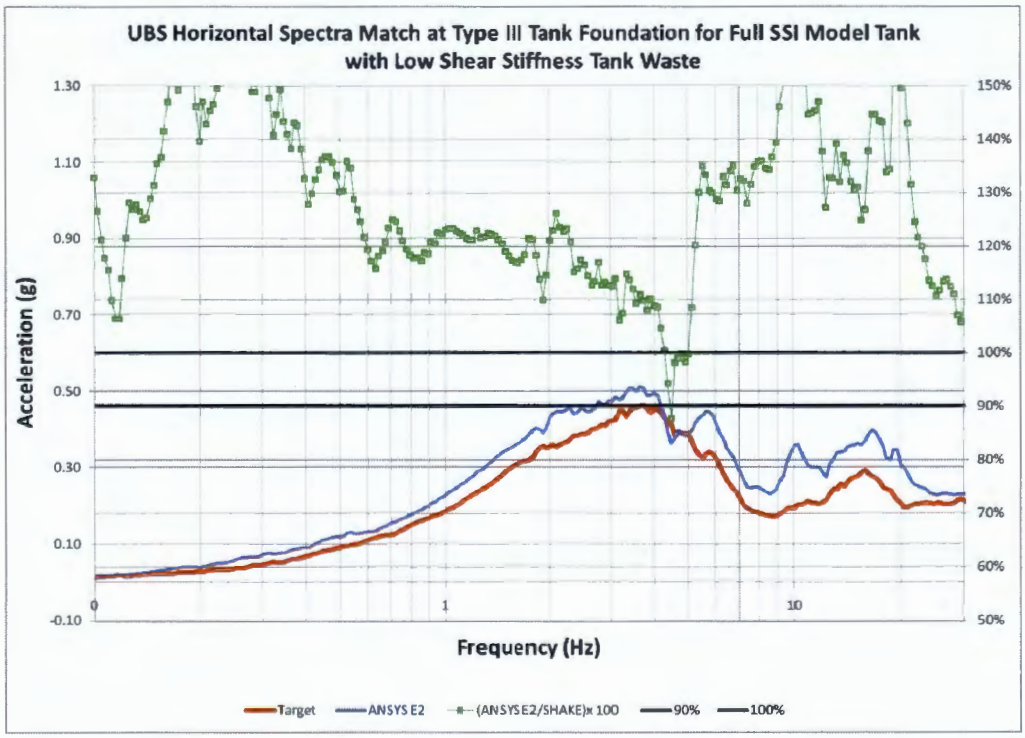

Figure 7.51. Comparison of Upper Bound Horizontal Tank Foundation Spectra with 5% Spectral Damping from the ANSYS® SSI Model with Low Shear Stiffness Tank Waste

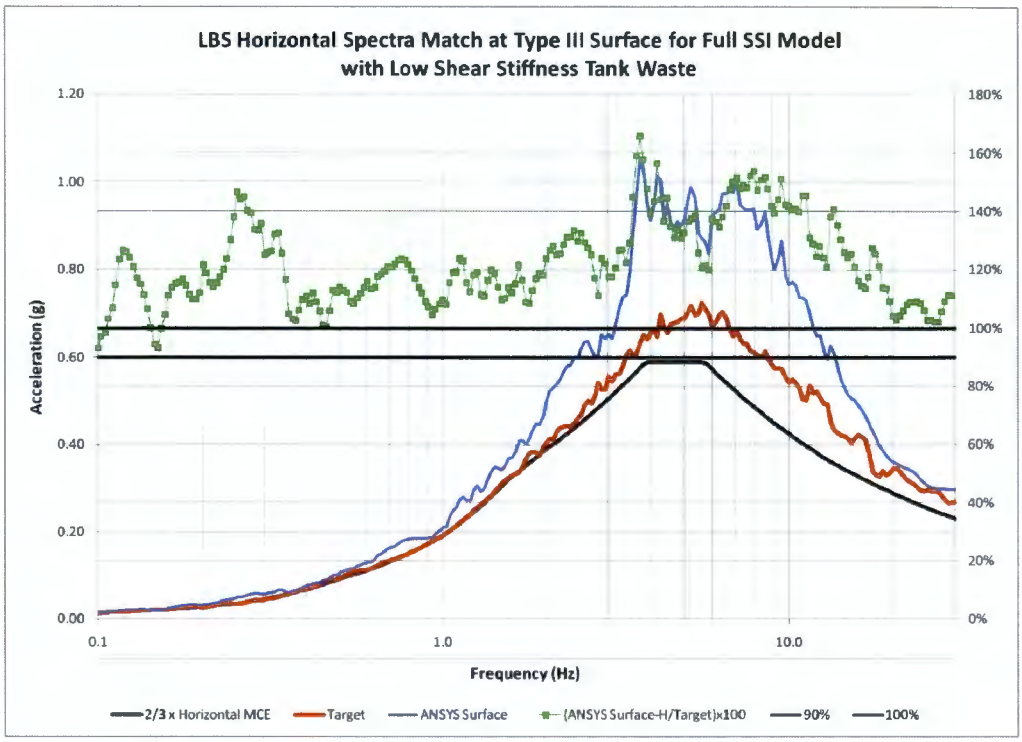

Figure 7.52. Comparison of Lower Bound Horizontal Surface Spectra with 5% Spectral Damping from the ANSYS® SSI Model with Low Shear Stiffness Tank Waste

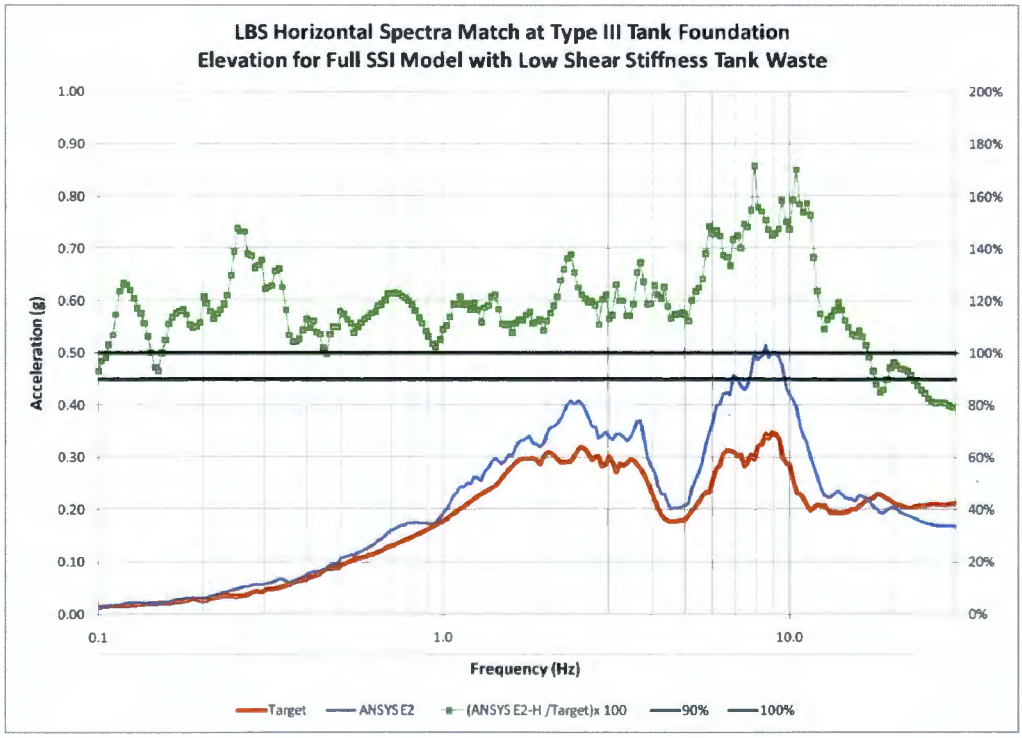

Figure 7.53. Comparison of Lower Bound Horizontal Tank Foundation Spectra with 5% Spectral Damping from the ANSYS® SSI Model with Low Shear Stiffness Tank Waste

Figure 7.54 shows the three soil profile surface spectra plotted against the smooth target spectrum. Figure 7.55 shows the surface spectral ratio curves for each soil profile and the maximum surface envelope (heavy black curve). It is clear that the upper bound envelope of ANSYS® SSI model surface spectra ratio exceeds 1.0 and 0.9 of the target spectrum for all of the frequencies shown.

The conclusion from this section is that adequate spectral matching has been achieved between the ANSYS® SSI model and the target spectra generated by SHAKE in the frequency range of 0.1 to 30.0 Hz. The limiting runs are the tank foundation response of the UB soil profile, which will be addressed by further evaluation of the tank demands. In general, there is a very conservative bias in the input time histories.

A sensitivity study was performed to investigate whether the model boundary of the UB soil profile is far enough away from the tank. The study is to extend the model boundary from 320-ft to 400-ft and 600-ft. The tank foundation spectral ratio curves of ANSYS® to the target for both the 400-ft and 600-ft case meets the spectral acceptance criteria. More specifically, the ordinate at 4.46 Hz of the spectral ratio curve of ANSYS® to the target is above 0.9 and there less than 3 ordinates below 1.0 in the frequency band of 4.36 to 5.0 Hz for both cases. The tank demands are evaluated and there are no changes.

Scaling the time histories of the baseline model is an option, but the conclusions from the tank demands and D/C ratios would not change. This option is deemed unnecessary because there would be no change to the tank performance. The spectrum for the UB soil profile is acceptable because tank performance would not change.

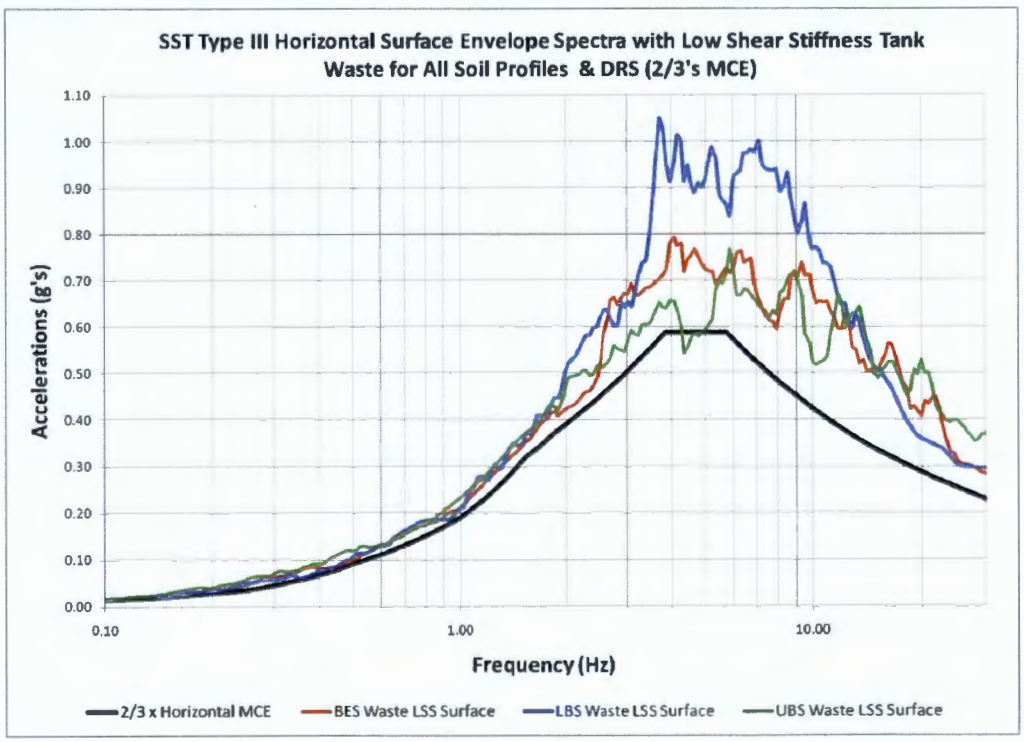

Figure 7.54. Surface Spectra Curves for Horizontal Time Histories for SSI Full Model with Low Shear Stiffness Tank Waste

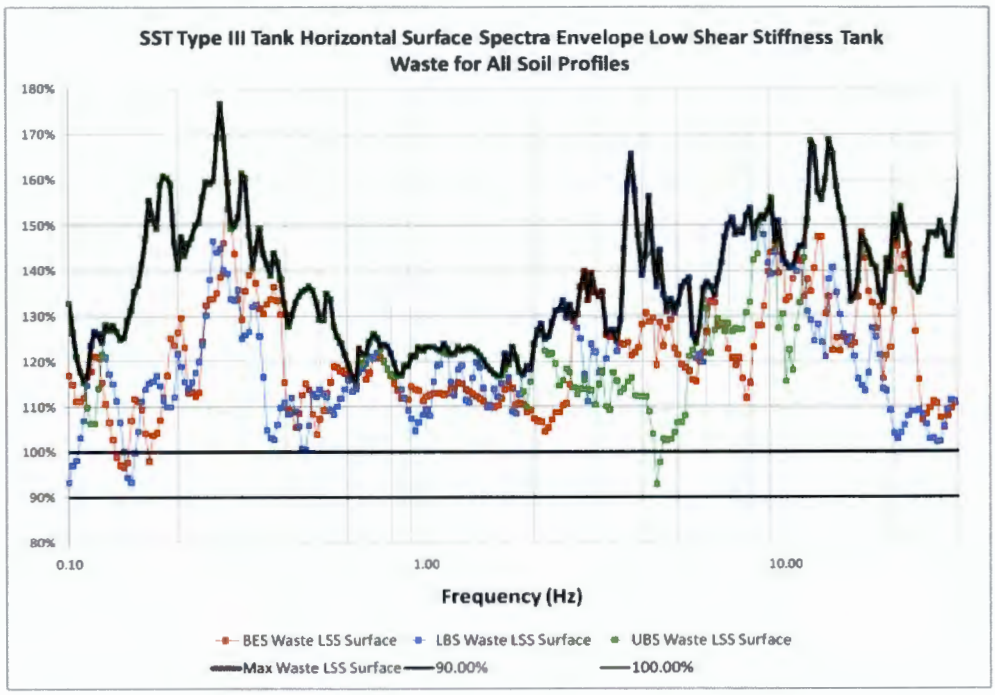

Figure 7.55. Surface Spectra Ratio Curves and Maximum Envelope Curve for Horizontal Time Histories for SSI Full Model with Low Shear Stiffness Tank Waste

7.9.2.4 Empty Tank Spectral Results with Vertical Time Histories

The previous section describe the spectral matching between the ANSYS® SSI model and SHAKE for horizontal input motions. This section repeats that process for the vertical input motion and shows spectra results for the empty tank case.

Figure 7.56 shows the vertical surface spectrum from the ANSYS® SSI model BE profile along with the SHAKE surface spectrum and the smooth vertical surface spectrum. The ratio of the ANSYS® to SHAKE surface spectrum is greater than 1.0 from 0.1 to 30 Hz.

Figure 7.57 shows the foundation-level response spectra for the BE soil profile. The plot indicates that the spectrum for the ANSYS® SSI model and the target in-column spectrum for a frequency range between 0.1 and 30 Hz. The ratio of the ANSYS® to SHAKE spectra dips below 1.0 at several intervals, but none of those intervals results in nine or more points below 1.0. The ratio of the two curves has a single point that is 0.9 at 16.20 Hz. However, this still meets the acceptance criteria because is it not below 0.9. Therefore, the BE foundation spectrum meets the acceptance criteria between 0.1 and 30.0 Hz.

Figure 7.58 shows the ANSYS® surface spectrum the ANSYS® SSI model and the UB soil profile target spectrum. The ratio of the two curves is greater than 1.0 between 0.1 and 30 Hz.

Figure 7.59 shows the foundation-level response spectra for the UB soil profile. The ratio of the two curves is greater than 1.0 at all frequencies between 0.1 and 30 Hz. Consequently, the vertical UB foundation spectrum meets the acceptance criteria described in Section 7.9.

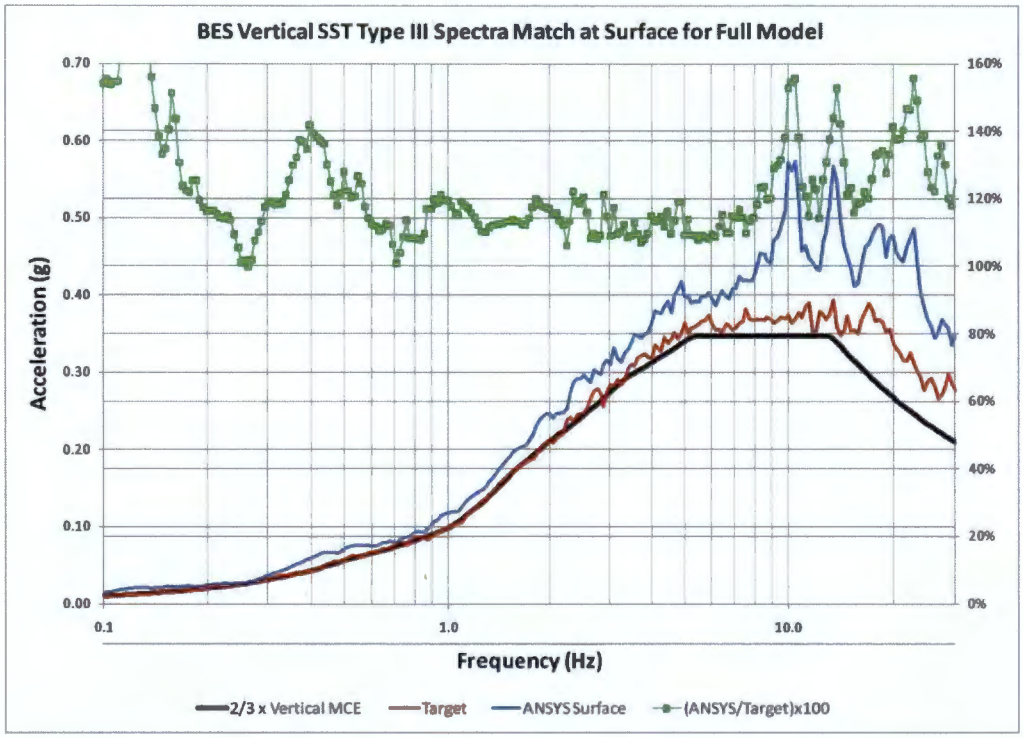

Figure 7.56. Comparison of Best Estimate Vertical Surface Spectra with 5% Spectral Damping from the ANSYS® SSI Model with Empty Tank

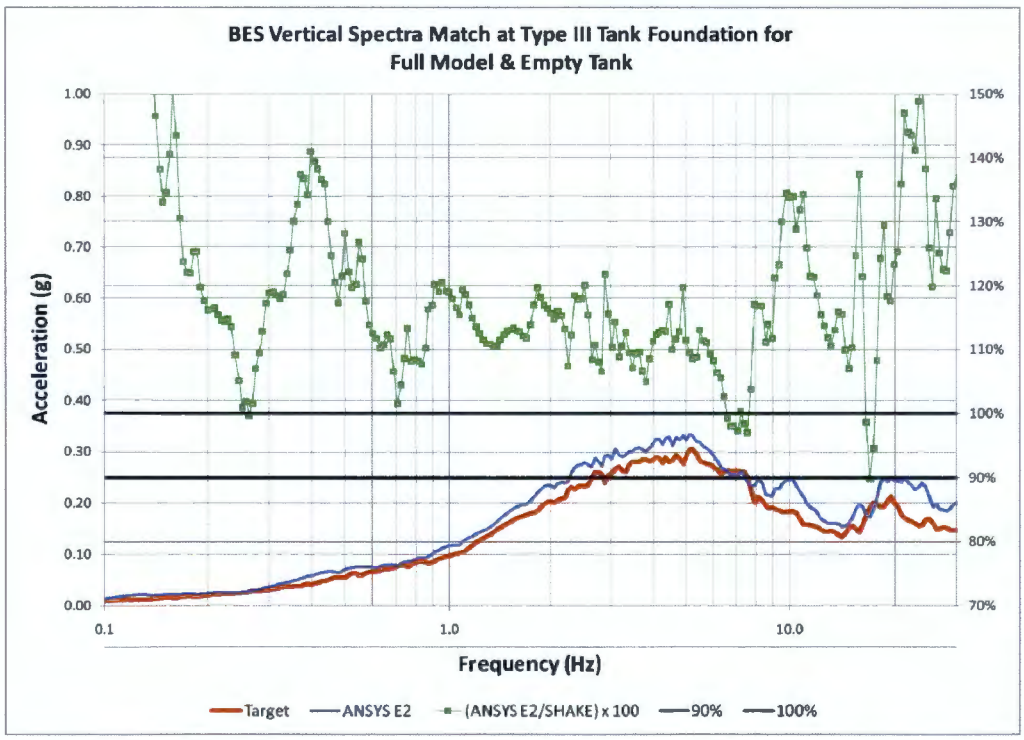

Figure 7.57. Comparison of Best Estimate Vertical Tank Foundation Spectra with 5% Spectral Damping from the ANSYS® SSI Model with Empty Tank

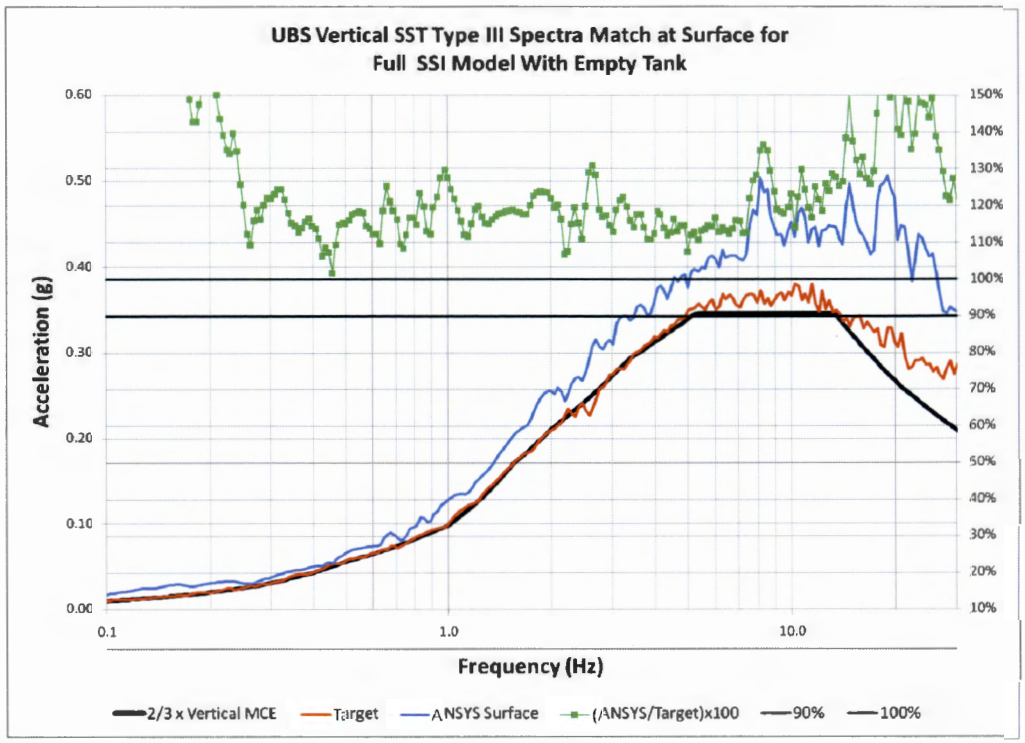

Figure 7.58. Comparison of Upper Bound Vertical Surface Spectra with 5% Spectral Damping from the ANSYS® SSI Model with Empty Tank

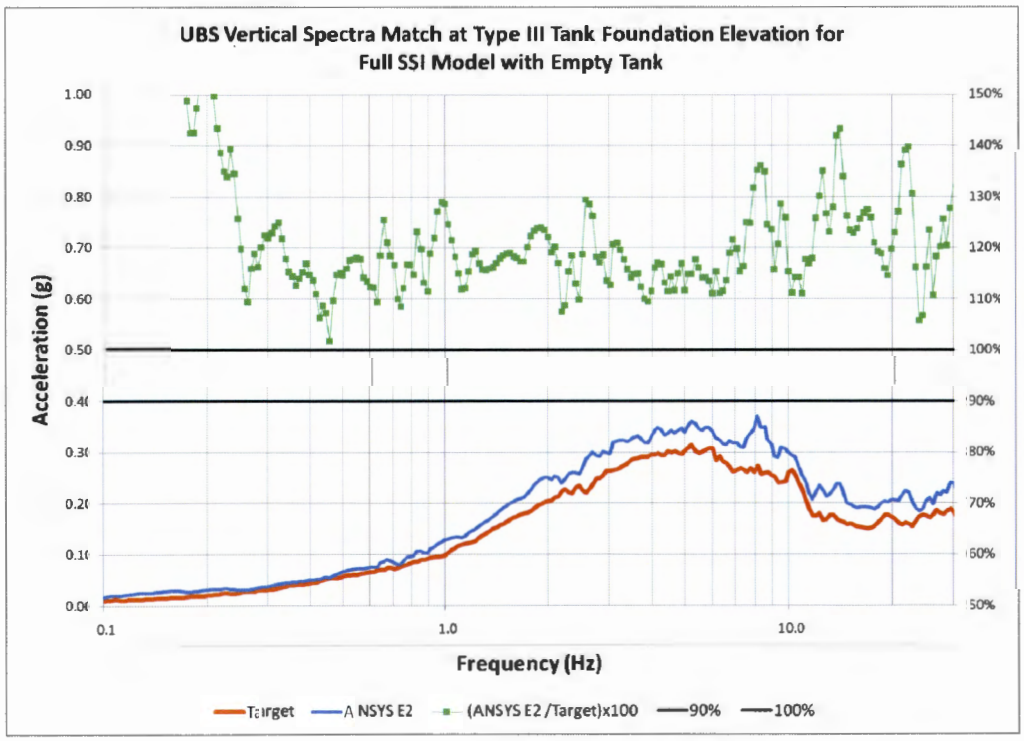

Figure 7.59. Comparison of Upper Bound Vertical Tank Foundation Spectra with 5% Spectral Damping from the ANSYS® SSI Model with Empty Tank

Figure 7.60 shows the ANSYS® surface spectrum from the full ANSYS® SSI model and the along with the SHAKE surface spectrum and the smooth target spectrum for the lower soil profile. The ratio of the ANSYS® to SHAKE spectra is greater than 1.0 between 0.1 and approximately 30.0 Hz. Figure 7.61 shows the ANSYS® LB spectrum from the ANSYS® SSI model and the LB soil profile target spectrum resulting from the tank foundation. The ratio of the two curves is greater than or equal to 1.0 between 0.1 and approximately 30.0 Hz except several intervals with several points below 1.0, but none of those intervals has more than 9 point consecutive points below 1.0 of the target. The ratio of the two curves never falls below 0.9. The ratio of the two curves meets the acceptance criteria described in Section 7.9 in the range of approximately 0.1 to 30 Hz.

Figure 7.62 shows the three soil profile surface spectra plotted against the smooth target spectrum. Figure 7.63 shows the ratio of the surface spectrum to the target for each soil profile. It is clear that the upper bound envelope of ANSYS® SSI model surface spectra ratios exceeds the 1.0 and 0.9 of the target spectrum at all frequencies shown and the acceptance criteria is met.

The conclusion from this section is that adequate spectral matching has been achieved between the ANSYS® SSI model and the target spectra generated by SHAKE in the frequency range of 0.1 to 30 Hz. In general, there is a very conservative bias in the input time histories.

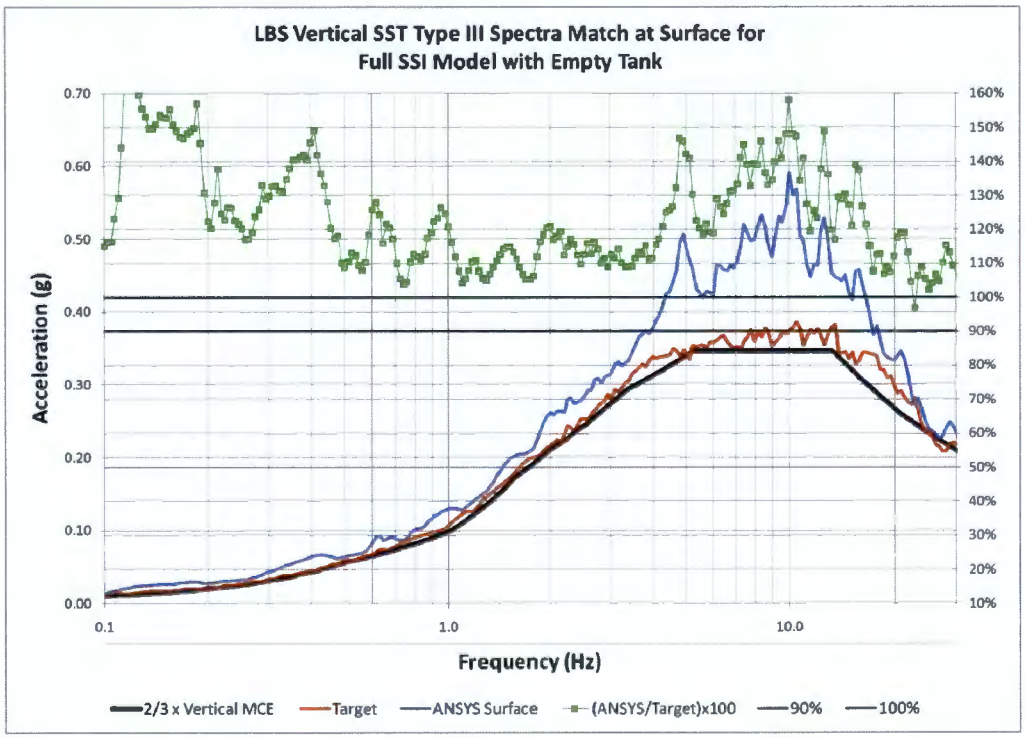

Figure 7.60. Comparison of Lower Bound Vertical Surface Spectra with 5% Spectral Damping from the ANSYS® SSI Model with Empty Tank

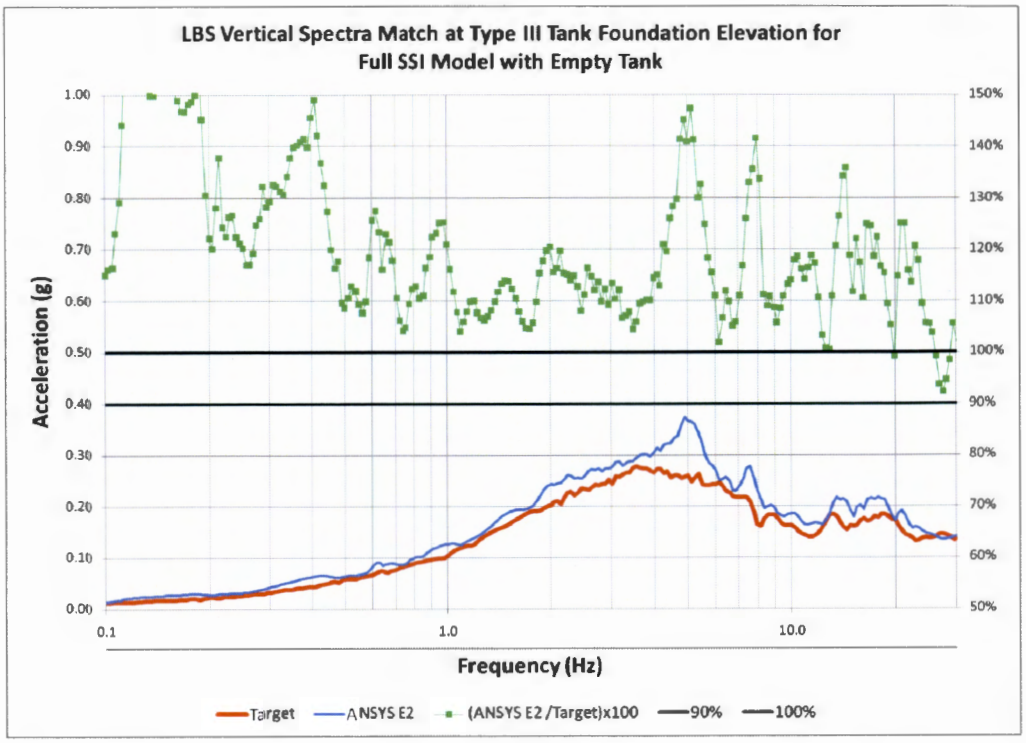

Figure 7.61. Comparison of Lower Bound Vertical Tank Foundation Spectra with 5% Spectral Damping from the ANSYS® SSI Model with Empty Tank

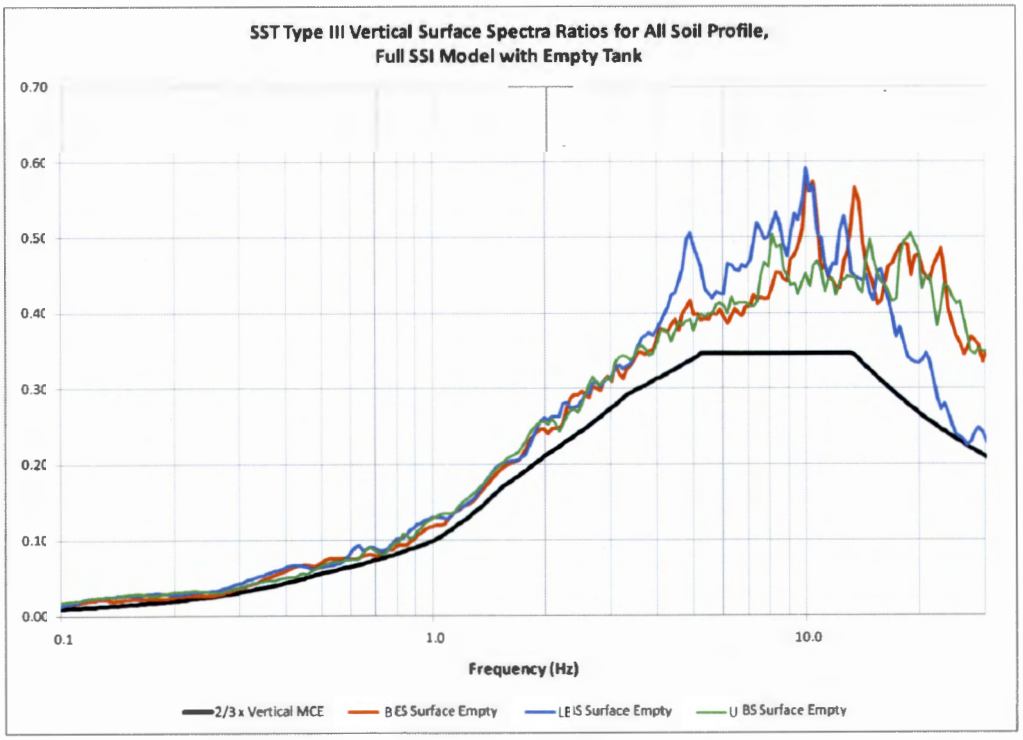

Figure 7.62. Surface Spectra Envelop Curves for Vertical Time Histories with Empty Tank

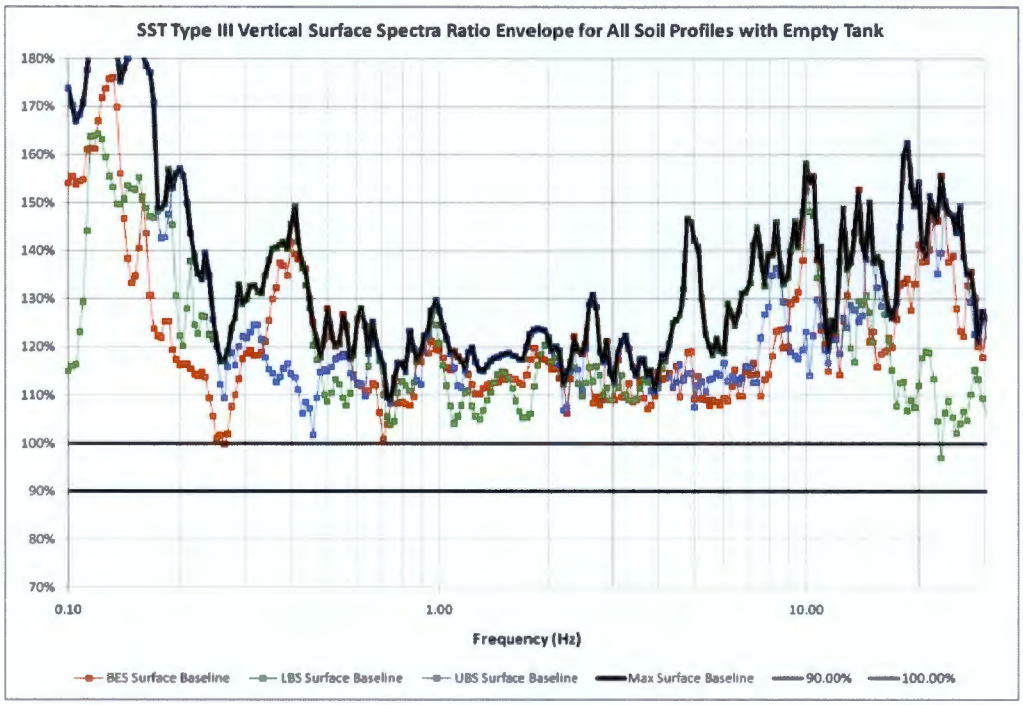

Figure 7.63. Surface Spectra Ratio Curves and Maximum Envelope Curve for Vertical Time Histories for SSI Full Model with Empty Tank

7.9.2.5 Spectral Results for SSI Full Model with High Shear Stiffness Tank Waste with Vertical Time Histories

The previous section described the spectral matching between the ANSYS® SSI model with an empty tank and SHAKE for vertical input motions. This section shows spectra results from vertical input motion for the tank waste characterized with high shear stiffness properties.

Figure 7.64 shows the vertical surface spectrum from the ANSYS® SSI model BE profile along with the SHAKE surface spectrum and the smooth vertical surface spectrum. The ratio of the ANSYS® to SHAKE surface spectrum is greater than or equal to 1.0 from 0.1 to 30 Hz.

Figure 7.65 shows the foundation-level response spectra for the BE soil profile. The plot indicates that the spectrum for the ANSYS® SSI model exceeds the target in-column spectrum between 0.1 and 30.0 Hz with one interval with seven points below 1.0 between 6.6 and 7.6 Hz and another interval with two points below 1.0 between 16.9 and 17.4 Hz. There are no frequency points that fall below 0.9 of the target. Therefore, the BE foundation spectrum meets the acceptance criteria as described in Section 7.9 from 0.1 to 30 Hz.

Figure 7.66 shows the ANSYS® surface spectrum the ANSYS® SSI model and the UB soil profile target spectrum. The ratio of the two curves is greater than 1.0 between 0.1 and 30 Hz.

Figure 7.67 shows the foundation-level response spectra for the UB soil profile. The ratio of the two curves is greater than 1.0 at all frequencies between 0.1 and 30 Hz. Consequently, the vertical UB foundation spectrum meets the acceptance criteria described in Section 7.9.

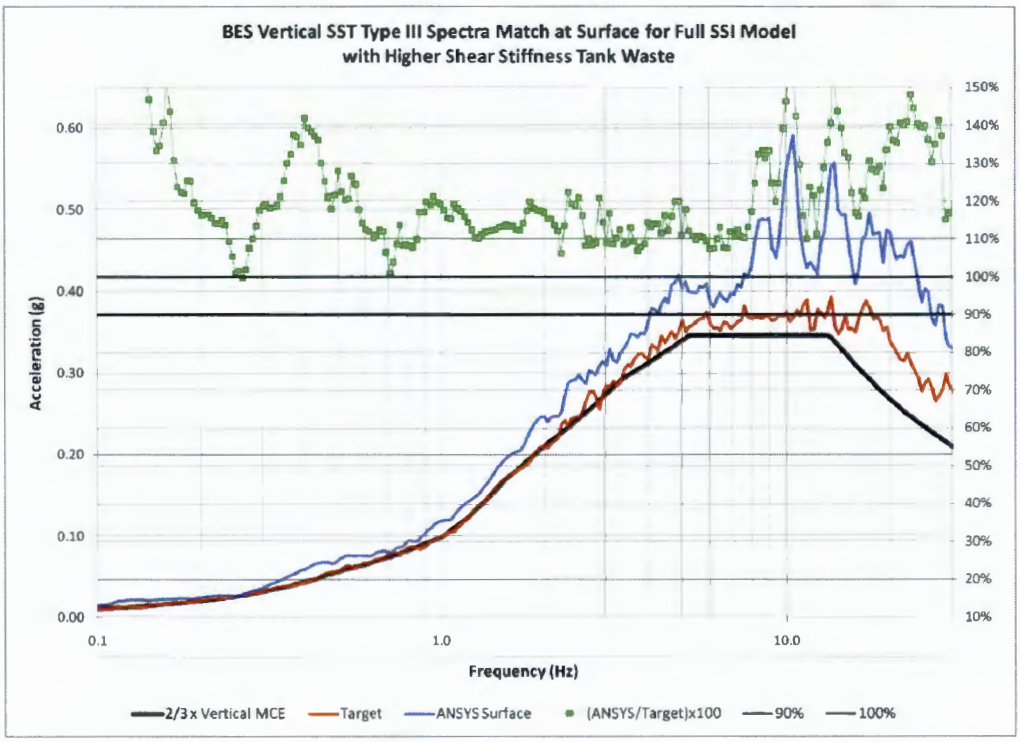

Figure 7.64. Comparison of Best Estimate Vertical Surface Spectra with 5% Spectral Damping from the ANSYS® SSI Model with High Shear Stiffness Tank Waste

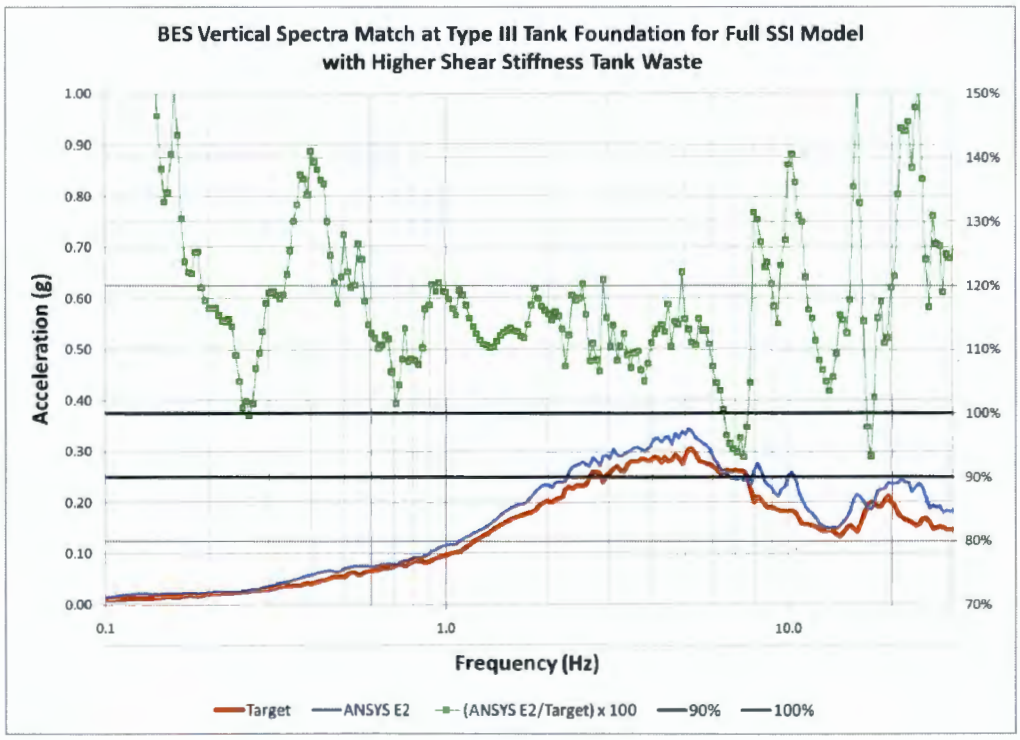

Figure 7.65. Comparison of Best Estimate Vertical Tank Foundation Spectra with 5% Spectral Damping from the ANSYS® SSI Model with High Shear Stiffness Tank Waste

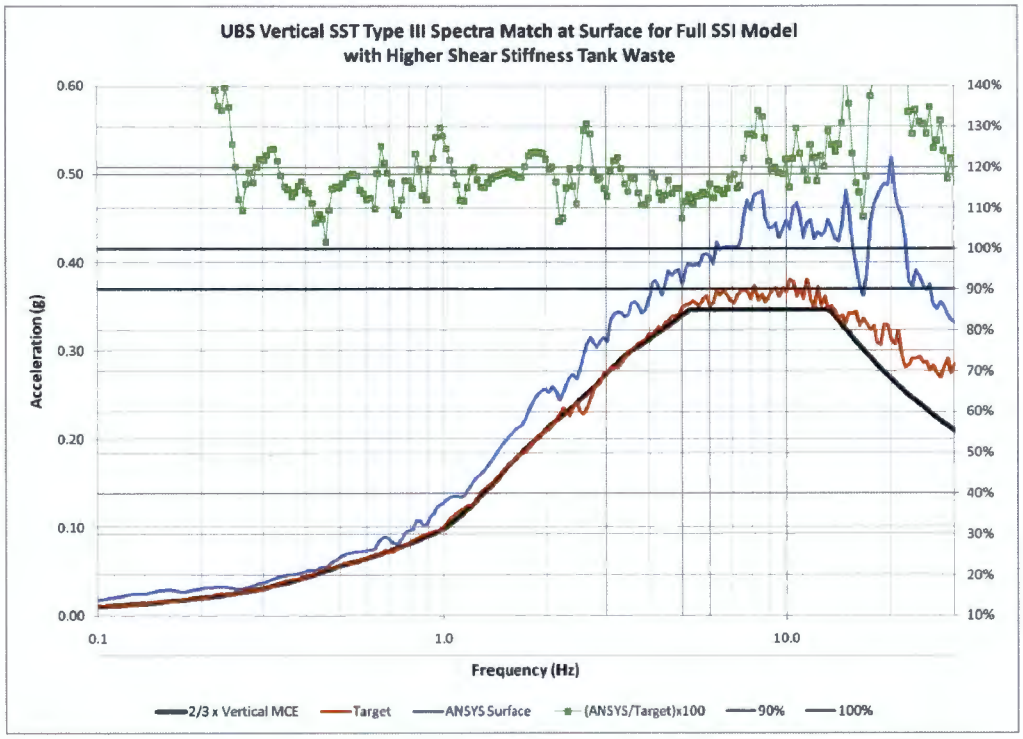

Figure 7.66. Comparison of Upper Bound Vertical Surface Spectra with 5% Spectral Damping from the ANSYS® SSI Model with High Shear Stiffness Tank Waste

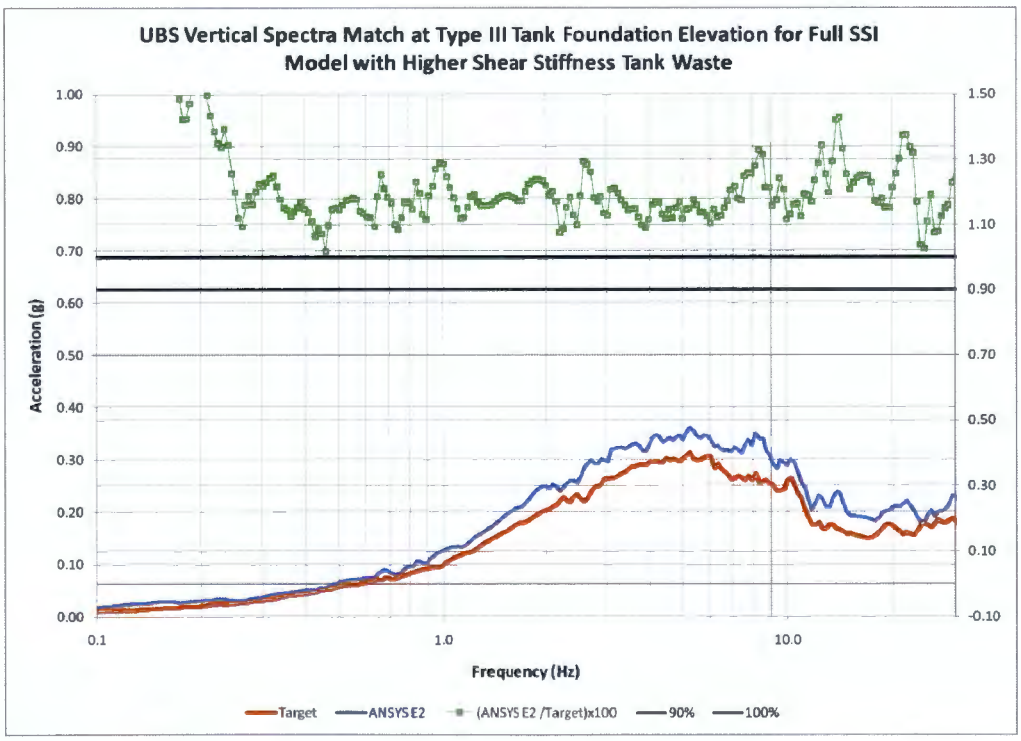

Figure 7.67. Comparison of Upper Bound Vertical Tank Foundation Spectra with 5% Spectral Damping from the ANSYS® SSI Model with High Shear Stiffness Tank Waste

Figure 7.68 shows the ANSYS® surface spectrum the ANSYS® SSI model and the along with the SHAKE surface spectrum and the smooth target spectrum for the lower bound soil profile. The ratio of the ANSYS® to SHAKE spectra is greater than 1.0 between 0.1 and approximately 30 Hz with a few points that are below 1.0 of the target.

Figure 7.69 shows the ANSYS® LB spectrum from the ANSYS® SSI model tank foundation and the LB soil profile target spectrum. The ratio of the two curves is greater than 1.0 between 0.1 and 26.3 Hz, after which five points are below 1.0 of the target. The two curves exceed 0.9 in the frequency range from 0.1 to 30 Hz. At frequency 27.54 Hz, one ordinate is exactly 0.9 of the target, which is still acceptable. Therefore, the ratio of the two curves meets the acceptance criteria from 0.1 and 30 Hz.

Figure 7.70 shows the three soil profile surface spectra plotted against the smooth target spectrum. Figure 7.71 shows the ratio of the ANSYS® SSI model surface spectrum to the target for each soil profile. It is clear that the upper bound envelope of surface spectra ratio exceeds the 1.0 and 0.9 target spectrum at all frequencies. Therefore, the surface spectrum meets the acceptance criteria described in Section 7.9.

The conclusion from this section is that adequate spectral matching has been achieved between the ANSYS® SSI model and the target spectra generated by SHAKE at the surface and tank foundation in the frequency range of 0.1 to 30 Hz. In general, there is a very conservative bias in the input time histories.

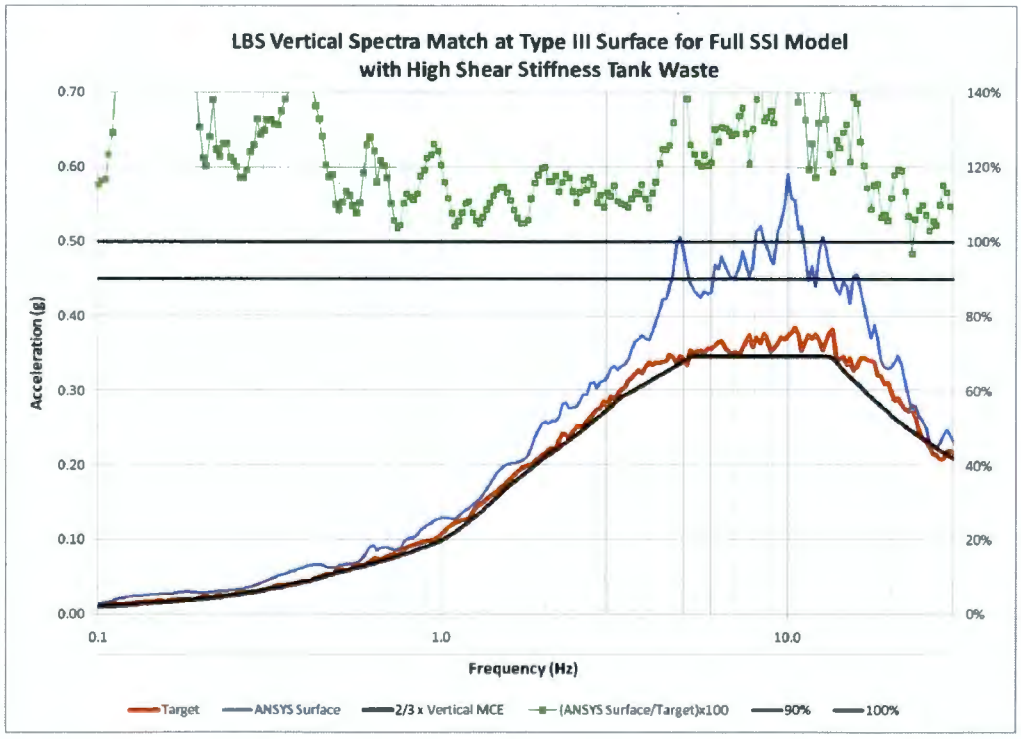

Figure 7.68. Comparison of Lower Bound Vertical Surface Spectra with 5% Spectral Damping from the ANSYS® SSI Model with High Shear Stiffness Tank Waste

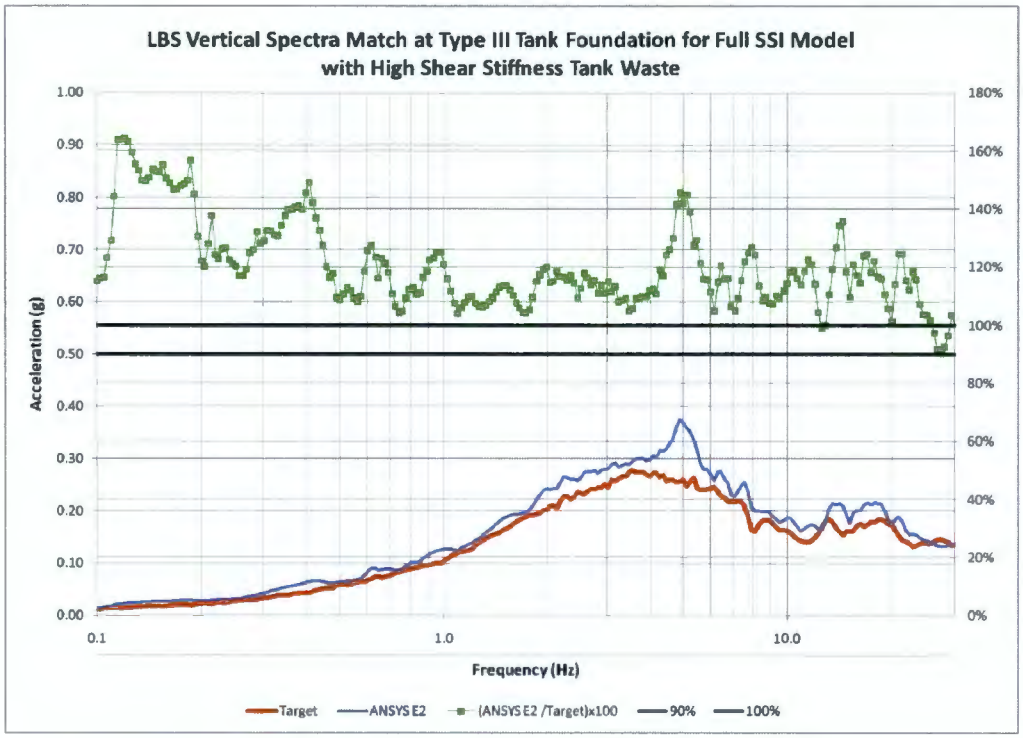

Figure 7.69. Comparison of Lower Bound Vertical Tank Foundation Spectra with 5% Spectral Damping from the ANSYS® SSI Model with High Shear Stiffness Tank Waste

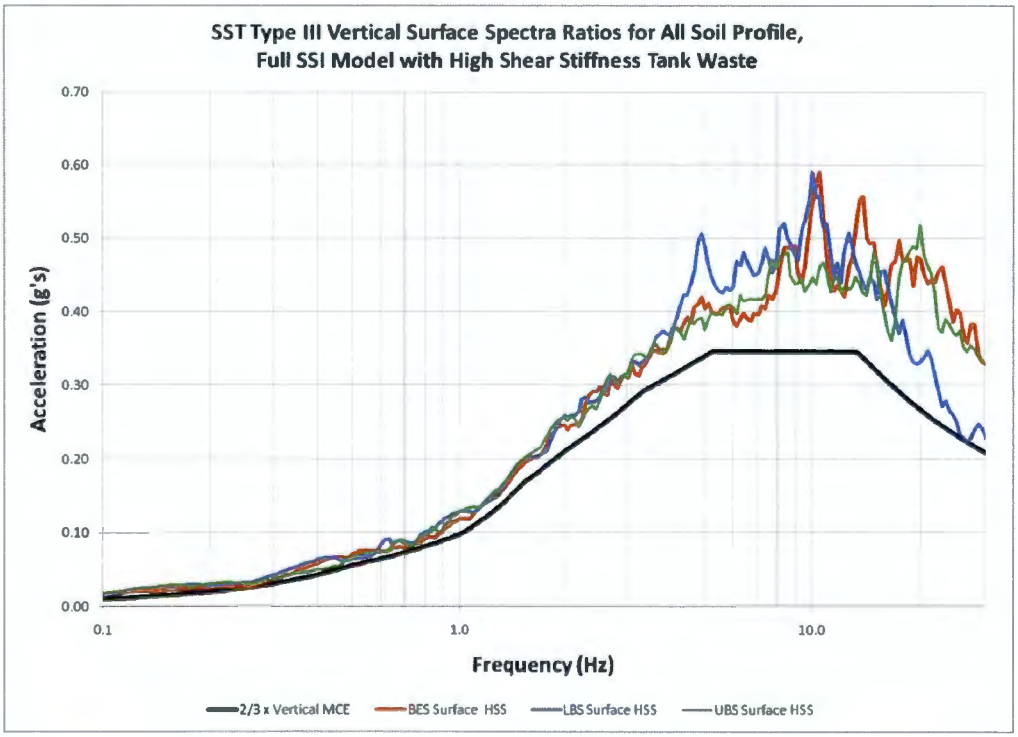

Figure 7.70. Surface Spectra Curves for Vertical Time Histories with High Shear Stiffness Tank Waste

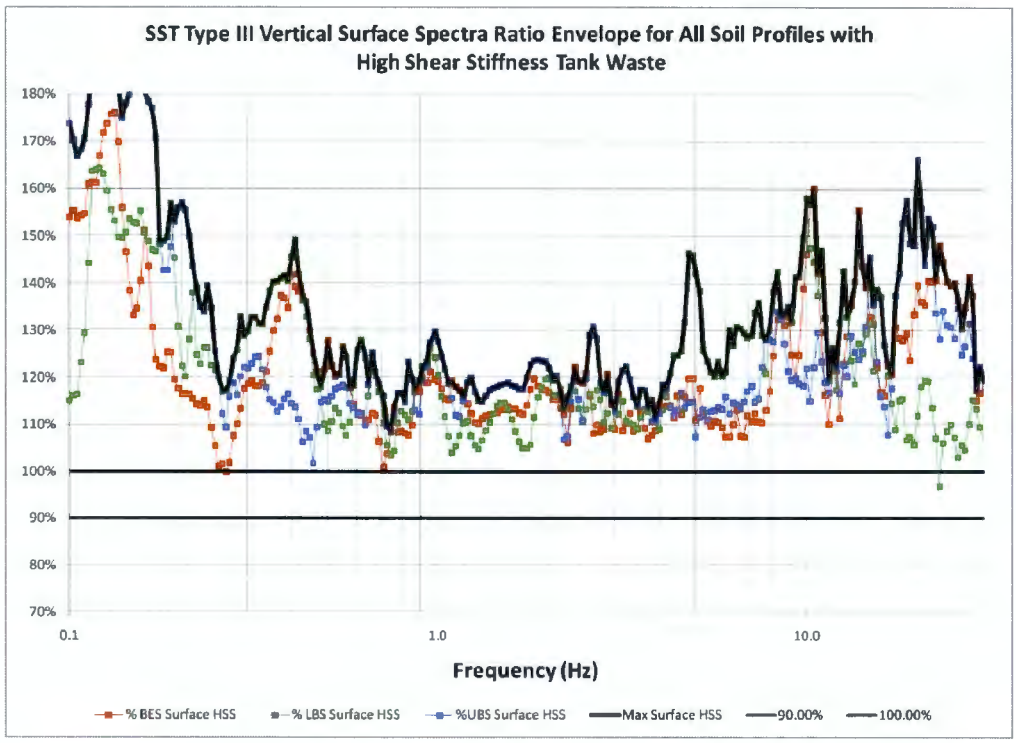

Figure 7.71. Surface Spectra ANSYS® to SHAKE Ratio Curves and Maximum Envelope Curve for Vertical Time Histories of the SSI Full Model with High Shear Stiffness Tank Waste

7.9.2.6 Spectra Results for SSI Full Model with Tank Waste as Low Shear Stiffness with Vertical Time Histories

The previous section described the spectral matching between the ANSYS® SSI model with tank waste and SHAKE for vertical input motions. This section shows spectra results from vertical input motion for the tank waste characterized with low shear stiffness (LSS) properties.

Figure 7.72 shows the vertical surface spectrum from the ANSYS® SSI model BE profile along with the SHAKE surface spectrum and the smooth vertical surface spectrum. The ratio of the ANSYS® to SHAKE surface spectrum is greater than or equal to 1.0 from 0.1 to 30 Hz.

Figure 7.73 shows the foundation-level response spectra for the BE soil profile. The plot indicates that the spectrum for the ANSYS® SSI model exceeds the target in-column spectrum between 0.1 and 30 Hz with one interval of six points falling below 1.0 between 6.6 and 7.6 Hz and a second interval of 2 points between 16.9 and 17.4 Hz. There are no frequency points that fall below 0.9 of the target. Therefore, the BE foundation spectrum meets the acceptance criteria described in Section 7.9.

Figure 7.74 shows the ANSYS® surface spectrum the ANSYS® SSI model and the UB soil profile target spectrum. The ratio of the two curves is greater than 1.0 between 0.1 and 30 Hz.

Figure 7.75 shows the foundation-level response spectra for the UB soil profile. The ratio of the two curves is greater than 1.0 at all frequencies between 0.1 and 30 Hz. Consequently, the vertical UB foundation spectrum meets the acceptance criteria described in Section 7.9 between 0.1 and 30 Hz.

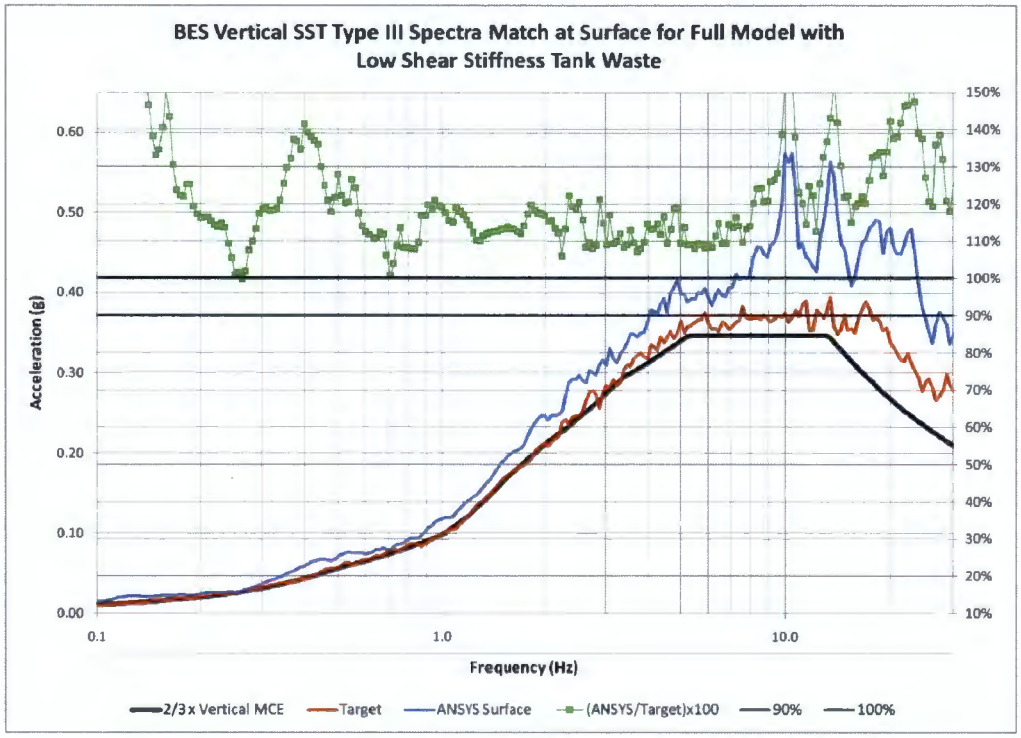

Figure 7.72. Comparison of Best Estimate Vertical Surface Spectra with 5% Spectral Damping from the ANSYS® SSI Model with Low Shear Stiffness Tank Waste

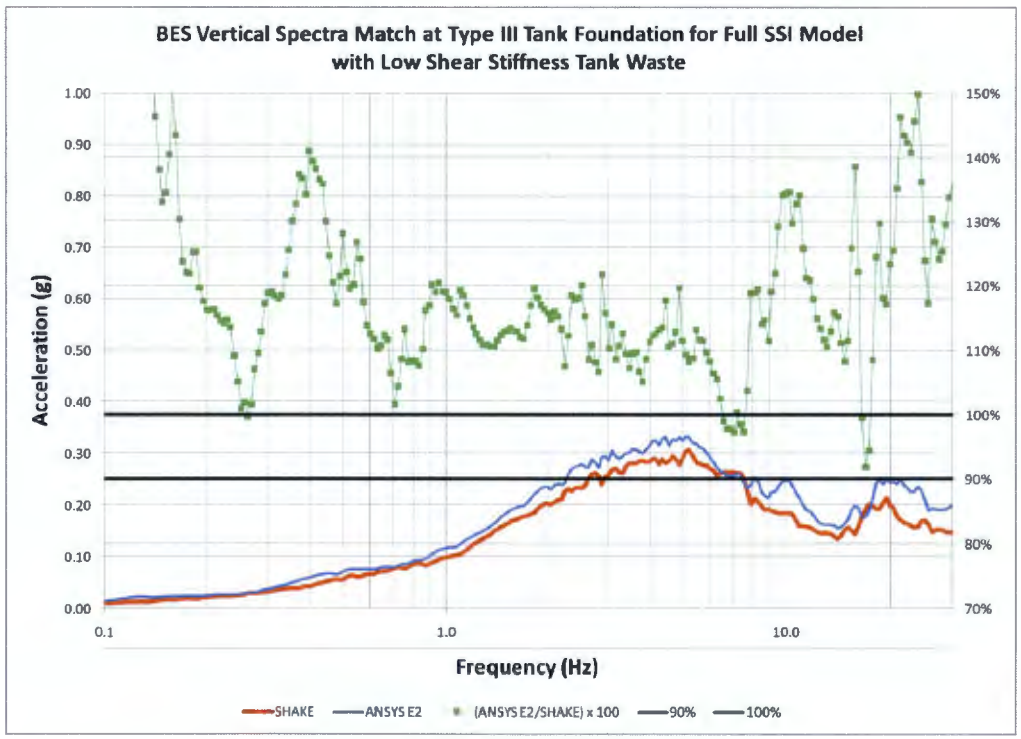

Figure 7.73. Comparison of Best Estimate Vertical Tank Foundation Spectra with 5% Spectral Damping from the ANSYS® SSI Model with Low Shear Stiffness Tank Waste

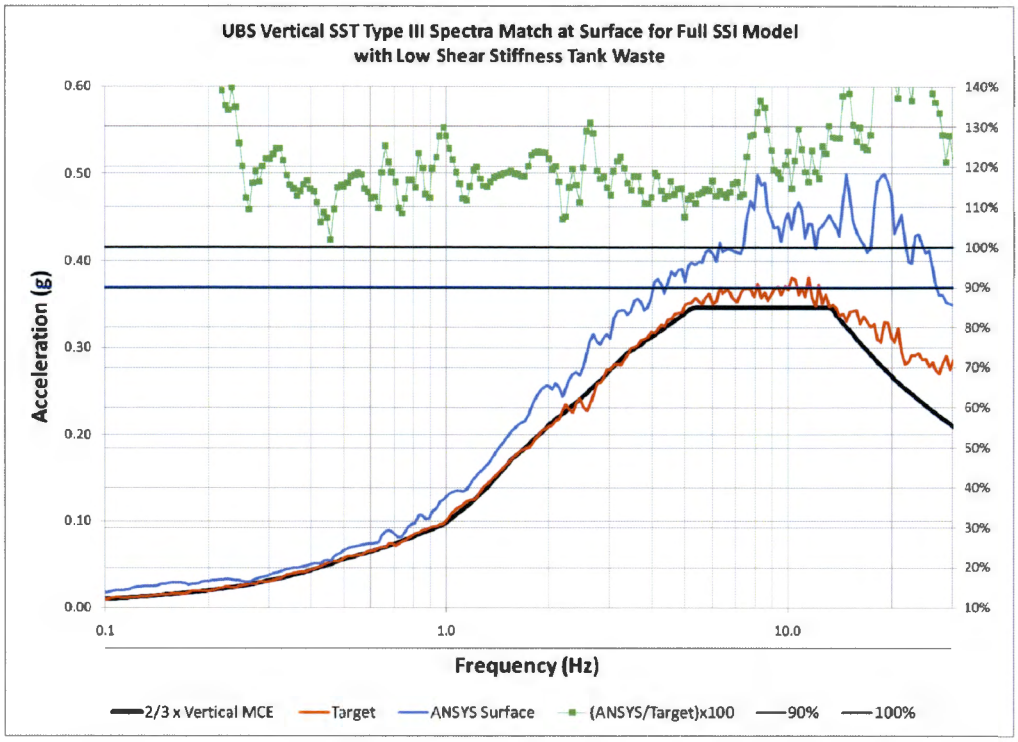

Figure 7.74. Comparison of Upper Bound Vertical Surface Spectra with 5% Spectral Damping from the ANSYS® SSI Model with Low Shear Stiffness Tank Waste

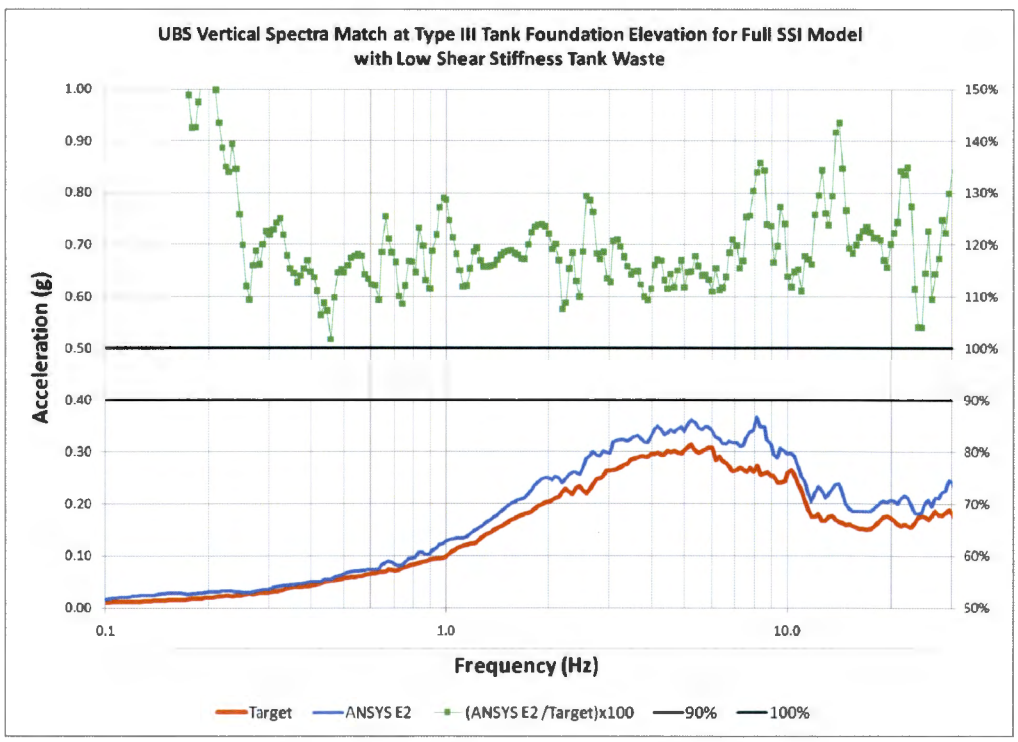

Figure 7.75. Comparison of Upper Bound Vertical Tank Foundation Spectra with 5% Spectral Damping from the ANSYS® SSI Model with Low Shear Stiffness Tank Waste

Figure 7.76 shows the ANSYS® surface spectrum of the ANSYS® SSI lower bound model and the along with the SHAKE surface spectrum and the smooth target spectrum. The ratio of the ANSYS® to SHAKE spectra is greater than 1.0 is greater than 1.0 between 0.1 and 30 Hz.

Figure 7.77 shows the ANSYS® LB spectrum from the ANSYS® SSI model tank foundation and the LB soil profile target spectrum. The ratio of the two curves dips below 1.0 with a few points, but there are less than nine consecutive points at these intervals. The ratio of the two curves falls is not below 0.9 between 0.1 and 30 Hz. The ratio of the two curves meets the acceptance criteria described in Section 7.9 in the range of approximately 0.1 to 30 Hz.

Figure 7.78 shows the three soil profile surface spectra plotted against the smooth target spectrum. It is clear that the upper bound envelope of ANSYS® SSI model surface spectra exceeds the smooth target spectrum at all frequencies shown. Figure 7.79 shows the ratio of the surface spectrum to the target for each soil profile and the maximum envelope curve showing the acceptance criteria is met.

The conclusion from this section is that adequate spectral matching has been achieved between the ANSYS® SSI model and the target spectra generated by SHAKE at the surface and tank foundation in the frequency range of 0.1 to 30 Hz. In general, there is a very conservative bias in the input time histories.

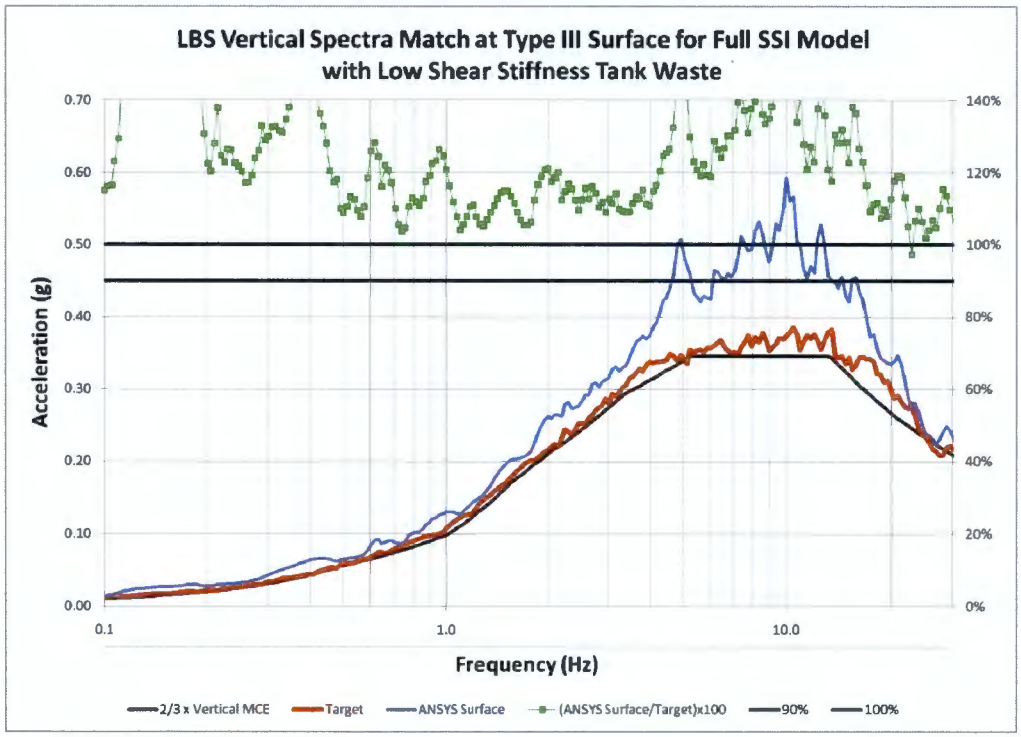

Figure 7.76. Comparison of Lower Bound Vertical Surface Spectra with 5% Spectral Damping from the ANSYS® SSI Model with Low Shear Stiffness Tank Waste

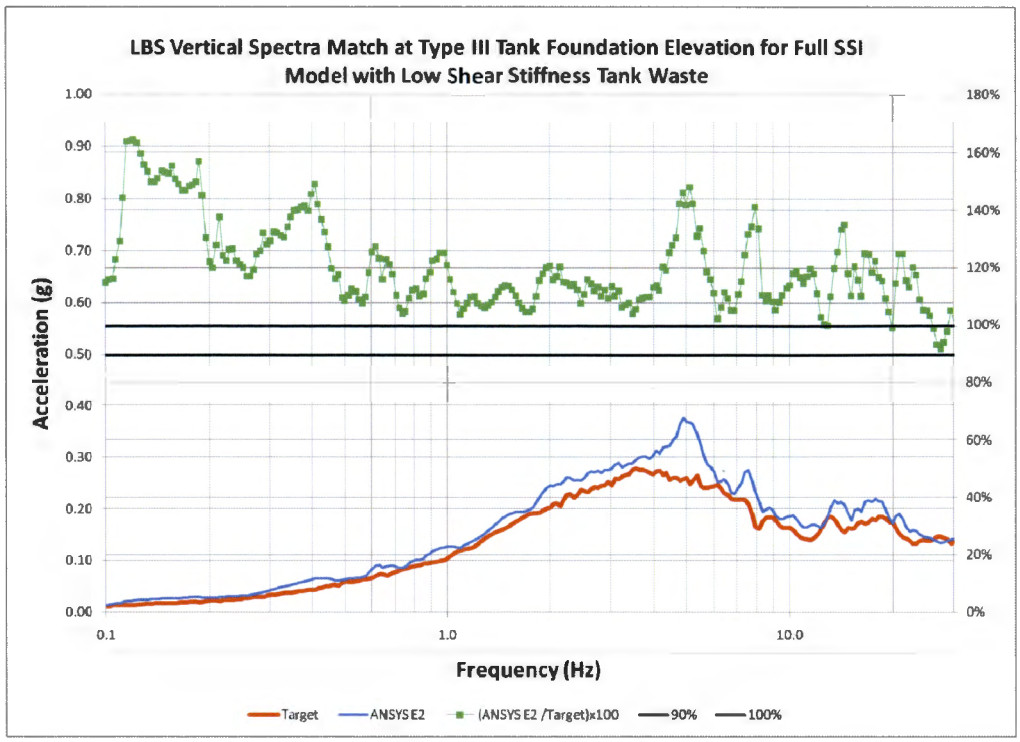

Figure 7.77. Comparison of Lower Bound Vertical Tank Foundation Spectra with 5% Spectral Damping from the ANSYS® SSI Model with Low Shear Stiffness Tank Waste

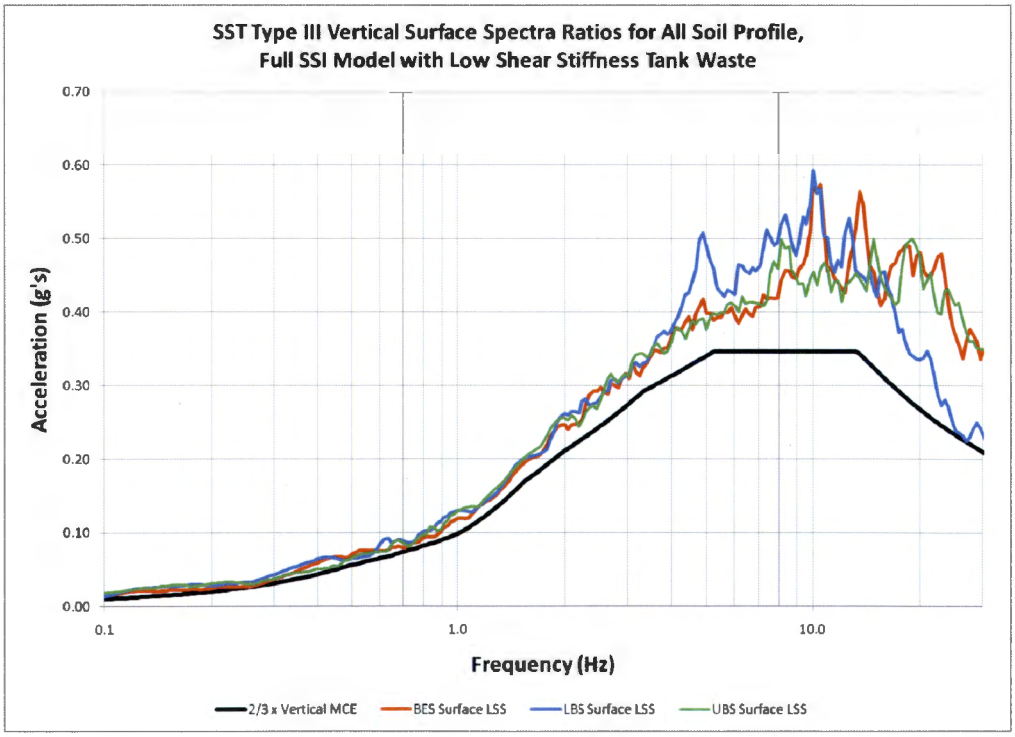

Figure 7.78. Surface Spectra Envelop Curves for Vertical Time Histories with Low Shear Stiffness Tank Waste

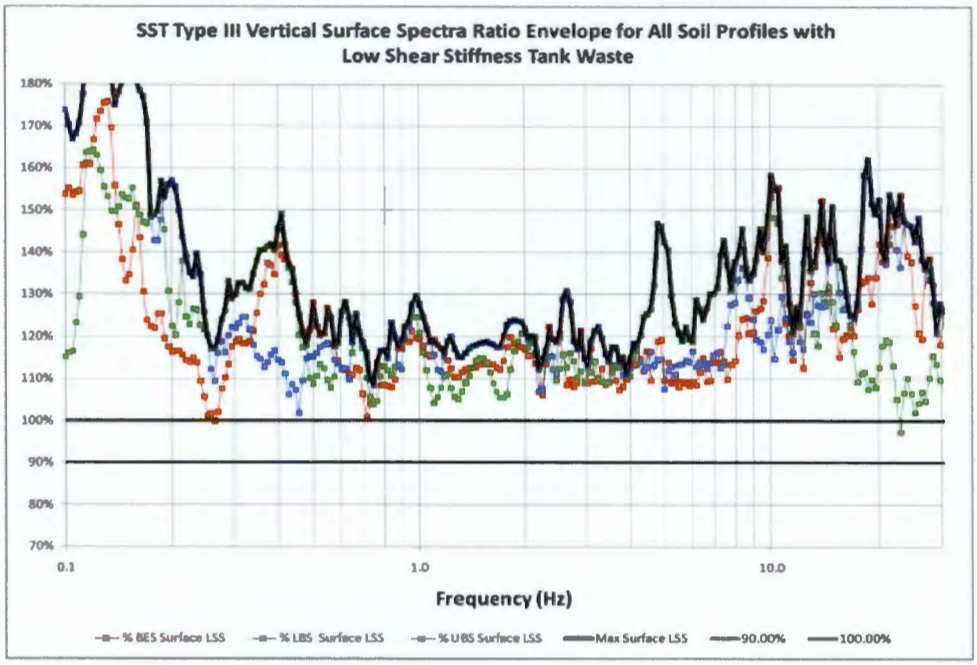

Figure 7.79. Surface Spectra ANSYS® to SHAKE Ratio Curves and Maximum Envelope Curve for Vertical Time Histories of the SSI Full Model with Low Shear Stiffness Tank Waste

7.10 Backfill Properties

The backfill soil properties are necessary in order to perform SSI evaluation of the tanks. The details about the backfill soil properties are shown in Appendix O of Rinker et al. (2011a), and they are summarized in this section. There are three backfill soil profiles – namely best estimate (BE), upper bound (UB) and lower bound (LB). The differences between the three soil profiles are a two-sigma variation between the lower bound, best estimate, upper bound shear velocity profiles. The surface and 60-feet shear velocities have been incorporated into the material properties of the three soil profiles.

At the recommendation of A. Rohay of PNNL, the backfill soil density is 129 lb/ft3 for the first 10-feet and tapers linearly to 108 lb/ft3 from 10-feet to 20-feet and remains constant at 108 lb/ft3 to 60-feet. Details of the soil density recommended values are shown in Appendix O of Rinker et al. (2011a).

Figure 7.80 shows the BE shear velocity of the far-field compared to the BE backfill shear velocity from the surface to an overall depth of 60 feet. In the same manner, Figure 7.81 and

Figure 7.82 show the shear velocity of the far-field compared to the backfill shear velocity from the surface for the LB and UB soil properties, respectively. It can be seen in Figure 7.80 that the slope of the backfill shear velocity curve is similar to the far-field shear velocity. Table 7.13 through 7.15 show the backfill properties including soil layer thickness, soil layer damping, soil layer density, Poisson's ratio, shear modulus, and modulus of elasticity for each soil layer. The soil layer depth, damping, density, and Poisson's ratio were chosen to be the same as the adjacent far-field soil layer properties. The shear velocities, shear modulus and modulus of elasticity are independent, but similar to the adjacent far-field soil layer properties.

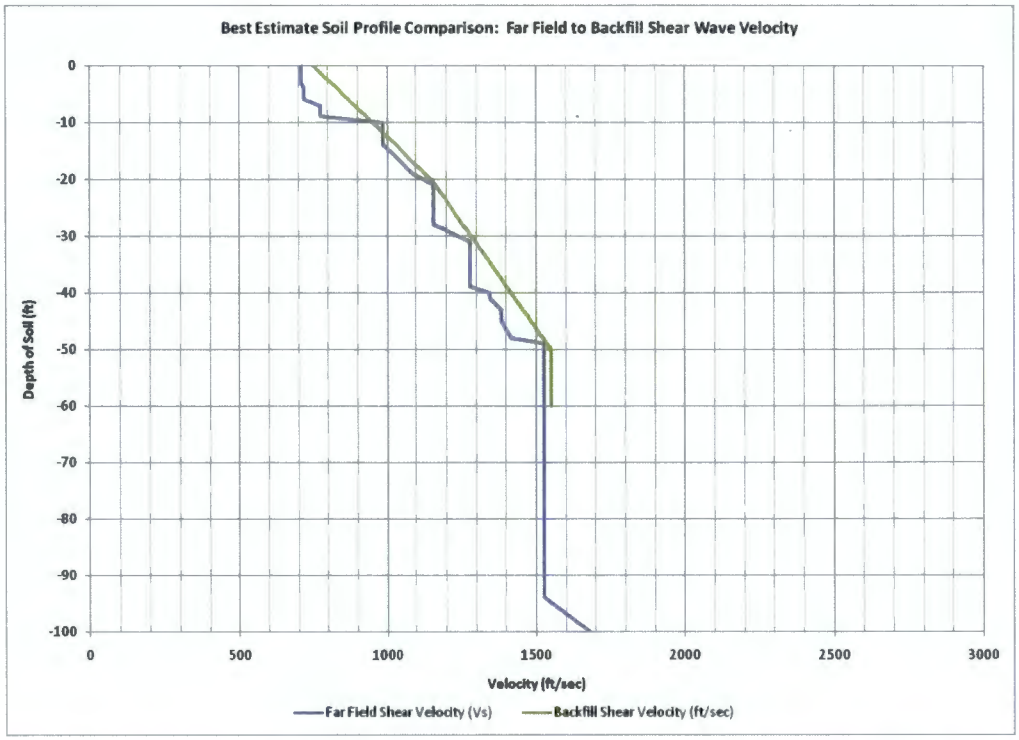

Figure 7.80. Best Estimate Soil Profile Comparison: Far Field to Backfill Shear Velocities

Table 7.13. Best Estimate Backfill Properties

Layer Number	Thickness (ft)	Elevation	Damping (in decimal)	Unit Weight (kip/ft^3)	Shear Velocity (ft/sec)	Poisson's Ratio	Shear Modulus (kip/ft^2)	Modulus of Elasticity (kip/ft^2)
1	1	-1	0.011	0.129	750	0.28	2253	5768.94
2	1	-2	0.015	0.129	770	0.28	2375	6080.72
3	1	-3	0.019	0.129	790	0.28	2500	6400.71
4	1	-4	0.022	0.129	810	0.28	2628	6728.90
5	1	-5	0.024	0.129	830	0.28	2759	7065.29
6	1	-6	0.029	0.129	850	0.28	2894	7409
7	1	-7	0.028	0.129	870	0.28	3032	7762
8	1	-8	0.032	0.129	890	0.28	3173	8123
9	1	-9	0.030	0.129	910	0.28	3317	8492
10	1	-10	0.029	0.129	930	0.28	3464	8870
11	4	-14	0.0357	0.123	1010	0.28	3887	9951
12	5	-19	0.0359	0.112	1110	0.28	4293.	10990
13	2	-21	0.0369	0.108	1150	0.28	4435	11355
14	2	-23	0.0379	0.108	1176	0.28	4643	11888
15	2	-25	0.0378	0.108	1203	0.28	4856	12433
16	3	-28	0.0404	0.108	1243	0.28	5184	13273
17	3	-31	0.0406	0.108	1283	0.28	5523	14141
18	4	-35	0.0348	0.108	1336	0.28	5992	15341
19	2	-37	0.0348	0.108	1363	0.28	6234	15959
20	2	-39	0.0351	0.108	1390	0.28	6480	16589
21	1	-40	0.0351	0.108	1403	0.28	6605	16909

Table 7.13. (contd)

Layer Number	Thickness (ft)	Elevation	Damping (in decimal)	Unit Weight (kip/ft3)	Shear Velocity (ft/sec)	Poisson's Ratio	Shear Modulus (kip/ft2)	Modulus of Elasticity (kip/ft2)
22	1	-41	0.0354	0.108	1416	0.28	6731	17232
23	2	-43	0.03515	0.108	1443	0.280	6987	17887
24	2	-45	0.03515	0.108	1470	0.280	7248	18554
25	3	-48	0.03548	0.108	1510	0.280	7648	19578
26	1	-49	0.03313	0.108	1523	0.280	7783	19925
27	1	-50	0.03313	0.108	1537	0.280	7920	20275
28	5	-55	0.03410	0.108	1550	0.280	8058	20629
29	2	-57	0.03445	0.108	1550	0.280	8058	20629
30	2	-59	0.03445	0.108	1550	0.280	8058	20629

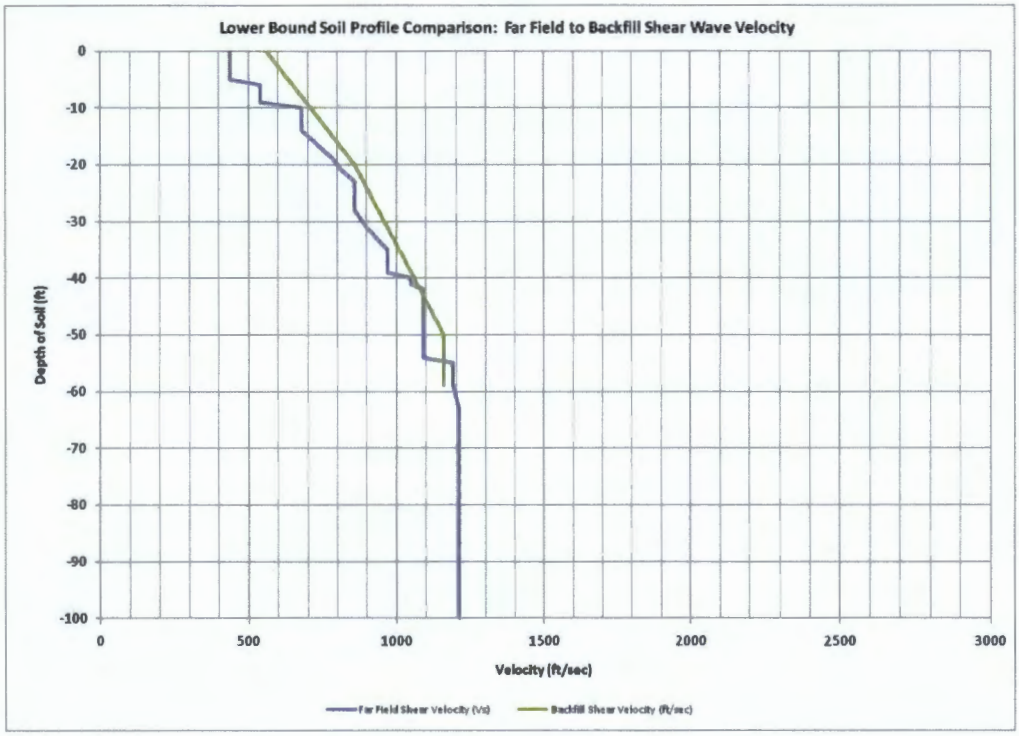

Figure 7.81. Lower Bound Soil Profile Comparison: Far Field to Backfill Shear Wave Velocity

Table 7.14. Lower Bound Backfill Properties

Layer Number	Thickness (ft)	Elevation	Damping (in decimal)	Unit Weight (kip/ft^3)	Shear Velocity (ft/sec)	Poisson's Ratio	Shear Modulus (kip/ft^2)	Modulus of Elasticity (kip/ft^2)
1	1	-1	0.015	0.129	560	0.28	1256	3216
2	1	-2	0.021	0.129	575	0.28	1324	3390
3	1	-3	0.028	0.129	590	0.28	1394	3570
4	1	-4	0.037	0.129	605	0.28	1466	3753
5	1	-5	0.043	0.129	620	0.28	1539	3942
6	1	-6	0.042	0.129	635	0.28	1615	4135
7	1	-7	0.043	0.129	650	0.28	1692	4333
8	1	-8	0.047	0.129	665	0.28	1771	4535
9	1	-9	0.050	0.129	680	0.28	1852	4742
10	1	-10	0.042	0.129	695	0.28	1935	4953
11	4	-14	0.043	0.123	755	0.28	2172	5560
12	5	-19	0.046	0.112	830	0.28	2400	6145
13	2	-21	0.049	0.108	860	0.28	2480	6350
14	2	-23	0.049	0.108	880	0.28	2597	6649
15	2	-25	0.055	0.108	900	0.28	2716	6954
16	3	-28	0.056	0.108	930	0.28	2900	7426
17	3	-31	0.057	0.108	960	0.28	3091	7913
18	4	-35	0.053	0.108	1000	0.28	3354	8586
19	2	-37	0.061	0.108	1020	0.28	3489	8933
20	2	-39	0.061	0.108	1040	0.28	3627	9286
21	1	-40	0.055	0.108	1050	0.28	3697	9466
22	1	-41	0.055	0.108	1060	0.28	3768	9647
23	1	-42	0.0508	0.108	1070	0.280	3840	9830
24	1	-43	0.0508	0.108	1080	0.280	3912	10015
25	2	-45	0.0508	0.108	1100	0.280	4058	10389
26	3	-48	0.0518	0.108	1130	0.280	4283	10964
27	1	-49	0.0517	0.108	1140	0.280	4359	11159
28	1	-50	0.0517	0.108	1150	0.280	4436	11355
29	4	-54	0.0499	0.108	1160	0.280	4513	11554
30	1	-55	0.0521	0.108	1160	0.280	4513	11554
31	2	-57	0.0521	0.108	1160	0.280	4513	11554
32	3	-59	0.0521	0.108	1160	0.280	4513	11554

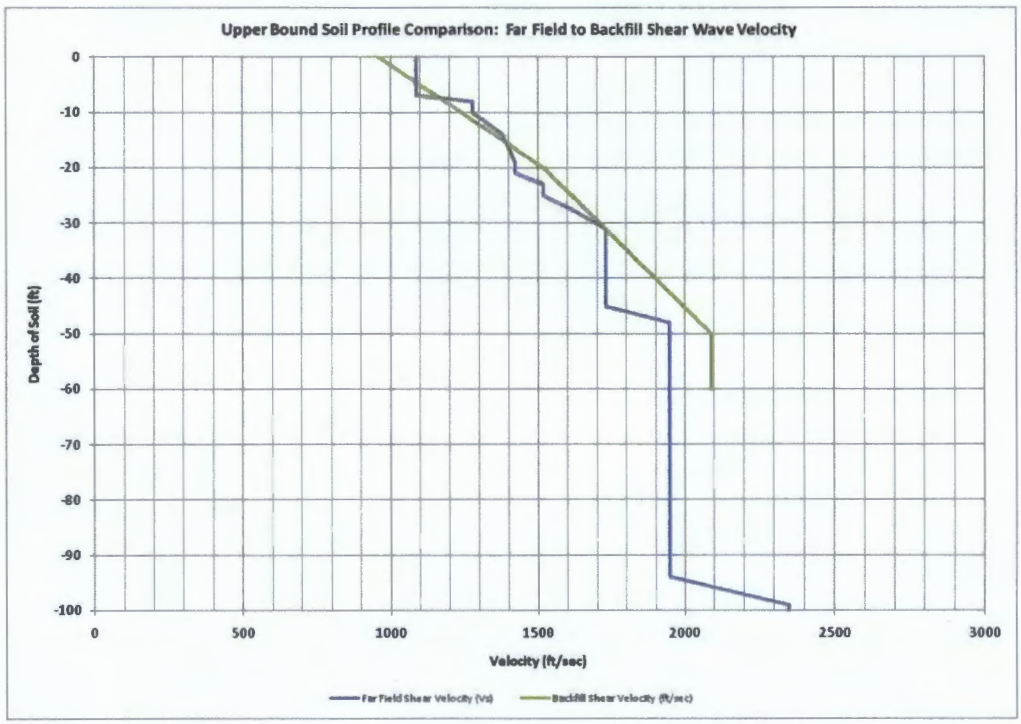

Figure 7.82. Upper Bound Soil Profile Comparison: Far Field to Backfill Shear Wave Velocity

Table 7.15. Upper Bound Back Fill Properties

Layer Number	Thickness (ft)	Elevation	Damping (in decimal)	Unit Weight (kip/ft^3)	Shear Velocity (ft/sec)	Poisson's Ratio	Shear Modulus (kip/ft^2)	Modulus of Elasticity (kip/ft^2)
1	1	-1	0.0087	0.129	960	0.28	3692	9451
2	1	-2	0.0102	0.129	988	0.28	3910	10011
3	1	-3	0.0122	0.129	1016	0.28	4135	10586
4	1	-4	0.0152	0.129	1044	0.28	4366	11178
5	1	-5	0.0164	0.129	1072	0.28	4603	11785
6	1	-6	0.0177	0.129	1100	0.28	4847	12409
7	1	-7	0.0183	0.129	1128	0.28	5097	13049
8	1	-8	0.0163	0.129	1156	0.28	5353	13705
9	1	-9	0.0177	0.129	1184	0.28	5616	14377
10	1	-10	0.0164	0.129	1212	0.28	5884	15065
11	4	-14	0.0195	0.123	1324	0.28	6679	17100
12	5	-19	0.0195	0.112	1464	0.28	7468	19118
13	2	-21	0.0204	0.108	1520	0.28	7749	19837
14	2	-23	0.0227	0.108	1558	0.28	8141	20842
15	2	-25	0.0210	0.108	1596	0.28	8543	21871
16	3	-28	0.0229	0.108	1653	0.28	9164	23461
17	3	-31	0.0204	0.108	1710	0.28	9807	25107
18	4	-35	0.0217	0.108	1786	0.28	10698	27388
19	2	-37	0.0244	0.108	1824	0.28	11158	28566

Table 7.15. (contd)

Layer Number	Thickness (ft)	Elevation	Damping (in decimal)	Unit Weight (kip/ft^3)	Shear Velocity (ft/sec)	Poisson's Ratio	Shear Modulus (kip/ft^2)	Modulus of Elasticity (kip/ft^2)
20	2	-39	0.0264	0.108	1862	0.28	11628	29769
21	1	-40	0.0212	0.108	1881	0.28	11867	30379
22	1	-41	0.0212	0.108	1900	0.28	12108	30996
23	2	-43	0.0198	0.108	1938	0.28	12597	32249
24	2	-45	0.0198	0.108	1976	0.28	13096	33526
25	3	-48	0.0219	0.108	2033	0.28	13863	35488
26	1	-49	0.0223	0.108	2052	0.28	14123	36155
27	1	-50	0.0223	0.108	2071	0.28	14386	36827
28	5	-55	0.0204	0.108	2090	0.28	14651	37506
29	2	-57	0.0211	0.108	2090	0.28	14651	37506
30	2	-59	0.0211	0.108	2090	0.28	14651	37506

7.11 Harmonic Analysis for the Full SSI Model with BE Soil Profile

A harmonic analysis of the ANSYS® SSI full model is performed to determine the natural frequencies of the concrete tank in the soil. The ANSYS® SSI model is described in Chapter 6. The figures presented in this section show horizontal and vertical amplification factors of the tank foundation, tank haunch and tank dome. The concrete tank features of interest are also shown in Figure 7.83.

The displacement amplification data is extracted from tank model at specific elevations. The tank dome data is extracted at the apex elevation, which is 11-ft below grade. The tank haunch data is extracted from the outer edge of the tank wall and at elevation -22.625-ft and the front X-Z plane. The tank foundation data is extracted from the outer edge of the tank footing at 41.58-ft, at elevation -40.1-ft and the front X-Z plane of the model.

With the BE soil profile, the ANSYS® SSI full model was modified for the harmonic analysis such that the friction surfaces between the tank and the soil are bonded and the empty tank. No changes were made to the cracked concrete material properties. An oscillating unit horizontal displacement is applied at the base of the soil column is the excitation for the horizontal harmonic analysis. The frequency range evaluated is from 0–20 Hz resulting in 200 frequency ordinates. In contrast to the full integration time domain analysis with mass and stiffness proportional damping, the harmonic analysis utilized a constant damping ratio, which for best estimate soil profile is 3.5% of critical damping. This is the median value calculated from the 41 soil layers each with a unique critical damping value as shown in Table 7.3.

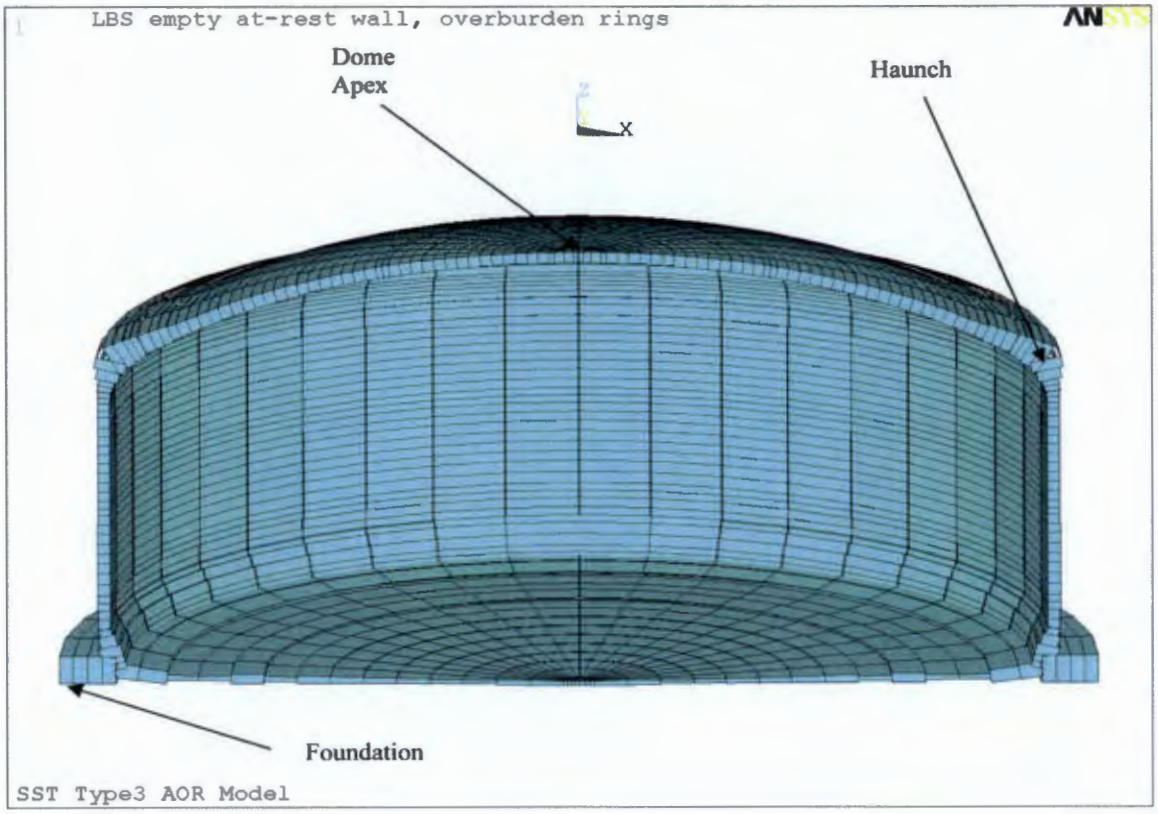

Figure 7.83. SST Type III Tank Model with Tank Features Shown

Figure 7.84 shows the horizontal amplification factors from the ANSYS® model at the Type III tank foundation elevation (49 feet below grade), the haunch elevation (20 feet below grade), and the dome apex elevation (11 feet below grade) at the far field boundary. The peak amplitudes of the soil column occur at 2.3, 5.2, 8.4, 11.6 and 14.5 Hz which agrees with Figure 7.1. Figure 7.85 shows the horizontal amplification factors of the dome apex and haunch which are normalized to the tank foundation.

Figure 7.85 shows the horizontal tank frequency recovered from the dome apex is 5.8 Hz when the peak amplitude of the dome is normalized to the peak amplitude of the tank foundation. Normalizing the dome displacements to the tank foundation displacements clearly identifies the independent character of the dome frequencies from the soil frequencies. The physical interpretation of this frequency corresponds to dome flexure associated with a lateral deformation of the tank walls.

The ANSYS® SSI full model is used to perform a vertical harmonic evaluation by replacing the horizontal displacement at the base of the model with a vertical displacement for the harmonic motion.

Figure 7.86 shows the vertical amplification factors for the tank foundation, the haunch, the dome apex, and the surface at the far field boundary of the ANSYS® model. Figure 7.86 shows the peak amplitudes of the BE soil at 4.5 Hz, 9.9 Hz, and 16.7 Hz, which agrees with the results shown in Figure 7.4. Figure 7.87 shows the vertical amplification factors of the dome apex and haunch normalized to the tank foundation. When the dome response is isolated from the supporting soil column response, the natural dome frequencies are approximately 5.0 Hz and 8.8 Hz with the fundamental natural frequency of 8.8 Hz.

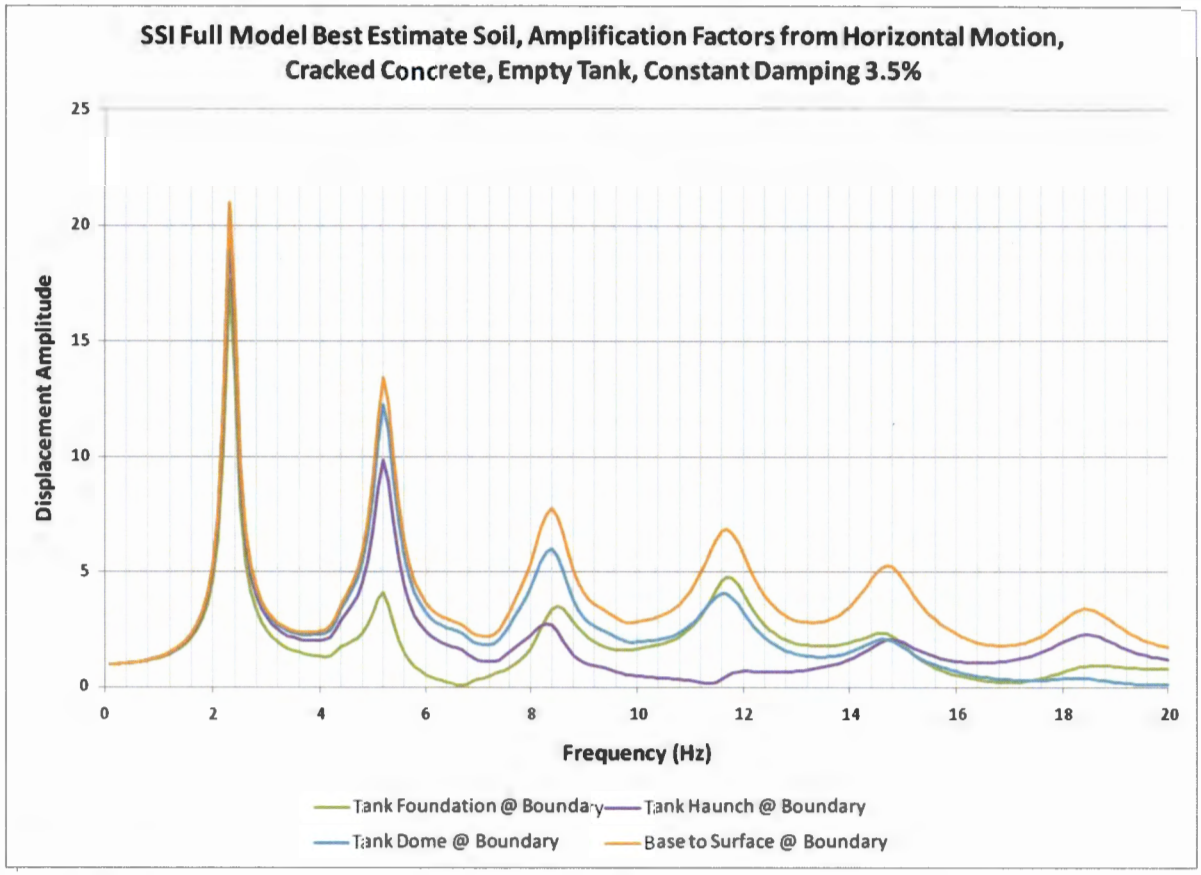

Figure 7.84. Horizontal Amplification Factors at the Far Field Boundary at the Tank Foundation, Haunch, Dome Apex, and Surface Elevations

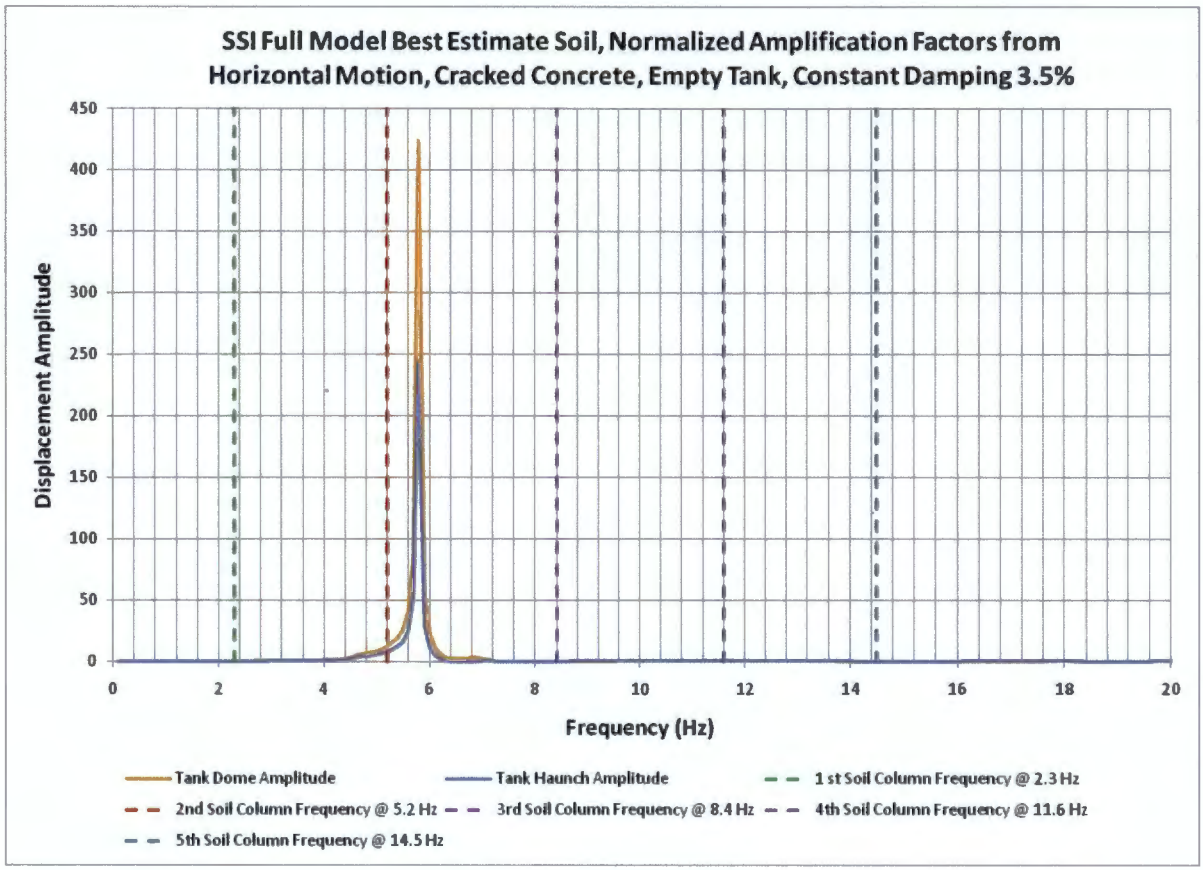

Figure 7.85. Horizontal Amplification Factors of the Dome Apex and Haunch Normalized to the Tank Foundation

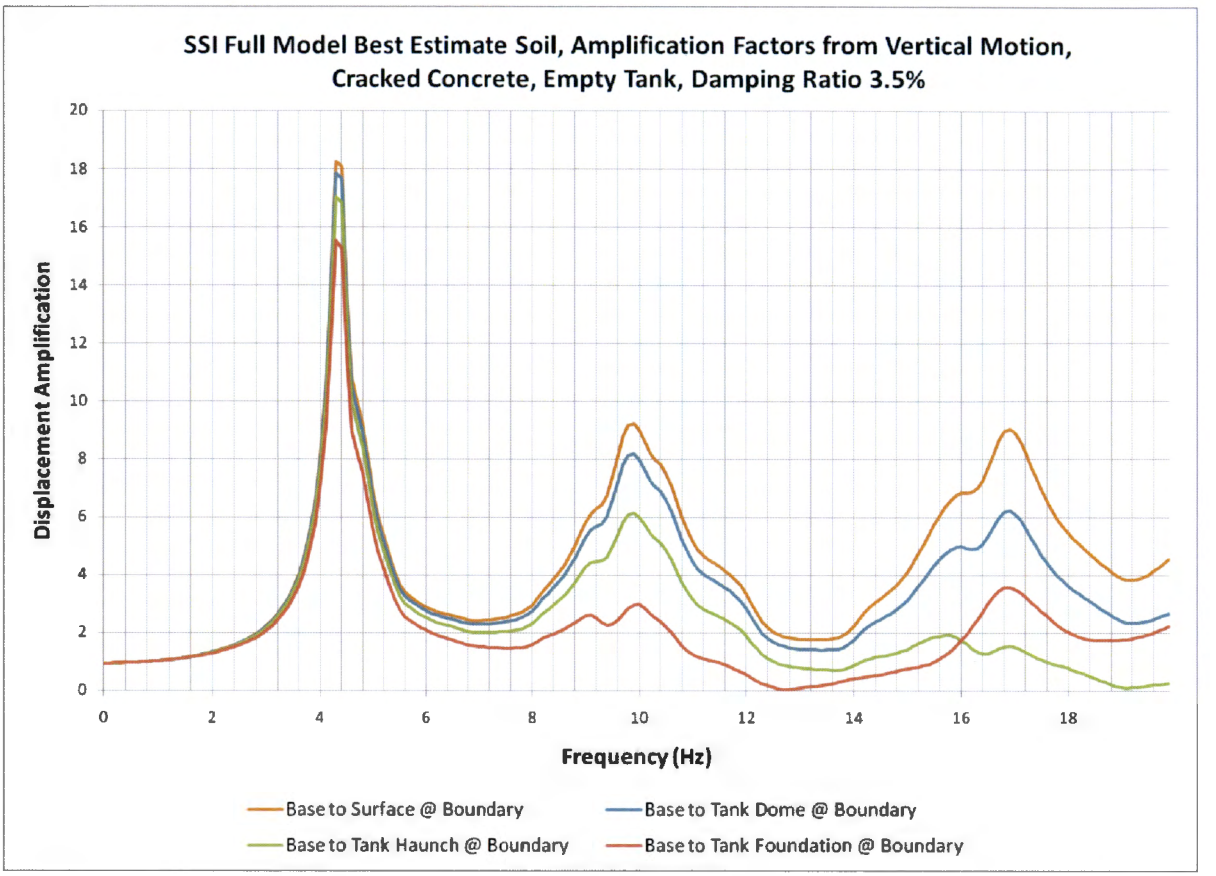

Figure 7.86. Vertical Amplification Factors at the Far Field Boundary for the Elevation of the Tank Foundation, Haunch, Dome Apex, and Surface

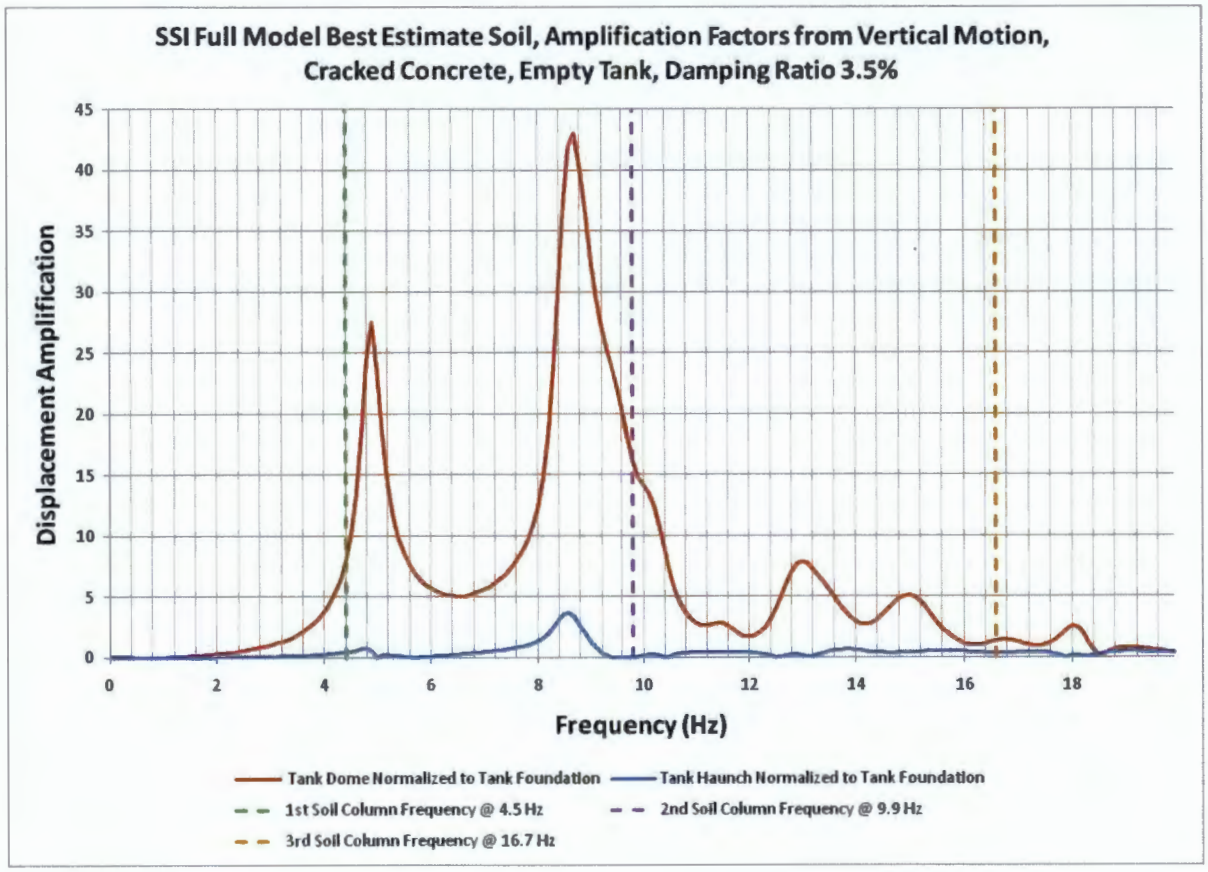

Figure 7.87. Vertical Amplification Factors of the Dome Apex, and Haunch Normalized to the Tank Foundation Amplitude

7.11.1 Conclusions Regarding Spectral Matching for the BE Soil Profile

Since the harmonic analysis has identified both horizontal and vertical modes of the dome and soil column, this information can be used to estimate the level of conservatism in the analysis based on the exceedance of the ANSYS® spectra relative to the target spectra at these structurally important frequencies. Figure 7.88 shows the tank foundation and surface horizontal spectra as the percentage above the target spectra between the frequencies of 0.1 Hz and 30 Hz. The solid black lines show the natural frequencies of the BE soil column, which are 2.3 Hz, 5.2 Hz, 8.4 Hz, 11.6 Hz and 14.5 Hz. The single solid green line shows the horizontal fundamental natural frequency at the dome apex, which is 6.8 Hz. The dome apex capacity at its fundamental natural frequency is of interest when evaluating the tank appurtenances response to horizontal motion. Therefore, the dome has margin between 20% and 40% above the target spectra.

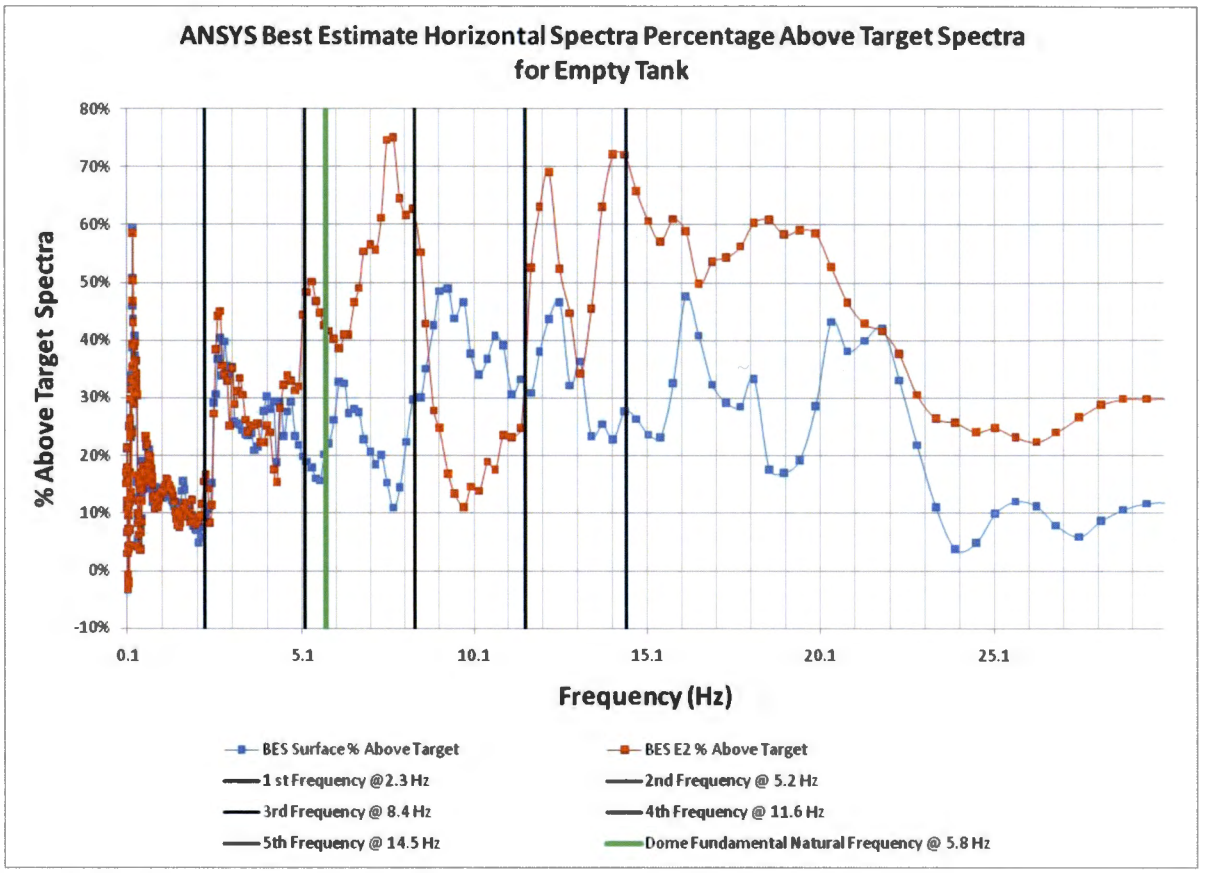

Figure 7.88. Horizontal spectra for SSI Model with Best Estimte Soil Profile Shown as a Percentage Above Target Spectra Along with the Natural Frequencies of the Soil Column and the Fundamental Natural Frequency of the Dome.

Figure 7.89 shows the tank foundation and surface vertical spectra as the percentage above the target spectra between the frequencies of 0.1 Hz and 30 Hz. The solid black line shows the natural frequencies of the BE soil column, which are 4.5 Hz, 9.9 Hz, and 16.7 Hz. The single purple line shows the first natural frequency of the dome apex, which is 5.0 Hz. The single green line shows the second natural frequency which is the fundamental natural frequency of the dome apex, which is 8.8 Hz. The plot shows that at the first dome natural frequency of 5.0 Hz, the ANSYS® spectra are between 6.4% and 9.5% above the target spectra. The plot shows that at the fundamental natural frequency of the dome is 8.8 Hz, the ANSYS® spectra are between 13.0% and 20.0% above the target spectra.

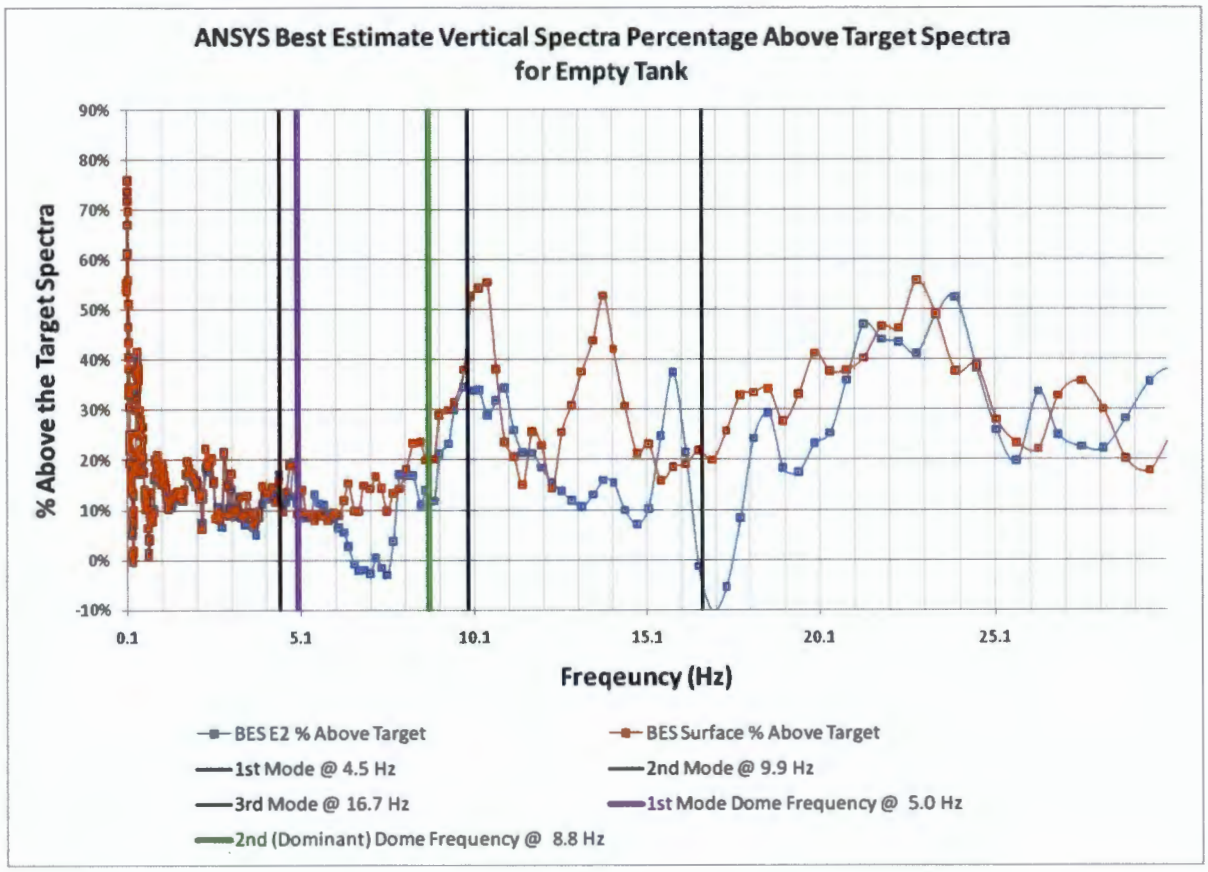

Figure 7.89. Vertical Spectra for SSI Model with Best Estimate Soil Profile Shown as a Percentage Above Target Spectra Along with the Fundamental Natual Frequencies of the Soil Column and Dome.

7.12 Harmonic Analysis for the Full SSI Model with LB Soil Profile

A harmonic analysis of the ANSYS® SSI full model is performed to determine the natural frequencies of the concrete tank in the soil. The ANSYS® SSI model is described in Chapter 6. The figures presented in this section show horizontal and vertical amplification factors of the tank foundation, tank haunch and tank dome. The concrete tank features of interest are shown in Figure 7.83 and the same tank locations where data is extracted as defined in the previous section.

With the LB soil profile, the ANSYS® SSI full model was modified such that the friction surfaces between the tank and the soil are bonded and no waste is present in the tank. No changes were made to the cracked concrete material properties. An oscillating unit horizontal displacement is applied at the base of the soil column is the excitation for the horizontal harmonic analysis. The frequency range evaluated is from 0–20 Hz resulting in 200 frequency ordinates. In contrast to the full integration time domain analysis with mass and stiffness proportional damping, the harmonic analysis utilized a constant damping ratio, which for lower bound soil profile is 5.5% of critical damping. This is the median value calculated from the 49 soil layers each with a unique critical damping value as shown in Table 7.2.

Figure 7.90 shows the horizontal amplification factors from the ANSYS® model at the Type III tank foundation elevation (49 feet below grade), the haunch elevation (20 feet below grade), and the dome apex elevation (11 feet below grade) at the far field boundary. The peak amplitude of the soil column occurs at 0.9 Hz, 2.4 Hz, 3.8 Hz, 5.2 Hz, and 6.7 Hz which agrees with Figure 7.2. Figure 7.91 shows the horizontal amplification factors of the dome apex and haunch which are normalized to the tank foundation.

Figure 7.91 shows the horizontal natural frequency recovered from the dome apex is 4.4 Hz when the peak amplitude of the dome is normalized to the peak amplitude of the tank foundation. The physical interpretation of this frequency corresponds to dome flexure associated with a lateral deformation of the tank walls.

The ANSYS® SSI full model is used to perform a vertical harmonic evaluation by replacing the horizontal displacement at the base of the model with a vertical displacement for the harmonic motion.

Figure 7.92 shows the vertical amplification factors for the tank foundation, the haunch, the dome apex, and the surface at the far field boundary of the ANSYS® model. Figure 7.92 shows the peak amplitudes of the LB soil at 1.8 Hz, 4.9 Hz, 7.8 Hz, 10.6 Hz, and 13.8 Hz, which agrees with the results shown in Figure 7.5. Figure 7.93 shows the vertical amplification factors of the dome apex and haunch normalized to the tank foundation. When the dome response is isolated from the supporting soil column response, the natural frequency of the dome is approximately 3.9 and 6.7 Hz with the fundamental natural frequency response at 6.7 Hz.

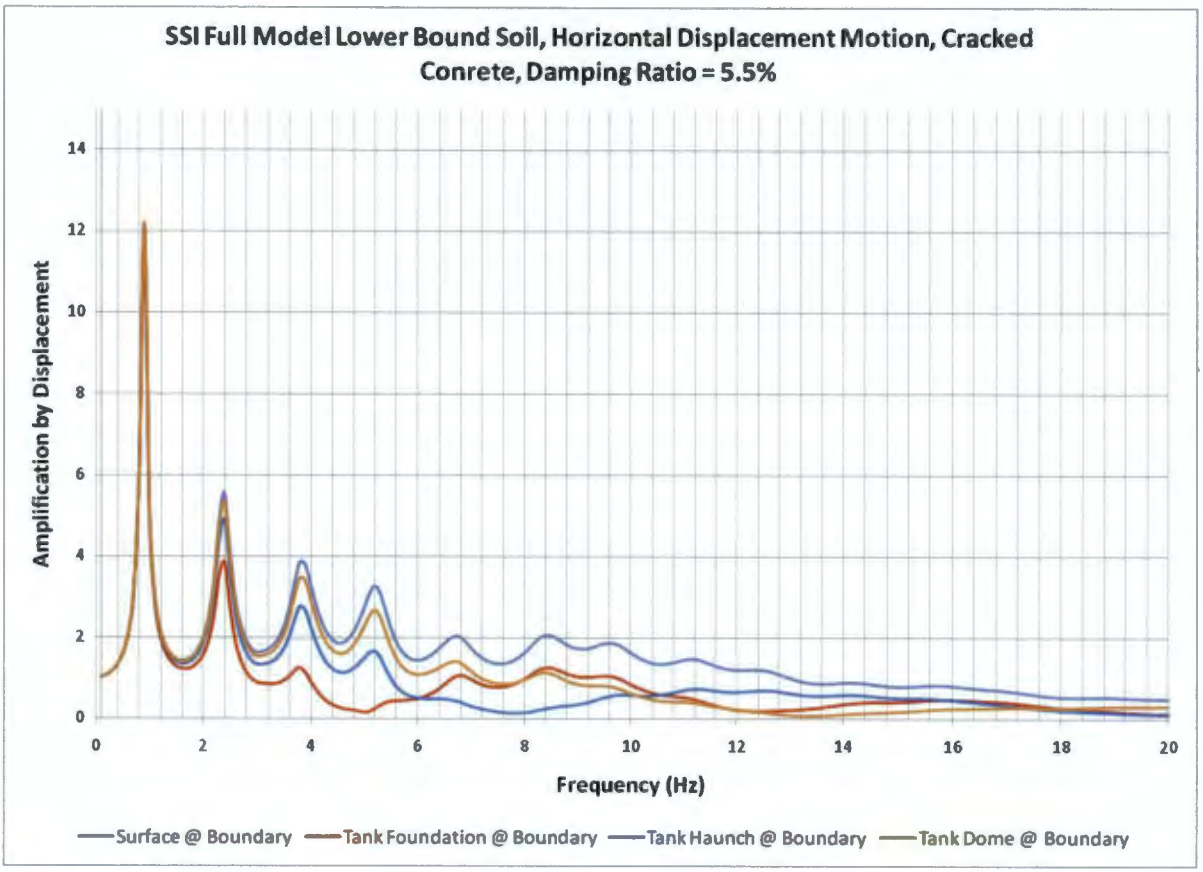

Figure 7.90. Horizontal Amplification Factors at the Far Field Boundary at the Tank Foundation, Haunch, Dome Apex, and Surface Elevations

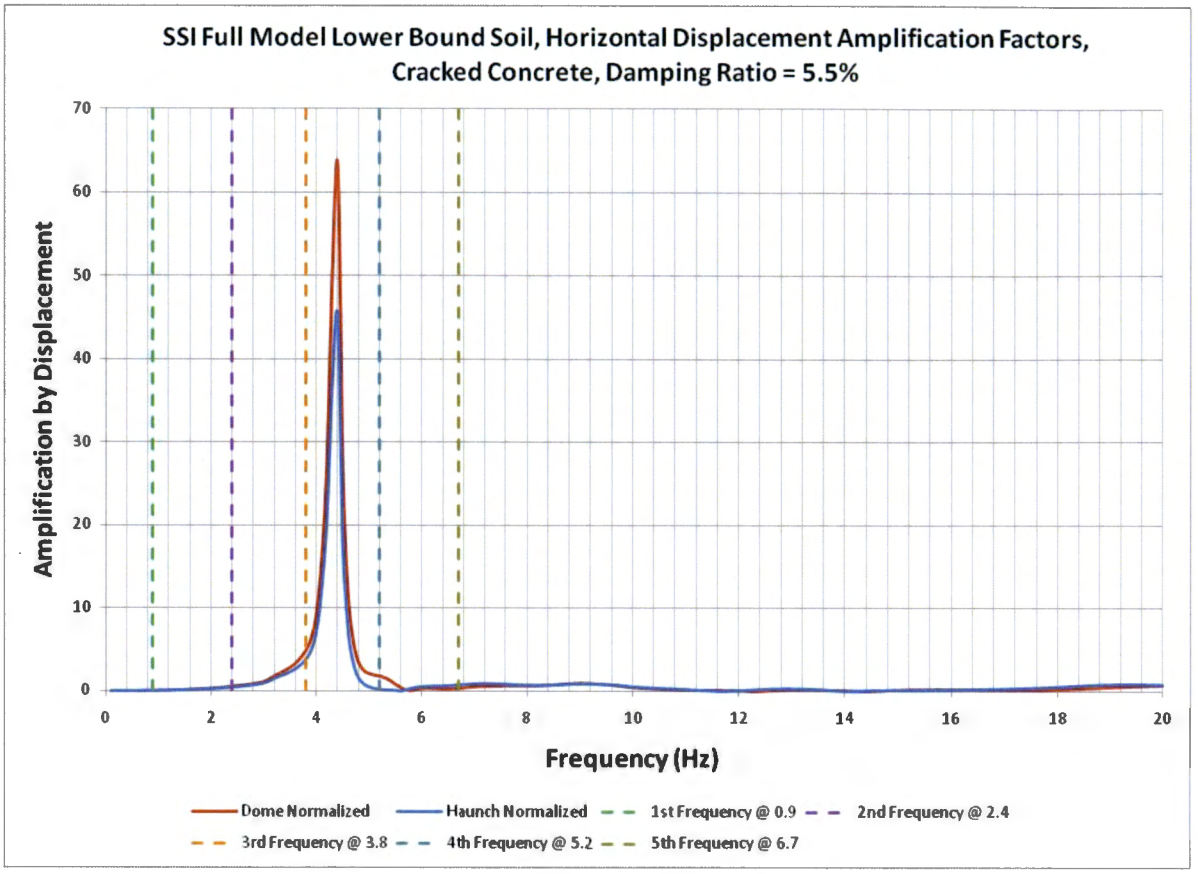

Figure 7.91. Horizontal Amplification Factors of the Dome Apex and Haunch Normalized to the Tank Foundation

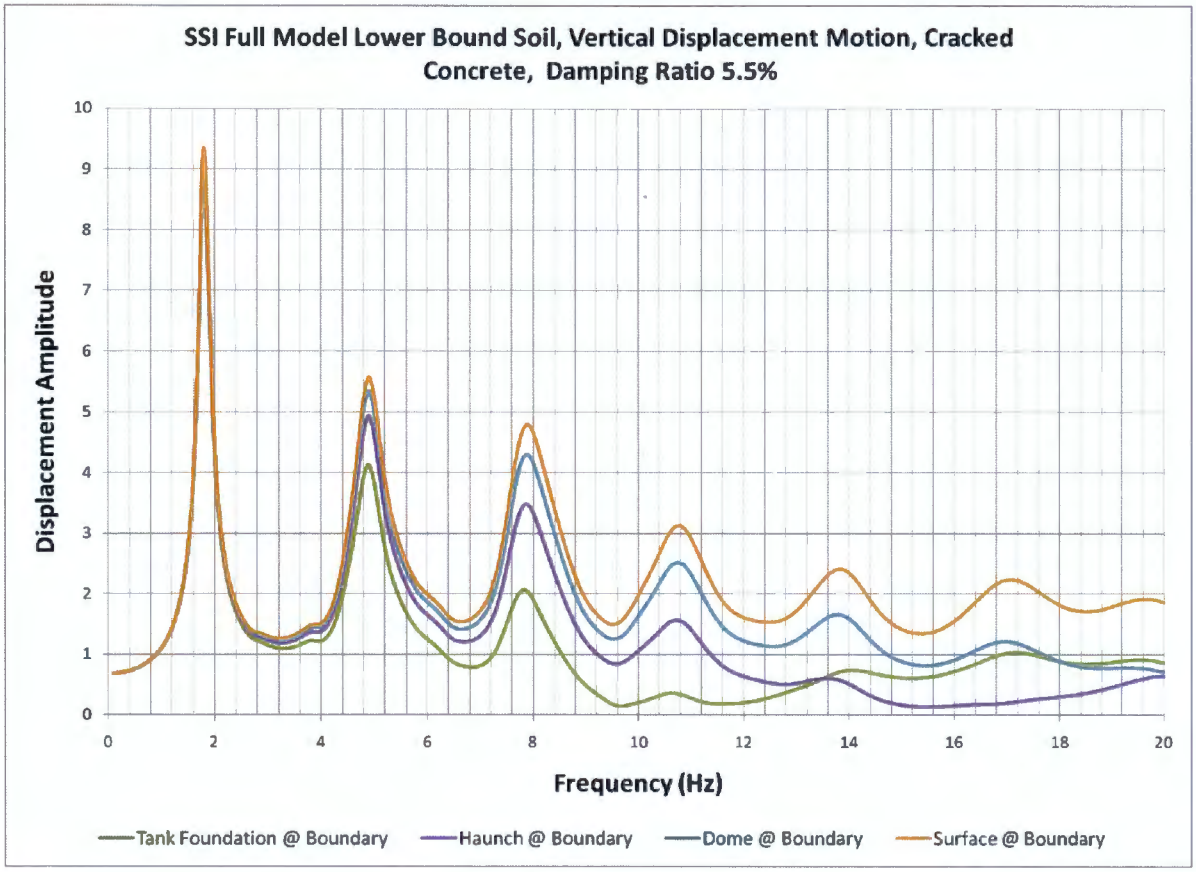

Figure 7.92. Vertical Amplification Factors at the Far Field Boundary for the Elevation of the Tank Foundation, Haunch, Dome Apex, and Surface

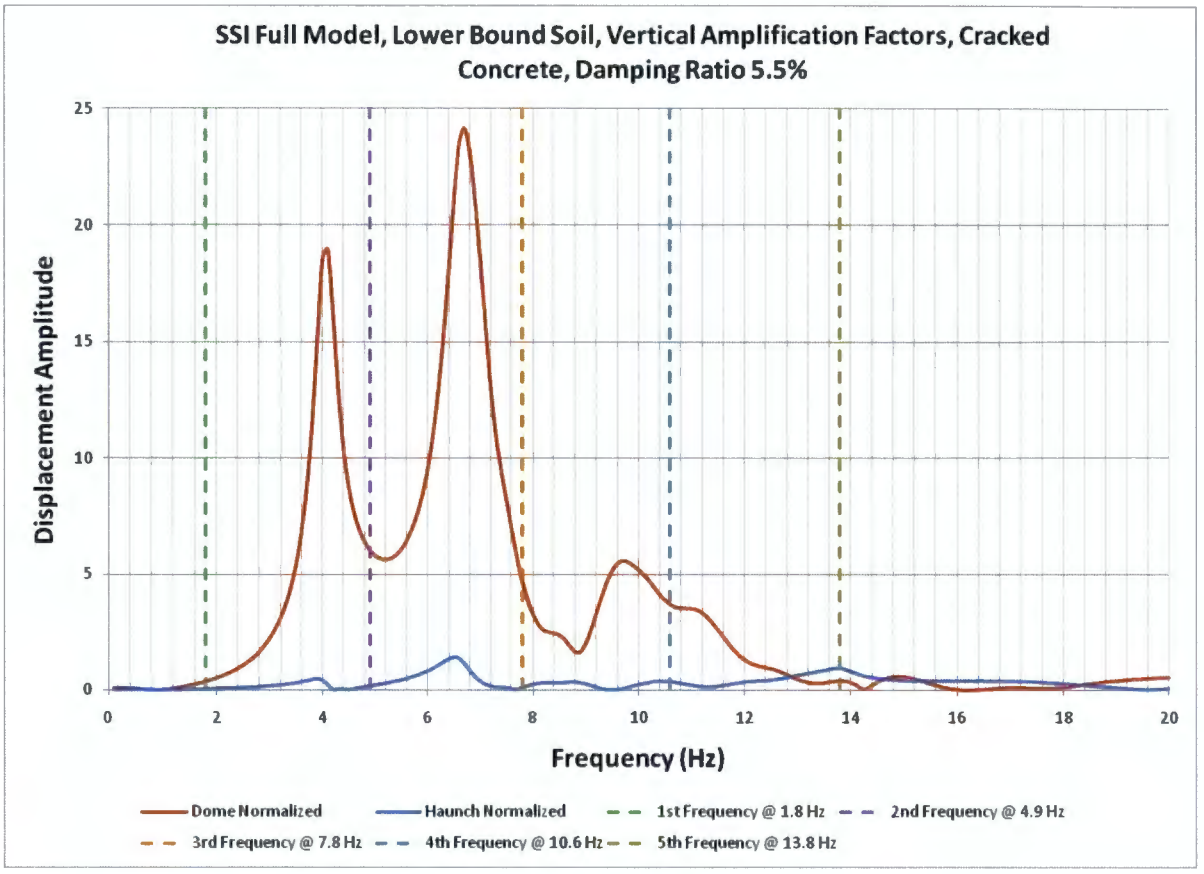

Figure 7.93. Vertical Amplification Factors of the Dome Apex, and Haunch Normalized to the Tank Foundation Amplitude

7.12.1 Conclusions Regarding Spectral Matching for the LB Soil Profile

Since the harmonic analysis has identified both horizontal and vertical modes of the dome and soil column, this information can be used to estimate the level of conservatism in the analysis based on the exceedance of the ANSYS® spectra relative to the target spectra at these structurally important frequencies. Figure 7.94 shows the tank foundation and surface horizontal spectra as the percentage above the target spectra between the frequencies of 0.1 Hz and 30 Hz. The solid black lines show the natural frequencies of the LB soil column, which are 0.9 Hz, 2.4 Hz, 3.8 Hz, 5.2 Hz, and 6.7 Hz. The single solid green line shows the fundamental natural frequency at the dome apex, which is 4.4 Hz. The dome apex capacity at its fundamental natural frequency is of interest when evaluating the tank appurtenances response to horizontal motion. The plot shows that at the fundamental natural frequency of 4.4 Hz, the ANSYS spectra are between 20% and 42% above the target spectra.

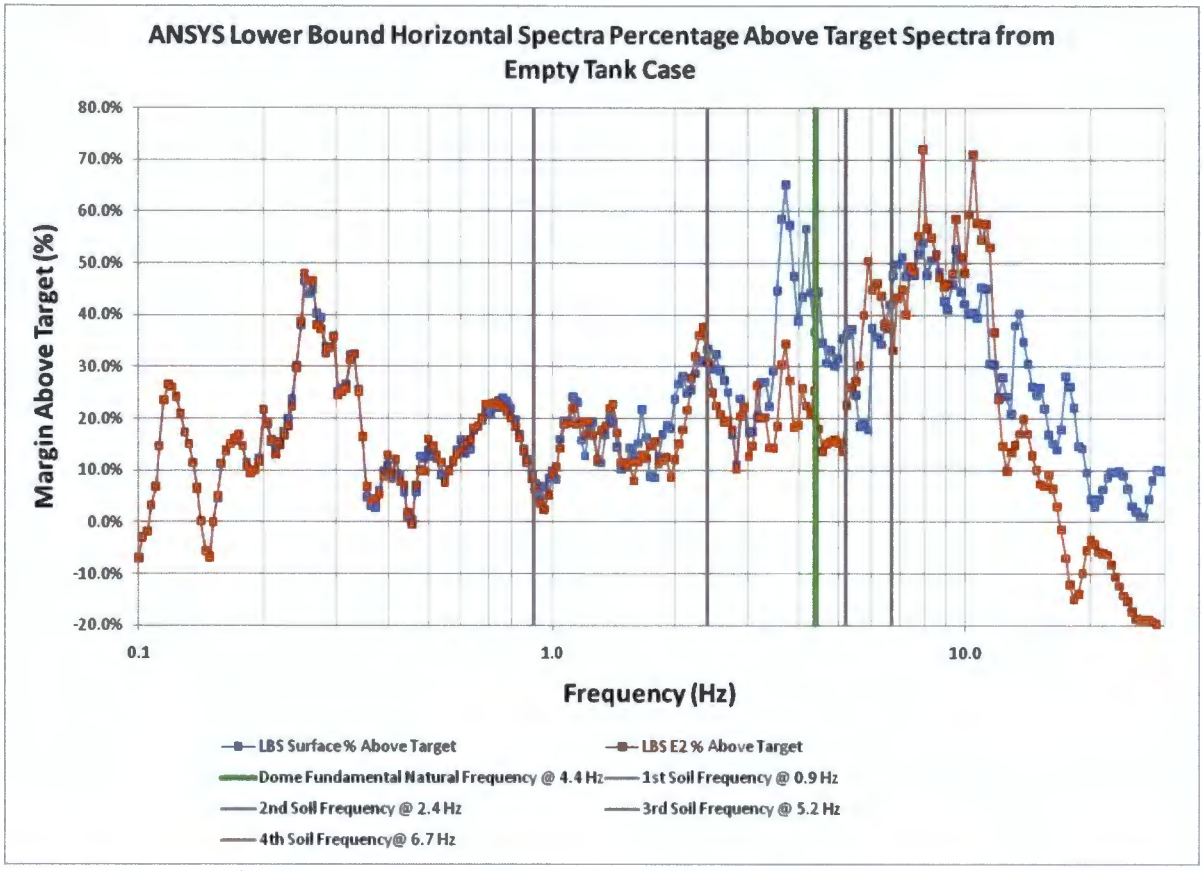

Figure 7.94. Horizontal spectra for SSI Model with Best Estimte Soil Profile Shown as a Percentage Above Target Spectra Along with the Natural Frequencies of the Soil Column and the Fundamental Natural Frequency of the Dome.

Figure 7.95 shows the tank foundation and surface vertical spectra as the percentage above the target spectra between the frequencies of 0.1 Hz and 30 Hz. The solid black line shows the natural frequencies of the LB soil column, which is 1.8 Hz, 4.9 Hz, 7.8 Hz, and 10.6 Hz. The single solid purple line shows the first natural freuquency of the dome apex, which is 3.9 Hz. The single solid green line shows the second and the fundamental natural freuqency of the dome apex, which is 6.7 Hz. The plot shows that at the first natural frequency of the dome is 3.9 Hz, the ANSYS® spectra are between 10% and 15% above the target spectra. The plot shows that at the fundamental natural frequency of the dome is 6.7 Hz, the ANSYS® spectra are between 10% and 30% above the target spectra.

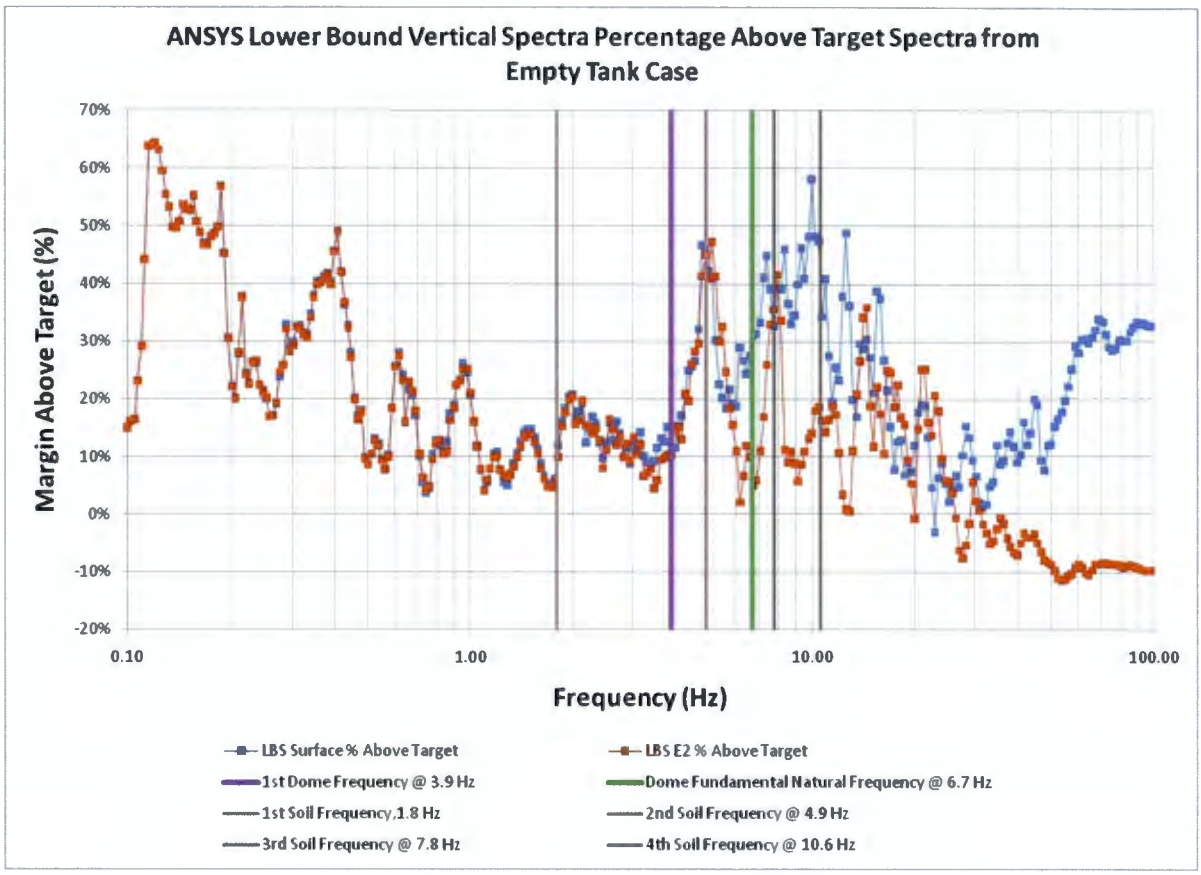

Figure 7.95. Vertical Spectra for SSI Model with Best Estimate Soil Profile Shown as a Percentage Above Target Spectra Along with the Fundamental Natual Frequencies of the Soil Column and Dome.

7.13 Harmonic Analysis for the Full SSI Model with UB Soil Profile

A harmonic analysis of the ANSYS® SSI full model is performed to determine the natural frequencies of the concrete tank in the soil. The ANSYS® SSI model is described in Chapter 6. The figures presented in this section show horizontal and vertical amplification factors of the tank foundation, tank haunch and tank dome. The concrete tank features of interest are shown Figure 7.83 and the same tank locations where data is extracted as defined in Section 7.11.

With the UB soil profile, the ANSYS® SSI full model was modified such that the friction surfaces between the tank and the soil are bonded and no waste is present in the tank. No changes were made to the cracked concrete material properties. An oscillating unit horizontal displacement is applied at the base of the soil column is the excitation for the horizontal harmonic analysis. The frequency range evaluated is from 0–20 Hz resulting in 200 frequency ordinates. In contrast to the full integration time domain analysis with mass and stiffness proportional damping, the harmonic analysis utilized a constant damping ratio, which for lower bound soil profile is 2.3% of critical damping. This is the median value calculated from the 35 soil layers each with a unique critical damping value as shown in Table 7.4.

Figure 7.96 shows the horizontal amplification factors from the ANSYS® model at the Type III tank foundation elevation (49 feet below grade), the haunch elevation (20 feet below grade), and the dome apex elevation (11 feet below grade) at the far field boundary. The peak amplitude of the soil column occurs at 4.4, 11.7 and 18.7 Hz, which agrees with Figure 7.3. Figure 7.97 shows the horizontal amplification factors of the dome apex and haunch which are normalized to the tank foundation.

Figure 7.97 shows the horizontal tank frequency recovered from the dome apex is 6.8 and 7.5 Hz when the peak amplitude of the dome is normalized to the peak amplitude of the tank foundation. The physical interpretation of this frequency corresponds to dome flexure associated with a lateral deformation of the tank walls.

The ANSYS® SSI full model is used to perform a vertical harmonic evaluation by replacing the horizontal displacement at the base of the model with a vertical displacement for the harmonic motion.

Figure 7.98 shows the vertical amplification factors for the tank foundation, the haunch, the dome apex, and the surface at the far field boundary of the ANSYS® model. Figure 7.98 shows the peak amplitudes of the UB soil at 8.4 Hz, which agrees with the results shown in Figure 7.6. Figure 7.99 shows the vertical amplification factors of the dome apex and haunch normalized to the tank foundation. When the dome response is isolated from the supporting soil column response, the natural frequency of the dome is approximately 5.5 and 10.3 Hz with the fundamental natural frequency response at 10.3 Hz.

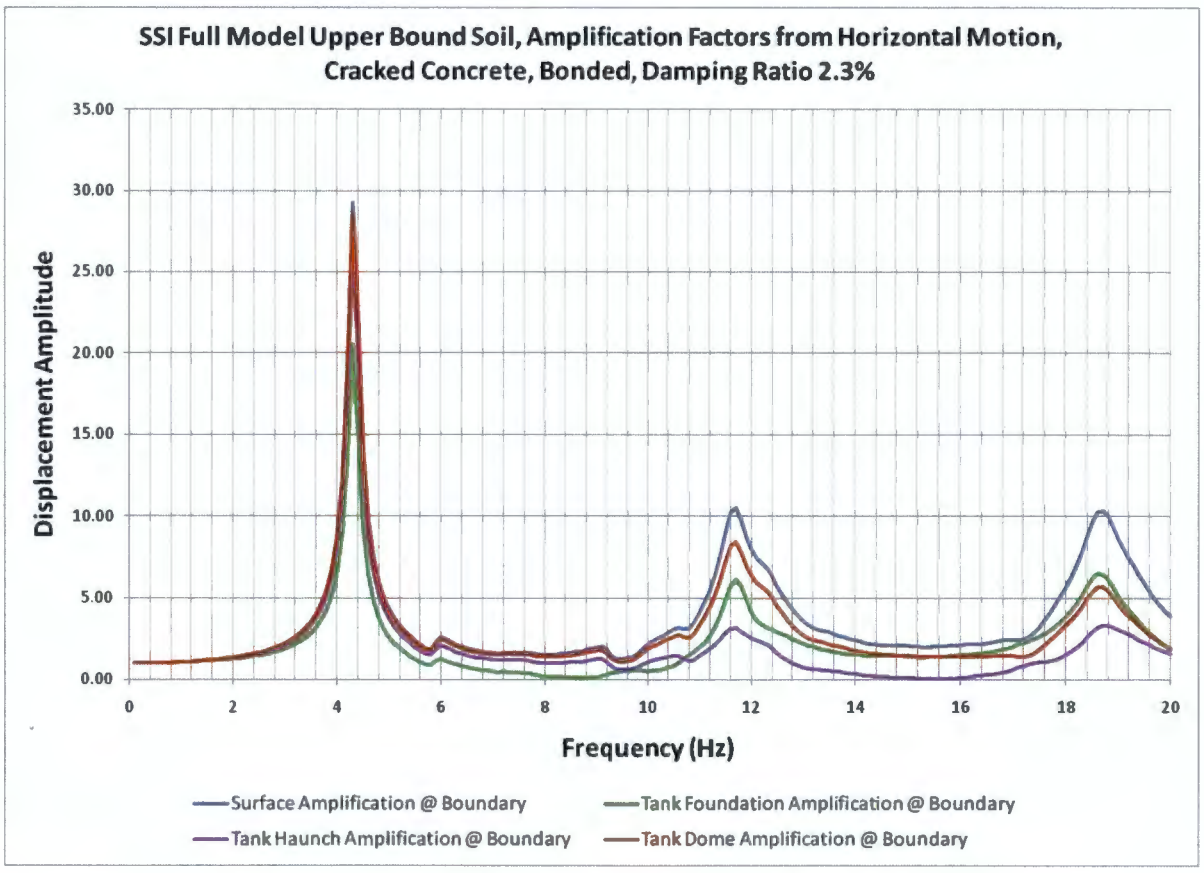

Figure 7.96. Horizontal Amplification Factors at the Far Field Boundary at the Tank Foundation, Haunch, Dome Apex, and Surface Elevations

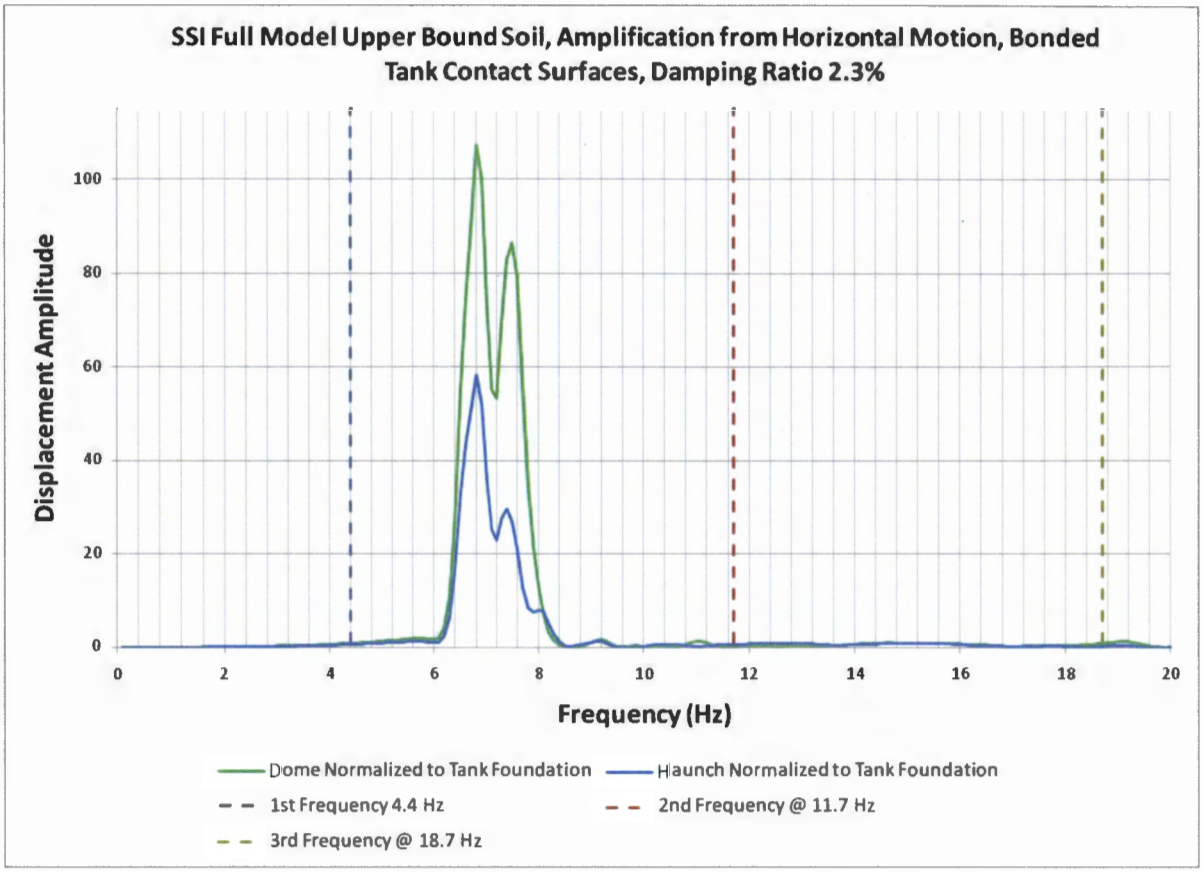

Figure 7.97. Horizontal Amplification Factors of the Dome Apex and Haunch Normalized to the Tank Foundation

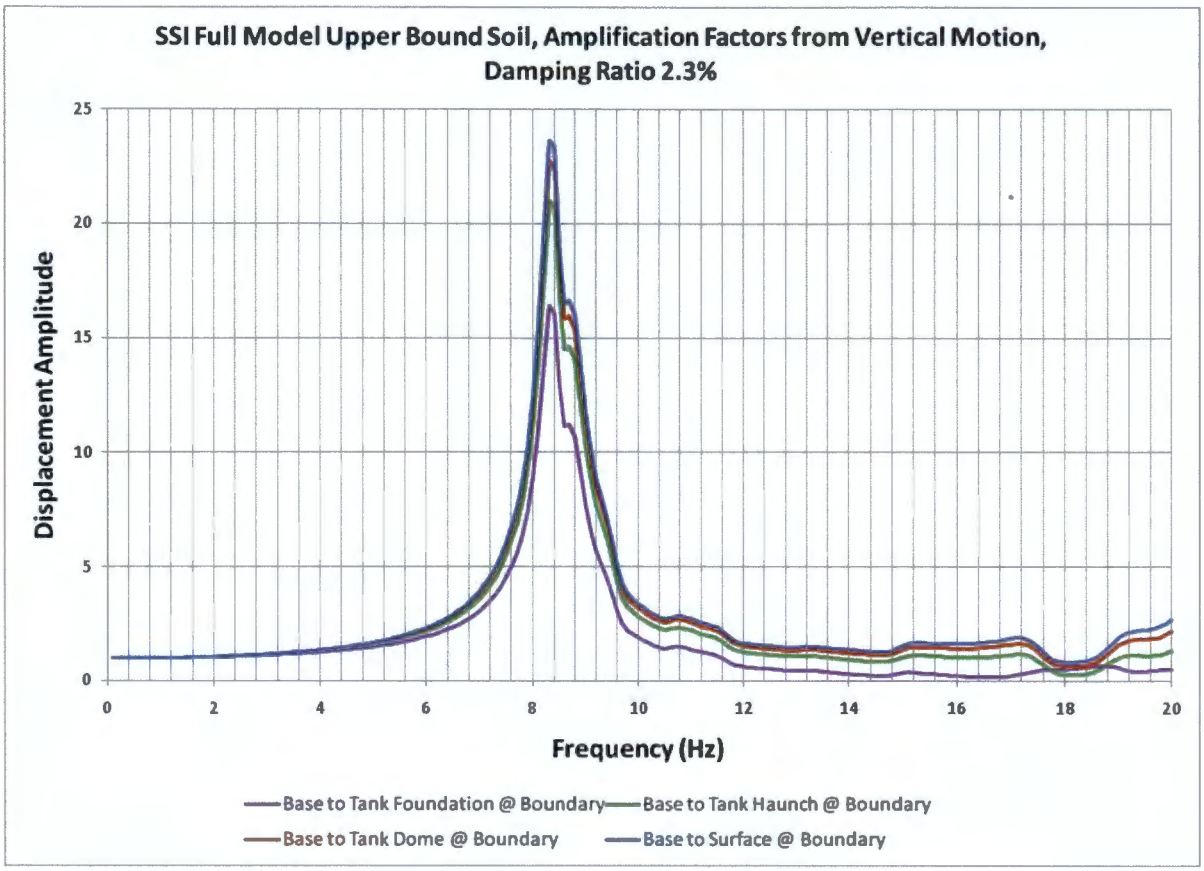

Figure 7.98. Vertical Amplification Factors at the Far Field Boundary for the Elevation of the Tank Foundation, Haunch, Dome Apex, and Surface

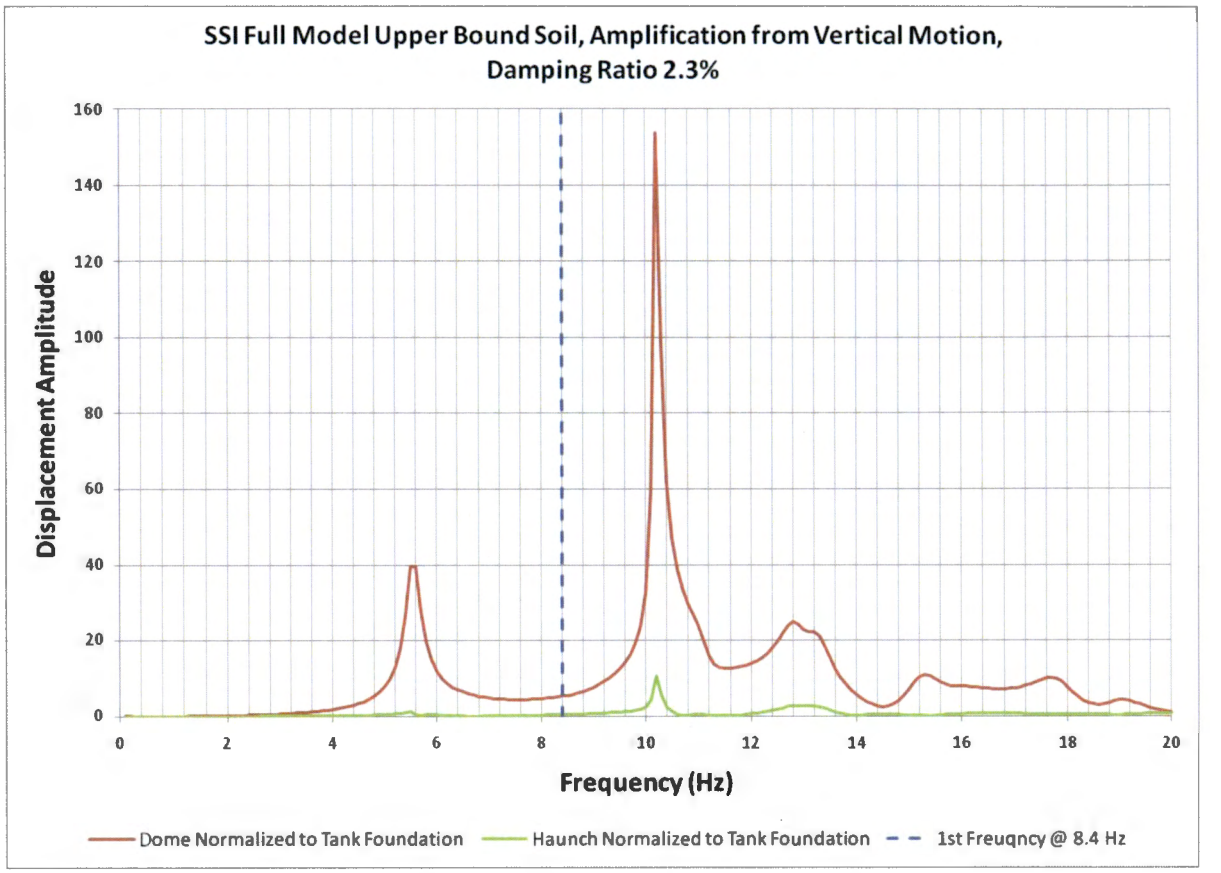

Figure 7.99. Vertical Amplification Factors of the Dome Apex, and Haunch Normalized to the Tank Foundation Amplitude

7.13.1 Conclusions Regarding Spectral Matching for the UB Soil Profile

Since the harmonic analysis has identified both horizontal and vertical modes of the dome and soil column, this information can be used to estimate the level of conservatism in the analysis based on the exceedance of the ANSYS® spectra relative to the target spectra at these structurally important frequencies. Figure 7.100 shows the tank foundation and surface horizontal spectra as the percentage above the target spectra between the frequencies of 0.1 Hz and 30 Hz. The solid black lines show the natural frequencies of the UB soil column, which are 4.4, 11.7 and 18.7 Hz. The single solid green line shows the fundamental natural frequency at the dome apex, which is 6.8 Hz. The dome apex capacity at its fundamental natural frequency is of interest when evaluating the tank appurtenances response to horizontal motion. The plot shows that at the fundamental natural frequency of 6.8 Hz, the ANSYS spectra are between 25% and 33% above the target spectra.

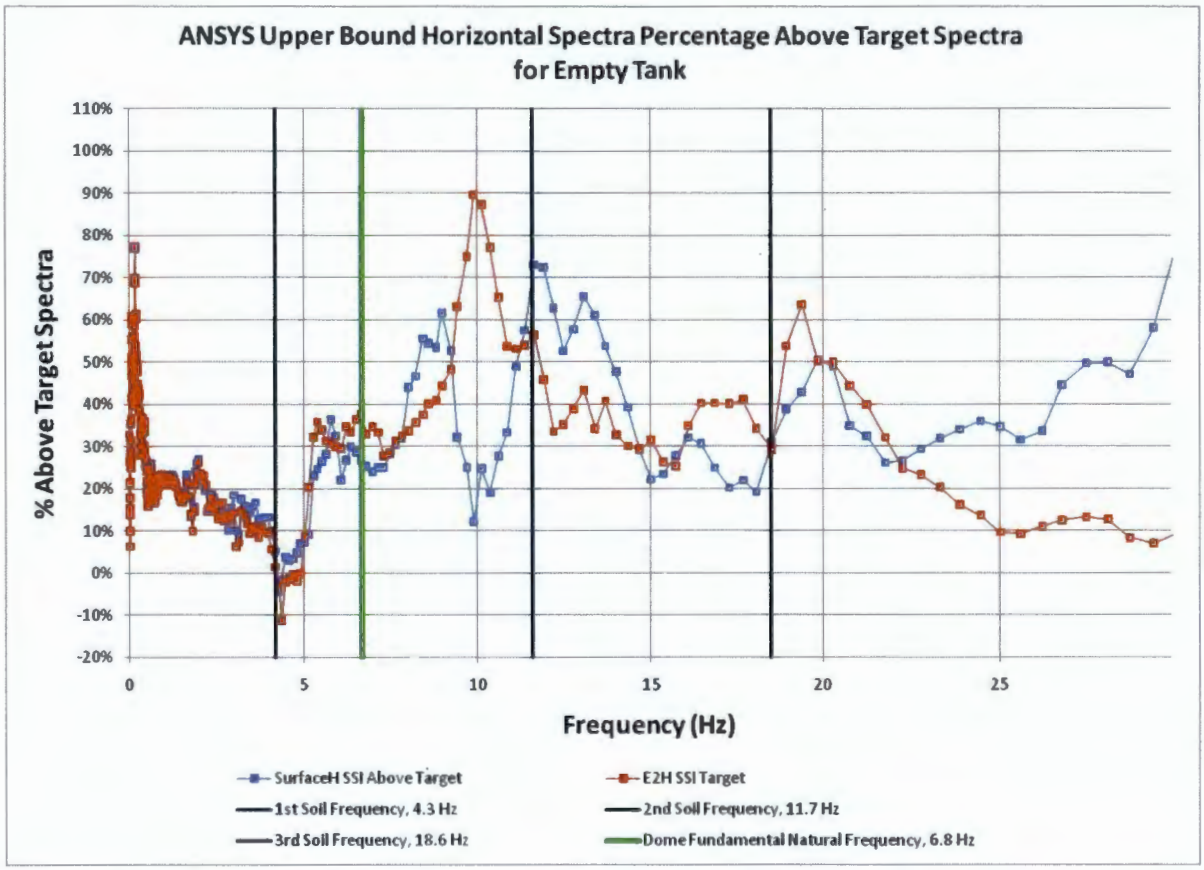

Figure 7.100. Horizontal Spectra for SSI Models with Upper Bound Soil Profile Shown as Percentage Above the Target Spectra Along with the Natural Frequencies of the Soil Column and the Fundamental Natural Freuquency of the Dome.

Figure 7.101 shows the tank foundation and surface vertical spectra as the percentage above the target spectra between the frequencies of 0.1 Hz and 30 Hz. The solid black line shows the fundamental frequency of the UB soil column, which is 8.4 Hz. The single solid green line shows the dominant mode of the dome apex, which is 10.3 Hz. The plot shows that at the fundamental natural frequency of the dome is 10.3 Hz, the ANSYS® spectra are between 11.0 and 14.2% above the target spectra.

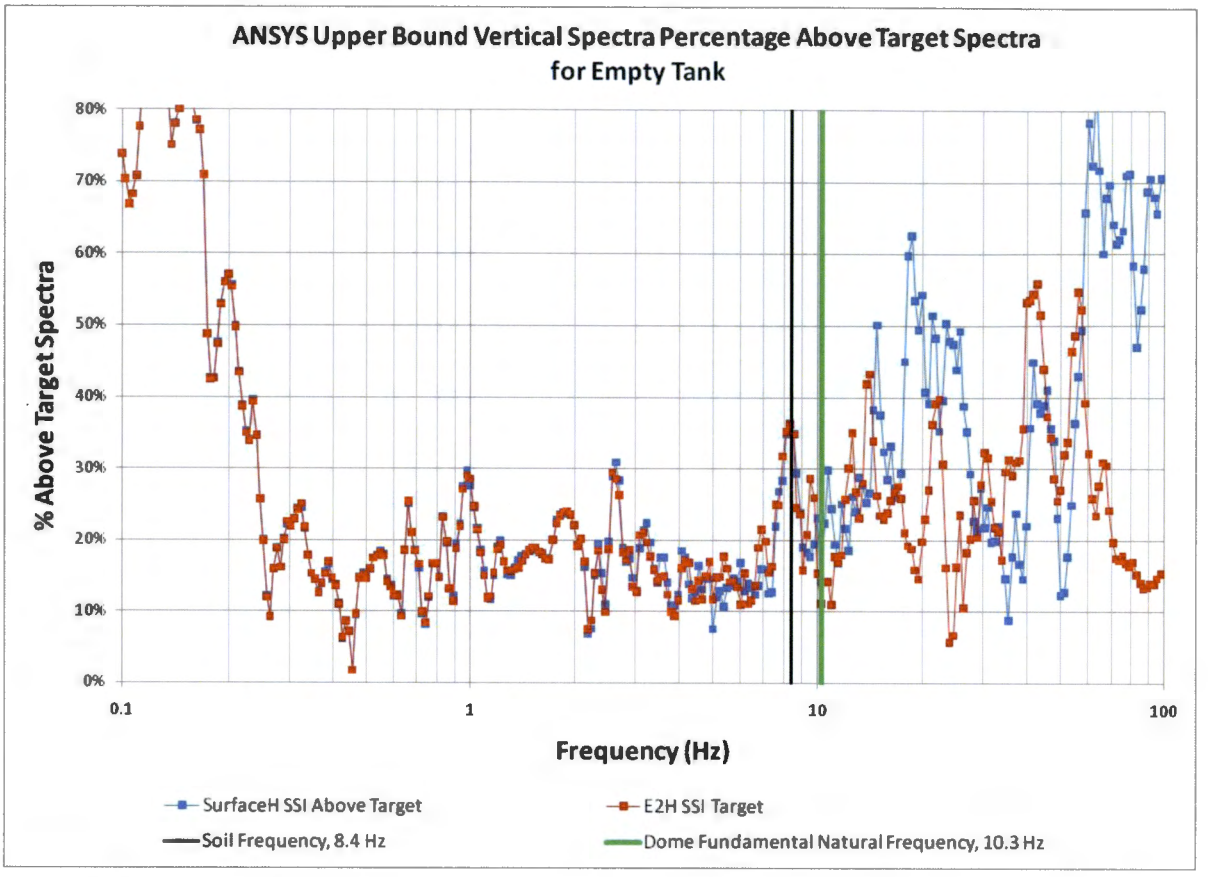

Figure 7.101. Vertical Spectra for SSI Model with Upper Bound Soil Profile Shown as Percentage Above Target Spectra Along with the Fundamental Natural Frequency of the Soil Column and Dome.

This page intentionally left blank.

8.0 Static Modeling Results

This chapter presents the TOLA static modeling results (without seismic) for the TOLA matrix runs given in Section 5.6 of Chapter 5.

8.1 Introduction

This section summarizes the results from the eight different TOLA runs described in Section 5 of this document. The primary focus is evaluation of the SST according to the criteria developed by Johnson et al. (2010) and summarized in Chapter 4 of this report. The ACI concrete evaluation for each run in Table 5.6 is presented. Run 1 is the baseline model with best estimate properties. TOLA matrix Runs 2 through 8 are combinations of bounding material property variations. These are called worst-case combinations because they are combined to bound the possible scenarios. For example, one would not expect to have zero creep under thermal loading with nominal or high concrete modulus; nonetheless, these are combined to understand the effect of concrete creep and soil modulus variation on the tank response. Runs 2 through 5, 7, and 8 have property variations ranging from 15% to 50% with either creep turned on or off in the model.

Each run was conducted in several steps as shown in Figure 4.2. The ACI evaluations are conducted at different points depending on the particular ACI load combination. Load combination 1 is a separate load path and is always conducted after the final 50°F load step. Load combinations 4 and 9 include temperature effects.

Load step numbers and years are referenced in various plots in the following evaluation sections. Table 4.4 gives the load step numbers as related to the year of the analysis and individual thermal load steps.

8.2 ACI Evaluations – Structural Concrete

The Evaluation Criteria report (Johnson et al. 2010) specifies that the reinforced concrete structure of the tanks shall be evaluated to the standards of ACI 349-06 (ACI 2007). The load factors to be applied in this analysis are a subset of the possible combinations specified in ACI 349-06. Chapter 4 of this report indicates that load combinations 1, 4, and 9 are relevant for this analysis.

Load combination 1 $\{U = 1.4D + 1.4F + 1.7L + 1.7H\}$ was achieved by running the model for an additional load step after the 50°F load step of thermal and waste-level history. This combination requires, in part, a factor of 1.4 on dead loads and a factor of 1.7 on lateral soil loads. This was achieved by placing the 1.4 factor on the gravitational acceleration and scaling the soil densities by the ratio of 1.7/1.4 except for soil overburden above the dome.

Load combination 4 (without seismic) $\{U = D + F + L + H + T_o + E_{ss}\}$ has load factors of 1.0 and includes thermal effects. This was achieved by cooling the waste temperature to 80°F after the thermal and waste-level history.

Load combination 9 {U = 1.05D + 1.05F + 1.3L + 1.3H + 1.05T_o} was achieved by running the load combination 4 model for an additional load step after the 80°F load step. This combination requires, in part, a factor of 1.05 on dead loads and a factor of 1.3 on lateral soil loads. This was achieved by placing the 1.05 factor on the gravitational acceleration and scaling the soil densities by the ratio of 1.3/1.05 except for soil overburden above dome. In addition, the temperature difference (tank temperature – the initial stress-free temperature) was multiplied by 1.05 T_o.

An ANSYS® macro, TypeIII_Rev4_ACI.inp, was developed to compute shear, meridional, and circumferential (hoop) forces and moments at 44 locations in the concrete tank. Figure 8.1 shows the locations of the sections. The sections in the concrete tank begin at the center of the dome and traverse through the haunch, down the wall, and back across the slab. Table 8.1 shows an excerpt of the computed shear, meridional, and circumferential (hoop) forces and moments at critical sections under the unfactored peak temperature loading for Run 1. Force-moment diagrams of all the 44 sections were developed using the ACI methodology described in the Evaluation Criteria report. The section properties used in the ACI capacity calculations are described in Table 8.2 and Table 8.3.

Figure 8.2 shows a typical force-moment diagram along with the definition of the demand/capacity ratio. The demand/capacity ratio is defined as the ratio of the vector length from the origin to the force-moment demand coordinate to the vector length from the origin to the capacity curve assuming the same ratio of force to moment. A demand/capacity ratio exceeding 1.0 indicates that the ACI requirements are not met. Caution should be observed to not interpret the demand/capacity ratio as a measure of safety factor, which is only applicable if the same ratio of force to moment is maintained under changing loads. Appendix J shows the implementation of the ACI methodology using section 14 under peak temperature as an example.

Figure 8.3 through Figure 8.9 show the force-moment diagrams at load step 6 (peak temperature step) for critical sections using Run 1. These figures illustrate the change in demand at different locations of the tank. The capacity curves also change with temperature, and the capacities plotted in these figures reflect the maximum temperature experienced by the section. Since high temperature irreversibly degrades the strength and stiffness of concrete, the ACI capacity curves are always calculated for the maximum temperature that the tank has experienced up to that point in time.

The results presented in this section are the demand/capacity ratios for each of the three ACI load combinations (1, 4, and 9) and for all the eight TOLA runs. The meridional, circumferential, and shear data are combined onto single plots.

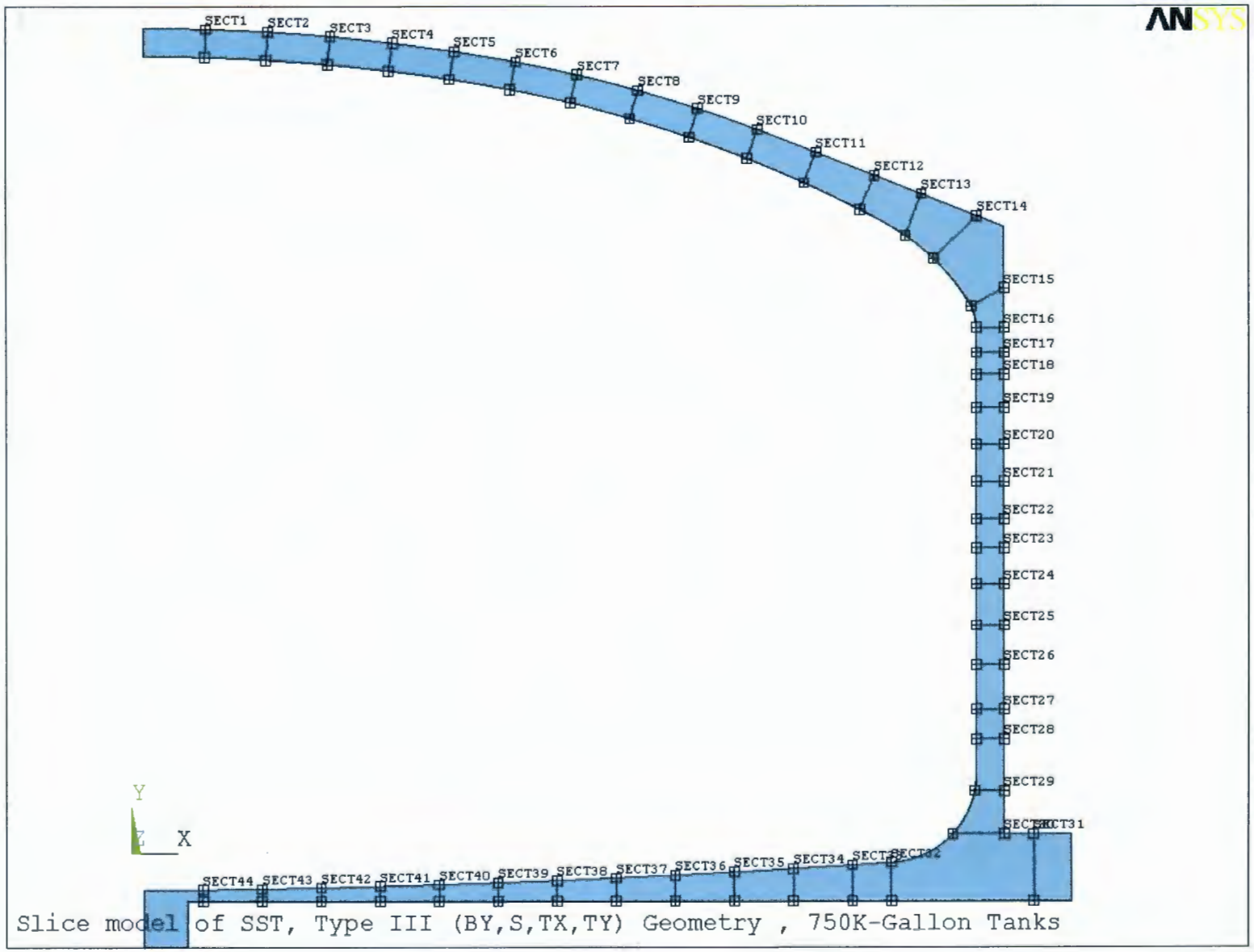

Figure 8.1. Reinforced Concrete Sections

Table 8.1. Computed Shear, Meridional, and Circumferential (hoop) Forces and Moments at Critical Sections Under Peak Temperatures for Run 1

Section #	Shear [kips/ft]	F-merid [kips/ft]	M-merid [kips-ft/ft]	F-hoop [kips/ft]	M-hoop [kips-ft/ft]	Tmin [°F]	Tmax [°F]	Tave [°F]	xbar [in]	ybar [in]	sect-thk [in]
13	-19	-64.7	33.1	-33.3	-3.3	202.8	219.3	210.7	417.2	368.9	23.72
14	-3.1	-65.9	60	-39.1	8.3	192.8	218.6	205.3	439.8	356.9	32.72
15	-4.7	-49.5	34.3	-20.3	-4.2	201.4	217.5	209.1	457.4	324.5	20.36
16	19	-69.9	24.9	-15.7	0.3	208.1	218	212.8	458.8	308	15
30	-8.7	-92.1	-3.2	-139.5	-0.4	225.4	256.3	240.5	452.3	36	27.88
31	-25.9	-62	13.8	-24	2.9	192.5	207.2	200.4	482	18	36
32	17.6	-83.7	22.4	-114.6	4.8	243.1	259.7	251.1	404.9	10.4	20.75

Table 8.2. Section Properties in Meridional Direction

Concrete Section		External Rebar			Internal Rebar			Notes/Schematic
No.	Thick (in.)	Bar Size	Depth d_1 (in.)	Spacing s (in.)	Bar Size	Depth d_2 (in.)	Spacing s (in.)	
1	15.00	6	3.000	12.00	6	12.000	12.00	For square mat in center
2	15.00	6	3.000	12.00	6	12.000	12.00	
3	15.00	6	4.000	11.08	6	13.000	11.08	
4	15.01	6	4.000	14.76	6	13.010	14.76	
5	15.01	6	4.000	9.22	6	13.010	9.22	
6	15.04	6	4.000	11.05	6	13.040	11.05	
7	15.20	6	4.000	12.86	6	13.200	12.86	
8	15.49	6	4.000	14.66	6	13.490	14.66	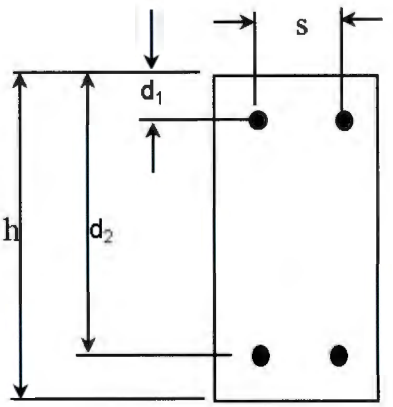
9	15.92	6	4.000	8.22	6	13.920	8.22	
10	16.49	6	4.000	9.09	6	14.490	9.09	
11	17.43	6	4.000	9.95	6	15.430	9.95	
12	19.81	6	4.000	10.81	6	17.810	10.81	
13	23.72	6	4.000	5.75	6	21.720	11.50	
14	32.72	6	4.000	6.06	6	30.720	12.12	
15	20.36	6	3.625	6.30	6	17.985	12.60	
16	15.00	6	3.625	12.01	6	12.625	12.01	
17	15.00	6	3.625	12.01	6	12.625	12.01	
18	15.00	6	3.625	12.01	6	12.625	12.01	
19	15.00	6	3.625	12.01	6	12.625	12.01	
20	15.00	6	3.625	12.01	6	12.625	12.01	
21	15.00	6	3.625	12.01	6	12.625	12.01	
22	15.00	6	3.625	12.01	6	12.625	12.01	
23	15.00	6	3.625	12.01	6	12.625	12.01	
24	15.00	6	3.625	12.01	6	12.625	12.01	
25	15.00	6	3.625	12.01	6	12.625	12.01	
26	15.00	6	3.625	12.01	6	12.625	12.01	
27	15.00	6	3.625	12.01	6	12.625	12.01	
28	15.00	6	3.625	12.01	6	12.625	12.01	
29	15.95	6	3.625	12.00	6	12.575	12.00	
30	27.88	6	3.625	12.00	6	12.625	12.00	
31	36.00	6	4.500	8.41	4	31.750	25.24	
32	20.62	4	4.500	12.00	-	-	NIR	
33	19.28	4	4.500	12.00	-	-	NIR	
34	17.46	4	4.500	12.00	-	-	NIR	
35	15.67	4	4.500	12.00	-	-	NIR	
36	14.02	4	4.500	12.00	-	-	NIR	
37	12.53	4	4.500	12.00	-	-	NIR	
38	11.19	4	4.500	12.00	-	-	NIR	No Internal Rebar (NIR)
39	10.00	4	4.500	12.00	-	-	NIR	
40	8.96	4	4.500	12.00	-	-	NIR	
41	8.07	4	4.500	12.00	-	-	NIR	
42	7.32	4	4.500	12.00	-	-	NIR	
43	6.73	4	4.500	12.00	-	-	NIR	
44	6.29	4	4.500	12.00	-	-	NIR	

Table 8.3. Section Properties in Circumferential Direction

Concrete Section		External Rebar			Internal Rebar			Middle Rebar			
No.	Thick (in.)	Bar Size	Depth d_1 (in.)	Spacing s (in.)	Bar Size	Depth d_2 (in.)	Spacing s (in.)	Bar Size	Depth d (in.)	Spacing s (in.)	Notes
1	15.00	6	2.250	12.00	6	12.750	12.00	-	-	-	For square mat in center
2	15.00	6	2.250	12.00	6	12.750	12.00	-	-	-	
3	15.00	6	3.250	12.00	6	12.250	12.00	-	-	-	-
4	15.01	6	3.250	12.00	6	12.260	12.00	-	-	-	-
5	15.01	6	3.250	12.00	6	12.260	12.00	-	-	-	-
6	15.04	6	3.250	12.00	6	12.290	12.00	-	-	-	-
7	15.20	6	3.250	12.00	6	12.450	12.00	-	-	-	-
8	15.49	6	3.250	12.00	6	12.740	12.00	-	-	-	-
9	15.92	6	3.250	12.00	6	13.170	12.00	-	-	-	-
10	16.49	6	3.250	12.00	6	13.740	12.00	-	-	-	-
11	17.43	9	3.063	16.00	6	14.680	12.00	-	-	-	1 in. square bars given as number 9 which has equivalent steel area, spacing knocked down for square bars, 6C1 bar not included as it is has not reached full development length.
12	19.81	9	3.063	12.00	9	16.873	12.00	-	-	-	
13	23.72	11	2.938	9.50	9	20.783	12.00	-	-	-	1.25 in. square bars given number 11 which conservatively has less steel area, spacing knocked down for square bars.
14	32.72	11	2.938	9.50	11	29.658	10.67	11	16.360	9.50	
15	20.36	11	2.563	6.67	11	16.923	16.10	11	14.760	6.67	
16	15.00	7	2.813	5.50	7	11.813	5.50	-	-	-	On boundary of wall and haunch - uses wall rebar.
17	15.00	7	2.813	5.50	7	11.813	5.50	-	-	-	-
18	15.00	7	2.813	5.50	7	11.813	5.50	-	-	-	-
19	15.00	7	2.813	10.00	7	11.813	10.00	-	-	-	-
20	15.00	7	2.813	10.00	7	11.813	10.00	-	-	-	-
21	15.00	7	2.813	10.00	7	11.813	10.00	-	-	-	-
22	15.00	7	2.813	10.00	7	11.813	10.00	-	-	-	-
23	15.00	7	2.813	9.00	7	11.813	9.00	-	-	-	-
24	15.00	7	2.813	8.00	7	11.813	8.00	-	-	-	-
25	15.00	7	2.813	7.00	7	11.813	7.00	-	-	-	-
26	15.00	7	2.813	7.00	7	11.813	7.00	-	-	-	-
27	15.00	7	2.813	6.00	7	11.813	6.00	-	-	-	-
28	15.00	8	2.750	7.00	8	11.750	7.00	-	-	-	-
29	15.95	8	2.750	6.00	8	11.700	6.00	-	-	-	-
30	27.88	8	2.750	6.00	8	11.750	6.00	-	-	-	-
31	36.00	9	3.563	11.67	9	30.938	11.67	-	-	-	1 in. square bars given number 9
32	20.62	4	5.000	12.00	-	-	NIR	-	-	-	No Internal Rebar (NIR)
33	19.28	4	5.000	12.00	-	-	NIR	-	-	-	
34	17.46	4	5.000	12.00	-	-	NIR	-	-	-	
35	15.67	4	5.000	12.00	-	-	NIR	-	-	-	
36	14.02	4	5.000	12.00	-	-	NIR	-	-	-	
37	12.53	4	5.000	12.00	-	-	NIR	-	-	-	
38	11.19	4	5.000	12.00	-	-	NIR	-	-	-	
39	10.00	4	5.000	12.00	-	-	NIR	-	-	-	
40	8.96	4	5.000	12.00	-	-	NIR	-	-	-	
41	8.07	4	5.000	12.00	-	-	NIR	-	-	-	
42	7.32	4	5.000	12.00	-	-	NIR	-	-	-	
43	6.73	4	5.000	12.00	-	-	NIR	-	-	-	
44	6.29	4	5.000	12.00	-	-	NIR	-	-	-	

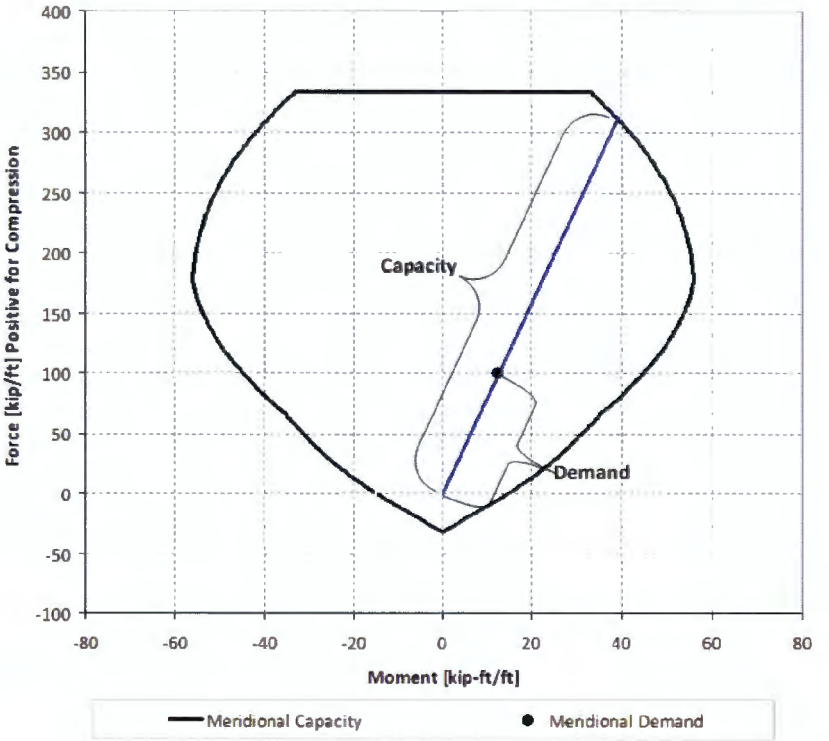

Figure 8.2. ACI Demand/Capacity Ratio Definition

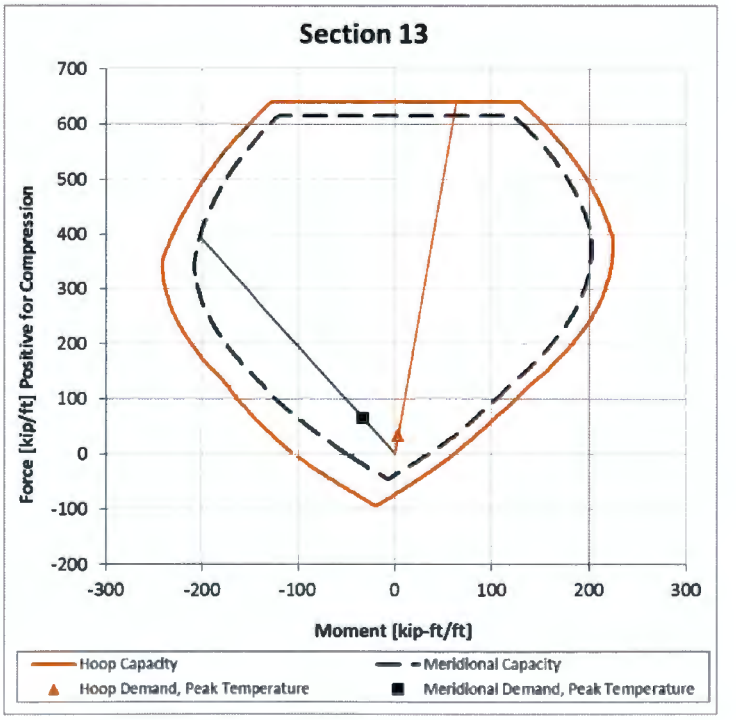

Figure 8.3. ACI – Force-Moment Diagram for Section 13. The results are for Run1 with best estimate material properties at the maximum tank temperature (Loadstep 6) and ACI load factors equal to 1.0.

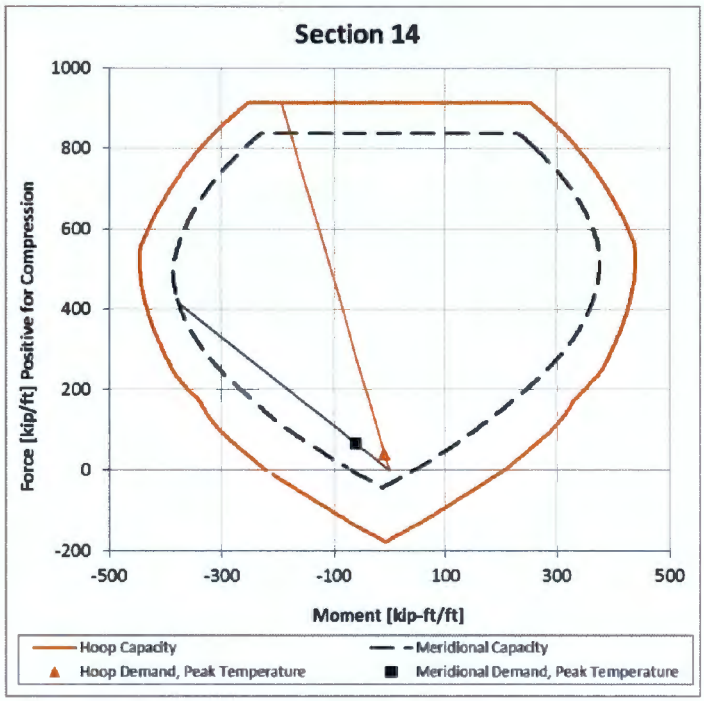

Figure 8.4. ACI – Force-Moment Diagram for Section 14. The results are for Run1 with best estimate material properties at the maximum tank temperature (Loadstep 6) and ACI load factors equal to 1.0.

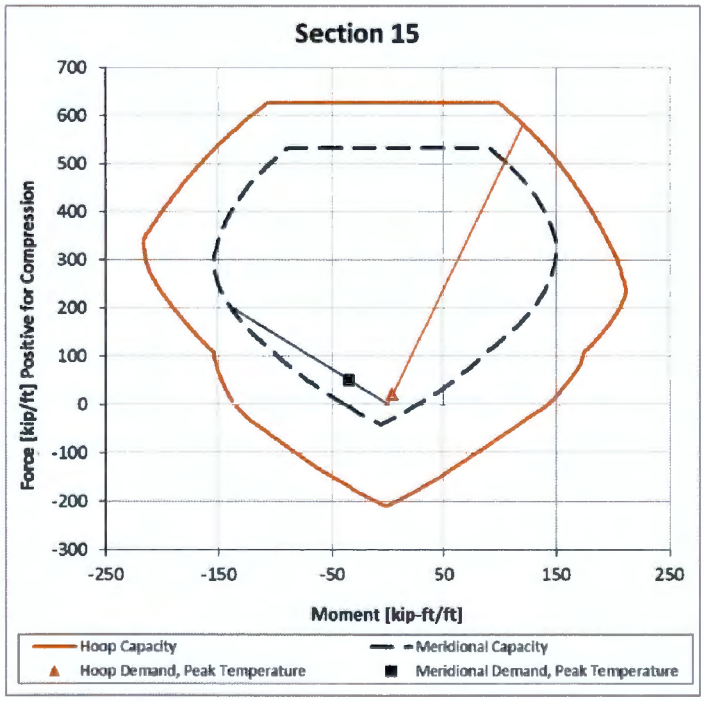

Figure 8.5. ACI – Force-Moment Diagram for Section 15. The results are for Run1 with best estimate material properties at the maximum tank temperature (Loadstep 6) and ACI load factors equal to 1.0.

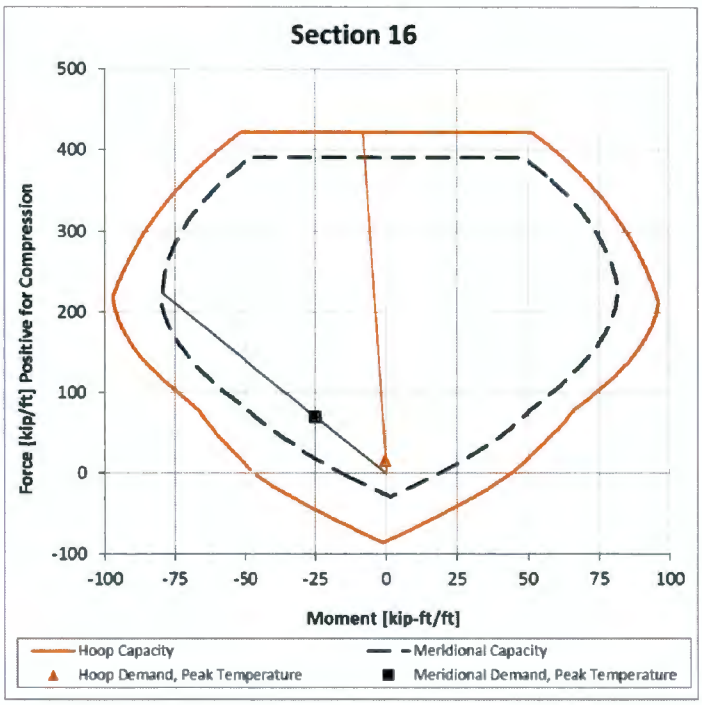

Figure 8.6. ACI – Force-Moment Diagram for Section 16. The results are for Run1 with best estimate material properties at the maximum tank temperature (Loadstep 6) and ACI load factors equal to 1.0.

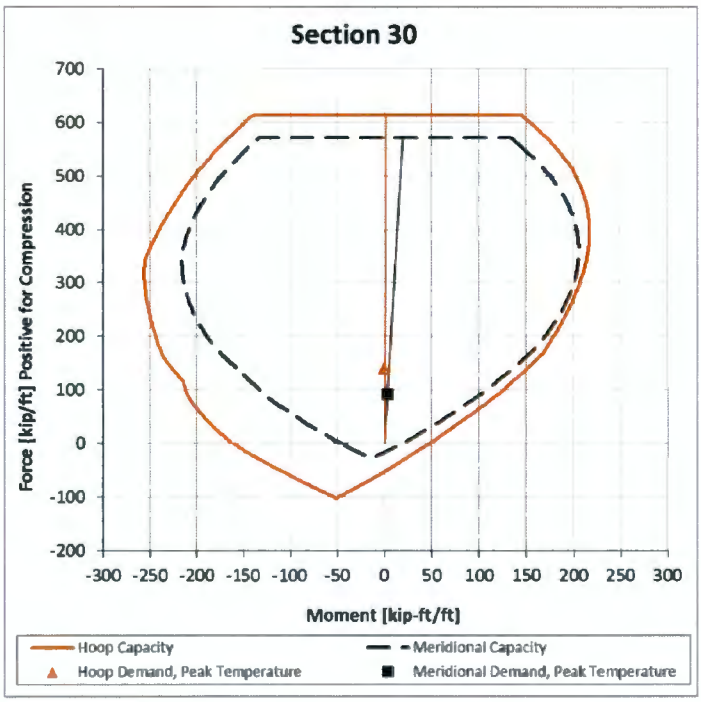

Figure 8.7. ACI – Force-Moment Diagram for Section 30. The results are for Run1 with best estimate material properties at the maximum tank temperature (Loadstep 6) and ACI load factors equal to 1.0.

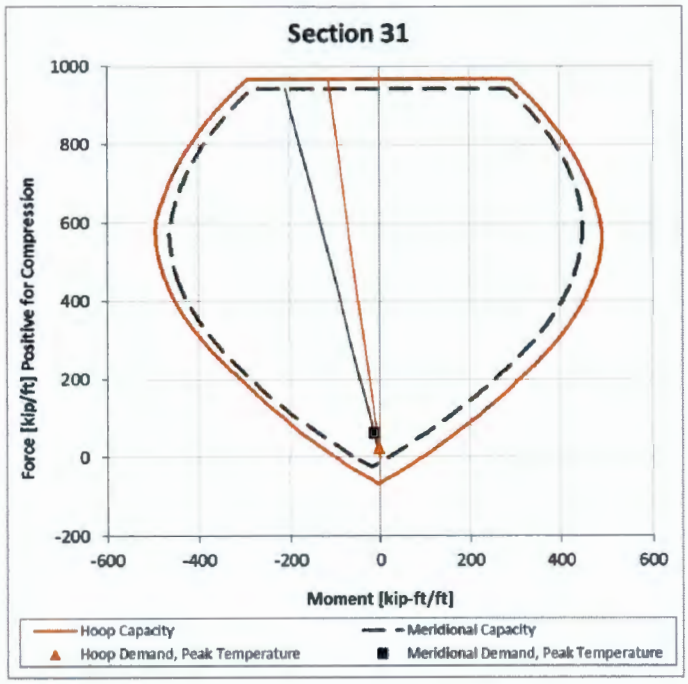

Figure 8.8. ACI – Force-Moment Diagram for Section 31. The results are for Run1 with best estimate material properties at the maximum tank temperature (Loadstep 6) and ACI load factors equal to 1.0.

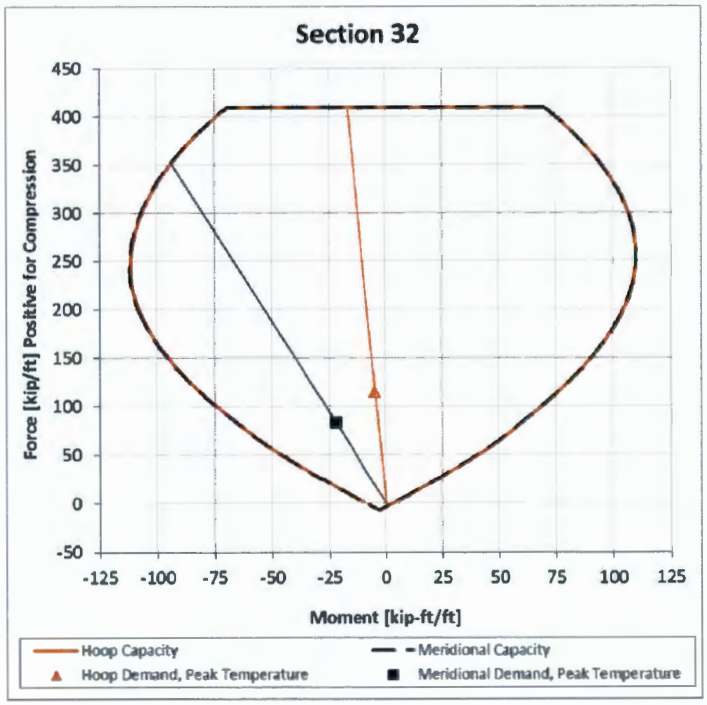

Figure 8.9. ACI – Force-Moment Diagram for Section 32. The results are for Run1 with best estimate material properties at the maximum tank temperature (Loadstep 6) and ACI load factors equal to 1.0.

8.3 Run 1, Baseline Case with Best Estimate Material Properties

This run uses the best estimate material properties (nominal soil modulus, nominal concrete modulus and near zero concrete tensile strength with creep turned on) and is considered to be the baseline run/ analysis. Figure 8.10 through Figure 8.13 show the demand/capacity ratios of this run at different load steps and load combinations. As requested by external reviewers in Appendix A of Rinker et al. (2011a), the demand/capacity ratios at peak temperatures are also provided . The demand/capacity ratios at peak temperatures and at all load combinations are less than 1.0 for shear, meridional and circumferential directions.

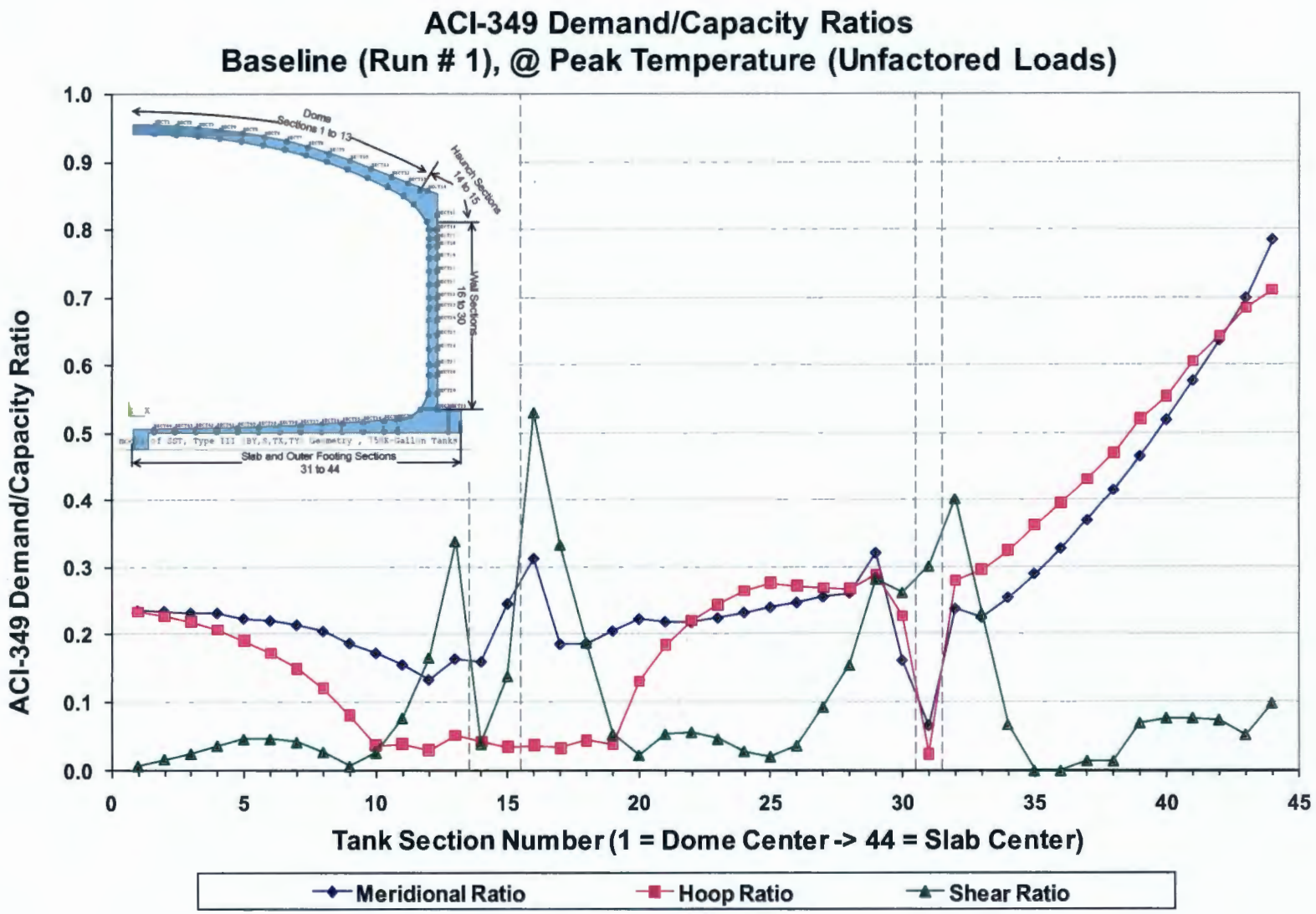

Figure 8.10. Run 1, ACI D/C Ratios at Peak Temperature. ACI load factors are equal to 1.0.

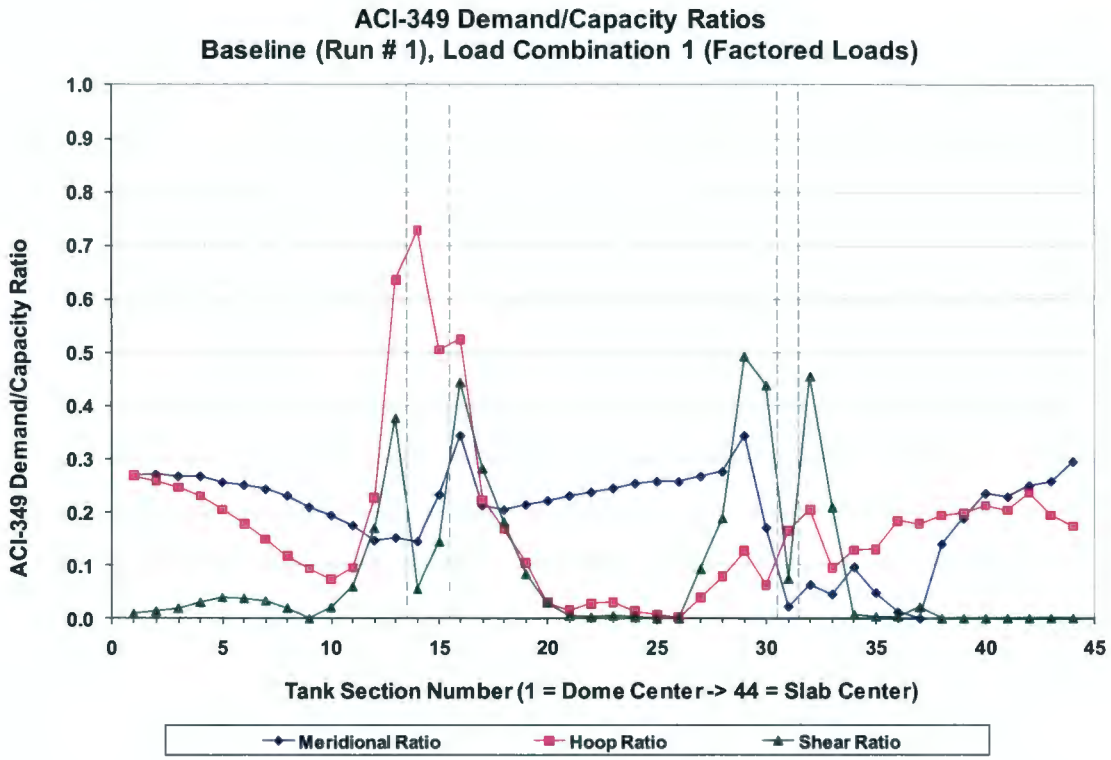

Figure 8.11. Run 1, ACI D/C Ratios for LC1

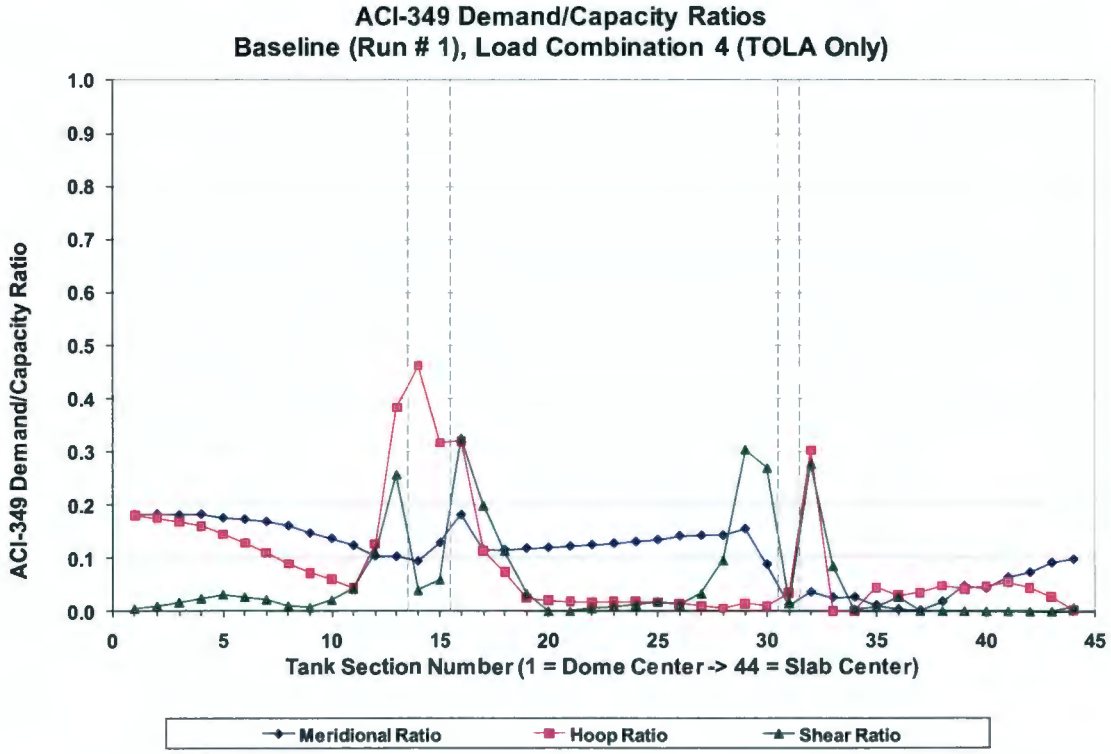

Figure 8.12. Run 1, ACI D/C Ratios for LC4 (TOLA results only – no seismic)

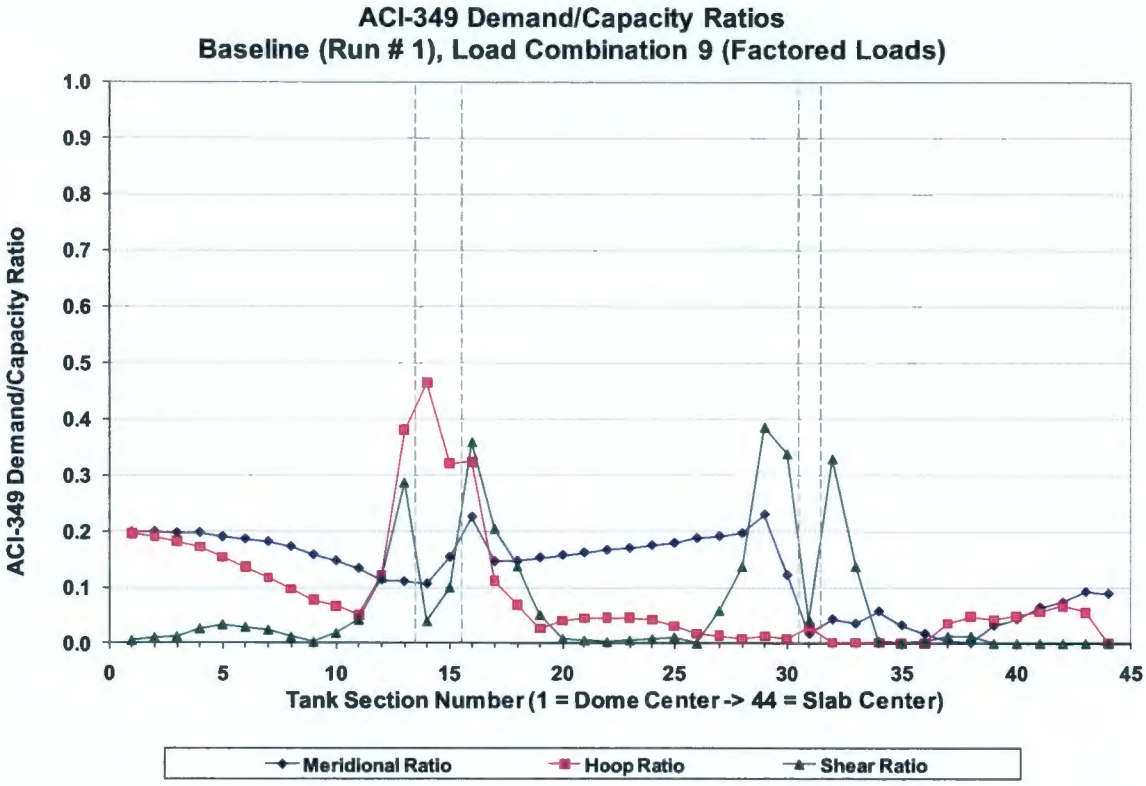

Figure 8.13. Run 1, ACI D/C Ratios for LC9

As demonstrated in Figure 8.10 through Figure 8.13, the best estimate case, Run 1, passes the ACI 349-06 (ACI 2007) evaluation for all sections.

To further understand the contribution of various loads to the demands on the tank, the total and incremental forces and moments for the baseline TOLA matrix Run 1 are presented in Appendix F. This includes the incremental changes due to gravity, waste, concentrated and uniform surface loads, thermal cycling, and load combinations 1 and 9. The incremental forces and moments demonstrate the effect each individual load has on the tank demands. Appendix F shows that generally the gravity load has the most dominant effect, even after load factors are applied. Waste load and surface loads have only minor effects on the tank demands. The thermal cycle to peak temperature has a large effect on the slab and lower wall but this effect is typically counteracted when the tank cools back down. The dome, haunch, and sidewall pressures for each load step in Run 1 are also presented in Appendix F. The dome and haunch pressures between load steps are similar except at the sensitive haunch corner. The sidewall pressures change significantly with loading. At the peak temperature, these pressures are the greatest but generally return to near gravity pressures upon cool-down. Application of the load factors brings the sidewall pressures to values greater than gravity at some depths and less than gravity at other depths.

8.4 Run 2, Nominal Soil Modulus, Nominal Concrete Modulus, Near Zero Concrete Tensile Strength, and No Creep

The material properties used in this analysis are similar to Run 1 except for concrete creep. Run 2 does not include concrete creep, whereas Run 1 includes it. Creep has the general effect of relieving stress in the concrete over time; therefore, not including concrete creep should provide increased concrete stresses. Any difference in the demand/capacity ratios between Run 2 and Run 1 is only due to the absence of creep in Run 2.

The demand/capacity ratios at peak temperature and load combinations 1, 4 (TOLA only), and 9 are less than 1.0 for meridional, circumferential, and shear directions (Figure 8.14 through Figure 8.17).

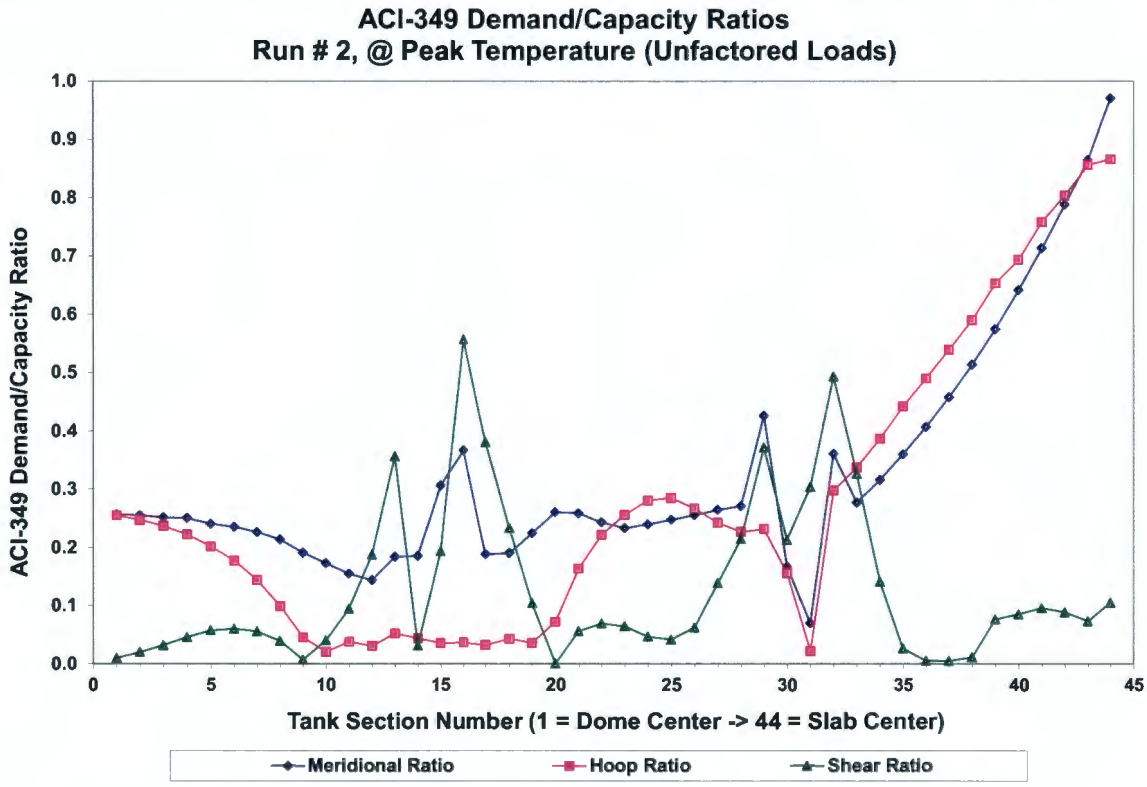

Figure 8.14. Run 2, ACI D/C Ratios at Peak Temperature. ACI load factors are equal to 1.0.

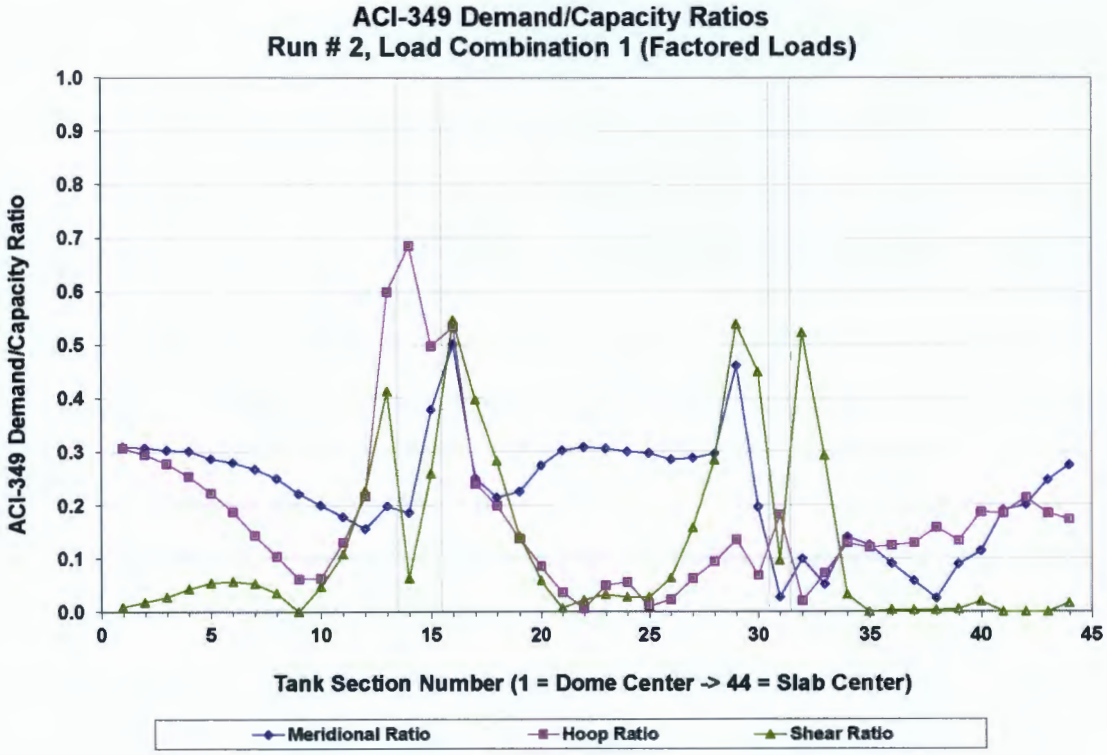

Figure 8.15. Run 2, ACI D/C Ratios for LC1

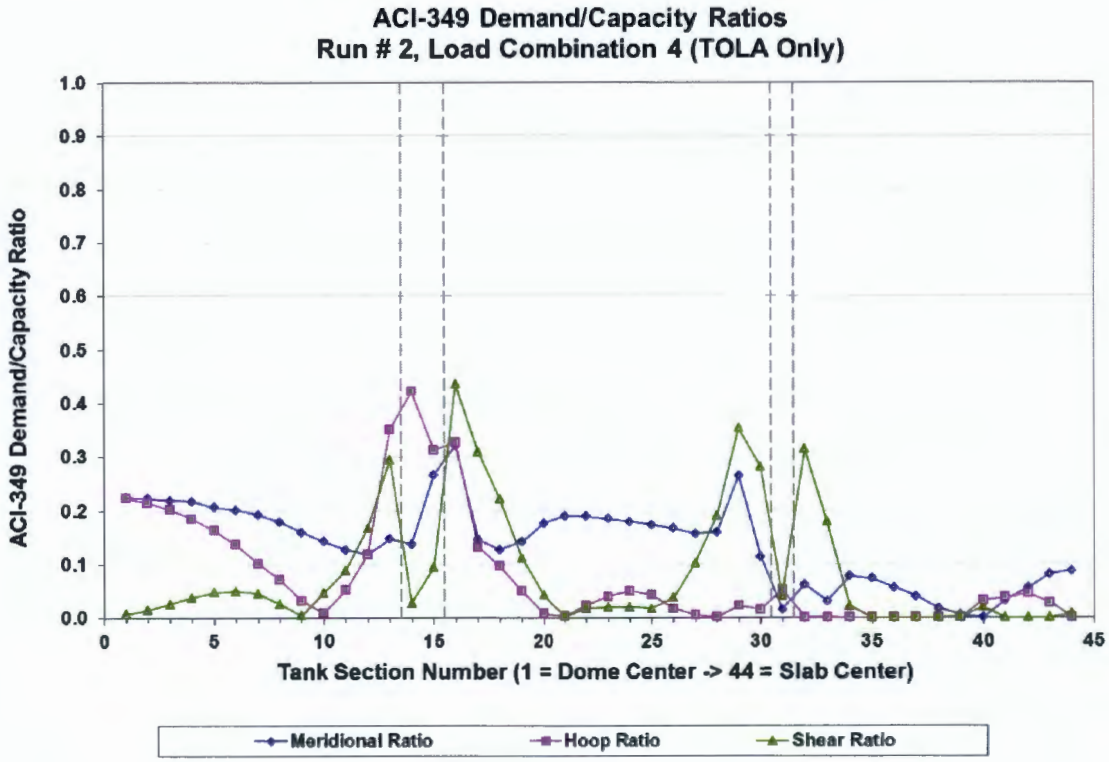

Figure 8.16. Run 2, ACI D/C Ratios for LC4 (TOLA results only – no seismic)

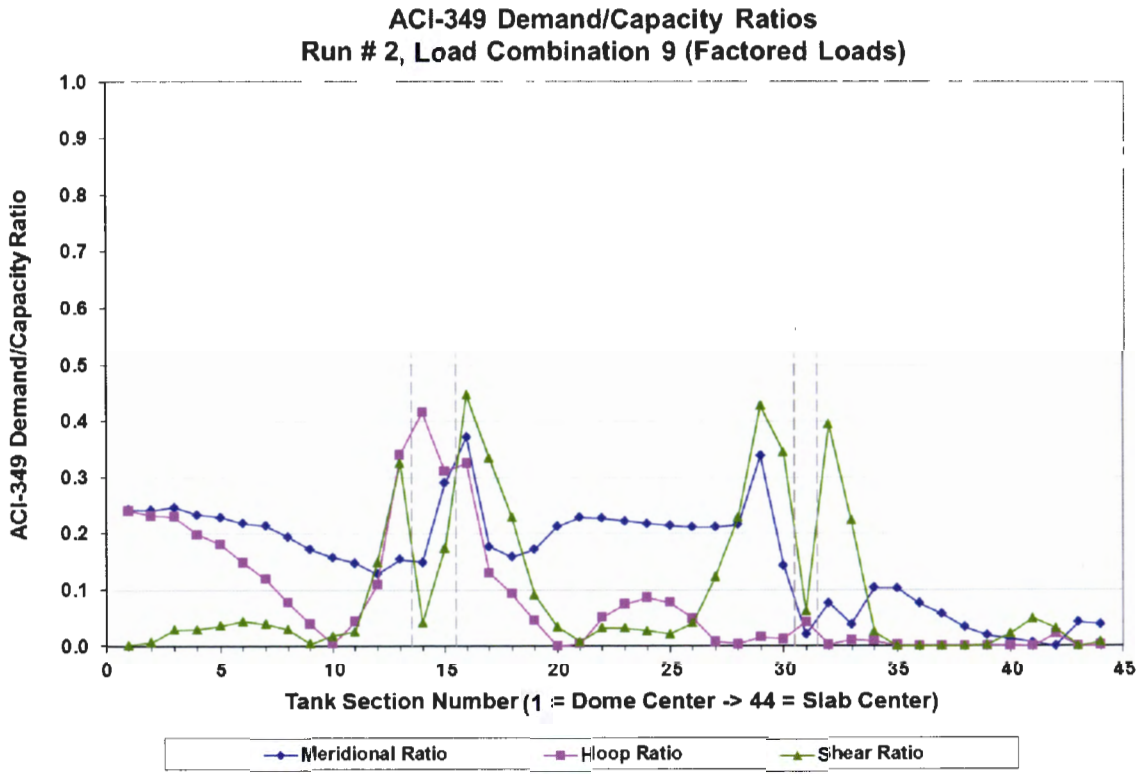

Figure 8.17. Run 2, ACI D/C Ratios for LC9

More details (in addition to the D/C ratios) near critical tank locations can be useful for understanding the tank structural response. In particular, stress contours can be used to determine if any concrete has crushed or any rebar has yielded. Stress contours are presented in Figure 8.18 to Figure 8.22 for Run 2 at peak temperature. Peak temperature stress contours are chosen to observe the tank response under maximum thermal loading. Run 2 is chosen as it has nominal properties with the exception of having no creep which will conservatively show higher stresses. Figure 8.20 shows the vertical stress contours in the concrete haunch, wall and slab. The maximum stress in the concrete (2268 psi) is less than the compressive strength of the concrete at peak temperature (2932 psi). Figure 8.19 and Figure 8.20 show the meridional and hoop rebars stress in the haunch/wall and knuckle regions. Note that the maximum rebar stress is less than the yield stress of 40 ksi.

Figure 8.18. Run 2, Concrete Stress (Sy in psi) in the Haunch and Wall

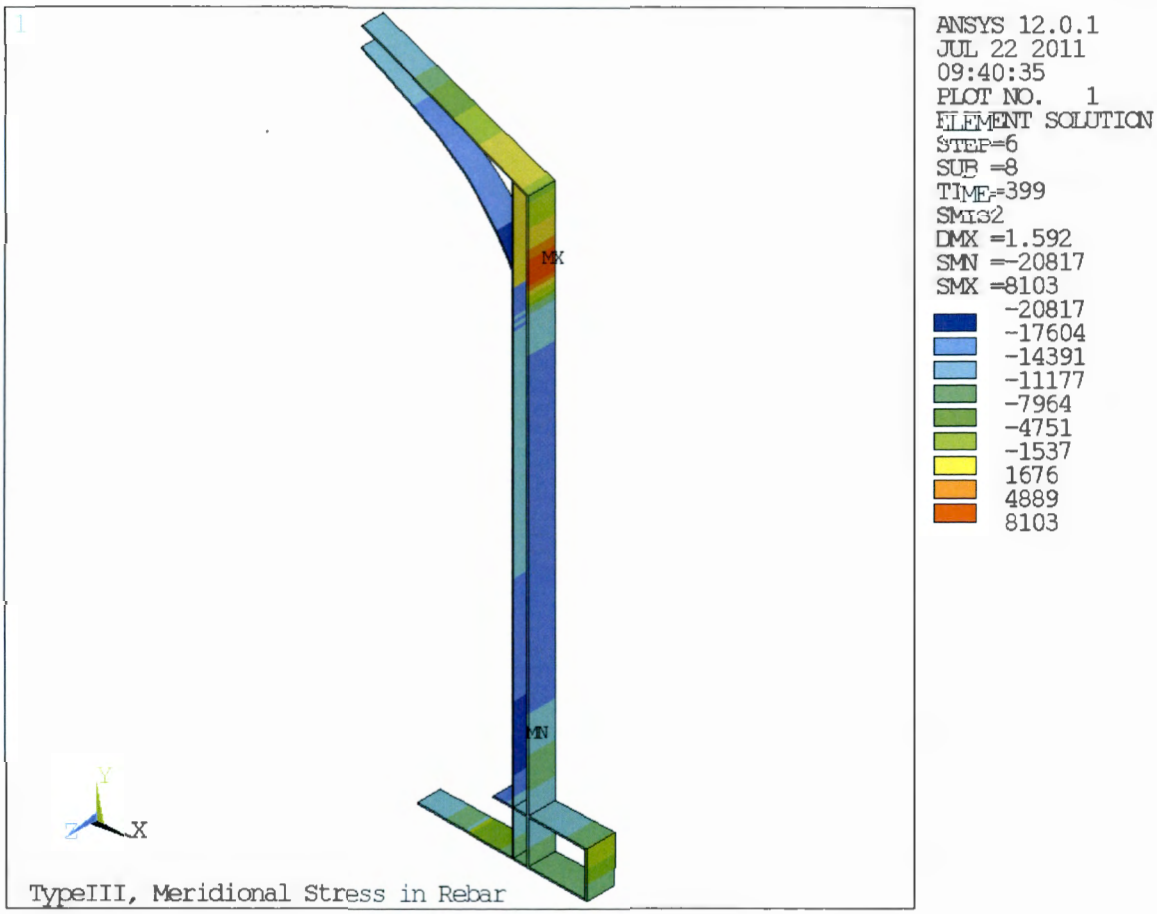

Figure 8.19. Run 2, Meridional Rebar Stress (psi) in Haunch, Wall and Knuckle Region

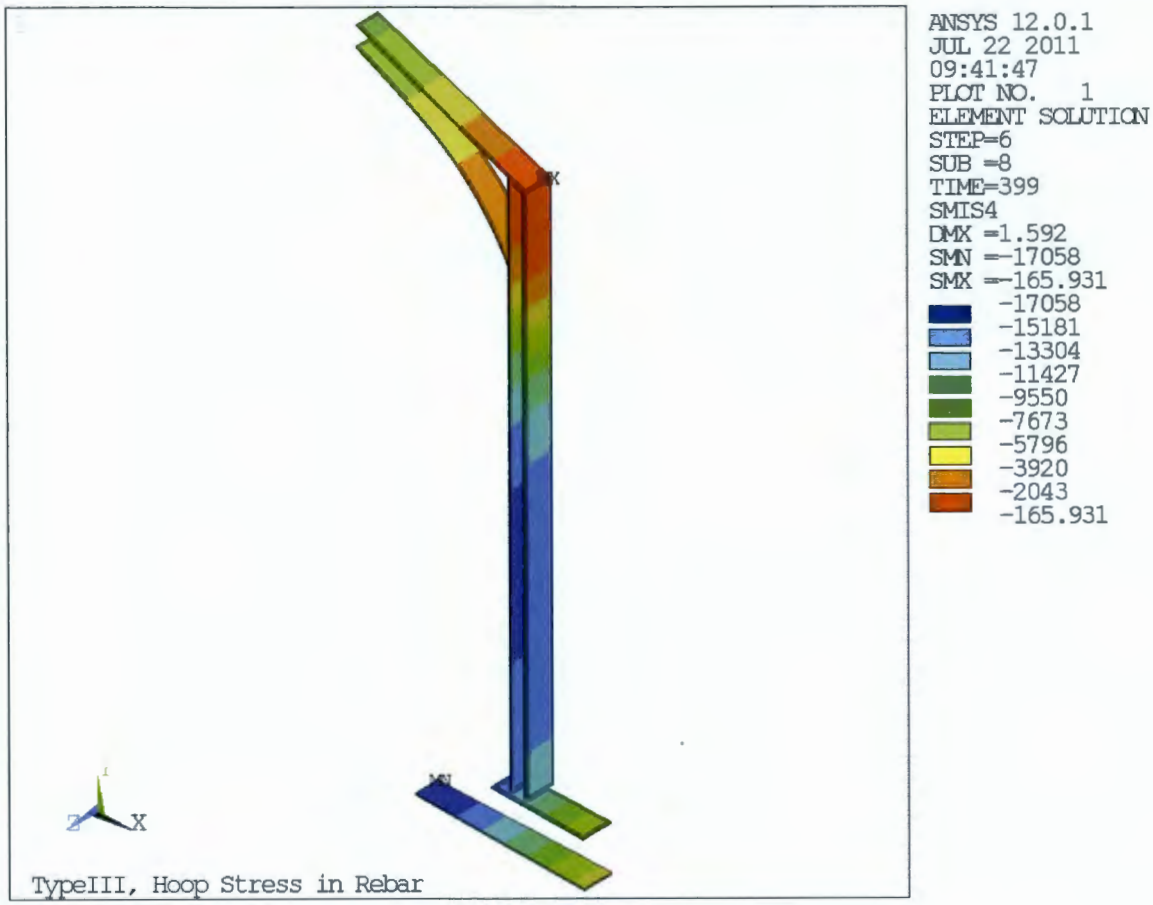

Figure 8.20. Run 2, Hoop Rebar Stress (psi) in Haunch, Wall and Knuckle Region

8.5 Run 3, Nominal Soil Modulus, High Concrete Modulus, Near Zero Concrete Tensile Strength, and No Creep

This run uses the nominal soil modulus, high concrete modulus, and near zero concrete tensile strength without creep. The two differences between the baseline run (Run 1) and this run (Run 3) are concrete modulus (nominal vs. high) and concrete creep (on vs. off). Omitting concrete creep provided higher stresses compared to the TOLA matrix run with creep. Similarly, higher concrete modulus should provide higher stresses.

The demand/capacity ratios for load combinations 1, 4 (TOLA only), and 9 are less than 1.0 for meridional, circumferential, and shear (Figure 8.22 through Figure 8.24). At peak temperature (Figure 8.21), meridional demand/capacity ratio is greater than 1.0 for section 44 (the center of the slab). The high temperature in the slab degrades the concrete strength (reduced capacity) and high compressive thermal expansion stresses (increases demand). The combination results in a demand/capacity ratio that is above 1.0. However, local exceedance at the slab center does not impact the structural stability of the tank.

A slab removal analysis study, similar to the Type II AOR (Rinker et al., 2011a), was performed for the Type III tanks. The slab removal results in Appendix E show that the ACI demand to capacity ratios in the dome, haunch, wall, and footing are not changed significantly by disconnecting the slab from the footing. In addition, the maximum shear offset between the slab and the footing is predicted to be less than 0.06 inch. This is only about one-sixth of the original nominal liner thickness of 0.375 inch. The bottom and knuckle of the tank are also covered with a tar-based mastic material that would act to cushion the transition. Therefore, it is likely that the liner would bridge the small displacement offset without being damaged.

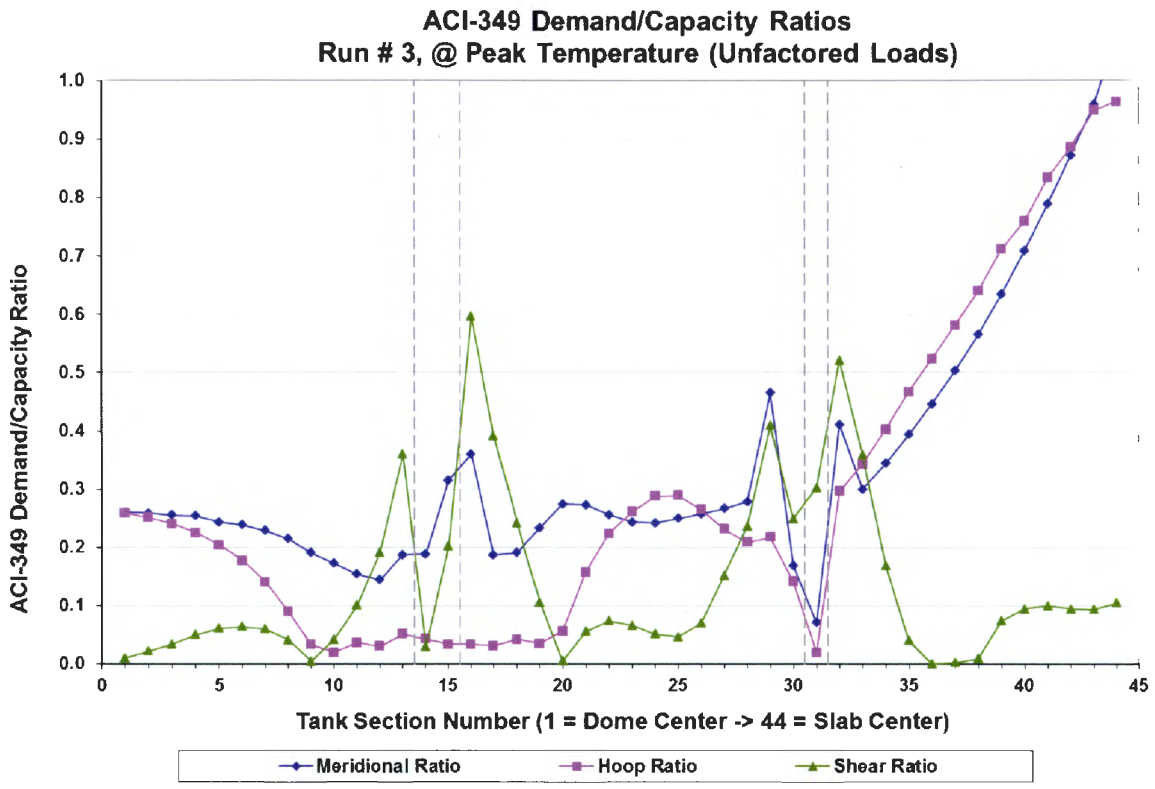

Figure 8.21. Run 3, ACI D/C Ratios at Peak Temperature. ACI load factors are equal to 1.0.

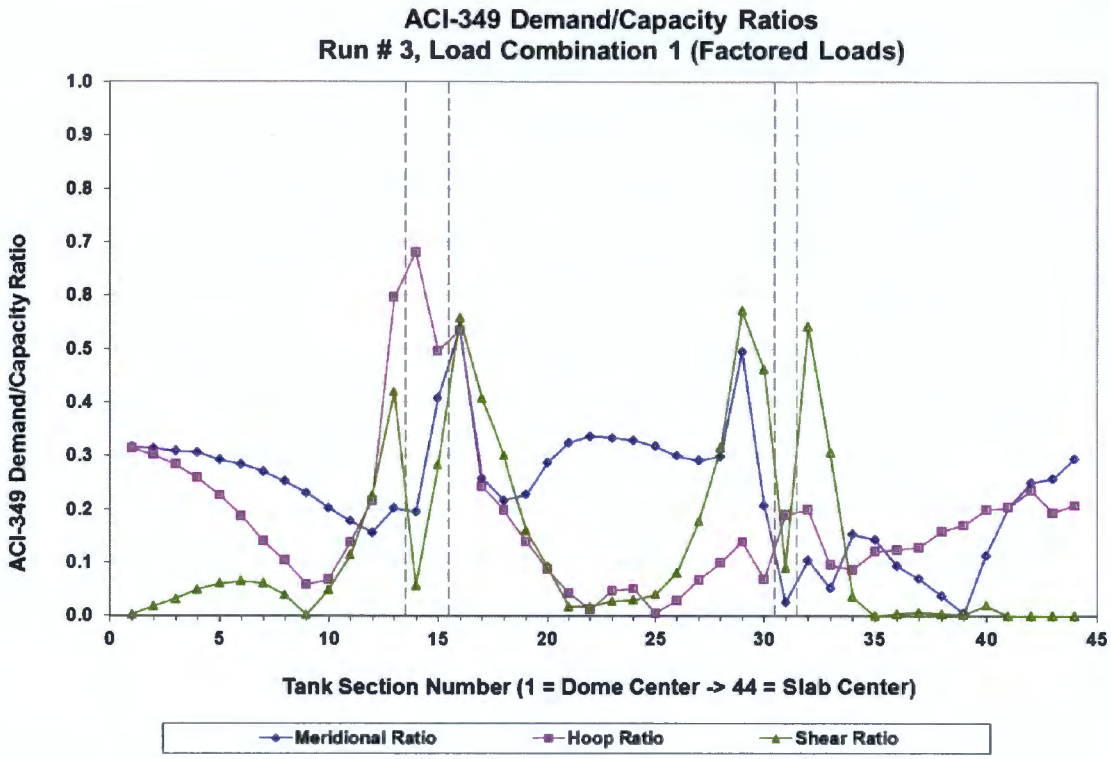

Figure 8.22. Run 3, ACI D/C Ratios for LC1

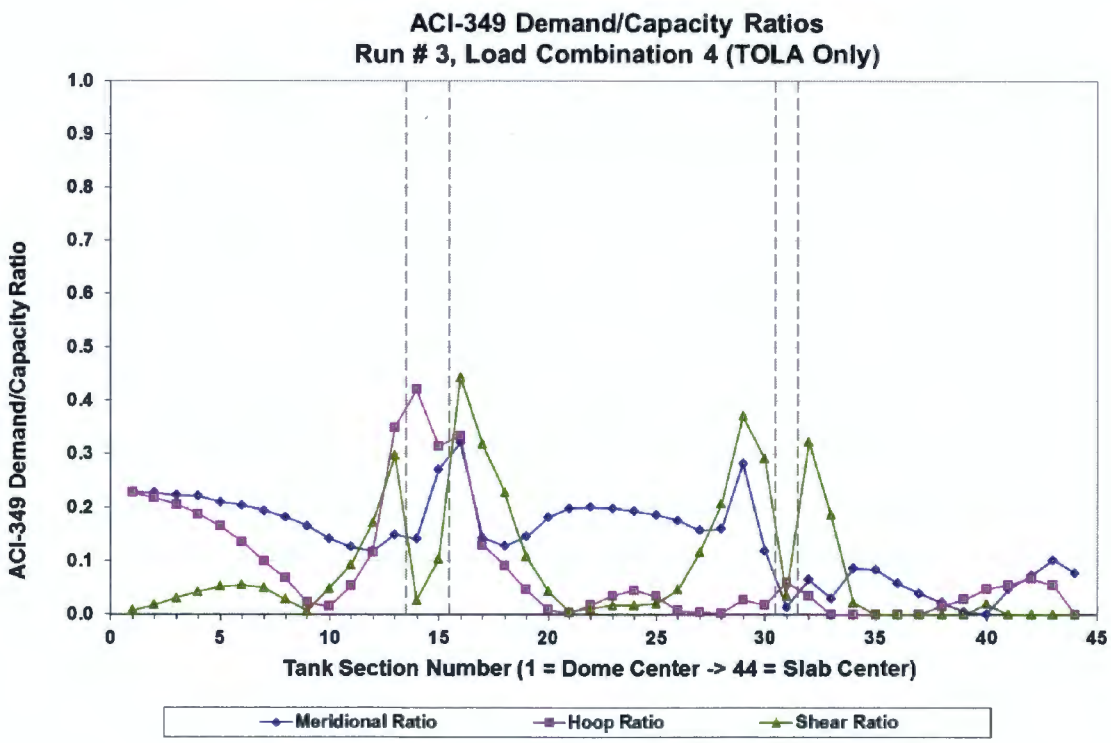

Figure 8.23. Run 3, ACI D/C Ratios for LC4 (TOLA results only – no seismic)

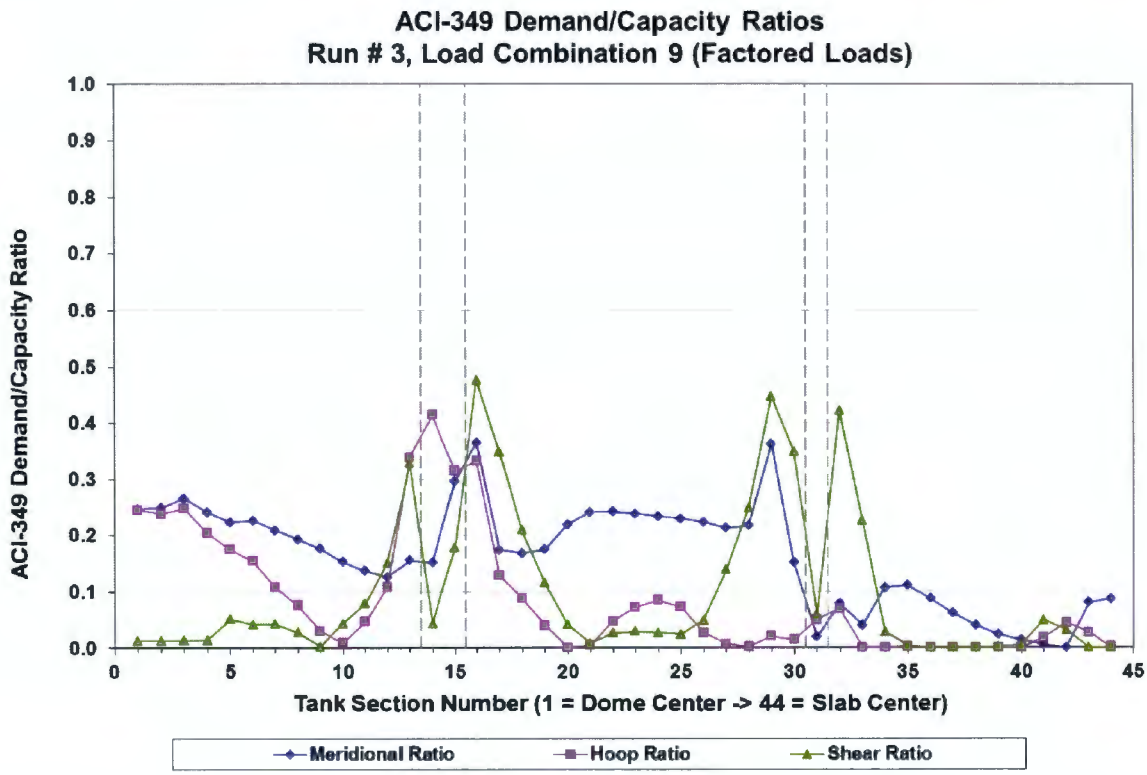

Figure 8.24. Run 3, ACI D/C Ratios for LC9

8.6 Run 4, Low Soil Modulus, High Concrete Modulus, Near Zero Concrete Tensile Strength, and No Creep

In addition to high concrete modulus and no creep, this run uses a low soil modulus. The low soil modulus will provide less support to the tank foundation and walls and increase the concrete stresses that were already higher due to the combination of high concrete modulus and no creep.

The demand/capacity ratios for the peak temperature load step and load combinations 1, 4 (TOLA only), and 9 are all less than 1.0 for the meridional, circumferential and shear directions (Figure 8.25 through Figure 8.28).

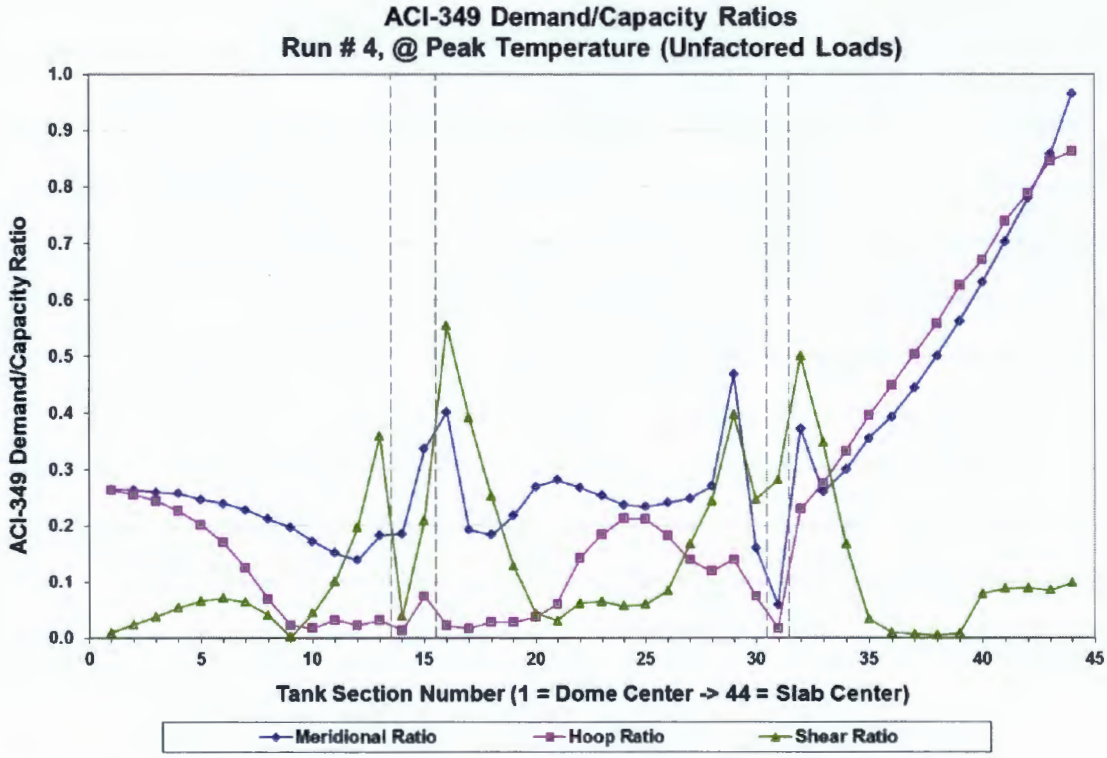

Figure 8.25. Run 4, ACI D/C Ratios at Peak Temperature. ACI load factors are equal to 1.0.

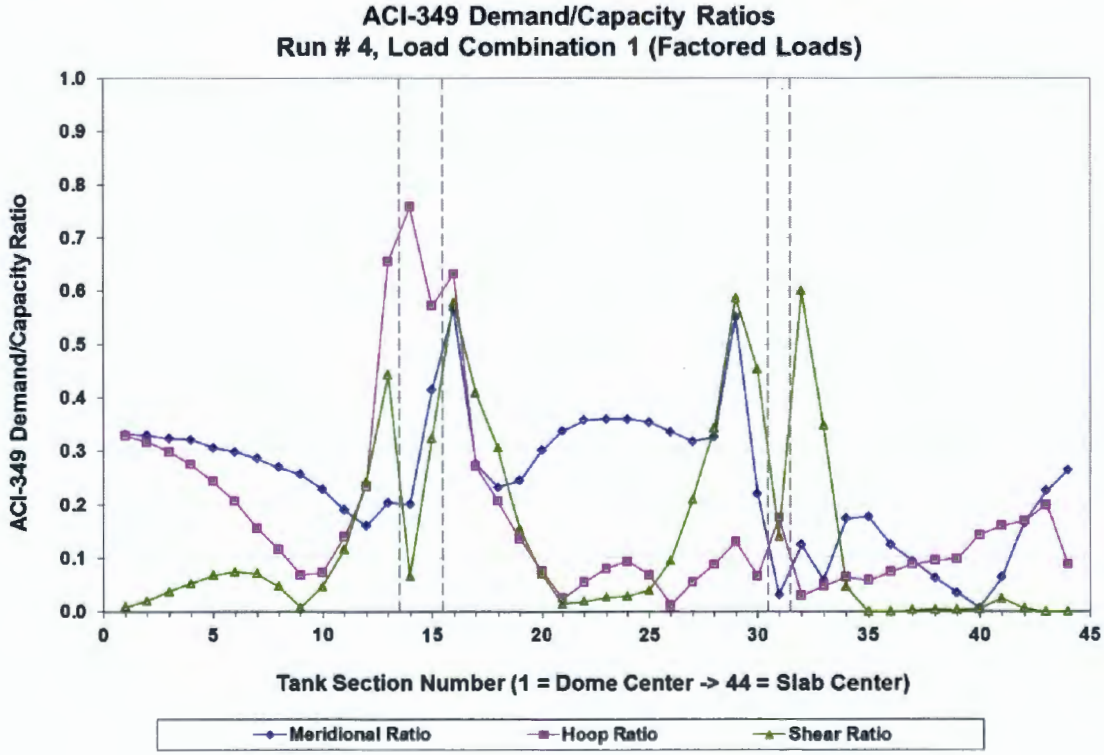

Figure 8.26. Run 4, ACI D/C Ratios for LC1

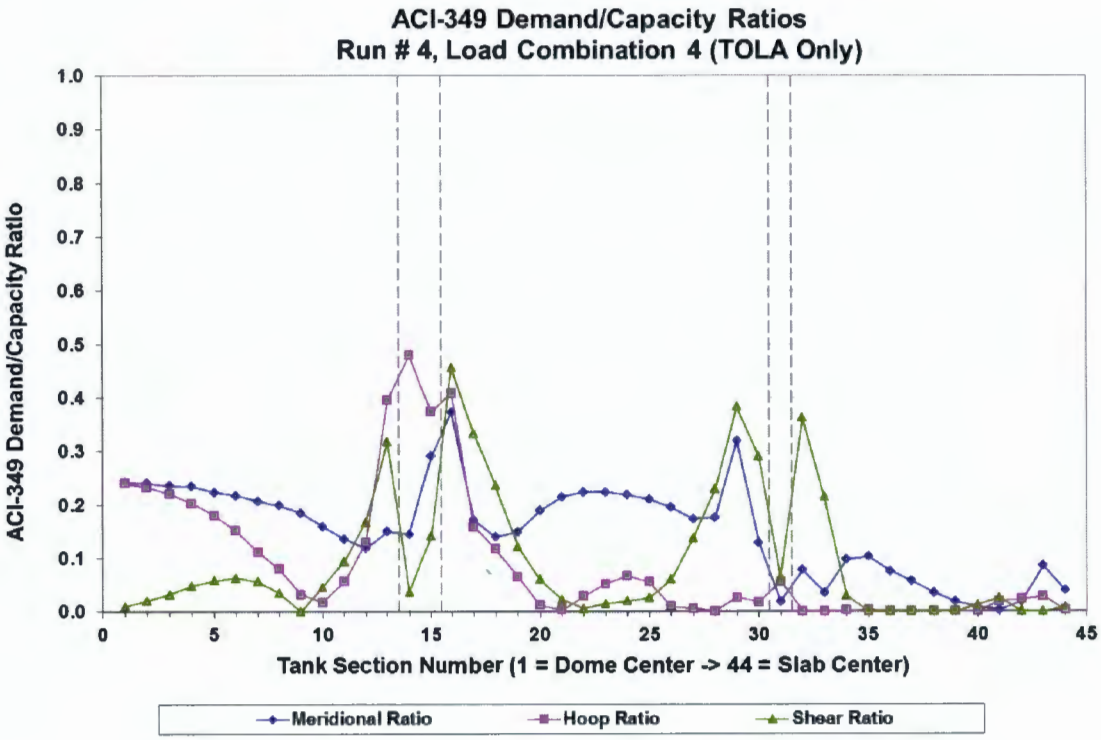

Figure 8.27. Run 4, ACI D/C Ratios for LC4 (TOLA results only – no seismic)

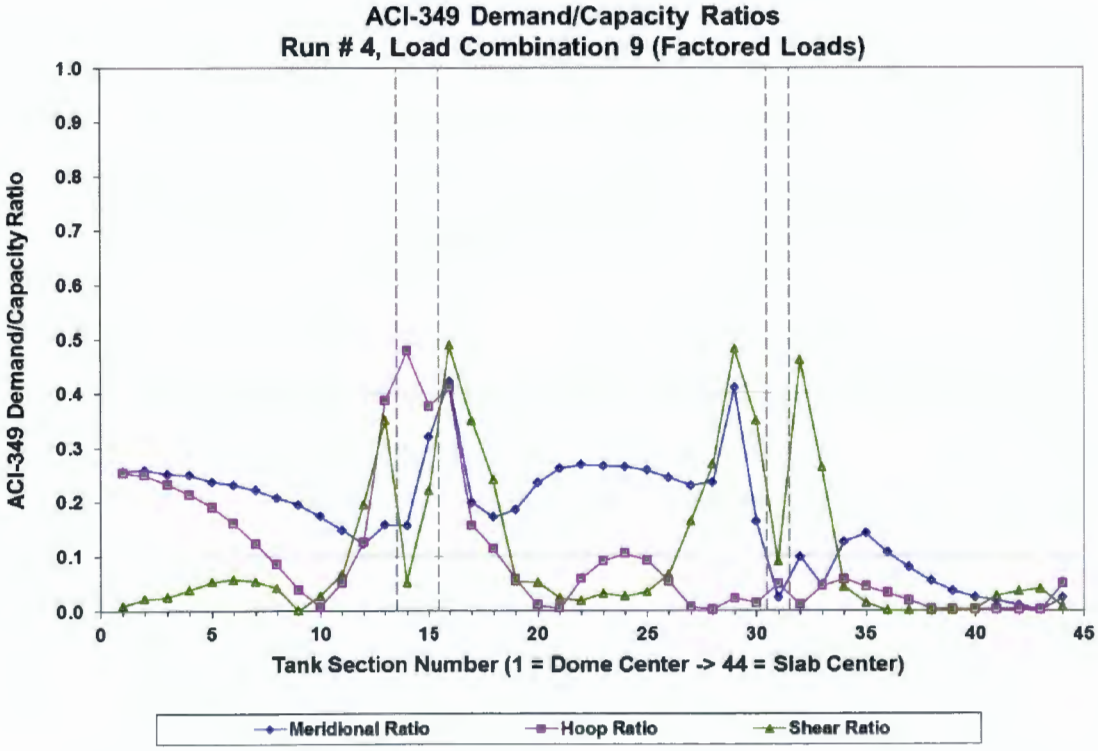

Figure 8.28. Run 4, ACI D/C Ratios for LC9

8.7 Run 5, Low Soil Modulus, Nominal Concrete Modulus, Near Zero Concrete Tensile Strength, and No Creep

This run uses a low soil modulus, nominal concrete modulus, and near zero concrete tensile strength without creep. As shown earlier, the combination of low soil modulus and no creep should increase the concrete stresses.

The demand/capacity ratios at peak temperatures and all load combinations (1, 4 [TOLA only], and 9) are less than 1.0 for the meridional, circumferential and shear directions (Figure 8.29 through Figure 8.32).

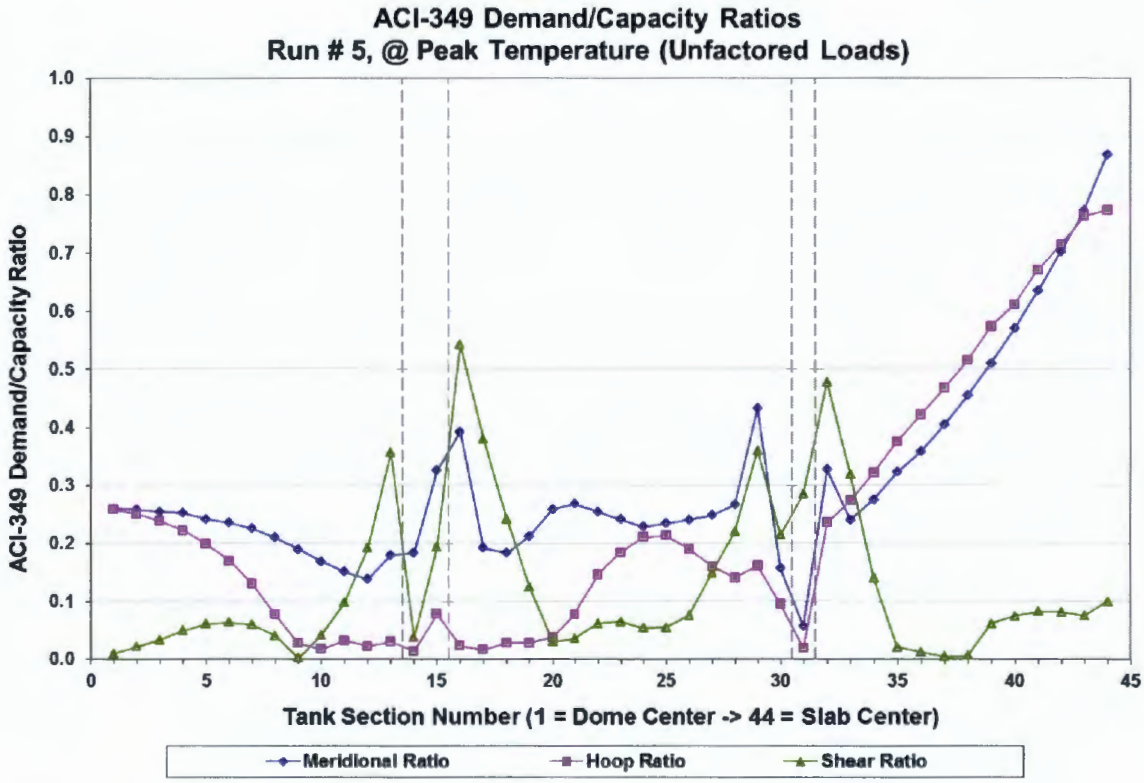

Figure 8.29. Run 5, ACI D/C Ratios at Peak Temperature. ACI load factors are equal to 1.0.

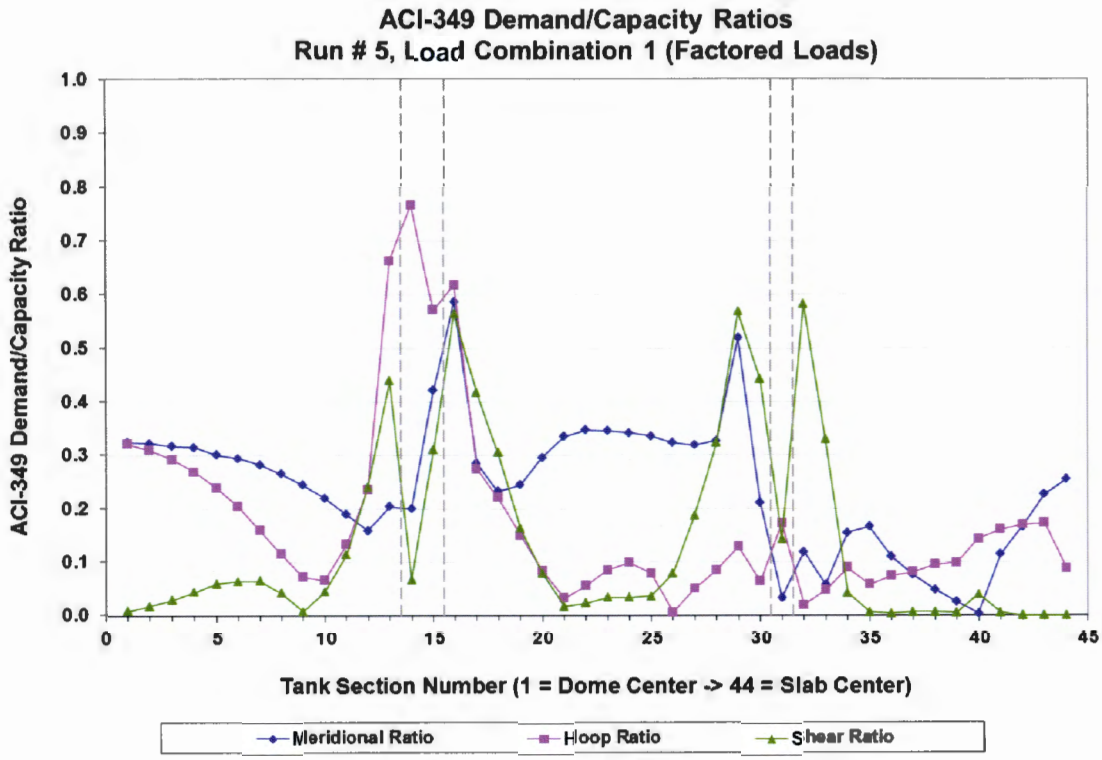

Figure 8.30. Run 5, ACI D/C Ratios for LC1

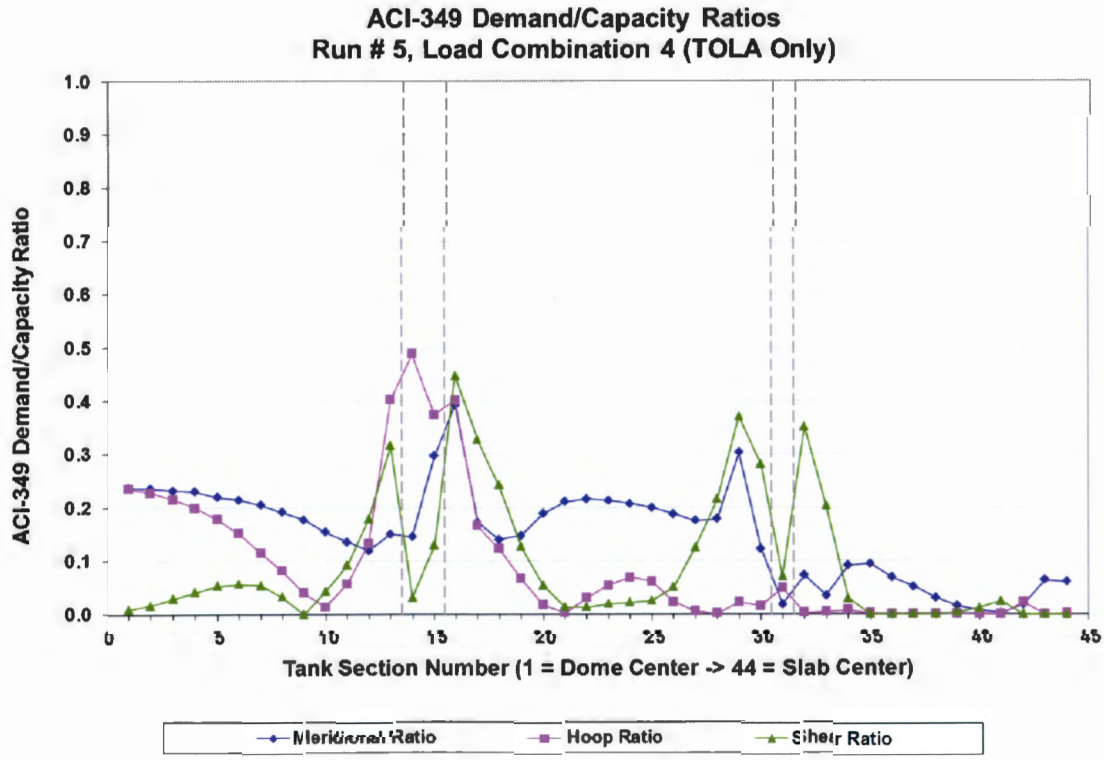

Figure 8.31. Run 5, ACI D/C Ratios for LC4 (TOLA results only – no seismic)

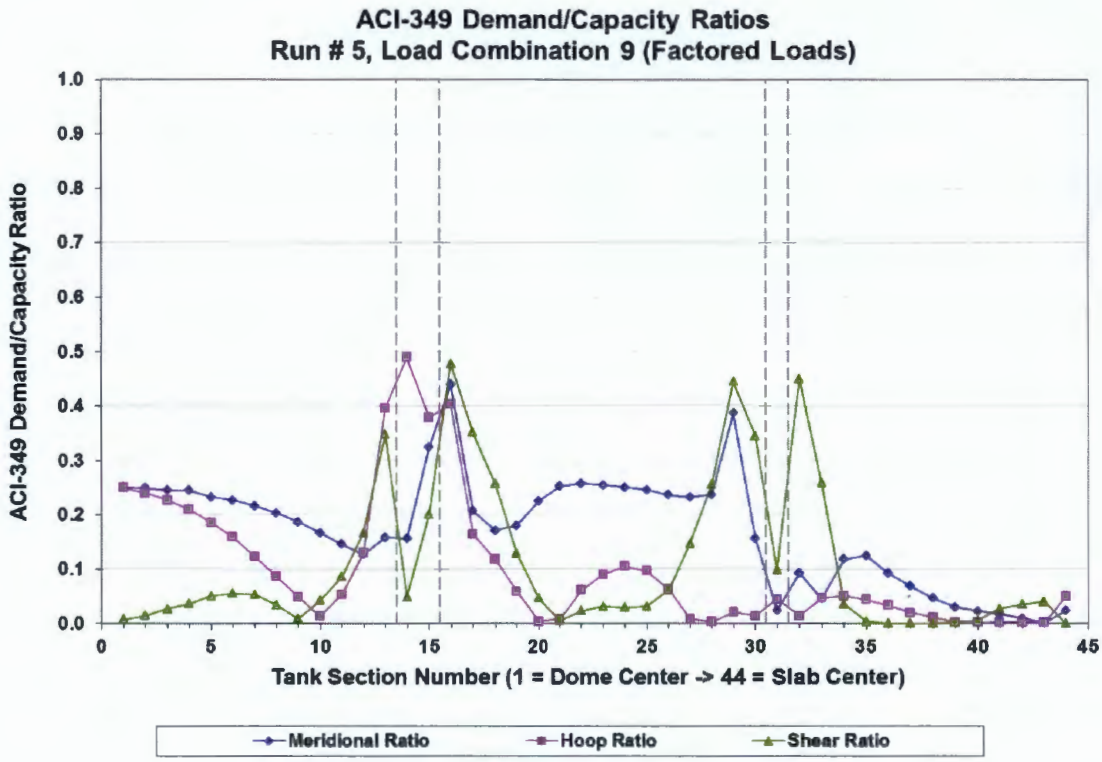

Figure 8.32. Run 5, ACI D/C Ratios for LC9

8.8 Run 6, Nominal Soil Modulus, Nominal Concrete Modulus, Nominal Concrete Tensile Strength with Creep

Run 6 was conducted to establish the degraded concrete condition at the start of the tank limit analysis described in Chapter 11. Run 6 was not evaluated using ACI because of the inconsistency between the ACI evaluation (which does not account for concrete tensile strength) vs. the analysis (which uses nominal tensile strength). The force, moment, and shear results from Run 6 are in the Appendix H for comparative purposes only.

8.9 Run 7, Low Soil Modulus, Nominal Concrete Modulus, Near Zero Concrete Tensile Strength with Creep

This run uses a low soil modulus, nominal concrete modulus, and near zero concrete tensile strength with creep. As shown earlier, the combination of low soil modulus and no creep should increase the concrete stresses.

The demand/capacity ratios at peak temperatures and all load combinations (1, 4 [TOLA only], and 9) are less than 1.0 for the meridional, circumferential and shear directions (Figure 8.33 through Figure 8.36).

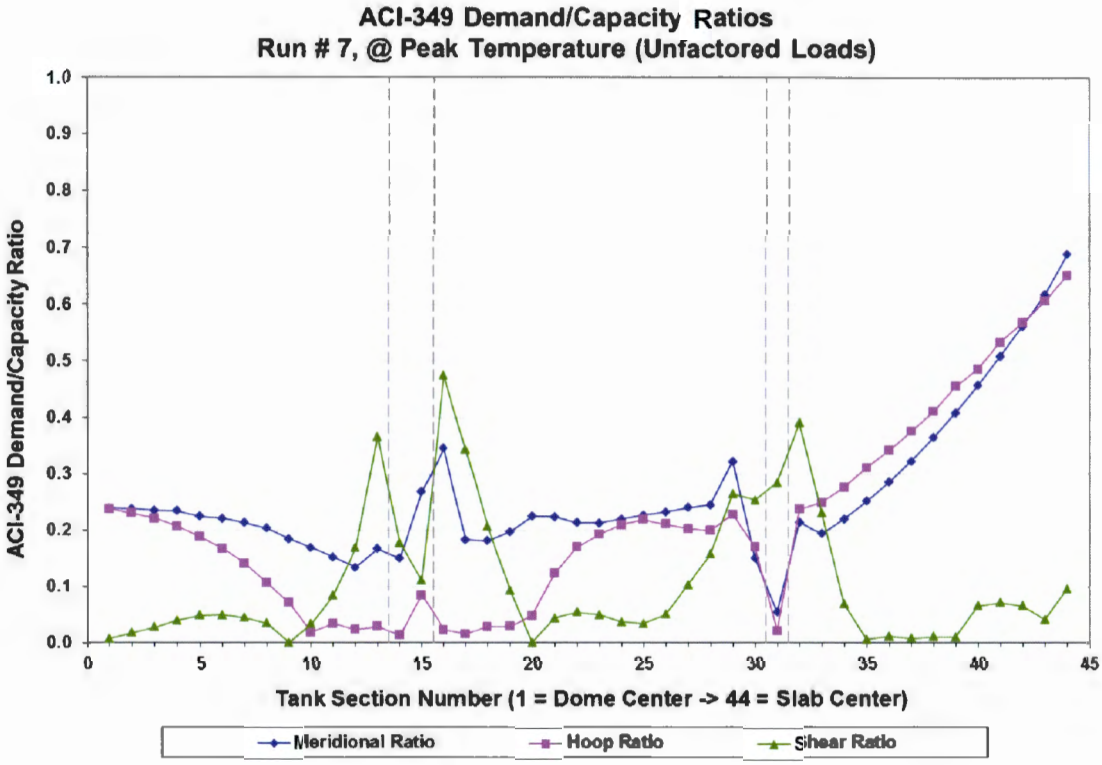

Figure 8.33. Run 7, ACI D/C Ratios at Peak Temperature. ACI load factors are equal to 1.0.

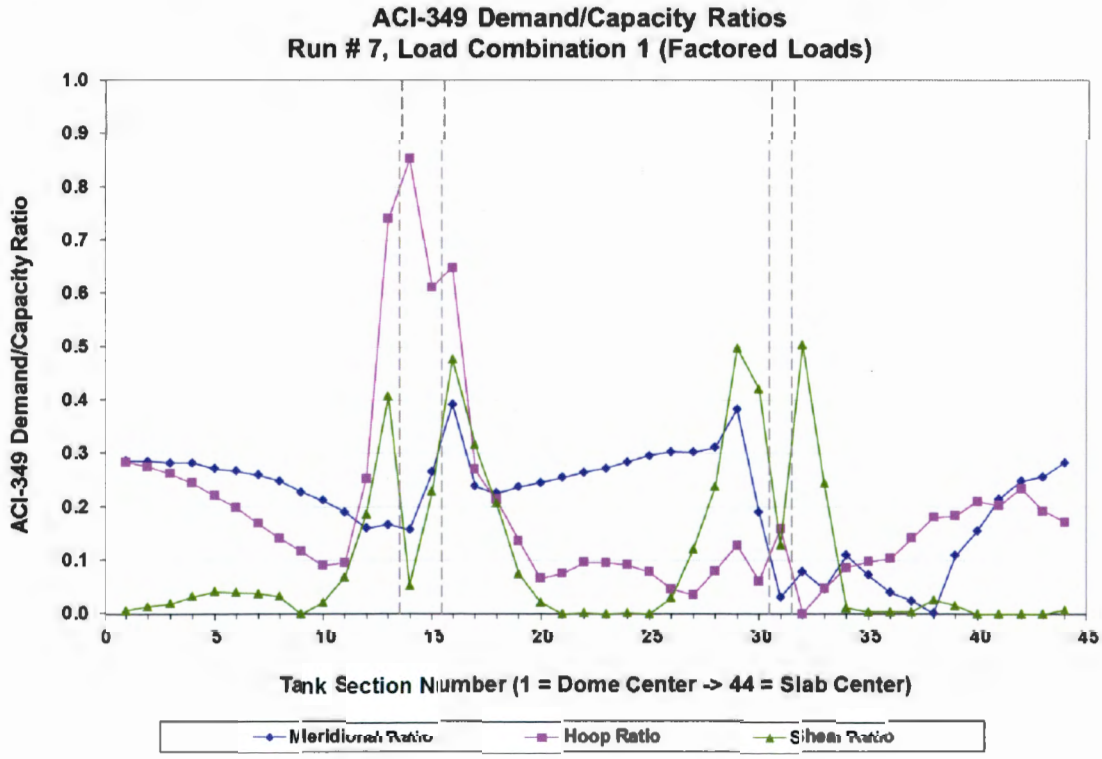

Figure 8.34. Run 7, ACI D/C Ratios for LC1

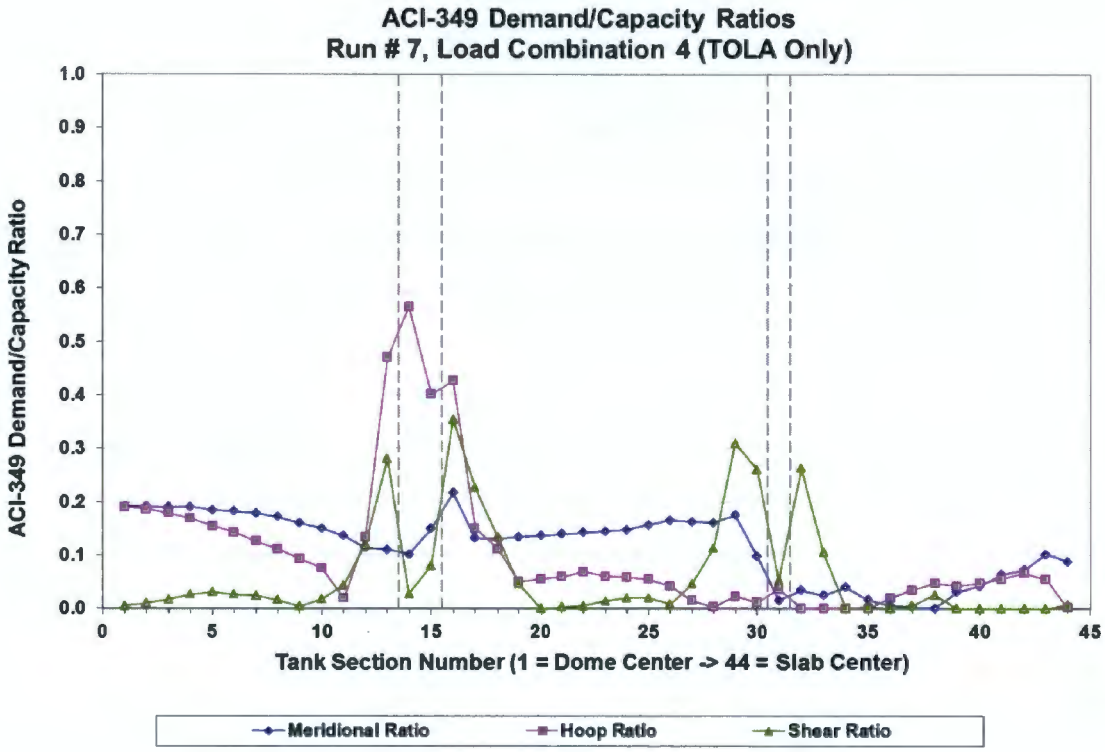

Figure 8.35. Run 7, ACI D/C Ratios for LC4 (TOLA results only – no seismic)

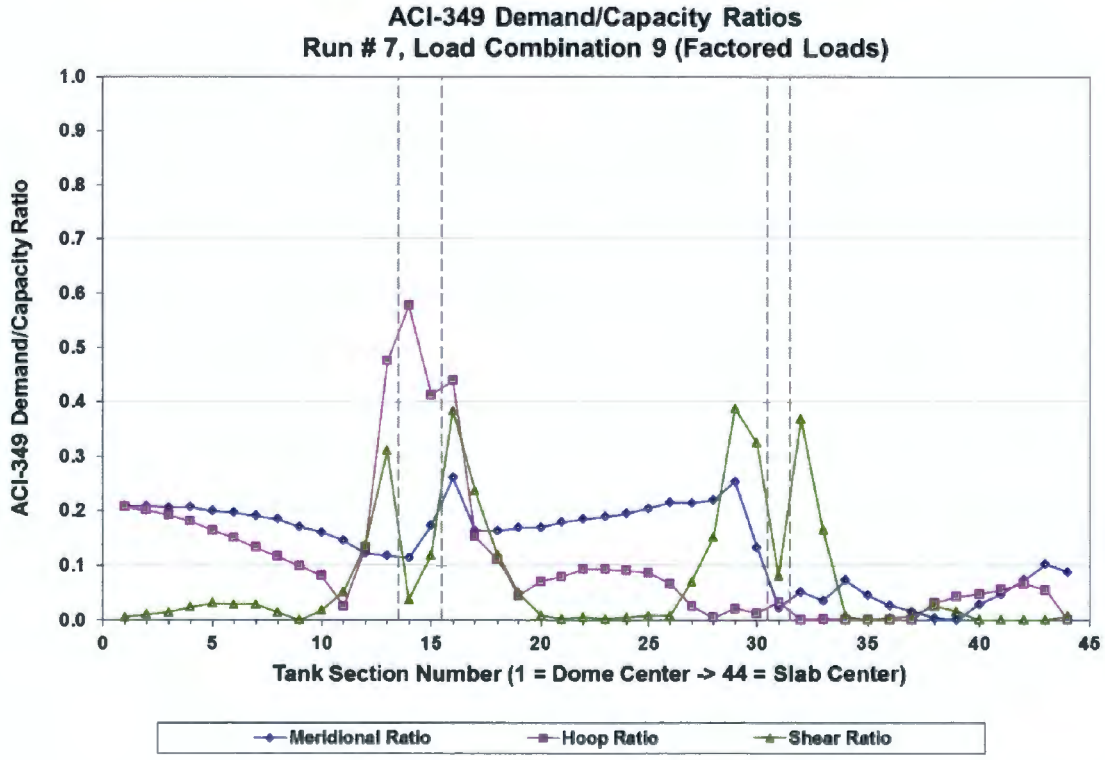

Figure 8.36. Run 7, ACI D/C Ratios for LC9

8.10 Run 8, High Soil Modulus, Nominal Concrete Modulus, Near Zero Concrete Tensile Strength with Creep

This run uses high soil modulus, nominal concrete modulus, and near zero concrete tensile strength with creep. In general high soil modulus tends to decrease the concrete stresses.

The demand/capacity ratios at peak temperatures and all load combinations (1, 4 [TOLA only], and 9) are less than 1.0 for the meridional, circumferential and shear directions (Figure 8.37 through Figure 8.40).

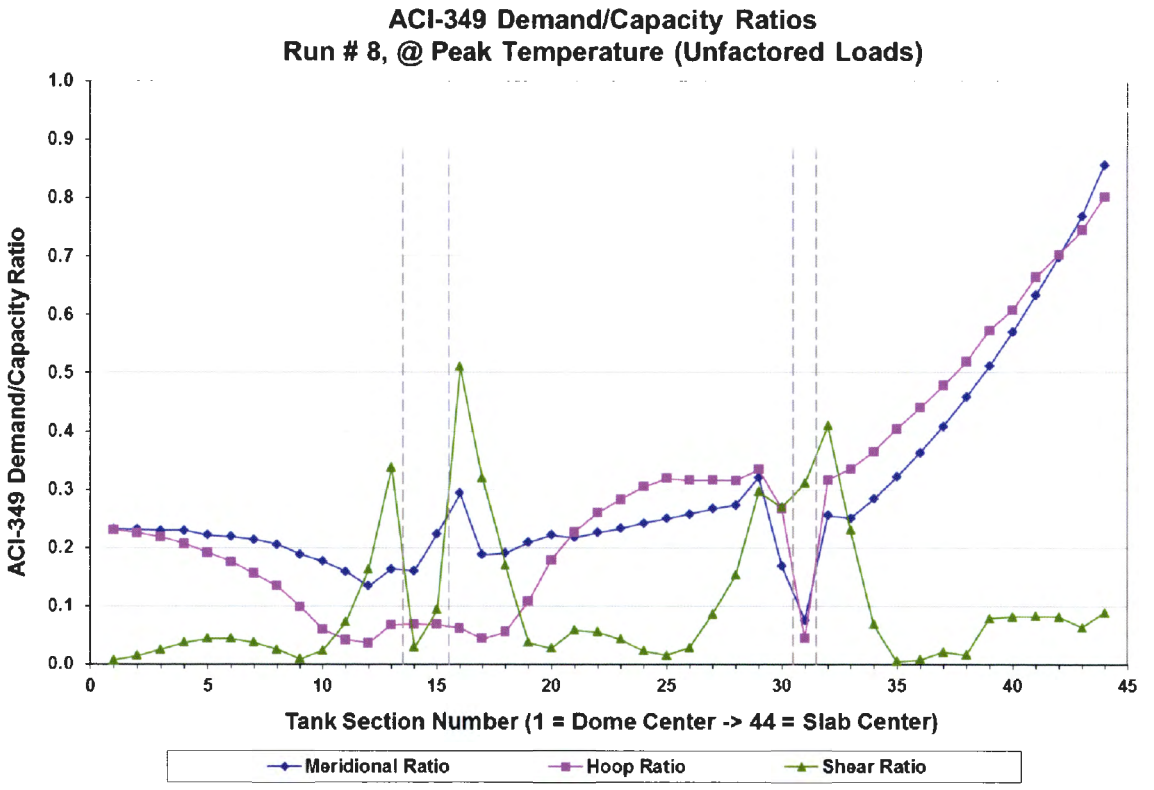

Figure 8.37. Run 8, ACI D/C Ratios at Peak Temperature. ACI load factors are equal to 1.0.

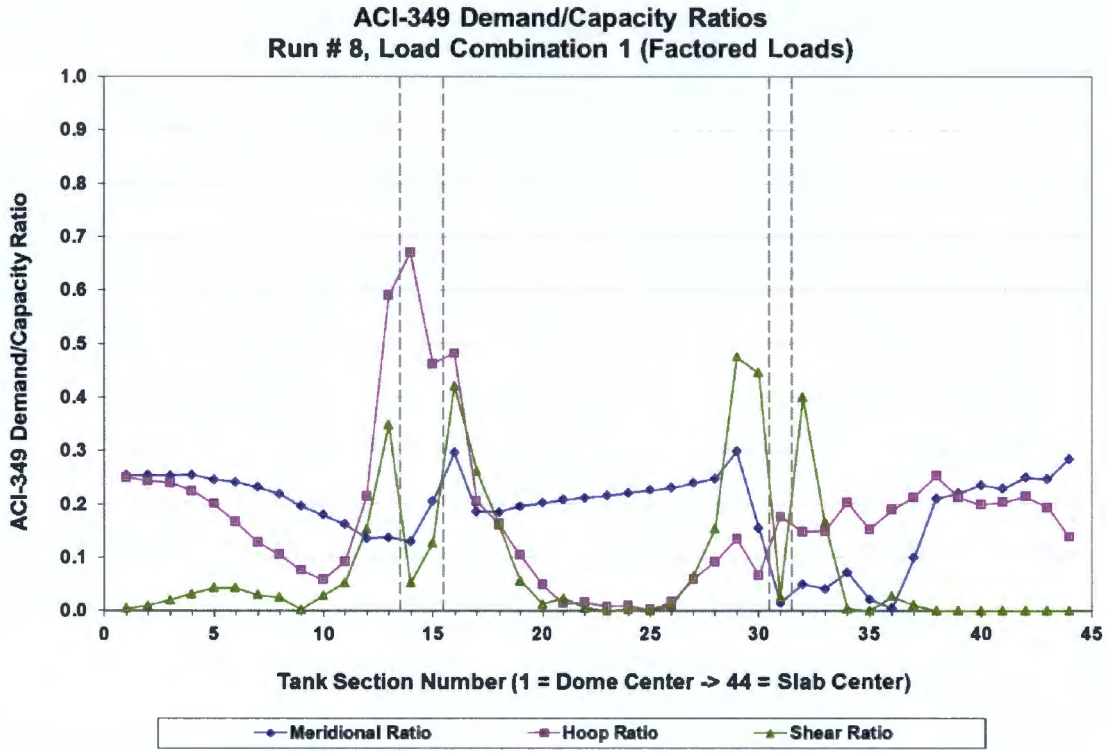

Figure 8.38. Run 8, ACI D/C Ratios for LC1

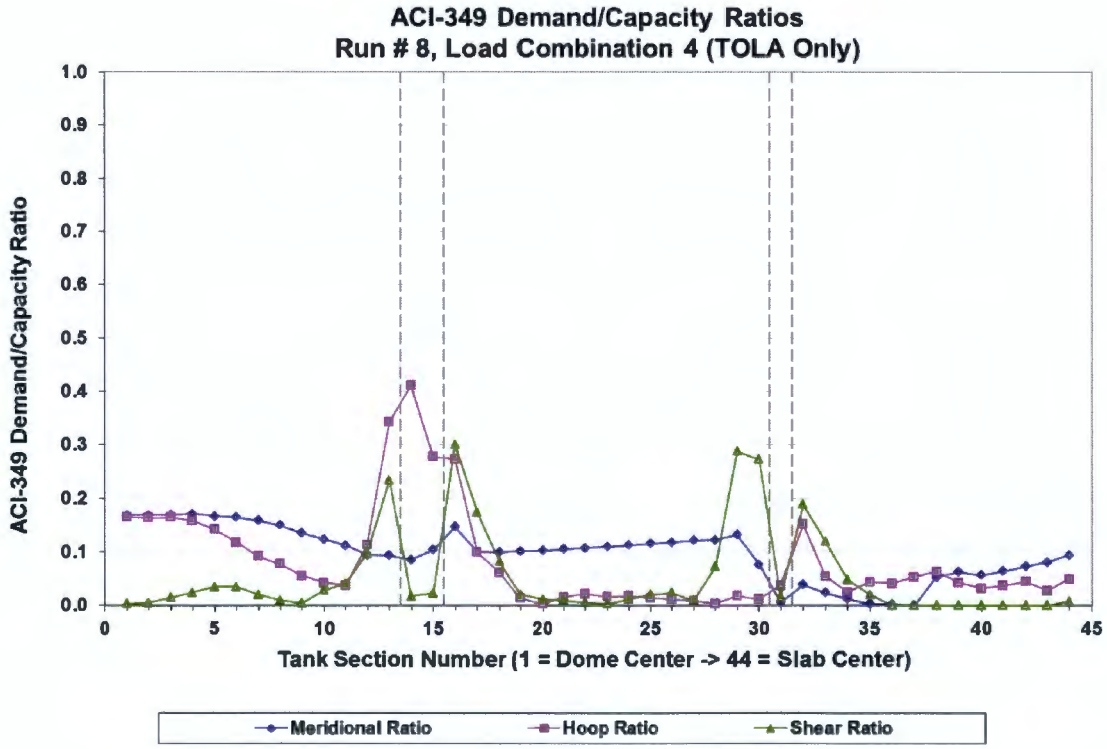

Figure 8.39. Run 8, ACI D/C Ratios for LC4 (TOLA results only – no seismic)

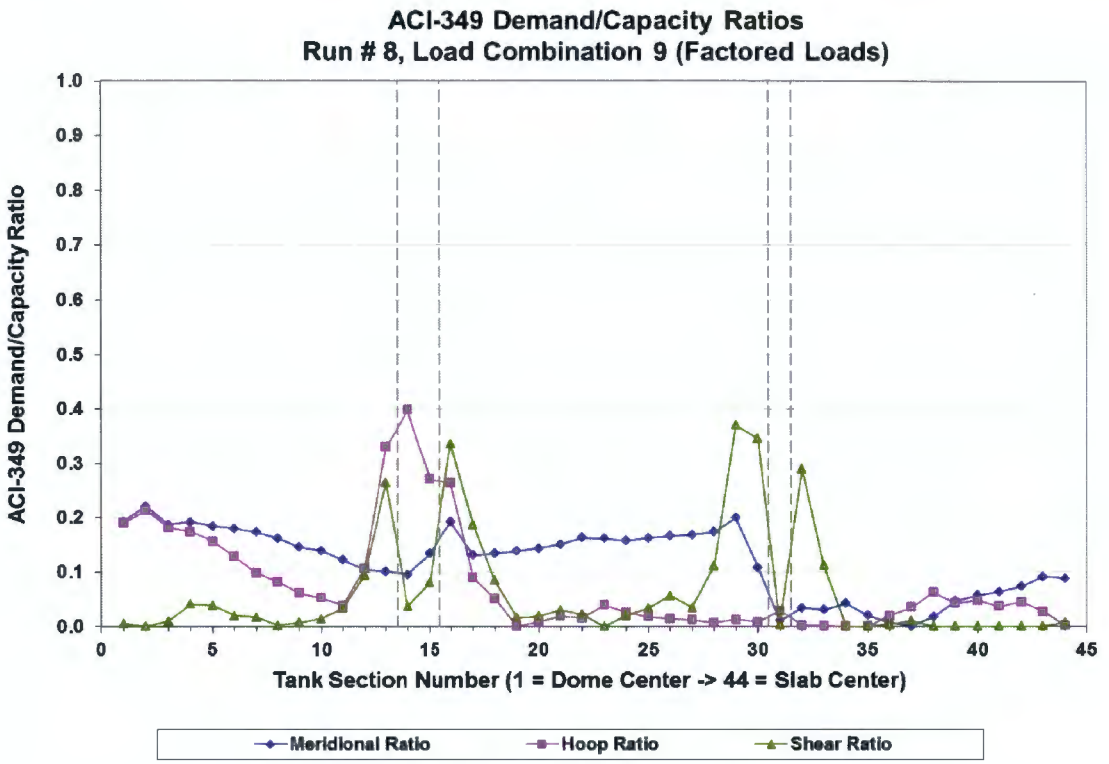

Figure 8.40. Run 8, ACI D/C Ratios for LC9

8.11 TOLA Run Matrix Conclusions

Table 8.4 through Table 8.6 show the summary of the range of ACI D/C ratios in meridional, circumferential, and shear for all the runs with the exception of Run 6. It is important to note that the D/C ratios of the dome, haunch, and wall are less than 1.0 for all load steps and load combinations. Therefore, all the tank regions that are critical to the structural stability of the Type III tanks pass the ACI 349-06 acceptance criteria for the design of new structures. This is true for the conservative combination of maximum recorded thermal loads and maximum soil overburden depth combined with the run matrix of bounding material property combinations. The summary tables also show a D/C ratio greater than 1.0 for slab locations at load step 6 (peak temperature). However, this only occurs at section 44 at the center of the tank where local concrete crushing (due to high thermal compression and reduced concrete strength) would not affect the structural stability of the tanks. Furthermore, the slab removal analysis presented in Appendix E also shows that structural isolation of the slab (due to cracking, crushing, or shear exceedance near the footing) will not affect the structural stability of the tanks.

Table 8.4. Meridional ACI Demand/Capacity Ratio Range

Meridional ACI Demand/Capacity Ratio Range	Run Matrix		Load Step	Dome	Haunch	Wall	Slab
				1 to 13	14 & 15	16 to 30	31 to 44
	Best Estimate	Run 1	LS 6 (Peak temperature)	0.13-0.24	0.16-0.25	0.16-0.32	0.07-0.78
			LS 18 (LC 1 - unfactored)	0.09-0.18	0.08-0.12	0.09-0.17	0.00-0.23
			LS 19 (LC 1 - factored)	0.15-0.27	0.15-0.23	0.17-0.34	0.00-0.29
			LS 18 (LC 9 - unfactored)	0.10-0.18	0.09-0.13	0.09-0.18	0.00-0.10
			LS 19 (LC 9 - factored)	0.11-0.20	0.11-0.15	0.12-0.23	0.00-0.09
	"Worst case combinations" using available material property bounds	Run 2	LS 6 (Peak temperature)	0.14-0.26	0.19-0.31	0.17-0.43	0.07-0.97
			LS 18 (LC 1 - unfactored)	0.11-0.22	0.13-0.26	0.12-0.32	0.02-0.26
			LS 19 (LC 1 - factored)	0.16-0.31	0.19-0.38	0.20-0.50	0.03-0.27
			LS 18 (LC 9 - unfactored)	0.12-0.22	0.14-0.27	0.11-0.32	0.00-0.09
			LS 19 (LC 9 - factored)	0.13-0.25	0.15-0.29	0.14-0.37	0.00-0.10
		Run3	LS 6 (Peak temperature)	0.14-0.26	0.19-0.32	0.17-0.47	0.07-1.08
			LS 18 (LC 1 - unfactored)	0.11-0.23	0.13-0.28	0.12-0.34	0.01-0.28
			LS 19 (LC 1 - factored)	0.16-0.32	0.19-0.41	0.21-0.54	0.00-0.29
			LS 18 (LC 9 - unfactored)	0.12-0.23	0.14-0.27	0.12-0.32	0.00-0.10
			LS 19 (LC 9 - factored)	0.13-0.27	0.15-0.30	0.15-0.37	0.00-0.11
		Run 4	LS 6 (Peak temperature)	0.14-0.26	0.19-0.34	0.16-0.47	0.06-0.97
			LS 18 (LC 1 - unfactored)	0.11-0.24	0.14-0.28	0.13-0.37	0.01-0.26
			LS 19 (LC 1 - factored)	0.16-0.33	0.20-0.42	0.22-0.56	0.01-0.26
			LS 18 (LC 9 - unfactored)	0.12-0.24	0.15-0.29	0.13-0.37	0.00-0.10
			LS 19 (LC 9 - factored)	0.12-0.26	0.16-0.32	0.16-0.42	0.00-0.14
		Run 5	LS 6 (Peak temperature)	0.14-0.26	0.18-0.33	0.16-0.43	0.06-0.87
			LS 18 (LC 1 - unfactored)	0.12-0.23	0.14-0.29	0.13-0.39	0.01-0.23
			LS 19 (LC 1 - factored)	0.16-0.33	0.20-0.42	0.21-0.59	0.00-0.25
			LS 18 (LC 9 - unfactored)	0.12-0.24	0.15-0.30	0.12-0.39	0.00-0.09
			LS 19 (LC 9 - factored)	0.13-0.25	0.16-0.32	0.16-0.44	0.00-0.12
		Run 7	LS 6 (Peak temperature)	0.13-0.24	0.15-0.27	0.15-0.35	0.05-0.69
			LS 18 (LC 1 - unfactored)	0.11-0.19	0.09-0.14	0.09-0.21	0.00-0.24
			LS 19 (LC 1 - factored)	0.16-0.29	0.16-0.27	0.19-0.39	0.00-0.28
			LS 18 (LC 9 - unfactored)	0.11-0.19	0.10-0.15	0.10-0.22	0.00-0.10
			LS 19 (LC 9 - factored)	0.12-0.21	0.11-0.17	0.13-0.26	0.00-0.10
		Run 8	LS 6 (Peak temperature)	0.13-0.23	0.16-0.22	0.17-0.32	0.08-0.86
			LS 18 (LC 1 - unfactored)	0.08-0.17	0.07-0.10	0.08-0.14	0.00-0.23
			LS 19 (LC 1 - factored)	0.14-0.25	0.13-0.20	0.16-0.30	0.00-0.28
			LS 18 (LC 9 - unfactored)	0.09-0.17	0.09-0.10	0.08-0.15	0.00-0.09
			LS 19 (LC 9 - factored)	0.10-0.22	0.10-0.13	0.11-0.20	0.00-0.09

Table 8.5. Hoop/Circumferential ACI Demand/Capacity Ratio Range

	Run Matrix		Load Step	Dome	Haunch	Wall	Slab
				1 to 13	14 & 15	16 to 30	31 to 44
Hoop ACI Demand/Capacity Ratio Range	Best Estimate	Run 1	LS 6 (Peak temperature)	0.03-0.23	0.03-0.04	0.03-0.29	0.02-0.71
			LS 18 (LC 1 - unfactored)	0.06-0.53	0.41-0.60	0.00-0.43	0.10-0.62
			LS 19 (LC 1 - factored)	0.07-0.64	0.50-0.73	0.00-0.52	0.09-0.24
			LS 18 (LC 9 - unfactored)	0.04-0.38	0.32-0.46	0.01-0.32	0.00-0.30
			LS 19 (LC 9 - factored)	0.05-0.38	0.32-0.46	0.01-0.32	0.00-0.07
	"Worst case combinations" using available material property bounds	Run 2	LS 6 (Peak temperature)	0.02-0.25	0.04-0.04	0.03-0.28	0.02-0.87
			LS 18 (LC 1 - unfactored)	0.04-0.49	0.40-0.56	0.03-0.43	0.09-0.20
			LS 19 (LC 1 - factored)	0.06-0.60	0.50-0.68	0.01-0.53	0.02-0.21
			LS 18 (LC 9 - unfactored)	0.01-0.35	0.31-0.42	0.00-0.33	0.00-0.05
			LS 19 (LC 9 - factored)	0.00-0.34	0.31-0.42	0.00-0.33	0.00-0.04
		Run3	LS 6 (Peak temperature)	0.02-0.26	0.03-0.04	0.03-0.29	0.02-0.96
			LS 18 (LC 1 - unfactored)	0.04-0.49	0.40-0.56	0.04-0.44	0.12-0.21
			LS 19 (LC 1 - factored)	0.06-0.60	0.50-0.68	0.01-0.53	0.09-0.24
			LS 18 (LC 9 - unfactored)	0.02-0.35	0.31-0.42	0.00-0.33	0.00-0.07
			LS 19 (LC 9 - factored)	0.01-0.34	0.32-0.41	0.00-0.33	0.00-0.07
		Run 4	LS 6 (Peak temperature)	0.02-0.26	0.01-0.08	0.02-0.21	0.02-0.86
			LS 18 (LC 1 - unfactored)	0.05-0.51	0.44-0.59	0.02-0.49	0.10-0.20
			LS 19 (LC 1 - factored)	0.07-0.66	0.57-0.76	0.01-0.63	0.03-0.20
			LS 18 (LC 9 - unfactored)	0.02-0.39	0.37-0.48	0.00-0.41	0.00-0.06
			LS 19 (LC 9 - factored)	0.01-0.39	0.38-0.48	0.00-0.41	0.00-0.06
		Run 5	LS 6 (Peak temperature)	0.02-0.26	0.01-0.08	0.02-0.21	0.02-0.77
			LS 18 (LC 1 - unfactored)	0.05-0.52	0.44-0.60	0.01-0.48	0.08-0.18
			LS 19 (LC 1 - factored)	0.07-0.66	0.57-0.77	0.01-0.62	0.02-0.17
			LS 18 (LC 9 - unfactored)	0.01-0.40	0.38-0.49	0.00-0.40	0.00-0.05
			LS 19 (LC 9 - factored)	0.01-0.40	0.38-0.49	0.00-0.40	0.00-0.05
		Run 7	LS 6 (Peak temperature)	0.02-0.24	0.01-0.08	0.02-0.23	0.02-0.65
			LS 18 (LC 1 - unfactored)	0.05-0.59	0.47-0.68	0.01-0.51	0.02-0.24
			LS 19 (LC 1 - factored)	0.09-0.74	0.61-0.85	0.04-0.65	0.00-0.24
			LS 18 (LC 9 - unfactored)	0.02-0.47	0.40-0.57	0.00-0.43	0.00-0.07
			LS 19 (LC 9 - factored)	0.03-0.48	0.41-0.58	0.00-0.44	0.00-0.07
		Run 8	LS 6 (Peak temperature)	0.04-0.23	0.07-0.07	0.04-0.33	0.04-0.80
			LS 18 (LC 1 - unfactored)	0.04-0.51	0.38-0.57	0.01-0.41	0.09-0.24
			LS 19 (LC 1 - factored)	0.06-0.59	0.46-0.67	0.00-0.48	0.14-0.25
			LS 18 (LC 9 - unfactored)	0.04-0.34	0.28-0.41	0.00-0.27	0.02-0.15
			LS 19 (LC 9 - factored)	0.04-0.33	0.27-0.40	0.00-0.26	0.00-0.06

Table 8.6. Shear ACI Demand/Capacity Ratio Range

	Run Matrix		Load Step	Dome 1 to 13	Haunch 14 & 15	Wall 16 to 30	Slab 31 to 44
Shear ACI Demand/Capacity Ratio Range	Best Estimate	Run 1	LS 6 (Peak temperature)	0.01-0.34	0.04-0.14	0.02-0.53	0.00-0.40
			LS 18 (LC 1 - unfactored)	0.01-0.24	0.03-0.06	0.01-0.32	0.00-0.20
			LS 19 (LC 1 - factored)	0.00-0.38	0.06-0.14	0.00-0.49	0.00-0.46
			LS 18 (LC 9 - unfactored)	0.01-0.26	0.04-0.06	0.00-0.33	0.00-0.28
			LS 19 (LC 9 - factored)	0.00-0.29	0.04-0.10	0.00-0.39	0.00-0.33
	"Worst case combinations" using available material property bounds	Run 2	LS 6 (Peak temperature)	0.01-0.36	0.03-0.19	0.00-0.56	0.00-0.49
			LS 18 (LC 1 - unfactored)	0.01-0.28	0.03-0.07	0.00-0.41	0.00-0.29
			LS 19 (LC 1 - factored)	0.00-0.41	0.06-0.26	0.01-0.55	0.00-0.52
			LS 18 (LC 9 - unfactored)	0.00-0.29	0.03-0.09	0.00-0.43	0.00-0.31
			LS 19 (LC 9 - factored)	0.00-0.33	0.04-0.17	0.01-0.45	0.00-0.39
		Run3	LS 6 (Peak temperature)	0.00-0.36	0.03-0.20	0.01-0.60	0.00-0.52
			LS 18 (LC 1 - unfactored)	0.00-0.28	0.03-0.09	0.00-0.41	0.00-0.30
			LS 19 (LC 1 - factored)	0.00-0.42	0.06-0.28	0.02-0.57	0.00-0.54
			LS 18 (LC 9 - unfactored)	0.01-0.30	0.03-0.10	0.01-0.44	0.00-0.32
			LS 19 (LC 9 - factored)	0.00-0.33	0.04-0.18	0.01-0.48	0.00-0.42
		Run 4	LS 6 (Peak temperature)	0.00-0.36	0.04-0.21	0.03-0.55	0.00-0.50
			LS 18 (LC 1 - unfactored)	0.00-0.31	0.03-0.14	0.00-0.43	0.00-0.35
			LS 19 (LC 1 - factored)	0.01-0.44	0.07-0.32	0.01-0.59	0.00-0.60
			LS 18 (LC 9 - unfactored)	0.00-0.32	0.04-0.14	0.01-0.46	0.00-0.36
			LS 19 (LC 9 - factored)	0.00-0.35	0.05-0.22	0.02-0.49	0.00-0.46
		Run 5	LS 6 (Peak temperature)	0.00-0.36	0.04-0.19	0.03-0.54	0.00-0.48
			LS 18 (LC 1 - unfactored)	0.00-0.31	0.03-0.12	0.00-0.43	0.00-0.34
			LS 19 (LC 1 - factored)	0.01-0.44	0.07-0.31	0.02-0.57	0.00-0.58
			LS 18 (LC 9 - unfactored)	0.00-0.32	0.03-0.13	0.01-0.45	0.00-0.35
			LS 19 (LC 9 - factored)	0.01-0.35	0.05-0.20	0.01-0.48	0.00-0.45
		Run 7	LS 6 (Peak temperature)	0.00-0.37	0.11-0.18	0.00-0.48	0.01-0.39
			LS 18 (LC 1 - unfactored)	0.01-0.27	0.06-0.08	0.01-0.33	0.00-0.30
			LS 19 (LC 1 - factored)	0.00-0.41	0.05-0.23	0.00-0.50	0.00-0.50
			LS 18 (LC 9 - unfactored)	0.00-0.28	0.03-0.08	0.00-0.35	0.00-0.26
			LS 19 (LC 9 - factored)	0.00-0.31	0.04-0.12	0.00-0.39	0.00-0.37
		Run 8	LS 6 (Peak temperature)	0.01-0.34	0.03-0.09	0.02-0.51	0.01-0.41
			LS 18 (LC 1 - unfactored)	0.01-0.21	0.01-0.03	0.01-0.31	0.00-0.14
			LS 19 (LC 1 - factored)	0.00-0.35	0.05-0.13	0.00-0.48	0.00-0.40
			LS 18 (LC 9 - unfactored)	0.00-0.23	0.02-0.02	0.00-0.30	0.00-0.19
			LS 19 (LC 9 - factored)	0.00-0.26	0.04-0.08	0.00-0.37	0.00-0.29

8.12 Shear Friction at Construction Joints

In addition to the through wall shear D/C ratio checks provided in the previous sections, shear friction checks must be performed at locations of construction joints in the tanks. Figure 8.41 shows the four construction joints located in the walls of the Type III tanks. These four construction joints align with the Type III ACI sections (shown in Figure 8.1) 18, 22, 26, and 30. No changes are required in the model to check the shear friction at the construction joints. However, the through wall shear demands must be compared to the shear friction capacities which differ from the through wall shear capacity.

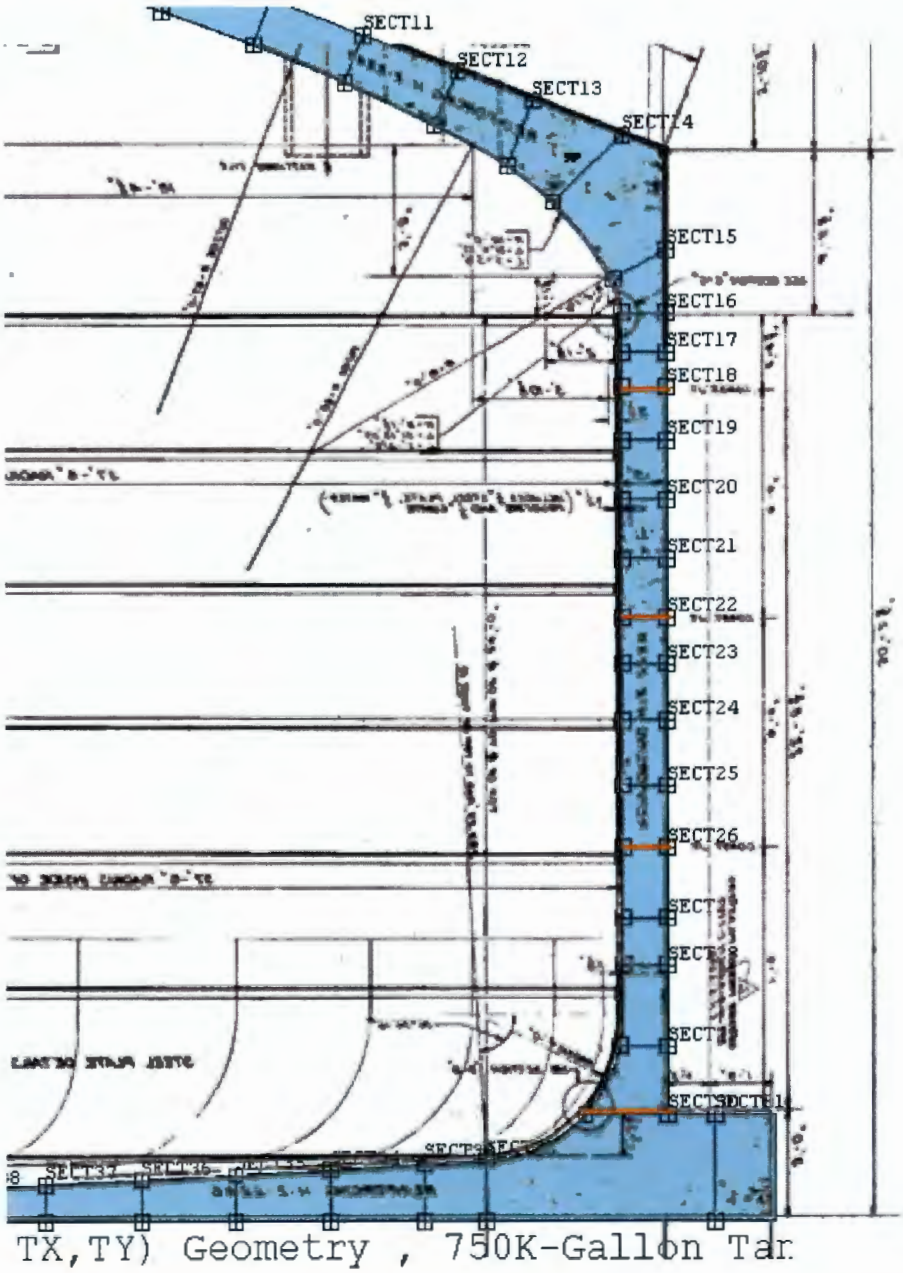

Figure 8.41. Construction Joints in Type III Tanks (Drawing H-2-2244, Rev. 2) Highlighted on the Type III ACI Sections

As stated in the Structural Evaluation Criteria (Johnson et al. 2010), shear friction at construction joints should be checked according to ACI 349-06 (ACI 2007), Section 11.7, where the allowable shear across the construction joint is calculated as follows:

$$\textit{Shear friction capacity} = \textit{lesser of}\ \{\varphi A_{vf} f_y \mu\ ,\ \varphi(0.2A_c)\ f_c',\ \varphi(800)A_c\} \tag{8.1}$$

where φ = Capacity reduction factor for shear, per ACI 349-06 Appendix C = 0.85[5]
A_{vf} = Area of shear friction reinforcement normal to the construction joint
f_c' = Compressive strength of concrete adjusted for temperature
f_y = Yield strength of the rebar adjusted for temperature
μ = Coefficient of friction per ACI 349-06, Section 11.7.4.3
A_c = Area of concrete section resisting shear transfer.

Given the lack of knowledge about the procedures used between different concrete pours during the time of tank construction, the minimum value of $\mu = 0.6$ from ACI 349-06 was chosen. Because of their locations in the tanks, the construction joints are always in compression. Section 11.7.7 of ACI 349-06 states that if there exists permanent net compression across the shear plane, this net compression is permitted to be taken as additive to $A_{vf}f_y$.

Shear friction was checked at these sections for all of the material property runs that were evaluated according to ACI 349-06, matrix Runs 1 through 5, 7, and 8. Tables 8.7 through 8.10 show the shear friction D/C calculations in the various load steps for the run matrix. The maximum D/C ratios for sections 18, 22, 26, and 30 were 0.19, 0.05, 0.09, and 0.54 respectively. Shear friction at the construction joints for the Type III SSTs meet ACI 349-06 requirements under TOLA loads.

[5] $\phi = 0.75$ is incorrectly specified in Johnson et al. 2010 based on ACI 349-06 Section 11.7 rather than $\phi = 0.85$ from ACI 349-06 Appendix C which is identified as the appropriate criteria in Johnson et al. 2010.

Table 8.7. Section 18 Shear Friction D/C Ratios

Run	load step	Shear Demand [kip/ft]	Axial [kip/ft]	A_{vf} [in^2/ft]	A_c [in^2/ft]	μ	f_y [psi]	f_c' [psi]	$800A_c$ [kip/ft]	$0.2f_c'A_c$ [kip/ft]	$A_{vf}f_y\mu$ [kip/ft]	ϕ	Capacity [kip/ft]	D/C
1	6	7.5	-72.2	0.88	180	0.6	36300	4338	144.00	156.17	62.55	0.85	53.17	**0.14**
	18-50F	3.1	-40.9	0.88	180	0.6	40000	4338	144.00	156.17	45.73	0.85	38.87	**0.08**
	LC1	6.7	-80.0	0.88	180	0.6	40000	4338	144.00	156.17	69.19	0.85	58.81	**0.11**
	18-80F	3.7	-44.9	0.88	180	0.6	40000	4338	144.00	156.17	48.13	0.85	40.91	**0.09**
	LC9	4.7	-57.0	0.88	180	0.6	40000	4338	144.00	156.17	55.39	0.85	47.08	**0.10**
2	6	9.3	-73.6	0.88	180	0.6	36300	4338	144.00	156.17	63.39	0.85	53.88	**0.17**
	18-50F	6.9	-45.5	0.88	180	0.6	40000	4338	144.00	156.17	48.49	0.85	41.22	**0.17**
	LC1	10.5	-83.5	0.88	180	0.6	40000	4338	144.00	156.17	71.29	0.85	60.60	**0.17**
	18-80F	7.4	-49.5	0.88	180	0.6	40000	4338	144.00	156.17	50.89	0.85	43.26	**0.17**
	LC9	8.0	-62.0	0.88	180	0.6	40000	4338	144.00	156.17	58.39	0.85	49.63	**0.16**
3	6	9.7	-74.4	0.88	180	0.6	36300	4338	144.00	156.17	63.87	0.85	54.29	**0.18**
	18-50F	7.3	-45.8	0.88	180	0.6	40000	4338	144.00	156.17	48.67	0.85	41.37	**0.18**
	LC1	11.2	-84.1	0.88	180	0.6	40000	4338	144.00	156.17	71.65	0.85	60.90	**0.18**
	18-80F	7.6	-49.9	0.88	180	0.6	40000	4338	144.00	156.17	51.13	0.85	43.46	**0.17**
	LC9	7.4	-65.6	0.88	180	0.6	40000	4338	144.00	156.17	60.55	0.85	51.47	**0.14**
4	6	10.0	-71.3	0.88	180	0.6	36300	4338	144.00	156.17	62.01	0.85	52.71	**0.19**
	18-50F	7.6	-51.5	0.88	180	0.6	40000	4338	144.00	156.17	52.09	0.85	44.28	**0.17**
	LC1	11.6	-90.7	0.88	180	0.6	40000	4338	144.00	156.17	75.61	0.85	64.27	**0.18**
	18-80F	8.0	-54.4	0.88	180	0.6	40000	4338	144.00	156.17	53.83	0.85	45.76	**0.17**
	LC9	8.5	-67.1	0.88	180	0.6	40000	4338	144.00	156.17	61.45	0.85	52.23	**0.16**
5	6	9.6	-71.3	0.88	180	0.6	36300	4338	144.00	156.17	62.01	0.85	52.71	**0.18**
	18-50F	7.4	-51.7	0.88	180	0.6	40000	4338	144.00	156.17	52.21	0.85	44.38	**0.17**
	LC1	11.6	-90.8	0.88	180	0.6	40000	4338	144.00	156.17	75.67	0.85	64.32	**0.18**
	18-80F	8.2	-54.6	0.88	180	0.6	40000	4338	144.00	156.17	53.95	0.85	45.86	**0.18**
	LC9	9.1	-66.8	0.88	180	0.6	40000	4338	144.00	156.17	61.27	0.85	52.08	**0.17**
7	6	8.2	-70.2	0.88	180	0.6	36300	4338	144.00	156.17	61.35	0.85	52.15	**0.16**
	18-50F	4.2	-48.3	0.88	180	0.6	40000	4338	144.00	156.17	50.17	0.85	42.65	**0.10**
	LC1	7.8	-88.1	0.88	180	0.6	40000	4338	144.00	156.17	74.05	0.85	62.94	**0.12**
	18-80F	4.5	-51.0	0.88	180	0.6	40000	4338	144.00	156.17	51.79	0.85	44.02	**0.10**
	LC9	4.2	-63.7	0.88	180	0.6	40000	4338	144.00	156.17	59.41	0.85	50.50	**0.08**
8	6	6.8	-74.1	0.88	180	0.6	36300	4338	144.00	156.17	63.69	0.85	54.14	**0.13**
	18-50F	2.2	-33.5	0.88	180	0.6	40000	4338	144.00	156.17	41.29	0.85	35.10	**0.06**
	LC1	5.8	-72.2	0.88	180	0.6	40000	4338	144.00	156.17	64.51	0.85	54.84	**0.11**
	18-80F	2.9	-38.9	0.88	180	0.6	40000	4338	144.00	156.17	44.53	0.85	37.85	**0.08**
	LC9	3.2	-52.3	0.88	180	0.6	40000	4338	144.00	156.17	52.57	0.85	44.69	**0.07**
													Max	**0.19**

Table 8.8. Section 22 Shear Friction D/C Ratios

Run	load step	Shear Demand [kip/ft]	Axial [kip/ft]	A_{vf} [in^2/ft]	A_c [in^2/ft]	μ	f_y [psi]	f_c' [psi]	$800A_c$ [kip/ft]	$0.2f_c'A_c$ [kip/ft]	$A_{vf}f_y\mu$ [kip/ft]	ϕ	Capacity [kip/ft]	D/C
1	6	2.2	-78.2	0.88	180	0.6	36148	4006	144.00	144.22	66.07	0.85	56.16	**0.04**
	18-50F	0.4	-41.2	0.88	180	0.6	40000	4006	144.00	144.22	45.91	0.85	39.03	**0.01**
	LC1	0.1	-84.8	0.88	180	0.6	40000	4006	144.00	144.22	72.07	0.85	61.26	**0.00**
	18-80F	0.2	-45.0	0.88	180	0.6	40000	4006	144.00	144.22	48.19	0.85	40.96	**0.00**
	LC9	0.1	-60.1	0.88	180	0.6	40000	4006	144.00	144.22	57.25	0.85	48.66	**0.00**
2	6	2.7	-80.4	0.88	180	0.6	36148	4006	144.00	144.22	67.39	0.85	57.28	**0.05**
	18-50F	0.1	-46.3	0.88	180	0.6	40000	4006	144.00	144.22	48.97	0.85	41.63	**0.00**
	LC1	0.9	-90.3	0.88	180	0.6	40000	4006	144.00	144.22	75.37	0.85	64.07	**0.01**
	18-80F	0.6	-50.9	0.88	180	0.6	40000	4006	144.00	144.22	51.73	0.85	43.97	**0.01**
	LC9	1.2	-65.9	0.88	180	0.6	40000	4006	144.00	144.22	60.73	0.85	51.62	**0.02**
3	6	2.9	-81.2	0.88	180	0.6	36148	4006	144.00	144.22	67.87	0.85	57.69	**0.05**
	18-50F	0.0	-46.7	0.88	180	0.6	40000	4006	144.00	144.22	49.21	0.85	41.83	**0.00**
	LC1	0.7	-91.1	0.88	180	0.6	40000	4006	144.00	144.22	75.85	0.85	64.47	**0.01**
	18-80F	0.4	-51.1	0.88	180	0.6	40000	4006	144.00	144.22	51.85	0.85	44.07	**0.01**
	LC9	1.0	-66.4	0.88	180	0.6	40000	4006	144.00	144.22	61.03	0.85	51.88	**0.02**
4	6	2.4	-76.4	0.88	180	0.6	36148	4006	144.00	144.22	64.99	0.85	55.24	**0.04**
	18-50F	0.4	-52.7	0.88	180	0.6	40000	4006	144.00	144.22	52.81	0.85	44.89	**0.01**
	LC1	0.8	-98.3	0.88	180	0.6	40000	4006	144.00	144.22	80.17	0.85	68.15	**0.01**
	18-80F	0.2	-55.9	0.88	180	0.6	40000	4006	144.00	144.22	54.73	0.85	46.52	**0.00**
	LC9	0.7	-71.6	0.88	180	0.6	40000	4006	144.00	144.22	64.15	0.85	54.53	**0.01**
5	6	2.4	-76.7	0.88	180	0.6	36148	4006	144.00	144.22	65.17	0.85	55.40	**0.04**
	18-50F	0.1	-53.3	0.88	180	0.6	40000	4006	144.00	144.22	53.17	0.85	45.20	**0.00**
	LC1	1.0	-98.6	0.88	180	0.6	40000	4006	144.00	144.22	80.35	0.85	68.30	**0.01**
	18-80F	0.5	-56.4	0.88	180	0.6	40000	4006	144.00	144.22	55.03	0.85	46.78	**0.01**
	LC9	0.9	-71.9	0.88	180	0.6	40000	4006	144.00	144.22	64.33	0.85	54.68	**0.02**
7	6	2.1	-74.4	0.88	180	0.6	36148	4006	144.00	144.22	63.79	0.85	54.22	**0.04**
	18-50F	0.7	-48.5	0.88	180	0.6	40000	4006	144.00	144.22	50.29	0.85	42.75	**0.02**
	LC1	0.1	-93.9	0.88	180	0.6	40000	4006	144.00	144.22	77.53	0.85	65.90	**0.00**
	18-80F	0.2	-51.4	0.88	180	0.6	40000	4006	144.00	144.22	52.03	0.85	44.23	**0.00**
	LC9	0.2	-67.0	0.88	180	0.6	40000	4006	144.00	144.22	61.39	0.85	52.18	**0.00**
8	6	2.2	-81.2	0.88	180	0.6	36148	4006	144.00	144.22	67.87	0.85	57.69	**0.04**
	18-50F	0.4	-34.0	0.88	180	0.6	40000	4006	144.00	144.22	41.59	0.85	35.35	**0.01**
	LC1	0.2	-76.5	0.88	180	0.6	40000	4006	144.00	144.22	67.09	0.85	57.03	**0.00**
	18-80F	0.2	-39.0	0.88	180	0.6	40000	4006	144.00	144.22	44.59	0.85	37.90	**0.01**
	LC9	0.8	-59.1	0.88	180	0.6	40000	4006	144.00	144.22	56.65	0.85	48.15	**0.02**
													Max	**0.05**

Table 8.9. Section 26 Shear Friction D/C Ratios

Run	load step	Shear Demand [kip/ft]	Axial [kip/ft]	A_{vf} [in^2/ft]	A_c [in^2/ft]	μ	f_y [psi]	f_c' [psi]	$800A_c$ [kip/ft]	$0.2f_c'A_c$ [kip/ft]	$A_{vf}f_y\mu$ [kip/ft]	ϕ	Capacity [kip/ft]	D/C
1	6	1.4	83.6	0.88	180	0.6	36061	3761	144.00	135.40	19.11	0.85	16.24	**0.09**
	18-50F	0.2	-42.3	0.88	180	0.6	40000	3761	144.00	135.40	46.57	0.85	39.59	**0.01**
	LC1	1.1	-87.7	0.88	180	0.6	40000	3761	144.00	135.40	73.81	0.85	62.74	**0.02**
	18-80F	0.4	-46.0	0.88	180	0.6	40000	3761	144.00	135.40	48.79	0.85	41.47	**0.01**
	LC9	0.0	-62.5	0.88	180	0.6	40000	3761	144.00	135.40	58.69	0.85	49.89	**0.00**
2	6	2.4	-86.3	0.88	180	0.6	36061	3761	144.00	135.40	70.89	0.85	60.25	**0.04**
	18-50F	1.4	-47.3	0.88	180	0.6	40000	3761	144.00	135.40	49.57	0.85	42.14	**0.03**
	LC1	2.5	-94.0	0.88	180	0.6	40000	3761	144.00	135.40	77.59	0.85	65.95	**0.04**
	18-80F	1.3	-52.0	0.88	180	0.6	40000	3761	144.00	135.40	52.39	0.85	44.53	**0.03**
	LC9	1.5	-69.5	0.88	180	0.6	40000	3761	144.00	135.40	62.89	0.85	53.46	**0.03**
3	6	2.7	-87.3	0.88	180	0.6	36061	3761	144.00	135.40	71.49	0.85	60.76	**0.04**
	18-50F	1.6	-47.7	0.88	180	0.6	40000	3761	144.00	135.40	49.81	0.85	42.34	**0.04**
	LC1	3.2	-95.1	0.88	180	0.6	40000	3761	144.00	135.40	78.25	0.85	66.51	**0.05**
	18-80F	1.6	-52.3	0.88	180	0.6	40000	3761	144.00	135.40	52.57	0.85	44.69	**0.04**
	LC9	1.8	-70.3	0.88	180	0.6	40000	3761	144.00	135.40	63.37	0.85	53.87	**0.03**
4	6	3.2	-81.2	0.88	180	0.6	36061	3761	144.00	135.40	67.83	0.85	57.65	**0.06**
	18-50F	2.3	-54.0	0.88	180	0.6	40000	3761	144.00	135.40	53.59	0.85	45.55	**0.05**
	LC1	3.9	-104.3	0.88	180	0.6	40000	3761	144.00	135.40	83.77	0.85	71.21	**0.05**
	18-80F	2.1	-57.4	0.88	180	0.6	40000	3761	144.00	135.40	55.63	0.85	47.29	**0.04**
	LC9	2.5	-75.9	0.88	180	0.6	40000	3761	144.00	135.40	66.73	0.85	56.72	**0.04**
5	6	2.9	-81.5	0.88	180	0.6	36061	3761	144.00	135.40	68.01	0.85	57.80	**0.05**
	18-50F	2.1	-54.7	0.88	180	0.6	40000	3761	144.00	135.40	54.01	0.85	45.91	**0.05**
	LC1	3.2	-104.4	0.88	180	0.6	40000	3761	144.00	135.40	83.83	0.85	71.26	**0.04**
	18-80F	1.8	-58.0	0.88	180	0.6	40000	3761	144.00	135.40	55.99	0.85	47.59	**0.04**
	LC9	2.3	-76.3	0.88	180	0.6	40000	3761	144.00	135.40	66.97	0.85	56.93	**0.04**
7	6	1.9	-78.7	0.88	180	0.6	36061	3761	144.00	135.40	66.33	0.85	56.38	**0.03**
	18-50F	0.2	-49.4	0.88	180	0.6	40000	3761	144.00	135.40	50.83	0.85	43.21	**0.00**
	LC1	1.2	-99.3	0.88	180	0.6	40000	3761	144.00	135.40	80.77	0.85	68.66	**0.02**
	18-80F	0.3	-52.4	0.88	180	0.6	40000	3761	144.00	135.40	52.63	0.85	44.74	**0.01**
	LC9	0.3	-70.8	0.88	180	0.6	40000	3761	144.00	135.40	63.67	0.85	54.12	**0.01**
8	6	1.1	-87.3	0.88	180	0.6	36061	3761	144.00	135.40	71.49	0.85	60.76	**0.02**
	18-50F	0.2	-35.6	0.88	180	0.6	40000	3761	144.00	135.40	42.55	0.85	36.17	**0.01**
	LC1	0.4	-78.4	0.88	180	0.6	40000	3761	144.00	135.40	68.23	0.85	58.00	**0.01**
	18-80F	0.8	-40.2	0.88	180	0.6	40000	3761	144.00	135.40	45.31	0.85	38.52	**0.02**
	LC9	2.0	-56.7	0.88	180	0.6	40000	3761	144.00	135.40	55.21	0.85	46.93	**0.04**
													Max	**0.09**

Table 8.10. Section 30 Shear Friction D/C Ratios

Run	load step	Shear Demand [kip/ft]	Axial [kip/ft]	A_{vf} [in^2/ft]	A_c [in^2/ft]	μ	f_y [psi]	f_c' [psi]	$800A_c$ [kip/ft]	$0.2f_c'A_c$ [kip/ft]	$A_{vf}f_y\mu$ [kip/ft]	ϕ	Capacity [kip/ft]	D/C
1	6	8.7	92.1	0.88	335	0.6	35937	3488	267.65	233.39	19.06	0.85	16.20	**0.54**
	18-50F	16.7	-46.3	0.88	335	0.6	40000	3488	267.65	233.39	49.00	0.85	41.65	**0.40**
	LC1	28.3	-98.5	0.88	335	0.6	40000	3488	267.65	233.39	80.32	0.85	68.27	**0.41**
	18-80F	15.7	-50.3	0.88	335	0.6	40000	3488	267.65	233.39	51.40	0.85	43.69	**0.36**
	LC9	20.6	-69.6	0.88	335	0.6	40000	3488	267.65	233.39	62.98	0.85	53.53	**0.38**
2	6	13.6	-95.4	0.88	335	0.6	35937	3488	267.65	233.39	76.30	0.85	64.86	**0.21**
	18-50F	17.8	-51.7	0.88	335	0.6	40000	3488	267.65	233.39	52.24	0.85	44.40	**0.40**
	LC1	29.3	-104.9	0.88	335	0.6	40000	3488	267.65	233.39	84.16	0.85	71.53	**0.41**
	18-80F	16.6	-56.3	0.88	335	0.6	40000	3488	267.65	233.39	55.00	0.85	46.75	**0.36**
	LC9	21.3	-76.2	0.88	335	0.6	40000	3488	267.65	233.39	66.94	0.85	56.90	**0.37**
3	6	16.0	-96.6	0.88	335	0.6	35937	3488	267.65	233.39	77.02	0.85	65.47	**0.24**
	18-50F	18.3	-51.8	0.88	335	0.6	40000	3488	267.65	233.39	52.30	0.85	44.45	**0.41**
	LC1	30.2	-106.0	0.88	335	0.6	40000	3488	267.65	233.39	84.82	0.85	72.09	**0.42**
	18-80F	17.2	-56.4	0.88	335	0.6	40000	3488	267.65	233.39	55.06	0.85	46.80	**0.37**
	LC9	21.6	-76.6	0.88	335	0.6	40000	3488	267.65	233.39	67.18	0.85	57.10	**0.38**
4	6	15.6	-89.7	0.88	335	0.6	35937	3488	267.65	233.39	72.88	0.85	61.95	**0.25**
	18-50F	18.5	-58.3	0.88	335	0.6	40000	3488	267.65	233.39	56.20	0.85	47.77	**0.39**
	LC1	30.1	-114.7	0.88	335	0.6	40000	3488	267.65	233.39	90.04	0.85	76.53	**0.39**
	18-80F	17.3	-61.5	0.88	335	0.6	40000	3488	267.65	233.39	58.12	0.85	49.40	**0.35**
	LC9	21.8	-82.3	0.88	335	0.6	40000	3488	267.65	233.39	70.60	0.85	60.01	**0.36**
5	6	13.6	-89.8	0.88	335	0.6	35937	3488	267.65	233.39	72.94	0.85	62.00	**0.22**
	18-50F	18.0	-59.1	0.88	335	0.6	40000	3488	267.65	233.39	56.68	0.85	48.17	**0.37**
	LC1	29.4	-115.0	0.88	335	0.6	40000	3488	267.65	233.39	90.22	0.85	76.68	**0.38**
	18-80F	16.8	-62.3	0.88	335	0.6	40000	3488	267.65	233.39	58.60	0.85	49.81	**0.34**
	LC9	21.6	-83.0	0.88	335	0.6	40000	3488	267.65	233.39	71.02	0.85	60.36	**0.36**
7	6	8.3	-86.3	0.88	335	0.6	35937	3488	267.65	233.39	70.84	0.85	60.21	**0.14**
	18-50F	16.8	-53.4	0.88	335	0.6	40000	3488	267.65	233.39	53.26	0.85	45.27	**0.37**
	LC1	27.7	-109.3	0.88	335	0.6	40000	3488	267.65	233.39	86.80	0.85	73.78	**0.38**
	18-80F	15.4	-56.3	0.88	335	0.6	40000	3488	267.65	233.39	55.00	0.85	46.75	**0.33**
	LC9	20.1	-76.9	0.88	335	0.6	40000	3488	267.65	233.39	67.36	0.85	57.25	**0.35**
8	6	9.0	-96.5	0.88	335	0.6	35937	3488	267.65	233.39	76.96	0.85	65.42	**0.14**
	18-50F	16.7	-39.0	0.88	335	0.6	40000	3488	267.65	233.39	44.62	0.85	37.92	**0.44**
	LC1	28.2	-89.0	0.88	335	0.6	40000	3488	267.65	233.39	74.62	0.85	63.42	**0.44**
	18-80F	15.7	-43.9	0.88	335	0.6	40000	3488	267.65	233.39	47.56	0.85	40.42	**0.39**
	LC9	20.7	-62.3	0.88	335	0.6	40000	3488	267.65	233.39	58.60	0.85	49.81	**0.42**
													Max	**0.54**

9.0 Seismic Results

9.1 Concrete Tank

Concrete tank forces and moments are extracted from the model using the post-processing methods described in Section 6.2.12. Figures are grouped in sets showing the force or moment for the seismic portion. In each condition only the bounding values are presented. The seismic-only load is the difference between the full transient loading and gravity loading. The greatest difference between the minima or maxima of each loading is reported, which may not be the same as the difference in the bounding values of each loading as explained in Section 6.2.

The forces and moments are plotted against a "path" that starts at the dome apex and increases to the floor center. Forces and moments have been enveloped circumferentially for these plots. Concrete force/moment plots are as follows:

- Figure 9.1. Best Estimate Soil (BES): Concrete Tank Meridional Force – Seismic Only
- Figure 9.2. Best Estimate Soil (BES): Concrete Tank Hoop Force – Seismic Only
- Figure 9.3. Best Estimate Soil (BES): Concrete Tank Meridional Moment – Seismic Only
- Figure 9.4. Best Estimate Soil (BES): Concrete Tank Hoop Moment – Seismic Only
- Figure 9.5. Best Estimate Soil (BES): Concrete Tank Through-Wall Shear Force – Seismic Only
- Figure 9.6. Best Estimate Soil (BES): Concrete Tank In-Plane Shear Force – Seismic Only
- Figure 9.7. Lower Bound Soil (LBS): Concrete Tank Meridional Force – Seismic Only
- Figure 9.8. Lower Bound Soil (LBS): Concrete Tank Hoop Force – Seismic Only
- Figure 9.9. Lower Bound Soil (LBS): Concrete Tank Meridional Moment – Seismic Only
- Figure 9.10. Lower Bound Soil (LBS): Concrete Tank Hoop Moment – Seismic Only
- Figure 9.11. Lower Bound Soil (LBS): Concrete Tank Through-Wall Shear Force – Seismic Only
- Figure 9.12. Lower Bound Soil (LBS): Concrete Tank In-Plane Shear Force – Seismic Only
- Figure 9.13. Upper Bound Soil (UBS): Concrete Tank Meridional Force – Seismic Only
- Figure 9.14. Upper Bound Soil (UBS): Concrete Tank Hoop Force – Seismic Only
- Figure 9.15. Upper Bound Soil (UBS): Concrete Tank Meridional Moment – Seismic Only
- Figure 9.16. Upper Bound Soil (UBS): Concrete Tank Hoop Moment – Seismic Only
- Figure 9.17. Upper Bound Soil (UBS): Concrete Tank Through-Wall Shear Force – Seismic Only
- Figure 9.18. Upper Bound Soil (UBS): Concrete Tank In-Plane Shear Force – Seismic Only

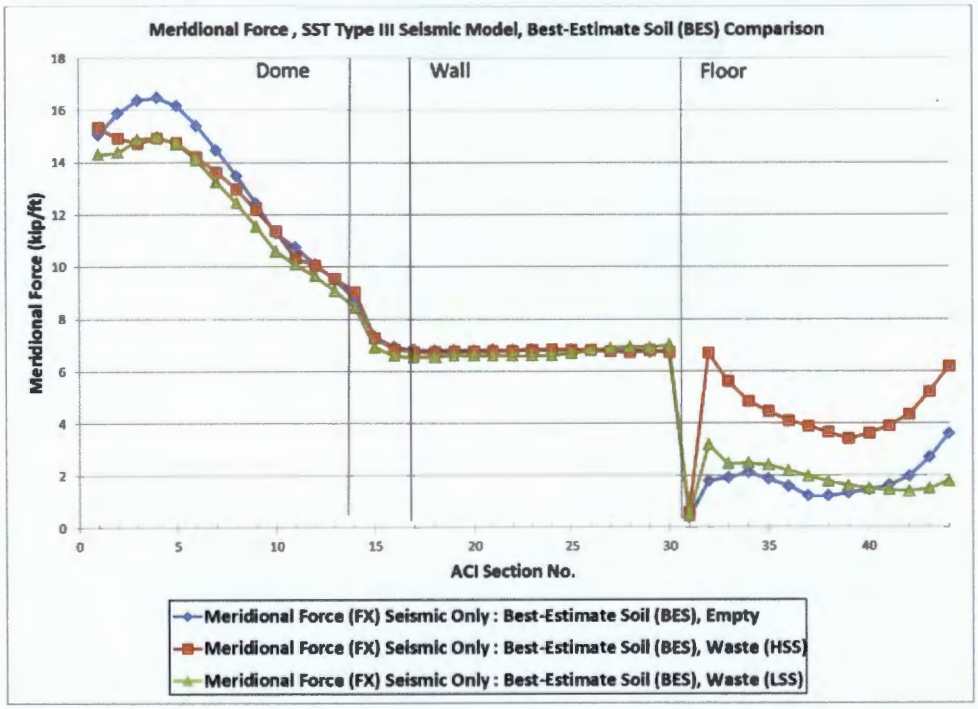

Figure 9.1. Best Estimate Soil (BES): Concrete Tank Meridional Force – Seismic Only

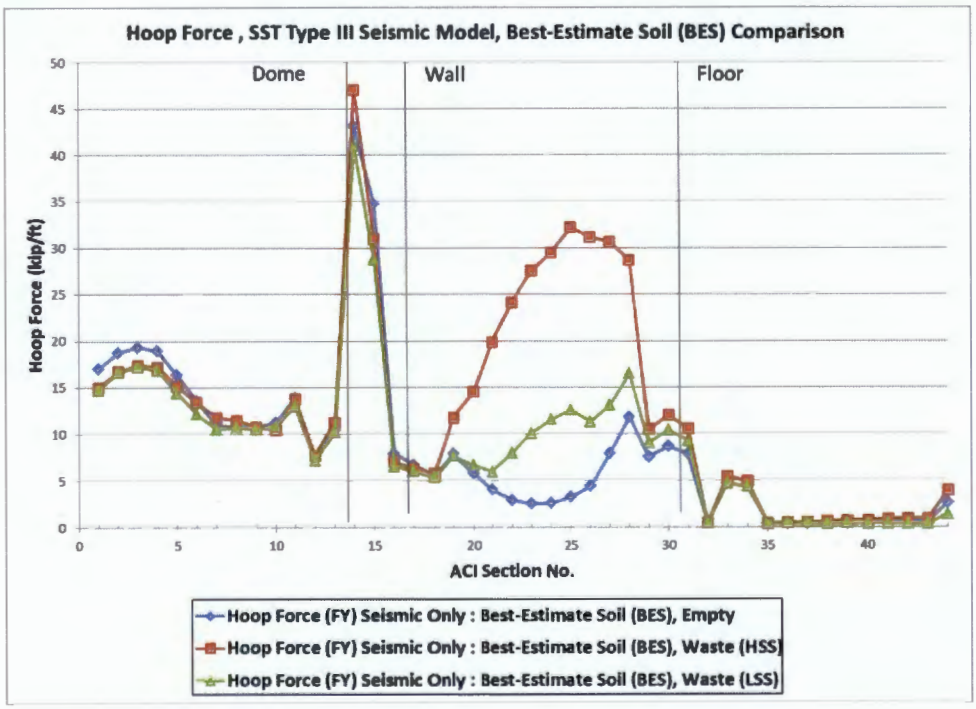

Figure 9.2. Best Estimate Soil (BES): Concrete Tank Hoop Force – Seismic Only

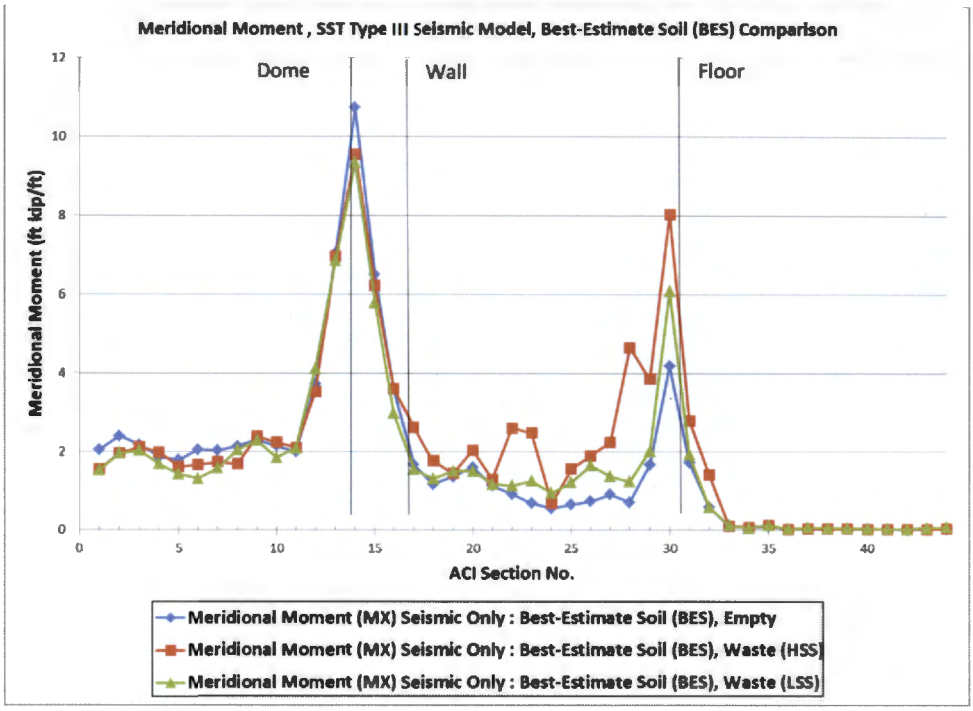

Figure 9.3. Best Estimate Soil (BES): Concrete Tank Meridional Moment – Seismic Only

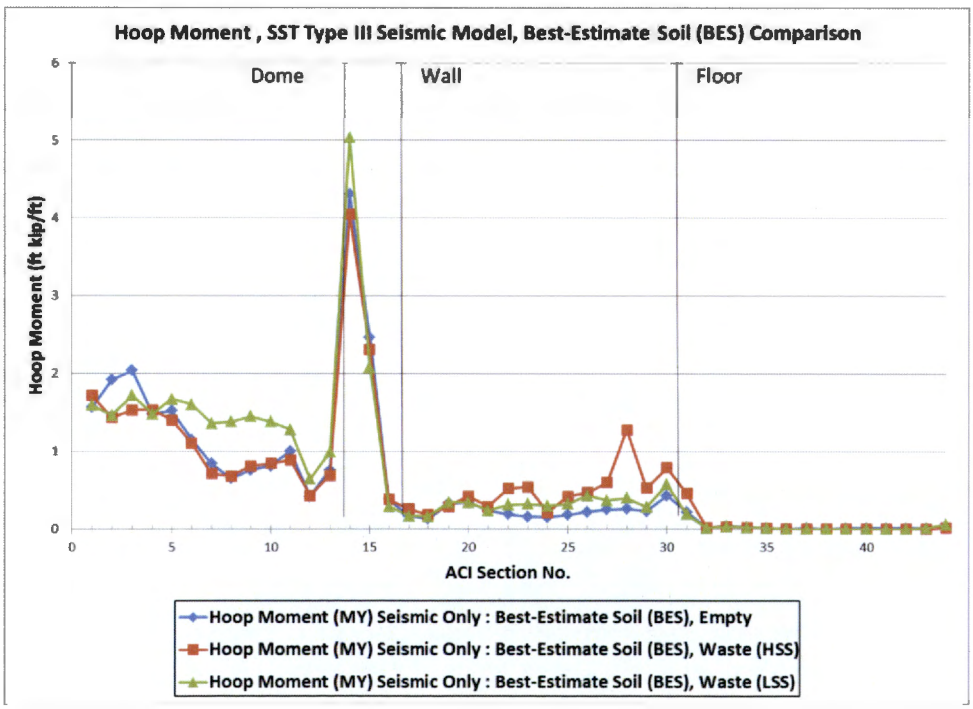

Figure 9.4. Best Estimate Soil (BES): Concrete Tank Hoop Moment – Seismic Only

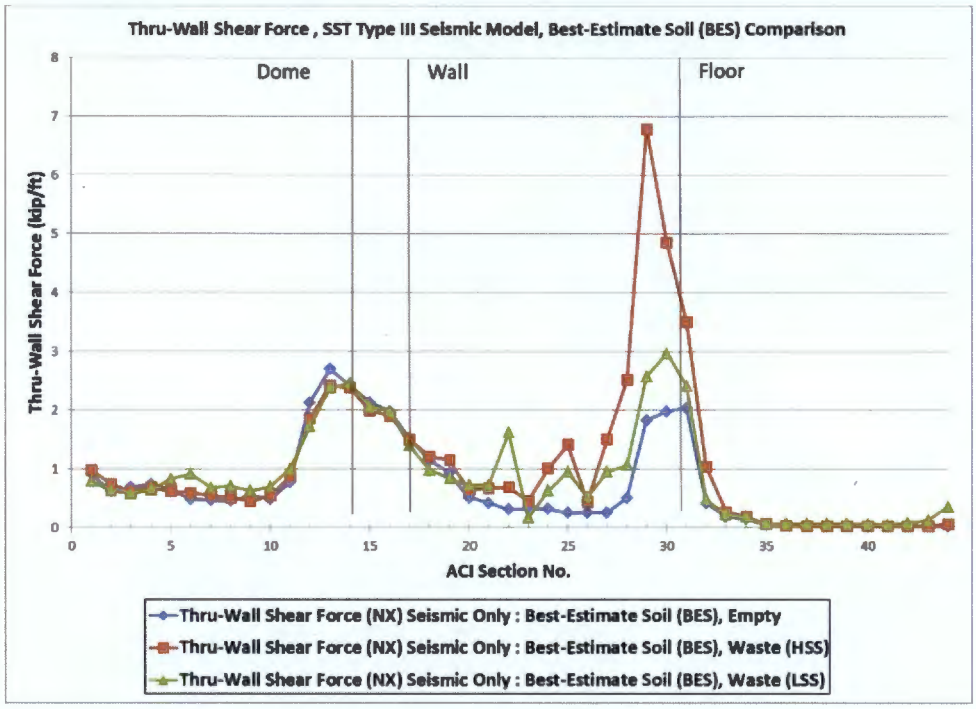

Figure 9.5. Best Estimate Soil (BES): Concrete Tank Through-Wall Shear Force – Seismic Only

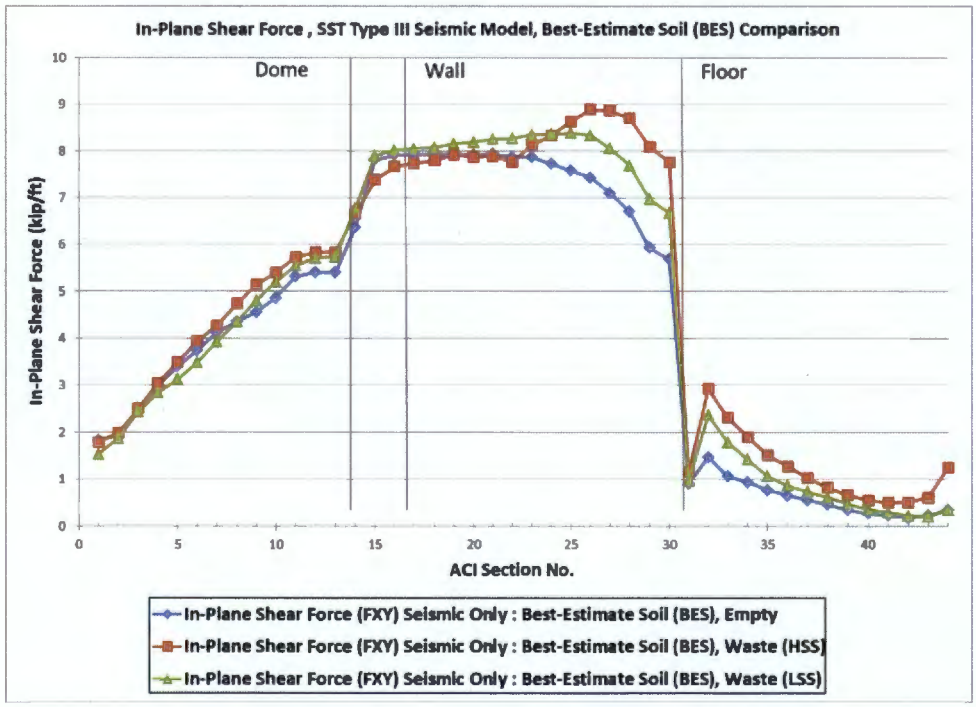

Figure 9.6. Best Estimate Soil (BES): Concrete Tank In-Plane Shear Force – Seismic Only

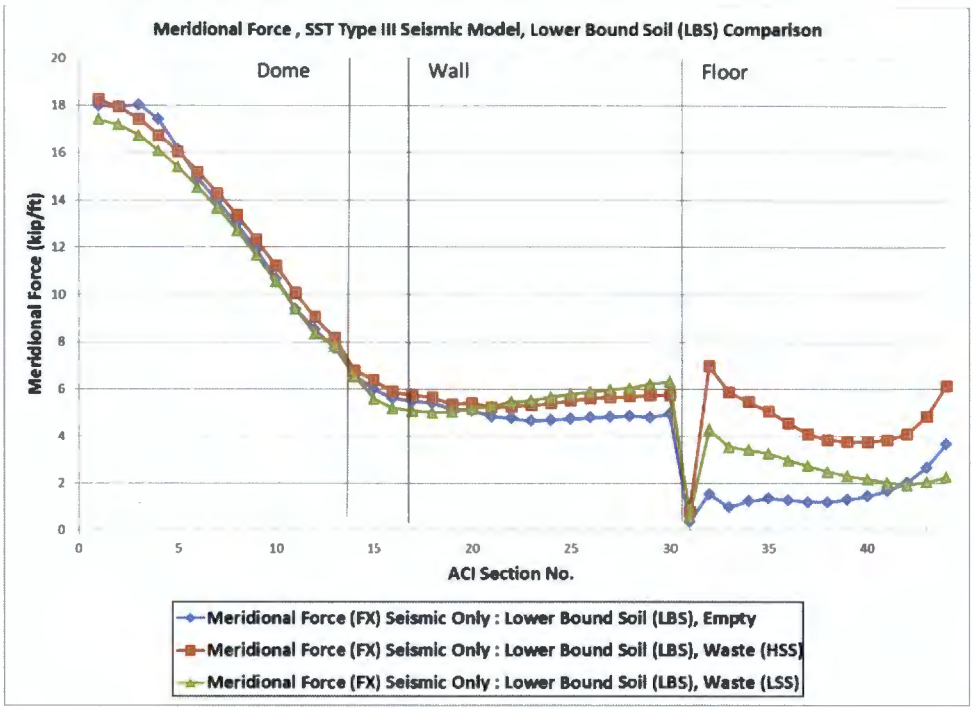

Figure 9.7. Lower Bound Soil (LBS): Concrete Tank Meridional Force – Seismic Only

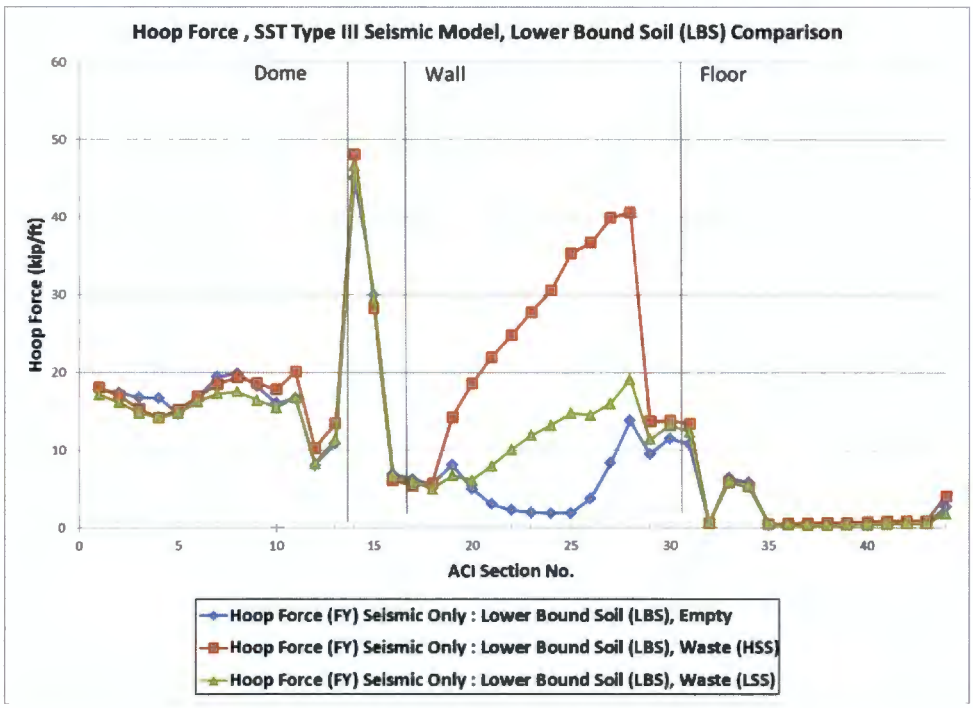

Figure 9.8. Lower Bound Soil (LBS): Concrete Tank Hoop Force – Seismic Only

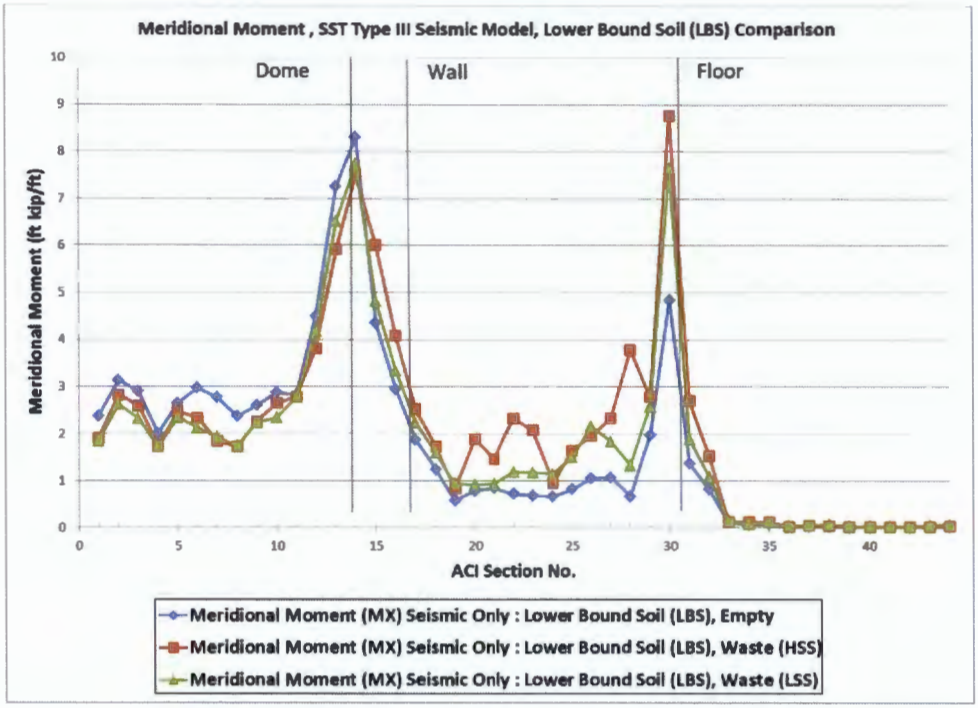

Figure 9.9. Lower Bound Soil (LBS): Concrete Tank Meridional Moment – Seismic Only

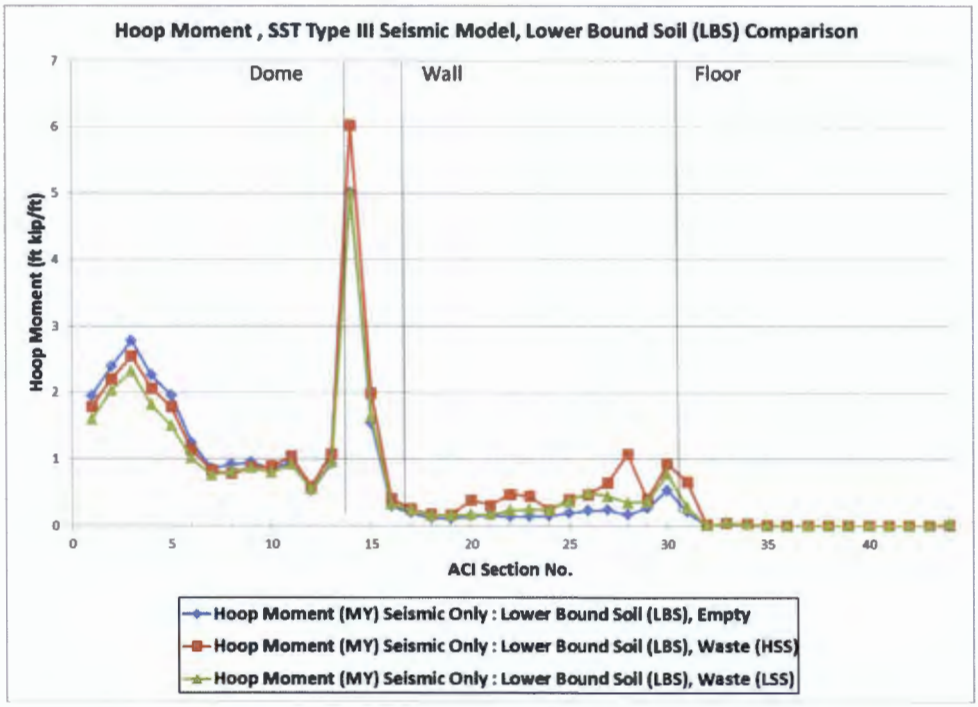

Figure 9.10. Lower Bound Soil (LBS): Concrete Tank Hoop Moment – Seismic Only

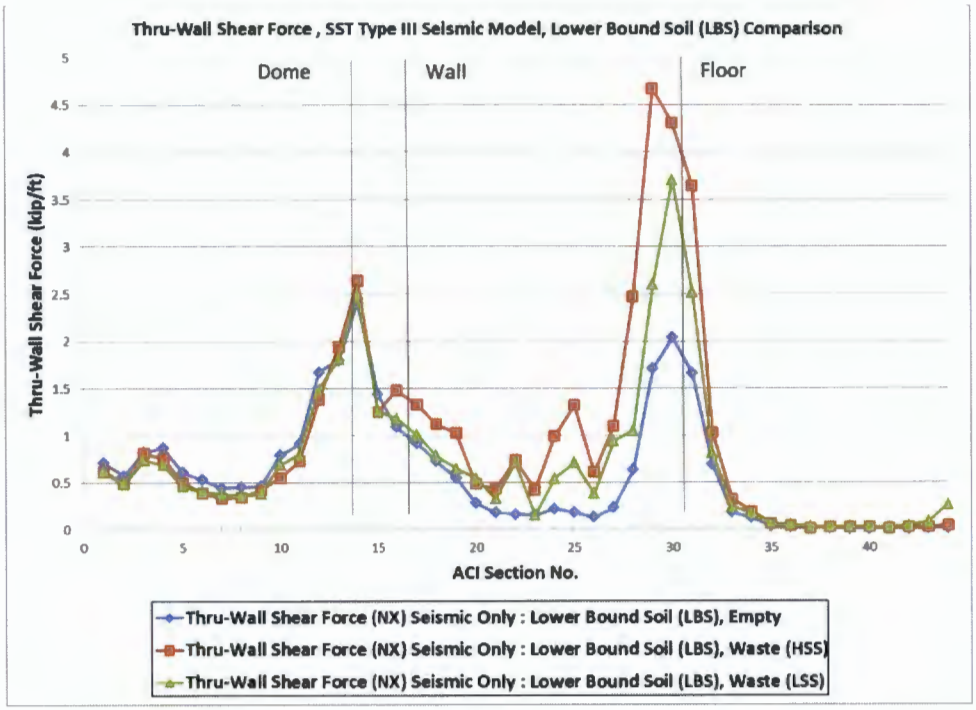

Figure 9.11. Lower Bound Soil (LBS): Concrete Tank Through-Wall Shear Force – Seismic Only

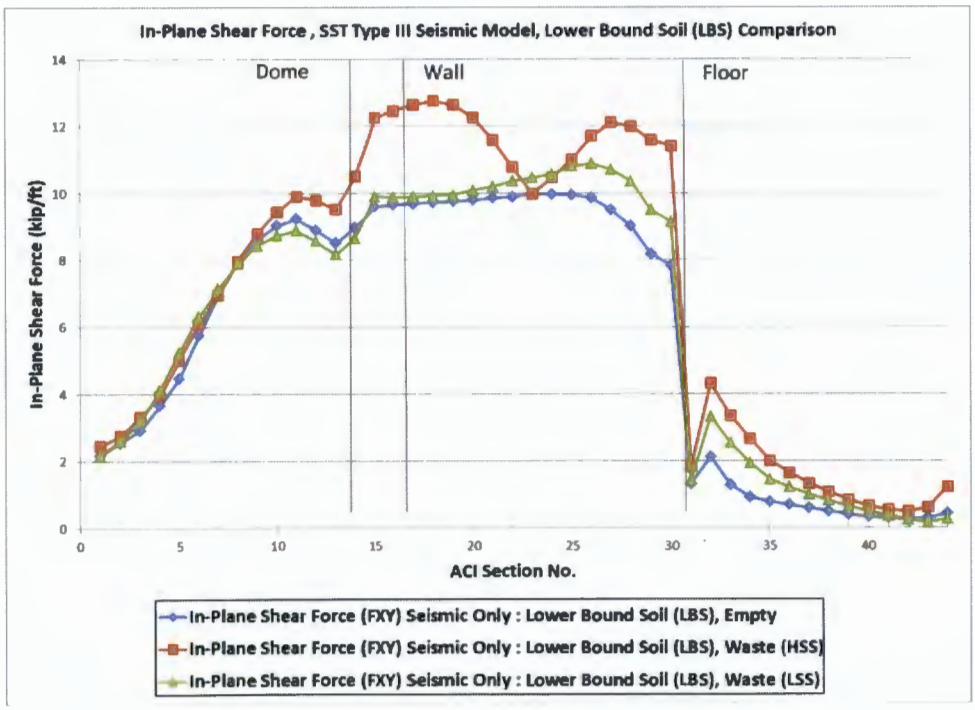

Figure 9.12. Lower Bound Soil (LBS): Concrete Tank In-Plane Shear Force – Seismic Only

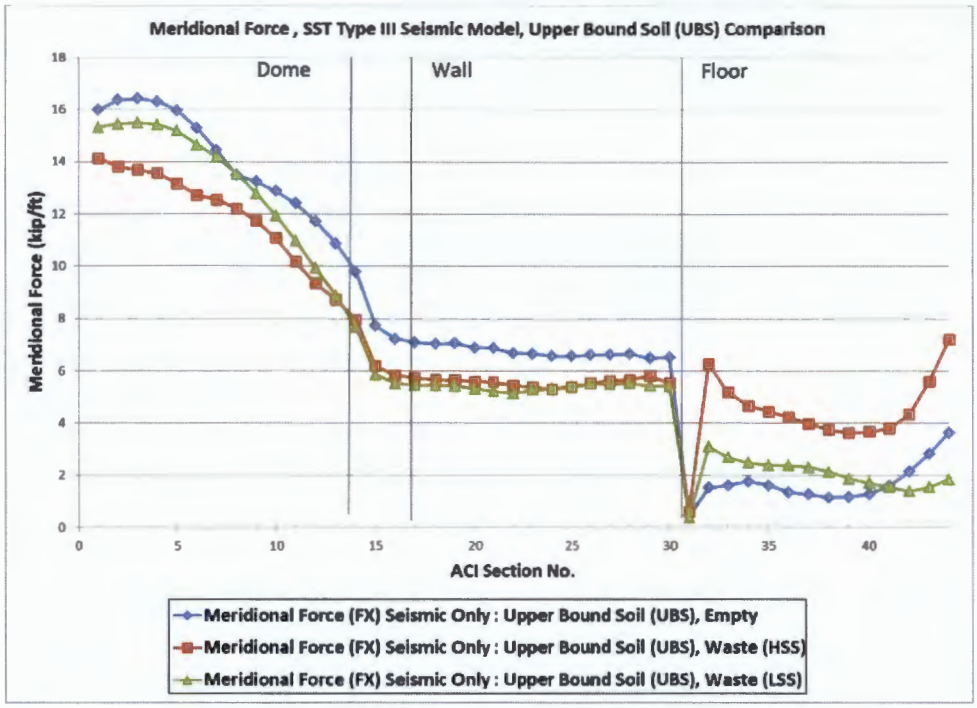

Figure 9.13. Upper Bound Soil (UBS): Concrete Tank Meridional Force – Seismic Only

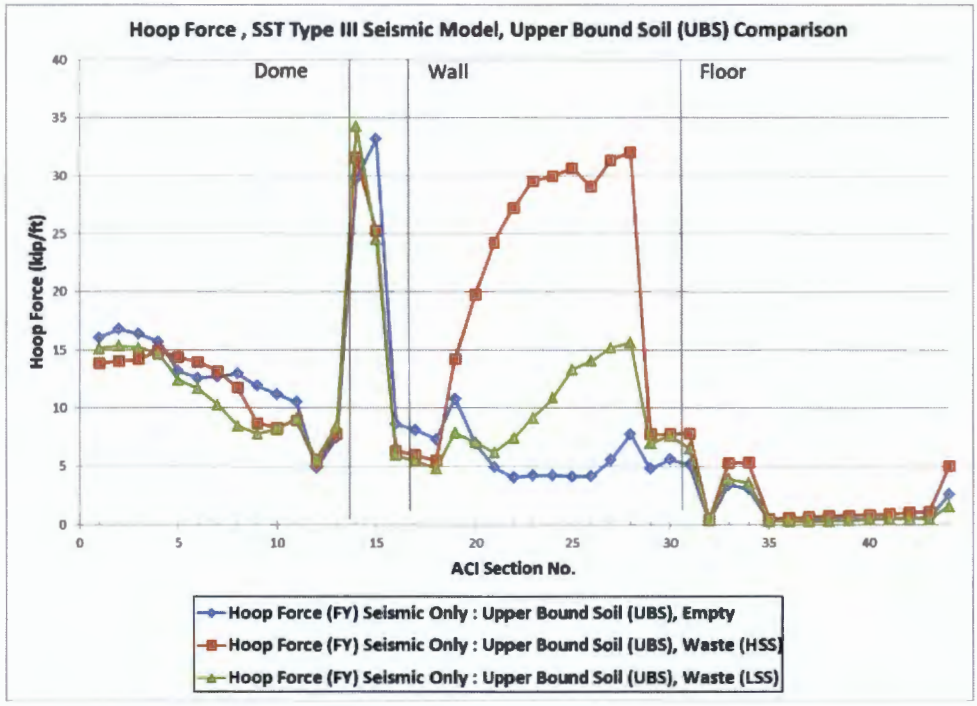

Figure 9.14. Upper Bound Soil (UBS): Concrete Tank Hoop Force – Seismic Only

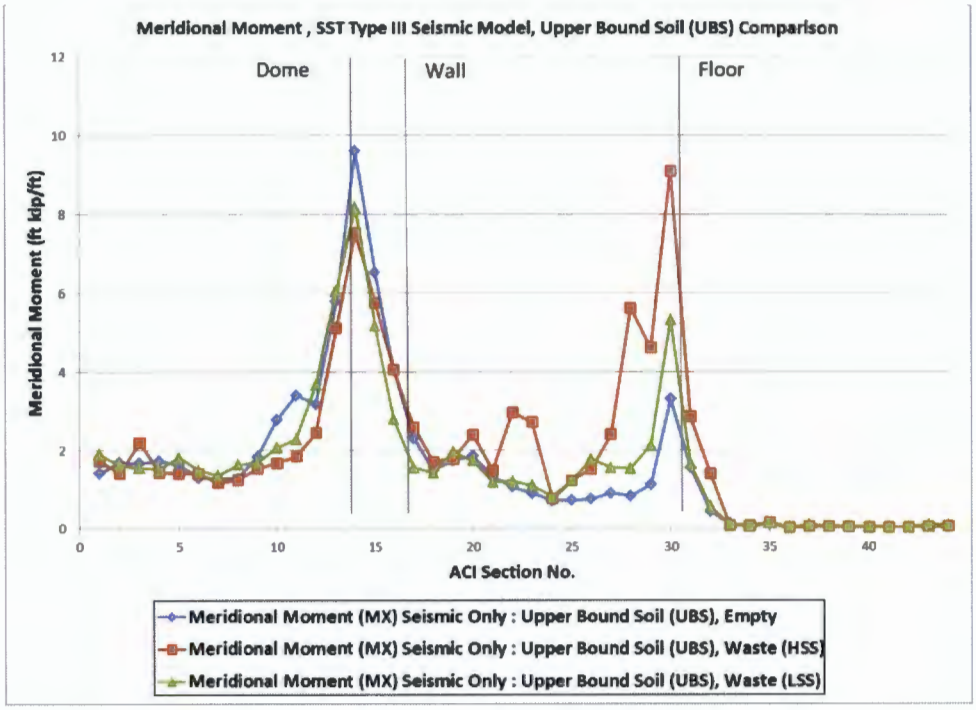

Figure 9.15. Upper Bound Soil (UBS): Concrete Tank Meridional Moment – Seismic Only

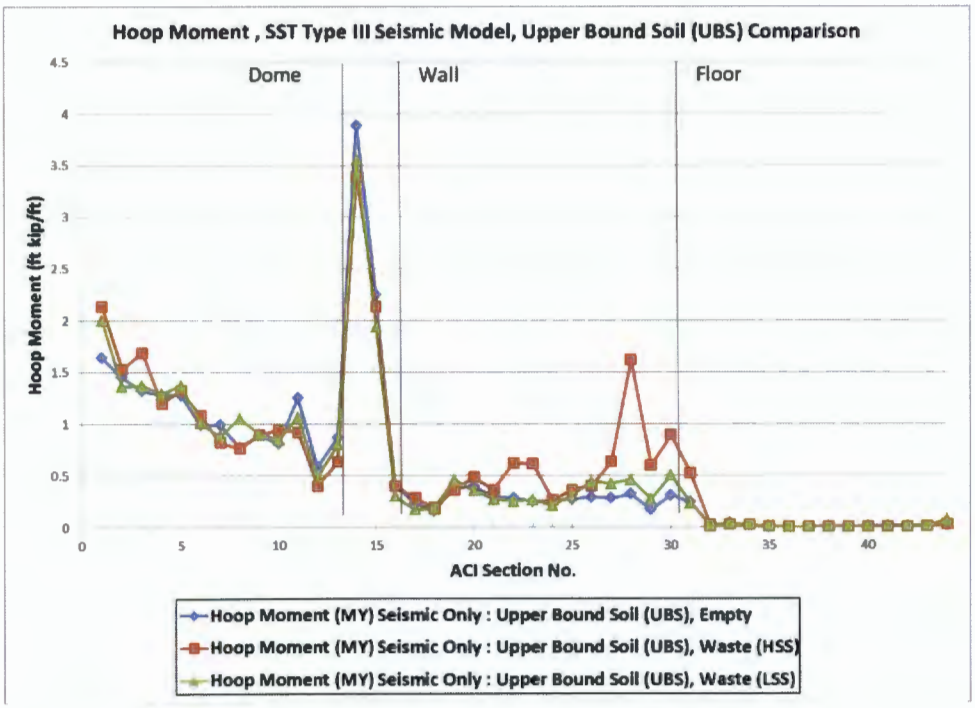

Figure 9.16. Upper Bound Soil (UBS): Concrete Tank Hoop Moment – Seismic Only

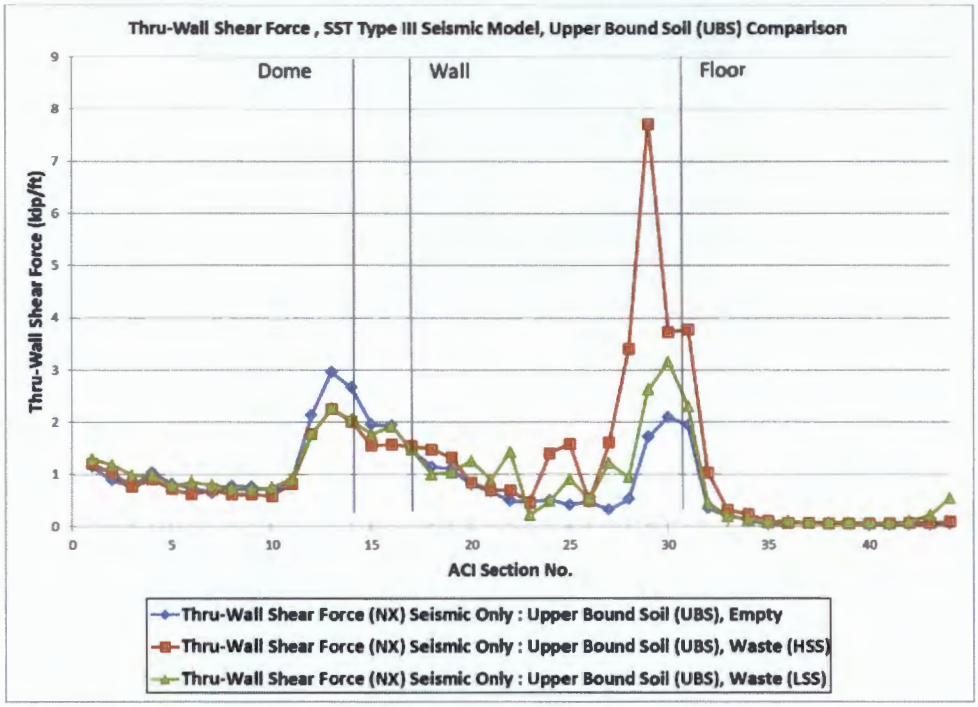

Figure 9.17. Upper Bound Soil (UBS): Concrete Tank Through-Wall Shear Force – Seismic Only

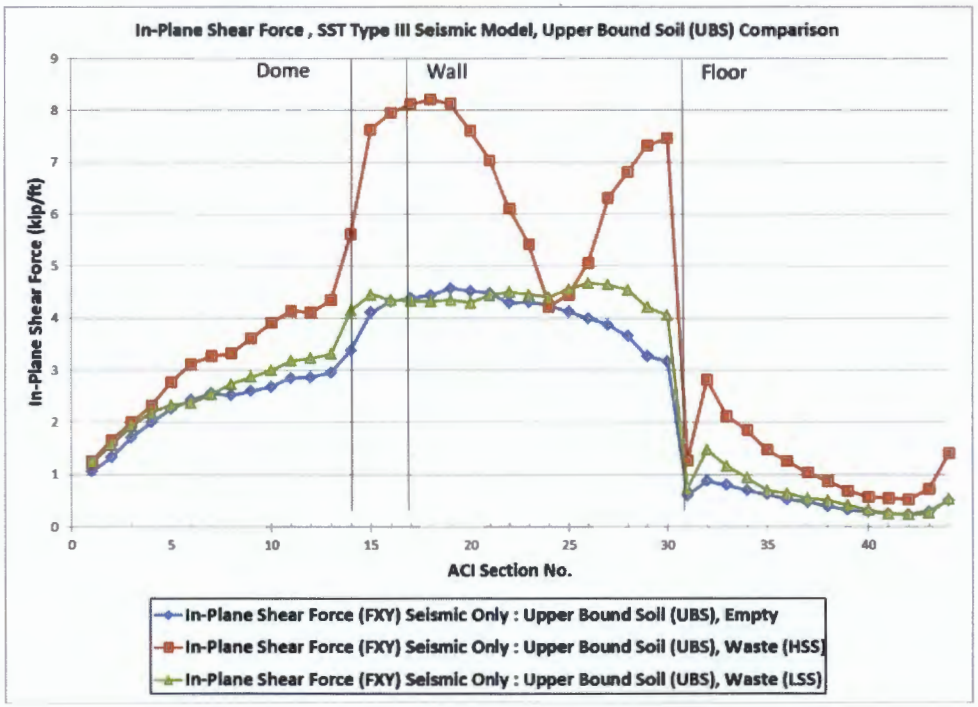

Figure 9.18. Upper Bound Soil (UBS): Concrete Tank In-Plane Shear Force – Seismic Only

Figure 9.1 through Figure 9.18 showed concrete demands for each of the soil cases. Figure 9.19 through Figure 9.24 show the same information, but include all soil cases on one plot in order to identify trends in the demands.

The seismic-only meridional forces in Figure 9.19 show similar trends in the dome and wall. The greatest demands in the slab are for a full tank higher modulus waste and the least demands are for an empty tank.

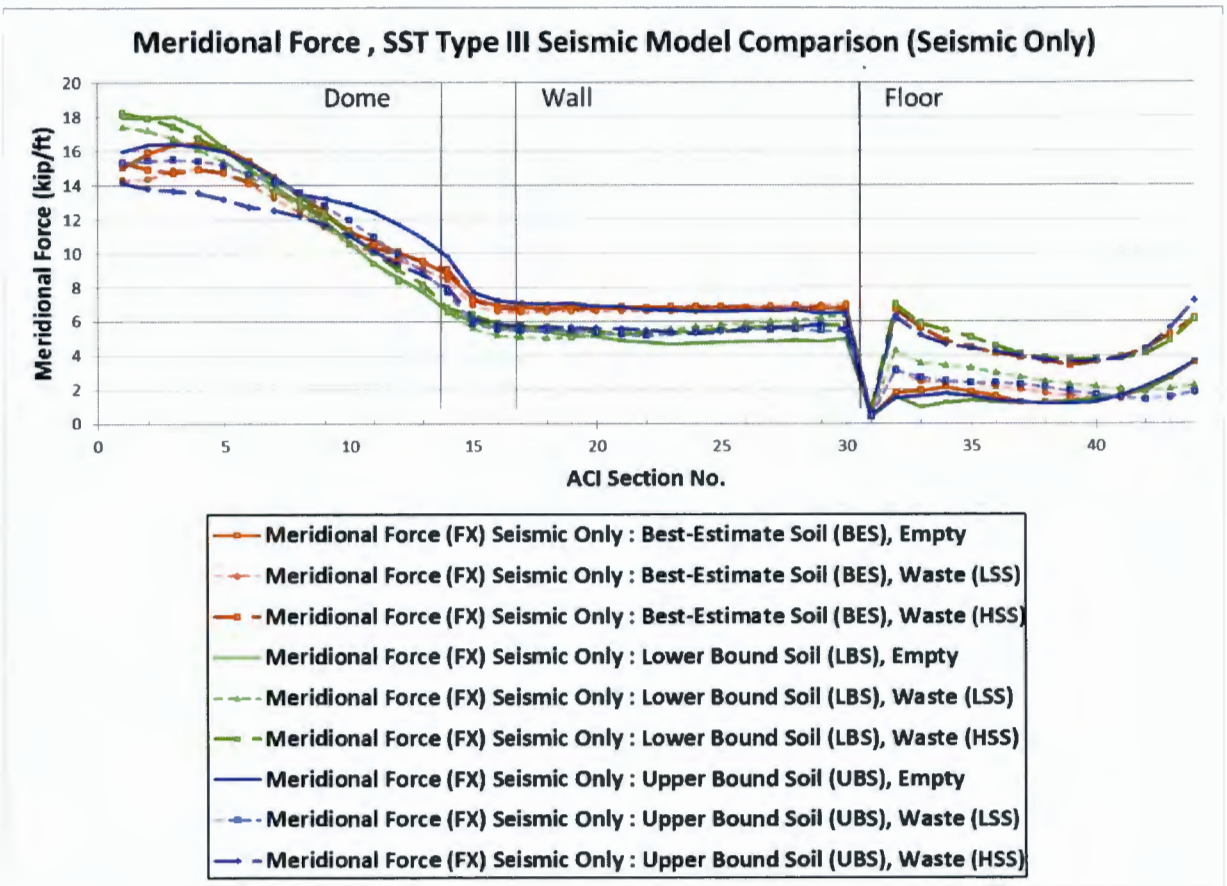

Figure 9.19. Seismic Results: Concrete Tank Meridional Force – Seismic Only

The seismic-only hoop forces in Figure 9.20 show that the hoop force in the dome tends to increase for the softer soil. In the wall, the presence of waste increases hoop force demands, with greater increases coming from stiffer waste. Demands in the slab are all low.

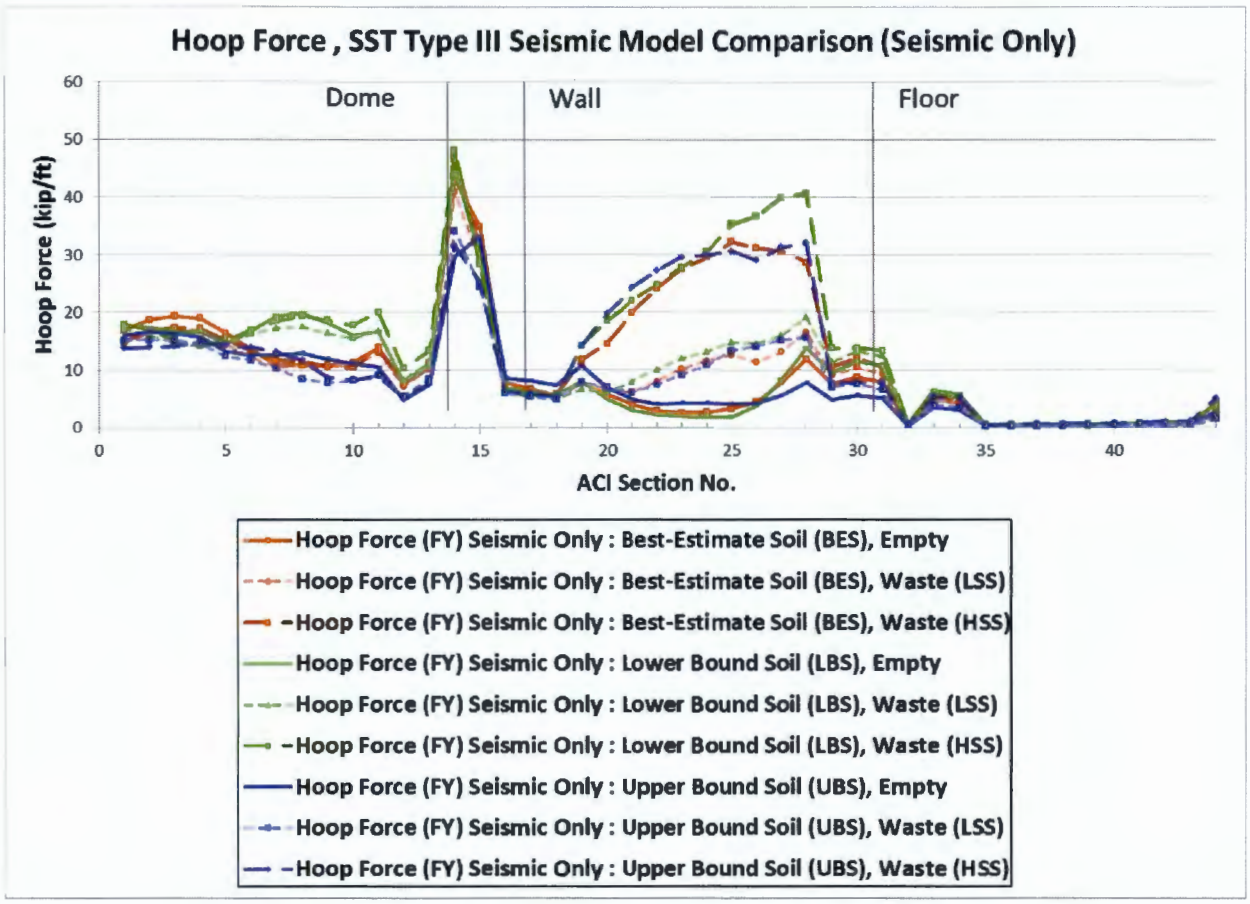

Figure 9.20. Seismic Results: Concrete Tank Hoop Force – Seismic Only

The seismic-only meridional moments in Figure 9.21 show that the greatest demands in the dome are for LBS, and the least demands are for UBS. The greatest demands in the wall are for full tank higher modulus waste, and the least demands are for an empty tank. Demands in the slab are all low.

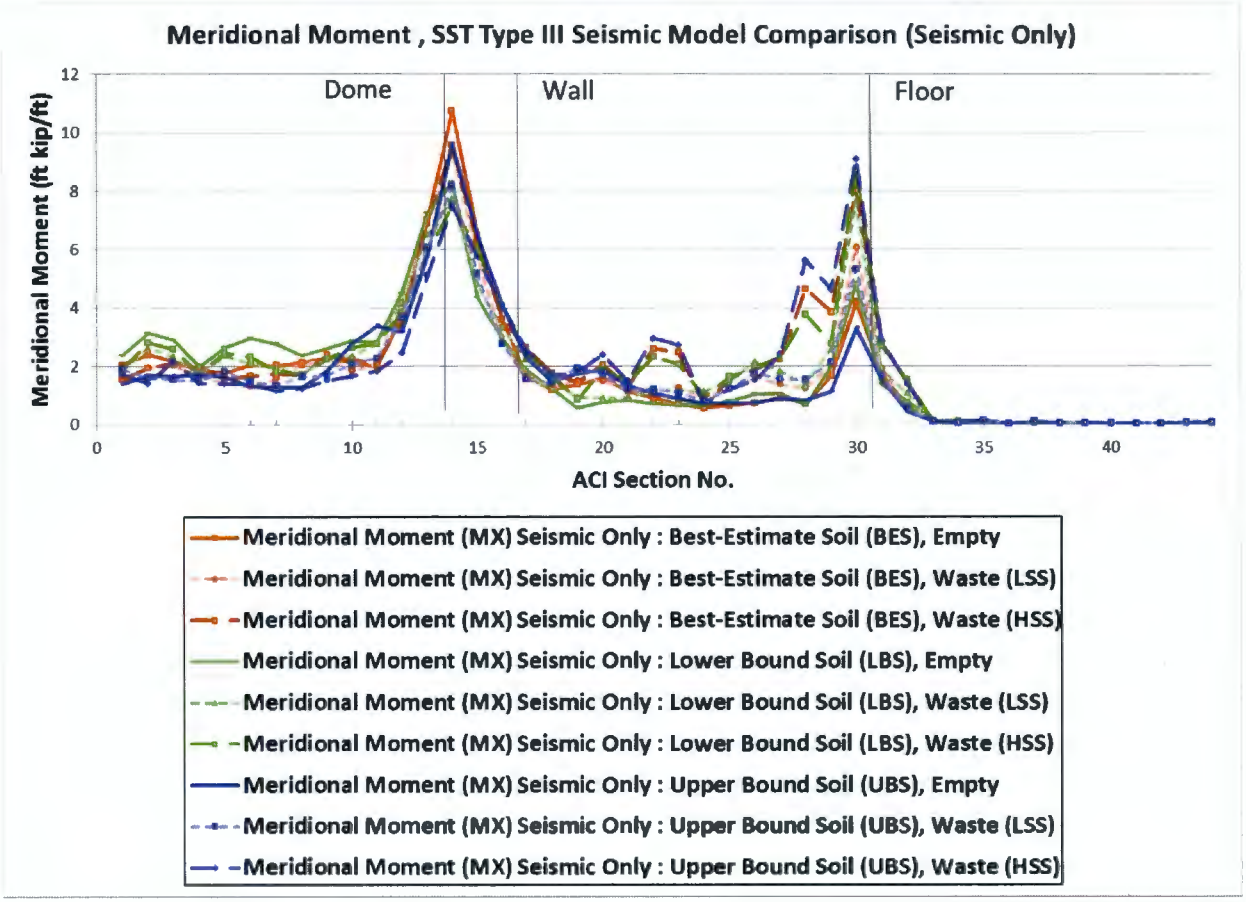

Figure 9.21. Seismic Results: Concrete Tank Meridional Moment – Seismic Only

The seismic-only hoop moments in Figure 9.22 show that higher demands in the dome and haunch occur for softer soil. Limited evidence of grouping can be seen at several points in the wall, with the greatest demands in the wall for full tank higher modulus waste, and the least demands for an empty tank. Demands in the slab are negligible in all cases.

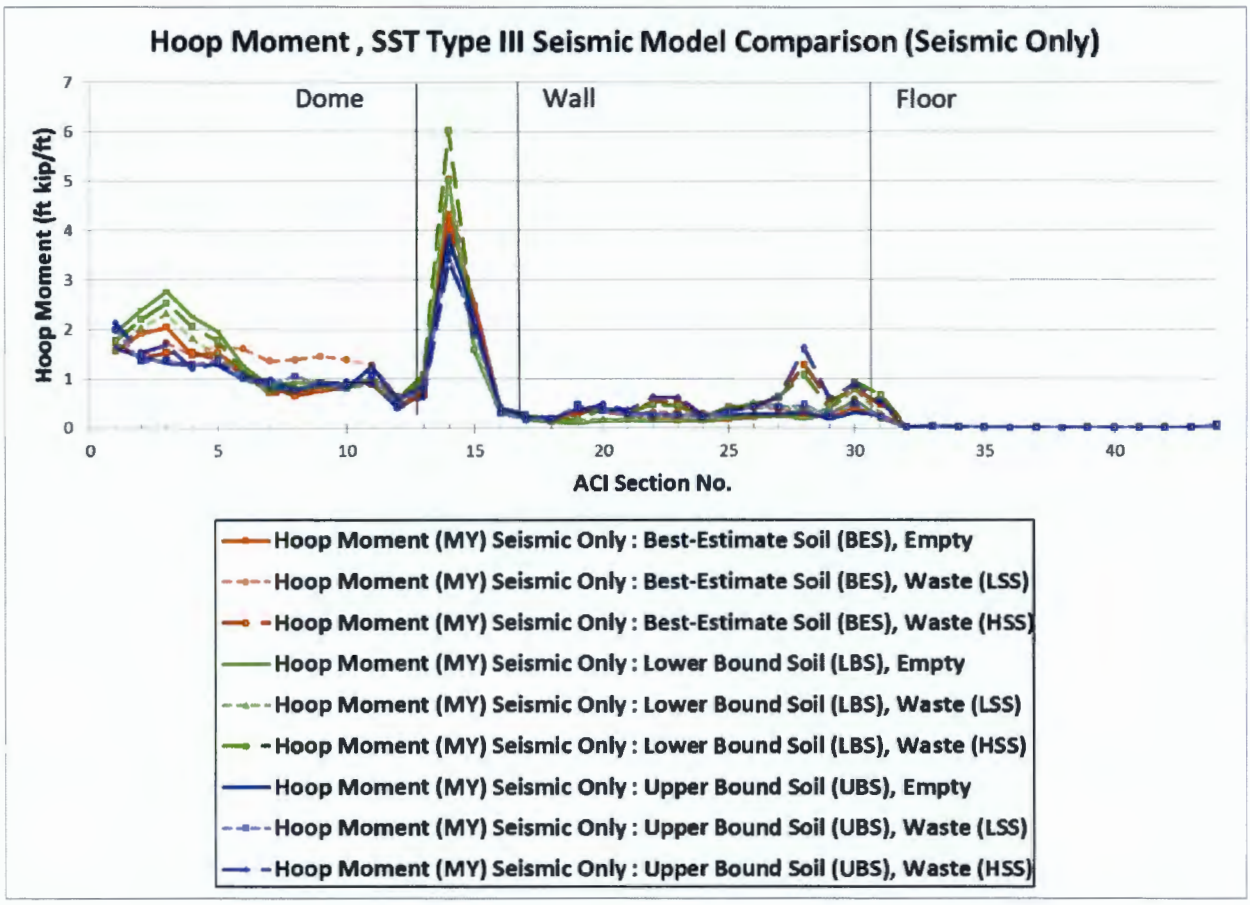

Figure 9.22. Seismic Results: Concrete Tank Hoop Moment – Seismic Only

The seismic-only through-wall shear forces in Figure 9.23 show the greatest demands in the dome are for UBS and the least demands are for LBS. The greatest demands in the wall are for full tank lower modulus waste, and the least demands are for empty tank. Demands in the slab are negligible in all cases.

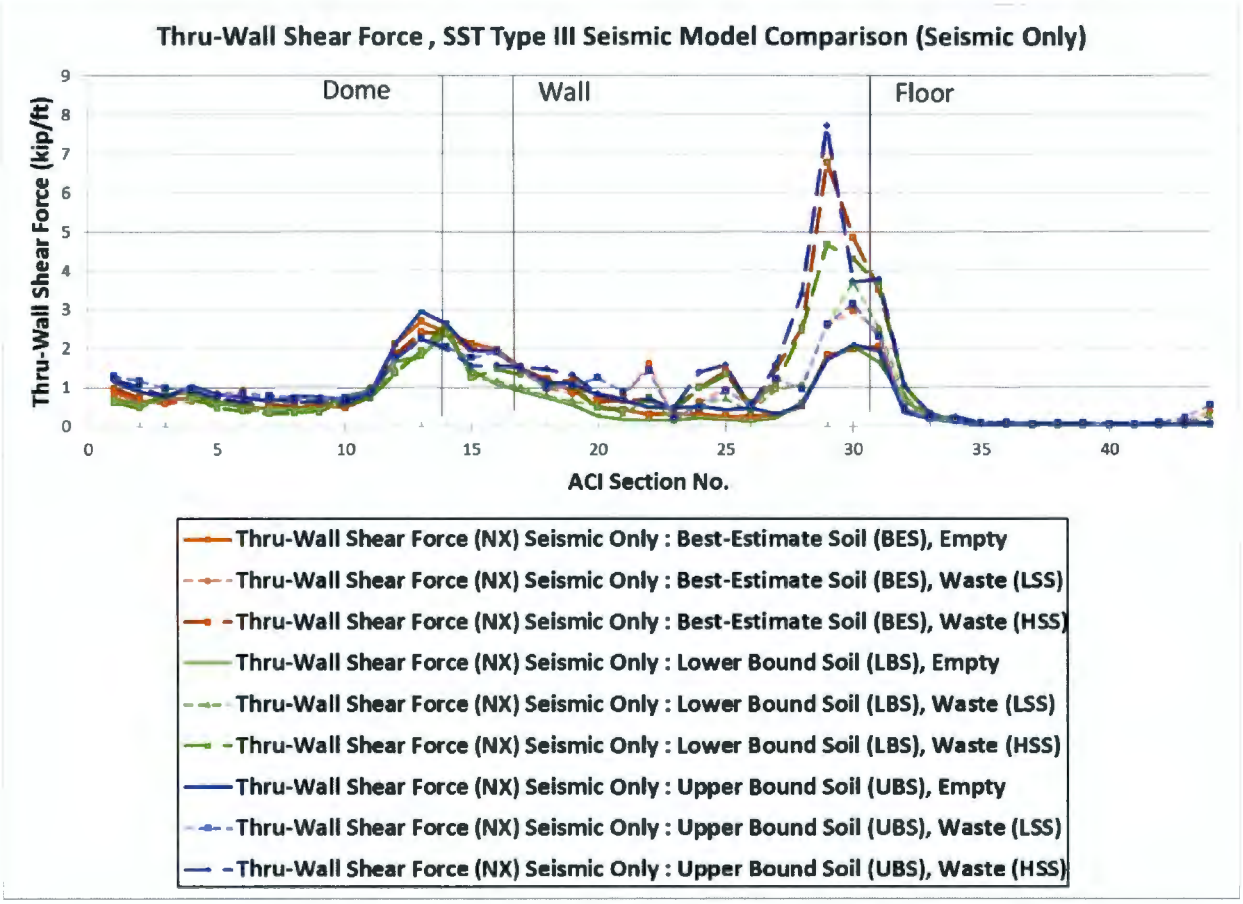

Figure 9.23. Seismic Results: Concrete Tank Through-Wall Shear Force – Seismic Only

The seismic-only in-plane shear forces in Figure 9.24 show grouping in the dome and wall based on soil configuration, transitioning to grouping in the slab based on the waste configuration, and converging toward the center of the slab. The greatest demands are for LBS and the least demands are for UBS. Among the groupings according to soil configuration, the greatest demands are generally for full tank higher modulus waste, and the least demands are for empty tank. Thus, demands in the dome and wall generally decrease as a function of increasing soil stiffness.

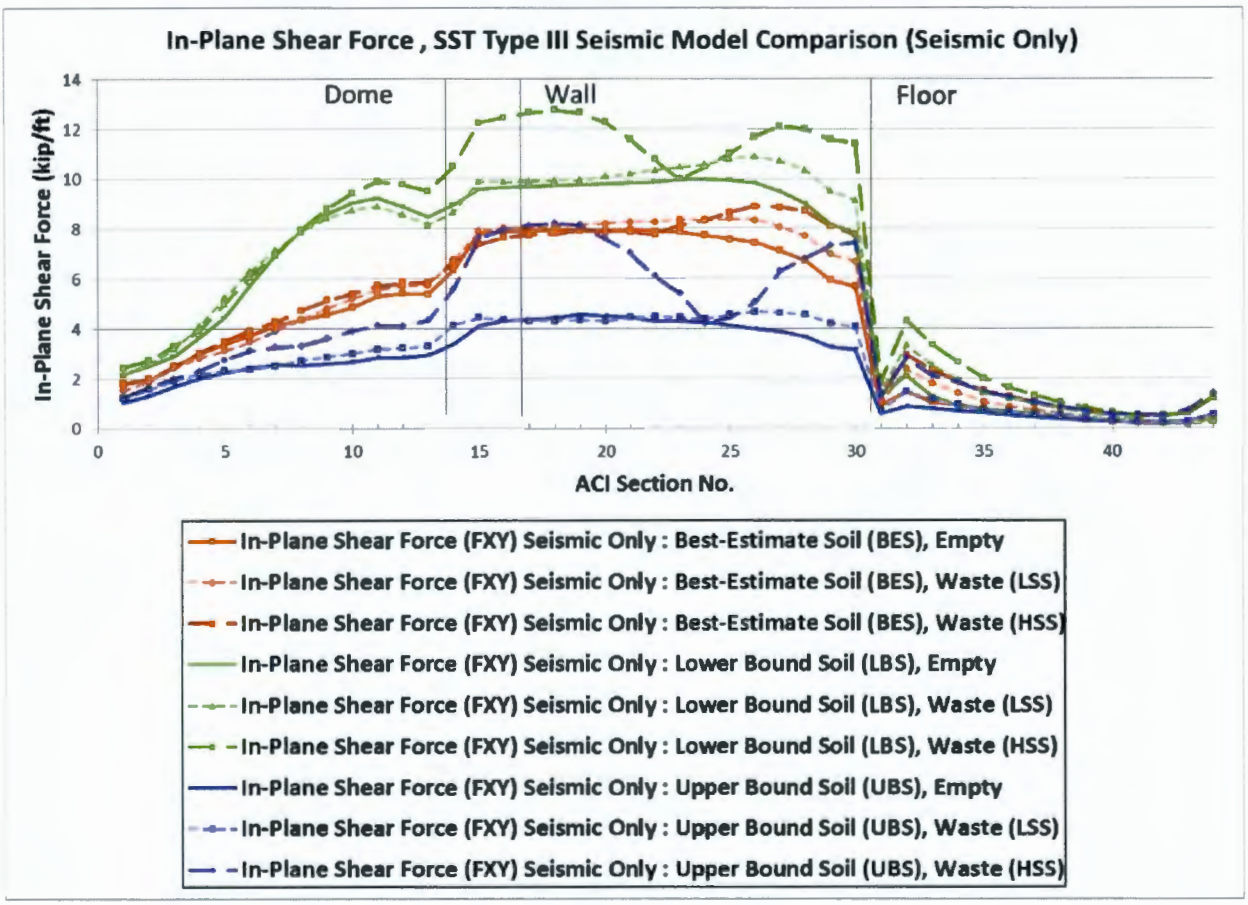

Figure 9.24. Seismic Results: Concrete Tank In-Plane Shear Force – Seismic Only

9.1.1 Summary of Seismic Demands

Seismic forces and moments typically show maximum values in the haunch, or near the footing. Smaller peaks can often be seen in the lower wall. Meridional force starts at a maximum at the apex, decreasing toward the slab. Hoop force is maximum at the haunch, then dropping sharply before increasing again in the lower wall. Meridional moment is greatest near the haunch and footing. Hoop moment is greatest near the haunch. Through-wall shear forces peak in the lower wall. In-plane shear is maximum in the wall, decreasing toward the dome and slab. All seismic demands in the floor are small relative to other locations.

LBS tends to create the greatest demands overall. The dome is sensitive primarily to the soil configuration and insensitive to the waste configuration. The wall shows a stronger sensitivity to the waste configuration, but overall tends to be varied in sensitivity to either the soil or waste configuration.

Where the influence of waste in the wall is significant, the demands in the wall are greatest for full tank higher modulus (stiff) waste, and the least demands are for empty tank. The in-plane shear forces in the wall show the most sensitivity to the soil configuration. The hoop forces in the wall show the most sensitivity to the waste configuration.

9.2 Soil Contact Results

Soil contact results are post-processed using the same methods as for the concrete tank forces and moments. Figures are grouped in sets showing the force or moment for gravity-only first, then only the seismic portion. The contact results are plotted against a "path" which starts at the dome apex and increasing to the floor center. Contact results have been enveloped circumferentially for these plots. Contact results plots are as follows:

- Figure 9.25. Soil/Concrete Contact Element Normal Pressure – Soil/Concrete Contact Element Normal Pressure – Gravity Only
- Figure 9.26. Soil/Concrete Contact Element Bounding Normal Pressure – Soil/Concrete Contact Element Bounding Normal Pressure – Seismic Only
- Figure 9.27. Soil/Concrete Contact Element Meridional Shear – Soil/Concrete Contact Element Meridional Shear – Seismic Only
- Figure 9.28. Soil/Concrete Contact Element Hoop Shear – Soil/Concrete Contact Element Hoop Shear – Seismic Only
- Figure 9.29. Soil/Concrete Contact Element Lateral Displacement (Sliding) – Seismic Only
- The contact pressure gravity results are included to demonstrate the effectiveness of the slip planes in the soil overburden above the dome and the at-rest adjustments in the wall. For more details, see Section 6.2. The other contact results are of secondary importance.

The gravity-only soil/concrete contact element normal pressures in Figure 9.25 all follow the theoretical at-rest profile in the dome and wall. The soil/concrete contact element normal pressures show little sensitivity to the soil or waste configuration. The trends diverge significantly from the wall into the slab, with full tank configurations highest and empty tanks as the lowest.

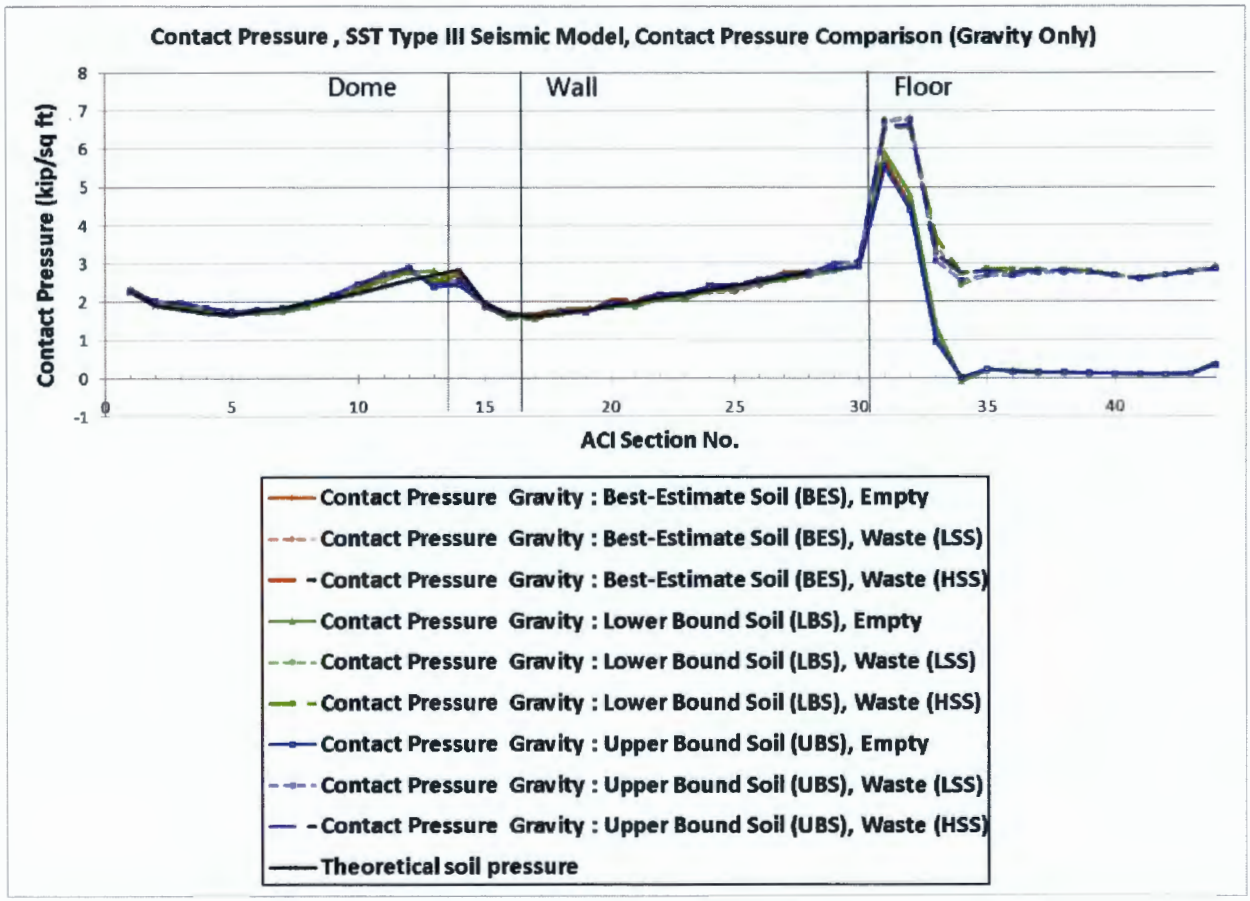

Figure 9.25. Soil/Concrete Contact Element Normal Pressure – Gravity Only

The seismic-only soil/concrete contact element bounding normal pressure in Figure 9.26 shows no clear grouping in the dome. There is grouping in the wall and slab based on waste configuration, with the greatest demands in the wall and slab are for higher modulus waste and the least demands for an empty tank. Among the waste configuration groupings in the wall and slab, UBS tends to create the highest demand and LBS the least demand.

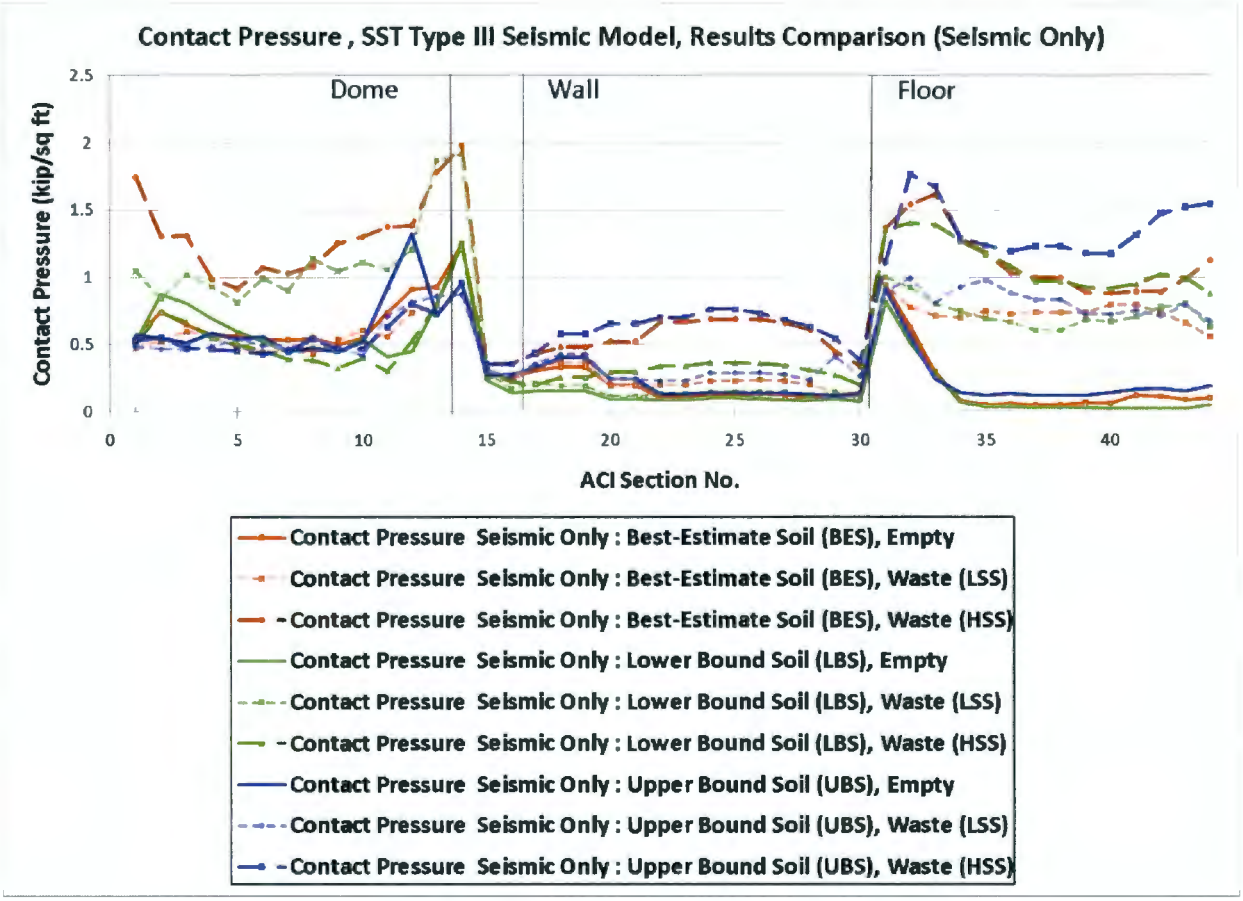

Figure 9.26. Soil/Concrete Contact Element Bounding Normal Pressure – Seismic Only

The seismic-only soil/concrete contact element meridional shear in Figure 9.27 shows grouping in the inner dome based on soil configuration. The demands in the wall are all similar. For groupings in the dome according to soil configuration, LBS (BES is similar) has the greatest demand and UBS has the least demand.

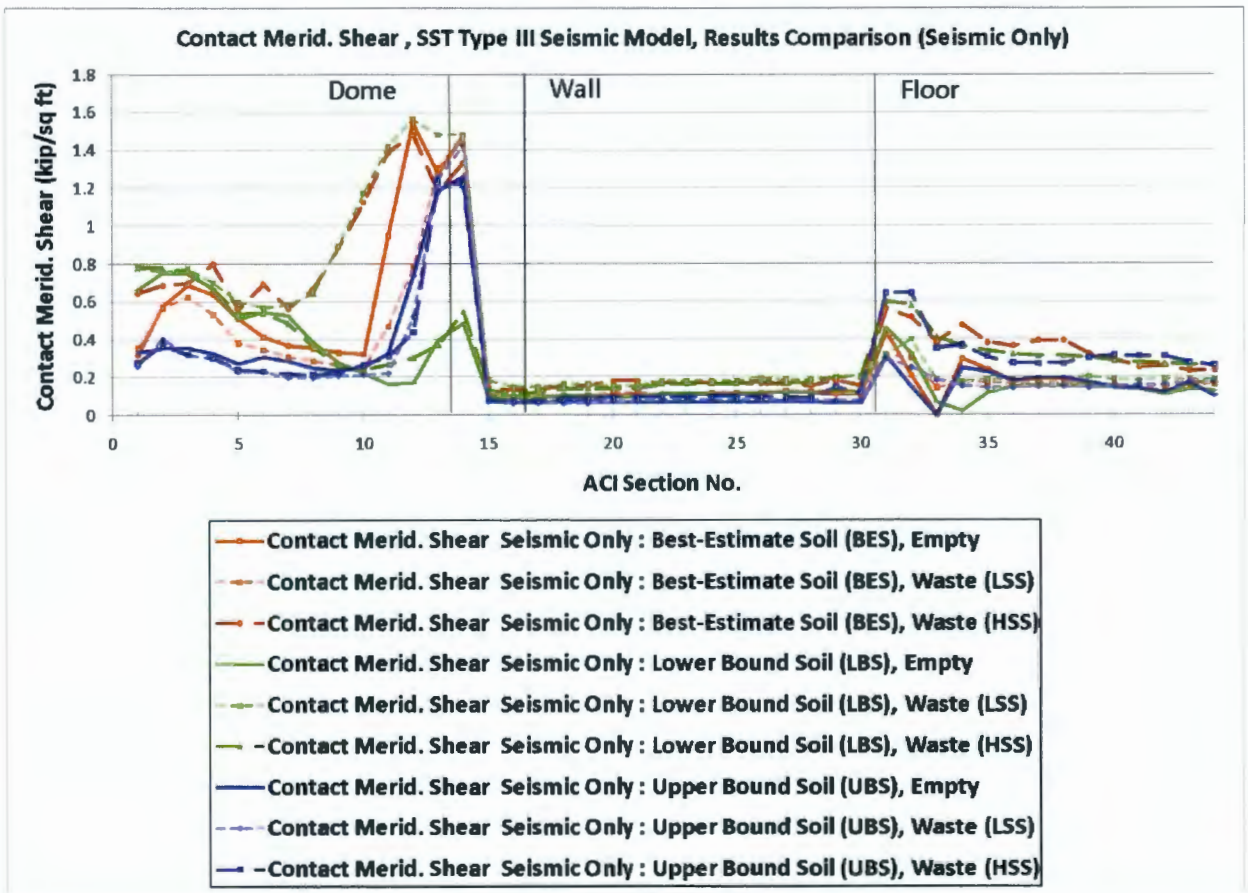

Figure 9.27. Soil/Concrete Contact Element Meridional Shear – Seismic Only

The seismic-only soil/concrete contact element hoop shear in Figure 9.28 shows grouping in the dome based on soil configuration, transitioning to grouping in the slab based on waste configuration. For groupings in the dome according to soil configuration, LBS has the greatest demand and UBS has the least demand. The demands in the haunch tend to increase with decreasing soil stiffnes. For groupings in the wall and slab according to waste configuration, higher modulus waste has the greatest demand and empty tank has the least demand.

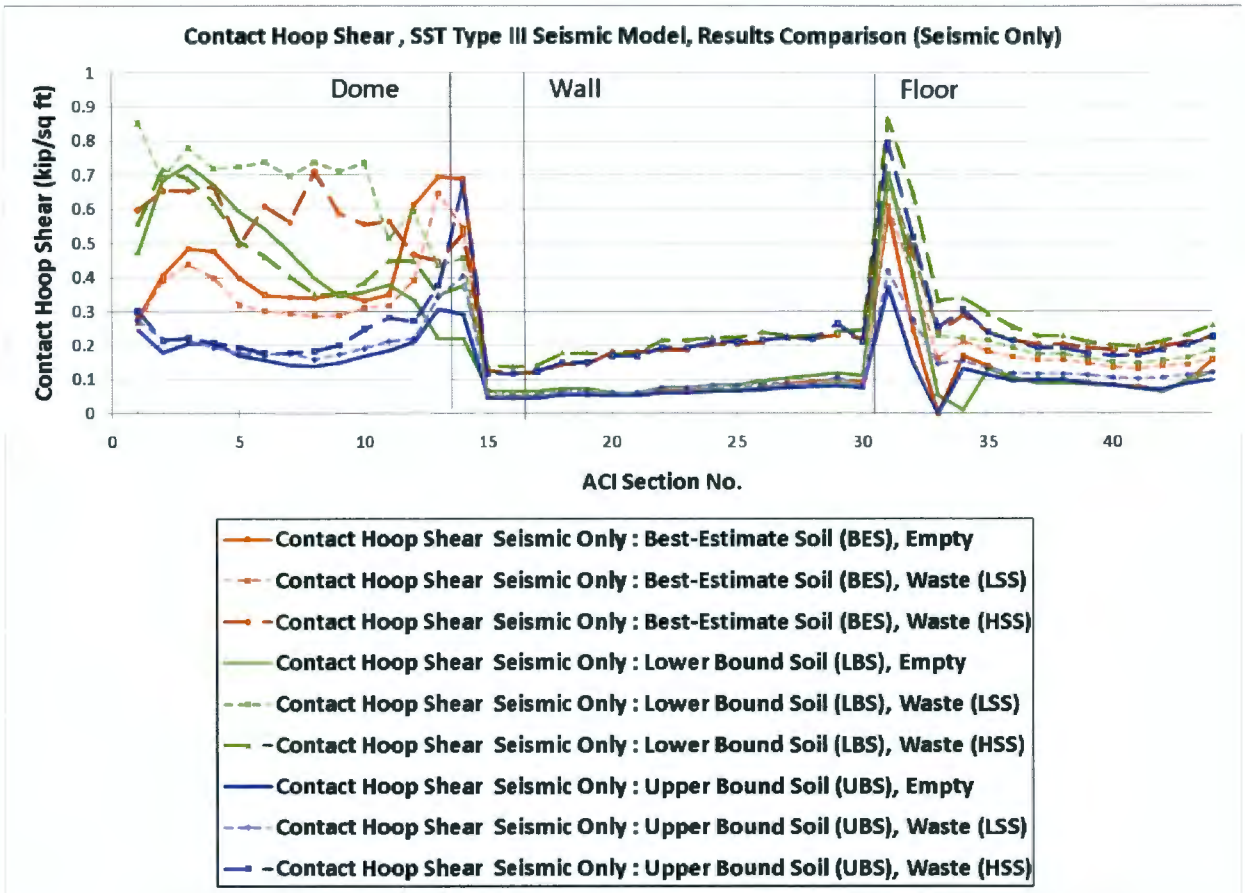

Figure 9.28. Soil/Concrete Contact Element Hoop Shear – Seismic Only

The seismic-only soil/concrete contact element lateral displacement in Figure 9.29 shows clear grouping in the dome based on soil configuration transitioning to grouping in the slab based on waste configuration. Within groupings in the wall according to soil configuration, an empty tank has the least displacement. Trends in the slab generally follow a similar pattern, except that the empty tank configurations all show increased displacements relative to the other locations. Thus, the waste has a significant influence at the slab. At all locations, the LBS group typically has the greatest displacement and the UBS group has the least displacement.

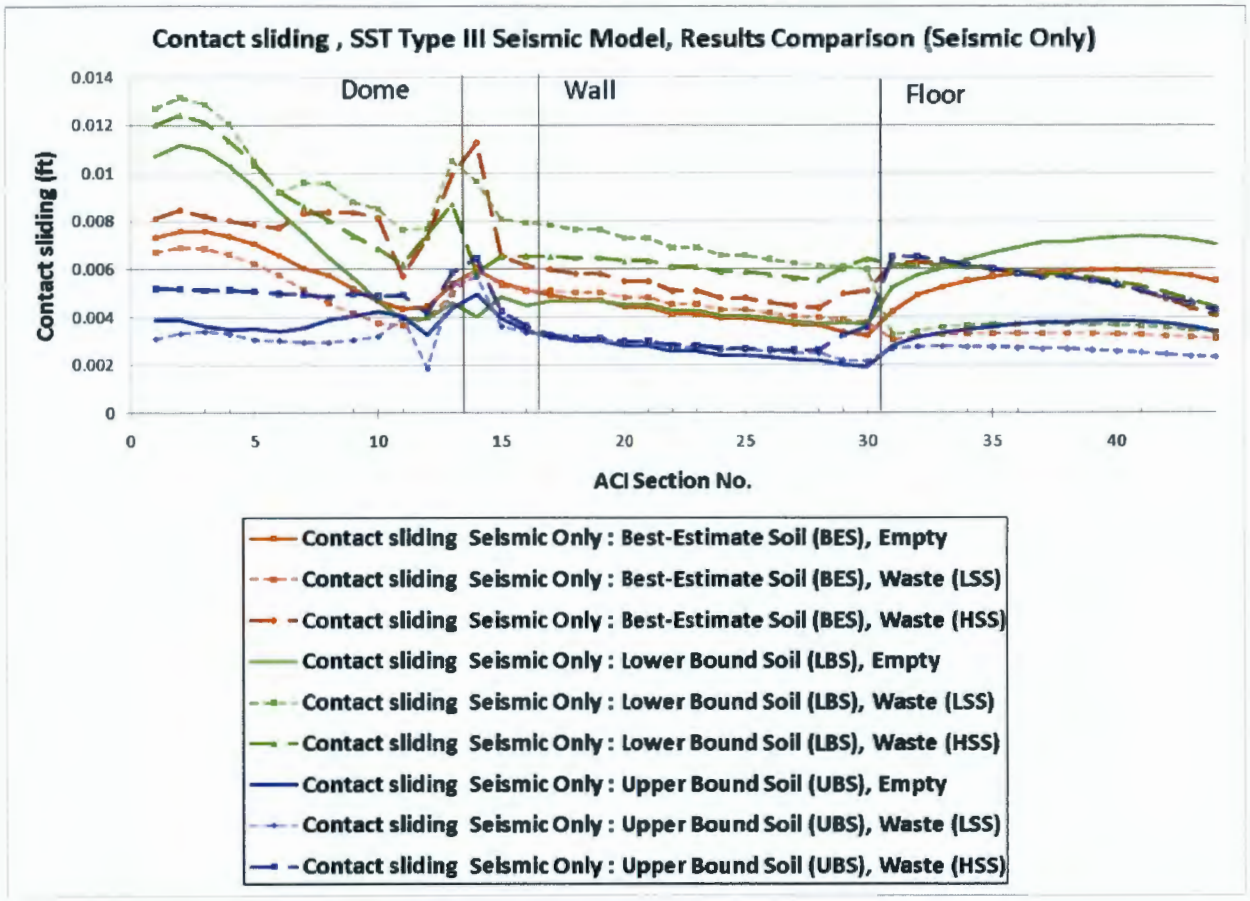

Figure 9.29. Soil/Concrete Contact Element Lateral Displacement (Sliding) – Seismic Only

9.2.1 Summary of Contact Results

Contact pressures show maximum values in the haunch and the footing for all load configurations, as expected. Gravity-only contact pressures follow the theoretical at-rest pressure profile due to the slip planes in the soil overburden above the dome and the manual adjustment in the wall. The contact shear forces peak in the haunch and the footing. The contact sliding generally decreases from the dome apex through the slab.

For seismic-only contact pressure in the wall, the full tank configurations tend to have greater pressures than the empty tank configurations. For seismic-only contact meridional and hoop shear in the dome, LBS and BES tend to create the greatest demands in the dome, and full tank higher modulus waste tends to create the greatest demands in the wall and slab. For seismic-only contact sliding in the dome, LBS tends to create the greatest displacements and UBS tends to create the least displacements.

Altogether, the contact results are more sensitive to the soil configuration than the waste configuration. For almost all contact results, the higher modulus waste has the greater demand and empty tank has the lesser demand. Contact sliding sensitivity to waste configuration is primarily based on the soil configuration.

9.3 TOLA and Seismic Combination Procedure

ACI LC4 is the only applicable load combination that contains earthquake demands. The seismic demands from the nine seismic runs described previously must be combined with the demands from the appropriate TOLA runs. The appropriate TOLA runs are those runs that have the same soil classification as the seismic runs; best estimate soil (BES), lower bound soil (LBS), or upper bound soil (UBS). Table 5.6 shows that TOLA Run 1 has nominal concrete properties and BES properties, TOLA Run 7 has nominal concrete properties and LBS properties, and TOLA Run 8 has nominal concrete properties and UBS properties. In addition, Table 4.4 indicates that the waste height at the end of the thermal history is 10 ft at 1.7 SpG. A final load step on the TOLA LC4 runs (Runs 1, 7, and 8) was solved where the waste height was made to match the appropriate waste conditions of the seismic run considered; either empty or full to 20.3 ft at 1.94 SpG per Section 6.3.2. Table 9.1 shows seismic and TOLA runs used for the nine LC4 combined runs.

Table 9.1. Combined Seismic and TOLA Runs

	Seismic Properties			TOLA Properties				
		Waste				Concrete		
Combined Run	Soil	Modulus	Height	Run Used	Soil	Modulus	Tensile Strength	Creep
1	BES	High	Full	1	BES	BES	Near Zero	Yes
2	BES	Low	Full	1	BES	BES	Near Zero	Yes
3	BES	-	Empty	1	BES	BES	Near Zero	Yes
4	LBS	High	Full	7	LBS	BES	Near Zero	Yes
5	LBS	Low	Full	7	LBS	BES	Near Zero	Yes
6	LBS	-	Empty	7	LBS	BES	Near Zero	Yes
7	UBS	High	Full	8	UBS	BES	Near Zero	Yes
8	UBS	Low	Full	8	UBS	BES	Near Zero	Yes
9	UBS	-	Empty	8	UBS	BES	Near Zero	Yes

Because the earthquake ground motions could theoretically come from the reverse direction than which they are applied to the seismic model (i.e., the ground motions are reversible), the seismic forces and moments must be combined with the TOLA forces and moments in both a positive and negative way. This leads to four combinations for ACI LC4 for both the meridional and hoop demands:

- F+M+: TOLA force + seismic force and TOLA moment + seismic moment
- F+M-: TOLA force + seismic force and TOLA moment – seismic moment
- F-M+: TOLA force – seismic force and TOLA moment + seismic moment
- F-M-: TOLA force – seismic force and TOLA moment – seismic moment

The highest D/C ratio of these four combinations for both meridional and hoop directions is reported as the D/C ratio for combined runs 1–9. Figure 9.30 shows an example P-M diagram with these four demand combinations as well as the TOLA-only demand. The upper right point in this case would have the highest D/C ratio based on the demand and capacity definitions defined in Figure 8.2. In addition, the through-wall shear capacity depends on the meridional force and moment values. Again, four through wall shear D/C ratios are calculated and the highest values are reported in the next section.

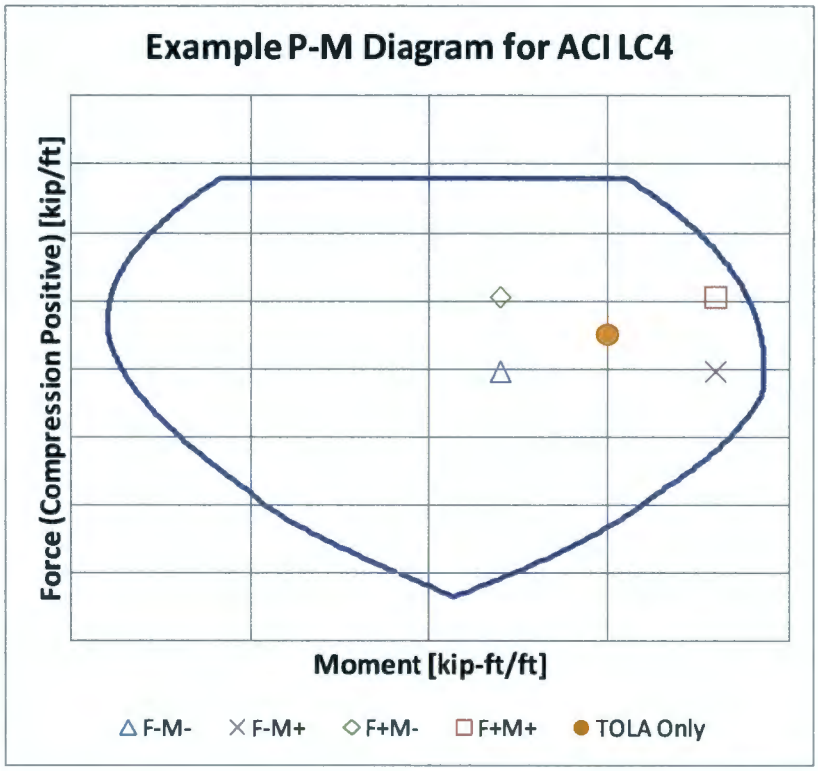

Figure 9.30. Example P-M Diagram with Four Possible Seismic Combinations

Shear friction D/C ratios are also checked for the construction joints under LC4. For the shear demands, the absolute value of shears are combined. The shear capacity is a function of the axial (meridional) force. The seismic axial force is combined with the TOLA axial force to produce a lower combined compressive force. This is a conservative choice, as the capacity decreases with a reduction in axial compression.

Finally, unlike the axisymmetric TOLA runs that only had axisymmetric loading, in-plane shear is present as a result of the non symmetric seismic loads. As recommended in the Structural Evaluation Criteria (Johnson et al. 2010), the in-plane shear capacity is evaluated by ACI 349-06 equation 11-29. D/C ratios for in-plane shear are also reported in the next section.

9.4 ACI Load Combination 4 Results

The ACI 349-06 LC4 D/C ratios ranges for combined runs 1–9 are summarized in Table 9.2. Generally, the LBS cases resulted in the highest D/C ratios while the UBS cases resulted in the lowest D/C ratios. The table shows that for all combined runs D/C ratios are less than one in the dome, haunch, and wall. In the slab, D/C ratios greater than one are seen in combined runs 1–8 in the hoop direction and in combined runs 1, 4, and 7 (all three G_{high} runs) in the meridional direction. Three slab removal runs were performed and are presented in Appendix E. The slab removal runs demonstrate that even if the slab is not intact the rest of the tank remains structurally sound.

Table 9.2. LC4 Combined TOLA and Seismic ACI Demand/Capacity Ratio Range

Combined ACI Demand/Capacity Ratio Range		Dome	Haunch	Wall	Slab
Combined Run		1 to 13	14 to 15	16 to 30	31 to 44
Run 1	Meridional	0.12-0.22	0.14-0.27	0.10-0.22	0.03-1.61
Seismic: BES G_{high}	Hoop	0.10-0.53	0.47-0.73	0.14-0.43	0.14-1.53
TOLA: BES	Shear	0.02-0.30	0.09-0.20	0.02-0.46	0.00-0.42
Run 2	Meridional	0.12-0.22	0.14-0.25	0.10-0.21	0.02-0.59
Seismic: BES G_{low}	Hoop	0.10-0.52	0.45-0.70	0.08-0.40	0.10-1.33
TOLA: BES	Shear	0.02-0.30	0.09-0.20	0.01-0.40	0.01-0.17
Run 3	Meridional	0.12-0.23	0.15-0.28	0.10-0.24	0.02-0.94
Seismic: BES empty	Hoop	0.09-0.53	0.49-0.71	0.02-0.42	0.05-1.25
TOLA: BES	Shear	0.02-0.31	0.11-0.22	0.01-0.39	0.00-0.22
Run 4	Meridional	0.13-0.24	0.13-0.30	0.11-0.29	0.04-1.59
Seismic: LBS G_{high}	Hoop	0.14-0.66	0.54-0.85	0.17-0.50	0.00-1.67
TOLA: LBS	Shear	0.02-0.32	0.05-0.19	0.01-0.43	0.00-0.41
Run 5	Meridional	0.13-0.24	0.13-0.27	0.11-0.27	0.03-0.84
Seismic: LBS G_{low}	Hoop	0.14-0.63	0.54-0.84	0.09-0.50	0.00-1.70
TOLA: LBS	Shear	0.02-0.32	0.05-0.19	0.01-0.41	0.00-0.35
Run 6	Meridional	0.13-0.24	0.14-0.27	0.11-0.28	0.03-0.89
Seismic: LBS empty	Hoop	0.14-0.63	0.54-0.84	0.05-0.51	0.03-1.69
TOLA: LBS	Shear	0.02-0.32	0.06-0.22	0.01-0.40	0.00-0.27
Run 7	Meridional	0.11-0.22	0.13-0.24	0.09-0.20	0.01-1.85
Seismic: UBS G_{high}	Hoop	0.10-0.47	0.41-0.61	0.11-0.47	0.12-1.80
TOLA: UBS	Shear	0.02-0.28	0.08-0.15	0.03-0.43	0.01-0.36
Run 8	Meridional	0.11-0.22	0.13-0.23	0.09-0.18	0.01-0.77
Seismic: UBS G_{low}	Hoop	0.10-0.48	0.40-0.62	0.04-0.35	0.08-1.11
TOLA: UBS	Shear	0.03-0.28	0.08-0.16	0.02-0.41	0.01-0.32
Run 9	Meridional	0.12-0.22	0.15-0.29	0.10-0.23	0.01-0.93
Seismic: UBS empty	Hoop	0.11-0.47	0.44-0.60	0.02-0.38	0.08-0.95
TOLA: UBS	Shear	0.03-0.30	0.11-0.18	0.01-0.39	0.00-0.19

Figure 9.31 shows the D/C ratios for LC4 combined run 1. Hoop and meridional demands in the slab are the only demands greater than capacity. Figure 9.32 shows the hoop capacity of section 33 near the tension side of the P-M diagram. Also shown in Figure 9.32 is the TOLA only demand and the four combined TOLA and seismic demands for LC4. The TOLA only demand is a small compressive force with a very small moment that would result in a small TOLA only D/C ratio. However, in combining an additional small seismic demand, two of the four combinations fall in the tension side of the P-M diagram, both of which lie outside of the capacity curve.

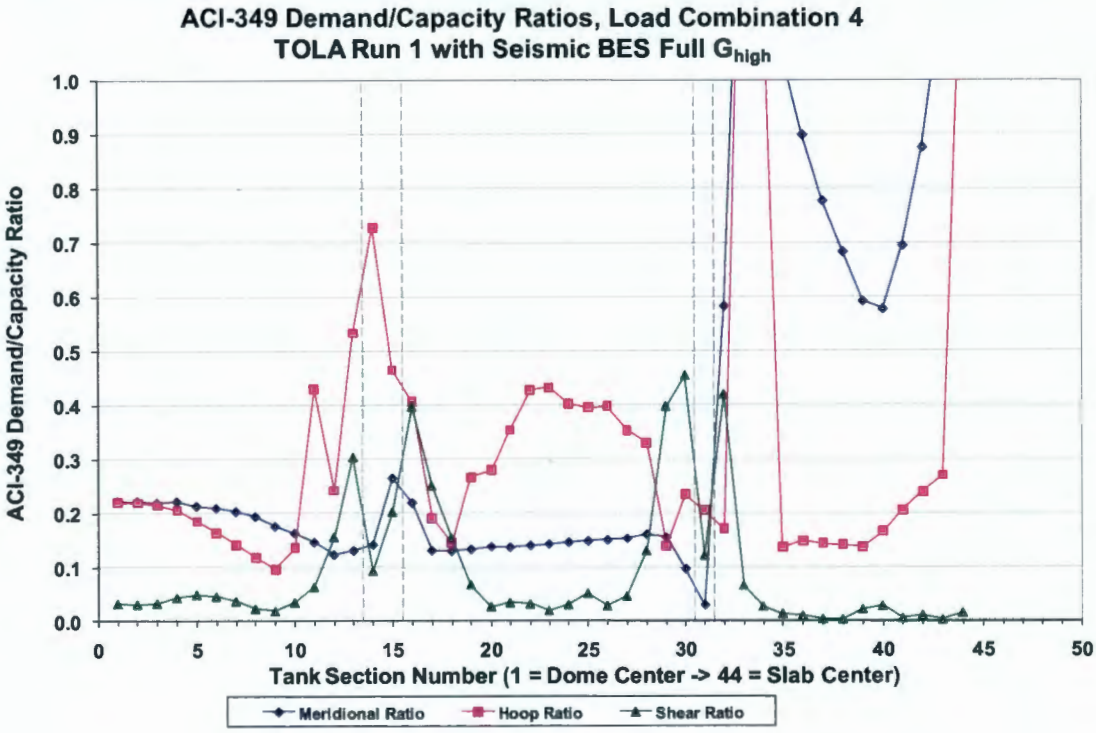

Figure 9.31. LC4 Combined Run 1 ACI D/C Ratios

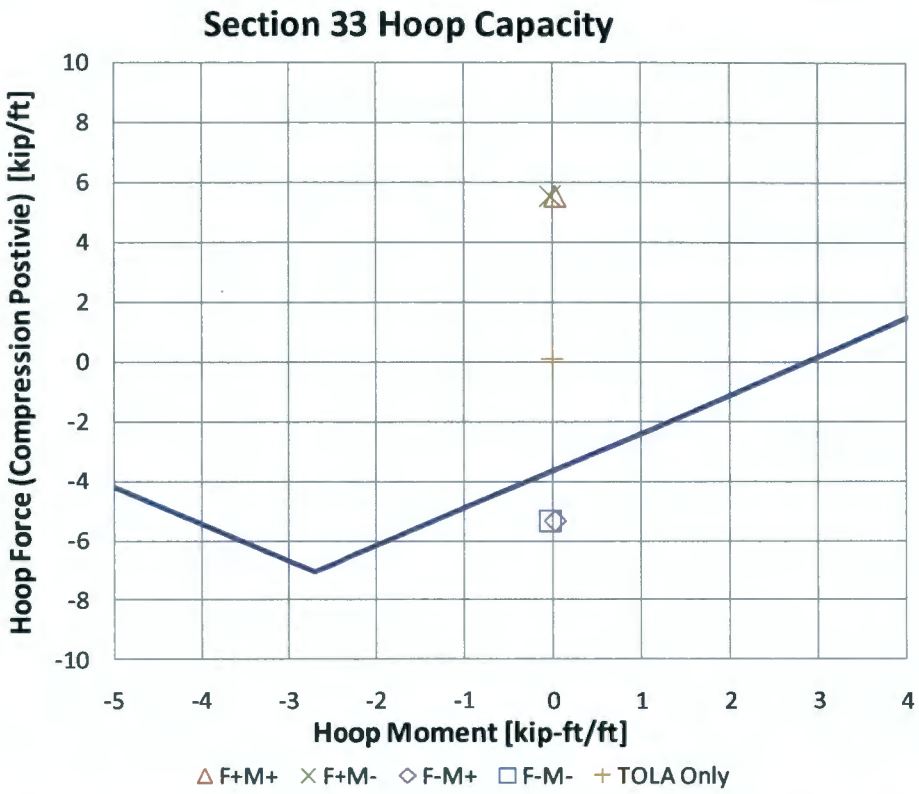

Figure 9.32. Section 33 Hoop Capacity and LC4 Combined Run 1 Demands

The slab has very little tension capacity compared with the rest of the tank. The ACI 349 slab tension capacity only exists due to one layer of ½-in.-diameter steel bars at a 12-in. center-to-center spacing. Even though the combined forces and moments within section 33 are relatively small, these sections have very little capacity in tension. This results in several occurrences of meridional and hoop D/C ratios greater than one within the slab.

The D/C ratios for the other BES combined runs, runs 2 and 3, are shown in Figure 9.33 and Figure 9.34, respectively. The meridional and shear D/C ratios are all less than one for both combined runs. As with combined run 1, combined runs 2 and 3 show the hoop demand exceeds capacity in two slab sections.

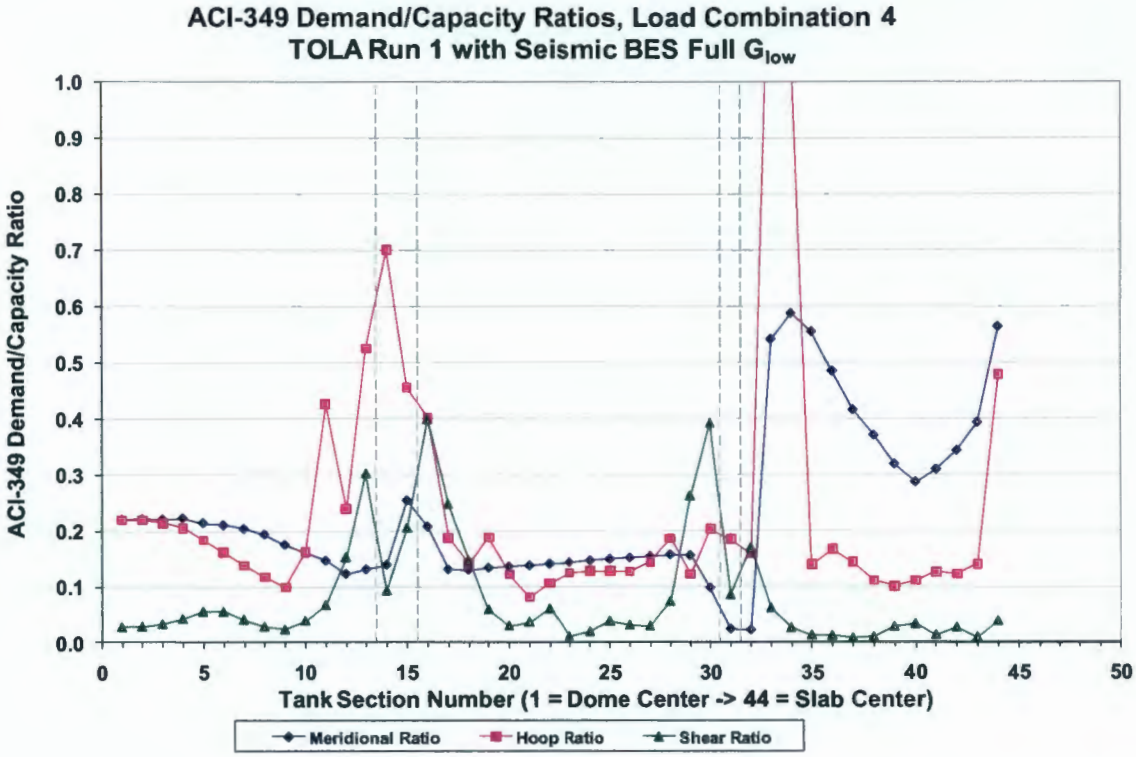

Figure 9.33. LC4 Combined Run 2 ACI D/C Ratios

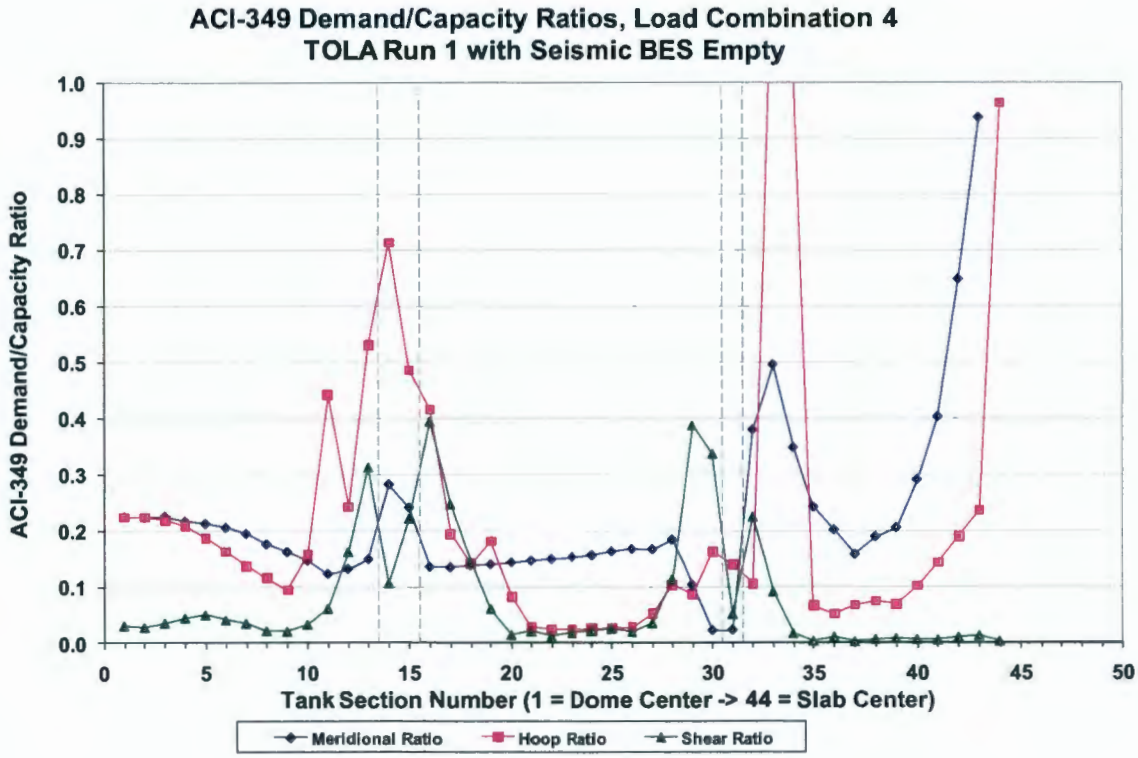

Figure 9.34. LC4 Combined Run 3 ACI D/C Ratios

The D/C ratios for the LBS combined runs (runs 4–6) are shown in Figure 9.35, Figure 9.36, and Figure 9.37. Again, all the D/C ratios are less than one for all three runs in the dome, haunch, and wall. The hoop D/C ratios are greater than one in some slab sections for all three combined runs. The meridional D/C ratios are greater than one in some slab sections in combined run 4.

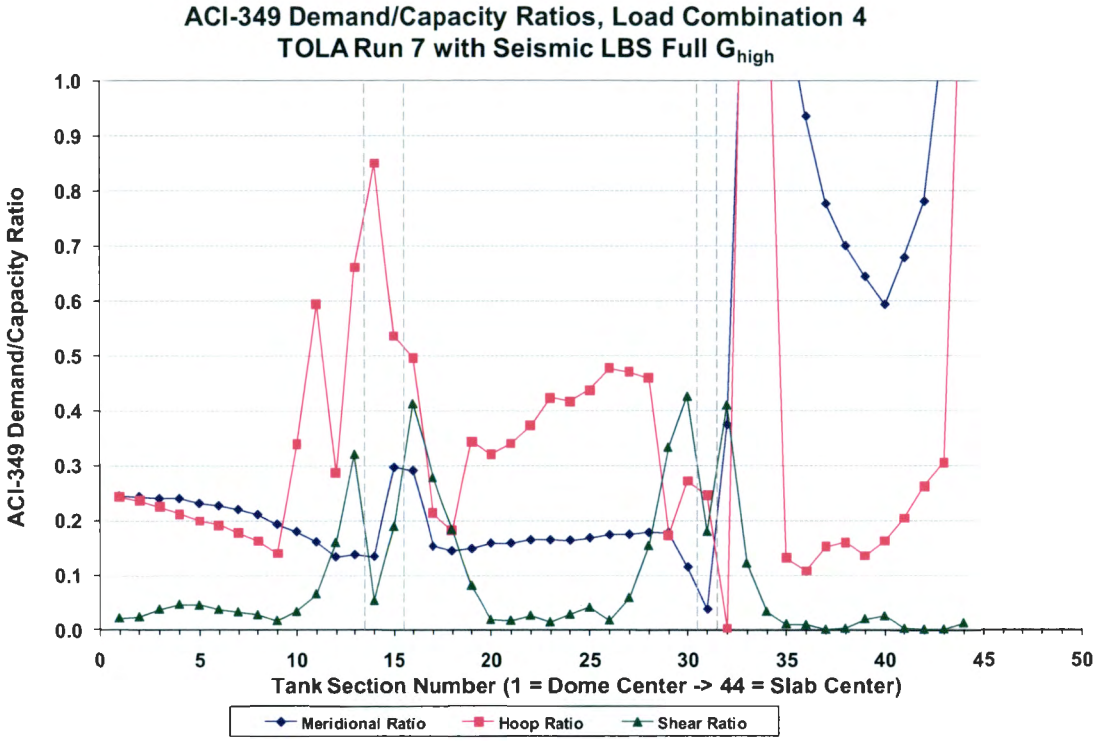

Figure 9.35. LC4 Combined Run 4 ACI D/C Ratios

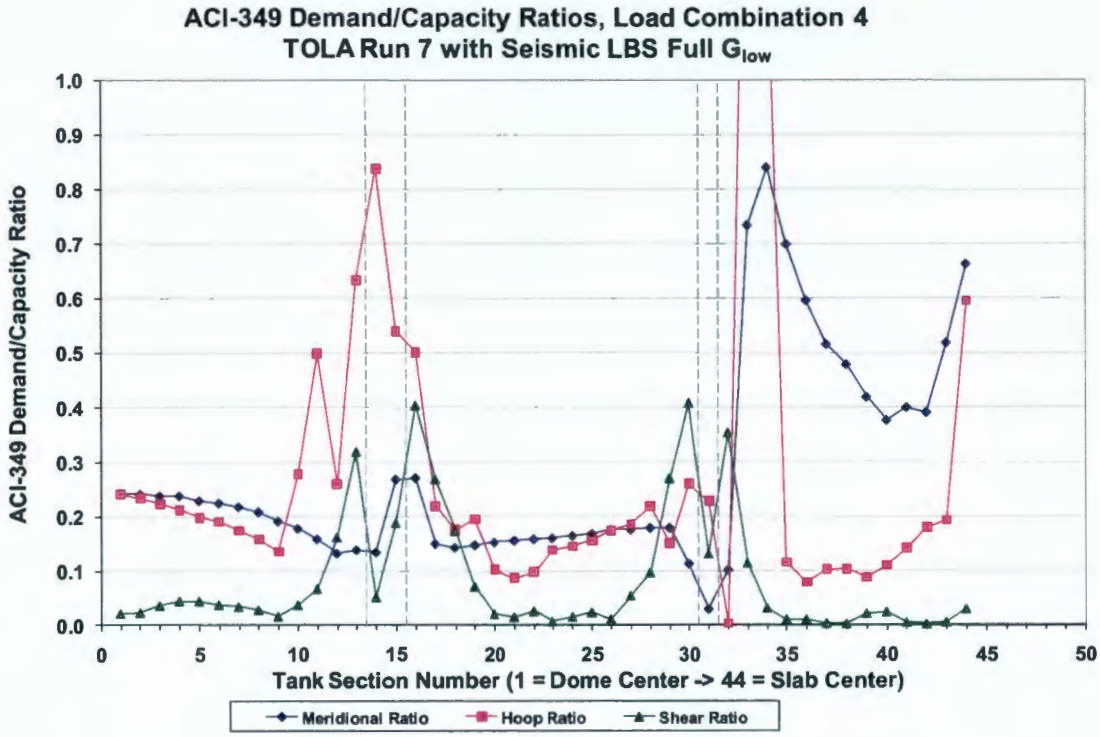

Figure 9.36. LC4 Combined Run 5 ACI D/C Ratios

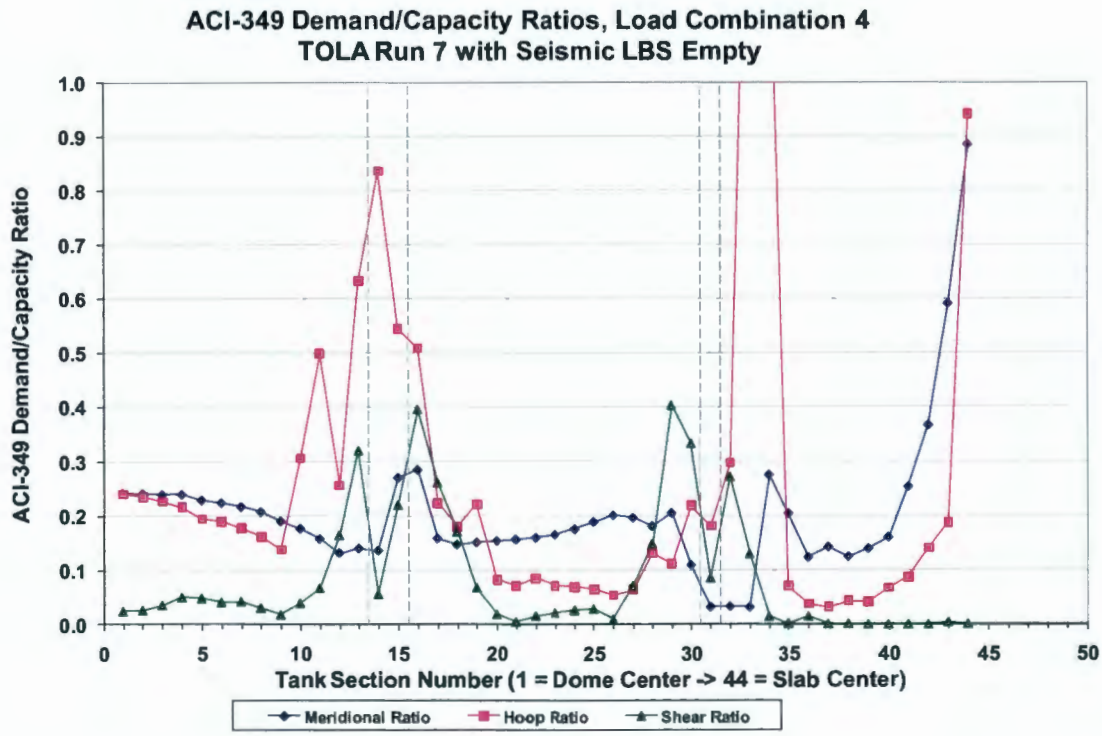

Figure 9.37. LC4 Combined Run 6 ACI D/C Ratios

The D/C ratios for the UBS combined runs, runs 7–9, are shown in Figure 9.38, Figure 9.39, and Figure 9.40. Again, all the D/C ratios are less than one for all three runs in the dome, haunch, and wall. The empty tank run, combined run 9, results in all D/C ratios less than one in the slab as well. The meridional D/C ratios only exceed one in the slab in combined run 7. The hoop D/C ratios exceed one in the slab in combined runs 7 and 8.

In-plane shear D/C ratios for all combined runs 1–9 are shown in Figure 9.41. In-plane shear demands are generally low with a maximum of 0.30 occurring at section 19 for combined run 4.

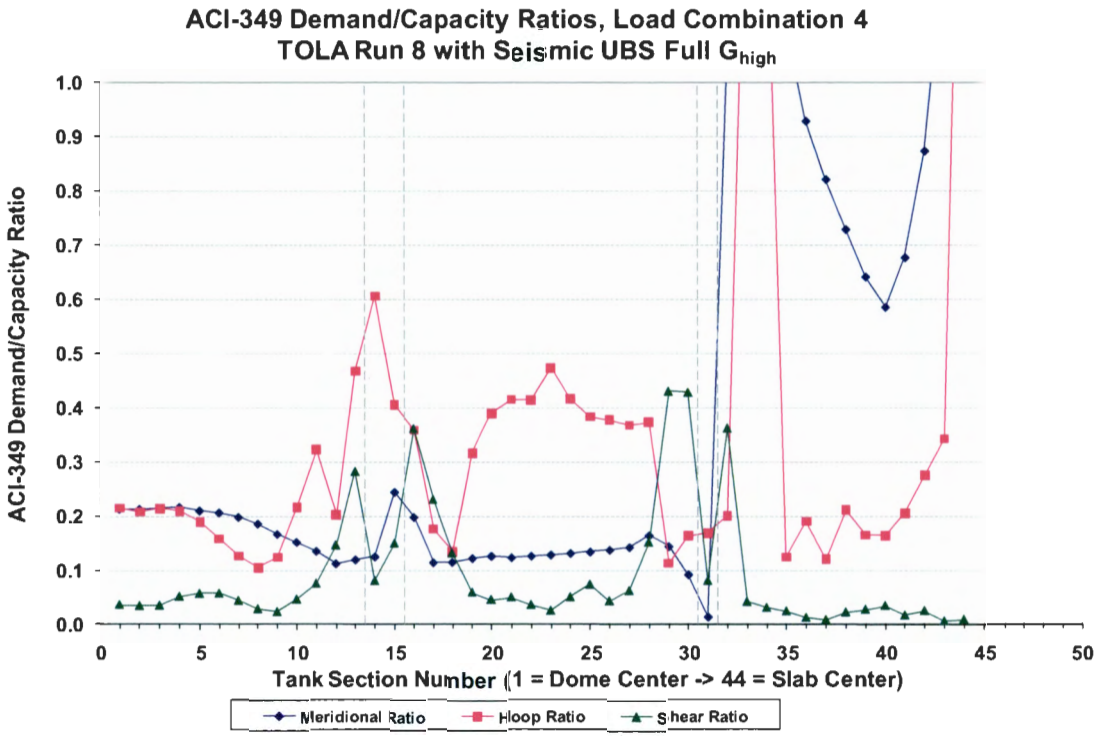

Figure 9.38. LC4 Combined Run 7 ACI D/C Ratios

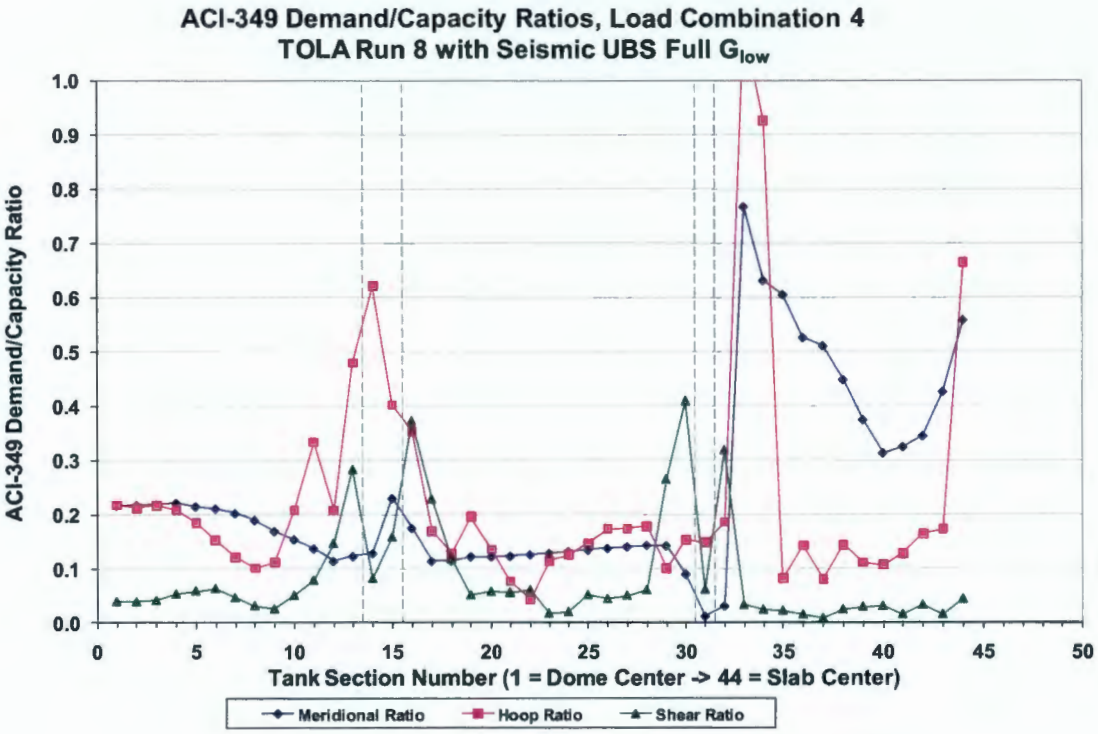

Figure 9.39. LC4 Combined Run 8 ACI D/C Ratios

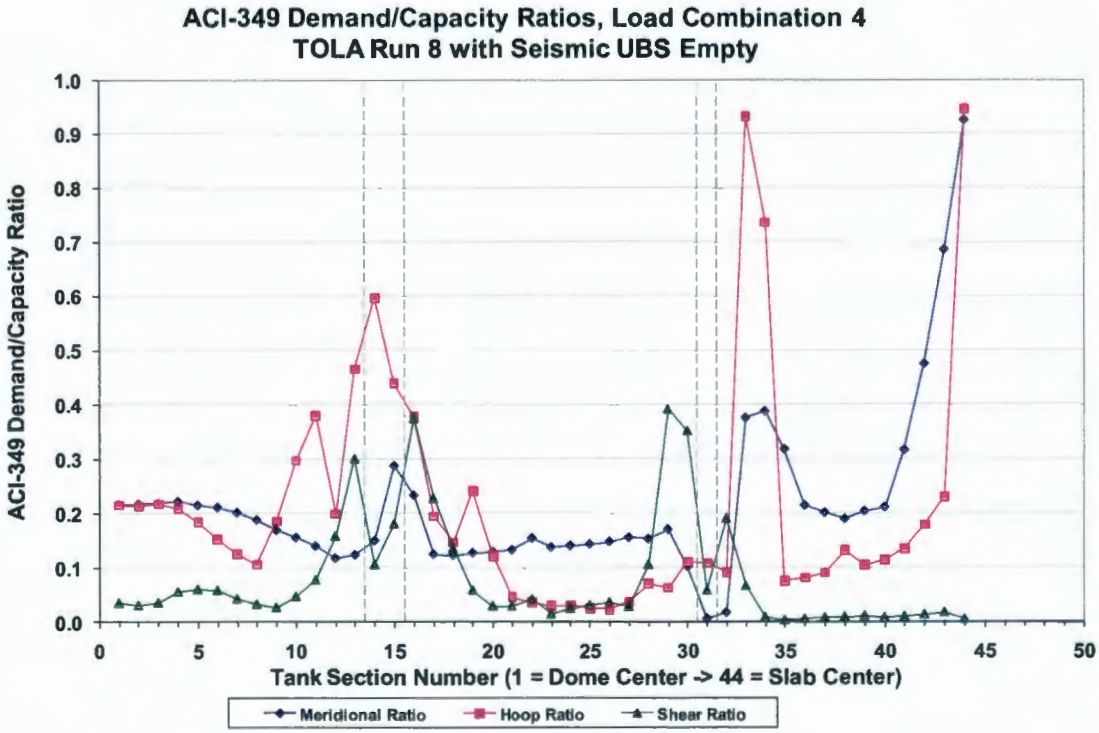

Figure 9.40. LC4 Combined Run 9 ACI D/C Ratios

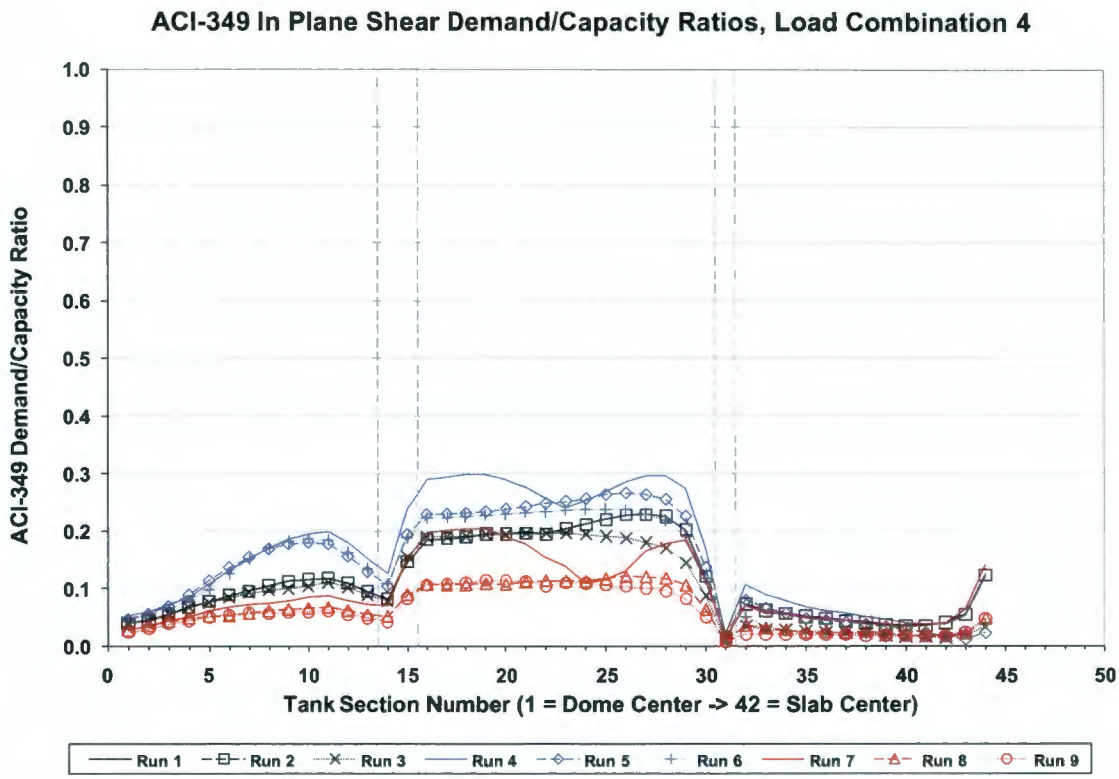

Figure 9.41. In-Plane Shear D/C Ratios for all Nine Seismic Runs

Table 9.3, Table 9.4, Table 9.5, and Table 9.6 show the shear friction D/C calculations for construction joints in the tank walls near sections 18, 22, 26, and 30 for the combined runs 1–9. The shear friction demand is the resultant vector shear from both the through wall shear and the in-plane shear. The combined axial demand is the TOLA meridional force less the seismic meridional force. All D/C ratios for the construction joints are less than one. The maximum D/C ratio is 0.55 occurring in section 30 for combined run 1.

Table 9.3. LC4 Combined Shear Friction D/C Calculations for Section 18

Combined Run	Combined Shear [kip/ft]	Combined Axial [kip/ft]	A_{vf} [in^2/ft]	A_c [in^2/ft]	μ	f_y [psi]	f_c' [psi]	$800A_c$ [kip/ft]	$0.2f_c'A_c$ [kip/ft]	$A_{vf}f_y\mu$ [kip/ft]	ϕ	Capacity [kip/ft]	D/C
1	9.2	-38.2	0.88	180	0.6	40000	4338	144.00	156.17	44.10	0.85	37.49	**0.25**
2	9.3	-38.4	0.88	180	0.6	40000	4338	144.00	156.17	44.20	0.85	37.57	**0.25**
3	9.3	-38.1	0.88	180	0.6	40000	4338	144.00	156.17	44.06	0.85	37.45	**0.25**
4	13.9	-45.4	0.88	180	0.6	40000	4338	144.00	156.17	48.40	0.85	41.14	**0.34**
5	11.2	-46.0	0.88	180	0.6	40000	4338	144.00	156.17	48.79	0.85	41.47	**0.27**
6	11.0	-45.6	0.88	180	0.6	40000	4338	144.00	156.17	48.55	0.85	41.26	**0.27**
7	9.3	-33.2	0.88	180	0.6	40000	4338	144.00	156.17	41.14	0.85	34.97	**0.27**
8	5.8	-33.5	0.88	180	0.6	40000	4338	144.00	156.17	41.27	0.85	35.08	**0.17**
9	6.0	-31.9	0.88	180	0.6	40000	4338	144.00	156.17	40.31	0.85	34.27	**0.18**
												Max	**0.34**

Table 9.4. LC4 Combined Shear Friction D/C Calculations for Section 22

Combined Run	Combined Shear [kip/ft]	Combined Axial [kip/ft]	A_{vf} [in²/ft]	A_c [in²/ft]	μ	f_y [psi]	f_c' [psi]	$800A_c$ [kip/ft]	$0.2f_c'A_c$ [kip/ft]	$A_{vf}f_y\mu$ [kip/ft]	ϕ	Capacity [kip/ft]	D/C
1	7.8	-38.2	0.88	144	0.6	40000	4006	115.20	115.37	44.12	0.85	37.50	**0.21**
2	8.5	-38.4	0.88	144	0.6	40000	4006	115.20	115.37	44.24	0.85	37.60	**0.23**
3	7.9	-38.2	0.88	144	0.6	40000	4006	115.20	115.37	44.11	0.85	37.50	**0.21**
4	10.8	-46.1	0.88	144	0.6	40000	4006	115.20	115.37	48.87	0.85	41.54	**0.26**
5	10.4	-46.0	0.88	144	0.6	40000	4006	115.20	115.37	48.76	0.85	41.45	**0.25**
6	9.9	-46.6	0.88	144	0.6	40000	4006	115.20	115.37	49.18	0.85	41.80	**0.24**
7	6.2	-33.6	0.88	144	0.6	40000	4006	115.20	115.37	41.33	0.85	35.13	**0.18**
8	4.8	-33.9	0.88	144	0.6	40000	4006	115.20	115.37	41.51	0.85	35.29	**0.14**
9	4.3	-32.3	0.88	144	0.6	40000	4006	115.20	115.37	40.58	0.85	34.50	**0.13**
												Max	**0.26**

Table 9.5. LC4 Combined Shear Friction D/C Calculations for Section 26

Combined Run	Combined Shear [kip/ft]	Combined Axial [kip/ft]	A_{vf} [in²/ft]	A_c [in²/ft]	μ	f_y [psi]	f_c' [psi]	$800A_c$ [kip/ft]	$0.2f_c'A_c$ [kip/ft]	$A_{vf}f_y\mu$ [kip/ft]	ϕ	Capacity [kip/ft]	D/C
1	8.9	-39.2	0.88	180	0.6	40000	3761	144.00	135.40	44.71	0.85	38.01	**0.23**
2	8.4	-39.2	0.88	180	0.6	40000	3761	144.00	135.40	44.71	0.85	38.01	**0.22**
3	7.5	-39.2	0.88	180	0.6	40000	3761	144.00	135.40	44.71	0.85	38.00	**0.20**
4	11.7	-46.8	0.88	180	0.6	40000	3761	144.00	135.40	49.27	0.85	41.88	**0.28**
5	10.9	-46.5	0.88	180	0.6	40000	3761	144.00	135.40	49.10	0.85	41.74	**0.26**
6	9.9	-47.6	0.88	180	0.6	40000	3761	144.00	135.40	49.76	0.85	42.29	**0.23**
7	5.2	-34.7	0.88	180	0.6	40000	3761	144.00	135.40	41.99	0.85	35.69	**0.15**
8	4.9	-34.7	0.88	180	0.6	40000	3761	144.00	135.40	42.01	0.85	35.71	**0.14**
9	4.2	-33.6	0.88	180	0.6	40000	3761	144.00	135.40	41.34	0.85	35.14	**0.12**
												Max	**0.28**

Table 9.6. LC4 Combined Shear Friction D/C Calculations for Section 30

Combined Run	Combined Shear [kip/ft]	Combined Axial [kip/ft]	A_{vf} [in²/ft]	A_c [in²/ft]	μ	f_y [psi]	f_c' [psi]	$800A_c$ [kip/ft]	$0.2f_c'A_c$ [kip/ft]	$A_{vf}f_y\mu$ [kip/ft]	ϕ	Capacity [kip/ft]	D/C
1	22.0	-43.6	0.88	335	0.6	40000	3488	267.65	233.39	47.36	0.85	40.26	**0.55**
2	19.8	-43.3	0.88	335	0.6	40000	3488	267.65	233.39	47.19	0.85	40.11	**0.49**
3	18.6	-43.5	0.88	335	0.6	40000	3488	267.65	233.39	47.30	0.85	40.21	**0.46**
4	22.8	-50.5	0.88	335	0.6	40000	3488	267.65	233.39	51.54	0.85	43.81	**0.52**
5	21.2	-50.0	0.88	335	0.6	40000	3488	267.65	233.39	51.20	0.85	43.52	**0.49**
6	19.1	-51.4	0.88	335	0.6	40000	3488	267.65	233.39	52.03	0.85	44.23	**0.43**
7	20.8	-38.4	0.88	335	0.6	40000	3488	267.65	233.39	44.24	0.85	37.60	**0.55**
8	19.3	-38.5	0.88	335	0.6	40000	3488	267.65	233.39	44.30	0.85	37.66	**0.51**
9	18.1	-37.4	0.88	335	0.6	40000	3488	267.65	233.39	43.64	0.85	37.10	**0.49**
												Max	**0.55**

In addition to these normal shear friction checks, a check was performed to determine the minimum effective steel area required to resist the shear friction at the lower construction joint. Here, an explicit reduction of steel in the model was not performed. Instead, using the same combined LC4 demands, the effective steel area is simply reduced in the shear friction capacity until there is no more steel left or the D/C ratio has reached one.

For LC4, the minimum required effective steel area at the lower construction joint for eight of the nine combined runs is zero. For these runs the meridional compression is large enough to provide enough shear friction capacity to resist the combined shear. As shown in Table 9.7, for combined run 7, only 0.06 in^2/ft of meridional steel, or 7% of the total initial steel amount, is required to have demands meet the capacity.

Table 9.7. LC4 Combined Shear Friction D/C Calculations for Reduction in Steel at Section 30

Combined Run	Combined Shear [kip/ft]	Combined Axial [kip/ft]	A_{vf} [in2/ft]	A_c [in2/ft]	μ	f_y [psi]	f_c' [psi]	$800A_c$ [kip/ft]	$0.2fc'A_c$ [kip/ft]	$A_{vf}f_y\mu$ [kip/ft]	ϕ	Capacity [kip/ft]	D/C
1	22.0	-43.6	0.00	276	0.6	40000	3674	220.80	202.80	26.15	0.85	22.23	**0.99**
2	19.8	-43.3	0.00	276	0.6	40000	3674	220.80	202.80	25.97	0.85	22.08	**0.90**
3	18.6	-43.5	0.00	276	0.6	40000	3674	220.80	202.80	26.09	0.85	22.17	**0.84**
4	22.8	-50.5	0.00	276	0.6	40000	3674	220.80	202.80	30.32	0.85	25.78	**0.88**
5	21.2	-50.0	0.00	276	0.6	40000	3674	220.80	202.80	29.99	0.85	25.49	**0.83**
6	19.1	-51.4	0.00	276	0.6	40000	3674	220.80	202.80	30.82	0.85	26.19	**0.73**
7	20.8	-38.4	0.06	276	0.6	40000	3674	220.80	202.80	24.51	0.85	20.83	**1.00**
8	19.3	-38.5	0.00	276	0.6	40000	3674	220.80	202.80	23.09	0.85	19.62	**0.98**
9	18.1	-37.4	0.00	276	0.6	40000	3674	220.80	202.80	22.43	0.85	19.06	**0.95**

9.5 LC4 Combined Results Summary

The results presented in the previous section indicate that for ACI 349-06 LC4, the shear friction at construction joints and in-plane shear demands are well within the respective capacities. The hoop, meridional, and through-wall shear demands are all less than the capacities (D/C ratios < 1) in the dome, haunch, and wall, hence ACI 349-06 requirements are met. The hoop and meridional demands exceed capacity in the slab; however, as shown in the slab removal runs in Appendix E, the tank will remain structurally sound even with the slab not intact.

This page intentionally left blank.

10.0 Tank Appurtenances

The Type III single-shell tanks (SSTs) evaluated in this report contain a variety of appurtenances (such as pits, risers, penetrations, piping and pads) that may have an effect on the tank structural response and in turn the structural integrity. The effect of appurtenances on tank structural integrity has not been examined in past tank AORs (Bander et al. 1994; Julyk and Mackey 2003; Ramble 1983). This chapter presents a state-of-the-art AOR to address tank appurtenances. Some prior tank structural analyses have examined the effect of penetrations up to 55-inches in diameter on tank structural integrity (McCluskey 2005; Rinker et al. 2011b). The Type II SST AOR (Rinker et al. 2011a) evaluated the effect of pits and penetrations (post-construction and during construction) on the Type II SSTs using both a "pits only" model and a "pits and penetrations" model. It was found that the effect of the penetrations, in combination with the pits, was limited to a small region in the vicinity of the penetrations.

A complete review of the Type III SST appurtenances is presented in Appendix B. Appendix B provides details regarding all Type III tank appurtenances and concludes that the design of tank-to-tank piping, fill line piping, small-diameter risers (12 inches or less), and ancillary equipment is such that these appurtenances have a negligible effect on structural demands. As discussed in Appendix B, the Type III SST penetrations are no larger and no further from the dome center than those penetrations in Type II SSTs. Because of this, no penetrations need to be modeled in this Type III SST AOR. Some pits are expected to have a significant impact due to their heavy net weight. Appendix B does identify a necessary Type III pit configuration to be evaluated. This configuration is modeled and subjected to TOLA and/or seismic loads using an appropriate set of material properties.

Pits included in the appurtenance model are those with the heaviest net weight, as these pits are expected to apply the largest concentrated load on the dome. The dome load record data reports (Hundal 2004a, 2004b, 2004c, 2004d) calculate the net weight of all appurtenances above each of the Type III SSTs. The net weight is the weight of the pit and weight of any risers or equipment in the pit minus the weight of the displaced soil. As identified in Section B.5, the heaviest pit over the center of a Type III tank is the Pump pit on tank 241-TX-115, with a net weight of 23.2 kips (Hundal 2004c). The heaviest offset pits are the Sluice pits on tanks 241-TY-101 and 241-TY-102 with a net weight of 58.8 kips (Hundal 2004d). Each of these tanks has two sluice pits weighing 58.8 kips each. As defined in Section 4.1.2, the baseline concentrated dome load for the 100-Series SSTs is 200,000 lbf. Because the appurtenances add net weight to the dome, the additional concentrated load on the soil over the center of the tank will be reduced due to the addition of appurtenance weights.

Since the heavy offset pits are located on the 241-TY-101/102 tanks, these pit configurations will be used for the appurtenance models. The net weight of the central pit on these tanks will be increased to match that of the Pump pit on tank 241-TX-115. Figure 10.1 shows a centerline cut of the pit configuration on tanks 241-TY-101/102 as well as the dome penetrations in these pits. Based on the results of the Type II SST AOR, modeling of these penetrations is not necessary. For the Type III appurtenance model, this configuration is adjusted so that the pits are arranged symmetrically to allow for models less than the full tank. Figure 10.2 shows a plan view of the adjusted pit configuration that was used in the appurtenance models. The central pit is relocated to be centered directly above the dome apex. The offset pits are symmetrically spaced from the central pit. The height of the soil above the dome apex is increased to 11-ft to match the soil height used in all Type III axisymmetric analyses (as defined in Section 4.1.2). Figure 10.3 shows the centerline cut view of the pit configuration used in the

appurtenance models. The pits are seen as symmetrically spaced and the soil height is increased. The height of the base concrete between the pit and the dome is increased to have a soil height of 11-ft without altering the shape of the pits. The density of the pit concretes are adjusted such that the net weights of the pits are 22.3 kips for the center pit and 58.8 kips for each offset pit.

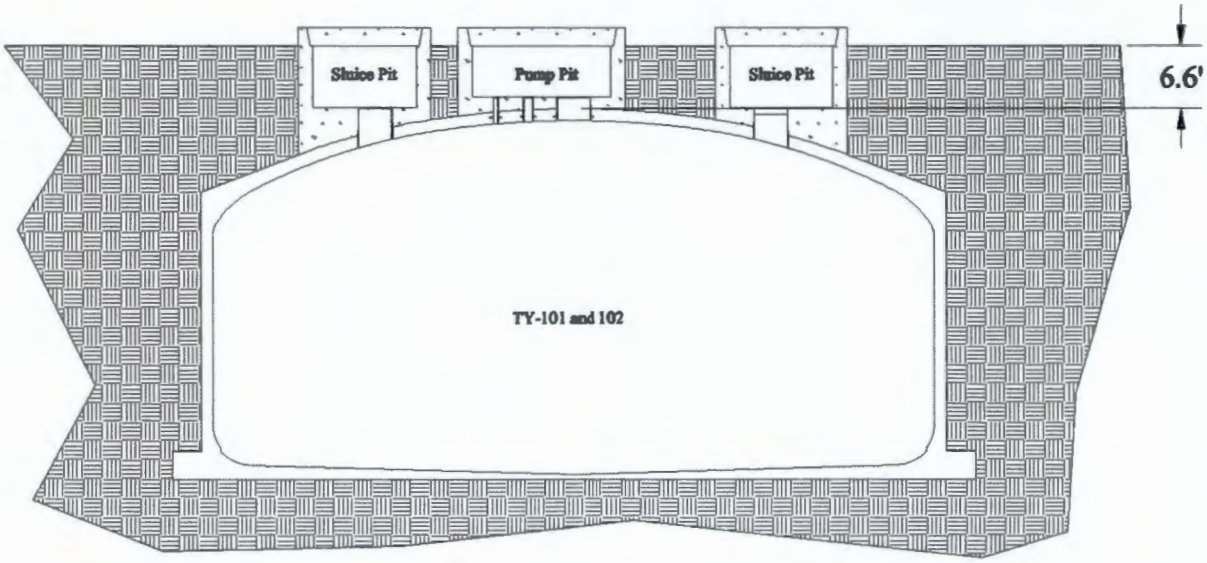

Figure 10.1. Centerline Cut View of TY-101/102 Appurtenance Configuration. Units in feet.

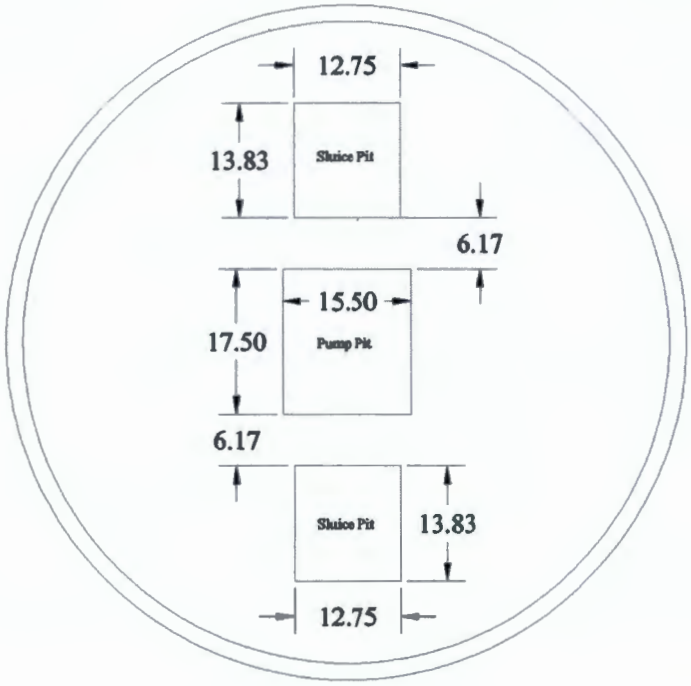

Figure 10.2. Plan View of Appurtenance Configuration used in Appurtenance Models. Units in feet.

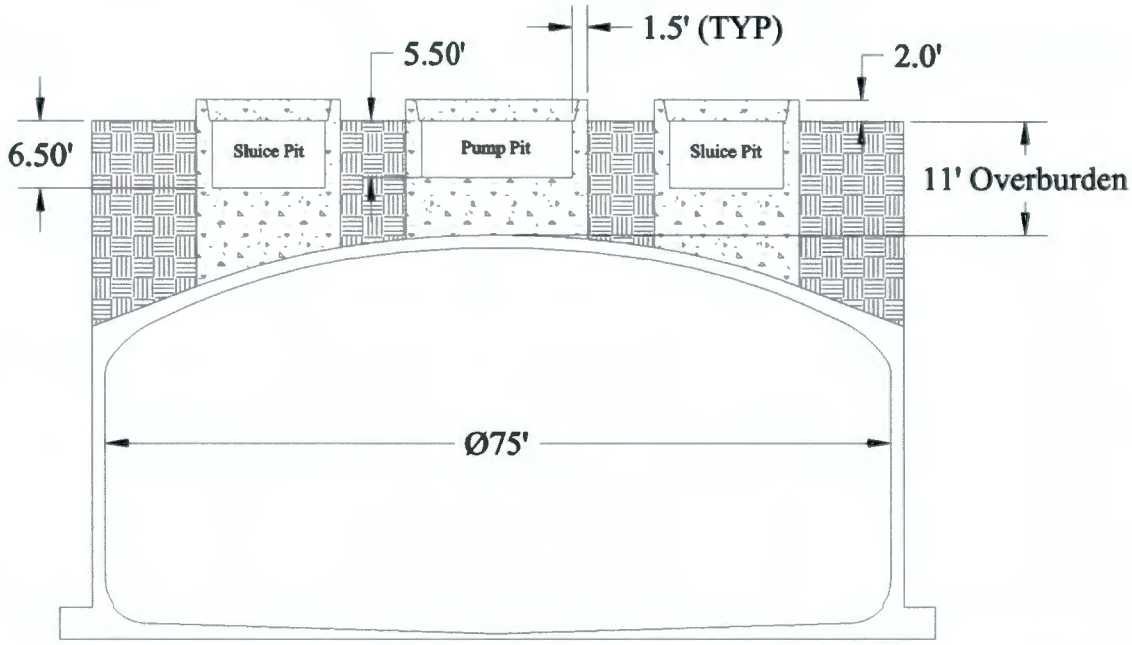

Figure 10.3. Centerline Cut View of Appurtenance Configuration used in Appurtenance Models. Units in feet.

10.1 Type III SST TOLA Appurtenance Models

The TOLA appurtenance models were constructed from the axisymmetric TOLA model presented in Chapter 5. Rather than modeling an entire tank, which would result in a prohibitively large finite element model, a 90° section of the tank was modeled with symmetric boundary conditions. The single element wide 2° axisymmetric slice was modified to a 3° slice. This 3° slice was rotated and repeated to achieve a 90° section of the tank and surrounding soil. The pits were added to the 90° tank section. Figure 10.4 shows a plan view of the TOLA appurtenance configuration. The hatched 90° section is the portion of the tank that was modeled. Symmetric boundary conditions were applied along the 0° and 90° boundaries. Figure 10.5 shows a close up of the tank and pits in the TOLA appurtenance model along with the mesh used. The 90° model has over 1.8 million simultaneous equations to solve. To reduce solving time the model was run using the ANSYS® parallel processing solver.

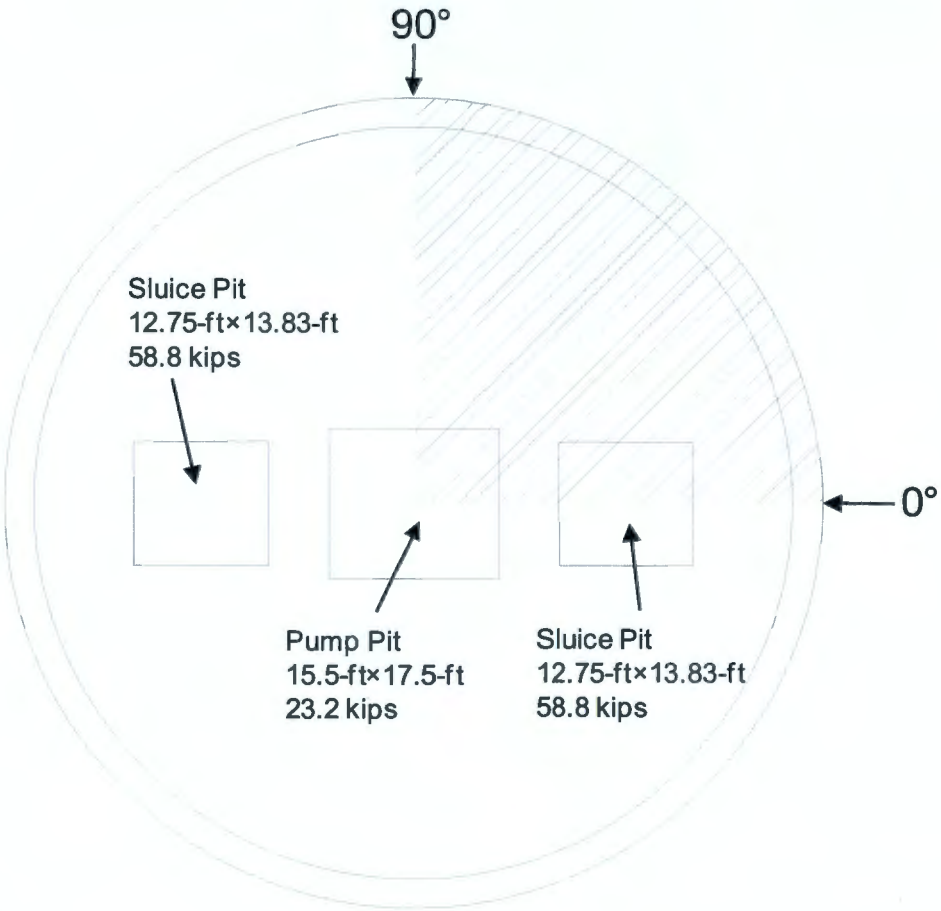

Figure 10.4. Plan View of TOLA Appurtenance Configuration. Hatched area is modeled with symmetric boundary conditions.

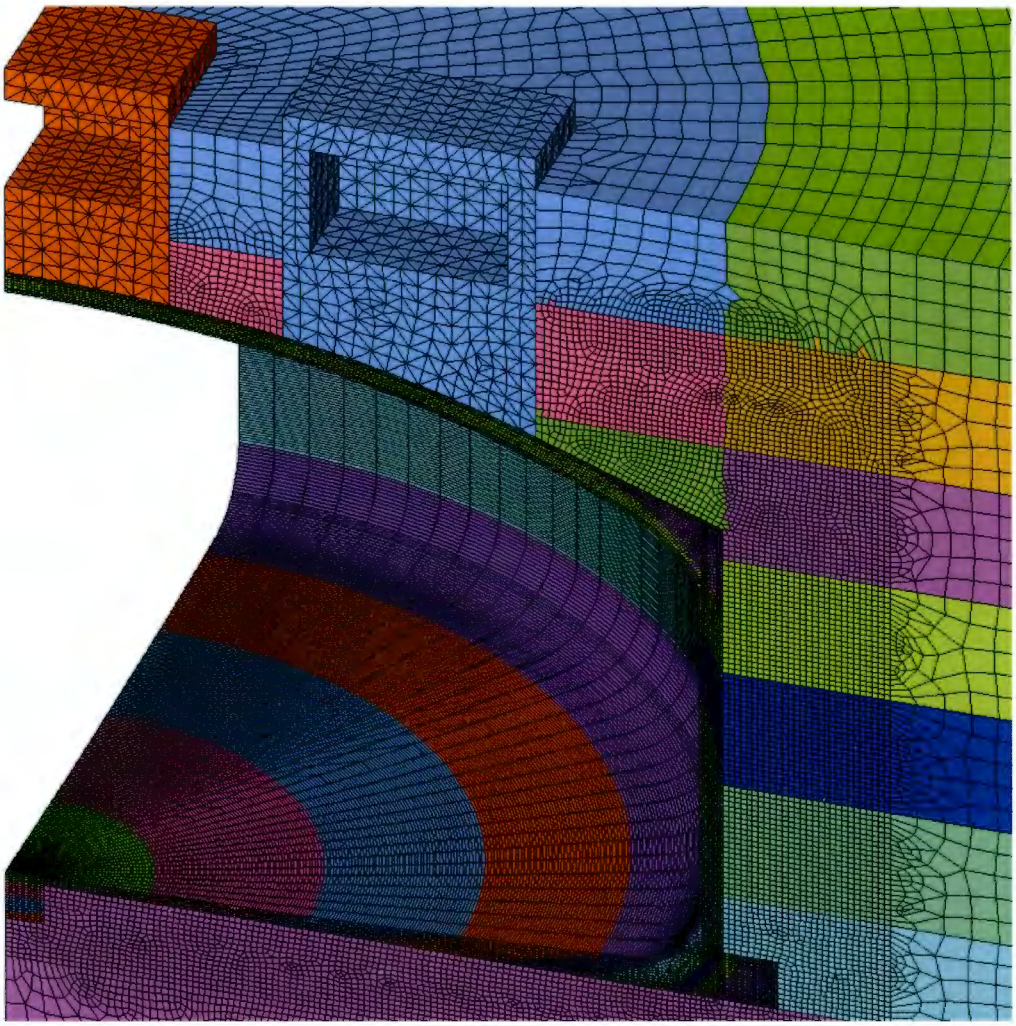

Figure 10.5. TOLA Appurtenance Model with Mesh. Coloring is by material properties after thermal degradation of the concrete has occurred.

To reduce the number of time steps needed to be solved, the thermal history applied to the axisymmetric TOLA models (see Section 5.7) was simplified. Figure 10.6 shows the maximum tank temperature history for the axisymmetric models and the simplified history used for the appurtenance models. At the initial uniform temperature of 53°F mechanical loads are applied to the tank. These mechanical loads are the same as for the axisymmetric models (see Table 4.4) with the exception that the 200 kips concentrated surface load is reduced to 59.2 kips; the sum of the net pit weights and this 59.2 kips concentrated surface load is 200 kips. The maximum temperature reaches a peak at 300°F and then drops down to 80°F over a period of 59 years. After this cool-down to 80°F the tank history splits for different ACI-349 load combinations. If ACI-349 LC1 is applied, the tank is cooled further to a uniform 50°F. Then ACI-349 LC1 load factors, as described in Equation 4.1a, are applied and the LC1 structural demands are extracted from the results. Otherwise the tank remains at 80°F where either the ACI-349 LC4 TOLA demands (no factors are required for LC4) are extracted or the ACI-349 LC9 load factors, as described in Equation 4.1c, are applied and LC9 demands are extracted. The LC4 TOLA demands are later combined with the seismic demands to evaluated the LC4 D/C ratios. Figure 10.7 shows the flow plan for the loading history of the TOLA appurtenance model just described.

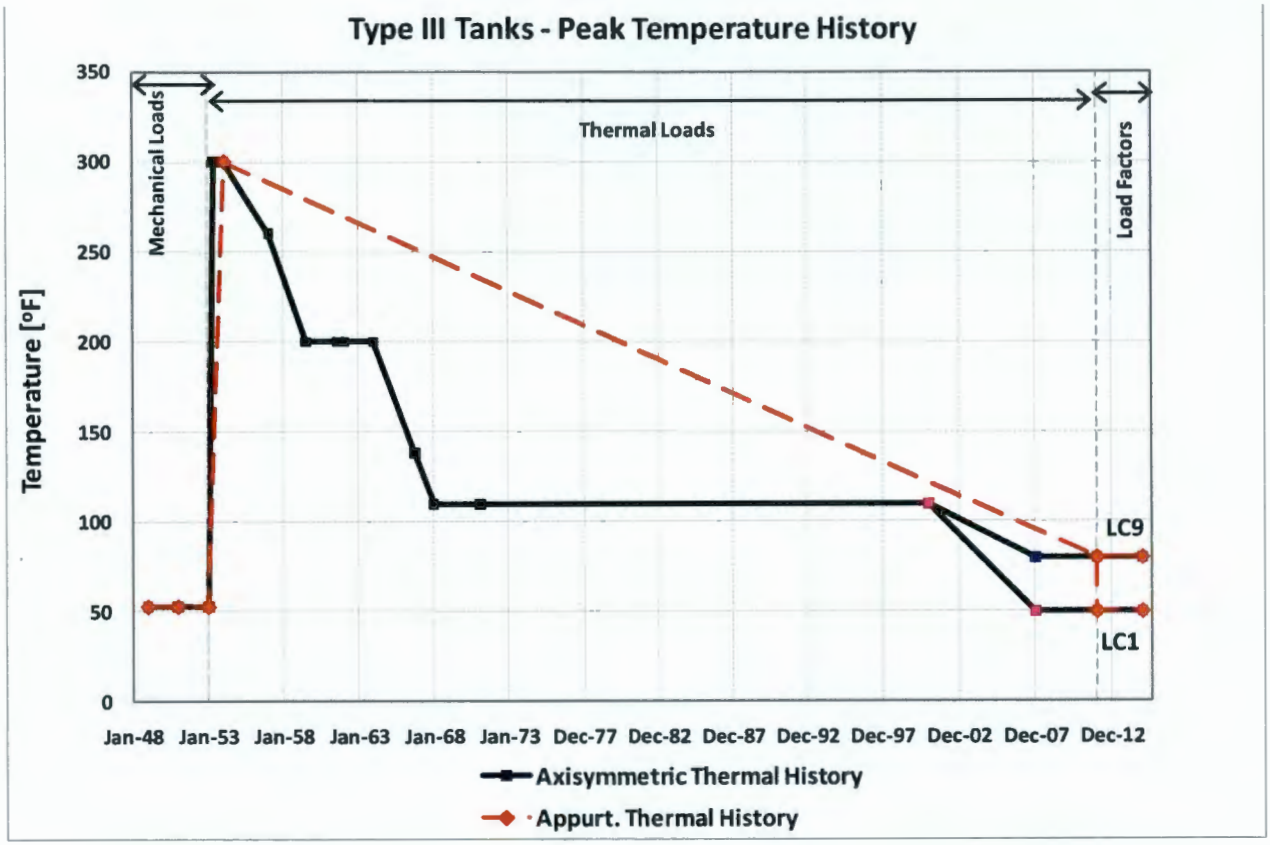

Figure 10.6. Appurtenance Model Thermal History Compared to Axisymmetric Thermal History

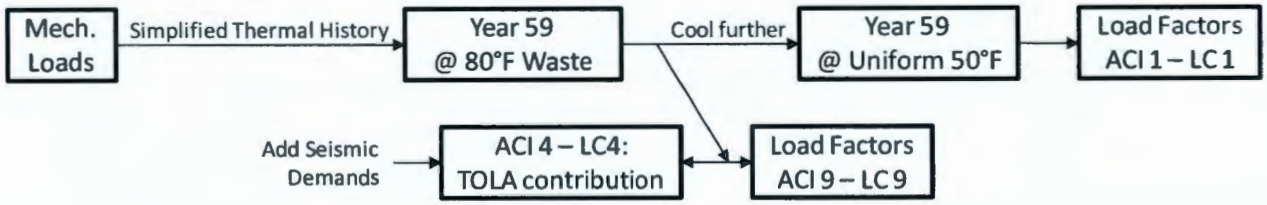

Figure 10.7. Appurtenance Loading History Flow Plan

To obtain accurate thermal profiles at the peak temperature of 300°F and the cool-down temperature of 80°F, nodal temperatures for the concrete tank were extracted from the axisymmetric model at these load steps. Two steady-state thermal models of the appurtenance model were created where these extracted nodal temperatures were applied to the 90° section of the tank. No thermal variation was introduced in the hoop direction; i.e., within the tank concrete the temperatures are axisymmetric. These two steady-state thermal models were solved to obtain temperatures in the surrounding soil and pit concrete creating full appurtenance model thermal profiles at 300°F and 80°F. Figure 10.8 and Figure 10.9 show close up views of these thermal profiles at 300°F and 80°F respectively. These full thermal profiles were then applied as body temperatures into the structural analysis of the appurtenance model at the appropriate load step. Uniform temperature profiles, such as the LC1 50°, can be directly input as body temperatures into the structural model without these additional steps.

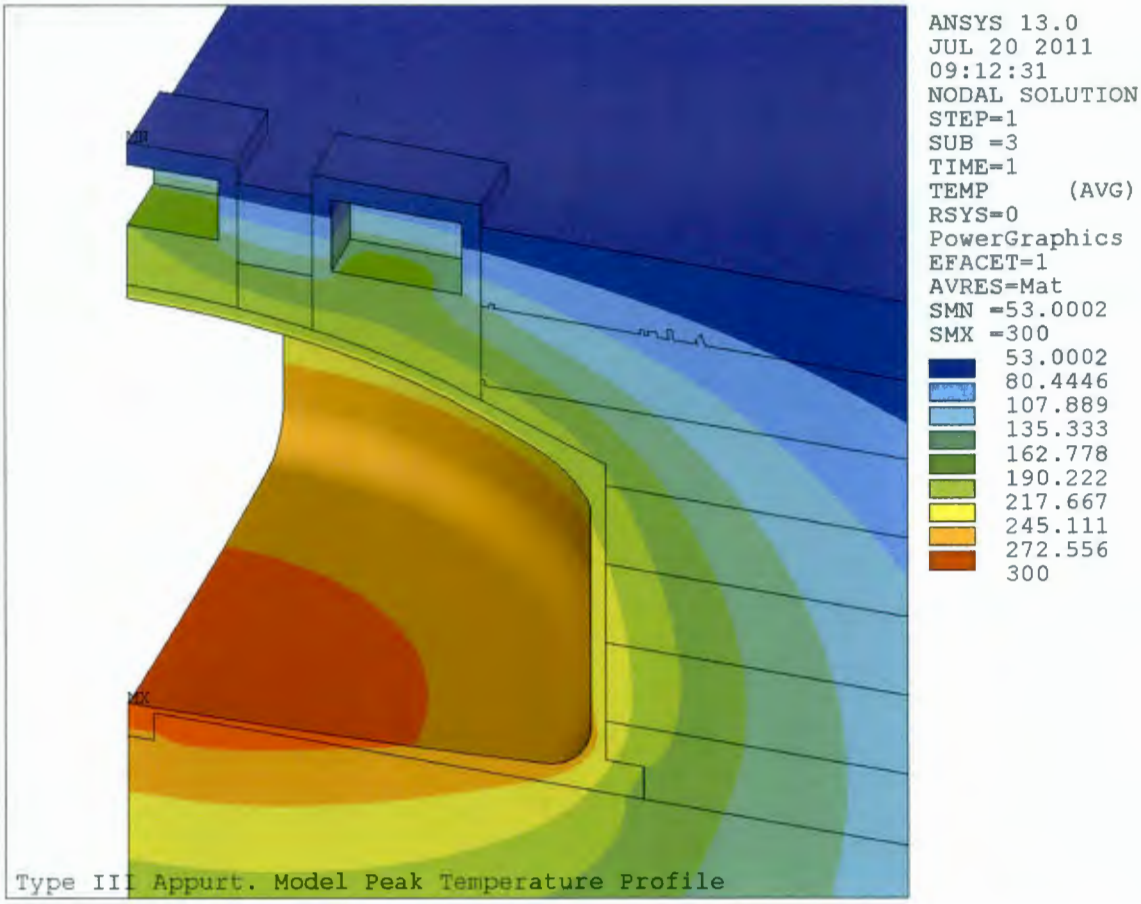

Figure 10.8. Temperature Profile at Peak Temperature in Appurtenance Model

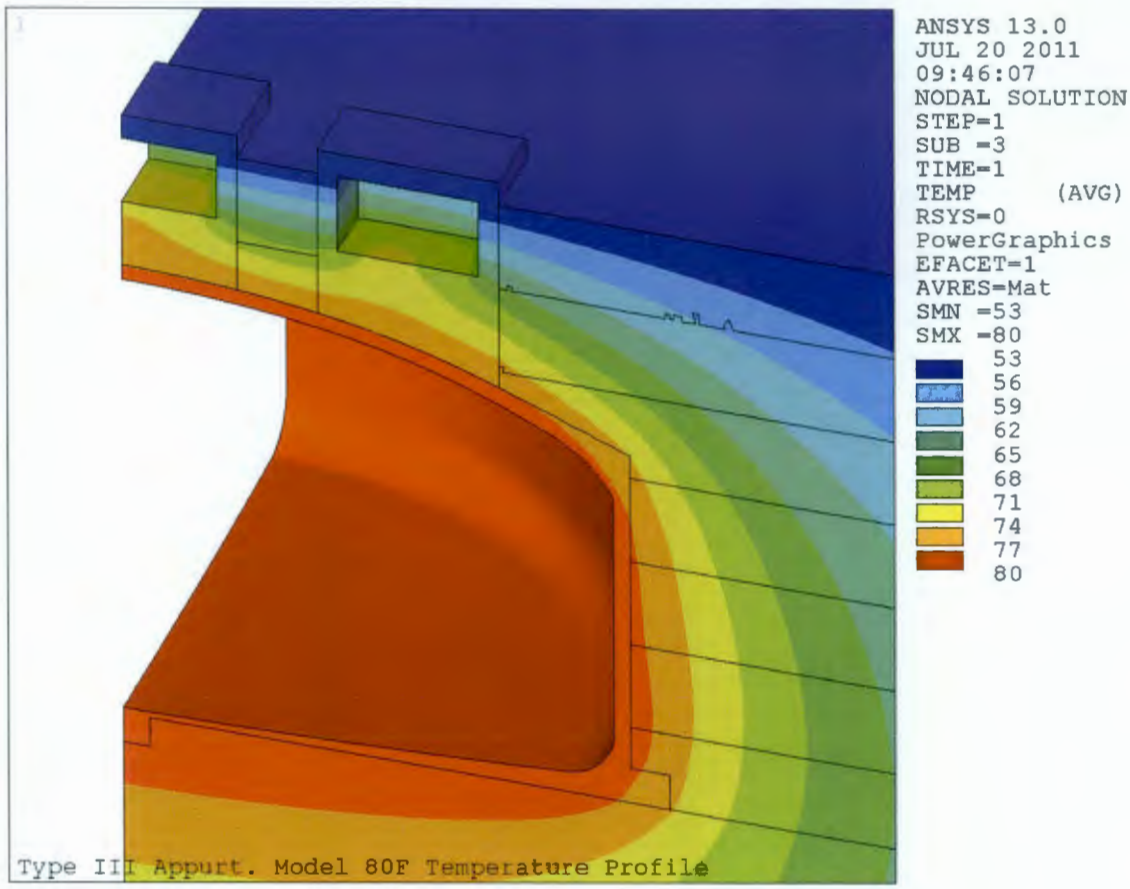

Figure 10.9. Temperature Profile at 80°F in Appurtenance Model

Material properties for the TOLA appurtenance models follow those for axisymmetric Run 2 presented in Section 8.4; nominal concrete modulus, near zero concrete tensile strength, nominal soil properties, and no concrete creep. If creep were included then the final creep strain accumulated over the simplified thermal history may not be accurate. Neglecting creep is also a conservative choice as creep relaxes stresses that would otherwise lead to higher demands. Just as in the axisymmetric TOLA models, after the peak temperature is reached the concrete properties in the tank are degraded according to their maximum temperature. The pits are assigned linear concrete material properties and do not undergo degradation in this model. The density of the pit concrete is adjusted such that the proper net weight for the center pit and the offset pit is achieved. Coefficients of friction for the contact surfaces between the tank and the soil are the same as in the axisymmetric TOLA model. The new vertical contact surface between the pits and the soil is assigned the same coefficient of friction as the tank sidewall. The new contact surfaces between the pit bottoms and tank dome are given a coefficient of friction of 0.6 for all loadsteps.

10.2 Type III SST Seismic Modeling with Appurtenances

Tank-to-tank overflow piping and process piping were not directly analyzed in the seismic analysis. The pipe-in-pipe design as described in Section B.7 in Appendix B for the tank-to-tank overflow piping is not expected to produce significant demand on the tank wall because the inner 3-inch-diameter pipe is free to slide axially and the outer 8-inch-diameter pipe is in contact with soil and supported by a reinforced concrete beam that is strain limited by the surrounding soil. In addition, the side nozzle design details mitigate moment transfers from soil induced pipe motion. These design features mitigate pipe axial loads and moment transfers to the tank wall. Similar design details associated with the small-diameter (3-inch) direct-buried tank process fill piping and support system as described in Section B.8 in Appendix B mitigate axial loads and moment transfers to the tank wall. The Type III SST small-diameter (4- and 12-inch) penetrations and risers were not analyzed in the seismic analysis (see Section B.4 in Appendix B). The larger 42-inch-diameter manhole penetrations were not analyzed as well because the riser is not directly tied to the tank dome at the dome penetration. The large-diameter post-construction riser and any equipment installed in the riser are supported by the pit floor. The pit is supported by the tank dome.

The dome load record data documents (Hundal 2004a through 2004d) determined the net additional loading on the dome from pits and installed equipment on the SSTs. These documents were used to find the maximum loading of pits and/or equipment for each tank type. Soil is removed when the pit is added above the tank. To be conservative the net maximum Type III pit weight including installed equipment for each pit type will be used. Table 10.1, lists the heaviest net weight pits that are expected to apply the largest concentrated dome load on a Type III tank.

Table 10.1. Type III SST Pit Appurtenances Maximum Net Weights

Appurtenance	Maximum Net Weight[a]	Type III SST Number	Reference
Pump Pit	23,200 lb	241-TX-115	Hundal (2004c), *241-TX*
Sluice Pit	58,800 lb	241-TY-101/102	Hundal (2004d), *241-TY*

(a) Maximum net weight with addition of appurtenance and subtraction of excavated soil weight.

10.2.1 Type III SST Pit Appurtenances Model Development

The Type III SST Appurtenances model development is the same as the Type III SST baseline seismic model except for the differences listed below. A more detailed description of the SST Type III baseline seismic model is provided in Chapter 6.

10.2.2 Pit Appurtenances Model Soil and Concrete Properties

Best-Estimate Soil (BES) and fully cracked concrete (FCC) properties have been used in the Type III SST pit appurtenances analysis. The FCC properties are the best estimate of expected concrete condition. This configuration is run as a full nonlinear (interface elements are only nonlinear elements in seismic model) seismic time history including gravity, and separately as a gravity-only analysis. The difference between the two cases provides the seismic only response.

10.2.3 Type III SST Pit Appurtenances Model Description

The Type III SST Appurtenance Seismic model contains the tank, soil, (2) sluice pits, and (1) pump pit. To reduce model size, a 180° model was used. The maximum net gain of weight for each pit for a Type III SST configuration will be included in the model (see Table 10.2 and Table 10.3). This model was used to analyze the tank structure for seismic loading with the additional weight of the pits (see Table 10.4). Figures 10.10 through 10.15 display an overall view of the Type III seismic appurtenances model containing one central pump pit and two offset sluice pits. Note that the modeled pit configuration is typical for Type III SSTs. The analyzed configuration was selected for consistency with the TOLA 90° model. Due to unsymmetrical pit dimensions two SST Type III seismic models were created to determine the worst case concrete demands during the time history. Configuration 1 has a 15.5-foot by 17.5-foot (1) pump pit and a 12.75- by 13.83-foot (2) sluice pit, the sluice pit is located at 0° and 180° on the Type III Seismic Appurtenances model (see Figures 10.12 and 10.14). Configuration 2 has a 15.5- by 17.5-foot (1) pump pit and a 12.75- by 13.83-foot (1) sluice pit, the sluice pit is located at 90° on the Type III Seismic Appurtenances model (see Figures 10.13 and 10.15). The concrete of the pit and the Type III SST dome are connected with interface elements. The modeling dimension of the pump pit and sluice pit are shown in Figures 10.10 and 10.11. The pits are modeled using SOLID45 elements, which is an eight-node element with three translational degrees-of-freedom at each node (see Figures 10.14, 10.15, and 10.16). Modeling and weight properties for the Pit Appurtenances model are shown in Table 10.2 through Table 10.4.

Table 10.2. Type III SST Pit Appurtenances Model Weights

Appurtenance	Removed Soil Volume	Removed Soil Weight[(a)]	Appurtenance Net Increase	Appurtenance Gross Weight
Pump Pit	15.5'x17.5'x11'	195.71 kip	11.6 kip	207.31 kip
Sluice Pit (2)	12.75'x13.83'x11'	313.10 kip	58.8 kip	371.90 kip

(a) Soil Density is assumed to be 129 lb/ft^3. See Section 7.10 for details.

Table 10.3. Type III SST Pit Appurtenances Dome Load

Appurtenance	Appurtenance Net Increase	Axisymmetric Model Factor	Dome Net Load Increase
Pump Pit	11.6 kip	2	23.2 kip
Sluice Pit (2)	58.8 kip	2	117.6 kip
Total			140.8 kip

Table 10.4. Type III SST Seismic Pit Appurtenance Model Loading Conditions

Load Type	Value
Uniform Load/Vapor Pressure	none
Concentrated Dome Load[(a)]	(200-140.8) kip = 59.2 kip
Tank Fluid Height/Density	none
Seismic Overburden Soil Height/Density	11 ft/129 lb/ft^3

(a) Distributed over Pump Pit area, centered over dome apex.

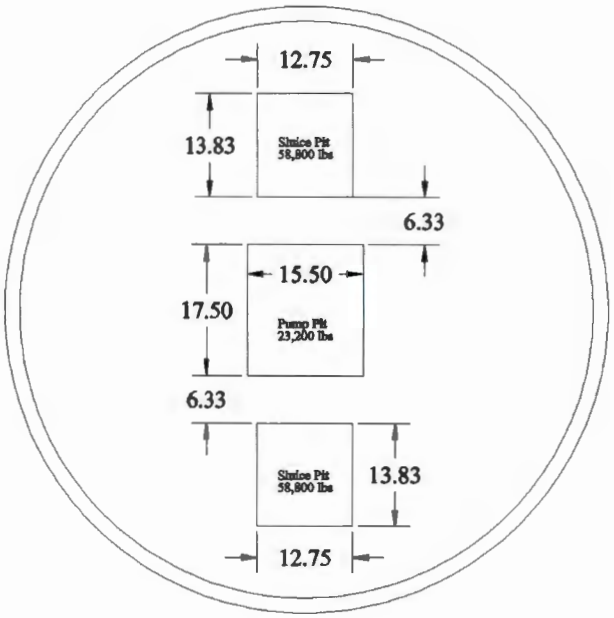

Figure 10.10. Type III SST Seismic Model Plan View with Pit Appurtenances (net weights indicated)

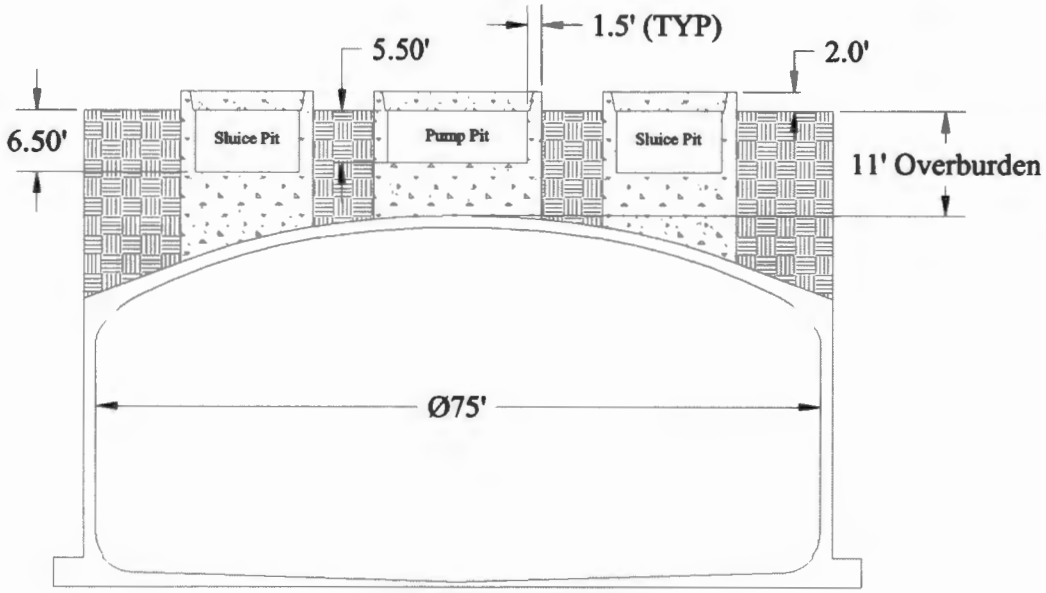

Figure 10.11. Type III SST Seismic Model Section View with Pit Appurtenances

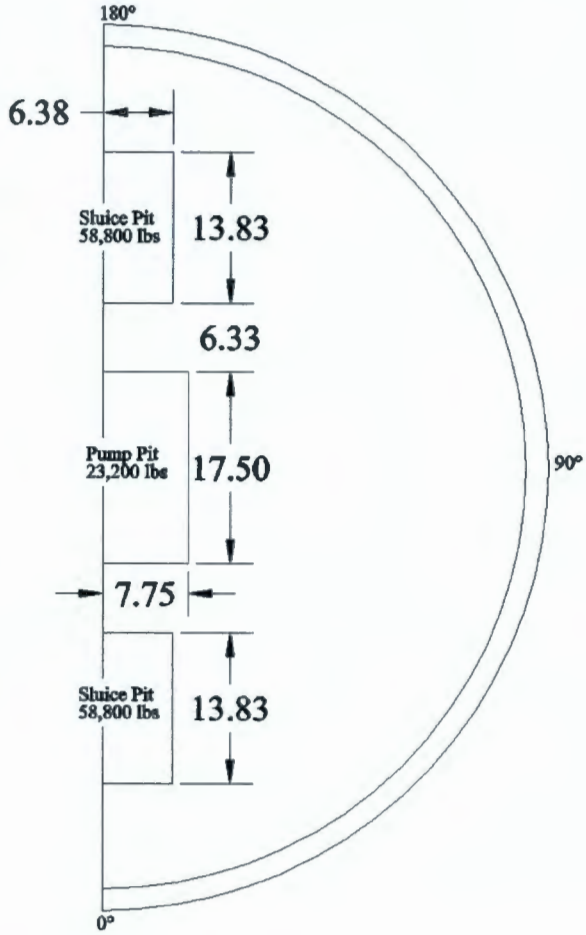

Figure 10.12. Type III SST Seismic Pit Appurtenances Model Configuration 1

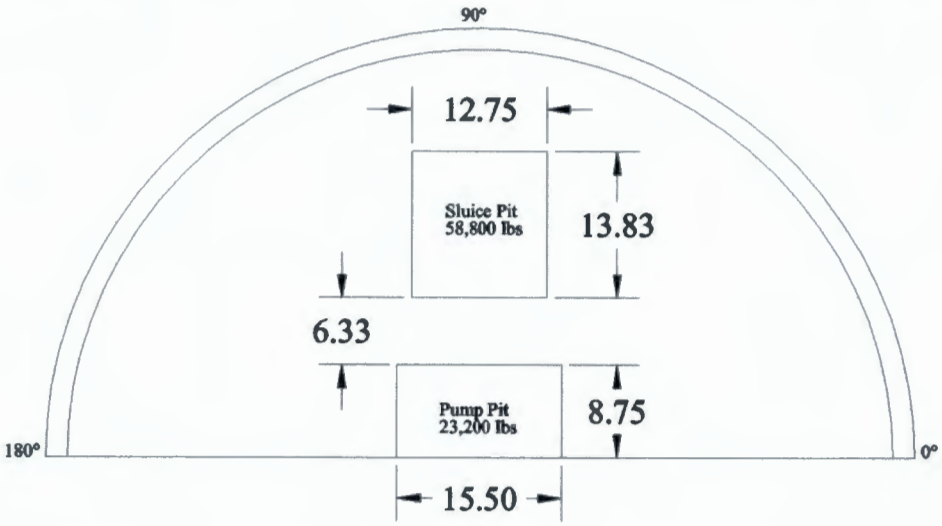

Figure 10.13. Type III SST Seismic Pit Appurtenances Model Configuration 2

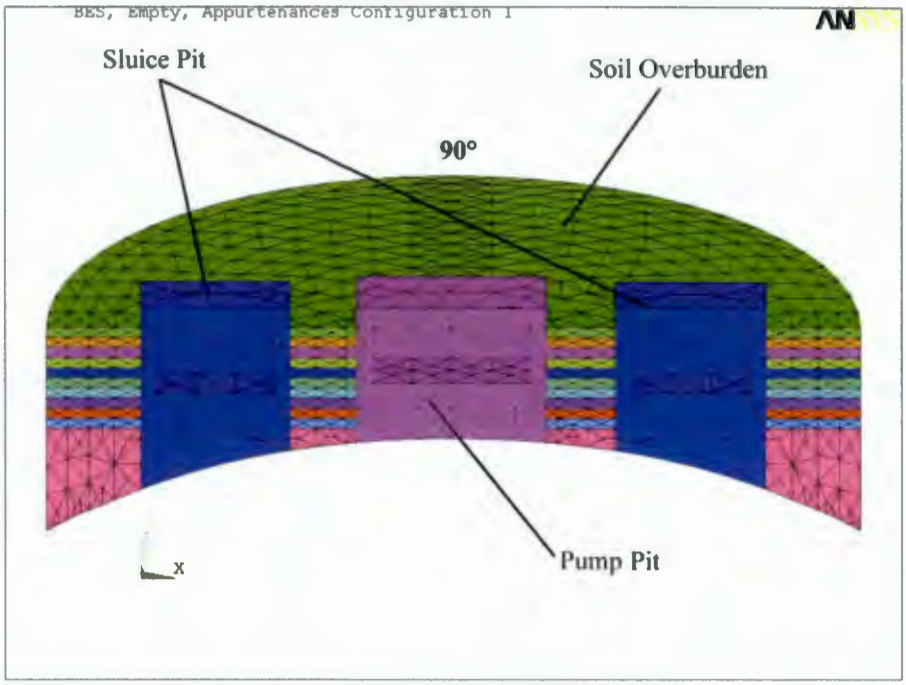

Figure 10.14. Type III SST Seismic Pit Appurtenances ANSYS® Model Configuration 1

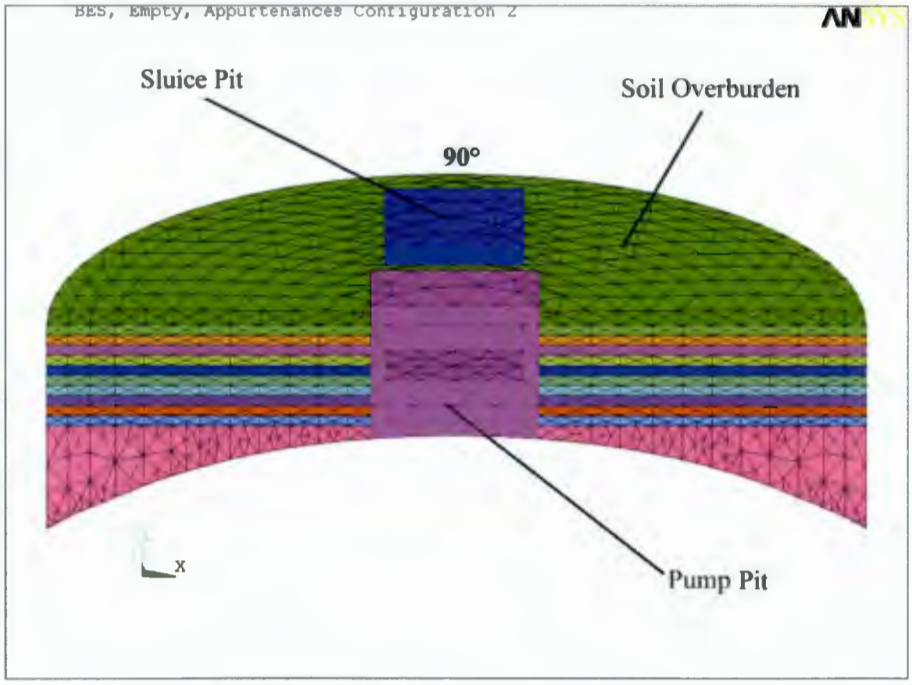

Figure 10.15. Type III SST Seismic Pit Appurtenances ANSYS® Model Configuration 2

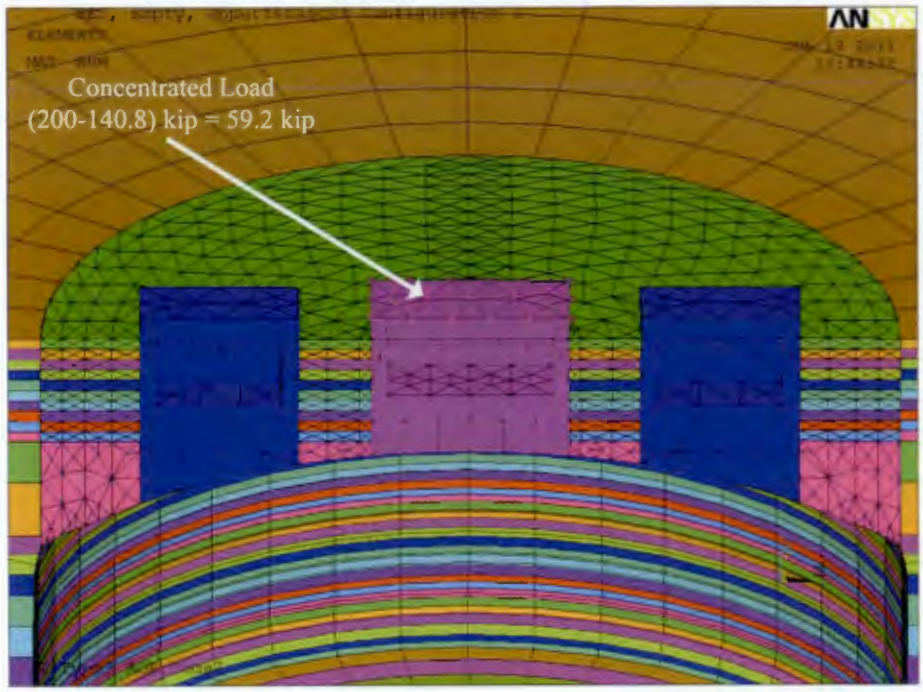

Figure 10.16. Type III SST ANSYS® Seismic Pit Appurtenances Model Elemental Plot

10.2.3.1 Concrete Pit/Concrete Tank Interface

A combination of TARGE170 and CONTA173 elements was used to model the interface between the concrete pit and the concrete tank. The concrete dome is the target surface and the concrete pit is the contact surface. The surfaces are allowed to slide and separate (standard contact). A coefficient of friction of 0.6 was used in both the gravity step of the and the seismic time history. See Figure 10.17 for the locations of model contact surfaces. The mesh of the bottom of concrete pit does not match mesh of the concrete dome but the contact elements allow proper load transfer.

10.2.3.2 Concrete Pit/Overburden Soil Fill Interface

A combination of TARGE170 and CONTA173 elements was used to model the interface between the concrete pit and the overburden soil. The overburden soil is the target surface and the concrete pit is the contact surface. Initial geometrical penetration or gap and offset are both excluded. A coefficient of friction of 0.005 was used in the gravity step of the seismic model and a coefficient of friction of 0.6 was used during seismic time history. See Figure 10.17 for the locations of model contact surfaces. The mesh of the concrete pit does not match mesh of the soil overburden but the contact elements allow proper load transfer.

Table 10.5. Summary of Type III SST Seismic Pit Appurtenances Model Interface Friction Properties

Interface	Initial Gravity Step Friction Value	Seismic Time History Friction Value
Soil to Tank: Dome down to top of sidewall	0.3	0.3
Soil to Tank: Sidewall	0.05	0.5
Soil to Tank: Footing top surface	0.6	0.6
Soil to Tank: Floor	0.6	0.6
Pits to Soil	0.005	0.6
Pits to Tank Dome	0.6	0.6
Tank Dome Overburden soil ring to ring	0.05	0.2

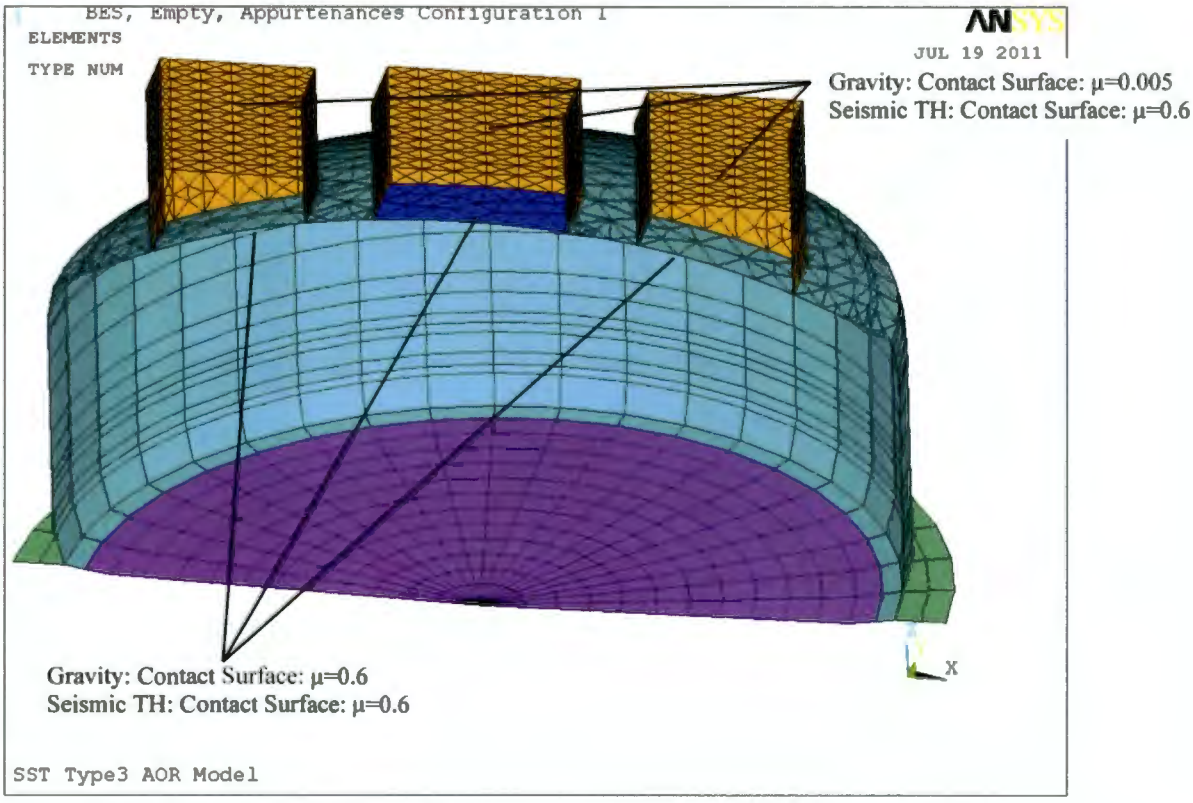

Figure 10.17. Type III SST ANSYS® Seismic Pit Appurtenances Model Contact Surfaces

10.2.4 Type III SST Seismic Pit Appurtenances Model Run Matrix

The combinations used for the appurtenances seismic runs are listed in Table 10.6. The pit locations in relation to the ACI sections are shown in Figure 10.15. An initial at-rest soil pressure is imposed along the vertical wall of the tank. The run matrix includes the empty tank case although the choice is immaterial because the critical ACI sections, 14–16, of the tank will not be influenced by waste in the tank as shown in Section 9.1, Figures 9.1 through Figure 9.6. These figures show little or no change in the tank demands for the three cases, empty tank, high shear modulus tank waste and low shear modulus tank waste.

Table 10.6. Type III SST Seismic Pit Appurtenances Model Run Matrix

Run	Soil	Backfill	Time History	Tank Concrete	Waste	At Rest	Configuration
1	BES	BE	BES H + V	FCC	Empty	Wall	1
2	BES	BE	BES H + V	FCC	Empty	Wall	2

BES = Best Estimate Soil
FCC = Fully Cracked Concrete Properties

10.2.5 Pit Appurtenances Type III SST Seismic Results

10.2.5.1 Concrete Tank

Concrete tank force moment and shear stress resultants are extracted from the model using the post-processing methods described in Chapter 6. The seismic-only load is the difference between the full transient loading and gravity only. The greatest difference between the minima or maxima of each shell section stress resultant is reported, which may not be the same as the difference in the bounding values of each stress resultant (see example in Section 6).

The concrete shell force moment and shear stress resultants are plotted against a "path" that starts at the dome apex and increasing to the floor center shown in Figure 10.18. The stress resultants have been enveloped circumferentially for these "paths" plots. In addition, surfaced plots are provided that show the circumferential variation of the stress resultants. Concrete force moment and shear stress resultant plots are as follows.

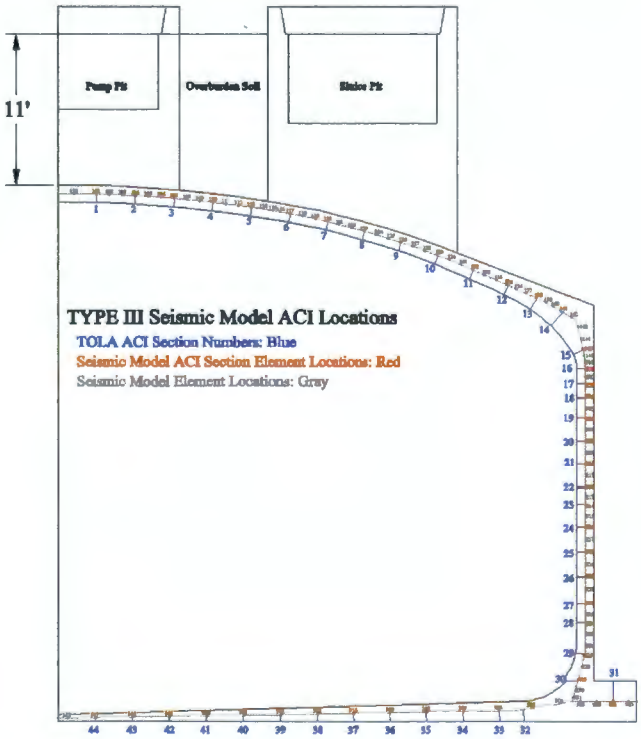

Figure 10.18. Type III SST ANSYS® Seismic Pit Appurtenances Model ACI Locations

Figure 10.19 through Figure 10.30 display the seismic-only force, moment, and shear stress resultant surface plots for Best-Estimate Soil (BES) Empty Tank with pit appurtenances for Configuration 1 and 2. The pump pit is located at ACI sections 1–3 and the sluice pits are located at ACI sections 5–10 (see Figure 10.16 through Figure 10.18). Figure 10.31 through Figure 10.36 compare the corresponding maximum seismic-only force, moment, and shear stress resultants with and without appurtenances.

The appurtenances seismic model produces a different dome response due to the location of the pits and redistribution relative to the baseline of the 200-kip concentrated loading on the dome. There are some differences in the meridional and hoop forces between the Type III SST Pit Appurtenances, Best-Estimate Soil, Empty tank runs compared to the Type III SST baseline, Best-Estimate Soil, Empty tank run (see Figure 10.31 and Figure 10.32). The additional demand results only showed small differences at pit locations in the dome between the Type III SST baseline, Best-Estimate Soil, Empty tank run. and the Type III SST Pit Appurtenances, Best-Estimate Soil, Empty tank run (see Figure 10.33 through Figure 10.36). The Pit Appurtenances Configuration 1 and Configuration 2 seismic results will be enveloped taking the maximum demand at each section before being combined with TOLA for an ACI code evaluation.

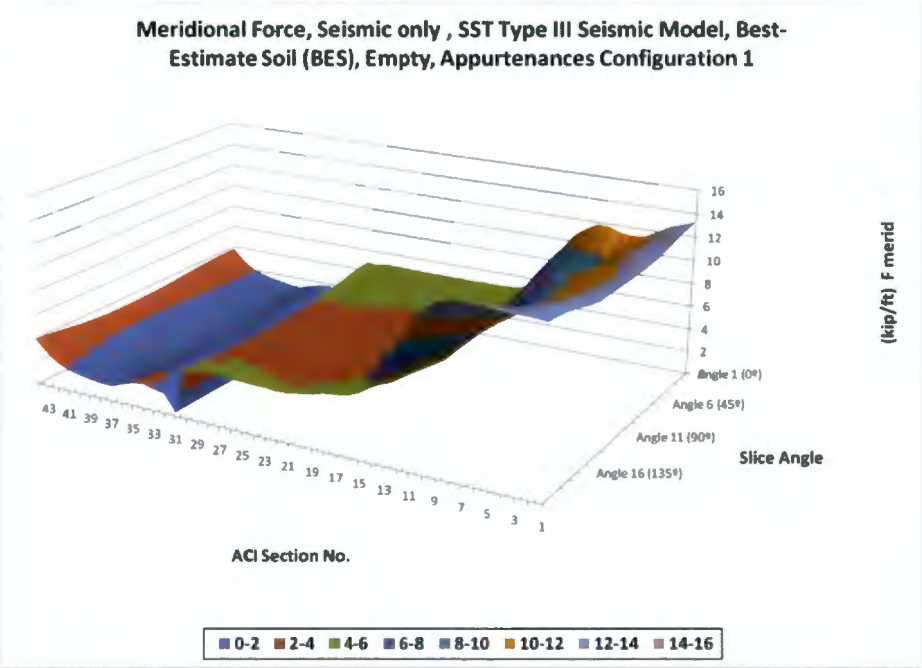

Figure 10.19. Concrete Tank Maximum Meridional Force: Type III SST (BES, Empty) Pit Appurtenances Model Configuration 1 (Seismic Only)

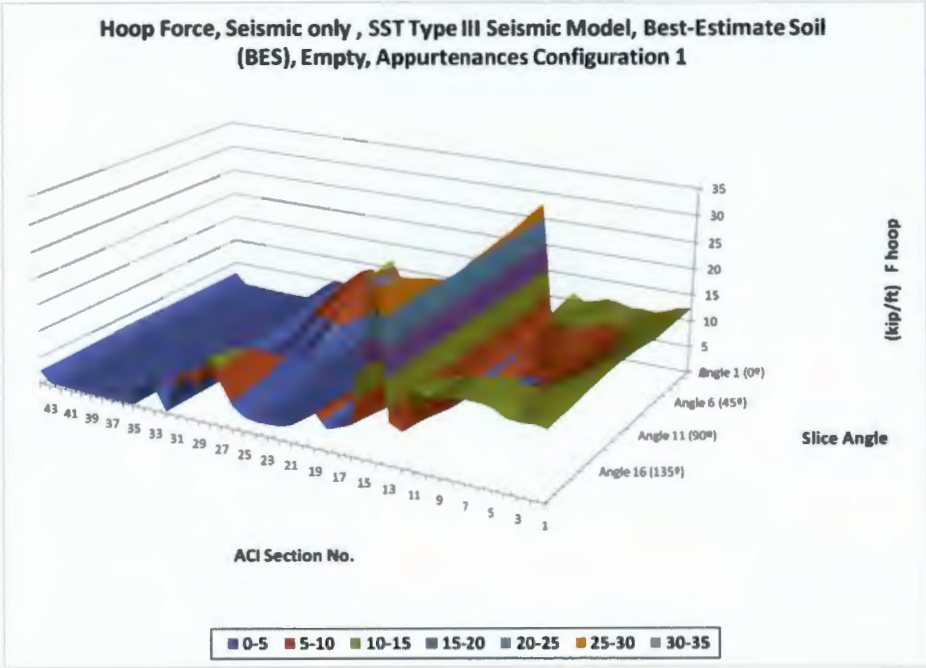

Figure 10.20. Concrete Tank Maximum Hoop Force: Type III SST (BES, Empty) Pit Appurtenances Model Configuration 1 (Seismic Only)

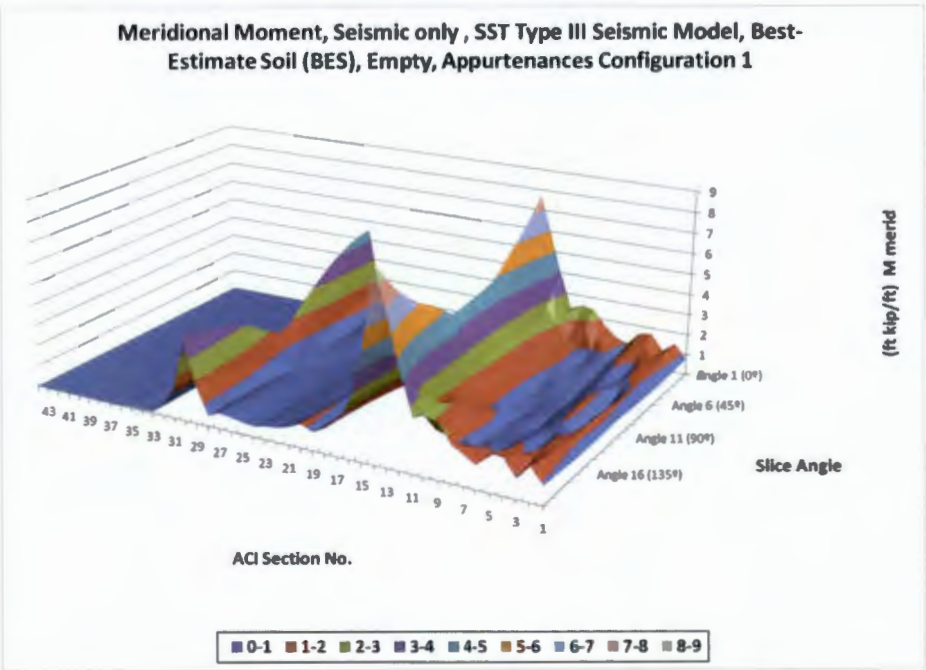

Figure 10.21. Concrete Tank Maximum Meridional Moment: Type III SST (BES, Empty) Pit Appurtenances Model Configuration 1 (Seismic Only)

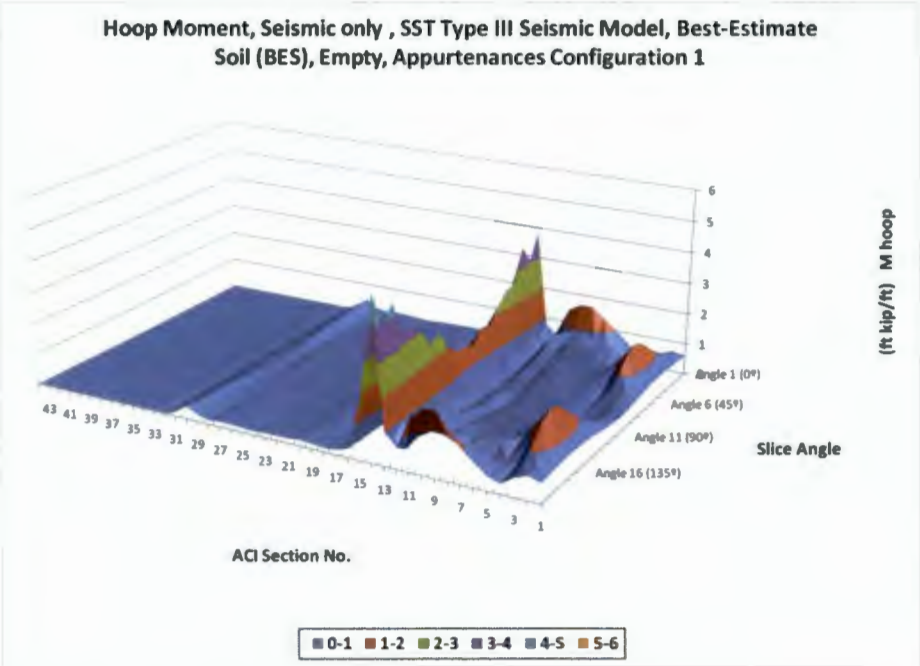

Figure 10.22. Concrete Tank Maximum Hoop Moment: Type III SST (BES, Empty) Pit Appurtenances Model Configuration 1 (Seismic Only)

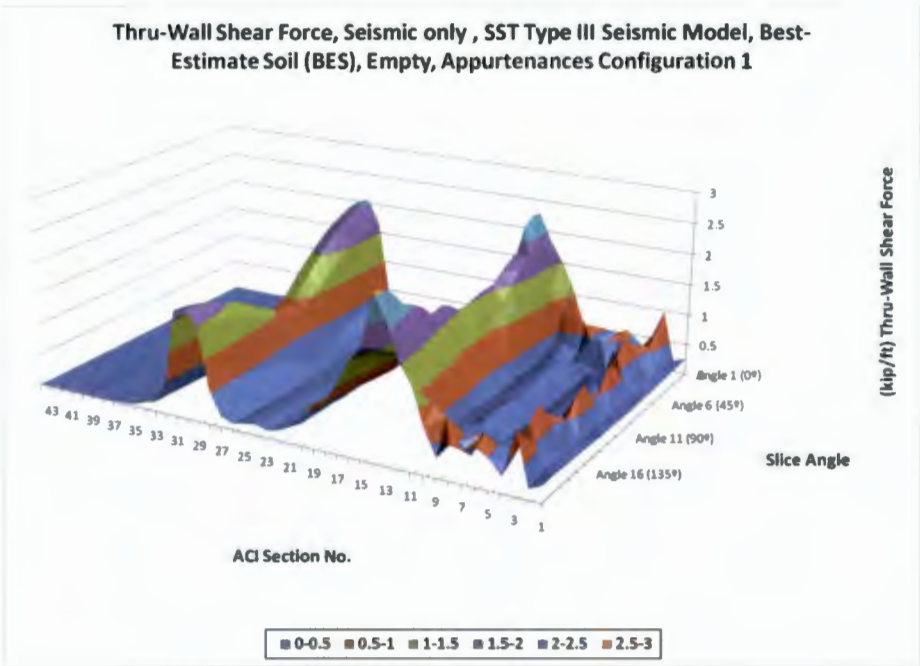

Figure 10.23. Concrete Tank Maximum Through-Wall Shear Force: Type III SST (BES, Empty) Pit Appurtenances Model Configuration 1 (Seismic Only)

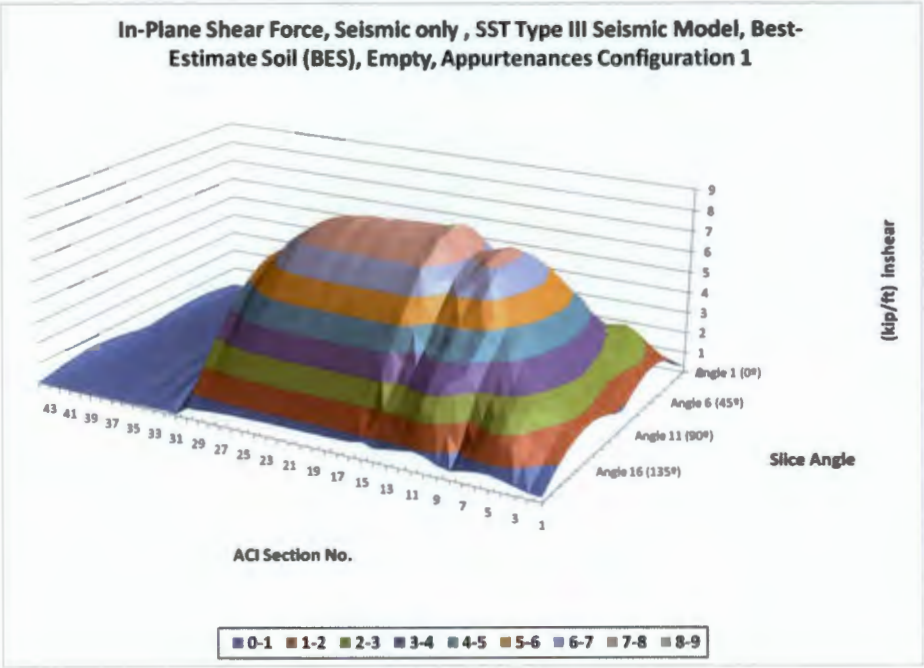

Figure 10.24. Concrete Tank Maximum In-Plane Shear Force: Type III SST (BES, Empty) Pit Appurtenances Model Configuration 1 (Seismic Only)

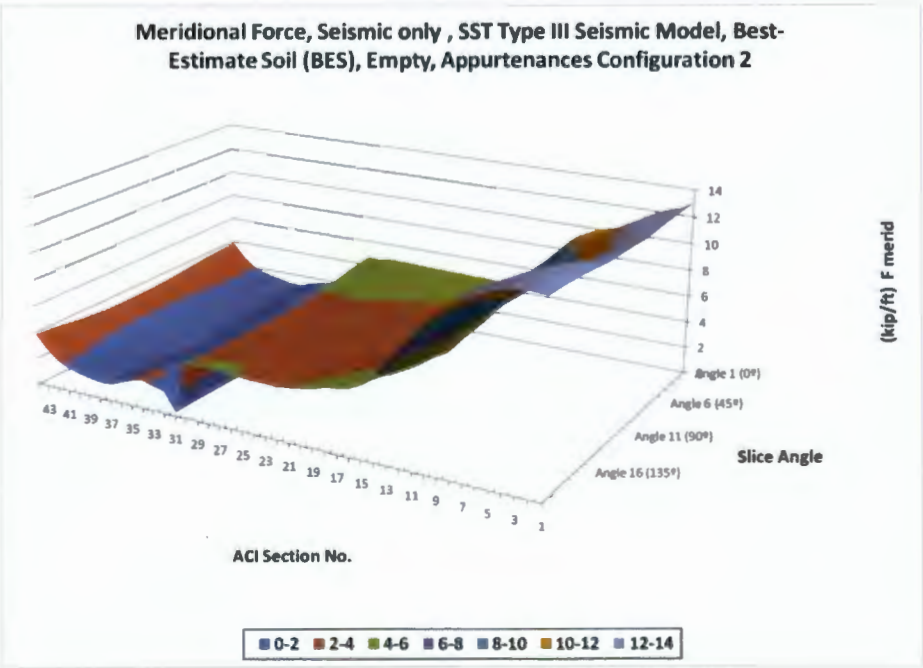

Figure 10.25. Concrete Tank Maximum Meridional Force: Type III SST (BES, Empty) Pit Appurtenances Model Configuration 2 (Seismic Only)

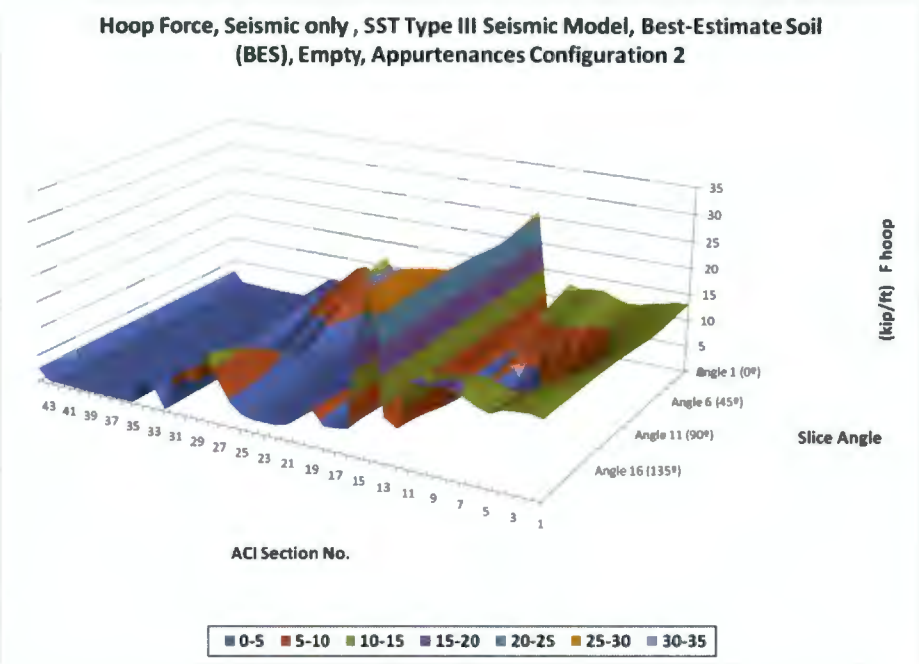

Figure 10.26. Concrete Tank Maximum Hoop Force: Type III SST (BES, Empty) Pit Appurtenances Model Configuration 2 (Seismic Only)

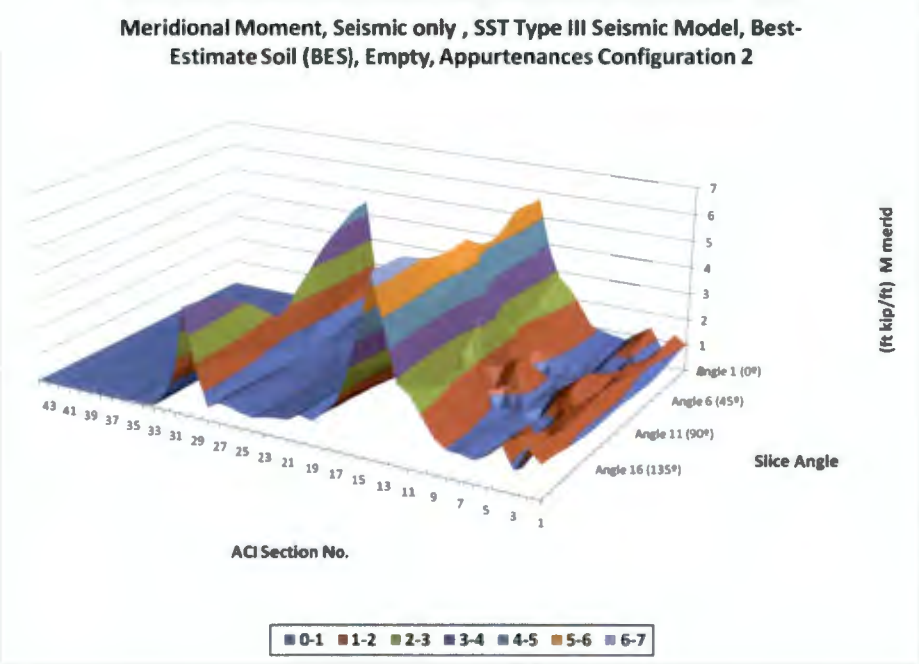

Figure 10.27. Concrete Tank Maximum Meridional Moment: Type III SST (BES, Empty) Pit Appurtenances Model Configuration 2 (Seismic Only)

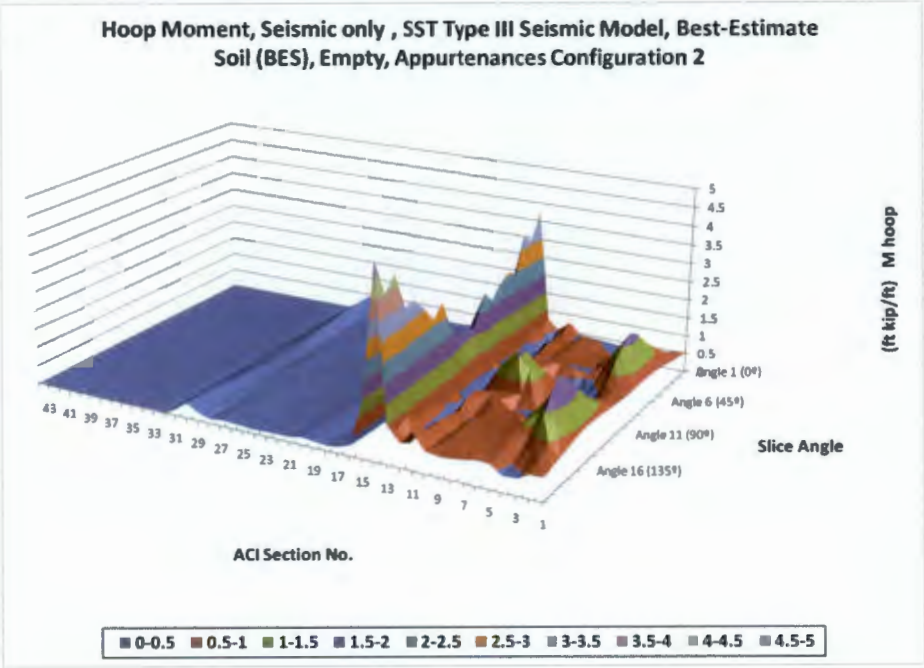

Figure 10.28. Concrete Tank Maximum Hoop Moment: Type III SST (BES, Empty) Pit Appurtenances Model Configuration 2 (Seismic Only)

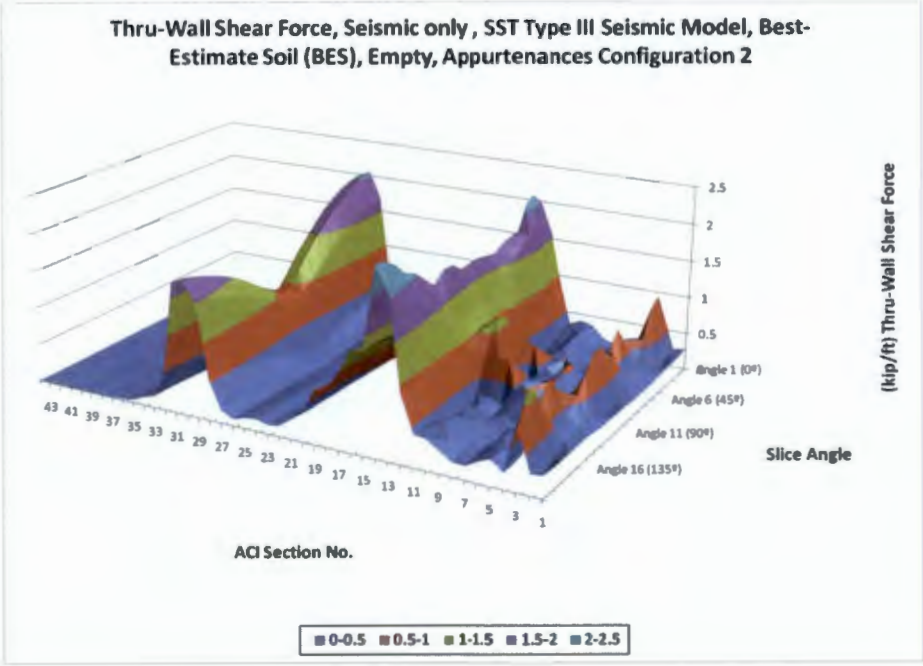

Figure 10.29. Concrete Tank Maximum Through-Wall Shear Force: Type III SST (BES, Empty) Pit Appurtenances Model Configuration 2 (Seismic Only)

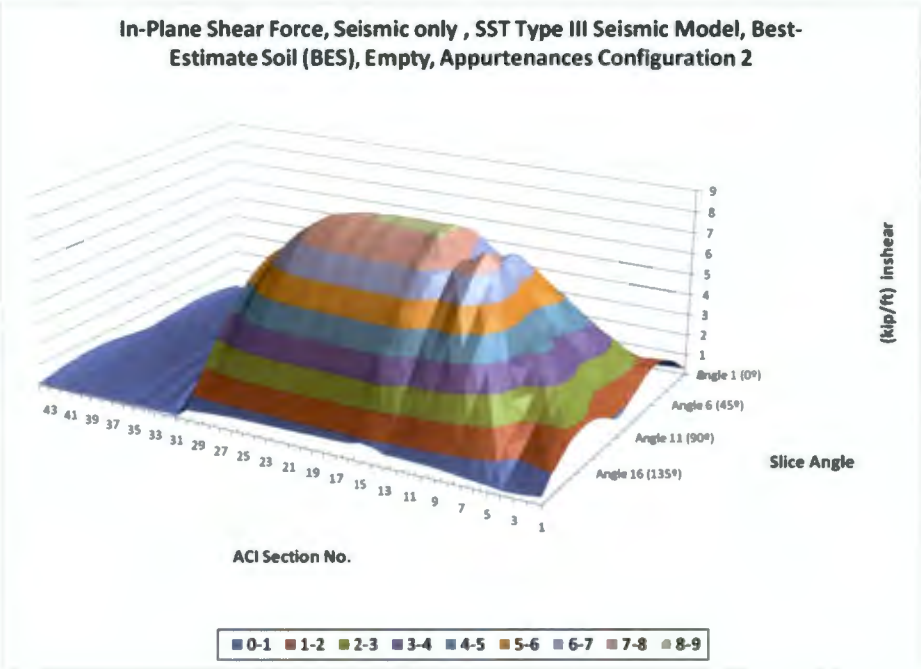

Figure 10.30. Concrete Tank Maximum In-Plane Shear Force: Type III SST (BES, Empty) Pit Appurtenances Model Configuration 2 (Seismic Only)

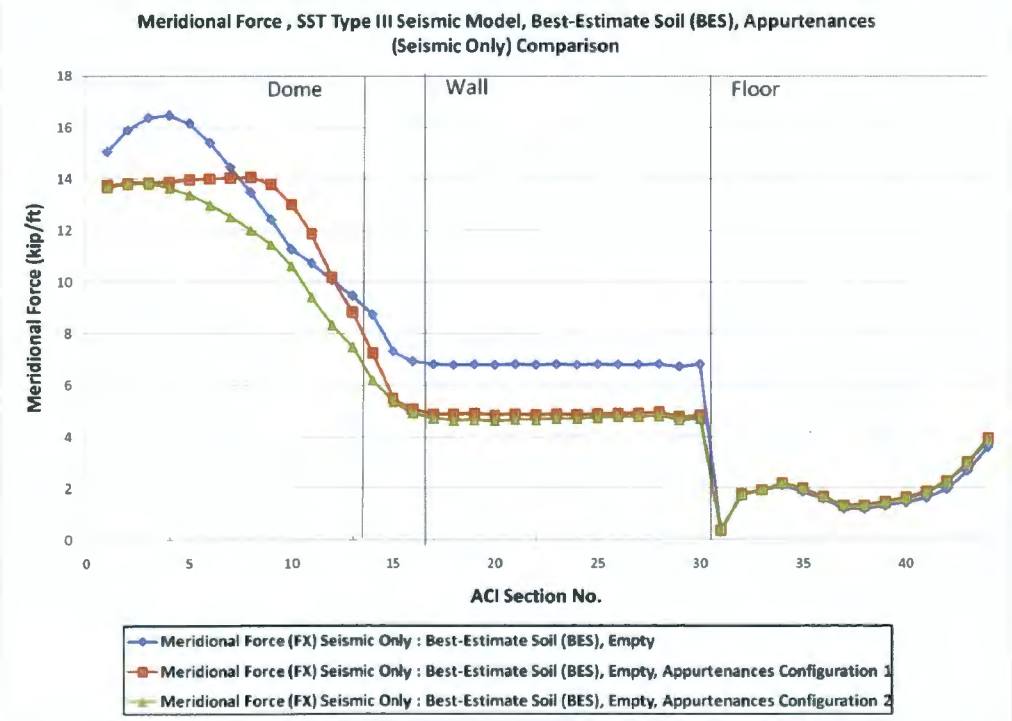

Figure 10.31. Concrete Tank Maximum Meridional Force – Type III SST (BES, Empty) Comparison with and without Pit Appurtenances (Seismic Only)

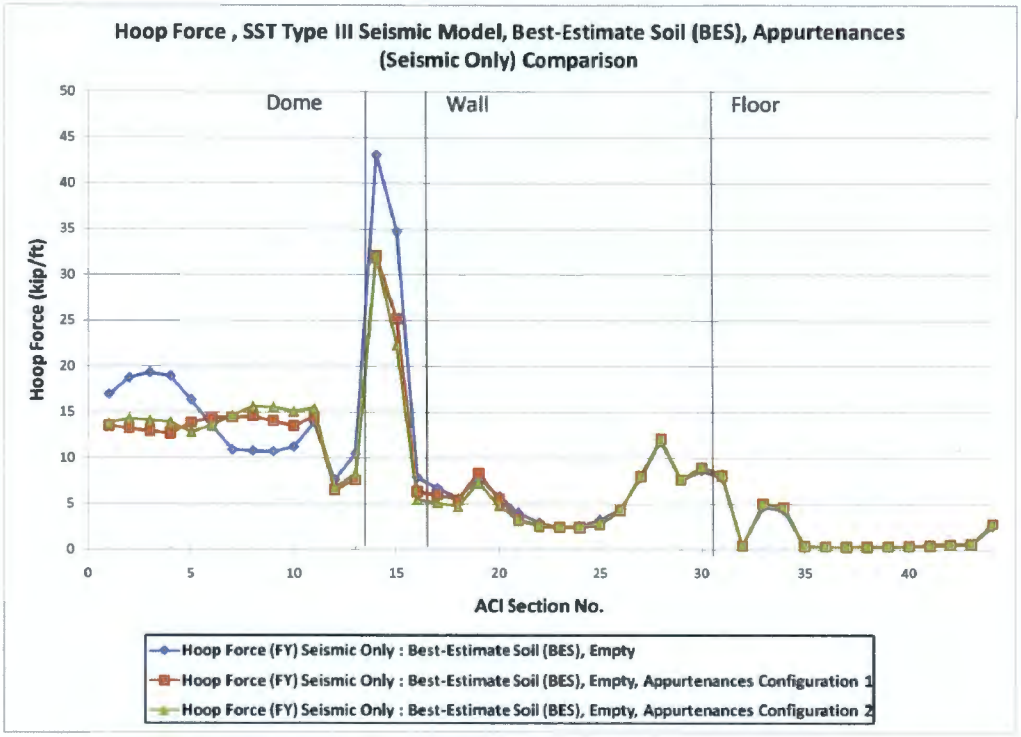

Figure 10.32. Concrete Tank Maximum Hoop Force – Type III SST (BES, Empty) Comparison with and without Pit Appurtenances (Seismic Only)

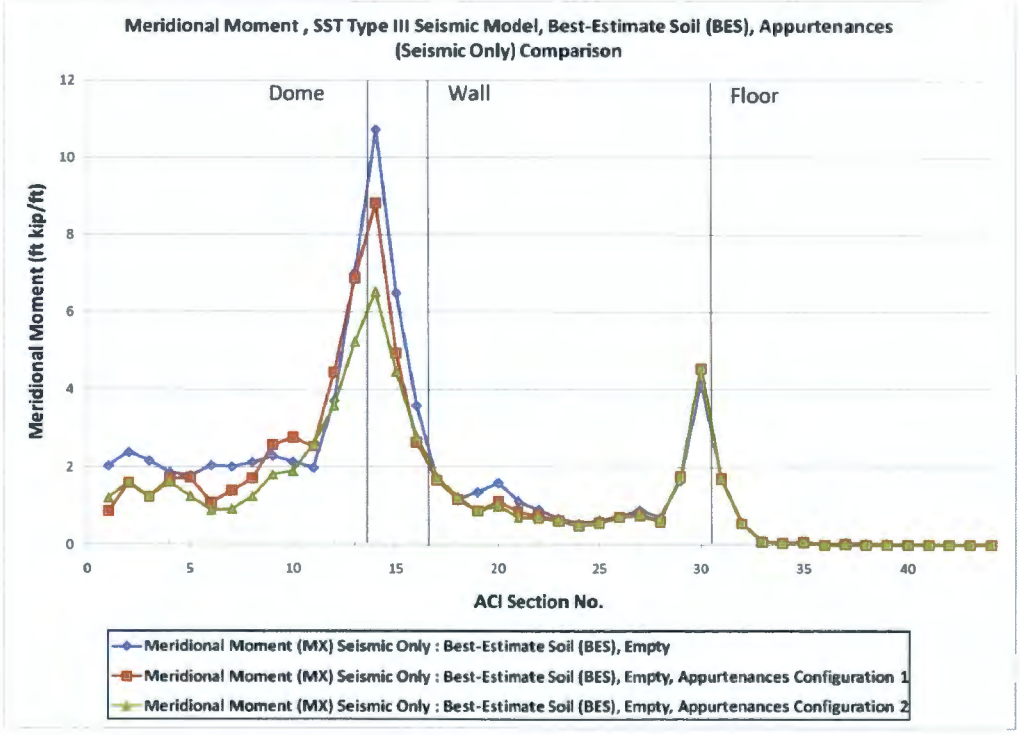

Figure 10.33. Concrete Tank Maximum Meridional Moment – Type III SST (BES, Empty) Comparison with and without Pit Appurtenances (Seismic Only)

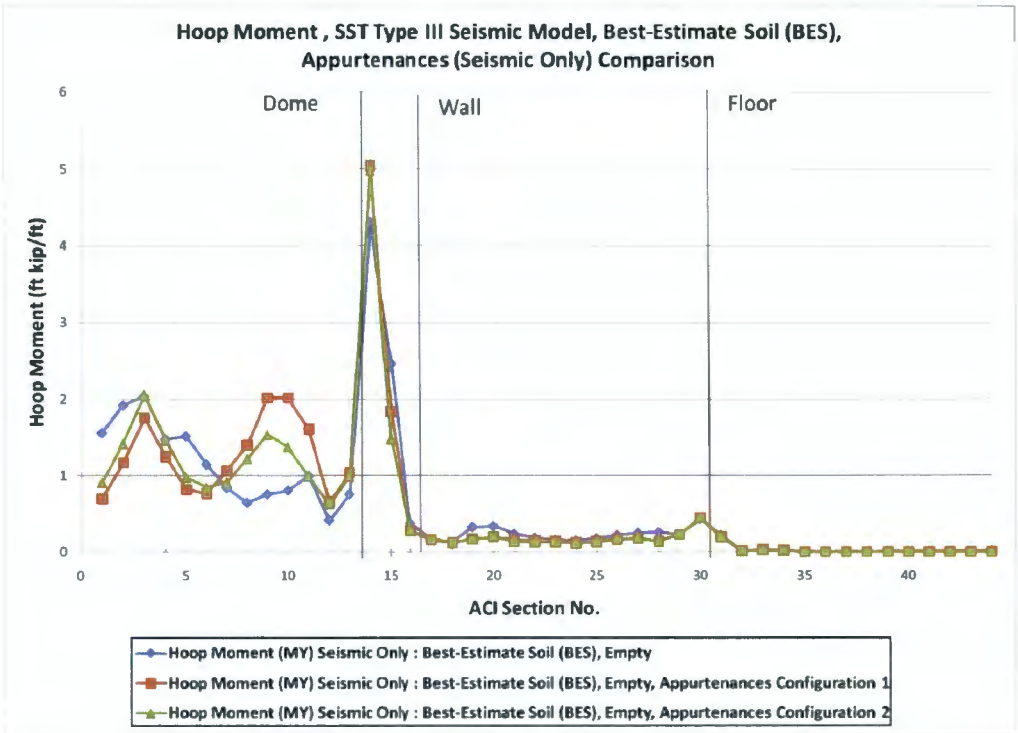

Figure 10.34. Concrete Tank Maximum Hoop Moment – Type III SST (BES, Empty) Comparison with and without Pit Appurtenances (Seismic Only)

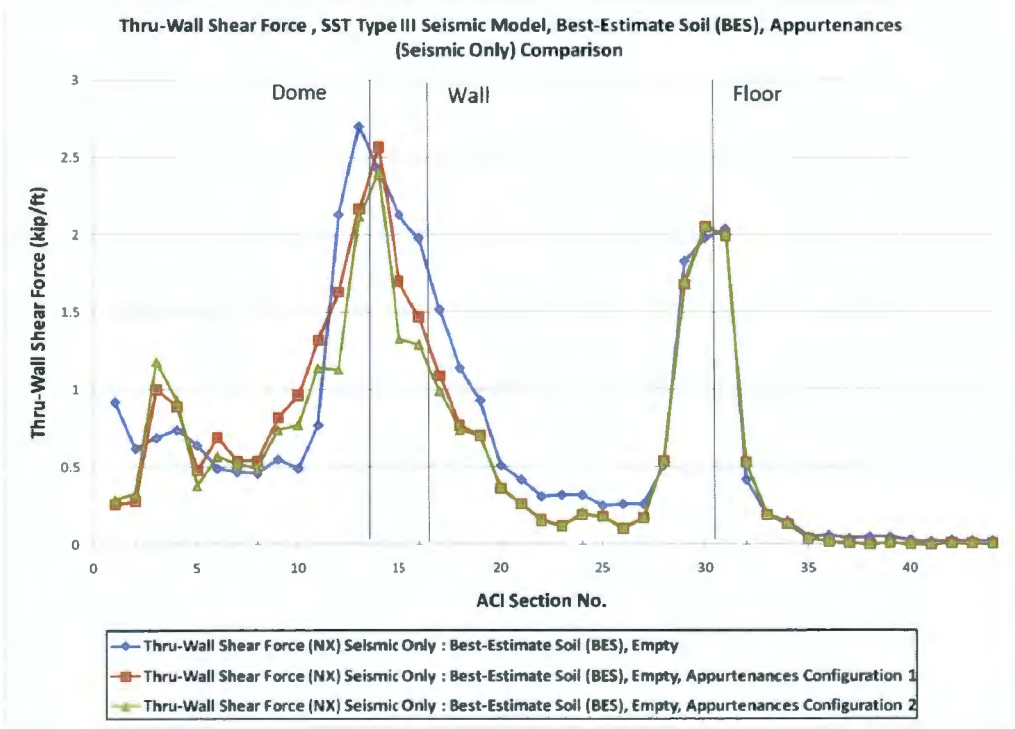

Figure 10.35. Concrete Tank Maximum Through-Wall Shear – Type III SST (BES, Empty) Comparison with and without Pit Appurtenances (Seismic Only)

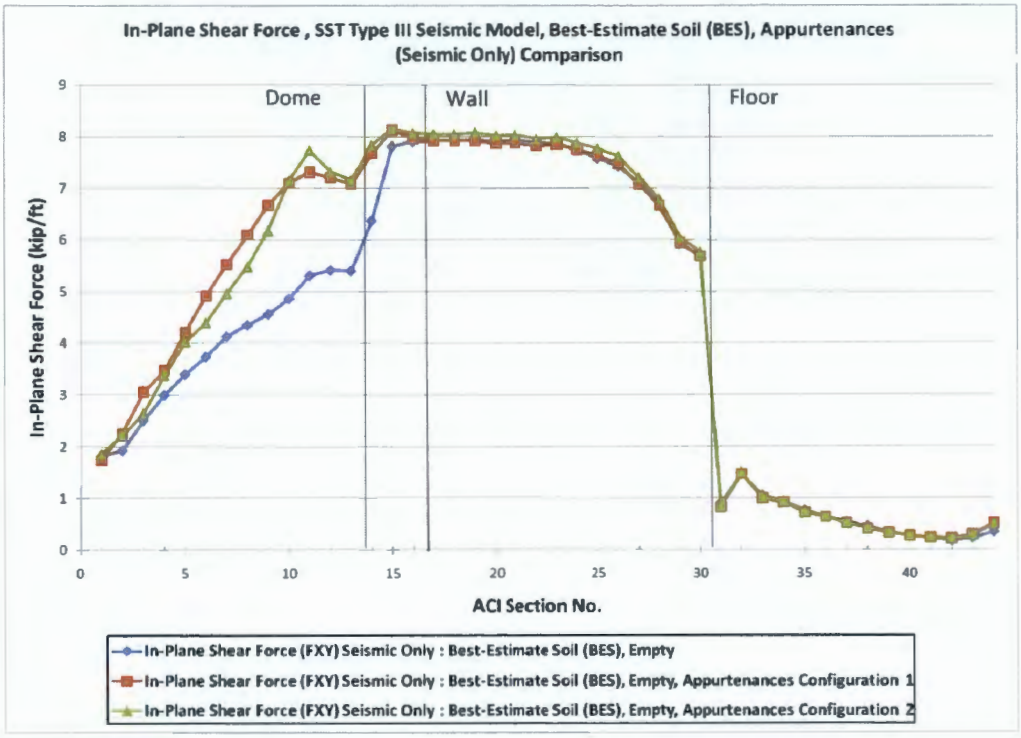

Figure 10.36. Concrete Tank Maximum In-Plane Shear – Type III SST (BES, Empty) Comparison with and without Pit Appurtenances (Seismic Only)

10.3 Appurtenance Demand to Capacity Ratios

Demands were extracted from the TOLA appurtenance model at the peak temperature as well as at LC1, LC4, and LC9 load steps. Just as in the axisymmetric runs, ACI D/C ratios were evaluated at the same 44 sections from the dome through the slab shown in Figure 8.1. However, in the appurtenance model, this evaluation was performed for 44 sections on each 3° increment from the 0° boundary to the 90° boundary. For the seismic appurtenance model, demands were enveloped over the time history to report the maximum value at element centroids for both appurtenance configurations. For ACI LC4 the maximum seismic demands from the two configurations over all angles from 0° to 180° (not angle specific seismic demands) were combined with the angle specific TOLA demands. Again, four possible force/moment combinations are evaluated as described in Section 9.2 with the maximum D/C ratio being reported.

Figure 10.37 shows the D/C ratios for the appurtenance model under the peak temperature. The left column shows a three dimensional representation tank with the D/C ratios represented by the coloring. The right column shows a representation of the same D/C ratio (y-axis) versus the section number (x-axis) and angle (y-axis). Recall the offset pit is centered along the 0° boundary. At the peak temperature loads are unfactored. Shear D/C ratios are shown in the top row, meridional D/C ratios are shown in the middle row, and hoop D/C ratios are shown in the bottom row. At peak temperatures all D/C ratios are less than one. Apart from the dome where the pits are located, there is very little variation along the angle from 0° to 90°. These appurtenance D/C ratios can be compared to the axisymmetric D/C ratios for Run 2 at peak temperature shown in Figure 8.16. The variation along the section numbers of the appurtenance D/C

ratios matches very closely to the axisymmetric D/C ratios. This indicates that the pits modeled have little influence on the structural response in the haunch, wall, and slab. In-plane shear D/C ratios were also calculated for peak temperatures but are not shown here as all values were less than 0.08.

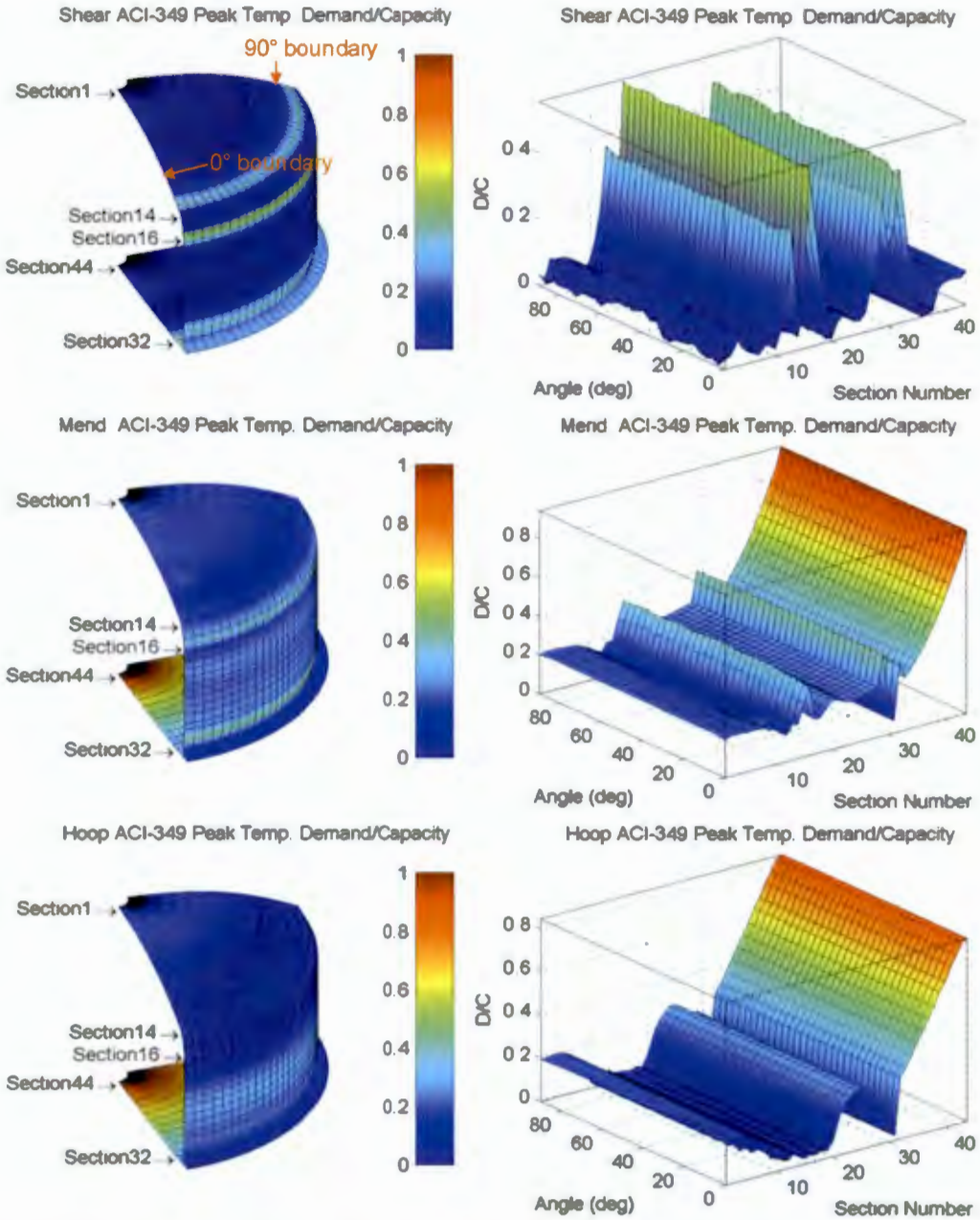

Figure 10.37. Peak Temperature D/C Ratios for Through Wall Shear (top), Meridional (middle), and Hoop (bottom)

Figure 10.38 shows the D/C ratios for the appurtenance model under ACI-349 LC1. Again, shear D/C ratios are shown in the top row, meridional D/C ratios are shown in the middle row, and hoop D/C ratios are shown in the bottom row. Under ACI-349 LC1 factors, all D/C ratios are less than one. There is very little variation along the angle from 0° to 90° except for in the dome near the pits and in the slab.

The variation in the slab is the result of the low capacities in the slab, particularly in tension as described in Section 9.4, which gives rise to slab D/C ratios that are very sensitive to the demands. These appurtenance D/C ratios can be compared to the axisymmetric D/C ratios for Run 2 under LC1 shown in Figure 8.15. Again, the variation along the section numbers of the appurtenance D/C ratios match very closely to the axisymmetric D/C ratios. This indicates that the pits modeled have little influence on the structural response in the haunch, wall, and slab under LC1. In-plane shear D/C ratios were also calculated for LC1 but are not shown here as all values were less than 0.12.

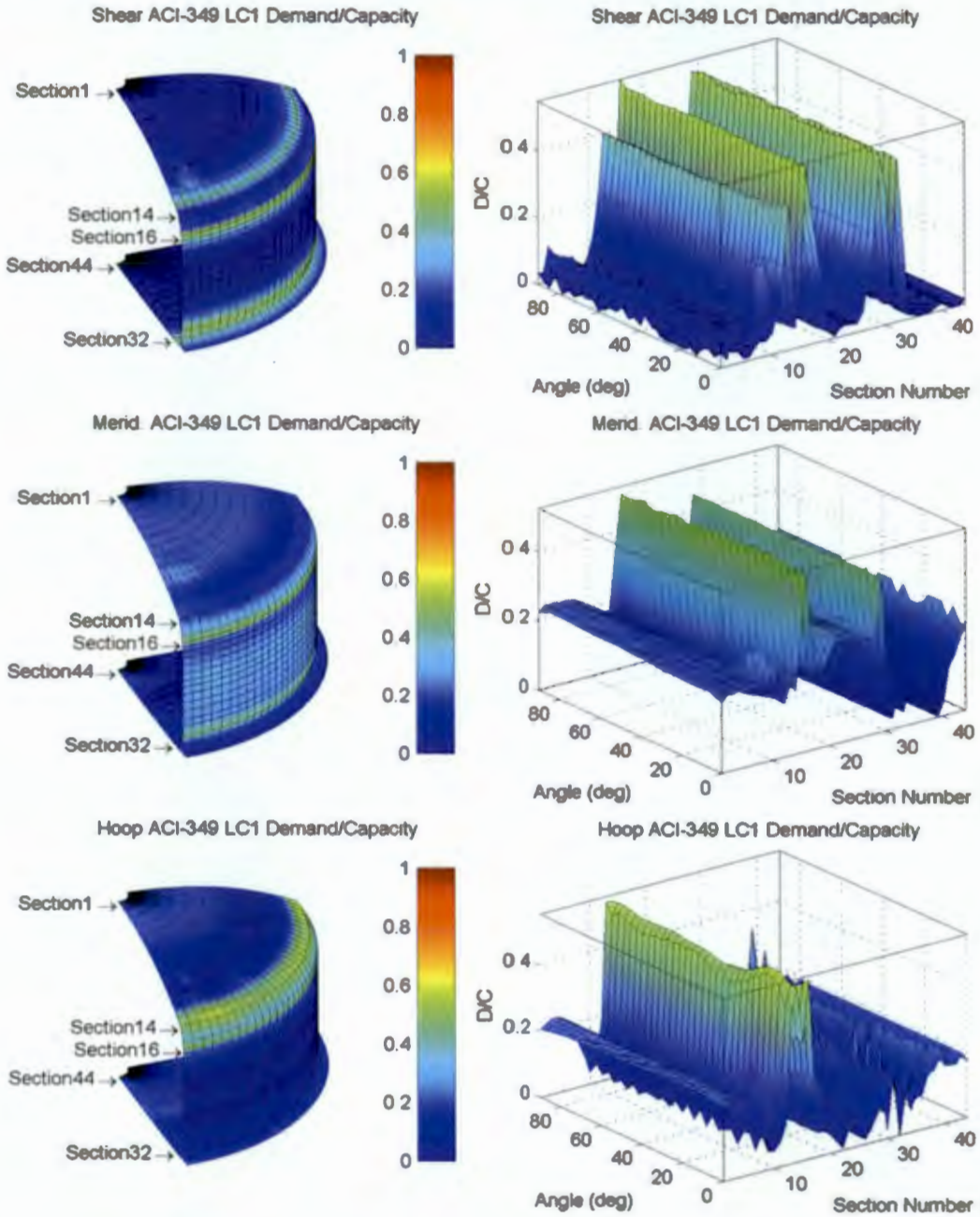

Figure 10.38. ACI LC1 D/C Ratios for through Wall Shear (top), Meridional (middle), and Hoop (bottom)

Figure 10.39 shows the D/C ratios for the appurtenance model under ACI-349 LC9. Again, shear D/C ratios are shown in the top row, meridional D/C ratios are shown in the middle row, and hoop D/C ratios are shown in the bottom row. As with the previous cases, under ACI-349 LC9 factors all D/C ratios are less than one. There is little variation along the angle from 0° to 90° except for in the dome near the pits. These appurtenance D/C ratios can be compared to the axisymmetric D/C ratios for Run 2 under LC9 shown in Figure 8.28. Again, the variation along the section numbers of the appurtenance D/C ratios match very closely to the axisymmetric D/C ratios indicating that the pits modeled have little influence on the structural response in the haunch, wall, and slab under LC9. In-plane shear D/C ratios were also calculated for LC9 but are not shown here as all values were less than 0.09.

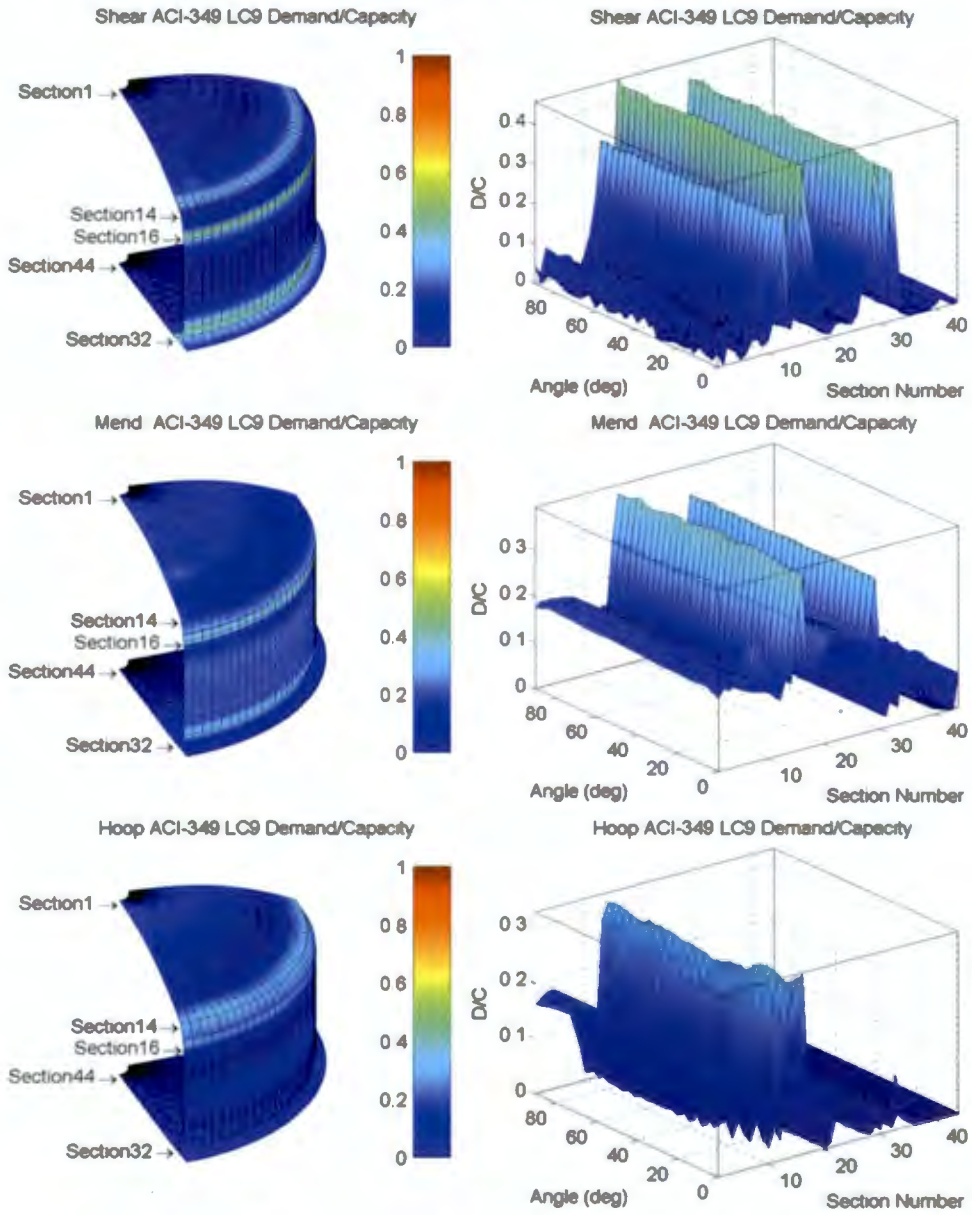

Figure 10.39. ACI LC9 D/C Ratios for Through Wall Shear (top), Meridional (middle), and Hoop (bottom)

Finally, Figure 10.40 shows the D/C ratios for the appurtenance model under ACI-349 LC4. These D/C ratios are the maximum of the four seismic and TOLA combinations for LC4. Again, shear D/C ratios are shown in the top row, meridional D/C ratios are shown in the middle row, and hoop D/C ratios are shown in the bottom row. Under ACI-349 LC4 all D/C ratios in the dome, haunch, wall, and outer footing are less than one. The hoop D/C ratio exceeds one in the slab. The shear D/C ratio peaks along the top of the wall at a value of about 0.89. There is little variation along the angle from 0° to 90° outside of the dome and haunch. The variation of D/C ratios in the haunch indicate that there is a slightly larger region of influence of the pits in the seismic analysis. These appurtenance D/C ratios can best be compared to the axisymmetric D/C ratios for combined Run 1 under LC4 as shown in Figure 9.31. Unlike this appurtenance model, the concrete in combined Run 1 includes creep. Here there are some differences between the two sets of D/C ratios. The shear D/C ratios in both sets peak at the same location but the shear peak in the appurtenance run is more than twice the value in the axisymmetric run. The meridional D/C ratios have spikes in the same sections but in some sections the appurtenance run shows greater spikes while in others the axisymmetric run shows greater spikes. The hoop D/C ratios in both sets also show similar behaviors. Both hoop D/C ratios exceed one in the slab and have spikes in the outer dome and haunch. However, the spikes in the hoop D/C ratios in the haunch for the axisymmetric run have larger values. Lastly, in Figure 10.41 ACI-349 LC4 in-plane shear D/C ratios are shown. All in-plane shear D/C ratios are less than 0.25.

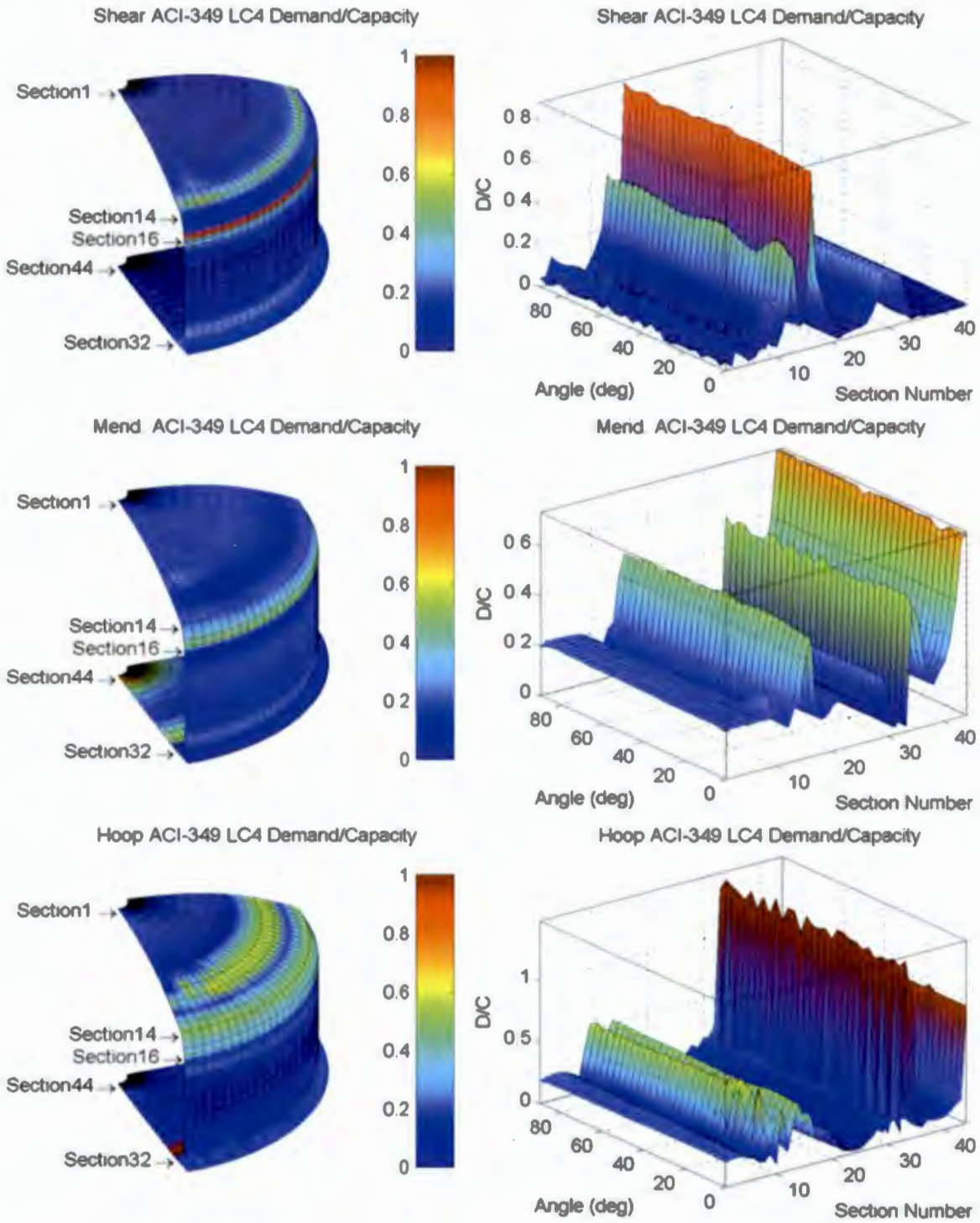

Figure 10.40. ACI LC4 D/C Ratios for Through Wall Shear (top), Meridional (middle), and Hoop (bottom)

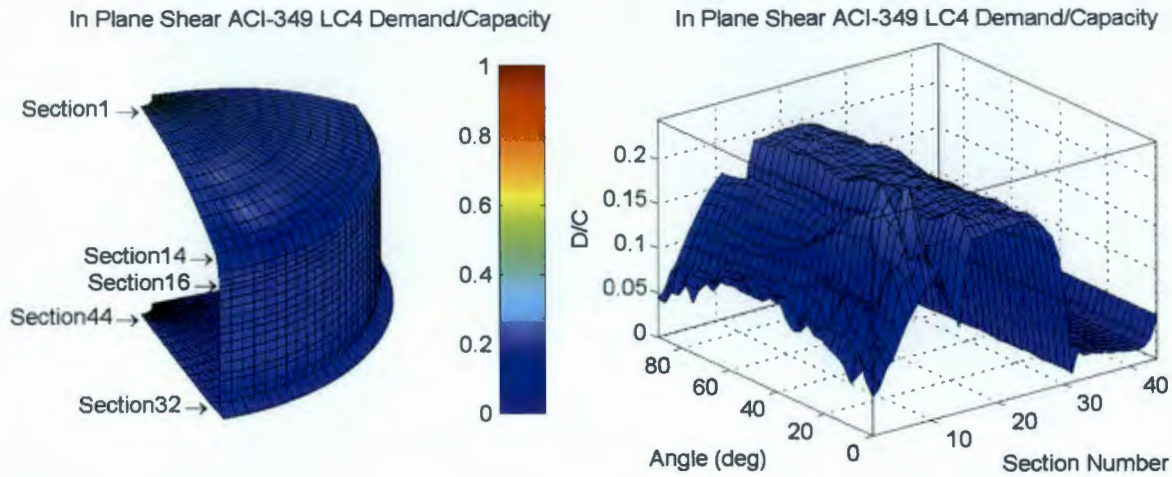

Figure 10.41. ACI LC4 D/C Ratios for In-Plane Shear

The appurtenance model under peak temperature, LC1, and LC9 shows that D/C ratios for through wall shear are very similar to the axisymmetric cases while the in-plane shear is negligible. This indicates that the shear friction D/C at the construction joints should not vary much from the values for the axisymmetric model presented in Section 8.12. However, through wall shear D/C ratios in LC4 are significantly greater than the axisymmetric results at the top of the wall. In addition, the in-plane shear D/C ratios are no longer negligible. Therefore, shear friction D/C ratios at the construction joints are calculated for the appurtenance model under LC4. Table 10.7 shows the D/C ratios for shear friction under LC4 for the appurtenance model. Here, the maximum combined shear includes the vector combination of the maximum seismic plus TOLA through wall shear over all angles and the maximum seismic plus TOLA in-plane shear over all angles. The maximum combined axial includes the combination of seismic and TOLA meridional force that produces the least compressive force across the construction joints. All the shear friction D/C ratios are less than one with the maximum value of 0.30 located in section 18 near the top of the wall.

Table 10.7. Shear Friction D/C Ratios for LC4 Appurtenance Model

Section Number	Max Combined Shear [kip/ft]	Max Combined Axial [kip/ft]	A_{vf} [in^2/ft]	A_c [in^2/ft]	μ	f_y [psi]	f_c' [psi]	$800A_c$ [kip/ft]	$0.2f_c'A_c$ [kip/ft]	$A_{vf}f_y\mu$ [kip/ft]	ϕ	Capacity [kip/ft]	D/C
18	11.8	-42.6	0.88	180	0.6	40000	4338	144.00	156.17	46.76	0.85	39.75	**0.30**
22	8.4	-44.2	0.88	180	0.6	40000	4006	144.00	144.22	47.74	0.85	40.58	**0.21**
26	8.2	-45.1	0.88	180	0.6	40000	3761	144.00	135.40	48.24	0.85	41.00	**0.20**
30	12.1	-49.4	0.88	335	0.6	40000	3488	267.65	233.39	50.83	0.85	43.21	**0.28**

10.4 Summary of the Type III Appurtenance Model Evaluations

A review of the Type III SST appurtenances concluded that an appurtenance configuration with three heavy pits should be analyzed within this AOR. A TOLA appurtenance model was subjected to a simplified thermal history and ACI load factors while two seismic models (same configuration with symmetry boundary in different locations) where subjected to seismic loading. The appurtenance analysis

was not performed for all the material property combinations as it is not part of the baseline Type III model. The particular pit configuration analyzed has a conservative geometry for all the Type III tanks, therefore, additional material property conservatisms are not necessary.

The TOLA only load combinations, peak temperature and load combinations 1 and 9, showed that no D/C ratios exceeded one. Furthermore, the D/C ratios for these loads are generally very similar to the axisymmetric Run 2 D/C ratios (see Section 8.4) outside of the region on the dome where the pits were located. The D/C ratios under LC4, the combined TOLA and seismic load combination, show a little more variation from the axisymmetric combined Run 1 D/C ratios (see Figure 9.31). However, just as in the axisymmetric combined run, the appurtenance LC4 D/C ratios are all less than one in the dome, haunch, and wall. Also just as in the axisymmetric combined runs, the D/C ratios for LC4 only exceed one in the inside slab. The slab removal runs in Appendix E demonstrated that even with D/C ratios greater than one in the slab the structural integrity of the tank remains intact.

In summary, the appurtenance modeling shows that the variations in D/C ratios are generally restricted to localized regions near the pits. At other locations the ACI D/C ratios closely follow the baseline TOLA model. The combined TOLA and seismic D/C ratios show a little more variation but still generally follow the most appropriate axisymmetric ratios. Because of these close D/C ratios and lack of variation in ratios over the angles in the model, it is not necessary to conduct a full series of analyses over the entire range of material property combinations. For the Type III SSTs, the baseline material properties were adequate to evaluate the effects of the appurtenances.

This page intentionally left blank.

11.0 Tank Limit Analysis

The methodology for assessing the tank limit loads is described in the Evaluation Criteria report (Johnson et al. 2010). The specifics of that methodology were developed in the C-106 Structural Integrity Evaluation (Bander et al. 1994). The tank limit loads were evaluated relative to both the in situ soil-load condition and relative to future loading conditions. The in situ limit load was determined by applying a uniformly distributed load over the entire soil surface. The load is increased until the tank offers little or no resistance to additional load. The tank limit load relative to future loading conditions was determined by applying a local load on the soil surface over a 20-ft diameter about the center of the tank. Again, the load is increased until the tank offers little or no resistance to additional load.

The load-displacement curve for each analysis is presented in addition to the tabular limit load results. The displacement in these curves is the vertical displacement of the dome center relative to the haunch. It is anticipated that these may be of value in on-going dome monitoring programs.

The tank limit loads were applied following the full thermal history shown in Table 5.7. The tank limit loads were applied at a uniform 53°F. The 53°F temperature corresponds to the initial stress-free temperature of the model at the beginning of the 59 year thermal analysis.

The limit load analyses were conducted with both nominal and lower bound concrete properties. The concrete tensile strength was taken either as nominal or lower bound, rather than the near zero value prescribed in Chapter 4. In addition, the concrete moduli and compressive strengths were selected to be best estimates or lower bound estimates of currently existing concrete. The limit load is governed by compressive forces on the concrete and either compressive or tensile yielding of the rebar as discussed below. Consequently, the concrete tensile strength is not expected to have any effect on the limit load and side studies have confirmed that hypothesis. The nominal soil overburden depth was taken as 11 ft as specified in Section 4.2. The analyses were repeated with 6.85 ft of soil overburden to illustrate the effects of the variation in soil overburden that is present with each individual tank.

The in situ limit load analysis presented in this chapter differs from previous analyses (Bander et al. 1994) in that the load was applied over the entire soil surface rather than being limited to the projected area of the dome. This load distribution was deemed more representative of the natural phenomena loads. In addition, potential barrier covers would most likely cover the whole farm and even extend out beyond the farm.

The limit load safety factor is defined as the ratio of the limit load plus the equivalent surface load divided by the equivalent surface load. The equivalent surface load is defined as the load that results in the same dome center deflection as the in situ loads of soil and dome weight. For the uniform surface load, this is an equivalent uniform pressure applied at the surface of the soil. For the local surface load, this is the equivalent local pressure over a 20-ft diameter that also gives the in situ dome deflection. This equivalent load was determined for each case by extrapolating the dome load-displacement curve back to zero displacement. This procedure is illustrated in Figure 11.1 for the local surface load on the nominal concrete, 6.85 ft soil case. This procedure was repeated for all combinations of uniform or local load distribution, concrete and soil depth.

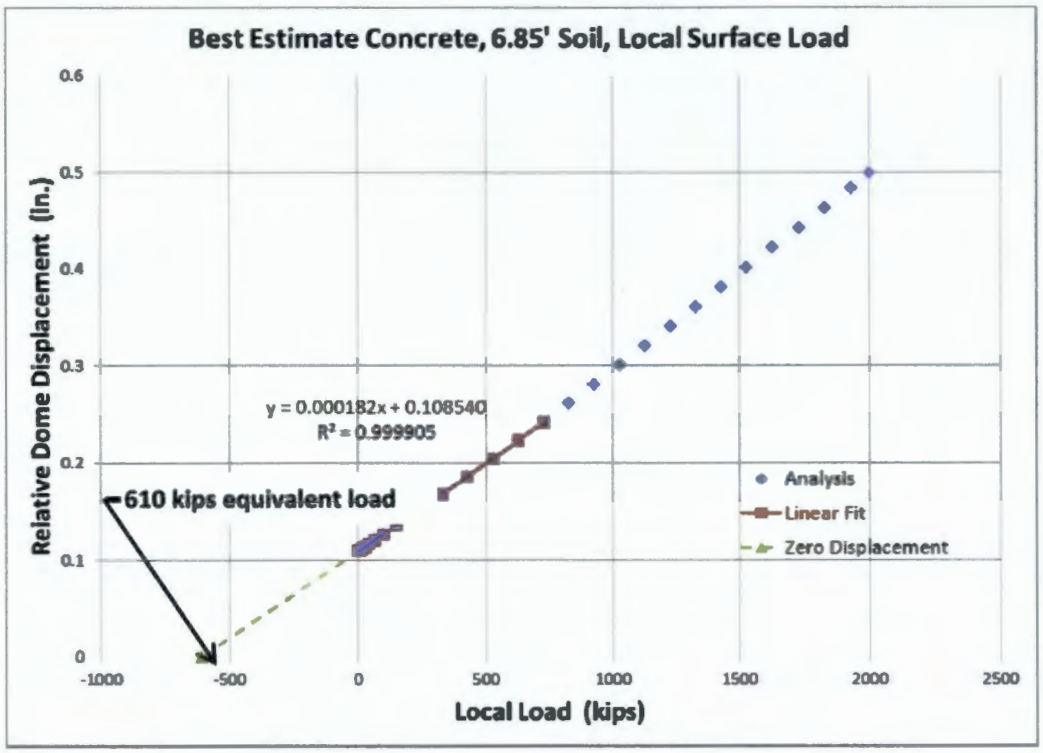

Figure 11.1. Equivalent Local Surface Load Calculation

In Figure 11.1, the "analysis" data is the displacement response of the dome centerline (relative to the haunch) as the local surface load (distributed over the 20-ft-diameter area) is increased on the model with undegraded nominal concrete. The 0.1-inch relative displacement at zero load reflects the in-situ displacement of the dome under the effects of gravity on the dome and 6.85 ft soil overburden. A "linear fit" is established through the initial portion of the load-displacement data. The slope of this line is affected by both the soil depth, concrete stiffness (i.e., elastic modulus) and load distribution (uniform surface vs. local). The "analysis" data are then extrapolated using this slope to "zero displacement." The 610 kips load at the 0.0-inch intercept is defined as the equivalent surface load for this case. This procedure was repeated for all combinations of soil depth, concrete properties and load distribution.

Another perspective on this procedure, in this case for the uniform surface load on 11-ft soil, is provided in Figure 11.2 and Figure 11.3. The equivalent surface load calculation is illustrated in Figure 11.2. Extrapolating the original 0.16-inch displacement back to zero displacement gives an equivalent load of 10.8 psi. Figure 11.3 confirms that the ANSYS® model with a uniform surface load of 10.8 psi (and gravity removed) gives the same 0.16-inch displacement.

The equivalent in situ uniform surface load for the nominal concrete case is 10.8 psi. The equivalent local load for the nominal concrete is 1130 kips. The corresponding values for the lower bound concrete are 10.1 psi and 1160 kips. The 6.85-ft soil, nominal concrete analysis generated equivalent loads of 7.1 psi and 610 kips. The 6.85-ft soil, lower bound concrete analysis gave equivalent loads of 7.2 psi and 620 kips as summarized in Table 11.1.

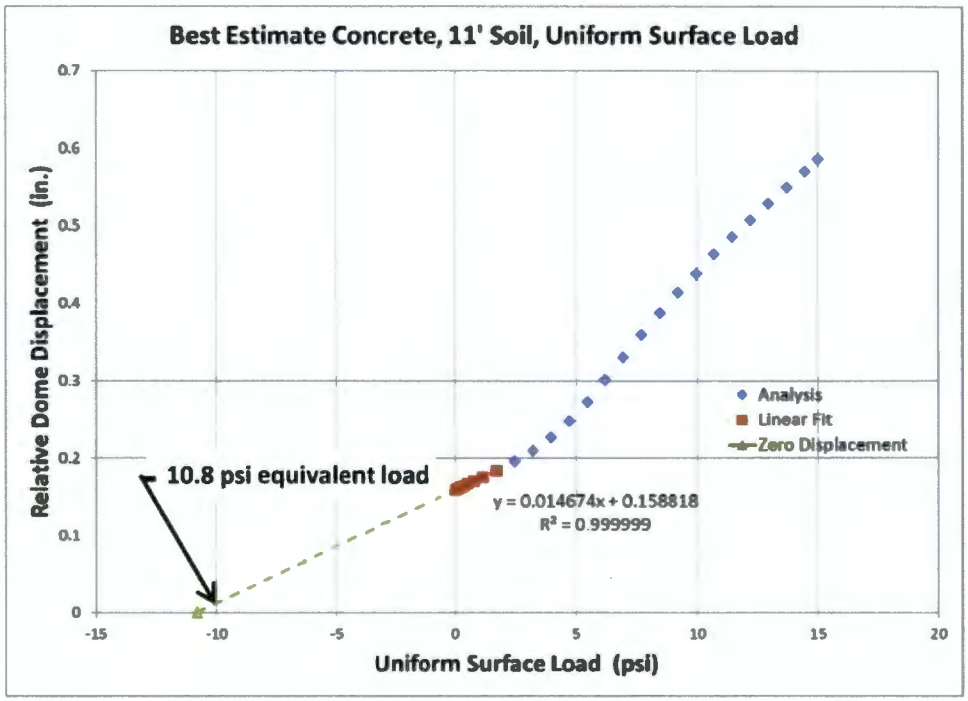

Figure 11.2. Equivalent Uniform Surface Load Calculation

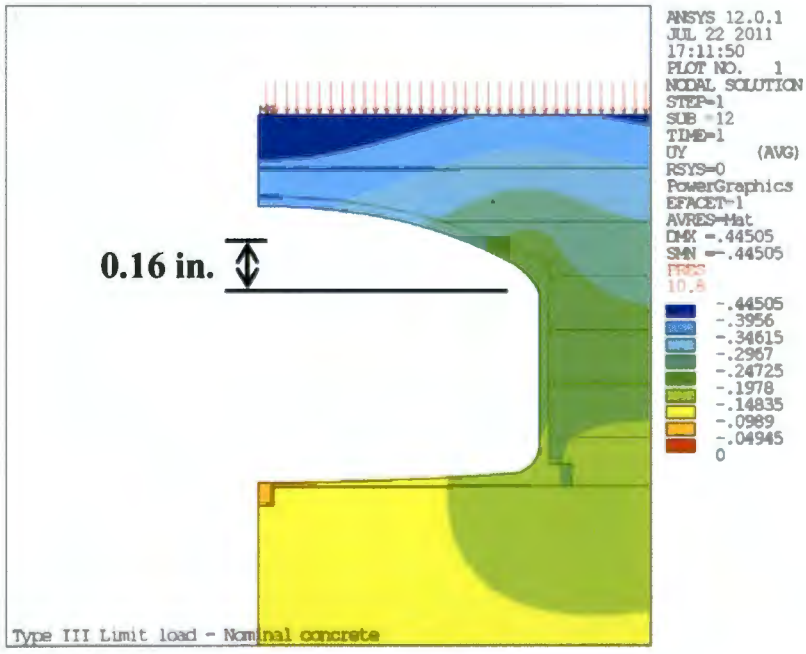

Figure 11.3. Equivalent Local Load

Table 11.1. Summary of Limit Load Analysis

Concrete	Limit Load - uniform (psi)	Limit Load - local (kips)	Equiv load - uniform (psi)	Equiv load - local (kips)	Safety Factor (uniform)	Safety Factor (local)
11' Soil LB	40.0	6190	10.1	1160	5.0	6.3
11' Soil Nom.	46.3	6940	10.8	1130	5.3	7.1
6.85' Soil LB	38.3	5070	7.2	620	6.3	9.2
6.85' Soil Nom.	40.8	5740	7.1	610	6.7	10.4

The Evaluation Criteria report, in keeping with previous analyses, recommends use of the ASME Boiler & Pressure Vessel Code methodology of identifying the limit load as the intersection of the load-displacement curve with a line drawn through the origin at two times the slope of the initial linear portion of the load-displacement curve. The ASME methodology proved to be difficult to apply consistently in both the current analyses and the C-106 Structural Integrity Evaluation as reported by Bander et al. (1994). Extensive cracking in the dome and haunch leads to a "jump" in the load-deflection curve as illustrated in Figure 11.4. Literal application of the ASME methodology for this case would lead to grossly conservative limit loads. In addition, the lower bound concrete cases as illustrated in Figure 11.4 and Figure 11.5, exhibit concrete crushing and rebar yielding before the ASME line intersects the load-displacement curve. Bander et al. (1994) and the reviewers of this analysis [Appendix A-2 of Rinker et al. (2011a)] comment that, "the combination of concrete crushing and rebar yielding is the critical failure mode." Accordingly, the limit load was taken to be the load at the onset of concrete crushing and rebar yield.

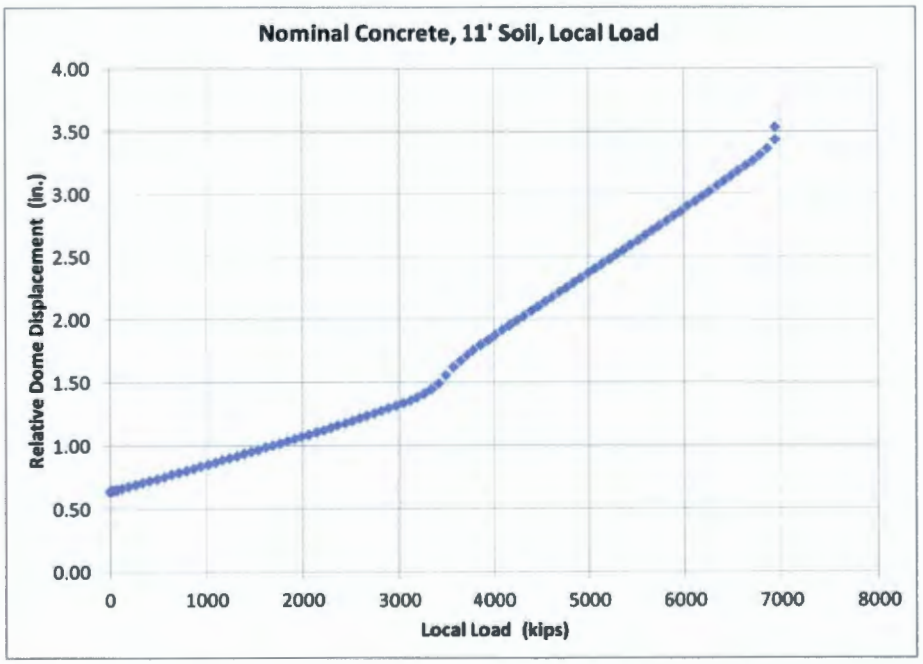

Figure 11.4. Load-Displacement Response of Nominal Concrete under Local Load

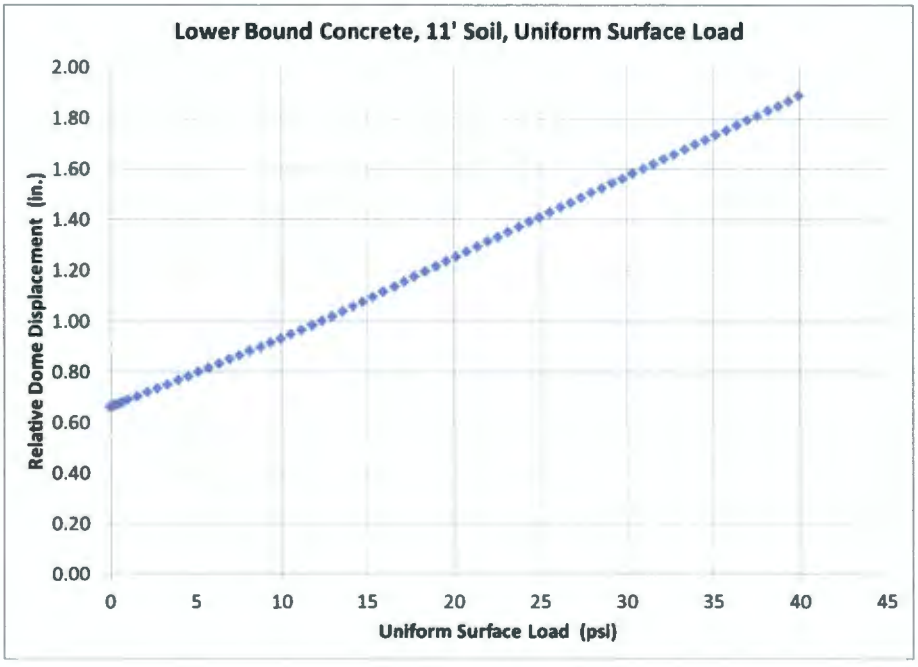

Figure 11.5. Load-Displacement Response of Lower Bound Concrete under Uniform Surface Load

The current analysis demonstrates, as did the C-106 Structural Integrity Evaluation, that the critical location changes with the load distribution. Figure 11.6 demonstrates the tank deformation (exaggerated scale for clarity) under the local limit load. The bending of the center of the dome is indicative of the loss of stiffness caused by crushing of the concrete on the top surface of the dome at the tank centerline.

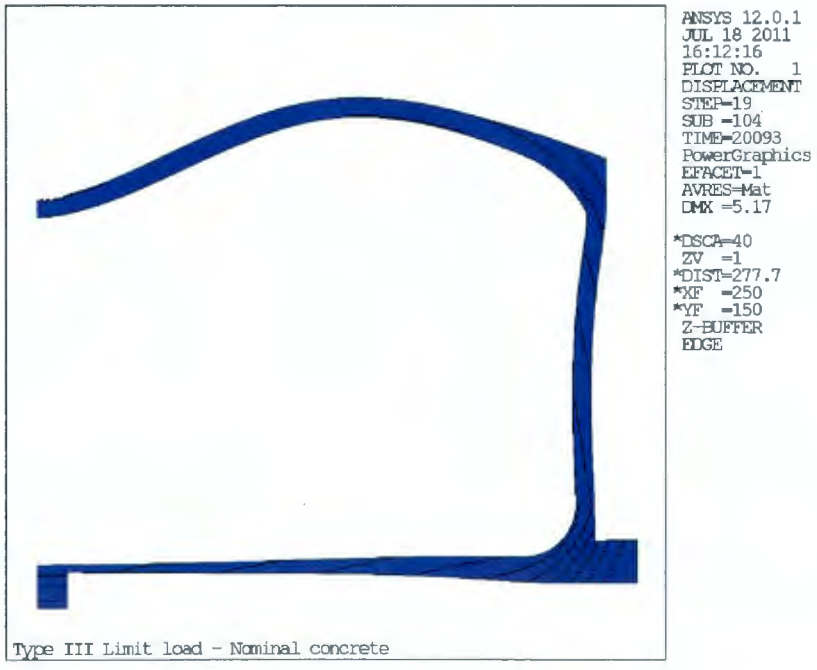

Figure 11.6. Local Load Tank Deformation (Scale Factor = 40)

In contrast, Figure 11.7 illustrates the tank deformation under the uniform surface load. The dome flattens relatively uniformly, but the top of the wall deforms significantly in the radial direction. The bending of the wall is indicative of the loss of stiffness caused by crushing of the concrete at the top inner face of the wall.

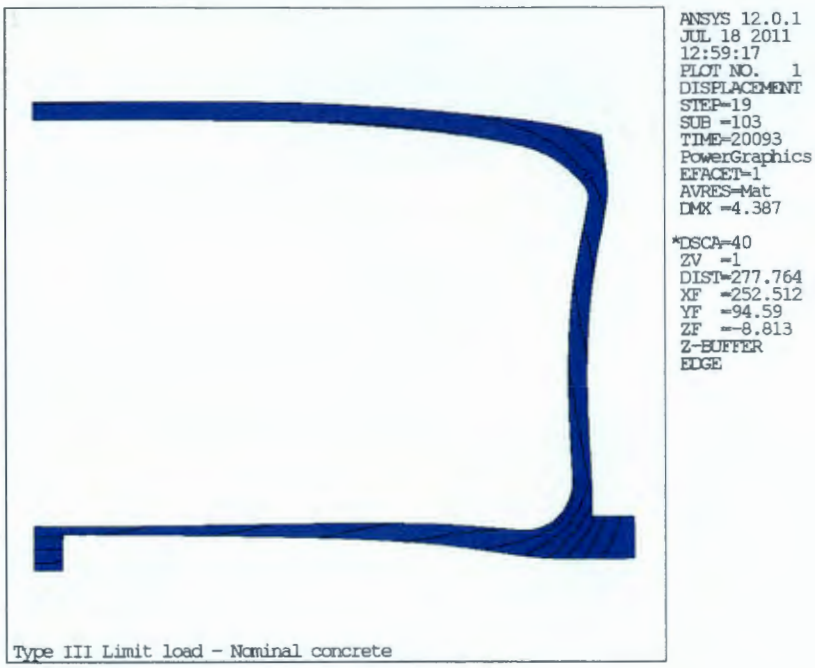

Figure 11.7. Uniform Surface Load Tank Deformation (Scale Factor = 40)

Figure 11.8 shows the response of the best estimate concrete under uniform surface load. The limit load is identified as 46.3 psi. Figure 11.4 shows the response of the best estimate concrete under local load with the limit load identified as 6940 kips.

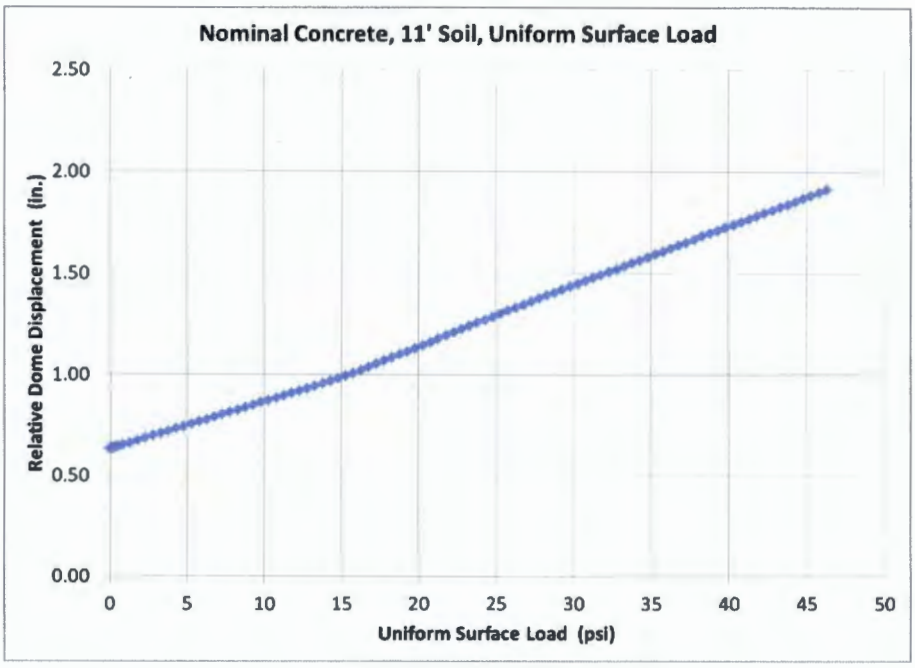

Figure 11.8. Load-Displacement Response of Nominal Concrete under Uniform Surface Load

Figure 11.5 shows the limit load of 40.0 psi for the lower bound concrete, uniform surface load case, and Figure 11.9 shows the limit load of 6190 kips for the lower bound concrete, local load case.

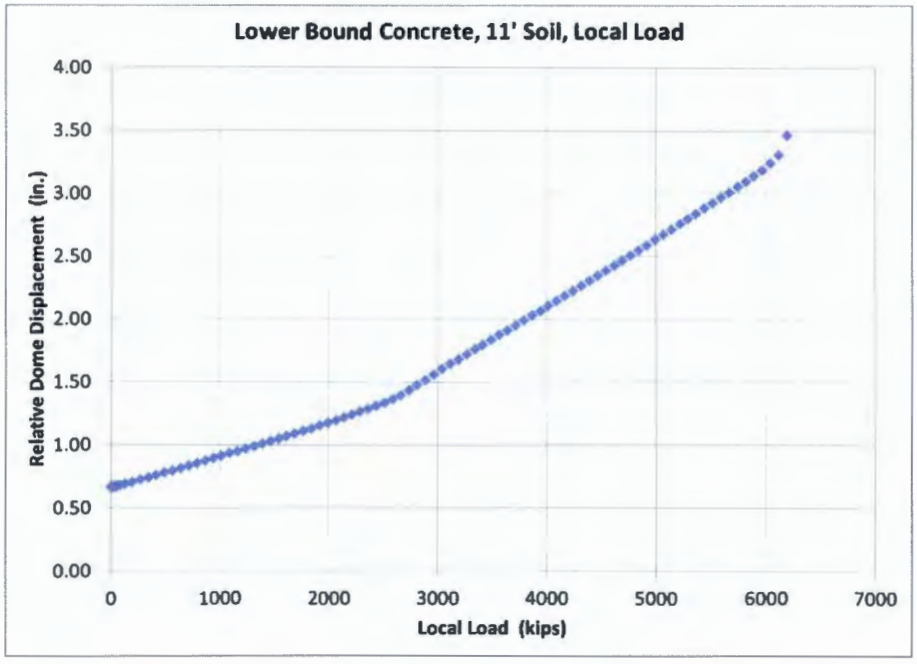

Figure 11.9. Load-Displacement Response of Lower Bound Concrete under Local Load

Figure 11.10 shows the response of the nominal concrete with 6.85 ft of soil overburden under uniform surface load. The limit load is 40.8 psi. The local load response is shown in Figure 11.11 with a limit load of 5740 kips.

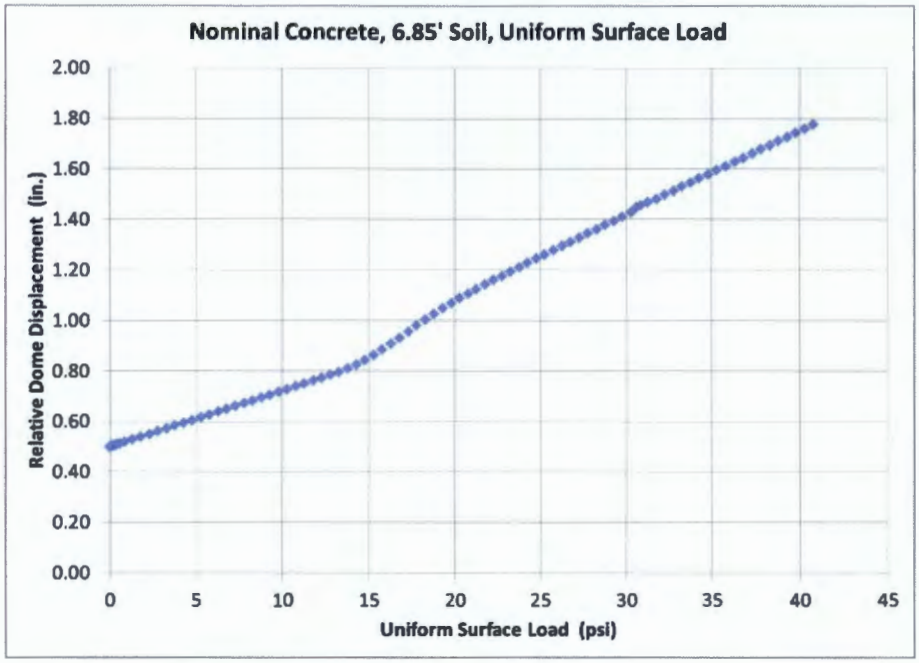

Figure 11.10. Load-Displacement Response of Nominal Concrete under 6.85 ft of Soil with Uniform Load

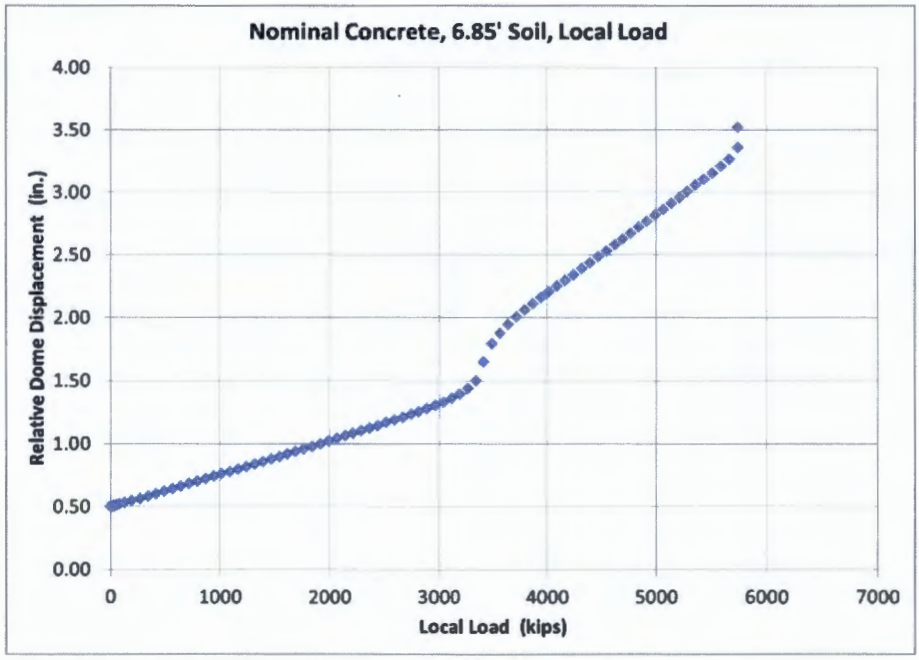

Figure 11.11. Load-Displacement Response of Nominal Concrete under 6.85 ft of Soil with Local Load

Figure 11.12 shows the response of the lower bound concrete with 6.85 ft of soil overburden under uniform surface load. The limit load is 38.3 psi. The local load response is shown in Figure 11.13 with a limit load of 5070 kips.

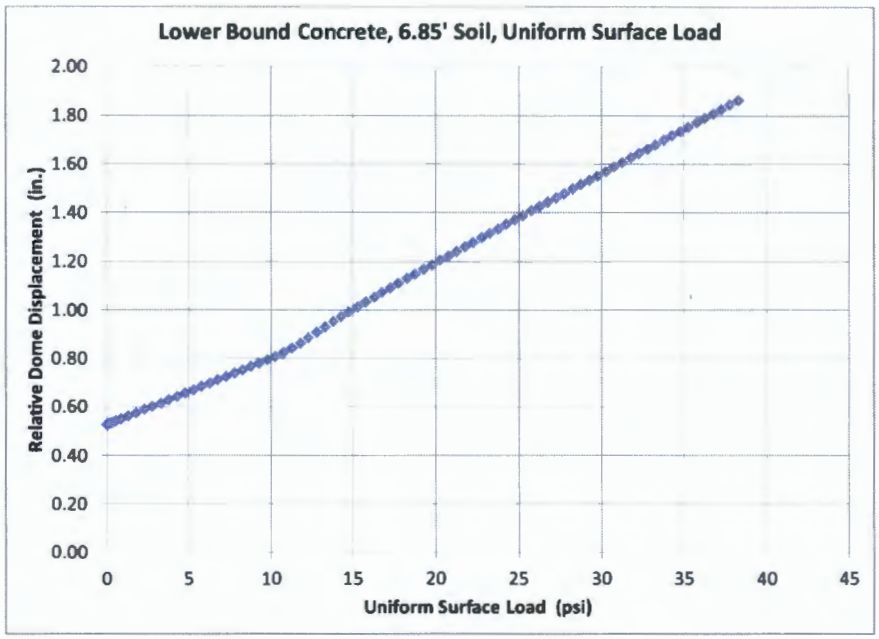

Figure 11.12. Load-Displacement Response of Lower Bound Concrete under 6.85 ft of Soil with Uniform Load

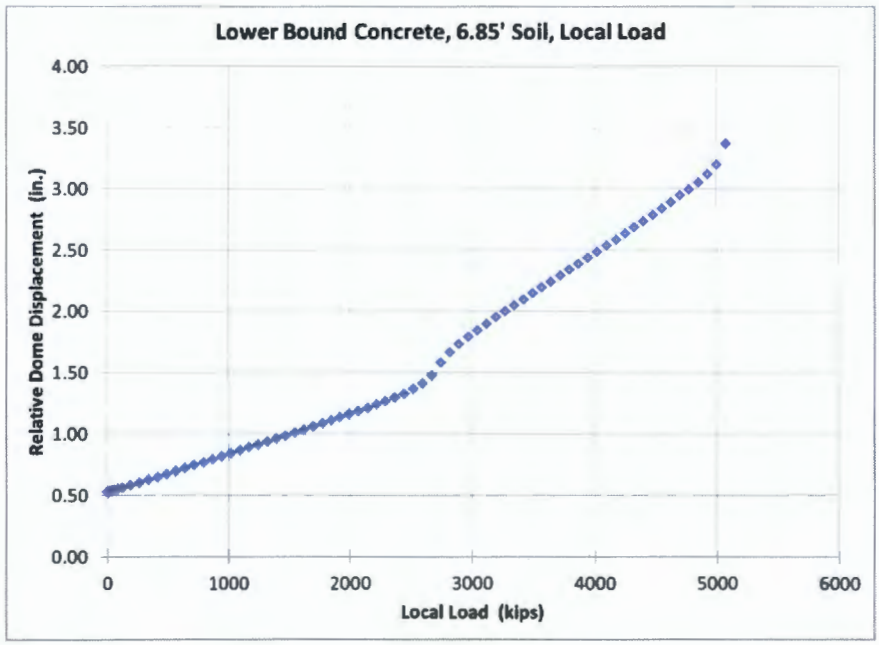

Figure 11.13. Load-Displacement Response of Lower Bound Concrete under 6.85 ft of Soil with Local Load

The limit loads and safety factors are summarized in Table 11.1. The safety factors are calculated as: (total load + equivalent load) / equivalent load. The safety factors are greater than the 3.0 recommended in the Evaluation Criteria report. This demonstrates that the current dome load limits (Mackey, 2004b) are adequate.

These results are comparable to others previously reported. The ability of the tank to carry more load if the total load is distributed evenly over the entire dome is clearly demonstrated (Bander et al. 1994). The uniform surface limit load of 46.3 psi for the 11 ft soil, nominal concrete case corresponds to a total applied load of 32000 kips, a factor a 4.6 times greater than the calculated limit load of 6940 kips. The approximately 15% decrease in limit load with the decrease in concrete strength from nominal to lower bound was also reported by Bander et al. (1994). The effects of soil overburden depth generally reflect those reported in Mackey and Julyk (2004) and Julyk et al. (2003).

The limit load for the case of uniform surface load on 6.85 ft of soil is lower than that suggested by a simple scaling of the other uniform surface load results. It is noted that the limit analysis is nonlinear due in part to the concrete cracking. This implies that the tank stiffness is path dependent and that the conditions of the tanks with differing soil overburden are not necessarily identical at the end of the thermal transient. Therefore the limit load is a function of the previous history of the tank. Accordingly, it is recommended that these results not be extrapolated to individual tanks but that tank specific analyses be conducted to address specific variations in soil overburden and soil density.

12.0 Concrete Shell Buckling Analysis

This chapter presents the results of the concrete shell buckling analysis for the Type III single-shell tanks studied in this report.

Buckling occurs when a structure is subjected to a compressive load and an infinitesimal increase in the load results in a large increase in the deflection of the structure or a large change in the equilibrium configuration of the structure. The mode of buckling may be characterized either by a split in the equilibrium path to an adjacent equilibrium configuration (bifurcation) or by a sudden jump to a new equilibrium configuration (snap-through) as the applied load is increased infinitesimally. In general for thin-shell structures, the magnitude of the buckling load depends on the shell geometry, boundary restraints, material properties, and the type of load. The effects of large displacements and geometric imperfections are important considerations in correlating experimental results with theoretical analyses. For concrete shell structures like the SSTs, the effects of inelastic behavior, creep, reinforcement, and cracking need to be considered.

The buckling mode of the tank dome can be related to that of a spherical cap and may be either bifurcation or snap-through depending on the relative shallowness of the cap as well as the extent of the applied load. There are two interacting modes of buckling that must be addressed for the cylindrical tank wall: (1) buckling under uniform axial compression and (2) buckling under external lateral pressure. Parameters of potential significance to the buckling capacity of the tank dome and the cylindrical tank wall include the following:

- Type of loading: uniform, concentrated, axisymmetric, or asymmetric
- Post-buckling behavior
- Initial geometric imperfection
- Creep
- Cracking and the amount and type of reinforcement
- Nonlinear behavior of concrete in compression.

Chapter 19 of ACI 349-06 (ACI 2007) requires the investigation of thin shells for instability, including the consideration of the possible reduction in buckling capacity caused by large deflections, creep effects, temperature, cracking, and deviations between the actual and theoretical shell geometry. Referring to the commentary in Chapter 19 of ACI 318-05, ACI 349-06 identifies ACI SP-67, *Concrete Shell Buckling* (ACI 1981), as a source of approaches for determining the critical buckling loads of reinforced concrete shells. A practical procedure for determining critical buckling loads of reinforced concrete shells, as given by the International Association for Shell and Spatial Structures (IASS) Working Group No. 5, *Recommendations for Reinforced Concrete Shells and Folded Plates*, is discussed in the ACI SP-67 document (ACI 1981).

Scordelis (1981) summarizes the IASS recommendations in SP-67 with the following equations:

$$P_b^{red} = \alpha_1 \alpha_2 \alpha_3 \alpha_4 P_b^{lin} = \alpha P_b^{lin} \tag{12.1}$$

$$P_b^{allow} = P_b^{red}/SF_b \tag{12.2}$$

where

P_b^{red} = Reduced buckling load

P_b^{lin} = Linear "classical" critical buckling load

P_b^{allow} = Allowable buckling load

α_1 = Geometric imperfection-sensitivity reduction factor

α_2 = Creep reduction factor

α_3 = Reduction factor to account for cracking and amount and type of reinforcement

α_4 = Reduction factor to account for material nonlinearity of concrete under high stresses

α = Combined buckling load-reduction factor = $\alpha_1 \alpha_2 \alpha_3 \alpha_4$

SF_b = Buckling safety factor

12.1 Unfactored Theoretical Buckling Loads

Computation of the "classical" buckling load as predicted by linear buckling theory for an ideal shell geometry assuming gross uncracked concrete is based on the end-of-life degraded concrete modulus. The following section provides equations that may be used to determine the linear buckling load for the dome and the cylindrical wall of the tank.

12.1.1 Dome Buckling

This section presents solutions for the theoretical buckling load of the tank dome under uniform pressure and a concentrated pressure load. Two concentrated load solutions are compared, one for a point load applied to a spherical cap and the second for a local pressure load over a circular area. The point load solution was previously used in the C-106 analysis by Bander et al. (1994), and it was recommended for use on the Single-Shell Tank Analysis of Record (SST AOR) by the Evaluation Criteria report (Johnson et al. 2010). However, comparing the two methods shows that the locally distributed pressure solution more accurately describes the actual loading condition and it has a lower critical buckling load than the point load solution. Therefore, the more realistic and conservative local pressure load solution was used in the current buckling evaluation.

In lieu of an eigenvalue buckling analysis that considers the changing curvature and wall thickness of the tank dome, a conservative calculation of the dome linear buckling load, P_b^{lin}, can be obtained by idealizing the dome as a clamped spherical cap. For uniform pressure, $P_{b_u}^{lin}$ can be obtained by conservatively applying the following equation for a clamped spherical cap under uniform pressure with a shallowness parameter, λ, of 4 (Zarghamme and Heger 1983):

$$P_{b_u}^{lin} = 0.66E\left(\frac{t}{R}\right)^2 \tag{12.3}$$

where E = Young's modulus for concrete
t = Dome minimum wall thickness
R = Dome maximum mid-wall radius of curvature

The shallowness parameter, λ, is given by

$$\lambda = \left[12\left(1-\nu^2\right)\right]^{\frac{1}{4}}\left(\frac{R}{t}\right)^{\frac{1}{2}} 2\sin\frac{\varphi}{2} \tag{12.4}$$

where ν = Poisson's ratio for concrete
φ = Half the included angle of the spherical cap.

According to Baker et al. (1972), for spherical caps with clamped edges, theory indicates that buckling will not occur under a concentrated loading if the shallowness parameter, λ, is less than about 8. For values of λ between 8 and 9, axisymmetric snap-through is the expected buckling mode, with the shell continuing to carry load. For larger values of λ, asymmetric buckling is expected to occur first, but again the shell will continue to carry load. Baker cites experimental results that indicate that limit loads of clamped spherical caps loaded over a small area are conservatively estimated by the load determined from Figure 12.1 (Baker et al. 1972).

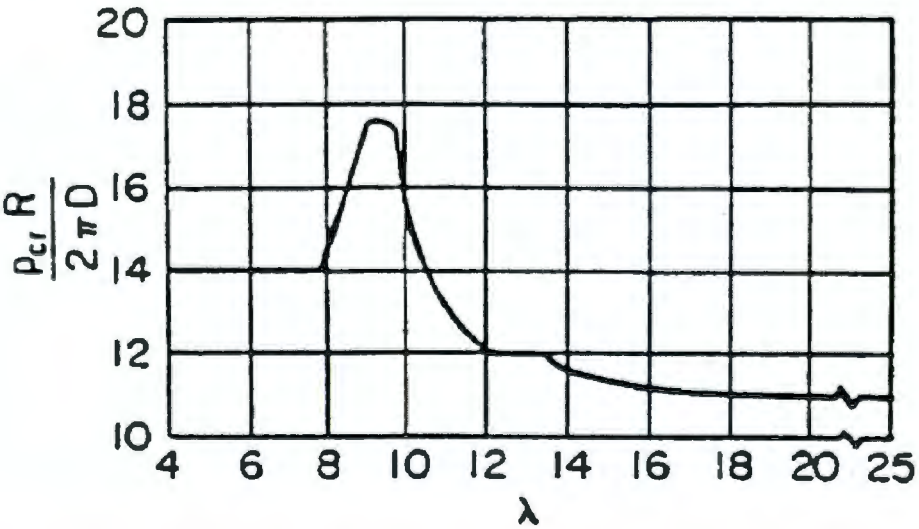

Figure 12.1. Theoretical Buckling Loads for Clamped Spherical Cap Under Concentrated Load (Figure 10-34 of Baker et al. 1972)

For a concentrated load at the dome apex, $\alpha_1 P_{b_c}^{lin}$ can be estimated for Hanford SSTs by conservatively applying the following equation for a clamped spherical cap loaded over a small area with a shallowness parameter, λ, of 4 to 8 (Figure 12.1):

$$\alpha_1 P_{b_c}^{lin} = \frac{28\pi D}{R} \tag{12.5}$$

where $D = \frac{Et^3}{12(1-\nu^2)}$ = Flexural stiffness of the concrete shell

E = Young's modulus for concrete

v = Poisson's ratio for concrete

t = Dome minimum wall thickness

R = Dome maximum mid-wall radius of curvature

The value of $\alpha_1 P_{b_c}^{lin}$, determined from Figure 12.1 is based on experimental determinations that are considered to include the effects of the geometric imperfection factor, α_1.

However, the 200-kip "concentrated load" limit specified by tank operations is actually distributed over a 10-ft radius circle at the dome apex. The soil overburden further spreads the pressure load over a larger circle as a function of the overburden depth and the internal friction angle of the soil. Fitch and Budiansky (1970) present the buckling solution for a spherical cap loaded by a local pressure distributed over a circle with radius, R_{cl}. They present the solution as a function of the parameter, λ_{bar}, which is in turn a function of the loading radius, R_{cl}, the dome radius of curvature, R, the dome thickness, t, and the Poisson's ratio, v.

$$\lambda_{bar} = [12(1-\nu^2]^{\frac{1}{4}}\left(\frac{t}{R}\right)^{\frac{1}{2}}\left(\frac{R_{cl}}{t}\right) \tag{12.6}$$

The radius of the load circle at the dome surface is estimated using the following function of soil depth, h_s, and internal friction angle, φ.

$$R_{cl} = R_{surface} + h_s \tan(\varphi) \tag{12.7}$$

The load radius, R_{cl}, is 17.7 ft for an 11-ft soil depth and internal friction angle of 35°. The Type III dome geometry gives λ_{bar} equal to 3. The total buckling load corresponding to the local pressure is calculated from the following equation.

$$\alpha_1 P_{bcl}^{lin} = p_c 2\pi R_{cl}^2 \frac{E}{\sqrt{3(1-\nu^2)}}\left(\frac{t}{R}\right)^2 \tag{12.8}$$

where p_c is the buckling sensitivity parameter in the upper graph of Figure 12.2 from Fitch and Budiansky (1970). For λ_{bar} equal to 3, p_c is approximately 0.42.

The concentrated buckling load was calculated for both the methods in Equations (12.5) and (12.8). The solution for the local pressure load in Equation (12.8) gave a critical buckling load that is about 50% of the concentrated point load solution in Equation (12.5). Therefore, the local pressure solution from Equation (12.8) was used for conservatism. In addition, Fitch and Budiansky (1970) report that for $\lambda_{bar} > 2$, buckling is accompanied by a reduced load-carrying capacity. This is contrary to the increasing post-buckling load capacity reported by Baker (1972) for the point load. Therefore, it is more appropriate

to use a safety factor of 3.5 on the concentrated dome load buckling evaluation rather than the 1.75 factor recommended for conditions with an increasing post-buckling load capacity (see Section 12.3). The factor of two reduction in theoretical buckling load combined with the factor of two increase in safety factor increases the buckling fraction for the concentrated load by a factor of four over the method used in the C-106 analysis (Bander et al. 1994).

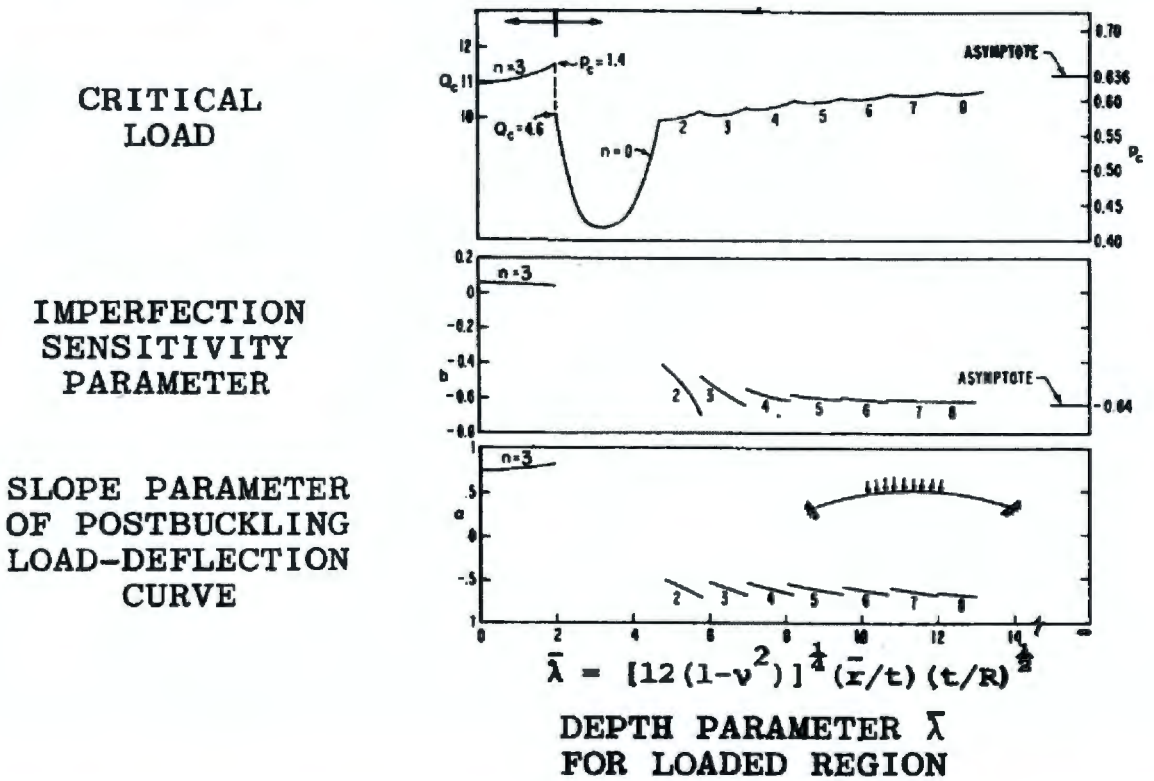

Figure 12.2. Buckling and Post-Buckling Behavior of a Spherical Cap Under Distributed Load (Fitch and Budiansky 1970)

12.1.2 Cylindrical Wall Buckling

The linear buckling load for axial compression in the tank cylindrical wall, $P_{b_a}^{lin}$, is derived from the equation for the critical buckling stress presented by Seide (1981):

$$\sigma_{b_a}^{lin} = \frac{1}{\sqrt{3(1-\nu^2)}} E\left(\frac{t}{R}\right) \tag{12.9}$$

which is transformed to the corresponding total dome load

$$P_{b_a}^{lin} = 2\pi R t \sigma_{b_a}^{lin} = \frac{2\pi}{\sqrt{3(1-\nu^2)}} E t^2 \tag{12.10}$$

where E = Young's modulus for concrete
ν = Poisson's ratio for concrete
t = Tank minimum wall thickness
R = Tank cylinder mid-wall radius of curvature

The theoretical buckling pressure of the cylindrical wall loaded by external lateral pressure is given by Flugge (1960) as:

$$P_{bL}^{lin} = \frac{E}{1-\nu^2}\cdot\sqrt{12\cdot k}\cdot\varphi_{cr} \tag{12.11}$$

where:

$$\varphi_{cr} := \frac{\left(1-\nu^2\right)\cdot(n\cdot\lambda)^4 + k\cdot\left[\left[(n\cdot\lambda)^2+m^2\right]^4 - 2\cdot\left[\begin{array}{l}\nu\cdot(n\cdot\lambda)^6 + 3\cdot(n\cdot\lambda)^4\cdot m^2 \ldots \\ +(4-\nu)\cdot(n\cdot\lambda)^2\cdot m^4 + m^6\end{array}\right]\ldots \\ +2\cdot(2-\nu)\cdot(n\cdot\lambda)^2\cdot m^2 + m^4\right]}{m^2\left[(n\cdot\lambda)^2+m^2\right]^2 - m^2\left[3\cdot(n\cdot\lambda)^2+m^2\right]} \tag{12.12}$$

$$\lambda = \pi\cdot\frac{R}{L} \tag{12.13}$$

$$k = \frac{t^2}{12\cdot R^2} \tag{12.14}$$

n = the integer describing the half wave buckling mode along the length.
$2m$ = the integer describing the half wave buckling mode along the circumference.

Whereas the linear buckling load for external lateral pressure is determined for a uniform distribution along the length of the cylindrical wall, the actual distribution of pressure is linearly varying from a minimum value at the top to a maximum value at the base of the wall. Seide et al. (1979) identify theoretical results for a pressure distribution that varies linearly in the longitudinal direction. The critical equivalent uniform pressure is found to be the length average of the positive pressure distribution. If the lateral pressure is entirely positive along the full length of the cylinder, this corresponds to the average lateral pressure. Therefore, the at-rest soil pressure at the mid-height of the tank wall was used in the buckling calculations.

12.2 Buckling Load-Reduction Factors

The buckling load-reduction factor, α_l, accounts for the imperfection sensitivity (i.e., deviation between the actual and theoretical shell geometry) of the structure. Seide (1981) develops a lower bound correlation equation as a function of radius-to-thickness ratio based on experimental buckling data for axially loaded cylindrical shells. The use of this lower bound correlation is appropriate when imperfections are unknown. Experimental values presented for axially compressed cylindrical shells, while exhibiting considerable scatter, indicate that the discrepancy between theory and experiment tends to increase as the R/t of the shell increases. Seide attributes this phenomenon to decreased bending

stiffness of the relatively thinner shells, which renders them more susceptible to imperfections during construction. Seide (1981) presents the following conservative design formula as a lower bound representation of the experimental data:

$$\alpha_1 = 1 - 0.9\left(1 - e^{\frac{-1}{16}\sqrt{\frac{R}{t}}}\right) \tag{12.15}$$

for cylinders with $100 < R/t < 3{,}000$ and $0.5 < L/R < 5$, where L is the length of the cylinder. The applicability of knockdown factors developed for axially compressed cylinders to the dome under radial pressure is recognized by Popov and Medwadowski (1981) in their account of the IASS recommendations. They state that if no solution is available for shells of a given geometry and load, the curves applicable to an axially compressed cylinder and a spherical cap should be used.

The upper bound R/t for the typical Hanford SST dome is 84, which is somewhat outside the range where Equation (12.14) is applicable. By taking R/t at the lower bound of the acceptable range ($R/t = 100$), a conservative value of α_1 is calculated to be 0.58. The R/t for the Type III tank wall is 31. Therefore, a calculated value for α_1 of 0.58 is also a conservative lower bound for the wall under axial compression. A conservative value of α_1 for the wall under external lateral pressure is based on Seide's (1981) recommendation of 0.75.

The buckling load-reduction factor, α_2, accounts for concrete creep. The creep reduction factor is defined as E_{c2}/E_c where E_c is the initial concrete modulus at the time of first loading and $E_{c2} = E_c/(1 + C_u)$ is the reduced concrete modulus resulting from creep strains. The ultimate creep coefficient for the concrete, C_u, is the ratio of the ultimate creep strain divided by the initial elastic strain. The values of C_u should be based on a creep analysis for an upper bound thermal history of the structure. If a creep analysis is not available, Popov and Medwadowski (1981) recommend that the ultimate creep coefficient be estimated as $C_u = 4 - 2\log(f_c)$, where f_c is the concrete compressive strength at the time of loading in MPa. Both methods of calculating C_u were checked in the current buckling analysis and the maximum C_u was applied to conservatively calculate the minimum creep reduction factor. The C_u value calculated from finite element creep strains governed in all cases for the Type III SST with the bounding thermal history. This is opposite to the SST Type II analysis where the approximation by Popov and Medwadowski (1981) gave the higher ultimate creep coefficient. Comparing with the Type II analysis, the creep strains were higher in the Type III analysis because the maximum tank temperatures occurred earlier in the operating history of tank S-104 compared to the thermal history of the C-106 Type II tank. This occurred because the concrete is characterized by a time dependent creep rate so that the concrete becomes more resistant to creep as it ages (Johnson et al. 2010). The same α_2 factor was applied conservatively to all loads addressed during a particular service period of the tank despite the fact that for short-term loads such as live loads, the effect of creep is considered to be insignificant.

$$\dot{\varepsilon}_{cr} = C_1 \sigma^{C_2} t^{C_3} e^{-C_4/T} \tag{12.16}$$

The buckling load-reduction factor, α_3, accounts for the effect of cracking and the amount and type of reinforcement in the cross-section. Following the IASS procedure cited in SP-67 (Popov and Medwadowski 1981), $n = E_s/E_{c2}$ where E_s is the elastic modulus of the steel reinforcement and E_{c2} is the reduced concrete modulus caused by creep computed as before, except that a conservative initial concrete

modulus corresponding to the end-of-life degraded concrete is applied. The steel ratio $p = A_s/A_c$ is determined, where A_s is the total steel area per unit width of shell in one direction and A_c is the concrete area. The product $\eta\rho$ is used to determine a Ψ factor from Figure 12.3 (Scordelis 1981, p. 100). From Figure 12.4 (Scordelis 1981), a value of w_o/h (the ratio of the imperfection size divided by the wall thickness) is selected that corresponds to α_1. Finally, α_3 is estimated from Figure 12.5 (Scordelis 1981) as a function of w_o/h.

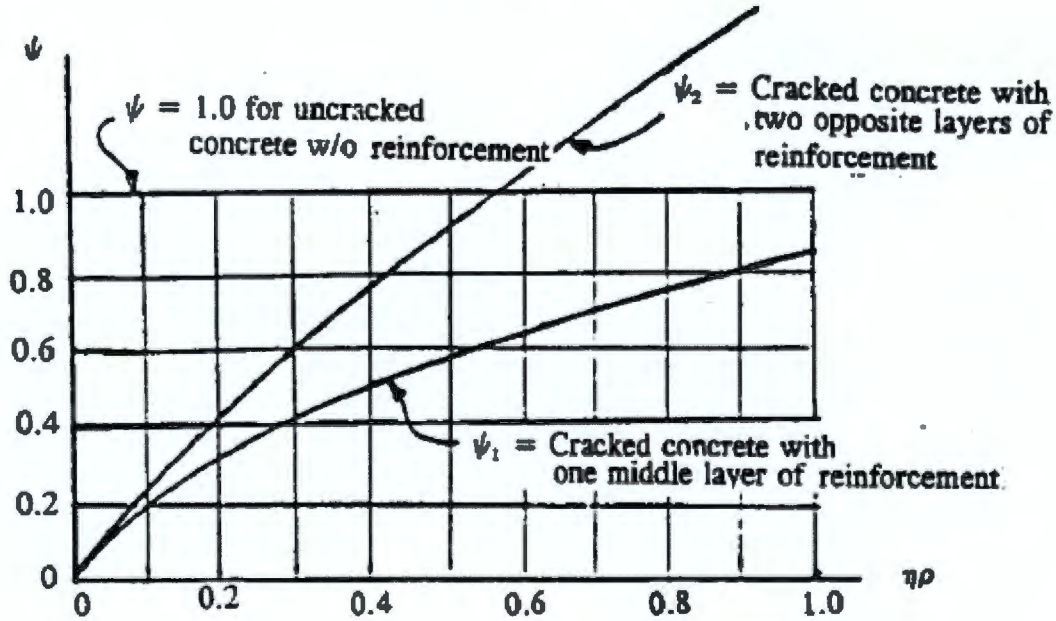

Figure 12.3. Values of ψ for Effect of Concrete Cracking and Amounts and Type of Reinforcement (Figure 4 of Scordelis 1981)

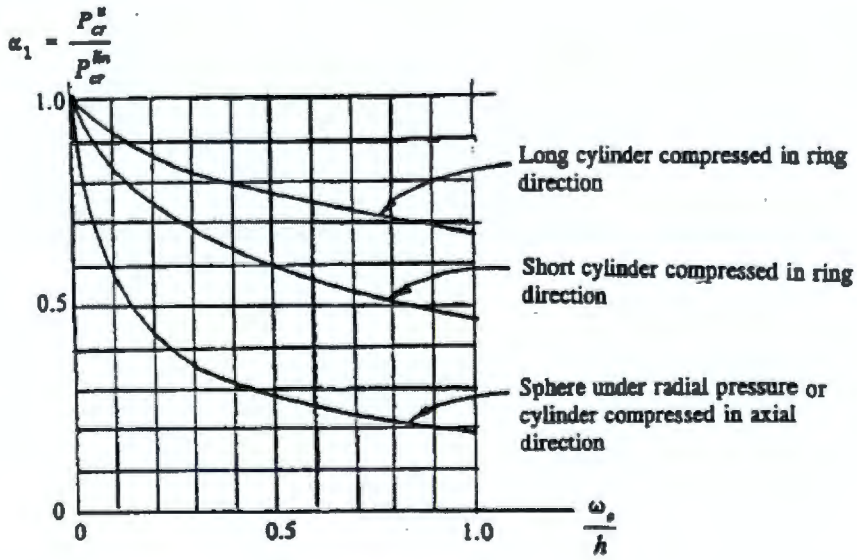

Figure 12.4. Effect of Geometric Imperfections on Buckling Load (Figure 3 of Scordelis 1981)

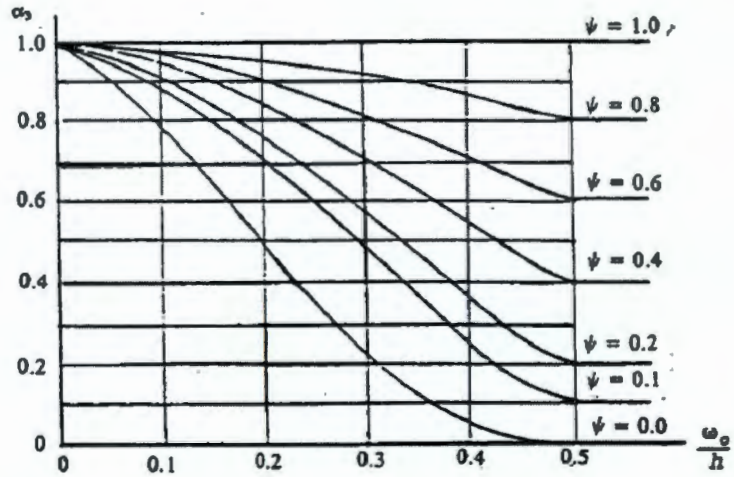

Figure 12.5. Reduction Factor α_3 for Concrete Cracking and Amounts and Type of Reinforcement (Figure 5 of Scordelis 1981)

The buckling load-reduction factor, α_4, is associated with material nonlinearity of the concrete under high stresses. The α_4 is determined from the semi-quadratic interaction equation (Scordelis 1981):

$$\left(\frac{P_b^{red}}{P_{ult}}\right)^2 + \left(\frac{P_b^{red}}{P_s}\right) = 1 \tag{12.17}$$

or

$$\alpha_4^2\left(\frac{P_s}{P_{ult}}\right)^2 + \alpha_4 = 1 \tag{12.18}$$

where $P_3 = \alpha_1\alpha_2\alpha_3 P_b^{lin}$

P_{ult} = ultimate externally applied load that the shell can carry as governed by the ultimate strength of the reinforced concrete shell section, independent of any buckling consideration.

P_{ult_u} = for the SST dome under uniform pressure may be based on predictions from the limit load analysis for a uniform load applied at the soil surface.

P_{ult_c} = for the SST dome under concentrated loading is based on predictions from the limit load analysis for loads applied at the soil surface over a local region about the center of the tank.

P_{ult_a} = for the SST cylindrical wall under axial compressive loading is computed based on obtaining a uniform circumferential compressive stress equal to the predicted degraded concrete compressive strength of the cylindrical wall at the end of its service.

P_{ult_L} = for the SST cylindrical wall under uniform external lateral pressure is computed based on obtaining a uniform circumferential compressive stress equal to the predicted degraded concrete compressive strength of the cylindrical wall at the end of its service.

12.3 Buckling Load-Interaction and Safety Factors

The buckling evaluation requires consideration of the combined loads on the dome and wall. Dome buckling must consider the combined uniform and concentrated loads, whereas tank wall buckling must consider the combined effect of axial compression and lateral earth pressure loads. Baker et al. (1972), for dome loading, and Seide (1981), for wall loading, recommend that a linear interaction equation be applied. Then, when appropriate safety factors are introduced for the load conditions on the dome and wall, the linear interaction equations become:

Dome Buckling:

$$SF_{bu}\left(\frac{P_u}{P_{bu}^{red}}\right)+SF_{bc}\left(\frac{P_c}{P_{bc}^{red}}\right)\leq 1 \tag{12.19}$$

Wall Buckling:

$$SF_{ba}\left(\frac{P_a}{P_{ba}^{red}}\right)+SF_{bL}\left(\frac{P_L}{P_{bL}^{red}}\right)\leq 1 \tag{12.20}$$

The subscripts "u" and "c" stand for the dome uniform and concentrated loads and subscripts "a" and "L" stand for the axial and lateral loads on the tank wall.

The buckling safety factors depend on the type of shell structure and its characteristic post-buckling behavior. The buckling safety factors are specified as 1.75 for shells with increasing load capacities in the post-buckling regime, and 3.5 for shells with decreasing load capacities after buckling.

The safety factor, SF_{bu}, for dome buckling under uniform load is based on the similarity between the buckling behavior of a spherical cap under uniform external pressure and that of an axially compressed cylinder (Popov and Medwadowski 1981). Popov and Medwadowski characterize the post-buckling behavior of an axially compressed circular cylinder by a decreasing post-buckling capacity. Therefore, a safety factor of 3.5 is applied to buckling of the tank dome under uniform pressure.

The safety factor, SF_{bc}, for dome buckling under a concentrated load is based on the observations of Fitch and Budiansky (1970). For a spherical cap with λ_{bar} >2 (Equation 12.5) and a locally applied pressure load, the post-buckling response is characterized by reduced load-carrying capacity. Therefore, a safety factor of 3.5 is applied to tank dome buckling under a concentrated center load.

The safety factor, SF_{ba}, applicable to buckling of the tank wall under axial compression is 3.5 based on the above discussion noting the similarities of an axially compressed cylinder and a sphere with uniform external pressure (Popov and Medwadowski 1981).

The safety factor, SF_{bL}, for buckling of the tank wall under lateral pressure is established by considering the source of the pressure load and the confinement of the surrounding soil:

- The nature of the applied external soil pressure is somewhat self-limiting. That is, the local soil loads tend to reduce for those circumferential segments of the wall whose radial deflections are inward (away for the soil) for the critical buckling shape.
- Conversely, the soil tends to resist the outward radial deflections of the critical buckling shape.

- In addition, the presence of the steel liner with the four ring stiffeners (5 × 3½ × 5/16-in. angle iron, spaced 4-ft 6-in. apart) tends to increase the buckling capacity of the cylindrical wall for external lateral pressure loads.

Therefore, both the construction of the Type III tank wall and the confining nature of the lateral soil load suggest that the post-buckling deformation mode will be stable and the applied soil loads are self-limiting. Hence, a safety factor of 1.75 was used for the lateral pressure load on the tank wall.

12.4 Results of the Type III Tank Buckling Evaluation

Three loading conditions were considered in the buckling evaluation of the Type III SSTs:

The Baseline Tank Analysis – The maximum Type III thermal history of the S-104 tank was analyzed with a bounding soil overburden depth of 11 feet.

Maximum Thermal History with Actual Overburden – The maximum thermal history corresponding to the S-104 tank was analyzed with the actual S-104 overburden depth of 6.85 feet, soil density of 125 lb/ft3, and the maximum concentrated load of 434 kips specified in RPP-16363 (Julyk and Mackey 2003).

Actual Thermal History for the Tank with Maximum Overburden – The maximum overburden depth for Type III tanks is 10.4 feet over the TX-108 tank (Rifaey 2002). However, the maximum temperature of the TX-108 tank has only reached 116°F (Rifaey 2002). Therefore, the third buckling analysis considered a Type III tank with a soil depth of 11-feet and a maximum tank temperature of 116°F.

All three analyses used the 95/95 lower bound concrete strength and elastic modulus degraded at the maximum temperature observed during the operating history. For the third buckling case the 95/95 concrete properties remained un-degraded at the low 116°F temperature. The steel properties correspond to 80°F, which is the estimated current and future operating temperature of the Type III tanks.

The buckling analysis methods outlined in Sections 12.1 through 12.3 were implemented in separate Mathcad™ worksheets for the tank dome and the tank wall. The Mathcad™ worksheets for the three buckling evaluations of the dome and tank wall are listed in Appendix I of this document. Table 12.1 lists the Type III tank dimensions used in the buckling analyses. The dome buckling evaluations are summarized in Table 12.2 and the wall buckling cases are summarized in Table 12.3. The unfactored critical buckling loads for uniform and concentrated loads on the dome are a strong function of the elastic modulus of the concrete. Therefore, thermal degradation of the concrete modulus strongly influences the critical buckling loads.

The buckling reduction factors are also listed in Table 12.2. The geometric reduction factor, α_1=0.58, corresponds to a geometric defect equal to 10% of the wall thickness. Equations in Kollar and Dulacska (1984) confirm that this is a reasonable estimate for reinforced concrete constructed in rigid forms. The creep reduction factor, α_2, was calculated two ways, first based on the maximum predicted creep strain component in the finite element tank model and second using the approximate equation in ACI SP-67 (Popov and Medwadowski 1981). The governing creep reduction factor, α_2, was calculated from the maximum creep strains in cases 1 and 2 (α_2=0.31 for dome buckling, α_2=0.33 for wall buckling). The creep strain is near zero for the low temperature case 3 and the governing α_2=0.50 is produced by the SP-67 method, which is a function of the concrete strength.

Table 12.1. Tank Dimensions for the Buckling Analysis

Item	Value
Dome mid-thickness radius of curvature, ft	95.6
Dome thickness, inch	15
Dome half arc angle, degrees, $\sin^{-1}(R_c / R_d)$	23.6
Shallowness Parameter, λ, Eq. 12.4	6.6
Tank mid-wall radius, ft	38
Minimum wall thickness, inch	15
Height of cylindrical wall, inch	363
Total tank height, footing to dome apex, ft	39
Soil density, lb/ft^3	125
Soil internal friction angle, φ, °	35
At-rest soil pressure coefficient [1-sin(φ)]	0.426
Soil overburden depth at dome apex, ft	11/6.9
Soil depth from surface to mid-wall, ft	34.9/30.8

Interpolating from the curves by Scordelis (1981), the reduction factor, α_3, for concrete cracking and loading of steel reinforcement is estimated to be 0.94 for a dome temperature of 221°F and 0.91 for a dome temperature of 80°F. Medwadowski (2004) takes the position that prior to buckling the stresses in at least one direction (i.e., radial for the tank dome) will be compressive and cracking would not tend to reduce the shell stiffness in that direction. He further states that tension in the other direction (i.e., hoop tension in the outer perimeter of the dome) would tend to decrease the danger of buckling. Based on these observations Medwadowski proposed a value of α_3=1.0. However, the more conservative values of α_3 equal to 0.94 or 0.91 are used in the current dome buckling evaluations.

The reduction factor for nonlinear concrete behavior, α_4, was estimated using the limit loads calculated for the tank dome. The ultimate uniform surface pressure above the tank and the ultimate concentrated load within a 10-foot radius at the center of the tank were estimated using the finite element model of the Type III tank (Chapter 10). The ultimate load was taken from the limit load analyses as the load at the onset of concrete crushing. The α_4 factors range from 0.60 to 0.31 for the uniform dome load and 0.53 to 0.27 for the concentrated dome load. Medwadowski (2004) provides an alternate equation that gives slightly larger (less conservative) values for α_4.

Table 12.2 shows that the total buckling reduction factor (the product of α_1, α_2, α_3, and α_4) is in the range of 0.08 to 0.10 for the uniform load and 0.07 to 0.09 for the concentrated load. This illustrates that the theoretical buckling loads must be reduced very significantly to account for the geometric defects and material property uncertainties present in reinforced concrete. The reduced allowable dome buckling loads are therefore only 7% to 10% of the theoretical values. A further margin of safety is then applied by multiplying the applied dome loads by safety factors of 3.5 for uniform dome pressure and concentrated dome loads before comparing with the allowable reduced dome loads.

Table 12.2. Summary Results of the Dome Buckling Analysis

Item	Case 1. Baseline Max. Temp. Max. Soil	Case 2. Max. Temp. Actual Soil	Case 3. Actual Temp. Max. Soil
Maximum Dome Temperature, T_{max}, °F	221	221	116
Current and Future Wall Temperature, T_{oper}, °F	80	80	80
Overburden Depth, ft	11	6.85	11
Concrete Compressive Strength, f_c, psi	4338	4338	4600
Concrete elastic modulus at T_{max}, 10^6 psi	2.75	2.75	4.33
Concrete Poisson's ratio at T_{max}	0.15	0.15	0.15
Concrete density, lbf/ft^3	145	145	145
Steel elastic modulus at T_{oper} = 80°F, 10^6 psi	29.4	29.4	29.4
Steel Poisson's ratio at T_{oper} = 80°F	0.30	0.30	0.30
Unfactored critical uniform dome pressure, psi	310	310	488
α_1, geometric reduction factor	0.58	0.58	0.58
α_2, creep reduction factor	0.31	0.37	0.50
α_3, cracking reduction factor	0.94	0.94	0.91
α_4, nonlinear material reduction factor	0.60	0.51	0.32
Total Reduction Factor, $\alpha_1 \times \alpha_2 \times \alpha_3 \times \alpha_4$	0.10	0.10	0.08
Reduced uniform dome pressure, psi	31.7	31.9	41.3
Unfactored critical concentrated dome load, lb	56.3×10^6	45.0×10^6	88.7×10^6
α_1, geometric reduction factor	0.58	0.58	0.58
α_2, creep reduction factor	0.31	0.37	0.50
α_3, cracking reduction factor	0.94	0.94	0.91
α_4, nonlinear material reduction factor	0.53	0.46	0.27
Total Reduction Factor, $\alpha_1 \times \alpha_2 \times \alpha_3 \times \alpha_4$	0.09	0.09	0.07
Reduced concentrated dome load, lb	5.05×10^6	4.18×10^6	6.3×10^6
Finite Element Results			
Maximum ultimate creep strain in dome, ε_c	13.8×10^{-5}	10.5×10^{-5}	0
Maximum initial elastic strain in dome, ε_{el}	6.26×10^{-5}	6.16×10^{-5}	6.26×10^{-5}
Ultimate uniform dome load, psi	50.1	45.5	50.1
Ultimate concentrated dome load, kip	7350	5690	7350
Applied Pressure on Dome, psi	11.1	7.48	11.1
Applied Concentrated Dome Load, kip	200	434	200
Combined Buckling Demand/Capacity			
D/C Ratio for SF = 3.5 uniform/3.5 concentrated	1.36	1.18	1.05
Safety Factors Achieved at D/C=1 Unif./Conc.	2.57/2.57	2.95/2.95	3.33/3.33

Table 12.2 shows that the Case 1 Baseline Tank Analysis has a combined dome buckling demand-to-capacity (D/C) ratio of 1.36 based on the 3.5 safety factors. The achieved safety factors in this case are 2.57, which are somewhat below the recommended values. Medwadowski (2004) provides an alternate equation by Kollar for the safety factor where buckling governs over the ultimate load capacity. The following equation allows for the steepness of the buckling load with the size of the imperfection

$$\text{Safety Factor} = 2.5 + e^{\left[-1.5\frac{w_0}{h}\right]} \tag{12.21}$$

where w_0/h is the geometric imperfection size divided by the dome thickness. The resulting safety factor is 3.36 for the value $w_0/h=0.1$, which is appropriate for the single-shell tank construction. It is also important to note that the baseline case is a bounding combination of the maximum temperature history with the maximum upper bound soil depth. The D/C ratio for Case 2 is 1.18 (giving a realized safety factor of 2.95) for the maximum temperature history of the S-104 tank with the actual soil depth of 6.85 feet. Note that the maximum concentrated load is 434 kips for Tank S-104 with 6.85 ft soil depth at 125 lb/ft^3 (Julyk and Mackey 2003). For Case 3, the lower concrete temperature of tank TX-108 (116°F) does not cause degradation of the elastic modulus. This results in higher theoretical buckling loads for both the uniform and concentrated loads. Load Case 3 gives a combined D/C ratio of 1.05 for the 11-foot soil depth that conservatively bounds the TX-108 tank conditions (reported soil depth of 10.4 feet).

Table 12.3 summarizes the buckling analysis of the cylindrical tank wall loaded by axial compression and external lateral pressure. The applied axial load at the mid-wall of the tank (section 23) was obtained from the finite element models of the Type III tank with 11-foot and 6.85-foot soil depths. The models include the 40 lb/ft^2 uniform live load across the entire soil surface plus the 200,000-pound concentrated load distributed over a 10-foot radius at the dome center. The applied lateral pressure on the outside of the wall was calculated as the at-rest soil pressure at the mid-wall soil depths of 34.88 and 30.73 feet corresponding to overburden depths or 11 and 6.85 feet. Table 12.3 shows that the D/C ratios for the three cases are significantly below 1.0. Therefore, wall buckling is not the governing failure mode for the Type III SSTs. The baseline bounding case has a D/C ratio of 0.73. Case 2, which represents the S-104 tank, has a D/C ratio of 0.60. Case 3, which approximates the loading conditions of the TX-108 tank, has a D/C ratio of 0.48.

Table 12.3. Summary Results of the Wall Buckling Analysis

Item	Case 1. Baseline Max. Temp. Max. Soil	Case 2. Max. Temp. Actual Soil	Case 3. Actual Temp. Max. Soil
Maximum Wall Temperature, T_{max}, °F	256	256	116
Current and Future Wall Temperature, T_{oper}, °F	80	80	80
Overburden Depth, ft	11	6.85	11
Concrete Compressive Strength, f_c, psi	3440	3440	4600
Concrete elastic modulus at T_{max}, 10^6 psi	2.45	2.45	4.33
Concrete Poisson's ratio at T_{max}	0.15	0.15	0.15
Concrete density, lb/ft^3	145	145	145
Steel elastic modulus at T_{oper} = 80°F, 10^6 psi	29.4	29.4	29.4
Steel Poisson's ratio at T_{oper} = 80°F	0.30	0.30	0.30
Axial Compression on Cylinder			
Theoretical axial buckling load, lb	2.02×10^9	2.02×10^9	3.58×10^9
α_1, geometric reduction factor	0.58	0.58	0.58
α_2, creep reduction factor	0.33	0.37	0.50
α_3, cracking reduction factor	0.94	0.94	0.91
α_4, nonlinear material reduction factor	0.34	0.30	0.19
Total Reduction Factor, $\alpha_1 \times \alpha_2 \times \alpha_3 \times \alpha_4$	0.06	0.06	0.05
Reduced axial buckling load, lb	1.21×10^8	1.24×10^8	1.79×10^8
External Lateral Pressure on Cylinder			
Theoretical lateral buckling pressure, psi	606	606	1071
α_1, geometric reduction factor	0.75	0.75	0.75
α_2, creep reduction factor	0.33	0.37	0.50
α_3, cracking reduction factor	0.90	0.90	0.78
α_4, nonlinear material reduction factor	0.56	0.52	0.38
Total Reduction Factor, $\alpha_1 \times \alpha_2 \times \alpha_3 \times \alpha_4$	0.12	0.13	0.11
Reduced lateral buckling pressure, psi	74.5	78.2	118.6
Finite element ultimate creep strain in wall	13.7×10^{-5}	11.8×10^{-5}	0
Finite element initial elastic strain in wall	6.6×10^{-5}	6.9×10^{-5}	6.6×10^{-5}
Ultimate axial wall load, lbf	1.49×10^8	1.49×10^8	1.99×10^8
Ultimate lateral wall pressure, psi	112.5	112.5	150.4
Axial wall force at mid-wall section 23, lbf	14.9×10^6	11.6×10^6	14.9×10^6
At-Rest Soil Pressure at mid-wall depth, psi	12.9	11.4	12.9
Combined Buckling Demand/Capacity			
D/C Ratio for SF = 3.5 Axial/1.75 Lateral	0.73	0.58	0.48
Safety Factors Achieved at D/C = 1 Axial/Lateral	4.77/2.39	6.0/3.0	7.27/3.63

12.5 Summary of the Type III Tank Buckling Evaluation

A buckling analysis was performed for the dome and sidewalls of the Type III SSTs using the methods specified in the Evaluation Criteria report (Johnson et al. 2010). Several additional solutions were identified subsequent to release of the Evaluation Criteria report that better represent the geometry and loading conditions of the tanks. These solutions are used in the present analysis to better approximate the buckling loads on the Type III tanks. The allowable buckling loads were estimated as the theoretical buckling loads reduced by factors that account for geometric imperfections, concrete creep, cracking and loading of the reinforcing steel, and the nonlinear stress-strain behavior of concrete at high compressive stress. The dome was evaluated for the combined effect of uniform pressure plus a concentrated load distributed over a local area at the dome apex. The tank wall was evaluated for combined axial compression plus lateral soil pressure on the outside of the tank. Three loading cases were evaluated representing the bounding case (maximum temperature and soil overburden depth) plus two more realistic cases that approximate the S-104 tank (with the maximum temperature history) and the TX-108 tank (the maximum soil overburden). The dome evaluation showed that the bounding case has a realized safety factor of 2.57 for both uniform and concentrated loads, which is somewhat below the recommended safety factor of 3.5. The more realistic S-104 dome evaluation has a calculated safety factor of 3.54, and the TX-108 evaluation has a safety factor of 3.33, which are both very close to the recommended values. The 11-foot soil depth results in loads that are near the buckling limits for both the high temperature (S-104) and the low temperature (TX-108) cases. The buckling evaluation of the tank wall showed that each of the three load cases has safety factors that significantly exceed the recommended values of 3.5 (axial load) and 1.75 (lateral pressure). Therefore, sidewall buckling is of less concern than dome buckling.

13.0 Conclusions

The structural analyses discussed in this report do not reveal any deficiencies with the structural integrity of the Type III Hanford single-shell tanks (SSTs). Furthermore, rebar yielding was not observed in any of the analysis runs conducted. The analyses represent 59 years of use. The loads imposed on the model for the finite element analyses are significantly more severe than any service to date or currently planned for the future. The analyses treated the most severe combinations of soil and concrete stiffness and based the structural evaluation on lower bound concrete strength.

The Type III tank model was subjected to a 200-kip concentrated load on the soil surface, a 40 lb/ft^2 surface load, a typical waste load, and a 59-year thermal history that peaked at 300°F. The ACI 349-06 code evaluations show that tank demands are lower than the capacities for all locations in the dome, upper haunch, and wall. The best estimate condition of the Type III tanks with 11 feet of soil overburden and best estimate material properties is that the non-seismic ACI 349-06 load demands are at most 34%, 73%, 53% of the meridional, hoop, and shear capacities, respectively, in the dome, upper haunch, and wall. In addition, the maximum tank section forces and moments over the time history were extracted from the seismic model and combined with the non-seismic forces and moments to evaluate the American Concrete Institute (ACI) seismic load combination. The seismic ACI evaluation results indicate that tank demands are lower than the ACI 349-06 capacities for all locations in the dome, upper haunch, and wall. For the best estimate material property runs, with any of the seismic waste properties, the seismic ACI load combination resulted in demands that were at most 28%, 73%, and 46% of the meridional, hoop, and shear capacities, respectively, in the dome, upper haunch, and wall.

The reinforced concrete structure was evaluated in the manner required by ACI 349. Load combinations 1, 4 (which includes the seismic load), and 9 of the ACI codes were evaluated for each variation of soil and concrete properties. The axial load and moment were evaluated on the load-moment diagram for each individual cross-section. The demand was demonstrated to be lower than the capacity at all locations in the dome, haunch, and wall for all load combinations. One or more locations in the slab displayed demands higher than capacity for load combination 4 for several material property combinations. One of the bounding cases (Run #3) under load combination 1 also showed a D/C ratio exceeding 1.0 for a section in the slab. However, the slab is supported on soil and the concrete cracking and displacements are displacement controlled. To further address the slab concerns, three analysis cases with upper bound, lower bound and best estimate soil properties were repeated with the slab effectively separated at the inner edge of the tank footing so that it could not provide structural support to the rest of the tank. The results demonstrate that isolating the slab does not adversely affect the structural stability and integrity of the tank. The slab removal analyses predicted that the maximum shear offset between the slab and footing would be less than 0.06 inch; less than one-sixth of the original nominal liner thickness of 0.375 inch. The bottom and knuckle of the tank are also covered with a tar-based mastic material that would act to cushion the transition so it is unlikely that the liner would incur any damage. In summary, the occurrence of slab sections with ACI capacity lower than demand will not negatively impact the tank structural integrity. Cracks in the slab do not adversely affect the structural stability of the tank dome, walls, and footing.

The soil overburden is the largest load on the tank and it is the largest contributor to the static tank demands. Waste and soil surface loads produced only secondary effects. Thermal loads were significant in the slab and lower wall where the temperatures were highest (exceeding 300°F). Including the load-relieving effects of concrete creep reduces the demands by 5–16%. The material combination of upper bound concrete modulus and lower bound soil modulus increased the concrete section demands.

To assess the impact of various tank appurtenances, conservative Type III appurtenance configurations were also modeled and evaluated according to the ACI code. The demand was shown to be less than the capacity at all locations in the tank for load combinations (LC1, LC9) that do not include a seismic demand. For load combination 4, which includes seismic, the demands were less than the capacity in all dome, haunch, and wall locations while they were greater than the capacity in some sections in the slab (just as in the axisymmetric TOLA loads analysis). The appurtenance modeling shows some increased D/C ratios restricted to local regions near the pits and penetrations. At all other locations the ACI D/C ratios follow the baseline TOLA model very closely. This suggests that it is not necessary to conduct a full series of analyses over the entire range of material property combinations but the analysis with the baseline material properties is adequate to evaluate the effects of appurtenances. For the Type III SSTs, the baseline material properties were adequate to evaluate the effects of the appurtenances.

The tank limit load analyses have safety factors greater than the recommended value of 3.0. This confirms the adequacy of the current dome load limits. The bounding case dome buckling evaluation calculated safety factors that were below the recommended value of 3.5 due to the conservative combination of the maximum temperature history and the maximum 11 ft soil overburden of the Type III tanks. However, the more realistic combinations of maximum temperature with the actual overburden (tank S-104) and the maximum overburden with the actual temperature (tank TX-108) gave safety factors that were closer to the recommended value of 3.5. The wall buckling evaluation calculated safety factors that significantly exceed the recommended values, showing that sidewall buckling is of less concern than dome buckling. The limit load results for the case of uniform surface load using a lower bound soil overburden of 6.85 ft also showed factors of safety above the recommended values. However, these results are lower than that suggested by a simple scaling of the other uniform surface load results, suggesting that these results are not scalable due to the significant nonlinearities in the model.

Additional analyses, documented as appendices to this report, were conducted to address the external reviewer comments and recommendations while performing the Type II AOR. The appendices address the usage of 11 ft soil overburden, the appurtenance configuration used in the analysis based on Type III tanks features, the extent of backfill in the seismic model, improvements in modeling soil above the tanks (using soil rings), the waste height sensitivity (empty vs. full tank scenarios), slab detachment scenarios, Mathcad™ buckling analyses, and a detailed example of the ACI evaluation methods. Additional appendices present analysis results showing the effects of individual load components, alternate load factor studies, and force and moment plots for Run #6 with nominal strength concrete. These additional studies were performed to gain a more complete understanding of the Type III SSTs and to ensure that the models present an accurate representation of tank structural integrity.

14.0 References

ACI. 2007. American Concrete Institute Code Requirements for Nuclear Safety Related Concrete Structures. ACI 349-06, American Concrete Institute, Farmington Hills, Michigan.

Bander TJ, JP Day, AD Dyrness, RJ James, LJ Julyk, RS Marlow, CJ Moore, EW Pianka, YR Rashid, JS Shulman, and MP Weis. 1994. Tank 241-C-106 Structural Integrity Evaluation for In situ Conditions. WHC-SD-W320-ANAL-001, Revision 0, Volumes I and II, Westinghouse Hanford Company, Richland, Washington.

Berman HS. 2009. "Hanford Single-Shell Tank Integrity Program." Single-Shell Tank Integrity Project-Workshop, July 29, 2009. WRPS-40224-VA, Richland, Washington.

BNL 1995, "Seismic Design and Evaluation Guidelines for the Department of Energy High-Level Waste Tanks and Appurtenances," BNL 52361, Engineering Research and Applications Division, Department of Advanced Technology, Brookhaven National Laboratory, Associated Universities, Inc., Upton, New York.

Boomer KD. 2009. "Presentations to the Single-Shell Tank Integrity Panel- Single-Shell Tank History." Single-Shell Tank Integrity Project-Workshop, January 26-28, 2009. WRPS-40224-VA, Richland, Washington.

DOE. 2002. Natural Phenomena Hazards Design and Evaluation Criteria for Department of Energy Facilities. DOE-STD-1020-2002. U.S. Department of Energy, Washington, D.C.

Ewer KL, JW Funk, RG Hale, GA Lisle, CV Salois, and MR Umphrey. 1997. Supporting Document for the Historical Tank Content Estimate for S Tank Farm. HNF-SD-WM-ER-323, Rev. 1, Fluor Daniel Northwest, Inc., Richland, Washington.

Fitch JR and B Budiansky. 1970. "Buckling and Postbuckling Behavior of Spherical Caps under Axisymmetric Load." AIAA Journal 8(4):686–693.

Flugge W. 1960. Stresses in Shells, Springer-Verlag, New York, New York.

GE. 1953a. Design and Construction History 241-BY Tank Farm 200 East Area. HW-24800-30, General Electric Hanford Works, Richland, Washington.

GE. 1953b. Design and Construction History 241-TX Tank Farm 200 West. HW-24800-35, General Electric Hanford Works, Richland, Washington.

Geomatrix. 2007 . Updated site response analyses for the Waste Treatment Plant, DOE Hanford Site

Washington: GMX-9995.002-001, Revision 00, June.

Han FC. 1998. Structural Integrity and Potential Failure Modes of the Hanford High-Level Waste Tanks. WHC-SD-TWR-RPT-002. Lockheed Martin Hanford Company, Richland, Washington.

Harvey RW. 1970. Management of Radioactive Wastes Stored in underground Tanks at Hanford. ARH-R-43, Rev. 2, Atlantic Richfield Hanford Company, Richland, Washington.

Hundal TS. 2004a. 241-BY Tank Farm Historic Dome Load Record Data. RPP-20448, Rev. 0, COGEMA Engineering Corporation, Richland, Washington.

Hundal TS. 2004b. 241-S Tank Farm Historic Dome Load Record Data. RPP-20450, Rev. 0, COGEMA Engineering Corporation, Richland, Washington.

Hundal TS. 2004c. 241-TX Tank Farm Historic Dome Load Record Data. RPP-20453, Rev. 0, COGEMA Engineering Corporation, Richland, Washington.

Hundal TS. 2004d. 241-TY Tank Farm Historic Dome Load Record Data. RPP-20454, Rev. 0, COGEMA Engineering Corporation, Richland, Washington.

IBC. 2003. International Building Code 2003. International Code Council. Inc.

Irish, E.R. 1953. Temperature of Redox Process Waste Storage Tanks. Letter from E.R. Irish to C. A. Rohrmann, November 4, 1953. LET-110453

Johnson KI, JE Deibler, FG Abatt, and MW Rinker. 2010. Single-Shell Tank Structural Evaluation Criteria. RPP-46442, Rev. 0, Pacific Northwest National Laboratory, Richland, Washington.

Julyk LJ. 2003. LHMC Letter 74731-98-LJJ-001: 100-Series Single-Shell Tank dome Load Reassessment for Revised Soil Loading. RPP-11423, Rev. 0B, CH2M HILL Hanford Group, Inc., Richland, Washington.

Julyk LJ and TC Mackey. 2003. Tank-Specific Allowable Dome Load for Hanford-Site 100-Series Single-Shell Tanks. RPP-16363, Rev. 0, CH2M HILL Hanford Group, Inc., Richland, Washington.

Kollar L and E Dulacska. 1984. Buckling of Shells for Engineers, Wiley-Interscience, John Wiley & Sons, New York, New York.

Mackey TC. 2004a. Design Loads for Tank Farm Facilities. TFC-ENG-STD-06. CH2M HILL Hanford Group, Inc., Richland, Washington.

Mackey TC. 2004b. Design and Dome Load Criteria for Hanford Waste Storage Tanks. RPP-20473, Rev. 1, CH2M HILL Hanford Group, Imc., Richland, Washington.

Mackey TC and LJ Julyk. 2004a. Soil Load Above Hanford Waste Storage Tanks. WHC-SD-WM-TI-665, Rev. 0D, CH2M HILL Hanford Group, Inc., Richland, Washington.

Mackey TC and LJ Julyk. 2004b. Analysis of Record Summary for Single-Shell Tanks. RPP-11802, Rev. 1, CH2M HILL Hanford Group, Inc., Richland, Washington.

Mackey TC and LJ Julyk. 2004c. Soil Weight at Hanford Storage Tank Locations. WHC-SC-WM-SOIL-001, Rev. 0A, CH2M HILL Hanford Group, Inc., Richland, Washington.

McCluskey PR. 2005. SST Analysis for Installation of Additional Risers. RPP-21840, Rev. 0, CH2M HILL Hanford Group Inc., Richland, Washington.

McKnight, JP. 1970. Design Criteria Waste Concentrate Facilities for the 241-T and 241-B Farm Complexes. ARH-1845, Atlantic Richfield Hanford Company, Richland, Washington.

Medwadowski SJ. 2004. "Buckling of Concrete Shells: An Overview." Journal of the International Association for Shell and Spatial Structures 2004, No. 144 pp. 51–63.

Mercier PF, MD Wonacott, and C DeFigh-Price. 1981. Survey of the Single-Shell Tank Thermal Histories. RHO-CD-1172, Rockwell Hanford Operations, Richland, Washington.

Overbeck WP. 1946. Project Proposal Additional Underground Waste Tank Facilities 241-B-Tank Farm. H-7-5264, Hanford Engineer Works, Richland, Washington.

Popov EP and SJ Medwadowski. 1981. "Stability of Reinforced Concrete Shells: State-of-the-Art Overview." In Concrete Shell Buckling, ACI SP-67, American Concrete Institute, Detroit, Michigan.

Ramble AL. 1983. Single-Shell Waste Tank Load Sensitivity Study. SD-RE-TI-012 Rev. A-0. Rockwell Hanford Operations, Richland, Washington.

Rifaey SH. 2002. Single Shell Tank System Integrity Assessment Report. RPP-10435, Rev. 0, CH2M HILL Hanford Group, Inc., Richland, Washington.

Rinker MW, SK Bapanapalli JE Deibler, CE Guzman-Leong, KI Johnson, NK Karri, SP Pilli, and SE Sanborn. 2010. Single-Shell Tank Integrity Project Analysis of Record: Preliminary Modeling Plan for Thermal and Operating Loads. RPP-46644, Rev. 0, PNNL-19338. Pacific Northwest National Laboratory, Richland, Washington.

Rinker MW, BG Carpenter, C Hendrix, and FG Abatt. 2008. Hanford Thermal and Seismic Project – ANSYS Seismic Analysis of Hanford Double-Shell Tanks. RPP-RPT-28966 Rev. 1, PNNL-15720 Rev. 1, Pacific Northwest National Laboratory, Richland, Washington.

Rinker MW, KI Johnson, SK Bapanapalli, NK Karri, JE Deibler, SP Pilli, CE Guzman-Leong, SE Sanborn, FG Abatt, JA Dewberry, BM Larsen, KL Stoops, and LJ Julyk. 2011a. Single-Shell Tank Integrity Project Analysis of Record: Hanford Type II Single-Shell Tank Thermal and Operating Loads and Seismic Analysis. RPP-RPT-49989, Rev. 0, Pacific Northwest National Laboratory, Richland, Washington.

Rinker MW, NK Karri, CE Guzman-Leong, SP Pilli, JE Deibler, FG Abatt, and KI Johnson. 2011b. An Evaluation of Single-Shell Tank 241-C-107 for the Addition of a large Penetration in the Tank Dome. RPT-CALC-43416, Rev. 1, Pacific Northwest National Laboratory, Richland, Washington.

Rohay AC and SP Reidel. 2005. Site-Specific Seismic Site Response Model for the Waste Treatment Plant, Hanford, Washington. Report prepared by Pacific Northwest National Laboratory for the U.S. Department of Energy, Office of River Protection, under Contract DE-AC05-76RL01830, March.

Rutherford MJ. 1948. Additional Waste Storage Facilities 200 East Area. HW 3783, General Electric Company, Hanford Works, Richland, Washington.

Rutherford MJ. 1949. Specifications for Construction of Waste Disposal Facilities 241-S, 216-S, and 207-S 200 West Area. HW-3937, General Electric Company, Hanford Works, Richland, Washington.

Rutherford MJ. 1951. Waste Disposal Facilities 241-BZ and TY Tank Farms 200 East and West Areas. HW 4696, General Electric Company, Hanford Works, Richland, Washington.

Scordelis AC. 1981. "Stability of Reinforced Concrete Domes and Hyperbolic Paraboloid Shells." In Concrete Shell Buckling, ACI SP-67, American Concrete Institute, Detroit, Michigan.

Seide P, V Weingarten, and S Masri. 1979. Buckling Criteria and Application of Criteria to Design of Steel Containment Shell. Final Report, NUREG/CR-0793, January 1978-March 1979, U.S. Nuclear Regulatory Commission, Washington, D.C.

Seide P. 1981. "Stability of Cylindrical Reinforced Concrete Shells." In Concrete Shell Buckling, ACI SP-67, American Concrete Institute, Detroit, Michigan.

Stivers HW. 1955. A Study to Determine the Economical Tank Size for Radioactive Waste Disposal. HW-34860, General Electric Company, Hanford Atomic Products Operation, Richland, Washington.

Stivers HW. 1957. Hazards Study Self-Boiling Radioactive Wastes Storage Facilities - Process Technology – Recommendation Report. HW-53641, General Electric Company, Hanford Atomic Products Operation, Richland, Washington.

Weber RA. 2009. Methodology and Calculations for the Assignment of Waste Groups for the Large Underground Waste Storage Tanks at the Hanford Site. RPP-10006, Rev. 8, Washington River Protection Solutions, LLC, Richland, Washington.

Appendix A

SST AOR Guidance, March 28, 2011

This page intentionally left blank.

Appendix A

SST AOR Guidance, March 28, 2011

From: Rast, Richard S
Sent: Monday, March 28, 2011 4:00 PM
To: Sanborn, Scott E
Cc: Pilli, Siva P; Karri, Naveen K; Deibler, John E; Johnson, Kenneth I; Rinker, Michael W; Scott, Mark A; Mackey, Thomas C; Rast, Richard S
Subject: RE: Type III soil overburden and concentrated loads

Dr. Sanborn,

Please be advised that the Type III SST AOR model should reflect a soil overburden depth = 11 ft.

If you have any questions, please let me know.

Thanks,

Rick Rast, P.E.
Civil/Structural Engineer
509-376-6056 office
509-376-6249 fax
503-753-7773 cell
richard_s_rast@rl.gov
MSIN E6-47

Technical Integration Central Process
Double-Shell Tank and Single-Shell Tank Integrity
Washington River Protection Solutions

From: Sanborn, Scott E [mailto:Scott.Sanborn@pnl.gov]
Sent: Wednesday, March 23, 2011 10:40 AM
To: Rast, Richard S
Cc: Pilli, Siva P; Karri, Naveen K; Deibler, John E
Subject: Type III soil overburden and concentrated loads

Rick,

I've reviewed the documents we discussed and listed below are my findings. I think we could use 125 lb/ft3 soil with either 200 kip concentrated load and 10.59 ft of soil or 200 kip concentrated load and 10.38 ft of soil (max of Type III tanks). What do you think?

-Scott

* RPP-16363, Rev 0 list different combinations of soil density, height, and concentrated load. We can choose the combination that we want but if we stick with 125 lb/ft3 soil and 200 kip concentrated load for the Type III tanks then the soil depth is 10.59 ft (or we can choose the largest Type III soil depth at 10.38 ft and a concentrated load of 218 kip). This 10.59 ft case is listed as the baseline case from RPP-11802, Rev 0. RPP-16363, Rev 0A does not have any updates to the Type III tanks. As a side note, in our Type II analysis we are exceeding the recommendations for soil height and concentrated load combinations at 125 lb/ft3 density; we have analyzed 10ft and 200kips where as at 200kips RPP-16363 recommends a max of 8.83ft for 125 lb/ft3.

* RPP-11802, Rev 0 lists 200kip concentrated load (pg 7) with 10.59 ft and 125 lb/ft3 soil for the Type III farms (pg 8) and references SD-RE-TI-012 and RPP-11423 as the AORs where the load limits come from.

* RPP-11802, Rev 1 is updated according to RPP-16363, Rev 0 (circular referencing here) and has individual allowable concentrated loads for each tank's actual soil depth and soil density (all Type III tanks are 125 lb/ft3). RPP-11802, Rev1A and Rev1B don't change the Type III allowable loads.

* RPP-11423, Rev 0 finds that in switching to 125 lb/ft3 density and using current soil heights some tanks in TX farm exceed previously set (SD-RE-TI-012) dome load limits. Type III farms show that given 125 lb/ft3 soil and 200 kip concentrated load the revised maximum soil height is 10.59 ft (Table 3). RPP-11423 Rev 0A and Rev 0B don't have any updates to Type III tanks.

* SD-RE-TI-012, Rev A-0 recommends for all 75-ft diameter tanks a limit of 10 ft soil depth, 200 kip concentrated load for 115 lb/ft3 soil.

Appendix B
Appurtenance Review

This page intentionally left blank.

Appendix B

Appurtenance Review

The following sections present a review of the appurtenances on the Type III single-shell tanks (SSTs) at Hanford.

B.1 Appurtenances

The appurtenances on the Hanford SSTs include pits, piping, risers, and other ancillary equipment. Although appurtenances are not expected to significantly affect the structural demand on the tank, this must be verified by appropiate analysis. The purpose of this appendix is to identify configurations of the appurtenances for the Type III SSTs in particular and to establish a strategy for determining the effect of the appurtenances on the TOLA and seismic response of the tank. The focus of this analysis is not on the structural integrity of the appurtenances but rather on their influence to the tank structural demands. Type III SSTs consist of the 100-Series 241-BY, S, TX, and TY tanks with a waste storage capacity of 758,000 gallons. A typical Type III SST configuration is shown in Figure B.1.

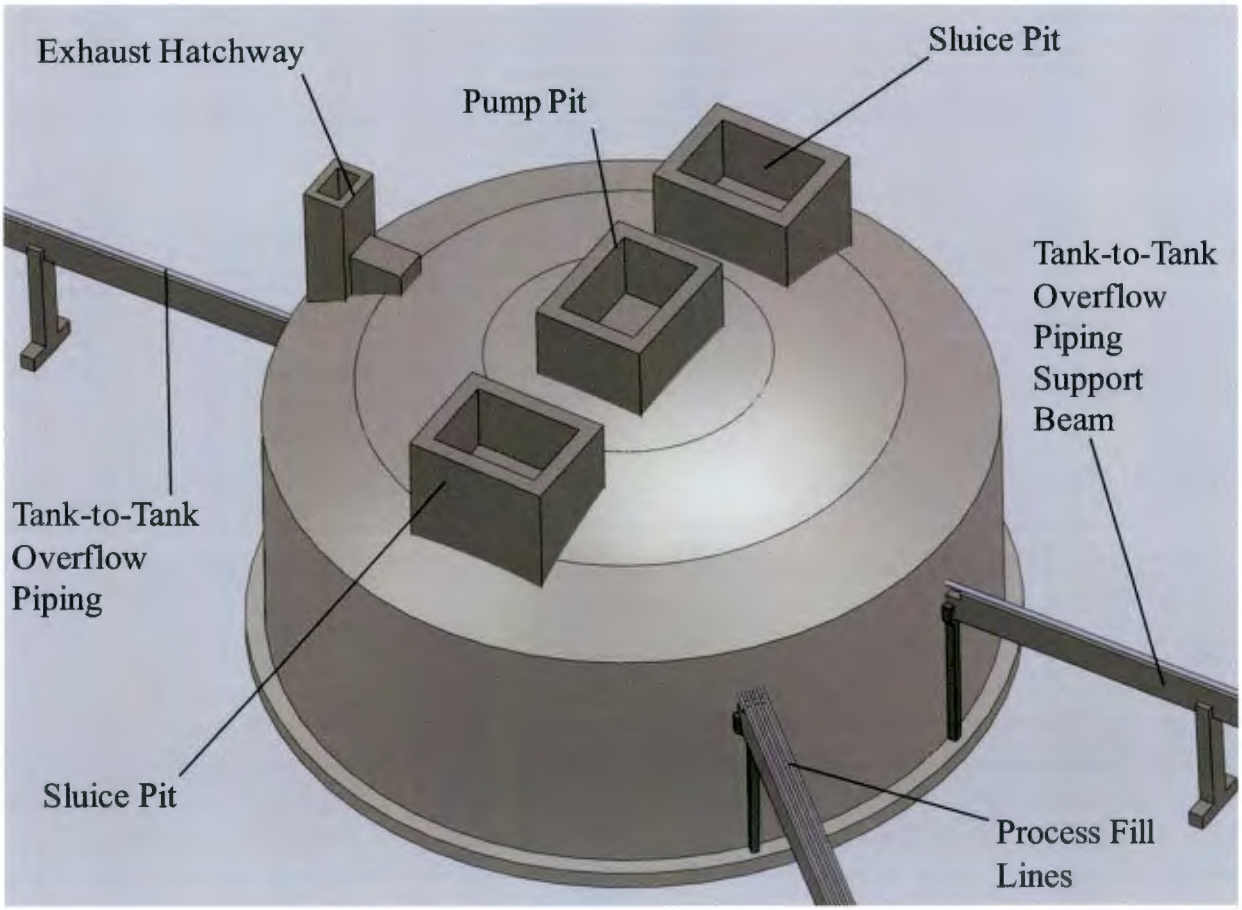

Figure B.1. Typical Type III SST Appurtenance Configuration

The Type III SSTs are arranged in batteries of six, twelve, or eighteen tanks. Tank-to-tank overflow piping and supports exist between rows of tanks. Process fill lines bring processed waste to the tank farm typically through one exterior row of tanks. A typical Type III SST farm arrangement is shown in Figure B.2.

(Ref: 241-S, H-2-1774)

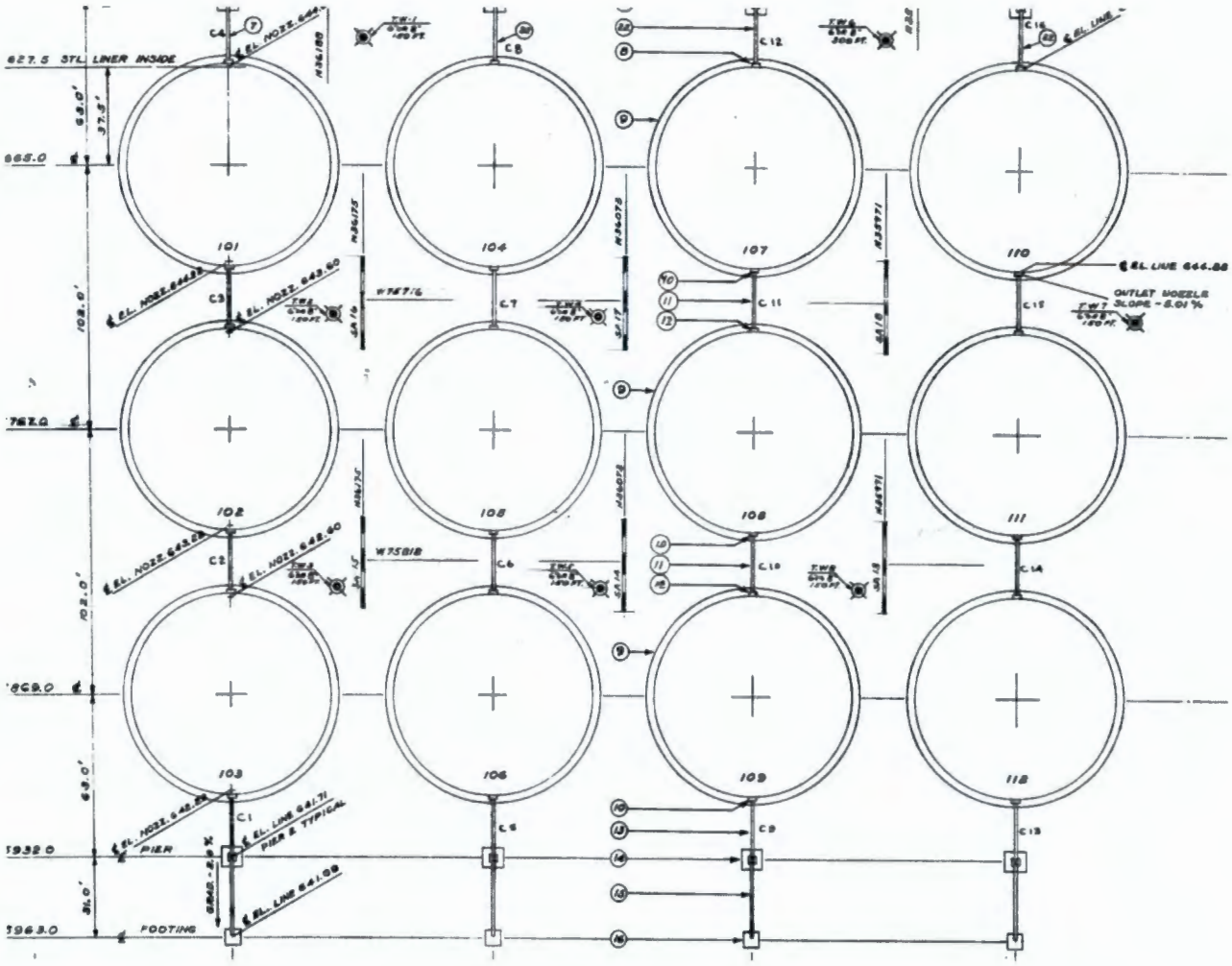

Figure B.2. Type III SST S-Farm Arrangement Showing Tank-to-Tank Piping

B.2 Dome Penetrations

Type III SSTs have both original construction (see Figure B.3) and post-construction penetrations for risers. Original construction penetrations for Type III tanks have diameters of 4 inches, 12 inches, 42 inches, and 42-inch manhole. Figure B.4 through Figure B.7 display a plan view of each Type III tank with the locations of original construction penetrations (blue) and the post-construction penetrations (red) in the tank domes.

(Ref: 241-TX, H-2-807)

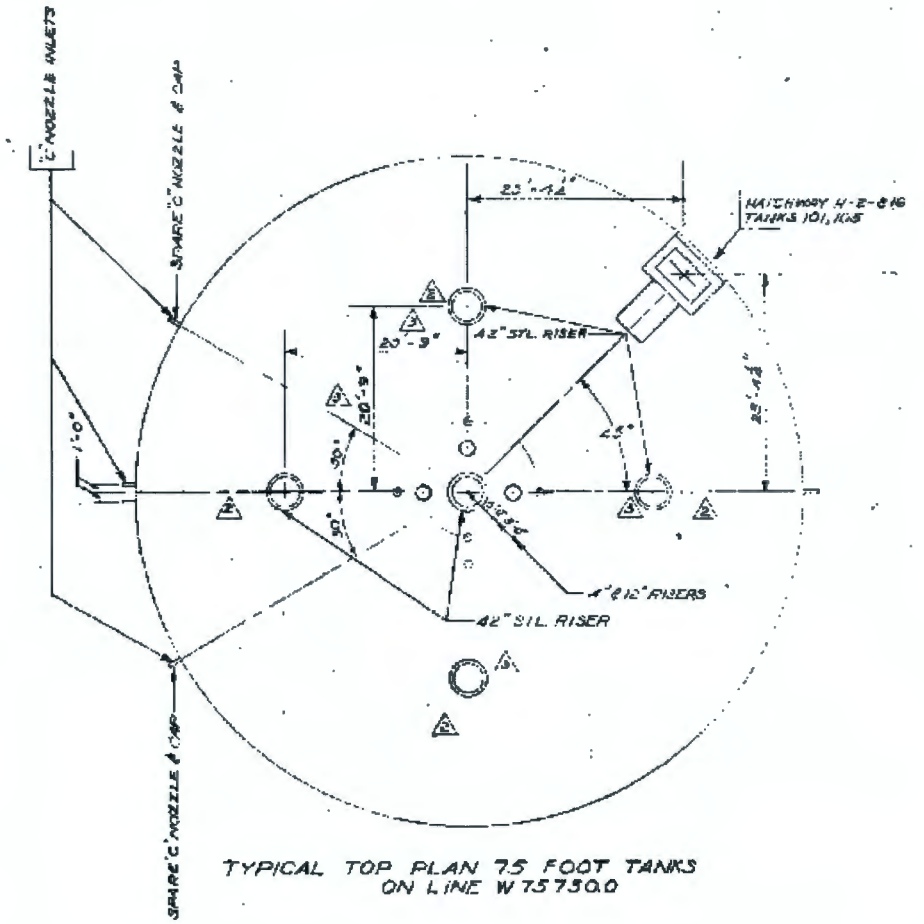

Figure B.3. Typical Type III SST Original Construction Dome Penetration Layout

Previous analyses have modeled the affect of penetrations in the dome (Watwood 1977; Rinker et al. 2009; McCluskey 2005). Rinker et al. (2011b) showed a Type II SST with a 55-inch-diameter post-construction hole at the center to be structurally sound. McCluskey (2005) analyzed the affect of potential post-construction penetrations in 100-Series SST domes ranging in size from 4 inches, 12 inches, 26 inches to 42 inches in diameter out to a radial distance of 29 feet from the center of the dome and concluded that the tank dome would remain structurally adequate as long as the holes were spaced at least three diameter spacings apart. The Type II SST AOR (Rinker et al., 2011a) analyzed 42-inch diameter converted manways at a radial distance of 32-ft 6-inches as well as a central post-construction 36-inch diameter penetration, and found there is little structural influence of the penetrations outside of their immediate area. Some of the Type III SSTs include 42-inch-diameter manholes (see Section B.3) at 32 feet 6 inches from the center; however the reinforced manhole covers remain in place for these manholes. The Type III SSTs include some small diameter penetrations at radial distances beyond those studied previously (see Figure B.7 for example), however these penetrations are all smaller than the dome thickness and are expected to have a negligible effect on the structural response. Based on the previous analyses, none of the dome penetrations in the Type III SSTs are expected to have a significant effect on the structural response of the tanks.

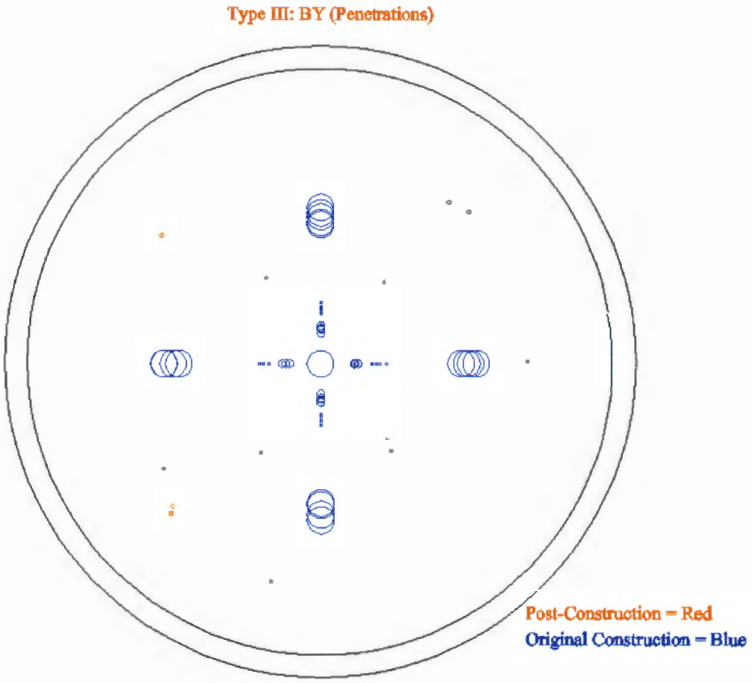

Figure B.4. Type III SST BY Penetration Plan View

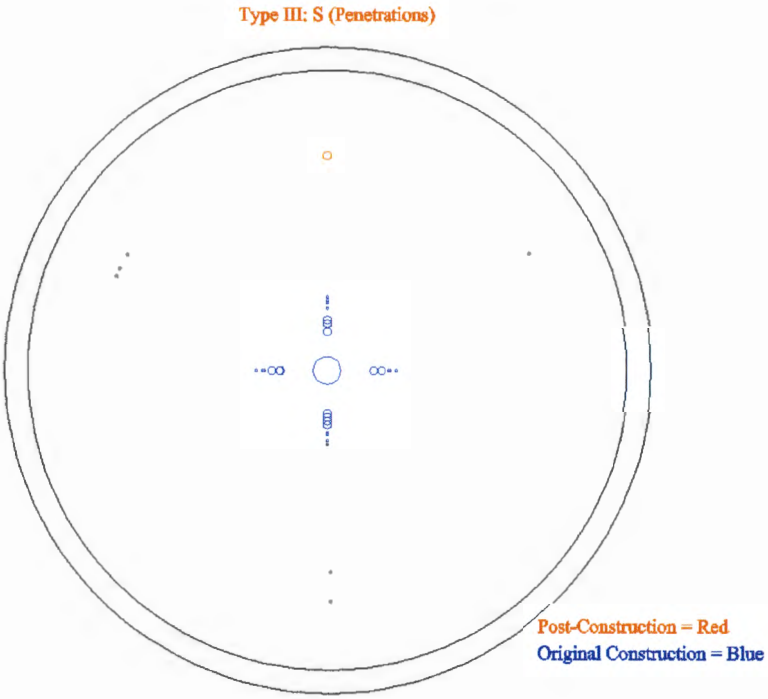

Figure B.5. Type III SST S Penetration Plan View

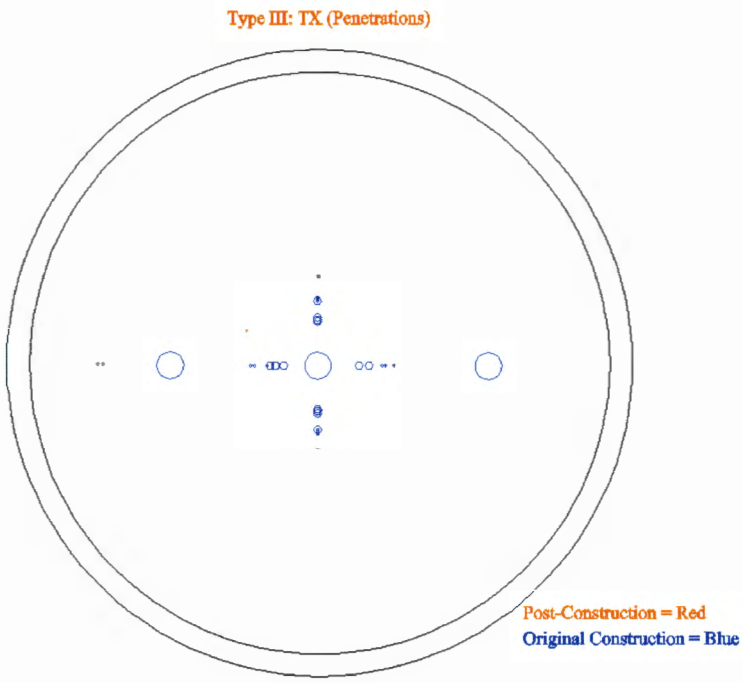

Figure B.6. Type III SST TX Penetration Plan View

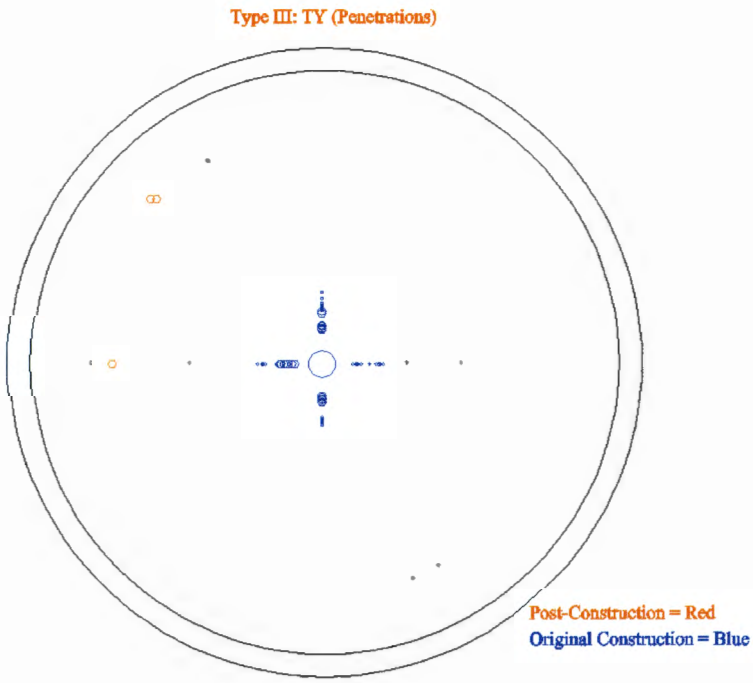

Figure B.7. Type III SST TY Penetration Plan View

B.3 Manhole Penetrations and Cover

Manhole covers are used to cover the 42-inch manhole penetrations[1] located approximately 18.50 feet to 22.75 feet from the center of the Type III SST dome. Each manhole cover is constructed of reinforced concrete as shown in Figure B.8. This reinforced manhole cover and penetration is not expected to significantly affect the demand on the tank dome during a seismic event or under TOLA loads.

(Ref: 241-S, H-2-1814)

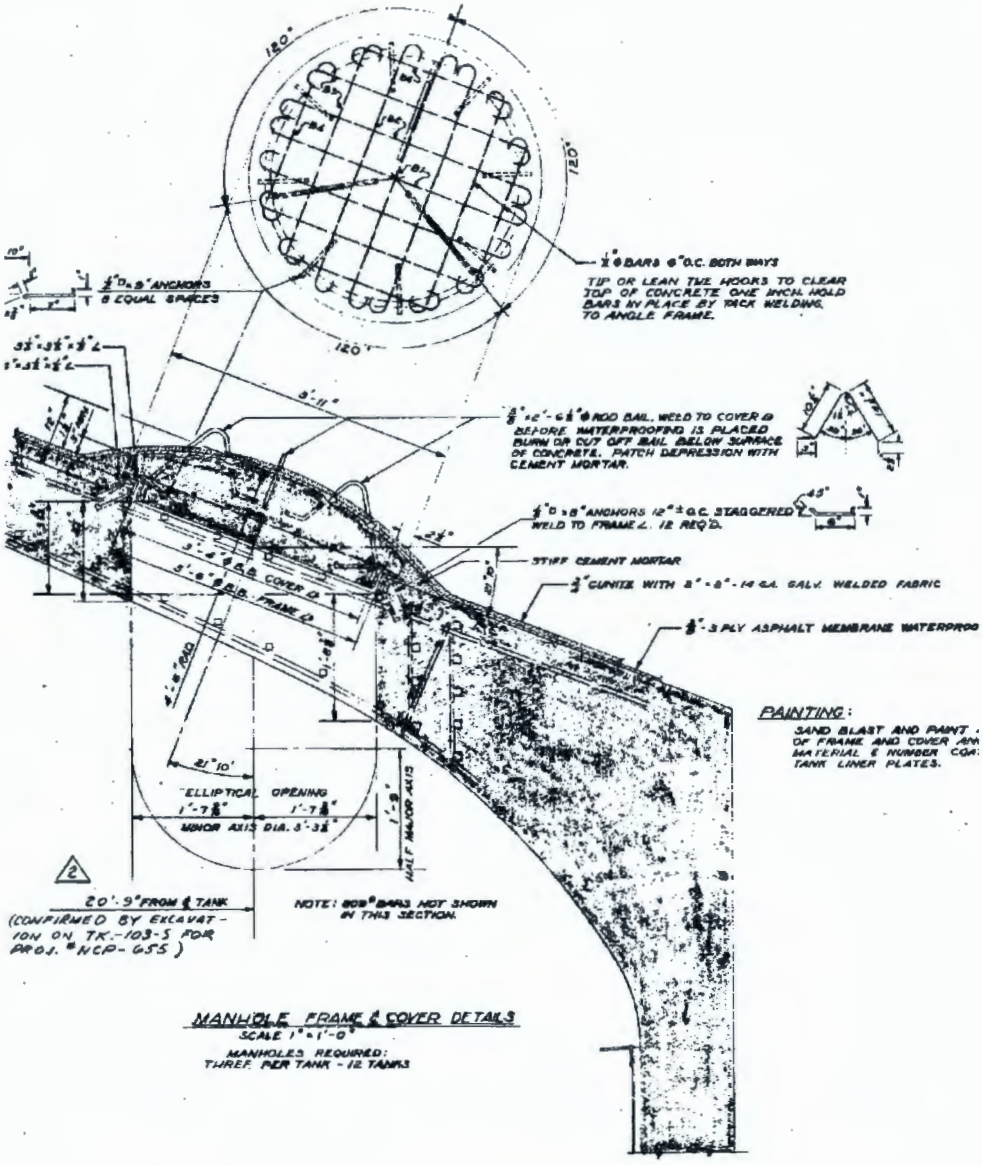

Figure B.8. Type III SST 42-inch Manhole Penetration and Cover

[1] Note that the 42 inches refers to the size of the major axis of the elliptical opening at the top surface of the dome. The diameter of the hole through the dome is 39.125 inches, which is the size of the minor axis of the elliptical opening at the top surface of the dome.

B.4 Risers

Original construction non-pit riser details consist of a pipe encapsulated into the concrete dome with local rebar reinforcement as shown in Figure B.9. Post-construction non-pit risers are not locally reinforced but are grouted into the newly formed dome penetrations. These small-diameter non-pit risers are not expected to significantly affect the demand on the tank dome under TOLA loads or during a seismic event. The movement of the steel riser that extends from the dome to slightly above grade (approximately one foot) is strain-controlled by the surrounding soil mitigating the transfer of moments to the dome.

(Ref: 241-TX, H-2-817)

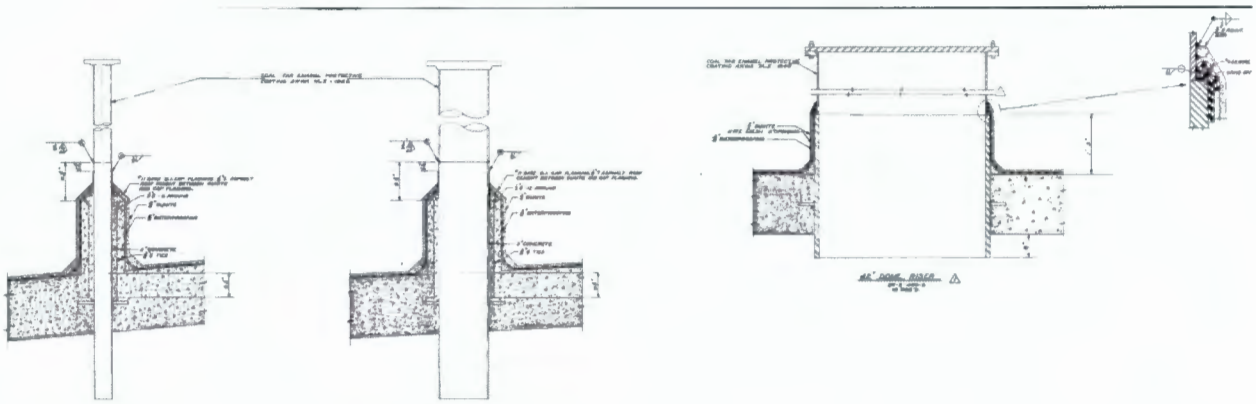

Figure B.9. Type III SST Original Construction Riser Details

B.5 Pits

Pits are reinforced concrete boxes that extend just enough above grade to prevent flooding by surface water. The pits have removable reinforced concrete cover blocks or steel plates to allow entry for work. The SST pit types include pump pits, heel pits, sluicing pits, flush pits, instrument enclosure pits, condensor pits, and distribution pits. Pits may contain jumpers, pumps, monitoring equipment, sluicing equipment or other miscellaneous equipment. The configuration and extent of this equipment have continued to change as mission changes have required different equipment. Pits may be part of the original construction or added (post-construstion) as needed to meet process mission requirements.

The dome load record documents (Hundal 2004a, 2004b, 2004c, and 2004d) calculated the net weight of all structures above the Type III SST domes. The pit net weight was calculated by taking the calculated pit and equipment weight and subtracting the weight of the removed soil. The heaviest Type III SST net weight pit is an offset 73.2 kip heat exchanger pit. However, this pit mostly above the soil surface and only buried to a depth less than 2-ft. This allows this pit to distribute its load through the soil to a larger area on the dome surface. Essentially this is no different than an offset concentrated surface load. Of more concern from a structural response perspective are heavy pits that load the tank dome directly. The heaviest SST Type III central pit above the tank is a Pump pit on tank 241-TX-115 that has a net weight of approximately 23.2 kip (Hundal 2004c). The heaviest SST Type III offset pit located above the 42-inch-diameter converted manway is a Sluice pit on tank 241-TY-101/102 that has a net weight of approximately 58.8 kip (Hundal 2004d).

Pits over the tanks were not included during the original construction of Type III SSTs. Hence, Type III SST pits are not doweled directly into the dome. The pits were constructed over original risers (or in some cases added risers). Figure B.10 through Figure B.13 show the details of typical pump pits and sluice pits on tanks 241-TY-101 and TY-102. Figure B.14 through Figure B.18 show the post-construction sequence for the installation of a pump pit and riser in tank 241-TY-101 and TY-102.

(Ref: 241-TY, H-2-2293)

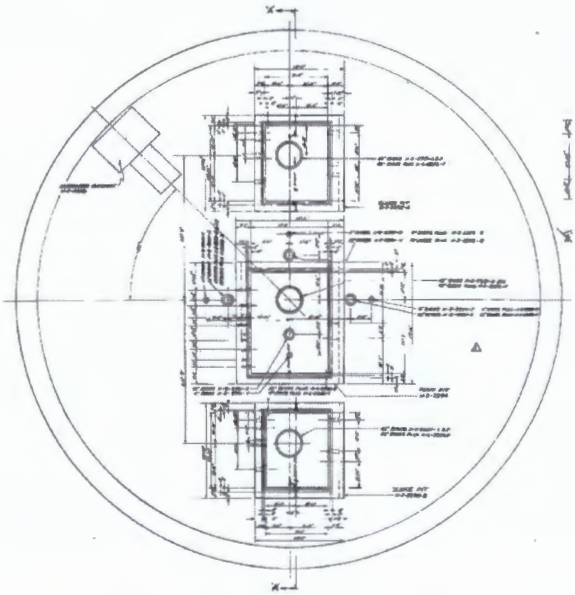

Figure B.10. Type III SST Plan View of Pump & Sluice Pit Details

(Ref: 241-TY, H-2-2293)

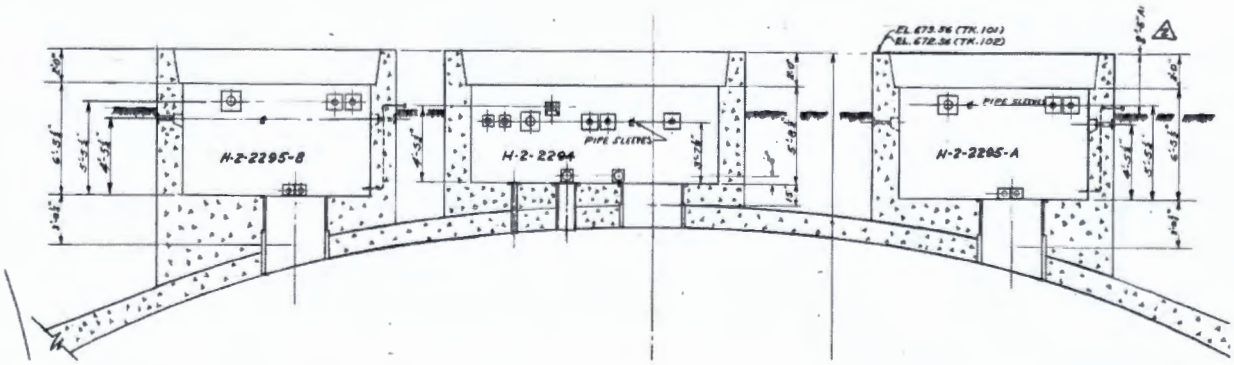

Figure B.11. Type III SST Pump & Sluice Pit Details

(Ref: 241-TY, H-2-2294)

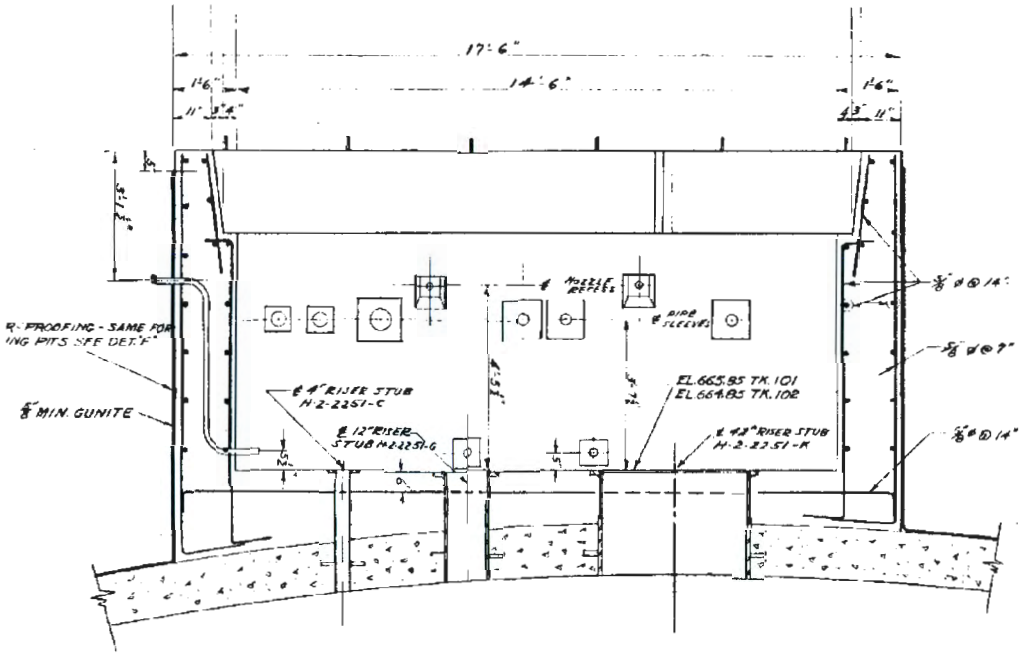

Figure B.12. Type III SST Pump Pit Details

(Ref: 241-TY, H-2-2295)

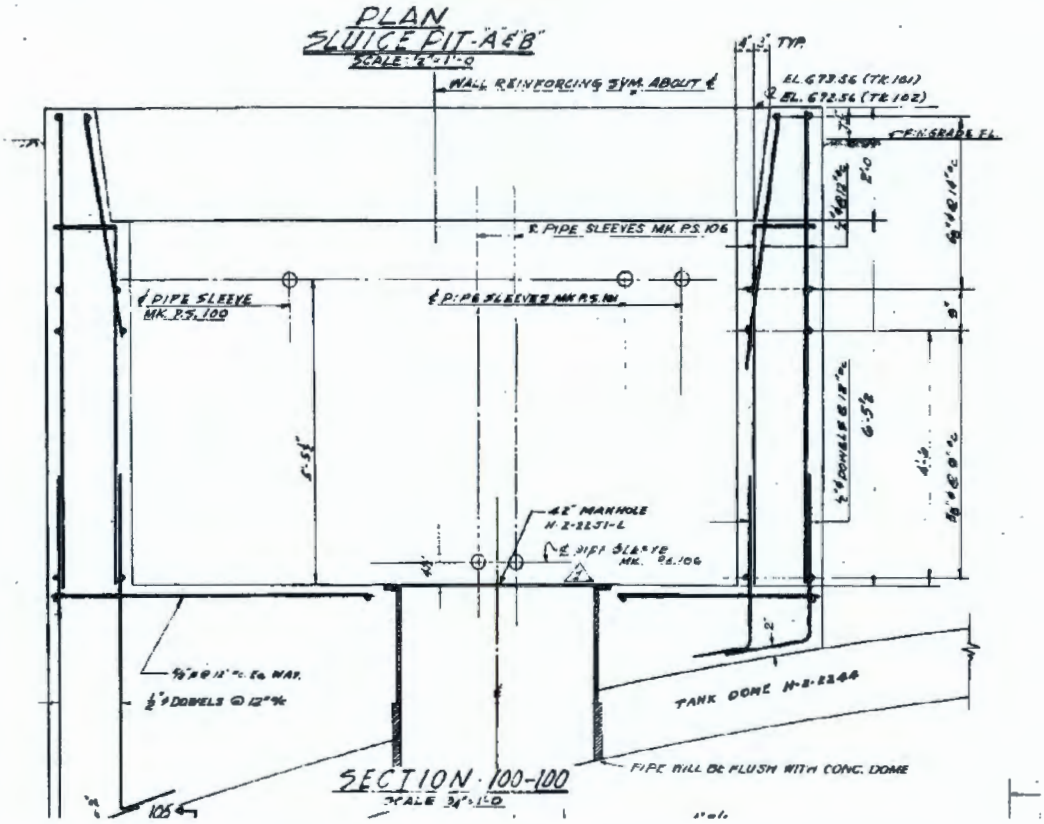

Figure B.13. Type III SST Sluice Pit Details

B.5.1 Type III SST Post-Construction Pump Pit and Riser Installation

Stage One: Excavate Area "A" & "B" to elevation shown in Figure B.14 and to the maximum slope as shown. Insert shield in all risers (remote operations). Weld lugs to existing risers.

(Ref: 241-BY, H-2-42150)

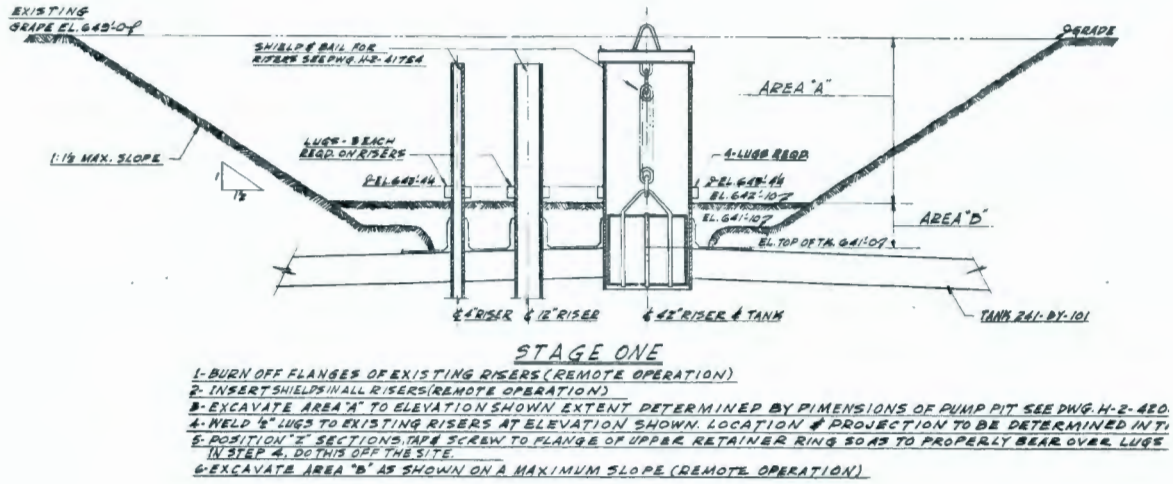

Figure B.14. Type III SST Pit Installation Stage One (Post-Construction)

Stage Two: Remove shields. Place the thread retainer ring centrally located about the exposed riser so that the 2-inch sections rest on the riser lugs. Insert shield in the risers. Place compacted backfill as shown in Figure B.15.

(Ref: 241-BY, H-2-42150)

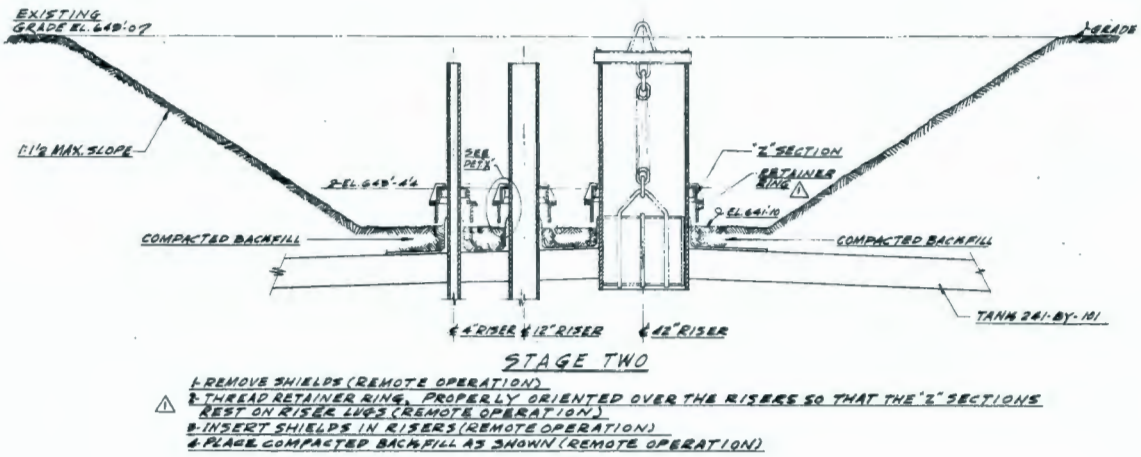

Figure B.15. Type III SST Pit Installation Stage Two (Post-Construction)

(Ref: 241-BY, H-2-42150)

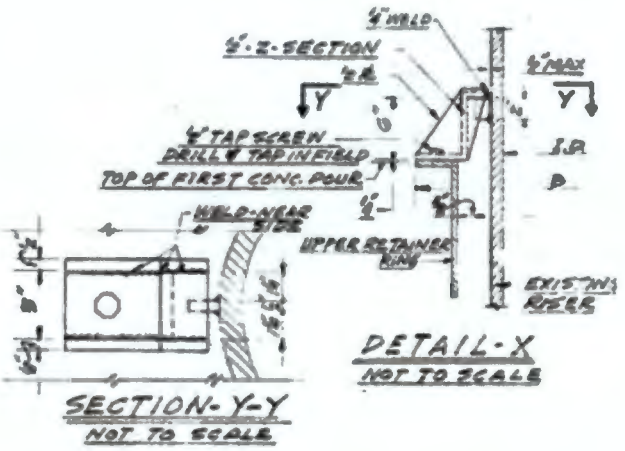

Figure B.16. Retainer Ring Details

Stage Three: Place prefabricated reinforced steel material and pour 12-inch concrete base slab to elevation shown in Figure B.17. Unbolt the 2-inch section from the retainer rings (Figure B.16). Weld gussets to risers and maintain contact of the bearing pads with concrete slab. There are four gussets on the 42-inch riser and three gussets on the 12-inch and 4-inch risers. Tie shield bails to gussets. Place steel bearing plates on concrete between the base of the gussets and the concrete pad. Grout over or chip away concrete as required. Fill space between retainer ring and riser stub with bituminous mastic to within one inch of top of pipe. Remove shields, bails, gussets and upper sections of risers.

(Ref: 241-BY, H-2-42150)

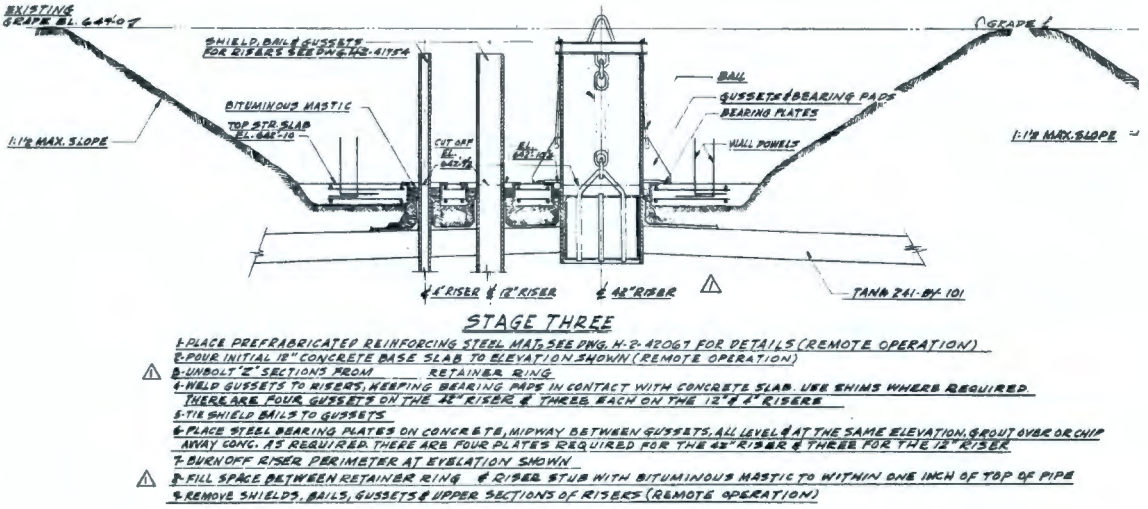

Figure B.17. Type III SST Pit Installation Stage Three (Post-Construction)

Stage Four: Remotely place adapter ring and dummy cover plug assembly into riser. Shim adapter ring to elevation shown in Figure B.18, orient ring as shown and tack weld to upper retainer ring. Install other adapter rings and remote disconnects as directed in the mechanical erection specifications.

(Ref: 241-BY, H-2-42150)

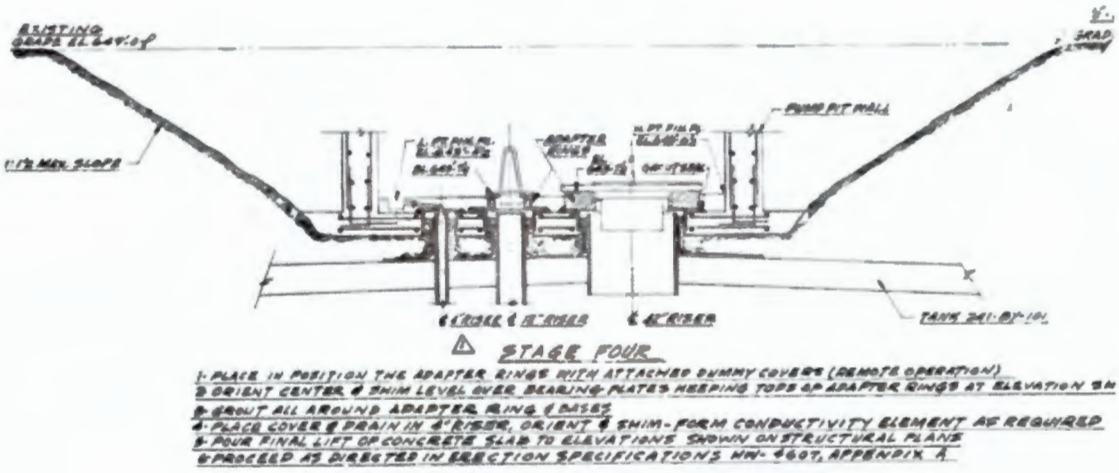

Figure B.18. Type III SST Pit Installation Stage Four (Post-Construction)

The steel riser shown in Figure B.18 has an inner diameter of 42-inch and a wall thickness of 3/8 inches (H-2-41267, Rev. 1), which is welded to an 8-inch-thick adaptor ring supported by the pit floor. The riser extends through the retaining ring assembly and the 42-inch manhole (through hole in dome is 39.125 inches). Thus, there is a radial gap of 1.1875 inches between the riser and the manhole penetration. Hence, the riser is not directly tied to the tank dome at the dome penetration. The large-diameter post-construction riser and any equipment installed in the riser are supported by the pit floor. The pit is supported by a layer of lean concrete and soil that is supported by the tank dome.

B.6 Exhaust Hatchways

Exhaust hatchways are also below-grade reinforced concrete boxes, but with a different configuration than the pits described above. The exhaust hatchways contain a pipe that is surrounded by concrete. The SST hatchways are doweled directly into the concrete dome of the tank. Type III SSTs have one hatchway design (see Figure B.19 though Figure B.21).

(Ref: 241-TY, H-2-2248)

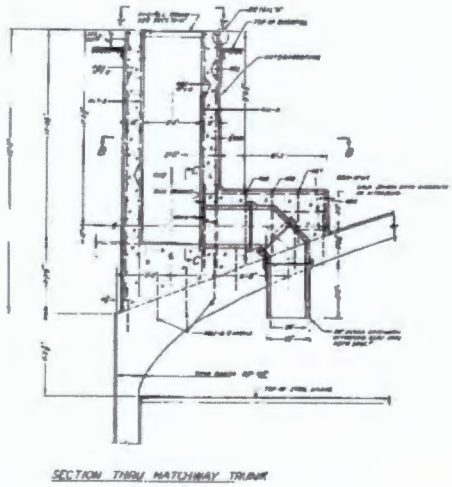

Figure B.19. Type III SST Typical Exhaust Hatchway

(Ref: 241-TY, H-2-2248)

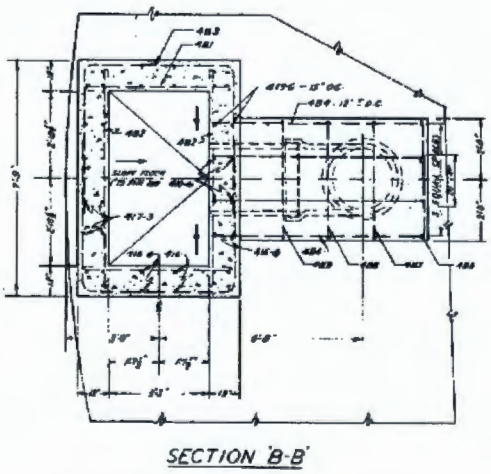

Figure B.20. Type III SST Typical Exhaust Hatchway Plan View

(Ref: 241-TY, H-2-2248)

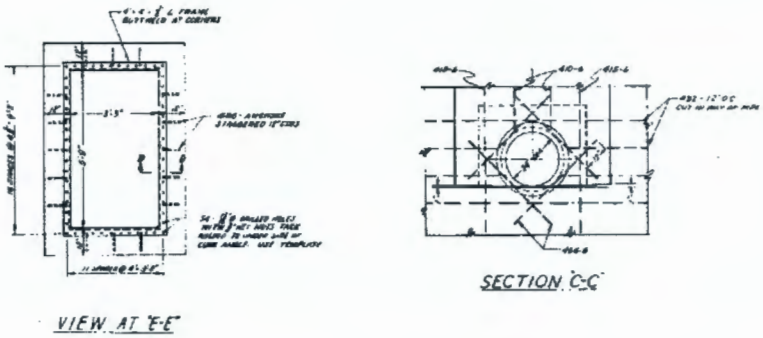

Figure B.21. Type III SST Typical Exhaust Hatchway Details

B.7 Tank-To-Tank Overflow Piping

A typical SST tank-to-tank overflow piping layout is shown in Figure B.22. Also shown are the tank process fill lines running from the diversion box to the tanks (see Section B.8). The overflow piping was designed to allow excess waste to flow to the next tank down line in a cascading fashion when the waste level is too high in the "uphill" tank. The overflow piping is a pipe-in pipe design. The inner 3-inch-diameter pipe is the waste overflow pipe contained within an outer 8-inch-diameter pipe that is in contact with the soil (see Figure B.23). The 3-inch-diameter waste pipe is centered and vertically supported within the 8-inch-diameter pipe by a long 7-inch-wide plate that is welded to the inner surface of the 8-inch-diameter pipe (see Figure B.25). The 8-inch-diameter pipe slips over the tank nozzle that penetrates the concrete walls of adjacent tanks but is not welded to the nozzles (see Figure B.23 and Figure B.24). The 8-inch diameter outer pipe is free to slide along each tank nozzle within a 3-inch space between the tank wall and the 8-inch-diameter pipe end ring. The tank overflow nozzle is a short pipe-in-pipe arrangement consisting of an outer 6-inch-diameter pipe that is doweled into the tank concrete wall and an inner 4-inch-diameter pipe that is welded to the tank inner steel liner. The 3-inch-diameter waste pipe is welded at one end to the 4-inch-diameter inner nozzle pipe. At the other end of the 3-inch-diameter waste pipe (see Figure B.23) the space between the 3-inch-diameter waste pipe and 4-inch-diameter inner nozzle pipe is packed tightly with asbestos wick. Thus, the 3-inch-diameter waste pipe is free to expand axially. The 8-inch-diameter outer pipe that is in contact with the soil is grouted to a 2 feet, 10 inches-thick by 3 feet, 2 inches-high by 23-feet 9 ½ inches long concrete reinforced pre-cast beam (see Figure B.30). A 2-inch-thick layer of felt impregnated with asphalt is provided between the ends of the pre-cast beam and the tank walls. The pre-cast beam reinforced concrete end supports are anchored to the tank wall (see Figure B.27). These design features mitigate pipe axial loads and moment transfers to the tank wall. In addition, seismically induced movement of the pipe and beam support is strain limited by the soil. Hence, the tank-to-tank overflow piping is not expected to significantly affect the demands on the SST wall, and thus the tank-to-tank piping will not be considered any further in the TOLA and seismic modeling of the Type III tanks.

B.8 Tank Process Fill Pipes

The process fill piping allows waste to be transferred into the tanks. The process fill lines running from the diversion box to the SST Farm are shown in the piping layout in Figure B.22. All SST process fill lines have been isolated as part of the SST Interim Stabilization Program. The process piping is a direct-buried pipe design. The process fill pipe is a 3-inch-diameter stainless steel pipe. Three to four process fill pipelines are routed from the diversion box to each tank row and connect to the below-grade process fill nozzles in the SST wall. The nozzle design is shown in Figure B.28. The nozzle consist of an inner 4-inch-diameter pipe sleeve that is welded to the inner steel tank liner and passes through the outer 6-inch-diameter pipe sleeve that is embedded in the tank concrete wall. The 4-inch-diameter pipe sleeve is centered in the 6-inch-diameter pipe sleeve by an 8-inch-diameter collar with an end washer plate welded to the one end and the inner hole providing a close fit alignment to the 6-inch-diameter pipe sleeve as shown in Figure B.28. The 3-inch-diameter process fill pipe passes through the 4-inch diameter nozzle sleeve with space between the 3- and 4-inch pipes packed tightly with asbestos wick before the 5-inch inner diameter collar/cap is welded to the 3-inch-diameter process fill pipe. The 5-inch inner diameter collar/cap is installed so that the process pipe is free to move axially up to 2 inches before contacting the end of the 4-inch-diameter nozzle sleeve.

(Ref: 241-S, H-2-1776)

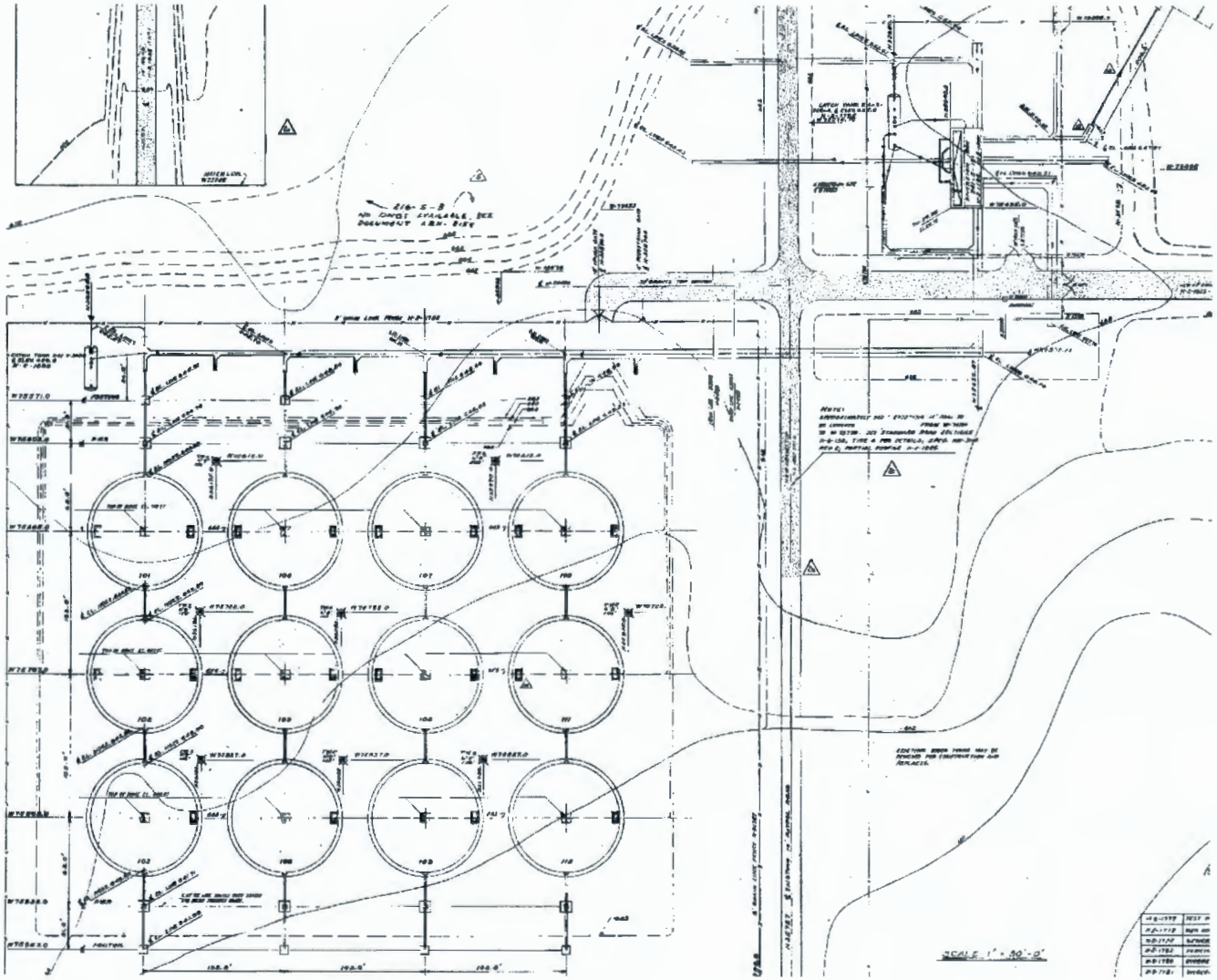

Figure B.22. Type III SST Process Fill and Tank-to-Tank Overflow Piping Layout

(Ref: 241-TY, H-2-2277)

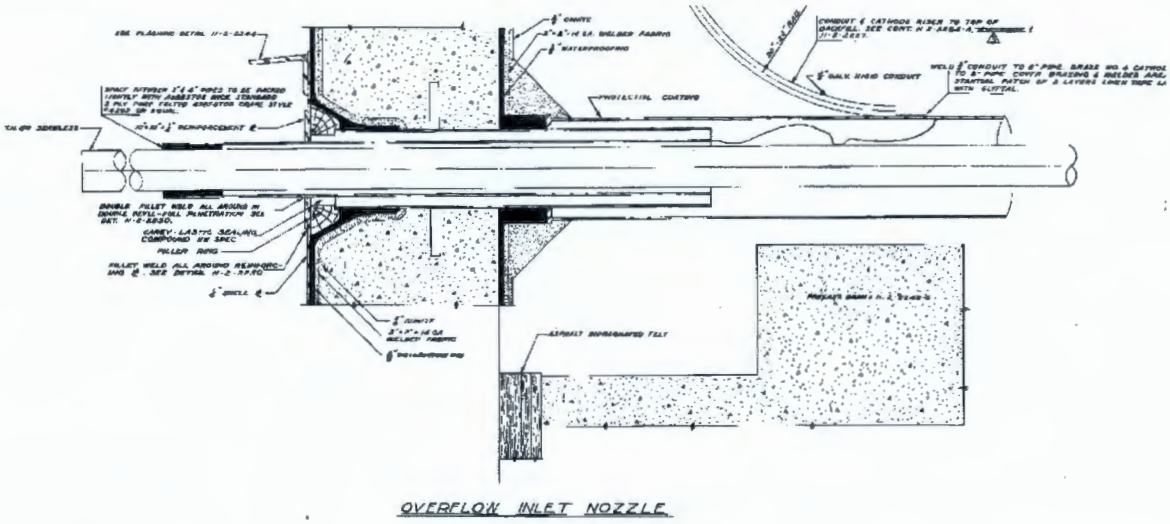

Figure B.23. Type III SST Tank-to-Tank Overflow Inlet Piping and Nozzle Arrangement

(Ref: 241-TY, H-2-2277)

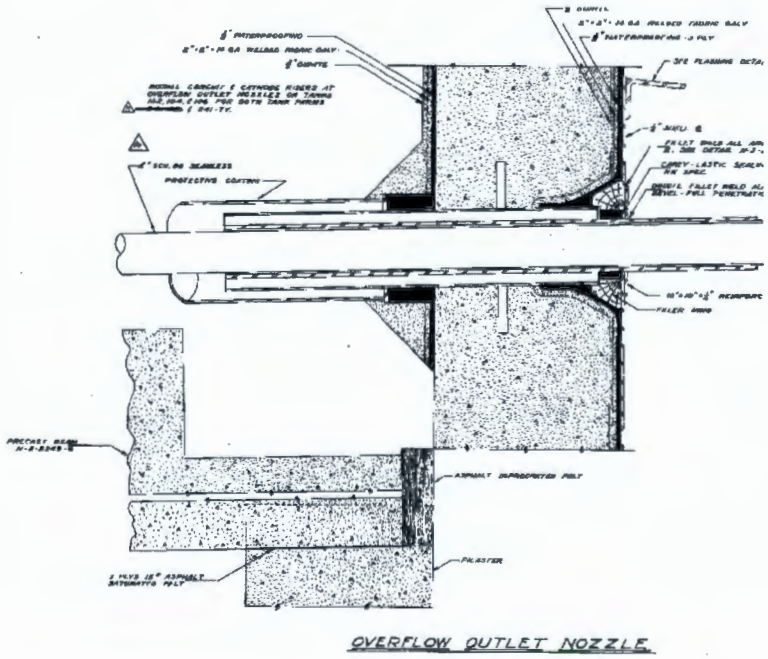

Figure B.24. Type III SST Tank-to-Tank Overflow Outlet Piping and Nozzle Arrangement

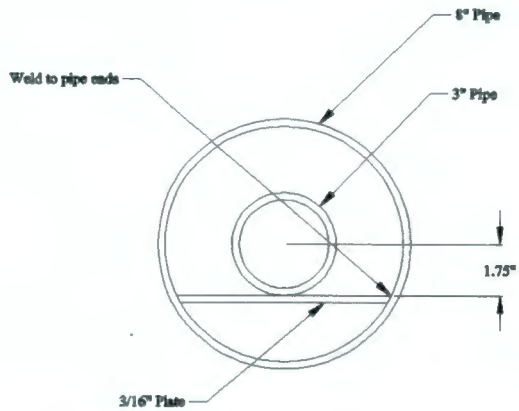

Figure B.25. Type III SST Tank-to-Tank Overflow Piping Cross Section

The 3-inch-diameter process fill pipelines are supported by a reinforced concrete beam system extending from the tank wall to the undisturbed outer soil slope of the excavation. See Figure B.30 for details of the reinforced concrete beam system and Figure B.29 for an example of beam layout in the BY Farm. Note that a 2-inch-thick layer of felt impregnated with asphalt is provided between the ends of the reinforced concrete beam and the tank walls. The beam reinforced concrete end supports at the tank walls are anchored to the tank wall (see detail in Figure B.27 and Figure B.30). In addition, footed column supports are provided at 15-foot spaced increments along the beam. The concrete beam becomes wider to align with the nozzles at the tank wall (see Figure B.31).

The design features mitigate pipe axial loads and moment transfers to the tank wall. In addition, seismically induced movement of the pipe and beam support is strain limited by the soil. Hence, the tank process fill piping is not expected to significantly affect the demands on the SST wall, and thus the tank process fill piping will not be considered any further in the TOLA and seismic modeling of the Type III tanks.

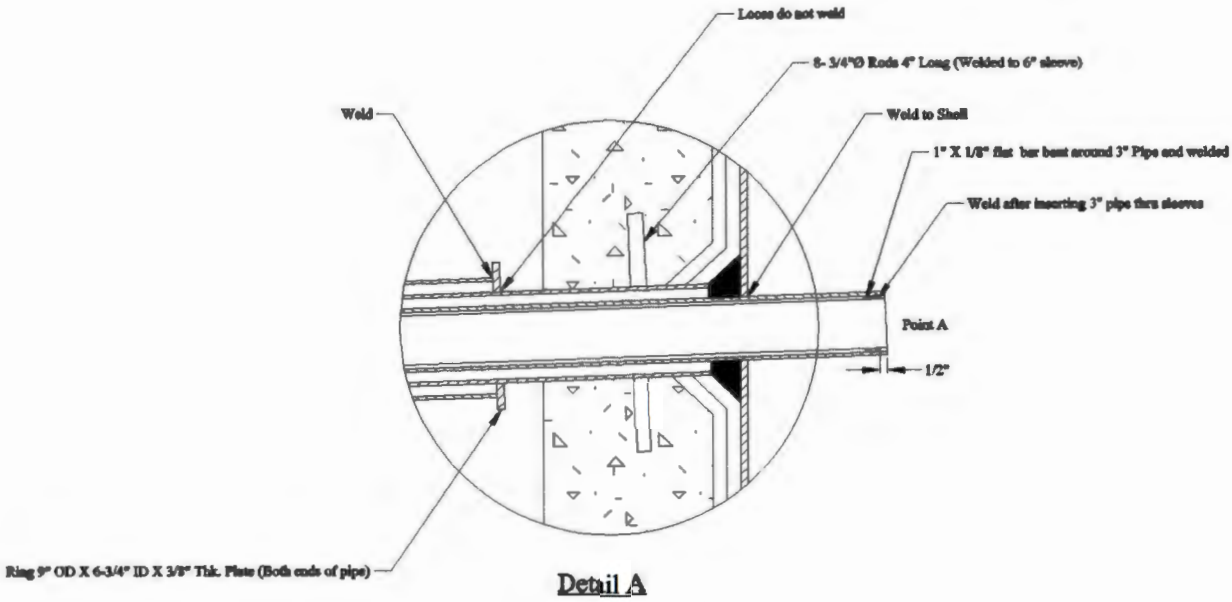

Figure B.26. Type III SST Tank-to-Tank Overflow Piping Detail A

(Ref: 241-S, H-2-1788)

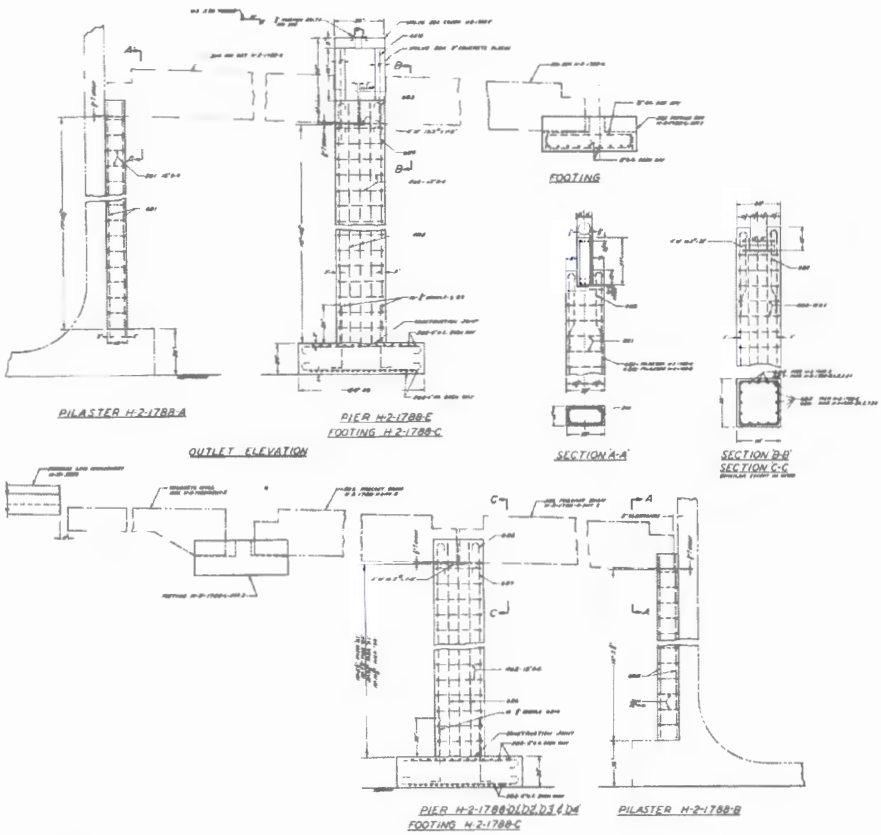

Figure B.27. Type III SST Tank-to-Tank Overflow Piping Beam Support

(Ref: 241-TY, H-2-2277)

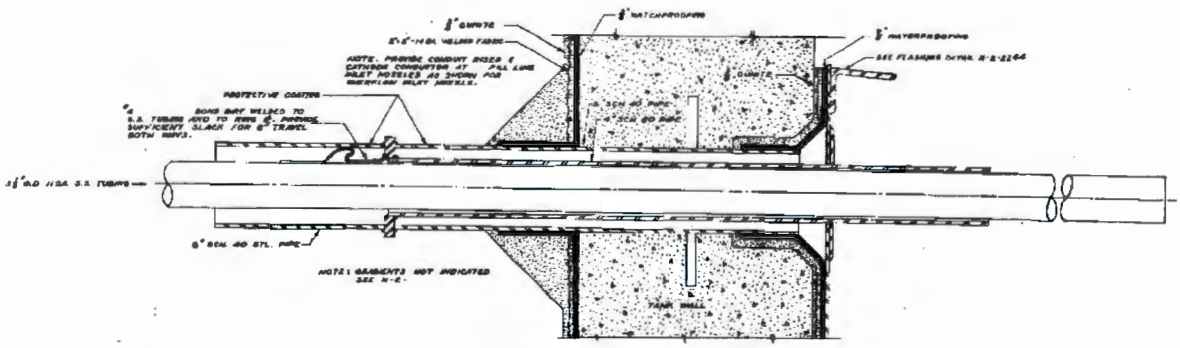

Figure B.28. Type III SST Process Fill Nozzle with 3-inch-Diameter Fill Pipe

(Ref: 241-BY, H-2-1308)

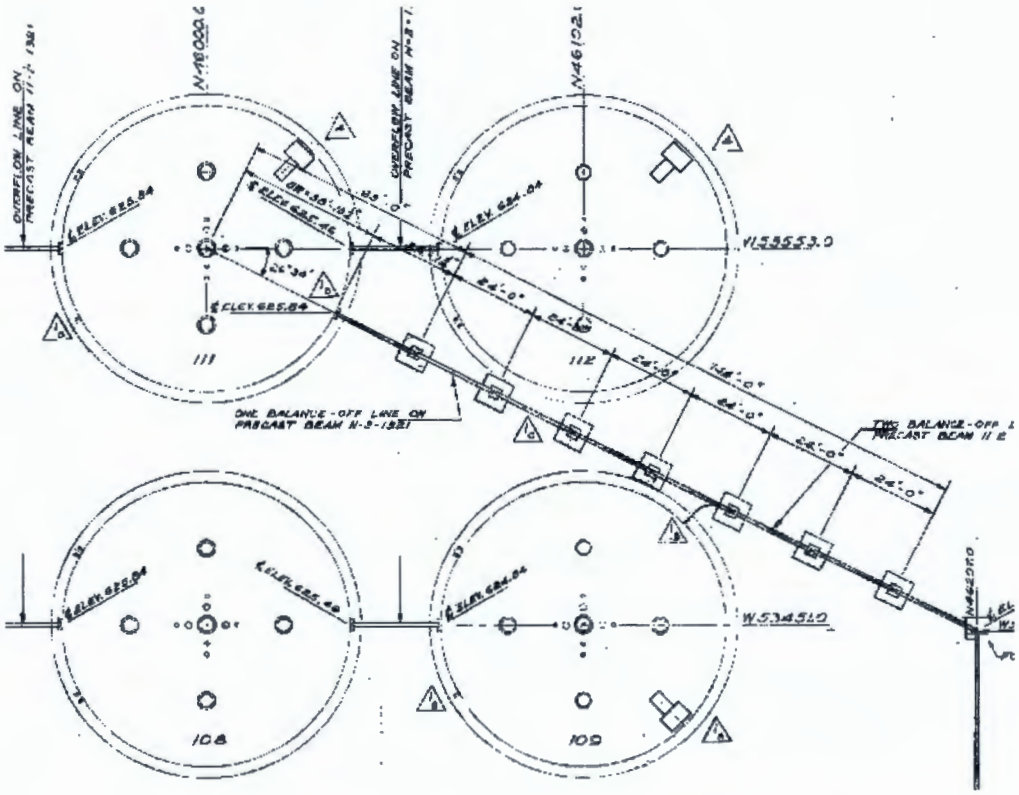

Figure B.29. Example Type III SST Process Fill Pipe Support Beam Layout

(Ref: 241-BY, H-2-1316)

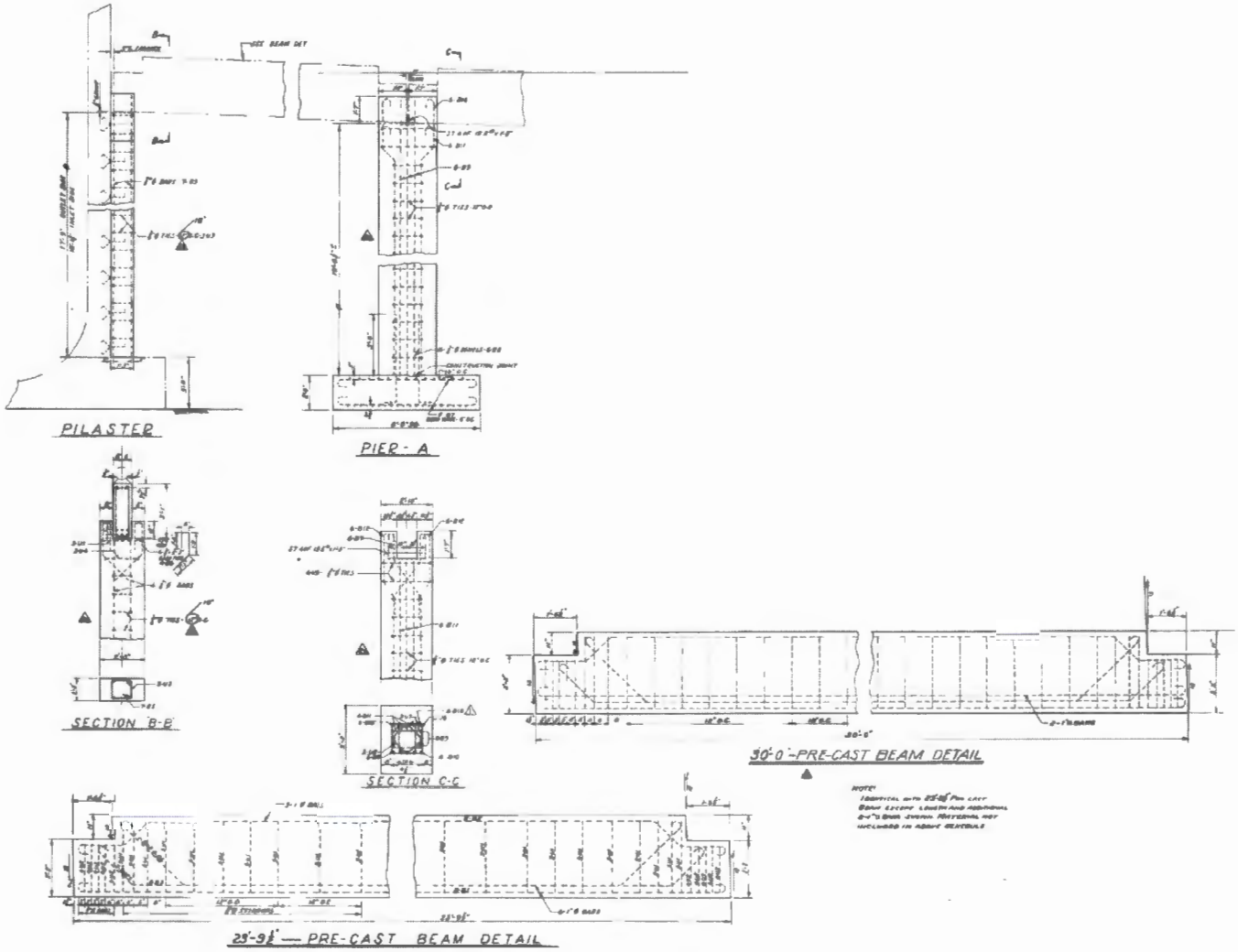

Figure B.30. Type III SST Process Fill Pipe Support Beam Detail for Tank 241-BY-110

(Ref: 241-S, H-2-1788, Sheet 2)

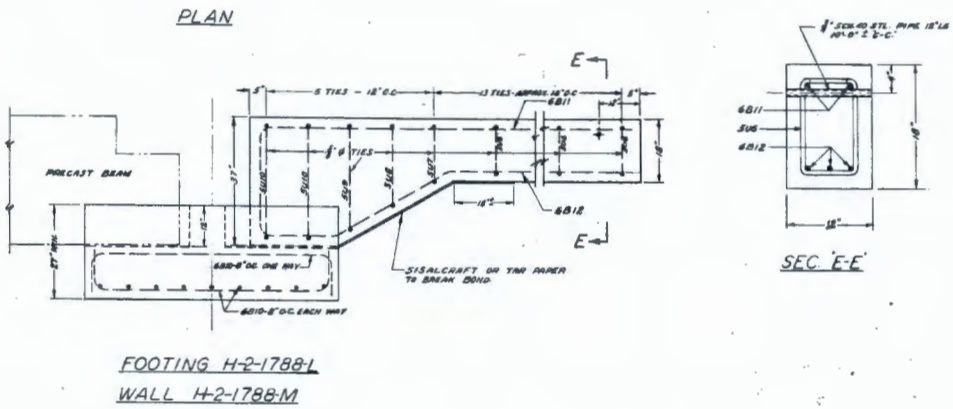

Figure B.31. Type III SST Process Fill Pipe Support Details

B.9 Ancillary Equipment

Ancillary equipment includes installed pumps, monitoring equipment, sluicing equipment or other miscellaneous equipment. Typically the more massive equipment such as pumps is supported on the pit floor and extend through a riser into the waste. Although the interaction of the equipment with the waste during a seismic event can lead to potential impacting between the equipment and the riser, the mounting system and equipment to riser clearance are typically designed to mitigate such interactions.

B.10 References

Hanford Drawing H-2-807, Rev. 11

Hanford Drawing H-2-817, Rev. 5

Hanford Drawing H-2-1308, Rev. 7.

Hanford Drawing H-2-1316, Rev. 3.

Hanford Drawing H-2-1774, Rev. 6.

Hanford Drawing H-2-1776, Rev. 0.

Hanford Drawing H-2-1788, Rev. 1.

Hanford Drawing H-2-1814, Rev. 2

Hanford Drawing H-2-2248, Rev. 2

Hanford Drawing H-2-2277, Rev. 3.

Hanford Drawing H-2-2293, Rev. 2

Hanford Drawing H-2-2294, Rev. 1

Hanford Drawing H-2-2295, Rev. 1

Hanford Drawing H-2-42150, Rev. 1.

Hundal TS. 2004a. *241-BY Tank Farm Historic Dome Load Record Data.* RPP-20448, Rev. 0, COGEMA Engineering Corporation, Richland, Washington.

Hundal TS. 2004b. *241-S Tank Farm Historic Dome Load Record Data.* RPP-20450, Rev. 0, COGEMA Engineering Corporation, Richland, Washington.

Hundal TS. 2004c. *241-TX Tank Farm Historic Dome Load Record Data.* RPP-20453, Rev. 0, COGEMA Engineering Corporation, Richland, Washington.

Hundal TS. 2004d. *241-TY Tank Farm Historic Dome Load Record Data.* RPP-20454, Rev. 0, COGEMA Engineering Corporation, Richland, Washington.

McCluskey PR. 2005. *SST Analysis for Installation of Additional Risers.* RPP-21840, Rev. 0, CH2M HILL Hanford Group Inc., Richland, Washington.

Rinker MW, KI Johnson, SK Bapanapalli, NK Karri, JE Deibler, SP Pilli, CE Guzman-Leong, SE Sanborn, FG Abatt, JA Dewberry, BM Larsen, KL Stoops, and LJ Julyk. 2011a. *Single-Shell Tank Integrity Project Analysis of Record: Hanford Type II Single-Shell Tank Thermal and Operating Loads and Seismic Analysis.* RPP-RPT-49989, Rev. 0, Pacific Northwest National Laboratory, Richland, Washington.

Rinker MW, NK Karri, CE Guzman-Leong, SP Pilli, JE Deibler, FG Abatt, and KI Johnson. 2011b. *An Evaluation of Single-Shell Tank 241-C-107 for the Addition of a large Penetration in the Tank Dome.* RPT-CALC-43416, Rev. 1, Pacific Northwest National Laboratory, Richland, Washington.

Watwood VB. 1977. *Analysis and Evaluation of the 241 U Concrete Waste Tank with Added Access Holes in Roof.* ARH-C-19, Atlantic Richfield Hanford Company, Richland, Washington.

This page intentionally left blank.

Appendix C

Backfill Soil Evaluation

This page intentionally left blank.

Appendix C

Backfill Soil Evaluation

C.1 Backfill Soil Evaluation

This section presents the resolution to the May 2011 reviewer's comment, which is shown below.

> *The reviewers would have preferred that the backfill around the tank in the seismic model was extended through the entire radial distance of the model, as was done for the model used in the TOLA analysis. However, considering that the backfill and native soil properties are quite similar, the results would not be expected to be significantly different.*

This evaluation shows the sensitivity of the Type III seismic model when extending the backfill to the boundary, as shown in Figure C.1, by comparison of tank demands from the Type III seismic baseline model to the tank demands of the Type III seismic extended backfill model. The backfill soil properties are not appreciably different from the native soil properties. D/C ratios will be calculated to show acceptable tank performance.

Spectral matching at the model boundary was considered as an additional acceptance criterion. The time histories and spectral targets have been calibrated only to the native soil. Comparing the extended backfill spectra to the target spectra is not appropriate without re-calibrating the time histories and generating new spectral targets. If the tank demands are not sensitive to extending the backfill soil to the boundary, then this additional criterion may not be meaningful in determining acceptable seismic performance.

Figure C.2 through Figure C.19 in the following sections shows the tank seismic demands for the baseline case compared to the extended backfill case for each of the three SSI Type III Seismic Models, Upper Bound, Best-Estimate and Lower Bound Soil. All three models include the empty tank case only.

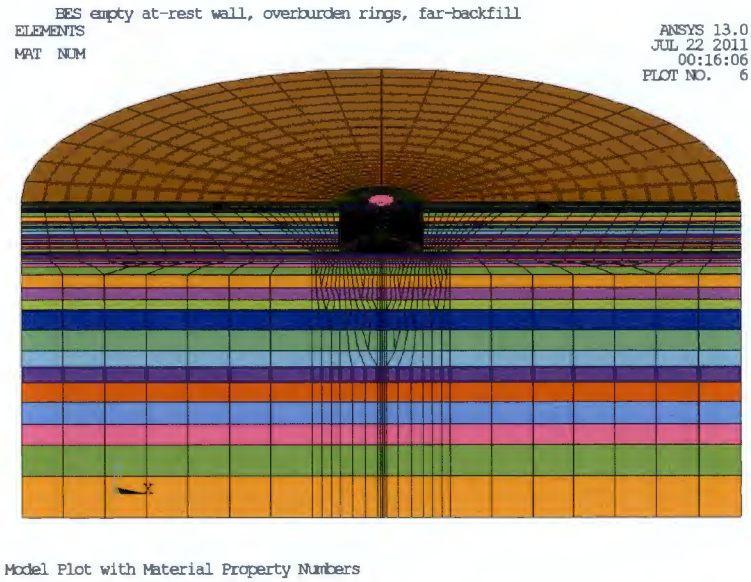

Figure C.1. Type III BES SST Seismic Model with Extended Backfill to Model Boundary

C.2 SST Type III Upper Bound Seismic Model Tank Demands

This section shows that tank demands for the Type III Seismic Model with the Upper Bound Soil (UBS). Each plot contains a comparison of the tank seismic demands from the Type III baseline model and the tank seismic demands from the Type III extended backfill soil model. The results and conclusions are summarized in Section C.5.

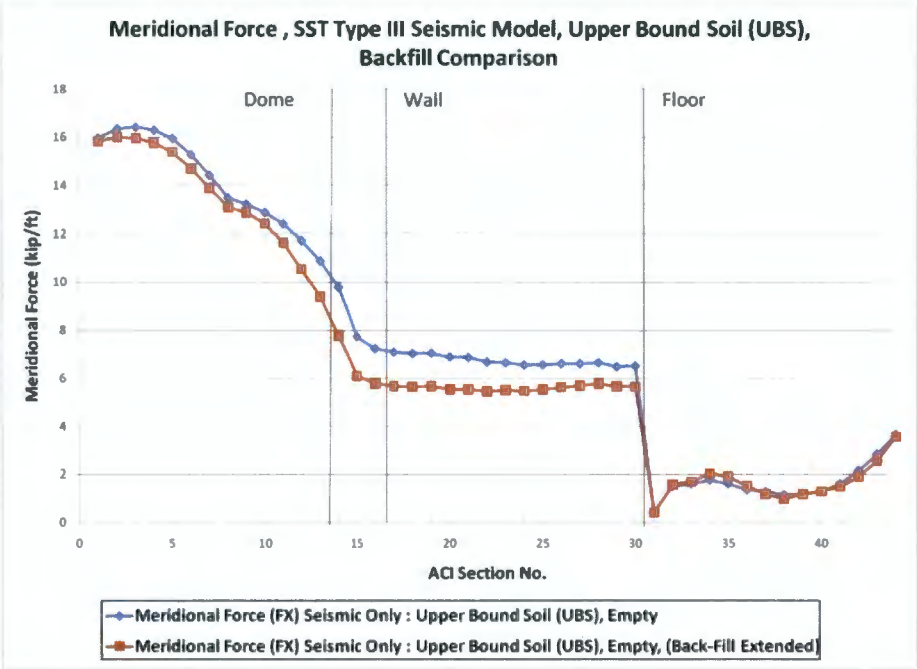

Figure C.2. Meridional Force, SST Type III Seismic Model, Upper Bound Soil (UBS), Comparison Between the Type III Seismic Baseline Model and the Type III Seismic Extended Backfill Model.

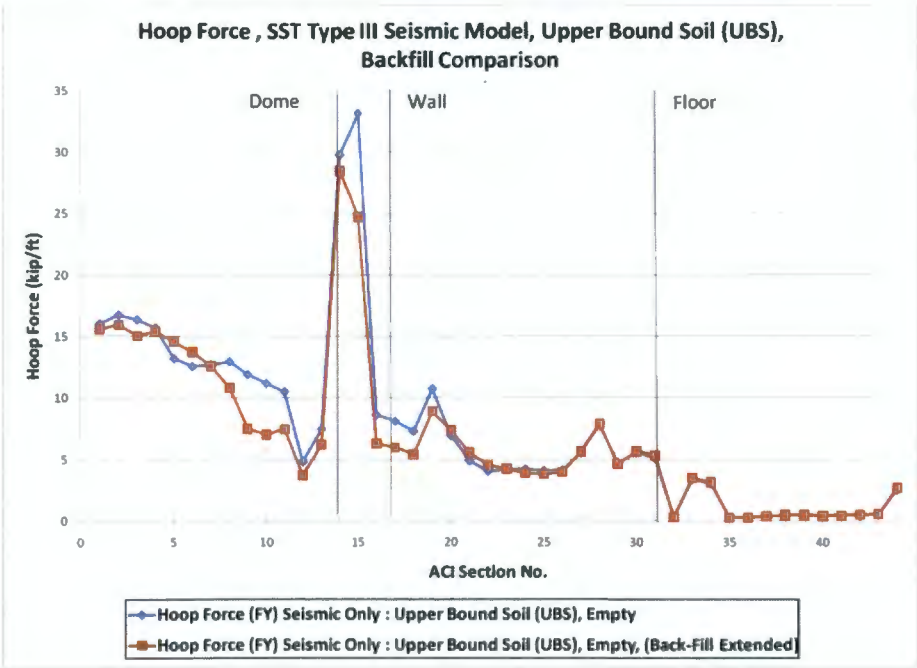

Figure C.3. Hoop Force, SST Type III Seismic Model, Upper Bound Soil (UBS), Comparison Between the Type III Seismic Baseline Model and the Type III Seismic Extended Backfill Model

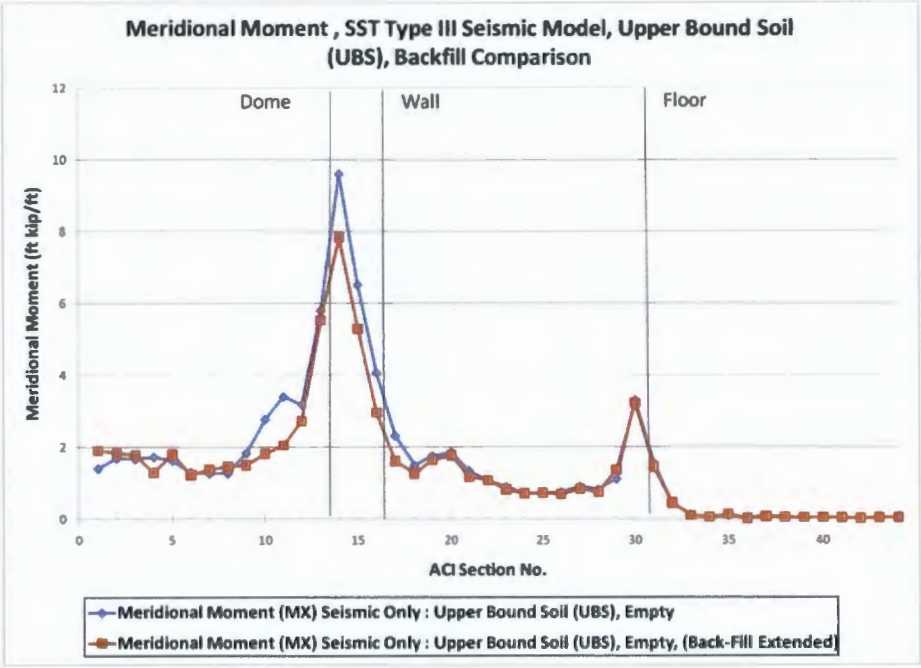

Figure C.4. Meridional Moment, SST Type III Seismic Model, Upper Bound Soil (UBS), Comparison Between the Type III Seismic Baseline Model and the Type III Seismic Extended Backfill Model

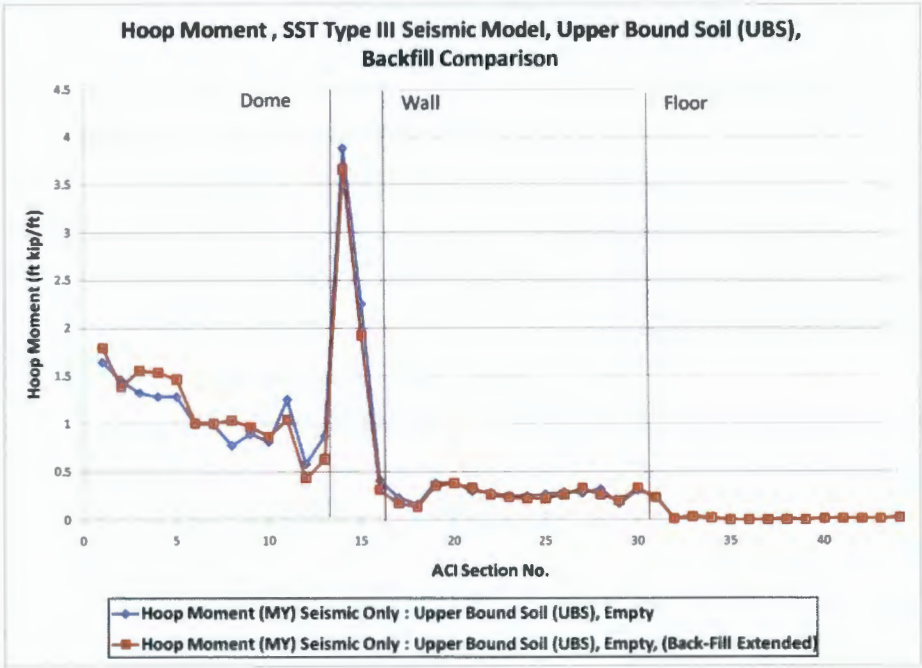

Figure C.5. Hoop Moment, SST Type III Seismic Model, Upper Bound Soil (UBS), Comparison Between the Type III Seismic Baseline Model and the Type III Seismic Extended Backfill Model

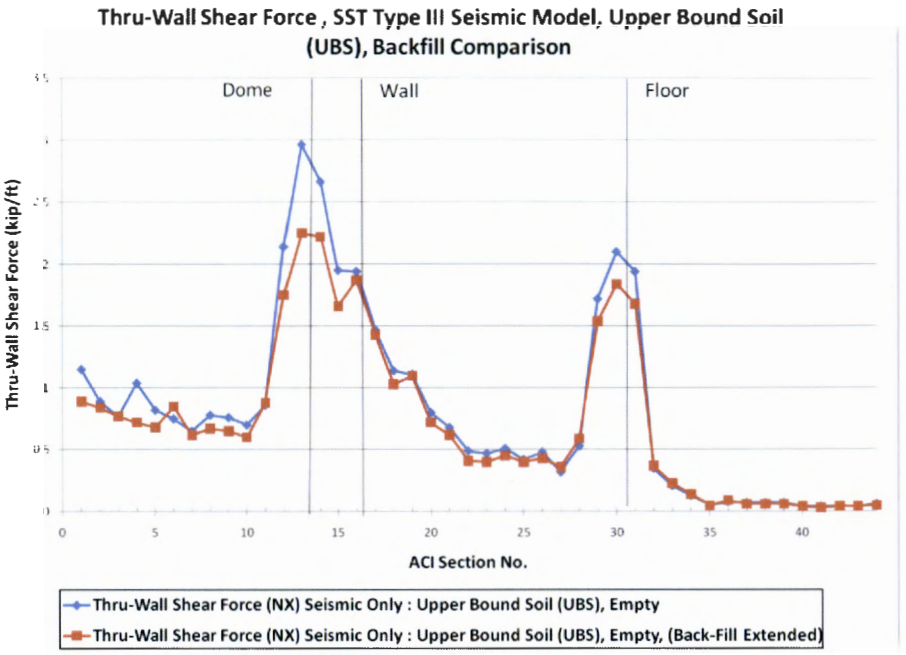

Figure C.6. Through-Wall Shear, SST Type III Seismic Model, Upper Bound Soil (UBS), Comparison Between the Type III Seismic Baseline Model and the Type III Seismic Extended Backfill Model

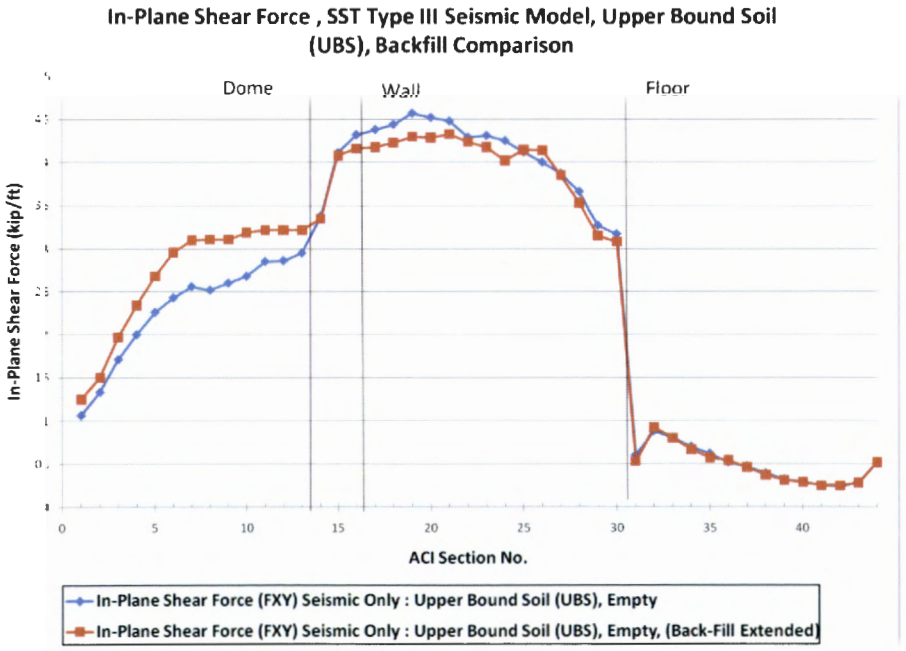

Figure C.7 In-Plane Shear, SST Type III Seismic Model, Upper Bound Soil (UBS), Comparison Between the Type III Seismic Baseline Model and the Type III Seismic Extended Backfill Model

C.3 SST Type III Best Estimate Seismic Model Tank Demands

This section shows that tank demands for the Type III Seismic Model with the Best-Estimate Soil (BES). Each plot contains a comparison of the tank seismic demands from the Type III baseline model and the tank seismic demands from the Type III extended backfill soil model. The results and conclusions are summarized in Section C.5.

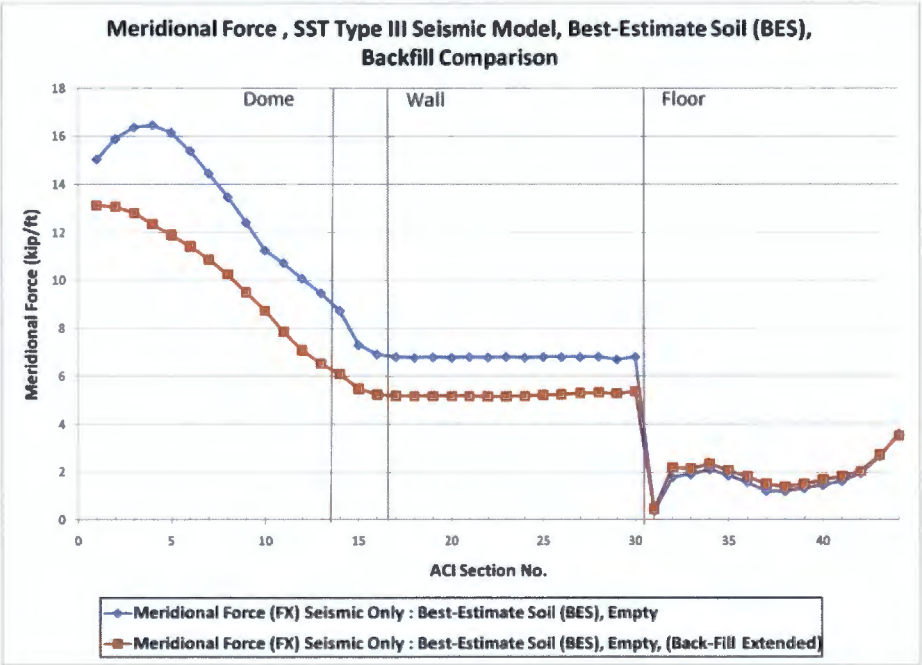

Figure C.8. Meridional force, SST Type III Seismic Model, Best-Estimate Soil (BES), Comparison Between the Type III Seismic Baseline Model and the Type III Seismic Extended Backfill Model

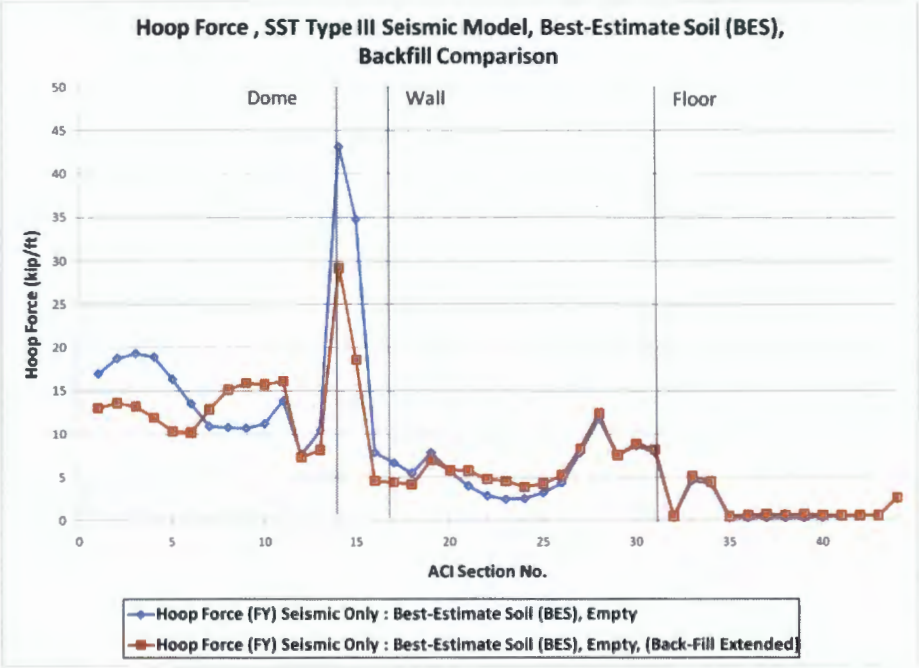

Figure C.9. Hoop force, SST Type III Seismic Model, Best-Estimate Soil (BES), Comparison Between the Type III Seismic Baseline Model and the Type III Seismic Extended Backfill Model

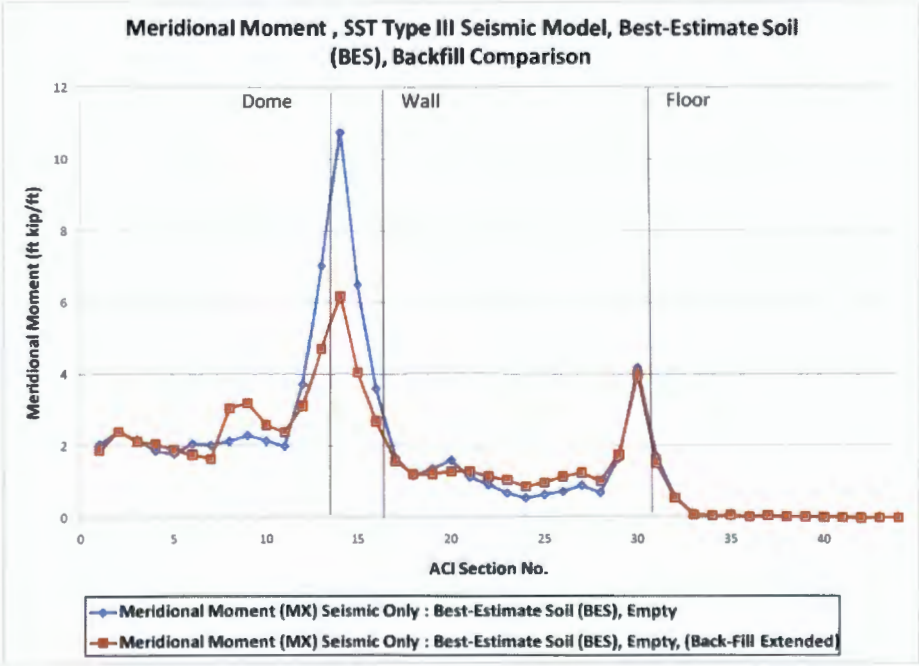

Figure C.10. Meridional Moment, SST Type III Seismic Model, Best-Estimate Soil (BES), Comparison Between the Type III Seismic Baseline Model and the Type III Seismic Extended Backfill Model

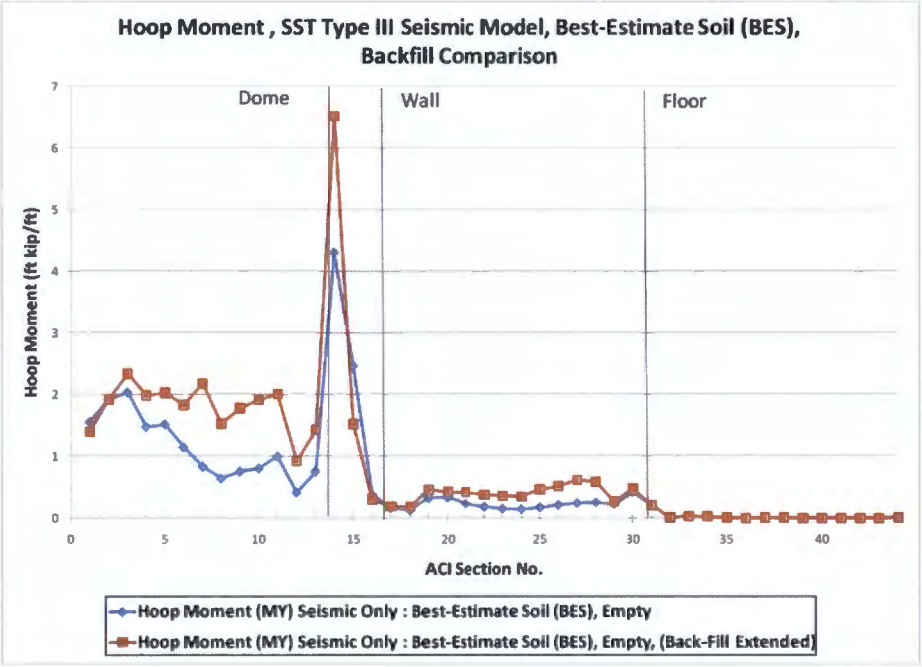

Figure C.11. Hoop Moment, SST Type III Seismic Model, Best-Estimate Soil (BES), Comparison Between the Type III Seismic Baseline Model and the Type III Seismic Extended Backfill Model

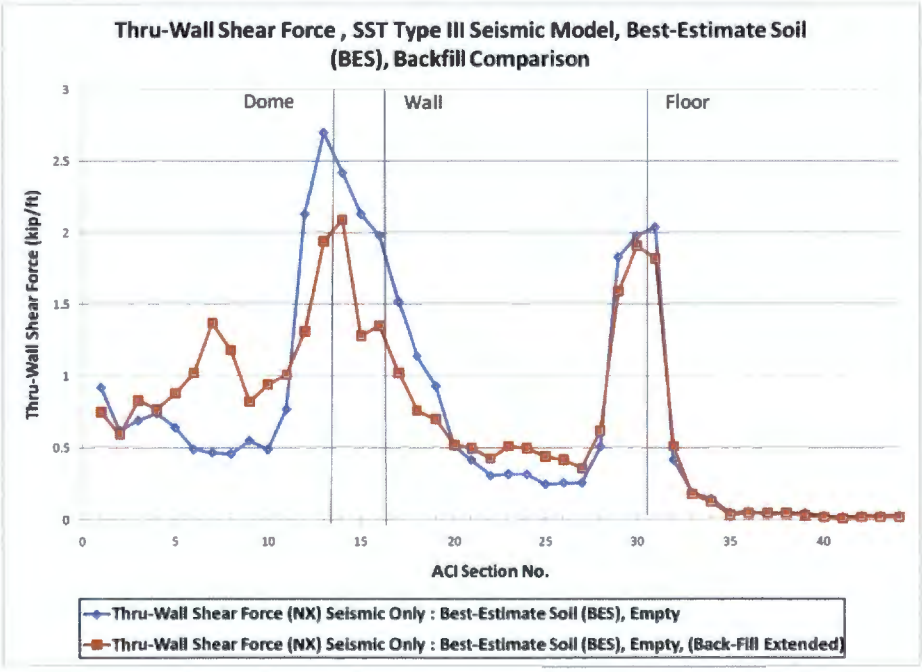

Figure C.12. Through-Wall Shear Force, SST Type III Seismic Model, Best-Estimate Soil (BES), Comparison Between the Type III Seismic Baseline Model and the Type III Seismic Extended Backfill Model

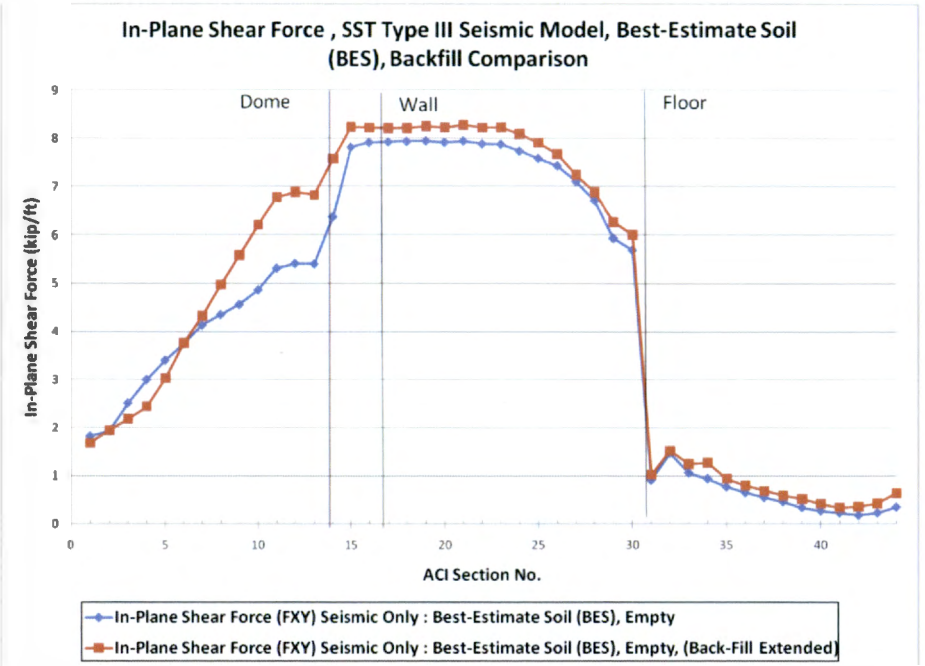

Figure C.13. In-Plane Shear Force, SST Type III Seismic Model, Best-Estimate Soil (BES), Comparison Between the Type III Seismic Baseline Model and the Type III Seismic Extended Backfill Model

C.4 SST Type III Lower Bound Seismic Model Tank Demands

This section shows that tank demands for the Type III Seismic Model with the Lower Bound Soil (LBS). Each plot contains a comparison of the tank seismic demands from the Type III baseline model and the tank seismic demands from the Type III extended backfill soil model. The results and conclusions are summarized in Section C.5.

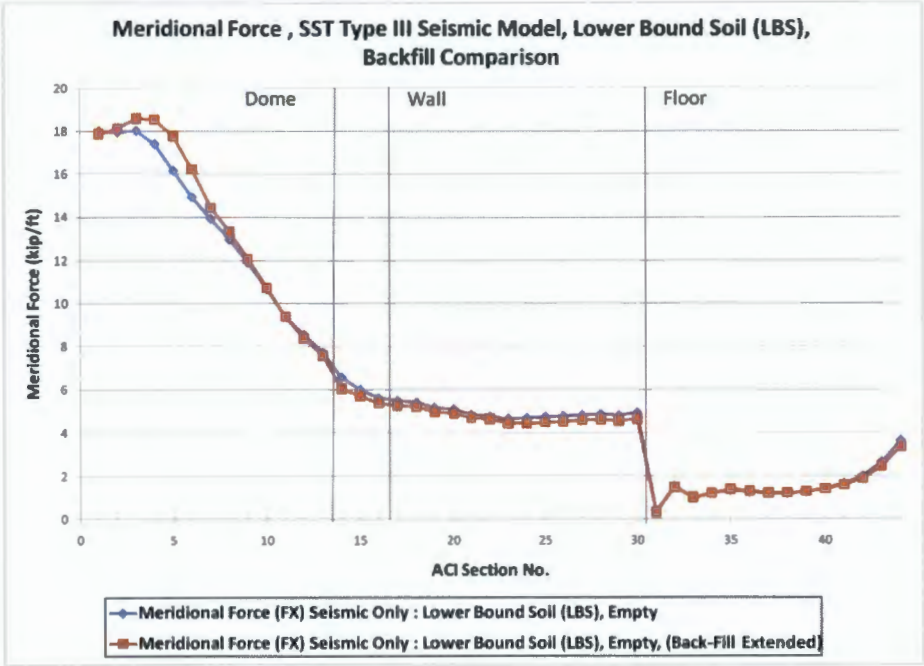

Figure C.14. Meridional Force, SST Type III Seismic Model, Lower Bound Soil (LBS), Comparison Between the Type III Seismic Baseline Model and the Type III Seismic Extended Backfill Model

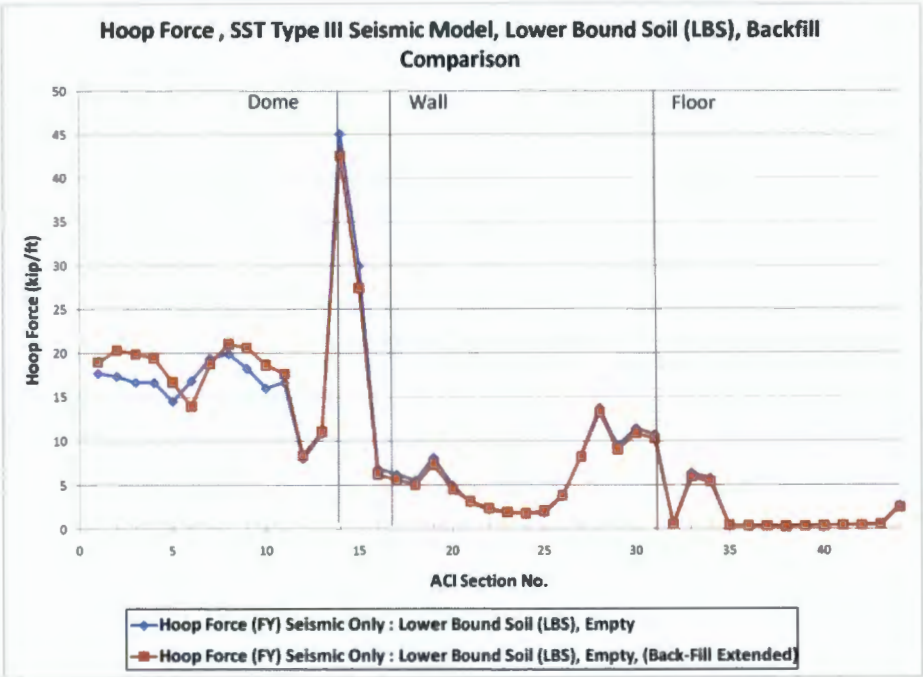

Figure C.15. Hoop Force, SST Type III Seismic Model, Lower Bound Soil (LBS), Comparison Between the Type III Seismic Baseline Model and the Type III Seismic Extended Backfill Model

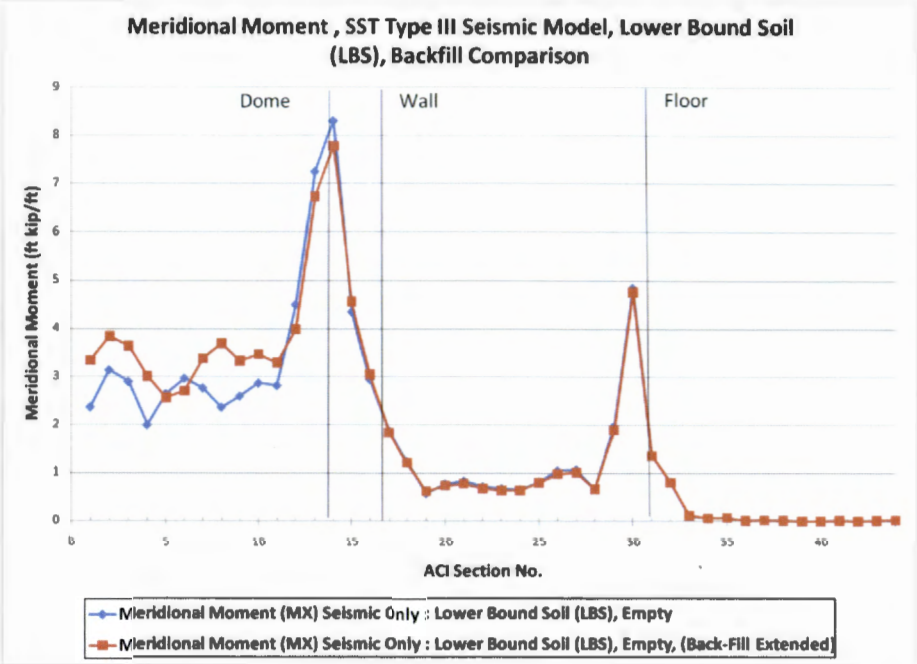

Figure C.16. Meridional Moment, SST Type III Seismic Model, Lower Bound Soil (LBS), Comparison Between the Type III Seismic Baseline Model and the Type III Seismic Extended Backfill Model

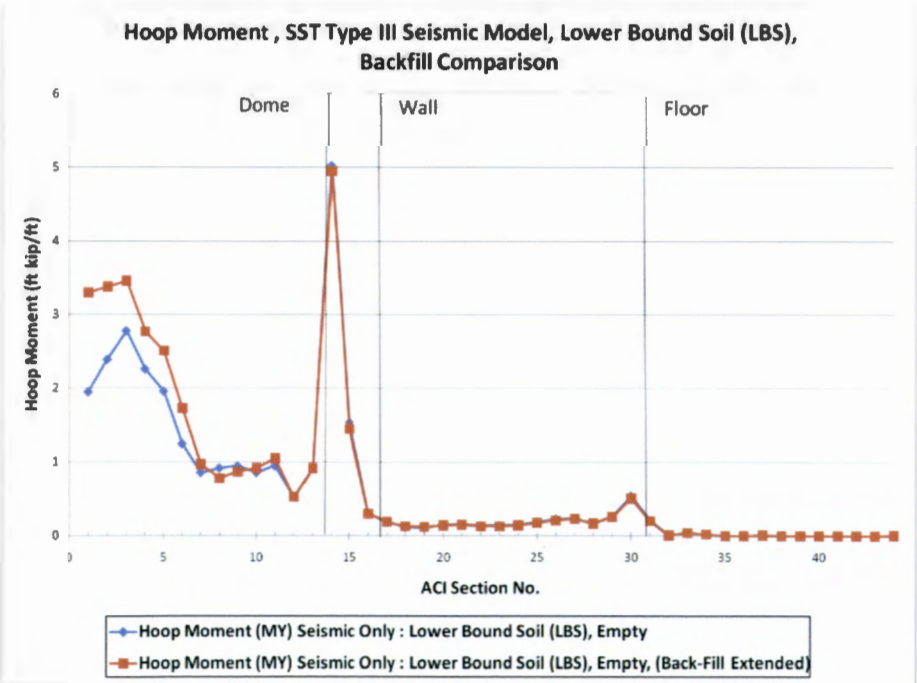

Figure C.17. Hoop Moment, SST Type III Seismic Model, Lower Bound Soil (LBS), Comparison Between the Type III Seismic Baseline Model and the Type III Seismic Extended Backfill Model

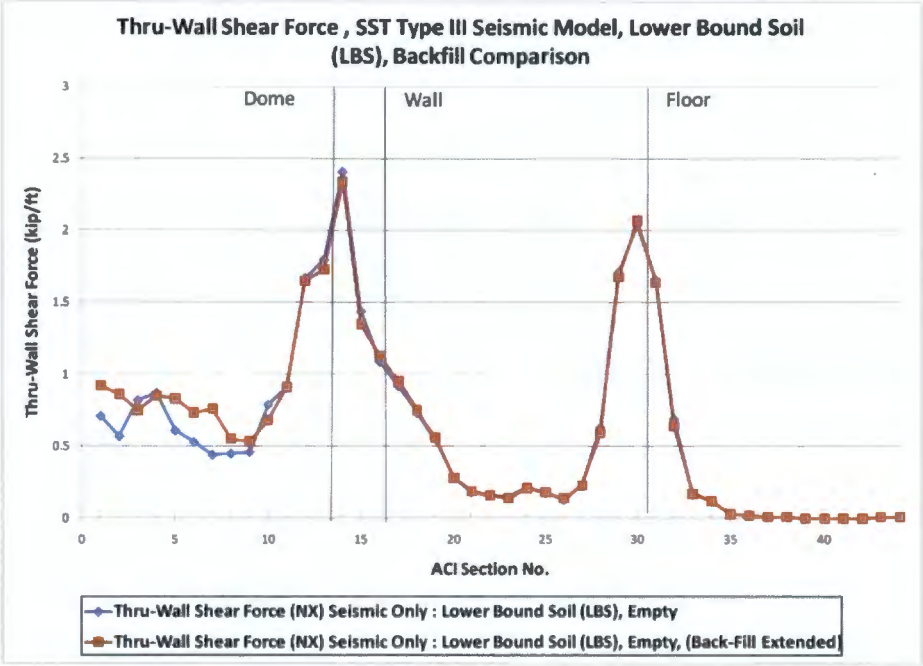

Figure C.18. Through-Wall Shear, SST Type III Seismic Model, Lower Bound Soil (LBS), Comparison Between the Type III Seismic Baseline Model and the Type III Seismic Extended Backfill Model

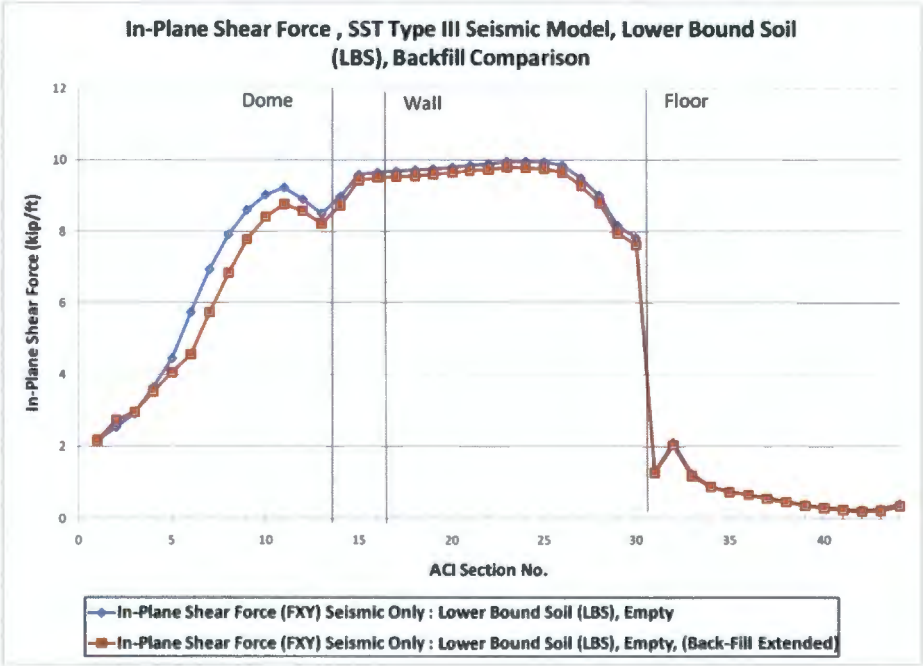

Figure C.19. In-Plane Shear, SST Type III Seismic Model, Lower Bound Soil (LBS), Comparison Between the Type III Seismic Baseline Model and the Type III Seismic Extended Backfill Model

C.5 SST Type III D/C Ratio Results and Conclusions

This section presents the D/C ratios for the tank demands for the extended backfill case. Acceptable results are those ratios that are less than 1.0 of the ACI-349 calculated capacity. The following figures show the D/C results for the Best Estimate, the Lower Bound, and Upper Bound Soil profiles. In the following figures, the demand/capacity ratios exceed 1.0 in the slab region (ACI Sections 32 through 44). This does not indicate unacceptable results because the slab is not critical to tank integrity.

Figure C.20 shows the ACI-349 demand/capacity ratios for the BES empty tank seismic demands combined with the TOLA demands for meridional, hoop, and shear. The demand/capacity ratios curves are less than 1.0 of the calculated capacity in the ACI Sections1 through 31, except in ACI Sections 32 through 44 in the slab. The demand/capacity ratio curves for both nominal backfill and extended backfill cases are very similar. The nominal backfill hoop curve is slightly greater than the extended backfill hoop curves which peaks near 0.75 as the dome curve transitions to the haunch region. Both the nominal and extended backfill demand/capacity ratio curves are very similar for meridional and shear where the trends of the curve peak in the regions where the dome transitions to the haunch and at the wall transition to the tank footing, but all of the peaks are less than hoop curve peaks. The tank demands results for both nominal and extended backfill are acceptable because none of the curves exceed 1.0, excluding the slab region.

Figure C.21 shows the ACI-349 demand/capacity ratios for the LBS empty tank seismic demands combined with the TOLA demands for meridional, hoop, and shear. The demand/capacity ratios curves are less than 1.0 of the calculated capacity in the ACI Sections 1 through 31, except in ACI Sections 32 through 44 in the slab. The demand/capacity ratios for the nominal backfill and extended backfill are very similar for meridional, hoop and shear. Each set of curves trend together and the set of curves for hoop peaks at approximately 0.85 as the dome transitions to the haunch region. Excluding the slab region, it is concluded that the nominal backfill and extended backfill tank demands results are acceptable because none of the curves exceed 1.0.

Figure C.22 shows the ACI-349 demand/capacity ratios for the UBS empty tank seismic demands combined with the TOLA demands for meridional, hoop, and shear. The demand/capacity ratios curves for the nominal backfill and extended backfill are very similar for meridional, hoop and shear. All of the sets of the demand/capacity ratios curves are less than 1.0 of the calculated capacity in all locations. The nominal backfill demand/capacity ratio curve for hoop at ACI Section 11 exceeds the extended backfill demand/capacity ratio curve. The set of hoop curves then trend together a maximum of 0.6 as the dome transitions to the haunch region. The tank demand results are acceptable because none of the curves in the critical regions exceed 1.0.

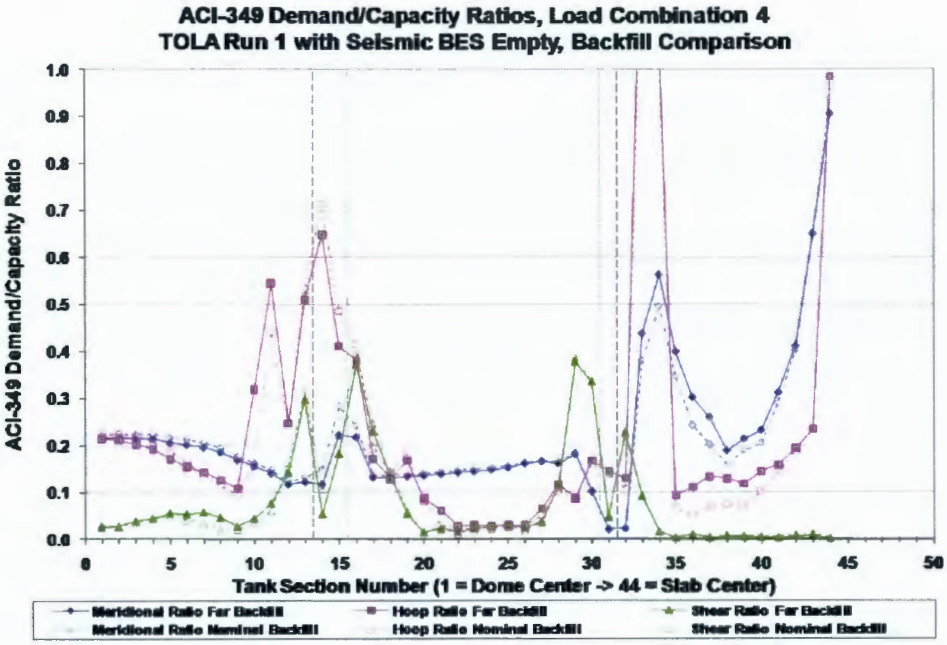

Figure C.20. ACI-349 Demand/Capacity Ratios, Load Combination 4, TOLA Run 1 with Seismic BES Empty Tank Case

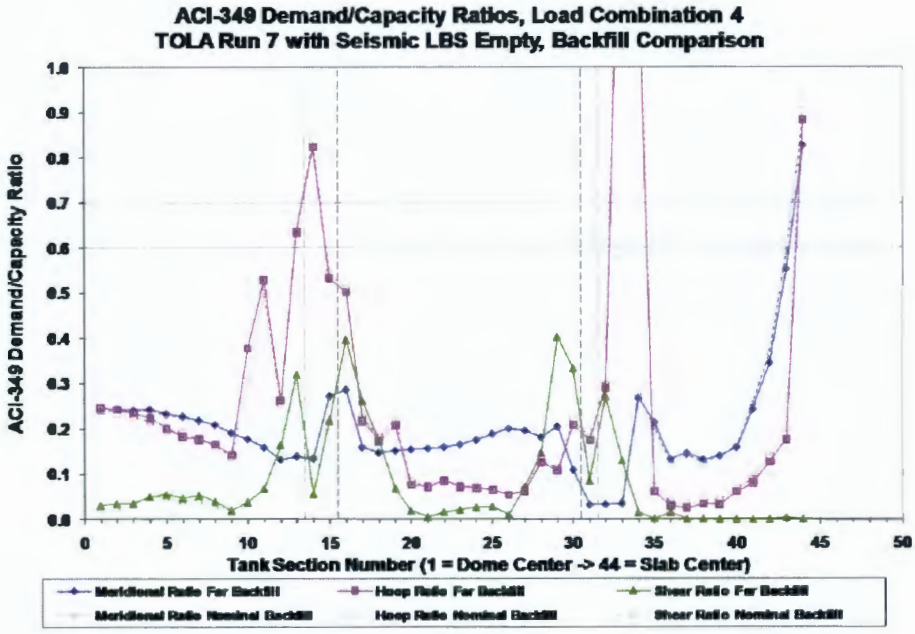

Figure C.21. ACI-349 Demand/Capacity Ratios, Load Combination 4 TOLA Run 7 with Seismic LBS Empty Tank Case

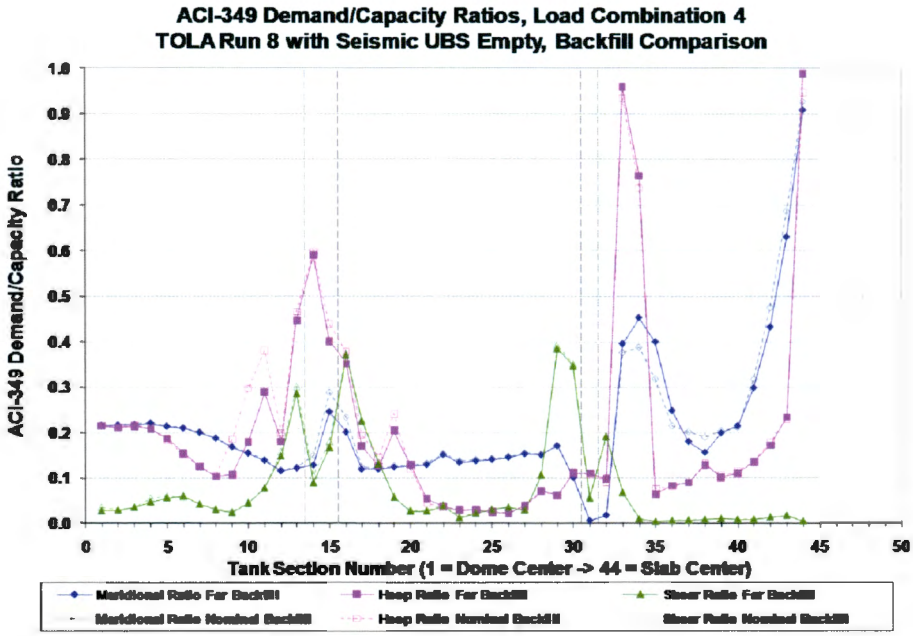

Figure C.22. ACI-349 Demand/Capacity Ratios, Load Combination 4, TOLA Run 8 with Seismic UBS Empty Tank Case

The tank demand results from extending the backfill to the model boundary are very similar to the nominal backfill case for each soil profile and resultant loadings in the critical tank regions. The demand/capacity ratio curves for TOLA and seismic tank demands do not exceed 1.0 in the ACI Sections 1 through 31. The D/C ratios results are acceptable. In many of the loading cases, there are wide margins of capacity. Therefore, it is concluded that extending the backfill to model boundary has very little effect on acceptable tank behavior.

This page intentionally left blank.

Appendix D

Waste Height Sensitivity Analysis

This page intentionally left blank.

Appendix D

Waste Height Sensitivity Analysis

D.1 Full Waste

A run matrix was developed to account for uncertainties in soil modulus, concrete modulus; concrete tensile strength, and concrete creep (see Table 5.16). For all these runs, a variable waste height history was used. The Type III representative tank waste height history was generated based on available S-101 and S104 tank waste-level histories . The waste height profile was a representative worst-case scenario before interim stabilization date (approximately year 1975) followed by an adjusted waste height to represent a near-empty tank.

To account for waste-level uncertainties, Run 1 from the run matrix was investigated for both empty and full conditions. The empty tanks analysis assume no waste is present in the tanks where as the full condition considers the current maximum waste height level in any of the Type III tanks (in BY,S,TX,TY farms). Both profiles (empty and full) had the representative historical waste height information before interim stabilization date after which the height was adjusted to represent either a near full (current max) or empty tank. Representative waste height profiles are shown in Figure D.1.

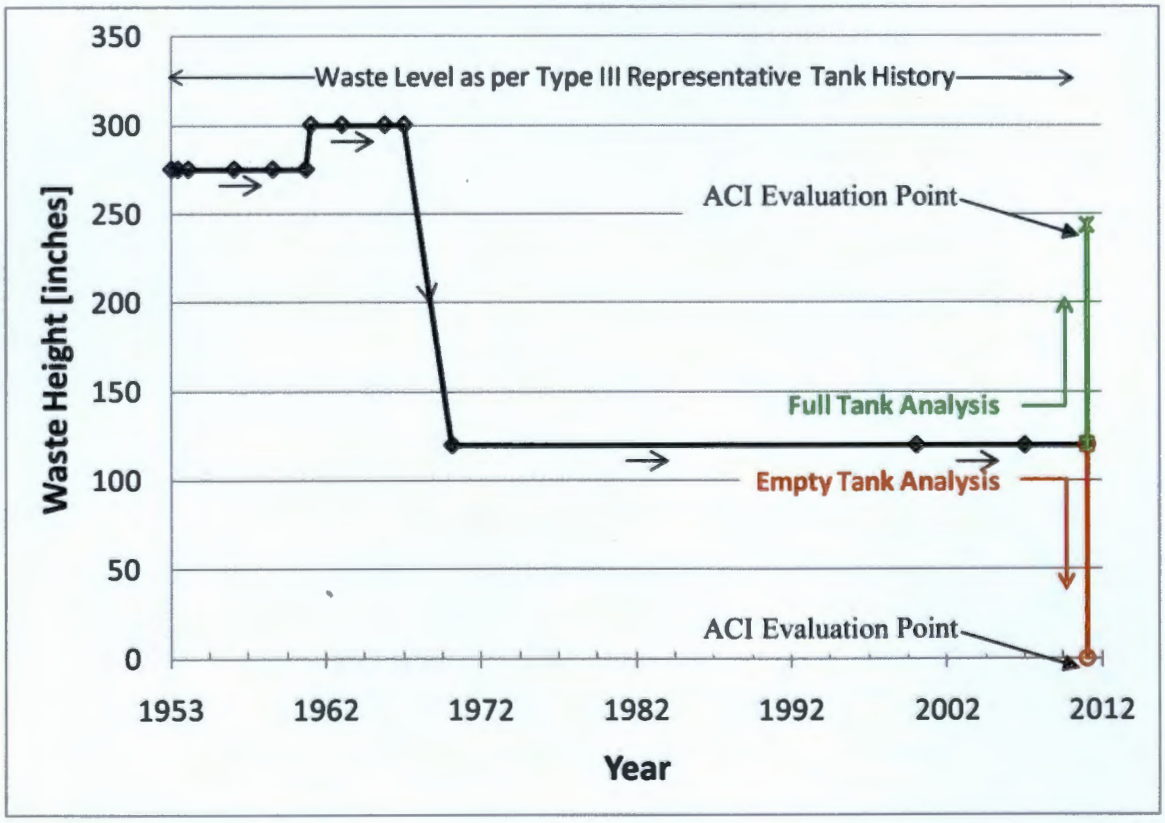

Figure D.1. Representative Waste Height Profiles Used for Type II SST-AOR

The empty and full tank analysis cases were carried out by continuing the analysis from Run 1 of the run matrix Load Step 16 (LS-16) as shown in the TOLA thermal history (Table 4.4). From this point the tank is cooled to either uniform 53F (for LC1) or 80F (LC9) in load step 17 and kept at the same conditions till the end of LS-18. Relevant ACI load factors are applied in load step 19. It is at this point(LS 19) the previous hydrostatic (waste) loads are removed and the simulations are performed for empty or full tank conditions by imposing corresponding hydrostatic loads under both the ACI load combinations 1 and 9.

The results at the end of load steps 18 (unfactored) and 19 (factored) are compared for both waste height conditions and both ACI load combinations. Load step 4 (or 5), which is a peak temperature load step, was not compared here because the changes in waste height happen after the peak temperature i.e., at the end of 59 year history. Figures D.2 through D.7 show the demand/capacity ratio plots for meridional, circumferential, and shear for un-factored and factored loads for both ACI load combinations. The change in demand/capacity for these cases is insignificant except for the shear in the lower wall, which is expected. However, the shear D/C ratios at these locations are all 0.5 or less. These trends are similar to those noted during the waste height sensitivity analysis for Type-II tanks (Rinker et al. 2011a). From this comparative study, it can be concluded that waste height is not a significant contributor to the tank demands.

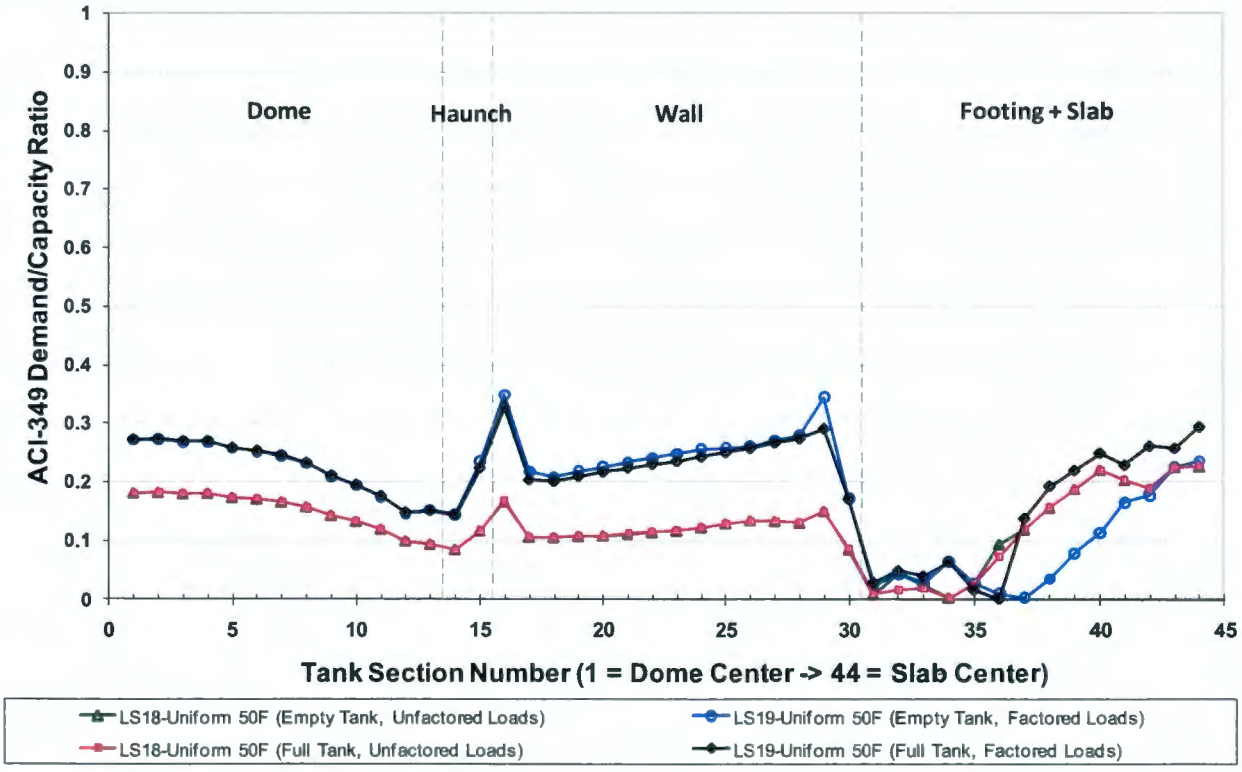

Figure D.2. Meridional ACI D/C Ratios – Load Combination 1

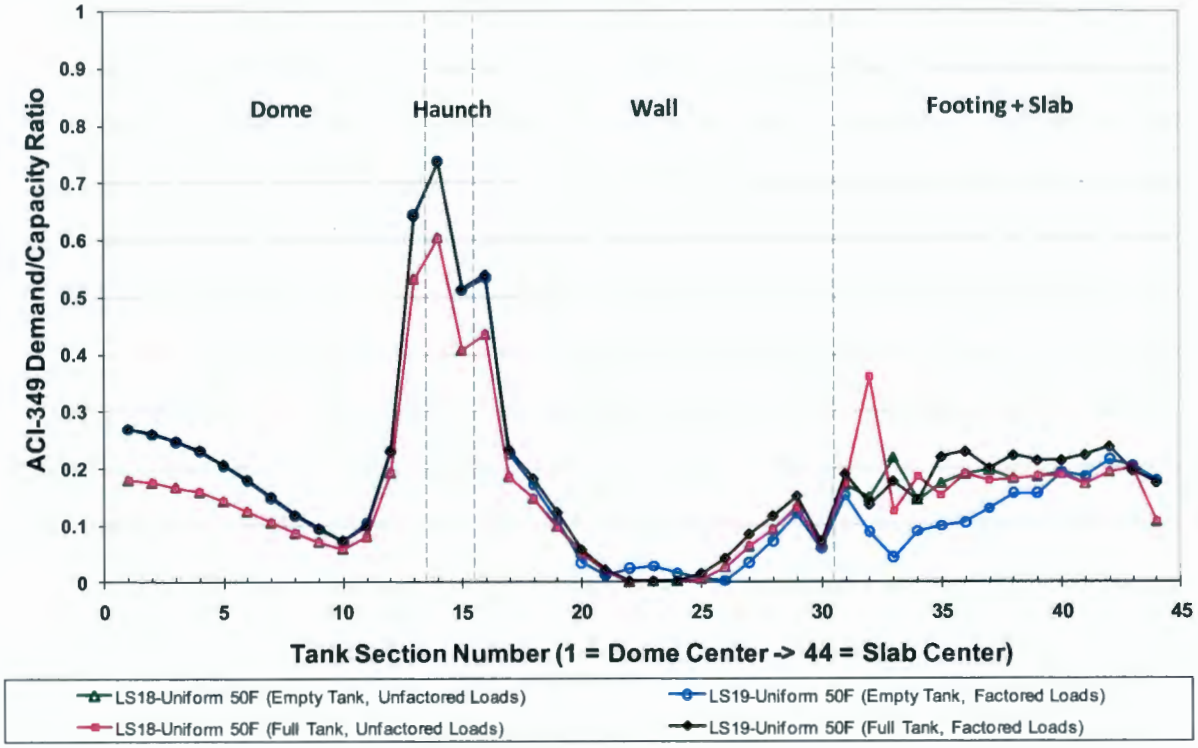

Figure D.3. Circumferential ACI D/C Ratios – Load Combination 1

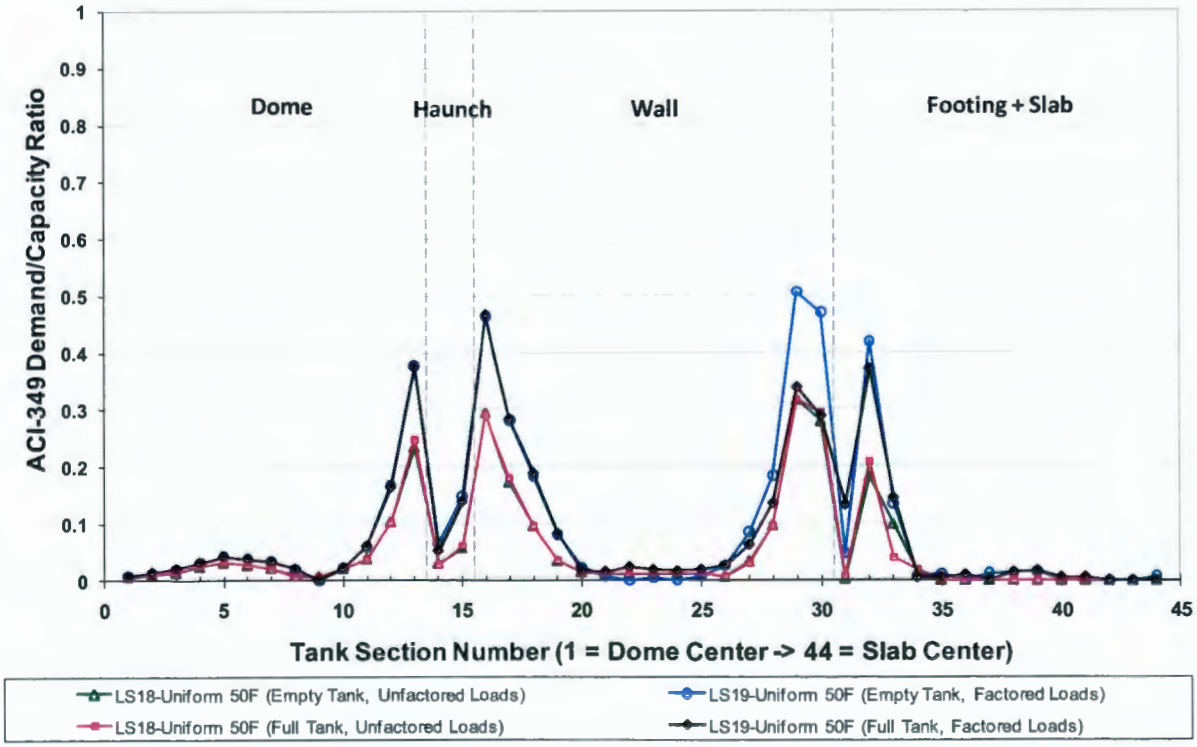

Figure D.4. Shear ACI D/C Ratios – Load Combination 1

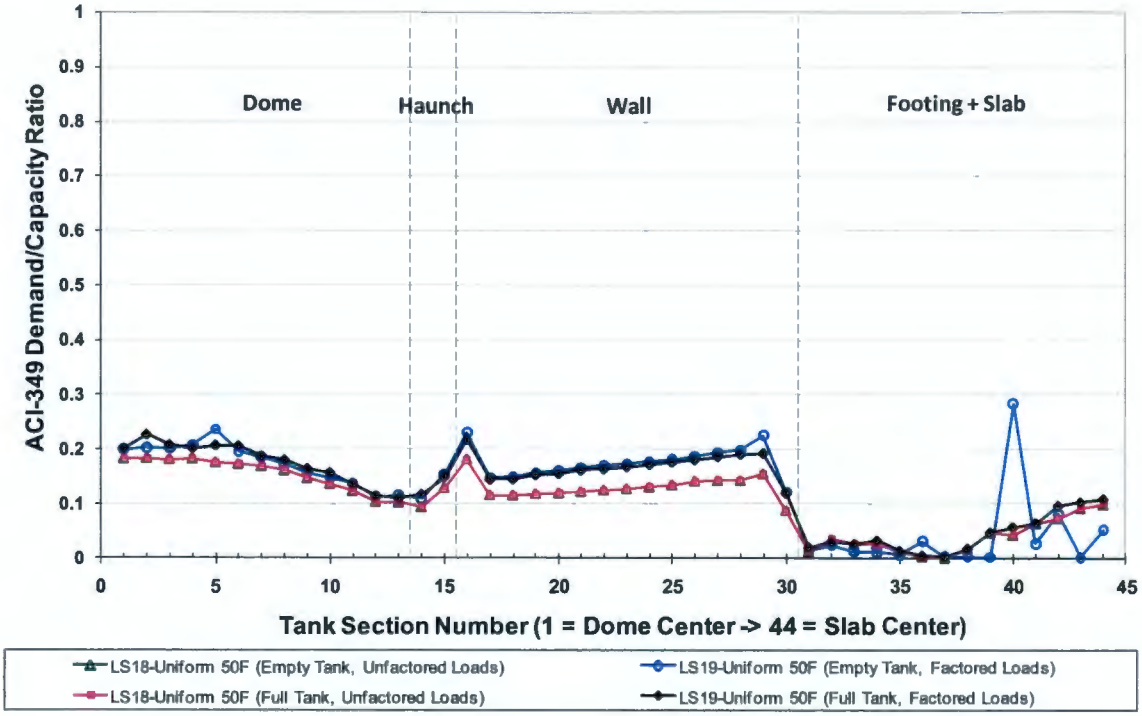

Figure D.5. Meridional ACI D/C Ratios – Load Combination 9

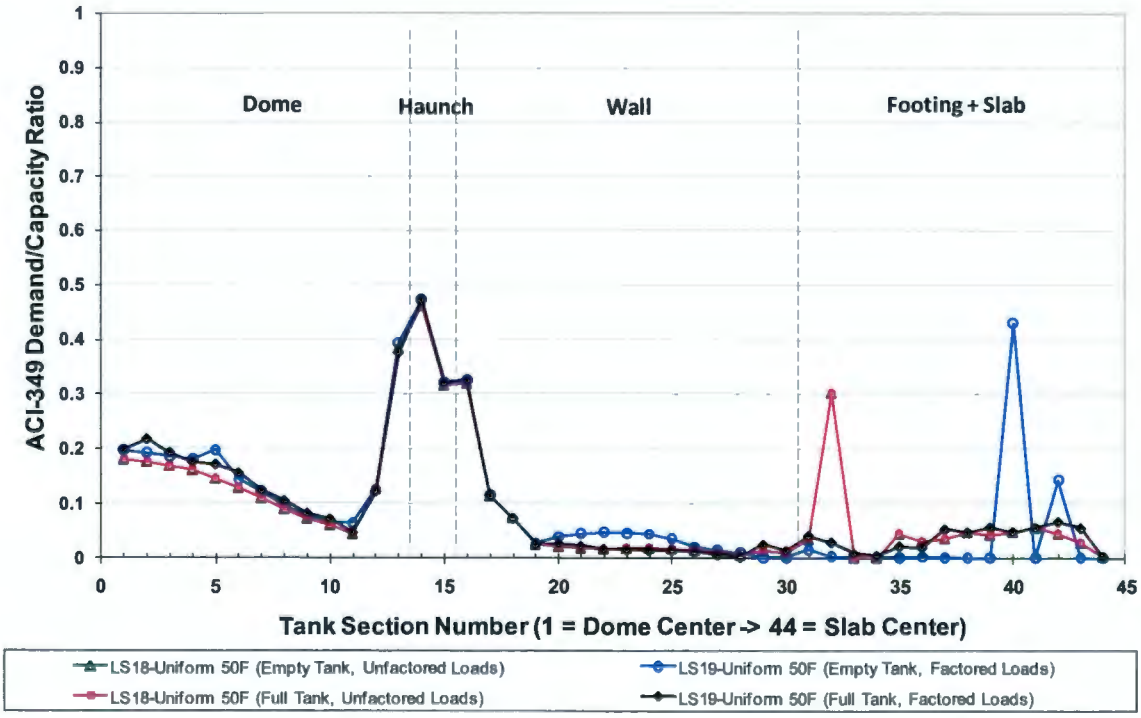

Figure D.6. Circumferential ACI D/C Ratios – Load Combination 9

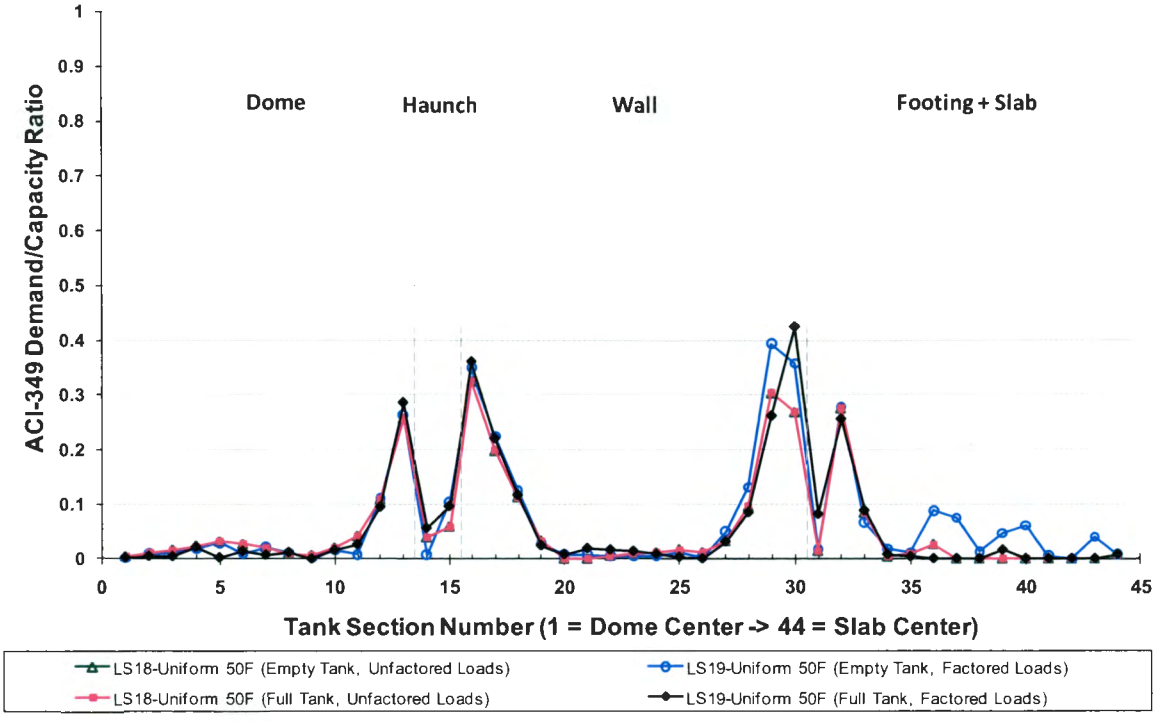

Figure D.7. Shear ACI D/C Ratios – Load Combination 9

This page intentionally left blank.

Appendix E

Slab Removal Study

This page intentionally left blank.

Appendix E

Slab Removal Study

The purpose of this slab removal sensitivity study is to understand the impact of potential slab shear exceedance on the structural integrity of the Type III tanks.

The ACI evaluations under the thermal and operating loads analysis (TOLA) of Type III tanks indicated that the demands at various sections in the tank are all less than the ACI capacities except for one case in Run 3 of the TOLA run matrix (with nominal soil modulus, high concrete modulus and no creep as listed in Table 5.6) where the D/C ratio in the meridional direction at the peak temperature of 310°F is about 1.08 near the center of the base slab (section #44). However, when these TOLA demands with low, nominal, and high soil modulii are combined with corresponding cases of seismic demands, all the cases of seismic run matrix (listed in Table 6.19) except for combined Run 9 showed demands exceeding capacities in the base slab in either circumferential, shear or meridional directions. Hence, a few analysis cases with nominal, low and high soil modulus were run where the slab was physically detached from the rest of the tank after the peak temperature load step in the analysis.

E.1 Run 1: Slab Element Removal

Removal of the section 32 slab elements was accomplished using the ANSYS® EKILL command. The EKILL command "kills" an element by reducing the stiffness of the specified elements by a factor of 10^{-6}. By "killing" these elements only insignificant force can be transferred from the rest of the tank to the slab. The slab is effectively isolated from the rest of the tank and provides no structural support. This removal is illustrated in Figure E.1.

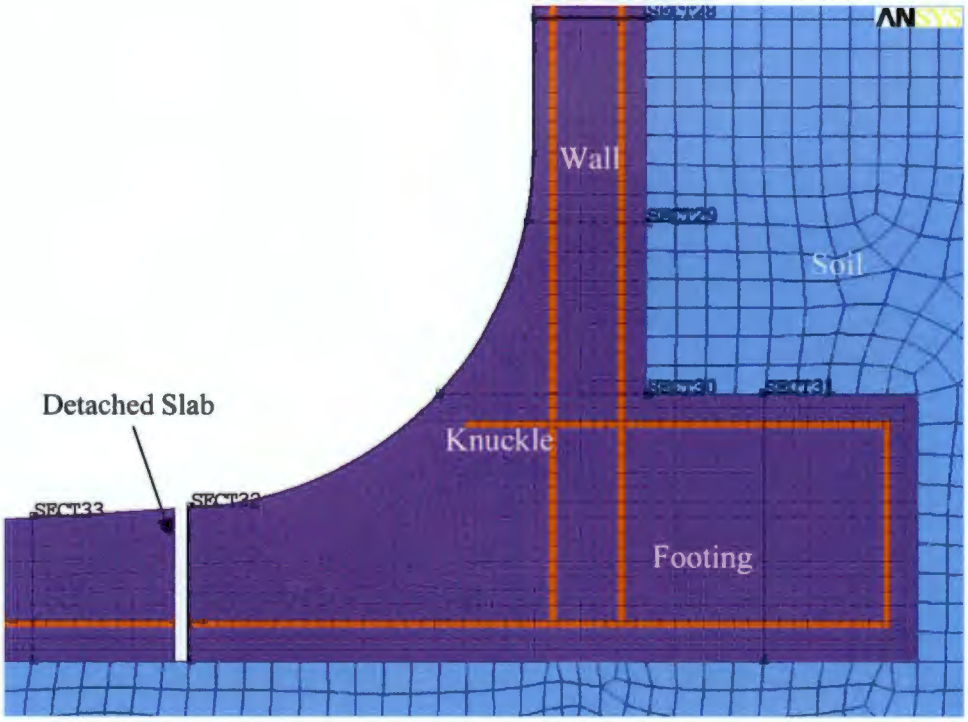

Figure E.1. Lower Knuckle region with Killed Elements at Section 32

Upon application of ACI 349-06 LC1 load factors, D/C ratios were calculated through the dome, haunch, wall, and outer footing. Since the slab is isolated from the rest of the tank no section D/C ratios were calculated in the slab after section 32. Figure E.2 shows the D/C ratios for this analysis with the break at section 32 compared with the nominal Run 1 ratios. In this plot the legend entries starting with DS correspond to the detached slab results. The slab removal study shows little difference from the nominal TOLA matrix Run 1 in all sections except section 32. The section 30 and 31 meridional hoop and shear D/C ratios decreased slightly. Clearly the removal of section 32, or any other slab section, does not adversely affect the structural integrity of the tank from an ACI 349-06 perspective.

Upon removal of the slab, or isolation of the slab from the rest of the tank, the tank wall and footing may now be free to punch into the soil below. To assure this is not the case, the total vertical displacement of the bottom of the wall of Run 1 with section 32 removed was compared to the corresponding displacement for the nominal Run 1. Total vertical displacement of the bottom of the wall for Run 1 under ACI 349-06 LC1 is –1.982 inches. The total vertical displacement of the bottom of the wall for Run 1 with section 32 removed under ACI 349-06 LC1 is –1.991 inches. This insignificant difference of 0.009 inches in displacement indicates that punching of the wall and footing into the soil is not a realistic yielding scenario. In addition, the relative vertical displacement across the gap in section 32 under ACI 349-06 LC1 is 0.0379 inches. Again, this minor relative displacement indicates that wall and footing are not expected to punch into the soil.

In addition to checking the displacements, a calculation is made to check the soil-bearing capacity under the footing no longer connected to the slab. Soil-bearing capacity is calculated using the modified general ultimate bearing capacity equation (Das 2002):

$$q_u = q\lambda_{qs}\lambda_{qd}\lambda_{qi}N_q + \tfrac{1}{2}\lambda_{\gamma s}\lambda_{\gamma d}\lambda_{\gamma i}\gamma B N_\gamma \tag{E.1}$$

where q_u = the ultimate bearing capacity

q = the surcharge

γ = the soil density

B = the width of the footing remaining outboard of the location where the slab was detached from the footing.

Here the term associated with the soil cohesion has not been included as the soil is assumed cohesionless (Johnson et al. 2010) and only the terms associated with the surcharge and the soil density remain.

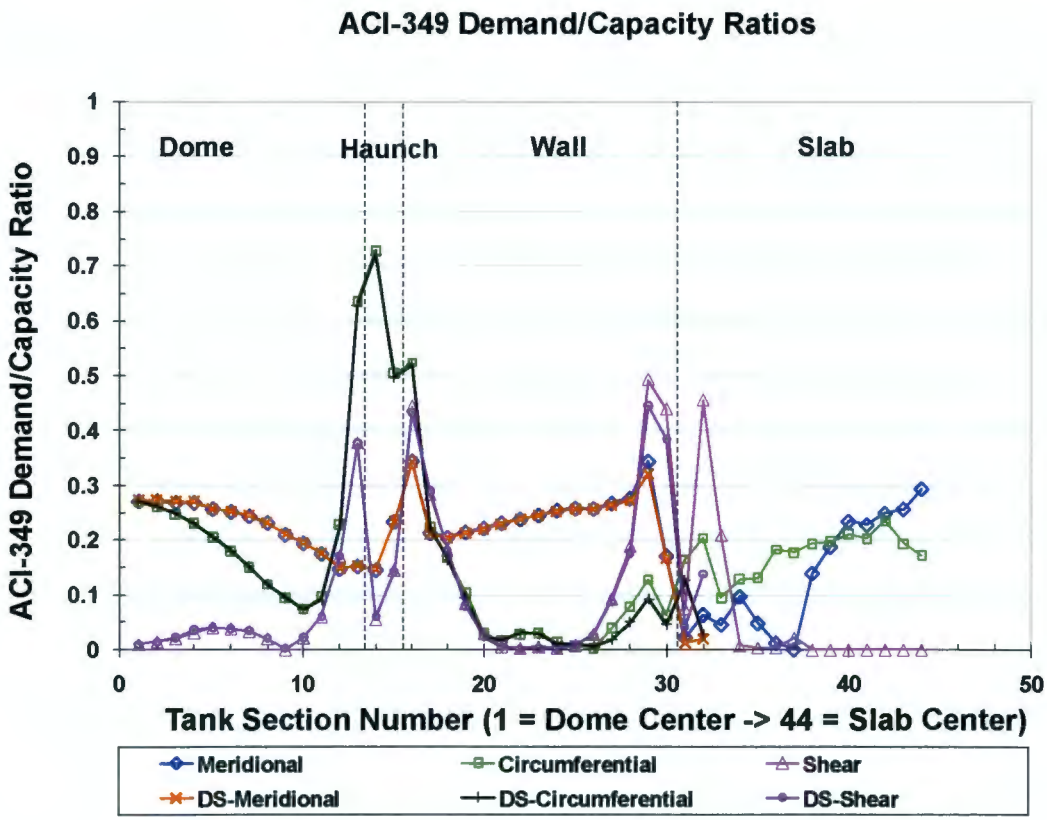

Figure E.2. ACI D/C Ratios for Run 1, LC1 with and without Detached Slab

N_q and N_γ are determined from Terzaghi's equations:

$$N_q = e^{\pi \tan\phi'} \tan^2(45 + \phi'/2) \quad \text{(E.2)}$$

$$N_\gamma = (N_q - 1)\tan(1.4\phi') \quad \text{(E.3)}$$

As the water table is well below the tanks, the drained friction angle is the friction angle given for the surrounding soil, 35°. This gives an $N_q = 33.30$ and $N_\gamma = 37.15$.

Given an inner wall radius of 37.5 ft, the ring foundation is treated as an infinite strip footing. The shape factors, λ_{qs} and $\lambda_{\gamma s}$, both are equal to 1 under this assumption. The depth factors, λ_{qd} and $\lambda_{\gamma d}$, are determined from Meyerhof's equations:

$$\lambda_{qd} = \lambda_{\gamma d} = 1 + 0.1(D_f/B)\tan(45 + + \phi'/2) \quad \text{(E.4)}$$

where D_f is the depth of the soil above the footing. For the footing width in the tank interior, the depth of the soil is zero, giving depth factors of 1.0. For the tank exterior, the depth of the footing is 49.99 ft, giving depth factors of 2.18. The inclination factors, λ_{qi} and $\lambda_{\gamma i}$, are also given by Meyerhof's equations:

$$\lambda_{qi} = (1 - \alpha°/90°) \quad \text{(E.5)}$$

$$\lambda_{qi} = (1 - \alpha°/\phi'°) \quad \text{(E.6)}$$

Here $\alpha°$ is the angle of inclination of the resultant force applied by the footing on the soil in degrees. The resultant force under ACI LC1 is determined by integrating the shear stress and normal stress along the contact elements between the concrete and the soil under the footing. The angle, $\alpha°$, was found to be 14.31° and the average resultant stress on the soil was 115.94 psi.

The surcharge in Eq. (E.1) is calculated separately for the tank footing interior and the tank footing exterior. The interior surcharge is 10.79 psi, which includes the pressure on the footing due to the tank liquid 8.55 psi, plus the weight of the concrete slab ~2.24 psi. The exterior surcharge is 43.39 psi, which is due to the weight of the soil above the footing.

Eq. (E.1) is used to calculate the ultimate bearing capacity for the soil under both the interior and the exterior of the footing. The interior ultimate bearing capacity is the lowest at 294.32 psi. Given the previously mentioned average resultant stress of 115.94 psi, a factor of safety of 2.54 is calculated. The factor of safety is conservative for two reasons. This factor of safety is calculated for the tank under ACI LC1 factored loads: 1.4 (D + F) + 1.7 (L + H). In addition, the bearing capacity equation does not account for the stiffness of any intact slab in the interior of the tank that would resist any soil deformation due to general shear yielding of the soil at the interior surface. This safety factor, which is greater than

one even for factored loads, indicates that the wall and footing will remain supported by the soil even if the slab is not completely intact.

Furthermore, the D/C ratios ≥1.0 in the slab region are primarily due to the seismic loads. The stresses due to these thermal loads are secondary and self-relieving. The slab is also displacement controlled and is limited to cracking and crushing only. Based on this analysis and observations, any ACI exceedance in shear, meridional, and circumferential directions, in the slab region (sections 32 through 44) is considered to be of no structural significance.

E.2 Run 7 and Run 8: Slab Element Removal

As done for Run 1 (nominal soil modulus), the slab removal run was repeated with Run 7 (low) and Run 8 (high) properties because the combined TOLA+Seismic D/C ratios exceeded 1.0 in one of the directions in the base slab sections. Figure E.3 and Figure E.4 compares the D/C ratios at various sections in the tank with and without the slab for Run 7 and Run 8 respectively under ACI LC1 factors. With the higher modulus soil, the wall and footing may show a lower tendency to punch into the soil and vice versa when section 32 is removed. It was found that the difference in the total vertical displacement at the bottom of the wall for Run 7 with section 32 removed relative to nominal Run 7 under ACI 349-06 LC1 was about, 0.013 inches and for Run 8 with section 32 removed relative to nominal Run 8 under ACI 349-06 LC1 was negligible, 0.006 inches. Also, the relative vertical displacements across the gap in section 32 under ACI 349-06 LC1 are about 0.0556 and 0.0277 inches for Run 7 and Run 8 slab removal studies respectively. These minor displacement values indicate that the wall and footing are not expected to punch into the soil, even for the lower bound soft soil (Run 7). Again, the soil-bearing capacity was checked according to Eq. (E.1). The minimum safety factor, found for the soil on the interior of the footing, under ACI 349-06 LC1 loading was 2.48 and 2.60 for Run 7 and Run 8, respectively. This safety factor, which is greater than two even for factored loads, indicates that the wall and footing will remain supported by the soil even if the slab is not completely intact.

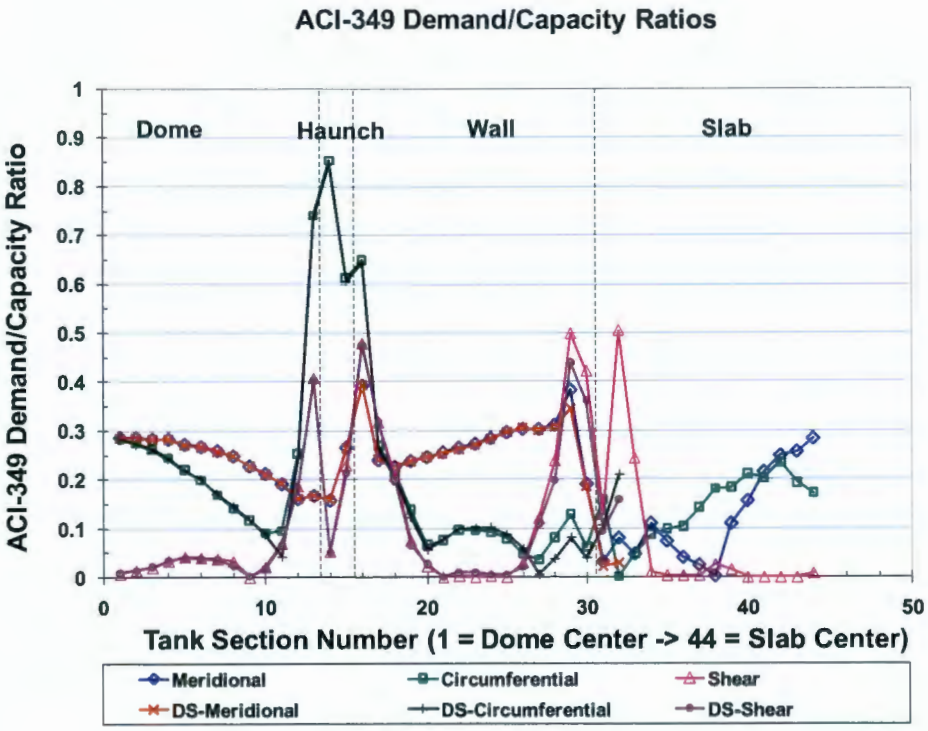

Figure E.3. ACI D/C Ratios for Run 7, LC1 with and without Detached Slab

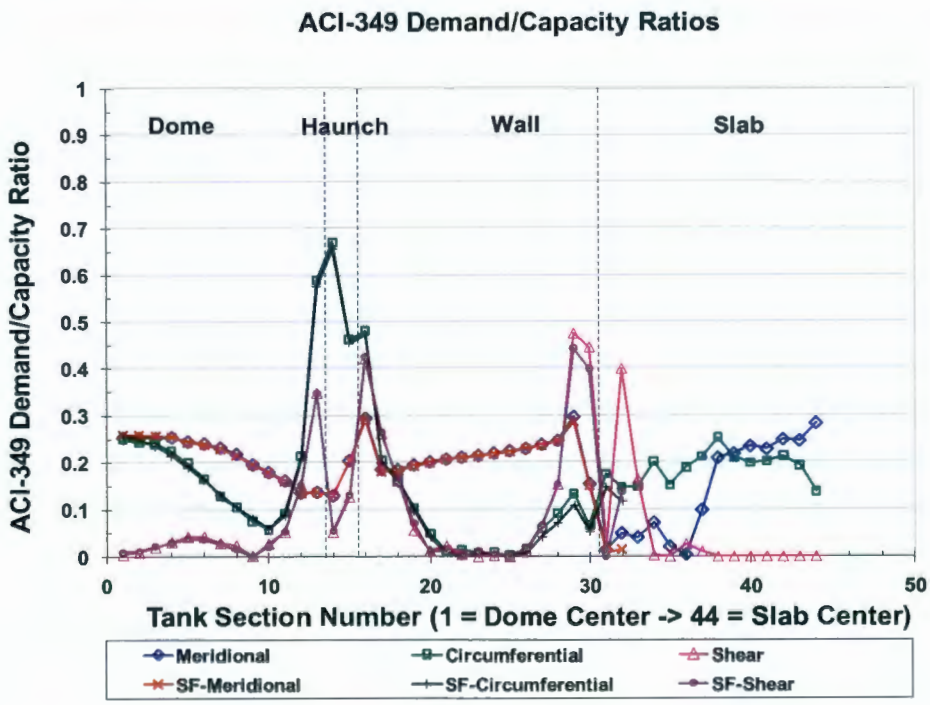

Figure E.4. ACI D/C Ratios for Run 8, LC1 with and without Detached Slab

Appendix F

Run 1, Baseline Case with Best EstimateMaterial Properties: Load Contributions

This page intentionally left blank.

Appendix F

Run 1, Baseline Case with Best Estimate Material Properties: Load Contributions

F.1 Individual Load Effect on Tank Forces and Moments

To understand the effect of each individual load on the tank demands, Figures F.1 through F.10 show the total forces and moments as well as the incremental forces and moments in the tank sections for each of the loads. The total force and moment figures (F.1, F.3, F.5, F.7, and F.9) show the total force or moment under the load steps for gravity only, ls2, ls3, ls6, ls18_50F, ls19_50F, ls18_80F, and ls19_80F. Ls2 includes the effects of gravity and the waste load. Ls3 includes the effects of all mechanical loads – that is, gravity, waste load, and the concentrated load and surface load. Ls6 includes the effects of these mechanical loads and the thermal cycle-to-peak temperature. Ls18_50F or Ls18_80F include the effects of these mechanical loads and the thermal cycle through the cool-down to stress-free temperature (50°F) or to the present day temperature (80°F). Ls19_50F includes the effect of the mechanical loads through cool-down to stress-free temperature plus the effect of the ACI 349-06 load combination 1 load factors. Ls19_80F includes the effect of the mechanical loads through cool-down to present-day temperature plus the effect of the ACI 349-06 load combination 9 load factors.

The incremental force and moment figures (F.2, F.4, F.6, F.8, and F.10) show the incremental force or moment demands for these load steps. To show the effect of adding a particular load to the tank, the force or moment of prior loads are subtracted. The TOLA model has non-linearities so the effect of the loading would be different if the loading order was different. The forces and moments of the gravity load remain the same as the total force and moment plots as the gravity load is the first applied. The incremental plots show that gravity typically dominates the other incremental forces and moments in many of the tank sections.

Figure F.2 shows the incremental meridional force. Gravity load is shown to introduce large compressive forces in the dome, haunch, and wall, and smaller compressive forces in the slab. Adding waste load to the tank has little effect on the meridional force in the dome and haunch, as expected, and adds a very small amount of tensile forces in the wall and slab. Adding the concentrated surface load and uniform surface load adds some meridional compression to the dome, a little compression to the haunch and wall, and has an insignificant effect on the slab. Heating the tank to the peak temperature has minor effects in the dome and haunch, adds some compression in the wall, and adds a lot of compression in the slab. As the tank heats up, the slab, which is the hottest part, expands. This expansion is resisted by the surrounding soil and compression is introduced into the slab. The figure shows the thermal cycle through cool-down (to either 50°F or 80°F) by subtracting the mechanical loads (gravity, waste, and surface loads) from these cool-down steps (ls18_50F or ls18_80F). The effect of the entire thermal cycle through cool-down is to add meridional tension to the dome, haunch, wall, and slab. However, this added tension is small compared to the compression added by the mechanical loads; therefore, as seen in Figure F.1, the dome, haunch, and wall remain in compression and the slab transitions to very miniscule tension in some sections. The addition of load factors for ACI 349-06 LC1 adds significant compression to the dome, haunch, and wall, as well as some compression to the slab. The addition of load factors for ACI 349-06 LC9 also adds compression to the dome, haunch, and wall, but has only a minor effect on the slab.

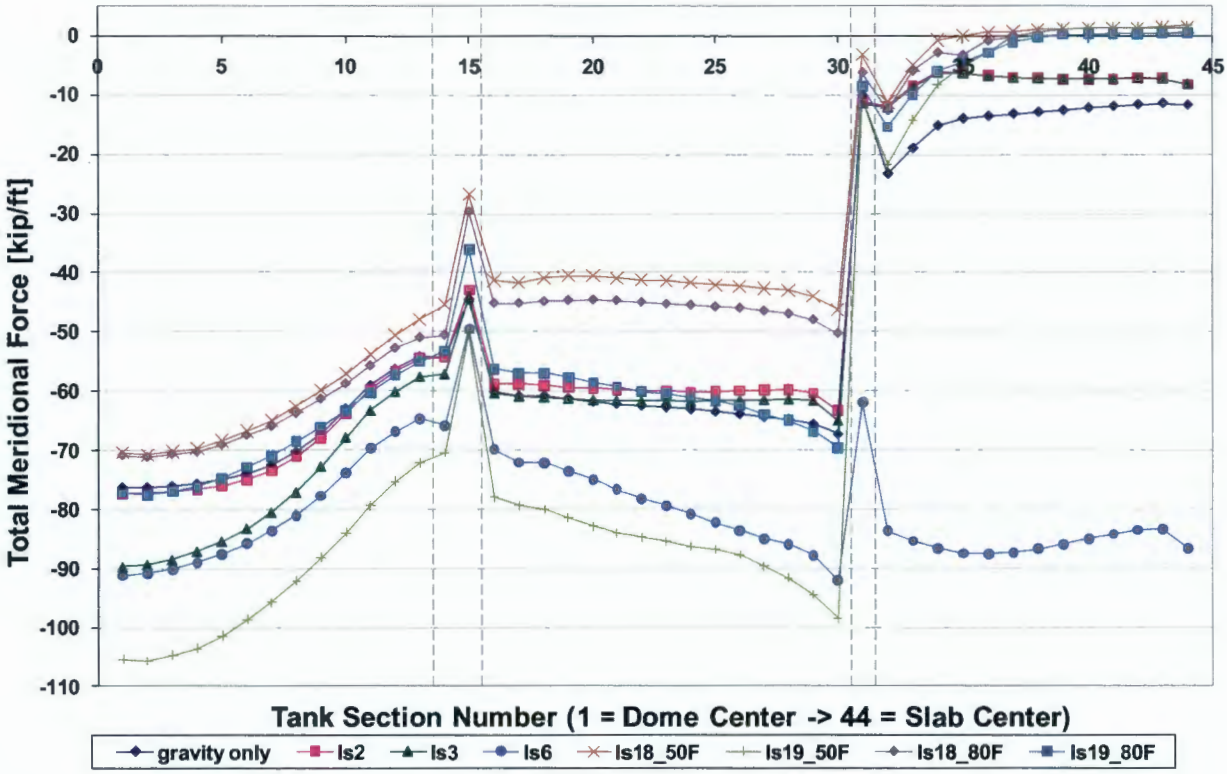

Figure F.1. Total Meridional Force for Run 1

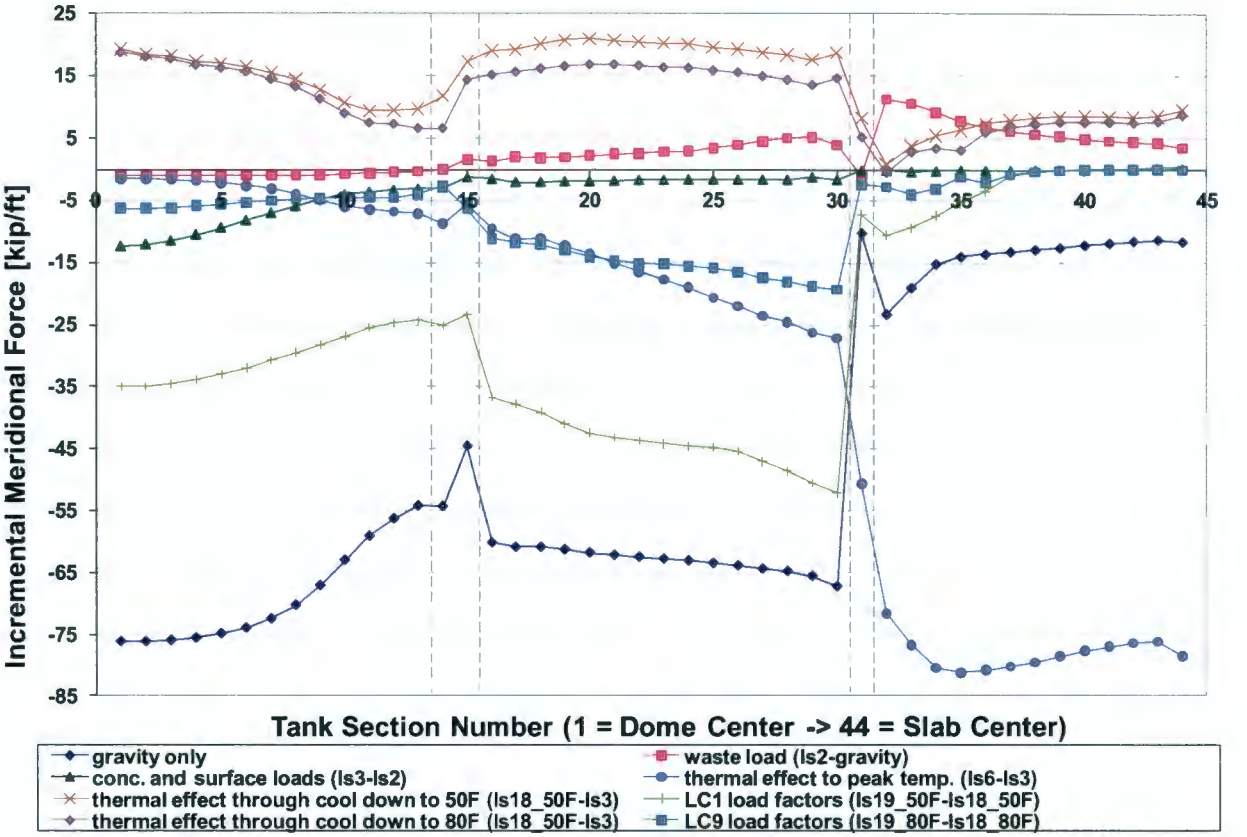

Figure F.2. Incremental Meridional Force for Run 1

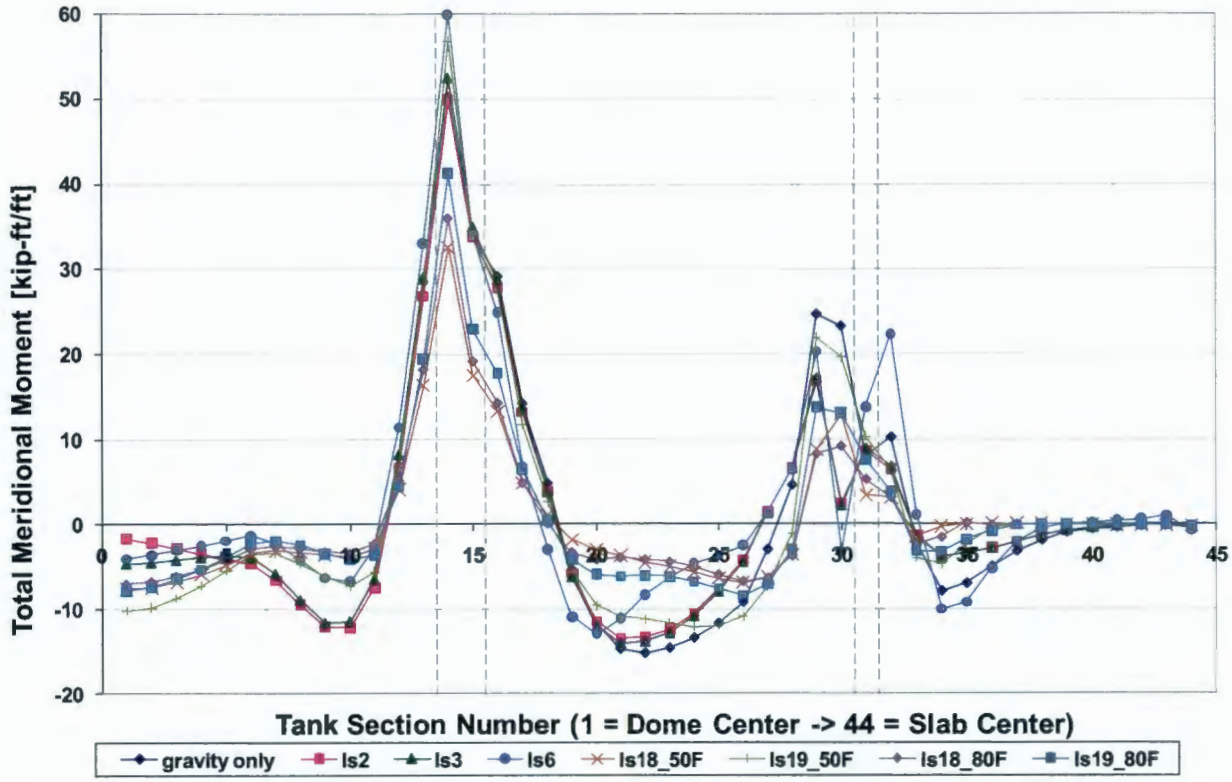

Figure F.3. Total Meridional Moment for Run 1

Figure F.4 shows the incremental meridional moment. Gravity load adds significant moment to the outer dome, haunch, and wall and small moment to the outer slab. Waste loads and concentrated and uniform surface loads have little effect on the meridional moment throughout the tank. The effect of the thermal cycle through peak temperature is to reduce the total moment in the dome while adding a small amount of moment to the haunch and wall. The effect of the thermal cycle through either of the two cool down temperatures is to reduce the moment in the outer dome, haunch, wall, and outer slab. The load factors from both ACI 349-06 LC1 and LC9 tend to add a small moment to the outer dome, haunch, wall, and outer slab.

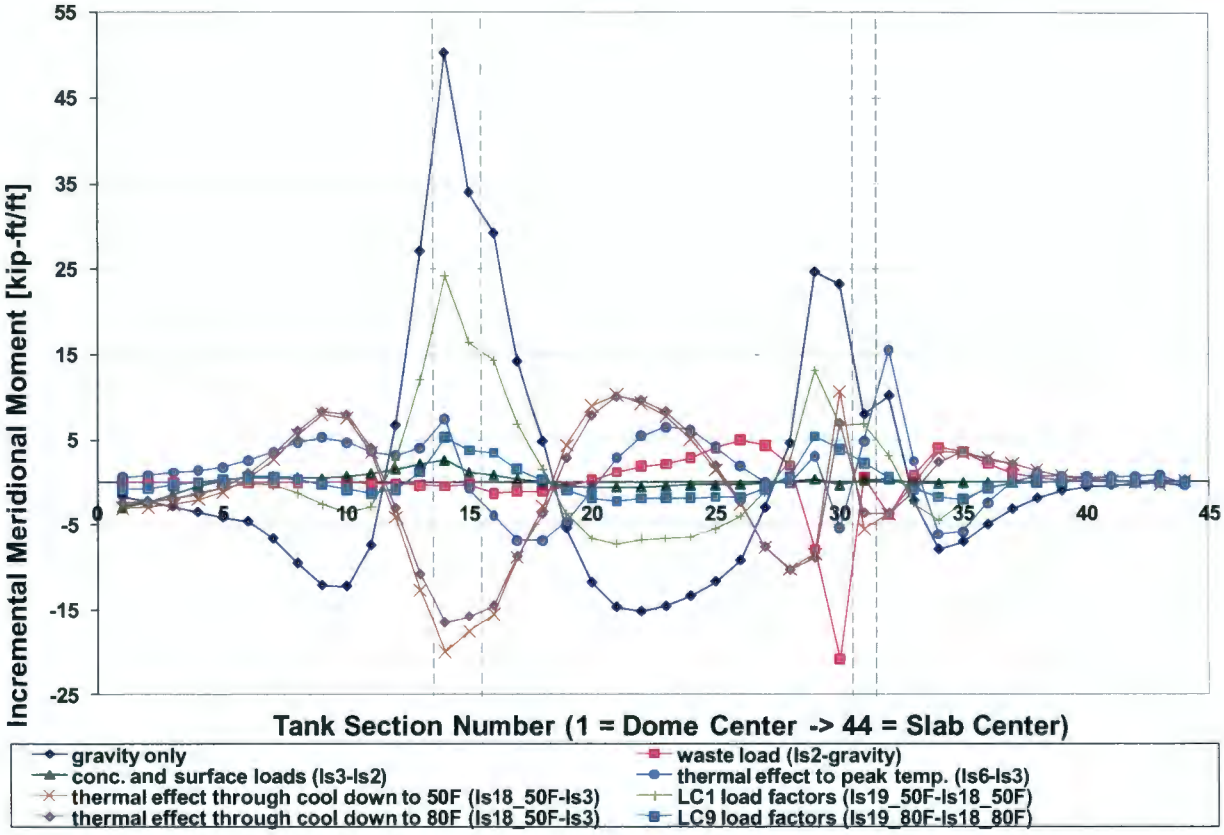

Figure F.4. Incremental Meridional Moment for Run 1

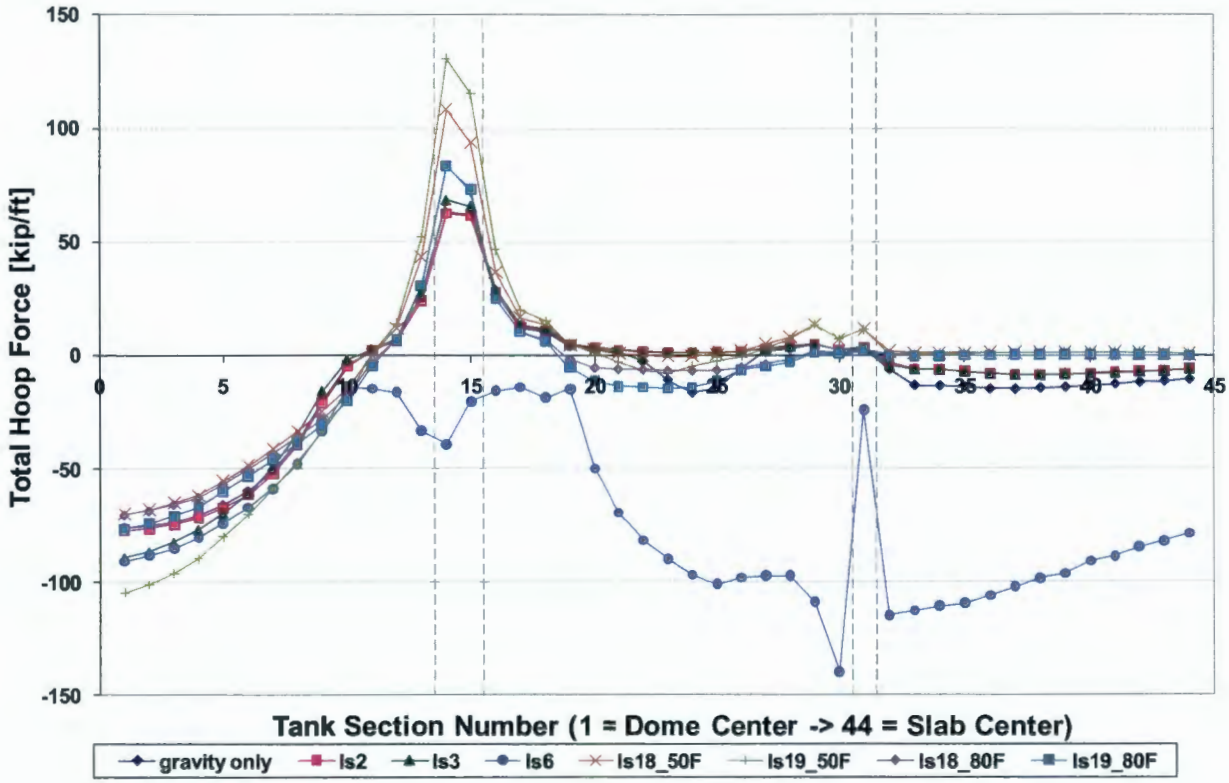

Figure F.5. Total Hoop Force for Run 1

Figure F.6 shows the incremental hoop force. Gravity load adds hoop compression to the dome, hoop tension to the haunch, minor hoop tension or compression to the wall, and minor hoop compression to the slab. The waste load has almost no effect on the hoop force throughout the dome, haunch, and upper wall and adds some small hoop tension to the wall and slab. The addition of the concentrated and uniform surface loads adds some hoop compression in the center of the dome, adds some hoop tension in the outer dome and haunch, and has little effect in the wall or slab. The effect of the thermal cycle to peak temperature is to add significant hoop compression to the haunch, wall, and slab. Again, this is expected. As the tank heats up the surrounding soil resists the tank expansion, resulting in hoop compression. The effect of the thermal cycle through either of the cool-down states is to add some hoop tension to the dome center, haunch, lower wall, and slab while adding minor hoop compression to the outer dome and middle wall. However, as can be seen in Figure F.5, the compression added by the mechanical loads keeps the dome and slab in compression or practically zero. Only the haunch, upper and lower wall, and outer footing are in tension. The effect of the load factors for both ACI 349-06 LC1 and LC9 is to add hoop compression to the dome, some tension to the haunch, and almost no force to the wall or slab.

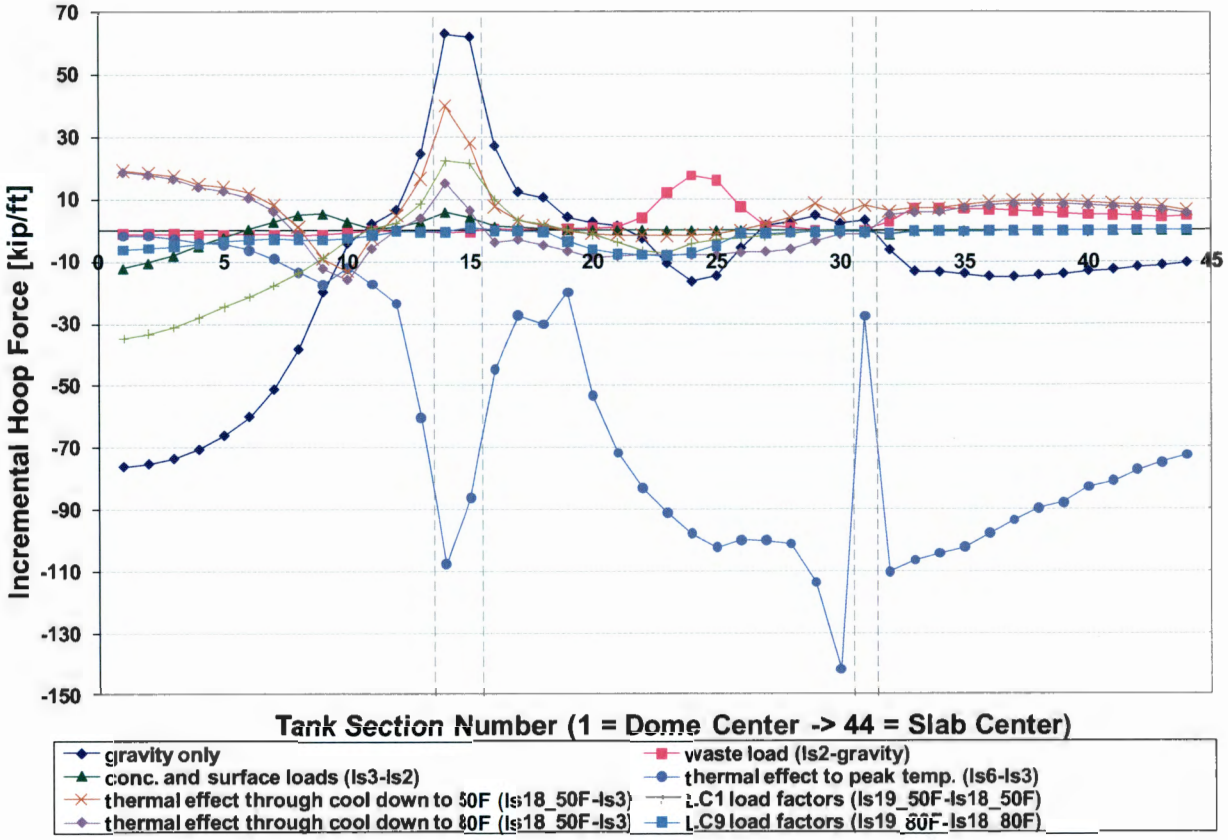

Figure F.6. Incremental Hoop Force for Run 1

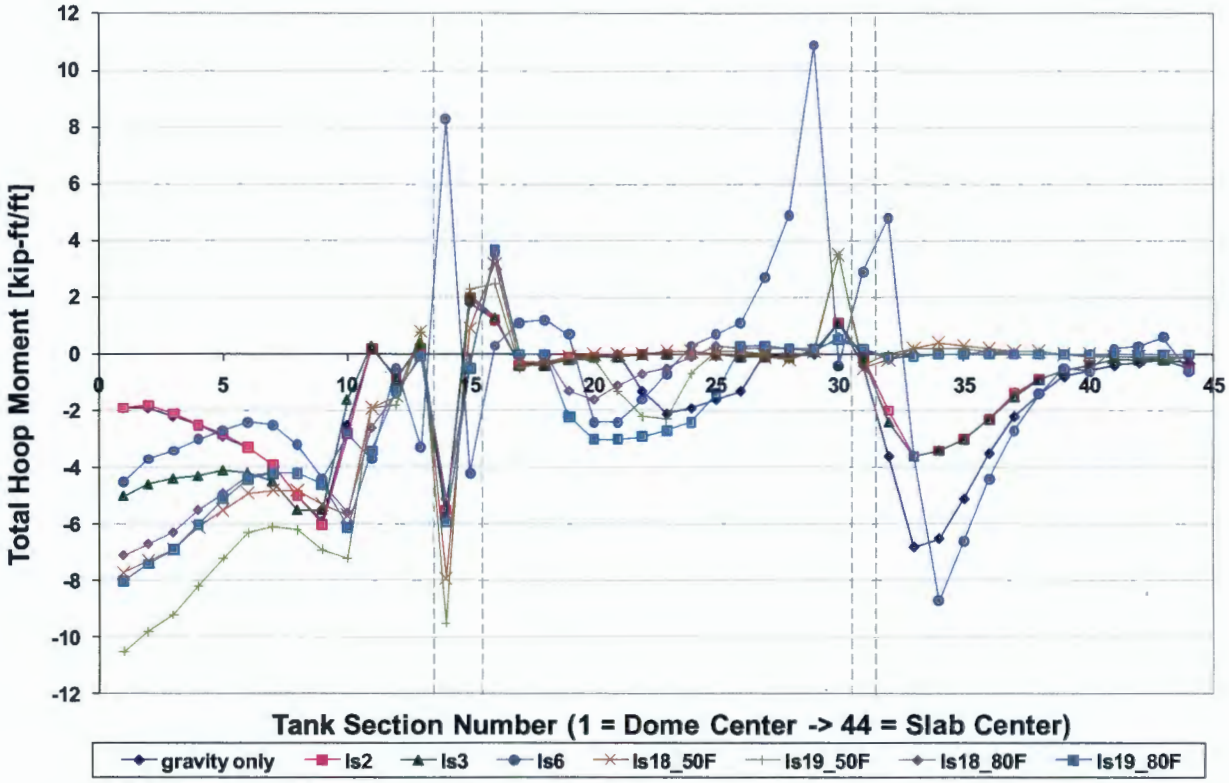

Figure F.7. Total Hoop Moment for Run 1

Figure F.8 shows the incremental hoop moment. In general, the hoop moments on the tank are small in magnitude. Gravity load and the thermal cycle through peak temperature have the largest effect on the hoop moment. The other loads each change the hoop moment by 4 kip-ft/ft or less throughout the tank. The highest total hoop moments under any load are less than 11 kip-ft/ft and are seen in the center of the dome and the lower wall (Figure F.7).

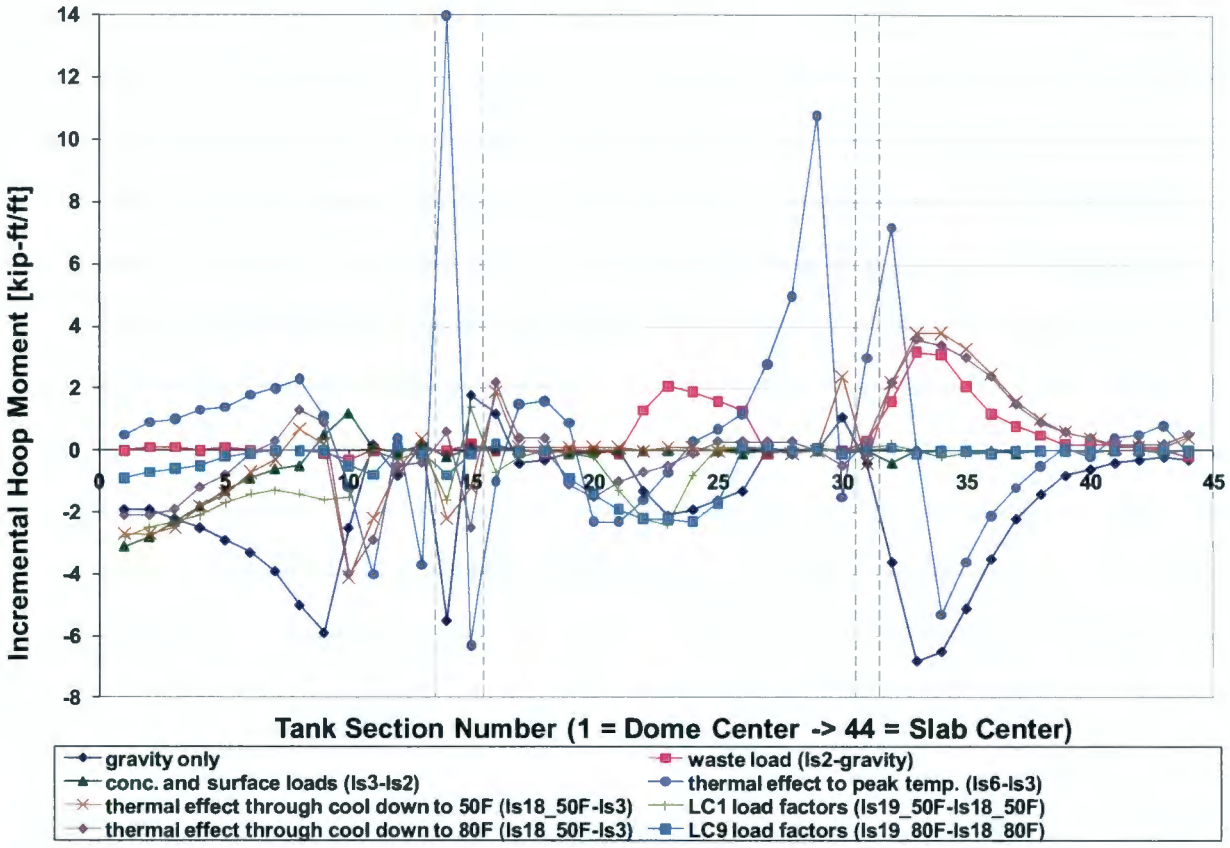

Figure F.8. Incremental Hoop Moment for Run 1

Figure F.9 shows the total shear force is greatest in the outer dome, top and bottom of the wall, and the footing and outer slab. Figure F.10 shows the incremental shear forces. The gravity load has the greatest effect on the shear load in the outer dome, wall, and footing and outer slab. The waste load has little effect on the shear in the dome and haunch, and reduces the shear in the bottom of the wall and the outer slab. The concentration and uniform surface loads have little effect on the shear throughout the tank. The thermal cycle through peak has minor effects to the shear at the top and bottom of the wall as well as to the outer slab and a larger effect on the outer footing. The effect of the thermal cycle through the two cool-down states decreases the shear in the haunch, wall, and outer footing and slab. The additional load factors for ACI 349-06 LC1 and LC9 slightly increase the shear in the dome, haunch, wall, and outer slab.

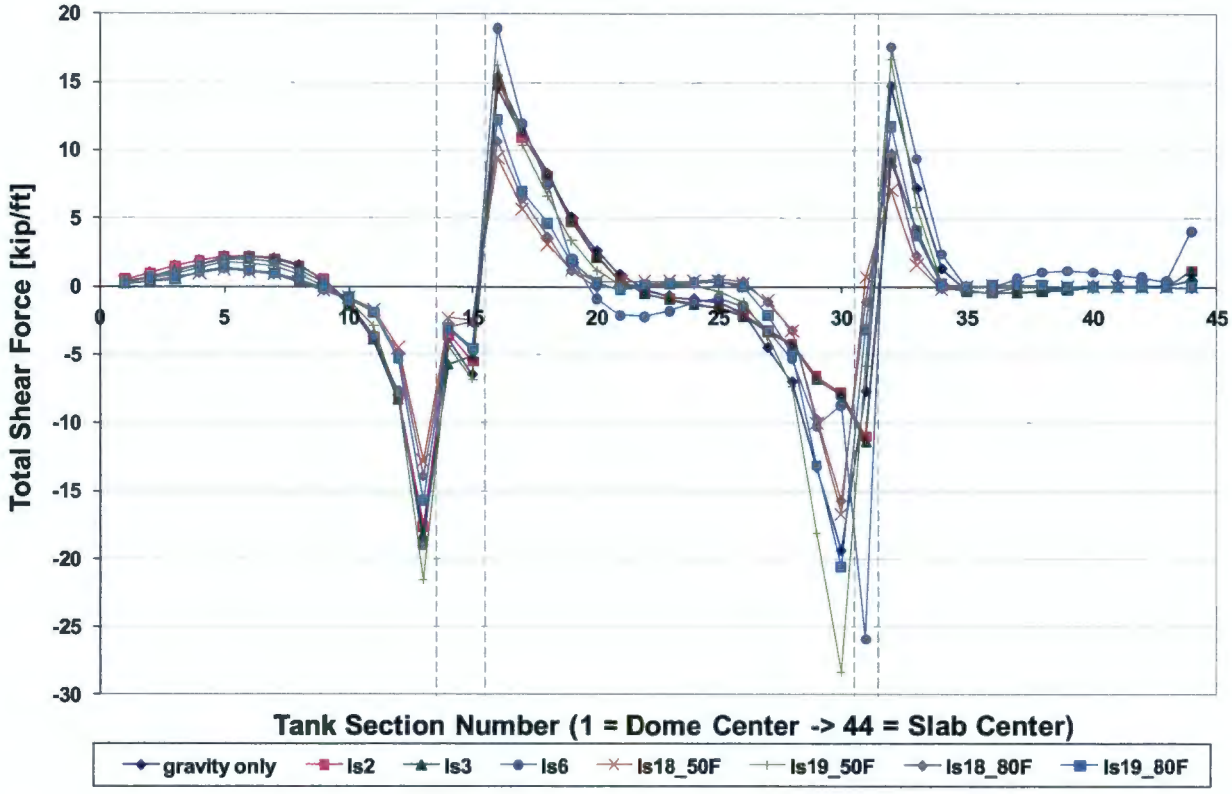

Figure F.9. Total Shear Force for Run 1

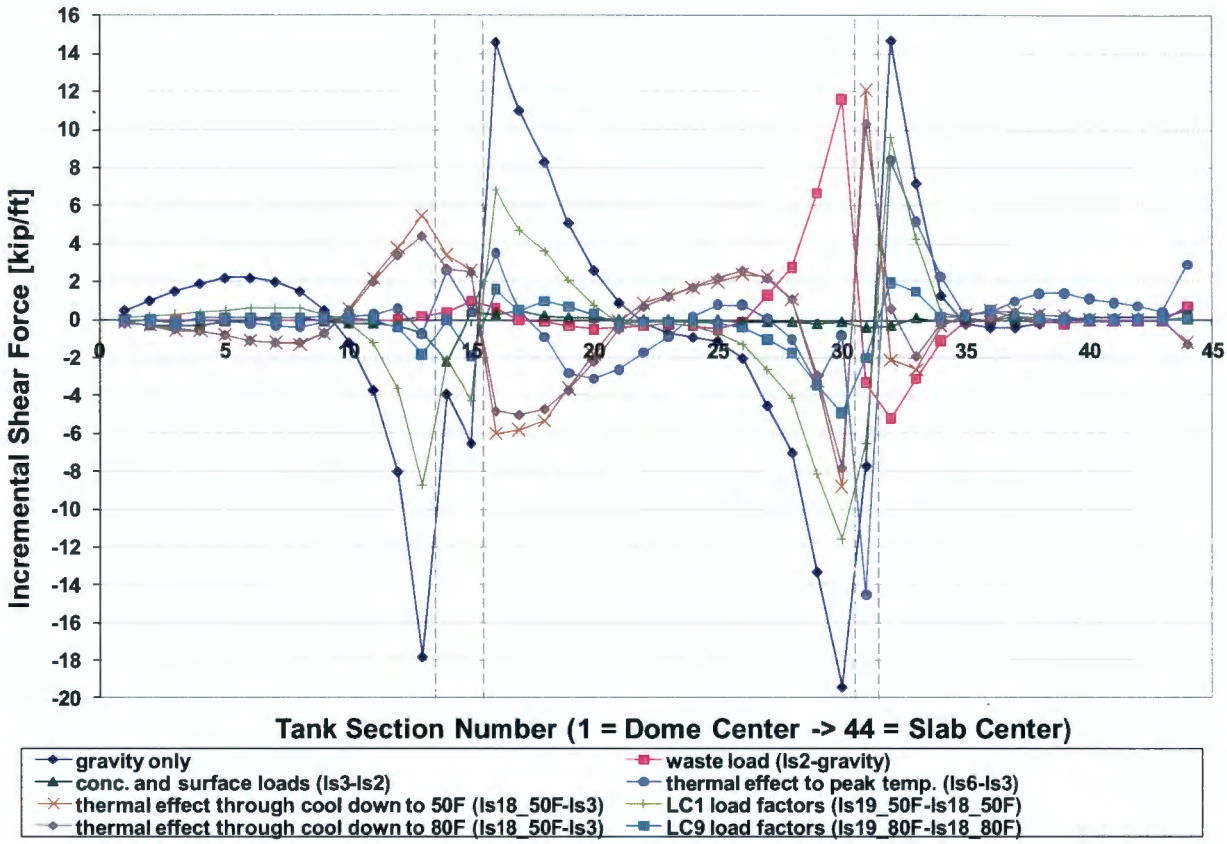

Figure F.10. Incremental Shear Force for Run 1

F.2 Load Effect on Dome and Sidewall Pressures

To further understand the effect that each load has, pressures the soil exerts on the tank, dome, haunch, and sidewall are plotted for each load of Run 1. Figure F.11 shows the dome and haunch pressures for each load step as well as the weight of the soil above the tank for comparison. It can be seen that the outer haunch is the most sensitive to the loads. As demonstrated in Appendix H of the Type II SST AOR (Rinker et al., 2011a), this sharp corner is a location of high soil plasticity; nonetheless the haunch here carries some additional load from soil outside of the soil directly above the tank. Figure F.12 shows the sidewall pressures for each load step along with the at-rest pressure. The at-rest pressure is defined as the at-rest pressure coefficient (0.426) times the weight of the soil above that depth. The lower wall and footing are the most sensitive to the loads, particularly the thermal cycle. Upon completion of the thermal cycle the sidewall pressures are less than those under gravity only in the wall center but slightly greater than those due to the gravity near the top and bottom of the wall. The application of load combinations 1 and 9 causes the peak pressures to exceed those due to gravity only even further; however, the pressure in the middle of the wall remains lower than that due to gravity only.

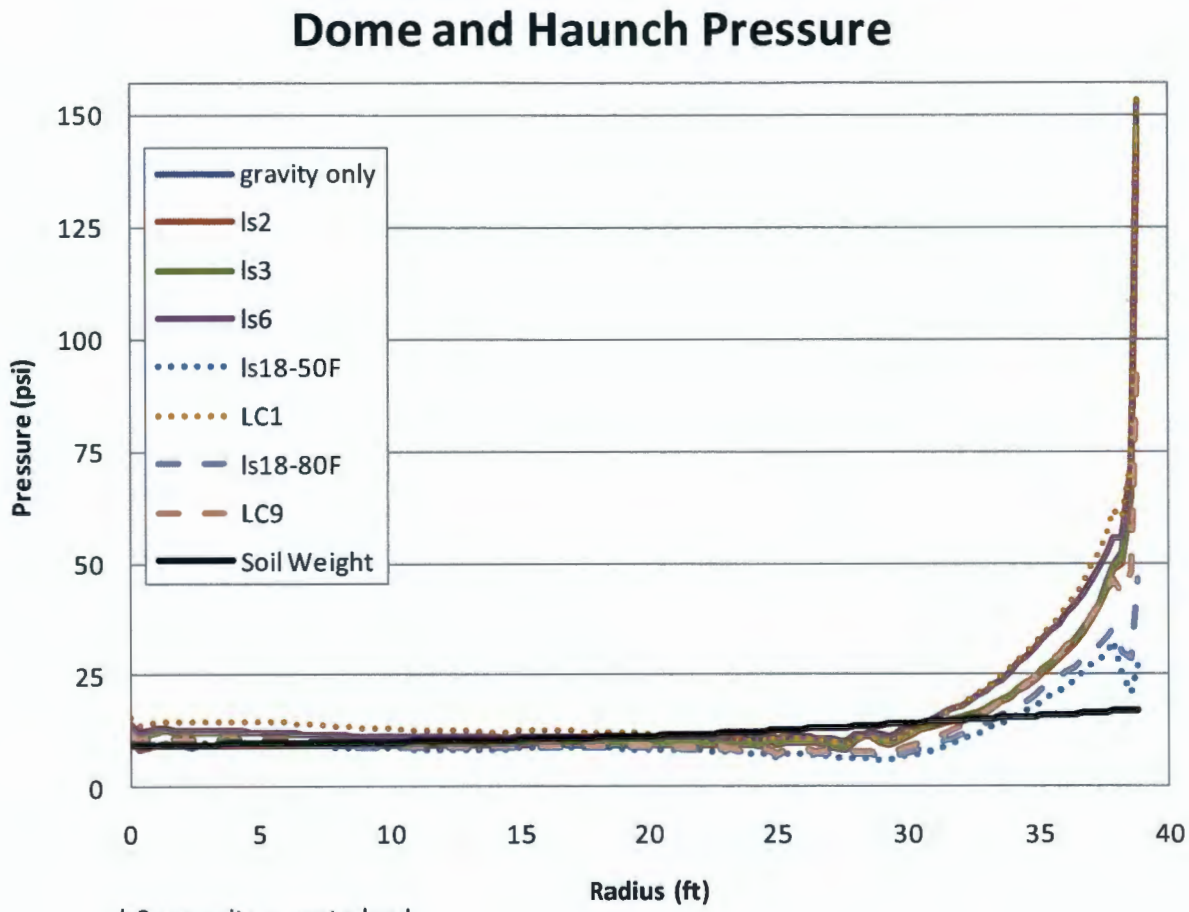

ls2 = gravity + waste load
ls3 = all mechanical loads (gravity + waste load + conc. and surface load)
ls6 = mechanical loads + thermal cycle to peak temp.
ls18-50F = mechanical loads + thermal cycle through cool down to stress free temp.
ls18-80F = mechanical loads + thermal cycle through cool down to present day temp.

Figure F.11. Pressures on Dome and Haunch due to Different Loads for Run 1

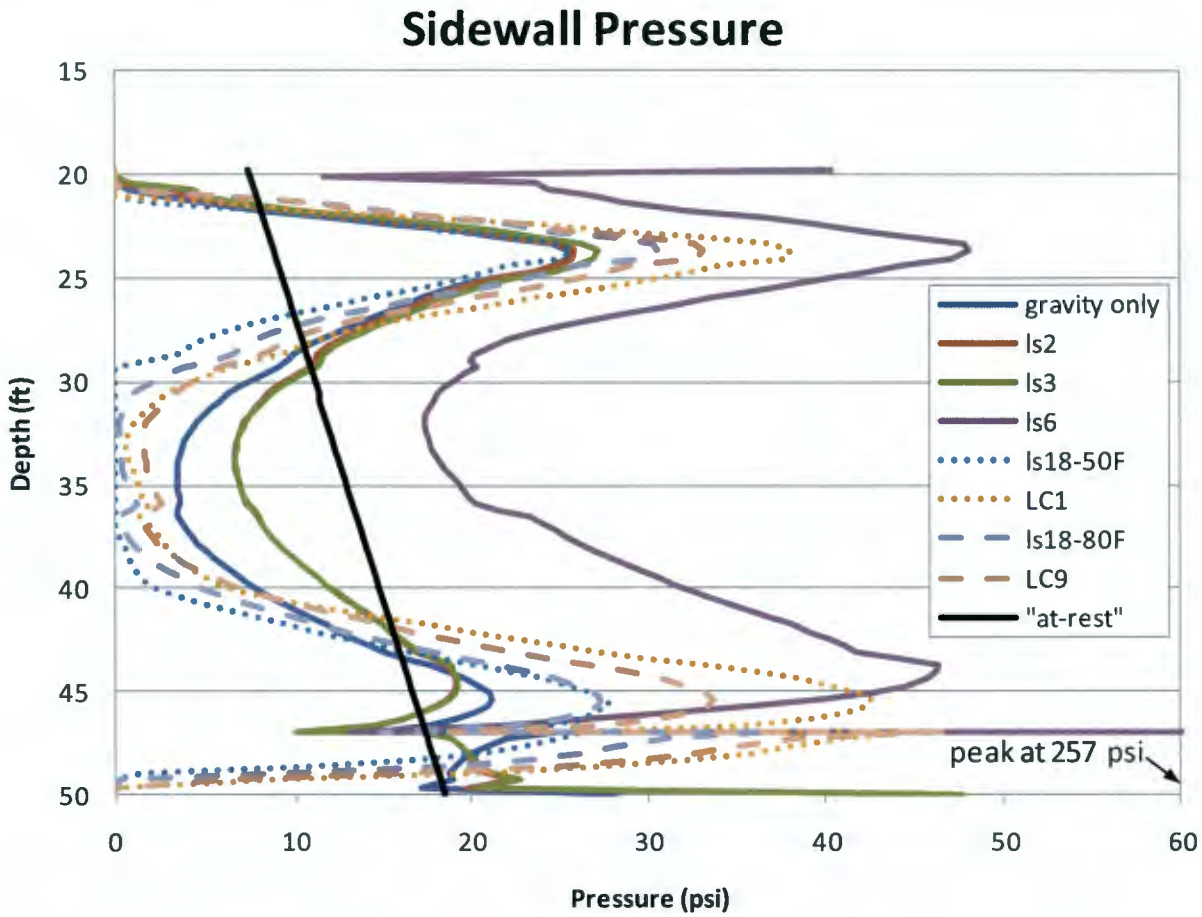

ls2 = gravity + waste load
ls3 = all mechanical loads (gravity + waste load + conc. and surface load)
ls6 = mechanical loads + thermal cycle to peak temp.
ls18-50F = mechanical loads + thermal cycle through cool down to stress free temp.
ls18-80F = mechanical loads + thermal cycle through cool down to present day temp.

Figure F.12. Pressures on Sidewall due to Different Loads for Run 1

F.3 Reference

ACI. 2007. American Concrete Institute Code Requirements for Nuclear Safety Related Concrete Structures. ACI 349-06, American Concrete Institute, Farmington Hills, Michigan.

Rinker MW, KI Johnson, SK Bapanapalli, NK Karri, JE Deibler, SP Pilli, CE Guzman-Leong, SE Sanborn, FG Abatt, JA Dewberry, BM Larsen, KL Stoops, and LJ Julyk. 2011a. Single-Shell Tank Integrity Project Analysis of Record: Hanford Type II Single-Shell Tank Thermal and Operating Loads and Seismic Analysis. RPP-RPT-49989, Rev. 0, Pacific Northwest National Laboratory, Richland, Washington.

This page intentionally left blank.

Appendix G

Alternate Load Factor Study

This page intentionally left blank.

Appendix G

Alternate Load Factor Study

Section 4.1.3 of this report shows the applicable load combinations. In addition to the load combinations presented in Section 4.1.3, Section 9.2.3 of ACI 349 states that "If any load reduces the effects of other loads, the load factors for that load shall be reduced to 0.9 if it is always present or occurs simultaneously with other loads. Otherwise the load factors for that load shall be taken as zero in the additional load case." An alternative load factor case was performed using run #1 to understand the effect of the reduced load factors. This alternative load factor case essentially reduces the lateral soil loads and should be bounded by the low soil runs (Runs 4 and 5). A comparison of the load combination 1 and the alternative load factors is provided here. Table G.1 gives the nominal load values with the corresponding load factors for load combination 1 and the alternative load combination. Figure G.1 shows a typical layout of a single-shell tank along with the soil boundaries used in load and load factor definitions.

Table G.1. Load Combinations

Loading Type	Load	Nominal Value	Load Factor (LC1)	Alternative Load Factors
Structure	Body Load (D)	1 g	1.4	1.4
Structure	Soil Cover (D) (depth at apex of dome)	11 ft	N/A (density is factored)	N/A (density is factored)
Structure	Soil Density – backfill overburden (D)	125 lbf/ft^3	1.4	1.4
	Soil Density – backfill side soil (H)	125 lbf/ft^3	1.7	0.9
	Soil Density – undisturbed	110 lbf/ft^3	N/A	N/A
Normal Op	Uniform Surface Load (L)	40 lbf/ft^2	1.7	1.7
Extended Op	Concentrated Load at dome center (L)	200 kip	1.7	1.7
Normal Op	Waste Specific Gravity (F)	1.7	1.4	1.4
Normal Op	Waste Level	120 in.	N/A (density is factored)	N/A (density is factored)
Normal Op	Thermal cycle as shown in Figure 5.5	Peak of 300°F (tank center bottom)	N/A	N/A

N/A = Not applicable.

Figures G.2, G.3, and G.4 show the demand/capacity plots for meridional, circumferential, and shear for both ACI LC1 and alternative ACI load combination. The D/C values of alternative load cases are slightly higher in the circumferential direction. This is due to the decrease in lateral soil load defined by the new load factor. In general, this alternative load factor case reduces the lateral soil loads, which is similar to the effect of having low soil modulus (Runs 4 and 5).

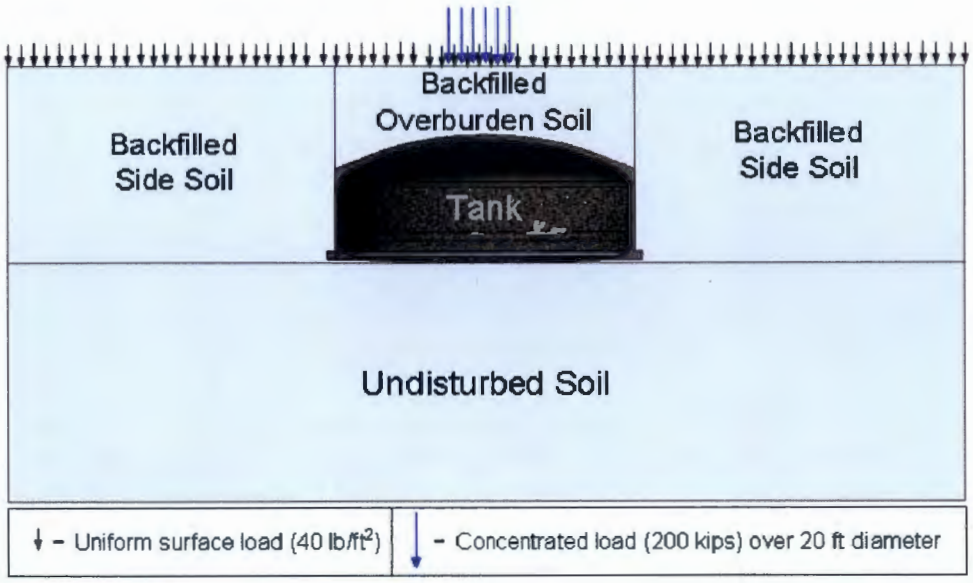

Figure G.1. Typical Layout of a Single-Shell Tank (not to scale)

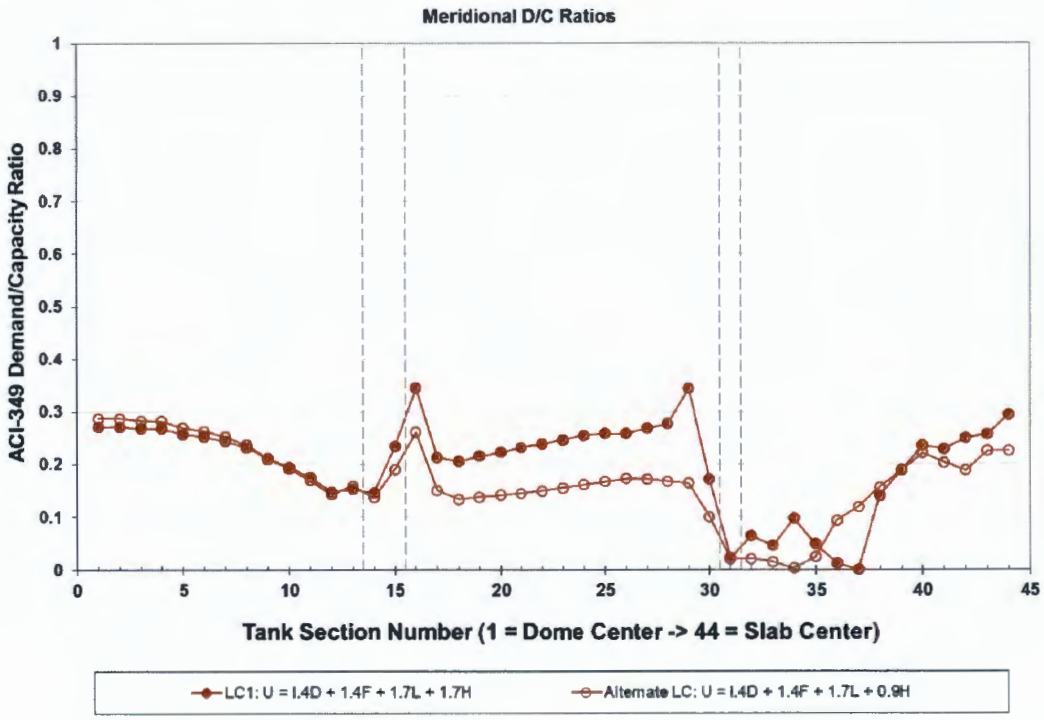

Figure G.2. Meridional ACI D/C Ratios

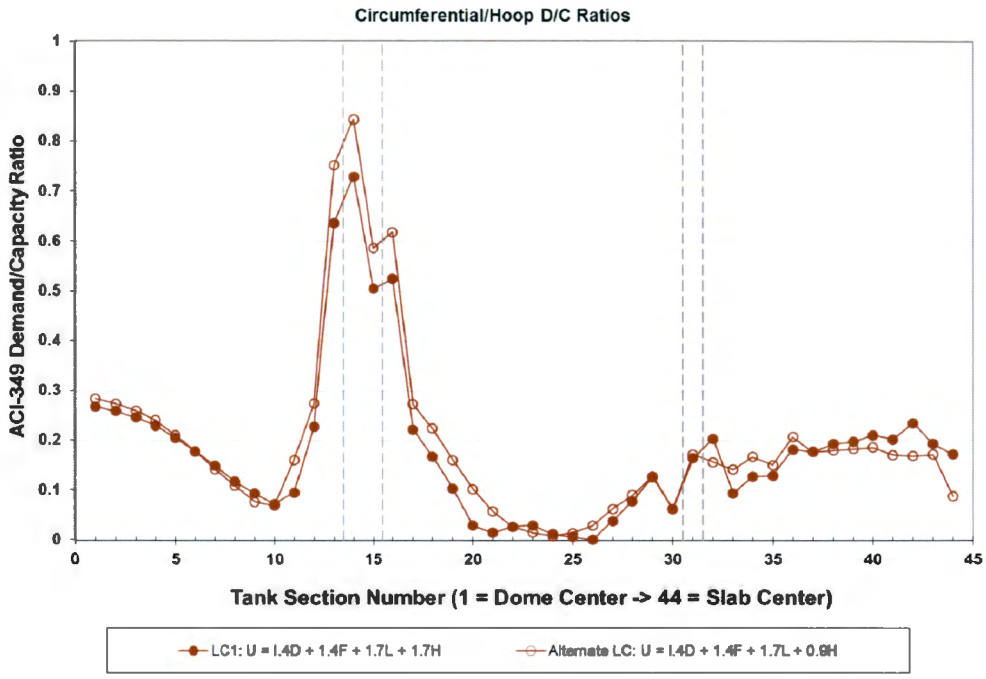

Figure G.3. Circumferential ACI D/C Ratios

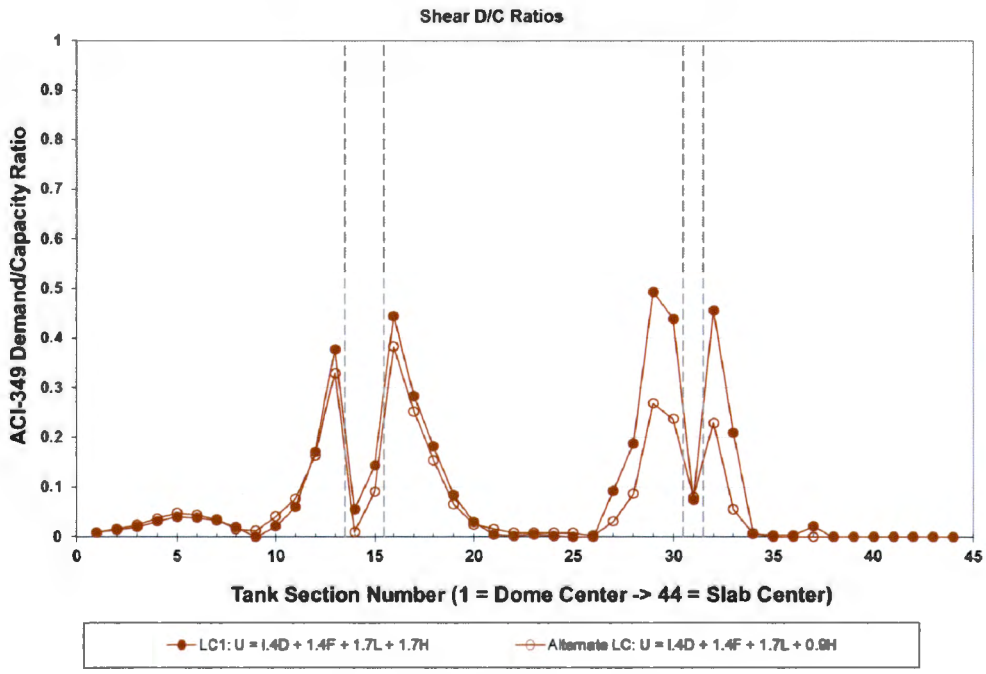

Figure G.4. Shear ACI D/C Ratios

G.1 Reference

ACI. 2007. American Concrete Institute Code Requirements for Nuclear Safety Related Concrete Structures. ACI 349-06, American Concrete Institute, Farmington Hills, Michigan.

Appendix H

Run 6, Forces and Moments

This page intentionally left blank.

Appendix H

Run 6, Forces and Moments

The following figures, Figure H.1 through Figure H.5, show forces and moments of Run 6. Run 6 uses nominal soil modulus, nominal concrete modulus, and nominal concrete tensile strength with creep turned on. ACI evaluation for this run was not performed because of the use of nominal concrete tensile strength.

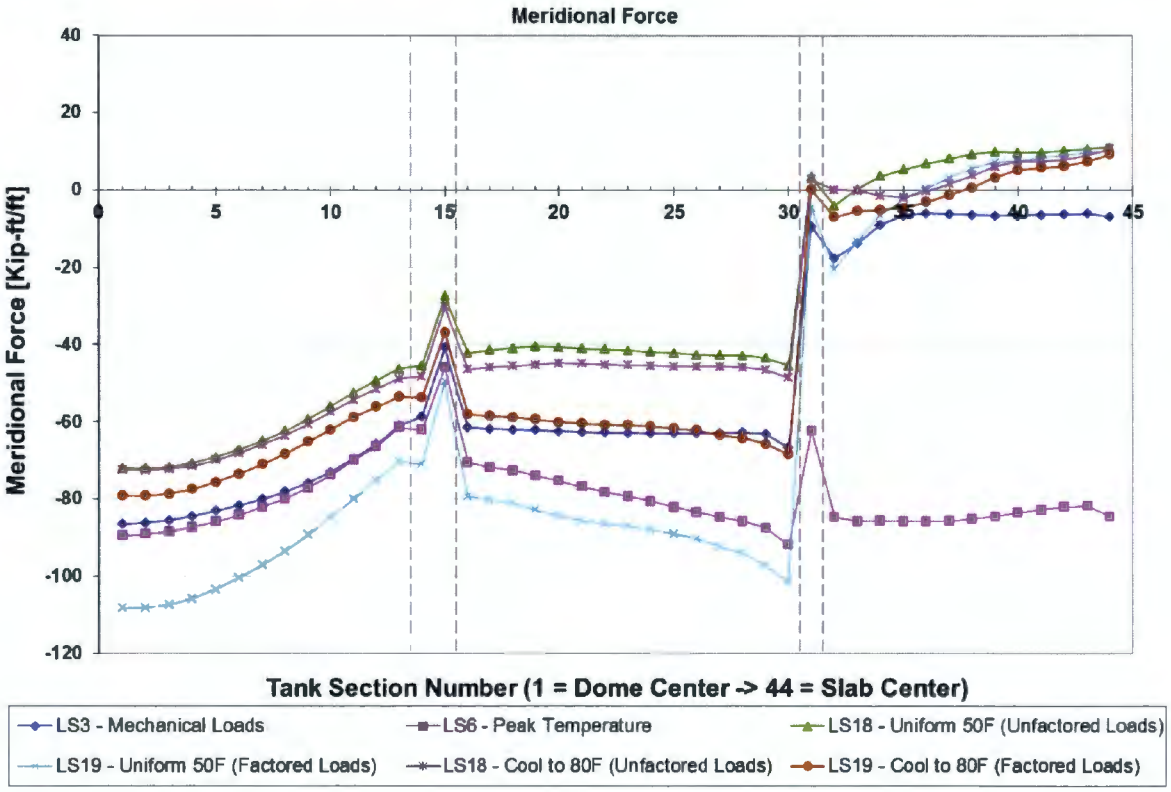

Figure H.1. Run 6, Meridional Force

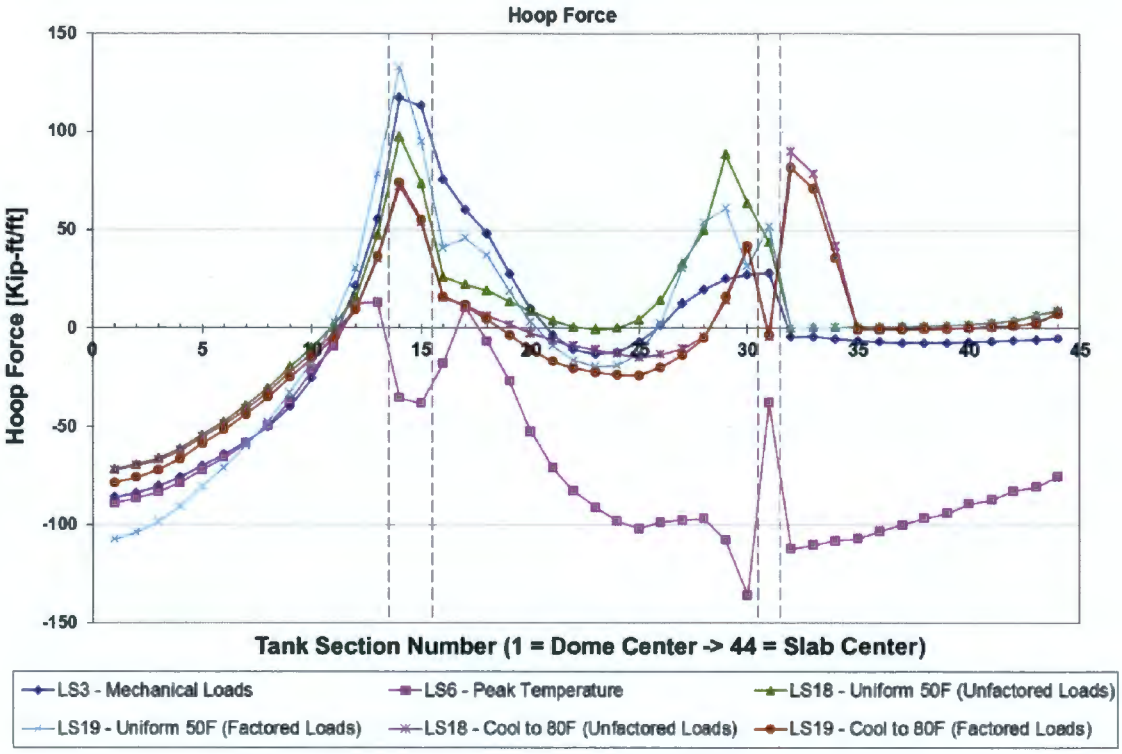

Figure H.2. Run 6, Hoop/Circumferential Force

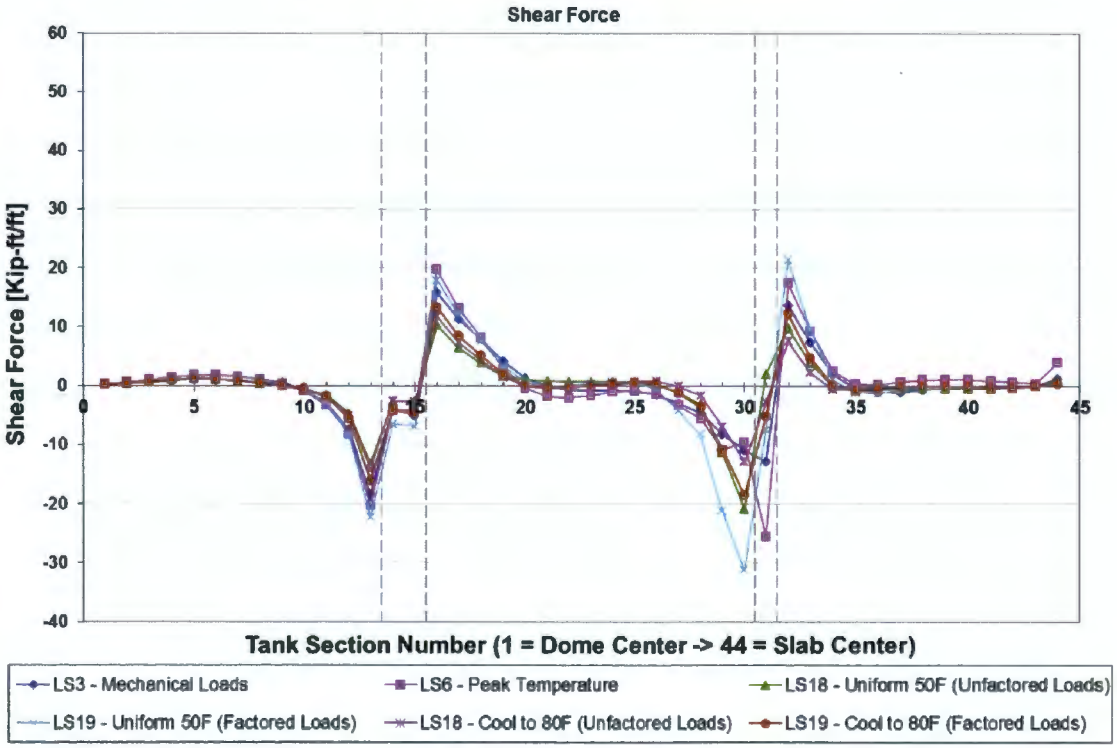

Figure H.3. Run 6, Shear Force

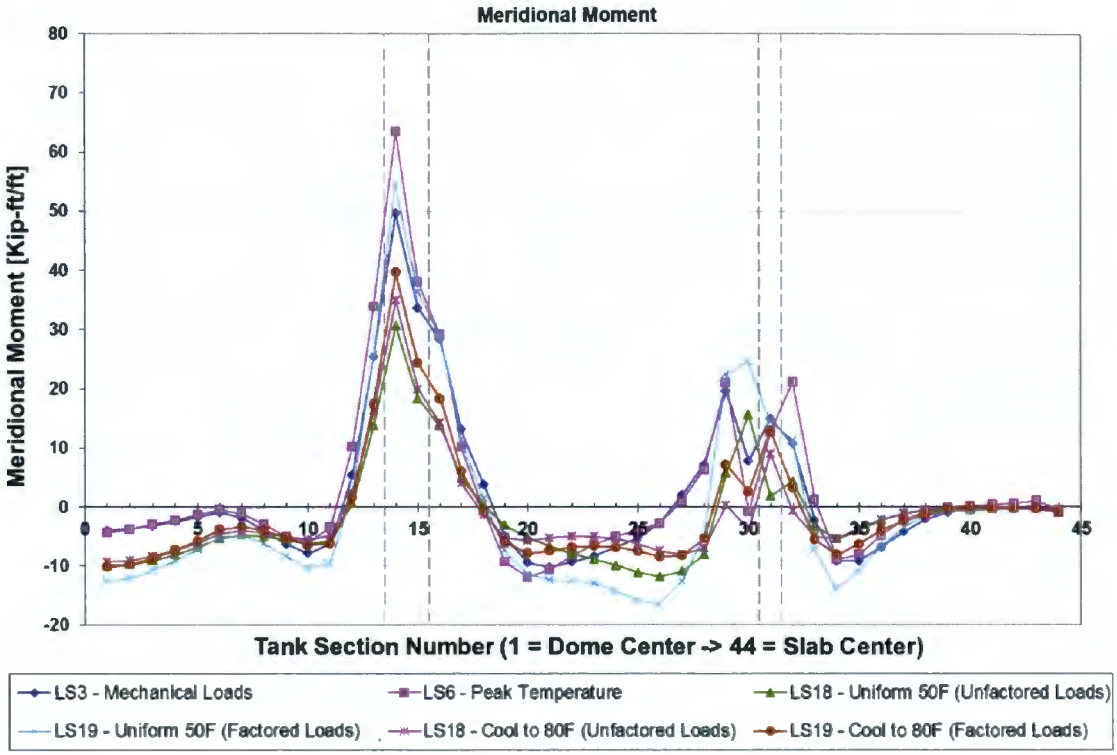

Figure H.4. Run 6, Meridional Moment

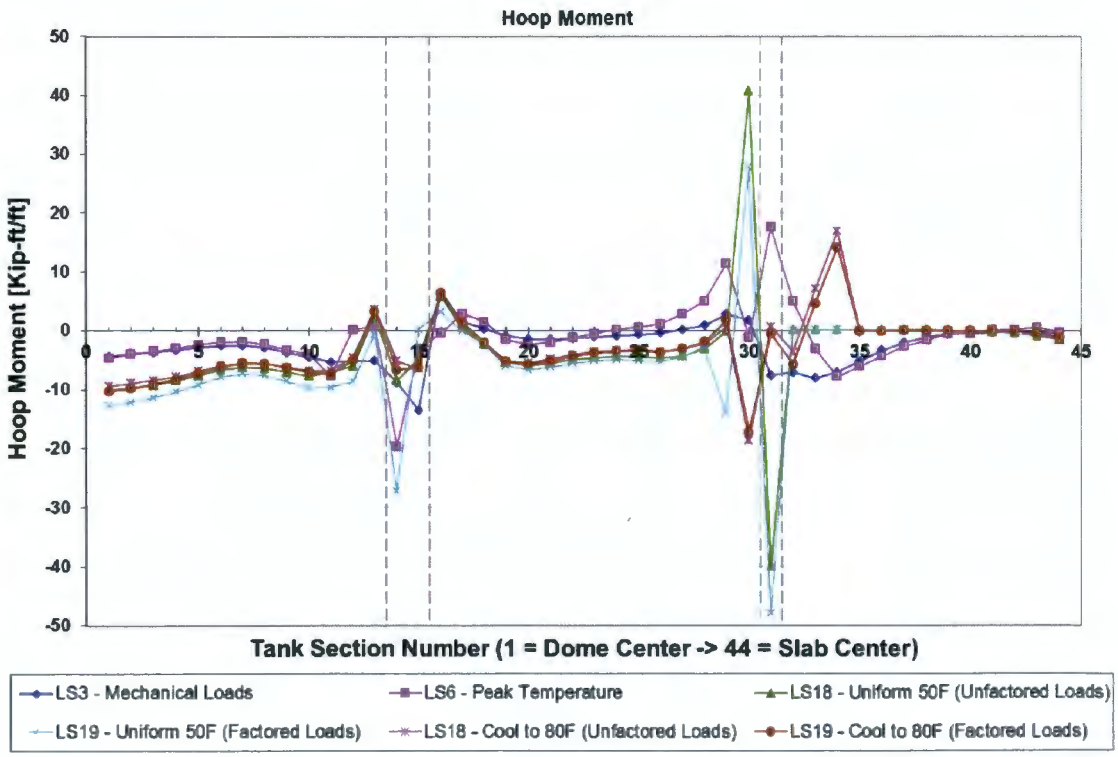

Figure H.5. Run 6, Hoop/Circumferential Moment

This page intentionally left blank.

Appendix I

Buckling Calculation in MathCAD™

This page intentionally left blank.

Appendix I

Buckling Calculations in Mathcad™

This appendix presents the concrete shell buckling calculations that were performed using the Mathcad™ software for the Type III single-shell tank analysis of record. The results of these calculations are summarized in Chapter 12 of this report. The Mathcad™ calculation sheets implement the buckling evaluation methods recommended by Johnson et al. (2010) and they provide easy visualization of both the equations and the results. The same calculation files (with different input data) were used in the buckling evaluation of the Type II single-shell tanks. These methods will also be used in the later buckling analysis of the Type I and IV single-shell tanks. Separate calculation sheets were developed for evaluating the dome and wall of the Type III tanks. This appendix contains the following set of calculations in order:

1. Case 1 dome buckling evaluation for bounding temperature and soil overburden.
2. Case 2 dome buckling evaluation for bounding temperature with actual soil overburden.
3. Case 3 dome buckling evaluation for actual temperature with bounding soil overburden.
4. Case 1 wall buckling evaluation for bounding temperature and soil overburden.
5. Case 2 wall buckling evaluation for bounding temperature with actual soil overburden.
6. Case 3 wall buckling evaluation for actual temperature with bounding soil overburden.

I.1 Reference

Johnson KI, JE Deibler, FG Abatt, and MW Rinker. 2010. *Single-Shell Tank Structural Evaluation Criteria.* RPP-46442, Rev. 0, Pacific Northwest National Laboratory, Richland, Washington.

Calculations for Case 1 – Dome Buckling Evaluation for Bounding Temperature and Soil Overburden

Tank Dome Buckling
Case 1. Type III Baseline, 11-ft Soil, Bounding Temperatures, 95/95 Lower Bound Concrete Properties

The following tank buckling evaluation method is described in:

KI Johnson, JE Deibler, FG Abatt and MW Rinker. 2010. *Single Shell Tank Structural Evaluation Criteria*. PNNL-18837, Rev. 1. Pacific Northwest National Laboratory, Richland, Washington.

Tank Dome Degraded Concrete Properties **Tank Dome Reinforcing Steel Properties**

Maximum Dome temperature during tank life = 221 F Current maximum temp = 80 F for Type III SSTs

Elastic Modulus (95/95 at Temp) $E_c := 2.75 \times 10^6 \text{psi}$ $E_s := 29.4 \times 10^6 \text{psi}$

Concrete Strength (95/95 at Temp), psi $f_{c_min} := 4338 \cdot \text{psi}$

Concrete Density, $d_c := 145 \cdot \text{pcf}$

Poisson's Ratio $\nu := 0.15$ $\nu_s := 0.30$

Tank Geometry - from SST Type III Drawing # H-2-808

Dome minimum wall thickness, t_d, inches $t_d := 15\text{in}$

Dome maximum mid-wall radius of curvature, R_d, feet $R_d := \left[\frac{(96.25 + 95) \cdot \text{ft}}{2}\right] = 95.6 \cdot \text{ft}$

Tank Wall Inner and Outer Radii $r_i := 37\text{ft} + 7.25\text{in} = 37.604\,\text{ft}$ $r_o := r_i + 15 \cdot \text{in} = 466.25 \cdot \text{in}$

Tank cylinder mid-wall radius of curvature, R_c, inches $R_c := \frac{r_i + r_o}{2} = 458.75 \cdot \text{in}$

Tank minimum wall thickness, t_w, inch $t_w := 15\text{in}$

Unfactored Critical Dome Buckling Loads

Uniform Pressure Load $P_{du} := 0.66 \cdot E_c \cdot \left(\frac{t_d}{R_d}\right)^2 = 310.1\,\text{psi}$

Concentrated Center Load

ϕ is half the included angle of the dome $\phi := \text{asin}\left(\frac{R_c}{R_d}\right) = 23.6 \cdot \text{deg}$

Shallowness Parameter, λ $\lambda := \left[12 \cdot \left(1 - \nu^2\right)\right]^{\frac{1}{4}} \cdot \left(\frac{R_d}{t_d}\right)^{\frac{1}{2}} \cdot 2 \cdot \sin\left(\frac{\phi}{2}\right) = 6.6$

According to Baker (1972):

$\lambda < 7$ Buckling will not occur.

$8 < \lambda < 9$ Axisymmetric snap-through is the expected buckling mode, but the shell will continue to take load.

$\lambda > 9$ Asymmetric buckling is expected first, but the shell will continue to carry load.

Pacific Northwest National Laboratory
Tank Dome Buckling, Type-III Single Shell Tanks
Case 1, Bounding Temperature and Soil Depth, 95/95 Lower Bound Concrete

Page 2 of 8
Date: 7/28/2011 By: K. I. Johnson
Chkd: 8/7/2011 By: L. J. Julyk
Revised: 8/10/2011 By: K. I. Johnson

$$D := \frac{E_c t_d^3}{12\cdot\left(1-\nu^2\right)} = 7.912\times 10^8\cdot lbf\cdot in$$

Concentrated Point Load at the Center

$$\alpha 1 P_{dc} := \frac{28\cdot\pi\cdot D}{R_d} = 6.065\times 10^7\cdot lbf$$

Fitch and Budiansky (1970) present the buckling solution for a spherical cap loaded by a local pressure distributed over a circle of radius, Rcl. They present the solution as a function of the parameter, λbar, which is in turn a function of the loading radius, the dome radius, the dome thickness, and the Poisson's ratio.

The tank operating limits specify a 200-kip concentrated load over a circle of 10-ft radius at the dome center. The soil overburden depth further distributes the pressure load over a larger radius, which is a function of the overburden depth and the internal friction angle of the soil.

Load Radius $R_l := 10\cdot ft$ Soil depth $h_s := 11\cdot ft$ Soil Friction Angle $\phi_s := 35\cdot deg$

Load radius at the tank dome $R_{cl} := R_l + h_s\cdot\tan\left(\phi_s\right) = 17.702\,ft$

$$\lambda_{bar} := \left[12\cdot\left(1-\nu^2\right)\right]^{\frac{1}{4}}\cdot\left(\frac{t_d}{R_d}\right)^{\frac{1}{2}}\cdot\left(\frac{R_{cl}}{t_d}\right) = 3$$

$p_c := 0.42$ See plot below

The buckling sensitivity parameter, p_c, is interpolated from the right vertical axis of the plot below (Fitch and Budiansky, 1970).

CRITICAL LOAD

IMPERFECTION SENSITIVITY PARAMETER

SLOPE PARAMETER OF POSTBUCKLING LOAD-DEFLECTION CURVE

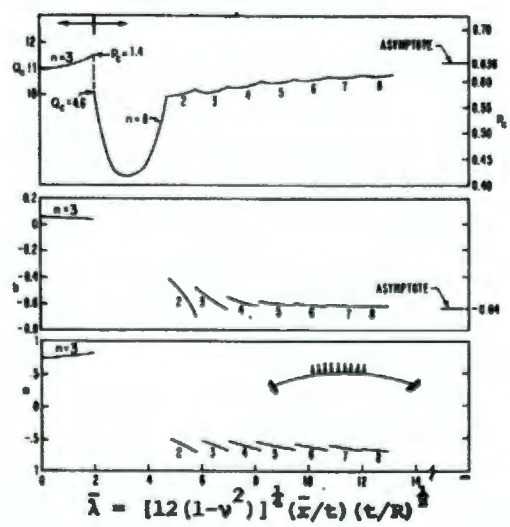

DEPTH PARAMETER $\bar{\lambda}$ FOR LOADED REGION

Total buckling force of a pressure acting over a 10-ft radius circle at the soil surface

$$\alpha 1P_{dL} := p_c \cdot 2\pi \cdot R_{cl}^2 \cdot \frac{E_c}{\sqrt{3 \cdot (1-\nu^2)}} \cdot \left(\frac{t_d}{R_d}\right)^2 = 3.268 \times 10^7 \cdot lbf$$

This is 54% of the buckling point load $\frac{\alpha 1P_{dL}}{\alpha 1P_{dc}} = 0.54$

Use the minimum of the concentrated load estimates $\alpha 1P_{dconc} := \min(\alpha 1P_{dc}, \alpha 1P_{dL}) = 3.268 \times 10^7$ lbf

Buckling Load Reduction Factors

α_1 = The Geometric Imperfection Factor

Seide (1981) provides the following equation for the lower bound fit of buckling experiments of cylindrical shells in compression. Popov and Medwadowski (1981) recommend this approximation of α_1 for other shell geometries (including shallow domes) when no specific solution is available.

Dome, α_{1d}

$$\alpha_{1d} := 1 - 0.9 \cdot \left(1 - \exp\left(\frac{-1}{16} \cdot \sqrt{\frac{R_d}{t_d}}\right)\right) = 0.621$$

which is valid for $100 \le \frac{R}{t} \le 3000$

but for the dome: $\frac{R_d}{t_d} = 76.5$ Therefore, the SST Structural Evaluation Criteria conservatively assumes R/t=100 for the dome.

Recommended Value for both uniform and concentrated loads

$$\alpha_{1d} := 1 - 0.9 \cdot \left(1 - \exp\left(\frac{-1}{16} \cdot \sqrt{100}\right)\right) = 0.58$$

α_2 = The Creep Buckling Load-Reduction Factor

Creep strains were predicted by the ANSYS finite element mode of the Type-III tank. The maximum temperature history for Type-III tanks was applied over the 60-year current life of the tanks.

C_u = ultimate creep strain / initial elastic strain

C_u is from Type III ANSYS model, hoop strains in Dome

$$C_{ua} := \frac{1.38 \times 10^{-4}}{6.26 \times 10^{-5}} = 2.204$$

$$\alpha_{2a} := \frac{1}{(1 + C_{ua})} = 0.312$$

If a creep analysis is not available, Popov and Medwadowski (1981) recommend the following as an estimate of the ultimate creep coefficient, C_u:

$C_u = 4 - 2\log(f_c)$ where f_c is the concrete strength at the time of loading in N/mm².

$$f_c := \frac{f_{c_min}}{1ksi} \cdot 6.895 = 29.9 \quad C_{ub} := 4 - 2\log(f_c) = 1.048 \quad \alpha_{2b} := \frac{1}{(1 + C_{ub})} = 0.488$$

Use the maximum C_u to obtain the minimum creep reduction factor

$$C_u := \max(C_{ua}, C_{ub}) = 2.204$$

$$\alpha_2 := \frac{1}{(1 + C_u)} = 0.312$$

Pacific Northwest National Laboratory
Tank Dome Buckling, Type-III Single Shell Tanks
Case 1: Bounding Temperature and Soil Depth, 95/95 Lower Bound Concrete

Page 4 of 8
Date: 7/28/2011 By: K.I. Johnson
Chkd: 8/7/2011 By: L.J. Julyk
Revised: 8/10/2011 By: K.I. Johnson

α_3 = The Buckling Load-Reduction Factor Accounting for Cracking and the Amount and Type of Reinforcement.

E_{C2eol} is the effective concrete modulus in the dome accounting for creep strain and end-of-life degraded concrete modulus, E_{Ceol}.

Must use the degraded concrete modulus based on thermal history

$E_{Ceol} := E_C = 2.75 \times 10^6$ psi $\qquad E_{C2eol} := \frac{E_{Ceol}}{(1 + C_u)} = 8.582 \times 10^5$ psi

Rebar Size and Spacing from SST Type-III Drawing # H-2-813

$\eta := \frac{E_s}{E_{C2eol}} = 34.259$ $\qquad$ $Bar := 6$ Rebar Size (in 1/8th of an inch)

$S_p := 12$ Bar Spacing near inner and outer surfaces. Varies from 6 to 12 inch in the dome. Use 12 inch for conservatism

$A_s := 2 \cdot \left(\frac{Bar}{8}\right)^2 \cdot \frac{\pi}{4} \cdot \frac{12}{S_p} = 0.884$ Steel Area, in²/ft

$A_c := 12 \cdot \frac{t_d}{in} = 180$ Concrete Area, in²/ft $\qquad \rho := \frac{A_s}{A_c} = 0.00491$

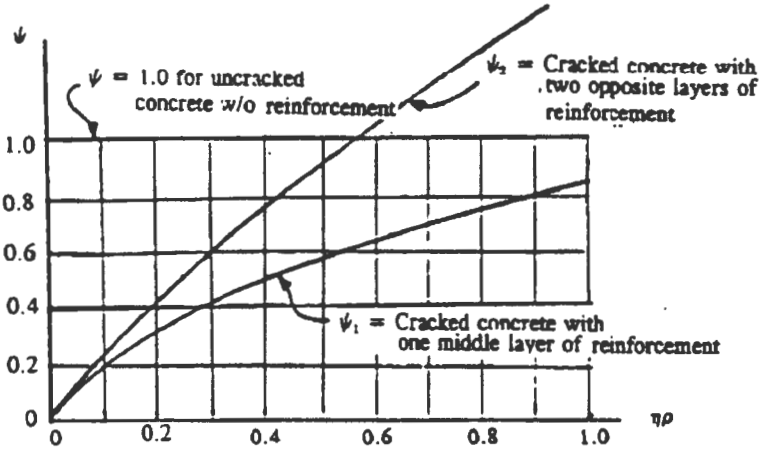

Values of ψ for Effect of Concrete Cracking And Amounts and Type of Reinforcement (Figure 4 of Scordelis 1981).

Must interpolate by eye

From the above plot for cracked concrete with two opposite layers of reinforcement. $\qquad \eta \cdot \rho = 0.168 \qquad \psi := 0.35$

Pacific Northwest National Laboratory
Tank Dome Buckling, Type-III Single Shell Tanks
Case 1, Bounding Temperature and Soil Depth, 95/95 Lower Bound Concrete

Page 5 of 8
Date: 7/28/2011 By: K. I. Johnson
Chkd: 8/7/2011 By: L. J. Julyk
Revised: 8/10/2011 By: K. I. Johnson

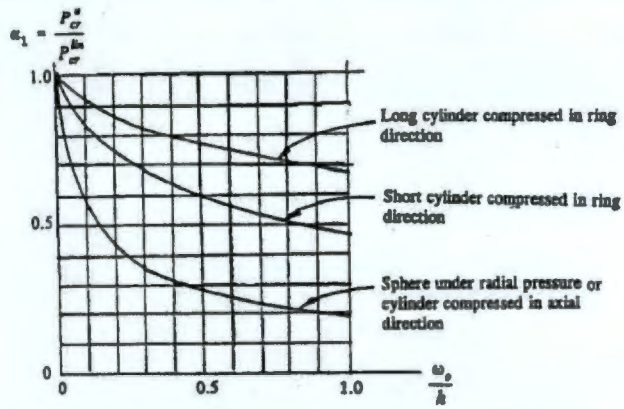

Effect of Geometric Imperfections on Buckling Load (Figure 3 of Scordelis 1981). ω_0/h factors for different geometries for specified geometric imperfection factor, α_1.

Must interpolate by eye

Dome = Sphere under radial pressure $\alpha_{1d} = 0.58$ $\omega_{ohd} := 0.1$

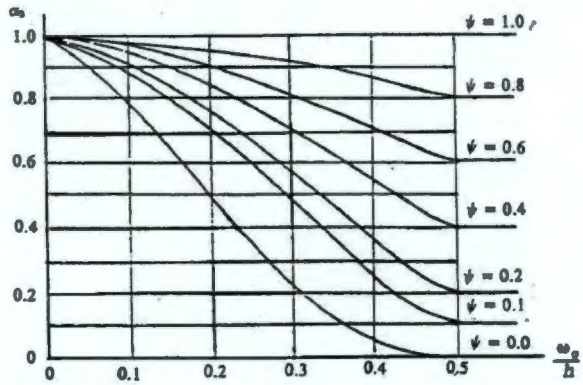

Reduction Factor α_3 for Concrete Cracking and Amount and Type of Reinforcement (Figure 5 of Scordelis 1981)

Must interpolate by eye

Dome = Sphere under radial pressure

$\alpha_{1d} = 0.58$ $\omega_{ohd} = 0.1$ $\psi = 0.35$ $\alpha_{3d} := 0.94$

Calculate $P_3 = \alpha_1\alpha_2\alpha_3 P_{buckle}$ and α_4 for highly loaded nonlinear concrete material effects

Uniform Dome Pressure, psi

$P_{3du} := \alpha_{1d}\cdot\alpha_2\cdot\alpha_{3d}\cdot P_{du} = 52.9\,psi$ This is based on the closed-form theoretical buckling load

Uniform Ultimate Pressure Load from SST Finite Element Analysis - NOTE, this pressure is the total effective ultimate dome pressure including:

- Dome weight (Concrete density=145 pcf)
- Soil overburden =11 ft at 125 pcf
- Pressure over dome diameter at the ultimate load capacity.

$P_{ult_u} := 50.1\cdot psi$ Type-III finite element ultimate load analysis for 95/95 lower bound properties

$$Ru(\alpha_4) := (\alpha_4)^2\left(\frac{P_{3du}}{P_{ult_u}}\right)^2 + (\alpha_4 - 1) \qquad \alpha_{4du} := root(Ru(\alpha_4), \alpha_4, 0.01, 0.99) = 0.599$$

Reduced Uniform Dome Buckling Load $P_{du_red} := \alpha_{4du}\cdot P_{3du} = 31.7\,psi$

Total Uniform Load Reduction Factor $\alpha_{dc} := \alpha_{1d}\cdot\alpha_2\cdot\alpha_{3d}\cdot\alpha_{4du} = 0.1$

Concentrated Ultimate Dome Load, lbf

$P_{3dc} := \alpha_2\cdot\alpha_{3d}\cdot\alpha 1 P_{dconc} = 9.585\times 10^6\,lbf$

Concentrated Ultimate Load from SST Finite Element Analysis - NOTE, this is the total effective ultimate concentrated dome load accounting for the effects of:

- Dome weight (Concrete density=145 pcf)
- Soil overburden =11 ft at 125 pcf
- Pressure over dome diameter at the ultimate load capacity.

$P_{ult_c} := 3675\cdot tonf$ Type-III finite element ultimate load analysis for 95/95 lower bound

$$Rc(\alpha_4) := (\alpha_4)^2\left(\frac{P_{3dc}}{P_{ult_c}}\right)^2 + (\alpha_4 - 1) \qquad \alpha_{4dc} := root(Rc(\alpha_4), \alpha_4, 0.01, 0.99) = 0.527$$

Reduced Concentrated Dome Buckling Load $P_{dc_red} := \alpha_{4dc}\cdot P_{3dc} = 5.05\times 10^6\,lbf$

Total Concentrated Load Reduction $\alpha_{dc} := \alpha_{1d}\cdot\alpha_2\cdot\alpha_{3d}\cdot\alpha_{4dc} = 0.09$

Buckling Safety Factors

From the IASS Working Group No. 5, *Recommendations for Reinforced Concrete Shells and Folded Plates*, (IASS, 1979):
For shells that do not experience a reduction in load-carrying capacity in the post-buckling regime, a factor of safety of 1.75 is recommended. For shells that do experience a reduction in the load-carrying capacity in the post-buckling regime, a factor of safety of 3.5 is recommended.

Dome Uniform Pressure $SF_{du} := 3.5$ Post Buckling = Reduced Load Capacity

Dome Concentrated Load $SF_{dc} := 1.75$ Post Buckling = Increasing Load Capacity

But for a distributed local load with $\lambda_{bar} > 2$, the buckling will be accompanied by a loss of load carrying capacity. $\lambda_{bar} = 2.88$ so the safety factor should be 3.5

Dome Local Distributed Center Load $SF_{dlc} := 3.5$ Post Buckling = Reduced Load Capacity

Applied Loads on the Tank Dome

Dome Uniform Pressure = Concrete Dome Weight + Soil Overburden + Design Live Load

Dome Thickness, inch $t_d = 1.25\,ft$ Concrete Density, pcf $d_c = 145 \cdot pcf$ $P_d := t_d \cdot d_c = 1.259\,psi$

Soil Depth, h_s $h_s = 11\,ft$ Soil Density, d_s $d_s := 125\,pcf$ Soil Pressure $P_s := h_s \cdot d_s = 9.549\,psi$

Uniform Live Load $L_u := 40\,psf$ Total Uniform Load $Pr_{du} := P_d + P_s + L_u = 11.085\,psi$

Dome Specified Concentrated Load, $F_{dc} := 200000\,lbf$

Dome Buckling - Linear Combination of Uniform and Concentrated Loads

Applied Pressure on the Dome, psi $Pr_{du} = 11.09\,psi$

Reduced Uniform Dome Pressure Capacity, psi $P_{du_red} = 31.72\,psi$

Applied Concentrated Dome Load, lbf $F_{dc} = 2 \times 10^5\,lbf$

Reduced Concentrated Dome Load Capacity, lbf $P_{dc_red} = 5.054 \times 10^6\,lbf$

Uniform Load Fraction of Dome Buckling Capacity

$$R_{Uniform} := SF_{du} \cdot \left(\frac{Pr_{du}}{P_{du_red}}\right) = 1.223$$

Concentrated Load Fraction of Dome Buckling Capacity

$$R_{Concentrated} := SF_{dc} \cdot \left(\frac{F_{dc}}{P_{dc_red}}\right) = 0.139$$

Combined Fraction of Dome Buckling Capacity

$$R_{dome} := SF_{du} \cdot \left(\frac{Pr_{du}}{P_{du_red}}\right) + SF_{dc} \cdot \left(\frac{F_{dc}}{P_{dc_red}}\right) = 1.362$$

What Safety Factors give a Demand/Capacity Ratio of 1.0?

Uniform Load Safety Factor on Dome Buckling

$$SF_{act_U} := \frac{SF_{du}}{R_{dome}} = 2.57$$

Concentrated Load Safety Factor on Dome Buckling

$$SF_{act_C} := \frac{SF_{dc}}{R_{dome}} = 2.57$$

References

Baker EH, L Kovalevsky, and FL Rish. 1972. *Structural Analysis of Shells.* McGraw-Hill, New York, New York.

Fitch, JR and B Budiansky. 1970. "Buckling and Postbuckling Behavior of Spherical Caps under Axisymmetric Load." AIAA Journal, Vol. 8, No. 4, pp. 686-693.

IASS. 1979. *Recommendations for Reinforced Concrete Shells and Folded Plates.* Prepared by the Working Group No. 5 of The International Association for Shell and Spatial Structures (IASS), Stefan J. Medwadowski, Chairman. International Association for Shell and Spatial Structures, Madrid, Spain.

KI Johnson, JE Deibler, FG Abatt and MW Rinker. 2010. *Single Shell Tank Structural Evaluation Criteria.* PNNL-18837, Rev. 1. Pacific Northwest National Laboratory, Richland, Washington.

Popov EP and SJ Medwadowski. 1981. "Stability of Reinforced Concrete Shells: State-of-the-Art Overview." In *Concrete Shell Buckling*, ACI SP-67, American Concrete Institute, Detroit, Michigan.

Scordelis AC. 1981. "Stability of Reinforced Concrete Domes and Hyperbolic Paraboloid Shells." In *Concrete Shell Buckling*, ACI SP-67, American Concrete Institute, Detroit, Michigan.

Calculations for Case 2 – Dome Buckling Evaluation for Bounding Temperature with Actual Soil Overburden

Pacific Northwest National Laboratory
Tank Dome Buckling, Type-III Single Shell Tanks
Case 2. Bounding Temperature with 6.85-ft Soil Depth, 95/95 Lower Bound Concrete

Page 1 of 8
Date: 7/28/2011 By: K. I. Johnson
Chkd: 8/7/2011 By: L. J. Julyk
Revised: 8/10/2011 By: K. I. Johnson

Tank Dome Buckling
Case 2. Type III, 6.85-ft Soil, 434 Kip Concentrated Load, Bounding Temperatures, 95/95 Lower Bound Concrete Properties

The following tank buckling evaluation method is described in:

KI Johnson, JE Deibler, FG Abatt and MW Rinker. 2010. *Single Shell Tank Structural Evaluation Criteria*. PNNL-18837, Rev. 1. Pacific Northwest National Laboratory, Richland, Washington.

Tank Dome Degraded Concrete Properties | **Tank Dome Reinforcing Steel Properties**

Maximum Dome temperature during tank life = 221 F | Current maximum temp = 80 F for Type III SSTs

Elastic Modulus (95/95 at Temp) $E_c := 2.75 \times 10^6 \text{psi}$ $E_s := 29.4 \times 10^6 \text{psi}$

Concrete Strength (95/95 at Temp), psi $f_{c_min} := 4338 \cdot \text{psi}$

Concrete Density, $d_c := 145 \cdot \text{pcf}$

Poisson's Ratio $\nu := 0.15$ $\nu_s := 0.30$

Tank Geometry - from SST Type III Drawing # H-2-808

Dome minimum wall thickness, t_d, inches $t_d := 15\text{in}$

Dome maximum mid-wall radius of curvature, R_d, inches $R_d := \left[\frac{(96.25 + 95) \cdot \text{ft}}{2}\right] = 95.6 \cdot \text{ft}$

Tank Wall Inner and Outer Radii $r_i := 37\text{ft} + 7.25\text{in} = 37.604\text{ft}$ $r_o := r_i + 15 \cdot \text{in} = 466.25 \cdot \text{in}$

Tank cylinder mid-wall radius of curvature, R_c, inches $R_c := \frac{r_i + r_o}{2} = 458.75 \cdot \text{in}$

Tank minimum wall thickness, t_w, inch $t_w := 15\text{in}$

Unfactored Critical Dome Buckling Loads

Uniform Pressure Load $P_{du} := 0.66 \cdot E_c \cdot \left(\frac{t_d}{R_d}\right)^2 = 310.1\,\text{psi}$

Concentrated Center Load

ϕ is half the included angle of the dome $\phi := \text{asin}\left(\frac{R_c}{R_d}\right) = 23.6 \cdot \text{deg}$

Shallowness Parameter, λ $\lambda := \left[12 \cdot \left(1 - \nu^2\right)\right]^{\frac{1}{4}} \cdot \left(\frac{R_d}{t_d}\right)^{\frac{1}{2}} \cdot 2 \cdot \sin\left(\frac{\phi}{2}\right) = 6.6$

According to Baker (1972):

$\lambda < 7$ Buckling will not occur.

$8 < \lambda < 9$ Axisymmetric snap-through is the expected buckling mode, but the shell will continue to take load.

$\lambda > 9$ Asymmetric buckling is expected first, but the shell will continue to carry load.

$$D := \frac{E_c t_d^3}{12\cdot(1-\nu^2)} = 7.912\cdot 10^8\cdot lbf\cdot in$$

Concentrated Point Load at the Center

$$\alpha 1P_{dc} := \frac{28\cdot\pi\cdot D}{R_d} = 6.065\cdot 10^7\cdot lbf$$

Fitch and Budiansky (1970) present the buckling solution for a spherical cap loaded by a local pressure distributed over a circle of radius, Rcl. They present the solution as a function of the parameter, λbar, which is in turn a function of the loading radius, the dome radius, the dome thickness, and the Poisson's ratio.

The tank operating limits specify a maximum 434-kip concentrated load for Tank S-104 (6.85 ft of soil at 125 lb/ft^3) over a circle of 10-ft radius at the dome center. The soil overburden depth further distributes the pressure load over a larger radius, which is a function of the overburden depth and the internal friction angle of the soil.

Load Radius $R_l := 10\cdot ft$ Soil depth $h_s := 6.85\cdot ft$ Soil Friction Angle $\phi_s := 35\cdot deg$

Load radius at the tank dome $R_{cl} := R_l - h_s\cdot\tan(\phi_s) = 14.796\,ft$

$$\lambda_{bar} := \left[12\cdot(1-\nu^2)\right]^{\frac{1}{4}}\cdot\left(\frac{t_d}{R_d}\right)^{\frac{1}{2}}\cdot\left(\frac{R_{cl}}{t_d}\right) = 2.5 \qquad p_c := 0.48 \quad \text{See plot below}$$

The buckling sensitivity parameter, p_c, is interpolated from the right vertical axis of the plot below (Fitch and Budiansky, 1970).

CRITICAL LOAD

IMPERFECTION SENSITIVITY PARAMETER

SLOPE PARAMETER OF POSTBUCKLING LOAD-DEFLECTION CURVE

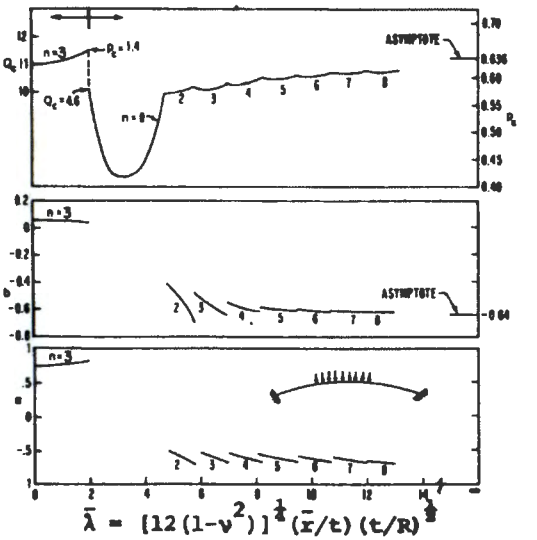

DEPTH PARAMETER $\bar{\lambda}$ FOR LOADED REGION

Total buckling force of a pressure acting over a 10-ft radius circle at the soil surface

$$\alpha 1P_{dL} := p_c \cdot 2\pi \cdot R_d^2 \cdot \frac{E_c}{\sqrt{3 \cdot (1-\nu^2)}} \cdot \left(\frac{t_d}{R_d}\right)^2 = 2.609 \times 10^7 \cdot \text{lbf}$$

This is 43% of the buckling point load $\frac{\alpha 1P_{dL}}{\alpha 1P_{dc}} = 0.43$

Use the minimum of the concentrated load estimates $\alpha 1P_{dconc} := \min(\alpha 1P_{dc}, \alpha 1P_{dL}) = 2.609 \times 10^7 \text{ lbf}$

Buckling Load Reduction Factors

α_1 = The Geometric Imperfection Factor

Seide (1981) provides the following equation for the lower bound fit of buckling experiments of cylindrical shells in compression. Popov and Medwadowski (1981) recommend this approximation of α_1 for other shell geometries (including shallow domes) when no specific solution is available.

Dome, α_{1d}

$$\alpha_{1d} := 1 - 0.9 \cdot \left(1 - \exp\left(\frac{-1}{16} \cdot \sqrt{\frac{R_d}{t_d}}\right)\right) = 0.621$$

which is valid for $100 \le \frac{R}{t} \le 3000$

but for the dome: $\frac{R_d}{t_d} = 76.5$ Therefore, the SST Structural Evaluation Criteria conservatively assumes R/t=100 for the dome.

Recommended Value for both uniform and concentrated loads

$$\alpha_{1d} := 1 - 0.9 \cdot \left(1 - \exp\left(\frac{-1}{16} \cdot \sqrt{100}\right)\right) = 0.58$$

α_2 = The Creep Buckling Load-Reduction Factor

Creep strains were predicted by the ANSYS finite element model of the Type-III tank. The maximum temperature history for Type-III tanks was applied over the 60-year current life of the tanks.

C_u = ultimate creep strain / initial elastic strain

C_u is from Type III ANSYS model, hoop strains in Dome

$$C_{ua} := \frac{10.5 \times 10^{-5}}{6.16 \times 10^{-5}} = 1.705$$

$$\alpha_{2a} := \frac{1}{(1 + C_{ua})} = 0.37$$

If a creep analysis is not available, Popov and Medwadowski (1981) recommend the following as an estimate of the ultimate creep coefficient, C_u:

$C_u = 4 - 2\log(f_c)$ where f_c is the concrete strength at the time of loading in N/mm^2.

$$f_c := \frac{f_{c_min}}{1\text{ksi}} \cdot 6.895 = 29.9 \quad C_{ub} := 4 - 2\log(f_c) = 1.048 \quad \alpha_{2b} := \frac{1}{(1 + C_{ub})} = 0.488$$

Use the maximum C_u to obtain the minimum creep reduction factor

$$C_u := \max(C_{ua}, C_{ub}) = 1.705$$

$$\alpha_2 := \frac{1}{(1 + C_u)} = 0.37$$

Pacific Northwest National Laboratory
Tank Dome Buckling, Type-III Single Shell Tanks
Case 2: Bounding Temperature with 6.85-ft Soil Depth, 95/95 Lower Bound Concrete

Page 4 of 8
Date: 7/28/2011 By: K. I. Johnson
Chkd: 8/7/2011 By: L. J. Julyk
Revised: 8/10/2011 By: K. I. Johnson

α_3 = The Buckling Load-Reduction Factor Accounting for Cracking and the Amount and Type of Reinforcement

E_{C2eol} is the effective concrete modulus in the dome accounting for creep strain and end-of-life degraded concrete modulus, E_{Ceol}.

Must use the degraded concrete modulus based on thermal history

$E_{Ceol} := E_c = 2.75 \times 10^6$ psi $\qquad E_{C2eol} := \frac{E_{Ceol}}{(1 + C_u)} = 1.017 \times 10^6$ psi

Rebar Size and Spacing from SST Type-III Drawing #H-2-813

$\eta := \frac{E_s}{E_{C2eol}} = 28.914$ $\qquad$ Bar := 6 $\qquad$ Rebar Size (in 1/8th of an inch)

$S_p := 12$ $\qquad$ Bar Spacing near inner and outer surfaces. Varies from 6 to 12 inch in the dome. Use 12 inch for conservatism

$A_s := 2 \cdot \left(\frac{Bar}{8}\right)^2 \cdot \frac{\pi}{4} \cdot \frac{12}{S_p} = 0.884$ $\qquad$ Steel Area, in²/ft

$A_c := 12 \cdot \frac{t_d}{in} = 180$ $\qquad$ Concrete Area, in²/ft $\qquad \rho := \frac{A_s}{A_c} = 0.00491$

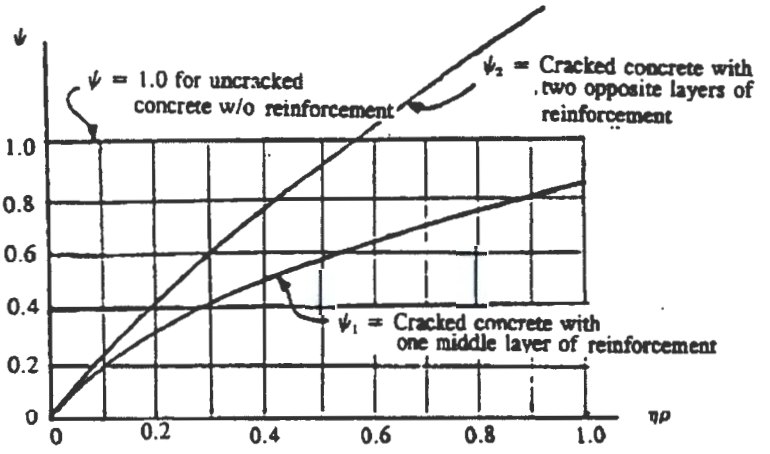

Values of ψ for Effect of Concrete Cracking And Amounts and Type of Reinforcement (*Figure 4* of Scordelis 1981).

Must interpolate by eye

From the above plot for cracked concrete with two opposite layers of reinforcement. $\eta \cdot \rho = 0.142$ $\qquad \psi := 0.35$

Pacific Northwest National Laboratory
Tank Dome Buckling, Type-III Single Shell Tanks
Case 2, Bounding Temperature with 6.85-ft Soil Depth, 95/95 Lower Bound Concrete

Page 5 of 8
Date: 7/28/2011 By: K. I. Johnson
Chkd: 8/7/2011 By: L. J. Julyk
Revised: 8/10/2011 By: K. I. Johnson

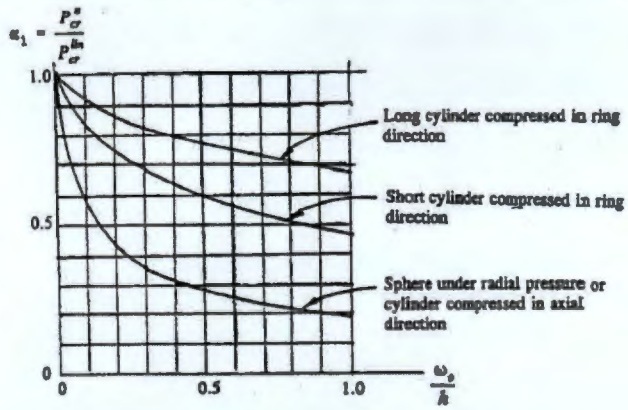

Effect of Geometric Imperfections on Buckling Load (Figure 3 of Scordelis 1981). ω_o/h factors for different geometries for specified geometric imperfection factor, α_1.

Must interpolate by eye

Dome = Sphere under radial pressure $\alpha_{1d} = 0.58$ $\omega_{ohd} := 0.1$

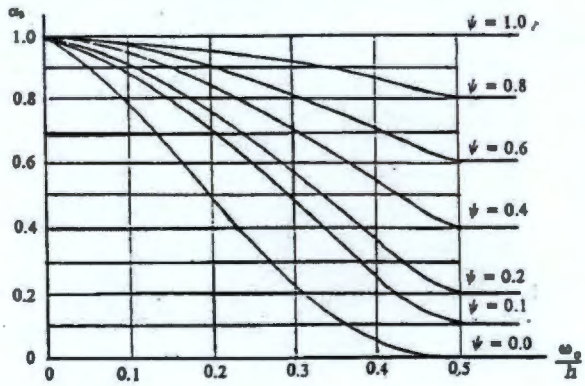

Reduction Factor α_3 for Concrete Cracking and Amount and Type of Reinforcement (Figure 5 of Scordelis 1981)

Must interpolate by eye

Dome = Sphere under radial pressure

$\alpha_{1d} = 0.58$ $\omega_{ohd} = 0.1$ $\psi = 0.35$ $\alpha_{3d} := 0.94$

Calculate $P_3 = \alpha_1\alpha_2\alpha_3 P_{buckle}$ and α_4 for highly loaded nonlinear concrete material effects

Uniform Dome Pressure, psi

$P_{3du} := \alpha_{1d}\cdot\alpha_2\cdot\alpha_{3d}\cdot P_{du} = 62.7\,psi$ This is based on the closed-form theoretical buckling load

Uniform Ultimate Pressure Load from SST Finite Element Analysis - NOTE, this pressure is the total effective ultimate dome pressure including:

- Dome weight (Concrete density=145 pcf)
- Soil overburden =6.85 ft at 125 pcf
- Pressure over dome diameter at the ultimate load capacity.

$P_{ult_u} := 45.5\cdot psi$ Type-III finite element ultimate load analysis for 95/95 lower bound properties

$$Ru(\alpha_4) := (\alpha_4)^2\left(\frac{P_{3du}}{P_{ult_u}}\right)^2 + (\alpha_4 - 1) \qquad \alpha_{4du} := root(Ru(\alpha_4), \alpha_4, 0.01, 0.99) = 0.509$$

Reduced Uniform Dome Buckling Load $P_{du_red} := \alpha_{4du}\cdot P_{3du} = 31.9\,psi$

Total Uniform Load Reduction Factor $\alpha_{dc} := \alpha_{1d}\cdot\alpha_2\cdot\alpha_{3d}\cdot\alpha_{4du} = 0.1$

Concentrated Ultimate Dome Load, lbf

$P_{3dc} := \alpha_2\cdot\alpha_{3d}\cdot\alpha 1 P_{dconc} = 9.068\times 10^6\,lbf$

Concentrated Ultimate Load from SST Finite Element Analysis - NOTE, this is the total effective ultimate concentrated dome load accounting for the effects of:

- Dome weight (Concrete density=145 pcf)
- Soil overburden =11 ft at 125 pcf
- Pressure over dome diameter at the ultimate load capacity.

$P_{ult_c} := 2845\cdot tonf$ Type-III finite element ultimate load analysis for 95/95 lower bound properties

$$Rc(\alpha_4) := (\alpha_4)^2\left(\frac{P_{3dc}}{P_{ult_c}}\right)^2 + (\alpha_4 - 1) \qquad \alpha_{4dc} := root(Rc(\alpha_4), \alpha_4, 0.01, 0.99) = 0.461$$

Reduced Concentrated Dome Buckling Load $P_{dc_red} := \alpha_{4dc}\cdot P_{3dc} = 4.18\times 10^6\,lbf$

Total Concentrated Load Reduction Factor $\alpha_{dc} := \alpha_{1d}\cdot\alpha_2\cdot\alpha_{3d}\cdot\alpha_{4dc} = 0.09$

Buckling Safety Factors

From the IASS Working Group No. 5, *Recommendations for Reinforced Concrete Shells and Folded Plates*, (IASS, 1979):
For shells that do not experience a reduction in load-carrying capacity in the post-buckling regime, a factor of safety of 1.75 is recommended. For shells that do experience a reduction in the load-carrying capacity in the post-buckling regime, a factor of safety of 3.5 is recommended.

Dome Uniform Pressure	$SF_{du} := 3.5$	Post Buckling = Reduced Load Capacity
Dome Concentrated Load	$SF_{dc} := 1.75$	Post Buckling = Increasing Load Capacity

But for a distributed local load with $\lambda_{bar} > 2$, the buckling will be accompanied by a loss of load carrying capacity, $\lambda_{bar} = 2.88$ so the safety factor should be 3.5

Dome Local Distributed Center Load	$SF_{dc} := 3.5$	Post Buckling = Reduced Load Capacity

Applied Loads on the Tank Dome

Dome Uniform Pressure = Concrete Dome Weight + Soil Overburden + Design Live Load

Dome Thickness, inch $t_d = 1.25\,ft$ Concrete Density, pcf $d_c = 145 \cdot pcf$ $P_d := t_d \cdot d_c = 1.259\,psi$

Soil Depth, h_s $h_s = 6.85\,ft$ Soil Density, d_s $d_s := 125\,pcf$ Soil Pressure $P_s := h_s \cdot d_s = 5.946\,psi$

Uniform Live Load $L_u := 40\,psf$ Total Uniform Load $Pr_{du} := P_d + P_s + L_u = 7.483\,psi$

Dome Specified Concentrated Load, $F_{dc} := 434000\,lbf$

Dome Buckling - Linear Combination of Uniform and Concentrated Loads

Applied Pressure on the Dome, psi $Pr_{du} = 7.48\,psi$

Reduced Uniform Dome Pressure Capacity, psi $P_{du_red} = 31.89\,psi$

Applied Concentrated Dome Load, lbf $F_{dc} = 4.34 \times 10^5\,lbf$

Reduced Concentrated Dome Load Capacity, lbf $P_{dc_red} = 4.178 \times 10^6\,lbf$

Uniform Load Fraction of Dome Buckling Capacity

$$R_{Uniform} := SF_{du} \cdot \left(\frac{Pr_{du}}{P_{du_red}}\right) = 0.821$$

Concentrated Load Fraction of Dome Buckling Capacity

$$R_{Concentrated} := SF_{dc} \cdot \left(\frac{F_{dc}}{P_{dc_red}}\right) = 0.364$$

Combined Fraction of Dome Buckling Capacity

$$R_{dome} := SF_{du} \cdot \left(\frac{Pr_{du}}{P_{du_red}}\right) + SF_{dc} \cdot \left(\frac{F_{dc}}{P_{dc_red}}\right) = 1.18$$

What Safety Factors give a Demand/Capacity Ratio of 1.0?

Uniform Load Safety Factor on Dome Buckling $SF_{act_U} := \frac{SF_{du}}{R_{dome}} = 2.95$

Concentrated Load Safety Factor on Dome Buckling $SF_{act_C} := \frac{SF_{dc}}{R_{dome}} = 2.95$

References

Baker EH, L Kovalevsky, and FL Rish. 1972. *Structural Analysis of Shells*. McGraw-Hill, New York, New York.

Fitch, JR and B Budiansky. 1970. "Buckling and Postbuckling Behavior of Spherical Caps under Axisymmetric Load." AIAA Journal, Vol. 8, No. 4, pp. 686-693.

IASS. 1979. *Recommendations for Reinforced Concrete Shells and Folded Plates*. Prepared by the Working Group No. 5 of The International Association for Shell and Spatial Structures (IASS), Stefan J. Medwadowski, Chairman. International Association for Shell and Spatial Structures, Madrid, Spain.

KI Johnson, JE Deibler, FG Abatt and MW Rinker. 2010. *Single Shell Tank Structural Evaluation Criteria*. PNNL-18837, Rev. 1. Pacific Northwest National Laboratory, Richland, Washington.

Popov EP and SJ Medwadowski. 1981. "Stability of Reinforced Concrete Shells: State-of-the-Art Overview." In *Concrete Shell Buckling*, ACI SP-67, American Concrete Institute, Detroit, Michigan.

Scordelis AC. 1981. "Stability of Reinforced Concrete Domes and Hyperbolic Paraboloid Shells." In *Concrete Shell Buckling*, ACI SP-67, American Concrete Institute, Detroit, Michigan.

Calculations for Case 3 – Dome Buckling Evaluation for Actual Temperature with Bounding Soil Overburden

Tank Dome Buckling
Case 3. Type III Baseline, 11-ft Soil, Actual Temperatures, 95/95 Lower Bound Concrete Properties

The following tank buckling evaluation method is described in:

KI Johnson, JE Deibler, FG Abatt and MW Rinker. 2010. *Single Shell Tank Structural Evaluation Criteria.* PNNL-18837, Rev. 1. Pacific Northwest National Laboratory, Richland, Washington.

Tank Dome Degraded Concrete Properties **Tank Dome Reinforcing Steel Properties**

Maximum Dome temperature during tank life = 116 F Current maximum temp = 80 F for Type III SSTs

Elastic Modulus (95/95 at Temp) $E_c := 4.33 \times 10^6 \text{psi}$ $E_s := 29.4 \times 10^6 \text{psi}$

Concrete Strength (95/95 at Temp), psi $f_{c_min} := 4600 \cdot \text{psi}$

Concrete Density, $d_c := 145 \cdot \text{pcf}$

Poisson's Ratio $\nu := 0.15$ $\nu_s := 0.30$

Tank Geometry - from SST Type III Drawing # H-2-808

Dome minimum wall thickness, t_d, inches $t_d := 15\text{in}$

Dome maximum mid-wall radius of curvature, R_d, feet $R_d := \left[\frac{(96.25 + 95) \cdot \text{ft}}{2}\right] = 95.6 \cdot \text{ft}$

Tank Wall Inner and Outer Radii $r_i := 37\text{ft} + 7.25\text{in} = 37.604\text{ft}$ $r_o := r_i + 15 \cdot \text{in} = 466.25 \cdot \text{in}$

Tank cylinder mid-wall radius of curvature, R_c, inches $R_c := \frac{r_i + r_o}{2} = 458.75 \cdot \text{in}$

Tank minimum wall thickness, t_w, inch $t_w := 15\text{in}$

Unfactored Critical Dome Buckling Loads

Uniform Pressure Load $P_{du} := 0.66 \cdot E_c \cdot \left(\frac{t_d}{R_d}\right)^2 = 488.3\,\text{psi}$

Concentrated Center Load

ϕ is half the included angle of the dome $\phi := \text{asin}\left(\frac{R_c}{R_d}\right) = 23.6 \cdot \text{deg}$

Shallowness Parameter, λ $\lambda := \left[12 \cdot \left(1 - \nu^2\right)\right]^{\frac{1}{4}} \cdot \left(\frac{R_d}{t_d}\right)^{\frac{1}{2}} \cdot 2 \cdot \text{sin}\left(\frac{\phi}{2}\right) = 6.6$

According to Baker (1972):

$\lambda < 7$ Buckling will not occur.

$8 < \lambda < 9$ Axisymmetric snap-through is the expected buckling mode, but the shell will continue to take load.

$\lambda > 9$ Asymmetric buckling is expected first, but the shell will continue to carry load.

$$D := \frac{E_c t_d^3}{12\cdot(1 - \nu^2)} = 1.246 \cdot 10^9 \cdot lbf\cdot in$$

Concentrated Point Load at the Center

$$\alpha 1P_{dc} := \frac{28\cdot\pi\cdot D}{R_d} = 9.55 \cdot 10^7 \cdot lbf$$

Fitch and Budiansky (1970) present the buckling solution for a spherical cap loaded by a local pressure distributed over a circle of radius, Rcl. They present the solution as a function of the parameter, λbar, which is in turn a function of the loading radius, the dome radius, the dome thickness, and the Poisson's ratio.

The tank operating limits specify a 200-kip concentrated load over a circle of 10-ft radius at the dome center. The soil overburden depth further distributes the pressure load over a larger radius, which is a function of the overburden depth and the internal friction angle of the soil.

Load Radius R_l: 10·ft Soil depth h_s: 11·ft Soil Friction Angle ϕ_s: 35·deg

Load radius at the tank dome $R_{cl} := R_l + h_s\cdot\tan(\phi_s) = 17.702\,ft$

$$\lambda_{bar} := \left[12\cdot(1 - \nu^2)\right]^{\frac{1}{4}}\cdot\left(\frac{t_d}{R_d}\right)^{\frac{1}{2}}\cdot\left(\frac{R_{cl}}{t_d}\right) = 3$$

$p_c := 0.42$ See plot below

The buckling sensitivity parameter, p_c, is interpolated from the right vertical axis of the plot below (Fitch and Budiansky, 1970).

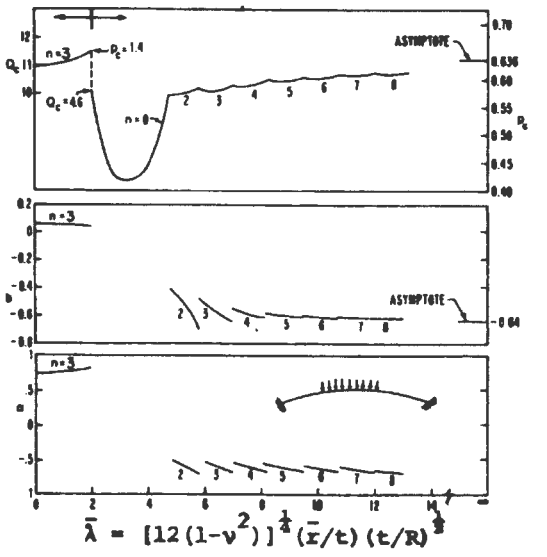

Total buckling force of a pressure acting over a 10-ft radius circle at the soil surface

$$\alpha 1P_{dL} := p_c \cdot 2\pi \cdot R_{cl}^2 \cdot \frac{E_c}{\sqrt{3\cdot(1-\nu^2)}} \cdot \left(\frac{t_d}{R_d}\right)^2 = 5.145\times 10^7 \cdot lbf$$

This is 54% of the buckling point load $\frac{\alpha 1P_{dL}}{\alpha 1P_{dc}} = 0.54$

Use the minimum of the concentrated load estimates $\alpha 1P_{dconc} := \min(\alpha 1P_{dc}, \alpha 1P_{dL}) = 5.145\times 10^7$ lbf

Buckling Load Reduction Factors

α_1 = The Geometric Imperfection Factor

Seide (1981) provides the following equation for the lower bound fit of buckling experiments of cylindrical shells in compression. Popov and Medwadowski (1981) recommend this approximation of α_1 for other shell geometries (including shallow domes) when no specific solution is available.

Dome, α_{1d}

$$\alpha_{1d} := 1 - 0.9\cdot\left(1 - \exp\left(\frac{-1}{16}\cdot\sqrt{\frac{R_d}{t_d}}\right)\right) = 0.621$$

which is valid for $100 \le \frac{R}{t} \le 3000$

but for the dome: $\frac{R_d}{t_d} = 76.5$ Therefore, the SST Structural Evaluation Criteria conservatively assumes R/t=100 for the dome.

Recommended Value for both uniform and concentrated loads

$$\alpha_{1d} := 1 - 0.9\cdot\left(1 - \exp\left(\frac{-1}{16}\cdot\sqrt{100}\right)\right) = 0.58$$

α_2 = The Creep Buckling Load-Reduction Factor

Creep strains were predicted by the ANSYS finite element mode of the Type-III tank. The maximum temperature history for Type-III tanks was applied over the 60-year current life of the tanks.

C_u = ultimate creep strain / initial elastic strain

C_u is from Type III ANSYS model, hoop strains in Dome

$$C_{ua} := \frac{0}{6.26\times 10^{-5}} = 0$$

$$\alpha_{2a} := \frac{1}{(1+C_{ua})} = 1$$

If a creep analysis is not available, Popov and Medwadowski (1981) recommend the following as an estimate of the ultimate creep coefficient, C_u:

$C_u = 4 - 2\log(f_c)$ where f_c is the concrete strength at the time of loading in N/mm^2.

$$f_c := \frac{f_{c_min}}{1ksi}\cdot 6.895 = 31.7 \quad C_{ub} := 4 - 2\log(f_c) = 0.997 \quad \alpha_{2b} := \frac{1}{(1+C_{ub})} = 0.501$$

Use the maximum C_u to obtain the minimum creep reduction factor

$$C_u := \max(C_{ua}, C_{ub}) = 0.997$$

$$\alpha_2 := \frac{1}{(1+C_u)} = 0.501$$

α_3 = The Buckling Load-Reduction Factor Accounting for Cracking and the Amount and Type of Reinforcement.

E_{C2eol} is the effective concrete modulus in the dome accounting for creep strain and end-of-life degraded concrete modulus, E_{Ceol}.

Must use the degraded concrete modulus based on thermal history

$E_{Ceol} := E_c = 4.33 \times 10^6$ psi $\qquad E_{C2eol} := \dfrac{E_{Ceol}}{(1 + C_u)} = 2.168 \times 10^6$ psi

Rebar Size and Spacing from SST Type-III Drawing # H-2-813

$\eta := \dfrac{E_s}{E_{C2eol}} = 13.562$ $\qquad$ Bar := 6 $\qquad$ Rebar Size (in 1/8th of an inch)

$S_p := 12$ $\qquad$ Bar Spacing near inner and outer surfaces. Varies from 6 to 12 inch in the dome. Use 12 inch for conservatism

$A_s := 2 \cdot \left(\dfrac{Bar}{8}\right)^2 \cdot \dfrac{\pi}{4} \cdot \dfrac{12}{S_p} = 0.884$ $\qquad$ Steel Area, in²/ft

$A_c := 12 \cdot \dfrac{t_d}{in} = 180$ $\qquad$ Concrete Area, in²/ft $\qquad \rho := \dfrac{A_s}{A_c} = 0.00491$

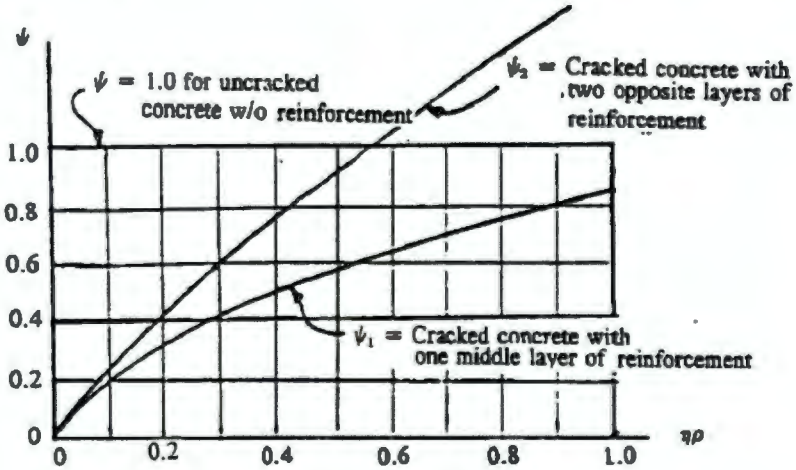

Values of ψ for Effect of Concrete Cracking And Amounts and Type of Reinforcement (Figure 4 of Scordelis 1981).

Must interpolate by eye

From the above plot for cracked concrete with two opposite layers of reinforcement. $\qquad \eta \cdot \rho = 0.067 \qquad \psi := 0.20$

Pacific Northwest National Laboratory
Tank Dome Buckling, Type-III Single Shell Tanks
Case 3, Actual Temperature and 11-ft Soil Depth, 95/95 Lower Bound Concrete

Page 5 of 8
Date: 7/28/2011 By: K. I. Johnson
Chkd: 8/7/2011 By: L. J. Julyk
Revised: 8/10/2011 By: K. I. Johnson

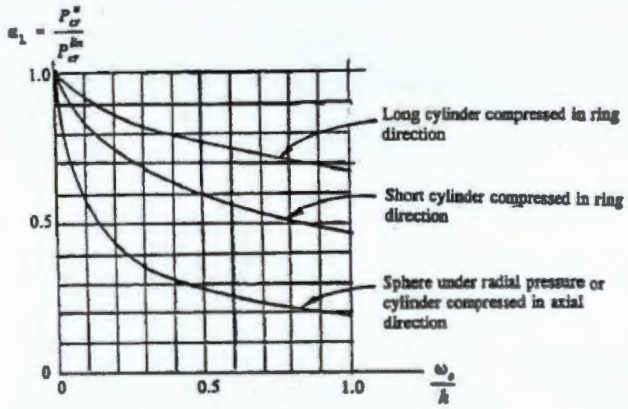

Effect of Geometric Imperfections on Buckling Load (Figure 3 of Scordelis 1981). ω_o/h factors for different geometries for specified geometric imperfection factor, α_1.

Must interpolate by eye

Dome = Sphere under radial pressure $\alpha_{1d} = 0.58$ $\omega_{ohd} := 0.1$

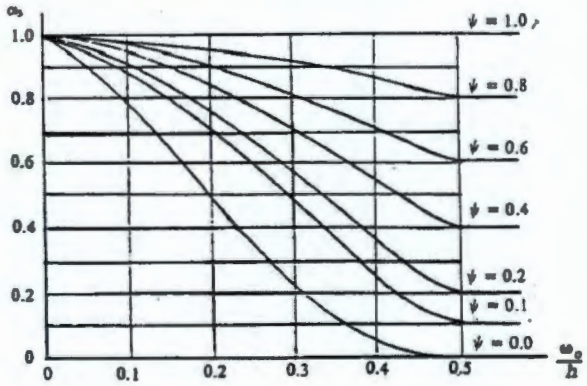

Reduction Factor α_3 for Concrete Cracking and Amount and Type of Reinforcement (Figure 5 of Scordelis 1981)

Must interpolate by eye

Dome = Sphere under radial pressure

$\alpha_{1d} = 0.58$ $\omega_{ohd} = 0.1$ $\psi = 0.2$ $\alpha_{3d} := 0.91$

Calculate $P_3 = \alpha_1\alpha_2\alpha_3 P_{buckle}$ and α_4 for highly loaded nonlinear concrete material effects

Uniform Dome Pressure, psi

$P_{3du} := \alpha_{1d}\cdot\alpha_2\cdot\alpha_{3d}\cdot P_{du} = 129.4\,psi$ This is based on the closed-form theoretical buckling load

Uniform Ultimate Pressure Load from SST Finite Element Analysis - NOTE, this pressure is the total effective ultimate dome pressure including:

- Dome weight (Concrete density=145 pcf)
- Soil overburden =11 ft at 125 pcf
- Pressure over dome diameter at the ultimate load capacity.

$P_{ult_u} := 50.1\cdot psi$ Type-III finite element ultimate load analysis for 95/95 lower bound properties

$$Ru(\alpha_4) := (\alpha_4)^2\left(\frac{P_{3du}}{P_{ult_u}}\right)^2 + (\alpha_4 - 1) \qquad \alpha_{4du} := root(Ru(\alpha_4), \alpha_4, 0.01, 0.99) = 0.319$$

Reduced Uniform Dome Buckling Load $P_{du_red} := \alpha_{4du}\cdot P_{3du} = 41.3\,psi$

Total Uniform Load Reduction Factor $\alpha_{dc} := \alpha_{1d}\cdot\alpha_2\cdot\alpha_{3d}\cdot\alpha_{4du} = 0.08$

Concentrated Ultimate Dome Load, lbf

$P_{3dc} := \alpha_2\cdot\alpha_{3d}\cdot\alpha 1 P_{dconc} = 2.344\times 10^7\,lbf$

Concentrated Ultimate Load from SST Finite Element Analysis - NOTE, this is the total effective ultimate concentrated dome load accounting for the effects of:

- Dome weight (Concrete density=145 pcf)
- Soil overburden =11 ft at 125 pcf
- Pressure over dome diameter at the ultimate load capacity.

$P_{ult_c} := 3675\cdot tonf$ Type-III finite element ultimate load analysis for 95/95 lower bound properties

$$Rc(\alpha_4) := (\alpha_4)^2\left(\frac{P_{3dc}}{P_{ult_c}}\right)^2 + (\alpha_4 - 1) \qquad \alpha_{4dc} := root(Rc(\alpha_4), \alpha_4, 0.01, 0.99) = 0.268$$

Reduced Concentrated Dome Buckling Load $P_{dc_red} := \alpha_{4dc}\cdot P_{3dc} = 6.29\times 10^6\,lbf$

Total Concentrated Load Reduction Factor $\alpha_{dc} := \alpha_{1d}\cdot\alpha_2\cdot\alpha_{3d}\cdot\alpha_{4dc} = 0.07$

Buckling Safety Factors

From the IASS Working Group No. 5, *Recommendations for Reinforced Concrete Shells and Folded Plates*, (IASS, 1979):
For shells that do not experience a reduction in load-carrying capacity in the post-buckling regime, a factor of safety of 1.75 is recommended. For shells that do experience a reduction in the load-carrying capacity in the post-buckling regime, a factor of safety of 3.5 is recommended.

Dome Uniform Pressure	$SF_{du} := 3.5$	Post Buckling = Reduced Load Capacity
Dome Concentrated Load	$SF_{dc} := 1.75$	Post Buckling = Increasing Load Capacity

But for a distributed local load with $\lambda_{bar} > 2$, the buckling will be accompanied by a loss of load carrying capacity. $\lambda_{bar} = 2.88$ so the safety factor should be 3.5

Dome Local Distributed Center Load	$SF_{dc} := 3.5$	Post Buckling = Reduced Load Capacity

Applied Loads on the Tank Dome

Dome Uniform Pressure = Concrete Dome Weight + Soil Overburden + Design Live Load

Dome Thickness, inch $t_d = 1.25\,ft$ Concrete Density, pcf $d_c = 145 \cdot pcf$ $P_d := t_d \cdot d_c = 1.259\,psi$

Soil Depth, h_s $h_s = 11\,ft$ Soil Density, d_s $d_s := 125pcf$ Soil Pressure $P_s := h_s \cdot d_s = 9.549\,psi$

Uniform Live Load $L_u := 40psf$ Total Uniform Load $Pr_{du} := P_d + P_s + L_u = 11.085\,psi$

Dome Specified Concentrated Load, $F_{dc} := 200000lbf$

Dome Buckling - Linear Combination of Uniform and Concentrated Loads

Applied Pressure on the Dome, psi $Pr_{du} = 11.09\,psi$

Reduced Uniform Dome Pressure Capacity, psi $P_{du_red} = 41.33\,psi$

Applied Concentrated Dome Load, lbf $F_{dc} = 2 \times 10^5\,lbf$

Reduced Concentrated Dome Load Capacity, lbf $P_{dc_red} = 6.287 \times 10^6\,lbf$

Uniform Load Fraction of Dome Buckling Capacity

$$R_{Uniform} := SF_{du} \cdot \left(\frac{Pr_{du}}{P_{du_red}}\right) = 0.939$$

Concentrated Load Fraction of Dome Buckling Capacity

$$R_{Concentrated} := SF_{dc} \cdot \left(\frac{F_{dc}}{P_{dc_red}}\right) = 0.111$$

Combined Fraction of Dome Buckling Capacity

$$R_{dome} := SF_{du} \cdot \left(\frac{Pr_{du}}{P_{du_red}}\right) + SF_{dc} \cdot \left(\frac{F_{dc}}{P_{dc_red}}\right) = 1.05$$

What Safety Factors give a Demand/Capacity Ratio of 1.0?

Uniform Load Safety Factor on Dome Buckling $SF_{act_U} := \frac{SF_{du}}{R_{dome}} = 3.33$

Concentrated Load Safety Factor on Dome Buckling $SF_{act_C} := \frac{SF_{dc}}{R_{dome}} = 3.33$

References

Baker EH, L Kovalevsky, and FL Rish. 1972. *Structural Analysis of Shells*. McGraw-Hill, New York, New York.

Fitch, JR and B Budiansky. 1970. "Buckling and Postbuckling Behavior of Spherical Caps under Axisymmetric Load." AIAA Journal, Vol. 8, No. 4, pp. 686-693.

IASS. 1979. *Recommendations for Reinforced Concrete Shells and Folded Plates*. Prepared by the Working Group No. 5 of The International Association for Shell and Spatial Structures (IASS), Stefan J. Medwadowski, Chairman. International Association for Shell and Spatial Structures, Madrid, Spain.

KI Johnson, JE Deibler, FG Abatt and MW Rinker. 2010. *Single Shell Tank Structural Evaluation Criteria*. PNNL-18837, Rev. 1. Pacific Northwest National Laboratory, Richland, Washington.

Popov EP and SJ Medwadowski. 1981. "Stability of Reinforced Concrete Shells: State-of-the-Art Overview." In *Concrete Shell Buckling*, ACI SP-67, American Concrete Institute, Detroit, Michigan.

Scordelis AC. 1981. "Stability of Reinforced Concrete Domes and Hyperbolic Paraboloid Shells." In *Concrete Shell Buckling*, ACI SP-67, American Concrete Institute, Detroit, Michigan.

Calculations for Case 1 – Wall Buckling Evaluation for Bounding Temperature and Soil Overburden

Pacific Northwest National Laboratory
Tank Wall Buckling, Type-III Single Shell Tanks
Case 1, Baseline, Bounding Temperature and Soil Depth

Page 1 of 9
Date: 7/28/2011 By: K. I. Johnson
Chkd: 8/7/2011 By: L. J. Julyk
Revised: 8/10/2011 By: K. I. Johnson

Tank Wall Buckling
Case 1. Type III Baseline, 11-ft Soil, Bounding Temperatures, 95/95 Lower Bound Concrete

The following tank buckling evaluation method is described in:
KI Johnson, JE Deibler, FG Abatt and MW Rinker. 2010. *Single Shell Tank Structural Evaluation Criteria*. PNNL-18837, Rev. 1. Pacific Northwest National Laboratory, Richland, Washington.

Tank Wall Degraded Concrete Properties		**Tank Wall Reinforcing Steel Properties**
Maximum wall temperature during tank history = 256 F		Current maximum temp = 80 F for Type III SSTs
Elastic Modulus (95/95 at Temp)	$E_c := 2.45 \times 10^6 \text{psi}$	$E_s := 29.4 \times 10^6 \text{psi}$
Concrete Strength (95/95 at Temp), psi	$f_{c_min} := 3440 \cdot \text{psi}$	
Concrete Density,	$d_c := 145 \cdot \text{pcf}$	
Poisson's Ratio	$\nu := 0.15$	$\nu_s := 0.30$

Tank Geometry - from SST Type III Drawing # H-2-808

Dome minimum wall thickness, t_d, inches $t_d := 15\text{in}$

Dome maximum mid-wall radius of curvature, R_d, inches $R_d := \left[\frac{(96.25 + 95) \cdot \text{ft}}{2}\right] = 95.6 \cdot \text{ft}$

Tank Wall Inner and Outer Radii $r_i := 37\text{ft} + 7.24\text{in} = 37.603\text{ft}$ $r_o := r_i + 15 \cdot \text{in} = 38.853 \cdot \text{ft}$

Tank cylinder mid-wall radius of curvature, R_c, inches $R_c := \frac{r_i + r_o}{2} = 38.228 \cdot \text{ft}$

Tank minimum wall thickness, t_w, inch $t_w := 15\text{in}$

Equivalent Tank Height - including half of Dome and Floor Heights

Dome Height - top of haunch to dome apex $h_d := 8 \cdot \text{ft} + 9.25 \cdot \text{in} = 105.25 \cdot \text{in}$

Wall Height - bottom of footing to haunch $h_w := 30 \cdot \text{ft} + 2.625 \cdot \text{in} = 362.625 \cdot \text{in}$

Dished Floor Depth (Type-III floor is flat) $h_f := 0 \cdot \text{in}$

Equivalent Tank Height, L_{eq} $L_{eq} := h_w + \frac{h_d}{2} + \frac{h_f}{2} = 415.25 \cdot \text{in}$

Tank Cylindrical Wall Buckling

Axial

$$\sigma_{ca} := \frac{1}{\sqrt{3 \cdot (1 - \nu^2)}} \cdot E_c \cdot \left(\frac{t_w}{R_c}\right) = 4.678 \times 10^4 \text{psi} \qquad P_{ca} := 2 \cdot \pi \cdot R_c \cdot t_w \sigma_{ca} = 2.023 \times 10^9 \text{lbf}$$

Lateral Uniform Pressure on Tank Wall (Average Soil Pressure)

$h := t_w = 1.25\text{ft}$ $a := R_c = 38.228\text{ft}$ $E := E_c = 2.45 \times 10^6 \text{psi}$

$$k := \frac{h^2}{12 \cdot a^2} = 8.91 \times 10^{-5} \quad \lambda := \pi \cdot \frac{a}{L_{eq}} = 3.471 \quad \frac{L_{eq}}{a} = 0.905 \quad \frac{a}{h} = 30.583 \quad \beta := \frac{L_{eq}^2}{a \cdot h} = 25.1$$

Flugge, W., 1960, *Stresses in Shells*, Springer-Verlag, New York, New York.

page 432, Eqn 20

$$\varphi_{Flugge}(m,n,\nu,\lambda,k) := \frac{\left(1-\nu^2\right)\cdot(n\cdot\lambda)^4 + k\cdot\left[\left[(n\cdot\lambda)^2+m^2\right]^4 - 2\cdot\left[\begin{array}{l}\nu\cdot(n\cdot\lambda)^6 + 3\cdot(n\cdot\lambda)^4\cdot m^2 \ldots \\ + (4-\nu)\cdot(n\cdot\lambda)^2\cdot m^4 + m^6\end{array}\right] \ldots \right.}{\left. + 2\cdot(2-\nu)\cdot(n\cdot\lambda)^2\cdot m^2 + m^4\right]}{m^2\cdot\left[(n\cdot\lambda)^2+m^2\right]^2 - m^2\cdot\left[3\cdot(n\cdot\lambda)^2+m^2\right]}$$

$m := 2 \quad n := 2$

Given

$m \ge 2$
$n \ge 1$

$\varphi_{Flugge}(m,n,\nu,\lambda,k) \ge 0$

$P(\nu,\lambda,k) := \text{Minimize}\left(\varphi_{Flugge}, m, n\right)$

$m_{min}(\nu,\lambda,k) := \text{round}\left(P(\nu,\lambda,k)_0\right)$

$n_{min}(\nu,\lambda,k) := \text{round}\left(P(\nu,\lambda,k)_1\right)$

$\varphi_{cr_Flugge}(\nu,\lambda,k) := \varphi_{Flugge}\left(m_{min}(\nu,\lambda,k), n_{min}(\nu,\lambda,k), \nu, \lambda, k\right)$

$p_{cr_Flugge}(E,\nu,\lambda,k) := \frac{E}{1-\nu^2}\cdot\sqrt{12\cdot k}\cdot\varphi_{cr_Flugge}(\nu,\lambda,k)$

Theoretical Lateral Buckling Pressure, P_{cl} $P_{cl} := p_{cr_Flugge}(E,\nu,\lambda,k) = 605.7\,\text{psi}$

Buckling Load Reduction Factors

α_1 = The Geometric Imperfection Factor

For the Cylindrical wall under uniform lateral pressure $\alpha_{1c_lat} = 0.75$ (Seide, 1981)

For cylindrical wall under axial load $\quad \alpha_{1c_axi} = 1 - 0.9\cdot\left(1 - \exp\left(\frac{-1}{16}\cdot\sqrt{\frac{R}{t}}\right)\right)$

which is valid for $\quad 100 \le \frac{R}{t} = \frac{a}{h} \le 3000 \quad$ and $\quad 0.5 \le \frac{L}{R} = \frac{L_{eq}}{a} \le 5$

but $\quad \frac{a}{h} = 30.583 \quad \frac{L_{eq}}{a} = 0.905$

Hence, conservatively assume R/t=100 $\quad \alpha_{1c_axi} := 1 - 0.9\cdot\left(1 - \exp\left(\frac{-1}{16}\cdot\sqrt{100}\right)\right) = 0.582$

Recommended Values

$\alpha_{1c_axi} := 0.58$ for axial compression of a cylinder

$\alpha_{1c_lat} := 0.75$ for external lateral pressure

α_2 = The Creep Buckling Load-Reduction Factor

C_u = ultimate creep strain / initial elastic strain

C_u from ANSYS Type II TOLA Model, creep in axial compression mid-wall

$$C_{ua} := \frac{1.37 \times 10^{-4}}{6.6 \times 10^{-5}} = 2.076$$

$$\alpha_{2a} := \frac{1}{(1 + C_{ua})} = 0.325$$

If a creep analysis is not available, Popov and Medwadowski (1981) recommend the following as an estimate of the ultimate creep coefficient, C_u:

$C_u = 4 - 2\log(f_c)$ where f_c is the concrete strength (N/mm^2) at the time of sustained loading .

$$f_c := \frac{f_{c_min}}{\frac{N}{mm^2}} = 23.7 \qquad C_{ub} := 4 - 2 \cdot \log(f_c) = 1.25 \qquad \alpha_{2b} := \frac{1}{(1 + C_{ub})} = 0.444$$

Use the maximum C_u to obtain minimum creep reduction factor

$$C_u := \max(C_{ua}, C_{ub}) = 2.076$$

$$\alpha_2 := \frac{1}{(1 + C_u)} = 0.325$$

α_3 = The Buckling Load-Reduction Factor Accounting for Cracking and the Amount and Type of Reinforcement.

E_{C2eol} is the effective concrete modulus in the dome accounting for creep strain and end-of-life degraded concrete modulus, E_{Ceol}.

Use the degraded concrete modulus based on thermal history

$$E_{Ceol} := E_c = 2.45 \times 10^6 \text{ psi} \qquad E_{C2eol} := \frac{E_{Ceol}}{(1 + C_u)} = 7.966 \times 10^5 \text{ psi}$$

$$\eta := \frac{E_s}{E_{C2eol}} = 36.909$$

Rebar Reinforcement Fractions

Meriidional Rebar - from SST Type III drawing # H-2-812

$Bar_m := 6$ Rebar Size (in 1/8th of an inch).

$S_{pm} := 12$ Bar Spacing (inches) near inner and outer wall surfaces

$$A_{sm} := 2 \cdot \left(\frac{Bar_m}{8}\right)^2 \cdot \frac{\pi}{4} \cdot \frac{12}{S_{pm}} = 0.884 \text{ Steel Area, in}^2\text{/ft}$$

$$A_c := 12 \cdot \frac{t_w}{in} = 180 \qquad \text{Concrete Area, in}^2\text{/ft} \qquad \rho_m := \frac{A_{sm}}{A_c} = 0.00491$$

Pacific Northwest National Laboratory
Tank Wall Buckling, Type-III Single Shell Tanks
Case 1, Baseline, Bounding Temperature and Soil Depth

Page 4 of 9
Date: 7/28/2011 By: K. I. Johnson
Chkd: 8/7/2011 By: L. J. Julyk
Revised: 8/10/2011 By: K. I. Johnson

Hoop Rebar - from SST Type III drawing # H-2-812

$Bar_h := 7$ Rebar Size (in 1/8th of an inch).

$S_{ph} := 10$ Bar Spacing (inches) near inner and outer wall surfaces. (Varies from 8 inch at lower wall to 10" at top of wall. Conservatively assume 10 inch)

$$A_{sh} := 2 \cdot \left(\frac{Bar_h}{8}\right)^2 \cdot \frac{\pi}{4} \cdot \frac{12}{S_{ph}} = 1.443 \quad \text{Steel Area, in}^2\text{/ft} \qquad \rho_h := \frac{A_{sh}}{A_c} = 0.00802$$

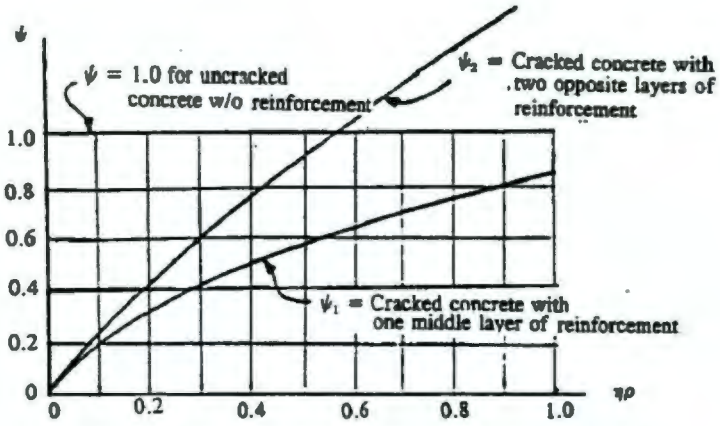

Values of ψ for Effect of Concrete Cracking And Amounts and Type of Reinforcement (Figure 4 of Scordelis 1981).
Must interpolate by eye

From the above plot for cracked concrete with two opposite layers of reinforcement.

Meridional Rebar $\eta \cdot \rho_m = 0.181$ $\psi_m := 0.40$

Hoop Rebar $\eta \cdot \rho_h = 0.296$ $\psi_h := 0.60$

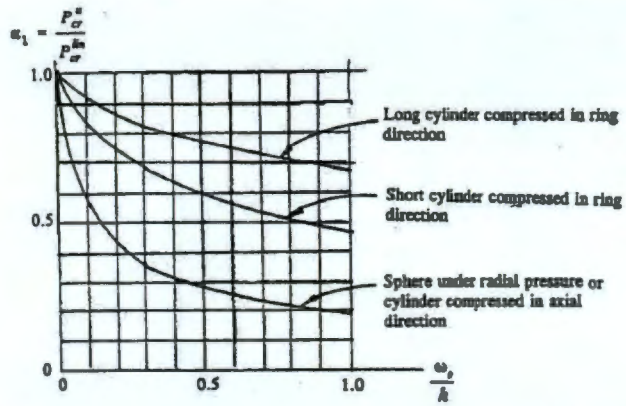

Effect of Geometric Imperfections on Buckling Load (Figure 3 of Scordelis 1981).
ω_0/h factors for different geometries for specified geometric imperfection factor, α_1.

Must interpolate by eye

Tank Wall, Axial Load: Cylinder compressed in axial direction

$\alpha_{1c_axi} = 0.58$ $\omega_{ohc_axi} := 0.1$

Tank Wall, Lateral Pres: Short cylinder compressed in ring direction

$\alpha_{1c_lat} = 0.75$ $\omega_{ohc_lat} := 0.2$

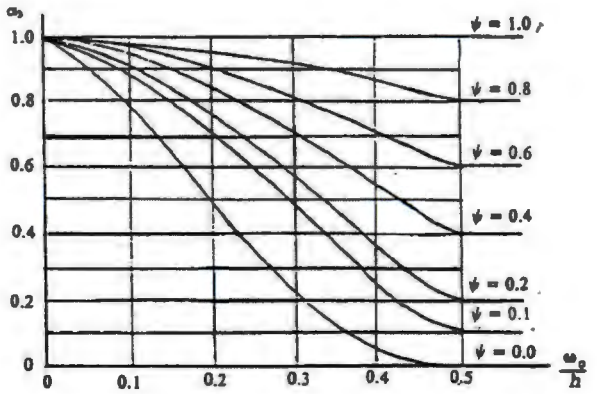

Reduction Factor α_3 for Concrete Cracking and Amount and Type of Reinforcement (Figure 5 of Scordelis 1981)

Must interpolate by eye

Tank Wall, Axial Load: cylinder compressed in axial direction (Meridional Rebar)

$\alpha_{1c_axl} = 0.58$ $\omega_{ohc_axl} = 0.1$ $\psi_m = 0.4$ $\alpha_{3c_axl} := 0.94$

Tank Wall, Lateral Pres: short cylinder compressed in ring direction (Hoop Rebar)

$\alpha_{1c_lat} = 0.75$ $\omega_{ohc_lat} = 0.2$ $\psi_h = 0.6$ $\alpha_{3c_lat} := 0.90$

Calculate $P_3 = \alpha_1\alpha_2\alpha_3 P_{buckle}$ and α_4 for highly loaded nonlinear concrete material effects

Axial Compressive Pressure on Cylindrical Wall, psi

$P_{3c_axi} := \alpha_{1c_axi} \cdot \alpha_2 \cdot \alpha_{3c_axi} \cdot \sigma_{ca} = 8292.3\,psi$

Ultimate axial force of concrete

Degraded Concrete Strength $f_{c_min} = 3440\,psi$ $F_{ult_axi} := 2 \cdot \pi \cdot R_c \cdot t_w \cdot f_{c_min} = 1.49 \times 10^8\,lbf$

$Raxi(\alpha_4) := (\alpha_4)^2 \left(\frac{P_{3c_axi}}{f_{c_min}}\right)^2 + (\alpha_4 - 1)$ $\alpha_{4axi} := root(Raxi(\alpha_4), \alpha_4, 0.01, 0.99) = 0.338$

Total Axial Load Reduction Factor $\alpha_{dc} := \alpha_{1c_axi} \cdot \alpha_2 \cdot \alpha_{3c_axi} \cdot \alpha_{4axi} = 0.06$

Reduced Axial Wall Buckling Pressure, psi $P_{c_axi_red} := \alpha_{4axi} \cdot P_{3c_axi} = 2799.7\,psi$

Reduced Axial Wall Buckling Force, psi $F_{c_axi_red} := P_{c_axi_red} \cdot 2 \cdot \pi R_c \cdot t_w = 1.21 \times 10^8\,lbf$

$tons := F_{c_axi_red} = 60523 \cdot tonf$

Lateral Compressive Pressure on **Short** Cylindrical Wall, psi

$P_{3c_lat} := \alpha_{1c_lat} \cdot \alpha_2 \cdot \alpha_{3c_lat} \cdot P_{cl} = 132.9\,psi$

Cylinder compressive hoop stress $\sigma_{hoop} := \frac{P_{3c_lat} \cdot R_c}{t_w} = 4065.2\,psi$

$Rlat(\alpha_4) := (\alpha_4)^2 \left(\frac{\sigma_{hoop}}{f_{c_min}}\right)^2 + (\alpha_4 - 1)$ $\alpha_{4lat} := root(Rlat(\alpha_4), \alpha_4, 0.01, 0.99) = 0.561$

Total Lateral Pressure Reduction Factor $\alpha_{dlat} := \alpha_{1c_lat} \cdot \alpha_2 \cdot \alpha_{3c_lat} \cdot \alpha_{4lat} = 0.12$

Reduced Lateral Buckling Pressure, Short Wall $P_{c_lat_red} := \alpha_{4lat} \cdot P_{3c_lat} = 74.5\,psi$

Ultimate Lateral Pressure for concrete strength $P_{ult_lat} := f_{c_min} \cdot \frac{t_w}{R_c} = 112.48\,psi$

Buckling Safety Factors

From the IASS Working Group No. 5, *Recommendations for Reinforced Concrete Shells and Folded Plates*, (IASS, 1979):
For shells that do not experience a reduction in load-carrying capacity in the post-buckling regime, a factor of safety of 1.75 is recommended. For shells that do experience a reduction in the load-carrying capacity in the post-buckling regime, a factor of safety of 3.5 is recommended.

Wall Uniform Axial Compression	$SF_{c_axi} := 3.5$	Post Buckling = Reduced Load Capacity
Wall Lateral Pressure	$SF_{c_lat} := 1.75$	Post Buckling = Displacement Controlled Loading, Soil Pressure is Self Relieving

Applied Loads on the Tank Wall

Axial Compressive Stress at the Mid-Height of the Wall

This includes the total weight of the soil, uniform live load, concentrated live load, and the weight of the dome and wall concrete.

Finite Element Results for Axial Compression at the Mid-Height of the Wall, Section 23 (F = 62 kip/ft)

Meridional Section Force, Loadstep 3, Gravity Loads $F_{c_axi} := 62\frac{kip}{ft}\,2\cdot\pi\cdot R_c = 1.49\times 10^{7}\,lbf$

Wall Lateral Earth Pressure calculated as the at rest soil pressure at depth=34.88-ft, Type-III tank ht=31'-11" from bottom of footing to top of dome, Soil depth=11-ft.

Soil internal friction angle, φ $\varphi := 35deg$ $k_o := 1 - \sin(\varphi) = 0.426$

Soil Density, d_s $d_s := 125pcf$

Soil Overburden Depth $h_{soil} := 11ft$

Soil Depth at Midwall $h_{mid} := \frac{h_w}{2} + h_d + h_{soil} = 34.88\,ft$

Lateral Soil Pressure at Mid-Wall $P_{lat} := k_o\cdot d_s\cdot h_{mid} = 12.9\,psi$

Wall Buckling - Linear Combination of Axial and Lateral Loads

Applied Axial Wall Compression, lbf	$F_{c_axi} = 1.489\times 10^{7}\,lbf$
Reduced Axial Wall Capacity, lbf	$F_{c_axi_red} = 1.21\times 10^{8}\,lbf$
Applied Lateral Wall Pressure, psi	$P_{lat} = 12.9psi$
Reduced Lateral Wall Pressure Capacity, psi	$P_{c_lat_red} = 74.5psi$

Axial Compression Fraction of Wall Buckling Capacity

$$R_{Axial} := SF_{c_axi}\cdot\left(\frac{F_{c_axi}}{F_{c_axi_red}}\right) = 0.431$$

Lateral Pressure Fraction of Wall Buckling Capacity

$$R_{Lateral} := SF_{c_lat}\cdot\left(\frac{P_{lat}}{P_{c_lat_red}}\right) = 0.303$$

Combined Fraction of Wall Buckling Capacity

$$R_{wall} := SF_{c_axi}\cdot\left(\frac{F_{c_axi}}{F_{c_axi_red}}\right) + SF_{c_lat}\cdot\left(\frac{P_{lat}}{P_{c_lat_red}}\right) = 0.734$$

What Safety Factors give a Demand/Capacity Ratio of 1.0?

Lateral Pressure Safety Factor on Wall Buckling $SF_{lat} := \frac{SF_{c_lat}}{R_{wall}} = 2.39$

Axial Compression Safety Factor on Wall Buckling $SF_{axi} := \frac{SF_{c_axi}}{R_{wall}} = 4.77$

References

Baker EH, L Kovalevsky, and FL Rish. 1972. *Structural Analysis of Shells*. McGraw-Hill, New York, New York.

Flugge, W. 1960. *Stresses in Shells*, Springer-Verlag, New York, New York.

IASS. 1979. *Recommendations for Reinforced Concrete Shells and Folded Plates*. Prepared by the Working Group No. 5 of The International Association for Shell and Spatial Structures (IASS), Stefan J. Medwadowski, Chairman. International Association for Shell and Spatial Structures, Madrid, Spain.

KI Johnson, JE Deibler, FG Abatt and MW Rinker. 2010. *Single Shell Tank Structural Evaluation Criteria*. PNNL-18837, Rev. 1. Pacific Northwest National Laboratory, Richland, Washington.

Popov EP and SJ Medwadowski. 1981. "Stability of Reinforced Concrete Shells: State-of-the-Art Overview." In *Concrete Shell Buckling*, ACI SP-67, American Concrete Institute, Detroit, Michigan.

Scordelis AC. 1981. "Stability of Reinforced Concrete Domes and Hyperbolic Paraboloid Shells." In *Concrete Shell Buckling*, ACI SP-67, American Concrete Institute, Detroit, Michigan.

Calculations for Case 2 – Wall Buckling Evaluation for Bounding Temperature with Actual Soil Overburden

Pacific Northwest National Laboratory
Tank Wall Buckling, Type-III Single Shell Tanks
Case 2. Actual 6.85 ft Soil Depth with Bounding Temperature

Page 1 of 9
Date: 7/28/2011 By: K. I. Johnson
Chkd: 8/7/2011 By: L. J. July
Revised: 8/10/2011 By: K. I. Johnson

Tank Wall Buckling
Case 2. Type III, Actual 6.85-ft Soil, Bounding Temperatures, 95/95 Lower Bound Concrete

The following tank buckling evaluation method is described in:
KI Johnson, JE Deibler, FG Abatt and MW Rinker. 2010. *Single Shell Tank Structural Evaluation Criteria*. PNNL-18837, Rev. 1. Pacific Northwest National Laboratory, Richland, Washington.

Tank Wall Degraded Concrete Properties		Tank Wall Reinforcing Steel Properties
Maximum wall temperature during tank history = 256 F		Current maximum temp = 80 F for Type III SSTs
Elastic Modulus (95/95 at Temp)	$E_c := 2.45 \times 10^6 \text{psi}$	$E_s := 29.4 \times 10^6 \text{psi}$
Concrete Strength (95/95 at Temp), psi	$f_{c_min} := 3440 \cdot \text{psi}$	
Concrete Density,	$d_c := 145 \cdot \text{pcf}$	
Poisson's Ratio	$\nu := 0.15$	$\nu_s := 0.30$

Tank Geometry - from SST Type III Drawing # H-2-808

Dome minimum wall thickness, t_d, inches $t_d := 15\text{in}$

Dome maximum mid-wall radius of curvature, R_d, inches $R_d := \left[\frac{(96.25 + 95) \cdot \text{ft}}{2}\right] = 95.6 \cdot \text{ft}$

Tank Wall Inner and Outer Radii $r_i := 37\text{ft} + 7.24\text{in} = 37.603\text{ft}$ $r_o := r_i + 15 \cdot \text{in} = 38.853 \cdot \text{ft}$

Tank cylinder mid-wall radius of curvature, R_c, inches $R_c := \frac{r_i + r_o}{2} = 38.228 \cdot \text{ft}$

Tank minimum wall thickness, t_w, inch $t_w := 15\text{in}$

Equivalent Tank Height - including half of Dome and Floor Heights

Dome Height - top of haunch to dome apex $h_d := 8 \cdot \text{ft} + 9.25 \cdot \text{in} = 105.25 \cdot \text{in}$

Wall Height - bottom of footing to haunch $h_w := 30 \cdot \text{ft} + 2.625 \cdot \text{in} = 362.625 \cdot \text{in}$

Dished Floor Depth (Type-III floor is flat) $h_f := 0 \cdot \text{in}$

Equivalent Tank Height, L_{eq} $L_{eq} := h_w + \frac{h_d}{2} + \frac{h_f}{2} = 415.25 \cdot \text{in}$

Tank Cylindrical Wall Buckling

Axial Compression

$$\sigma_{ca} := \frac{1}{\sqrt{3 \cdot (1 - \nu^2)}} \cdot E_c \cdot \left(\frac{t_w}{R_c}\right) = 4.678 \times 10^4 \text{psi} \qquad P_{ca} := 2 \cdot \pi \cdot R_c \cdot t_w \sigma_{ca} = 2.023 \times 10^9 \text{lbf}$$

Lateral Uniform Pressure on Tank Wall (Average Soil Pressure)

$h := t_w = 1.25\text{ft}$ $a := R_c = 38.228\text{ft}$ $E := E_c = 2.45 \times 10^6 \text{psi}$

$$k := \frac{h^2}{12 \cdot a^2} = 8.91 \times 10^{-5} \quad \lambda := \pi \cdot \frac{a}{L_{eq}} = 3.471 \quad \frac{L_{eq}}{a} = 0.905 \quad \frac{a}{h} = 30.583 \quad \beta := \frac{L_{eq}^2}{a \cdot h} = 25.1$$

Flugge, W., 1960, *Stresses in Shells*, Springer-Verlag, New York, New York.

page 432, Eqn 20

$$\varphi_{Flugge}(m,n,\nu,\lambda,k) := \frac{(1-\nu^2)\cdot(n\cdot\lambda)^4 + k\cdot\left[\left[(n\cdot\lambda)^2+m^2\right]^4 - 2\cdot\left[\nu\cdot(n\cdot\lambda)^6 + 3\cdot(n\cdot\lambda)^4\cdot m^2 \ldots + (4-\nu)\cdot(n\cdot\lambda)^2\cdot m^4 + m^6\right] \ldots + 2\cdot(2-\nu)\cdot(n\cdot\lambda)^2\cdot m^2 + m^4\right]}{m^2\cdot\left[(n\cdot\lambda)^2+m^2\right]^2 - m^2\cdot\left[3\cdot(n\cdot\lambda)^2+m^2\right]}$$

$m := 2 \quad n := 2$

Given

$m \geq 2$
$n \geq 1$

$\varphi_{Flugge}(m,n,\nu,\lambda,k) \geq 0$

$P(\nu,\lambda,k) := \text{Minimize}(\varphi_{Flugge}, m, n)$

$m_{min}(\nu,\lambda,k) := \text{round}(P(\nu,\lambda,k)_0)$

$n_{min}(\nu,\lambda,k) := \text{round}(P(\nu,\lambda,k)_1)$

$\varphi_{cr_Flugge}(\nu,\lambda,k) := \varphi_{Flugge}(m_{min}(\nu,\lambda,k), n_{min}(\nu,\lambda,k), \nu, \lambda, k)$

$p_{cr_Flugge}(E,\nu,\lambda,k) := \frac{E}{1-\nu^2}\cdot\sqrt{12\cdot k}\cdot\varphi_{cr_Flugge}(\nu,\lambda,k)$

Theoretical Lateral Buckling Pressure, P_{cl} $\quad P_{cl} := p_{cr_Flugge}(E,\nu,\lambda,k) = 605.7\,\text{psi}$

Buckling Load Reduction Factors

α_1 = The Geometric Imperfection Factor

For the Cylindrical wall under uniform lateral pressure $\alpha_{1c_lat} = 0.75$ (Seide, 1981)

For cylindrical wall under axial load $\quad \alpha_{1c_axi} = 1 - 0.9\cdot\left(1 - \exp\left(\frac{-1}{16}\cdot\sqrt{\frac{R}{t}}\right)\right)$

which is valid for $\quad 100 \leq \frac{R}{t} = \frac{a}{h} \leq 3000$ and $0.5 \leq \frac{L}{R} = \frac{L_{eq}}{a} \leq 5$

but $\frac{a}{h} = 30.583 \quad \frac{L_{eq}}{a} = 0.905$

Hence, conservatively assume R/t=100 $\quad \alpha_{1c_axi} := 1 - 0.9\cdot\left(1 - \exp\left(\frac{-1}{16}\cdot\sqrt{100}\right)\right) = 0.582$

Recommended Values

$\alpha_{1c_axi} := 0.58$ for axial compression of a cylinder

$\alpha_{1c_lat} := 0.75$ for external lateral pressure

α_2 = The Creep Buckling Load-Reduction Factor

C_u = ultimate creep strain / initial elastic strain

C_u from ANSYS Type II TOLA Model, creep in axial compression mid-wall

$$C_{ua} := \frac{11.8 \times 10^{-5}}{6.93 \times 10^{-5}} = 1.703$$

$$\alpha_{2a} := \frac{1}{(1 + C_{ua})} = 0.37$$

If a creep analysis is not available, Popov and Medwadowski (1981) recommend the following as an estimate of the ultimate creep coefficient, C_u:

$C_u = 4 - 2\log(f_c)$ where f_c is the concrete strength (N/mm^2) at the time of sustained loading .

$$f_c := \frac{f_{c_min}}{\frac{N}{mm^2}} = 23.7 \qquad C_{ub} := 4 - 2 \cdot \log(f_c) = 1.25 \qquad \alpha_{2b} := \frac{1}{(1 + C_{ub})} = 0.444$$

Use the maximum C_u to obtain minimum creep reduction factor

$$C_u := \max(C_{ua}, C_{ub}) = 1.703$$

$$\alpha_2 := \frac{1}{(1 + C_u)} = 0.37$$

α_3 = The Buckling Load-Reduction Factor Accounting for Cracking and the Amount and Type of Reinforcement.

E_{C2eol} is the effective concrete modulus in the dome accounting for creep strain and end-of-life degraded concrete modulus, E_{Ceol}.

Use the degraded concrete modulus based on thermal history

$$E_{Ceol} := E_c = 2.45 \times 10^6 \text{psi} \qquad E_{C2eol} := \frac{E_{Ceol}}{(1 + C_u)} = 9.065 \times 10^5 \text{psi}$$

$$\eta := \frac{E_s}{E_{C2eol}} = 32.433$$

Rebar Reinforcement Fractions

Meriidional Rebar - from SST Type III drawing # H-2-812

$Bar_m := 6$ Rebar Size (in 1/8th of an inch).

$S_{pm} := 12$ Bar Spacing (inches) near inner and outer wall surfaces

$$A_{sm} := 2 \cdot \left(\frac{Bar_m}{8}\right)^2 \cdot \frac{\pi}{4} \cdot \frac{12}{S_{pm}} = 0.884 \quad \text{Steel Area, in}^2\text{/ft}$$

$$A_c := 12 \cdot \frac{t_w}{in} = 180 \qquad \text{Concrete Area, in}^2\text{/ft} \qquad \rho_m := \frac{A_{sm}}{A_c} = 0.00491$$

Pacific Northwest National Laboratory
Tank Wall Buckling, Type-III Single Shell Tanks
Case 2, Actual 6.85 ft Soil Depth with Bounding Temperature

Date: 7/28/2011 By: K. I. Johnson
Chkd: 8/7/2011 By: L. J. July
Revised: 8/10/2011 By: K. I. Johnson

Hoop Rebar - from SST Type III drawing # H-2-812

$Bar_h := 7$ Rebar Size (in 1/8th of an inch).

$S_{ph} := 10$ Bar Spacing (inches) near inner and outer wall surfaces. (Varies from 6 inch at lower wall to 10" at top of wall. Conservatively assume 10 inch)

$A_{sh} := 2 \cdot \left(\frac{Bar_h}{8}\right)^2 \cdot \frac{\pi}{4} \cdot \frac{12}{S_{ph}} = 1.443$ Steel Area, in^2/ft $\rho_h := \frac{A_{sh}}{A_c} = 0.00802$

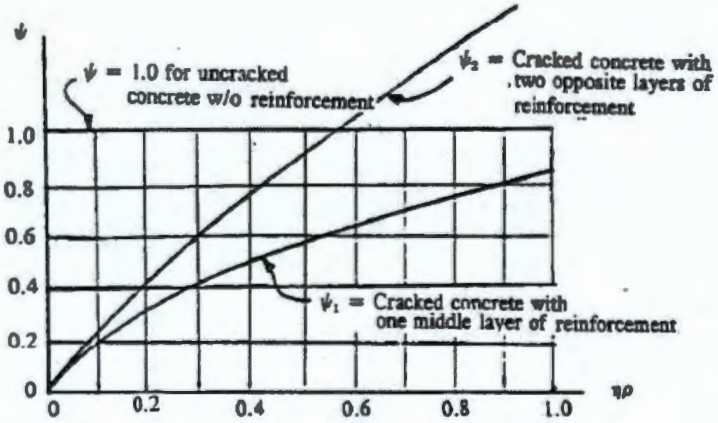

Values of ψ for Effect of Concrete Cracking And Amounts and Type of Reinforcement (Figure 4 of Scordelis 1981).
Must interpolate by eye

From the above plot for cracked concrete with two opposite layers of reinforcement.

Meridional Rebar $\eta \cdot \rho_m = 0.159$ $\psi_m := 0.40$

Hoop Rebar $\eta \cdot \rho_h = 0.26$ $\psi_h := 0.60$

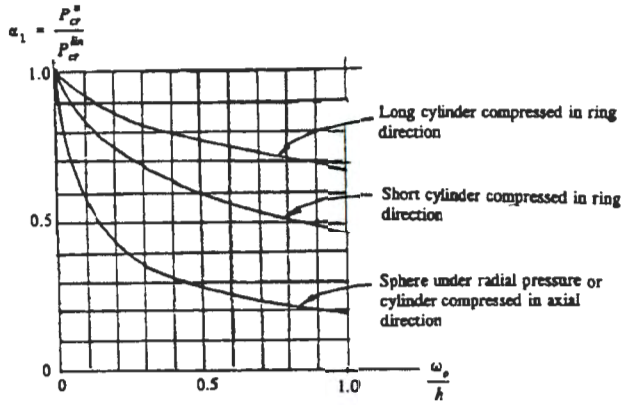

Effect of Geometric Imperfections on Buckling Load (Figure 3 of Scordelis 1981). ω_0/h factors for different geometries for specified geometric imperfection factor, α_1.

Must interpolate by eye

Tank Wall, Axial Load: Cylinder compressed in axial direction

$\alpha_{1c_axi} = 0.58$ $\omega_{ohc_axi} := 0.1$

Tank Wall, Lateral Pres: Short cylinder compressed in ring direction

$\alpha_{1c_lat} = 0.75$ $\omega_{ohc_lat} := 0.2$

Pacific Northwest National Laboratory
Tank Wall Buckling, Type-III Single Shell Tanks
Case 2, Actual 6.85 ft Soil Depth with Bounding Temperature

Page 8 of 9
Date: 7/28/2011 By: K. I. Johnson
Chkd: 8/7/2011 By: L. J. July
Revised: 8/10/2011 By: K. I. Johnson

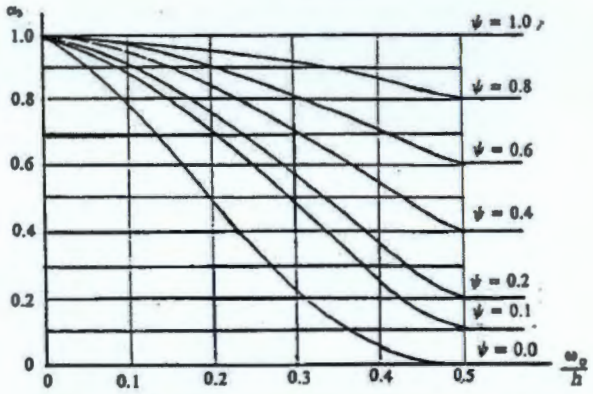

Reduction Factor α_3 for Concrete Cracking and Amount and Type of Reinforcement (Figure 5 of Scordelis 1981)

Must interpolate by eye

Tank Wall, Axial Load: cylinder compressed in axial direction (Meridional Rebar)

$\alpha_{1c_axi} = 0.58$ $\omega_{ohc_axi} = 0.1$ $\psi_m = 0.4$ $\alpha_{3c_axi} := 0.94$

Tank Wall, Lateral Pres: short cylinder compressed in ring direction (Hoop Rebar)

$\alpha_{1c_lat} = 0.75$ $\omega_{ohc_lat} = 0.2$ $\psi_h = 0.6$ $\alpha_{3c_lat} := 0.90$

Calculate $P_3 = \alpha_1\alpha_2\alpha_3 P_{buckle}$ and α_4 for highly loaded nonlinear concrete material effects

Axial Compressive Pressure on Cylindrical Wall, psi

$P_{3c_axi} := \alpha_{1c_axi} \cdot \alpha_2 \cdot \alpha_{3c_axi} \cdot \sigma_{ca} = 9436.8\,psi$

Ultimate axial force of concrete strength

Degraded Concrete Strength $f_{c_min} = 3440\,psi$ $F_{ult_axi} := 2 \cdot \pi \cdot R_c \cdot t_w \cdot f_{c_min} = 1.49 \times 10^8\,lbf$

$Raxi(\alpha_4) := (\alpha_4)^2 \left(\frac{P_{3c_axi}}{f_{c_min}}\right)^2 + (\alpha_4 - 1)$ $\alpha_{4axi} := root(Raxi(\alpha_4), \alpha_4, 0.01, 0.99) = 0.304$

Total Axial Load Reduction Factor $\alpha_{dc} := \alpha_{1c_axi} \cdot \alpha_2 \cdot \alpha_{3c_axi} \cdot \alpha_{4axi} = 0.06$

Reduced Axial Wall Buckling Pressure, psi $P_{c_axi_red} := \alpha_{4axi} \cdot P_{3c_axi} = 2869.7\,psi$

Reduced Axial Wall Buckling Force, psi $F_{c_axi_red} := P_{c_axi_red} \cdot 2 \cdot \pi R_c \cdot t_w = 1.241 \times 10^8\,lbf$

$tons := F_{c_axi_red} = 62036 \cdot tonf$

Lateral Compressive Pressure on **Short** Cylindrical Wall, psi

$P_{3c_lat} := \alpha_{1c_lat} \cdot \alpha_2 \cdot \alpha_{3c_lat} \cdot P_{cl} = 151.3\,psi$

Cylinder compressive hoop stress $\sigma_{hoop} := \frac{P_{3c_lat} \cdot R_c}{t_w} = 4626.3\,psi$

$Rlat(\alpha_4) := (\alpha_4)^2 \left(\frac{\sigma_{hoop}}{f_{c_min}}\right)^2 + (\alpha_4 - 1)$ $\alpha_{4lat} := root(Rlat(\alpha_4), \alpha_4, 0.01, 0.99) = 0.517$

Total Lateral Pressure Reduction Factor $\alpha_{dlat} := \alpha_{1c_lat} \cdot \alpha_2 \cdot \alpha_{3c_lat} \cdot \alpha_{4lat} = 0.13$

Reduced Lateral Buckling Pressure, Short Wall $P_{c_lat_red} := \alpha_{4lat} \cdot P_{3c_lat} = 78.2\,psi$

Ultimate Lateral Pressure for concrete strength $P_{ult_lat} := f_{c_min} \cdot \frac{t_w}{R_c} = 112.48\,psi$

Buckling Safety Factors

From the IASS Working Group No. 5, *Recommendations for Reinforced Concrete Shells and Folded Plates*, (IASS, 1979):
For shells that do not experience a reduction in load-carrying capacity in the post-buckling regime, a factor of safety of 1.75 is recommended. For shells that do experience a reduction in the load-carrying capacity in the post-buckling regime, a factor of safety of 3.5 is recommended.

Wall Uniform Axial Compression	$SF_{c_axi} := 3.5$	Post Buckling = Reduced Load Capacity
Wall Lateral Pressure	$SF_{c_lat} := 1.75$	Post Buckling = Displacement Controlled Loading, Soil Pressure is Self Relieving

Applied Loads on the Tank Wall

Axial Compressive Stress at the Mid-Height of the Wall

This includes the total weight of the soil, uniform live load, concentrated live load, and the weight of the dome and wall concrete.

Finite Element Results for Axial Compression at the Mid-Height of the Wall, Section 23 (F = 48.4 kip/ft)

Meridional Section Force, Loadstep 3, Gravity Loads $F_{c_axi} := 48.4\frac{kip}{ft}2\cdot\pi\cdot R_c = 1.16\times 10^7\,lbf$

Wall Lateral Earth Pressure calculated as the at rest soil pressure at depth=30.73-ft, Type-III tank ht=31'-11" from bottom of footing to top of dome, Soil depth=6.85-ft.

Soil internal friction angle, φ $\varphi := 35deg$ $k_o := 1 - \sin(\varphi) = 0.426$

Soil Density, d_s $d_s := 125pcf$

Soil Overburden Depth $h_{soil} := 6.85ft$

Soil Depth at Midwall $h_{mid} := \frac{h_w}{2} + h_d + h_{soil} = 30.73ft$

Lateral Soil Pressure at Mid-Wall $P_{lat} := k_o\cdot d_s\cdot h_{mid} = 11.4psi$

Wall Buckling - Linear Combination of Axial and Lateral Loads

Applied Axial Wall Compression, lbf $F_{c_axi} = 1.163\times 10^7\,lbf$

Reduced Axial Wall Capacity, lbf $F_{c_axi_red} = 1.241\times 10^8\,lbf$

Applied Lateral Wall Pressure, psi $P_{lat} = 11.4psi$

Reduced Lateral Wall Pressure Capacity, psi $P_{c_lat_red} = 78.2psi$

Axial Compression Fraction of Wall Buckling Capacity

$$R_{Axial} := SF_{c_axi}\cdot\left(\frac{F_{c_axi}}{F_{c_axi_red}}\right) = 0.328$$

Lateral Pressure Fraction of Wall Buckling Capacity

$$R_{Lateral} := SF_{c_lat}\cdot\left(\frac{P_{lat}}{P_{c_lat_red}}\right) = 0.255$$

Combined Fraction of Wall Buckling Capacity

$$R_{wall} := SF_{c_axi}\cdot\left(\frac{F_{c_axi}}{F_{c_axi_red}}\right) + SF_{c_lat}\cdot\left(\frac{P_{lat}}{P_{c_lat_red}}\right) = 0.583$$

What Safety Factors give a Demand/Capacity Ratio of 1.0?

Lateral Pressure Safety Factor on Wall Buckling

$$SF_{lat} := \frac{SF_{c_lat}}{R_{wall}} = 3$$

Axial Compression Safety Factor on Wall Buckling

$$SF_{axi} := \frac{SF_{c_axi}}{R_{wall}} = 6.01$$

References

Baker EH, L Kovalevsky, and FL Rish. 1972. *Structural Analysis of Shells*. McGraw-Hill, New York, New York.

Flugge, W. 1960. *Stresses in Shells*, Springer-Verlag, New York, New York.

IASS. 1979. *Recommendations for Reinforced Concrete Shells and Folded Plates*. Prepared by the Working Group No. 5 of The International Association for Shell and Spatial Structures (IASS), Stefan J. Medwadowski, Chairman. International Association for Shell and Spatial Structures, Madrid, Spain.

KI Johnson, JE Deibler, FG Abatt and MW Rinker. 2010. *Single Shell Tank Structural Evaluation Criteria*. PNNL-18837, Rev. 1. Pacific Northwest National Laboratory, Richland, Washington.

Popov EP and SJ Medwadowski. 1981. "Stability of Reinforced Concrete Shells: State-of-the-Art Overview." In *Concrete Shell Buckling*, ACI SP-67, American Concrete Institute, Detroit, Michigan.

Scordelis AC. 1981. "Stability of Reinforced Concrete Domes and Hyperbolic Paraboloid Shells." In *Concrete Shell Buckling*, ACI SP-67, American Concrete Institute, Detroit, Michigan.

Calculations for Case 3 – Wall Buckling Evaluation for Actual Temperature with Bounding Soil Overburden

Pacific Northwest National Laboratory
Tank Wall Buckling, Type-III Single Shell Tanks
Case 3. 11-ft Soil Depth with Actual Temperatures

Page 1 of 9
Date: 7/28/2011 By: K. I. Johnson
Chkd: 8/7/2011 By: L. J. Julyk
Revised: 8/10/2011 By: K. I. Johnson

Tank Wall Buckling
Case 3. Type III, 11-ft Soil, Actual Temperature, 95/95 Lower Bound Concrete

The following tank buckling evaluation method is described in:
KI Johnson, JE Deibler, FG Abatt and MW Rinker. 2010. *Single Shell Tank Structural Evaluation Criteria.* PNNL-18837, Rev. 1. Pacific Northwest National Laboratory, Richland, Washington.

Tank Wall Degraded Concrete Properties		**Tank Wall Reinforcing Steel Properties**
Maximum wall temperature during tank history = 116 F		Current maximum temp = 80 F for Type III SSTs
Elastic Modulus (95/95 at Temp)	$E_c := 4.33 \times 10^6 \text{psi}$	$E_s := 29.4 \times 10^6 \text{psi}$
Concrete Strength (95/95 at Temp), psi	$f_{c_min} := 4600 \cdot \text{psi}$	
Concrete Density,	$d_c := 145 \cdot \text{pcf}$	
Poisson's Ratio	$\nu := 0.15$	$\nu_s := 0.30$

Tank Geometry - from SST Type III Drawing # H-2-808

Dome minimum wall thickness, t_d, inches $t_d := 15\text{in}$

Dome maximum mid-wall radius of curvature, R_d, inches $R_d := \left[\frac{(96.25 + 95) \cdot \text{ft}}{2}\right] = 95.6 \cdot \text{ft}$

Tank Wall Inner and Outer Radii $r_i := 37\text{ft} + 7.24\text{in} = 37.603\text{ft}$ $r_o := r_i + 15 \cdot \text{in} = 38.853 \cdot \text{ft}$

Tank cylinder mid-wall radius of curvature, R_c, inches $R_c := \frac{r_i + r_o}{2} = 38.228 \cdot \text{ft}$

Tank minimum wall thickness, t_w, inch $t_w := 15\text{in}$

Equivalent Tank Height - including half of Dome and Floor Heights

Dome Height - top of haunch to dome apex $h_d := 8 \cdot \text{ft} + 9.25 \cdot \text{in} = 105.25 \cdot \text{in}$

Wall Height - bottom of footing to haunch $h_w := 30 \cdot \text{ft} + 2.625 \cdot \text{in} = 362.625 \cdot \text{in}$

Dished Floor Depth (Type-III floor is flat) $h_f := 0 \cdot \text{in}$

Equivalent Tank Height, L_{eq} $L_{eq} := h_w + \frac{h_d}{2} + \frac{h_f}{2} = 415.25 \cdot \text{in}$

Tank Cylindrical Wall Buckling

Axial

$$\sigma_{ca} := \frac{1}{\sqrt{3 \cdot (1 - \nu^2)}} \cdot E_c \cdot \left(\frac{t_w}{R_c}\right) = 8.268 \times 10^4 \text{psi} \qquad P_{ca} := 2 \cdot \pi \cdot R_c \cdot t_w \sigma_{ca} = 3.575 \times 10^9 \text{lbf}$$

Lateral Uniform Pressure on Tank Wall (Average Soil Pressure)

$h := t_w = 1.25\text{ft}$ $a := R_c = 38.228\text{ft}$ $E := E_c = 4.33 \times 10^6 \text{psi}$

$$k := \frac{h^2}{12 \cdot a^2} = 8.91 \times 10^{-5} \quad \lambda := \pi \cdot \frac{a}{L_{eq}} = 3.471 \quad \frac{L_{eq}}{a} = 0.905 \quad \frac{a}{h} = 30.583 \quad \beta := \frac{L_{eq}^2}{a \cdot h} = 25.1$$

Flugge, W., 1960, *Stresses in Shells*, Springer-Verlag, New York, New York.

page 432, Eqn 20

$$\varphi_{Flugge}(m,n,\nu,\lambda,k) := \frac{\left(1-\nu^2\right)\cdot(n\cdot\lambda)^4 + k\cdot\left[\left[(n\cdot\lambda)^2+m^2\right]^4 - 2\cdot\left[\begin{array}{l}\nu\cdot(n\cdot\lambda)^6 + 3\cdot(n\cdot\lambda)^4\cdot m^2 \ldots \\ + (4-\nu)\cdot(n\cdot\lambda)^2\cdot m^4 + m^6\end{array}\right]\ldots \\ + 2\cdot(2-\nu)\cdot(n\cdot\lambda)^2\cdot m^2 + m^4\right]}{m^2\cdot\left[(n\cdot\lambda)^2+m^2\right]^2 - m^2\cdot\left[3\cdot(n\cdot\lambda)^2+m^2\right]}$$

$m := 2 \quad n := 2$

Given

$m \ge 2$
$n \ge 1$

$\varphi_{Flugge}(m,n,\nu,\lambda,k) \ge 0$

$P(\nu,\lambda,k) := \text{Minimize}\left(\varphi_{Flugge}, m, n\right)$

$m_{min}(\nu,\lambda,k) := \text{round}\left(P(\nu,\lambda,k)_0\right)$

$n_{min}(\nu,\lambda,k) := \text{round}\left(P(\nu,\lambda,k)_1\right)$

$\varphi_{cr_Flugge}(\nu,\lambda,k) := \varphi_{Flugge}\left(m_{min}(\nu,\lambda,k), n_{min}(\nu,\lambda,k), \nu, \lambda, k\right)$

$p_{cr_Flugge}(E,\nu,\lambda,k) := \frac{E}{1-\nu^2}\cdot\sqrt{12\cdot k}\cdot\varphi_{cr_Flugge}(\nu,\lambda,k)$

Theoretical Lateral Buckling Pressure, P_{cl} $\quad P_{cl} := p_{cr_Flugge}(E,\nu,\lambda,k) = 1070.5\,\text{psi}$

Buckling Load Reduction Factors

α_1 = The Geometric Imperfection Factor

For the Cylindrical wall under uniform lateral pressure $\alpha_{1c_lat} = 0.75$ (Seide, 1981)

For cylindrical wall under axial load $\quad \alpha_{1c_axi} = 1 - 0.9\cdot\left(1 - \exp\left(\frac{-1}{16}\cdot\sqrt{\frac{R}{t}}\right)\right)$

which is valid for $\quad 100 \le \frac{R}{t} = \frac{a}{h} \le 3000 \quad$ and $\quad 0.5 \le \frac{L}{R} = \frac{L_{eq}}{a} \le 5$

but $\quad \frac{a}{h} = 30.583 \quad \frac{L_{eq}}{a} = 0.905$

Hence, conservatively assume R/t=100 $\quad \alpha_{1c_axi} := 1 - 0.9\cdot\left(1 - \exp\left(\frac{-1}{16}\cdot\sqrt{100}\right)\right) = 0.582$

Recommended Values

$\alpha_{1c_axi} := 0.58$ for axial compression of a cylinder

$\alpha_{1c_lat} := 0.75$ for external lateral pressure

α_2 = The Creep Buckling Load-Reduction Factor

C_u = ultimate creep strain / initial elastic strain

C_u from ANSYS Type II TOLA Model, creep in axial compression mid-wall

$$C_{ua} := \frac{0}{6.6 \times 10^{-5}} = 0$$

$$\alpha_{2a} := \frac{1}{(1 + C_{ua})} = 1$$

If a creep analysis is not available, Popov and Medwadowski (1981) recommend the following as an estimate of the ultimate creep coefficient, C_u:

$C_u = 4 - 2\log(f_c)$ where f_c is the concrete strength (N/mm^2) at the time of sustained loading .

$$f_c := \frac{f_{c_min}}{\frac{N}{mm^2}} = 31.7 \qquad C_{ub} := 4 - 2 \cdot \log(f_c) = 0.997 \qquad \alpha_{2b} := \frac{1}{(1 + C_{ub})} = 0.501$$

Use the maximum C_u to obtain minimum creep reduction factor

$$C_u := \max(C_{ua}, C_{ub}) = 0.997$$

$$\alpha_2 := \frac{1}{(1 + C_u)} = 0.501$$

α_3 = The Buckling Load-Reduction Factor Accounting for Cracking and the Amount and Type of Reinforcement.

E_{C2eol} is the effective concrete modulus in the dome accounting for creep strain and end-of-life degraded concrete modulus, E_{Ceol}.

Use the degraded concrete modulus based on thermal history

$$E_{Ceol} := E_c = 4.33 \times 10^6 \text{ psi} \qquad E_{C2eol} := \frac{E_{Ceol}}{(1 + C_u)} = 2.168 \times 10^6 \text{ psi}$$

$$\eta := \frac{E_s}{E_{C2eol}} = 13.562$$

Rebar Reinforcement Fractions

Meridional Rebar - from SST Type III drawing # H-2-812

$Bar_m := 6$ Rebar Size (in 1/8th of an inch).

$S_{pm} := 12$ Bar Spacing (inches) near inner and outer wall surfaces

$$A_{sm} := 2 \cdot \left(\frac{Bar_m}{8}\right)^2 \cdot \frac{\pi}{4} \cdot \frac{12}{S_{pm}} = 0.884 \text{ Steel Area, in}^2\text{/ft}$$

$$A_c := 12 \cdot \frac{t_w}{in} = 180 \qquad \text{Concrete Area, in}^2\text{/ft} \qquad \rho_m := \frac{A_{sm}}{A_c} = 0.00491$$

Pacific Northwest National Laboratory
Tank Wall Buckling, Type-III Single Shell Tanks
Case 3. 11-ft Soil Depth with Actual Temperatures

Page 4 of 9
Date: 7/28/2011 By: K. I. Johnson
Chkd: 8/7/2011 By: L. J. Julyk
Revised: 8/10/2011 By: K. I. Johnson

Hoop Rebar - from SST Type III drawing # H-2-812

$Bar_h := 7$ Rebar Size (in 1/8th of an inch).

$S_{ph} := 10$ Bar Spacing (inches) near inner and outer wall surfaces. (Varies from 6 inch at lower wall to 10" at top of wall. Conservatively assume 10 inch)

$$A_{sh} := 2 \cdot \left(\frac{Bar_h}{8}\right)^2 \cdot \frac{\pi}{4} \cdot \frac{12}{S_{ph}} = 1.443 \quad \text{Steel Area, in}^2\text{/ft} \qquad \rho_h := \frac{A_{sh}}{A_c} = 0.00802$$

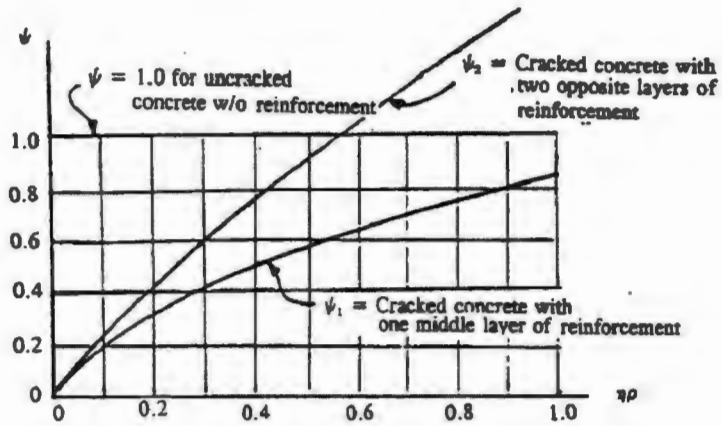

Values of ψ for Effect of Concrete Cracking And Amounts and Type of Reinforcement (*Figure 4 of* Scordelis 1981).

Must interpolate by eye

From the above plot for cracked concrete with two opposite layers of reinforcement.

Meridional Rebar $\eta \cdot \rho_m = 0.067$ $\psi_m := 0.20$

Hoop Rebar $\eta \cdot \rho_h = 0.109$ $\psi_h := 0.25$

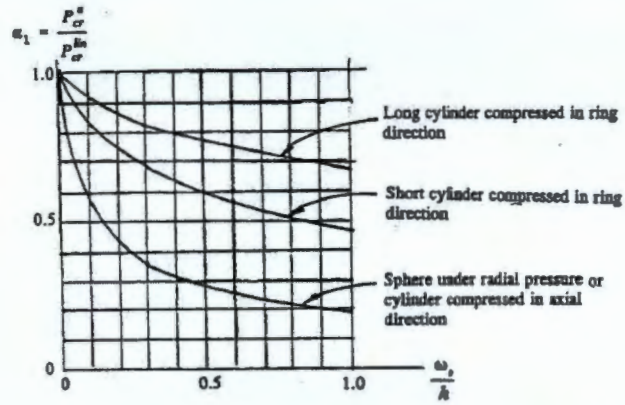

Effect of Geometric Imperfections on Buckling Load (Figure 3 of Scordelis 1981).
ω_0/h factors for different geometries for specified geometric imperfection factor, α_1.

Must interpolate by eye

Tank Wall, Axial Load: Cylinder compressed in axial direction

$\alpha_{1c_axi} = 0.58$ $\omega_{ohc_axi} := 0.1$

Tank Wall, Lateral Pres: Short cylinder compressed in ring direction

$\alpha_{1c_lat} = 0.75$ $\omega_{ohc_lat} := 0.2$

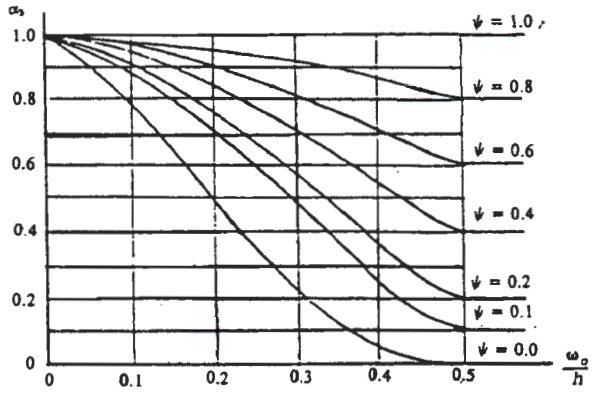

Reduction Factor α_3 for Concrete Cracking and Amount and Type of Reinforcement (Figure 5 of Scordelis 1981)

Must interpolate by eye

Tank Wall, Axial Load: cylinder compressed in axial direction (Meridional Rebar)

$\alpha_{1c_axi} = 0.58$ $\omega_{ohc_axi} = 0.1$ $\psi_m = 0.2$ $\alpha_{3c_axi} := 0.91$

Tank Wall, Lateral Pres: short cylinder compressed in ring direction (Hoop Rebar)

$\alpha_{1c_lat} = 0.75$ $\omega_{ohc_lat} = 0.2$ $\psi_h = 0.25$ $\alpha_{3c_lat} := 0.78$

Calculate $P_3 = \alpha_1\alpha_2\alpha_3 P_{buckle}$ and α_4 for highly loaded nonlinear concrete material effects

Axial Compressive Pressure on Cylindrical Wall, psi

$P_{3c_axi} := \alpha_{1c_axi} \cdot \alpha_2 \cdot \alpha_{3c_axi} \cdot \sigma_{ca} = 21846.8\,psi$

Ultimate axial force of concrete

Degraded Concrete Strength $f_{c_min} = 4600\,psi$ $F_{ult_axi} := 2 \cdot \pi \cdot R_c \cdot t_w \cdot f_{c_min} = 1.99 \times 10^8\,lbf$

$Raxi(\alpha_4) := (\alpha_4)^2 \left(\frac{P_{3c_axi}}{f_{c_min}}\right)^2 + (\alpha_4 - 1)$ $\alpha_{4axi} := root(Raxi(\alpha_4), \alpha_4, 0.01, 0.99) = 0.19$

Total Axial Load Reduction Factor $\alpha_{dc} := \alpha_{1c_axi} \cdot \alpha_2 \cdot \alpha_{3c_axi} \cdot \alpha_{4axi} = 0.05$

Reduced Axial Wall Buckling Pressure, psi $P_{c_axi_red} := \alpha_{4axi} \cdot P_{3c_axi} = 4141.1\,psi$

Reduced Axial Wall Buckling Force, psi $F_{c_axi_red} := P_{c_axi_red} \cdot 2 \cdot \pi R_c \cdot t_w = 1.79 \times 10^8\,lbf$

$tons := F_{c_axi_red} = 89522 \cdot tonf$

Lateral Compressive Pressure on **Short** Cylindrical Wall, psi

$P_{3c_lat} := \alpha_{1c_lat} \cdot \alpha_2 \cdot \alpha_{3c_lat} \cdot P_{cl} = 313.5\,psi$

Cylinder compressive hoop stress $\sigma_{hoop} := \frac{P_{3c_lat} \cdot R_c}{t_w} = 9588.1\,psi$

$Rlat(\alpha_4) := (\alpha_4)^2 \left(\frac{\sigma_{hoop}}{f_{c_min}}\right)^2 + (\alpha_4 - 1)$ $\alpha_{4lat} := root(Rlat(\alpha_4), \alpha_4, 0.01, 0.99) = 0.378$

Total Lateral Pressure Reduction Factor $\alpha_{dlat} := \alpha_{1c_lat} \cdot \alpha_2 \cdot \alpha_{3c_lat} \cdot \alpha_{4lat} = 0.11$

Reduced Lateral Buckling Pressure, Short Wall $P_{c_lat_red} := \alpha_{4lat} \cdot P_{3c_lat} = 118.6\,psi$

Ultimate Lateral Pressure for concrete strength $P_{ult_lat} := f_{c_min} \cdot \frac{t_w}{R_c} = 150.41\,psi$

Buckling Safety Factors

From the IASS Working Group No. 5, *Recommendations for Reinforced Concrete Shells and Folded Plates*, (IASS, 1979):
For shells that do not experience a reduction in load-carrying capacity in the post-buckling regime, a factor of safety of 1.75 is recommended. For shells that do experience a reduction in the load-carrying capacity in the post-buckling regime, a factor of safety of 3.5 is recommended.

Wall Uniform Axial Compression	$SF_{c_axi} := 3.5$	Post Buckling = Reduced Load Capacity
Wall Lateral Pressure	$SF_{c_lat} := 1.75$	Post Buckling = Displacement Controlled Loading, Soil Pressure is Self Relieving

Applied Loads on the Tank Wall

Axial Compressive Stress at the Mid-Height of the Wall

This includes the total weight of the soil, uniform live load, concentrated live load, and the weight of the dome and wall concrete.

Finite Element Results for Axial Compression at the Mid-Height of the Wall, Section 23 (F = 62 kip/ft)

Meridional Section Force, Loadstep 3, Gravity Loads $F_{c_axi} := 62\frac{kip}{ft}\,2\cdot\pi\cdot R_c = 1.49\times 10^7\,lbf$

Wall Lateral Earth Pressure calculated as the at rest soil pressure at depth=34.88-ft, Type-III tank ht=31'-11" from bottom of footing to top of dome, Soil depth=11-ft.

Soil internal friction angle, φ $\varphi := 35deg$ $k_o := 1 - \sin(\varphi) = 0.426$

Soil Density, d_s $d_s := 125pcf$

Soil Overburden Depth $h_{soil} := 11ft$

Soil Depth at Midwall $h_{mid} := \frac{h_w}{2} + h_d + h_{soil} = 34.88\,ft$

Lateral Soil Pressure at Mid-Wall $P_{lat} := k_o\cdot d_s\cdot h_{mid} = 12.9\,psi$

Wall Buckling - Linear Combination of Axial and Lateral Loads

Applied Axial Wall Compression, lbf	$F_{c_axi} = 1.489\times 10^7\,lbf$
Reduced Axial Wall Capacity, lbf	$F_{c_axi_red} = 1.79\times 10^8\,lbf$
Applied Lateral Wall Pressure, psi	$P_{lat} = 12.9\,psi$
Reduced Lateral Wall Pressure Capacity, psi	$P_{c_lat_red} = 118.6\,psi$

Axial Compression Fraction of Wall Buckling Capacity

$$R_{Axial} := SF_{c_axi}\cdot\left(\frac{F_{c_axi}}{F_{c_axi_red}}\right) = 0.291$$

Lateral Pressure Fraction of Wall Buckling Capacity

$$R_{Lateral} := SF_{c_lat}\cdot\left(\frac{P_{lat}}{P_{c_lat_red}}\right) = 0.191$$

Combined Fraction of Wall Buckling Capacity

$$R_{wall} := SF_{c_axi}\cdot\left(\frac{F_{c_axi}}{F_{c_axi_red}}\right) + SF_{c_lat}\cdot\left(\frac{P_{lat}}{P_{c_lat_red}}\right) = 0.482$$

What Safety Factors give a Demand/Capacity Ratio of 1.0?

Lateral Pressure Safety Factor on Wall Buckling

$$SF_{lat} := \frac{SF_{c_lat}}{R_{wall}} = 3.63$$

Axial Compression Safety Factor on Wall Buckling

$$SF_{axi} := \frac{SF_{c_axi}}{R_{wall}} = 7.27$$

References

Baker EH, L Kovalevsky, and FL Rish. 1972. *Structural Analysis of Shells*. McGraw-Hill, New York, New York.

Flugge, W. 1960. *Stresses in Shells*, Springer-Verlag, New York, New York.

IASS. 1979. *Recommendations for Reinforced Concrete Shells and Folded Plates*. Prepared by the Working Group No. 5 of The International Association for Shell and Spatial Structures (IASS), Stefan J. Medwadowski, Chairman. International Association for Shell and Spatial Structures, Madrid, Spain.

KI Johnson, JE Deibler, FG Abatt and MW Rinker. 2010. *Single Shell Tank Structural Evaluation Criteria*. PNNL-18837, Rev. 1. Pacific Northwest National Laboratory, Richland, Washington.

Popov EP and SJ Medwadowski. 1981. "Stability of Reinforced Concrete Shells: State-of-the-Art Overview." In *Concrete Shell Buckling*, ACI SP-67, American Concrete Institute, Detroit, Michigan.

Scordelis AC. 1981. "Stability of Reinforced Concrete Domes and Hyperbolic Paraboloid Shells." In *Concrete Shell Buckling*, ACI SP-67, American Concrete Institute, Detroit, Michigan.

Appendix J

Details of ACI-349 Demand/Capacity Calculations

This page intentionally left blank.

Appendix J

Details of ACI-349 Demand/Capacity Calculations

This appendix presents the details of the ACI-349 demand to capacity ratios that were calculated for meridional, hoop, and shear in each of the 44 tank sections presented throughout the body of this report. The hoop and meridional combined flexural capacities are determined by following the provisions in ACI-349-06 Section 10. The detailed calculation procedure is described in Section 3.2 of the SST Structural Evaluation Criteria report (Johnson et al. 2010). Assuming a linear strain profile, with a maximum strain in the concrete of 0.003 in/in, the forces and moments for the sections are calculated using a Whitney stress block approximation for the compressive concrete and elastic perfectly plastic behavior for the steel. A complete closed moment-axial force capacity curve (M-P diagram) can be calculated by varying the assumed depth of the neutral axis in the section as well as applying the appropriate strength reduction factors as described in ACI-349-06. Once the capacity interaction diagram is completed, the demand to capacity ratio is defined as the ratio of the length of the vector from the origin to the demand point over the length of the vector (in the same direction as the demand vector) from the origin to the capacity curve. Figure 8.2 illustrates this definition of D/C for the meridional and hoop directions. The through wall shear and in-plane shear capacity calculations are also described in the SST Structural Evaluation Criteria (Johnson et al., 2010). The shear capacity follows the provisions in ACI-349-06 Section 11.

The demand to capacity calculation was automated for all 44 ACI sections using an Excel document and a Mathcad™ document. The Mathcad™ document performs all the ACI-349-06 calculations necessary to develop the complete M-P diagram for capacity in both the hoop and meridional directions as well as the shear capacities. The Excel document contains all the necessary data to perform the calculations in Mathcad™. This data includes:

1. Section demands, current temperatures, and section locations and thicknesses for the specific load step extracted from the ANSYS® results. Table J.1 shows an example of the section demands, current temperatures, locations, and thicknesses for Run 1 under the peak temperature load step.
2. Section properties containing amounts and locations of reinforcing steel. These properties are shown in Tables 8.2 and 8.3.
3. Temperature dependent concrete compressive strengths and temperature dependent steel yield strength and modulus. These properties are described in Appendix A of the SST Structural Evaluation Criteria (Johnson et al. 2010).
4. Section maximum temperatures used to determine degraded concrete properties.

Table J.1. Example Table of Section Demands

Section	Shear [kips/ft]	F-merid [kips/ft]	M-merid [kips-ft/ft]	F-hoop [kips/ft]	M-hoop [kips-ft/ft]	Tmin [°F]	Tmax [°F]	Tave [°F]	xbar [in]	ybar [in]	sect-thk [in]	IP Shear [kips/ft]
1	0.3	-91.2	-4	-90.7	-4.5	209.9	221	215.2	34	460	15	0
2	0.7	-90.8	-3.6	-88.1	-3.7	210	221	215.3	67	458	15	0
3	1.1	-90.1	-3	-85	-3.4	210.2	221	215.4	101	456	15	0
4	1.6	-89	-2.5	-80.4	-3	210.4	221	215.5	134	453	15	0
5	2	-87.6	-1.9	-73.8	-2.7	210.8	221	215.6	167	448	15	0
6	2	-85.8	-1.3	-66.9	-2.4	210.8	221	215.7	200	443	15	0
7	1.8	-83.6	-2.2	-58.6	-2.5	211	221	215.9	233	436	15.2	0
8	1.2	-81	-4.2	-47.9	-3.2	211.1	221	215.9	266	427	15.5	0
9	0.3	-77.7	-6.3	-33	-4.4	211.1	221	215.9	298	418	15.9	0
10	-1.2	-73.8	-6.7	-13.8	-2.8	210.8	221	215.8	330	406	16.5	0
11	-3.6	-69.7	-2.7	-14.6	-3.7	210.1	221	215.4	361	394	17.4	0
12	-7.7	-66.9	11.4	-16.2	-0.5	207.4	220	213.7	392	381	19.8	0
13	-19	-64.7	33.1	-33.3	-3.3	202.8	219	210.7	417	369	23.7	0
14	-3.1	-65.9	60	-39.1	8.3	192.8	219	205.3	440	357	32.7	0
15	-4.7	-49.5	34.3	-20.3	-4.2	201.4	218	209.1	457	325	20.4	0
16	19	-69.9	24.9	-15.7	0.3	208.1	218	212.8	459	308	15	0
17	12	-72.1	6.8	-13.9	1.1	210.8	219	214.9	459	295	15	0
18	7.5	-72.2	-3	-18.6	1.2	213.1	220	216.8	459	283	15	0
19	2.1	-73.6	-10.9	-14.9	0.7	217.2	227	221.7	459	265	15	0
20	-0.9	-75	-12.9	-49.8	-2.4	220.7	229	225	459	245	15	0
21	-2.1	-76.7	-11.1	-69.3	-2.4	223.8	232	228	459	225	15	0
22	-2.2	-78.2	-8.3	-81.6	-1.6	226.6	235	230.9	459	205	15	0
23	-1.8	-79.4	-6.3	-89.7	-0.7	228.6	238	233.1	459	189	15	0
24	-1.1	-80.8	-4.6	-96.7	0.3	230.9	240	235.5	459	170	15	0
25	-0.8	-82.3	-3.7	-100.9	0.7	233.1	242	237.5	459	148	15	0
26	-1.4	-83.6	-2.5	-98	1.1	234.6	244	239.2	459	127	15	0
27	-3.2	-85	1.3	-97.1	2.7	236.2	246	241.1	459	103	15	0
28	-5.3	-85.9	6.5	-97.1	4.9	237.1	247	242.2	459	86.8	15	0
29	-10.2	-87.8	20.3	-108.7	10.9	237.1	255	245.3	458	59.2	16	0
30	-8.7	-92.1	-3.2	-139.5	-0.4	225.4	256	240.5	452	36	27.9	0
31	-25.9	-62	13.8	-24	2.9	192.5	207	200.4	482	18	36	0
32	17.6	-83.7	22.4	-114.6	4.8	243.1	260	251.1	405	10.4	20.8	0
33	9.4	-85.4	1.1	-112.5	-3.6	248.7	262	255.2	384	9.7	19.4	0
34	2.4	-86.6	-10	-110.5	-8.7	254.6	265	259.9	352	8.7	17.5	0
35	0	-87.5	-9.2	-109.4	-6.6	259.4	268	263.9	320	7.8	15.7	0
36	0	-87.6	-5.2	-105.8	-4.4	263.7	272	267.7	288	7	14	0
37	0.6	-87.3	-2.1	-102	-2.7	267.9	275	271.4	256	6.3	12.5	0
38	1.1	-86.7	-0.5	-98.2	-1.4	271.8	278	275	224	5.6	11.2	0
39	1.2	-85.9	0	-96.2	-0.5	275.6	281	278.5	192	5	10	0
40	1.1	-85	0.2	-90.7	-0.6	279.2	284	281.9	160	4.5	8.96	0
41	0.9	-84.2	0.4	-88.5	0.2	282.8	288	285.2	128	4	8.07	0
42	0.7	-83.5	0.6	-84.4	0.3	286.2	291	288.5	96	3.7	7.32	0
43	0.4	-83.4	1	-81.7	0.6	289.6	294	291.7	64	3.4	6.73	0
44	4.1	-86.6	-0.7	-78.5	-0.6	292.8	297	294.8	32	3.1	6.29	0

The Mathcad™ document loads the data from the Excel document and uses this to calculate the hoop, meridional, through wall shear and in-plane shear D/C ratios. While this Mathcad™ document was set up to automatically calculate all 44 sections using Mathcad™'s animate function, the document can also be used to evaluate individual sections. In this appendix, the Mathcad™ calculation sheets for section 14 are presented. This includes the hoop, meridional, through wall shear, and in-plane shear demand to capacity

calculations (for axisymmetric runs all of the in-plane shear demands are zero). After these calculations, the resulting D/C ratios, capacity curves, and demand vectors are output into external text files.

The Mathcad™ document performs the D/C calculations in eight sections:

1. Load data:

   Here the data from the Excel document is loaded for all 44 sections including the section properties, temperatures, and demands as well as the temperature dependent concrete and steel properties. Plots of tank geometry, temperature dependent concrete strength, section forces and moments, and temperature dependent steel modulus and yield strength are provided for quick verification that these inputs have been loaded correctly. Finally, the section number to be evaluated is entered into the Mathcad™ document. Alternatively, instead of one section number, "FRAME" can be entered and the animation function can be used to loop through all of the sections.

2. Global Parameters:

   Here, for a given section, the degraded concrete properties and reinforcing steel properties are set based on the maximum temperature experienced by that section and the current temperature of that section respectively. In addition, the section height (thickness), width, and gross area are calculated. In addition, the factor β_1 (the factor for the depth of the compressive stress block) is assigned somewhere from 0.65-0.85 depending on the concrete compressive strength according to ACI-349-06. Finally, the eccentricity factor α is also set and the axial load above where the strength reduction factor is 0.7 is determined.

3. Case-Specific Parameters and Geometry:

   Here, for a given section, section specific geometry properties (rebar depths, spacings, and areas and location of the plastic centroid) are calculated for both the meridional direction (left side) and circumferential (or hoop) direction (right side) for multiple layers of rebar in either direction. These section specific geometry properties are determined for both positive and negative bending moment in the meridional and circumferential directions. Finally, the pure compression strength reduction factor of 0.7 is applied to determine the maximum compression capacity (Point D) on the diagram.

4. Functions:

   Here, for a given section, functions are set up to calculate the axial force capacity, P, and positive or negative moment capacity, M_{pos} or M_{neg}. These capacities are set up as functions that depend on the neutral axis of strain, the rebar layer depths, the rebar layer areas, the plastic centroid location, the strength reduction factor, and the maximum compression capacity (Point D). The strength reduction factor, following the guidelines of ACI-349-06, is set to 0.7 for P (in compression) greater than $0.1f_c'A_g/0.7$, set to 0.9 for P in tension, and linearly interpolated for values in between.

5. Capacity Calculations:

   Here the capacity functions for P, M_{pos}, and M_{neg}, defined in the previous section are used to develop the complete diagram. First, the maximum possible neutral axis depth is determined. Then, the capacity functions are solved for 250 different neutral axis locations; for each given neutral axis the corresponding capacity axial force and moment are determined. Corresponding angles and vector lengths (from the origin to the capacity point) are determined to compare to the demands later. These 250 different capacity points are used to plot the complete diagrams in section 8 of the Mathcad™ document described below.

6. Demand Calculations:

   Here the meridional force and moments are used to determine the demand vector angle and length. For the given demand angle and length the capacity functions are solved again. This determines the exact capacity at that demand angle rather than interpolating between the 250 capacity points determined in the previous section. The D/C ratio for the meridional demand is then calculated. This process is repeated in the circumferential direction.

7. Shear Demand/Capacity Calculations:

   This section performs the through wall shear and in-plane shear D/C calculations. The shear capacity equations are from ACI-349-06 Section 11. The specific equation used to calculate the through wall capacity depends on the presence of flexure and axial tension or compression. The strength reduction factor of 0.85 is used to reduce the shear capacities. The through wall shear and in-plane shear D/C ratios are then calculated.

8. Results and Output:

   This section summarizes the D/C ratios in the circumferential, meridional, through wall shear, and in-plane shear directions. The circumferential and meridional capacity curves, demands, and D/C vectors are plotted on one M-P diagram. The D/C ratios are output to a text file. The capacity curves and the demand and capacity vectors are also output to separate text files.

J.1 Example Calculations for Hoop, Meridional, and Shear Demand/Capacity Ratios for Section 14

ACI Section Capacity/Demand Calculations
Tank Type II
Michael Schwendeman 7/14/10

SE Sanborn 10/13/10 Rev 4: Knocked down hoop rebar in haunch to 75%, added or logic to Case_c, case 4 to handle 0 moment with theta_c = theta min
SES 1/14/11 Rev 5: Reads in Rev5 excel sheet that counts middle layer of rebar in the haunch sections.
SES 2/3/11 Rev 6: Reads in Rev6 excel sheet that counts middle layer of rebar in sect 18
SES 3/30/11 Rev 7: Added in plane shear D/C for seismic demands
SES 4/25/11 Type III Rev 0: Modified for Type III tank
SES 5/12/11 Type III Rev 1: Reads in Rev1 Excel sheet
SES 5/19/11 Type III Rev 2: Reads in Rev2 Excel sheet
SES 5/20/11 Type III Rev 3: Reads in Rev3 Excel sheet
SES 5/26/11 Type III Rev 4: Reads in Rev4 Excel Sheet

Load Data:

Load Section Properties (excel): sectionprops := ACI-TypeIII[redacted]ta_Rev4.xls

Load Section Temperatures (excel): sectiontemps := ACI-TypeIII[redacted]ta_Rev4.xls

Load Concrete Compressive Strengths (excel): concretefc := ACI-TypeIII[redacted]ta_Rev4.xls

Load Bar Number Properties (excel): barprops := ACI-TypeIII[redacted]ta_Rev4.xls

Load Steel Yield Strengths (excel): steelstrengths := ACI-TypeIII[redacted]ta_Rev4.xls

Load Steel Modulus (excel): steelmodulus := ACI-TypeIII[redacted]ta_Rev4.xls

Load ANSYS Results (excel): ANSYS := ACI-TypeIII[redacted]ta_Rev4.xls

ORIGIN := 1 Defines first vector index as "1" rather than "0"

CALCULATE ALL SECTIONS INSTRUCTIONS:
1) Set Section:=FRAME
2) Find the function APPENDPRN at the bottom of the program
3) Specify a *unique* filename.txt and output vector (best if a horizontal vector beginning with section number) in APPENDPRN("filename.txt",outputVector)
4) Right-click APPENDPRN and choose "enable evaluation"
5) In Tools>Animation>Record, choose the range of Section numbers using "from" and "to"
6) With the Record Animation window open, drag to highlight the APPENPRN statement
7) Click "Animate" and wait for it to cycle through all the sections
8) When it finishes, click "cancel", close the animation playback window, and open filename.txt to access your data

Pacific Northwest National Laboratory
ACI-349-06 Demand/Capacity Calculation - Section 14 Example

Date: 7/14/2010 By: M.S. Schwendeman
Chkd: 8/2/2010 By: S.E. Sanborn
Revised: 5/26/2011 By: S.E.Sanborn

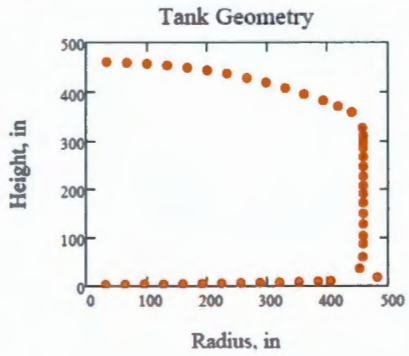

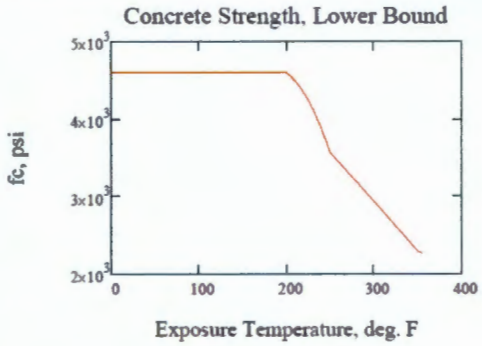

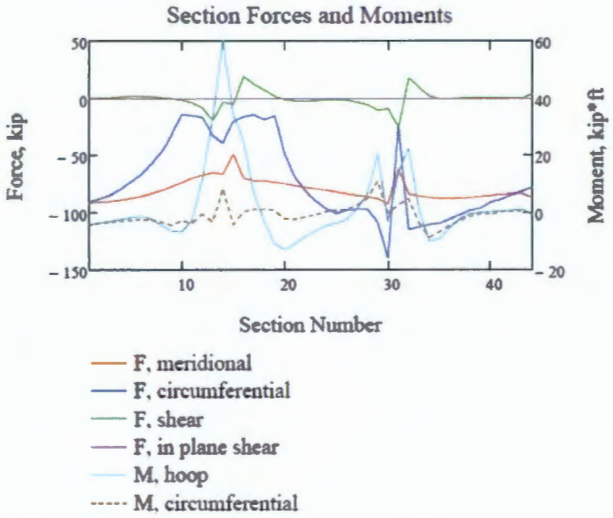

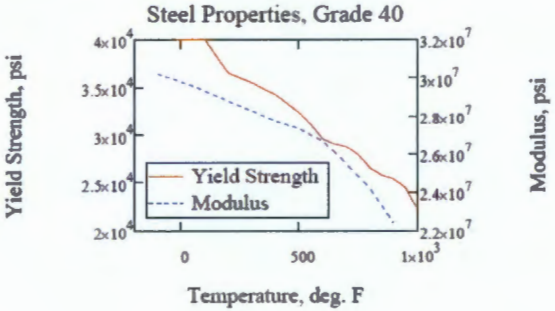

Input Section Number: Section := 14

Global Parameters:

Mechanical Properties:

Concrete: **max concrete temperature:** $T_{max} := \text{vlookup}(\text{Section}, \text{sectiontemps}, 2)_1 = 218.6$

Compressive strength: $f_c := \text{linterp}\left(\text{concretefc}^{\langle 1 \rangle}, \text{concretefc}^{\langle 2 \rangle}, T_{max}\right) \text{psi} = 4.362 \times 10^3 \text{ psi}$

Compressive strain: $\varepsilon_{cu} := 0.003 \frac{\text{in}}{\text{in}}$

Steel: **Grade:** $\text{grade} := \text{vlookup}(\text{Section}, \text{sectionprops}, 6)_1 = 40$

Average Section Temp: $\text{tempAve} := \text{vlookup}(\text{Section}, \text{ANSYS}, 9)_1 = 205.3$

Yield strength: $f_y := \frac{\text{grade}}{40} \text{linterp}\left(\text{steelstrengths}^{\langle 1 \rangle}, \text{steelstrengths}^{\langle 2 \rangle}, \text{tempAve}\right) 1000 \text{ psi} = 3.6447 \times 10^4 \text{ psi}$

Modulus: $E_s := \text{linterp}\left(\text{steelmodulus}^{\langle 1 \rangle}, \text{steelmodulus}^{\langle 2 \rangle}, \text{tempAve}\right) 10^6 \text{ psi} = 2.877 \times 10^7 \text{ psi}$

Yield strain: $\varepsilon_y := \frac{f_y}{E_s} = 1.267 \times 10^{-3}$

Section Geometry

Height: $h := \text{vlookup}(\text{Section}, \text{sectionprops}, 3)_1 \text{ in} = 32.72 \text{ in}$

Unit width: $b := 12\text{in}$ **Section area:** $A_g := b\,h = 392.64 \text{ in}^2$

Other Parameters

β_1, using section 10 of ACI 349-06:

$$\beta_1 := \begin{cases} \left[0.85 - \frac{0.05}{1000\text{psi}}\left(f_c - 4000\text{psi}\right)\right] & \text{if } \left[f_c < 4000\text{psi} + (0.85 - 0.65)\frac{1000\text{psi}}{0.05}\right] \\ 0.85 & \text{if } \left(f_c < 4000\text{psi}\right) \\ 0.65 & \text{otherwise} \end{cases} = 0.8319$$

α, factor to account for small eccentricity of axial load for columns $\alpha := 0.8$

$$P_\varphi := \frac{0.1\, f_c\, A_g}{0.7} = 244.644 \text{ kip}$$

Case-Specific Parameters and Geometry:

"mp"=Meridional, positive moment,
"mn"=Meridional, negative moment
"cp"=Circumferential, positive moment,

Cycle through all possible bars: $Bars_m := 4$ $\quad j := 1..Bars_m$

+M, meridional

Define vector of relative bar property cell distance for lookup [bar1, bar2, bar3, bar4], with bar1 being the most compressed bar, and bar4 the least: $k_p := (0\ \ 20\ \ 30\ \ 10)^T$

Bar size no.: $sizeNo_{mp_j} := vlookup(Section, sectionprops, 9 + k_{p_j})_1$

Depth: $d_{mp_j} := vlookup(Section, sectionprops, 10 + k_{p_j})_1\ in$

Diameter: $d_{b_mp_j} := vlookup(sizeNo_{mp_j}, barprops, 3)_1\ in$

Spacing: $s_{p_mp_j} := vlookup(Section, sectionprops, 11 + k_{p_j})_1\ in$

Area: $$A_{mp_j} := \begin{cases} \left[\pi\left(\frac{d_{b_mp_j}}{2}\right)^2 \frac{b}{s_{p_mp_j}}\right] & \text{if } s_{p_mp_j} \neq 0 \\ 0 & \text{otherwise} \end{cases}$$

Total Bar Geometry: Total area: $A_{st_m} := \sum A_{mp} = 1.312\ in^2$

Plastic Centroid: $$x_{p_mp} := \frac{\left[0.85\ b\ f_c \frac{h^2}{2} + f_y \sum \overrightarrow{(A_{mp}\ d_{mp})}\right]}{0.85 f_c\ b\ h + f_y \sum A_{mp}} = 16.25\ in$$

Cycle through possible bars (no fourth bar for circumferential): $Bars_c := 3$ $\quad r := 1..Bars_c$

+M, circumferential

Define vector of relative bar property cell distance for lookup [bar1, bar2, bar3], with bar1 being the most compressed bar, and bar3 the least: $s_p := (0\ \ 20\ \ 10)^T$

Bar size no.: $sizeNo_{cp_r} := vlookup(Section, sectionprops, 13 + s_{p_r})_1$

Depth: $d_{cp_r} := vlookup(Section, sectionprops, 14 + s_{p_r})_1\ in$

Diameter: $d_{b_cp_r} := vlookup(sizeNo_{cp_r}, barprops, 3)_1\ in$

Spacing: $s_{p_cp_r} := vlookup(Section, sectionprops, 15 + s_{p_r})_1\ in$

Area: $$A_{cp_r} := \begin{cases} \left[\pi\left(\frac{d_{b_cp_r}}{2}\right)^2 \frac{b}{s_{p_cp_r}}\right] & \text{if } s_{p_cp_r} \neq 0 \\ 0 & \text{otherwise} \end{cases}$$

Total Bar Geometry: Total area: $A_{st_c} := \sum A_{cp} = 5.422\ in^2$

Plastic Centroid: $$x_{p_cp} := \frac{\left[0.85\ b\ f_c \frac{h^2}{2} + f_y \sum \overrightarrow{(A_{cp}\ d_{cp})}\right]}{0.85 f_c\ b\ h + f_y \sum A_{cp}} = 16.295\ in$$

-M, meridional

Define vector of relative bar property cell distance for lookup [bar1, bar2, bar3, bar4], with bar1 being the most compressed bar, and bar4 the least: $k_n := (10\ \ 30\ \ 20\ \ 0)^T$

Bar size no.: $sizeNo_{mn_j} := vlookup\left(Section, sectionprops, 9 + k_{n_j}\right)_1$

Depth: $d_{mn_j} := h - \left(vlookup\left(Section, sectionprops, 10 + k_{n_j}\right)_1 in\right)$

Diameter: $d_{b_mn_j} := vlookup\left(sizeNo_{mn_j}, barprops, 3\right)_1 in$

Spacing: $s_{p_mn_j} := vlookup\left(Section, sectionprops, 11 + k_{n_j}\right)_1 in$

Area: $A_{mn_j} := \begin{cases} \pi\left(\dfrac{d_{b_mn_j}}{2}\right)^2 \dfrac{b}{s_{p_mn_j}} & \text{if } s_{p_mn_j} \neq 0 \\ 0 & \text{otherwise} \end{cases}$

Plastic Centroid: $x_{p_mn} := \dfrac{\left[0.85\, b\, f_c \dfrac{h^2}{2} + f_y \sum \overrightarrow{\left(A_{mn}\, d_{mn}\right)}\right]}{0.85 f_c\, b\, h + f_y \sum A_{mn}} = 16.47\ in$

Find Point "D" force value, which serves as upper bound on force capacity

Point D: $\varphi_D := 0.7$ $\quad P_{D_m} := \alpha\, \varphi_D \left[0.85\, f_c \left(A_g - A_{st_m}\right) + f_y A_{st_m}\right] = 839.212\ kip$

-M, meridional

Define vector of relative bar property cell distance for lookup [bar1, bar2, bar3], with bar1 being the most compressed bar, and bar3 the least: $s_n := (10\ \ 20\ \ 0)^T$

Bar size no.: $sizeNo_{cn_r} := vlookup\left(Section, sectionprops, 13 + s_{n_r}\right)_1$

Depth: $d_{cn_r} := h - \left(vlookup\left(Section, sectionprops, 14 + s_{n_r}\right)_1 in\right)$

Diameter: $d_{b_cn_r} := vlookup\left(sizeNo_{cn_r}, barprops, 3\right)_1 in$

Spacing: $s_{p_cn_r} := vlookup\left(Section, sectionprops, 15 + s_{n_r}\right)_1 in$

Area: $A_{cn_r} := \begin{cases} \left[\pi\left(\dfrac{d_{b_cn_r}}{2}\right)^2 \dfrac{b}{s_{p_cn_r}}\right] & \text{if } s_{p_cn_r} \neq 0 \\ 0 & \text{otherwise} \end{cases}$

Plastic Centroid: $x_{p_cn} := \dfrac{\left[0.85\, b\, f_c \dfrac{h^2}{2} + f_y \sum \overrightarrow{\left(A_{cn}\, d_{cn}\right)}\right]}{0.85 f_c\, b\, h + f_y \sum A_{cn}} = 16.425\ in$

Point D: $P_{D_c} := \alpha\, \varphi_D \left[0.85\, f_c \left(A_g - A_{st_c}\right) + f_y A_{st_c}\right] = 914.558\ kip$

Functions:

Moment and force (P) evaluated for given c (neutral axis of strain), d (vector of bar depths), A_s (vector of bar areas), x_p (plastic centroid), P_φ (determines φ factor), and P_D (maximum allowable force).

$$C_c(c) := 0.85\, f_c\, b\, \beta_1\, c$$

$$\varepsilon_s(c,d) := \begin{cases} \varepsilon_{cu}\dfrac{(c-d)}{c} & \text{if } c \neq 0 \\ \text{sign}(-d)\ 1\ 10^{10} & \text{otherwise} \end{cases} \qquad \text{A big number}$$

$$f_s(c,d) := \begin{cases} \min\left(E_s\, \varepsilon_s(c,d), f_y\right) & \text{if } \varepsilon_s(c,d) > 0 \\ \max\left(E_s\, \varepsilon_s(c,d), -f_y\right) & \text{otherwise} \end{cases}$$

$$F_s(c,d,A_s) := \begin{cases} \left(A_s\, f_s(c,d)\right) & \text{if } \beta_1\, c < d \\ \left[A_s\left(f_s(c,d) - 0.85\, f_c\right)\right] & \text{otherwise} \end{cases}$$

$$P_n(c,d,A_s,N) := C_c(c) + \sum_{m=1}^{N} F_s\left(c, d_m, A_{s_m}\right)$$

$$\varphi(c,d,A_s,N,P_\varphi) := \begin{cases} 0.9 & \text{if } P_n(c,d,A_s,N) < 0 \\ 0.7 & \text{if } P_n(c,d,A_s,N) > P_\varphi \\ \left[0.7 + \dfrac{(0.9-0.7)\left(P_\varphi - P_n(c,d,A_s,N)\right)}{P_\varphi}\right] & \text{otherwise} \end{cases}$$

$$M_{pos}(c,d,A_s,x_p,N,P_\varphi) := \varphi(c,d,A_s,N,P_\varphi)\left[C_c(c)\left(x_p - \frac{\beta_1\, c}{2}\right) + \sum_{m=1}^{N}\left[F_s\left(c,d_m,A_{s_m}\right)\left(x_p - d_m\right)\right]\right]$$

$$M_{neg}(c,d,A_s,x_p,N,P_\varphi) := -\varphi(c,d,A_s,N,P_\varphi)\left[C_c(c)\left(x_p - \frac{\beta_1\, c}{2}\right) + \sum_{m=1}^{N}\left[F_s\left(c,d_m,A_{s_m}\right)\left(x_p - d_m\right)\right]\right]$$

$$P(c,d,A_s,N,P_\varphi,P_D) := \min\left(P_D, \varphi(c,d,A_s,N,P_\varphi)\, P_n(c,d,A_s,N)\right)$$

Capacity Calculations:

Generates capacity curve for vector of c values

Meridional

determine c_{max} for calculations (meridional):

$c_{max_m} := root(M_{pos}(c, d_{mp}, A_{mp}, x_{p_mp}, Bars_m, P_\varphi) - M_{neg}(c, d_{mn}, A_{mn}, x_{p_mn}, Bars_m, P_\varphi), c, .1\ in, 50in) = 39.533\ in$

input desired number of points: $n := 250$

increment: $dc_m := \frac{c_{max_m}}{n-1} = 0.159\ in$

set up vector of c values for calculations

$i := 1..n$

$c_{m_i} := dc_m \cdot (i-1)$

+M

$P_{mp_i} := P(c_{m_i}, d_{mp}, A_{mp}, Bars_m, P_\varphi, P_{D_m})$

$M_{mp_i} := M_{pos}(c_{m_i}, d_{mp}, A_{mp}, x_{p_mp}, Bars_m, P_\varphi)$

-M

$P_{mn_i} := P(c_{m_i}, d_{mn}, A_{mn}, Bars_m, P_\varphi, P_{D_m})$

$M_{mn_i} := M_{neg}(c_{m_i}, d_{mn}, A_{mn}, x_{p_mn}, Bars_m, P_\varphi)$

concatenate +M and -M vectors

$M_m := stack(M_{mp}, M_{mn})$

$P_m := stack(P_{mp}, P_{mn})$

$i := 1..2n$

Circumferential

determine c_{max} for calculations (cirumferential):

$c_{max_c} := root(M_{pos}(c, d_{cp}, A_{cp}, x_{p_cp}, Bars_c, P_\varphi) - M_{neg}(c, d_{cn}, A_{cn}, x_{p_cn}, Bars_c, P_\varphi), c, .1in, 50in) = 39.888\ in$

input desired number of points: $n := n$ **(see left)**

increment: $dc_c := \frac{c_{max_c}}{n-1} = 0.16\ in$

set up vector of c values for calculations

$i := i$ **(see left)**

$c_{c_i} := dc_c \cdot (i-1)$

+M

$P_{cp_i} := P(c_{c_i}, d_{cp}, A_{cp}, Bars_c, P_\varphi, P_{D_c})$

$M_{cp_i} := M_{pos}(c_{c_i}, d_{cp}, A_{cp}, x_{p_cp}, Bars_c, P_\varphi)$

-M

$P_{cn_i} := P(c_{c_i}, d_{cn}, A_{cn}, Bars_c, P_\varphi, P_{D_c})$

$M_{cn_i} := M_{neg}(c_{c_i}, d_{cn}, A_{cn}, x_{p_cn}, Bars_c, P_\varphi)$

concatenate +M and -M vectors

$M_c := stack(M_{cp}, M_{cn})$

$P_c := stack(P_{cp}, P_{cn})$

$i := i$ **(see left)**

Calculate the angles and lengths of the capacity vectors, for comparision with demand vectors:

Angle: $\theta_{m_i} := \mathrm{atan2}\left(M_{m_i}\,kip^{-1}\,ft^{-1}, P_{m_i}\,kip^{-1}\right)$

Length: $r_{m_i} := \sqrt{\left(P_{m_i}\,kip^{-1}\right)^2 + \left(M_{m_i}\,kip^{-1}\,ft^{-1}\right)^2}$

For unit agreement, nondimensionalize forces and moments by reference force of 1 kip and reference length of 1 ft.

Define max and min angles

$\theta_{max_m} := \theta_{m_n} = 90.125\ deg$

$\theta_{min_m} := \theta_{m_1} = -105.569\ deg$

Create Ouput Matrix of P,M,θ,and r values and sort by θ

$MeridMatrix := augment\left(M_m\,kip^{-1}\,ft^{-1}, P_m\,kip^{-1}, r_m, \theta_m\right)$

$MeridOutput := csort(MeridMatrix, 4)$

Calculate the angles and lengths of the capacity vectors, for comparision with demand vectors:

$\theta_{c_i} := \mathrm{atan2}\left(M_{c_i}\,kip^{-1}\,ft^{-1}, P_{c_i}\,kip^{-1}\right)$

Length: $r_{c_i} := \sqrt{\left(P_{c_i}\,kip^{-1}\right)^2 + \left(M_{c_i}\,kip^{-1}\,ft^{-1}\right)^2}$

For unit agreement, nondimensionalize forces and moments by reference force of 1 kip and reference length of 1 ft.

Define max and min angles

$\theta_{max_c} := \theta_{c_n} = 90.124\ deg$

$\theta_{min_c} := \theta_{c_1} = -92.296\ deg$

Create Ouput Matrix of P,M,θ,and r values and sort by θ

$CircumMatrix := augment\left(M_c\,kip^{-1}\,ft^{-1}, P_c\,kip^{-1}, r_c, \theta_c\right)$

$CircumOutput := csort(CircumMatrix, 4)$

Demand Calculations:

Meridional Demand:

Force: $P_{u_m} := (-\text{vlookup}(\text{Section}, \text{ANSYS}, 3))_1 \text{ kip} = 65.9 \text{ kip}$

Moment: $M_{u_m} := (-\text{vlookup}(\text{Section}, \text{ANSYS}, 4))_1 \text{ kip ft} = -60 \text{ kip ft}$

For unit agreement, nondimensionalize forces and moments by reference force of 1 kip and length of 1 ft.

Demand angle and length:

Angle: $\theta_{u_m} := \begin{cases} \text{atan2}\left(M_{u_m} \text{kip}^{-1} \text{ft}^{-1}, P_{u_m} \text{kip}^{-1}\right) & \text{if } M_{u_m} \neq 0 \vee P_{u_m} \neq 0 \\ 0 & \text{otherwise} \end{cases} = 132.317°$

Length: $r_{u_m} := \sqrt{\left(P_{u_m} \text{kip}^{-1}\right)^2 + \left(M_{u_m} \text{kip}^{-1} \text{ft}^{-1}\right)^2} = 89.12244$

Ratio: $\text{MtoF}_m := \begin{cases} \dfrac{M_{u_m} \text{kip}^{-1} \text{ft}^{-1}}{P_{u_m} \text{kip}^{-1}} & \text{if } P_{u_m} \neq 0 \\ 1 & \text{otherwise} \end{cases} = -0.91$

Evaluate based on whether using +M terms (cases 1 and 2) or -M terms (cases 3 and 4) and whether P_u is positive (cases 1 and 3) or negative (cases 2 and 4) or zero (cases 5 and 6)

$$\text{Case}_m := \begin{cases} 1 & \text{if } (\theta_{u_m} \le \theta_{max_m}) \wedge (\theta_{u_m} \ge \theta_{min_m}) \wedge P_{u_m} > 0 = 3 \\ 2 & \text{if } (\theta_{u_m} \le \theta_{max_m}) \wedge (\theta_{u_m} \ge \theta_{min_m}) \wedge P_{u_m} < 0 \\ 3 & \text{if } (\theta_{u_m} > \theta_{max_m}) \\ 4 & \text{if } (\theta_{u_m} < \theta_{min_m}) \\ 5 & \text{if } P_{u_m} = 0 \wedge M_{u_m} \ge 0 \\ 6 & \text{if } P_{u_m} = 0 \wedge M_{u_m} < 0 \end{cases}$$

Find c_0, where P=0

$c_{0_mp} := \mathrm{root}(P(c, d_{mp}, A_{mp}, Bars_m, P_\varphi, P_{D_m}), c, 0, c_{max_m}) = 1.292\,in$

$c_{0_mn} := \mathrm{root}(P(c, d_{mn}, A_{mn}, Bars_m, P_\varphi, P_{D_m}), c, 0, c_{max_m}) = 1.292\,in$

solve for the c value that will give the correct angle for comparison with the demand

$$c_{cap_m} := \begin{cases} \mathrm{root}\left(M_{pos}(c, d_{mp}, A_{mp}, x_{p_mp}, Bars_m, P_\varphi)\,kip^{-1}\,ft^{-1} - MtoF_m\,P(c, d_{mp}, A_{mp}, Bars_m, P_\varphi, P_{D_m})\,kip^{-1}, c, c_{0_mp}, c_{max_m}\right) & \text{if } Case_m = 1 \\ \mathrm{root}\left(M_{pos}(c, d_{mp}, A_{mp}, x_{p_mp}, Bars_m, P_\varphi)\,kip^{-1}\,ft^{-1} - MtoF_m\,P(c, d_{mp}, A_{mp}, Bars_m, P_\varphi, P_{D_m})\,kip^{-1}, c, 0, c_{0_mp}\right) & \text{if } Case_m = 2 \\ \mathrm{root}\left(M_{neg}(c, d_{mn}, A_{mn}, x_{p_mn}, Bars_m, P_\varphi)\,kip^{-1}\,ft^{-1} - MtoF_m\,P(c, d_{mn}, A_{mn}, Bars_m, P_\varphi, P_{D_m})\,kip^{-1}, c, c_{0_mn}, c_{max_m}\right) & \text{if } Case_m = 3 \\ \mathrm{root}\left(M_{neg}(c, d_{mn}, A_{mn}, x_{p_mn}, Bars_m, P_\varphi)\,kip^{-1}\,ft^{-1} - MtoF_m\,P(c, d_{mn}, A_{mn}, Bars_m, P_\varphi, P_{D_m})\,kip^{-1}, c, 0, c_{0_mn}\right) & \text{if } Case_m = 4 \\ c_{0_mp} & \text{if } Case_m = 5 \\ c_{0_mn} & \text{if } Case_m = 6 \end{cases} = 16.447\,in$$

Calculate $M_{capacity}$ and $P_{capacity}$ for this angle

$$M_{cap_m} := \begin{cases} M_{pos}(c_{cap_m}, d_{mp}, A_{mp}, x_{p_mp}, Bars_m, P_\varphi) & \text{if } Case_m = 1 \vee Case_m = 2 \vee Case_m = 5 \\ M_{neg}(c_{cap_m}, d_{mn}, A_{mn}, x_{p_mn}, Bars_m, P_\varphi) & \text{otherwise} \end{cases} = -376.765\,kip\,ft$$

$$P_{cap_m} := \begin{cases} P(c_{cap_m}, d_{mp}, A_{mp}, Bars_m, P_\varphi, P_{D_m}) & \text{if } Case_m = 1 \vee Case_m = 2 \vee Case_m = 5 \\ P(c_{cap_m}, d_{mn}, A_{mn}, Bars_m, P_\varphi, P_{D_m}) & \text{otherwise} \end{cases} = 413.813\,kip$$

Find the demand/capacity ratio

$$r_{cap_m} := \sqrt{\left(P_{cap_m}\,kip^{-1}\right)^2 + \left(M_{cap_m}\,kip^{-1}\,ft^{-1}\right)^2} = 559.636$$

$$DCratio_m := \frac{r_{u_m}}{r_{cap_m}} = 0.159$$

Circumferential Demand:

Force: $P_{u_c} := (-\text{vlookup}(\text{Section}, \text{ANSYS}, 5))_1 \text{ kip} = 39.1 \text{ kip}$

Moment: $M_{u_c} := (-\text{vlookup}(\text{Section}, \text{ANSYS}, 6))_1 \text{ kip ft} = -8.3 \text{ kip ft}$

For unit agreement, nondimensionalize forces and moments by reference force of 1 kip and length of 1 ft.

Demand angle and length:

Angle: $\theta_{u_c} := \begin{cases} \text{atan2}\left(M_{u_c} \text{kip}^{-1} \text{ft}^{-1}, P_{u_c} \text{kip}^{-1}\right) & \text{if } M_{u_c} \neq 0 \vee P_{u_c} \neq 0 \\ 0 & \text{otherwise} \end{cases} = 101.985°$

Length: $r_{u_c} := \sqrt{\left(P_{u_c} \text{kip}^{-1}\right)^2 + \left(M_{u_c} \text{kip}^{-1} \text{ft}^{-1}\right)^2} = 39.971$

Ratio: $\text{MtoF}_c := \begin{cases} \dfrac{M_{u_c} \text{kip}^{-1} \text{ft}^{-1}}{P_{u_c} \text{kip}^{-1}} & \text{if } P_{u_c} \neq 0 \\ 1 & \text{otherwise} \end{cases} = -0.212$

Evaluate based on whether using +M terms (cases 1 and 2) or -M terms (cases 3 and 4) and whether P_u is positive (cases 1 and 3) or negative (cases 2 and 4) or zero (cases 5 and 6)

$$\text{Case}_c := \begin{cases} 1 & \text{if } (\theta_{u_c} \le \theta_{max_c}) \wedge (\theta_{u_c} \ge \theta_{min_c}) \wedge P_{u_c} > 0 \\ 2 & \text{if } (\theta_{u_c} \le \theta_{max_c}) \wedge (\theta_{u_c} \ge \theta_{min_c}) \wedge P_{u_c} < 0 \\ 3 & \text{if } (\theta_{u_c} > \theta_{max_c}) \\ 4 & \text{if } (\theta_{u_c} < \theta_{min_c}) \vee (\theta_{u_c} = \theta_{min_c}) \wedge (M_{u_c} = 0) \\ 5 & \text{if } P_{u_c} = 0 \wedge M_{u_c} \ge 0 \\ 6 & \text{if } P_{u_c} = 0 \wedge M_{u_c} < 0 \end{cases} = 3$$

Find c_0, where P=0

$c_{0_cp} := \mathrm{root}(P(c, d_{cp}, A_{cp}, Bars_c, P_\varphi, P_{D_c}), c, 0, c_{max_c}) = 3.171\,in$

$c_{0_cn} := \mathrm{root}(P(c, d_{cn}, A_{cn}, Bars_c, P_\varphi, P_{D_c}), c, 0, c_{max_c}) = 3.355\,in$

solve for the c value that will give the correct angle for comparison with the demand

$$c_{cap_c} := \begin{cases} \mathrm{root}\left(M_{pos}(c, d_{cp}, A_{cp}, x_{p_cp}, Bars_c, P_\varphi)\,kip^{-1}\,ft^{-1} - MtoF_c\,P(c, d_{cp}, A_{cp}, Bars_c, P_\varphi, P_{D_c})\,kip^{-1}, c, c_{0_cp}, c_{max_c}\right) & \text{if } Case_c = 1 \\ \mathrm{root}\left(M_{pos}(c, d_{cp}, A_{cp}, x_{p_cp}, Bars_c, P_\varphi)\,kip^{-1}\,ft^{-1} - MtoF_c\,P(c, d_{cp}, A_{cp}, Bars_c, P_\varphi, P_{D_c})\,kip^{-1}, c, 0, c_{0_cp}\right) & \text{if } Case_c = 2 \\ \mathrm{root}\left(M_{neg}(c, d_{cn}, A_{cn}, x_{p_cn}, Bars_c, P_\varphi)\,kip^{-1}\,ft^{-1} - MtoF_c\,P(c, d_{cn}, A_{cn}, Bars_c, P_\varphi, P_{D_c})\,kip^{-1}, c, c_{0_cn}, c_{max_c}\right) & \text{if } Case_c = 3 \\ \mathrm{root}\left(M_{neg}(c, d_{cn}, A_{cn}, x_{p_cn}, Bars_c, P_\varphi)\,kip^{-1}\,ft^{-1} - MtoF_c\,P(c, d_{cn}, A_{cn}, Bars_c, P_\varphi, P_{D_c})\,kip^{-1}, c, 0, c_{0_cn}\right) & \text{if } Case_c = 4 \\ c_{0_cp} & \text{if } Case_c = 5 \\ c_{0_cn} & \text{if } Case_c = 6 \end{cases} = 34.022\,in$$

Calculate $M_{capacity}$ and $P_{capacity}$ for this angle

$$M_{cap_c} := \begin{cases} M_{pos}(c_{cap_c}, d_{cp}, A_{cp}, x_{p_cp}, Bars_c, P_\varphi) & \text{if } Case_c = 1 \vee Case_c = 2 \vee Case_c = 5 \\ M_{neg}(c_{cap_c}, d_{cn}, A_{cn}, x_{p_cn}, Bars_c, P_\varphi) & \text{otherwise} \end{cases} = -194.139\,kip\,ft$$

$$P_{cap_c} := \begin{cases} P(c_{cap_c}, d_{cp}, A_{cp}, Bars_c, P_\varphi, P_{D_c}) & \text{if } Case_c = 1 \vee Case_c = 2 \vee Case_c = 5 \\ P(c_{cap_c}, d_{cn}, A_{cn}, Bars_c, P_\varphi, P_{D_c}) & \text{otherwise} \end{cases} = 914.558\,kip$$

Find the demand/capacity ratio

$$r_{cap_c} := \sqrt{\left(P_{cap_c}\,kip^{-1}\right)^2 + \left(M_{cap_c}\,kip^{-1}\,ft^{-1}\right)^2} = 934.937$$

$$DCratio_c := \frac{r_{u_c}}{r_{cap_c}} = 0.043$$

$$Mangle_m := \begin{pmatrix} 0 \\ M_{cap_m}\, kip^{-1}\, ft^{-1} \end{pmatrix} \qquad Mangle_c := \begin{pmatrix} 0 \\ M_{cap_c}\, kip^{-1}\, ft^{-1} \end{pmatrix}$$

For Plotting Vectors

$$Pangle_m := \begin{pmatrix} 0 \\ P_{cap_m}\, kip^{-1} \end{pmatrix} \qquad Pangle_c := \begin{pmatrix} 0 \\ P_{cap_c}\, kip^{-1} \end{pmatrix}$$

Shear Demand/Capacity Calculations:

Use ACI 349-06 eq. 11-4 to 11-8, using force and moment demand from meridional case, and $d=d_{mp2}$ for positive (and zero) moment and $d=d_{mn2}$ for negative moment (similarly with areas).

Through wall shear calculation

$V_u := \text{vlookup}(\text{Section}, \text{ANSYS}, 2)_1 \text{ kip} = -3.1 \text{ kip}$

$N_u := \begin{cases} P_{u_m} & \text{if } |P_{u_m}| > 1\text{kip} \\ 0 & \text{otherwise} \end{cases} = 65.9 \text{ kip}$

$M_u := |M_{u_m}| = 60 \text{ kip ft}$

$d := \begin{cases} d_{mnBars_m} & \text{if } M_{u_m} \le 0 \\ d_{mpBars_m} & \text{otherwise} \end{cases} = 28.72 \text{ in}$

$A_s := \begin{cases} A_{mnBars_m} & \text{if } M_{u_m} < 0 \\ A_{mpBars_m} & \text{otherwise} \end{cases} = 0.875 \text{ in}^2$

In-plane shear calculation

$V_{uip} := \text{vlookup}(\text{Section}, \text{ANSYS}, 13)_1 \text{ kip} = 0 \text{ kip}$

"Shear and Flexure only"

$$Vud_Mu := \begin{cases} \min\left(\left|\frac{V_u\, d}{M_u}\right|, 1\right) & \text{if } M_u \neq 0 \\ 1 & \text{otherwise} \end{cases} = 0.124$$ **calculate $V_u d/M_u$ with maximum value of 1.0**

$$\rho_w := \frac{A_s}{b\, d} = 2.538 \times 10^{-3}$$

$$V_{c1} := \left(1.9\sqrt{f'_c\, psi}^{\frac{1}{2}} + 2500\rho_w\, Vud_Mu\, psi\right) b\, d = 43.516\, kip$$

$$V_{c1_max} := 3.5\, psi^{\frac{1}{2}} \sqrt{f'_c}\, b\, d = 79.662\, kip$$

$$V_{c1_min} := 2\, psi^{\frac{1}{2}} \sqrt{f'_c}\, b\, d = 45.521\, kip$$

"Shear, Flexure, and Axial Compression

$$M_m := M_u - N_u\left(\frac{4\,h - d}{8}\right) = -10.129\, kip\, ft$$

$$lw := b = 12\, in$$

$$V_{c2_max} := 3.5\, psi^{\frac{1}{2}} \sqrt{f'_c}\, b\, d \sqrt{1 + \frac{N_u}{(500psi)\, b\, h}} = 92.067\, kip$$ **Also use for M_m<0**

$$V_{cip} := 3.3\, psi^{\frac{1}{2}} \sqrt{f'_c}\, h\, b + \frac{N_u\, b}{4\, lw} = 102.046\, kip$$

$$V_{c2} := \begin{cases} \left[\left(1.9\sqrt{f'_c\, psi}^{\frac{1}{2}} + 2500\, psi\, \rho_w \left|\frac{V_u\, d}{M_m}\right|\right) b\, d\right] & \text{if } M_m \neq 0 \\ V_{c2_max} & \text{otherwise} \end{cases} = 44.847\, kip$$

"Shear, Flexure, and Axial Tension"

$$V_{c3} := 2\,psi^{\frac{1}{2}}\left[1 + \frac{N_u}{(500psi)\,b\,h}\right]\sqrt{f_c}\,b\,d = 60.802\,kip$$

Calculate Shear Capacity:

$$V_c := \begin{cases} \max(V_{c1_min}, \min(V_{c1}, V_{c1_max})) & \text{if } N_u = 0 = 92.067\,kip \\ \min(V_{c2}, V_{c2_max}) & \text{if } N_u > 0 \wedge M_m \geq 0 \\ V_{c2_max} & \text{if } (N_u > 0 \wedge M_m < 0) \\ V_{c3} & \text{otherwise} \end{cases}$$

Factored Shear Capacity:

$$\varphi_{shear} := 0.85$$

$$V_{ua} := \varphi_{shear}\,V_c = 78.257\,kip$$

Shear Demand/Capacity Ratio:

$$DCratio_{shear} := \left|\frac{V_u}{V_c}\right| = 0.04$$

Factored In plane Shear Capacity:

$$V_{uip} := \varphi_{shear}\,V_{cip} = 86.739\,kip$$

Shear Demand/Capacity Ratio:

$$DCratio_{shearip} := \left|\frac{V_{uip}}{V_{cip}}\right| = 0$$

Results and Output:

$DCratio_c = 0.0428$ $DCratio_m = 0.1593$ $DCratio_{shear} = 0.0396$ $DCratio_{shearip} = 0$

$ratios := \left(Section\ \theta_{u_m}\ r_{u_m}\ r_{cap_m}\ DCratio_m\ \theta_{u_c}\ r_{u_c}\ r_{cap_c}\ DCratio_c\ V_u\ kip^{-1}\ V_c\ kip^{-1}\ DCratio_{shear}\ V_{uip}\ kip^{-1}\ V_{cip}\ kip^{-1}\ DCratio_{shearip}\right)$

$Section = 14$

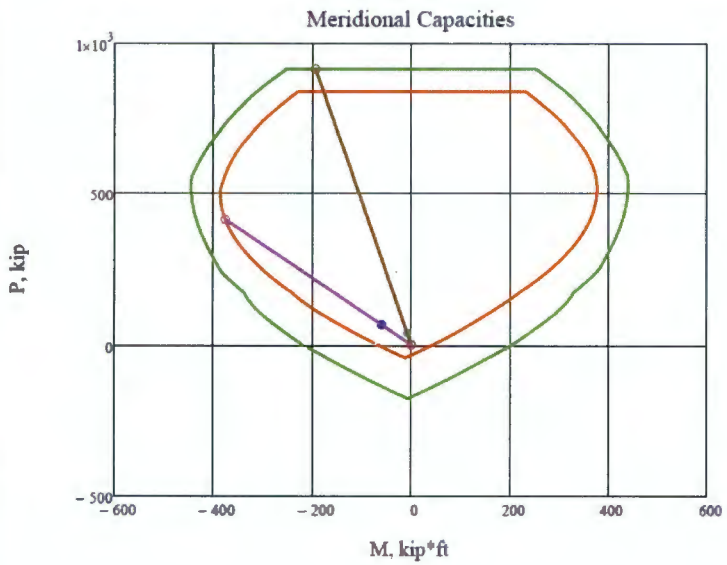

Output/Save Results:

$Output := augment(MeridOutput, CircumOutput)$

$append := APPENDPRN(\text{"ACItypeIII.txt"}, ratios)$

$vector := augment(Mangle_m, Pangle_m, Mangle_c, Pangle_c)$

capacityvector.txt
vector

ACItypeIIICURVE.txt
Output

J.2 References

ACI. 2007. *American Concrete Institute Code Requirements for Nuclear Safety Related Concrete Structures*. ACI 349-06, American Concrete Institute, Farmington Hills, Michigan.

Johnson KI, JE Deibler, FG Abatt, and MW Rinker. 2010. *Single-Shell Tank Structural Evaluation Criteria*. RPP-46442, Rev. 0, Pacific Northwest National Laboratory, Richland, Washington.

Appendix K

Seismic Soil Overburden Modeling Technique

This page intentionally left blank.

Appendix K

Seismic Soil Overburden Modeling Technique

K.1 Purpose

The Type III soil overburden modeling technique was changed to improve initial gravity loading, remove amplified acceleration caused by soft soil, support the soil overburden and pits more realistically in the lateral direction, and remove conservatism in seismic loading. In the seismic analysis of the Type II SSTs documented in Rinker et al. (2011a), the overburden soil included softened soil zones (soft soil modeling technique) as a mechanism to minimize the potential for soil arching in the vertical direction of the overburden soil above the dome. In contrast, the seismic model for the Type III SSTs employed vertical slip rings (soil rings modeling technique) to minimize arching during the initial gravity loading leading to a more accurate dead weight loading on the dome. In addition, replacing the soft soil regions with the soil rings modeling technique more accurately simulates the soil behavior in the horizontal direction during a seismic time history leading to more realistic seismic loading.

Details and comparisons between the two approaches are presented in this appendix.

Sensitivity studies were conducted to determine the differences between Type II and Type III SST Seismic model soil overburden modeling techniques by evaluating the sensitivity of tank demands to the soil overburden modeling. The following cases were run for a comparison between modeling techniques:

1. Type III, SST, Best-Estimate Soil (BES), Empty, Soil Rings Modeling Technique
2. Type III, SST, Best-Estimate Soil (BES), Empty, Soft Soil Modeling Technique
3. Type III, SST, Best-Estimate Soil (BES), Empty, Appurtenances, Soil Rings Modeling Technique
4. Type III, SST, Best-Estimate Soil (BES), Empty, Appurtenances, Soft Soil Modeling Technique

The soil overburden in Type III SST seismic analysis was simulated using soil rings rather than using the Type II SST seismic analysis soil overburden soft soil technique. The soft soil modeling technique used in the Type II SST AOR seismic model consisted of two soft soil regions. The soft soil modeling technique was replaced in the Type III analysis with the soil rings modeling technique consisting of a series of soil rings and contact elements. The soil rings allow the soil to slide vertically without separation from adjacent soil thus reducing soil arching and eliminating the undesirable effects of the soft soil regions in the seismic analysis.

This study will demonstrate that the soil rings modeling technique for the Type III seismic analysis has the following modeling improvements:

- Vertical response has improved with more accurate dome loading (less arching) in static gravity.
- Horizontal response has improved with more realistic lateral support for soil overburden and pits. The unrealistic soft soil regions are replaced with more realistic soil-to-soil contact elements to provide adequate horizontal support for soil overburden and pits. Physically unrealistic modes resulting from inadequate lateral support of soil overburden have been removed by using the soil rings approach, thus reducing conservatism in tank demands during the seismic time history.

K.2 Soil Rings Modeling Technique for Type III SST Seismic Model

The soil rings modeling technique consists of vertical slip planes inserted into the soil overburden (soil above the dome within the radius of the wall) as shown in Figure K.1. The locations of the contact surfaces are consistently placed halfway between the ACI sections to ensure uniform loading. A combination of TARGE170 and CONTA173 elements is used to model the interface between the soil rings. The contact behavior is specified as "no separation," this allows for the potential of sliding between the surfaces, but the surfaces remain in contact. To establish the initial gravity condition, a low coefficient of friction of 0.05 is used between the soil rings above the dome, which allows the soil to settle consistently with the dome deformation under initial gravity load step. A coefficient of friction of 0.2 was used in the vertical slip ring contacts during the seismic analysis. A "static" coefficient of friction of approximately 0.5 was calculated by taking the internal friction angle of the soil, but the lower coefficient of friction of 0.2 was chosen due to the "dynamic" nature of the seismic analysis. A sensitivity study shown below compares a Type III, SST, Best-Estimate Soil (BES), empty tank with a 0.2 and 0.5 seismic coefficient of friction for the soil rings modeling technique.

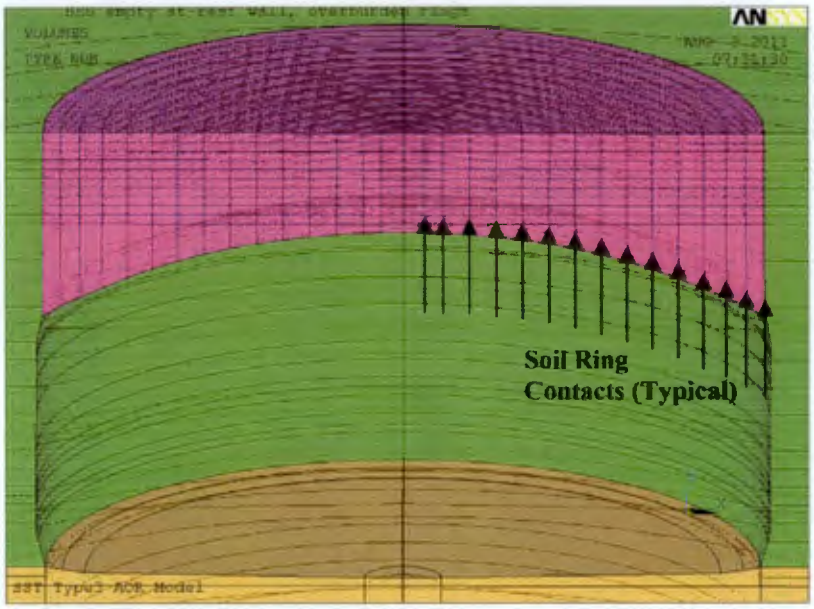

Figure K.1. Type III SST Seismic Model Soil Overburden: Series of Soil Rings with contact friction interfaces between Soil Rings

There is a decrease in the meridional and hoop forces in the dome with a coefficient of friction of 0.5 as shown in Figures K.2 and K.3. There are higher demands for the dome in the hoop moment, through-wall shear, and in-plane shear with the ring friction value of 0.5 as shown in Figures K.5, K.6, and K.7. The higher friction causes resistance to upward movement in the soil rings, which increases the demand in portions of the dome during a seismic time history. A higher coefficient of friction between the soil rings leads to dynamic soil arching which is not expected for the ground shaking during the seismic event. For this reason, the friction coefficient of 0.2 was selected to provide a more realistic dynamic response of the soil overburden during the seismic analysis. Figure K.8 displays the ACI-349 demand/capacity (D/C) ratios for the Type III SST (BES, Empty) combined TOLA plus Seismic comparison for friction coefficients of 0.2 and 0.5. The soil rings modeling technique with a coefficient of friction of 0.5 increased approximately 0.2 for the Hoop D/C in ACI Section 11, but this section is not critical. In the critical ACI Section 14, the results for the two friction cases are the same. Hence, even with the assumed higher coefficient of friction of 0.5 between the soil rings, the tank response is acceptable.

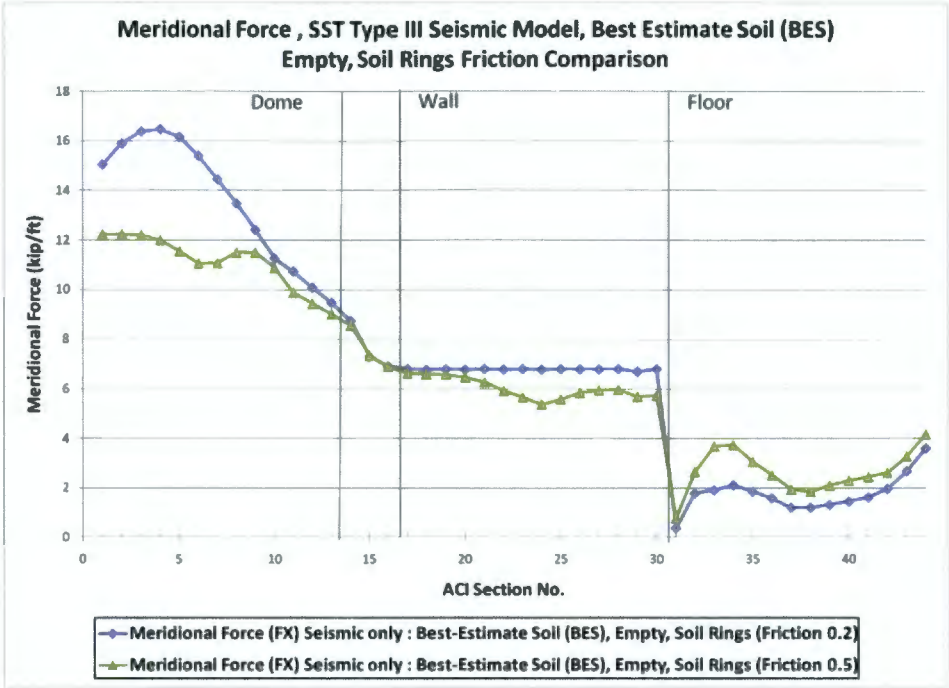

Figure K.2. Concrete Tank Meridional Force (Seismic Only): Type III SST (BES, Empty) Seismic Model, Soil Rings Modeling Technique Coefficient of Friction Comparison

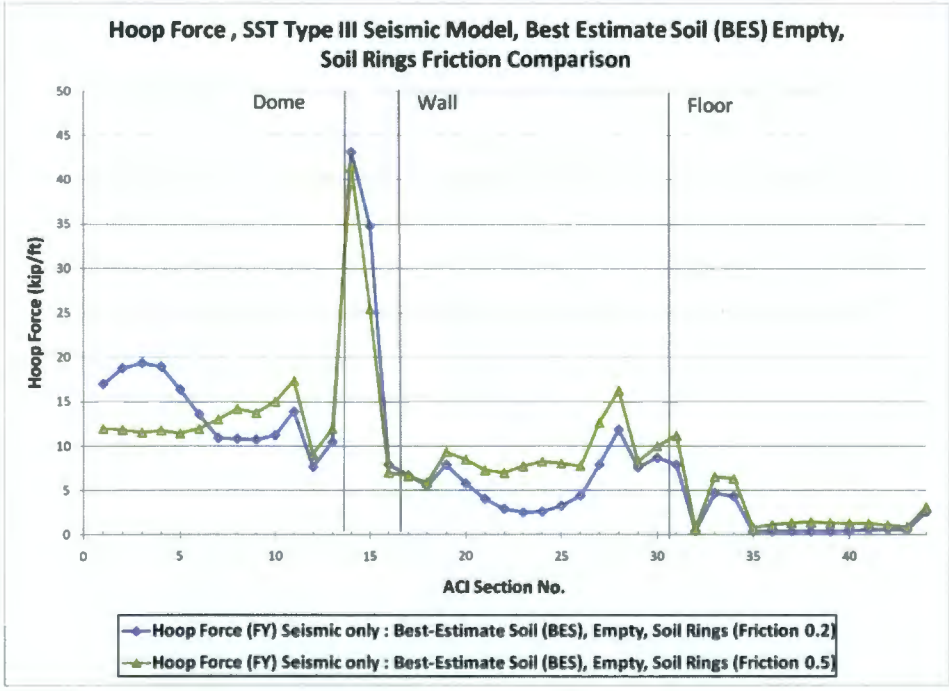

Figure K.3. Concrete Tank Hoop Force (Seismic Only): Type III SST (BES, Empty) Seismic Model, Soil Rings Modeling Technique Coefficient of Friction Comparison

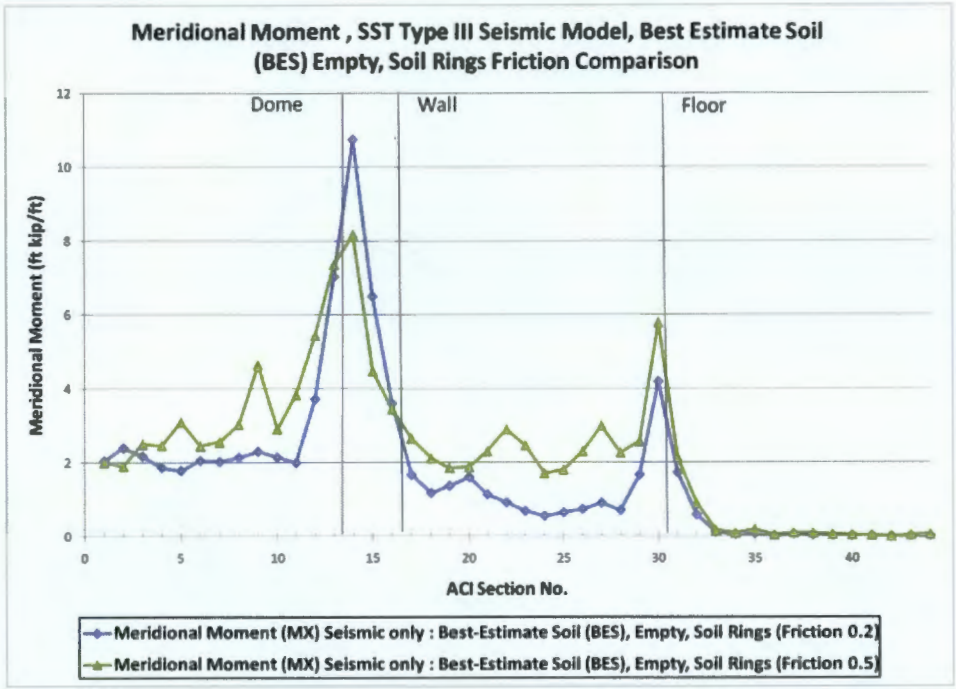

Figure K.4. Concrete Tank Meridional Moment (Seismic Only): Type III SST (BES, Empty) Seismic Model, Soil Rings Modeling Technique Coefficient of Friction Comparison

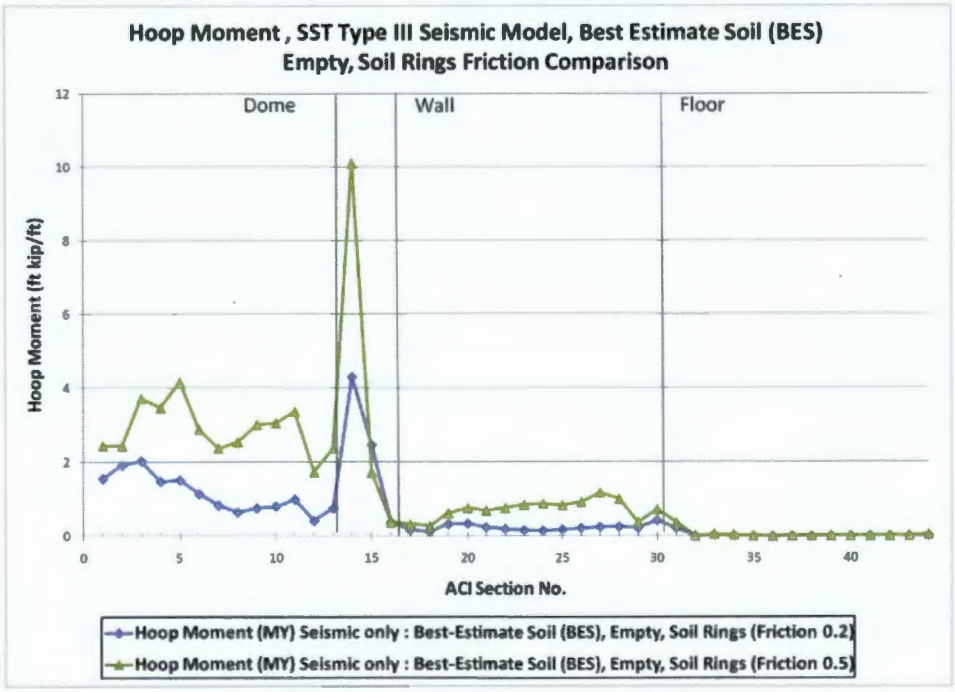

Figure K.5. Concrete Tank Hoop Moment (Seismic Only): Type III SST (BES, Empty) Seismic Model, Soil Rings Modeling Technique Coefficient of Friction Comparison

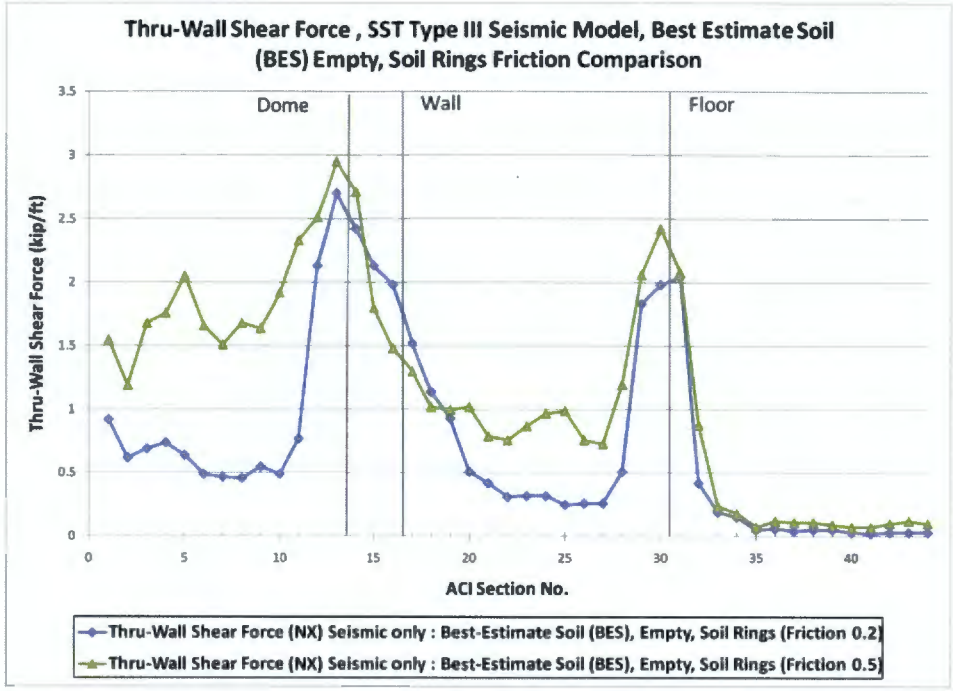

Figure K.6. Concrete Tank Through-Wall Shear Force (Seismic Only): Type III SST (BES, Empty) Seismic Model, Soil Rings Modeling Technique Coefficient of Friction Comparison

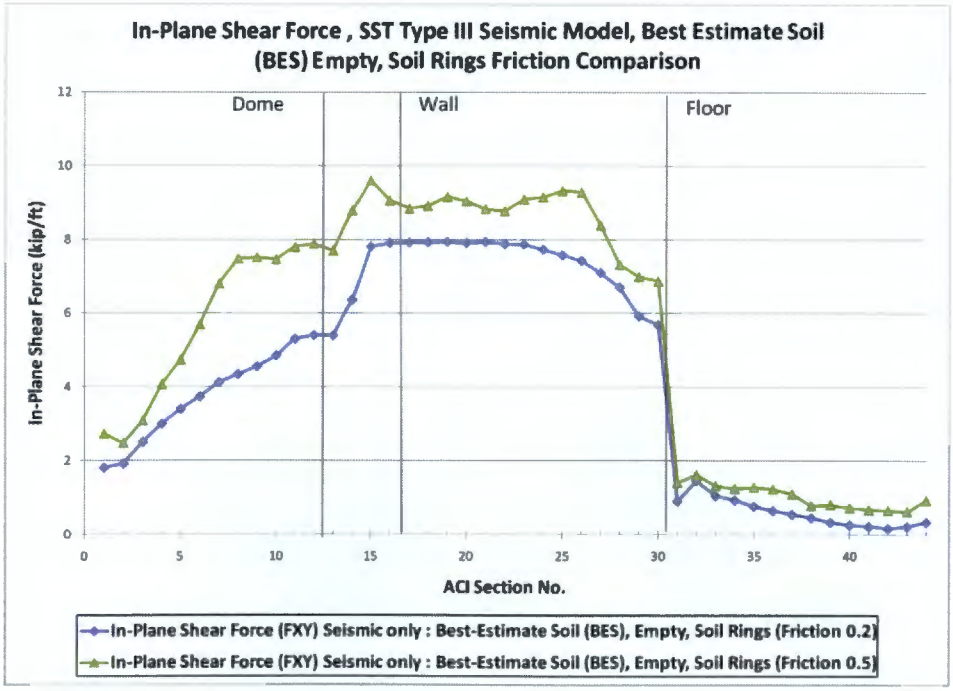

Figure K.7. Concrete Tank In-Plane Shear Force (Seismic Only): Type III SST (BES, Empty) Seismic Model, Soil Rings Modeling Technique Coefficient of Friction Comparison

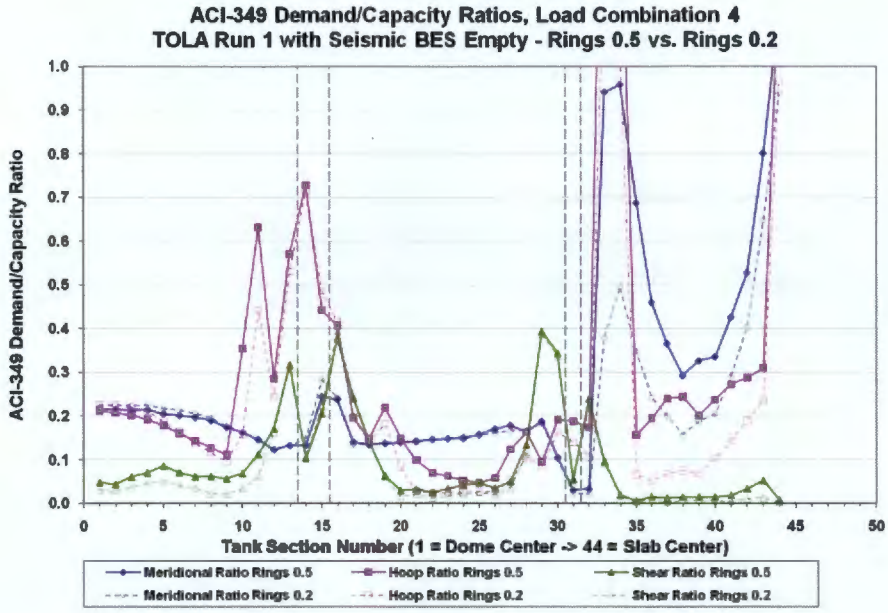

Figure K.8. LC4 Combined TOLA Run1 plus Seismic ACI D/C Ratios: Type III SST (BES, Empty), Soil Rings Modeling Technique Coefficient of Friction Comparison

K.3 Soft Soil Modeling Technique for Type II SST Seismic Model

The soft soil modeling technique consists of regions of the soil over the tank dome that are softened to minimize the effects of soil arching. Figure K.9 demonstrates soil zones (shown with leaders over tank haunch and apex not following soil layering pattern) for which Modulus of Elasticity was modified from a Best-Estimate Soil Range of (5,769 - 10,991) kip/ft^2 to 250 kip/ft^2. The intent of adding softened soil zones is to create a break in the soil through which only limited tension or compression can be carried. The ring over the tank sidewall isolates the soil over the tank, changing it from "fixed" at the edges, to "simply supported." A zone over the center of the dome was also softened to break the "beam action" over the dome, essentially preventing a moment being carried over the dome. See Section 6 of Rinker et al. (2011a) for further discussion.

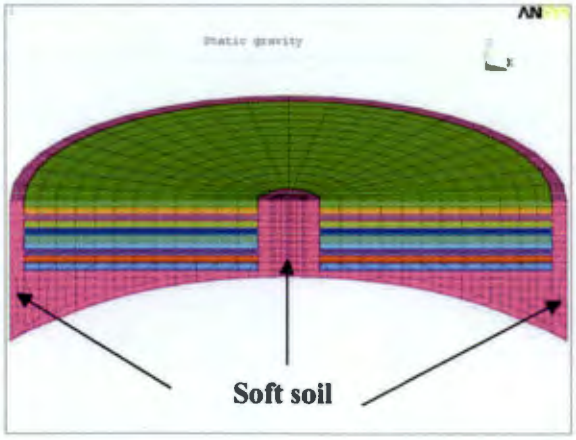

Figure K.9. Type III SST Seismic Model with Soft Soil Overburden Regions: Softened Soil Zones

K.3.1 Contact Pressure for Dead Weight

As discussed previously, a modeling technique was necessary to minimize soil arching in the soil over the tank dome under gravity and during seismic loading. The soft soil modeling approach was used in the Type II SST analysis. The purpose of the soil ring modeling technique was to obtain more accurate loading on the tank dome. Previous tank analyses, including the analysis of Type II SSTs and DSTs, used softened regions in the soil overburden. The Type III SST seismic analysis utilizes soil ring slip planes in the soil overburden instead of the soft soil regions.

The application of the soil rings modeling technique for the soil above the dome allows loading on the dome to be much closer to the theoretical value expected during dead weight (initial gravity load step). In Figure K.10, results from the initial gravity loading on a Type III SST [Best-Estimate Soil (BES), Empty tank] using soft soil modeling technique are compared to the theoretical contact pressure corresponding results using soil rings modeling technique and theoretical contact pressure. The soil rings modeling technique clearly provides a more accurate method for properly loading the dome under dead weight loading (initial gravity load step).

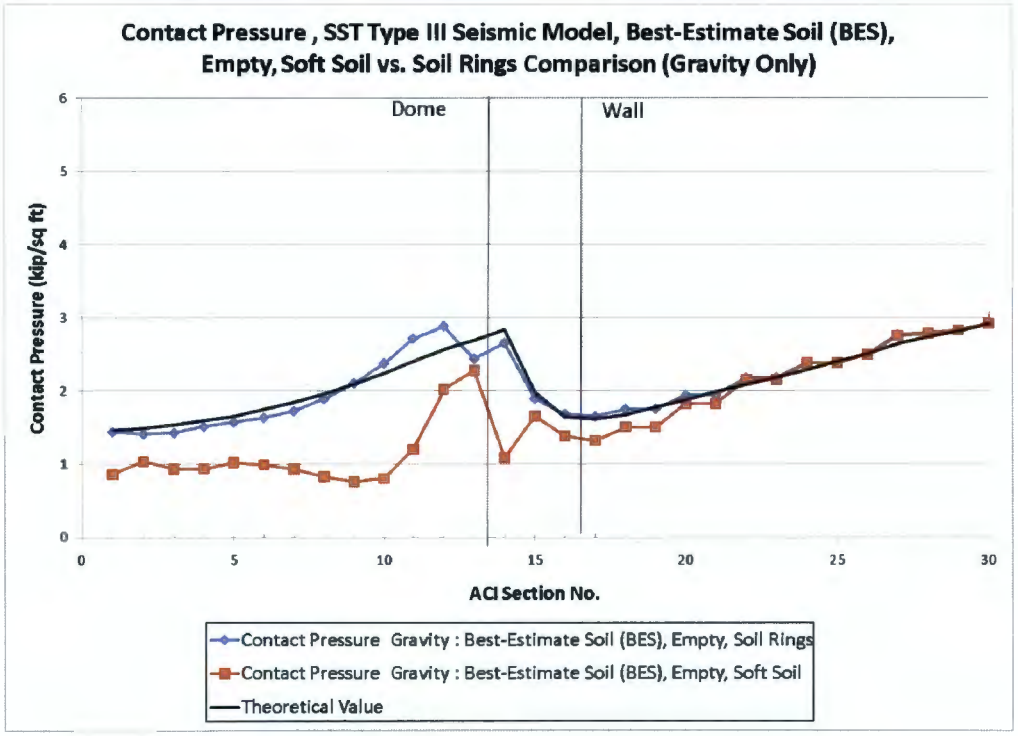

Figure K.10. Type III SST Seismic Model Dead Weight Contact Pressure Comparison

K.4 Type III SST (BES, Empty) Seismic Demand Comparison Between Soft Soil and Soil Rings Modeling Techniques

Results from the Type III SST (BES, Empty) seismic analysis are compared between the soft soil and soil rings modeling techniques in Figures K.11 through K.16. The soft soil modeling technique produced higher meridional, hoop, and in-plane shear forces in the dome and the wall as compared to the soil rings modeling technique with the coefficient of friction between rings equal to 0.2.

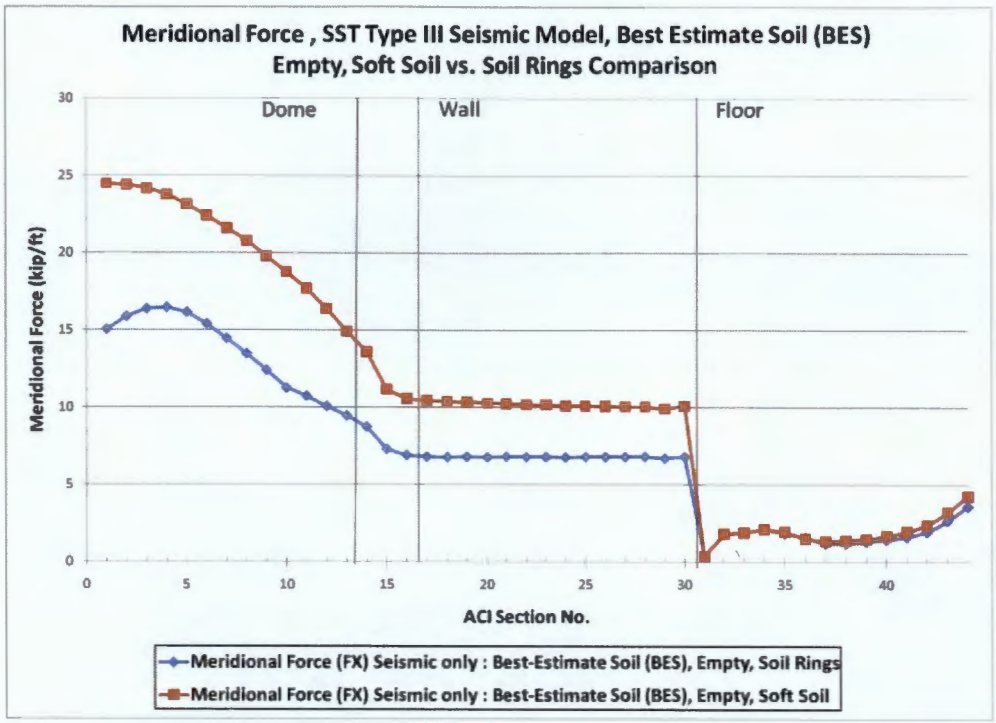

Figure K.11. Concrete Tank Meridional Force: Type III SST (BES, Empty) Overburden Soil Modeling Technique Comparison (Seismic Only)

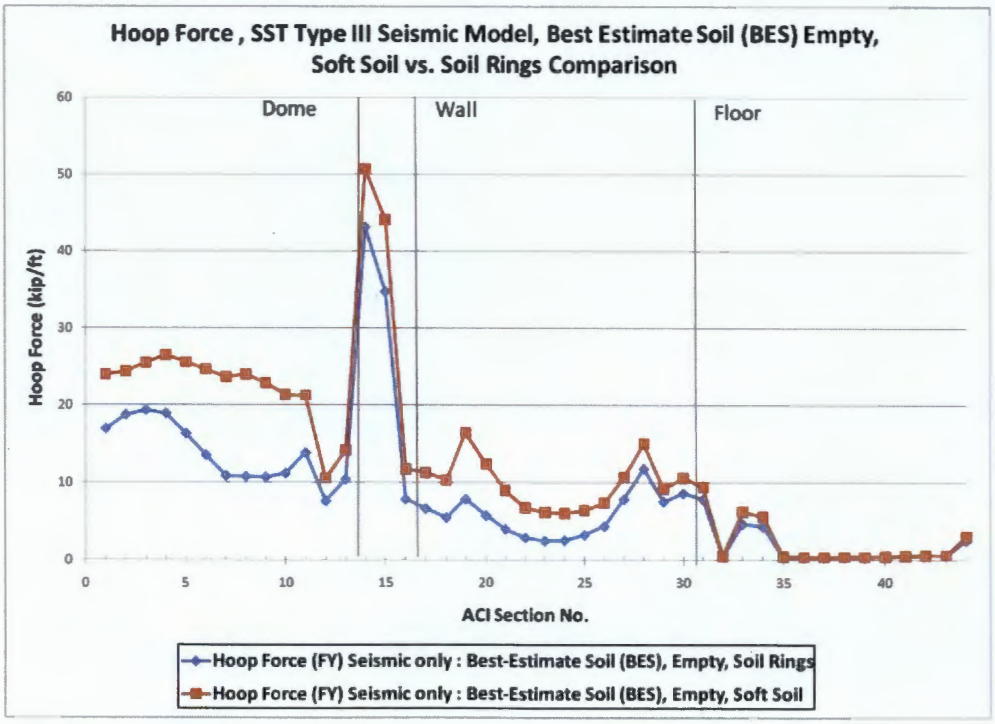

Figure K.12. Concrete Tank Hoop Force: Type III SST (BES, Empty) Overburden Soil Modeling Technique Comparison (Seismic Only)

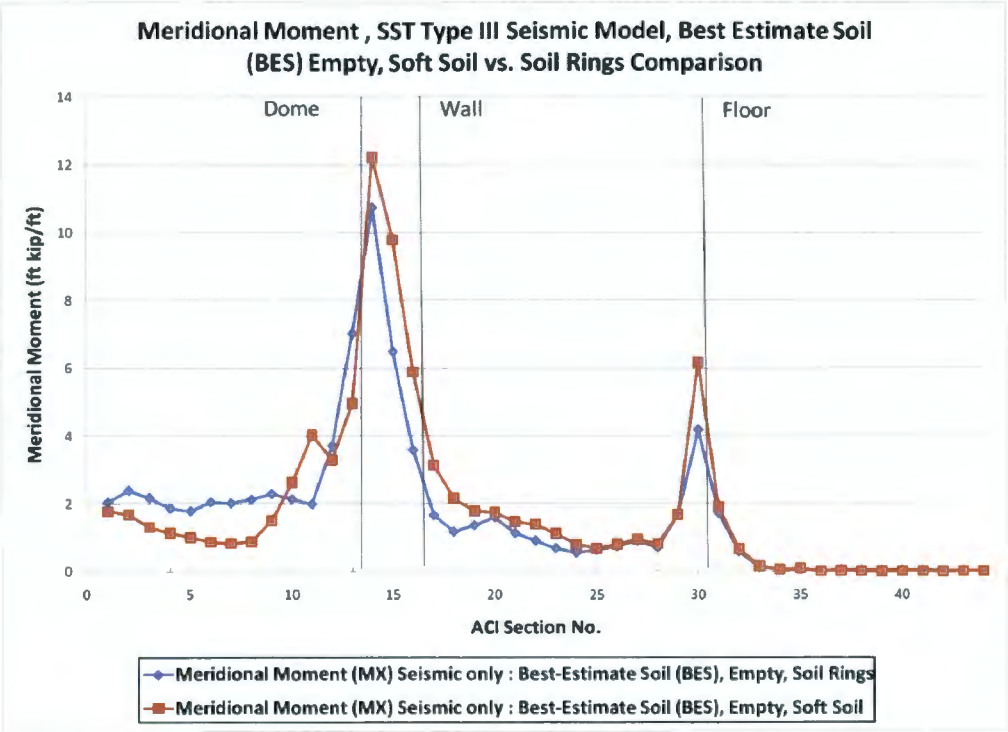

Figure K.13. Concrete Tank Meridional Moment: Type III SST (BES, Empty) Overburden Soil Modeling Technique Comparison (Seismic Only)

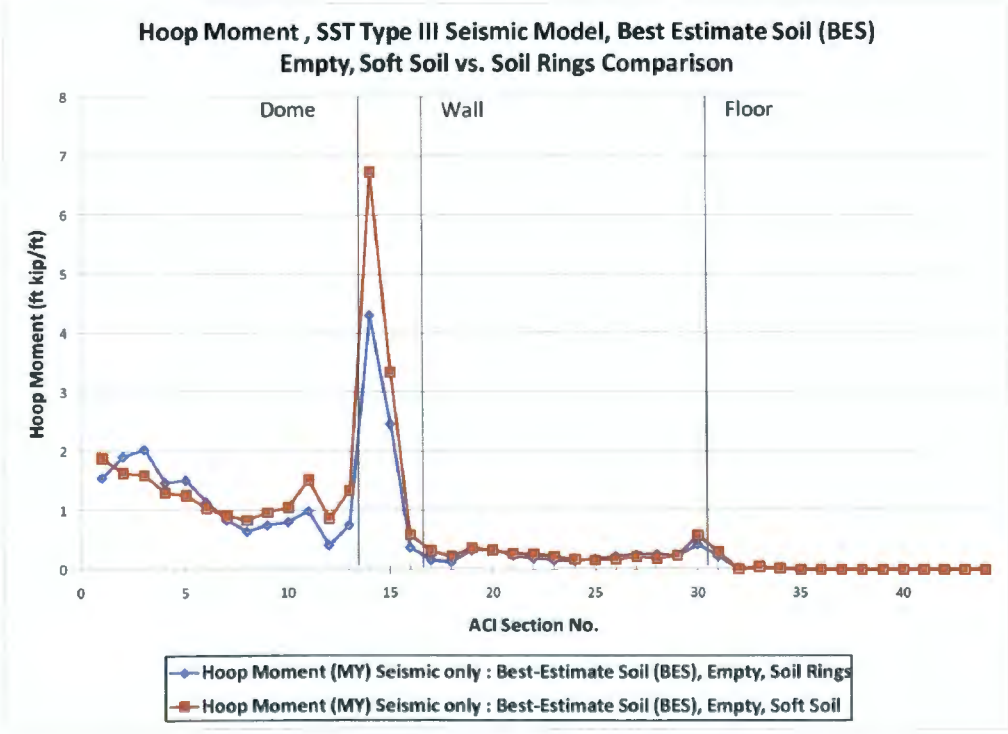

Figure K.14. Concrete Tank Hoop Moment: Type III SST (BES, Empty) Overburden Soil Modeling Technique Comparison (Seismic Only)

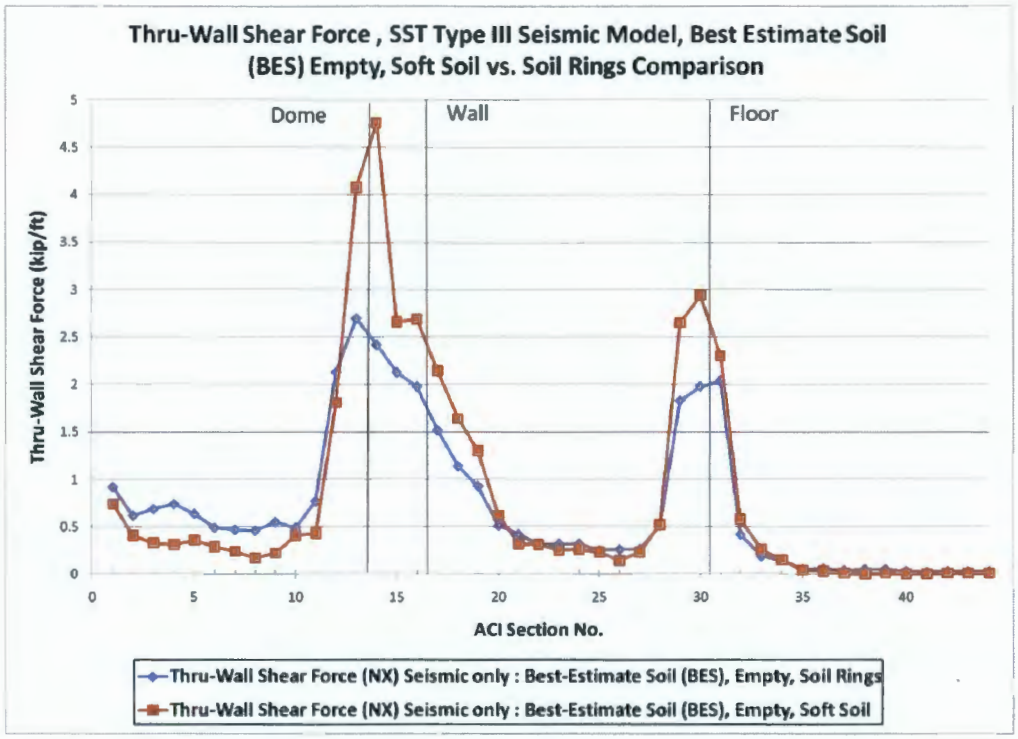

Figure K.15. Concrete Through-Wall Shear Force: Type III SST (BES, Empty) Overburden Soil Modeling Technique Comparison (Seismic Only)

Figure K.16. Concrete Tank In-Plane Shear Force: Type III SST (BES, Empty) Overburden Soil Modeling Technique Comparison (Seismic Only)

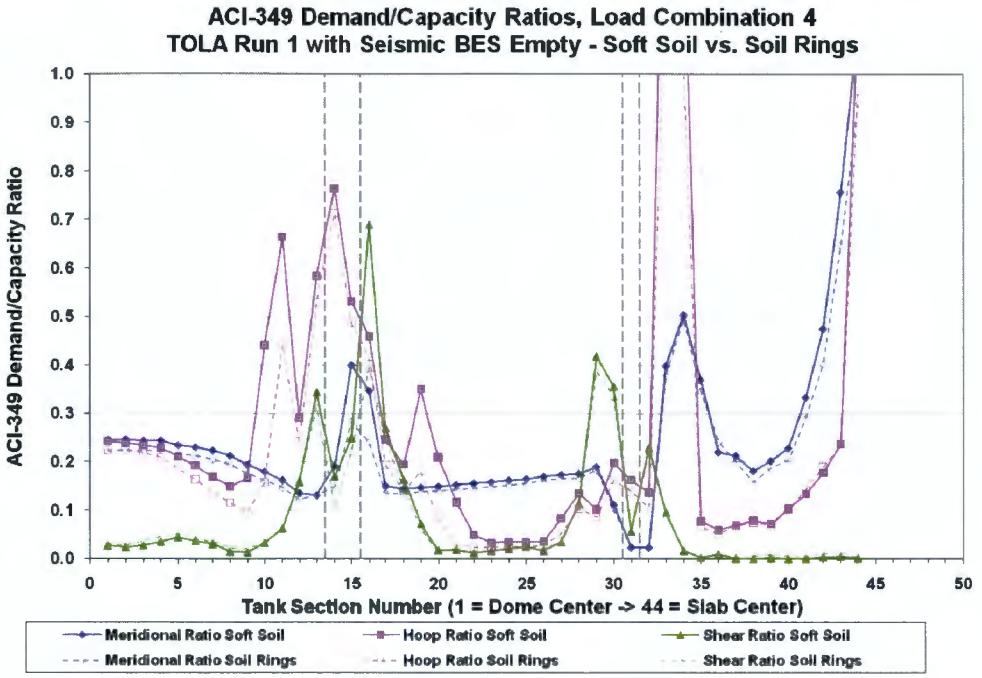

Figure K.17. LC4 Combined TOLA Run1 plus Seismic ACI D/C Ratios: Type III SST (BES, Empty) Overburden Soil Modeling Technique Comparison

Figure K.17 displays the ACI-349 demand/capacity (D/C) ratios for the Type III SST (BES, Empty) combined TOLA plus Seismic comparison between results from overburden soft soil and soil rings modeling techniques. Acceptable results are those D/C ratios that are less than 1.0 for the ACI-349 calculated capacity. The demand/capacity ratios curves are less than 1.0 for the calculated capacity in the ACI Sections 1 through 31. The soil rings modeling technique reduces the Hoop D/C ratio most significantly in Sections 9-11 and Section 18-21 as compared to results from the soft soil modeling technique. More importantly, the hoop D/C ratio in the critical ACI Section 14 is only slightly different between the two cases.

K.5 Type III SST Pit Appurtenances Seismic Analysis Comparison Between Results using Overburden Soft Soil and Soil Rings Modeling Techniques

The soil overburden in Type III SST seismic pit appurtenances analysis was modified from the Type II SST seismic analysis soil overburden which used the soft soil technique. For comparison both the soft soil and soil rings modeling techniques were applied. The two soft soil regions for the Type III SST pit appurtenances seismic model as shown in Figure K.18, were used similar to the method used in the Type II SST AOR seismic appurtenances model. This modeling technique was then replaced with a series of soil rings with contact elements as shown in Figure K.19. The soil rings are allowed to slide vertically without separation from the adjacent soil ring. The Type III SST seismic appurtenances modeling is otherwise unchanged so that a direct comparison can be made.

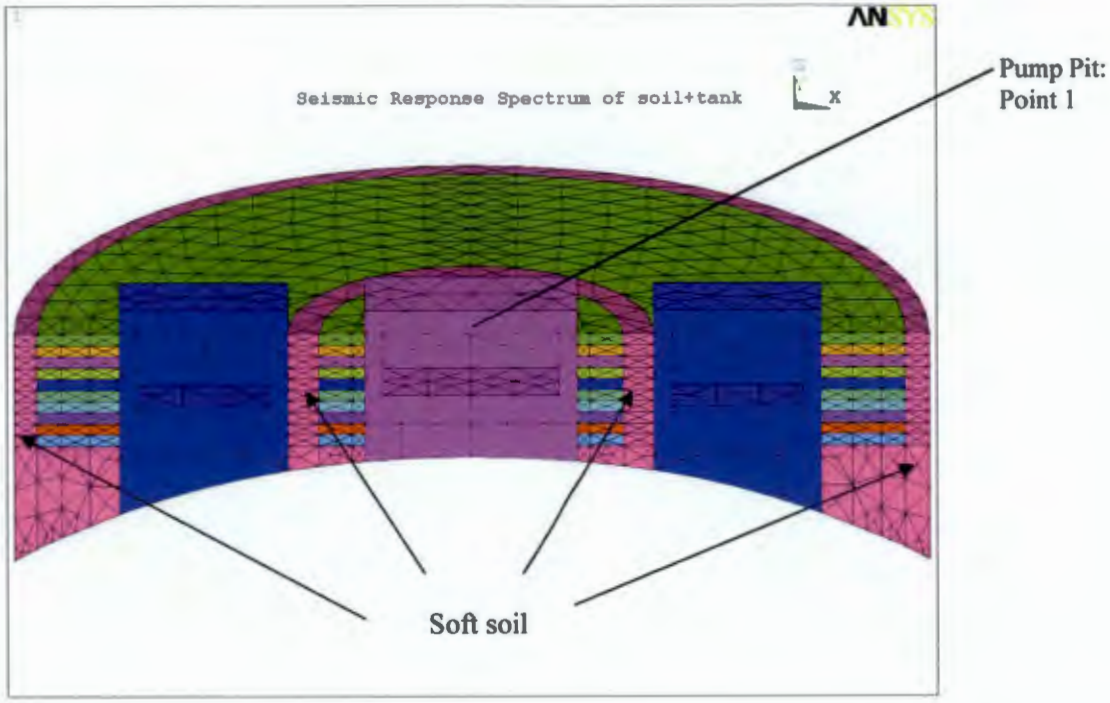

Figure K.18. Type III SST Appurtenances Seismic Model Soil Overburden: Softened Soil Zones

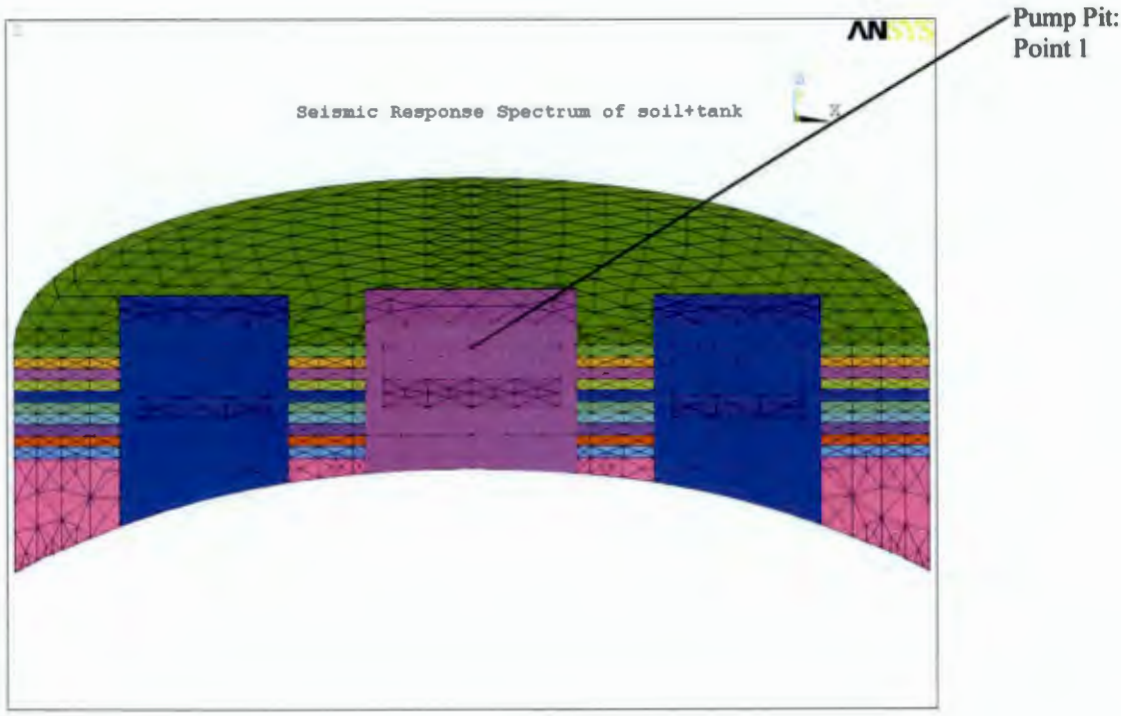

Figure K.19. Type III SST Appurtenances Seismic Model Soil Overburden: Series of Soil Rings with Contact Friction Interfaces between Soil Rings

K.6 Appurtenances Horizontal and Vertical Acceleration

The concrete pits are supported by adjacent soil which provides lateral support during a seismic event. The soft soil regions (Figure K.18) in the soft soil modeling technique utilize a very low Young's modulus, thus providing less resistance to lateral motion. The resulting increased displacement in the lateral direction during the seismic loading produces overly conservative loading on the dome. In addition, the soft soil modeling technique amplifies the acceleration in the horizontal and vertical direction due to the soft soil. As shown in Figure K.20, the horizontal acceleration in the X-direction for the central pump pit at point one (See Figure K.18 and K.19) is compared between the soft soil modeling technique and the soil rings modeling technique. The soft soil modeling technique results in a minimum of twice the horizontal acceleration at point 1 compared to the response using the soil rings modeling technique. In addition, as shown in Figure K.21, the soft soil modeling technique produces a minimum of 1.5 times the vertical acceleration in the Z-direction at point 1 compared to the soil rings modeling technique. Application of the soft soil modeling technique in the pit appurtenances model is conservative due to amplified acceleration loads induced in the pits of the model. This amplification of acceleration and lack of proper lateral stabilization support for the pit appurtenances significantly increases the seismic tank demands for the soft soil appurtenances model. Therefore, a more realistic modeling technique for the pit appurtenances model is to utilize the soil rings modeling methodology.

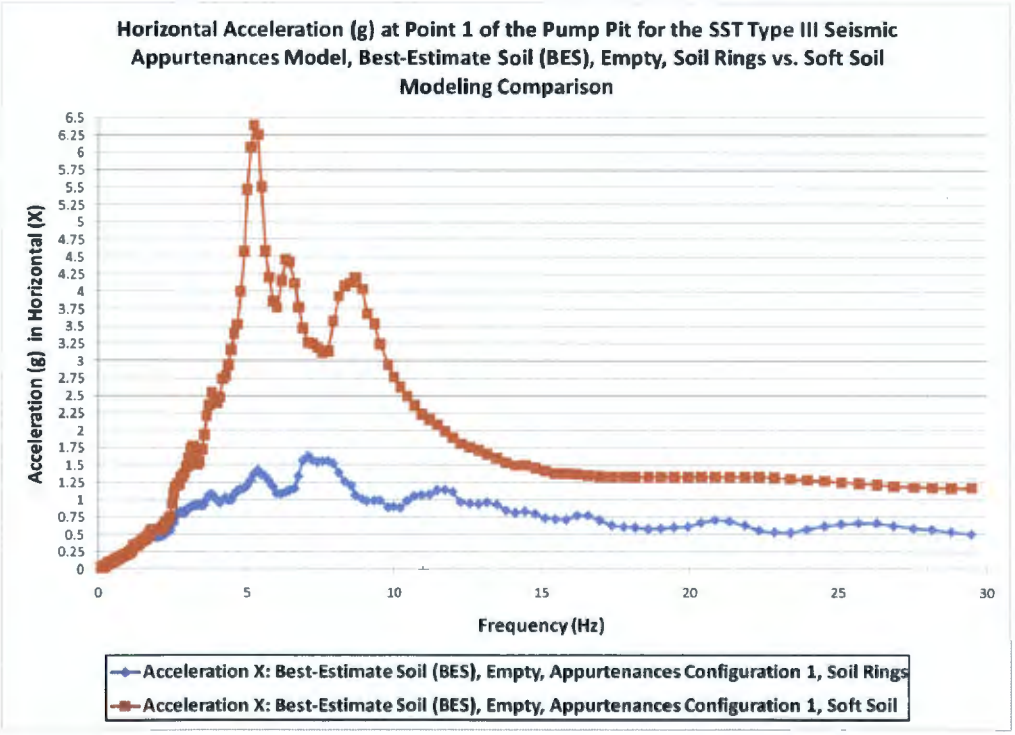

Figure K.20. Point 1, Horizontal Acceleration (X) Comparison, Type III SST Appurtenances Seismic Model Soil Overburden

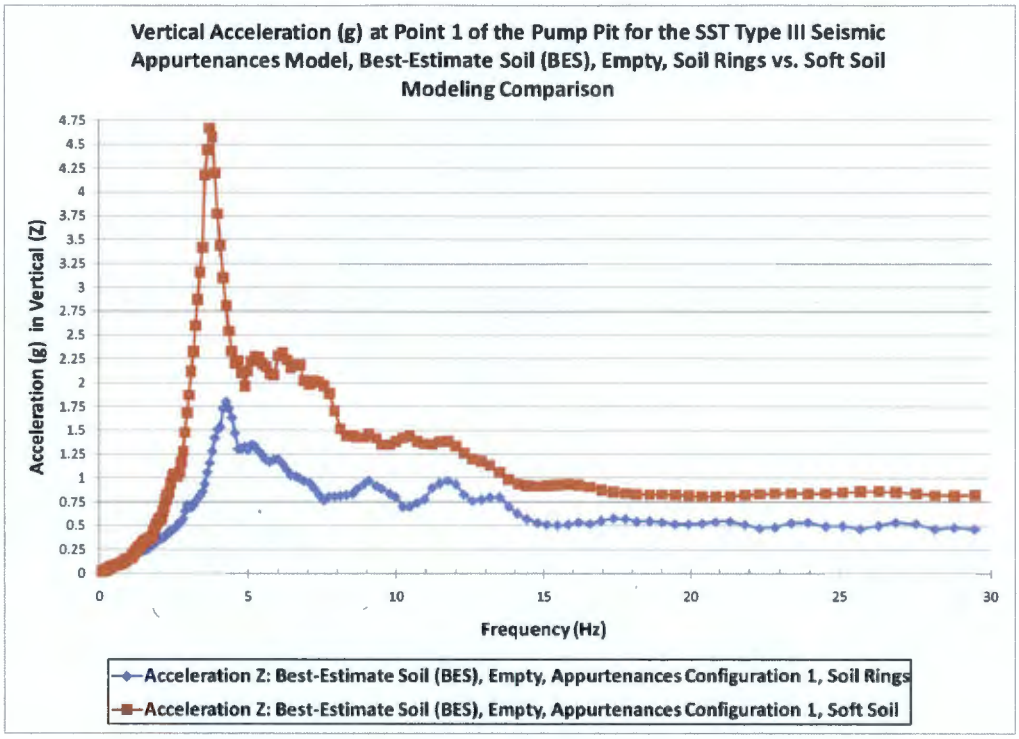

Figure K.21. Point 1, Vertical Acceleration (Z) Comparison, Type III SST Appurtenances Seismic Model Soil Overburden:

K.7 Seismic Demand Comparison for Type III SST (BES, Empty) Seismic Appurtenances Model

Figures K.22 through K.27 compare the Type III SST (BES, Empty) seismic only demands with and without pit appurtenances utilizing the soft soil and soil rings modeling techniques. Application of the soft soil modeling technique resulted in higher demands in all forces and moments for the dome and the wall as compared to the results using the soil rings modeling technique.

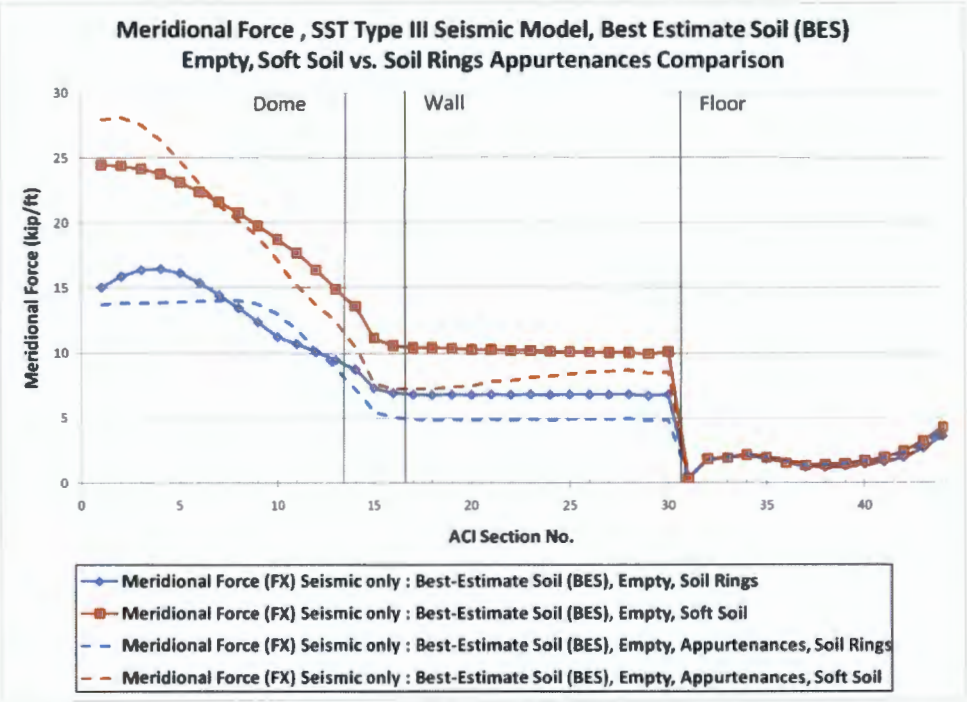

Figure K.22. Concrete Tank Meridional Force (Seismic Only): Type III SST (BES, Empty) Seismic Model with and without Pit Appurtenances Utilizing the Soft Soil and Soil Rings Modeling Techniques

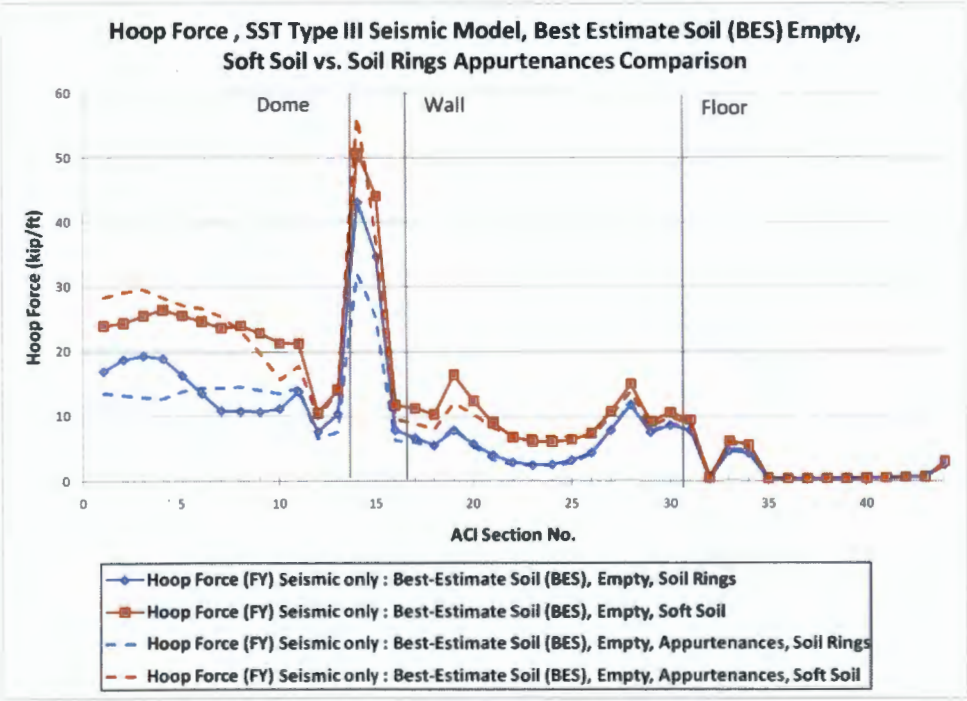

Figure K.23. Concrete Tank Hoop Force (Seismic Only): Type III SST (BES, Empty) Seismic Model with and without Pit Appurtenances Utilizing the Soft Soil and Soil Rings Modeling Techniques

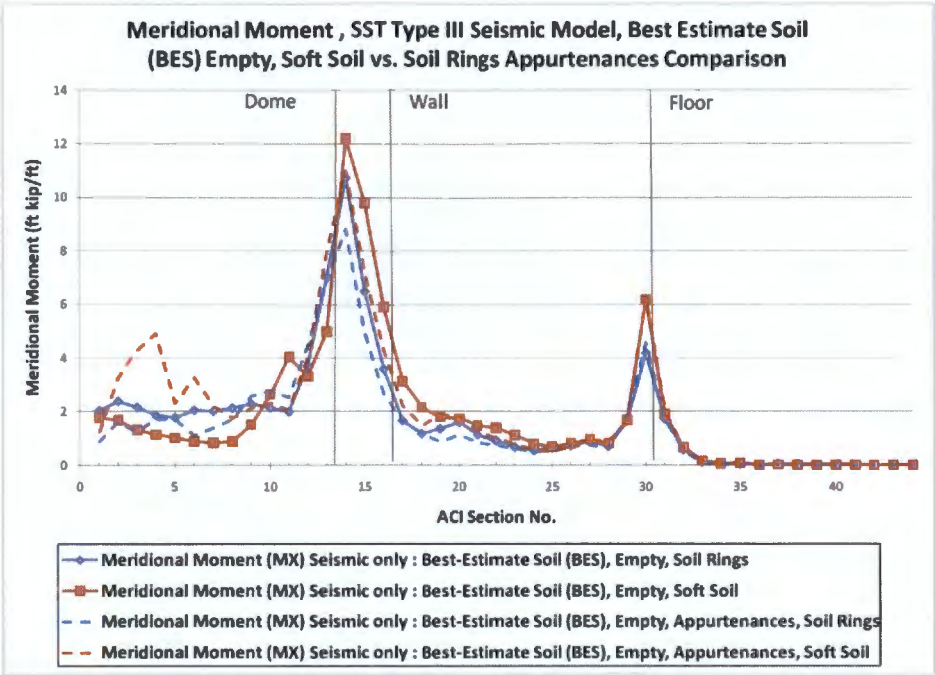

Figure K.24. Concrete Tank Meridional Moment (Seismic Only): Type III SST (BES, Empty) Seismic Model with and without Pit Appurtenances Utilizing the Soft Soil and Soil Rings Modeling Techniques

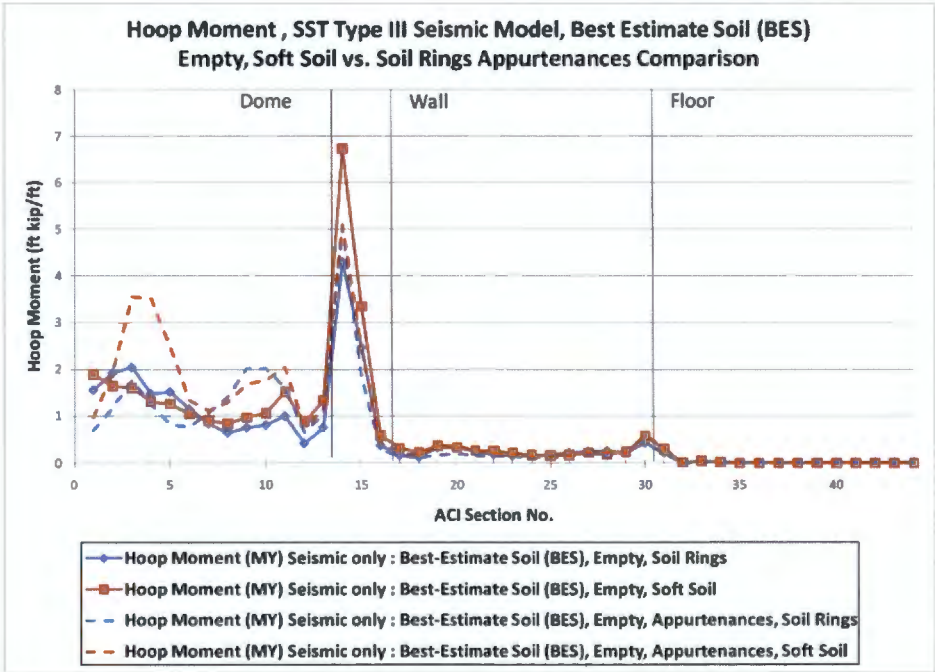

Figure K.25. Concrete Tank Hoop Moment (Seismic Only): Type III SST (BES, Empty) Seismic Model with and without Pit Appurtenances Utilizing the Soft Soil and Soil Rings Modeling Techniques

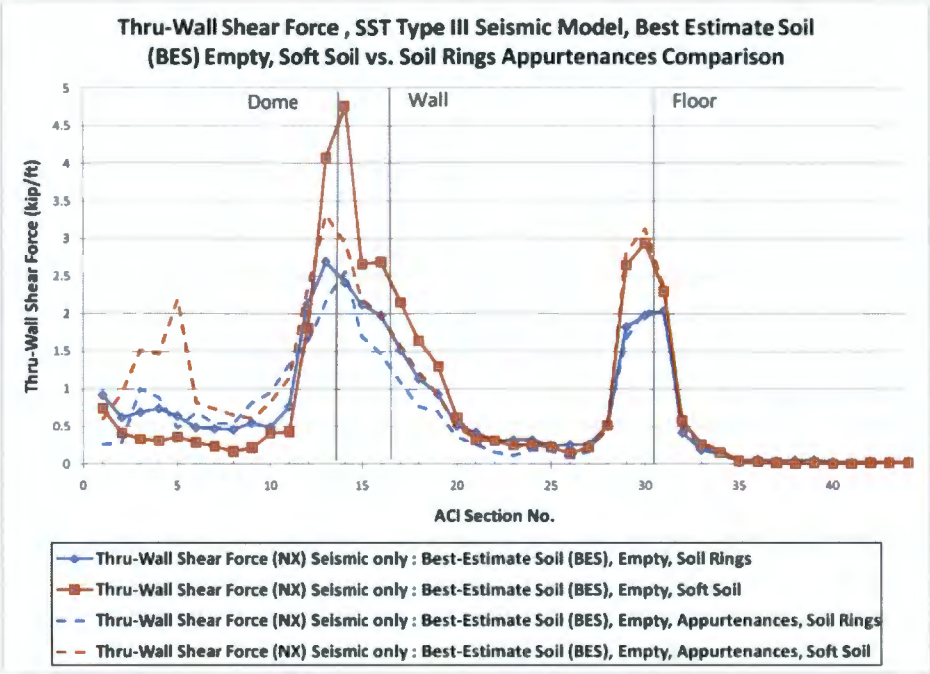

Figure K.26. Concrete Tank Through-Wall Shear Force (Seismic Only): Type III SST (BES, Empty) Seismic Model with and without Pit Appurtenances Utilizing the Soft Soil and Soil Rings Modeling Techniques

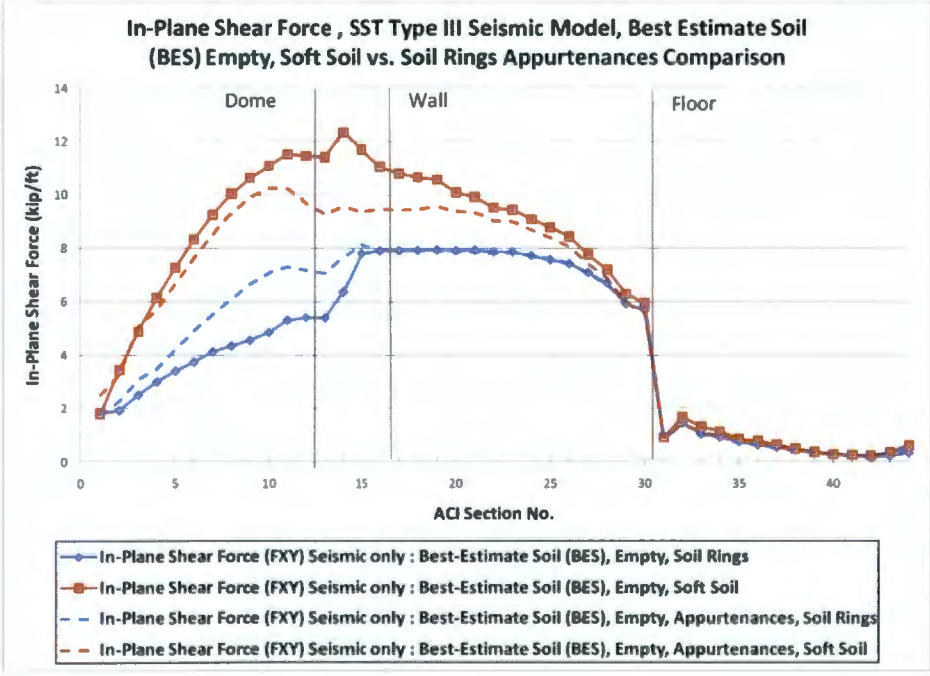

Figure K.27. Concrete Tank In-Plane Shear Force (Seismic Only): Type III SST (BES, Empty) Seismic Model with and without Pit Appurtenances Utilizing the Soft Soil and Soil Rings Modeling Techniques

Figures K.28 through K.31 display the LC4 (TOLA plus seismic) ACI-349 demand/capacity (D/C) ratio differences ($D/C_{soft\ soil} - D/C_{soil\ rings}$) for the Type III SST (BES, Empty) pit appurtenances model. The pit appurtenances seismic model D/C ratios are higher in the dome and section 32 utilizing the soft soil modeling technique. However, none of the sections resulted in a D/C ratio difference greater than approximately ±0.2.

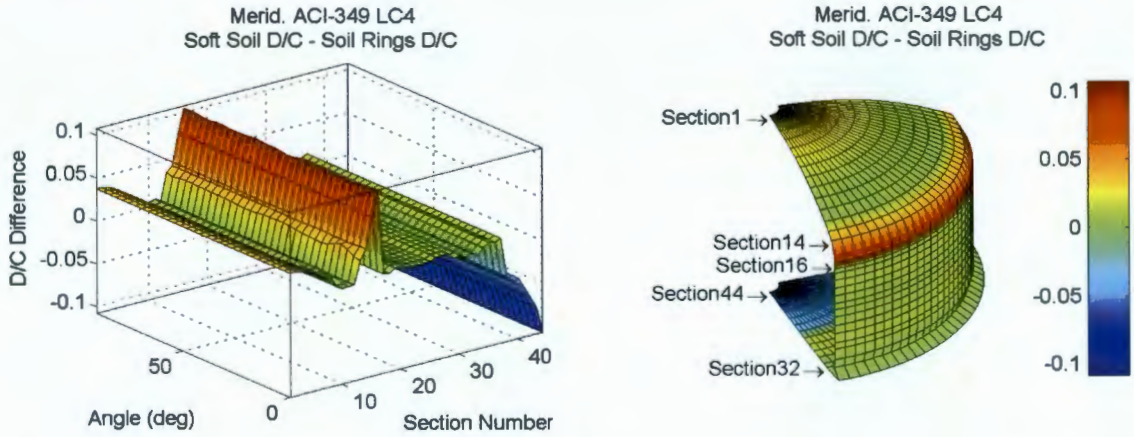

Figure K.28. LC4 ACI-349 Meridional D/C Ratio Differences ($D/C_{soft\ soil} - D/C_{soil\ rings}$): Type III SST (BES, Empty) Pit Appurtenances Soil Overburden Modeling Comparison

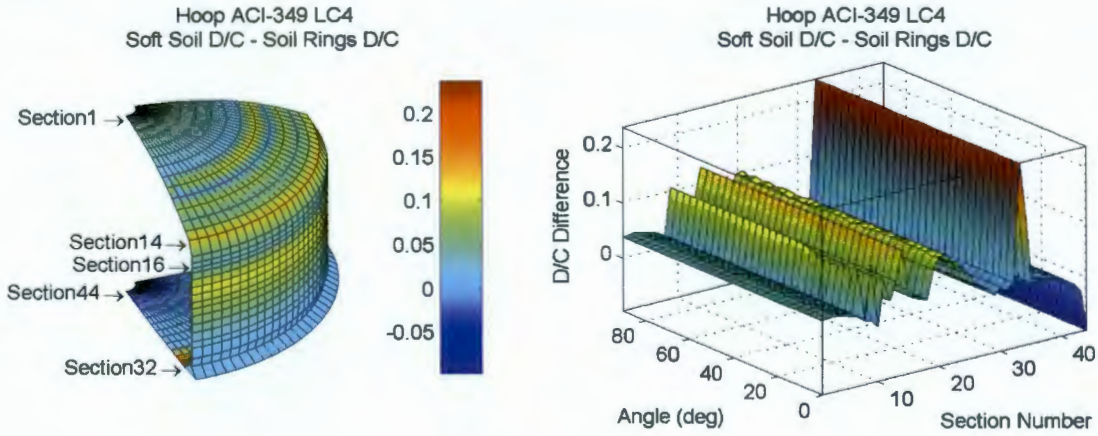

Figure K.29. LC4 ACI-349 Hoop D/C Ratio Differences ($D/C_{soft\ soil} - D/C_{soil\ rings}$): Type III SST (BES, Empty) Pit Appurtenances Soil Overburden Modeling Comparison

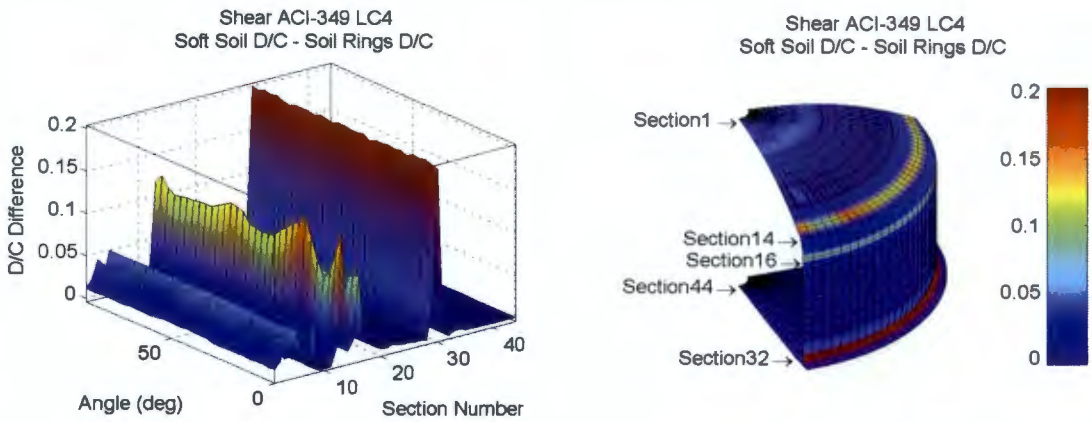

Figure K.30. LC4 ACI-349 Through-Wall Shear D/C Ratio Differences ($D/C_{soft\ soil} - D/C_{soil\ rings}$): Type III SST (BES, Empty) Pit Appurtenances Soil Overburden Modeling Comparison

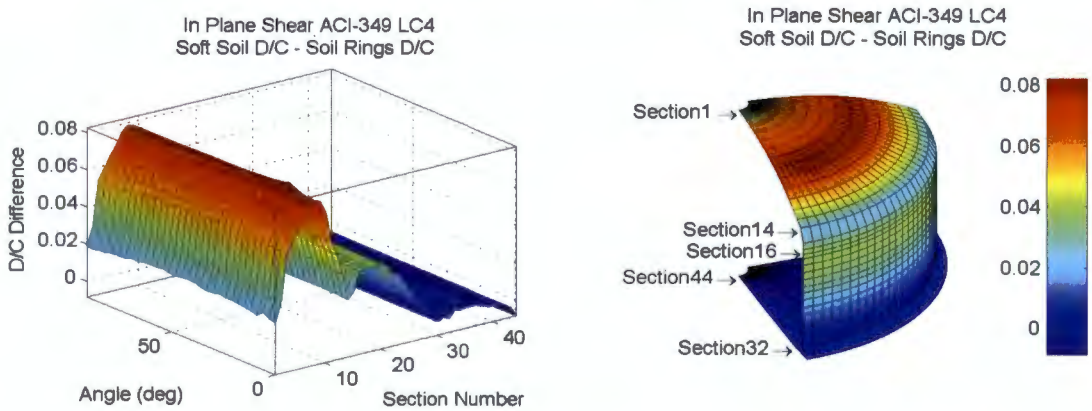

Figure K.31. LC4 ACI-349 In-Plane Shear D/C Ratio Differences ($D/C_{soft\ soil} - D/C_{soil\ rings}$): Type III SST (BES, Empty) Pit Appurtenances Soil Overburden Modeling Comparison

As shown in the comparison plots in Figure K.28 through K.31, the demands are higher for the soft soil modeling technique. The demand trends are very similar between soft soil modeling technique and the soil rings modeling techniques for all cases. Even though the demands are higher for the soft soil modeling technique the D/C ratios are very similar to the soil ring modeling technique except for increased D/C ratios in certain sections of the dome and footing regions.

K.8 Conclusion

The soil rings modeling technique is a more realistic technique for modeling the soil above the dome in the seismic SST model. The Type III soil overburden modeling technique improves initial gravity loading, removes amplified acceleration from soft soil, and supports the soil more realistically in the lateral direction. The soil rings modeling technique allows for a more accurate dead weight loading without interfering with the horizontal behavior as found in the soft soil modeling technique during a seismic time history. The removal of the soft soil eliminates extraneous non-physical modes and associated seismic acceleration, reducing the potential for excessive conservatism in the analysis. In addition, the soil rings modeling technique allows for adequate lateral support for the pit during the appurtenances seismic analysis.

This page intentionally left blank.

Appendix L

External Reviewer Comments

This page intentionally left blank.

Appendix L

External Reviewer Comments

September 7, 2011

Jim Castleberry
MS R3-26
Washington River Protection Solutions
PO Box 1500
Richland, WA 99352

Re: Comments and Recommendations on the Report on the Draft *Single-Shell Tank Integrity Project Analysis of Record, Hanford Type III Single-Shell Tank Thermal and Operating Loads and Seismic Analysis,* RPP-RPT-49990, Rev. 0.

Jim:

The analyses in this report are similar to those presented in the report for the Type II tanks (RPP-RPT-49989, Rev. 0, *Single-Shell Tank Integrity Project Analysis of Record, Hanford Type II Single-Shell Tank Thermal and Operating Loads and Seismic Analysis*) and are equally comprehensive and acceptable. Our comments, which are similar to those for the Type II tanks, are included in Attachment A.

Please feel free to contact Mike Terry with any questions or concerns that you might have.

Sincerely,

Dr. R. P. Kennedy

Dr. A. S. Veletsos

Attachment A

Comments and Recommendations on RPP-RPT-49990, Rev. 0, *Single-Shell Tank Integrity Project Analysis of Record, Hanford Type III Single-Shell Tank Thermal and Operating Loads and Seismic Analysis* by MW Rinker et al, 2011

by

R. P. Kennedy and A. S. Veletsos

Due to its similarity to the Type II report, RPP-RPT-49989, Rev. 0, *Single-Shell Tank Integrity Project Analysis of Record, Hanford Type II Single-Shell Tank Thermal and Operating Loads and Seismic Analysis*, we see no need for any additional studies or changes to the Type III Report, but feel that it would be highly desirable if a few brief, clarifying statements were added regarding the three issues identified below.

- The interaction effects among tanks are not considered in the Report. However, reference is made to a previous study, which concluded that, the effects "for tanks separated by one-half tank radius or more did not cause any significant increase in stress levels". It would, of course, be highly desirable to know how substantive both the thermal and seismic effects are for the tanks of interest. While no additional studies are proposed at this time, it is recommended that a statement be included in the Report to the effect that this issue will be examined in connection with the analyses of the Type IV tanks, and that depending on the results obtained, its effects on the Type III tanks may have to be considered at a later date.

  Addressed in Section 2.0.

- It would be helpful if the discussion near the end of Section 7.7 of the Report concerning the selection of the beta damping factor for the soil layers were clarified. It is especially desirable to identify the rational of Eq. (7.3) and the basis of selecting the indicated values for the factor DF. It would also be desirable to note that, while the variations with frequency of the percentage of critical damping corresponding to the alpha and beta damping factors for the soil layers is not realistic, the indicated values lead to conservative estimates of the maximum seismic effects.

  Addressed in Section 7.7.

- On the issue of slab element removal and its effect on the integrity of the liner addressed in Appendix E of the Report, the document should discuss the consequences of the vertical footing/slab offset. A potential comment might be: "The predicted displacement offset between the footing and slab is only about 0.05 inch. For reference, this is only about one-fourth of the original nominal liner thickness of 0.25 inch. The bottom and knuckle of the tank are also covered with a tar-based mastic material. Therefore, it is likely that the liner would bridge the small displacement offset without causing damage to the liner."

  Addressed in the Summary, Chapter 8, and Conclusion sections of the report.

This page intentionally left blank.

Pacific Northwest
NATIONAL LABORATORY

Proudly Operated by Battelle *Since 1965*

902 Battelle Boulevard
P.O. Box 999
Richland, WA 99352
1-888-375-PNNL (7665)
www.pnl.gov

U.S. DEPARTMENT OF
ENERGY